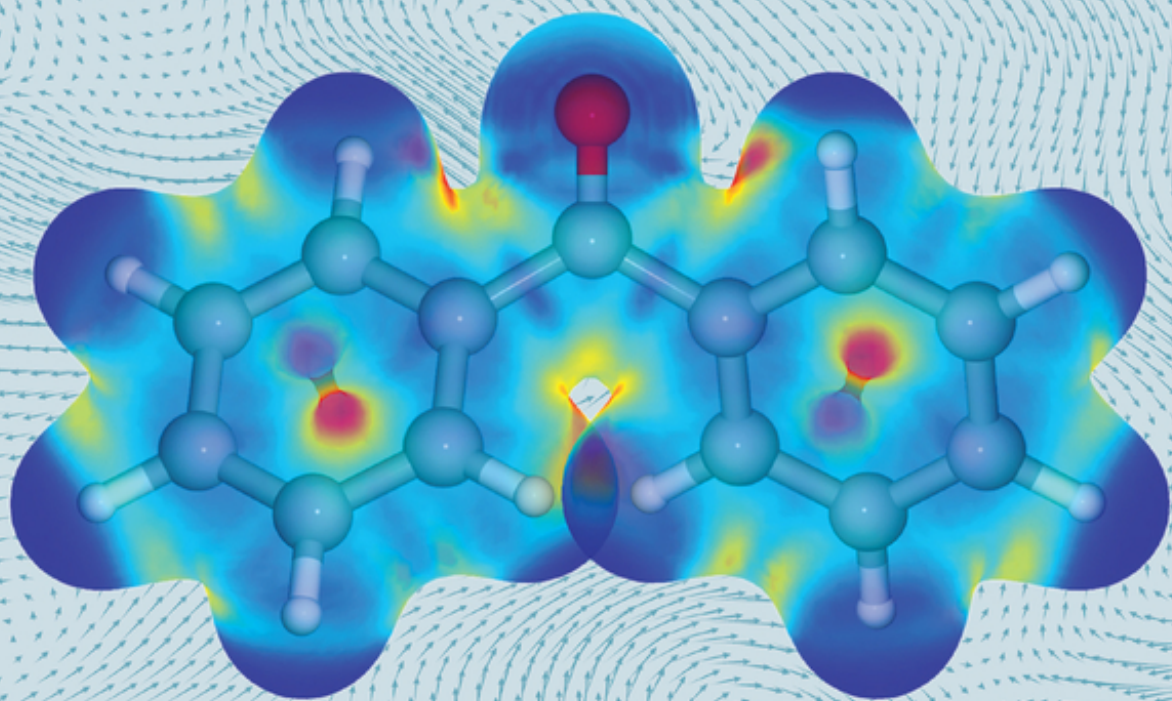


Edited by Shubin Liu

# Conceptual Density Functional Theory

Towards a New Chemical Reactivity Theory



## **Conceptual Density Functional Theory**

# **Conceptual Density Functional Theory**

Towards a New Chemical Reactivity Theory

Volume 1

*Edited by*  
*Shubin Liu*

**WILEY-VCH**

# **Conceptual Density Functional Theory**

Towards a New Chemical Reactivity Theory

Volume 2

*Edited by*  
*Shubin Liu*

**WILEY-VCH**

**Editor**

**Prof. Shubin Liu**

University of North Carolina  
Research Computing Center  
211 Manning Drive  
CB# 3420  
North Carolina  
United States

**Cover:** © GarryKillian/Shutterstock;  
Courtesy of Dong-Xia Zhao

■ All books published by **WILEY-VCH** are carefully produced. Nevertheless, authors, editors, and publisher do not warrant the information contained in these books, including this book, to be free of errors. Readers are advised to keep in mind that statements, data, illustrations, procedural details or other items may inadvertently be inaccurate.

**Library of Congress Card No.:** applied for

**British Library Cataloguing-in-Publication Data**

A catalogue record for this book is available from the British Library.

**Bibliographic information published by  
the Deutsche Nationalbibliothek**

The Deutsche Nationalbibliothek lists this publication in the Deutsche Nationalbibliografie; detailed bibliographic data are available on the Internet at <<http://dnb.d-nb.de>>.

© 2022 WILEY-VCH GmbH, Boschstr. 12,  
69469 Weinheim, Germany

All rights reserved (including those of translation into other languages). No part of this book may be reproduced in any form – by photoprinting, microfilm, or any other means – nor transmitted or translated into a machine language without written permission from the publishers. Registered names, trademarks, etc. used in this book, even when not specifically marked as such, are not to be considered unprotected by law.

**Print ISBN:** 978-3-527-35119-0

**ePDF ISBN:** 978-3-527-82992-7

**ePub ISBN:** 978-3-527-82993-4

**oBook ISBN:** 978-3-527-82994-1

**Typesetting** Straive, Chennai, India

**Printing and Binding**

Printed on acid-free paper

10 9 8 7 6 5 4 3 2 1

*This book is dedicated to the memory of the founding father of  
Conceptual Density Functional Theory,*

***Robert Ghormley Parr***

## Contents

### Volume 1

**Preface** *xv*

**Foreword** *xvii*

### Part I Foundations 1

#### 1 **Historic Overview** 3

*Paul Geerlings*

- 1.1 Introduction: From DFT to Conceptual DFT 3
- 1.1.1 But, Where Is Conceptual DFT in This Story? 5
- 1.2 The Birth of Conceptual DFT: The Identification of the Electronic Chemical Potential (1978) 5
- 1.3 The Early Years (1978–1985): Completing the Launching of Conceptual DFT 6
- 1.4 The Ever-Growing Tree of Response Functions and Its Associated or Derived Quantities (1985-) 8
- 1.5 Principles (1978;1985-) 10
- 1.6 Applications 12
- 1.7 The Present and the Future 12
- 1.8 Conclusions 13
- References 14

#### 2 **Basic Functions** 17

*Frank De Proft*

- 2.1 Introduction: Density Functional Theory 17
- 2.2 The Electronic Chemical Potential and the Electron Density as First Order Response Functions 20
- 2.3 Second and Higher Order Global Derivatives and Derived Quantities 23
- 2.4 Second- and Third-Order Local Quantities: The Fukui Function and the Dual Descriptor 26

- 2.5 Local Softness and Local Hardness 31
- 2.6 The Linear Response Function, Softness, and Hardness Kernels 33
- 2.7 The Perturbational Perspective on Chemical Reactivity 36
- 2.8 Conclusion 38
- Acknowledgment 39
- References 39

### **3 Basic Formalism 47**

*Paul W. Ayers and Shubin Liu*

- 3.1 Legendre Transform 48
- 3.2 Four Ensembles in CDFT 49
- 3.3 Basic Relations in the Canonical Ensemble 50
- 3.4 Basic Relations in the Grand Canonical Ensemble 52
- 3.5 Basic Relations in the Isomorphic Ensemble 53
- 3.6 Basic Relations in the Grand Isomorphic Ensemble 54
- 3.7 Relations Among Quantities from Different Ensembles 54
- 3.8 Second-order Taylor Expansions in the Four Ensembles 55
- 3.9 Generalized Considerations 57
- References 58

### **4 Basic Principles 61**

*Debdutta Chakraborty and Pratim K. Chattaraj*

- 4.1 Introduction 61
- 4.2 Global and Local Reactivity Descriptors 63
- 4.3 Electronic Structure Principles 65
  - 4.3.1 Electronegativity-Based Principle 65
  - 4.3.2 Hardness-Based Principles 66
  - 4.3.3 Electrophilicity-Based Principles 67
  - 4.3.4 Electronic Entropy-Based Principle 68
- 4.4 Conclusion 69
- Acknowledgments 69
- References 69

## **Part II Extensions 75**

### **5 Conceptual DFT and Excited States 77**

*Frédéric Guégan, Lynda Merzoud, Henry Chermette, and Christophe Morell*

- 5.1 Introduction 77
- 5.2 Reactivity and Selectivity of Excited States 77
  - 5.2.1 Photochemical Reactivity 77
  - 5.2.2 Insight from Frontier MO Theory 78
  - 5.2.3 Chemical Potential Locality 79
  - 5.2.4 In Summary 81
- 5.3 Excited States Used to Describe the Ground State 81



- 5.3.1 Reactivity from Excitation Energy: An Early Formulation of the Maximum Hardness Principle 81
- 5.3.2 States-Specific Dual Descriptors 83
- 5.3.3 Electron Polarization Rationalized with Excited States 85
- 5.3.4 In Summary 89
- 5.4 Conclusion and Perspectives 89
- References 90

## 6 Chemical Response Functions in (Quasi-)Degenerate States 93

*Patrick Bultinck and Carlos Cárdenas*

- 6.1 Introduction 93
- 6.2 Theory 95
  - 6.2.1 An Illustrative Example 99
- 6.3 Impact of Degeneracy on Chemical Concepts 100
  - 6.3.1 Electron Density 100
  - 6.3.2 Electrostatic Potential 102
  - 6.3.3 Atomic Charges 103
  - 6.3.4 Fukui Function 104
- 6.4 Further Considerations 105
- 6.5 Conclusions 106
- Acknowledgments 106
- References 107

## 7 Spin-Polarized CDFT 111

*Eduardo Chamorro*

- 7.1 Introduction 111
- 7.2 Non-relativistic Spin Density Functional Theory 112
- 7.3 Conceptual SP-DFT: Electronic Descriptors 114
  - 7.3.1 On Global and Local Electronic Descriptors 116
  - 7.3.2 Non-local Electronic Descriptors 117
  - 7.3.3 The Finite-Difference Approximations for Spin-Resolved Descriptors Within Kohn–Sham Theory 117
- 7.4 Conceptual SP-DFT: Nuclei-Related Descriptors 118
- 7.5 Brief Update Concerning Conceptual SP-DFT Applications (2010–2020) 119
- 7.6 Illustrating the Usefulness of Local SP-DFT Fukui Descriptors 121
- 7.7 Concluding Remarks and Perspectives 123
- Acknowledgments 124
- References 125

## 8 Finite Temperature Conceptual Density Functional Theory 137

*José L. Gázquez and Marco Franco-Pérez*

- 8.1 Introduction 137

- 8.2 First-Order Response Functions in the Grand Canonical Ensemble 139
- 8.3 Second-Order Response Functions in the Grand Canonical Ensemble 145
- 8.4 Response Functions to Changes in the Temperature and Their Central Role in a Chemical Event 148
- 8.5 Concluding Remarks 150  
Acknowledgment 151  
References 151
  
- 9 Chemical Reactivity in Time-Dependent Situations 161**  
*Utpal Sarkar and Pratim Kumar Chattaraj*
- 9.1 Introduction 161
- 9.2 Theoretical Background 163
- 9.3 An Atom Interacting with an External Electric Field 164
- 9.4 An Atom Interacting with an External Electric Field in a Confined Environment 167
- 9.5 A Molecule Interacting with an External Electric Field in a Confined Environment 167
- 9.6 An Atom Interacting with an External Magnetic Field in a Confined Environment 176
- 9.7 A Molecule Interacting with an External Magnetic Field in a Confined Environment 176
- 9.8 Ion–Atom Collision 178
- 9.9 Ion–Molecule Collision 179
- 9.10 Conclusion 180  
Acknowledgments 180  
References 180
  
- 10 Selectivity: An Electron Density Perspective 187**  
*Mar Ríos-Gutiérrez and Ramón Alain Miranda-Quintana*
- 10.1 Introduction 187
- 10.2 Conceptual Density Functional Theory 188
  - 10.2.1 The Fukui Function and Frontier Molecular Orbitals 188
  - 10.2.2 Calculating the Fukui Function 190
  - 10.2.3 Matching Criteria Based on the Fukui Function 193
  - 10.2.4 The Dual Descriptor 195
- 10.3 Molecular Electron Density Theory 196
  - 10.3.1 Pseudocyclic Selectivity in Polar DA (P-DA) Reactions 196
    - 10.3.1.1 Competitive [2 + 4] vs. [4 + 2] Cycloadditions 196
    - 10.3.1.2 Competitive [4 + 2] vs. [2 + 2] Cycloadditions 198
  - 10.3.2 Regioselectivity in [3 + 2] Cycloaddition (32CA) Reactions 199
  - 10.3.3 Chemoselectivity in 32CA Reactions 202
- 10.4 Conclusions and Perspective 203  
References 204

<b>11</b>	<b>Charge Transfer Models in Conceptual DFT</b>	209
	<i>Alberto Vela, José L. Gázquez, and Ulises Orozco-Valencia</i>	
11.1	Introduction	209
11.2	Taylor Expansion of the Energy	210
11.3	One-Parabola Model: The Venerable Parr and Pearson Model	211
11.4	Derivative Discontinuities	213
11.5	Two-Parabola Model	214
11.6	Association Reaction	216
11.6.1	Partitioning of the Charge Transferred in the PP Model	217
11.6.2	Global Charge Transfer in the Two-Parabola Model	218
11.6.3	Local Charge Transfer in the Two-Parabola Model	220
11.7	An Illustrative Application	221
11.8	Summary and Perspectives	223
	References	225
<b>12</b>	<b>Reaction Electronic Flux</b>	229
	<i>Luis Rincon and F. Javier Torres</i>	
12.1	Introduction	229
12.2	Reaction Force	230
12.2.1	Definition	230
12.2.2	Interpretation	233
12.3	Reaction Electronic Flux	233
12.3.1	The Chemical Potential	233
12.3.2	The Reaction Electronic Flux Concept	235
12.3.3	REF Application	236
12.4	Conclusions	239
	Bibliography	239
<b>13</b>	<b>Mechanical Force</b>	245
	<i>Tom Bettens and Frank De Proft</i>	
13.1	Introduction	245
13.2	Quantum Mechanochemistry	247
13.3	Mechanical Force and Conceptual DFT	249
13.3.1	Importance of a Small Force	249
13.3.2	Mechanochemical Response Functions	251
13.3.3	Chemical Bonds Stressed by Mechanical Force	252
13.3.4	Bond Angles Stressed by Mechanical Force	255
13.4	Conclusions and Outlook	258
	Bibliography	259
<b>14</b>	<b>The Hard/Soft Acid/Base Rule: A Perspective from Conceptual Density-Functional Theory</b>	263
	<i>Paul W. Ayers, Menatalla Mohamed, and Farnaz Heidar-Zadeh</i>	
14.1	Introduction	263

- 14.2 Acid/Base Strength, Hardness, and Reactivity from Conceptual DFT 265
- 14.3 Summary and Future Directions 269  
Acknowledgments 270  
References 270
- 15 Information-Theoretic Approach 281**  
*Chunying Rong, Donghai Yu, and Shubin Liu*
- 15.1 Introduction 281
- 15.2 Theoretical Framework 282
- 15.2.1 Three Representations 282
- 15.2.2 Three Principles in ITA 285
- 15.2.3 Relationships Among ITA Quantities 287
- 15.3 Applications 288
- 15.3.1 Steric Effect and Stereoselectivity 288
- 15.3.2 Electrophilicity and Nucleophilicity 291
- 15.3.3 Strong Covalent Interactions 292
- 15.3.4 Cooperativity in Noncovalent Systems 294
- 15.3.5 Aromaticity and Antiaromaticity 295
- 15.4 Concluding Remarks 297  
References 298
- 16 The Linear Response Function 301**  
*Paul Geerlings*
- 16.1 Introduction 301
- 16.2 Theory and Computational Aspects 303
- 16.3 Applications 307
- 16.3.1 Atoms: Shell Structure 307
- 16.3.2 Molecules: Inductive and Mesomeric Effects, Electron Delocalization, and Aromaticity 310
- 16.3.3 The Link Between the Linear Response Function and Molecular Conductivity 313
- 16.3.4 Alchemical Derivatives and Their Relationship with the Linear Response Function 315
- 16.4 Conclusions 320  
Acknowledgments 320  
References 321
- 17 Valence-State Concepts and Implications for CDFT 325**  
*László von Szentpály and Romola A. Bernard*
- 17.1 Introduction 325
- 17.2 Ground-State vs. Valence-State Energies 326
- 17.3 Valence-Pair-Affinity, its Equilibration, and Partial Charges 329
- 17.4 Valence-Pair-Equilibration and Thermodynamic Cycles 336
- 17.5 Partial Charges from Valence-Pair-Equilibration in Polyatomics 340
- 17.6 Electric Dipole Moments 342

- 17.7 Summary and Conclusions 344  
References 344
- Volume 2**
- Preface** xvii
- 18 **Chemical Information** 349  
*Rubén Laplaza, Julen Munárriz, and Julia Contreras-García*
- 19 **Molecular Face** 375  
*Dong-Xia Zhao, Hong Huang, and Zhong-Zhi Yang*
- 20 **Bridging Conceptual Density Functional and Valence Bond Theories** 391  
*Thijs Stuyver and Sason Shaik*
- Part III Applications** 417
- 21 **A Conceptual Density Functional Theoretic View of Chemical Binding** 419  
*Swapan K. Ghosh*
- 22 **Molecular Acidity, PCET, and Metal Specificity** 443  
*Dongbo Zhao and Shubin Liu*
- 23 **On the Mechanisms of Chemical Reactions** 463  
*Soledad Gutiérrez-Oliva, Angie Carolay Forero-Girón, Nery Villegas-Escobar, and Alejandro Toro-Labbé*
- 24 **Application of Reactivity Indices in the Study of Polar Diels–Alder Reactions** 481  
*Luis R. Domingo and Mar Ríos-Gutiérrez*
- 25 **Interaction Locality in Molecular Crystals** 503  
*Kanupriya Verma and Tonglei Li*
- 26 **A Conceptual DFT Approach Toward Analyzing Hydrogen Storage Potential** 533  
*Arindam Chakraborty, Sukanta Mondal, Rakesh Parida, Santanab Giri, and Pratim K. Chattaraj*
- 27 **The Fukui Function in Extended Systems: Theory and Applications** 555  
*Carlos Cárdenas, Andrea Echeverry, Trinidad Novoa, Andrés Robles-Navarro, T. Gomez, and Patricio Fuentealba*

- 28**      **Fermi Softness: A Local Perspective on Surface Activity** 573  
*Bing Huang and Lin Zhuang*
- 29**      **ABEEM Polarizable Force Field** 587  
*Dong-Xia Zhao and Zhong-Zhi Yang*
- 30**      **Charge Transfer and Polarization in Force Fields: An *Ab Initio* Approach Based on the (Atom-Condensed) Kohn–Sham Equations, Approximated by Second-Order Perturbation Theory About the Reference Atoms (ACKS2)** 603  
*Paul W. Ayers*
- Part IV Implementations** 631
- 31**      **Realization of Conceptual Density Functional Theory and Information-Theoretic Approach in Multiwfn Program** 633  
*Tian Lu and Qinxue Chen*
- 32**      **ChemTools: Gain Chemical Insight from Quantum Chemistry Calculations** 649  
*Leila Pujal, Alireza Tehrani, and Farnaz Heidar-Zadeh*
- Index** 663

## Contents

### Volume 1

**Preface** *xv*

**Foreword** *xvii*

### Part I Foundations 1

**1** **Historic Overview** 3

*Paul Geerlings*

**2** **Basic Functions** 17

*Frank De Proft*

**3** **Basic Formalism** 47

*Paul W. Ayers and Shubin Liu*

**4** **Basic Principles** 61

*Debdutta Chakraborty and Pratim K. Chattaraj*

### Part II Extensions 75

**5** **Conceptual DFT and Excited States** 77

*Frédéric Guégan, Lynda Merzoud, Henry Chermette, and Christophe Morell*

**6** **Chemical Response Functions in (Quasi-)Degenerate States** 93

*Patrick Bultinck and Carlos Cárdenas*

**7** **Spin-Polarized CDFT** 111

*Eduardo Chamorro*

- 8 Finite Temperature Conceptual Density Functional Theory** 137  
*José L. Gázquez and Marco Franco-Pérez*
- 9 Chemical Reactivity in Time-Dependent Situations** 161  
*Utpal Sarkar and Pratim Kumar Chattaraj*
- 10 Selectivity: An Electron Density Perspective** 187  
*Mar Ríos-Gutiérrez and Ramón Alain Miranda-Quintana*
- 11 Charge Transfer Models in Conceptual DFT** 209  
*Alberto Vela, José L. Gázquez, and Ulises Orozco-Valencia*
- 12 Reaction Electronic Flux** 229  
*Luis Rincon and F. Javier Torres*
- 13 Mechanical Force** 245  
*Tom Bettens and Frank De Proft*
- 14 The Hard/Soft Acid/Base Rule: A Perspective from Conceptual Density-Functional Theory** 263  
*Paul W. Ayers, Menatalla Mohamed, and Farnaz Heidar-Zadeh*
- 15 Information-Theoretic Approach** 281  
*Chunying Rong, Donghai Yu, and Shubin Liu*
- 16 The Linear Response Function** 301  
*Paul Geerlings*
- 17 Valence-State Concepts and Implications for CDFT** 325  
*László von Szentpály and Romola A. Bernard*

## Volume 2

### Preface xvii

- 18 Chemical Information** 349  
*Rubén Laplaza, Julen Munárriz, and Julia Contreras-García*
- 18.1 Introduction 349
- 18.2 The Electron Density 350
- 18.2.1 General Shape 350
- 18.2.2 Extracting Chemical Information: QTAIM 352
- 18.2.2.1 Critical Points of the Electron Density 353
- 18.3 Electron Density-Derived Functions 355



- 18.3.1 The Reduced Density Gradient 356
- 18.3.2 The Laplacian of the Electron Density 360
- 18.3.3 Kinetic Energy Densities 361
  - 18.3.3.1 LOL 361
  - 18.3.3.2 ELF 363
- 18.4 Assessing the Quality of Chemical Information 366
  - 18.4.1 Electron Density Errors 366
  - 18.4.2 Electron Localization Errors 368
- 18.5 Summary and Conclusions 371
  - Bibliography 372
  
- 19 Molecular Face 375**  
*Dong-Xia Zhao, Hong Huang, and Zhong-Zhi Yang*
  - 19.1 Introduction 375
  - 19.2 Atomic and Ionic Radii 376
    - 19.2.1 Turning Radius of a Hydrogen Atom 377
    - 19.2.2 Atomic Turning Radii for Many-Electron Atoms 378
  - 19.3 Molecular Face Formalism 379
    - 19.3.1 Potential Acting on One Electron in a Molecule 380
    - 19.3.2 Kohn–Sham One-Electron Potential 382
    - 19.3.3 Molecular Intrinsic Characteristic Contour – A Classical Turning Surface 382
  - 19.4 Frontier Electron Density on the Molecular Face, Revealing the Reaction and Interaction Between the Molecules 382
    - 19.4.1 Molecular Face Indicating the Hydrogen, Halogen, and Pnicogen Bonds Between the Molecules 383
    - 19.4.2 Molecular Face Picture Indicating the Interactions and Reactions Between Atoms and Molecules 384
    - 19.4.3 Showing Reactivity Ability by the Frontier Electron Density and Steric Force on the Molecular Face 387
  - 19.5 Summary 388
    - Acknowledgment 388
    - References 389
  
- 20 Bridging Conceptual Density Functional and Valence Bond Theories 391**  
*Thijs Stuyver and Sason Shaik*
  - 20.1 Introduction 391
  - 20.2 Qualitative VB Reactivity Theory 393
  - 20.3 How Does Delocalization Affect the Shape of the Curves in the VB Diagram? 395
  - 20.4 The Spin Density Distribution as a Probe for the Regioselective Preference in Radical Reactions 398
  - 20.5 Extending the VB Delocalization Perspective to Other Local Reactivity Descriptors: The Case of the Fukui Function 399

- 20.6 Hardness and Softness from a VB Perspective 402
- 20.7 Regioselectivity in Protonation Reactions: Sometimes Consideration of a Single Spin-pairing/Orbital Interaction Descriptor Is Not Enough! 405
- 20.8 Revisiting the Reactivity of the Ambident Vinyloxy Anion 409
- 20.9 Conclusions 411
- Acknowledgments 412
- References 412

### Part III Applications 417

- 21 A Conceptual Density Functional Theoretic View of Chemical Binding 419**  
*Swapan K. Ghosh*
  - 21.1 Introduction 419
  - 21.2 Physical Foundation of Chemical Concepts: A View Through Conceptual DFT Window 421
  - 21.3 Energy Change of Spin-Polarized Many-Electron Systems: A Perturbation Theoretic Approach 424
  - 21.4 Density Functional Perturbation Approach to Energy Changes in Molecule Formation: A Coarse-Grained Procedure 429
  - 21.5 A Coarse-Graining Procedure: Lattice Model for Molecular Systems 430
  - 21.6 Miscellaneous Aspects: Inclusion of Bond Space, Covalent Binding, and Correct Asymptotics 438
  - 21.7 Concluding Remarks 440
  - Acknowledgments 440
  - References 440
  
- 22 Molecular Acidity, PCET, and Metal Specificity 443**  
*Dongbo Zhao and Shubin Liu*
  - 22.1 Introduction 443
  - 22.2 Molecular Acidity 443
  - 22.3 Proton-coupled Electron Transfer 449
  - 22.4 Metal Specificity 452
  - 22.5 Concluding Remarks 460
  - References 460
  
- 23 On the Mechanisms of Chemical Reactions 463**  
*Soledad Gutiérrez-Oliva, Angie Carolay Forero-Girón, Nery Villegas-Escobar, and Alejandro Toro-Labbé*
  - 23.1 Introduction 463
  - 23.2 Theory of the Mechanism of Chemical Reactions 466
    - 23.2.1 The Reaction Force Analysis 466
    - 23.2.2 The Marcus Potential Function 469
    - 23.2.3 The Reaction Force Analysis of  $E^{(m)}(\xi)$  469

23.3	The Reaction Electronic Flux	470
23.3.1	Physical Partition of the REF	471
23.3.2	Chemical Partition of the REF	471
23.3.3	REF, Electronic Populations, and Bond Orders	472
23.4	Selected Applications	472
23.4.1	Reaction Force Analysis and REF	472
23.4.2	Physical and Chemical Partition of REF	474
23.5	Conclusions	474
	Acknowledgments	476
	References	476
<b>24</b>	<b>Application of Reactivity Indices in the Study of Polar Diels–Alder Reactions</b>	<b>481</b>
	<i>Luis R. Domingo and Mar Ríos-Gutiérrez</i>	
24.1	Introduction	481
24.2	The Diels–Alder Reaction. The Polar Mechanism	481
24.3	The Electrophilicity $\omega$ and Nucleophilicity $N$ Indices in the Study of P-DA Reactions	482
24.4	P-DA Reactions of Forward (FEDF) and Reverse (REDF) Electron Density Flux	485
24.5	Lewis Acid–Catalyzed P-DA Reactions of FEDF	486
24.6	P-DA Reactions of REDF. The H-DA Reactions	487
24.7	P-DA Reactions Between Electrophilic Species. A Challenge for the FMO Theory	490
24.8	Regioselectivity and Chemoselectivity in P-DA Reactions. The Parr Functions	493
24.8.1	The Parr Functions	493
24.8.2	Regioselectivity in P-DA Reactions	496
24.8.3	Chemoselectivity in P-DA Reactions	497
24.9	Conclusions	498
	Acknowledgments	499
	References	499
<b>25</b>	<b>Interaction Locality in Molecular Crystals</b>	<b>503</b>
	<i>Kanupriya Verma and Tonglei Li</i>	
25.1	Introduction	503
25.2	Characterizing Solid-state Reaction of Organic Crystals	505
25.2.1	Reactivity of Pharmaceutical Crystals	506
25.2.2	Reactivity of Energetic Materials	508
25.3	Crystal–Solvent Interaction and Wettability Anisotropy	511
25.4	Atomic Libration in Organic Crystals	514
25.5	Hydrogen-bonding Strength	516
25.6	Locality of Intermolecular Interactions in Organic Crystals	519
25.7	Conclusion	525
	References	525

- 26      A Conceptual DFT Approach Toward Analyzing Hydrogen Storage Potential    533**  
*Arindam Chakraborty, Sukanta Mondal, Rakesh Parida, Santanab Giri, and Pratim K. Chattaraj*
- 26.1      Introduction    533
- 26.2      Conceptual DFT Approach for Hydrogen Storage Materials    535
- 26.3      Computational Details    537
- 26.4      Designing of Hydrogen-Binding Building Blocks    537
- 26.5      Concluding Remarks    547
- Acknowledgments    548
- References    548
- 
- 27      The Fukui Function in Extended Systems: Theory and Applications    555**  
*Carlos Cárdenas, Andrea Echeverry, Trinidad Novoa, Andrés Robles-Navarro, T. Gomez, and Patricio Fuentealba*
- 27.1      Introduction    555
- 27.2      Models of Local Softness: The Case of Metallic Carbon Nanotubes    558
- 27.2.1      Carbon Nanotube    559
- 27.3      Models of Fukui Function: The Case of Alkaline Metal Oxides Bulks and (100) Surfaces    561
- 27.3.1      Application to Surfaces    565
- 27.4      Conclusions    568
- Acknowledgments    568
- References    568
- 
- 28      Fermi Softness: A Local Perspective on Surface Activity    573**  
*Bing Huang and Lin Zhuang*
- 28.1      Introduction    573
- 28.1.1      Fermi Softness    575
- 28.1.1.1      Basic Idea    575
- 28.1.1.2      Fermi Softness vs. d-Band Center    579
- 28.2      Applications    580
- 28.2.1      Correlation with Adsorption Energy    580
- 28.2.2      Active Sites of MoS<sub>2</sub>    582
- 28.3      Conclusion and Outlook    582
- Acknowledgments    584
- Bibliography    584
- 
- 29      ABEEM Polarizable Force Field    587**  
*Dong-Xia Zhao and Zhong-Zhi Yang*
- 29.1      Introduction    587
- 29.2      Classical Force Fields with the Fixed Atomic Partial Charges    587
- 29.2.1      The Potential Energy Function in a Force Field    588

29.2.2	Charge Distribution and Polarization	589
29.3	Polarizable Force Fields	590
29.3.1	Induced Dipole Moment (Multipole) Model and Drude Model	591
29.3.2	Electronegativity Equalization Method for Calculating the Charge Distribution	592
29.3.2.1	EEM Method	592
29.3.2.2	Atom–Bond Electronegativity Equalization Method (ABEEM)	593
29.3.3	Calibration of the Parameters	595
29.4	Molecular Dynamic Simulations	595
29.4.1	Water Clusters and Water Solution	595
29.4.2	Chemical and Biological Systems as Well as in Their Aqueous Solution	597
	Acknowledgment	598
	References	598
<b>30</b>	<b>Charge Transfer and Polarization in Force Fields: An <i>Ab Initio</i> Approach Based on the (Atom-Condensed) Kohn–Sham Equations, Approximated by Second-Order Perturbation Theory About the Reference Atoms (ACKS2)</b>	<b>603</b>
	<i>Paul W. Ayers</i>	
30.1	Introduction	603
30.2	Motivation: Where Do Current Approaches Fail	604
30.2.1	Challenge: Molecular Polarizability and Hyperpolarizability	604
30.2.2	Challenge: Charge and Spin States	605
30.2.3	Challenge: Molecular Dissociation and Long-Range Electron Transfer	605
30.2.4	Challenge: (Near) Degeneracy	606
30.3	The Atom-Condensed Kohn–Sham Framework	606
30.3.1	Explicit Demonstration That Atomistic Force Fields Can Be Derived from DFT	606
30.3.2	Atoms in a Molecule (AIM)	608
30.3.3	Energy Difference from Changes in Molecular Density	608
30.3.4	The Electronegativity Equalization Method (EEM): Energy Difference from Changes in Atomic Densities	609
30.3.5	<i>Ab Initio</i> Parameterization of EEM	610
30.3.6	Kohn–Sham DFT: Fixing the Failures of Orbital-Free DFT and Traditional EEM	611
30.3.7	Atom-Condensed Kohn–Sham DFT (ACKS-DFT)	611
30.4	Recapitulation	613
30.5	Challenges	615
30.5.1	Parameterization of the ACKS2 Model	615
30.5.2	Tests for Atomistic Force-Field Models	616
	Acknowledgments	618
	References	618

**Part IV Implementations 631****31 Realization of Conceptual Density Functional Theory and Information-Theoretic Approach in Multiwfn Program 633***Tian Lu and Qinxue Chen*

- 31.1 Introduction 633
- 31.2 Some Relevant Knowledge 633
  - 31.2.1 Basic Features of Multiwfn 633
  - 31.2.2 Evaluation of Electron Density 634
  - 31.2.3 Atomic Space Partition and Integration 635
- 31.3 Conceptual Density Functional Theory Analysis in Multiwfn 636
  - 31.3.1 Automatic Calculation of Common CDFT Quantities 636
  - 31.3.2 Orbital-Weighted Fukui Function and dual Descriptor 637
  - 31.3.3 Evaluation of Contribution of Orbitals to Fukui Function 639
  - 31.3.4 Other CDFT Analyses 641
- 31.4 Information-Theoretic Approach Analysis in Multiwfn 642
  - 31.4.1 Shannon Entropy 642
  - 31.4.2 Fisher Information and Ghosh–Berkowitz–Parr Entropy 643
  - 31.4.3 Relative Shannon Entropy and Relative Fisher Entropy 643
  - 31.4.4 Rényi Entropy 644
  - 31.4.5 Other Quantities Theoretically Related to ITA 644
- 31.5 Concluding Remarks 645
- References 645

**32 ChemTools: Gain Chemical Insight from Quantum Chemistry Calculations 649***Leila Pujal, Alireza Tehrani, and Farnaz Heidar-Zadeh*

- 32.1 Introduction 649
- 32.2 Getting Started with ChemTools 650
  - 32.2.1 Input and Output 650
  - 32.2.2 Example Gallery 651
- 32.3 ChemTools Features 652
  - 32.3.1 Conceptual Density Functional Theory 652
  - 32.3.2 Atoms-in-Molecules Partitioning Schemes 653
  - 32.3.3 Chemical Topological Analysis 653
  - 32.3.4 Density Functional Theory Tools 653
  - 32.3.5 Conceptual Density Matrix Functional Theory 653
  - 32.3.6 Molecular Orbital Theory 653
- 32.4 ChemTools Design Principles 654
  - 32.4.1 Open-Source Software 654
  - 32.4.2 Modularity 655
  - 32.4.3 Robustness and Quality Assurance 655
  - 32.4.4 Ease of Extension and Contribution 657

32.5	Future Prospects	657
	Acknowledgments	658
	References	658
	<b>Index</b>	<b>663</b>

## Preface

Conceptual density functional theory (CDFT), pioneered by Robert G. Parr and coworkers, has been with us for over 30 years. As witnessed by the 32 chapters presented in this book, there have been tremendous interests and enormous developments on CDFT in the literature. Nevertheless, there has never been a book dedicated to this topic. With the sad passing of Bob Parr, our beloved teacher, mentor, collaborator, and friend, the goal for us to put collective efforts along that direction had become more urgent. That was the reason why we held CCTC2018 Symposium in Changsha, China, where a roundtable discussion led to a CDFT status report on *Theoretical Chemical Accounts*. When Aron Urbatsch of Wiley VCH approached me in January 2020 with the book idea and I subsequently consulted major players in CDFT about the possibility, the feedback that I obtained was overwhelmingly positive. That's how and when this book project got started in the first place.

Coincidentally, that's also when the global pandemic of COVID-19 got started. Only people who experienced it firsthand knew how hard and miserable life became during that period. Amazingly, we still could get this book done as proposed. I am deeply indebted and sincerely grateful to all authors who spent days and nights during this extremely tough time working on their contributions. I wish also to thank the publishers for their hard work and flexibility. Without the commitment and dedication of all of them, this book is simply impossible.

To wrap up, let us remember what Bob told us: "There is another whole side of DFT which has concerned and still concerns many of us, the 'conceptual' side. This side is rich in potential, and it is not without accomplishment. The concepts of DFT neatly tie into older chemical reasoning, and they are useful for discussing molecules in course of reaction as well as for molecules in isolation. Where solid state physics has Fermi energy, chemical potential, band gap, density of states, and local density of states, quantum chemistry has ionization potential, electron affinity, hardness, softness, and local softness. Much more too."

10 January 2022

*Shubin Liu*  
*Chapel Hill, North Carolina, USA*



## Foreword

It was a great pleasure to read this book edited by Dr. Shubin Liu. The comprehensive collection of articles from leading scientist covers the field of conceptual density functional theory (CDFT) from historical perspectives, didactic presentations, chemical insights, critical analysis, and frontier ideas to computational software and applications in chemistry. This is the book to read for students and researchers.

Density functional theory (DFT) has become the most widely used method for computational chemistry and materials science because of the optimal balance between the accuracy of prediction on measurable physical quantities and the cost of computation. In view of the power of computational predictions from DFT, what is the role of CDFT? What is CDFT anyway?

Let us think over the meaning of conceptual. “The definition of conceptual is something having to do with the mind, or with mental concepts or philosophical or imaginary ideas”, according to a dictionary (<https://www.yourdictionary.com/conceptual>). “Something is conceptual when it deals primarily with abstract or original thoughts”, based on another one (<https://www.vocabulary.com/dictionary/conceptual>). This appears to fit our appreciation of CDFT.

Chemical concepts are indeed mental or philosophical ideas of chemists about molecules and their properties. Chemical concepts are therefore in general different from physical quantities, which are observables, such as the ionization potentials, electron affinities and the geometry of a molecule in its ground state. Chemical concepts are in the mind of a chemist and are apparently not directly related to observables. For examples, the concept of electronegativity describes the capability of a molecule to attract electrons, and the concept of chemical hardness is related to intrinsic chemical reactivities of a molecule. Chemical concepts are traditionally somewhat fuzzy, without a mathematical definition. They are a very useful part of the chemical language and chemical thinking framework.

In contrast, physical observables can often be directly computed from the electron density or the wavefunction of a molecule, or the density matrix or the Green's functions of the statistical ensemble of a condensed matter. While wave function methods can in principle rely on systematic improvement based on some natural orders or hierarchy in the theory, density functional methods had (and still have) to fight with a way to find good approximations. Thus, wave function methods had to find the

best way to converge to the exact result, while the DFT framework stimulates one to find out what approximate methods really do.

When a method is created, it is intended for users ultimately. Of course, calculations should produce numbers that can be compared to experiments. Validation of computational predictions is critical for developing and accessing theoretical methods. It was the successful validation of DFT calculations that led the broad application of DFT in chemistry and materials science and engineering. There is also a more ambitious objective: we would like our calculations to be predictive. Of course, “numbers don’t lie”, but there is something more we would like to produce from our calculations. The users should get have some tools that they can apply on the results of the calculations that should allow them to think further, to connect the results with existing knowledge. In other words, to apply some concepts to the results obtained.

Let us exemplify the statement above. Ionization potentials and electron affinities are quantities that can be measured, and also be computed. The concept of reactivity is vague. However, it is widely used. There are several definitions for electronegativity, but this does not mean that a given definition is not based on quantities that cannot be derived from experimental measurements. For example, the electronegativity can be defined as half the sum of the ionization potential and the electron affinity.

Clearly different from the commonly used computational prediction aspect of DFT, as shown throughout the chapters in this book, CDFT is a framework of mathematical definitions of chemical concepts and application of the concepts to describing chemical systems, based mainly on DFT. Therefore, CDFT provides the quantitative connections to the concepts in the minds of chemists and the associated quantitative understanding of chemical reactivities, using electronic structure theory, mainly DFT. The 1978 identification by Parr and coworkers of electronegativity of atoms and molecules as the negative of chemical potentials averaged over the two limits of electron addition and removal is a great example, marking the birth of the field of CDFT.

What aspects of DFT are uniquely important for quantitative connections to chemical concepts? Using electron density, a reduced variable and much simpler object, leads to more direct connection to conceptual thinking. Furthermore, the definition on electronegativity highlights the feature of DFT in treating electron number as a continuous variable (fractionals). Yes, fractional number of electrons can occur as a grand canonical ensemble in quantum theory. However, there is no direct connection from a grand canonical ensemble description to an isolated molecule in its ground state. In other words, an isolated molecule in its ground state does not need an ensemble description. Similarly, in DFT, fractional numbers of electrons can occur in an ensemble. But there is an inherently more important role of fractional numbers of electrons in DFT; namely, fractional numbers of electrons are the manifestation in the electron density, a classical variable, of the quantum mechanical principle of state degeneracy. As a result of the linearity of the Schrodinger equation, any linear combination of degenerate eigenstate wavefunctions is also an eigenstate with the same energy. In DFT with the basic variable being the electron density,

any convex linear combination of electron density for the degenerate states has the same total energy. This naturally leads to fractional charges and spins in the electron density and their corresponding exact conditions, which are critical for developing functional approximations.

As with electronegativity, a large part of CDFT has been developed for describing responses of the system to changes in electron numbers and/or external potentials. The corresponding total energy derivatives play a central role in CDFT. They have been applied in broad fields of chemistry and materials. On the other hand, many interesting mathematical definitions of chemical concepts are not expressed as such energy derivatives. Two outstanding examples are the electron localization function (ELF), capturing the electron localization features, and the non-covalent interaction (NCI), revealing noncovalent interactions in molecules and bulk systems. Both ELF and NCI are not about measurable quantities, but they describe quantitatively what is in the minds of chemists. All these are featured in this book.

Many concepts used in interpreting results of density functional calculations could be also computed from experimental densities if they were accurate enough. Electronegativity, ELF and NCI are such examples. Even the fractional occupation numbers, a construct of the Kohn-Sham method that shows up in situations when (near-)degeneracy is important enter this category: once we have a density, we can construct the exact Kohn-Sham potential, and check if fractional occupation numbers show up.

Looking forward, CDFT would benefit from developing sets of standards or benchmarks to evaluate concepts developed. The validation was critical for the development and success of computational DFT and should be expected to further promote the field of CDFT – it is important for CDFT to spread out to users. This measures its success. However, challenges remain on how to develop such test sets.

The Editor of this book, Dr. Shubin Liu is a leader in CDFT, having been trained with the late Professor Robert G. Parr, the founding father of CDFT. Dr. Liu has assembled a team of distinguished scientists. Together, they provide a feast of CDFT for all to enjoy.

Durham, NC  
Paris, France  
February 2022

*Weitao Yang*  
Duke University  
*Andreas Savin*  
CNRS and Sorbonne University

## **Part I**

### **Foundations**

# 1

## Historic Overview

Paul Geerlings

Vrije Universiteit Brussel, Research Group of General Chemistry (ALGC), Faculty of Science and Bioengineering Science, Pleinlaan 2, Brussels 1050, Belgium

### 1.1 Introduction: From DFT to Conceptual DFT

Density Functional Theory goes back to the early days of Quantum Mechanics when, in 1926, Thomas and Fermi [1–3] presented a model to study the electronic structure of atoms on the basis of the electron density  $\rho(\mathbf{r})$  instead of the wave function. The simplification is spectacular: for an  $N$ -electron system, one passes from an immensely complicated wave function  $\Psi(\mathbf{x}^N)$ , a function of  $4N$  variables (three spatial variables and one spin variable for each electron, gathered in a 4-vector  $\mathbf{x}$ ) to just three variables in the density  $\rho(x, y, z)$ . The results for atoms were encouraging, but the approach failed dramatically for (diatomic) molecules not being able to account for their stability. Was the loss of information when passing from a wave function to the density (in fact, an integration over  $4N-3$  variables) too drastic? An important step was taken by Slater in the 1950s. In his  $X_\alpha$  method [4], he presented a simplification of the Hartree–Fock method replacing the complicated nonlocal Fock operator with a local, single parameter, operator involving the density. The method turned out to be a quite efficient technique for electronic structure calculations on molecules and solids.

One has, however, to wait until 1964 when Hohenberg and Kohn [5] turned density-based *models* into a full-fledged *theory* through their two famous theorems. The first theorem is an existence theorem presenting the ground-state energy of a system as functional of the density. The proof, based on a *reductio ad absurdum*, is, as quoted by Parr and Yang [6], “disarmingly simple.” The second theorem offers a variational principle, and so, at least in principle, a road to the “best” density: look for the one yielding the lowest energy, as known for decades in wave function quantum mechanics. The crux of the first theorem is that it is proven that for a given  $N$ -electron system, its ground-state density  $\rho(\mathbf{r})$  is compatible with a single external potential  $v(\mathbf{r})$ , i.e. the potential felt by the electrons due to the nuclei, in the

absence of external fields. This single external potential is equivalent to a unique constellation of nuclei: their number, position, and charge. To put it all succinctly:  $\rho$  determines  $v$ , and as it also determines  $N$  by integration, it also determines the Hamiltonian, and at least in principle, “everything.” Coming back to the second theorem, the variational procedure leads to the Euler equation of the problem

$$v(\mathbf{r}) + \delta F_{\text{HK}}/\delta \rho(\mathbf{r}) = \mu \quad (1.1)$$

where  $F_{\text{HK}}$  is the Hohenberg–Kohn functional and  $\mu$  the Lagrangian Multiplier introduced during the variational procedure ensuring that the density remains properly normalized to  $N$ . Equation (1.1) is the analogue of the time-independent Schrödinger equation  $H\psi = E\psi$ , which also can be obtained in a variational ansatz, where the Lagrangian Multiplier ensuring proper normalization of the wave function  $\psi$  is at the end identified with the system’s energy  $E$ . The analogy is striking, but two aspects of this equation deserve further consideration. What is  $F_{\text{HK}}$ , and what is the physical interpretation of  $\mu$ ? The Hohenberg–Kohn functional is a universal functional (i.e.  $v$ -independent), which contains unknown parts governing electron correlation and exchange assembled in the exchange–correlation functional  $E_{\text{xc}}[\rho]$ , which will be highlighted in other chapters in the “Fundamentals” part in this book. Quintessentially, it’s the price to be paid for the simplification when passing from a wave function to the density, still retaining its essential information content. By introducing, in the context of a non-interacting reference system, orbitals in the variational procedure, Kohn and Sham [7] were able to cast the variational equation into a series of pseudo-one-electron eigenvalue equations, similar to the Hartree–Fock equations, be it, again, that part of the concerned operator is unknown: the functional derivative of  $E_{\text{xc}}$  with respect to  $\rho(\mathbf{r})$ ,  $\delta E_{\text{xc}}/\delta \rho(\mathbf{r})$ , termed the exchange–correlation potential  $v_{\text{xc}}(\mathbf{r})$ .

The history of DFT is (among others) a quest for finding better and better approximations for this unknown  $v_{\text{xc}}(\mathbf{r})$ . The simplest approximation, of standard use, mainly by solid-state physicists, in the 1970s and the 1980s was the local density approximation (LDA) [7], showing however substantial over-binding in molecules [8]. Things became more interesting for chemists in the second half of the 1980s when the generalized gradient approximations (GGA) were launched [9, 10]. The great breakthrough, with the wide acceptance of DFT by the Quantum-Chemical community, came in the early 1990s when hybrid functionals were introduced, in which a fraction of the GGA exchange was replaced with exact HF exchange, with as most prominent example the still ubiquitous B3LYP functional [8–10]. This approach yielded at that time unsurpassed quality/computing time ratios, the latter aspect being reinforced by its implementation in Pople’s widely used GAUSSIAN package [11]. At that time, DFT was on its way to become the standard method for obtaining an optimal quality/cost ratio for studying properties and reactions of not too exotic systems of varying sizes. Afterward, its “popularity” grew at incredible pace. In his excellent 2012 *Journal of Chemical Physics* perspective, Burke [12] plots the number of papers retrieved from the Web of Science when searching for DFT as a function of time, reaching in 1996 about 1000 papers, 5000 in 2005, and 8000 in 2010. Nowadays, DFT is the workhorse “par excellence” used, not only by theoreticians

but also by experimentalists, in combined experimental–computational papers, when exploring structure, stability, electronic properties, reactivity, and reactions of molecules, polymers, and solids in the most diverse subdomains of chemistry [8].

### 1.1.1 But, Where Is Conceptual DFT in This Story?

As highlighted at the very beginning of this chapter, the variational Eq. (1.1) stands central in DFT, just as the Schrödinger equation in wave function theory. Besides the quest for the exact Hohenberg–Kohn functional, we already mentioned that a second fundamental question in relation to this equation arises: what is the physical/chemical meaning of the Lagrangian multiplier  $\mu$ ? Its identification by Parr et al. [13] can be considered as the birth of Conceptual DFT.

This genesis, its early years, and evolution with a short reflection on its present status and its future will be described in the following paragraphs. Note that detailed explanations and derivations leading to the various concepts, formulas, and equations will mostly not be given in view of space limitations and because the reader will find them in Part I (Foundations) and, in case of more recent developments, in Part II (Extensions) of this book. This is also the reason why the number of references is kept to the most essential ones. For the most extensive reviews on Conceptual DFT, we can now already refer the reader to items [14–20] in the reference list.

## 1.2 The Birth of Conceptual DFT: The Identification of the Electronic Chemical Potential (1978)

In a landmark paper in 1978, Parr et al. [13] showed that the Lagrangian Multiplier in the DFT variational equation could be written as the partial derivative of the system's energy with respect to the number of electrons at fixed external potential.

$$\mu = (\partial E / \partial N)_v \quad (1.2)$$

The chemical importance of this demystification of the Lagrangian Multiplier shows up when going back to the early 1960s, when Iczkowski and Margrave [21] presented evidence, on the basis of experimental ionization energies and electron affinities, that the energy of an atom could reasonably well be written as a polynomial in  $n$  (the number of electrons  $N$  minus the nuclear charge) around  $n = 0$  as

$$E = E(n) = an^4 + bn^3 + cn^2 + dn \quad (n = N - Z) \quad (1.3)$$

Assuming continuity and differentiability of  $E$ , the slope at  $n = 0$  and at fixed nuclear charge  $Z$ ,  $(\partial E / \partial n)_{n=0}$ , could easily be seen as a measure of electronegativity  $\chi$  of the neutral system

$$\chi = -(\partial E / \partial N)_Z = -(\partial E / \partial n)_Z \quad (1.4)$$

As it was recognized that the cubic and quartic terms were negligible, Mulliken's electronegativity definition [22]

$$\chi = \frac{1}{2}(I + A) \quad (1.5)$$

where  $I$  and  $A$  are the first ionization and electron affinity, respectively, were regained as a special case, so that within this approximation

$$\mu = -\chi = -\frac{1}{2}(I + A) \quad (1.6)$$

Generalizing the constant  $Z$  condition for atoms to a constant  $\nu$  condition for molecules, the Lagrangian Multiplier of the Euler Eq. (1.1) has now been identified with a cornerstone of (physical) chemistry: electronegativity. *A bridge between Density Functional Theory and (concepts in) Chemistry has thereby been established.*

The analogy between  $\mu$  and (the expression for) the macroscopic chemical potential of component  $i$  in a system at given pressure  $p$  and temperature  $T$  is beautiful. Indeed,  $\mu_i$  can be written as [23]

$$\mu_i = (\partial G / \partial n_i)_{nj \neq i, p, T} \quad (1.7)$$

with  $G$  the Gibbs free energy and  $n_i$  the number of moles of component  $i$ . The resemblance between Eqs (1.4) and (1.7) was at the origin of later, even up to the present moment, endeavor to scrutinize analogies between macroscopic thermodynamics and "microscopic" Conceptual DFT.

### 1.3 The Early Years (1978–1985): Completing the Launching of Conceptual DFT

Further exploring the  $E = E(N)$  function Parr and Pearson identified in 1983, quite soon after Parr's 1978 landmark paper, Pearson's hardness as the second derivative of  $E$  with respect to  $N$  at constant  $\nu$ , denoted as  $\eta$  [24]

$$\eta = (\partial^2 E / \partial N^2)_{\nu} \quad (1.8)$$

Pearson had introduced the hardness concept in the early 1960s [25] in the context of the study of generalized acid–base reactions, where he proposed a classification of favorably interacting acids and bases, mainly built on the polarizability, terming low polarizable species as "hard" and highly polarizable species as "soft." Combining this classification and the terminology then yields the famous hard-soft acid-base (HSAB) principle: hard acids preferentially interact with hard bases; soft acids preferentially interact with soft bases. But... no quantification of this hardness/softness concept was available, be it a way to calculate it. It was the identification of  $\eta$  as the second derivative Eq. (1.8), which paved the way to quantitative studies on the hardness of atoms and molecules and to use it as such or in the context of the HSAB principle: *a second achievement where a chemical concept is linked to DFT, as indeed  $(\partial^2 E / \partial N^2)_{\nu}$  is nothing else than the  $N$  derivative of the Lagrangian Multiplier  $\mu$ .* Both  $\mu$  and  $\eta$  are called *global* descriptors as they are associated to an overall characteristic of the system.



Soon after, in 1984, Parr and Yang [26] launched the first *local*, i.e.  $\mathbf{r}$ -dependent or varying from place to place descriptor, which further established the bridge between DFT and chemistry. They generalized and extended Fukui's frontier Molecular Orbital concept [27] by considering a mixed second-order derivative  $f(\mathbf{r}) = (\partial^2 E / \partial N \delta v(\mathbf{r}))$ . Its chemical significance is clear when realizing that it can be easily deduced from perturbation theory [6, 15] that

$$(\delta E / \delta v(\mathbf{r}))_N = \rho(\mathbf{r}) \quad (1.9)$$

so that  $f(\mathbf{r})$  can also be written as  $(\partial \rho(\mathbf{r}) / \partial N)_v$ , indicating how a system partitions the added or subtracted electrons in space. When the orbitals are kept unchanged (frozen) upon adding or subtracting electrons, it is easily seen that  $f(\mathbf{r})$  boils down to the highest occupied molecular orbital (HOMO) or lowest occupied molecular orbital (LUMO) density (for decreasing or increasing  $N$ , respectively) and can thereby directly be linked to the basic ingredients of Fukui's reactivity descriptors. In the early 1950s, Fukui emphasized the predominant role of the frontier orbitals in (certain types of) reactions. His Frontier MO theory was considered both a milestone and a guiding principle in studying chemical reactions and reactivity. One of the most prominent examples are the celebrated Woodward–Hoffmann rules [28], highlighting the conservation of orbital symmetry (with particular emphasis on the frontier MOs) in the course of concerted reactions. In honor of Fukui, this local descriptor  $f(\mathbf{r})$  was termed the Fukui function.

Note that when writing  $\rho(\mathbf{r})$  as  $(\delta E / \delta v(\mathbf{r}))_N$ ,  $f(\mathbf{r})$  can also be written as  $(\delta \mu / \delta v(\mathbf{r}))_N$ , stressing again the link with the content of the variational Eq. (1.1).

Two points should be stressed. *Again, a DFT routed quantity, the functional derivative of the Lagrangian Multiplier with respect to the external potential, has been connected to a chemical “cornerstone,” this time at stake when scrutinizing reactivity.* On top of that, and almost unnoticed, the electron density itself also entered this series of descriptors, in fact, as Eq. (1.9) shows, as the “first” local one: the derivative of  $E$  with respect to  $v(\mathbf{r})$ . It's useful to reconsider the fundamental equation of DFT, Eq. (1.1), again and to note that three of its main ingredients  $E$ ,  $v(\mathbf{r})$ , and  $\mu$ , and the number of electrons are retrieved as pillars when establishing the link between the physicist's DFT and what was later on termed “the Chemist's DFT,” “Chemical DFT,” or most commonly “Conceptual DFT” [20, 29].

It can safely be said that at that time, i.e. around 1985, the launching of DFT was completed. Remarkably, and when going back to the history of DFT, this moment is situated in a period when DFT was not yet that popular in the quantum-chemical community. The pioneering work by Parr and his school, not only in Conceptual DFT but ongoing in other aspects of DFT too, undoubtedly further raised the chemists' interest in DFT in the post-1985 period. The publication, some years later, of Parr and Yang's “Density Functional Theory of Atoms and Molecules” is a remarkable synthesis of that endeavor and this book largely contributed to the acceptance, by chemists, of DFT, from the early 1990s on, as a highly valuable alternative to wave function theory. It has influenced now already several generations of chemists, convincing them on both the conceptual richness and the amazing computational advantages of DFT.

The following paragraphs will highlight this post-1985 evolution along three main themes, with the obvious danger of simplification and personal taste in this kind of exercise in this limited space. As pillars or themes along which CDFT grew and blossomed after its birth and launching, we would like to discern: (1°) the ever-growing tree of response functions and its congeners, the so-called derived descriptors; (2°) the formulation and use of principles governing chemical reactions; and (3°) the applications of CDFT.

## 1.4 The Ever-Growing Tree of Response Functions and Its Associated or Derived Quantities (1985-)

Looking back at the aforementioned DFT-based atomic and molecular descriptors  $\rho(\mathbf{r})$ ,  $\mu$ ,  $\eta$ , and  $f(\mathbf{r})$ , a common feature emerges: they are all functional, partial, or mixed derivatives of the energy with respect to  $N$  and/or  $v$ . They can be identified as *response functions* characterizing the sensitivity of the system's energy to perturbations in its number of electrons  $N$  and/or its external potential  $v(\mathbf{r})$ . These perturbations are essentially those occurring during a chemical reaction from which the *chemical* relevance of these particular response functions emerges. Response functions, called “the bread and butter of theoretical physics” [30], thereby enter the chemist's playground. They find their place in a natural way when considering the  $E = E[N, v(\mathbf{r})]$  functional as extensively commented in Parr and Yang's book. Changes in  $N$  and  $v$  of a given species due to the interaction/reaction with a second species yield an energy change of the former species, which, up to first order, can be written as

$$dE = (\partial E / \partial N)_{v(\mathbf{r})} dN + \int (\delta E / \delta v(\mathbf{r})) N \delta v(\mathbf{r}) d\mathbf{r} = \mu dN + \int \rho(\mathbf{r}) \delta v(\mathbf{r}) d\mathbf{r} \quad (1.10)$$

The identification of  $\mu$  and  $\rho(\mathbf{r})$  as response functions is obvious, as is the possibility to increase its number and diversity when passing to higher-order terms with associated higher-order derivatives. It became standard to group these functions, which can be written in general as  $\partial^n E / \partial N^m \delta v(\mathbf{r}_1) \delta v(\mathbf{r}_2) \cdots \delta v(\mathbf{r}_{m'})$  with  $n = m + m'$  in a response function tree (see, for example, Senet [31] and Chermette [14]) that can be found in many of the review papers mentioned in Section 1.1 and which is extensively discussed in Chapters 2–4 of this book. Note that we will restrict ourselves to the case of the Canonical Ensemble with the associated  $E = E[N, v(\mathbf{r})]$  functional; other ensembles (Grand Canonical, Isomorphic, and Grand Isomorphic) give rise to an analogous construction but are based on a different starting functional, Legendre transformed from the  $E = E[N, v]$  functional [32].

Entering the response function tree for  $n = 3$  is the hyper-hardness  $(\partial^3 E / \partial N^3)_v$ , introduced by Fuentealba and Parr [33]; it, however, received relatively restricted attention due to its apparently limited chemical significance. The  $n = 3$  derivative, which received by far the most interest and turned out to be the most rewarding  $n = 3$  response function from a chemical point of view, is the dual descriptor  $f^{(2)}$

( $\mathbf{r}$ ) introduced by Morell et al. [34] as the  $N$ -derivative of the Fukui function:  $(\partial f(\mathbf{r})/\partial N)_v$ . It indeed turned out that this descriptor displays a one-shot picture of both electrophilic and nucleophilic regions in a molecule. The remaining (cf Section 1.3)  $n = 2$  derivative is  $(\delta^2 E/\delta v(\mathbf{r}) \delta v(\mathbf{r}'))_N$ , termed the linear response function as it represents the linear term in the response of the density  $\rho(\mathbf{r})$  to a perturbation  $v$  at a point  $\mathbf{r}'$ :  $(\delta \rho(\mathbf{r})/\delta v(\mathbf{r}'))_N$ . Though present in earlier schemes and used before in its time-dependent form in the solid-state community, it was scrutinized in a Conceptual DFT context by Geerlings et al. [35, 36] only in the last 10 years, addressing its computability, interpretation, and especially its chemical relevance.

Another way to extend the response function tree is increasing the number of variables in the  $E = E[N, v]$  functional. Natural extensions were presented in 1986 by Galvan et al. [37] by including spin polarization, and in 1994, by Ghanty and Ghosh [38] by resolving the number of electrons into its spin components by considering the functionals  $E = E[N, N_S, v, \mathbf{B}]$  and  $E = E[N_\alpha, N_\beta, v_\alpha, v_\beta]$ , respectively, where  $N_S$ , the spin number, is the difference between the number of  $\alpha$  and  $\beta$  electrons ( $N_\alpha$  and  $N_\beta$ ). This approach allows to consider the energy and reactivity change of a system when its spin state is perturbed, typically by a magnetic field  $\mathbf{B}$  or by spin transfer from its environment or another reagent.

Another extension was the introduction of external electric and magnetic fields, promoted by Chattaraj and coworkers, in 2003 and 2014, respectively [39, 40]. Not addressed frequently until now, the Brussels group is presently taking this subject at heart, concentrating on the influence of oriented external electric fields (OEEFs) on reactivity, including aspects of electric field-induced enantioselectivity and on the changes of global descriptors like atomic electronegativity and hardness for high magnetic fields, where changes in the atomic electronic configurations play a preponderant role [41, 42]. In the same vein, this group recently (2019) introduced the inclusion of an external mechanical force, different in nature from an electromagnetic one [43, 44]. This issue is at stake in mechanochemistry, which, although existing for centuries in its “macroscopic” form, has only recently been downscaled to the molecular level [45].

An important step has been the introduction of temperature by the Ayers group to cope with the  $N$  differentiability problem of the  $E = E[N, v]$  functional whose  $N$  dependence was shown by Perdew to be a series of straight lines intersecting at integer  $N$  in the zero-temperature limit of the (thermal) expectation value of the electronic energy [46]. Average electronic energy (and its derivatives) becomes the central quantity in finite temperature chemical reactivity theory, analogous in form/interpretation but different in evaluation to those from traditional approaches [47, 48]. Although the temperature values at which the deviation from the zero-temperature limit becomes meaningful exceed by far the usual laboratory conditions, the temperature-dependent approach, besides setting the differentiability problem, also provides a new perspective and has led to new reactivity descriptors such as heat capacity [49] and local heat capacity [50].

The reader will observe that most of the above-mentioned extensions are addressed as separate chapters in the Extension (Part II) of this book. As a proviso to this paragraph enlightening the fundamental importance of response functions as

molecular (reactivity) descriptors, it should be remarked that those are not the only acceptable descriptors. Other descriptors derived from the  $E = E[N,\nu]$  functional and exploiting its characteristics (e.g. the position of the minimum in the quadratic interpolation for  $E(N)$ ) are perfectly acceptable and often boil down to combinations of response functions. Parr's electrophilicity [51] is the most prominent example referring to the system's maximal uptake of electrons from an electron reservoir, leading to the expression

$$\omega = \mu^2/\eta \quad (1.11)$$

where two response functions  $\mu$  and  $\eta$  are combined. Countless applications (*vide infra*) using this "derived" descriptor have been published since its introduction in 1999, as evidenced in Chattaraj's 2003/2006 Chemical Reviews [52]. What, however, should be avoided is combining reactivity descriptors (response functions) in an ad hoc fashion without conferring them any physical or chemical meaning as opposed to the case of electrophilicity.

To close this more fundamental pillar of the history of CDFT, it should be noticed that its evolution since 1985, and certainly the one in the last 20 years, has (much) more to offer but is less easily systematized than this dominating response tree evolution. The treatment of degeneracy (Bultinck and coworkers [53, 54]), excited-state reactivity, whereas DFT, is in essence, a ground-state theory Morell et al. [55], the coupling of CDFT with reaction path calculations by Toro-Labbé's group in his reaction force ansatz (the derivative of the electronic chemical potential with respect to the reaction coordinate) [56] introducing also the reaction electronic flux as a key indicator for chemical reactions [57], are prominent examples of these efforts. We finally mention the intertwining of CDFT and the Information Theory [58], which, after the pioneering work by Parr and coworkers [59], witnessed major developments by Liu's group in an endeavor to join the best of both worlds [60, 61]. All these subjects will be treated in separate chapters in Part II (Extensions).

## 1.5 Principles (1978;1985-)

When browsing through the history of Conceptual DFT, it emerges that in the majority of papers, the above-discussed concepts (response functions and derived descriptors) were used "as such" but that in an important part of the literature, they were used in the context of "principles," which can broadly be characterized as rules of thumb to interpret/predict the direction of a reaction, sometimes concentrating on its kinetic aspects, sometimes on its thermodynamics. This important line of the history of CDFT will be separately presented, though obviously intertwined with the two other pillars (Response functions and Applications).

In view of the above-formulated characterization of these principles, the first one, the *Electronegativity Equalization Principle*, is to some extent an outlier as it essentially concentrates on charge distributions. Formulated already in 1951 by Sanderson [62], long before the advent of DFT, let it be CDFT, it postulates that upon molecule formation, the electronegativities of all constituent atoms equalize,

yielding a molecular electronegativity equal to the geometrical mean of the original atomic electronegativities [63]. This principle has been proven by Donnelly and Parr [64] shortly after the electronegativity/electronic chemical potential identification: they showed the constancy of the electronic chemical potential over the considered system and proved that the electronegativities or chemical potentials of the natural orbitals of a molecule in the ground state are equal. In 1982, Parr and Bartolotti [65] presented theoretical and numerical evidence for the geometrical mean postulate. A decisive step passing from an Electronegativity Equalization Principle toward an Electronegativity Equalization Method was taken by Mortier et al. around 1985 [66, 67], turning the principle into an easy-to-implement computational ansatz capable of calculating charge distributions in polyatomic molecules. Later on, further refinements (e.g. by Bultinck et al. in 2002) [68] combined with the ever-increasing computing power advanced EEM to the stage where nowadays it can be used to yield a reasonable first estimate of charge distributions in large series of (not too exotic) large molecules, e.g. at stake in drug discovery research. Its implementation in popular molecular mechanics/force field packages largely contributed to its popularity and consolidated the success of a CDFT-based method.

The second principle in which CDFT-based descriptors were incorporated in a natural way is, as already mentioned in Section 1.3, the *Hard and Soft Acids and Bases* principle with the pioneering work by Parr and Pearson on hardness and softness in 1983 [24]. In 1991, a formal proof was given by Chattaraj et al. [69] for its application at global, i.e. molecular, level, whereas Mendez and Gazquez presented its counterpart at the local level in 1994 [70], focusing on the interaction characteristics between (only) the relevant atoms of the acid and the base. In the former case, the stability issue (thermodynamic in nature) is at stake; in the latter case, the reactivity aspect (kinetic in nature) is predominant. In the subsequent period, the CDFT approach to the HSAB principle knew not only many successes with extensive literature but also some failures (probably underreported). The principle has found a firm place not only in the CDFT community but also in the much broader “general chemistry” context and has been widely used both by experimentalists and theoreticians. Over the years, it became, however, clear (cf. the above-mentioned “failures”) that the conditions under which the HSAB principle can safely be applied deserve more attention. In this way, one copes, for example, with Pearson’s caveat when he formulated the principle stating that “all other things being equal, hard acids prefer binding to hard bases and soft acids to soft bases” [71]. The “all other things being equal” caveat is often forgotten, and, although never perfectly satisfied, the conditions under which the HSAB principle is applied should always be scrutinized. One of the Extension Chapters will deepen the discussion on this “second principle.”

The third principle is Pearson’s *Maximum Hardness Principle* (MHP) (1987) [72], which in its verbal statement sounds that “there seems to be a rule of nature that molecules arrange themselves to be as hard as possible” and for which Parr and Chattaraj presented a proof in 1991 [73]. Overall, the MHP has found less acceptance, outside the CDFT community, than the HSAB principle. However, its importance in CDFT is unquestionable, as witnessed, for example, by the about 1000 citations to Parr and Chattaraj’s proof. A possible reason for its more limited acceptance is that

the constraints under which the MHP is rigorously valid (e.g. constant chemical and external potential) are highly restrictive, leading to an even more important caveat in its application than in the case of the HSAB principle.

As a companion to the MHP Chattaraj and Sengupta [74] formulated in 1996, the *Minimum Polarizability Principle* (MPP), not unnatural as a positive correlation between the softness, the inverse of the hardness, and the polarizability was put forward already in 1987 by Politzer [75], later on, quantified by Gazquez and Fuentealba and coworkers [76, 77]. The principle states that “the natural direction of evolution of a system is towards a state of minimum polarizability.” A recent statistical analysis on its validity has been successful though, in general, the domain of applicability should also be scrutinized further. This concern turns out to be a general issue for the principles described in this paragraph, as advocated in the recent “Status, Issues, and Prospects” paper by a group of CDFT experts [20].

To end this chapter, Chattaraj’s Minimum Electrophilicity Principle (2003) [78] should be mentioned, for which recent detailed studies showed encouraging statistical performance data as compared to the MHP.

## 1.6 Applications

The volume of the CDFT literature has recently been estimated to exceed 4000 papers [20], illustrating that CDFT as a subfield of DFT has been the subject of intense intellectual activity in the past decades. Whereas, after its launching in 1978, the number of papers remained relatively small in the 1980s, most papers being fundamental in nature, a steady increase manifested itself in the 1990s with a balance between fundamental and applied studies, turning after 2000 to an avalanche of papers where applications clearly dominate. The applications in the early years mainly concentrated on reactivity studies in “classical” organic reactions scrutinizing different types of organic reaction types/mechanisms, (general) acid–base and complexation reactions, and an already important series of studies on clusters and catalysis with Mortier’s work on zeolites as pioneering work (as witnessed in the 2003 review by Geerlings et al. [15], presenting an almost complete literature survey on both fundamental and applied CDFT). The literature, after, say, 2000, shows not only the aforementioned quantitative explosion but also a hard-to-describe extension of the field of applications. Nowadays, applications are published across really all branches of chemistry, from inorganic and materials chemistry to organic, organometallic and polymer chemistry, and biochemistry. Therefore, almost the full scope of reaction types is covered, from gas-phase reactions to reactions in solutions to reactions/rearrangements in solids and reactions at phase boundaries. A remarkable example is the range of applications of the electrophilicity concept as summarized in Chattaraj’s Chemical Reviews [52], extending to biological activity and toxicity.

## 1.7 The Present and the Future

The present situation of CDFT has already been succinctly addressed in the final parts of the previous three paragraphs. The reader may find an alternative view

of the present status of DFT in the aforementioned paper in *Theoretical Chemical Accounts* [20], concentrating, among others, on accomplishments in the last 20 years. Even more important, in our view, is that in this paper, experts reflect on the future of DFT and highlight issues (both from a fundamental and a methodological point of view) that should be considered in the near future, and suggest directions both for fundamental and applied/computational research. Therefore, a combination of respect for the basic philosophy of CDFT, and the ambition to switch from interpretation to prediction, thereby enlarging the impact of CDFT, is a guiding principle.

This philosophy behind CDFT, though implicitly present from the early, more fundamental CDFT literature, has – remarkably – never been written down explicitly until recently in Ref. [20] (for a preliminary account, see [79, 80]), and in view of its importance for future developments/applications of CDFT, we summarize it here. CDFT’s philosophy can be traced back to three fundamental precepts: (i) Observability: meaning that an understanding of chemical events should be based on quantum mechanical observables: the density, the energy, and their derivatives; (ii) Universality: the tools that are used should not depend on the type of calculation (wave function, DFT, Quantum Monte Carlo); and (iii) Mathematical rigor: the tools should fit in a well-defined mathematical framework. These are simple rules ensuring that CDFT further evolves as a physically and mathematically sound approach to understand/interpret chemical phenomena.

This passage from an interpretative mode (“explaining”) to a predictive mode (“forecasting”) should absolutely be realized to increase the acceptance of CDFT in a still broader chemical community. The development of user-friendly and well-documented software packages that can be coupled to the existing quantum-chemical packages is an essential condition for this endeavor and should be undertaken. This issue is addressed in the two Part IV Chapters on Implementation by Heidar-Zadeh and the Ayers group discussing the ChemTools package [81] and by Lu and Chen’s presenting the capabilities of the MultiWFN program [82].

## 1.8 Conclusions

The birth and early years of Conceptual DFT (1978–1985) can be situated in a time frame where DFT was not that popular/accepted yet in the (quantum) chemists’ community. Its “chemical” approach undoubtedly promoted DFT into this community, together, of course, with the spectacular evolution in the development of approximate but already remarkably efficient exchange-correlation potentials. This “density”-based approach was steadily growing in the quantum-chemical community toward and at the beginning of the 1990s. Of course, Bader’s contribution to incite chemists on focusing on the density in his “Atoms in Molecules” [83] theory, with the book with the same name published in 1990, should be mentioned here with deep respect.

In globo, after the early years, Conceptual DFT witnessed impressive developmental/fundamental research along the extension of the response function concept, the extension and refinement of principles, and many other issues strengthening

its mathematical/physical foundations. An avalanche of papers on applications has meanwhile been published covering a large variety of subfields of chemistry and neighboring sciences.

Looking ahead, at the end of this historic overview, this combination of deepening and widening the basic theory and its use in a well-thought and critical way in the most diverse subfields of chemistry via dedicated software is the way in which CDFT could and should ensure and strengthen its position as a full-fledged theory. Characterized by a remarkable entwining of mathematical and physical rigor with chemical intuition, it offers an intellectually rich approach to interpret and finally predict chemical phenomena and thus contribute to the chemistry of the future.

## References

- 1 Fermi, E. (1928). *Z. Phys. A* 48: 73–79.
- 2 Thomas, L.H. (1927). *Proc. Cambridge Philos. Soc.* 23: 542–548.
- 3 For a comprehensive account see Bransden, B. and Joachain, C.J. (2003). *Physics of Atoms and Molecules*, 2e. Harlow: Prentice Hall.
- 4 Slater, J.C. (1951). *Phys. Rev.* 81: 385–390.
- 5 Hohenberg, P. and Kohn, W. (1964). *Phys. Rev. B* 136: 864–871.
- 6 Parr, R.G. and Yang, W. (1989). *Density Functional Theory of Atoms and Molecules*. New York: Oxford University Press.
- 7 Kohn, W. and Sham, L.J. (1965). *Phys. Rev. A* 140: 1133–1138.
- 8 For an account on the performance of various, basic types of functionals see Koch, W. and Holthausen, M.C. (2002). *A Chemist's Guide to Density Functional Theory*, 2e. Weinheim: Wiley-VCH.
- 9 Lee, C., Yang, W., and Parr, R.G. (1988). *Phys. Rev. B* 37: 785–789.
- 10 Becke, A.D. (1988). *Phys. Rev. A* 38: 3098–3100.
- 11 Frisch, M.J., Trucks, G.W., Schlegel, H.B. et al. (2016). *Gaussian 16*. Wallingford: Gaussian Inc.
- 12 Burke, K. (2012). *J. Chem. Phys.* 136: 150901.
- 13 Parr, R.G., Donnelly, R.A., Levy, M., and Palke, W.E. (1978). *J. Chem. Phys.* 68: 3801–3807.
- 14 Chermette, H. (1999). *J. Comput. Chem.* 20: 129–154.
- 15 Geerlings, P., De Proft, F., and Langenaeker, W. (2003). *Chem. Rev.* 103: 1793–1873.
- 16 Ayers, P.W., Anderson, J., and Bartolotti, L.J. (2005). *Int. J. Quantum Chem.* 101: 520–524.
- 17 Geerlings, P. and De Proft, F. (2008). *Phys. Chem. Chem. Phys.* 10: 3028–3042.
- 18 Gazquez, J.L. (2008). *J. Mex. Chem. Soc.* 52: 8–10.
- 19 Liu, S.B. (2009). *Acta Phys. Chem. Sin.* 25: 590–600.
- 20 Geerlings, P., Chamorro, E., Chattaraj, P.K. et al. (2020). *Theor. Chim. Acta* 139: i36.
- 21 Iczkowski, R.P. and Margrave, J.L. (1961). *J. Am. Chem. Soc.* 83: 3547–3551.
- 22 Mulliken, R.S. (1934). *J. Chem. Phys.* 2: 782–793.



- 23 See for example, Atkins, P.W. and De Paula, J. (2006). *Atkins' Physical Chemistry*, Chapter 5, 8e. Oxford: Oxford University Press.
- 24 Parr, R.G. and Pearson, R.G. (1983). *J. Am. Chem. Soc.* 105: 7512–7516.
- 25 For an authoritative account see Pearson, R.G. (1993). *Chemical Hardness: Applications from Molecules to the Solid State*. Weinheim: Wiley-VCH.
- 26 Parr, R.G. and Yang, W. (1984). *J. Am. Chem. Soc.* 106: 4049–4050.
- 27 Fukui, K., Yonezawa, Y., and Shingu, H. (1952). *J. Chem. Phys.* 30: 722–725.
- 28 Woodward, R.B. and Hoffmann, R.W. (1971). *The Conservation of Orbital Symmetry*. Verlag Chemie: Weinheim.
- 29 Parr, R.G. and Yang, W. (1995). *Annu. Rev. Phys.Chem.* 46: 701–728.
- 30 Martin, R.M. (2004). *Electronic Structure: Basic Theory and Practical Methods*, Appendix D. Cambridge, New York: Cambridge University Press.
- 31 Senet, P. (1997). *J. Chem. Phys.* 107: 2516–2524.
- 32 Nalewajski, R.F. and Parr, R.G. (1982). *J. Chem. Phys.* 77: 393–407.
- 33 Fuentealba, P. and Parr, R.G. (1991). *J. Chem. Phys.* 94: 5559–5564.
- 34 Morell, C., Grand, A., and Toro-Labbé, A. (2005). *J. Phys. Chem. A* 109: 205–212.
- 35 Geerlings, P., Fias, S., Boisdenghien, Z., and De Proft, F. (2014). *Chem. Soc. Rev.* 43: 4989–5008.
- 36 Geerlings, P., Fias, S., Stuyver, T. et al. (2019). New insights and horizons from the linear response function in conceptual DFT. In: *Density Functional Theory*, Chapter 1 (ed. D.G. Mitnik), 3–29. London: IntechOpen.
- 37 Galvan, M., Gazquez, J.L., and Vela, A. (1986). *J. Chem. Phys.* 85: 2337–2338.
- 38 Ghanty, T.K. and Ghosh, S.K. (1994). *J. Am. Chem. Soc.* 116: 3943–3948.
- 39 Parthasarathi, R., Subramanian, V., and Chattaraj, P.K. (2003). *Chem. Phys. Lett.* 382: 48–56.
- 40 Khatua, M., Sarkar, U., and Chattaraj, P.K. (2014). *Eur. J. Phys. D* 68: 2.
- 41 Bettens, T., Stuyver, T., De Proft, F., and Geerlings, P. (2021). *Phys. Chem. Chem. Phys.* 23: 990–1005.
- 42 Francotte, R., Irons, T.J.P., Teale, A., De Proft, F., and Geerlings, P. submitted.
- 43 Bettens, T., Alonso, M., Geerlings, P., and De Proft, F. (2019). *Phys. Chem. Chem. Phys.* 21: 7378–7388.
- 44 Bettens, T., Alonso, M., Geerlings, P., and De Proft, F. (2020). *Chem. Sci.* 11: 1431–1439.
- 45 Stauch, T. and Dreuw, A. (2016). *Chem. Rev.* 116: 14137–14180.
- 46 Perdew, J.P., Parr, R.G., Levy, M., and Balduz, J.L. (1982). *Phys. Rev. Lett.* 49: 1691–1694.
- 47 Franco-Perez, M., Ayers, P.W., Gazquez, J.L., and Vela, A. (2015). *J. Chem. Phys.* 143: 244117.
- 48 Gazquez, J.L., Franco-Perez, M., Ayers, P.W., and Vela, A. (2019). *Int. J. Quantum Chem.* 119: e25797.
- 49 Ayers, P.W. and Gazquez, J.L. (2016). *Theor. Chem. Acc.* 135: 199.
- 50 Franco-Perez, M., Ayers, P.W., Gazquez, J.L., and Vela, A. (2017). *J. Chem. Phys.* 147: 094105.
- 51 Parr, R.G., Von Szentpaly, L., and Liu, S.B. (1999). *J. Am. Chem. Soc.* 121: 1922–1924.

- 52 (a) Chattaraj, P.K., Sarkar, U., and Roy, D.R. (2006). *Chem. Rev.* 106: 2065–2091.  
(b) Chattaraj, P.K. and Roy, D.R. (2007). *Chem. Rev.* 107: PR64–PR74.
- 53 Cardenas, C., Ayers, P.W., and Cedillo, A. (2011). *J. Chem. Phys.* 134: 174103.
- 54 Bultinck, P., Cardenas, C., Fuentealba, P., and Johnson, P.A. (2013). *J. Chem. Theor. Comput.* 9: 4779–4788.
- 55 Morell, C., Labet, V., Grand, A. et al. (2009). *J. Chem. Theor. Comput.* 9: 2274–2283.
- 56 Toro-Labbé, A. (1999). *J. Phys. Chem. A* 103: 4398–4403.
- 57 Echegaray, E. and Toro-Labbé, A. (2008). *J. Phys. Chem. A* 112: 11801–11807.
- 58 Shannon, C.E. (1948). *Bell Syst. Tech. J.* 27: 379–423.
- 59 Sears, S.B., Parr, R.G., and Dinur, U. (1980). *Isr. J. Chem.* 19: 165–173.
- 60 Liu, S. (2007). *J. Chem. Phys.* 126: 244103.
- 61 Rong, C., Wang, B., Zhao, D., and Liu, S. (2019). *WIREs Comput. Mol. Sci.* 10 (4).
- 62 Sanderson, R.T. (1951). *Science* 114: 670–672.
- 63 Sanderson, R.T. (1976). *Chemical Bonds and Bond Energies*. New York: Academic Press.
- 64 Donnelly, R.A. and Parr, R.G. (1978). *J. Chem. Phys.* 69: 4431–4439.
- 65 Parr, R.G. and Bartolotti, L.J. (1982). *J. Am. Chem. Soc.* 104: 3801–3803.
- 66 Mortier, W.J., Van Genechten, K., and Gasteiger, R.A. (1985). *J. Am. Chem. Soc.* 107: 829–835.
- 67 Mortier, W.J., Ghosh, S.K., and Shankar, S. (1986). *J. Am. Chem. Soc.* 108: 4315–4320.
- 68 Bultinck, P., Langenaeker, W., Lahorte, P. et al. (2002). *J. Phys. Chem. A* 106: 7887–7894.
- 69 Chattaraj, P.K., Lee, H., and Parr, R.G. (1991). *J. Am. Chem. Soc.* 113: 1855–1856.
- 70 Mendez, F. and Gazquez, J.L. (1994). *J. Am. Chem. Soc.* 116: 9298–9301.
- 71 See e.g. Pearson, R.G. and Chattaraj, P.K. (2008). *Chemtracts-Inorg. Chem.* 21: 1–7.
- 72 Pearson, R.G. (1987). *J. Chem. Educ.* 64: 561–567.
- 73 Parr, R.G. and Chattaraj, P.K. (1991). *J. Am. Chem. Soc.* 113: 1854–1855.
- 74 Chattaraj, P.K. and Sengupta, S. (1996). *J. Phys. Chem.* 100: 16126–16130.
- 75 Politzer, P. (1987). *J. Chem. Phys.* 86: 1072–1073.
- 76 Vela, A. and Gazquez, J.L. (1990). *J. Am. Chem. Soc.* 112: 1490–1492.
- 77 Simon-Manso, Y. and Fuentealba, P. (1998). *J. Phys. Chem. A* 102: 2029–2032.
- 78 Chamorro, E., Chattaraj, P.K., and Fuentealba, P. (2003). *J. Phys. Chem. A* 107: 7068–7072.
- 79 Johnson, P.A., Bartolotti, L.J., Ayers, P.W. et al. (2012). Charge density and chemical reactions: A unified view from conceptual DFT. In: *Modern Charge Density Analysis*, Chapter 21 (ed. L. Gatti and P. Macchi), 715–764. Dordrecht: Springer-Verlag.
- 80 De Proft, F., Ayers, P.W., and Geerlings, P. (2014). *Fundamental Aspects of Chemical Bonding*, Chapter 4. New York: Wiley.
- 81 Heidar-Zadeh, F., Richer, M., Fias, S. et al. (2016). *Chem. Phys. Lett.* 660: 307–312.
- 82 Lu, T. and Chen, F. (2012). *J. Comput. Chem.* 33: 580–592.
- 83 Bader, R.F.W. (1990). *Atoms in Molecules. A Quantum Theory*. Oxford: Clarendon Press.

## 2

## Basic Functions

Frank De Proft

Research Group of General Chemistry (ALGC), Vrije Universiteit Brussel (VUB), Pleinlaan 2, 1050 Brussels, Belgium

## 2.1 Introduction: Density Functional Theory

Density functional theory (DFT) uses the electron density  $\rho(\mathbf{r})$  as the basic variable for an atom, molecule, or solid instead of the wavefunction  $\Psi$  as is common in wavefunction quantum chemistry [1–11]. It is based on the famous Hohenberg–Kohn theorems [1], of which the first one states that the external potential of the system  $v(\mathbf{r})$  (for an isolated system, this is the potential due to the nuclei) is determined, within an trivial, additive constant, by the electron density. As a result, the energy of the system  $E$  can be written as a functional of the density  $\rho(\mathbf{r})$ , i.e.  $E = E[\rho(\mathbf{r})]$ , comparable to writing  $E = E[\Psi]$  in wave function theory. More specifically, the ground state energy can be written as

$$E[\rho(\mathbf{r})] = T[\rho(\mathbf{r})] + V_{\text{ne}}[\rho(\mathbf{r})] + V_{\text{ee}}[\rho(\mathbf{r})] = V_{\text{ne}}[\rho(\mathbf{r})] + F_{\text{HK}}[\rho(\mathbf{r})] \quad (2.1)$$

with  $T[\rho(\mathbf{r})]$  the kinetic energy,  $V_{\text{ne}}[\rho(\mathbf{r})]$  the nucleus–electron attraction energy, and  $V_{\text{ee}}[\rho(\mathbf{r})]$  the electron–electron repulsion. As can be seen, in the second part of Eq. (2.1),  $T$  and  $V_{\text{ee}}$  have been grouped in the so-called Hohenberg–Kohn functional  $F_{\text{HK}}$ .

The  $V_{\text{ne}}[\rho(\mathbf{r})]$  is exactly expressed as

$$V_{\text{ne}}[\rho(\mathbf{r})] = \int \rho(\mathbf{r})v(\mathbf{r})d\mathbf{r} \quad (2.2)$$

The second Hohenberg–Kohn theorem establishes the variational principle within DFT [1]. Given a trial density  $\tilde{\rho}(\mathbf{r})$ , such that  $\tilde{\rho}(\mathbf{r}) \geq 0, \forall \mathbf{r}$  and  $\int \tilde{\rho}(\mathbf{r})d\mathbf{r} = N$  (with  $N$  the number of electrons of the system), then  $E_0 \leq E[\tilde{\rho}(\mathbf{r})]$ , with  $E_0$  the exact ground state energy of the system. Minimizing the energy (Eq. (2.1)) with respect to changes in the electron density under the constraint that the density should at all times integrate to the number of electrons  $N$  of the system yields

$$\frac{\delta}{\delta\rho(\mathbf{r})} \left[ E - \mu \left( \int \rho(\mathbf{r})d\mathbf{r} - N \right) \right] = 0 \quad (2.3)$$

where  $\mu$  is the Lagrange multiplier attached to the above-mentioned constrained. Working out this minimization yields

$$\mu = v(\mathbf{r}) + \frac{\delta T_{\text{HK}}}{\delta \rho(\mathbf{r})} + \frac{\delta V_{\text{ee}}[\rho(\mathbf{r})]}{\delta \rho(\mathbf{r})} = v(\mathbf{r}) + \frac{\delta F_{\text{HK}}}{\delta \rho(\mathbf{r})} \quad (2.4)$$

This Euler equation is sometimes called the DFT analog of the Schrödinger equation. It implies that at all points in space, the sum of the local quantities  $v(\mathbf{r})$  and  $\frac{\delta F_{\text{HK}}}{\delta \rho(\mathbf{r})}$  should be constant and equal to  $\mu$ . The Hohenberg–Kohn functional  $F_{\text{HK}}$  is unfortunately unknown and represents a large quantity. Consequently, only the slightest (relative) error in its approximation will have a large impact.

In order to circumvent this problem, Kohn and Sham re-introduced orbitals in the DFT minimization problem invoking a noninteracting reference system for which the density is exactly the exact ground state density of the interacting system. A single Slater determinant is an exact wavefunction for a system of independent noninteracting electrons, and it will be presumed that this density expression spans all possible  $N$ -electron densities, interacting or not. The electron density for the noninteracting system can be written as

$$\rho(\mathbf{r}) = \sum_{i=1}^N |\psi_i(\mathbf{r})|^2 \quad (2.5)$$

where the  $\psi_i(\mathbf{r})$  are the spin-orbitals in the Slater determinant.

For this noninteracting system, the kinetic energy, denoted  $T_s$  is exactly given as

$$T_s = \sum_{i=1}^N \left\langle \psi_i \left| -\frac{1}{2} \nabla^2 \right| \psi_i \right\rangle \quad (2.6)$$

The quantity

$$t(\mathbf{r}) = -\frac{1}{2} \sum_{i=1}^N \psi_i^*(\mathbf{r}) \nabla^2 \psi_i(\mathbf{r}) \quad (2.7)$$

can be termed a kinetic energy density, although this definition is not unique [12]. Another expression for this quantity is the so-called “del dot del” [12] formula, given as

$$t(\mathbf{r}) = \sum_{i=1}^N \frac{(\nabla \psi_i(\mathbf{r}))^* \cdot \nabla \psi_i(\mathbf{r})}{2} \quad (2.8)$$

The local temperature  $T(\mathbf{r})$  is then introduced as

$$T(\mathbf{r}) = \frac{2t(\mathbf{r})}{3k_{\text{B}}\rho(\mathbf{r})} \quad (2.9)$$

with  $k_{\text{B}}$  is the Boltzmann constant. This quantity was put forward as a measure of the “nighness” of an electron pair [12] and was additionally proposed as a reactivity index [13]; the time-dependent version of this quantity was used to compute the time-dependent entropy in collision processes and resulted in the formulation of a maximum entropy principle [14].

It is a reasonable assumption that the kinetic energy  $T_s$  is a good approximation to  $T$  in the Hohenberg–Kohn energy functional. It is also reasonable to approximate  $V_{\text{ee}}[\rho]$  by the classical Coulomb self-repulsion  $J[\rho]$ , given as

$$J[\rho] = \frac{1}{2} \int \int \frac{\rho(\mathbf{r})\rho(\mathbf{r}')}{|\mathbf{r} - \mathbf{r}'|} d\mathbf{r}d\mathbf{r}' \quad (2.10)$$

The error made by these approximations (which turns out to be a small quantity as compared to the other exactly known contributions) was called the exchange-correlation energy  $E_{\text{XC}}$ :

$$F_{\text{HK}}\rho(\mathbf{r}) = T[\rho(\mathbf{r})] + V_{\text{ee}}[\rho(\mathbf{r})] = T_s[\rho(\mathbf{r})] + J[\rho(\mathbf{r})] + E_{\text{XC}}[\rho(\mathbf{r})] \quad (2.11)$$

with

$$E_{\text{XC}}[\rho(\mathbf{r})] = (T[\rho(\mathbf{r})] - T_s[\rho(\mathbf{r})]) + (V_{\text{ee}}[\rho(\mathbf{r})] - J[\rho(\mathbf{r})]) \quad (2.12)$$

The Kohn–Sham total energy functional is thus given as

$$E_{\text{KS}}[\rho(\mathbf{r})] = T_s[\rho(\mathbf{r})] + J[\rho(\mathbf{r})] + \int \rho(\mathbf{r})v(\mathbf{r})d\mathbf{r} + E_{\text{XC}}[\rho(\mathbf{r})] \quad (2.13)$$

Again minimizing this energy with respect to the electron density with the constraint that the density should at all times integrate to the number of electrons yields

$$\mu = v(\mathbf{r}) + \int \frac{\rho(\mathbf{r}')}{|\mathbf{r} - \mathbf{r}'|} d\mathbf{r}' + \frac{\delta E_{\text{XC}}}{\delta \rho(\mathbf{r})} + \frac{\delta T_s}{\delta \rho(\mathbf{r})} \quad (2.14)$$

Introducing the exchange-correlation potential  $v_{\text{XC}}(\mathbf{r})$

$$v_{\text{XC}}(\mathbf{r}) = \frac{\delta E_{\text{XC}}}{\delta \rho(\mathbf{r})} \quad (2.15)$$

and

$$v_J(\mathbf{r}) = \int \frac{\rho(\mathbf{r}')}{|\mathbf{r} - \mathbf{r}'|} d\mathbf{r}' \quad (2.16)$$

yields

$$\mu = v(\mathbf{r}) + v_J(\mathbf{r}) + v_{\text{XC}}(\mathbf{r}) + \frac{\delta E_{\text{XC}}}{\delta \rho(\mathbf{r})} + \frac{\delta T_s}{\delta \rho(\mathbf{r})} = v_{\text{KS}}(\mathbf{r}) + \frac{\delta T_s}{\delta \rho(\mathbf{r})} \quad (2.17)$$

with  $v_{\text{KS}}(\mathbf{r})$  the effective Kohn–Sham potential. When comparing Eq. (2.14) with Eq. (2.4), we now confirm the Kohn–Sham picture of a non-interacting systems ( $V_{\text{ee}} = 0$ ) where the electrons move in an effective potential  $v_{\text{KS}}(\mathbf{r})$ .

Minimization of the energy with respect to the occupied Kohn–Sham orbitals yields the celebrated Kohn–Sham equations,

$$\left( -\frac{1}{2}\nabla^2 + v_{\text{KS}}(\mathbf{r}) \right) = \psi_i = \epsilon_i \psi_i \quad (2.18)$$

where  $\epsilon_i$  are the Kohn–Sham orbital energies. Many papers have appeared discussing these orbital energies; a recent discussion was given in [15], focusing, among others, on differences in these quantities between finite systems (molecules) and extended systems (solids).

In this chapter, the basic functions, i.e. the “basic” chemical concepts from conceptual DFT are introduced. This chapter focuses on the zero temperature limit

and mainly considers the change in the number of electrons  $N$  and/or the external potential  $v(\mathbf{r})$  to probe the chemical reactivity of the system, as a chemical reaction means that the system will undergo changes in these variables. In addition, the reactivity concepts are introduced in a spin restricted manner, not considering any spin polarization. These concepts introduced are often used to study chemical reactivity, stability, and charge distributions as such or are adopted in the study of chemical reactivity and stability principles; the latter will be the subject of Chapter 4. Additionally, we will consider the various concepts for (isolated) individual molecules, and we will thus not treat concepts applied to two or more molecule simultaneously, e.g. during the course of a chemical reaction. It should thus be remarked that this chapter does not aim to provide an exhaustive introduction of all DFT-based chemical concepts, rather an outline of the basic concepts that will serve as a basis for more elaborate treatments throughout the course of this book.

## 2.2 The Electronic Chemical Potential and the Electron Density as First Order Response Functions

The number of electrons of the system  $N$  and the external potential  $v(\mathbf{r})$  both fix the Hamiltonian of the system and thus uniquely determine the energy  $E$ , so that  $E = E[N, v(\mathbf{r})]$ . The change in energy from one ground state to another can thus be written as

$$dE = \left( \frac{\partial E}{\partial N} \right)_v dN + \int \left[ \frac{\delta E}{\delta v(\mathbf{r})} \right]_N \delta v(\mathbf{r}) d\mathbf{r} \quad (2.19)$$

At constant external potential, the change in energy becomes

$$dE_v = \left( \frac{\partial E}{\partial N} \right)_v dN \quad (2.20)$$

Since the electron density integrates to the number of electrons, the infinitesimal change in electron number  $N$  at constant external potential is accompanied by an infinitesimal change in electron density with corresponding energy change

$$dE_v = \int \left[ \frac{\delta E}{\delta \rho(\mathbf{r})} \right]_v \delta \rho(\mathbf{r}) d\mathbf{r} \quad (2.21)$$

Taking the functional derivative of the energy expression in Equation (2.1) with respect to  $\rho$  at constant external potential yields

$$\left[ \frac{\delta E}{\delta \rho(\mathbf{r})} \right] = v(\mathbf{r}) + \frac{\delta F_{\text{HK}}}{\delta \rho(\mathbf{r})} = \mu \quad (2.22)$$

so that Eq. (2.21) becomes

$$dE_v = \int \mu \delta \rho(\mathbf{r}) d\mathbf{r} = \mu \int \delta \rho(\mathbf{r}) d\mathbf{r} = \mu dN \quad (2.23)$$

Comparing Eqs. (2.20) and (2.23) yields

$$\mu = \left( \frac{\partial E}{\partial N} \right)_v \quad (2.24)$$

As mentioned in Chapter 1, the birth of conceptual DFT [16–28] can be considered to be the identification of the Lagrange multiplier  $\mu$  in the DFT variational equation with the negative of the electronegativity of the system  $\chi$ , i.e. [29]

$$\mu = -\chi \quad (2.25)$$

in line with the earlier definition of Iczkowski and Margrave [30] for this concept. Electronegativity was initially introduced by Pauling as “the power of an atom in a molecule to attract electrons to itself” [31, 32]. A detailed account of different scales for this concept can e.g. be found in [33].

An important aspect in the evaluation of this quantity is the dependence of the energy of the system on its number of electrons [34]. It was shown that the exact  $E$  vs.  $N$  curve comprises a series of straight lines [35]; for a system with a fractional number of electrons  $N$  and with an external potential  $v(\mathbf{r})$ , the energy is a linear interpolation of the two neighboring integer energy points:

$$E[N, v] = E[N_0 + \delta, v] = (1 - \delta)E(N_0, v) + \delta E[N_0 + 1, v] \quad (2.26)$$

with  $0 \leq \delta \leq 1$  or, more general,

$$E[N, v] = (1 - N + [N])E([N], v) + ([N] - N)E([N], v) \quad (2.27)$$

where  $[N]$  and  $\lceil N \rceil$  are the floor and ceiling functions, respectively. This linearity condition was proven both using an ensemble [35] and pure state approach [36]. The violation of this condition for density functional approximations was termed the “delocalization error,” and is e.g. responsible for the underestimation of the energy for delocalized charge distributions [37, 38].

As a consequence of the linearity of  $E$  vs.  $N$ , the chemical potential  $\mu$  is constant between the integers and has a discontinuity at the integers; taking the derivative with respect to  $N$  of Eq. (2.27) on the electron deficient and abundant side, respectively, yields:

$$\frac{\partial E}{\partial N_{N-\lambda}} = -I \quad (2.28)$$

and

$$\frac{\partial E}{\partial N_{N+\lambda}} = -A \quad (2.29)$$

where  $I$  and  $A$  are the ionization energy and electron affinity, respectively. The derivative discontinuities at the integer  $N$  lead to discontinuities in the exact exchange-correlation potential; the exact potentials on the electron deficient and electron abundant sides of the integer, denoted  $v_{\text{XC}}^-$  and  $v_{\text{XC}}^+$ , will differ by a system-dependent positive constant  $\Delta_{\text{XC}}$  at all points in space

$$\Delta_{\text{XC}} = v_{\text{XC}}^+ - v_{\text{XC}}^- \quad (2.30)$$

For the removal of an electron from the highest occupied molecular orbital (HOMO), it can be shown that the HOMO eigenvalue associated with the exact  $v_{\text{XC}}^-$  equals the negative of the ionization energy [35]

$$\epsilon_{\text{HOMO}}^- = -I \quad (2.31)$$

For addition of an electron to the lowest unoccupied molecular orbital (LUMO), one finds

$$\epsilon_{\text{LUMO}}^+ = -A \quad (2.32)$$

where  $\epsilon_{\text{LUMO}}^+$  is the LUMO eigenvalue associated with  $v_{\text{XC}}^+$ .

Cohen et al. have shown that the chemical potential is related to the Kohn–Sham frontier orbital energies [39, 40]

$$\mu = \left\langle \phi_f \left| \hat{h}_{\text{KS}} \right| \phi_f \right\rangle \quad (2.33)$$

Taking the average of the left and right side derivative as an estimate of the chemical potential at the integer number of electrons  $N$  yields

$$\mu = -\chi = -\frac{I + A}{2} \quad (2.34)$$

which is the Mulliken definition for the electronegativity [41], writing this quantity as the arithmetic mean of the ground state ionization potential and electron affinity, respectively. This expression can also be obtained by using a quadratic model for the energy vs. the number of electrons. Within a Koopmans type of approximation [42], the electronegativity can be obtained as the average of the HOMO and LUMO energies [43]

$$\chi = -\frac{\epsilon_{\text{HOMO}} + \epsilon_{\text{LUMO}}}{2} \quad (2.35)$$

Returning to Eq. (2.16), a second derivative is present, i.e.  $\left[ \frac{\delta E}{\delta v(\mathbf{r})} \right]_N$

Using Rayleigh–Schrödinger perturbation theory, this functional derivative (which we will later call response function) can be proven to be equal to the electron density of the system, i.e.

$$\left[ \frac{\delta E}{\delta v(\mathbf{r})} \right]_N = \rho(\mathbf{r}) \quad (2.36)$$

Taking the functional derivative of Eq. (2.26) with respect to  $v(\mathbf{r})$  reveals that also the electron density of the fractionally charged system is a mixture of the  $N_0$  and  $N_0 + 1$  electron densities

$$\rho(N_0 + \delta) = (1 - \delta)\rho(N_0) + \delta\rho(N_0 + 1) \quad (2.37)$$

It thus becomes clear that the two first-order energy derivatives are central ingredients of the DFT variational equation and can thus be considered to be the cornerstone of conceptual DFT.

Parr and Bartolotti have introduced the shape function  $\sigma(\mathbf{r})$  (or the density per particle) as the ratio of the electron density and the number of electrons, i.e. [44]

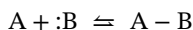
$$\sigma(\mathbf{r}) \equiv \frac{\rho(\mathbf{r})}{N} \quad (2.38)$$

It was shown by Ayers that also this quantity determines any observable quantity of a finite Coulombic system [45]. This quantity has also been used as a variable in the conceptual DFT reactivity framework [46–51].

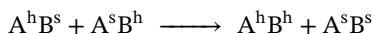


## 2.3 Second and Higher Order Global Derivatives and Derived Quantities

When studying generalized Lewis acid–base reactions of the type



in the 1960s, Pearson proposed, based on experimental thermochemical data, to classify Lewis acids and bases as hard or soft and formulated the Hard and Soft Acids and Bases (HSAB) principle: Hard acids prefer to bond to Hard bases and Soft acids prefer to bond to Soft bases [52, 53]. Ayers et al. have pointed, however, to the fact that the principle should be prefixed by “whenever other effects are similar” or “other things being equal” [54]. The principle implies that the process



should have a negative free energy change; in this equation  $A^h$  and  $A^s$  denote the harder and the softer acid and  $B^h$  and  $B^s$  the harder and the softer base, respectively.

Parr and Pearson introduced the absolute hardness  $\eta$  as [55]

$$\eta = \left( \frac{\partial^2 E}{\partial N^2} \right)_v = \left( \frac{\partial \mu}{\partial N} \right)_v \quad (2.39)$$

The chemical hardness measures the resistance of a chemical species toward charge transfer; the Parr and Pearson definition enables to quantify the hardness of different chemical species. Within the ensemble approach, however, the hardness would be zero for noninteger  $N$  and undefined for integer values of the electron number. One obtains values for this concept at integer  $N$  using a  $\Delta N = 1$  finite difference approximation of the chemical potentials  $\mu^+$  and  $\mu^-$  [56]

$$\eta = \mu^+ - \mu^- = I - A \quad (2.40)$$

This expression is also obtained using a quadratic  $E$  vs.  $N$  model. Using again a Koopmans type of approximation yields

$$\eta = \epsilon_{\text{LUMO}} - \epsilon_{\text{HOMO}} \quad (2.41)$$

i.e. the hardness is equal to the HOMO–LUMO gap of the system.

The chemical hardness is often evaluated through gas-phase computed  $I$  and  $A$  values. In many cases, however, gas phase electron affinities are negative and the anion is termed a temporary anion. This implies that the excess electron in the anion is not bound and that the anion is unstable with respect to electron loss. These metastable anions can readily be observed as sharp variations or resonances in electron transmission spectroscopy [57] and play important roles in different areas of chemistry [58]. Computation of these negative electron affinities is highly challenging although some computational methods are available (see e.g. [59] and the references cited in this paper). One solution consists in turning a resonance into a bound state by adding an artificial potential to the Hamiltonian [60, 61]. Since a negative electron affinity implies that the system accepts no electron at all, one can

argue that, in these cases, the electron affinity should be set to zero, implying the use of the ground state energy of the anion in the case of a negative electron affinity, i.e.

$$\eta = I - \text{Max}[0, A] \quad (2.42)$$

Cárdenas et al. aimed to establish the preference for using or ignoring or including the negative electron affinity in establishing the chemical hardness and advised for the use of negative electron affinities when available [62]. Tozer and De Proft [63] proposed a simple expression to determine the negative vertical electron affinities of neutral systems that the negative vertical electron affinities of neutral systems can be determined using the simple expression

$$A = -\epsilon_{\text{LUMO}}^{\text{GGA}} - \epsilon_{\text{HOMO}}^{\text{GGA}} - I^{\text{GGA}} \quad (2.43)$$

where  $\epsilon_{\text{LUMO}}$  and  $\epsilon_{\text{HOMO}}$  are the LUMO and HOMO eigenvalues, determined from a DFT calculation on the neutral system, using a local density approximation or generalized gradient approximation functional.  $I^{\text{GGA}}$  is the vertical ionization potential of the neutral system computed using the same GGA. Using this expression for the electron affinity, the global hardness can be computed as

$$\eta = \epsilon_{\text{LUMO}} - \epsilon_{\text{HOMO}}^{\text{GGA}} + 2(\epsilon_{\text{HOMO}}^{\text{GGA}} + I^{\text{GGA}}) \quad (2.44)$$

which can be considered as a corrected Koopmans type of approximation for the hardness.

The inverse of the chemical hardness is called the (global) softness  $S$  [64]

$$S = \frac{1}{\eta} = \left( \frac{\partial N}{\partial \mu} \right)_v \quad (2.45)$$

The global softness has been shown to be related to the polarizability and its cube root [65–71].

With now the global first- and second-order global derivatives established, we can write a Taylor series expansion for the energy  $E$  vs. the number of electrons  $N$  around a reference state with number of electrons  $N^0$  and external potential  $v^0$  (at constant external potential) up to second order,

$$E[N, v^0] = E[N^0, v^0] + \left( \frac{\partial E}{\partial N} \right)_{v=v^0} (N - N^0) + \frac{1}{2} \left( \frac{\partial^2 E}{\partial N^2} \right)_{v=v^0} (N - N^0)^2 \quad (2.46)$$

or

$$\Delta E = \mu \Delta N + \frac{1}{2} \eta \Delta N^2 \quad (2.47)$$

Using this equation, Parr et al. considered the case where an electrophile would be immersed in a free electron sea of chemical potential and derived the consequent maximum charge transfer  $\Delta N_{\text{max}}$  to this electrophile as [72]

$$\Delta N_{\text{max}} = -\frac{\mu}{\eta} \quad (2.48)$$

The negative of the accompanying energy lowering (to first order)  $\Delta E_{\text{max}}$  of the electrophile was introduced as the electrophilicity index  $\omega$  [72–74]

$$-\Delta E_{\text{max}} \equiv \omega = \frac{\mu^2}{2\eta} \quad (2.49)$$

In order to appreciate the importance of both left and right derivatives in the global quantities involved in this expression, Gázquez et al. considered the energy as a function of the number of electrons in the  $N - 1$  to  $N$  and  $N$  to  $N + 1$  regions, introducing the electrodonating and electroaccepting powers  $\omega^-$  and  $\omega^+$  as [75, 76]

$$\omega^- \equiv \frac{\mu^-}{2\eta^-} \quad (2.50)$$

and

$$\omega^+ \equiv \frac{\mu^+}{2\eta^+} \quad (2.51)$$

where  $\mu^-$ ,  $\mu^+$ ,  $\eta^-$ , and  $\eta^+$  are now the slopes and the curvatures in the two parabolas connecting the  $N - 1$  and  $N$  and  $N$  and  $N + 1$  points, respectively; these quantities allow to differentiate the response of the system when it either accepts or donates charge. Chattaraj et al. have additionally introduced the net electrophilicity  $\Delta\omega^\pm$  as [77]

$$\Delta\omega^\pm = \omega^+ - (-\omega^-) \quad (2.52)$$

In parallel, the net reactivity index (NRI) was developed to assess the reactivity between pairs of reactants on the basis of the difference of the electron-withdrawing power of the more electrophilic reactant and (minus) the electron-donating power of the less electrophilic reactant [78].

As can be seen, conceptual DFT allows the introduction of the concept of electrophilicity from first principles; a similar approach for the nucleophilicity is, however, not available and nucleophilicities thus have to be introduced ad hoc within the theory. Mayr has composed an extensive database of electrophilicities and nucleophilicities from experimental data [79–82]. The Mayr scale is based on the following expression for the rate constant (at 20 °C) for the combination of an electrophile and a nucleophile

$$\log k_{20} \text{ } ^\circ\text{C} = s_N(N + E) \quad (2.53)$$

In this equation,  $E$  and  $N$  are the electrophilicity and nucleophilicity, respectively.  $s_N$  is called a sensitivity parameter that is nucleophile and solvent dependent. It has been less straightforward to design an index for nucleophilicity within the framework of conceptual DFT [83–85]. Domingo et al. proposed a nucleophilicity index based on the difference between the Kohn–Sham HOMO orbital energy of the nucleophile and the HOMO energy of tetracyanoethylene; the latter molecule was used as a reference because of the low value of its HOMO. Tognetti et al. quantified electrophilicity and nucleophilicity by performing a partitioning of the dual descriptor (*vide infra*) [86]. These authors also introduced the concept of an atomic electronegativity in a molecule [87], partitioning an expression for the electronic chemical potential over atomic regions using Bader’s atoms in molecules (AIM) approach [88]. For a series of carbocations, these AIM electronegativities for C were found to be strongly correlated to the Mayr electrophilicities of these compounds. Additionally, a machine learning approach has been adopted to predict electrophilicities using different conceptual DFT and AIM descriptors [89].

The quadratic model in Eq. (2.46) was also used to propose the so-called electrofugality and nucleofugality indices, probing the quality of leaving groups [90, 91]. The dissociation or leaving energy of a nucleofuge  $\Delta E_{\text{nucleofuge}}$  and a electrofuge  $\Delta E_{\text{electrofuge}}$  from a neutral compound were defined as the energy difference between  $\Delta E_{\text{max}}$  and the energy of the anion and cation, respectively. The associated nucleofugality  $\lambda_N$  and electrofugality  $\lambda_E$  were defined as

$$\lambda_N \equiv e^{-\beta_N \Delta E_{\text{nucleofuge}}} \quad (2.54)$$

and

$$\lambda_E \equiv e^{-\beta_E \Delta E_{\text{electrofuge}}} \quad (2.55)$$

where the values of  $\beta_N$  and  $\beta_E$  were chosen so that the nucleofugality of the hydride anion and the the electrofugality of the proton are equal to 1.

The derivative of the chemical hardness with respect to the number of electrons was introduced by Parr and Fuentealba as the hyperhardness, a third-order derivative of the energy [92]

$$\gamma = \eta^{(2)} = \left( \frac{\partial^3 E}{\partial N^3} \right)_v = \left( \frac{\partial \eta}{\partial N} \right)_v \quad (2.56)$$

Fuentealba and Parr presented numerical values for the hyperhardness for atoms and monoatomic ions and concluded that the numerical values were small. Values for molecules were subsequently presented by Morell et al. [93] and Dunlap [94]. The former provided interpretation for the hyper-hardness values through, among others, a connection to the maximum hardness principle, stating that systems with a positive hyper hardness exhibit high stability, whereas species with negative hyper-hardness show high chemical reactivity. Further relationships between third-order reactivity indices were derived by Cárdenas et al. [95].

## 2.4 Second- and Third-Order Local Quantities: The Fukui Function and the Dual Descriptor

The change of the chemical potential  $\mu$  when going from one ground state to another is given by

$$d\mu = \left( \frac{\partial \mu}{\partial N} \right)_v dN + \int \left[ \frac{\delta \mu}{\delta v(\mathbf{r})} \right]_N \delta v(\mathbf{r}) d\mathbf{r} \quad (2.57)$$

Parr and Yang defined the Fukui function  $f(\mathbf{r})$  as [96, 97]

$$f(\mathbf{r}) = \left[ \frac{\delta \mu}{\delta v(\mathbf{r})} \right]_N = \left( \frac{\partial \rho(\mathbf{r})}{\partial N} \right)_v \quad (2.58)$$

which can be considered as an extension of the frontier-electron theory of chemical reactivity within the DFT framework. Note that in Eq. (2.58), a Maxwell relation has been used. In the same landmark paper, Parr and Yang put forward that the preferred approach of one reagent by another corresponds to the direction for which the initial  $|d\mu|$  is a maximum; since the first term of Eq. (2.57) is direction independent,

it can then be assumed that the preferred direction of approach is the one showing the largest value of the Fukui function at the reaction site. Recently, theoretical evidence for this rule has been given [98]. The Fukui function integrates to unity over space

$$\int f(\mathbf{r})d\mathbf{r} = 1 \quad (2.59)$$

Due to the discontinuity of the electron density with respect to the number of electrons, a Fukui function can be defined both on the electron deficient or abundant side of the integer  $N$ . The derivative on the electron deficient side is the Fukui function for an electrophilic attack, i.e.

$$f^-(\mathbf{r}) = \left( \frac{\partial \rho(\mathbf{r})}{\partial N} \right)_v^- = \rho_N(\mathbf{r}) - \rho_{N-1}(\mathbf{r}) \quad (2.60)$$

with  $\rho_N(\mathbf{r})$  and  $\rho_{N-1}(\mathbf{r})$  the electron density of the  $N$  and  $N - 1$  electron system, respectively. The Fukui function for a nucleophilic attack is given by the derivative on the electron abundant side,

$$f^+(\mathbf{r}) = \left( \frac{\partial \rho(\mathbf{r})}{\partial N} \right)_v^+ = \rho_{N+1}(\mathbf{r}) - \rho_N(\mathbf{r}) \quad (2.61)$$

where  $\rho_{N+1}(\mathbf{r})$  is now the electron density of the  $N + 1$  electron system. For a radical (neutral species) attack, the Fukui function  $f^0$  is introduced, the average of  $f^+$  and  $f^-$

$$f^0(\mathbf{r}) = \frac{f^-(\mathbf{r}) + f^+(\mathbf{r})}{2} \quad (2.62)$$

Based on Eq. (2.37), these expressions are in fact exact provided the exact electron densities of the  $N$ ,  $N + 1$ , or  $N - 1$  are used. Many aspects of the properties of this function were analyzed, such as, e.g. the cusp condition [99], its topography [100] and the fact that it can be negative in some molecular regions [101–107]. The Fukui function is typically used to discuss differences in reactivity between different sites within a molecule, more specifically reactivity in frontier molecular orbital controlled reactions (i.e. charge transfer reactions and orbital controlled reactions, i.e. soft–soft interactions) [108–111]. It was shown that the Fukui functions can be approximated as the densities of the Kohn–Sham frontier molecular orbitals [112], explicitly connecting the conceptual DFT framework with frontier molecular orbital theory [113]

$$f^-(\mathbf{r}) = \rho_{\text{HOMO}}(\mathbf{r}) \quad (2.63)$$

and

$$f^+(\mathbf{r}) = \rho_{\text{LUMO}}(\mathbf{r}) \quad (2.64)$$

$\rho_{\text{HOMO}}(\mathbf{r})$  and  $\rho_{\text{LUMO}}(\mathbf{r})$  are the densities of the HOMO and LUMO, respectively.

From the work of Yang et al., it is clear that the Fukui function contains information about not only the relevant frontier orbital but also about the change in the shape of the orbitals when electrons are either added to or subtracted from the system (the so-called orbital relaxation); an example where the latter are important was discussed in e.g. [114]. The importance of orbital relaxation effects was also

highlighted by Yang and coworkers who investigated the relaxation of Kohn–Sham orbitals upon addition or subtraction of a fractional number of electrons on a finite system using a perturbational approach [115]. Bultinck et al. introduced the Fukui matrix as a generalization of the Fukui function, allowing, among others, to gain insight into the occurrence of negative Fukui functions and to assess the quality of the frontier molecular orbital approximation as [116]

$$f(\mathbf{r}, \mathbf{r}') = \left( \frac{\partial \rho(\mathbf{r}, \mathbf{r}')}{\partial N} \right)_v \quad (2.65)$$

which can then be e.g. projected on the basis of the Kohn–Sham orbitals of the neutral system. Diagonalization of this matrix then yields the so-called Fukui orbitals and Fukui eigenvalues. In the case of a perfect frontier molecular orbital (FMO) approximation, only one eigenvalue will be different from zero (and equal to one); in this case, the Fukui orbital is composed only of the frontier molecular orbital of the neutral molecule. This approach bears resemblance to the Natural Orbitals for Chemical Valence approach of Michalak and coworkers, where the NOCVs are obtained by diagonalization of the deformation density, i.e. the change of the density of two interacting fragments A and B with respect to the densities of the individual A and B; these orbitals show great value in the characterization of charge transfer processes in molecular interactions [117].

In order to locally probe chemical reactivity, the Fukui functions are often visualized through contour plots, 3D isosurfaces or through mapping of the quantity on a specific representative molecular surface. In Figure 2.1, the Fukui function

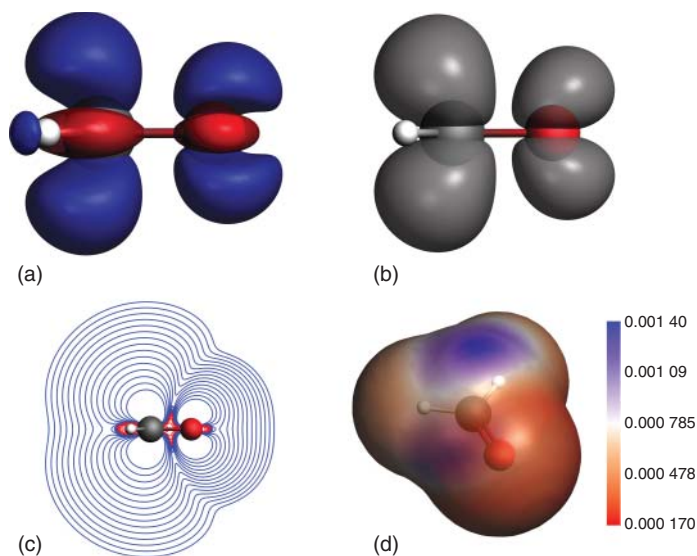


**Figure 2.1** 2D and 3D representations of the Fukui function  $f^+$  for a nucleophilic attack for  $\text{H}_2\text{CO}$ : (a)  $f^+$  0.008 a.u. isosurface with positive values depicted in blue and negative in red. (b) LUMO density (isovalue of 0.03 a.u.). (c) Contourplot with contours ranging from  $-0.02$  to  $0.02$ , with negative values depicted in red and positive in blue. (d)  $f^+$  plotted on the van der Waals surface.

for a nucleophilic attack is plotted for the formaldehyde molecule. As can be seen, the function shows the highest values around the carbon atom, correctly predicting this atom as the preferred site for a nucleophilic addition; for comparison, the LUMO density has been plotted as well, yielding the same conclusions about the regioselectivity for the addition of a nucleophile. These quantities were obtained using the ADF program [118], using the PBE exchange-correlation functional [119] and a DZP basis set [120].

A remark has to be made, however, on the evaluation of  $f^+$  in the gas phase. For a neutral compound, evaluation of  $f^+$  involves the evaluation of the molecular anion, which often is unbound in the gas phase and is unstable with respect to electron loss. In order to compute the electron density of the gas phase anion, two possible approaches consist in binding of the excess electron using either a compact basis set or a potential wall [60, 121].

For many applications, however, it is interesting to condense the function on an atom, since analyzing the Fukui function and its variation among different sites in a molecule cannot always be clearly appreciated from either the 2D or 3D spatial plots. Yang and Mortier introduced the atom-condensed Fukui functions by taking the difference of the atomic Mulliken populations [122] of the atom in the  $N$ ,  $N - 1$ , and  $N + 1$  systems; the Fukui functions condensed to an atom  $k$ , for an electrophilic, nucleophilic, and radical attack are then obtained as [123]

$$f_k^- = q_k(N) - q_k(N - 1) \quad (2.66)$$

$$f_k^+ = q_k(N + 1) - q_k(N) \quad (2.67)$$

and

$$f_k^0 = q_k(N + 1) - q_k(N - 1) \quad (2.68)$$

Since the atom-condensed Fukui functions can also be evaluated using other population analysis schemes, their values are dependent on the particular way to identify the atom in a molecule. This issue has been addressed in many papers, among others comparing different condensation schemes for this quantity [124–138]. In addition, Bultinck et al. also pointed to different expressions that could be used for the evaluation of the atom-condensed Fukui function, basically resulting from the order of the condensation and function evaluation. In the *Fragment of the Molecular Response* (FMR) approach to obtain the atom-condensed Fukui function, one first evaluates the molecular Fukui function, followed by a partitioning of the function over the atomic regions. Alternatively, one could first separately condense the constituent parts of the Fukui functions (i.e. the electron densities of the  $N$ ,  $N + 1$ , and  $N - 1$  electron systems) and then take the differences of these populations; this was termed the *response of the molecular fragment* (RMF) approach. Equations (2.69) and (2.70) illustrate the differences between the two approaches for a system containing  $N_0$  number of electrons; the FMR atom-condensed Fukui function is obtained as

$$f_{A,\text{FMR}}^\pm = w_A(\mathbf{r}, N^0) f^\pm(\mathbf{r}, N^0) \quad (2.69)$$

where  $w_A(\mathbf{r}, N^0)$  is a weight function to project the molecular function onto the atom  $A$  in the molecule.

The RMF Fukui function is computed as

$$f_{A,\text{RMF}}^{\pm} = \left( \frac{\partial [w_A(\mathbf{r}, N)\rho(\mathbf{r})]}{\partial N} \right)_v \quad (2.70)$$

Both approaches do not necessarily yield the same values for the atom-condensed Fukui function. In the case of the Mulliken [121] and Hirshfeld [139] population analyses schemes, both approaches yield the same results for the condensed Fukui functions. These Hirshfeld AIM have been derived from information theory [134, 140, 141]. A connection between conceptual DFT and information theory was further developed by Liu and coworkers [142].

Given the above-mentioned arbitrary choices, it thus might be appropriate to certainly also consider the local Fukui function next its atom condensed version. Alternatively, it has been suggested to condense Fukui functions to the different bonds in a molecule [143].

Morell et al. introduced the dual descriptor  $f^2(\mathbf{r})$  as the derivative of the Fukui function with respect to the number of electrons,

$$f^{(2)}(\mathbf{r}) = \left( \frac{\partial f(\mathbf{r})}{\partial N} \right)_v = \left( \frac{\delta \eta}{\delta v(\mathbf{r})} \right)_N = f^+(\mathbf{r}) - f^-(\mathbf{r}) \quad (2.71)$$

This quantity, a third-order energy derivative, was shown to provide a one-shot picture of both the nucleophilic and electrophilic regions in a chemical compound [144, 145]. It serves as an intramolecular reactivity index. In addition, it was found to play a crucial role in regaining the famous Woodward–Hoffmann rules for pericyclic reactions in conceptual DFT [25, 146]. In Figure 2.2, the dual descriptor is depicted for  $\text{H}_2\text{CO}$ , clearly showing positive (blue) regions where a nucleophilic attack is preferred and negative (red) regions where an electrophile is predicted to attach.

The dual descriptor was generalized to the state-specific dual descriptor  $\Delta f_i(\mathbf{r})$ , defined for an excited state  $i$  as [147]

$$\Delta f_i(\mathbf{r}) = \rho_i(\mathbf{r}) - \rho_0(\mathbf{r}) \quad (2.72)$$

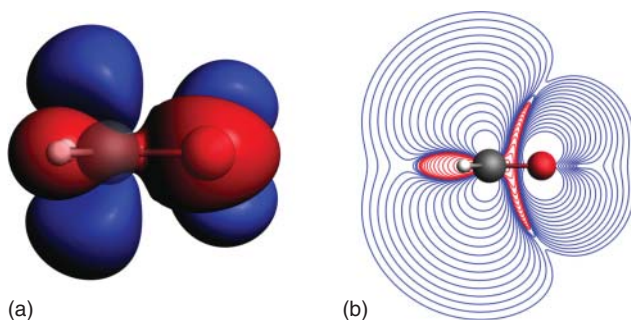


**Figure 2.2** 2D and 3D representation of the dual descriptor  $f^2$  for  $\text{H}_2\text{CO}$ : (a)  $f^2 \pm 0.003$  a.u. isosurface with positive values depicted in blue and negative in red. (b) Contourplot with contours ranging from  $-0.02$  to  $0.02$ , with negative values depicted in red and positive in blue.



where  $\rho_0(\mathbf{r})$  and  $\rho_i(\mathbf{r})$  are the electron densities of the ground state and excited state  $i$ , respectively. This quantity can be associated with the density polarization of the molecule resulting from an approaching reagent.

When a molecule undergoes a charge transfer during a chemical reaction, this will result in a change on the forces on the nuclei of its constituent atoms, from which an evaluation to a new equilibrium external potential will result. The magnitude of these forces on the nuclei upon change in number of electrons of the system is probed by the nuclear Fukui function  $\Phi_\alpha$  [148, 149]

$$\Phi_\alpha = \left( \frac{\partial \mathbf{F}_\alpha}{\partial N} \right)_v \quad (2.73)$$

This quantity can be considered to be a so-called nuclear reactivity index and probes the response of the nuclei toward changes in the number of electrons. The interplay between electronic and nuclear degrees of freedom was discussed among others by Nalewajski [150]. Different authors have obtained and discussed numerical values for this quantity and derived relations with other quantities from conceptual DFT [151–156]. Through the use of a Maxwell relationship, this quantity can be expressed as a function of the nuclear displacement as [151]

$$\Phi_\alpha = \left( \frac{\partial \mathbf{F}_\alpha}{\partial N} \right)_v = - \left( \frac{\delta \mu}{\delta \mathbf{R}_\alpha} \right)_N \quad (2.74)$$

where  $\mathbf{R}_\alpha$  indicates the position of nucleus  $\alpha$ . It was shown to be related to the electronic Fukui function through the Berlin binding function  $f_v(\mathbf{r})d\mathbf{r}$  [151], which divides the molecule into binding and antibinding regions [157]

$$-\sum_\alpha \Phi_\alpha \cdot \mathbf{R}_\alpha = \int f(\mathbf{r})f_v(\mathbf{r})d\mathbf{r} \quad (2.75)$$

The nuclear Fukui function was used in predicting the sites of DNA strand breaking due to electron attachment [158]. The derivative of the nuclear Fukui function with respect to the number of electrons is the nuclear stiffness [159]

$$G_\alpha = - \left( \frac{\partial \Phi_\alpha}{\partial N} \right)_v = - \left( \frac{\partial^2 \mathbf{F}_\alpha}{\partial N^2} \right)_v = \left( \frac{\delta \eta}{\delta \mathbf{R}_\alpha} \right)_N \quad (2.76)$$

It was shown to be qualitatively related to the Raman scattering intensity [160]. Higher order derivatives have additionally been considered [161].

## 2.5 Local Softness and Local Hardness

The definition of the Fukui function given in Eq. (2.58) can be written as

$$f(\mathbf{r}) = \left[ \frac{\delta \partial E}{\partial N \delta v(\mathbf{r})} \right] \quad (2.77)$$

It is the derivative of the state function of importance in the canonical ensemble  $E$  with respect to the two natural variables  $N$  and  $v$  in this ensemble [162]. In the grand canonical ensemble, with the grand potential  $\Omega$  as the state function and the

natural variables are  $v$  and  $\mu$  (Chapter 3), the local softness  $s(\mathbf{r})$  can be introduced as its counterpart, i.e. the derivative of  $\Omega$  with respect to both natural variables

$$s(\mathbf{r}) = \left[ \frac{\delta^2 \Omega}{\partial \mu \delta v(\mathbf{r})} \right] \quad (2.78)$$

with

$$\Omega = E - \mu N \quad (2.79)$$

Note that, besides  $E$  and  $\Omega$ , also other state functions exist which will be treated in Chapter 3.  $s(\mathbf{r})$  is the local counterpart of the global softness of the system. It equals

$$s(\mathbf{r}) = \left( \frac{\partial \rho(\mathbf{r})}{\partial \mu} \right)_v = \left( \frac{\partial \rho(\mathbf{r})}{\partial N} \right)_v \left( \frac{\partial N}{\partial \mu} \right)_v = Sf(\mathbf{r}) \quad (2.80)$$

As can be seen, the local softness distributes the global of the systems over the different regions of the system. It can thus be used as a quantity to probe differences in reactivity between molecules (i.e. through comparison of local softness values between different regions of different molecules). When integrated over space, the local softness yields to global softness of the system

$$\int s(\mathbf{r}) d\mathbf{r} = S \quad (2.81)$$

The local softness can, in analogy with the Fukui functions from Eqs. (2.60)–(2.62) be evaluated for an electrophilic, nucleophilic and radical attack, i.e.

$$s^\alpha(\mathbf{r}) = Sf^\alpha(\mathbf{r}) \quad (2.82)$$

with  $\alpha$  being either  $-$ ,  $+$ , or  $0$ . The condensed local softnesses are obtained in turn as

$$s_k^\alpha = Sf_k^\alpha \quad (2.83)$$

with, again,  $\alpha$  being either  $-$ ,  $+$ , or  $0$ . The Fukui function naturally emerges here as the partitioning function of global softness over space. It can be similarly applied to the global electrophilicity index giving rise to Chattaraj's philicity index [163]. In the case of e.g. electron uptake by an electrophile, this yields

$$\omega = \frac{\mu^2}{2\eta} = \frac{\mu^2 S}{2} = \frac{\mu^2 \int s^+(\mathbf{r}) d\mathbf{r}}{2} = \frac{\mu^2}{2\eta} \int f^+(\mathbf{r}) d\mathbf{r} \quad (2.84)$$

So that

$$\omega(\mathbf{r}) = \omega f^+(\mathbf{r}) \quad (2.85)$$

which is a local electrophilicity index. [163, 164] Using the dual descriptor to partition the electrophilicity over the different atomic regions  $k$  in the molecule yields the so-called multiphilic descriptor  $\Delta\omega_k$  [165]

$$\Delta\omega_k = \omega f_k^{(2)} \quad (2.86)$$

A related quantity is the electrophilicity excess introduced for functional groups [166]. The definition of a local counterpart of the chemical hardness has been proven to be much less straightforward, and its definition has been the subject of many

contributions [47, 48, 167–180]. Considering Eq. (2.80), a local counterpart of the hardness, the local hardness, may be defined as [167, 169]

$$\eta(\mathbf{r}) = \left( \frac{\delta\mu}{\delta\rho(\mathbf{r})} \right)_v \quad (2.87)$$

In this manner, the local softness and hardness integrate to 1 over space

$$\int s(\mathbf{r})\eta(\mathbf{r})d\mathbf{r} \quad (2.88)$$

Local softness and local hardness have been identified as measures of the local abundance of the corresponding global quantities [181, 182]. This definition turns out to be problematic, however, as it can be termed an “ambiguous constrained derivative” [167, 171, 174, 178, 183]; the problem lies in the fact that for a ground state, the electron density  $\rho(\mathbf{r})$  and  $v(\mathbf{r})$  are dependent because of the first Hohenberg–Kohn theorem.

Some additional remarks on the local hardness will be made later on in this chapter.

## 2.6 The Linear Response Function, Softness, and Hardness Kernels

The linear response function is defined as the second functional derivative of the energy with respect to the electron density, i.e.

$$\chi(\mathbf{r}, \mathbf{r}') = \left[ \frac{\delta^2 E}{\delta v(\mathbf{r})\delta v(\mathbf{r}')} \right]_N = \left[ \frac{\delta\rho(\mathbf{r})}{\delta v(\mathbf{r}')} \right]_N \quad (2.89)$$

This quantity expresses how the electron density at a given point  $\mathbf{r}$  changes following a change of the external potential at a point  $\mathbf{r}'$  and it is the static analogue of the frequency-dependent linear response function  $\chi(\mathbf{r}, \mathbf{r}', \omega)$ , an important quantity in time-dependent DFT [184]. It has been shown to be a quantity suitable of describing electron delocalization in molecules [26]. An in-depth discussion of this quantity and its use is given in Chapter 16.

Introducing the modified potential  $u(\mathbf{r}) = \mu - v(\mathbf{r})$ , the so-called softness kernel is introduced as [169]

$$s(\mathbf{r}, \mathbf{r}') = \frac{\delta\rho(\mathbf{r})}{\delta u(\mathbf{r}')} = \left[ \frac{\delta\rho(\mathbf{r})}{\delta v(\mathbf{r}')} \right]_\mu \quad (2.90)$$

The softness kernel is related to the linear response function through the Berkowitz–Parr relation [169],

$$\chi(\mathbf{r}, \mathbf{r}') = -s(\mathbf{r}, \mathbf{r}') + \frac{s(\mathbf{r})s(\mathbf{r}')}{S} \quad (2.91)$$

The local softness can be obtained straightforwardly from the softness kernel through integration over one of the spatial coordinates,

$$s(\mathbf{r}) = \int s(\mathbf{r}, \mathbf{r}')d\mathbf{r}' \quad (2.92)$$

The hardness kernel is defined as

$$\eta(\mathbf{r}, \mathbf{r}') = \frac{\delta u(\mathbf{r})}{\delta \rho(\mathbf{r}')} = \left[ \frac{\delta^2 F}{\delta \rho(\mathbf{r}) \delta \rho(\mathbf{r}')} \right]_{\mu} \quad (2.93)$$

The softness and hardness kernels are connected through

$$\int s(\mathbf{r}, \mathbf{r}') \eta(\mathbf{r}', \mathbf{r}'') d\mathbf{r}' = \delta(\mathbf{r} - \mathbf{r}'') \quad (2.94)$$

The hardness kernel plays a key role in the variational determination of the Fukui function [185]. Suppose that we construct a functional  $\eta[g]$  defined as

$$\eta[g] = \int \int g(\mathbf{r}) \eta(\mathbf{r}, \mathbf{r}') g(\mathbf{r}') d\mathbf{r} d\mathbf{r}' \quad (2.95)$$

where the function  $g(\mathbf{r})$  integrates to unity, minimizing  $\eta[g]$  under the constraint that  $g$  should at all times integrate to unity yields the exact Fukui function of the system; at the solution point,  $\eta[f] = \eta$  is the chemical hardness of the system. This implies that when a (suitable) expression for the hardness kernel would be available, one could variationally determine the Fukui function of the system.

Using Eqs. (2.1) and (2.4), Parr and Gázquez rewrote the  $E[\rho]$  functional as

$$E[\rho] = N\mu - H[\rho] \quad (2.96)$$

with

$$H[\rho] = \int \rho(\mathbf{r}) \frac{\delta F}{\delta \rho(\mathbf{r})} d\mathbf{r} - F[\rho] \quad (2.97)$$

the hardness functional [186].

Ghosh and Berkowitz now introduced the local hardness as [168]

$$\eta(\mathbf{r}) = \frac{1}{N} \int \frac{\delta^2 F}{\delta \rho(\mathbf{r}) \delta \rho(\mathbf{r}')} \rho(\mathbf{r}') d\mathbf{r}' \quad (2.98)$$

or, in terms of the hardness functional,

$$\eta(\mathbf{r}) = \frac{1}{N} \frac{\delta H[\rho]}{\delta \rho(\mathbf{r})} \quad (2.99)$$

This quantity was termed the “total local hardness” by Ayers and Parr [174]. With this definition, the local hardness can be approximated, within a Thomas-Fermi–Dirac ansatz [187], as the electronic part of the electrostatic potential divided by twice the number of electrons, i.e. [167, 172]

$$\eta(\mathbf{r}) = \frac{1}{2N} \int \frac{\rho(\mathbf{r}')}{|\mathbf{r} - \mathbf{r}'|} d\mathbf{r}' \quad (2.100)$$

Harbola et al. have proposed the following explicit form of the local hardness [171]

$$\eta(\mathbf{r}) = \int \frac{\delta^2 F}{\delta \rho(\mathbf{r}) \delta \rho(\mathbf{r}')} \lambda(\mathbf{r}') d\mathbf{r}' \quad (2.101)$$

where  $\lambda(\mathbf{r}')$  is an arbitrary function integrating to 1. It can easily be seen that for the Ghosh/Berkowitz definition,

$$\lambda(\mathbf{r}') = \frac{\rho(\mathbf{r}')}{N} \quad (2.102)$$

Another choice for this function, however, could be the Fukui function, yielding [170, 171]

$$\eta(\mathbf{r}) = \int \frac{\delta^2 F}{\delta \rho(\mathbf{r}) \delta \rho(\mathbf{r}')} f(\mathbf{r}') d\mathbf{r}' \quad (2.103)$$

Since however

$$\int \eta(\mathbf{r}, \mathbf{r}') f(\mathbf{r}') d\mathbf{r}' = \eta \quad (2.104)$$

This definition gives rise to a constant local hardness in space and was termed the frontier local hardness by Ayers and Parr [174]. The authors provided an alternative proposal for the definition of the local hardness, i.e. as the unconstrained derivative

$$\eta(\mathbf{r}) = \frac{\delta \mu}{\delta \rho(\mathbf{r})} \quad (2.105)$$

but also this quantity turns out not to be free from problems [176].

All in all, local hardness remains a challenging and difficult concept preventing its use on a routine basis in the study of chemical reactivity and stability. For the evaluation of hard-hard or charge-controlled interactions, the atomic charge appears to be of good quantity [109, 110]. A possibly connected reactivity index to probe charge-controlled processes is the molecular electrostatic potential, introduced as the interaction energy between a molecular system and a unit positive charge, neglecting polarization effects [188],

$$V(\mathbf{r}) = \sum_{A=1}^M \frac{Z_A}{|\mathbf{r} - \mathbf{R}_A|} - \int \frac{\rho(\mathbf{r}')}{|\mathbf{r} - \mathbf{r}'|} \quad (2.106)$$

As this indicator probes the interaction of the molecule with a hard system (i.e. a unit positive charge), a link with local hardness might be expected. For more complex cases, i.e. reactions that are neither charge- or orbital controlled, Ayers and coworkers have derived a so-called all purpose reactivity indicator that enables to probe the dual reactivity behavior and to quantify the shift in the reactivity (site-selectivity) depending on the nature of the electrophile (hard or soft) [189, 190]. Earlier, Geerlings and coworkers, in the framework of a study of the regioselectivity in electrophilic aromatic substitutions on monosubstituted benzenes, had proposed the following expression for a global reactivity index  $R(\mathbf{r})$ , consisting of a combination of the local softness  $s(\mathbf{r})$  and a local hardness estimate  $h(\mathbf{r})$ , both preceded by a local weight factor [172]

$$R(\mathbf{r}) = A(\mathbf{r})s(\mathbf{r}) + B(\mathbf{r})h(\mathbf{r}) \quad (2.107)$$

In the case of electrophilic aromatic substitution, the ratio  $A(\mathbf{r})/B(\mathbf{r})$  was expected to decrease with decreasing distance between the reagents, thus giving more weight to the local softness, in line with the description of the regioselectivity in the Wheland intermediate ( $\sigma$ -complex) of the reaction by this quantity. At larger distance, the local hardness would dominate, which is in agreement with this quantity describing the rate of the initial formation of the  $\pi$ -complex in this reaction.

## 2.7 The Perturbational Perspective on Chemical Reactivity

In Sections 2.2–2.6, we have been discussing a number of derivatives of the energy with respect to either  $N$  or  $v(\mathbf{r})$  or both, i.e.  $\frac{\partial^m \delta^k E}{\partial N^m \partial v(\mathbf{r})^k}$ . In many practical applications, the  $N$  derivatives are evaluated using a finite difference approach, although analytical expressions are available [191–199]. Fukui functions and dual descriptors have also been obtained as the  $v$  derivatives of, respectively,  $\mu$  and  $\eta$ , without resorting to changes in number of electrons [200]; a similar methodology was developed for the linear response function [201]. The implication of degeneracy on computed concepts and reactivity indicators has been scrutinized [202, 203]; Bultinck et al. additionally investigated the consequences for atomic charges and electrostatic potentials [204]. These energy derivatives are properties of an isolated system and can be considered as the response of a system when it is perturbed in  $N$  and/or  $v(\mathbf{r})$ . These are the changes characterizing the perturbations at a microscopic level when a system is undergoing a chemical reaction and can thus be termed response functions. Their evaluation affords to do comparative studies of chemical reactivity, either within a given systems (regioselectivity) or between different systems. Since all of these considerations are based on perturbations, one can term this a perturbational approach to chemical reactivity [20, 205]. Consider a reagent A characterized by a given number of electrons  $N_A^0$  and  $\Delta N_A, v_A^0(\mathbf{r})$ . These quantities define the Hamiltonian, and thus all properties  $\xi^0$  of A. During the chemical reaction, another molecule B is approaching A leading to a perturbation in both  $N_A^0$  and/or  $\Delta N_A, v_A^0(\mathbf{r})$ . Suppose that, upon this perturbation, both quantities change to  $N_A^0$  and  $\Delta N_A, v_A^0(\mathbf{r})$ , respectively, i.e.

$$N_A = N_A^0 + \Delta N_A \quad (2.108)$$

and

$$v_A(\mathbf{r}) = v_A^0(\mathbf{r}) + \Delta v_A(\mathbf{r}) \quad (2.109)$$

Analogously,  $N_A^0$  and  $\Delta N_A, v_A^0(\mathbf{r})$  determine all properties  $\xi$  of the molecule after the perturbation. One can then write a Taylor series expansion for  $\xi$  around the unperturbed situation  $\xi^0$  as

$$\begin{aligned} \xi &= \xi^0 + \Delta \xi \\ &= \xi^0 + \left( \frac{\partial \xi}{\partial N_A} \right)_{\substack{v_A(\mathbf{r}) = v_A^0(\mathbf{r}) \\ N_A = N_A^0}} \Delta N_A + \int \left[ \frac{\delta \xi}{\delta v_A(\mathbf{r})} \right]_{\substack{v_A(\mathbf{r}) = v_A^0(\mathbf{r}) \\ N_A = N_A^0}} \Delta v_A^0(\mathbf{r}) d\mathbf{r} \\ &\quad + \frac{1}{2} \left( \frac{\partial^2 \xi}{\partial N_A^2} \right)_{\substack{v_A(\mathbf{r}) = v_A^0(\mathbf{r}) \\ N_A = N_A^0}} \Delta N_A^2 + \Delta N_A \int \left[ \frac{\delta \partial \xi}{\partial N_A \delta v_A(\mathbf{r})} \right]_{\substack{v_A(\mathbf{r}) = v_A^0(\mathbf{r}) \\ N_A = N_A^0}} \Delta v_A^0(\mathbf{r}) d\mathbf{r} \\ &\quad + \frac{1}{2} \int \int \left[ \frac{\delta^2 \xi}{\delta v_A(\mathbf{r}) \delta v_A(\mathbf{r}')} \right]_{\substack{v_A(\mathbf{r}) = v_A^0(\mathbf{r}) \\ N_A = N_A^0}} \Delta v_A^0(\mathbf{r}) d\mathbf{r} \Delta N_A^2 \end{aligned} \quad (2.110)$$

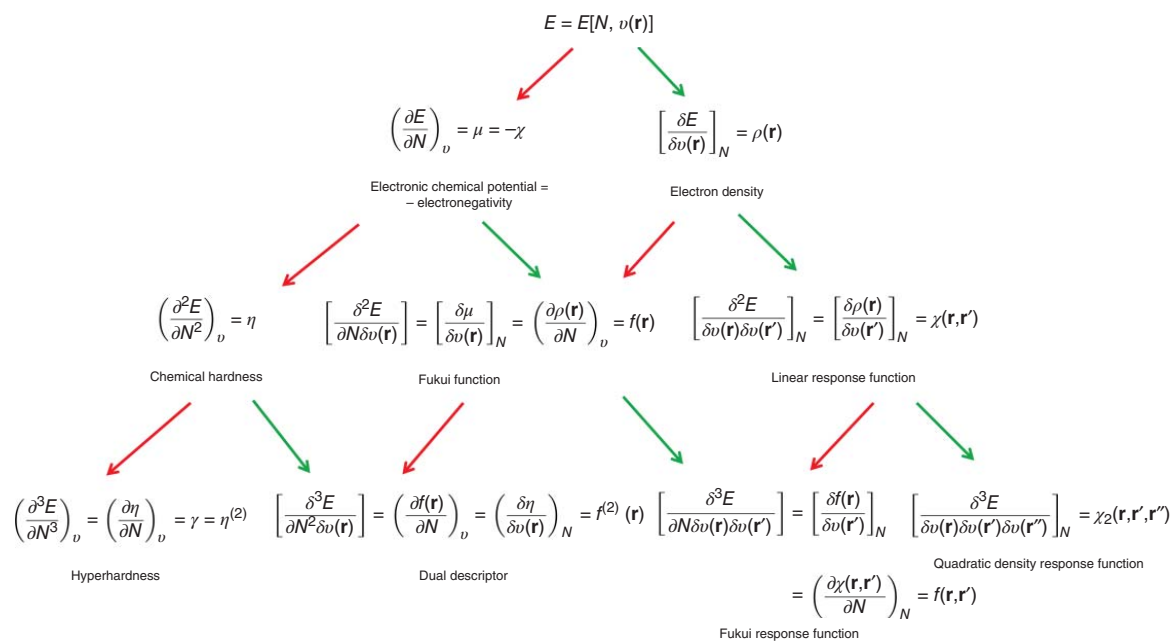


**Figure 2.3** Response function tree of the energy  $E$  vs. changes in the number of electrons  $N$  and the external potential  $v(\mathbf{r})$ . Red arrows indicate differentiation with respect to  $N$ , and green arrows indicate differentiation with respect to  $v(\mathbf{r})$ .

Putting  $\xi = E$ , truncating at second order and introducing the symbols for the different response functions introduced in this chapter, yields

$$\begin{aligned}
 E_A [N_A^0 + \Delta N_A, v_A^0(\mathbf{r}) + \Delta v_A(\mathbf{r})] &= E_A [N_A^0, v_A^0(\mathbf{r})] + \mu_A \Delta N_A + \frac{1}{2} \eta_A (\Delta N_A)^2 \\
 &+ \int \rho_A(\mathbf{r}) \Delta v_A(\mathbf{r}) d\mathbf{r} \Delta N_A + \int f_A(\mathbf{r}) \Delta N_A \Delta v_A(\mathbf{r}) d\mathbf{r} \\
 &+ \frac{1}{2} \int \int \chi_A(\mathbf{r}, \mathbf{r}') \Delta v_A(\mathbf{r}) \Delta v_A(\mathbf{r}') d\mathbf{r} d\mathbf{r}' \quad (2.111)
 \end{aligned}$$

The perturbational approach can thus be adopted to estimate the energy of the transition state (or other relevant points on the potential energy surface) through the properties of the isolated reactants; as such, it is expected to work best for cases where the transition state is not too far from the reactants on the surfaces, i.e. for early transition states [27] and when there is no crossing of competing reaction pathways. It can be considered to be a generalization of the Klopman–Salem equation [206], which has been used to rationalize frontier molecular orbital theory and the HSAB principle. The analysis and principle have been criticized; however, [207] a combination of conceptual DFT and the activation strain model [208] was used to gain further insight into the failure of the principle for ambident reactivity [209].

Two final remarks should be made:

1. The perturbation series is not guaranteed to converge, even if the necessary derivatives at all orders would be available; it is thus not possible to guarantee that one can accurately describe every point on the potential energy surface by considering the perturbation expansion
2. As pointed out by Yang and coworker [198], the derivatives with respect to  $N$  in Eq. (2.105) should be taken on either the electron deficient or abundant side, in view of the derivative discontinuity of the energy at integer  $N$ . These concepts can also be used to study density functional approximations in terms of their derivatives [197, 198] The effect of the discontinuities on reactivity indices was further scrutinized by Hellgren and Gross [210].

The response functions up to third order in the canonical ensemble are summarized in the so-called response function tree [211–214] (Figure 2.3).

## 2.8 Conclusion

This chapter has provided a general treatment of the basic functions introduced within the framework of conceptual DFT. The focus has been on derivatives of the energy with respect to either the number of electrons and/or the external potentials as basic variables describing chemical processes. Additionally, we have focused on the description of these properties at zero temperature for isolated molecules. In addition, we have not yet discussed the reactivity/stability principles in which these concepts are often used; these will be outlined in the following chapter. In subsequent chapters, extensions of both these functions will be discussed in more detail.



## Acknowledgment

The author would like to acknowledge Dr. Ana da Cunha for preparing Figures 2.1 and 2.2 in this chapter.

## References

- 1 Hohenberg, P. and Kohn, W. (1964). *Phys. Rev. B.* 136: 864.
- 2 Kohn, W. and Sham, L.J. (1965). *Phys. Rev. A* 140: 1133.
- 3 Parr, R.G. and Yang, W. (1989). *Density Functional Theory of Atoms and Molecules*. New York: Oxford University Press.
- 4 Dreizler, R.M. and Gross, E.K.U. (1990). *Density Functional Theory*. Berlin Heidelberg, New York: Springer-Verlag.
- 5 Parr, R.G. and Yang, W. (1995). *Annu. Rev. Phys. Chem.* 46: 710.
- 6 Kohn, W., Becke, A.D., and Parr, R.G. (1996). *J. Phys. Chem.* 100: 978.
- 7 Koch, W. and Holthausen, M. (2001). *A Chemists Guide to Density Functional Theory*, 2e. Weinheim: Wiley-VCH.
- 8 Cohen, A.J., Mori-Sánchez, P., and Yang, W. (2012). *Chem. Rev.* 112: 289.
- 9 Burke, K. (2012). *J. Chem. Phys.* 136: 150901.
- 10 Becke, A.D. (2014). *J. Chem. Phys.* 140: 18A301.
- 11 Jones, R.O. (2015). *Rev. Mod. Phys.* 87: 897.
- 12 Ayers, P.W., Parr, R.G., and Nagy, A. (2002). *Int. J. Quantum Chem.* 90: 309.
- 13 Guo, C., Rong, C., Lu, T. et al. (2021). *J. Phys. Chem. Lett.* 12: 5623.
- 14 Chattaraj, P.K. and Sengupta, S. (1997). *J. Phys. Chem. A* 101: 7893.
- 15 Baerends, E.J. (2018). *J. Chem. Phys.* 149: 054105.
- 16 Chermette, H. (1999). *J. Comput. Chem.* 20: 129.
- 17 Geerlings, P., De Proft, F., and Langenaeker, W. (1999). *Adv. Quantum Chem.* 33: 303.
- 18 De Proft, F. and Geerlings, P. (2001). *Chem. Rev.* 101: 1451.
- 19 Geerlings, P., De Proft, F., and Langenaeker, W. (2003). *Chem. Rev.* 103: 1793.
- 20 Ayers, P.W., Anderson, J.S.M., and Bartolotti, L.J. (2005). *Int. J. Quantum Chem.* 101: 520.
- 21 Gázquez, J.L. (2008). *J. Mex. Chem. Soc.* 52: 3.
- 22 Geerlings, P. and De Proft, F. (2008). *Phys. Chem. Chem. Phys.* 10: 3028.
- 23 Liu, S.B. (2009). *Acta Phys. Chem. China* 25: 590.
- 24 Chattaraj, P.K. (ed.) (2009). *Chemical Reactivity Theory: A Density Functional View*. Boca Raton, FL: Taylor and Francis/CRC Press.
- 25 Geerlings, P., Ayers, P.W., Toro-Labbé, A. et al. (2012). *Acc. Chem. Res.* 55: 683.
- 26 Geerlings, P., Fias, S., Biosdenghien, Z., and De Proft, F. (2014). *Chem. Soc. Rev.* 43: 4989.
- 27 Geerlings, P., Chamorro, E., Chattaraj, P.K. et al. (2020). *Theor. Chem. Acc.* 139: 36.
- 28 Chakraborty, D. and Chattaraj, P.K. (2021). *Chem. Sci.* <https://doi.org/10.1039/d0sc07017c>.

- 29 Parr, R.G., Donnelly, R.A., Levy, M., and Palke, W.A. (1978). *J. Chem. Phys.* 68: 3801.
- 30 Iczkowski, R.P. and Margrave, J.L. (1961). *J. Am. Chem. Soc.* 83: 3547.
- 31 Pauling, L. (1932). *J. Am. Chem. Soc.* 54: 3570.
- 32 Pauling, L. (1960). *The Nature of the Chemical Bond*, 3e. Ithaca: Cornell University Press.
- 33 Mullay, J. (1987). Estimation of atomic and group electronegativities. In: *Electronegativity, Structure and Bonding*, vol. 66 (ed. K.D. Sen and C.K. Jorgenson), 1. Berlin Heidelberg: Springer-Verlag.
- 34 Ayers, P.W. (2008). *J. Math. Chem.* 43: 285.
- 35 Perdew, J.P., Parr, R.G., Levy, M., and Balduz, J.L. Jr. (1982). *Phys. Rev. Lett.* 49: 1691.
- 36 Yang, W., Zhang, Y.K., and Ayers, P.W. (2000). *Phys. Rev. Lett.* 84: 5172.
- 37 Mori-Sánchez, P., Cohen, A.J., and Yang, W. (2008). *Phys. Rev. Lett.* 100: 146401.
- 38 Cohen, A.J., Mori-Sánchez, P., and Yang, W. (2008). *Science* 321: 792.
- 39 Cohen, A.J., Mori-Sánchez, P., and Yang, W. (2008). *Phys. Rev. B* 77: 115123.
- 40 Yang, W., Cohen, A.J., and Mori-Sánchez, P. (2012). *J. Chem. Phys.* 136: 204111.
- 41 Mulliken, R.S. (1934). *J. Chem. Phys.* 2: 782.
- 42 Koopmans, T. (1934). *Physica* 1: 104.
- 43 Pearson, R.G. (1986). *Proc. Natl. Acad. Sci. U.S.A.* 83: 8440.
- 44 Parr, R.G. and Bartolotti, L.J. (1983). *J. Phys. Chem.* 87: 2810.
- 45 Ayers, P.W. (2000). *Proc. Natl. Acad. Sci. U.S.A.* 97: 1959.
- 46 Cedillo, A. (1994). *Int. J. Quantum Chem.* 52 (S28): 231.
- 47 Baekelandt, B.G., Cedillo, A., and Parr, R.G. (1995). *J. Chem. Phys.* 103: 8548.
- 48 De Proft, F., Liu, S., and Parr, R.G. (1997). *J. Chem. Phys.* 107: 3000.
- 49 De Proft, F. and Geerlings, P. (1997). *J. Phys. Chem. A* 101: 5344.
- 50 Fuentealba, P. (1998). *J. Phys. Chem. A* 102: 4747.
- 51 De Proft, F., Ayers, P.W., Sen, K.D., and Geerlings, P. (2004). *J. Chem. Phys.* 120: 9969.
- 52 Pearson, R.G. (1973). *Hard and Soft Acids and Bases*. Stroudsburg, PA: Downen, Hutchinson and Ross.
- 53 Pearson, R.G. (1997). *Chemical Hardness*. New York: Wiley-VCH.
- 54 Ayers, P.W., Parr, R.G., and Pearson, R.G. (2006). *J. Chem. Phys.* 124: 194107.
- 55 Parr, R.G. and Pearson, R.G. (1983). *J. Am. Chem. Soc.* 105: 7512.
- 56 Ayers, P.W. and Parr, R.G. (2000). *J. Am. Chem. Soc.* 123: 2007.
- 57 Jordan, K.D. and Burrow, P.D. (1987). *Chem. Rev.* 87: 557.
- 58 Jagau, T.-C., Bravaya, K.B., and Krylov, A.I. (2017). *Annu. Rev. Phys. Chem.* 68: 525.
- 59 Vibert, C.P. and Tozer, D.J. (2018). *J. Chem. Theory Comput.* 15: 241 and references cited therein.
- 60 See e.g. Sablon, N., De Proft, F., Geerlings, P., and Tozer, D.J. (2007). *Phys. Chem. Chem. Phys.* 9: 5880 and references therein.
- 61 Jordan, K.D., Voora, K.D., and Simons, J. (2014). *Theor. Chem. Acc.* 133: 1445.
- 62 Cárdenas, C., Ayers, P.W., De Proft, F. et al. (2011). *Phys. Chem. Chem. Phys.* 13: 2285.

- 63 Tozer, D.J. and De Proft, F. (2005). *J. Phys. Chem. A* 109: 8923.
- 64 Yang, W. and Parr, R.G. (1985). *Proc. Natl. Acad. Sci. U.S.A.* 82: 6723.
- 65 Vela, A. and Gázquez, J.L. (1990). *J. Am. Chem. Soc.* 112: 1490.
- 66 (a) Ghanty, T.K. and Ghosh, S.K. (1993). *J. Phys. Chem.* 97: 4951; (b) Ghanty, T.K. and Ghosh, S.K. (1994). *J. Am. Chem. Soc.* 116: 8801.
- 67 Roy, R., Chandra, A.K., and Pal, S. (1994). *J. Phys. Chem.* 98: 10447.
- 68 Hati, S. and Datta, D. (1994). *J. Phys. Chem.* 98: 10451.
- 69 Simón-Manso, Y. and Fuentealba, P. (1998). *J. Phys. Chem. A* 102: 2029.
- 70 Ayers, P.W. (2007). *Faraday Discuss.* 135: 161.
- 71 Blair, S.A. and Thakkar, A.J. (2014). *J. Chem. Phys.* 141: 074306.
- 72 Parr, R.G., Von Szentpály, L., and Liu, S. (1999). *J. Am. Chem. Soc.* 121: 1922.
- 73 Maynard, A.T., Huang, M., Rice, W.G., and Covell, D.G. (1998). *Proc. Natl. Acad. Sci. U.S.A.* 95: 11578.
- 74 Chattaraj, P.K., Sarkar, U., and Roy, D.R. (2006). *Chem. Rev.* 106: 2065.
- 75 Gázquez, J.L., Cedillo, A., and Vela, A. (2007). *J. Phys. Chem. A* 111: 1966.
- 76 Morell, C., Gázquez, J.L., Vela, A. et al. (2014). *Phys. Chem. Chem. Phys.* 16: 26832.
- 77 Chattaraj, P.K., Chakraborty, A., and Giri, S. (2009). *J. Phys. Chem. A* 113: 10068.
- 78 Chakraborty, A., Das, R., Giri, S., and Chattaraj, P.K. (2011). *J. Phys. Org. Chem.* 24: 854.
- 79 Mayr, H. (1994). *Angew. Chem. Int. Ed. Engl.* 33: 938.
- 80 Mayr, H. and Ofial, A.R. (2005). *Pure Appl. Chem.* 77: 1807.
- 81 Mayr, H. and Ofial, A.R. (2008). *J. Phys. Org. Chem.* 21: 584.
- 82 Mayr, H. (2015). *Tetrahedron* 71: 5095.
- 83 Domingo, L.R., Chamorro, E., and Pérez, P. (2008). *J. Org. Chem.* 73: 4615.
- 84 Domingo, L.R. and Pérez, P. (2011). *Org. Biomol. Chem.* 9: 7168.
- 85 Domingo, L.R., Rios-Gutiérrez, M., and Pérez, P. (2016). *Molecules* 21: 748.
- 86 Tognetti, V., Morell, C., and Joubert, L. (2015). *J. Comput. Chem.* 36: 649.
- 87 Tognetti, V., Morell, C., and Joubert, L. (2015). *Chem. Phys. Lett.* 635: 111.
- 88 (a) Bader, R.F.W. (1990). *Atoms in Molecules: A Quantum Theory*. Oxford: Oxford University Press; (b) Popelier, P.L.A. (2000). *Atoms in Molecules: An Introduction*. Harlow: Pearson Education.
- 89 Hoffmann, G., Balcilar, M., Tognetti, V. et al. (2020). *J. Comput. Chem.* 41: 2124.
- 90 Ayers, P.W., Anderson, J.S.M., Rodriguez, J.I., and Jawed, Z. (2005). *Phys. Chem. Chem. Phys.* 7: 1918.
- 91 Broeckeaert, L., Moens, J., Roos, G. et al. (2008). *J. Phys. Chem. A* 112: 12164.
- 92 Parr, R.G. and Fuentealba, P. (1991). *J. Chem. Phys.* 94: 5559.
- 93 Morell, C., Grand, A., Toro-Labbé, A., and Chermette, H. (2013). *J. Mol. Model.* 19: 2893.
- 94 Dunlap, B.I. (2008). *J. Chem. Phys.* 129: 244109.
- 95 Cárdenas, C., Echegaray, E., Chakraborty, D. et al. (2009). *J. Chem. Phys.* 130: 244105.
- 96 Parr, R.G. and Yang, W. (1984). *J. Am. Chem. Soc.* 106: 4049.

- 97 For a perspective see Ayers, P.W. and Levy, M. (2000). *Theor. Chem. Acc.* 103: 353.
- 98 Miranda-Quintana, R.A., Heidar-Zadeh, F., and Ayers, P.W. (2018). *J. Phys. Chem. Lett.* 9: 4344.
- 99 Chattaraj, P.K., Cedillo, A., and Parr, R.G. (1995). *J. Chem. Phys.* 103: 10621.
- 100 Fuentealba, P., Florez, E., and Tiznado, W. (2010). *J. Chem. Theory Comput.* 6: 1470.
- 101 Roy, R.K., Pal, S., and Hirao, K. (1999). *J. Chem. Phys.* 110: 8236.
- 102 Roy, R.K., Pal, S., and Hirao, K. (2000). *J. Chem. Phys.* 113: 1372.
- 103 Bultinck, P., Carbo-Dorca, R., and Langenaeker, W. (2003). *J. Chem. Phys.* 118: 4349.
- 104 Bultinck, P. and Carbo-Dorca, R. (2003). *J. Math. Chem.* 34: 67.
- 105 Ayers, P.W. (2006). *Phys. Chem. Chem. Phys.* 8: 3387.
- 106 Melin, J., Ayers, P.W., and Ortiz, J.V. (2007). *J. Phys. Chem. A* 111: 10017.
- 107 Echegaray, E., Rabi, S., Cardenas, C. et al. (2014). *J. Mol. Model.* 20: 2162.
- 108 Berkowitz, M. (1987). *J. Am. Chem. Soc.* 109: 4823.
- 109 Chattaraj, P.K. (2001). *J. Phys. Chem. A* 105: 511.
- 110 Melin, J., Aparicio, F., Subramanian, V. et al. (2004). *J. Phys. Chem. A* 108: 2487.
- 111 Stuyver, T. and Shaik, S. (2020). *J. Am. Chem. Soc.* 142: 47, 20002.
- 112 Yang, W., Parr, R.G., and Pucci, R. (1984). *J. Chem. Phys.* 81: 2862.
- 113 (a) Fukui, K., Yonezawa, T., and Nagata, C. (1954). *Bull. Chem. Soc. Jpn.* 27: 423; (b) Fukui, K., Yonezawa, T., and Shingu, H. (1952). *J. Chem. Phys.* 20: 722; (c) Fukui, K. (1973). *Theory of Orientation and Stereoselection*. Berlin: Springer-Verlag; (d) Fukui, K. (1982). *Science* 218: 747.
- 114 Bartolotti, L.J. and Ayers, P.W. (2005). *J. Phys. Chem. A* 109: 1146.
- 115 Zhang, D., Zheng, X., Li, C., and Yang, W. (2015). *J. Chem. Phys.* 142: 154113.
- 116 Bultinck, P., Clarisse, D., Ayers, P.W., and Carbo-Dorca, R. (2011). *Phys. Chem. Chem. Phys.* 13: 6110.
- 117 (a) Mitoraj, M.P. and Michalak, A. (2007). *J. Mol. Model.* 13: 347; (b) Michalak, A., Mitoraj, M.P., and Ziegler, T. (2008). *J. Phys. Chem. A* 112: 1933; (c) Mitoraj, M.P., Michalak, A., and Ziegler, T. (2009). *J. Chem. Theory Comput.* 5: 962.
- 118 (a) te Velde, G., Bickelhaupt, F.M., Baerends, E.J. et al. (2001). *J. Comput. Chem.* 22: 931; (b) *ADF 2020*, SCM, Theoretical Chemistry. Amsterdam, The Netherlands: Vrije Universiteit. <http://www.scm.com> (accessed 29 October 2021).
- 119 Perdew, J.P., Burke, K., and Ernzerhof, M. (1996). *Phys. Rev. Lett.* 77: 3865.
- 120 van Lenthe, E. and Baerends, E.J. (2003). *J. Comput. Chem.* 24: 1142.
- 121 Tozer, D.J. and De Proft, F. (2007). *J. Chem. Phys.* 127: 034108.
- 122 (a) Mulliken, R.S. (1955). *J. Chem. Phys.* 23: 1833; (b) Mulliken, R.S. (1955). *J. Chem. Phys.* 23: 1841; (c) Mulliken, R.S. (1955). *J. Chem. Phys.* 23: 2338; (d) Mulliken, R.S. (1955). *J. Chem. Phys.* 23: 2343.
- 123 Yang, W. and Mortier, W.J. (1986). *J. Am. Chem. Soc.* 108: 5708.
- 124 De Proft, F., Martin, J.M.L., and Geerlings, P. (1996). *Chem. Phys. Lett.* 256: 400.

- 125 Arulmozhiraja, S. and Kolandaivel, P. (1997). *Mol. Phys.* 90: 55.
- 126 Gilardoni, F., Weber, J., and Chermette, H. (1998). *J. Phys. Chem. A* 102: 3607.
- 127 Fuentealba, P., Perez, P., and Contreras, R. (2000). *J. Chem. Phys.* 113: 2544.
- 128 Ayers, P.W., Morrison, R.C., and Roy, R.K. (2002). *J. Chem. Phys.* 116: 8731.
- 129 De Proft, F., Van Alsenoy, C., Peeters, A. et al. (2002). *J. Comput. Chem.* 23: 1198.
- 130 Thanikaivelan, P., Padmanabhan, J., Subramanian, V., and Ramasami, T. (2002). *Theor. Chem. Acc.* 107: 326.
- 131 Olah, J., Van Alsenoy, C., and Sannigrahi, A.B. (2002). *J. Phys. Chem. A* 106: 3885.
- 132 Bulat, F.A., Chamorro, E., Fuentealba, P., and Toro-Labbé, A. (2004). *J. Phys. Chem. A* 108: 342.
- 133 Tiznado, W., Chamorro, E., Contreras, R., and Fuentealba, P. (2005). *J. Phys. Chem. A* 109: 3220.
- 134 Bultinck, P., Van Alsenoy, C., Ayers, P.W., and Carbó-Dorca, R. (2007). *J. Chem. Phys.* 126: 144111.
- 135 Otero, N., Mandado, M., and Mosquera, R.A. (2007). *J. Chem. Phys.* 126: 234108.
- 136 Saha, S., Roy, R.K., and Ayers, P.W. (2009). *Int. J. Quantum Chem.* 109: 1790.
- 137 Zielinski, F., Tognetti, V., and Joubert, L. (2012). *Chem. Phys. Lett.* 527: 67.
- 138 Wang, B., Rong, C., Chattaraj, P.K., and Liu, S. (2019). *Theor. Chem. Acc.* 138: 1.
- 139 Hirshfeld, F.L. (1977). *Theor. Chim. Acta* 44: 129.
- 140 Nalewajski, R.F. and Parr, R.G. (2000). *Proc. Natl. Acad. Sci. U.S.A.* 97: 8879.
- 141 Parr, R.G., Ayers, P.W., and Nalewajski, R.F. (2005). *J. Phys. Chem. A* 109: 3957.
- 142 Rong, C., Wang, B., Zhao, D., and Liu, S. (2020). *WIREs Comput. Mol. Sci.* 10: e1461.
- 143 (a) Gonzalez-Suarez, M., Aizman, A., Soto-Delgado, J., and Contreras, R. (2012). *J. Org. Chem.* 77: 90; (b) Bultinck, P., Van Damme, S., and Cedillo, A. (2013). *J. Comput. Chem.* 34: 2421; (c) Sánchez-Márquez, J. (2016). *J. Chem. Phys.* 145: 194105; (d) Oña, O.B., De Clercq, O., Alcoba, D.R. et al. (2016). *ChemPhysChem* 17: 2881; (e) Franco-Perez, M., Polanco-Ramirez, C.-A., Ayers, P.W. et al. (2017). *Phys. Chem. Chem. Phys.* 19: 16095.
- 144 Morell, C., Grand, A., and Toro-Labbé, A. (2005). *J. Phys. Chem. A* 109: 205.
- 145 Morell, C., Grand, A., and Toro-Labbé, A. (2006). *Chem. Phys. Lett.* 425: 342.
- 146 Ayers, P.W., Morell, C., De Proft, F., and Geerlings, P. (2007). *Chem. Eur. J.* 13: 8240.
- 147 Tognetti, V., Morell, C., Ayers, P.W. et al. (2013). *Phys. Chem. Chem. Phys.* 15: 14465.
- 148 Cohen, M.H., Ganduglia-Pirovano, M.V., and Kudrnovsky, J. (1994). *J. Chem. Phys.* 101: 8988.
- 149 Cohen, M.H., Ganduglia-Pirovano, M.V., and Kudrnovsky, J. (1995). *J. Chem. Phys.* 103: 3543.
- 150 Nalewajski, R.F. (2006). *Adv. Quantum Chem.* 51: 235.
- 151 Baekelandt, B.G. (1996). *J. Chem. Phys.* 105: 4664.
- 152 De Proft, F., Liu, S., and Geerlings, P. (1998). *J. Chem. Phys.* 108: 7549.

- 153** Balawender, R. and Geerlings, P. (2001). *J. Chem. Phys.* 114: 682.
- 154** Balawender, R., De Proft, F., and Geerlings, P. (2001). *J. Chem. Phys.* 114: 4441.
- 155** Torrent-Sucarrat, M., Luis, J.M., Duran, M. et al. (2003). *J. Chem. Phys.* 119: 9393.
- 156** Cárdenas, C., Chamorro, E., Galvan, M., and Fuentealba, P. (2007). *Int. J. Quantum Chem.* 107: 807.
- 157** (a) Berlin, T. (1951). *J. Chem. Phys.* 19: 208; (b) Wang, X. and Peng, Z. (1993). *Int. J. Quantum Chem.* 47: 393.
- 158** Cauet, E., Bogatko, S., Lievin, J. et al. (2013). *J. Phys. Chem. B* 117: 9669.
- 159** Ordon, P. and Komorowski, L. (1998). *Chem. Phys. Lett.* 292: 22.
- 160** Torrent-Sucarrat, M., De Proft, F., and Geerlings, P. (2005). *J. Phys. Chem. A* 109: 6071.
- 161** Chamorro, E., Fuentealba, P., and Contreras, R. (2001). *J. Chem. Phys.* 115: 6822.
- 162** Nalewajski, R.F. and Parr, R.G. (1982). *J. Chem. Phys.* 77: 399.
- 163** Chattaraj, P.K., Maiti, B., and Sarkar, U. (2003). *J. Phys. Chem. A* 107: 4973.
- 164** Domingo, L.R., José Aurell, M., Pérez, P., and Contreras, R. (2002). *J. Phys. Chem. A* 106: 6871.
- 165** Padmanabhan, J., Parthasarathi, R., Elango, M. et al. (2007). *J. Phys. Chem. A* 111: 9130.
- 166** Roy, D.R., Chattaraj, P.K., and Subramanian, V. (2006). *Indian J. Chem., Sect. A* 45A: 2369.
- 167** Berkowitz, M., Ghosh, S.K., and Parr, R.G. (1985). *J. Am. Chem. Soc.* 107: 6811.
- 168** Ghosh, S.K. and Berkowitz, M. (1985). *J. Chem. Phys.* 83: 2976.
- 169** Berkowitz, M. and Parr, R.G. (1988). *J. Chem. Phys.* 88: 2554.
- 170** Ghosh, S.K. (1990). *Chem. Phys. Lett.* 172: 7782.
- 171** Harbola, M.K., Chattaraj, P.K., and Parr, R.G. (1991). *Isr. J. Chem.* 31: 395.
- 172** Langenaeker, W., De Proft, F., and Geerlings, P. (1995). *J. Phys. Chem.* 99: 6424.
- 173** Meneses, L., Tiznado, W., Contreras, R., and Fuentealba, P. (2004). *Chem. Phys. Lett.* 383: 181.
- 174** Ayers, P.W. and Parr, R.G. (2008). *J. Chem. Phys.* 128: 184108.
- 175** Chattaraj, P.K., Roy, D.R., Geerlings, P., and Torrent-Sucarrat, M. (2007). *Theor. Chem. Acc.* 118: 923.
- 176** Cuevas-Saavedra, R., Rabi, N., and Ayers, P.W. (2011). *Phys. Chem. Chem. Phys.* 13: 19594.
- 177** Gál, T., Geerlings, P., De Proft, F., and Torrent-Sucarrat, M. (2011). *Phys. Chem. Chem. Phys.* 13: 15003.
- 178** Gál, T. (2012). *Theor. Chem. Acc.* 131: 1223.
- 179** Heidar-Zadeh, F., Fuentealba, P., Cárdenas, C., and Ayers, P.W. (2014). *Phys. Chem. Chem. Phys.* 16: 6019.
- 180** (a) Polanco-Ramírez, C.A., Franco-Pérez, M., Carmona-Espíndola, J. et al. (2017). *Phys. Chem. Chem. Phys.* 19: 12355; (b) Guéguan F., Lamine, W., Chermette, H., and Morell, C. (2018). *Phys. Chem. Chem. Phys.* 20: 9006; (c) Polanco-Ramírez, C.A., Franco-Pérez, M., Carmona-Espíndola, J. et al. (2018). *Phys. Chem. Chem. Phys.* 20: 9011.

- 181 Torrent-Sucarrat, M., De Proft, F., Geerlings, P., and Ayers, P.W. (2008). *Chem. Eur. J.* 14: 8652.
- 182 Torrent-Sucarrat, M., De Proft, F., Ayers, P.W., and Geerlings, P. (2010). *Phys. Chem. Chem. Phys.* 12: 1072.
- 183 Gal, T. (2007). *J. Math. Chem.* 42: 661.
- 184 Ullrich, C.A. (2019). *Time Dependent Density Functional Theory: Concepts and Applications*. Oxford: Oxford University Press.
- 185 Chattaraj, P.K., Cedillo, A., and Parr, R.G. (1995). *J. Chem. Phys.* 103: 7645.
- 186 Gázquez, J.L. and Parr, R.G. (1993). *J. Phys. Chem.* 97: 3939.
- 187 (a) Thomas, L.H. (1927). *Proc. Cambridge Philos. Soc.* 23: 542; (b) Fermi, E. (1927). *Rend. Accad. Naz. Lincei* 6: 602; (c) Dirac, P.A.M. (1930). *Proc. Cambridge Philos. Soc.* 26: 376.
- 188 (a) Bonaccorsi, R., Scrocco, E., and Tomasi, J. (1970). *J. Chem. Phys.* 52: 5270; (b) Scrocco, E. and Tomasi, J. (1973). *Top. Curr. Chem.* 42: 95; (c) Politzer, P. and Truhlar, D.G. (eds.) (1981). *Chemical Applications of Atomic and Molecular Electrostatic Potentials*. New York: Plenum Press; (d) Naray-Szabo, G. and Ferenczy, G.G. (1995). *Chem. Rev.* 95: 829; (e) Murray, J.S. and Sen, K.D. (eds.) (1996). *Molecular Electrostatic Potentials - Concepts and Applications, Theoretical and Computational Chemistry*, vol. 3. Amsterdam: Elsevier; (f) Suresh, C.H. and Gadre, S.R. (1998). *J. Am. Chem. Soc.* 120: 7049; (g) Murray, J.S. and Politzer, P. (2011). *WIREs Comput. Mol. Sci.* 1: 153.
- 189 Anderson, J.S.M., Melin, J., and Ayers, P.W. (2007). *J. Chem. Theory Comput.* 3: 358.
- 190 Anderson, J.S.M., Melin, J., and Ayers, P.W. (2007). *J. Chem. Theory Comput.* 3: 375.
- 191 Liu, G. (1997). *J. Chem. Phys.* 106: 165.
- 192 Balawender, R. and Komorowski, L. (1998). *J. Chem. Phys.* 109: 5203.
- 193 Michalak, A., De Proft, F., Geerlings, P., and Nalewajski, R.F. (1999). *J. Phys. Chem. A* 103: 762.
- 194 Ayers, P.W. (2000). *Theor. Chem. Acc.* 106: 271.
- 195 Flores-Moreno, R. and Koster, A.M. (2008). *J. Chem. Phys.* 128: 134105.
- 196 Flores-Moreno, R., Melin, J., Ortiz, J.V., and Merino, G. (2008). *J. Chem. Phys.* 120: 224105.
- 197 Yang, W., Cohen, A.J., De Proft, F., and Geerlings, P. (2012). *J. Chem. Phys.* 136: 144110.
- 198 Peng, D. and Yang, W. (2013). *J. Chem. Phys.* 138: 184108.
- 199 Cedillo, A. (2019). *Theor. Chem. Acc.* 138: 79.
- 200 (a) Ayers, P.W., De Proft, F., Borgoo, A., and Geerlings, P. (2007). *J. Chem. Phys.* 126: 224107; (b) Sablon, N., De Proft, F., Ayers, P.W., and Geerlings, P. (2007). *J. Chem. Phys.* 126: 224108; (c) Fievez, T., Sablon, N., De Proft, F. et al. (2008). *J. Chem. Theory Comput.* 4: 1065.
- 201 Sablon, N., De Proft, F., Ayers, P.W., and Geerlings, P. (2010). *J. Chem. Theory Comput.* 6: 3671.
- 202 Cárdenas, C., Ayers, P.W., and Cedillo, A. (2011). *J. Chem. Phys.* 134: 174103.

- 203** Bultinck, P., Cárdenas, C., Fuentealba, P. et al. (2014). *J. Chem. Theory Comput.* 10: 202.
- 204** (a) Bultinck, P., Cárdenas, C., Fuentealba, P. et al. (2013). *J. Chem. Theory Comput.* 9: 4779; (b) Bultinck, P., Jayatilaka, D., and Cárdenas, C. (2015). *Comput. Theor. Chem.* 1053: 106.
- 205** (a) Ayers, P.W. and Parr, R.G. (2000). *J. Am. Chem. Soc.* 122: 2010; (b) Ayers, P.W. and Parr, R.G. (2001). *J. Am. Chem. Soc.* 123: 2007.
- 206** (a) Klopman, G. (1968). *J. Am. Chem. Soc.* 90: 223; (b) Salem, L. (1968). *J. Am. Chem. Soc.* 90: 543.
- 207** Mayr, H., Breugst, M., and Ofial, A.R. (2011). *Angew. Chem. Int. Ed.* 50: 6470.
- 208** Vermeeren, P., van der Lubbe, S.C.C., Fonseca Guerra, C. et al. (2020). *Nat. Protoc.* 15: 649.
- 209** Bettens, T., Alonso, M., De Proft, F. et al. (2020). *Chem. Eur. J.* 26: 3884.
- 210** Hellgren, M. and Gross, E.K.U. (2012). *J. Chem. Phys.* 136: 114102.
- 211** Nalewajski, R.F. and Korchowiec, J. (1997). *Charge Sensitivity Approach to Electronic Structure and Chemical Reactivity, Advanced Series in Physical Chemistry 8*. World Scientific.
- 212** Senet, P. (1996). *J. Chem. Phys.* 105: 6471.
- 213** Senet, P. (1997). *J. Chem. Phys.* 107: 2516.
- 214** Heidar-Zadeh, F., Richer, M., Fias, S. et al. (2016). *Chem. Phys. Lett.* 660: 307.



## 3

**Basic Formalism***Paul W. Ayers<sup>1</sup> and Shubin Liu<sup>2</sup>*

<sup>1</sup>McMaster University, Department of Chemistry & Chemical Biology, Main Street West, Hamilton, ON L8S 4M1, Canada

<sup>2</sup>University of North Carolina, Research Computing Center, 211 Manning Drive, Chapel Hill, NC 27599-3420, USA

In this chapter, we introduce the basic formalism of conceptual density functional theory (CDFT), whose foundation was laid out by Nalewajski and Parr [1] using the analog to classical thermodynamics, where the internal energy  $U$ , enthalpy  $H$ , Helmholtz free energy  $F$ , and Gibbs free energy  $G$  serve as the characteristic state functions for four ensembles, related to each other through Legendre transform. This framework was summarized in the book of Parr and Yang [2] and has been overviewed and reviewed elsewhere [3–7]. This system of ensembles was later expanded by Ghosh et al. [8–10] by introducing the concept of local temperature and improved by Cedillo [11] and Baekelandt et al. [12] by employing the shape function [13] to remove the interdependence of variables.

Here are the notations employed in this chapter and beyond. According to the fundamental theorems of density functional theory (DFT) [14], all observable properties of a molecular system, including its total energy, are functionals of the ground-state electron density. Functionals are real-valued functions whose domain is a space of functions. In DFT, the function space is a Banach space, not a Hilbert space, and Banach spaces are not vector spaces. They are represented by square brackets to avoid confusion with normal (multivariate) functions. For example, the universal density functional is represented by  $F[\rho]$ , a functional of the ground-state electron density  $\rho(\mathbf{r})$ . In CDFT, we take the same format, just that the variables could be different. They can be more than one variable, and they can also be global (independent of spaciuous variables) and/or local (i.e. a function of Cartesian coordinates  $x$ ,  $y$ , and  $z$ ). For example, the total energy  $E$  is a functional of the total electron number  $N$ , which is a global variable, and the external potential  $v(\mathbf{r})$ , which is local, so it can be written as  $E[N, v]$ . In addition, when a derivative for a quantity,  $q$ , is taken, different symbols to represent the different nature of this derivative are possible. Specifically, we denote total differential with  $dq$ , partial derivatives with  $\partial q$ , and functional derivatives with  $\delta q$ .

### 3.1 Legendre Transform

A Legendre transform converts a function or functional of one set of variables to another function or functional of a conjugate set of variables. Let us consider a function of two independent variables,  $F(x, y)$ , whose differential is

$$dF(x, y) = \left( \frac{\partial F}{\partial x} \right)_y dx + \left( \frac{\partial F}{\partial y} \right)_x dy \quad (3.1)$$

Defining  $u \equiv (\partial F/\partial x)_y$  and  $w \equiv (\partial F/\partial y)_x$ , we have

$$dF(x, y) = u dx + w dy \quad (3.2)$$

We call  $u$  and  $x$  a *conjugate* pair of variables, and likewise  $w$  and  $y$ . A Legendre-transformed function  $G$  is defined as follows

$$G \equiv F - \left( \frac{\partial F}{\partial y} \right)_x y = F - wy \quad (3.3)$$

and has the differential

$$dG = dF - d(wy) = u dx - y dw \quad (3.4)$$

So  $G$  can be regarded as the function of two new independent variables  $x$  and  $w$ ,  $G(x, w)$ . The variable change of  $y$  in  $F(x, y)$  to its conjugate variable  $w$  in  $G(x, w)$  is made possible by Legendre transform.

In thermodynamics, using Legendre transforms, one can convert between the internal energy  $U$ , enthalpy  $H$ , Helmholtz free energy  $F$ , and Gibbs free energy  $G$ , using conjugate variable pairs of pressure  $P$  and volume  $V$ , temperature  $T$  and entropy  $S$ , and the number of particles  $N$  and chemical potential  $\mu$ . According to the thermodynamic identity

$$dU = TdS - PdV + \mu dN \quad (3.5)$$

where  $T$ ,  $P$ , and  $\mu$  are therefore the variables conjugate to  $S$ ,  $V$ , and  $N$ , respectively, and, from Eq. (3.5), we also have

$$\left( \frac{\partial U}{\partial S} \right)_{V,N} = T, \quad \left( \frac{\partial U}{\partial V} \right)_{S,N} = -P, \quad \text{and} \quad \left( \frac{\partial U}{\partial N} \right)_{S,V} = \mu \quad (3.6)$$

We can use Legendre transform to convert  $U(N, S, V)$  to a new thermodynamic potential, enthalpy  $H(N, S, P)$

$$H(N, S, P) \equiv U(N, S, V) - \left( \frac{\partial U}{\partial V} \right)_S V = U(N, S, V) + PV \quad (3.7)$$

so its differential is as follows after Eq. (3.5) is applied,

$$dH(N, S, P) = TdS + VdP + \mu dN \quad (3.8)$$

with

$$\left( \frac{\partial H}{\partial S} \right)_{P,N} = T, \quad \left( \frac{\partial H}{\partial V} \right)_{S,N} = V, \quad \text{and} \quad \left( \frac{\partial H}{\partial N} \right)_{S,P} = \mu \quad (3.9)$$

Formulas for the Gibbs free energy  $G(N, P, T)$  and the Helmholtz free energy  $F(N, V, T)$  can be similarly obtained. In statistical mechanics, these thermodynamic quantities,  $U$ ,  $H$ ,  $F$ , and  $G$ , are the state functions in their respective ensembles, such as the canonical ensemble  $(N, V, T)$  and grand canonical ensemble  $(\mu, V, T)$ .

## 3.2 Four Ensembles in CDFT

In the spirit of classical thermodynamics, a molecular electronic ground state may be regarded as an equilibrium state at low temperature. For example, an atom or a functional group in a molecule can be described as an open system embedded in a bath that might be appropriately modeled at finite temperature. Since DFT focuses on the electron density distribution function  $\rho(\mathbf{r})$ , the canonical ensemble and grand canonical ensemble provide the most obvious ensemble descriptions, which both allow the electron density to fluctuate. In the microscopic world,  $V$  can be substituted by the external potential  $v(\mathbf{r})$ , which represents the attractive potential to the system's atomic nuclei, which binds the electrons to a particular region of space. In CDFT, ordinarily, the thermodynamic (but not necessarily the local [15–18]) temperature is assumed to equal zero, though temperature-dependent extensions of CDFT are emerging as a promising avenue for research [19–21], as introduced in Chapter 8 of this book.

Consider an electronic system consisting of  $N$  electrons moving in an external potential  $v(\mathbf{r})$ . The Schrödinger equation dictates that any ground-state property of such a system can be solved via the conventional variational principle, suggesting that the total energy  $E$  of the system can be thought of as a functional of  $N$  and  $v(\mathbf{r})$ ,

$$E = E[N, v] \quad (3.10)$$

As a consequence, one has the (generalized) Hellmann–Feynman formula for the energy change due to the infinitesimal change of these two variables,

$$dE = \left( \frac{\partial E}{\partial N} \right)_v dN + \int \left( \frac{\delta E}{\delta v(\mathbf{r})} \right)_N \delta v(\mathbf{r}) d\mathbf{r} \quad (3.11)$$

Assuming that  $E$  is differentiable with respect to  $N$  and  $v(\mathbf{r})$  and that  $N$  can be treated as a continuous variable, in DFT, one finds [2]

$$\left( \frac{\partial E}{\partial N} \right)_v = \mu \quad \text{and} \quad \left( \frac{\delta E}{\delta v(\mathbf{r})} \right)_N = \rho(\mathbf{r}) \quad (3.12)$$

From Eq. (3.11), according to Eq. (3.2), we can see that  $N$  and  $\mu$ , and  $\rho(\mathbf{r})$  and  $v(\mathbf{r})$  are two pairs of conjugate variables. In analog with classical thermodynamics, this representation is called the canonical ensemble in CDFT. It is consistent with the description of electronic systems in DFT, in which  $v(\mathbf{r})$  determines the density  $\rho(\mathbf{r})$  and the density is normalized to  $N$ ,

$$\int \rho(\mathbf{r}) d\mathbf{r} = N \quad (3.13)$$

While assuming that the (functional) derivatives exist is not rigorous mathematically, it is not too difficult to “patch up” the mathematics [22–25]. The easiest approach is to introduce a positive temperature, but this is not essential [20, 26, 27].

The Legendre transform allows one to convert the energy functional  $E[N, v]$  to other state functionals, defined using different sets of conjugate variables. Specifically, the ground-state independent variables  $N$  and  $v(\mathbf{r})$  for the state function  $E[N, v]$  can be replaced by the corresponding conjugate variables  $\mu$  and  $\rho(\mathbf{r})$ , respectively,

via Legendre transform. The three remaining natural functionals of the ground state defined by the Legendre transform of  $E[N, v]$  represent three other ensembles in CDFT. In the grand canonical ensemble, where  $\Omega$  is a functional of  $\mu$  and  $v(\mathbf{r})$ , defined by

$$\Omega[\mu, v] \equiv E - \left( \frac{\partial E}{\partial N} \right)_v N = E - \mu N \quad (3.14)$$

which is minimized by the equilibrium values of unconstrained internal variables of the system at constant  $\mu$  and  $v(\mathbf{r})$ . In the grand canonical ensemble, the system is said to be open in the sense that it can exchange both energy and particles with the reservoir so that various possible states of the system can differ in both their total energy and total number of particles. The system's shape and external potential are kept fixed in all possible states of the system. In this sense, the grand canonical ensemble is suitable for the description of the molecular formation processes, where charge transfer takes place among atoms. In the isomorphic ensemble,

$$F[N, \varrho] \equiv E - \int \left( \frac{\delta E}{\delta v(\mathbf{r})} \right)_N v(\mathbf{r}) d\mathbf{r} = E - \int \varrho(\mathbf{r}) v(\mathbf{r}) d\mathbf{r} \quad (3.15)$$

where  $F[N, \varrho]$  is a functional of natural variables  $N$  and  $\rho(\mathbf{r})$ . The last frequently used ensemble is the grand isomorphic ensemble,

$$R[\mu, \varrho] \equiv E - \left( \frac{\partial E}{\partial N} \right)_v N - \int \left( \frac{\delta E}{\delta v(\mathbf{r})} \right)_N v(\mathbf{r}) d\mathbf{r} = E - \mu N - \int \varrho(\mathbf{r}) v(\mathbf{r}) d\mathbf{r} \quad (3.16)$$

in which  $R[\mu, \rho]$  is a functional of natural variables  $\mu$  and  $\rho(\mathbf{r})$ . Because of Eq. (3.4),  $N$  and  $\rho(\mathbf{r})$  are dependent, a modified version for the isomorphic ensemble was provided by Cedillo [11] and Baekelandt et al. [12] in terms of the shape function  $\sigma(\mathbf{r})$  defined as

$$\sigma(\mathbf{r}) = \frac{\rho(\mathbf{r})}{N} \quad (3.17)$$

so

$$F[N, \sigma] \equiv E - N \int \sigma(\mathbf{r}) v(\mathbf{r}) d\mathbf{r} \quad (3.18)$$

Owing to the Hohenberg–Kohn theorem,  $\mu$  is a functional of  $\rho(\mathbf{r})$ , so the grand isomorphic ensemble can also be described as  $R[\mu, \sigma]$  or even  $R[\rho]$  [28].

### 3.3 Basic Relations in the Canonical Ensemble

In the canonical ensemble, the total energy  $E$  is represented as a functional of the global variable  $N$  and the local variable  $v(\mathbf{r})$ ,  $E[N, v]$ . Assuming  $E$  to be differentiable and using Eq. (3.10), one then has the following differential expression for  $E$

$$dE = \mu dN + \int \rho(\mathbf{r}) \delta v(\mathbf{r}) d\mathbf{r} \quad (3.19)$$

The Maxwell relation originates from the symmetry requirement on the second-order derivatives of a twice-differentiable function  $F(x,y)$ , i.e.  $\frac{\partial}{\partial x} \left( \frac{\partial F}{\partial y} \right) = \frac{\partial}{\partial y} \left( \frac{\partial F}{\partial x} \right)$ . These Maxwell relations are useful in connecting one set of derivatives with another set of derivatives. For Eq. (3.19), one has

$$\frac{\partial}{\partial N} \left( \frac{\delta E}{\delta v(\mathbf{r})} \right) = \frac{\delta}{\delta v(\mathbf{r})} \left( \frac{\partial E}{\partial N} \right) \quad (3.20)$$

With Eq. (3.10), so the Maxwell relation associated with Eq. (3.19) is the following

$$\left( \frac{\partial \rho(\mathbf{r})}{\partial N} \right)_v = \left( \frac{\delta \mu}{\delta v(\mathbf{r})} \right)_N = f(\mathbf{r}) \quad (3.21)$$

which is nothing but the definition of the Fukui function [29]. As will be discussed in detail in later chapters, this function can be utilized to predict electrophilic and nucleophilic attacks and thus recover the frontier molecular orbital theory by Fukui et al. [30]. With the Maxwell equation Eq. (3.21), it becomes clear that two definitions for the Fukui function are possible. Also, in the canonical ensemble, both chemical potential  $\mu$  and electron density  $\rho(\mathbf{r})$  are functionals of  $N$  and  $v(\mathbf{r})$ . The differential form for chemical potential  $\mu$ ,  $d\mu$ , is as follows.

$$d\mu = \eta dN + \int f(\mathbf{r}) \delta v(\mathbf{r}) d\mathbf{r} \quad (3.22)$$

where  $\eta$  is the hardness [31], defined as

$$\eta = \left( \frac{\partial^2 E}{\partial N^2} \right)_v = \left( \frac{\partial \mu}{\partial N} \right)_v \quad (3.23)$$

whose inverse is the softness  $S = 1/\eta$  [32]. For  $\rho(\mathbf{r})$ , one has the following differential form

$$d\rho(\mathbf{r}) = f(\mathbf{r})dN + \int \omega(\mathbf{r}, \mathbf{r}') \delta v(\mathbf{r}') d\mathbf{r}' \quad (3.24)$$

with the response function  $\omega(\mathbf{r}, \mathbf{r}')$  is defined by [33, 34]

$$\omega(\mathbf{r}, \mathbf{r}') = \left( \frac{\delta \rho(\mathbf{r})}{\delta v(\mathbf{r}')} \right)_N \quad (3.25)$$

The Maxwell relations for Eqs. (3.22, 3.24) are, respectively,

$$\left( \frac{\partial f(\mathbf{r})}{\partial N} \right)_v = \left( \frac{\delta \eta}{\delta v(\mathbf{r})} \right)_N \quad (3.26)$$

and

$$\left( \frac{\partial \omega(\mathbf{r}, \mathbf{r}')}{\partial N} \right)_v = \left( \frac{\delta f(\mathbf{r})}{\delta v(\mathbf{r}')} \right)_N \quad (3.27)$$

These quantities in Eqs. (3.26) and (3.27) are higher-order derivatives, which were first systematically investigated by Fuentealba and Parr [35]. Later, further studies led to actual applications of these higher-order derivatives as the dual descriptor and hardness responses [36–39].

### 3.4 Basic Relations in the Grand Canonical Ensemble

In the grand canonical ensemble, the natural variables are the chemical potential  $\mu$  and the external potential  $v(\mathbf{r})$ . The grand potential  $\Omega$  is defined in Eq. (3.14), whose differential form is as follows

$$d\Omega = -Nd\mu + \int \rho(\mathbf{r})\delta v(\mathbf{r})d\mathbf{r} \quad (3.28)$$

This equality is obtained by differentiating Eq. (3.14) and then employing Eq. (3.19). One thus has

$$\left(\frac{\partial\Omega}{\partial\mu}\right)_v = -N \quad \text{and} \quad \left(\frac{\delta\Omega}{\delta v(\mathbf{r})}\right)_\mu = \rho(\mathbf{r}) \quad (3.29)$$

The Maxwell relation associated with Eq. (3.28) brings in the definition of local softness  $s(\mathbf{r})$  [8]

$$\left(\frac{\partial\rho(\mathbf{r})}{\partial\mu}\right)_v = -\left(\frac{\delta N}{\delta v(\mathbf{r})}\right)_\mu = s(\mathbf{r}) \quad (3.30)$$

The other two variables,  $N$  and  $\rho(\mathbf{r})$ , can also be expressed as functionals of the chemical potential  $\mu$  and external potential  $v(\mathbf{r})$  in the grand canonical ensemble, leading to

$$dN = -Sd\mu + \int s(\mathbf{r})\delta v(\mathbf{r})d\mathbf{r} \quad (3.31)$$

and

$$d\rho(\mathbf{r}) = s(\mathbf{r})d\mu - \int s(\mathbf{r}, \mathbf{r}')\delta v(\mathbf{r}')d\mathbf{r}' \quad (3.32)$$

respectively, where the softness  $S$  is

$$S = \left(\frac{\partial N}{\partial\mu}\right)_v \quad (3.33)$$

and the softness kernel  $s(\mathbf{r}, \mathbf{r}')$  [10] is

$$s(\mathbf{r}, \mathbf{r}') = -\left(\frac{\delta\rho(\mathbf{r})}{\delta v(\mathbf{r}')}\right)_\mu \quad (3.34)$$

The Maxwell relations associated with Eqs. (3.31) and (3.32) are, respectively [35, 40],

$$-\left(\frac{\partial s(\mathbf{r})}{\partial\mu}\right)_v = -\left(\frac{\delta S}{\delta v(\mathbf{r})}\right)_\mu \quad (3.35)$$

and

$$-\left(\frac{\partial s(\mathbf{r}, \mathbf{r}')}{\partial\mu}\right)_v = -\left(\frac{\delta s(\mathbf{r})}{\delta v(\mathbf{r}')}\right)_\mu \quad (3.36)$$

### 3.5 Basic Relations in the Isomorphic Ensemble

In the isomorphic ensemble, the state function is  $F$ , which is also the universal functional in DFT [1, 2]. Its natural variables are  $N$  and  $\sigma(\mathbf{r})$ . Differentiating Eq. (3.18), one has

$$dF = \left[ \mu - \int \sigma(\mathbf{r})v(\mathbf{r})d\mathbf{r} \right] dN - N \int v(\mathbf{r})\delta\sigma(\mathbf{r})d\mathbf{r} \quad (3.37)$$

so we have

$$\left( \frac{\partial F}{\partial N} \right)_\sigma = \mu - \int \sigma(\mathbf{r})v(\mathbf{r})d\mathbf{r} \quad (3.38)$$

and

$$\left( \frac{\delta F}{\delta \sigma(\mathbf{r})} \right)_N = -Nv(\mathbf{r}) \quad (3.39)$$

The Maxwell relation with Eq. (3.37) gives [3, 11, 12]

$$h(\mathbf{r}) + g(\mathbf{r}) = \int q(\mathbf{r}, \mathbf{r}')\sigma(\mathbf{r}')d\mathbf{r}' \quad (3.40)$$

with

$$h(\mathbf{r}) = \frac{1}{N} \left( \frac{\delta \mu}{\delta \sigma(\mathbf{r})} \right)_N \quad (3.41)$$

$$g(\mathbf{r}) = \left( \frac{\partial v(\mathbf{r})}{\partial N} \right)_\sigma \quad (3.42)$$

and

$$q(\mathbf{r}, \mathbf{r}') = \frac{1}{N} \left( \frac{\delta v(\mathbf{r})}{\delta \sigma(\mathbf{r}')} \right)_N \quad (3.43)$$

The two other variables, chemical potential  $\mu$  and external potential  $v(\mathbf{r})$ , can also be represented by  $N$  and  $\sigma(\mathbf{r})$  in the isomorphic ensemble, whose differential forms are, respectively,

$$d\mu = \eta^\sigma dN + N \int h(\mathbf{r})\delta\sigma(\mathbf{r})d\mathbf{r} \quad (3.44)$$

and

$$dv(\mathbf{r}) = g(\mathbf{r})dN + N \int q(\mathbf{r}, \mathbf{r}')\delta\sigma(\mathbf{r}')d\mathbf{r}' \quad (3.45)$$

where

$$\eta^\sigma = \left( \frac{\partial \mu}{\partial N} \right)_\sigma \quad (3.46)$$

The corresponding Maxwell relation for Eq. (3.44) is

$$h(\mathbf{r}) + N \left( \frac{\partial h(\mathbf{r})}{\partial N} \right)_\sigma = \left( \frac{\delta \eta^\sigma}{\delta \sigma(\mathbf{r})} \right)_N \quad (3.47)$$

and that for Eq. (3.45) is

$$q(\mathbf{r}, \mathbf{r}') + N \left( \frac{\partial q(\mathbf{r}, \mathbf{r}')}{\partial N} \right)_\sigma = \left( \frac{\delta g(\mathbf{r})}{\delta \sigma(\mathbf{r}')} \right)_N \quad (3.48)$$

### 3.6 Basic Relations in the Grand Isomorphic Ensemble

Equation (3.16) represents the grand isomorphic ensemble, whose state function is  $R$  and natural variables are chemical potential  $\mu$  and electron density  $\rho(\mathbf{r})$ . Differentiating Eq. (3.16) with the use of Eq. (3.19) yields

$$dR = -Nd\mu - N \int v(\mathbf{r})\delta\rho(\mathbf{r})d\mathbf{r} \quad (3.49)$$

so we have

$$\left(\frac{\partial R}{\partial \mu}\right)_\rho = -N \quad (3.50)$$

and

$$\left(\frac{\delta R}{\delta \rho(\mathbf{r})}\right)_\mu = -v(\mathbf{r}) \quad (3.51)$$

The Maxwell relation associated with Eq. (3.49) is as follows

$$\left(\frac{\partial v(\mathbf{r})}{\partial \mu}\right)_\rho = \left(\frac{\delta N}{\delta \rho(\mathbf{r})}\right)_\mu = 1 \quad (3.52)$$

To express the other independent variables,  $N$  and  $v(\mathbf{r})$ , in the grand isomorphic ensemble, one has the following differential forms

$$dN = \left(\frac{\partial N}{\partial \mu}\right)_\rho d\mu + \int \left(\frac{\delta N}{\delta \rho(\mathbf{r})}\right)_\mu \delta\rho(\mathbf{r}) d\mathbf{r} = \int \delta\rho(\mathbf{r}) d\mathbf{r} \quad (3.53)$$

and

$$dv(\mathbf{r}) = \left(\frac{\partial v(\mathbf{r})}{\partial \mu}\right)_\rho d\mu + \int \left(\frac{\delta v(\mathbf{r})}{\delta \rho(\mathbf{r}')}\right)_\mu \delta\rho(\mathbf{r}') d\mathbf{r}' \quad (3.54)$$

with Eq. (3.52), Eq. (3.54) becomes

$$dv(\mathbf{r}) = d\mu + \int \eta(\mathbf{r}, \mathbf{r}')\delta\rho(\mathbf{r}') d\mathbf{r}' \quad (3.55)$$

where the hardness kernel is defined as [10]

$$\eta(\mathbf{r}, \mathbf{r}') = \left(\frac{\delta v(\mathbf{r})}{\delta \rho(\mathbf{r}')}\right)_\mu = \frac{\delta^2 F[\rho]}{\delta \rho(\mathbf{r})\delta \rho(\mathbf{r}')} \quad (3.56)$$

The Maxwell relation for Eq. (3.55) is

$$\left(\frac{\partial \eta(\mathbf{r}, \mathbf{r}')}{\partial \mu}\right)_\rho = 0 \quad (3.57)$$

### 3.7 Relations Among Quantities from Different Ensembles

Many relations among different quantities from different ensembles have been discovered [2, 3, 11, 12], including:

$$S = \int s(\mathbf{r})d\mathbf{r} \quad (3.58)$$



$$s(\mathbf{r}) = \int s(\mathbf{r}, \mathbf{r}') d\mathbf{r}' \quad (3.59)$$

$$s(\mathbf{r}) = S f(\mathbf{r}) \quad (3.60)$$

$$\eta = \int f(\mathbf{r}) \eta(\mathbf{r}) d\mathbf{r}' \quad (3.61)$$

$$\int s(\mathbf{r}) \eta(\mathbf{r}) d\mathbf{r} = 1 \quad (3.62)$$

with local hardness  $\eta(\mathbf{r})$  defined as

$$\eta(\mathbf{r}) = \left( \frac{\delta \mu}{\delta \rho(\mathbf{r})} \right)_v \quad (3.63)$$

Four other well-known relations [2, 3, 10–12] are

$$\omega(\mathbf{r}, \mathbf{r}') = \frac{s(\mathbf{r})s(\mathbf{r}')}{S} - s(\mathbf{r}, \mathbf{r}') \quad (3.64)$$

$$\eta^\sigma = \eta + \int h(\mathbf{r}) [f(\mathbf{r}) - \sigma(\mathbf{r})] d\mathbf{r} \quad (3.65)$$

$$h(\mathbf{r}) = \int f(\mathbf{r}') q(\mathbf{r}, \mathbf{r}') d\mathbf{r}' \quad (3.66)$$

and

$$g(\mathbf{r}) = \int q(\mathbf{r}, \mathbf{r}') [\sigma(\mathbf{r}') - f(\mathbf{r}')] d\mathbf{r}' \quad (3.67)$$

### 3.8 Second-order Taylor Expansions in the Four Ensembles

Now, let us consider in the canonical ensemble the following scenario where an attacking agent induces changes in the number of electrons and external potential of the system,  $\Delta N$  and  $\Delta v(\mathbf{r})$ . Using the Taylor expansion up to the second order, the subsequent change in the total energy reads

$$\begin{aligned} \Delta E &\equiv E[N + \Delta N, v(\mathbf{r}) + \Delta v(\mathbf{r})] - E[N, v(\mathbf{r})] \\ &= \left( \frac{\partial E}{\partial N} \right)_v \Delta N + \int \left( \frac{\delta E}{\delta v(\mathbf{r})} \right)_N \Delta v(\mathbf{r}) d\mathbf{r} \\ &\quad + \frac{1}{2!} \left\{ \left( \frac{\partial^2 E}{\partial N^2} \right)_v \Delta N^2 + 2 \int \left( \frac{\partial}{\partial N} \left( \frac{\delta E}{\delta v(\mathbf{r})} \right) \right)_N \Delta N \Delta v(\mathbf{r}) d\mathbf{r} \right. \\ &\quad \left. + \iint \left( \frac{\delta^2 E}{\delta v(\mathbf{r}) \delta v(\mathbf{r}')} \right)_N \Delta v(\mathbf{r}) \Delta v(\mathbf{r}') d\mathbf{r} d\mathbf{r}' \right\} \end{aligned} \quad (3.68)$$

where  $(\partial E / \partial N)_v$  and  $[\delta E / \delta v(\mathbf{r})]_N$  are the first-order partial derivatives of the total energy with respect to  $N$  and  $v(\mathbf{r})$  with  $v(\mathbf{r})$  and  $N$  fixed, respectively, and, similarly,  $(\partial^2 E / \partial N^2)_v$  and  $[\delta^2 E / \delta v^2(\mathbf{r})]_N$  are the corresponding second-order terms, whereby

$[\partial/\partial N (\delta E/\delta v)_N]_v$  is the second-order cross term. With the quantities introduced in the above sections, we have

$$\begin{aligned} \Delta E = & \mu \Delta N + \int \rho(\mathbf{r}) \Delta v(\mathbf{r}) d\mathbf{r} + \frac{1}{2} \left\{ \eta \Delta N^2 + 2 \Delta N \int f(\mathbf{r}) \Delta v(\mathbf{r}) d\mathbf{r} \right. \\ & \left. + \iint \omega(\mathbf{r}, \mathbf{r}') \Delta v(\mathbf{r}) \Delta v(\mathbf{r}') d\mathbf{r} d\mathbf{r}' \right\} \end{aligned} \quad (3.69)$$

where chemical potential  $\mu$ , hardness  $\eta$ , Fukui function  $f(\mathbf{r})$ , and linear response function  $\omega(\mathbf{r}, \mathbf{r}')$  are employed to obtain the total energy change.

Similarly, in the grand canonical ensemble,

$$\begin{aligned} \Delta \Omega \equiv & \Omega[\mu + \Delta \mu, v(\mathbf{r}) + \Delta v(\mathbf{r})] - \Omega[\mu, v(\mathbf{r})] \\ = & \left( \frac{\partial \Omega}{\partial \mu} \right)_v \Delta \mu + \int \left( \frac{\delta \Omega}{\delta v(\mathbf{r})} \right)_\mu \Delta v(\mathbf{r}) d\mathbf{r} \\ & + \frac{1}{2!} \left\{ \left( \frac{\partial^2 \Omega}{\partial \mu^2} \right)_v \Delta \mu^2 + 2 \int \left( \frac{\partial}{\partial \mu} \left( \frac{\delta \Omega}{\delta v(\mathbf{r})} \right)_\mu \right)_v \Delta \mu \Delta v(\mathbf{r}) d\mathbf{r} \right. \\ & \left. + \iint \left( \frac{\delta^2 \Omega}{\delta v(\mathbf{r}) \delta v(\mathbf{r}')} \right)_\mu \Delta v(\mathbf{r}) \Delta v(\mathbf{r}') d\mathbf{r} d\mathbf{r}' \right\} \end{aligned} \quad (3.70)$$

Again, with the quantities introduced above, we have

$$\begin{aligned} \Delta \Omega = & -N \Delta \mu + \int \rho(\mathbf{r}) \Delta v(\mathbf{r}) d\mathbf{r} - \frac{1}{2} \left\{ S \Delta \mu^2 - 2 \Delta \mu \int s(\mathbf{r}) \Delta v(\mathbf{r}) d\mathbf{r} \right. \\ & \left. + \iint s(\mathbf{r}, \mathbf{r}') \Delta v(\mathbf{r}) \Delta v(\mathbf{r}') d\mathbf{r} d\mathbf{r}' \right\} \end{aligned} \quad (3.71)$$

where softness  $S$ , local softness  $s(\mathbf{r})$ , and softness kernel  $s(\mathbf{r}, \mathbf{r}')$  are involved in determining the total  $\Delta \Omega$  change. In the isomorphic ensemble,

$$\begin{aligned} \Delta F \equiv & F[N + \Delta N, \sigma(\mathbf{r}) + \Delta \sigma(\mathbf{r})] - F[N, \sigma(\mathbf{r})] \\ = & \left( \frac{\partial F}{\partial N} \right)_\sigma \Delta N + \int \left( \frac{\delta F}{\delta \sigma(\mathbf{r})} \right)_N \Delta \sigma(\mathbf{r}) d\mathbf{r} + \frac{1}{2!} \left\{ \left( \frac{\partial^2 F}{\partial N^2} \right)_\sigma \Delta N^2 \right. \\ & \left. + 2 \int \left( \frac{\partial}{\partial N} \left( \frac{\delta F}{\delta \sigma(\mathbf{r})} \right)_N \right)_\sigma \Delta N \Delta \sigma(\mathbf{r}) d\mathbf{r} + \iint \left( \frac{\delta^2 F}{\delta \sigma(\mathbf{r}) \delta \sigma(\mathbf{r}')} \right)_N \Delta \sigma(\mathbf{r}) \Delta \sigma(\mathbf{r}') d\mathbf{r} d\mathbf{r}' \right\} \end{aligned} \quad (3.72)$$

with quantities introduced above, so

$$\begin{aligned} \Delta F = & \mu \Delta N - N \int v(\mathbf{r}) \Delta \sigma(\mathbf{r}) d\mathbf{r} + \frac{1}{2} \left\{ \eta^\sigma \Delta N^2 - 3 \Delta N \int g(\mathbf{r}) \Delta \sigma(\mathbf{r}) d\mathbf{r} \right. \\ & \left. + \int N^2 \iint q(\mathbf{r}, \mathbf{r}') \Delta \sigma(\mathbf{r}) \Delta \sigma(\mathbf{r}') d\mathbf{r} d\mathbf{r}' \right\} \end{aligned} \quad (3.73)$$

and in the grand isomorphic ensemble,

$$\Delta R \equiv R[\mu + \Delta \mu, \rho(\mathbf{r}) + \Delta \rho(\mathbf{r})] - R[\mu, \rho(\mathbf{r})]$$

$$\begin{aligned}
&= \left( \frac{\partial R}{\partial \mu} \right)_{\rho} \Delta \mu + \int \left( \frac{\delta R}{\delta \sigma(\mathbf{r})} \right)_{\mu} \Delta \rho(\mathbf{r}) d\mathbf{r} + \frac{1}{2!} \left\{ \left( \frac{\partial^2 R}{\partial \mu^2} \right)_{\rho} \Delta \mu^2 \right. \\
&\quad \left. + 2 \int \left( \frac{\partial}{\partial \mu} \left( \frac{\delta R}{\delta \rho(\mathbf{r})} \right) \right)_{\mu} \Delta \mu \Delta \rho(\mathbf{r}) d\mathbf{r} + \iint \left( \frac{\delta^2 R}{\delta \rho(\mathbf{r}) \delta \rho(\mathbf{r}')} \right)_{\mu} \Delta \rho(\mathbf{r}) \Delta \rho(\mathbf{r}') d\mathbf{r} d\mathbf{r}' \right\}
\end{aligned} \tag{3.74}$$

so

$$\Delta R = - \int v(\mathbf{r}) \Delta \rho(\mathbf{r}) d\mathbf{r} + \frac{1}{2} \iint \eta(\mathbf{r}, \mathbf{r}') \Delta \rho(\mathbf{r}) \Delta \rho(\mathbf{r}') d\mathbf{r} d\mathbf{r}' \tag{3.75}$$

### 3.9 Generalized Considerations

Assuming the existence of all derivatives, the preceding Taylor expansion can be generalized to any quantity  $Q$ , whose natural variables include one global parameter  $g$  and one local variable  $l(\mathbf{r})$ , as the following

$$\begin{aligned}
&\Delta Q[g, l] \equiv Q[g + \Delta g, l(\mathbf{r}) + \Delta l(\mathbf{r})] - Q[g, l(\mathbf{r})] \\
&= \left( \frac{\partial Q}{\partial g} \right)_l \Delta g + \int \left( \frac{\delta Q}{\delta l(\mathbf{r})} \right)_g \Delta l(\mathbf{r}) d\mathbf{r} + \frac{1}{2!} \left\{ \left( \frac{\partial^2 Q}{\partial g^2} \right)_l \Delta g^2 \right. \\
&\quad \left. + 2 \int \left( \frac{\partial}{\partial g} \left( \frac{\delta Q}{\delta l(\mathbf{r})} \right) \right)_g \Delta g \Delta l(\mathbf{r}) d\mathbf{r} + \iint \left( \frac{\delta^2 Q}{\delta l(\mathbf{r}) \delta l(\mathbf{r}')} \right)_N \Delta l(\mathbf{r}) \Delta l(\mathbf{r}') d\mathbf{r} d\mathbf{r}' \right\} +
\end{aligned} \tag{3.76}$$

$$\begin{aligned}
&\frac{1}{3!} \left\{ \left( \frac{\partial^3 Q}{\partial g^3} \right)_l \Delta g^3 + 3 \int \left( \frac{\partial^2}{\partial g^2} \left( \frac{\delta Q}{\delta l(\mathbf{r})} \right) \right)_g \Delta g^2 \Delta l(\mathbf{r}) d\mathbf{r} \right. \\
&\quad \left. + 3 \iint \left( \frac{\partial}{\partial g} \left( \frac{\delta^2 Q}{\delta l(\mathbf{r}) \delta l(\mathbf{r}')} \right) \right)_g \Delta g \Delta l(\mathbf{r}) \Delta l(\mathbf{r}') d\mathbf{r} d\mathbf{r}' + \iiint \left( \frac{\delta^3 Q}{\delta l(\mathbf{r}) \delta l(\mathbf{r}') \delta l(\mathbf{r}'')} \right)_g \right. \\
&\quad \left. \Delta l(\mathbf{r}) \Delta l(\mathbf{r}') \Delta l(\mathbf{r}'') d\mathbf{r} d\mathbf{r}' d\mathbf{r}'' \right\} + \dots + \\
&\quad \sum_{m=1}^n \int \dots \iint \frac{n!}{m!(n-m)!} \left( \frac{\partial^m Q}{\partial g^m} \right)_l \left( \frac{\delta^{n-m} Q}{\delta l(\mathbf{r}) \dots \delta l(\mathbf{r}^{n-m})} \right) \\
&\quad \Delta g^m \Delta l(\mathbf{r}) \dots \Delta l(\mathbf{r}^{n-m}) d\mathbf{r} \dots d\mathbf{r}^{n-m} + \dots
\end{aligned}$$

One question regularly coming up is whether higher-order derivatives are important in chemical processes. According to Fuentealba and Parr [35], the answer is seemingly no. Nevertheless, more recent works by Morell et al. [37–39] suggest otherwise. In that work, they defined a new CDFT quantity called the dual descriptor,

$$f^{(2)}(\mathbf{r}) = \left( \frac{\partial^2}{\partial^2 N} \left( \frac{\delta E}{\delta v(\mathbf{r})} \right) \right)_N = \left( \frac{\delta}{\delta v(\mathbf{r})} \left( \frac{\partial^2 E}{\partial^2 N} \right) \right)_N = \left( \frac{\partial f(\mathbf{r})}{\partial N} \right)_v = \left( \frac{\delta \eta}{\delta v(\mathbf{r})} \right)_N \tag{3.77}$$

which is the derivative of Fukui function  $f(\mathbf{r})$  with respect to the total number of electrons  $N$ . This third-order derivative recovers the Woodward–Hoffman rules [40–42], which were previously only understood using the symmetry of molecular orbitals. The significance of this work is that using density-based quantities, one can mimic what frontier molecular orbitals can do for explaining and predicting chemical reactivity. Nonetheless, CDFT is still valid in cases where frontier molecular orbital theory fails, e.g. because of strong orbital-relaxation or electron-correlation effects [43, 44].

The validity of the above formalism in CDFT is based on the following two assumptions. First, the response of a molecular system to the external impact during the process of chemical transformations can be approximated by a Taylor series. Second, the derivatives in the Taylor series are well behaved. That is, they are existent and continuous. As mentioned above, these assumptions are not mathematically rigorous, yet they work in practice. This is perhaps because for a reacting (sub)system, one is always considering a pseudo-mixed state, which mimics (to some reasonable approximation) a thermodynamic ensemble [19, 45–47]. This, however, is a topic for future research.

Before wrapping up, we notice in passing that there is another totally different expansion method in the literature in CDFT, called the functional expansion approach [3, 48], using the hierarchical identity of functional derivatives. Numerous applications of this functional expansion approach are available in the literature [49–56].

To summarize, these formulations form the foundation of CDFT and are expected to be insightful and/or useful in explaining chemical processes and transformations. More discussion about the basic functions and basic principles stemming from the above formulations will be ensued in the next chapters, followed by their numerous extensions in various scenarios and a variety of applications to solve real chemical problems.

## References

- 1 Nalewajski, R.F. and Parr, R.G. (1982). *J. Chem. Phys.* 77: 399.
- 2 Parr, R.G. and Yang, W. (1989). *Density Functional Theory of Atoms and Molecules*. Oxford: Oxford University Press.
- 3 Liu, S.B. and Parr, R.G. (1997). *J. Chem. Phys.* 106: 5578.
- 4 Chermette, H. (1999). *J. Comput. Chem.* 20: 129–154.
- 5 Geerlings, P., De Proft, F., and Langenaeker, W. (2003). *Chem. Rev.* 103: 1793–1873.
- 6 Chattaraj, P.R., Sarkar, U., and Roy, D.R. (2006). *Chem. Rev.* 106: 2065–2091.
- 7 Liu, S.B. (2009). *Acta Phys. Chem. Sin.* 25: 590–600.
- 8 Ghosh, S.K., Berkowitz, M., and Parr, R.G. (1984). *Proc. Natl. Acad. Sci. U. S. A.* 81: 8028–8031.
- 9 Nagy, A. and Parr, R.G. (1994). *Proc. Indian Acad. Sci. (Chem. Sci.)* 106: 217.
- 10 Berkowitz, M. and Parr, R.G. (1988). *J. Chem. Phys.* 88: 2554.

- 11 Cedillo, A. (1994). *Int. J. Quantum Chem.* 28: 231–240.
- 12 Baekelandt, B.G., Cedillo, A., and Parr, R.G. (1995). *J. Chem. Phys.* 103: 8548.
- 13 Ayers, P.W. (2000). *Proc. Natl. Acad. Sci. U. S. A.* 97: 1959–1964.
- 14 Hohenberg, P. and Kohn, W. (1964). *Phys. Rev.* B136: 864–871.
- 15 Ghosh, S.K. and Berkowitz, M. (1985). *J. Chem. Phys.* 83: 2976–2983.
- 16 Ayers, P.W., Parr, R.G., and Nagy, A. (2002). *Int. J. Quantum Chem.* 90: 309–326.
- 17 Nagy, A. and Parr, R.G. (1990). *Phys. Rev.* A42: 201–203.
- 18 Nagy, A., Parr, R.G., and Liu, S.B. (1996). *Phys. Rev.* A53: 3117–3121.
- 19 Miranda-Quintana, R.A. and Ayers, P.W. (2016). *Chem. Chem. Phys.* 18: 15070–15080.
- 20 Gázquez, J.L., Franco-Pérez, M., Ayers, P.W., and Vela, A. (2019). *Int. J. Quantum Chem.* 119: e25797.
- 21 Franco-Perez, M., Ayers, P.W., Gázquez, J.L., and Vela, A. (2017). *J. Chem. Phys.* 147: 094105.
- 22 Lieb, E.H. (1983). *Int. J. Quantum Chem.* 24: 243–277.
- 23 Ayers, P.W. (2008). *J. Math. Chem.* 43: 285–303.
- 24 Liu, S.B., Li, T.L., and Ayers, P.W. (2009). *J. Chem. Phys.* 131: 114106.
- 25 Cardenas, C., Ayers, P.W., and Cedillo, A. (2011). *J. Chem. Phys.* 134: 174103.
- 26 Perdew, J.P., Parr, R.G., Levy, M., and Balduz, J.L. (1982). *Phys. Rev. Lett.* 49: 1691–1694.
- 27 Zhang, Y.K. and Yang, W.T. (2000). *Theor. Chem. Acc.* 103: 346–348.
- 28 Ayers, P.W. and Cedillo, A. (2009). The shape function. In: *Chemical Reactivity Theory: A Density Functional View* (ed. P.K. Chattaraj), 269. Boca Raton, FL: Taylor and Francis.
- 29 Parr, R.G. and Yang, W. (1984). *J. Am. Chem. Soc.* 106: 4049–4050.
- 30 Fukui, K., Yonezawa, Y., and Shingu, H. (1952). *J. Chem. Phys.* 30: 722–725.
- 31 Parr, R.G. and Pearson, R.G. (1983). *J. Am. Chem. Soc.* 105: 7512–7516.
- 32 Yang, W.T. and Parr, R.G. (1985). *Proc. Natl. Acad. Sci. U. S. A.* 82: 6723–6726.
- 33 Langenaeker, W. and Liu, S.B. (2001). *J. Mol. Struct. THEOCHEM* 535: 279–286.
- 34 Geerlings, P., Fias, S., Boisdenghien, Z., and De Proft, F. (2014). *Chem. Soc. Rev.* 43: 4989–5008.
- 35 Fuentealba, P. and Parr, R.G. (1991). *J. Chem. Phys.* 94: 5559–5564.
- 36 Ayers, P.W., Morell, C., De Proft, F., and Geerlings, P. (2007). *Chem. Eur. J.* 13: 8240–8247.
- 37 Morell, C., Grand, A., and Toro-Labbé, A. (2005). *J. Phys. Chem.* A109: 205–212.
- 38 De Proft, F., Ayers, P.W., Fias, S., and Geerlings, P. (2006). *J. Chem. Phys.* 125: 214101.
- 39 Geerlings, P. and De Proft, F. (2008). *Phys. Chem. Chem. Phys.* 10: 3028–3042.
- 40 Cardenas, C., Rabi, N., Ayers, P.W. et al. (2009). *J. Phys. Chem.* A113: 8660–8667.
- 41 Geerlings, P., Ayers, P.W., Toro-Labbé, A. et al. (2012). *Acc. Chem. Res.* 45: 683–695.
- 42 Woodward, R.B. and Hoffmann, R.W. (1971). *The Conservation of Orbital Symmetry*. Weinheim: Verlag Chemie.
- 43 Bartolotti, L.J. and Ayers, P.W. (2005). *J. Phys. Chem.* A109: 1146–1151.

- 44 Johnson, P.A., Bartolotti, L.J., Ayers, P.W. et al. (2012). Charge density and chemical reactivity: a unified view from conceptual DFT. In: *Modern Charge Density Analysis* (ed. C. Gatti and P. Macchi), 715–764. New York: Springer.
- 45 Ayers, P.W. (2006). *Phys. Chem. Chem. Phys.* 8: 3387–3390.
- 46 Cohen, O. (1998). *Phys. Rev. Lett.* 80: 2493.
- 47 Ayers, P.W. (2007). *Theor. Chem. Acc.* 118: 371–381.
- 48 Parr, R.G., Liu, S.B., Kugler, A.A., and Nagy, A. (1995). *Phys. Rev. A* 52: 969–976.
- 49 Liu, S.B. and Parr, R.G. (1996). *Phys. Rev. A* 53: 2211–2219.
- 50 Liu, S.B., Sule, P., Lopez-Boada, R., and Nagy, A. (1996). *Chem. Phys. Lett.* 257: 68–74.
- 51 Liu, S.B. (1996). *Phys. Rev. A* 54: 1328–1336.
- 52 Liu, S.B. (1996). *Phys. Rev. A* 54: 4863–4867.
- 53 Liu, S.B. and Parr, R.G. (1997). *Phys. Rev. A* 55: 1792–1798.
- 54 Wang, Y.A., Liu, S.B., and Parr, R.G. (1997). *Chem. Phys. Lett.* 267: 14–22.
- 55 Liu, S.B., Nagy, A., and Parr, R.G. (1999). *Phys. Rev. A* 59: 1131–1134.
- 56 Liu, S.B., Morrison, R.C., and Parr, R.G. (2006). *J. Chem. Phys.* 125: 174109.

## 4

## Basic Principles

Debdutta Chakraborty<sup>1</sup> and Pratim K. Chattaraj<sup>2,3</sup>

<sup>1</sup>Birla Institute of Technology, Department of Chemistry, Mesra, Ranchi, Jharkhand 835215, India

<sup>2</sup>Indian Institute of Technology, Department of Chemistry, Kharagpur 721302, West Bengal, India

<sup>3</sup>Indian Institute of Technology Bombay, Department of Chemistry, Mumbai 400076, Maharashtra, India

## 4.1 Introduction

Although Dirac had assured us almost a century back, with a caveat, by saying:

“The underlying physical laws necessary for the mathematical theory of a large part of physics and the whole of chemistry are thus completely known, and the difficulty is only that the exact application of these laws leads to equations much too complicated to be soluble.” [1]

We are still not in a position to accurately predict the behavior of majority of the chemical systems. Since then, a major goal has been to develop appropriate numerical methods so that the time-independent (and time-dependent) Schrodinger equation for atoms and molecules could be solved. Once the wave function for the given problem is known, various observable properties for the system could be calculated, which can help to understand physical as well as chemical processes. However, obtaining the wave function, which is a function of several variables, is not a trivial task. Fortunately, density functional theory (DFT) [2–9] provides an effective alternative theoretical method. With the help of DFT, information concerning a given system could be obtained albeit at a much cheaper computational cost in comparison to *ab initio* wave-function-based methods. One can completely define the Hamiltonian ( $\hat{H}$ ) of an  $N$ -electron system by knowing  $N$  and the external potential  $v(r)$ . The solution of the Schrodinger equation for a given  $\hat{H}$  provides the  $3N$ -dimensional wave function  $\psi(r_1, r_2, \dots, r_N)$ . One can obtain the single-particle density  $\rho(\mathbf{r})$  by performing the following integration:

$$\rho(\mathbf{r}) = N \int \dots \int \psi^*(r, r_2, \dots, r_N) \psi(r, r_2, \dots, r_N) dr_2 \dots dr_N \quad (4.1)$$

where,

$$\int \rho(\mathbf{r}) d\mathbf{r} = N \quad (4.2)$$

*Conceptual Density Functional Theory: Towards a New Chemical Reactivity Theory*, First Edition.

Edited by Shubin Liu.

© 2022 WILEY-VCH GmbH. Published 2022 by WILEY-VCH GmbH.

It becomes quite clear that a mapping in between  $v(r)$  and  $\rho(\mathbf{r})$  exists. According to the Hohenberg and Kohn [4] theorem, an inverse mapping between  $\rho(\mathbf{r})$  and  $v(r)$  also exists. This observation lies at the heart of the formal development of DFT. Electron density is a three-dimensional quantity. Therefore, it becomes convenient to use  $\rho(\mathbf{r})$  to provide chemically meaningful interpretations [9]. The most important aspect of  $\rho(\mathbf{r})$  is that one can use it to develop various theoretical models. In this context, conceptual density functional theory (CDFT) [9–16] represents a major (and among the most celebrated) theoretical framework where  $\rho(\mathbf{r})$  is used to understand chemical reactivity.

Reactivity of a system could be gauged by its propensity in reacting against an action. The action could be generated by several external factors such as another atom/molecule, external electric/magnetic field, change in temperature or external pressure, catalyst, solvent, and confinement. The response of the system could be measured by reactivity when acted upon by any of the aforementioned external factors. As the Hamiltonian of the given system could be completely defined by fixing the values of  $N$  and  $v(r)$ , one could analyze the change in density or energy by varying  $N$ ,  $v(r)$  or both. In this way, one could understand the change in reactivity. To appreciate the reasoning behind the formulation of CDFT, one can invoke the Hohenberg–Kohn theorem, which provides a recipe of variational optimization of the energy functional  $E[\rho]$ , which attains the minimum value for the true density. The following associated Euler–Lagrange equation can be solved to obtain the density:

$$\frac{\delta E[\rho]}{\delta \rho} = \mu \quad (4.3)$$

Here, the electronic chemical potential,  $\mu$ , takes care of the normalization (Eq. (4.2)) as it is the related Lagrange multiplier. As shown by Parr et al. [17, 18], there exists a relationship in between the zero temperature limit of the chemical potential of the thermodynamic grand canonical ensemble and  $\mu$ . In addition, it was shown that  $\mu$  is the negative of electronegativity ( $\chi$ ). This consideration established a direct correlation in between chemical reactivity and CDFT [17]. Within a grand canonical ensemble, the atoms in a molecule can be considered as open systems. This assumption allows us to study the variation in electron density by using DFT. We note that  $E[\rho]$  attains the minimum value at the electronic ground state. Considering such a set of densities at a finite temperature, the equilibrium state could be identified with the help of the minimum Helmholtz free energy  $A[\rho]$  within a canonical ensemble. Similarly, within a grand canonical ensemble, grand potential functionals  $\Omega[\rho]$  could be utilized. One can consider the ground electronic state as the thermodynamic equilibrium state [9] at zero temperature. The aforementioned ideas form the backbone of the theoretical development of CDFT. Chemical reactions comprise change and redistribution of electron densities. Thus, different reactivity descriptors, both global and local, have been formulated within the premise of CDFT. These descriptors can be made use of in understanding various chemical processes [19, 20]. Associated electronic structure principles could also be utilized to shed light on a given problem of interest. The purpose of this chapter is to introduce the reader to these principles. Now, we would like



to introduce the readers to various reactivity descriptors and the associated basic electronic structure principles of CDFT.

## 4.2 Global and Local Reactivity Descriptors

As  $N$  and  $v(r)$  can fix the Hamiltonian of a system, by varying these quantities one can go from one ground electronic state to another, and the associated changes in energy and density corresponding to that process help us in developing different reactivity descriptors so that a comprehensive theory of chemical reactivity can be developed [9, 21].

Various reactivity descriptors are properly delineated in the previous chapter. Important global reactivity descriptors include electronegativity [9], hardness [22–25], softness [26], and electrophilicity [27, 28]. They are generally calculated [22, 29] using the electron affinity and ionization potential or by using Koopmans' theorem in terms of the energies of highest occupied and lowest unoccupied molecular orbitals.

Various other definitions of these descriptors exist for the charge acceptance and depletion processes [30, 31]. This is due to the fact that a discontinuity in energy vs.  $N$  curve is observed in several situations [18, 32]. To take care of this problem [33–36] in the definition of these quantities, an atom in a molecule is considered as a thermodynamic open system, and the zero temperature limit [18, 37–39] of a relevant grand canonical ensemble can be introduced. These global descriptors can take care of the reactivity and conversely the stability of a system.

For the chemical reactions where spin multiplicity changes, spin-polarized version of reactivity descriptors defined through the spin density ( $\rho_s(r)$ ) and the total charge density ( $\rho_C(r)$ ) can be used to understand reactivity [40–42].

In this context, it must be emphasized that the spin densities alone cannot uniquely determine effective and external potentials in spin-polarized DFT. We need to consider spin-polarized DFT to describe the properties of a system under the influence of magnetic fields. Similarly, in the cases of systems having odd number of electrons, spin-polarized DFT becomes important. We refer the reader to the following chapters in this book where these issues are discussed in detail.

To understand the site selectivity in a molecule, many local reactivity descriptors are defined. Important local reactivity descriptors include electron density and Fukui function ( $f(r)$ ) [43–50].

The condensed-to-atoms variants of the Fukui function ( $f_k$ ) [50] need the electronic population of the relevant atom in the molecule. Mulliken population analysis as well as Hirshfeld population analysis could be utilized to compute the values of the electronic population of the concerned atom within a given molecule. However, the Mulliken population analysis sometimes leads to the negative [51–53] values of the Fukui functions. Therefore, Hirshfeld population analysis [51–53] is usually recommended to evaluate the population. Thereby, the computed values of the Fukui functions would be positive in most cases if the Hirshfeld population analysis is utilized. We note, however, that there exist systems for which negative

Fukui functions are meaningful as they can shed some light on the nature of some processes [54–57].

These local reactivity descriptors are not suitable for gauging intermolecular reactivity. However, these descriptors can be used to analyze the intramolecular reactivity. When two moieties interact with each other at a large separation, the given moieties cannot “feel” the local reactivity changes. At large intermolecular distances, mainly the electrostatic effects dominate the intermolecular interactions, while the orbital interactions play a less significant role in such situations. In such cases, other reactivity descriptors such as local softness  $s^{\alpha}(r)$  [25, 58, 59] and philicity  $\omega(r)$  [60] could be used instead of the Fukui functions. It is possible to generate the corresponding group quantities by taking a sum over all condensed-to-atoms quantities over the group of corresponding atoms [61]. By following suitable variational procedures, the local reactivity descriptors such as  $s^{\alpha}(r)$ ,  $\omega^{\alpha}(r)$ ,  $\rho(r)$ , and  $f(r)$  can be evaluated.

There have been attempts to define a local hardness under some constraints [62–64]. Due to the inter-dependence of  $v(r)$  and  $\rho(r)$  within the realm of DFT, formal inconsistencies arise [65–69] for the simultaneous description of local hardness and local softness. While Hardness ( $\eta(r)$ ) provides an estimate of nuclear reactivity, softness ( $s(r)$ ) provides a measure of the electronic reactivity [70, 71].

Furthermore, many other local reactivity descriptors are also used to understand chemical reactivity. The most important examples in this category include the gradient ( $\nabla\rho(r)$ ) and Laplacian ( $\nabla^2\rho(r)$ ) of electron density [72], electron localization function [73], quantum potential [74, 75], multiphilic descriptor ( $\Delta\omega(r)$ ) [76], dual descriptors ( $\Delta f(r)$ ) [77–79], and molecular electrostatic potential [80–83]. By utilizing the kinetic energy density and density expressions for an ideal gas, a local temperature  $\Theta(r)$  has been defined [49, 84–87]. The local temperature could be defined in time-dependent situations [88–92]. It could be defined for the excited states possessing non-vanishing current density [88–92] as well. A condensed-to-atom variant of  $\Theta(r)$  has been proposed. However, such a condensation may face a formal limitation [93–95].  $\Theta(r)$  is non-linearly dependent on  $\rho(r)$ . Therefore, its condensation utilizing the concerned electron population becomes ad hoc. However, it does not suffer from any drawback in case population is not used. All of the above descriptors depend on the underlying density partitioning scheme used. Therefore, a careful examination is needed before employing these descriptors so that any unphysical behavior could be eradicated. Generally, in the cases of hard–hard interactions, atomic charge plays [96] the dominant role in deciding the nature of interaction and thus reactivity. So, in these instances, local reactivity descriptors based on atomic charges can characterize the reactivity satisfactorily [96–98]. However, in the instances of soft–soft interactions, the nature of interaction is dictated by frontier-orbitals. So, in such situations, intramolecular descriptors like Fukui function or the inter-molecular variants such as  $s(r)$  and  $\omega(r)$  can be used.

The global as well as local reactivity descriptors tend to adhere to some electronic structure principles, and they together form the backbone of the CDFT. In the next section, we will introduce these principles. Mostly they are of three types,

viz. similarity principles such as hard–soft acid–base (HSAB) principle, extremum principles like maximum hardness and entropy and minimum polarizability and electrophilicity as well as equalization principles, including electronegativity, hardness, and electrophilicity equalization principles.

## 4.3 Electronic Structure Principles

### 4.3.1 Electronegativity-Based Principle

Pauling [99] introduced the idea of electronegativity in chemistry. Electronegativity provides an estimate of the relative ability of electron donation and acceptance between two interacting species. Sanderson proposed that the electron transfer process continues until their electronegativity values become equal [100–103]. Sanderson’s electronegativity equalization principle (EEP) states that the final molecular electronegativity becomes equal to the geometric mean of the electronegativity values of constituent atoms at the isolated state. This is expressed as follows [100–103]:

$$\chi_{\text{GM}} \approx \left( \sum_{k=1}^P \chi_k \right)^{\frac{1}{P}} \quad (4.4)$$

Here, the given molecule comprises  $P$  atoms and  $\chi_k$  signifies the electronegativity value for the  $k$ th atom at the free state.

Let us consider a process where a complex  $X : Y$  is formed from acid  $X$  and base  $Y$ . In such situations, the amount of charge transfer ( $\Delta N$ ) and change in energy ( $\Delta E$ ) can be written in the following way [26]:

$$\Delta N = \frac{\chi_X^0 - \chi_Y^0}{\eta_X + \eta_Y} \quad (4.5)$$

$$\Delta E = -\frac{(\chi_X^0 - \chi_Y^0)^2}{2(\eta_X + \eta_Y)} \quad (4.6)$$

Parr and Pearson proposed the aforementioned equations. These equations have been utilized in several contexts. Equations (4.5) and (4.6) were used to find an analytical justification for the HSAB principle [104–112]. These equations proved their worth while defining an electrophilicity index [113–115] as well. Nevertheless, the aforementioned equations fail to take into account several crucial factors. These factors include entropy, solvent effects, and electrostatic interaction. This approach depends mainly on the charge transfer effects [116] and faces the derivative discontinuity issue [48, 49]. To find a solution to these issues, a relevant thermodynamic grand canonical ensemble in its zero temperature limit is introduced [18, 33–39]. To define reactivity descriptors at a finite temperature [9], concepts derived from statistical mechanics could be properly used. In this context, the softness could be described in terms of the number fluctuations [25] by borrowing concepts from statistical mechanics.

It has been argued that the chemical reactivity can be better analyzed within a grand canonical ensemble defined at a finite external temperature and considering its zero temperature limit [9, 38, 39]. Inclusion of temperature [117–119] within the definition of  $E[N, \nu]$  shifts the CDFT formalism from a canonical to a grand-canonical ensemble [18, 34–39]. In this temperature-dependent CDFT, the average electronic energy and its derivatives play the crucial role. As a result of the inclusion of finite temperature effects, the changes in the different response functions are negligible from their corresponding zero temperature counterparts. It is possible to define heat capacity (both global and local) [119] in such a temperature-dependent CDFT. Therefore, it becomes possible to study energy transfer processes by using the temperature-dependent CDFT. Other reactivity descriptors such as the thermodynamic hardness and dual descriptor have also been defined within the framework of temperature-dependent CDFT [119].

### 4.3.2 Hardness-Based Principles

The hardness sum represents an important descriptor to understand electron transfer processes. The hardness provides an estimate [26] for the reluctance of a chemical moiety for electron transfer. For both the directions of electron transfer in a molecule, the value of  $\Delta E$  is always negative. Therefore, the  $\Delta N$  values are to be considered to understand the direction of electron flow. The condensed-to-atom version of the Fukui function could be used to predict the direction of electron transfer.

Electronegativity alone cannot properly describe the reactivity of chemical systems. The corresponding values for hardness need to be considered as well to describe the reactivity of a system. Pearson [26] proposed the concept of hardness. The usefulness of this concept was verified while trying to describe the characteristics of acid–base reactions through his HSAB principle. The HSAB principle is stated as follows: “*Hard acids prefer to coordinate with hard bases and soft acids prefer to coordinate with soft bases for both their kinetic and thermodynamic properties.*” It has been shown that by using the definition of hardness within CDFT, the hard–soft nature of acids and bases can be explained, as obtained from several experiments. An extension of the HSAB principle to a local level is not straightforward [96].

Another electronic structure principle concerning the hardness is designated as the maximum hardness principle (MHP) [30, 120–125]. MHP states the following: “*There seems to be a rule of nature that molecules arrange themselves so as to be as hard as possible.*” In the cases of several physicochemical processes, the validity of MHP has been authenticated. In this regard it is prudent to mention a few examples as follows: the cases of various chemical reactions [126], Woodward–Hoffmann rules [127, 128], molecular vibrations and internal rotations [129–134], time-dependent situations [135], chaotic ionization from Rydberg states [136], aromaticity [137], etc. It has also been demonstrated [108, 109] that HSABP and MHP are intimately connected. In this context, it should be noted that a hardness equalization principle (HEP) has been proposed by considering two factors. The conceptual genesis for this principle lies at the EEP as well as in the observation that the global softness of a molecule could be denoted as the mean of the concerned local softness values of

the concerned atoms. As hardness is directly correlated with the electronegativity, one can arrive at the following expression for the HEP [138]:

$$\eta_{\text{GM}} \approx \left( \sum_{k=1}^P \eta_k \right)^{\frac{1}{P}} \quad (4.7)$$

Here,  $\eta_k$  represents the hardness values for the constituent atoms (in the corresponding free state) within a given molecule. In several situations, the aforementioned principle remains valid as evidenced by comparison in between computed and experimental hardness values. However, as a result of the ambiguities in the definition of local hardness, the universal validity of the HEP could be questioned. It has been argued that this ambiguity allows [62] us to equate local hardness with global hardness, a direct ramification of the HEP.

As hard systems are also less magnetizable as well as less polarizable, two more principles, viz. minimum magnetizability principle (MMP) and minimum polarizability principle (MPP), were proposed. MPP [135] states the following: “*The natural direction of evolution of any system is towards a state of minimum polarizability ( $\alpha$ )*”. On the other hand, MMP states [139]: “*A stable configuration/conformation of a molecule or a favourable chemical process is associated with a minimum value of the magnetizability ( $\xi$ )*.”

### 4.3.3 Electrophilicity-Based Principles

Utilizing  $\eta$  and  $\mu$ , one could calculate the extremum values of electrophilicity ( $\omega$ ) [140–142]. It was shown that a minimum electrophilicity principle (MEP) could remain operational in many situations [143–146]. In this context, by invoking concepts from classical electrostatics, it has been proposed [147] that MEP is implicitly described within the definition of Maynard–Parr description of  $\omega$ . When a chemical reaction takes place, the electrophilicity of an electrophile (which is an electron deficient species) decreases while the corresponding electrophilicity of the nucleophile (which is an electron rich species) increases. Due to this concept, an electrophilicity equalization principle might be proposed that may be valid in many situations. Since electrophilicity depends on hardness and chemical potential, it could be argued that in situations where hardness and chemical potential get simultaneously equalized, electrophilicity too would get equalized. Thus equalized electrophilicity could be expressed in the following way [148]:

$$\omega_{\text{GM}} = \frac{\chi_{\text{GM}}^2}{2\eta_{\text{GM}}} \approx \left( \sum_{k=1}^P \omega_k \right)^{\frac{1}{P}} \quad (4.8)$$

Here,  $\omega_k$  represents the electrophilicity values for the constituent atoms (in the corresponding free state) within a given molecule. During the course of a given chemical process, extrema in  $\omega$  arise in points when the following condition is satisfied [140–143]:

$$\frac{\partial \mu}{\partial \lambda} = \frac{\mu}{2\eta} \left[ \frac{\partial \eta}{\partial \lambda} \right] \quad (4.9)$$

$\lambda$  denotes the reaction coordinate for a chemical process. It could also represent any concerned internal degree of freedom. It should be noted that  $\eta$  is always positive while  $\mu$  is always negative. This property arises due to the convex nature of energy. As a result of this, electrophilicity attains the extremum value, when the interdependencies of  $\eta$  and  $\mu$  on  $\lambda$  are reversed.

#### 4.3.4 Electronic Entropy-Based Principle

Now it will be described as to how the concept of entropy is described and used within the premise of DFT. Upon considering an  $N$  electron system (comprising  $N$  non-interacting particles) under the influence of an effective potential  $v_{\text{eff}}(r, t)$ , entropy density in a time-dependent situation can be defined using an average density argument as [88, 136, 149]:

$$s(r, t) = \frac{5}{2}k\rho - k\rho \ln \rho + \frac{3}{2}k\rho \ln \left( \frac{k\theta}{2\pi} \right) \quad (4.10)$$

Here,  $k$  is the Boltzmann constant whereas  $\theta$  denotes a space-time dependent “temperature.” The kinetic energy density could be used to define  $\theta$  in the following manner:

$$t_s(r; \rho(r, t)) = \frac{3}{2}\rho(r, t)k\theta(r, t) + \left( \frac{|j|^2}{2\rho} \right) \quad (4.11)$$

Here,  $j$  denotes the current density. It should be noted that one can arrive at Eq. (4.11) by utilizing information theory as well. In this regard, the Shannon entropy for the entity could be defined in terms of the density of the concerned entity. Upon maximizing Shannon entropy under certain conditions, one can derive Eq. (4.11). The global entropy could be evaluated by integrating Eq. (4.11) over the complete space in the following manner:

$$S = \int s(r, t) dr \quad (4.12)$$

In several time-dependent situations, favorable processes are accompanied by the maximization of entropy. It could be stated that in such situations, a maximum entropy principle remains operational [125, 136]. Concepts emanating from information theory [150] could be used and suitable reactivity descriptors could be described to provide many important insights. The information theory has been helpful in understanding the theory of atoms-in-molecule [151]. Shannon entropy, when defined as a functional of  $\rho(r)$ , can on its own characterize Coulombic entities [152]. It has been proposed that the Shannon entropy has the potential to be as important as  $\rho(r)$ . Shannon entropy could be used to characterize several chemical processes. In this regard, several other density functionals are also proposed such as Onicescu information energy [153], Fisher information [154] as well as Rényi entropy [155]. Kullback–Leibler information measure also comprises significant insights [89]. The information conservation principle has been used to define [156–160] reactivity descriptors such as nucleophilicity, electrophilicity as well as regioselectivity.

## 4.4 Conclusion

As discussed above, in this chapter, we try to set the stage for the reader to understand and appreciate CDFT. In the following chapters, several formal as well as applied points of view of CDFT will be discussed. It will be seen in the following chapters, how one can employ CDFT-based reactivity descriptors to gain chemically intuitive information regarding several processes. The global and local reactivity descriptors are helpful in understanding stability, reactivity, dynamics, etc. These aspects are better appreciated through the use of the associated electronic structure principles. Therefore, one needs to understand the implication of the computed values of these descriptors in conjunction with these principles. The local reactivity descriptors, on the other hand, are useful in determining site selectivity. The CDFT has been shown to be capable of taking care of several interpretative aspects of chemical systems as well as processes and hopefully, in the course of time, the predictive [161–164] power of CDFT would be further improved.

## Acknowledgments

Pratim K. Chattaraj thanks DST, New Delhi, for the J. C. Bose National Fellowship (grant number SR/S2/JCB-09/2009). He would also like to thank Prof. S. Liu for his kind invitation.

## References

- 1 Dirac, P.A.M. (1929). *Proc. R. Soc. Lond. A* 123: 714.
- 2 Thomas, L.H. (1927). *Proc. Camb. Philos. Soc.* 23: 542.
- 3 Fermi, E. (1928). *Z. Phys.* 48: 73.
- 4 Hohenberg, P. and Kohn, W. (1964). *Phys. Rev. B* 136: 864.
- 5 Kohn, W. and Sham, L.J. (1965). *Phys. Rev.* 140: A1133.
- 6 Tong, B.Y. and Sham, L.J. (1966). *Phys. Rev.* 144: 1.
- 7 Ziegler, T. (1991). *Chem. Rev.* 91: 651.
- 8 March, N.H. and Deb, B.M. (ed.) (1987). *The Single Particle Density in Physics and Chemistry*. London: Academic Press.
- 9 Parr, R.G. and Yang, W. (1989). *Density Functional Theory of Atoms and Molecules*. Oxford: Oxford University Press.
- 10 Kohn, W., Becke, A.D., and Parr, R.G. (1996). *J. Phys. Chem.* 100: 12974.
- 11 Ayers, P.W. and Yang, W. (2003). Density functional theory. In: *Computational Medicinal Chemistry for Drug Discovery* (ed. P. Bultinck, H. de Winter, W. Langenaeker and J.P. Tollenaere), 571. New York: Dekker.
- 12 Parr, R.G. and Yang, W.T. (1995). *Annu. Rev. Phys. Chem.* 46: 701.
- 13 Chattaraj, P.K. and Parr, R.G. (1993). Density functional theory of chemical hardness. In: *Chemical Hardness, Structure and Bonding* (ed. K.D. Sen and D.M.P. Mingos), 11. Berlin: Springer-Verlag.

- 14 Chattaraj, P.K., Poddar, A., and Maiti, B. (2002). Chemical reactivity and dynamics within a density-based quantum mechanical framework. In: *Reviews in Modern Quantum Chemistry: A Celebration of the Contributions of Robert Parr* (ed. K.D. Sen), 871. Singapore: World Scientific.
- 15 Chattaraj, P.K., Nath, S., and Maiti, B. (2003). Reactivity descriptors. In: *Computational Medicinal Chemistry for Drug Discovery* (ed. J. Tollenaere, P. Bultinck, H.D. Winter and W. Langenaeker), 295. New York: Marcel Dekker.
- 16 Sarkar, U. and Chattaraj, P.K. (2021). *J. Phys. Chem. A* 125: 2051.
- 17 Parr, R.G., Donnelly, R.A., Levy, M., and Palke, W.E. (1978). *J. Chem. Phys.* 68: 3801.
- 18 Perdew, J.P., Parr, R.G., Levy, M., and Balduz, J.L. Jr, (1982). *Phys. Rev. Lett.* 49: 1691.
- 19 Geerlings, P., De Proft, F., and Langenaeker, W. (2003). *Chem. Rev.* 103: 1793.
- 20 Chattaraj, P.K. (ed.) (2009). *Chemical Reactivity Theory: A Density Functional View*. Boca Raton, FL: Taylor & Francis/CRC Press.
- 21 Ghosh, S.K. and Deb, B.M. (1982). *Phys. Rep.* 52: 1.
- 22 Pearson, R.G. (1986). *Proc. Natl. Acad. Sci. U. S. A.* 83: 8440.
- 23 Pearson, R.G. (1997). *Chemical Hardness: Applications from Molecules to Solids*. Weinheim: Wiley-VCH.
- 24 Parr, R.G. and Pearson, R.G. (1983). *J. Am. Chem. Soc.* 105: 7512.
- 25 Yang, W.T. and Parr, R.G. (1985). *Proc. Natl. Acad. Sci. U. S. A.* 82: 6723.
- 26 Pearson, R.G. (1973). *Hard and Soft Acids and Bases*. Stroudsburg, PA: Dowden, Hutchinson & Ross.
- 27 Maynard, A.T., Huang, M., Rice, W.G., and Covell, D.G. (1998). *Proc. Natl. Acad. Sci. U. S. A.* 95: 11578.
- 28 Parr, R.G., von Szentpály, L., and Liu, S. (1999). *J. Am. Chem. Soc.* 121: 1922.
- 29 Cohen, A.J., Mori-Sanchez, P., and Yang, W.T. (2008). *Phys. Rev. B* 77: 115123.
- 30 Ayers, P.W. and Parr, R.G. (2000). *J. Am. Chem. Soc.* 122: 2010.
- 31 Gazquez, J.L., Cedillo, A., and Vela, A. (2007). *J. Phys. Chem. A* 111: 1966.
- 32 Ayers, P.W. (2008). *J. Math. Chem.* 43: 285.
- 33 Cedillo, A., Chattaraj, P.K., and Parr, R.G. (2000). *Int. J. Quantum Chem.* 77: 403.
- 34 Cohen, M.H. and Wasserman, A. (2007). *J. Phys. Chem. A* 111: 2229.
- 35 Chattaraj, P.K., Liu, G.H., and Parr, R.G. (1995). *Chem. Phys. Lett.* 237: 171.
- 36 Chattaraj, P.K., Cedillo, A., and Parr, R.G. (1996). *Chem. Phys.* 204: 429.
- 37 Gyftopoulos, E.P. and Hatsopoulos, G.N. (1965). *Proc. Natl. Acad. Sci. U. S. A.* 60: 786.
- 38 Zhang, Y.K. and Yang, W.T. (2000). *Theor. Chem. Accounts* 103: 346.
- 39 Franco-Perez, M., Ayers, P.W., Gazquez, J.L., and Vela, A. (2017). *J. Chem. Phys.* 147: 094105.
- 40 Galván, M., Vela, A., and Gázquez, J.L. (1988). *J. Phys. Chem.* 92: 6470.
- 41 Ghanty, T.K. and Ghosh, S.K. (1994). *J. Am. Chem. Soc.* 116: 3943.
- 42 Garza, J., Vargas, R., Cedillo, A. et al. (2006). *Theor. Chem. Accounts* 115: 257.
- 43 Fukui, K. (1973). *Theory of Orientation and Stereoselection*. Berlin: Springer.
- 44 Fukui, K. (1982). *Science* 218: 747.



- 45 Parr, R.G. and Yang, W. (1984). *J. Am. Chem. Soc.* 106: 4049.
- 46 Ayers, P.W. and Levy, M. (2000). *Theor. Chem. Accounts* 103: 353.
- 47 Chattaraj, P.K., Cedillo, A., and Parr, R.G. (1995). *J. Chem. Phys.* 103: 7645.
- 48 Chattaraj, P.K., Cedillo, A., and Parr, R.G. (1995). *J. Chem. Phys.* 103: 10621.
- 49 Ayers, P.W. and Nagy, A. (2007). *J. Chem. Phys.* 126: 144108.
- 50 Yang, W. and Mortier, W.J. (1986). *J. Am. Chem. Soc.* 108: 5708.
- 51 Vanpoucke, D.E.P., Bultinck, P., and Van Driessche, I. (2013). *J. Comput. Chem.* 34: 405.
- 52 Bultinck, P., Ayers, P.W., and Carbó-Dorca, R. (2007). *J. Chem. Phys.* 126: 144111.
- 53 Ayers, P.W., Morrison, R.C., and Roy, R.K. (2002). *J. Chem. Phys.* 116: 8731.
- 54 Ayers, P.W. (2006). *Phys. Chem. Chem. Phys.* 8: 3387.
- 55 Melin, J., Ayers, P.W., and Ortiz, J.V. (2007). *J. Phys. Chem. A* 111: 10017.
- 56 Echegaray, E., Cardenas, C., Rabi, S. et al. (2013). *J. Mol. Model.* 19: 2779.
- 57 Echegaray, E., Rabi, S., Cardenas, C. et al. (2014). *J. Mol. Model.* 20: 2162.
- 58 Torrent-Sucarrat, M., De Proft, F., Ayers, P.W., and Geerlings, P. (2010). *Phys. Chem. Chem. Phys.* 12: 1072.
- 59 De Proft, F., Liu, S.B., and Parr, R.G. (1997). *J. Chem. Phys.* 107: 3000.
- 60 Chattaraj, P.K., Maiti, B., and Sarkar, U. (2003). *J. Phys. Chem. A* 107: 4973.
- 61 Parthasarathi, R., Padmanabhan, J., Elango, M. et al. (2004). *Chem. Phys. Lett.* 394: 225.
- 62 Harbola, M.K., Chattaraj, P.K., and Parr, R.G. (1991). *Isr. J. Chem.* 31: 395.
- 63 Chattaraj, P.K., Roy, D.R., Geerlings, P., and Torrent-Sucarrat, M. (2007). *Theor. Chem. Accounts* 118: 923.
- 64 Ayers, P.W. and Parr, R.G. (2008). *J. Chem. Phys.* 128: 184108.
- 65 Gal, T. (2012). *Theor. Chem. Accounts* 131: 1223.
- 66 Gal, T., Geerlings, P., De Proft, F., and Torrent-Sucarrat, M. (2011). *Phys. Chem. Chem. Phys.* 13: 15003.
- 67 Cuevas-Saavedra, R., Rabi, N., and Ayers, P.W. (2011). *Phys. Chem. Chem. Phys.* 13: 19594.
- 68 Berkowitz, M., Ghosh, S.K., and Parr, R.G. (1985). *J. Am. Chem. Soc.* 107: 6811.
- 69 Berkowitz, M. and Parr, R.G. (1988). *J. Chem. Phys.* 88: 2554.
- 70 De Proft, F., Liu, S., and Geerlings, P. (1998). *J. Chem. Phys.* 108: 7549.
- 71 Baekelandt, B.G. (1996). *J. Chem. Phys.* 105: 4664.
- 72 Bader, R.F.W. (1990). *Atoms in Molecules: A Quantum Theory*. Oxford, UK: Oxford University Press.
- 73 Silvi, B. and Savin, A. (1994). *Nature* 371: 683.
- 74 Holland, P.R. (1993). *The Quantum Theory of Motion*. Cambridge, UK: Cambridge University Press.
- 75 Chattaraj, P.K. (ed.) (2010). *Quantum Trajectories*. Boca Raton, FL: Taylor and Francis/CRC Press.
- 76 Padmanabhan, J., Parthasarathi, R., Elango, M. et al. (2007). *J. Phys. Chem. A* 111: 9130.
- 77 Morell, C., Grand, A., and Toro-Labbé, A. (2005). *J. Phys. Chem. A* 109: 205.
- 78 Morell, C., Grand, A., and Toro-Labbé, A. (2006). *Chem. Phys. Lett.* 425: 342.

- 79 De Proft, F., Ayers, P.W., Fias, S., and Geerlings, P. (2006). *J. Chem. Phys.* 125: 214101.
- 80 Murray, J.S. and Politzer, P. (1987). *Theor. Chim. Acta* 72: 507.
- 81 Gadre, S.R., Kulkarni, S.A., and Srivastava, I.H. (1992). *J. Chem. Phys.* 96: 5253.
- 82 Koster, A.M., Kolle, C., and Jug, K. (1993). *J. Chem. Phys.* 99: 244.
- 83 Naray-Szabo, G. and Ferenczy, G.G. (1995). *Chem. Rev.* 95: 829.
- 84 Ghosh, S.K., Berkowitz, M., and Parr, R.G. (1984). *Proc. Natl. Acad. Sci. U. S. A.* 81: 8028.
- 85 Parr, R.G., Rupnik, K., and Ghosh, S.K. (1986). *Phys. Rev. Lett.* 56: 1555.
- 86 Ayers, P.W., Parr, R.G., and Nagy, A. (2002). *Int. J. Quantum Chem.* 90: 309.
- 87 Ayers, P.W. (2007). *Chem. Phys. Lett.* 438: 148.
- 88 Deb, B.M. and Chattaraj, P.K. (1989). *Phys. Rev. A* 39: 1696.
- 89 Deb, B.M., Chattaraj, P.K., and Mishra, S. (1991). *Phys. Rev. A* 43: 1248.
- 90 Chattaraj, P.K. (1992). *Int. J. Quantum Chem.* 41: 845.
- 91 Chattaraj, P.K., Sengupta, S., and Poddar, A. (1998). *Int. J. Quantum Chem.* 69: 279.
- 92 Chattaraj, P.K. and Giri, S. (2009). *Annu. Rep. Prog. Chem. C* 105: 13.
- 93 Nagy, A., Parr, R.G., and Liu, S.B. (1996). *Phys. Rev. A* 53: 3117.
- 94 Gal, T. and Nagy, A. (1997). *Mol. Phys.* 91: 873.
- 95 Nagy, A. (2017). *Int. J. Quantum Chem.* 117: 25396.
- 96 Chattaraj, P.K. (2001). *J. Phys. Chem. A* 105: 511.
- 97 Melin, J., Aparicio, F., Subramanian, V. et al. (2004). *J. Phys. Chem. A* 108: 2487.
- 98 Hocquet, A., Toro-Labbé, A., and Chermette, H. (2004). *J. Mol. Struct. (THEOCHEM)* 686: 213.
- 99 Pauling, L. (1960). *The Nature of the Chemical Bond*. Ithaca, NY: Cornell University Press.
- 100 Sanderson, R.T. (1951). *Science* 114: 670.
- 101 Sanderson, R.T. (1954). *J. Chem. Educ.* 31: 238.
- 102 Sanderson, R.T. (1955). *Science* 121: 207.
- 103 Parr, R.G. and Bartolotti, L.J. (1982). *J. Am. Chem. Soc.* 104: 3801.
- 104 Chattaraj, P.K., Lee, H., and Parr, R.G. (1991). *J. Am. Chem. Soc.* 113: 1855.
- 105 Ayers, P.W. (2005). *J. Chem. Phys.* 122: 141102.
- 106 Ayers, P.W., Parr, R.G., and Pearson, R.G. (2006). *J. Chem. Phys.* 124: 194107/1.
- 107 Ayers, P.W. (2007). *Faraday Discuss.* 135: 161.
- 108 Chattaraj, P.K. and Ayers, P.W. (2005). *J. Chem. Phys.* 123: 086101.
- 109 Chattaraj, P.K., Ayers, P.W., and Melin, J. (2007). *Phys. Chem. Chem. Phys.* 9: 3853.
- 110 Chattaraj, P.K. and Schleyer, P.V.R. (1994). *J. Am. Chem. Soc.* 116: 1067.
- 111 Chattaraj, P.K., Gomez, B., Chamorro, E. et al. (2001). *J. Phys. Chem. A* 105: 8815.
- 112 Pearson, R.G. and Chattaraj, P.K. (2009). *Chemtracts-Inorg. Chem.* 21: 1.
- 113 Chattaraj, P.K., Sarkar, U., and Roy, D.R. (2006). *Chem. Rev.* 106: 2065.
- 114 Chattaraj, P.K. and Roy, D.R. (2007). *Chem. Rev.* 107: PR46.
- 115 Chattaraj, P.K., Giri, S., and Duley, S. (2011). *Chem. Rev.* 111: PR43.

- 116 Goodisman, J. (2007). *J. Chem. Phys.* 127: 066101/1.
- 117 Gázquez, J.L., Franco-Perez, M., Ayers, P.W., and Vela, A. (2019). *Int. J. Quantum Chem.* 119: e25797.
- 118 Franco-Perez, M., Ayers, P.W., and Gázquez, J.L. (2016). *Theor. Chem. Accounts* 135: 199.
- 119 Franco-Perez, M., Gázquez, J.L., Ayers, P.W., and Vela, A. (2018). *Acta Phys.-Chim. Sin.* 34: 683.
- 120 Pearson, R.G. (1987). *J. Chem. Educ.* 64: 561.
- 121 Parr, R.G. and Chattaraj, P.K. (1991). *J. Am. Chem. Soc.* 113: 1854.
- 122 Pearson, R.G. (1993). *Acc. Chem. Res.* 26: 250.
- 123 Pearson, R.G. and Palke, W.E. (1992). *J. Phys. Chem.* 96: 3283.
- 124 Torrent-Sucarrat, M., Luis, J.M., Duran, M., and Sola, M. (2001). *J. Am. Chem. Soc.* 123: 7951.
- 125 Chattaraj, P.K. and Sengupta, S. (1996). *J. Phys. Chem.* 100: 16126.
- 126 Ghanty, T.K. and Ghosh, S.K. (1996). *J. Phys. Chem.* 100: 12295.
- 127 Chattaraj, P.K., Fuentealba, P., Gomez, B., and Contreras, R. (2000). *J. Am. Chem. Soc.* 122: 348.
- 128 De Proft, F., Chattaraj, P.K., Ayers, P.W. et al. (2008). *J. Chem. Theor. Comput.* 4: 595.
- 129 Chattaraj, P.K., Fuentealba, P., Jaque, P., and Toro-Labbé, A. (1999). *J. Phys. Chem. A* 103: 9307.
- 130 Chattaraj, P.K., Nath, S., and Sannigrahi, A.B. (1994). *J. Phys. Chem.* 98: 9143.
- 131 Cárdenas-Jirón, G.I. and Toro-Labbé, A. (1995). *J. Phys. Chem.* 99: 12730.
- 132 Cárdenas-Jirón, G.I., Letelier, J.R., and Toro-Labbé, A. (1998). *J. Phys. Chem. A* 102: 7864.
- 133 Gutiérrez-Oliva, S., Letelier, J.R., and Toro-Labbé, A. (1999). *Mol. Phys.* 96: 61.
- 134 Chattaraj, P.K., Gutierrez-Oliva, S., Jaque, P., and Toro-Labbe, A. (2003). *Mol. Phys.* 101: 2841.
- 135 Chattaraj, P.K. and Sengupta, S. (1999). *J. Phys. Chem. A* 103: 6122.
- 136 Chattaraj, P.K. and Sengupta, S. (1997). *J. Phys. Chem. A* 101: 7893.
- 137 Chattaraj, P.K., Roy, D.R., Elango, M., and Subramanian, V. (2006). *J. Mol. Struct. (THEOCHEM)* 759: 109.
- 138 Datta, D. (1986). *J. Phys. Chem.* 90: 4216.
- 139 Tanwar, A., Pal, S., Roy, D.R., and Chattaraj, P.K. (2006). *J. Chem. Phys.* 125: 056101.
- 140 Chattaraj, P.K., Arun Murthy, T.V.S., Giri, S., and Roy, D.R. (2007). *J. Mol. Struct. (THEOCHEM)* 813: 63.
- 141 Chattaraj, P.K., Pérez, P., Zevallos, J., and Toro-Labbé, A. (2001). *J. Phys. Chem. A* 105: 4272.
- 142 Chamorro, E., Chattaraj, P.K., and Fuentealba, P. (2003). *J. Phys. Chem. A* 107: 7068.
- 143 Parthasarathi, R., Elango, M., Subramanian, V., and Chattaraj, P.K. (2005). *Theor. Chem. Accounts* 113: 257.
- 144 Pan, S., Sola, M., and Chattaraj, P.K. (2013). *J. Phys. Chem. A* 117: 1843.
- 145 Chattaraj, P.K. and Giri, S. (2007). *Ind. J. Phys.* 81: 871.

- 146** Noorizadeh, S. and Shakerzadeh, E. (2008). *J. Mol. Struct. (THEOCHEM)* 868: 22.
- 147** Chaquin, P. (2008). *Chem. Phys. Lett.* 458: 231.
- 148** Chattaraj, P.K., Giri, S., and Duley, S. (2010). *J. Phys. Chem. Lett.* 1: 1064.
- 149** Chattaraj, P.K., Chamorro, E., and Fuentealba, P. (1999). *Chem. Phys. Lett.* 314: 114.
- 150** Sears, S.B., Parr, R.G., and Dinur, U. (1980). *Isr. J. Chem.* 19: 165.
- 151** Nalawajski, R.F. and Parr, R.G. (2000). *Proc. Natl. Acad. Sci. U. S. A.* 97: 8879.
- 152** Nagy, A. (2013). *Chem. Phys. Lett.* 556: 355.
- 153** Onicescu, O. (1966). *C. R. Acad. Sci. A-B* 263: 841.
- 154** Fischer, R.A. (1925). *Math. Proc. Camb.* 22: 700.
- 155** Renyi, A. (1960). *Proceedings of Fourth Berkeley Symposium on Mathematical Statistics and Probability*, vol. 1, 547. Berkeley, CA: University of California Press.
- 156** Liu, S.B. (2007). *J. Chem. Phys.* 126: 244103.
- 157** Wu, J., Yu, D., Liu, S. et al. (2019). *J. Phys. Chem. A* 123: 6751.
- 158** Zhou, X.Y., Rong, C.Y., Lu, T. et al. (2016). *J. Phys. Chem. A* 120: 3634.
- 159** Liu, S.B., Rong, C., and Lu, T. (2014). *J. Phys. Chem. A* 118: 3698.
- 160** Wang, B., Rong, C., Chattaraj, P.K., and Liu, S.B. (2019). *Theor. Chem. Accounts* 138: 124.
- 161** Geerlings, P., Chamorro, E., Chattaraj, P.K. et al. (2020). *Theor. Chem. Accounts* 139: 36.
- 162** Geerlings, P., Ayers, P.W., Toro-Labbé, A. et al. (2012). *Acc. Chem. Res.* 45: 683.
- 163** Chakraborty, D. and Chattaraj, P.K. (2021). *Chem. Sci.* 12: 6264.
- 164** Guo, C., He, X., Rong, C. et al. (2021). *J. Phys. Chem. Lett.* 12: 5623.

## **Part II**

### **Extensions**

## 5

### Conceptual DFT and Excited States

Frédéric Guégan<sup>1</sup>, Lynda Merzoud<sup>2</sup>, Henry Chermette<sup>2</sup>, and Christophe Morell<sup>2</sup>

<sup>1</sup>IC2MP, ISA UMR 7285, Université de Poitiers – CNRS, 4, rue Michel Brunet,  
TSA 51106–86073 Cedex 9 Poitiers, France

<sup>2</sup>Université de Lyon, Institut des Sciences Analytiques, UMR 5280, CNRS, Université Lyon 1 - 5,  
rue de la Doua, 69100 Villeurbanne, France

#### 5.1 Introduction

Conceptual density functional theory (DFT) [1–3], by its explicit dependence over the first Hohenberg–Kohn theorem [4], is a ground state theory. Therefore, the very purpose of this chapter may then seem out of scope of conceptual DFT. How can one include excited states in a ground state only representation? And for which aim?

Several approaches were undertaken in the past years to embrace this topic, which we propose to revisit here. Broadly speaking, two axes can be drawn: either one is interested in characterizing the excited states properties, by studying them or conjecturing their properties from the ground state, or either one is interested in using the excited states to improve the representation of the ground state. Illustrations of both ideas are provided in Sections 5.1 and 5.2, respectively. Note, however, this chapter does not aim at being exhaustive. Noticeably, many developments were proposed over the years, especially at times when no efficient computational framework for excited states was available (before the advent of time-dependent density functional theory [TDDFT], so to say). Additionally, some works focused on the development of time-independent DFT models, looking for the definition and construction of either state-specific or generic energy density functionals [5, 6]. We believe such developments, though precious and meaningful, fall out of the scope of the chapter, and for the sake of clarity and concision we decided not to include them in the following.

#### 5.2 Reactivity and Selectivity of Excited States

##### 5.2.1 Photochemical Reactivity

Study of excited states properties is particularly interesting for photochemical reactions (reactions performed under photoexcitation) [7]. Experimentally, it is indeed

often observed that the course of a chemical reaction is altered when this reaction is performed under exposition to light. This is for instance the case of the electrocyclic reactions, whose reactivity is explained by the famous Woodward–Hoffmann rules [8].

In such photochemical reactions, one reactant is electronically excited to one of the very first excited states. Following Kasha's rule [9], light absorption may indeed lead to high excited singlet states, which quickly decay to the lowest excited one ( $S_1$ ). This singlet state may also convert to a lower energy triplet state  $T_1$  through intersystem crossing (ISC). Hence, among the excited states manifold, one may restrict the study to states  $S_1$  and  $T_1$  only to explain photochemical reactivity and selectivity.

The case of triplet state  $T_1$  is noteworthy. Formally speaking, this excited state is indeed a ground state for the triplet spin multiplicity. Hence, many photochemical reactions can be straightforwardly studied by the means of genuine ground state conceptual DFT tools. This has been nicely illustrated by a series of publication from Geerlings and de Proft group in the case of photochemical cycloadditions [10, 11]. They showed that the sign of the hardness variation at the onset of the reaction is a reliable indicator of the feasibility of the reaction (in connection with Woodward–Hoffmann rules) [12]. They also demonstrated, by deriving original spin-polarized descriptors (spin donicity and philicity), that selectivity in the [2+2] photochemical cycloaddition of enones with substituted alkenes is better explained by the differential spin coupling between reactive sites than by standard charge-transfer arguments [13].

### 5.2.2 Insight from Frontier MO Theory

Nonetheless, how can one address cases for which ISC is not active, or not leading to chemical reactivity? In such a case, a genuine excited state ( $S_1$ ) needs to be studied and a model for predicting its chemical behavior should be proposed.

At first, one may rely on the formalism of molecular orbital (MO) theory and employ “usual” approximations to delineate the chemical behavior of the first excited state. If one neglects orbital relaxation, the first excitation may be seen as arising from the promotion of one electron from the highest occupied molecular orbital (HOMO) to the lowest unoccupied molecular orbital (LUMO). The resulting excited state configuration can then be written as  $(\text{HO})^1(\text{LU})^1$ .

This approximate electron configuration can then be used to express usual conceptual density functional theory (C-DFT) descriptors. Let us for instance consider the electrophilic Fukui function [14]. Under the finite difference approximation, it is expressed as the following electron density difference:

$$f_{\text{ex}}^+(\mathbf{r}) = \rho_{N+1}(\mathbf{r}) - \rho_N(\mathbf{r}) \quad (5.1)$$

where the indices refer to the total number of electrons in the system. Here, one has to consider the neutral excited configuration and a configuration with one additional electron ( $N + 1$ ). Keeping the frozen orbital hypothesis, the lowest  $N + 1$  configuration in energy is  $(\text{HO})^2(\text{LU})^1$ . Hence, in the excited state and under the previous

approximations, the electrophilic Fukui function will equal the HOMO density:

$$f_{\text{ex}}^+(\mathbf{r}) = \rho_{\text{HO}}(\mathbf{r}) = f_{\text{gs}}^-(\mathbf{r}) \quad (5.2)$$

which is itself equal to the nucleophilic ground state Fukui function. Using the same line of arguments, one has  $f_{\text{ex}}^-(\mathbf{r}) = f_{\text{gs}}^+(\mathbf{r})$ . Ultimately, one may infer that the dual descriptor (DD) [15] in the excited state will be the opposite of that of the ground state:

$$\Delta f_{\text{ex}}(\mathbf{r}) = f_{\text{ex}}^+(\mathbf{r}) - f_{\text{ex}}^-(\mathbf{r}) = \rho_{\text{HO}}(\mathbf{r}) - \rho_{\text{LU}}(\mathbf{r}) = -\Delta f_{\text{gs}}(\mathbf{r}) \quad (5.3)$$

Sites with positive (respectively negative) values of  $\Delta f(\mathbf{r})$  will be nucleophilic (respectively electrophilic) in  $S_1$  and electrophilic (respectively nucleophilic) in the ground state. Such a simple development was used and allowed to retrieve the regioselectivity of photochemically induced cycloaddition (Woodward–Hoffmann rules) [16]. Even though this naive model holds and provides results in agreement with experiments, there is room for an improved and more grounded theory (Figure 5.1).

### 5.2.3 Chemical Potential Locality

So, how can one derive more general knowledge on the excited states, thus without the need to rely on the rather drastic frozen orbital hypothesis? One of the very few proposals rely on the electronic chemical potential.

Let us recall that the electronic chemical potential  $\mu$  is defined, according to Parr, as the functional derivative of the energy with respect to the electron density:

$$\mu = \left( \frac{\delta E}{\delta \rho(\mathbf{r})} \right)_N = v(\mathbf{r}) + \frac{\delta F_{\text{HK}}[\rho(\mathbf{r})]}{\delta \rho(\mathbf{r})} \quad (5.4)$$

This global quantity interestingly arises from the sum of two local quantities, namely the external potential and the Hohenberg–Kohn universal functional derivative against the density. Actually,  $\mu$  is constant because the ground state

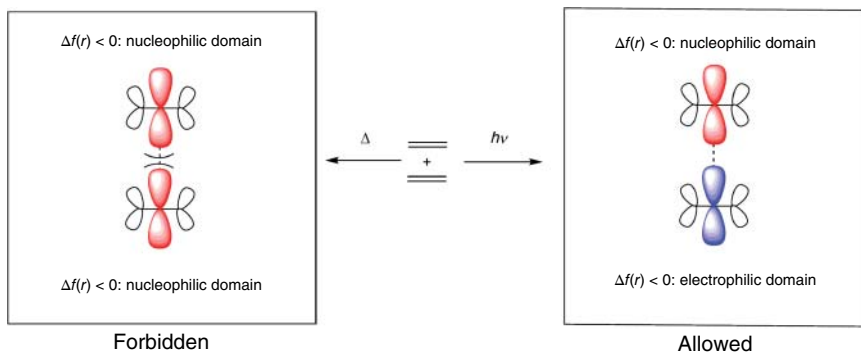


**Figure 5.1** [2+2] cycloaddition of ethylene explained by the dual descriptor. Molecules in the ground state are depicted in red, while molecules in the first excited state are depicted in blue.



electron density is stationary (it minimizes  $E$ ). In 2009, it was proposed to use a vertical excited state density  $\rho_k(\mathbf{r})$  (thus at constant external potential) instead of the ground state electron density in this derivative [17]:

$$\lambda_k(\mathbf{r}) = \left( \frac{\delta E}{\delta \rho_k(\mathbf{r})} \right)_N = v(\mathbf{r}) + \frac{\delta F_{\text{HK}}[\rho_k(\mathbf{r})]}{\delta \rho_k(\mathbf{r})} \quad (5.5)$$

The excited state concerned in the above equation is called Hot Excited State as it is both electronically and vibrationally excited. In this approach,  $\lambda_k$  is a local quantity, since the excited density does not minimize the ground state energy functional. Indeed, the above formulation uses the universal Hohenberg–Kohn functional that only works for ground states. This nonconstant chemical potential is thus fitted to translate the tendency of the electron density to relax to the ground state configuration, at fixed geometry through the integrated equation:

$$dE \approx \int \lambda_k(\mathbf{r}) \delta \rho(\mathbf{r}) d\mathbf{r} \quad (5.6)$$

Levy and Nagy proposed an excited state formulation of DFT in which the Hohenberg–Kohn functional is no longer universal, in the sense that it is a functional of both the electron density and the external potential [18]. To reach a stationary state, the external potential need to evolve (geometry relaxation)

$$E_k = \int \rho_k(\mathbf{r}) \delta v(\mathbf{r}) d\mathbf{r} + F_k[\rho_k(\mathbf{r}), v(\mathbf{r})] \quad (5.7)$$

$\lambda_k$  would have been global should this excited state formulation has been used.

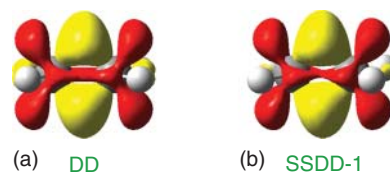
After some developments, it could be shown that for the low-lying excited states one may write

$$\lambda_k(\mathbf{r}) = \mu + \int \frac{\rho_k(\mathbf{r}') - \rho_0(\mathbf{r}')}{|\mathbf{r} - \mathbf{r}'|} d\mathbf{r}' = \mu + \int \frac{\Delta f_k(\mathbf{r}')}{|\mathbf{r} - \mathbf{r}'|} d\mathbf{r}' \quad (5.8)$$

with  $\rho_k$  the  $k$ th excited state electron density (0 meaning ground state), and  $\Delta f_k$  the so-called  $k$ th state-specific dual descriptor (SSDD). Hence, the difference between the global and local potentials is equal to the difference in the electrostatic potential induced by the electron density distributions in the ground and excited states. A site that lost electron density under excitation will then become attractive to electrons in the excited state (thus become electrophilic). Conversely, a site that gained electron density will become repulsive to electrons, thus bear some nucleophilicity.

If we now focus only on the first excited state, then we retrieve our previous results on the signification of the DD sign in the excited states. Indeed, it is often assumed that the first SSDD is equal to the “usual” C-DFT and ground state DD (*vide infra*). Thus, the ground state DD may indeed be used to retrieve the reactivity and selectivity in the first excited state, but the relation between the sign of the DD and the philicities is reversed (see Figure 5.2). Nucleophilic regions will be characterized by a positive sign of the DD in the excited state, while electrophilic regions are associated with a negative DD. Eventually, this model grounds the naive view that the opposite of the ground state DD can ascribe the electro/nucleophilicity of molecular regions. This approach has been successful to recover the Woodward–Hoffmann rules, predict the regioselectivity of Paterno–Buchi reactions [17], and has also been used for explaining DNA photochemically induced lesions [19].

**Figure 5.2** The ground state DD (a) and the first SSDD (b) of ethylen.



#### 5.2.4 In Summary

Very few attempts have been made to propose a theory able to predict the reactivity and selectivity of excited states. Generally, the proposed approaches intend to only tackle the low-lying excited states, which are expected to be the major player in photoreactivity. In fact, in several cases, these excited states are formally ground states for the triplet multiplicity; hence, ground state descriptors are perfectly working.

Otherwise, the electron densities can be described from a Taylor's expansion of the ground state density, allowing to delineate excited state properties using "standard" C-DFT developments. In this spirit, a descriptor based on a local chemical potential was proposed and successfully applied to predict the regioselectivity of various [2+2] photochemical cycloadditions.

### 5.3 Excited States Used to Describe the Ground State

The use of excited states to understand the reactivity of a ground state electron system goes back to a publication by Walsh in the 1940s [20]. At that time, Walsh was arguing that ethylene oxide and ethylene are more reactive than ethane because the first excited state wavelengths of the former are lower (respectively 1950 and 1745 Å) than that of the latter. After this first rough approach, the subject was left almost untouched till Pearson [21], Bader [22], and Salem [23] revived it up in the 1960s. In three different papers, they provided a series of conditions for an excited state to favor a chemical reaction. In this part, starting from their development, it is shown that lot of information about the ground state reactivity, region, and stereoselectivity can be obtained from the excited states.

#### 5.3.1 Reactivity from Excitation Energy: An Early Formulation of the Maximum Hardness Principle

In the late 1980s, Pearson was working on the physical meaning of the chemical potential and the absolute hardness. His main concern was chemical reactivity and how to compare the stability of molecules. In the following years, he was about to propose the Maximum Hardness Principle. In this context, he published an article in the journal of the American Chemical Society entitled "Electronic spectra and chemical reactivity" [24]. In this paper, actually a follow-up of the series of original papers published by Bader, Salem, and himself, he proposed a reactivity model based on the wavefunction and energy perturbation of a molecular fragment experiencing a modification of its surrounding, due for instance to the approach of another

molecule or an internal reorganization (isomerization). Its perturbed wavefunction, as it is common in this theory, was expanded through the set of the unperturbed eigenfunctions.

Following Pearson's notation, let  $U$  be the nuclear–nuclear and nuclear–electron potential energy, and  $Q$  be the reaction coordinate. The molecular (total) Hamiltonian can be expanded as a Taylor series:

$$H = H_0 + \left( \frac{\partial U}{\partial Q} \right) Q + \frac{1}{2} \left( \frac{\partial^2 U}{\partial Q^2} \right) Q^2 + \dots \quad (5.9)$$

and according to Rayleigh–Schrödinger perturbation theory ground state energy and wavefunction vary according to the perturbation as:

$$E = E_0 + \left\langle \psi_0 \left| \frac{\partial U}{\partial Q} \right| \psi_0 \right\rangle Q + \left\langle \psi_0 \left| \frac{\partial^2 U}{\partial Q^2} \right| \psi_0 \right\rangle \frac{Q^2}{2} + \sum_{k \neq 0} \frac{\left[ \left\langle \psi_0 \left| \frac{\partial U}{\partial Q} \right| \psi_k \right\rangle Q \right]^2}{E_0 - E_k} \quad (5.10)$$

$$\psi = \psi_0 + \sum_{k \neq 0} \frac{\left\langle \psi_0 \left| \frac{\partial U}{\partial Q} \right| \psi_k \right\rangle Q}{E_0 - E_k} \psi_k \quad (5.11)$$

where  $(E_0, \psi_0)$  and  $(E_k, \psi_k)$  are the unperturbed solutions of the Schrödinger equation for, respectively, the ground and  $k$ th excited state.

Pearson then used Eqs. (5.10) and (5.11) to deduce simple rules to evaluate the reactivity of a given compound. In the energy response, he noticed that the two first terms basically translate how the energy changes when nuclei move while electron density remains frozen. Obviously, if the reference geometry is a minimum, this contribution is positive (destabilization). On the other hand, the last contribution is stabilizing, since the numerator is by construction positive, while denominator is negative. This term translates the energy change experienced by the system as the electronic configuration is changed along the perturbation. As such, chemical reaction will take place only in cases where the last term has non-negligible values. This will be more likely to occur if transition energies  $E_k - E_0$  are small; thus, easily excitable compounds are expected to be rather reactive. Lot of examples were provided to support Pearson's statement that *the lower the excitation energy, the more reactive the molecule*. As for instance, the nucleophilic attack of carbonyl compounds that turn out to be easier in the following order:  $\text{HCOF}(45.5 \times 10^3 \text{ cm}^{-1}) > \text{CH}_3\text{COCl}(42.6 \times 10^3 \text{ cm}^{-1}) > \text{CH}_3\text{COCH}_3(35 \times 10^3 \text{ cm}^{-1}) > \text{CH}_3\text{CHO}(34 \times 10^3 \text{ cm}^{-1}) > \text{CH}_2 = \text{CHCHO}(26.5 \times 10^3 \text{ cm}^{-1})$ . Another example given was the decreasing bond strength of the following alkylhalides:  $\text{CH}_3\text{F}(75.4 \times 10^3 \text{ cm}^{-1}) > \text{CH}_3\text{Cl}(59 \times 10^3 \text{ cm}^{-1}) > \text{CH}_3\text{Br}(50 \times 10^3 \text{ cm}^{-1}) > \text{CH}_3\text{I}(38.5 \times 10^3 \text{ cm}^{-1})$ . The numbers between brackets are the first excitation wavenumbers. Later, it has been shown by Nagy [25] that the first excitation energy is very likely the best way to measure the hardness of a molecule. As a consequence, Pearson's article can be retrospectively regarded as an early formulation of the Principle of Maximum Hardness. A question naturally follows: would it be possible to get regioselectivity information by pursuing this research axis?

### 5.3.2 States-Specific Dual Descriptors

At the core of Pearson's and Bader's approaches, one finds perturbation theory, which basically states that response to perturbation of a given system can be developed on the basis of its unperturbed eigenstates. Then, treating chemical interaction as a perturbation and identifying eigenstates as the set of ground and excited states, it is possible to account for the ground state chemical properties through a careful analysis of the excited states.

In a related approach, it was proposed in 2013 that evolution of the electron density along a chemical process, that is, following a reaction coordinate, could also be extrapolated from a set of excited state electron densities [26]. More specifically, it was proposed that ground state electron density at a given point  $P$  on the potential energy surface, closer to the transition state of interest than the reagent  $R$  is, reads

$$\rho_{P,0}(\mathbf{r}) = \sum_{i \geq 0} \alpha_i \rho_{R,i}(\mathbf{r}) \quad (5.12)$$

where indices  $P$  and  $R$  refer to the geometry, and  $i$  to the energy state ( $i$ th excited state, 0 meaning ground state). From the conservation of the electron number, we directly obtain that

$$\sum_{i \geq 0} \alpha_i = 1 \quad (5.13)$$

from which we see that electron density reorganization from  $R$  to  $P$  is

$$\Delta \rho_{R \rightarrow P}(\mathbf{r}) = \sum_{i \geq 1} \alpha_i [\rho_{R,i}(\mathbf{r}) - \rho_{R,0}(\mathbf{r})] = \sum_{i \geq 1} \alpha_i \Delta f_{R,i}(\mathbf{r}) \quad (5.14)$$

Thus, one gets that electron density reorganization along a chemical process can be expressed thanks to the electron density reorganization under excitation of the reagent. Analytical formulas for the coefficients  $\alpha$  are unknown, but following Pearson's arguments it may be expected that high-lying excited states will not contribute significantly to the ground state reactivity. Following Fukui's development, one may even expect that the first excited state, likely stemming from a HO  $\rightarrow$  LU excitation, will be the principal player. Under a frozen orbital hypothesis, such a transition will indeed yield

$$\Delta f_{R,1}(\mathbf{r}) = \rho_{R,1}(\mathbf{r}) - \rho_{R,0}(\mathbf{r}) = \rho_{R,LU}(\mathbf{r}) - \rho_{R,HO}(\mathbf{r}) \approx \Delta f(\mathbf{r}) \quad (5.15)$$

Thus, the electron density reorganization from  $R$  to  $P$  will be roughly equal to the frontier molecular orbital (FMO) approximation of the DD. From this identification, it was proposed to coin  $\Delta f_i = \rho_i - \rho_0$  the  $i$ th SSDD.

Interestingly, though in most cases the correct reactivities and selectivities are grasped by the first SSDD (see Figure 5.2), situations arise where higher excitations are required (in line with Pearson's observation). This is obviously expected for cases where frontier molecular orbital theory (FMOT) itself is failing. But more interestingly, this is also often the case when one studies reactant complexes at the onset of a chemical reaction – thus with a rather large separation between reagents [27]. An illustrative example is given below. In Figure 5.3, both the second and third

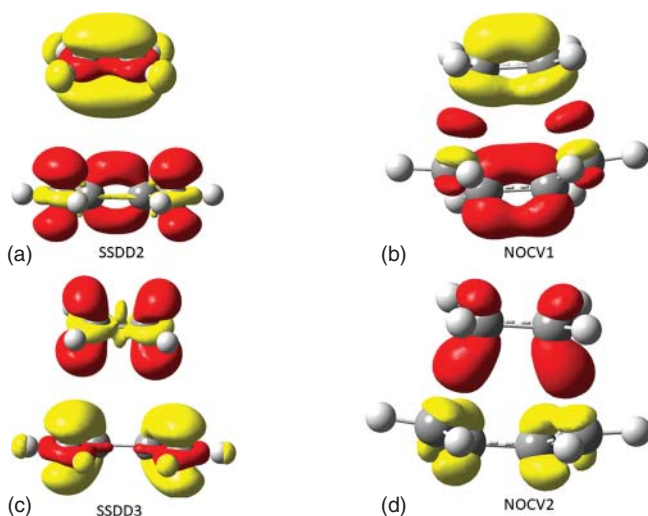


**Figure 5.3** SSDD and NOCV 3D maps pertaining to the [4+2] cycloaddition between ethylene (top) and butadiene (bottom): (a) second SSDD, (b) first NOCV, (c) third SSDD, and (d) second NOCV, in red regions where both functions are positive, in yellow regions where both functions are negative.

SSDDs are represented on the top and bottom left, and on the top and bottom right the electron density reorganisation associated to the first and second natural orbitals for chemical valence (NOCV) for a butadiene–ethylene complex. Basically, the NOCVs analyse in terms of orbitals the electron density deformation during a chemical reaction. The first SSDD actually consists on an intra-fragment excitation located on butadiene that quite likely suggests that butadiene is more prone to react with itself than with ethylene. It is in perfect line with the FMOT as both butadiene HOMO and LUMO are located in between those of ethylene making the [4+2] cyclo-adduct of butadiene with itself the major product of the reaction. Nonetheless, the first density reshuffling located on one reagent alone does not necessarily bring relevant information about reactivity or selectivity. On the other hand, charge transfers from one reagent to the other may be observed in higher excited states, and thus translate how electron density is likely to distort along the reaction path, especially regarding the direction of the easiest electron flow. SSDD may then ascertain the reagents relative to philicities and site selectivities, as expected for a DD avatar. Still on the example of cycloaddition between butadiene and ethylene, it can be observed on figure 5.3 that the second SSDD describes the electron donation from the ethylene to butadiene, while the third SSDD pictures the back donation from ethylene to butadiene. Interestingly, these inter-fragment SSDDs uncannily look like the first and second ETS-NOCVs density deformations calculated at the transition state structure [27].

Dewar [28] pointed out in his critic isoquinoline, as a usual heterocycle for which the use of FMOT fails to predict the correct orientation of electrophilic aromatic substitution (EAS). Using HOMO coefficients, FMOT suggests that the order of

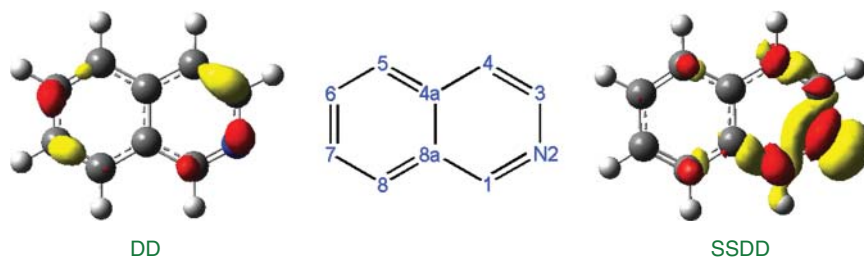


**Figure 5.4** The usual DD and SSDD for isoquinoline, in red regions where both functions are positive, in yellow regions where both functions are negative (Isovalue = 0.005 a.u.)

reactivity is  $C4 < C5 < C8$  and is not in good agreement with the experimental data. Indeed, the 4-derivative has never been observed. All the experimental results are consistent with a high reactivity of carbon C5 followed closely by carbon C8.

Concerning the regioselectivity of the EAS, it seems that the DFT-based descriptors, such as Fukui functions or the usual DD, are not better than FMOTs. As can be seen in Figure 5.4, the usual DD and the first SSDD calculated for isoquinoline are different. As can be seen, the usual DD does not give the correct prediction of regioselectivity. Therefore, for the usual DD, EAS should occur at carbons 3 and 7, the positions known to be nonreactive with respect to EAS. The first SSDD provides an alternative prediction. It indicates that the electrophiles should target the nitrogen lone pair. This example underlines the advantage of calculating the DD using excited states. Once protonated, the DD and the first SSDD of isoquinoline become identical.

In a final note, it is interesting to note that resorting to explicit evaluation of excited states has two significant advantages. First, since excited states are not restricted to single MO excitations, SSDDs are expected to incorporate fine details about the electron density reorganization, e.g.  $\sigma$  relaxation for a reaction involving unsaturated compounds. MO relaxation may thus be grasped, at least partially. Second, as a “side-product” of the excited state calculations, one ends up with charge transfer excitation energies. These energies could serve as quantitative reactivity indicators, as long as one is interested in comparable chemical systems. Interestingly, this point was overlooked so far.

### 5.3.3 Electron Polarization Rationalized with Excited States

In 2020, some of the present authors retraced Pearson's, Walsh', and Bader's footsteps and used explicit Rayleigh–Schrödinger perturbation theory to study the response of a chemical system [29]. The premises are thus known: let  $\mathcal{H}_{\text{pert}}$  be a perturbation Hamiltonian, acting on a system whose quantum states  $(E_n, |n\rangle)$  are known. From the first-order development of the ground state wavefunction,

$$|\psi\rangle = c_0 \left( |0\rangle + \sum_{k \neq 0} \frac{\langle k | \mathcal{H}_{\text{pert}} | 0 \rangle}{E_0 - E_k} |k\rangle \right) = c_0 \left( |0\rangle + \sum_{k \neq 0} c_k |k\rangle \right) \quad (5.16)$$

it is possible to express the perturbed electron density:

$$\rho_{\text{pert}}(\mathbf{r}) = \langle \psi | \hat{\rho}(\mathbf{r}) | \psi \rangle \approx \rho_0(\mathbf{r}) + 2 \sum_{k \neq 0} c_k \rho_k^0(\mathbf{r}) \quad (5.17)$$

In the previous expressions,  $c_0$  is a normalization constant, which is assumed to be close to unity (small perturbation), and  $\rho_k^0 = \langle k | \hat{\rho}(\mathbf{r}) | 0 \rangle$  is the transition density from the ground state to the excited state  $k$ .<sup>1</sup>

Electron density reshuffling under perturbation will thus be

$$\delta\rho(\mathbf{r}) = \rho_{\text{pert}}(\mathbf{r}) - \rho_0(\mathbf{r}) = 2 \sum_{k \neq 0} c_k \rho_k^0(\mathbf{r}) \quad (5.18)$$

hence be expressed as a weighted sum of transition densities, which can themselves be obtained from any TDDFT calculation. Several features of  $\delta\rho$  deserve to be delineated. First, if the perturbation is designed to mimic the approach of a reagent, then this quantity translates the electron density polarization caused by this approach. This is a missing term in usual reactivity developments (Klopman–Salem [30, 31] for instance) and relates to soft/hard interactions in the nomenclature of Pearson. Interestingly, it proves more relevant than expected to describe chemical reactivity and selectivity, as various known chemical properties can be grasped from such a quantity.

Second, since transition densities integrate to 0, so does  $\delta\rho$ : we indeed work at constant electron count. Regarding the  $c_k$  coefficients, it may be noted that they are decreasing as excitation energy increases, thus only the lowest excited states need to be computed. Nevertheless, and in perfect line with Pearson, one cannot rely on the very first excited states alone, since the numerator may be negligible for these states (poor overlap between unperturbed states through the perturbation). In fact, in the case of a simple point charge perturbation, it could be shown that the largest contribution could stem from rather high excited states – up to the 33rd excitation in the case of a cobalt complex!

Similarly, energy responses can be defined, up to the second order:

$$E^{(1)} = \langle 0 | \mathcal{H}_{\text{pert}} | 0 \rangle \quad (5.19)$$

$$E^{(2)} = - \sum_{k \neq 0} \frac{|\langle k | \mathcal{H}_{\text{pert}} | 0 \rangle|^2}{E_k - E_0} = - \sum_{k \neq 0} c_k^2 (E_k - E_0) \quad (5.20)$$

If the perturbation Hamiltonian is the electrostatic potential induced by a point charge at point  $\mathbf{r}$ ,  $E^{(1)}$  will then simply be proportional to the electronic component of the molecular electrostatic potential (MEP) at point  $\mathbf{r}$ . It will be stabilizing if the point charge is positive, and destabilizing otherwise.

On the other hand,  $E^{(2)}$  will always be a stabilizing contribution, translating the stabilization undergone by the system by distorting its electron density within the perturbing potential. Following Pearson, if we consider a perturbation potential mimicking the approach of a reagent, the favored geometry of approach should be

<sup>1</sup> Note this quantity is different from the  $k$ th SSDD,  $\Delta f_k(\mathbf{r}) = \langle k | \hat{\rho}(\mathbf{r}) | k \rangle - \langle 0 | \hat{\rho}(\mathbf{r}) | 0 \rangle$ .

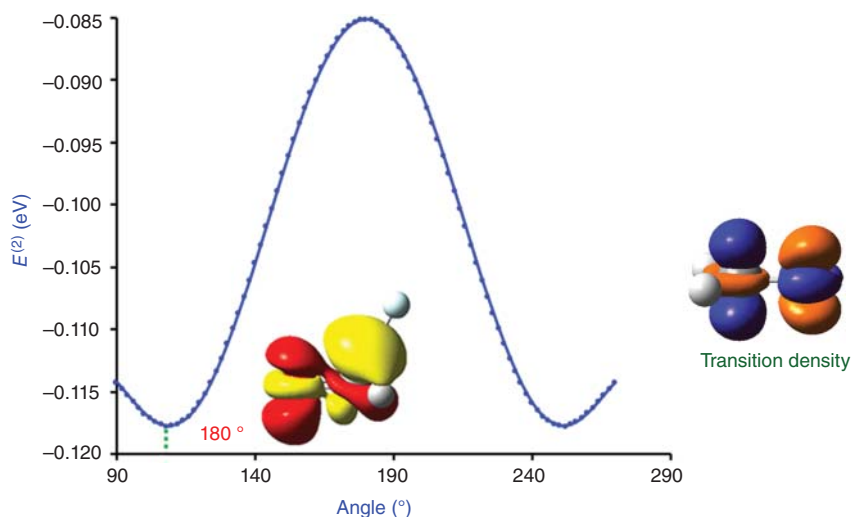


**Figure 5.5** Seventh formaldehyde transition density and electron density response for formaldehyde perturbed by a  $-0.5$  a.u. point charge placed at  $2 \text{ \AA}$  from the C atom, represented by the light blue sphere. Color scheme:  $\delta\rho > 0$ , red;  $\delta\rho < 0$ , yellow. Isodensity:  $0.0004$  a.u.

associated with the most negative (stabilizing) value of  $E^{(2)}$ . Hence, polarization energy can bring valuable information on reactivity and selectivity. And indeed, studying the evolution of  $E^{(2)}$  for carbonyl compounds perturbed by a negative point charge placed at a constant distance from the C and for various angles of attack on the C=O function, the well-known Bürgi–Dunitz angle of attack can be retrieved, see Figure 5.5. According to the density polarization sign, the main excited state involved in this charge transfer is associated with the promotion of a small fraction of electron of the  $\pi(\text{C}=\text{O})$  bonding orbital to the  $\pi^*(\text{C}=\text{O})$  antibonding orbital. The transition density that allows this electron excitation is represented in Figure 5.5.

In a further study, it could furthermore be shown that the more the system can spread its electron density reorganization, both through space and among the excited states manifold, the larger the second-order stabilization [32]. This could in fact be quantified. Recalling Eq. (5.16) and considering we now study a large number of replicas of the molecule under study, one may see that  $c_k^2$  will provide the proportion of molecules reaching excited state  $k$  as a consequence of perturbation. Thus, the collection of  $c_k^2$  values (including  $c_0^2 = 1 - \sum c_k^2$ ) is a statistical distribution of excited states populations induced by perturbation. According to Gibbs and Shannon, an entropy can be associated with this statistical distribution:

$$S = -k_B \sum_k c_k^2 \ln c_k^2 \quad (5.21)$$

It may be noted that the same entropy can be defined for the unperturbed system ( $c_k = \delta_{0k}$ ) but it equals 0. Hence,  $S$  here can be alternatively seen as the entropy of the perturbed configuration or the entropy change induced by the perturbation.



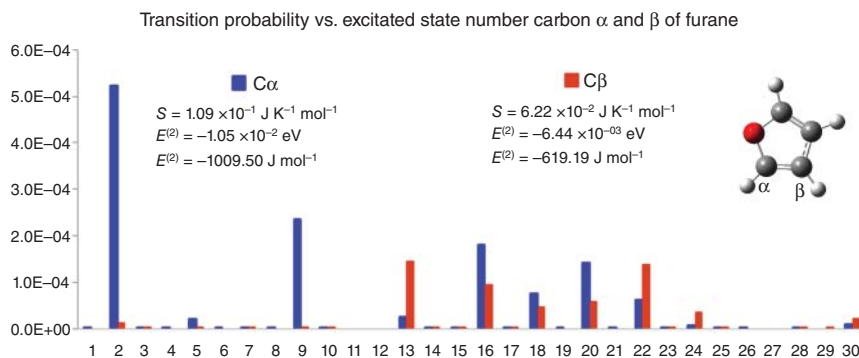


**Figure 5.6** Polarization spectrum when C $\alpha$  and C $\beta$  are perturbed by a  $0.1e$  point charge.

Strong correlations were observed between  $E^{(2)}$  and  $S$  values for a given system, confirming that most reactive positions in molecules lead to a maximal response in terms of excited states population.

This is, for instance, illustrated in the case of furan in Figure 5.6: placing a  $0.1e$  perturbing point charge on carbon atom C $\alpha$  results in a much larger polarization response, translated either in the transition probabilities for each excited state or in the total entropy, than placing the same charge on carbon atom C $\beta$ . At the same time, polarization energy is significantly more stabilizing in the case of a perturbation at C $\alpha$ , in the line with the expected higher reactivity on this position.

In fact, successively perturbing all nuclei in the furan molecule allows to draw a clear linear relation between entropy and energy, as shown in Figure 5.7. This linearity suggests that a statistical temperature,

$$T = \left( \frac{\partial E}{\partial S} \right) \quad (5.22)$$

could be constructed, if not rigorously defined. Here, one obtains  $T = 9300 \text{ K}$ , which is interestingly in agreement with the calculated temperature necessary to excite 1% of the total population of a collection of molecules in the first excited state.

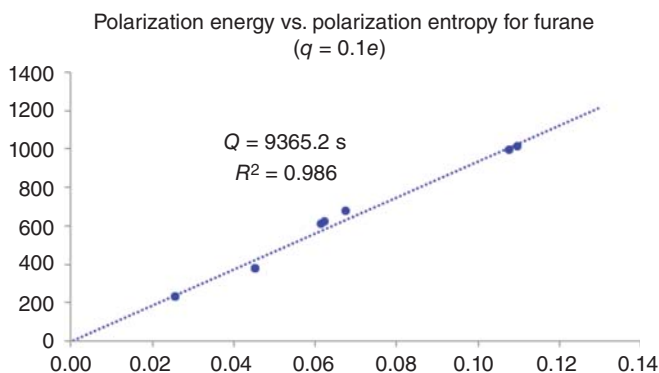


**Figure 5.7** Absolute polarization energy vs. entropy for furane;  $q = 0.1e$ .

Linearity in the  $E = f(S)$  plots was also shown in various other examples, suggesting this is a general feature. In the end, external perturbation can be seen as interaction with a “heat source,” and polarization as a heat exchange between the perturber and the system. Said otherwise, interaction of two reagents along a chemical reaction could be understood in terms of heating and cooling; it is then possible to say “how hot” or “how cold” an electron density is expected to become as a consequence of the approach of a reagent.

### 5.3.4 In Summary

To summarize, by its very vocabulary and concepts, chemistry invites to study chemical reactions through a “perturbation perspective.” As such, it is not surprising that mathematical expressions derived in this context rely explicitly on excited states. But, this is not a mere mathematical coincidence. In fact, as pointed out first by Walsh, a formal connection between reactivity and excitability is expected, since both properties are linked to the propensity of the electron distribution in a system to reorganize under external stress. It is also not surprising that Pearson came to the same idea, since he proposed to analyze reactivity through polarizability, which is also another way to describe the plasticity of the electron distribution. Overall, reactivity can then be conceived as “states-specific” excitation of a molecule induced by the approach of a reagent, or conversely excitation can be seen as a “reagent-specific” distortion of the electron cloud in view of a reaction.

## 5.4 Conclusion and Perspectives

In a more general conclusion, although C-DFT is usually conceived as a ground state theory, extensions to excited states are possible. As retraced previously, one can either focus on the properties of excited states themselves or try to extract ground state properties from excitations (through a perturbation framework). Formally speaking, both ideas were already present in early theoretical developments (in Walsh’s, Bader’s, Fukui’s, and Pearson’s papers, for instance). Nevertheless, it is only rather recently – say in the last 20 years or so – that they bloomed, owing to the developments of more and more efficient tools to compute excited states. Nowadays, excited state calculations are rather cheap, and computer developments allows the simultaneous calculation of large sets of excited states for relatively large systems; hence, “brute force” evaluations are now feasible.

Because of this, it could be tempting to declare that the perspectives are rather limited, since equations are known and can now be evaluated. Yet, the case of the electron density polarization illustrates that there is always room for more development. First, this phenomenon proved to be more relevant than expected, although polarization is the fifth wheel of usual reactivity model.

Second, a quantity displaying the features of a temperature could be constructed from polarization. What is the actual meaning and extent of this temperature? Could it be used to help developing T-dependent DFT models?

## References

- 1 Chermette, H. (1999). Chemical reactivity indexes in density functional theory. *J. Comput. Chem.* 20 (1): 129–154.
- 2 Geerlings, P., De Proft, F., and Langenaeker, W. (2003). Conceptual density functional theory. *Chem. Rev.* 103 (5): 1793–1873.
- 3 Geerlings, P., Chamorro, E., Chattaraj, P.K. et al. (2020). Conceptual density functional theory: status, prospects, issues. *Theor. Chem. Acc.* 139 (2).
- 4 Hohenberg, P. and Kohn, W. (1964). Inhomogeneous electron gas. *Phys. Rev.* 136: B864.
- 5 Görling, A. (1999). Density-functional theory beyond the Hohenberg–Kohn theorem. *Phys. Rev. A* 59: 3359–3374. <https://doi.org/10.1103/PhysRevA.59.3359>.
- 6 Ayers, P.W., Levy, M., and Nagy, A. (2012). Time-independent density-functional theory for excited states of coulomb systems. *Phys. Rev. A* 85: 042518. <https://doi.org/10.1103/PhysRevA.85.042518>.
- 7 International Union of Pure & Applied Chemistry (2020). "Photoreaction", IUPAC Compendium of Chemical Terminology – The Gold Book. <https://goldbook.iupac.org/terms/view/P04585> (accessed 18 October 2021).
- 8 Woodward, R.B. and Hoffmann, R. (1965). Stereochemistry of electrocyclic reactions. *J. Am. Chem. Soc.* 87 (2): 395–397.
- 9 Kasha, M. (1950). Characterization of electronic transitions in complex molecules. *Discuss. Faraday Soc.* 9: 14–19.
- 10 Pintér, B., De Proft, F., Veszprémi, T., and Geerlings, P. (2005). Regioselectivity in the [2+2] cyclo-addition reaction of triplet carbonyl compounds to substituted alkenes (Paterno–Buchi reaction): a spin-polarized conceptual DFT approach. *J. Chem. Sci.* 117 (5): 561–571.
- 11 De Proft, F., Ayers, P.W., Fias, S., and Geerlings, P. (2006). Woodward–Hoffmann rules in density functional theory: initial hardness response. *J. Chem. Phys.* 125 (21): 214101.
- 12 De Proft, F., Chattaraj, P.K., Ayers, P.W. et al. (2008). Initial hardness response and hardness profiles in the study of Woodward–Hoffmann rules for electrocyclizations. *J. Chem. Theor. Comput.* 4 (4): 595–602.
- 13 De Proft, F., Fias, S., Van Alsenoy, C., and Geerlings, P. (2005). Spin-polarized conceptual density functional theory study of the regioselectivity in the [2+2] photocycloaddition of enones to substituted alkenes. *J. Phys. Chem. A* 109 (28): 6335–6343.
- 14 Parr, R.G. and Yang, W. (1984). Density functional approach to the frontier-electron theory of chemical reactivity. *J. Am. Chem. Soc.* 106 (14): 4049–4050.
- 15 Morell, C., Grand, A., and Toro-Labbé, A. (2005). New dual descriptor for chemical reactivity. *J. Phys. Chem. A* 109 (1): 205–212.
- 16 Ayers, P.W., Morell, C., De Proft, F., and Geerlings, P. Understanding the Woodward–Hoffmann rules by using changes in electron density. *Chem. Eur. J.* 13 (29): 8240–8247.

- 17 Morell, C., Labet, V., Grand, A. et al. (2009). Characterization of the chemical behavior of the low excited states through a local chemical potential. *J. Chem. Theor. Comput.* 5 (9): 2274–2283.
- 18 Levy, M. and Nagy, A. (1999). Variational density-functional theory for an individual excited state. *Phys. Rev. Lett.* 83 (21): 4361–4364.
- 19 Morell, C., Labet, V., Ayers, P.W. et al. (2011). Use of the dual potential to rationalize the occurrence of some DNA lesions (pyrimidic dimers). *J. Phys. Chem. A* 115 (27): 8032–8040.
- 20 Walsh, A.D. (1949). The structures of ethylene oxide, cyclopropane, and related molecules. *Trans. Faraday Soc.* 45: 179–190.
- 21 Pearson, R.G. (1969). A symmetry rule for predicting molecular structure and reactivity. *J. Am. Chem. Soc.* 91 (5): 1252–1254.
- 22 Bader, R.F.W. (1962). Vibrationally induced perturbations in molecular electron distributions. *Can. J. Chem.* 40 (6): 1164–1175.
- 23 Salem, L. (1969). Conditions for favorable unimolecular reaction paths. *Chem. Phys. Lett.* 3 (2): 99–101.
- 24 Pearson, R.G. (1988). Electronic spectra and chemical reactivity. *J. Am. Chem. Soc.* 110 (7): 2092–2097.
- 25 Nagy, A. (2005). Hardness and excitation energy. *J. Chem. Sci.* 117 (5): 437–440.
- 26 Tognetti, V., Morell, C., Ayers, P.W. et al. (2013). A proposal for an extended dual descriptor: a possible solution when frontier molecular orbital theory fails. *Phys. Chem. Chem. Phys.* 15: 14465–14475.
- 27 De Proft, F., Forquet, V., Ourri, B. et al. (2015). Investigation of electron density changes at the onset of a chemical reaction using the state-specific dual descriptor from conceptual density functional theory. *Phys. Chem. Chem. Phys.* 17: 9359–9368.
- 28 Dewar, M.J.S. (1989). A critique of frontier orbital theory. *J. Mol. Struct. THEOCHEM* 200: 301–323.
- 29 Guégan, F., Pigeon, T., De Proft, F. et al. (2020). Understanding chemical selectivity through well selected excited states. *J. Phys. Chem. A* 124 (4): 633–641.
- 30 Klopman, G. (1968). Chemical reactivity and the concept of charge and Frontier-controlled reactions. *J. Am. Chem. Soc.* 90 (2): 223–234.
- 31 Salem, L. (1968). Intermolecular orbital theory of the interaction between conjugated systems. I. General theory. *J. Am. Chem. Soc.* 90 (3): 543–552. <https://doi.org/10.1021/ja01005a001>.
- 32 Guégan, F., Tognetti, V., Martínez-Araya, J.I. et al. (2020). A statistical thermodynamics view of electron density polarisation: application to chemical selectivity. *Phys. Chem. Chem. Phys.* 22: 23553–23562.

## 6

**Chemical Response Functions in (Quasi-)Degenerate States***Patrick Bultinck<sup>1</sup> and Carlos Cárdenas<sup>2,3</sup>*<sup>1</sup>*Ghent University, Department of Chemistry, Krijgslaan 281 (S3), 9000 Gent, Belgium*<sup>2</sup>*Centro para el Desarrollo de la Nanociencia y la Nanotecnología (CEDENNA), Avda. Ecuador 3493, Santiago 9170124, Chile*<sup>3</sup>*Departamento de Física, Facultad de Ciencias, Universidad de Chile, 653-Santiago, Chile***6.1 Introduction**

In density functional theory (DFT), the energy is a function of the electron density which is, in turn, intimately and uniquely linked to the external potential and the number of electrons [1]. Hence, the energy can also be expressed as  $E[N, v_{\text{ext}}]$ , where  $E$  is the energy,  $N$  is the number of electrons, and  $v_{\text{ext}}$  is the external potential and so a function of position  $\mathbf{r}$ , so  $v_{\text{ext}} \equiv v_{\text{ext}}(\mathbf{r})$  [1]. The intimate connection between the electron density  $\rho(\mathbf{r})$  and the external potential is central in the Hohenberg–Kohn theorem [2]. The first Hohenberg–Kohn theorem in its original proof is an *ex absurdo* proof. If one considers two systems  $A$  and  $B$  and thus two Hamiltonians that *only* differ in the external potential (but more than the addition of a constant), it is straightforward to show that the two systems cannot have the same density:  $\rho_A(\mathbf{r}) \neq \rho_B(\mathbf{r}) : \forall \mathbf{r}$ . So at some points the density may be the same but not for all points. This entails that the difference in the external potential is embedded in the electron density, and there is a unique correspondence between both. In fact, the so-called holographic electron density theorem [3] states that each and every positive volume density fragment already encodes the complete molecular information. The complete molecular information provided by the Hohenberg–Kohn theorem is already provided, in full, by any arbitrarily small electron density fragment. There is, however, a major caveat in the proof of the Hohenberg–Kohn theorem. The variation theorem is used with the exclusion of the equality, so the ground states cannot be degenerate. This constraint is admittedly relieved in Levy’s constrained search method [4] by including degenerate wave functions in the space of Hilbert that produces a given density. This, however, remains a problem in conceptual DFT.

The energy may be written as a Taylor expansion in terms of  $N$  and  $v_{\text{ext}}$ . Chemical interactions and reactions can be considered processes where for each of the reacting partners, these ingredients change as a function of the progress of the reaction [5].

Starting from a number of electrons  $N^0$  and external potential  $v_{\text{ext}}^0$ , the energy of a system for a number of electrons  $N$  and external potential  $v_{\text{ext}}$  is given by

$$\begin{aligned}
 E[v_{\text{ext}}, N] &= E[v_{\text{ext}}^0, N^0] + \left( \frac{\partial E[v_{\text{ext}}, N]}{\partial N} \right)_{\substack{v_{\text{ext}} = v_{\text{ext}}^0 \\ N = N^0}} (N - N^0) \\
 &+ \frac{1}{2} \left( \frac{\partial^2 E[v_{\text{ext}}, N]}{\partial N^2} \right)_{\substack{v_{\text{ext}} = v_{\text{ext}}^0 \\ N = N^0}} (N - N^0)^2 + \dots \\
 &+ \int \left( \frac{\delta E[v_{\text{ext}}, N]}{\delta v_{\text{ext}}(\mathbf{r})} \right)_{\substack{v_{\text{ext}} = v_{\text{ext}}^0 \\ N = N^0}} (v_{\text{ext}}(\mathbf{r}) - v_{\text{ext}}^0(\mathbf{r})) d\mathbf{r} + \dots \\
 &+ \int \left( \frac{\partial \delta E[v_{\text{ext}}, N]}{\partial N \delta v_{\text{ext}}(\mathbf{r})} \right)_{\substack{v_{\text{ext}} = v_{\text{ext}}^0 \\ N = N^0}} (N - N^0) (v_{\text{ext}}(\mathbf{r}) - v_{\text{ext}}^0(\mathbf{r})) d\mathbf{r} + \dots
 \end{aligned} \tag{6.1}$$

The entire area of conceptual DFT [1, 6–10] is built around the expansion coefficients and their use and meaning in chemical reactions. It is clear from the above that energy derivatives play a very major part in all of conceptual DFT. Many of the terms have a specific chemical meaning, but most often the theoretical background is only given based on nondegenerate states. Cardenas et al. [11] realized that the extension to degenerate states would become quite problematic as was confirmed with practical tests by the authors of this chapter and coworkers [12–16].

Take, for example, an atom with electron configuration  $1s^2 2s^2 2p^1$ . The p-orbital may be any of the three different p-orbitals with the same principal quantum number and all three states are degenerate. Now consider the interaction with some other system that can select one of the states (or a specific ensemble of some of the degenerate states). This other system may be something as simple as a point charge at a very far distance. Depending on the state considered, the interaction energy may result very different than the one of a non-degenerate case. Such a dependence is clearly undesirable as an infinite number of linear combinations of degenerate wavefunctions may be made that all lead to the same energy of the unperturbed system but may react radically differently with the point charge. The underlying reason is obviously that although the energy does not change when picking a different state, the key ingredient of DFT, the electron density, does change.

Given its central role in DFT, we first introduce it here starting from the one-density matrix. When no degeneracy is present, the one-density matrix for an  $N$ -electron system is given by

$$v(\mathbf{r}, \mathbf{r}') = \int d\mathbf{x}_1 \dots d\mathbf{x}_N d\mathbf{x}'_1 \dots d\mathbf{x}'_N \left[ \begin{array}{c} \Psi^*(\mathbf{x}_1, \dots, \mathbf{x}_N) \\ \left( \sum_{i=1}^N \delta(\mathbf{r}_i - \mathbf{r}) \delta(\mathbf{r}'_i - \mathbf{r}') \prod_{j \neq i} \delta(\mathbf{x}_j - \mathbf{x}'_j) \right) \\ \Psi(\mathbf{x}'_1, \dots, \mathbf{x}'_N) \end{array} \right] \tag{6.2}$$

$\mathbf{x}_i$  and  $\mathbf{r}_i$  stand for the collection of the space and spin coordinates of electron  $i$  or the space coordinates only, respectively. If no subscript is added, as in  $v(\mathbf{r}, \mathbf{r}')$ ,  $\mathbf{r}$  is simply a position in  $\mathbb{R}^3$ .  $\Psi(\mathbf{x}'_1, \dots, \mathbf{x}'_N)$  is the value of the nondegenerate (ground-state) wavefunction at the coordinates indicated and  $\delta(\mathbf{r}_i - \mathbf{r})$  is a Dirac delta function. Note that there are admittedly many other expressions for how to obtain  $v(\mathbf{r}, \mathbf{r}')$ . Among the more often encountered ones, one has

$$v(\mathbf{r}, \mathbf{r}') = N \int d\omega_1 \dots d\mathbf{x}_N \Psi^*(\mathbf{x}_1, \dots, \mathbf{x}_N) \delta(\mathbf{r}_1 - \mathbf{r}) \delta(\mathbf{r}'_1 - \mathbf{r}') \Psi(\mathbf{x}'_1, \dots, \mathbf{x}'_N) \quad (6.3)$$

The electron density corresponds to the diagonal of the density matrix, so

$$\rho(\mathbf{r}) \equiv v(\mathbf{r}, \mathbf{r}) = N \int d\omega_1 \dots d\mathbf{x}_N \Psi^*(\mathbf{x}_1, \dots, \mathbf{x}_N) \delta(\mathbf{r}_1 - \mathbf{r}) \Psi(\mathbf{x}_1, \dots, \mathbf{x}_N) \quad (6.4)$$

In what follows, wavefunctions will be assumed to be normalized and for the same system mutually orthogonal.

This chapter deals with the issue what happens when there is no longer one single  $\Psi$  that gives the same (ground-state) energy, so when a manifold of  $\{\Psi_i\}$  exist that all give the same energy. As is well known, any linear combination within this manifold is again an eigenfunction of the Hamiltonian with the same energy, and depending on what specific linear combination was used, the expectation values for other operators may differ. This is also true for the electron density. Depending on the coefficients  $\{c_i\}$ , a different electron density may be found. The electron density in the presence of a  $d$ -fold degeneracy is given by

$$\rho_c(\mathbf{r}) = \int d\mathbf{x}_1 \dots d\mathbf{x}_N d\mathbf{x}'_1 \dots d\mathbf{x}'_N \left[ \begin{array}{c} \sum_{i=1}^d c_i^* \Psi_i^*(\mathbf{x}_1, \dots, \mathbf{x}_N) \\ \left( \sum_{i=1}^N \delta(\mathbf{r}_i - \mathbf{r}) \delta(\mathbf{r}'_i - \mathbf{r}') \prod_{j \neq i}^N \delta(\mathbf{x}_j - \mathbf{x}'_j) \right) \\ \sum_{j=1}^d c_j \Psi_j(\mathbf{x}'_1, \dots, \mathbf{x}'_N) \end{array} \right] \quad (6.5)$$

$\rho_c$  denotes that the electron density has indeed become dependent on the set of coefficients  $c_i$ . So when a perturbation of a system arises that couples to the electron density, essentially any result is possible. This is rather discomfoting, but it will be shown that perturbation theory reveals effectively  $d$  different outcomes in a straightforward way. The nature of the perturbation will determine the coefficients.

This relationship between the nature of a perturbation and the set of coefficients will be illustrated for several cases. First, a coarse grain analysis of the electron density itself is considered through atoms in molecules, then the electrostatic potential as an example of an external potential perturbation, and finally the Fukui function as an example of a second-order effect.

## 6.2 Theory

As the major part of this chapter deals with electron density and (energy) response to external perturbations, it is appropriate to first establish the relation between

energy and electron density. Instead of moving immediately to the external potential, we first start with the Hamiltonian for an  $N$ -electron system with  $M$  nuclei with charges  $Z$  at positions  $\mathbf{R}$ . We do not include external fields and work within the Born–Oppenheimer approximation. The Hamiltonian therefore consists of the following terms:

$$\hat{H} = \hat{T} + \hat{V}_{ee} + \hat{V}_{NN} + \hat{V}_{Ne} \quad (6.6)$$

$$\hat{T} = \sum_{i=1}^N -\frac{1}{2} \hat{V}_i^2 \quad (6.7)$$

$$\hat{V}_{ee} = \sum_{i=1}^N \sum_{j>i}^N \frac{1}{|\mathbf{r}_i - \mathbf{r}_j|} \quad (6.8)$$

$$\hat{V}_{NN} = \sum_{A=1}^M \sum_{B>A}^N \frac{Z_A Z_B}{|\mathbf{R}_A - \mathbf{R}_B|} \quad (6.9)$$

$$\hat{V}_{Ne} = \sum_{i=1}^N \sum_{A=1}^M -\frac{Z_A}{|\mathbf{r}_i - \mathbf{R}_A|} \quad (6.10)$$

The energy is given by  $E = \langle \Psi | \hat{H} | \Psi \rangle = \langle \Psi | \hat{T} + \hat{V}_{ee} + \hat{V}_{NN} + \hat{V}_{Ne} | \Psi \rangle$ . In what follows, we will be particularly interested in  $\hat{V}_{Ne}$ . This is a scalar operator, meaning it is multiplicative and so one can arrive at

$$\begin{aligned} \langle \Psi | \hat{V}_{Ne} | \Psi \rangle &= \int d\mathbf{x}_1 \dots d\mathbf{x}_N \Psi^*(\mathbf{x}_1 \dots \mathbf{x}_N) \left[ \sum_{i=1}^N \sum_{A=1}^M -\frac{Z_A}{|\mathbf{r}_i - \mathbf{R}_A|} \right] \Psi(\mathbf{x}_1 \dots \mathbf{x}_N) \\ &= \int d\mathbf{x}_1 \dots d\mathbf{x}_N \left[ \sum_{i=1}^N \sum_{A=1}^M -\frac{Z_A}{|\mathbf{r}_i - \mathbf{R}_A|} \right] \Psi^*(\mathbf{x}_1 \dots \mathbf{x}_N) \Psi(\mathbf{x}_1 \dots \mathbf{x}_N) \end{aligned} \quad (6.11)$$

In DFT, often use is made of a quantity called the external potential, which replaces the above expressions with one that in the operator does not hold reference to an electron label and allows for the introduction of electron density. A natural way of doing it is as follows:

$$\begin{aligned} \langle \Psi | \hat{V}_{Ne} | \Psi \rangle &= \int d\mathbf{x}_1 \dots d\mathbf{x}_N \Psi^*(\mathbf{x}_1 \dots \mathbf{x}_N) \left[ \sum_{i=1}^N \sum_{A=1}^M -\frac{Z_A}{|\mathbf{r}_i - \mathbf{R}_A|} \right] \Psi(\mathbf{x}_1 \dots \mathbf{x}_N) \\ &= \int d\mathbf{r} \sum_{A=1}^M -\frac{Z_A}{|\mathbf{r} - \mathbf{R}_A|} \int d\mathbf{x}_1 \dots d\mathbf{x}_N d\mathbf{x}'_1 \dots d\mathbf{x}'_N \Psi^*(\mathbf{x}_1 \dots \mathbf{x}_N) \\ &\quad \times \left( \sum_{i=1}^N \delta(\mathbf{r}_i - \mathbf{r}) \delta(\mathbf{r}'_i - \mathbf{r}) \prod_{j \neq i}^N \delta(\mathbf{x}_j - \mathbf{x}'_j) \right) \Psi(\mathbf{x}'_1 \dots \mathbf{x}'_N) \\ &= \int d\mathbf{r} v_{\text{ext}}(\mathbf{r}) \rho(\mathbf{r}) \end{aligned} \quad (6.12)$$

This properly introduces the external potential as a scalar function of  $\mathbf{r}$  that upon multiplication with  $\rho(\mathbf{r})$  and integration gives the desired energy contribution. The



external potential is then given by

$$v_{\text{ext}}(\mathbf{r}) = \sum_{A=1}^M -\frac{Z_A}{|\mathbf{r} - \mathbf{R}_A|} \quad (6.13)$$

Starting again with a nondegenerate case, we first establish that the electron density – in this case – is the functional derivative of the energy with respect to the external potential. We work field-free, so we do not consider an external magnetic or external field and write the energy as a function of the number of electrons  $N$  in a system and as a function of the external potential  $\hat{v}(\mathbf{r})$ :  $E[N, v]$ . Imagine that another source of the external potential is added:

$$v'_{\text{ext}}(\mathbf{r}) = v_{\text{ext}}(\mathbf{r}) + \epsilon \eta(\mathbf{r}) \quad (6.14)$$

$\eta(\mathbf{r})$  could correspond to adding a nucleus or a simple point charge at some point in space and rests unspecified.  $\epsilon$  is a real number that “scales” the added potential. The energy change, at fixed density, corresponds to

$$E[N, v'] - E[N, v] = \epsilon \int d\mathbf{r} \eta(\mathbf{r}) \rho(\mathbf{r}) \quad (6.15)$$

The functional derivative of  $E$  with respect to a change in the external potential is denoted  $\frac{\delta E}{\delta v(\mathbf{r})}$  and is defined as

$$\lim_{\epsilon \rightarrow 0} \frac{E[N, v + \epsilon \eta] - E[N, v]}{\epsilon} = \int d\mathbf{r} \eta(\mathbf{r}) \frac{\delta E}{\delta v(\mathbf{r})} \quad (6.16)$$

By comparison, it is clear that

$$\frac{\delta E}{\delta v(\mathbf{r})} = \rho(\mathbf{r}) \quad (6.17)$$

The electron density at some point in space is equal to the functional derivative of the energy with respect to a change in the external potential field at that point.

This was the case of a nondegenerate state. When a  $d$ -fold degeneracy occurs, problems arise. As shown in Eq. (6.5), the electron density depends on the choice of coefficients in a linear combination of the  $d$  degenerate wavefunctions. It is unacceptable to equate a density that has such degree of freedom to the functional derivative that should be a unique energy response to some perturbation. However, the impact of a perturbation at a point  $\mathbf{r}$  may be calculated using perturbation theory. Degenerate perturbation theory is ideally suited to establish a new form of assessing the energy response without appealing to functional derivatives that are ill-defined in degenerate states. We return to the original Hamiltonian and add a perturbation. The perturbation in the Hamiltonian is  $\sum_{i=1}^N \eta(\mathbf{r}_i)$ , and  $\epsilon$  plays the role of the scaling parameter that tunes the strength of the perturbation. The Hamiltonian is altered to

$$\hat{H} = \hat{H}^0 + \epsilon \sum_{i=1}^N \eta(\mathbf{r}_i) \quad (6.18)$$

In the case of a system with degenerate states, rather than having simply a first-order energy change  $\langle \Psi | \sum_{i=1}^N \eta(\mathbf{r}_i) | \Psi \rangle$ , the first-order energy correction is obtained from

diagonalizing the perturbation matrix:

$$\mathbf{P} = \begin{bmatrix} \left\langle \Psi_1 \left| \sum_{i=1}^N \eta(\mathbf{r}_i) \right| \Psi_1 \right\rangle & \left\langle \Psi_1 \left| \sum_{i=1}^N \eta(\mathbf{r}_i) \right| \Psi_2 \right\rangle & \cdots & \left\langle \Psi_1 \left| \sum_{i=1}^N \eta(\mathbf{r}_i) \right| \Psi_d \right\rangle \\ \left\langle \Psi_2 \left| \sum_{i=1}^N \eta(\mathbf{r}_i) \right| \Psi_1 \right\rangle & \left\langle \Psi_2 \left| \sum_{i=1}^N \eta(\mathbf{r}_i) \right| \Psi_2 \right\rangle & \cdots & \left\langle \Psi_2 \left| \sum_{i=1}^N \eta(\mathbf{r}_i) \right| \Psi_d \right\rangle \\ \vdots & \vdots & \ddots & \vdots \\ \left\langle \Psi_d \left| \sum_{i=1}^N \eta(\mathbf{r}_i) \right| \Psi_1 \right\rangle & \left\langle \Psi_d \left| \sum_{i=1}^N \eta(\mathbf{r}_i) \right| \Psi_2 \right\rangle & \cdots & \left\langle \Psi_d \left| \sum_{i=1}^N \eta(\mathbf{r}_i) \right| \Psi_d \right\rangle \end{bmatrix} \quad (6.19)$$

where  $\Psi_{1\dots d}$  are the degenerate wavefunctions. The diagonal elements of this matrix may be expressed using the electron density obtained from a specific wavefunction, but a small generalization of electron density to transition electron density allows to write

$$\mathbf{P} = \begin{bmatrix} \int d\mathbf{r} \eta(\mathbf{r}) \rho_{11}(\mathbf{r}) & \int d\mathbf{r} \eta(\mathbf{r}) \rho_{12}(\mathbf{r}) & \cdots & \int d\mathbf{r} \eta(\mathbf{r}) \rho_{1d}(\mathbf{r}) \\ \int d\mathbf{r} \eta(\mathbf{r}) \rho_{21}(\mathbf{r}) & \int d\mathbf{r} \eta(\mathbf{r}) \rho_{22}(\mathbf{r}) & \cdots & \int d\mathbf{r} \eta(\mathbf{r}) \rho_{2d}(\mathbf{r}) \\ \vdots & \vdots & \ddots & \vdots \\ \int d\mathbf{r} \eta(\mathbf{r}) \rho_{d1}(\mathbf{r}) & \int d\mathbf{r} \eta(\mathbf{r}) \rho_{d2}(\mathbf{r}) & \cdots & \int d\mathbf{r} \eta(\mathbf{r}) \rho_{dd}(\mathbf{r}) \end{bmatrix} \quad (6.20)$$

The transition density matrix corresponds to

$$v_{ij}(\mathbf{r}, \mathbf{r}') = \int d\mathbf{x}_1 \dots d\mathbf{x}_N d\mathbf{x}'_1 \dots d\mathbf{x}'_N \left[ \begin{array}{c} \Psi_i^*(\mathbf{x}_1, \dots, \mathbf{x}_N) \\ \left( \sum_{i=1}^N \delta(\mathbf{r}_i - \mathbf{r}) \delta(\mathbf{r}'_i - \mathbf{r}') \prod_{j \neq i} \delta(\mathbf{x}_j - \mathbf{x}'_j) \right) \\ \Psi_j(\mathbf{x}'_1, \dots, \mathbf{x}'_N) \end{array} \right] \quad (6.21)$$

from which the transition density is obtained:

$$\rho_{ij}(\mathbf{r}) \equiv v_{ij}(\mathbf{r}, \mathbf{r}) \quad (6.22)$$

The matrix (6.20) is generally not diagonal, and its eigenvalues correspond to different responses of the degenerate system to a perturbation  $\eta(\mathbf{r})$ . These are the first-order changes in energy  $E^{(1)}$ . Finding the eigenvectors of the matrix (6.19) corresponds to finding those linear combinations of degenerate eigenfunctions of the unperturbed Hamiltonian that diagonalize the matrix. These eigenvectors give rise to the electron density that, however, cannot be equated to a functional derivative because the derivative does not exist. Hence, it is not so that the response of the energy with respect to the perturbation does not correspond to a density, it is rather that it corresponds to a very specific density obtained from a linear combination of degenerate wavefunctions. A further observation is that the matrix depends on a specific perturbation. For example, imagine that one adds a point charge in the molecule. The external potential changes by an amount:

$$\eta(\mathbf{r}) = -\frac{Q}{|\mathbf{r} - \mathbf{R}_Q|} \quad (6.23)$$

where  $Q$  is the magnitude of the point charge and  $\mathbf{R}_Q$  is its position. Depending on the sign of the charge and its location, the matrix changes and so do its eigenvalues and eigenvectors.

### 6.2.1 An Illustrative Example

To sketch the impact of degeneracy, consider first a 4-electron atomic or ionic system that is in its ground state with electron configuration  $1s^2 2s^2$ . The response to a point charge placed at some point  $\mathbf{R}_Q$  corresponds to the integral  $-\int d\mathbf{r} \frac{Q}{|\mathbf{r}-\mathbf{R}_Q|} \rho(\mathbf{r})$  where  $\rho(\mathbf{r})$  is the density of this nondegenerate wavefunction. If we put the nucleus in the origin and move the point charge on a sphere around the origin, the same response results. If we change the sign of the point charge, the response again remains the same in magnitude but opposite sign.

Now imagine a 5-electron atomic or ionic system with electron configuration  $1s^2 2s^2 2p^1$ . In an orbital picture, there are three 2p orbitals that can be populated. The corresponding three wavefunctions denoted  $\Psi_x$ ,  $\Psi_y$ , and  $\Psi_z$  are degenerate and so any linear combination

$$\Psi(\mathbf{r}) = \sum_{i=\{x,y,z\}} c_i \Psi_i(\mathbf{r}) \quad (6.24)$$

is again an eigenfunction of the Hamiltonian for this anion. From this  $\Psi$ , one can construct the electron density by quadrature as was done above. Now consider a perturbation with a point charge. A perturbation matrix needs to be composed. The diagonal elements are readily computed, showing that depending on the position of the point charge, the three diagonal elements may differ. Suppose that we put a unit point charge along the  $z$ -axis. The matrix element  $\left\langle \Psi_z \left| \frac{-Q}{|\mathbf{r}-\mathbf{R}_Q|} \right| \Psi_z \right\rangle$  is definitely different from the other two diagonal elements. Suppose, however, that one would only consider  $\Psi_z$ . The first-order energy change is

$$E^{(1)}(Q, \mathbf{R}_Q) = -Q \int \frac{|\Psi_z(\mathbf{r})|^2(\mathbf{r})}{|\mathbf{r}-\mathbf{R}_Q|} d\vec{r} \quad (6.25)$$

A different diagonal element is

$$-Q \int \frac{|\Psi_x(\mathbf{r})|^2(\mathbf{r})}{|\mathbf{r}-\mathbf{R}_Q|} d\vec{r} \quad (6.26)$$

If we keep the point charge at the same location on the  $z$ -axis, the last term definitely differs from the previous one. The arbitrariness of hand-picking a degenerate wavefunction is alleviated if we consider the perturbation matrix (6.19). The wavefunctions  $\Psi_{x,y,z}$  differ in only one orbital; as the perturbing operator is a one-electron operator, there are clearly also off-diagonal elements such as

$$-Q \int \frac{\Psi_x^*(\mathbf{r})\Psi_z(\mathbf{r})}{|\mathbf{r}-\mathbf{R}_Q|} d\vec{r} \quad (6.27)$$

Depending on the position and sign of the point charge, all matrix elements can change and so do the eigenvalues and eigenvectors. With  $d = 3$ , three eigenvalues and three eigenvectors can be distinguished. Although the perturbation matrix may completely lift the degeneracy, this is not required, and it may also not be lifted completely. The important issue is that the interaction energy changes as the perturbation changes, and so it becomes parametrically dependent on the parameters that characterize the perturbation.

The importance of considering the entire perturbation matrix can hardly be stressed enough. Several authors have, in case of degeneracies, used some ad hoc averages [17–21] over the diagonal elements of the perturbation matrix. This is a purely pragmatic but unfounded approach as it again does not take degeneracy into account properly. As a further note, the above concentrates on the “quantum contributions” due to the electronic wavefunction. One needs to include also the extra Coulombic interaction with the nucleus. However, this is computed classically, so an energy change  $\sum_{A=1}^M \frac{Z_A Q}{|\mathbf{R}_Q - \mathbf{R}_A|}$  must also be added. This will reduce the energetic impact of the electronic interaction with the point charge, but the difference between perturbation matrix eigenvalues remains the same.

## 6.3 Impact of Degeneracy on Chemical Concepts

In this section, a didactic approach is used to illustrate the importance of properly taking into account the effect of degeneracy on many chemical concepts. The main focus lies on concepts that are directly related to electron density but where the “usual” relationships cannot be used anymore.

### 6.3.1 Electron Density

According to the most common interpretation of quantum mechanics, the wavefunction in itself has not much meaning beyond being a good vehicle to extract relevant information from a system. This information is encapsulated in expectation values for which the electron density is one. In a one-electron system, the electron density is immediately related to probability. The electron density at some point multiplied with an infinitesimal volume element  $dV$  gives the probability of finding the electron in that volume element around that point.

$$P(\mathbf{x}) = \rho(\mathbf{x})dV \quad (6.28)$$

$dV$  includes both the spatial components and spin. The probability density function  $\rho$  must obviously be positive and the probability must have norm equal to 1. There is little confusion at this stage in the meaning of the electron density as linked to probability and the electron density is obtained from quadrature of the wavefunction for the one-electron system.

$$\rho(\mathbf{x}) = \Psi^*(\mathbf{x})\Psi(\mathbf{x}) \quad (6.29)$$

Matters get somewhat more complicated in the case of a multielectron system. Taking a two-electron system, the probability is introduced for finding electron 1 in a volume element  $dV_1$  and electron 2 in a volume element  $dV_2$ :

$$P(\mathbf{x}_1, \mathbf{x}_2) = \Psi^*(\mathbf{x}_1, \mathbf{x}_2)\Psi(\mathbf{x}_1, \mathbf{x}_2)dV_1dV_2 \quad (6.30)$$

Some confusion sometimes arises for these probabilities and the connection to what is called electron density in DFT on the one hand and other chemical interpretation tools [22]. When considering the so-called marginal probability  $P_m$  to find electron 1 in some volume element  $dV_1$  around  $\mathbf{x}_1$ , the second electron in the joint distribution is integrated over all space, including again the space  $dV_1$ .

$$P_m(\mathbf{x}_1) = dV_1 \int_{-\infty}^{+\infty} \Psi^*(\mathbf{x}_1, \mathbf{x}_2)\Psi(\mathbf{x}_1, \mathbf{x}_2)dV_2 \quad (6.31)$$

This marginal probability from Eq. (6.31) is then recast in the shape of Eq. (6.28) by defining

$$\rho(\mathbf{x}_1) = \int_{-\infty}^{+\infty} \Psi^*(\mathbf{x}_1, \mathbf{x}_2)\Psi(\mathbf{x}_1, \mathbf{x}_2)dV_2 \quad (6.32)$$

Electron density is often described as the probability density amplitude for finding electron 1 at  $\mathbf{x}_1$ , but it should always be included explicitly “irrespective of where the other electrons are.” The total probability of finding an electron at  $\mathbf{x}$  is then obtained as the sum of the probability of finding electron 1 summed with that of finding electron 2:

$$\rho(\mathbf{x}) = 2 \int_{-\infty}^{+\infty} \Psi^*(\mathbf{x}, \mathbf{x}_2)\Psi(\mathbf{x}, \mathbf{x}_2)dV_2 \quad (6.33)$$

The contributions are the same for any electron thanks to the anti-symmetry and equivalence of all electrons, but each individual contribution always integrates out all other electrons. When reporting  $\rho(\mathbf{x})$  and interpreting in terms of a probability density amplitude, it is important to remain aware that it counts the probability of finding at least one electron in the volume element. In the two-electron case, it holds the probability of having only one electron in  $dV$  but also having two electrons in that same volume element. That is, it counts the average number of electrons in  $dV$ . So the marginal probability should be kept separate from the conditional or joint probability that are used elsewhere in DFT concepts and chemical bond methods such as domain-averaged Fermi holes [23], maximum probability domains [24], and electron distribution statistics [25], for example.

The chief problem with systems with degenerate states lies in the fact that for the same energy, there are several different states that may yield totally different electron densities. Any concept based on the electron density can then give a different answer depending on the linear combination of eigenstates chosen. For example, we consider the electrostatic potential and Fukui functions. In both cases, a specific external perturbation is required to reveal precisely what a linear combination of degenerate states is required for a specific response. The electrostatic potential is often mimicked through atoms-in-molecules charges, which are in turn in many atomic charge methods derived from the electron density. Hence, also atomic charges become ill-defined and extra input in the shape of a specific perturbation is required.

### 6.3.2 Electrostatic Potential

As a second example, we consider the electrostatic potential. The electrostatic potential is defined in terms of the energy in the following way. The charged species inside a molecule generate a potential  $\Phi(\mathbf{r})$  at every point in space  $\mathbf{r}$ . Essentially, it can be computed easily as

$$\Phi(\mathbf{r}) = \sum_{A=1}^M \frac{Z_A}{|\mathbf{r} - \mathbf{R}_A|} - \int d\mathbf{r}' \frac{\rho(\mathbf{r}')}{|\mathbf{r} - \mathbf{r}'|} \quad (6.34)$$

This poses no problem for a nondegenerate state. The electron density is easily obtained from quadrature. However, what with degenerate states? As argued above, the density is a rather problematic quantity. There is also another way to approach the problem. The electrostatic potential at some point in space is equal to the electrostatic potential energy  $U$  generated by a point charge put at this same point:

$$U(\mathbf{r}) = Q(\mathbf{r})\Phi(\mathbf{r}) \quad (6.35)$$

This means that we put a point charge at  $\mathbf{r}$  and compute the change in energy. The ratio between the energy and the value of the point charge equals the potential. When degenerate states come into play, the electrostatic potential has to be computed by effectively putting a point charge at some point in space and computing the change in energy. This change in energy may be computed using perturbation theory, and the potential equals the first-order response divided by the value of the point charge. The issue that arises is that depending on the nature of the perturbation, a different linear combination of zero-order wavefunctions will be obtained from the perturbation matrix and hence a different electron density. One immediately realizes that the sign of the point charge will also matter. Taking as an example again the  $1s^2 2s^2 2p^1$  electron configuration, this is easily rationalized appealing to the symmetry of the p orbitals. When a positive charge approaches the atom along the  $z$  direction, an electron will be attracted to it and the energy is minimized when the  $p_z$  orbital is populated by the single valence electron. Contrary, in the case of a negative charge the  $p_z$  orbital will remain empty while the electron occupies a linear combination of  $p_y$  and  $p_x$ . There is, however, a link between the perturbation caused by a positive and a negative charge. The perturbation matrix elements simply are opposite sign, so the magnitude of the eigenvalues is the same but the sign opposite. As we choose the lowest energy response, what is the lowest energy for one charge becomes the highest energy response when we change the sign of the probe charge.

To illustrate the effect of the sign of the point charge (probe) on the electrostatic potential, we performed CASSCF(1,3)/6-31G\* calculations for  $N^{2+}$  in the presence of a point charge placed at different distances from the nucleus. The perturbation matrix was set up and diagonalized. To ensure that the response falls within the linear regime of perturbation, smaller and smaller charges were used at every point and a linear regression was used to estimate the limit in which  $q \rightarrow 0$ . For both a negative and a positive point charge, the lowest energy solution was obtained from the perturbation matrix. As Figure 6.1 shows, the electrostatic potential for a positive probe,  $\Phi^+$ , is always larger than that for a negative one,  $\Phi^-$ . Although the difference is small for large distances, it is more than  $100 \text{ kcal mol}^{-1}$  at the covalent radius of  $N$ ,

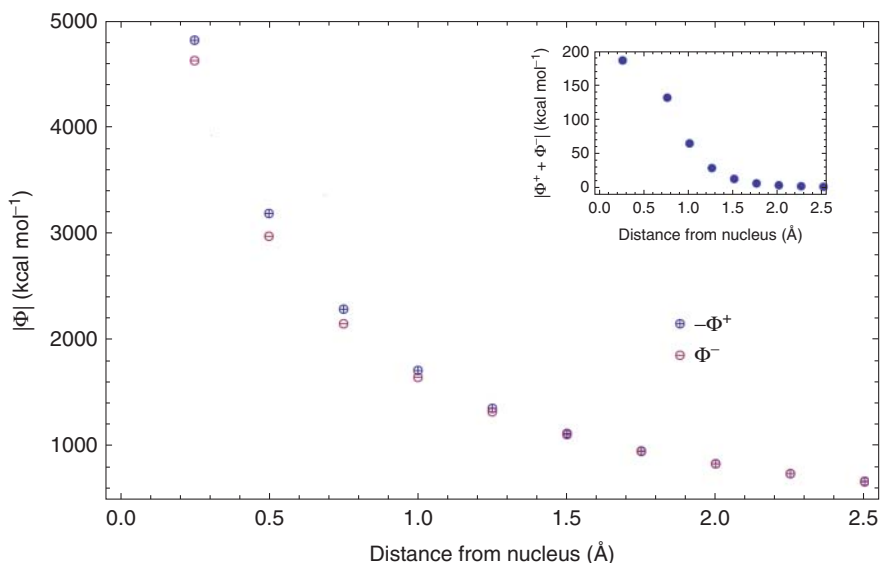


**Figure 6.1** Electrostatic potential,  $\Phi$ , of  $N^{2+}$ . A positive (blue) and a negative (red) point charge were used as probes.

which is the order of the chemically relevant distances (see the inset in Figure 6.1). This means that computing ‘the “electrostatic potential” is an ill-posed question and that one can only compute such a quantity with an explicit specification of the probe charge and position used. This result clearly confirms that care must be taken when treating degenerate states in conceptual DFT. Any attempt at using any sort of average of the diagonal elements in the perturbation matrix is sure to fail.

### 6.3.3 Atomic Charges

There exists a wealth of methods [26, 27] to compute atomic charges including those based on the attachment between a basis function and atomic nucleus (the so-called Mulliken population analysis [28]), statistical methods such as those where the electrostatic potential at a selection of points is used to fit an atomic charge [29–32] and atomic density methods where not only a charge is obtained but a true density from which other properties can also be computed. Here, focus is on atomic density methods. The ill-defined nature of the electrostatic potential makes those atomic charges also depend parametrically on the position and magnitude of the precise perturbation used. Atomic density methods are methods based on the general scheme

$$\rho_A(\mathbf{r}) = w_A(\mathbf{r})\rho_{\text{Mol}}(\mathbf{r}) \quad (6.36)$$

where  $w_A(\mathbf{r})$  is a weight coefficient with value between 0 and 1 and whose sum  $\sum_{A=1}^M w_A(\mathbf{r}) = 1$ . Different methods exist with both binary weights including the Quantum Theory of Atoms and Molecules [33, 34] and fuzzy weights such as in diverse information-theory-based methods [35]. The main issue remains that  $\rho_{\text{Mol}}(\mathbf{r})$  depends on the method of perturbation used and its parameters. The electrostatic

potential is just one such method that holds as parameters the magnitude, sign, and position of the atomic charge but other methods could be conceived. The chapter authors have previously [12] shown that, for instance, CAS(3,4)/cc-pVDZ Hirshfeld-I [36, 37] and QTAIM [33, 34] atomic charges on one and the same atom in the trans butadiene radical cation, with three near-degenerate states, may change sign depending on where the electrostatic potential probe was put. Such complete reversal of even the sign of the atomic charge is obviously dramatic. The reason for this effect was shown to be due to the change of the coefficients of the quasi-degenerate states in the lowest energy eigenvector of the perturbation matrix. The source of the problem is fundamental and is not, in any way, due to a specific choice of the atoms-in-molecules method although symmetry may sometimes hide the problem [21].

### 6.3.4 Fukui Function

As another example, we may consider the Fukui function [38–40]. This is a second-order term in the Taylor expansion of the energy in terms of the number of electrons  $N$  and the external potential [41, 42]. It is an  $\mathbf{r}$  dependent quantity, defined by

$$f(\mathbf{r}) = \left[ \frac{\partial \left[ \frac{\delta E}{\delta v_{\text{ext}}(\mathbf{r})} \right]_N}{\partial N} \right]_{v_{\text{ext}}} \quad (6.37)$$

Most often, it is also written as

$$f(\mathbf{r}) = \left[ \frac{\partial \rho(\mathbf{r})}{\partial N} \right]_{v_{\text{ext}}} \quad (6.38)$$

But this is again problematic for a degenerate state where the electron density is not the functional derivative of the energy vs. the external potential. It is therefore highly recommendable to always work with energy derivatives and delay any substitution in the Taylor series coefficients to a later stage once the intricacies of the system are known. This entails that the Fukui function for a degenerate state will depend again on where the probe charge was put as well as its value. Moreover, since the Fukui function is most often computed via finite differences, care must be taken to check whether the charged system is also not degenerate. This would be the case for adding an electron to  $N^{2+}$ , for example. Hence, in every calculation of a Fukui function, one must consider carefully whether none of the calculated systems has a degenerate state.

(Quasi-)Degeneracy has a pronounced effect on the Fukui function. While in the case of nondegenerate states and single determinant theories (and Kohn–Sham theory) the so-called Fukui matrix [13, 43, 44] eigenvalues have a very specific eigenvalue spectrum, the need to include more states here makes that the Fukui matrix has the characteristic properties following from a correlated method. Again also notice that the effect of degeneracy on the Fukui function does not only appear in its atom condensed form [45] but in general. The extra complications induced



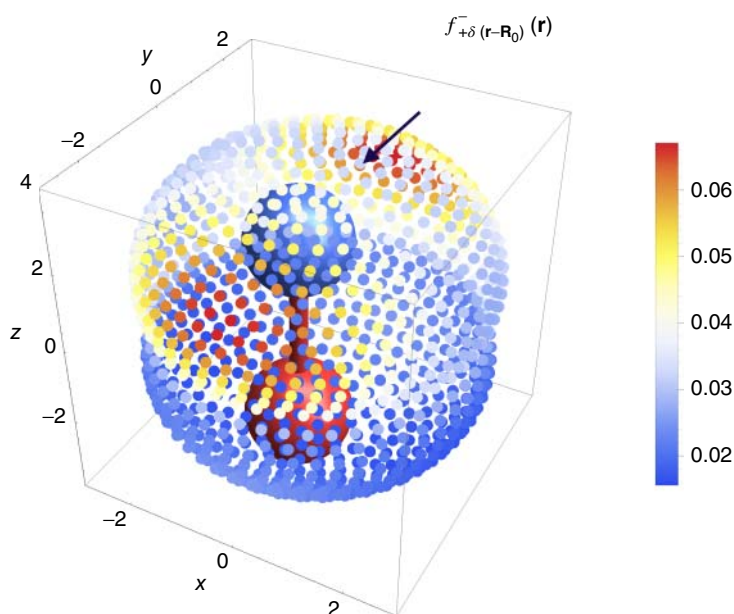


**Figure 6.2** Fukui function  $f_{+\delta}^-(\mathbf{r})$  originating from an attractive Dirac delta perturbation located at the point indicated (arrow).

by degeneracy especially manifest in the case of the Fukui matrix as not only there are  $\mathbf{r}$ -like in a density matrix  $\mathbf{r}$  and  $\mathbf{r}'$  coordinates but also the parametric dependence on the choice of the perturbing potential, including the sign of the charge and its location in the case of a point charge [13].

As an example, take the NO molecule whose ground state is doubly degenerate. If neither the ground state nor its vertical cations were degenerate, the Fukui function would have the axial symmetry of the molecule ( $C_{\infty v}$ ). However, this is not the case of NO, and the resulting symmetry of the Fukui function depends on the type and location of the perturbation. Figure 6.2 shows, in a color code, the values of the Fukui function  $f^-(\mathbf{r})$  for NO when an attractive Dirac delta acts as a perturbation. The perturbation is located at the point indicated with an arrow, and the points of the plot correspond to the van der Waals surface of the molecule. Contrary to what intuition gained in nondegenerate states, the perturbation breaks the symmetry, and the Fukui function in this case has only symmetry ( $C_{2v}$ ).

## 6.4 Further Considerations

The need to treat the full perturbation matrix is clear from the above discussion, but the question as to what perturbation must be considered in practice remains, that is, can a point charge mimic an approaching molecule? Probably a point charge it is too simple and crude a model and a more realistic model could be a set of small point

charges that mimic the entire electrostatic field of an approaching molecule. Every other set of point charges or other perturbing operator will, in general, result in a different response density. This naturally makes use of conceptual DFT to predict, rather than to a posteriori explain, the outcome of a much more difficult chemical reaction. Moreover, not only point charges are a possibility, but Dirac delta functions are also a useful perturbing operator.

Another relevant question is when one should start worrying about quasi-degeneracy. Quasi-degenerate states should be treated in the same way as degenerate states. We have proposed to use the Fermi level (i.e. the energy halfway between the highest occupied molecular orbital [HOMO] and lowest unoccupied molecular orbital [LUMO] orbitals) as a reference. If there are orbitals within 0.25 Hartree of this level, we propose to consider them quasi-degenerate. Also note that although we have only considered here a subset of chemical concepts, the problem is universal and will also appear in the chemical potential, dual descriptor, etc. However, the effect must not always be immediately visible, and, e.g., symmetry may occasionally hide the underlying necessity to use a full perturbation matrix treatment [21].

## 6.5 Conclusions

The calculation of many conceptual DFT quantities becomes highly problematic or they simply become ill-defined when (quasi-)degenerate states occur in the system(s) considered. The underlying reason is that ‘the’ “density” no longer has meaning and that the proper density to use is rather determined by the source of the perturbation associated with the concept considered. The dramatic effect is illustrated for concepts intimately related to the functional derivative of the energy with respect to the external potential. In the of degenerate eigenfunctions of the Hamiltonian, this quantity becomes ill-defined. Notably, its calculation using perturbation theory shows that it depends on the nature of the perturbation used. If a point charge is used, there is a clear dependence on the sign of the point charge. This makes it clear that degeneracies do have a possibly dramatic effect on the proper calculation of chemical concepts and that more attention to their calculation is needed.

The present results also show that using an average of densities of degenerate states is not accounted for. The transition density (matrix) elements definitely play a role as well and must be properly considered.

## Acknowledgments

P.B. acknowledges financial support by the National Fund for Scientific Research – Flanders for continuous support. C.C. acknowledges financial support by: (i) FONDECYT through project No. 1181121, (ii) CONICYT, REDES 190102, and (iii) Center for the Development of Nanoscience and Nanotechnology CEDENNA AFB180001. Powered@NLHPC: This research was partially supported by the supercomputing infrastructure of the NLHPC (ECM-02).

## References

- 1 Parr, R.G. and Yang, W. (1989). *Density Functional Theory of Atoms and Molecules*. Oxford: Oxford University Press, Inc.
- 2 Hohenberg, P. and Kohn, W. (1964). Inhomogeneous electron gas. *Phys. Rev. B* 136: 864–871.
- 3 Mezey, P.G. (2017). The Holographic Electron Density Theorem, de-quantization, re-quantization, and nuclear charge space extrapolations of the Universal Molecule Model. *AIP Conference Proceedings*, Volume 1906, 020001.
- 4 Levy, M. (1979). Universal variational functionals of electron-densities, 1st-order density-matrices, and natural spin-orbitals and solution of the v-representability problem. *Proc. Natl. Acad. Sci. U.S.A.* 76: 6062–6065.
- 5 Ayers, P.W., Anderson, J.S.M., and Bartolotti, L.J. (2005). Perturbative perspectives on the chemical reaction prediction problem. *Int. J. Quantum Chem.* 101: 520–534.
- 6 Geerlings, P., De Proft, F., and Langenaeker, W. (2003). Conceptual density functional theory. *Chem. Rev.* 103: 1793–1873.
- 7 Liu, S.B. (2009). Conceptual density functional theory and some recent developments. *Acta Phys. Chim. Sin.* 25: 590–600.
- 8 Gazquez, J. (2008). Perspectives on density functional theory of chemical reactivity. *J. Mex. Chem. Soc.* 52: 3–10.
- 9 Fuentealba, P. and Cardenas, C. (2015). Density functional theory of chemical reactivity. In: *Chemical Modelling*, vol. 11 (ed. J.-O.J. Michael Springborg), 151–174. The Royal Society of Chemistry.
- 10 Johnson, P.A., Bartolotti, L.J., Ayers, P.W. et al. (2012). Charge density and chemical reactions: a unified view from conceptual DFT. In: *Modern Charge Density Analysis* (ed. C. Gatti and P. Macchi), 715–764. New York: Springer.
- 11 Cardenas, C., Ayers, P.W., and Cedillo, A. (2011). Reactivity indicators for degenerate states in the density-functional theoretic chemical reactivity theory. *J. Chem. Phys.* 134: 174103.
- 12 Bultinck, P., Cardenas, C., Fuentealba, P. et al. (2013). Atomic charges and the electrostatic potential are ill-defined in degenerate ground states. *J. Chem. Theory Comput.* 9: 4779–4788.
- 13 Bultinck, P., Cardenas, C., Fuentealba, P. et al. (2014). How to compute the Fukui matrix and function for systems with (quasi-)degenerate states. *J. Chem. Theory Comput.* 10: 202–210.
- 14 Bultinck, P., Jayatilaka, D., and Cardenas, C. (2015). A problematic issue for atoms in molecules: impact of (quasi-)degenerate states on Quantum Theory Atoms in Molecules and Hirshfeld-I properties. *Comput. Theor. Chem.* 1053: 106–111.
- 15 Pino-Rios, R., Yaez, O., Inostroza, D. et al. (2017). Proposal of a simple and effective local reactivity descriptor through a topological analysis of an orbital-weighted Fukui function. *J. Comput. Chem.* 38: 481–488.

- 16 Pino-Rios, R., Inostroza, D., Cárdenas-Jirón, G., and Tiznado, W. (2019). Orbital-weighted dual descriptor for the study of local reactivity of systems with (quasi-)degenerate states. *J. Phys. Chem. A* 123: 10556–10562.
- 17 Meneses, L., Tiznado, W., Contreras, R., and Fuentealba, P. (2004). A proposal for a new local hardness as selectivity index. *Chem. Phys. Lett.* 383: 181–187.
- 18 Chamorro, E. and Perez, P. (2005). Condensed-to-atoms electronic Fukui functions within the framework of spin-polarized density-functional theory. *J. Chem. Phys.* 123: 114107.
- 19 Cardenas, C., De Proft, F., Chamorro, E. et al. (2008). Theoretical study of the surface reactivity of alkaline earth oxides: local density of states evaluation of the local softness. *J. Chem. Phys.* 128: 034708.
- 20 Martinez, J. (2009). Local reactivity descriptors from degenerate frontier molecular orbitals. *Chem. Phys. Lett.* 478: 310–322.
- 21 Flores-Moreno, R. (2010). Symmetry Conservation in Fukui functions. *J. Chem. Theory Comput.* 6: 48–54.
- 22 Acke, G., De Baerdemacker, S., Martin Pendas, A., and Bultinck, P. (2020). Hierarchies of quantum chemical descriptors induced by statistical analyses of domain occupation number operators. *Wiley Interdiscip. Rev. Comput. Mol. Sci.* 10: e1456.
- 23 Ponec, R. (1997). Electron pairing and chemical bonds. Chemical structure, valences and structural similarities from the analysis of the Fermi holes. *J. Math. Chem.* 21: 323–333.
- 24 Savin, A. (2002). Probability distributions and valence shells in atoms. In: *Reviews of Modern Quantum Chemistry: A Celebration of the Contributions of Tobert G. Parr* (ed. K. Sen), 43–62. Singapore: World Scientific.
- 25 Martin Pendas, A.M. and Francisco, E. (2019). Chemical bonding from the statistics of the electron distribution. *ChemPhysChem* 20: 2722–2741.
- 26 Bachrach, S.M. (1994). Population analysis and electron-densities from quantum mechanics. *Rev. Comput. Chem.* 5: 171–227.
- 27 Bultinck, P. and Popelier, P.L.A. (2009). In: *Theory of Chemical Reactivity* (ed. P. Chattaraj), 215–227. Boca Raton, FL: CRC Press.
- 28 Mulliken, R.S. (1955). Electronic population analysis on LCAO-MO molecular wave functions.1. *J. Chem. Phys.* 23: 1833–1840.
- 29 Breneman, C.M. and Wiberg, K.B. (1990). Determining atom-centered monopoles from molecular electrostatic potentials - the need for high sampling density in formamide conformational-analysis. *J. Comput. Chem.* 11: 361–373.
- 30 Spackman, M.A. (1996). Potential derived charges using a geodesic point selection scheme. *J. Comput. Chem.* 17: 1–18.
- 31 Francl, M.M., Carey, C., Chirlian, L.E., and Gange, D.M. (1996). Charges fit to electrostatic potentials.2. Can atomic charges be unambiguously fit to electrostatic potentials? *J. Comput. Chem.* 17: 367–383.
- 32 Francl, M.M. and Chirlian, L.E. (2000). The pluses and minuses of mapping atomic charges to electrostatic potentials. *Rev. Comput. Chem.* 14: 1–31.
- 33 Bader, R.F.W. (1990). *Atoms in Molecules, A Quantum Theory*. Oxford Science Publications.

- 34 Bader, R.F.W. (1991). A quantum-theory of molecular structure and its applications. *Chem. Rev.* 91: 893–928.
- 35 Heidar-Zadeh, F., Ayers, P.W., Verstraelen, T. et al. (2018). Information-theoretic approaches to atoms-in-molecules: Hirshfeld family of partitioning schemes. *J. Phys. Chem. A* 122: 4219–4245.
- 36 Bultinck, P., Van Alsenoy, C., Ayers, P.W., and Carbo-Dorca, R. (2007). Critical analysis and extension of the Hirshfeld atoms in molecules. *J. Chem. Phys.* 126: 144111.
- 37 Bultinck, P., Ayers, P.W., Fias, S. et al. (2007). Uniqueness and basis set dependence of iterative Hirshfeld charges. *Chem. Phys. Lett.* 444: 205–208.
- 38 Parr, R.G. and Yang, W.T. (1984). Density functional approach to the frontier-electron theory of chemical reactivity. *J. Am. Chem. Soc.* 106: 4049–4050.
- 39 Yang, W., Parr, R.G., and Pucci, R. (1984). Electron density, Kohn–Sham frontier orbitals, and Fukui functions. *J. Chem. Phys.* 81: 2862–2863.
- 40 Fuentealba, P., Cardenas, C., Pino-Rios, R., and Tiznado, W. (2016). *Applications of Topological Methods in Molecular Chemistry*, 227–241. Springer International Publishing.
- 41 Parr, R.G. and Yang, W. (1984). Density functional-approach to the frontier-electron theory of chemical-reactivity. *J. Am. Chem. Soc.* 106: 4049–4050.
- 42 Ayers, P. and Parr, R. (2000). Variational principles for describing chemical reactions: the Fukui function and chemical hardness revisited. *J. Am. Chem. Soc.* 122: 2010–2018.
- 43 Bultinck, P., Clarisse, D., Ayers, P.W., and Carbo-Dorca, R. (2011). The Fukui matrix: a simple approach to the analysis of the Fukui function and its positive character. *Phys. Chem. Chem. Phys.* 13: 6110–6115.
- 44 Bultinck, P., Van Neck, D., Acke, G., and Ayers, P.W. (2012). Influence of electron correlation and degeneracy on the Fukui matrix and extension of frontier molecular orbital theory to correlated quantum chemical methods. *Phys. Chem. Chem. Phys.* 14: 2408–2416.
- 45 Yang, W. and Mortier, W.J. (1986). The use of global and local molecular-parameters for the analysis of the gas-phase basicity of amines. *J. Am. Chem. Soc.* 108: 5708–5711.

## 7

## Spin-Polarized CDFT

Eduardo Chamorro

Universidad Andres Bello, Facultad de Ciencias Exactas, Departamento de Ciencias Químicas, Avenida República 275, Santiago 8370146, Chile

### 7.1 Introduction

A perspective about the current status and prospect of the so-called conceptual density functional theory (CDFT) framework has been presented very recently by Geerlings et al. [1]. The aim, fundamentals, philosophy, accomplishments, and a brief of several possible exciting directions for future development of the CDFT were discussed. This work has already become one of the *Highly Cited Papers* as defined from the Essential Science Indicators of the Web of Science Core Collection. CDFT provides a “*nonempirical, mathematically and physically sound, density-based, quantum-mechanical theory for interpreting and predicting chemical phenomena, especially chemical reactions*” [1]. The DFT framework [2] offers a formal mathematical structure for the interpretation/prediction of experimental/theoretical chemical reactivity patterns based on a series of responses of state functions (e.g. the electronic energy) to changes or perturbations in essential ground-state variables (e.g. the number of electrons or the external potential  $v(\mathbf{r})$ ) [3, 4]. These descriptors configure complete hierarchies defined in terms of Taylor series expansions of the energy functional within Legendre-transformed ensemble representations (e.g. *canonical, grand-canonical, isomorphic, and grand-isomorphic*) [5] of DFT with impact on several areas of chemistry. The advances in this field are related to both *conceptual* and *computational* aspects, being the subject of extensive discussions connected with the so-called *electronic descriptors*. The CDFT framework is nowadays intrinsically connected with the rationalization of the *electronegativity equalization principle* [6], the *hard and soft acids and bases principle* [7, 8], and the *maximum hardness principle* [9, 10]. These rationalizing principles impact a great variety of applications, including, for instance, the interplay of *electrophilicity-nucleophilicity* patterns of reactivity [11], the understanding of *polar interactions* in pericyclic reactions [12, 13], and the consideration of *finite-temperature based* approaches [8, 14–16]. In this chapter, we just intend a pedagogically focused revision of the most fundamental aspects of the so-called

*spin-polarized conceptual DFT framework* (SP-CDFT) [17, 18], which is associated with the *non-relativistic limit* of *spin-dependent DFT* (SDFT) [19, 20]. Our emphasis is primarily intended to provide a bird's-eye view of the subject, including reference to critical applications of the formalisms and its conceptual implications, which could be attractive, in the author's very subjective opinion, for non-experts and graduate students entering for the first place in the field. Detailed authoritative reviews on the many aspects of the SP-CDFT conceptual extensions are also available [21–24].

## 7.2 Non-relativistic Spin Density Functional Theory

Let us start recalling that within the realm of non-relativistic spin-resolved density functional theory (S-DFT) [21–24], the *ad hoc* consideration of the  $\alpha$ -spin electron density  $\rho_\alpha(\mathbf{r})$  and the  $\beta$ -spin electron density  $\rho_\beta(\mathbf{r})$  plays a crucial role as fundamental variables. The introduction of the electron spin degrees of freedom is oriented to properly treat the electronic problem for  $N$ -electron  $M$ -nuclei systems with open-shell structures featuring spin-uncompensated (i.e. spin-polarized) electron distributions, either in isolated systems or as the result of the electronic interaction with an external magnetic field  $\mathbf{B}(\mathbf{r})$ . In the most basic approach to the electronic problem, the *scalar* field originated by the  $M$  nuclei  $(v(\mathbf{r}) = -\sum_k^M Z_k / |\mathbf{r} - \mathbf{R}_k|)$  as well as the external *vector* magnetic field ( $\mathbf{B}(\mathbf{r})$ ) couples with the spin magnetization density ( $\mathbf{m}(\mathbf{r})$ ) arising from the electron spin angular momentum vector, i.e.  $\mathbf{m}(\mathbf{r}) = -2\mu_B \langle \Psi[\rho, \mathbf{m}] | \sum_i^N \boldsymbol{\sigma}_i \delta(\mathbf{r} - \mathbf{r}_i) | \Psi[\rho, \mathbf{m}] \rangle$ . Note that the angular component is here not included. In this expression,  $\mu_B$  is the Bohr magneton and  $\sigma_i$  are the  $2 \times 2$  Hermitian Pauli matrices [20]. Hence, the electronic energy is explicitly considered to depend on both scalar and vector fields, namely (all equations are written in atomic units),

$$E_{V,\mathbf{B}}[\rho, \mathbf{m}] = F[\rho, \mathbf{m}] + \int \rho(\mathbf{r})v(\mathbf{r})d\mathbf{r} - \int \mathbf{B}(\mathbf{r}) \cdot \mathbf{m}(\mathbf{r})d\mathbf{r} \quad (7.1)$$

The universal functional  $F[\rho, \mathbf{m}]$  refers specifically to the sum of the total kinetic electronic energy  $T_e[\rho, \mathbf{m}]$  and the total electron–electron repulsion  $V_{ee}[\rho, \mathbf{m}]$  [20], i.e.

$$F[\rho, \mathbf{m}] = \langle \Psi[\rho, \mathbf{m}] | \hat{T}_e + \hat{V}_{ee} | \Psi[\rho, \mathbf{m}] \rangle \quad (7.2)$$

In such a general case of Eqs (7.1) and (7.2), the  $v$ -representability problem is severe, given the nontrivial still open problem associated with the non-uniqueness map between the set of potentials, i.e.  $(v(\mathbf{r}), \mathbf{B}(\mathbf{r}))$ , and densities, i.e.  $(\rho(\mathbf{r}), \mathbf{m}(\mathbf{r}))$  [25–29].

Both theoretical and computational simplifications arise by considering only *one-component magnetic fields*, i.e.  $\mathbf{B}(\mathbf{r}) = (0, 0, \gamma(r))$ , for which the one-to-one correspondence between the density and the non-vanishing component of magnetization is *granted*. The magnetic field and magnetization  $\mathbf{m}(\mathbf{r})$  are thus entirely *collinear*, e.g. along the  $z$ -component for instance. In such a case, Eq. (7.1) becomes [23, 28, 30, 31].

$$E[\rho^\alpha, \rho^\beta] = F[\rho^\alpha, \rho^\beta] + \int v^\alpha(\mathbf{r})\rho^\alpha(\mathbf{r})d\mathbf{r} + \int v^\beta(\mathbf{r})\rho^\beta(\mathbf{r})d\mathbf{r} \quad (7.3)$$

given that  $m_z(\mathbf{r}) = -\mu_B(\rho^\alpha(\mathbf{r}) - \rho^\beta(\mathbf{r})) = -\mu_B\rho_S(\mathbf{r})$ , and where  $v^\alpha(\mathbf{r}) = v(\mathbf{r}) + \mu_B\gamma(\mathbf{r})$  and  $v^\beta(\mathbf{r}) = v(\mathbf{r}) - \mu_B\gamma(\mathbf{r})$  [22, 32]. Note that we here explicitly use the selected component of the magnetic field  $\gamma(\mathbf{r})$  to expressly emphasize the imposed limitations of the approach. Of course, the universal functional Eq. (7.2) now stands for  $F[\rho^\alpha, \rho^\beta] = \langle \Psi[\rho^\alpha, \rho^\beta] | \hat{T}_e + \hat{V}_{ee} | \Psi[\rho^\alpha, \rho^\beta] \rangle$ , and can be appropriately considered within the context of the Hohenberg–Kohn theorem holding for spin densities [32, 33]. The minimization of the energy functional in Eq. (7.3) for both  $\rho^\alpha(\mathbf{r})$  and  $\rho^\beta(\mathbf{r})$ , subject to the constraints  $\int \rho^\alpha(\mathbf{r}) = N_\alpha$  and  $\int \rho^\beta(\mathbf{r}) = N_\beta$ , yields the fundamental Euler–Lagrange S-DFT equations,

$$\mu_\alpha = \left[ \frac{\delta F}{\delta \rho^\alpha} \right]_{\rho_\beta} + v^\alpha(\mathbf{r}), \text{ and } \mu_\beta = \left[ \frac{\delta F}{\delta \rho^\beta} \right]_{\rho_\alpha} + v^\beta(\mathbf{r}) \quad (7.4)$$

that would provide the ground-state minimum energy associated to the fixed pair values of  $N_\alpha$  and  $N_\beta$ . Equation (7.4) can also be written as

$$\mu_N = \left[ \frac{\delta F}{\delta \rho} \right]_{\rho_S} + v(\mathbf{r}), \text{ and } \mu_S = \left[ \frac{\delta F}{\delta \rho_S} \right]_{\rho} - \mu_B\gamma(\mathbf{r}) \quad (7.5)$$

Within the spirit of the Kohn–Sham (KS) approach, one-electron (spin) orbitals  $\psi_{i\alpha}(\mathbf{r}) = \phi_{i\alpha}(\mathbf{r})\alpha(s)$  and  $\psi_{i\beta}(\mathbf{r}) = \phi_{i\beta}(\mathbf{r})\beta(s)$ , are introduced to deal with the kinetic energy  $T_S[\rho^\alpha, \rho^\beta]$  of a reference system of noninteracting electrons with densities  $\rho^\alpha(\mathbf{r})$  and  $\rho^\beta(\mathbf{r})$ ,

$$T_S[\rho^\alpha, \rho^\beta] = \sum_{i\sigma} n_{i\sigma} \left\langle \phi_{i\sigma}(\mathbf{r}) \left| \left( -\frac{1}{2} \nabla^2 \right) \right| \phi_{i\sigma}(\mathbf{r}) \right\rangle \quad (7.6)$$

$\phi_{i\alpha}(\mathbf{r})$  and  $\phi_{i\beta}(\mathbf{r})$  denote the spatial orbitals of each spin symmetry described by the spin functions  $\alpha(s)$  and  $\beta(s)$ . This fact is just an *ad hoc* introduction of spin in such a non-relativistic limit for an S-DFT framework. Henceforth, the energy functional in Eq. (7.3) becomes a functional of *spin orbitals*, and we can write that

$$E[\rho^\alpha, \rho^\beta] = T_S[\rho^\alpha, \rho^\beta] + J[\rho^\alpha, \rho^\beta] + E_{XC}[\rho^\alpha, \rho^\beta] + \int v^\alpha(\mathbf{r})\rho^\alpha(\mathbf{r})d\mathbf{r} + \int v^\beta(\mathbf{r})\rho^\beta(\mathbf{r})d\mathbf{r} \quad (7.7)$$

where  $J[\rho^\alpha, \rho^\beta]$  and  $E_{XC}[\rho^\alpha, \rho^\beta]$  stand for the electrostatic Coulomb interaction and the exchange-correlation functional, respectively. Correspondingly, Eq. (7.4) becomes,

$$\mu_\alpha = \frac{\delta T_S[\rho^\alpha, \rho^\beta]}{\delta \rho^\alpha(\mathbf{r})} + v_{\text{eff}}^\alpha(\mathbf{r}), \text{ and } \mu_\beta = \frac{\delta T_S[\rho^\alpha, \rho^\beta]}{\delta \rho^\beta(\mathbf{r})} + v_{\text{eff}}^\beta(\mathbf{r}) \quad (7.8)$$

where effective potentials can be defined as

$$v_{\text{eff}}^\alpha(\mathbf{r}) = \int \frac{\delta \rho(\mathbf{r}')}{|\mathbf{r} - \mathbf{r}'|} d\mathbf{r}' + \frac{\delta E_{XC}[\rho^\alpha, \rho^\beta]}{\delta \rho^\alpha(\mathbf{r})} + v(r) + \mu_B\gamma(\mathbf{r}), \text{ and} \\ v_{\text{eff}}^\beta(\mathbf{r}) = \int \frac{\delta \rho(\mathbf{r}')}{|\mathbf{r} - \mathbf{r}'|} d\mathbf{r}' + \frac{\delta E_{XC}[\rho^\alpha, \rho^\beta]}{\delta \rho^\beta(\mathbf{r})} + v(r) - \mu_B\gamma(\mathbf{r}) \quad (7.9)$$

Note we are pointing out an explicit consideration of the one-component nature of the magnetic field. To deal with Eq. (7.7), the KS approach implies solving  $N(=N_\alpha + N_\beta)$  one-electron equations,

$$\left[ -\frac{1}{2} \nabla^2 + v_{\text{eff}}^\alpha(\mathbf{r}) \right] \phi_{i\alpha}(\mathbf{r}) = \varepsilon_{i\alpha} \phi_{i\alpha}(\mathbf{r}) \text{ and } \left[ -\frac{1}{2} \nabla^2 + v_{\text{eff}}^\beta(\mathbf{r}) \right] \phi_{i\beta}(\mathbf{r}) = \varepsilon_{i\beta} \phi_{i\beta}(\mathbf{r}) \quad (7.10)$$



where the normalization constraints are  $\langle \phi_{i\alpha} | \phi_{i\alpha} \rangle = 1$  and  $\langle \phi_{i\beta} | \phi_{i\beta} \rangle = 1$ . Thus, after a suitable model for the spin-resolved exchange-correlation functional and/or associated potential is defined, i.e.  $v_{XC}^{\alpha\beta}(\mathbf{r}) \equiv \delta E_{XC}[\rho^\alpha, \rho^\beta] / \delta \rho^{\alpha\beta}(\mathbf{r})$ , a self-consistent iterative procedure implying Eqs. (7.8–7.10) yields the optimum spin densities consistent with the chosen selection of the total number of electrons  $N$  and a given spin number  $N_S (= N_\alpha - N_\beta)$ , i.e.

$$\rho^\alpha(\mathbf{r}) = \sum_i^{N_\alpha} n_{i\alpha} |\phi_{i\alpha}(\mathbf{r})|^2 \text{ and } \rho^\beta(\mathbf{r}) = \sum_i^{N_\beta} n_{i\beta} |\phi_{i\beta}(\mathbf{r})|^2 \quad (7.11)$$

The electron spin-density functions are considered the primary carriers of information on the system within such a framework.

It is important to emphasize that the above non-relativistic and collinear magnetic field restricted version of S-DFT, has served as a basic framework for developing what has been named a *conceptual spin-polarized version of DFT (SP-DFT)* treatment of chemical reactivity [21–24]. It is clear that within such a conceptual SP-DFT context [23, 32], equivalent representations can be built based on both  $\rho(\mathbf{r})$  and  $\rho_S(\mathbf{r})$  or both  $\rho^\alpha(\mathbf{r})$  and  $\rho^\beta(\mathbf{r})$  as pairs of essential variables. It can be noted that by fixing  $N_S$  and  $N$ , non-uniqueness can be removed, providing a *conceptual spin-resolved framework to describe reactivity involving both charge transfer and spin polarization*. It was indeed pointed out by Gal et al. [34] that even the non-uniqueness of  $\mathbf{B}(\mathbf{r})$  implies the nonexistence of the total derivative of  $E_{v(\mathbf{r}), \mathbf{B}(\mathbf{r})}(\rho(\mathbf{r}), \rho_S(\mathbf{r}))$  with respect to  $\rho_S(\mathbf{r})$ , it does not inhibit the associated one-sided derivatives, providing a sound basis for the concept of spin potential [34]. Hence, and within a perturbative perspective to chemical reactivity [22], the SP-DFT formalism can be conveniently exploited using suited Legendre-transformed [21, 23, 24] ensemble representations based on the  $[\rho, \rho_S]$  (or  $[N, N_S]$ ) and  $[\rho_\alpha, \rho_\beta]$  (or  $[N_\alpha, N_\beta]$ ) equivalent representations. It has been shown that the derivation of critical identities linking the  $[N, N_S]$  and  $[N_\alpha, N_\beta]$  SP-DFT representations is possible using a simple *matrix-vector notation* [21–24]. Indeed, it has been emphasized that, in terms of such notation (and associated transformation rules), *all* formal identities involving chemical descriptors of the conceptual DFT share essentially *the same* mathematical structure [22].

### 7.3 Conceptual SP-DFT: Electronic Descriptors

It is clear that within the so-called “*perturbative approximation to chemical reactivity*” [3, 4, 33, 35, 36], *global*, *local*, and *non-local* electronic hierarchies of descriptors arise from the Taylor series expansion associated with the variation of energy-related functionals, described in terms of essential variables of any chosen suitable (ensemble)-representation. The coefficients of such a series expansion are there identified with the different chemical reactivity responses. Chemical reactivity becomes thus represented and understood in terms of *responses against perturbations*. These descriptors are the essential ingredients entering any conceptual rationalization of both *charge transfer* and/or *spin polarization* (i.e. *spin-transfer*), within

the limits of applicability associated with the SP-DFT framework. Correspondingly, and using a matrix notation [21, 23, 24], we can express the change in the *state functions* representing the electronic energy  $E$ , the grand potential,  $\Omega = E - \bar{\mu} \cdot \bar{N}$ , and even the universal functional,  $F = E - \int \overleftrightarrow{\rho}(\mathbf{r}) \cdot \bar{v}(\mathbf{r}) d\mathbf{r}$ , of any system, as [22],

$$\begin{aligned} \Delta E = & \bar{\mu} \cdot \Delta \bar{N} + \int \bar{\rho}(\mathbf{r}) \cdot (\Delta \bar{v}(\mathbf{r})) d\mathbf{r} + \frac{1}{2!} [(\Delta \bar{N})^T \cdot \overleftrightarrow{\eta} \cdot (\Delta \bar{N})] + \\ & \int (\Delta \bar{v}(\mathbf{r}))^T \cdot \overleftrightarrow{f}(\mathbf{r}) \cdot (\Delta \bar{N}) d\mathbf{r} + \frac{1}{2!} \iint (\Delta \bar{v}(\mathbf{r}))^T \cdot \overleftrightarrow{\chi}(\mathbf{r}, \mathbf{r}') \cdot (\Delta \bar{v}(\mathbf{r}')) d\mathbf{r} d\mathbf{r}' + \dots \end{aligned} \quad (7.12)$$

$$\begin{aligned} \Delta \Omega = & -\bar{N} \cdot \Delta \bar{\mu} + \int \bar{\rho}(\mathbf{r}) \cdot (\Delta \bar{v}(\mathbf{r})) d\mathbf{r} - \frac{1}{2!} [(\Delta \bar{\mu})^T \cdot \overleftrightarrow{S} \cdot (\Delta \bar{\mu})] + \\ & \int (\Delta \bar{v}(\mathbf{r}))^T \cdot \overleftrightarrow{s}(\mathbf{r}) \cdot (\Delta \bar{\mu}) d\mathbf{r} - \frac{1}{2!} \iint (\Delta \bar{v}(\mathbf{r}))^T \cdot \overleftrightarrow{s}(\mathbf{r}, \mathbf{r}') \cdot (\Delta \bar{v}(\mathbf{r}')) d\mathbf{r} d\mathbf{r}' + \dots \end{aligned} \quad (7.13)$$

$$\Delta F = - \int \bar{u}(\mathbf{r}) \cdot (\Delta \bar{\rho}(\mathbf{r})) d\mathbf{r} + \frac{1}{2!} \iint (\Delta \bar{v}(\mathbf{r}))^T \cdot \overleftrightarrow{\eta}(\mathbf{r}, \mathbf{r}') \cdot (\Delta \bar{\rho}(\mathbf{r}')) d\mathbf{r} d\mathbf{r}' + \dots \quad (7.14)$$

representing the way the ground-state function responds to changes in proper state variables defining a closed-system (i.e.  $E$  is the state function), an open-system ( $\Omega$  is the state function), and/or a density (e.g.  $F$  is the state function) representation, respectively. In Eqs (7.12)–(7.14), the global quantities corresponding to the number of electrons  $\bar{N}$ , the chemical potential  $\bar{\mu}$ , softness  $\overleftrightarrow{S}$ , and hardness  $\overleftrightarrow{\eta}$ ; the *local* descriptors such as the electron density  $\bar{\rho}(\mathbf{r})$ , the external potential  $\bar{v}(\mathbf{r})$ , the grand potential  $\bar{u}(\mathbf{r})$ , the softness  $\overleftrightarrow{s}(\mathbf{r})$ , and the Fukui function  $\overleftrightarrow{f}(\mathbf{r})$ ; and the *non-local* indices such as the linear response of density function  $\overleftrightarrow{\chi}(\mathbf{r}, \mathbf{r}')$ , the softness  $\overleftrightarrow{s}(\mathbf{r}, \mathbf{r}')$  and hardness  $\overleftrightarrow{\eta}(\mathbf{r}, \mathbf{r}')$  define complete sets of reactivity hierarchies. The *global* descriptors characterize the system as a single entity, being associated with global responses against global perturbations. Such global responses are intrinsically connected to electronic or even thermodynamic stability. The local indicators (i.e.  $\mathbf{r}$ -dependent) on the other hand, are associated with both global or local responses against local or global perturbations, respectively. Such local descriptors can thus be connected to chemical concepts of regional selectivity. The *non-local* indices  $\mathbf{r}$ -,  $\mathbf{r}'$ -dependent) correspond to local responses against local perturbations, and they can be associated with activation/deactivation concepts of chemical reactivity. The universal matrix–vector notation for conceptual DFT enables the efficient transferring of results to *any* formulation of S-DFT and even to spin-free conceptual DFT (see Ref. [22] for complete details), offering a unifying perspective on conceptual DFT as a whole [21–24].

The link between the *global*, *local*, and *non-local* reactivity indicators that features the CDFT framework, including the inverse relationships between the global softness and global hardness [37, 38], the inverse relationship between the hardness kernel and the softness kernel [37, 39, 40], the Berkowitz–Parr identity [37],  $\overleftrightarrow{\chi}(\mathbf{r}, \mathbf{r}') = \overleftrightarrow{f}(\mathbf{r}) \cdot \overleftrightarrow{S} \cdot (\overleftrightarrow{f}(\mathbf{r}'))^T - \overleftrightarrow{s}(\mathbf{r}, \mathbf{r}')$ , which links the Fukui function and

the local softness, and the Harbola–Chattaraj–Cedillo–Parr identity [22, 41, 42],  $\vec{\eta} = \int \vec{\eta}(\mathbf{r}, \mathbf{r}') \cdot \vec{f}(\mathbf{r}') d\mathbf{r}'$ , are straightforward examples. These facts are valuable in the analysis of electrophilicity/nucleophilicity interactions, as well as in testing the general validity of chemical principles (e.g. maximum hardness principle (MHP) [9, 43], hard-soft acid–base principle (HSAB) [6, 7, 43]) in the context of a chemical process involving both charge transfer and spin polarization effects.

### 7.3.1 On Global and Local Electronic Descriptors

Spin-resolved *global* and *local* chemical reactivity descriptors were presented for the first time by Galván et al. [17] within the  $[N, N_S]$  representation, and later by Ghanty and Ghosh within a  $[N_\alpha, N_\beta]$  representation in 1994 [18]. We will explicitly consider the  $[N, N_S]$  representation, where the Euler–Lagrange multipliers  $\mu_N$  and  $\mu_S$  in Eq. (7.5) constitute indeed  $N_S$ -constant *chemical potential* and  $N$ -constant *spin potential*, respectively [44], namely [21, 23, 24]

$$\mu_N = [\partial E / \partial N]_{N_S, v(\mathbf{r}), \gamma(\mathbf{r})} \text{ and } \mu_S = [\partial E / \partial N_S]_{N, v(\mathbf{r}), \gamma(\mathbf{r})} \quad (7.15)$$

*These quantities describe constrained responses of the entire system against global perturbations.* Their changes with respect to variations in the number of electrons  $N$ , at constant  $N_S$  (i.e. constrained charge transfer), or in the spin number  $N_S$  at constant  $N$  (i.e. spin-polarization processes) are identified as a different type of hardness responses, i.e.

$$\begin{aligned} \eta_{NN} &= [\partial \mu_N / \partial N]_{N_S, v(\mathbf{r}), \gamma(\mathbf{r})}, \eta_{NS} = [\partial \mu_N / \partial N_S]_{N, v(\mathbf{r}), \gamma(\mathbf{r})}, \\ \eta_{SN} &= [\partial \mu_S / \partial N]_{N_S, v(\mathbf{r}), \gamma(\mathbf{r})}, \text{ and } \eta_{SS} = [\partial \mu_S / \partial N_S]_{N, v(\mathbf{r}), \gamma(\mathbf{r})} \end{aligned} \quad (7.16)$$

Spin-resolved extensions for the electrophilicity index [22] arise naturally, i.e.  $2\omega = (\vec{\mu})^T \cdot \vec{S} \cdot \vec{\mu} = (\vec{\mu})^T \cdot (\vec{\eta})^{-1} \cdot \vec{\mu}$ . Intended to *study local regioselectivity*, the  $[N, N_S]$  SP-DFT Fukui functions [21, 23, 24] arise from the derivatives of  $\mu_N$  and  $\mu_S$  potentials with respect to variations in  $v(\mathbf{r})$  and  $v_S(\mathbf{r})$  at  $N$  and/or  $N_S$  held constant, namely,

$$\begin{aligned} f_{NN}(\mathbf{r}) &= [\partial \rho(\mathbf{r}) / \partial N]_{N_S, v(\mathbf{r}), \gamma(\mathbf{r})}, f_{NS}(\mathbf{r}) = [\partial \rho(\mathbf{r}) / \partial N_S]_{N, v(\mathbf{r}), \gamma(\mathbf{r})}, \\ f_{SN}(\mathbf{r}) &= [\partial \rho_S(\mathbf{r}) / \partial N]_{N_S, v(\mathbf{r}), \gamma(\mathbf{r})}, \text{ and } f_{SS}(\mathbf{r}) = [\partial \rho_S(\mathbf{r}) / \partial N_S]_{N, v(\mathbf{r}), \gamma(\mathbf{r})} \end{aligned} \quad (7.17)$$

Note that Maxwell relations allow us a direct connection with variations of  $\rho(\mathbf{r})$  and  $\rho_S(\mathbf{r})$  against changes in  $N$  and/or  $N_S$ ,

$$\begin{aligned} f_{NN}(\mathbf{r}) &= [\delta \mu_N / \delta v(\mathbf{r})]_{N, N_S, \gamma(\mathbf{r})}, f_{NS}(\mathbf{r}) = [\delta \mu_N / \delta \gamma(\mathbf{r})]_{N, N_S, v(\mathbf{r})}, \\ f_{SN}(\mathbf{r}) &= [\delta \mu_S / \delta v(\mathbf{r})]_{N, N_S, \gamma(\mathbf{r})}, \text{ and } f_{SS}(\mathbf{r}) = [\delta \mu_S / \delta \gamma(\mathbf{r})]_{N, N_S, v(\mathbf{r})} \end{aligned} \quad (7.18)$$

Evaluation of the simplest condensed-to-atom SP-DFT model of Fukui functions [45] is straightforward within the KS framework. Even though there is a complicated coupling between *electron transfer* and *spin transfer* in higher-order terms within a  $[N, N_S]$  representation [21, 23, 24], such a framework has demonstrated to be helpful for the characterization of both excitation/deexcitation processes implying singlet-triplet multiplicities [21–24] and radical reactions [46, 47]. Straightforward

extensions concerning other descriptors include local electrophilicities and dual descriptors [48] and reaction indicators [49–51].

### 7.3.2 Non-local Electronic Descriptors

Local responses to local perturbations constitute non-local electronic responses [39, 40, 45, 52, 53]. In such a context, linear responses associated with density  $\chi(\mathbf{r}, \mathbf{r}') = [\delta\rho(\mathbf{r})/\delta v(\mathbf{r}')]_N$  [54], Fukui function  $f(\mathbf{r}, \mathbf{r}') = [\delta f(\mathbf{r})/\delta v(\mathbf{r}')]_N$ , and softness  $s(\mathbf{r}, \mathbf{r}') = [\delta\rho(\mathbf{r})/\delta v(\mathbf{r}')]_\mu$  [37] are well-known examples in non-spin-polarized CDFT. Reactivity kernels for hardness and softness hierarchies of reactivity in the SP-DFT framework were discussed by Chamorro et al. [55]. Fias and coworkers [56, 57] have presented analytical expressions for the SP-DFT linear response functions in the  $[N_\alpha, N_\beta]$  representation,

$$\chi_{\sigma\tau}(\mathbf{r}, \mathbf{r}') = \frac{\delta\rho_\sigma(\mathbf{r})}{\delta v_\tau(\mathbf{r}')} = -2 \sum_{ia} \left( \sum_{jb} (M^{-1})_{ia\sigma, jb\tau} \phi_{j\tau}(\mathbf{r}') \phi_{b\tau}^*(\mathbf{r}') \phi_{i\sigma}(\mathbf{r}) \phi_{a\sigma}^*(\mathbf{r}) \right) \quad (7.19)$$

which, as immediately noted, is linearly related to the corresponding  $[N, N_S]$  representation. In this expression, we have that,  $M_{ia\sigma, jb\tau} = (\epsilon_c - \epsilon_j) \delta_{\sigma\tau} \delta_{ij} \delta_{bc} + 2\langle \phi_{i\sigma} \phi_{j\tau} | \phi_{a\sigma} \phi_{b\tau} \rangle + 2\langle \phi_{i\sigma} \phi_{j\tau} | f_{XC}(\mathbf{r}, \mathbf{r}') | \phi_{a\sigma} \phi_{b\tau} \rangle$ , where  $f_{XC}(\mathbf{r}, \mathbf{r}') = \delta^2 E_{XC} / \delta\rho(\mathbf{r}) \delta\rho(\mathbf{r}')$ . The radial distribution of the associated kernels has been discussed for first- and second-row atoms, including open-shell configurations [56], and noble gases [57].

### 7.3.3 The Finite-Difference Approximations for Spin-Resolved Descriptors Within Kohn–Sham Theory

Ayers and Miranda–Quintana have presented a critical discussion concerning working formulae for spin-resolved CDFT descriptors based on Kohn–Sham formalism [58]. Finite-difference approximations to spin-resolved global reactivity indicators require a parabolic interpolation model for the dependence of the energy on  $N_\alpha$  and  $N_\beta$  (i.e. two-side spin-reactivity descriptors), yielding the central-difference approximation for the spin potentials and hardness responses,

$$\begin{aligned} \mu_\alpha^0 &\approx \frac{1}{2} (\epsilon_L^\alpha + \epsilon_H^\alpha), \mu_\beta^0 \approx \frac{1}{2} (\epsilon_L^\beta + \epsilon_H^\beta), \eta_{\alpha\alpha}^0 \approx \epsilon_L^\alpha - \epsilon_H^\alpha, \eta_{\beta\beta}^0 \approx \epsilon_L^\beta - \epsilon_H^\beta \\ \mu_N^0 &\approx \frac{1}{2} (\mu_\alpha^0 + \mu_\beta^0), \mu_S^0 \approx \frac{1}{2} (\mu_\alpha^0 - \mu_\beta^0), \eta_{SS}^0 \approx \eta_{NN}^0 \approx \frac{1}{4} (\eta_\alpha^0 + \eta_\beta^0) \end{aligned} \quad (7.20)$$

Preliminary numerical results concerning the estimation of spin potentials and spin philicities indicate better performance than results using only linear interpolation models or mixed combinations [58]. An analysis comparing frozen-core and finite-differences approximations for evaluating both global and local descriptors was earlier presented by Garza et al. [59], also emphasizing the straightforward linear transformation connecting the  $[N, N_S]$  and  $[N_\alpha, N_\beta]$  SP-DFT representations. Vargas et al. [60] discussed the impact of Koopmans'-like approximations on evaluating reactivity indicators within a Kohn–Sham context. A general discussion

concerning a proper formulation of CDFT reactivity indicators for degenerate and quasi-degenerate ground states has been presented by Ayers and coworkers [61]. It should be noted at this point that all the above-defined global, local, and non-local DFT electronic hierarchy of descriptors essentially describes electron or spin-density responses against perturbations at some specific fixed nuclei configuration. A complete picture of chemical reactivity should also incorporate the nucleus responses.

## 7.4 Conceptual SP-DFT: Nuclei-Related Descriptors

Following Cohen's formulations [62], the so-called nuclear reactivity indices  $\Phi_{N,k}$  and  $\Phi_{S,k}$  extensions to the spin-polarized density functional theory were first presented by Chamorro et al. [63] and also discussed by Cardenas et al. [64], i.e.

$$\begin{aligned}\Phi_{N,k} &= \left[ \frac{\partial \mathbf{F}_k}{\partial N} \right]_{N_S} = - \left[ \frac{\delta \mu_N}{\delta \mathbf{R}_k} \right]_{\{\mathbf{R}_l \neq k\}} = Z_k \int \frac{f_{NN}(\mathbf{r})}{|\mathbf{r} - \mathbf{R}_k|^3} (\mathbf{r} - \mathbf{R}_k) d\mathbf{r}, \text{ and} \\ \Phi_{S,k} &= \left[ \frac{\partial \mathbf{F}_k}{\partial N_S} \right]_N = - \left[ \frac{\delta \mu_S}{\delta \mathbf{R}_k} \right]_{\{\mathbf{R}_l \neq k\}} = Z_k \int \frac{f_{NS}(\mathbf{r})}{|\mathbf{r} - \mathbf{R}_k|^3} (\mathbf{r} - \mathbf{R}_k) d\mathbf{r}\end{aligned}\quad (7.21)$$

where  $\mathbf{F}_k$  is the Hellmann–Feynman force on the  $k$ -nucleus in the system, i.e. [62, 65–67].

$$\mathbf{F}_k = Z_k \int \frac{\rho(\mathbf{r})(\mathbf{r} - \mathbf{R}_k)}{|\mathbf{r} - \mathbf{R}_k|^3} d\mathbf{r} - Z_k \sum_{l \neq k} \frac{Z_l(\mathbf{R}_l - \mathbf{R}_k)}{|\mathbf{R}_l - \mathbf{R}_k|^3}\quad (7.22)$$

Note that the spin-resolved nuclear Fukui functions also represent the change of the restrained electronic chemical potential and spin potentials [defined in Eqs (7.5) and (7.18)] upon nuclear displacement. The  $[N_\alpha, N_\beta]$  SP-DFT representation becomes simply,

$$\Phi_k^\sigma = \left[ \frac{\partial \mathbf{F}_k}{\partial N_\sigma} \right]_{\sigma'} = - \left[ \frac{\delta \mu^\sigma}{\delta \mathbf{R}_k} \right]_{\{\mathbf{R}_l \neq k\}} = Z_k \int \frac{f^{\sigma\sigma}(\mathbf{r}) + f^{\sigma\sigma'}(\mathbf{r})}{|\mathbf{r} - \mathbf{R}_k|^3} (\mathbf{r} - \mathbf{R}_k) d\mathbf{r}\quad (7.23)$$

where  $\sigma$  stands for the  $\{\alpha|\beta\}$ -spin symmetries. These nuclear reactivity descriptors can be understood within a perturbative approach by explicitly considering the nuclei position dependence of the external potential  $v(\mathbf{r})$  on the nuclei coordinates  $\{\mathbf{R}_k\}$  [4]. Thus, for instance, within a canonical  $[N, N_S]$  representation of the total energy of the system  $W = E + V_{nn}$  (i.e. adding the nuclear–nuclear interaction term to the electronic energy), it is clear that the Hellmann–Feynman force on nuclei is  $\mathbf{F}_k = -(\delta W / \delta \mathbf{R}_k)_{N, N_S, \gamma(\mathbf{r})}$ . Indeed, further considerations of such a force in terms of the basic variables of the  $[N, N_S]$  SP-DFT representation allow us to write the second terms in Eq. (7.23), given that  $\mu_N = -(\partial W / \partial N)_{N_S, \{\mathbf{R}_k\}, \gamma(\mathbf{r})}$  and  $\mu_S = -(\partial W / \partial N_S)_{N, \{\mathbf{R}_k\}, \gamma(\mathbf{r})}$ . The treatment of nuclei changes becomes thus related to the explicit consideration, within the realm of validity of the Born–Oppenheimer approximation, of changes in the nuclei forces.

The applicability of such a nuclei-related descriptor in connection with the spin-resolved framework of electronic indicators can be explored in terms of the local Berlin function  $\vartheta_v(\mathbf{r})$ ,

$$\begin{aligned}\sum_k \Phi_{N,k} \mathbf{R}_k &= - \int f_{NN}(\mathbf{r}) \vartheta_v(\mathbf{r}) d\mathbf{r}, \text{ and} \\ \sum_k \Phi_{S,k} \mathbf{R}_k &= - \int f_{NS}(\mathbf{r}) \vartheta_v(\mathbf{r}) d\mathbf{r}\end{aligned}\quad (7.24)$$

where  $\vartheta_v(\mathbf{r}) \equiv - \sum_k Z_k \mathbf{R}_k \cdot (\mathbf{r} - \mathbf{R}_k) / |\mathbf{r} - \mathbf{R}_k|^3$ . The usefulness of such descriptors has been less explored. However, illustrative examples devoted to measuring the magnitude of the onset of the perturbation (note, not the actual response of the potential) in the spin number in excitation/deexcitation processes are available for simple systems, including water, formaldehyde, and substituted nitrenes and phosphinidenes [63], as well as triatomic carbenic species [64].

## 7.5 Brief Update Concerning Conceptual SP-DFT Applications (2010–2020)

The current literature indicates a diversity of discoveries over the last ten years, evidencing a continuous activity concerning the development and application of SP-DFT descriptors, which we shall outline in the following. Ghashghaee and Ghambarian have explored the usefulness of the spin-resolved chemical potential, hardness, and philicity indices to characterize *ZnO-doped black phosphorene monolayer slabs for sensing nitrogen dioxide* [68]. Anota and coworkers [69] used global SP-DFT descriptors to rationalize the *adsorption of caffeine on boron nitride fullerene, the interaction between the octahedral  $B_{12}N_{12}$  cage and iron clusters  $Fe_n$*  [70], the *global stability of boron nitride cages  $B_xN_y$  ( $x + y = 28$ )* [69], the *interactions of  $B_{12}N_{12}$  fullerenes on graphene and boron nitride nanosheets* [71], and the *adsorption processes of CO on magnetic  $BNF^-$  and on the  $[BNF:B_6]^-$  and  $[BNF:C_6]^-$  composites* [72]. An SP-DFT analog to the reaction flux descriptor, namely,  $J(\xi) = -\partial\mu_N/\partial\xi$  has been introduced by Vargas and coworkers [73] to understand energy profiles and reactivity patterns associated with *hydrogen-atom transfer mechanisms in phenolic compounds toward radicals*. Based on the previously established connection between pairing energies and the SP-DFT spin potential [44], Galván and coworkers [74] have analyzed *confinement effects on the spin potential (within Kohn–Sham formalism) of first-row transition metals*. The *global spin reactivity of carbenes, silylenes, and germynes was re-examined using descriptors based on proper interpolation formulas for the energy* either as a function of the basic variables of both the  $[N_\alpha, N_\beta]$  and  $[N, N_S]$  representations [58]. Peng and Yang [75] have proposed *analytical expressions for the spin-resolved Fukui function and other response functions within the consideration of non-local fractional systems*. Lamsabhi et al. [76] have explored the usefulness of the  $[N, N_S]$  SP-DFT global and philicity derived indicators in the *rationalization of the spin-allowedness nature concerning the oxygenation of phenylhalocarbenes*. The

$[N, N_S]$  SP-DFT global and philicity descriptors were applied by Du et al. [77] in the analysis of *spin-catalysis effects of tantalum clusters cations*. The vertical lower-upper spin energies are found linearly correlated with spin-philicity descriptors [77]. Gal and Geerlings [78] have presented an SP-DFT *generalization for the Perdew–Parr–Levy–Balduz relationship* within the  $E[N, N_S]$  SP-DFT representation, providing a formal basis for a proper discussion of the energy surface  $E[N, N_S]$  and its *implications on chemical potentials, highest-occupied and lowest-unoccupied KS spin energies, and derivative discontinuities* [78]. General considerations associated with *fractional particle and spin numbers connected to the Lieb functional* were also discussed [79]. Geerlings and coworkers [80] rationalized the *intrinsic stability pattern and reactivity of series of silylenes and p-benzynes intermediates exhibiting a different degree of biradical character* using global SP-DFT  $[N, N_S]$  descriptors. Pérez and Chamorro [81] described the *stability and regional selectivity associated with to series of N-heterocyclic carbenes incorporating B and P atoms*. As is the case for analog systems [45, 82], the philicities for spin polarization and the vertical energy gap are shown to be linearly correlated [81]. The role played by the *local spin-density distribution in directing the reactivity of (di/poly)radical compounds to participate in radical reactions* [83], and the way it contributes to *model potential energy surfaces in connection to qualitative valence bond theories* has been discussed [84]. López-Albarrán and coworkers [85] applied the  $[N, N_S]$  Fukui functions, within the frozen-core approximation, to study the *key role of monoligols in lignin polymerization processes*. As measured through the  $[N, N_S]$  SP-DFT *hyper-softness*,  $s_{NNN}(\mathbf{r}) \simeq S_{NN}^2 f_{NNN}(\mathbf{r})$ , Fe centers' local reactivity *has been related to the catalytic activity* by Martínez-Araya and Glossman-Mitnik [86] *in ethylene polymerization processes*. Morrison used  $[N_\alpha, N_\beta]$  Fukui functions to characterize *attached electrons' effect in temporary anion resonance states* in  $\text{Be}^-$ ,  $\text{Mg}^-$ , and  $\text{Ca}^-$  [87]. Martínez-Araya et al. have discussed the importance of the spin-resolved dual descriptor components [88], i.e.  $f^{(2)}(\mathbf{r}) = (\partial f_{NN}(\mathbf{r}) / \partial N)_{N_S, \nu(\mathbf{r}), \gamma(\mathbf{r})} = (f_{\Delta N_S < 0}^{(2)}(\mathbf{r}) + f_{\Delta N_S > 0}^{(2)}(\mathbf{r})) / 2$ , in the *assessment of substituent effects in open-shell systems such as molybdenum-oxo complexes* [89], and the *rationalization of catalytic activity in polymerization processes driven by Bis(imino)pyridine (BIMP)-Fe(II) cations* [90]. Martínez explored the *usefulness of working equations based on frontier molecular orbital densities on open-shell systems*, including NO, O, and cyclic saturated carbenes [91]. Salas-Reyes and coworkers [92] used SP-DFT Fukui functions to analyze *the reaction mechanism proposed for the aprotic-medium electrochemical oxidation of amides derived from Feluric acid*. Chamorro et al. [13] have associated the  $f_{\alpha\alpha}^\pm(\mathbf{r})$  SP-DFT Fukui function to the so-called *electrophilic and nucleophilic Parr functions*  $P^\pm(\mathbf{r})$  empirically introduced by Domingo et al. [93] in the context of *rationalizing polar chemical reactions within a free radical-like perspective*. Kovalenko and coworkers [94] have presented a *methodological framework for evaluating Fukui functions, based on the extended Koopmans' approximation for multiconfigurational Green's functions*. Chamorro and coworkers [95] have explored the usefulness of the condensed-to-atoms approach to the  $f_{NN}^\pm(\mathbf{r})$  SP-DFT Fukui in *predicting the intramolecular cyclization process's selectivity of 2'aminochalcones*. Lain and coworkers [96] have presented a *matrix implementation for the SP-DFT Fukui and dual-descriptor functions applied to both*

closed- and open-shell systems of arbitrary spin symmetry and uncorrelated/correlated level of theory. SP-DFT Fukui function's usefulness was also demonstrated by Zhong et al. [97] in analyzing  $H_2S$  bonding to metal(II) porphyrin complexes. Gal et al. [98] have proposed new definitions for the  $[N_\alpha, N_\beta]$  SP-DFT chemical hardness based on the definition of local chemical potentials. De Proft and coworkers [99] used the SP-DFT dual descriptor  $\Delta f_{NN}(\mathbf{r}) = f_{NN}^+(\mathbf{r}) - f_{NN}^-(\mathbf{r})$  for the suitable rationalization of the observed regioselectivity of radical additions to substituted alkenes. Liu applied both global and local  $[N, N_S]$  SP-DFT to the analysis of a series of (pyridine) $_n$  – metal (II) – porphyrin complexes with metal = Mg, Ca, Cr, Mn, Fe, Co, Ni, Cu, Zn, Ru, and Cd and  $n = 0, 1, \text{ and } 2$ , revealing the unique selectivity and specificity of Fe-porphyrin complexes [100].

## 7.6 Illustrating the Usefulness of Local SP-DFT Fukui Descriptors

In the following section and within a pedagogical approach, we focus on the widespread finite-difference frozen-core condensed-to-atom implementation [45] of the SP-DFT Fukui descriptors defined by Eq. (7.17). Such an implementation is a key basis for evaluating philicities [53] and dual descriptors [88] within the same context of atom-based resolution of descriptors. By considering that the norms of the spin-orbitals  $\varphi_i^\sigma(\mathbf{r}) \equiv |\phi_{i\sigma}(\mathbf{r})|^2$  as shape factors of densities [entering in Eq. (7.11)] can be expanded in any atomic basis set  $\{\chi_\mu(\mathbf{r})\}$ ,

$$\varphi_i^\sigma(\mathbf{r}) = \sum_\mu \sum_\nu c_{\mu,i}^\sigma c_{\nu,i}^\sigma \chi_\mu(\mathbf{r}) \chi_\nu(\mathbf{r}) \quad (7.25)$$

the “condensation” of the local response to a given atom  $k$  arises by summing only on the basis set contributions directly associated to such a center and by taking the complete overlap matrices  $S_{\mu\nu} \equiv \int \chi_\mu(\mathbf{r}) \chi_\nu(\mathbf{r}) d\mathbf{r}$ , namely,

$$\varphi_{i,k}^\sigma \equiv |\phi_{i\sigma,k}|^2 = \sum_{\mu \in k} \sum_\nu c_{\mu,i}^\sigma c_{\nu,i}^\sigma S_{\mu\nu} \quad (7.26)$$

Average shape factors can be indeed considered in evaluating Eq. (7.26) by summing over the complete number of degenerate spin-orbitals (if any) of each given  $\sigma$ -spin state [45]. It should be emphasized that this approach corresponds to a simple Mulliken-type partition at the frontier spin orbitals. Hence, a frozen-core approximation to Eq. (7.17), within the general validity of Eqs (7.25) and (7.26), yields simple expressions in terms of the highest occupied (HO) and lowest unoccupied (LU) spin orbitals, namely [17, 23, 45, 59],

$$\begin{aligned} f_{NN,k}^- &\approx \frac{1}{2} \left[ \varphi_{HO,k}^\alpha + \varphi_{HO,k}^\beta \right], \quad \text{and} \quad f_{NN,k}^+ \approx \frac{1}{2} \left[ \varphi_{LU,k}^\alpha + \varphi_{LU,k}^\beta \right]; \\ f_{NS,k}^- &\approx \frac{1}{2} \left[ \varphi_{HO,k}^\alpha - \varphi_{LU,k}^\beta \right], \quad \text{and} \quad f_{NS,k}^+ \approx \frac{1}{2} \left[ \varphi_{LU,k}^\alpha - \varphi_{HO,k}^\beta \right]; \\ f_{SN,k}^- &\approx \frac{1}{2} \left[ \varphi_{HO,k}^\alpha - \varphi_{HO,k}^\beta \right], \quad \text{and} \quad f_{SN,k}^+ \approx \frac{1}{2} \left[ \varphi_{LU,k}^\alpha - \varphi_{LU,k}^\beta \right]; \\ f_{SS,k}^- &\approx \frac{1}{2} \left[ \varphi_{HO,k}^\alpha + \varphi_{LU,k}^\beta \right], \quad \text{and} \quad f_{SS,k}^+ \approx \frac{1}{2} \left[ \varphi_{LU,k}^\alpha + \varphi_{HO,k}^\beta \right] \end{aligned} \quad (7.27)$$



**Table 7.1** SP-DFT condensed-to-atoms Fukui descriptors for  $^2\text{NO}$  optimized at the (U)wB97XD/6-31G(d) level of theory.

Atom $k$	$f_{NN,k}^+$	$f_{NN,k}^-$	$f_{SN,k}^+$	$f_{SN,k}^-$	$f_{NS,k}^+$	$f_{NS,k}^-$	$f_{SS,k}^+$	$f_{SS,k}^-$
N	+0.6495	+0.6712	-0.0098	-0.0494	-0.0405	-0.0187	+0.6801	+0.6406
O	+0.3505	+0.3288	+0.0098	+0.0494	+0.0405	+0.0187	+0.3199	+0.3594

Evaluation of working Eq. (7.27) is straightforward from results of any quantum mechanical program [101, 102]. Indeed, the MS Jaguar suite of programs [101] provides direct access to the evaluation of Fukui functions and Fukui atomic indices based on such approaches [45]. As a simple illustrative example, we will consider the characterization of the intrinsic reactive patterns in both charge transfer processes and spin polarization phenomena for nitric oxide NO, a ubiquitous species implied in the catalytic regulation of several biological processes as well as in spin catalytic reactions [103]. Table 7.1 reports the values of SP-DFT condensed-to-atoms Fukui descriptors evaluated from Gaussian 16 [102] results for optimizations. The keyword *IOP* (3/33 = 1) has been used to output the required overlap matrix of Eq. (7.26).

The predicted reactivity trends are the same as discussed earlier in Ref. [45]. For instance, concerning spin polarization processes occurring at constant number of electrons (i.e. spin-flip phenomena centered at NO), the negative (positive) value of  $f_{NS,k}^-$  at nitrogen (oxygen) indicates that charge density  $\rho(\mathbf{r})$  is accumulated (depleted) on the N (O) center in a  $\alpha \rightarrow \beta$  transition, associated to the doublet state. The positive  $f_{SS,k}^-$  indicators at N and O reveal that in such a spin-flip situation, the spin density  $\rho_S(\mathbf{r})$  is consistently twofold decreased at the N center. By considering  $\beta \rightarrow \alpha$  which increases the spin multiplicity of the system, the predicted responses in both density and spin density are inferred from the  $f_{NS,k}^+$  and  $f_{SS,k}^+$  responses. Charge density rearrangement is predicted to polarize the system whereas spin density is expected to increase at N by a factor of 1.8 compared to the O center. This fact points out to the N center as the active one within the arsenal of spin catalysis interests [103].

In Figure 7.1, we present isosurface maps for each of these descriptors. The rendering has been produced via the VMD [104] and Multiwfn [105] packages using cube files generated for the  $\mathbf{r}$ -dependent frozen-core approximations to Eq. (7.17) [whose condensed-to-atom resolution are Eq. (7.27)]. Panels (a) and (c) reveal the response in  $\rho(\mathbf{r})$  and  $\rho_S(\mathbf{r})$ , respectively, for the spin-flip  $\alpha \rightarrow \beta$  process associated with the doublet state. Panels (b) and (d) are the corresponding responses for the spin-flip  $\beta \rightarrow \alpha$  increasing the spin multiplicity from 2 to 4. Given the underlying finite-difference approach to Eq. (7.17),  $f_{NS}^-(\mathbf{r}) > 0$  regions are associated with those with  $\Delta\rho(\mathbf{r}) < 0$ , and vice versa. The opposite “rule” holds for the  $f_{NS}^+(\mathbf{r})$  responses. Within the same context, the decrease (or increase) of  $\rho_S(\mathbf{r})$  is easily associated with  $f_{SS}^-(\mathbf{r})$  (or  $f_{SS}^+(\mathbf{r})$ ) maps given the change in spin number is negative (positive) definite.

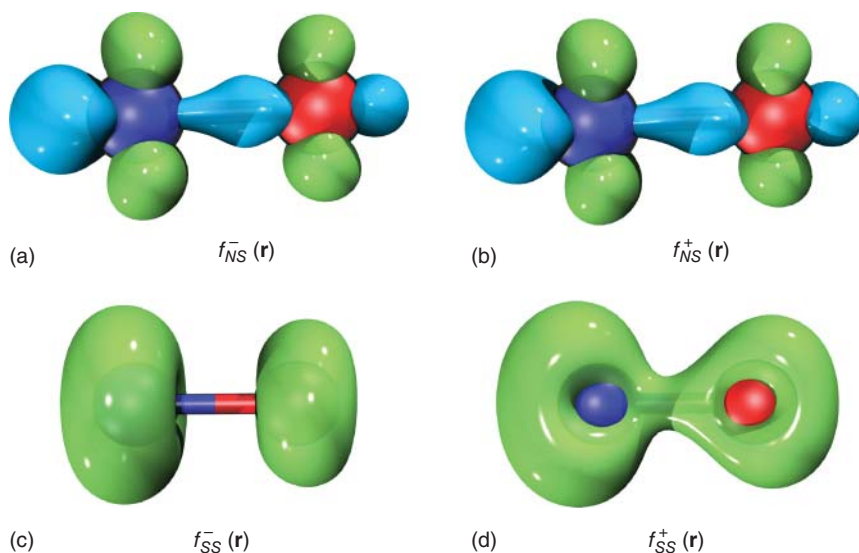


**Figure 7.1** Isosurface maps for the SP-DFT Fukui descriptors for spin-polarization phenomena evaluated at the doublet of the NO species. A positive iso value of +0.05 is depicted in green color and the negative one of  $-0.05$  in blue. (a)  $f_{NS}^-(\mathbf{r})$ , (b)  $f_{NS}^+(\mathbf{r})$ , (c)  $f_{SS}^-(\mathbf{r})$ , (d)  $f_{SS}^+(\mathbf{r})$ .

It can be instructive to highlight in this point about the increasing number of studies focused on the characterization of *selectivity in drug discovery* and *material-related sciences* on the basis of these straightforward available implementations [101] based on Eq. (7.27) [17, 45]. Valuable results in such specific context include for instance new insights for selectivity characterization of derivatives based on structures of *quinoline* [106–108], *thiourea* [109–113], *benzoxazole* [114–116], *benzene* [117], *xylene* [118], *imidazole* [119–123], *oxadiazole* [124, 125], *triazole* [126], *thiazole* [127], *pyrazine* [125, 128], *semicarbazide* [129], *amide* [130–136], *acids* [137, 138], *pyrazole* [139], *chalcone* [140], *quinoline* [141–143], *pyridoxylidene aminoguanidine* [144], *arylpiperazine* [145], *oxime* [146], *isoindoline* [147], *pyrimidine* [148, 149], *pyrrolizidine alkaloids* [150], and *peptides* [151]. In all these explorations, the local SP-DFT Fukui functions have probed its usefulness in characterizing the most reactive sites, as it has been also the case along polar organic chemical reactions, including [3 + 2] and [4 + 2] cycloadditions [12, 13, 93, 96, 152, 153].

## 7.7 Concluding Remarks and Perspectives

This work has presented fundamental aspects of the *conceptual* SP-DFT framework, also called spin-polarized CDFT (SP-CDFT). It is the non-relativistic limit of spin-DFT, where spin becomes incorporated just in the form of spin orbitals. Our revision is introductory and pedagogical [21–24]. The conceptual SP-DFT framework

allows us, within a perturbative approach, to explore *both charge transfer* processes and *spin-polarization* phenomena. The exact relationships between *electronic* [40, 45, 53] and *nuclei-forces* related chemical descriptors [154, 155] certainly provide a general reference framework for exploring chemical responses as exemplified through the exciting applications of SP-DFT reported in several areas of chemical sciences. A defying focus for further conceptual SP-DFT applications is the characterization of magnetic responses and/or materials for spintronic-derived technologies. The development of this field, even the limitations imposed for the underlying non-relativistic frameworks, is far away to be complete. Examples of areas where further work is desirable include extensions of arbitrarily defined Legendre-transformed ensemble representations. Practical applications for older and new relationships connecting both electrophilicity and nucleophilicity spin-related responses with nuclei rearrangements in chemical reactions [22, 154] are also open to further research. The subject offers several possibilities for developing theoretical and/or computational approaches that broaden the scope of applicability of chemical principles aimed to improve our understanding and interpretation of chemical phenomena and reactivity [1]. Areas for future development of spin-dependent formalisms include (i) finite-temperature extensions [8, 14, 16] and free-energy-based formalisms for SP-DFT [156, 157]; (ii) development of a fully relativistic treatment of spin-dependent electronic and nuclei-related chemical “reactivity”, (iii) time-dependent considerations of reactivity hierarchies defined within the spirit of the SP-DFT approaches, and (iv) exploration of SP-DFT nuclei-related reactivities considering static and dynamic approaches to modeling chemical reactions involving different electronic states.

Despite the above generalizations, we should undoubtedly be aware that proper and complete incorporation of *spin* (within a density-related framework) should be intrinsically related to conceptual aspects derived from a full *quantum electrodynamical density functional theory framework*. This field [158–163] remains completely open and fully defying for the entire scientific community seeking for the establishment of a formal and deeply theoretical basis for many of the successful classical principles employed in rationalizing chemical facts. Certainly, such formal advancements will contribute to strongly extend the range of standard applications, broadening the possibilities for interpretation of chemical reactivity based on development for new concepts firmly grounded within the framework offered by the mathematical structure of density-functional theory and its extensions [1].

## Acknowledgments

The author is grateful to FONDECYT (Chile) for continuous support through Grants Nos. 1030173 (2003–2007), 1070378 (2007–2010), 1100277 (2010–2014), 1140343 (2014–2018), and 1181582 (2018–2022).

## References

- 1 Geerlings, P., Chamorro, E., Chattaraj, P.K. et al. (2020). Conceptual density functional theory: status, prospects, issues. *Theor. Chem. Acc.* 139 (2): 18.
- 2 Parr, R.G. and Yang, W. (1989). *Density Functional Theory of Atoms and Molecules*. Oxford: Oxford University Press.
- 3 Ayers, P.W., Anderson, J.S.M., and Bartolotti, L.J. (2005). Perturbative perspectives on the chemical reaction prediction problem. *Int. J. Quantum Chem.* 101 (5): 520–534.
- 4 Ayers, P.W. and Parr, R.G. (2001). Variational principles for describing chemical reactions. Reactivity indices based on the external potential. *J. Am. Chem. Soc.* 123 (9): 2007–2017.
- 5 Cedillo, A. (1994). A new representation for ground states and its Legendre transforms. *Int. J. Quantum Chem., Quantum Chem. Sympos.* 28: 231–240.
- 6 Ayers, P.W. (2005). An elementary derivation of the hard/soft-acid/base principle. *J. Chem. Phys.* 122 (14): 141102.
- 7 Ayers, P.W. (2007). The physical basis of the hard/soft acid/base principle. *Faraday Discuss.* 135: 161–190.
- 8 Miranda-Quintana, R.A., Kim, T.D., Cardenas, C., and Ayers, P.W. (2017). The HSAB principle from a finite-temperature grand-canonical perspective. *Theor. Chem. Acc.* 136 (12): 6.
- 9 Pearson, R.G. (1997). *Chemical Hardness*. Oxford: Wiley.
- 10 Miranda-Quintana, R.A. and Ayers, P.W. (2019). The “ $|\Delta\mu|$  big is good” rule, the maximum hardness, and minimum electrophilicity principles. *Theor. Chem. Acc.* 138 (3): 6.
- 11 Chattaraj, P.K., Giri, S., and Duley, S. (2011). Update 2 of: electrophilicity index. *Chem. Rev.* 111 (2): PR43–PR75.
- 12 Domingo, L.R., Ríos-Gutiérrez, M., and Pérez, P. (2016). Applications of the conceptual density functional indices to organic chemistry reactivity. *Molecules* 2: 748.
- 13 Chamorro, E., Perez, P., and Domingo, L.R. (2013). On the nature of parr functions to predict the most reactive sites along organic polar reactions. *Chem. Phys. Lett.* 582: 141–143.
- 14 Miranda-Quintana, R.A., Chattaraj, P.K., and Ayers, P.W. (2017). Finite temperature grand canonical ensemble study of the minimum electrophilicity principle. *J. Chem. Phys.* 147 (12): 4.
- 15 Franco-Perez, M., Ayers, P.W., Gazquez, J.L., and Vela, A. (2015). Local and linear chemical reactivity response functions at finite temperature in density functional theory. *J. Chem. Phys.* 143 (24): 9.
- 16 Gazquez, J.L., Franco-Perez, M., Ayers, P., and Vela, A. (2019). Temperature-dependent approach to chemical reactivity concepts in density functional theory. *Int. J. Quantum Chem.* 119 (2): e25797.
- 17 Galvan, M., Vela, A., and Gazquez, J.L. (1988). Chemical reactivity in spin-polarized density functional theory. *J. Phys. Chem.* 92 (22): 6470–6474.

- 18 Ghanty, T.K. and Ghosh, S.K. (1994). Spin-polarized generalization of the concepts of electronegativity and hardness and the description of chemical binding. *J. Am. Chem. Soc.* 116 (9): 3943–3948.
- 19 Jacob, C.R. and Reiher, M. (2012). Spin in density-functional theory. *Int. J. Quantum Chem.* 112 (23): 3661–3684.
- 20 Engel, E. and Dreizler, R.M. (2011). *Density Functional Theory. An Advanced Course*. Berlin, Heidelberg, Dordrecht, London, New York: Springer-Verlag.
- 21 Vargas, R., Cedillo, A., Garza, J., and Galvan, M. (2002). Reactivity criteria in spin-polarized density functional theory. In: *Reviews of Modern Quantum Chemistry: A Celebration of the Contributions of Robert G Parr* (ed. R.G. Parr and K.D. Sen), 936–965. Singapore: World Scientific Publishing Company.
- 22 Perez, P., Chamorro, E., and Ayers, P.W. (2008). Universal mathematical identities in density functional theory: results from three different spin-resolved representations. *J. Chem. Phys.* 128 (20): 204108.
- 23 Vargas, R. and Galván, M. (2009). Spin-polarized density functional theory: chemical reactivity. In: *Chemical Reactivity Theory: A Density Functional View*, Chapter 10 (ed. P.K. Chattaraj), 137–153. Boca Raton, FL: CRC Press Taylor & Francis Group.
- 24 De Proft, F., Chamorro, E., Pérez, P. et al. (2009). Spin-polarized reactivity indices from density functional theory: theory and applications. In: *Specialist Periodical Reports: Chemical Modeling : Applications and Theory* (ed. M. Springborg), 63–111. Cambridge: The Royal Society of Chemistry (RSC) Publishing.
- 25 Capelle, K. and Libero, V.L. (2005). Spin-density functional theory: some open problems and application to inhomogeneous Heisenberg models. *Int. J. Quantum Chem.* 105 (6): 679–686.
- 26 Gritsenko, O.V. and Baerends, E.J. (2004). The spin-unrestricted molecular Kohn–Sham solution and the analogue of Koopmans’s theorem for open-shell molecules. *J. Chem. Phys.* 120 (18): 8364–8372.
- 27 Capelle, K. and Vignale, G. (2002). Nonuniqueness and derivative discontinuities in density-functional theories for current-carrying and superconducting systems. *Phys. Rev. B* 65 (11): 113106-1–113106-4.
- 28 Eschrig, H. and Pickett, W.E. (2001). Density functional theory of magnetic systems revisited. *Solid State Commun.* 118: 123.
- 29 Capelle, K. and Vignale, G. (2001). Nonuniqueness of the potentials of spin-density-functional theory. *Phys. Rev. Lett.* 86 (24): 5546–5549.
- 30 Holas, A. and Balawender, R. (2006). Comment on “Legendre-transform functionals for spin-density-functional theory”. *J. Chem. Phys.* 125: 247101.
- 31 Ullrich, C.A. (2005). Nonuniqueness in spin-density-functional theory on lattices. *Phys. Rev. B* 72: 073102.
- 32 Ayers, P.W. and Yang, W.T. (2006). Legendre-transform functionals for spin-density-functional theory. *J. Chem. Phys.* 124 (22): 224108.
- 33 Ayers, P.W., Golden, S., and Levy, M. (2006). Generalizations of the Hohenberg-Kohn theorem: I. Legendre transform constructions of variational

- principles for density matrices and electron distribution functions. *J. Chem. Phys.* 124 (5): 054101.
- 34 Gal, T., Ayers, P.W., De Proft, F., and Geerlings, P. (2009). Nonuniqueness of magnetic fields and energy derivatives in spin-polarized density functional theory. *J. Chem. Phys.* 131 (15): 7.
- 35 Ayers, P.W., Morrison, R.C., and Roy, R.K. (2002). Variational principles for describing chemical reactions: condensed reactivity indices. *J. Chem. Phys.* 116 (20): 8731–8744.
- 36 Ayers, P.W., Fias, S., and Heidar-Zadeh, F. (2018). The axiomatic approach to chemical concepts. *Comput. Theor. Chem.* 1142: 83–87.
- 37 Berkowitz, M. and Parr, R.G. (1988). Molecular hardness and softness, local hardness and softness, hardness and softness kernels, and relations among these quantities. *J. Chem. Phys.* 88 (4): 2554–2557.
- 38 Morell, C., Ayers, P.W., Grand, A. et al. (2008). Rationalization of Diels-Alder reactions through the use of the dual reactivity descriptor  $\Delta f(r)$ . *Phys. Chem. Chem. Phys.* 10 (48): 7239–7246.
- 39 Chamorro, E., Contreras, R., and Fuentealba, P. (2000). Some relationships within the nonlocal (pair-site) chemical reactivity formalism of density functional theory. *J. Chem. Phys.* 113 (24): 10861–10866.
- 40 Chamorro, E., De Proft, F., and Geerlings, P. (2005). Hardness and softness reactivity kernels within the spin-polarized density-functional theory. *J. Chem. Phys.* 123 (15): 154104.
- 41 Harbola, M.K., Parr, R.G., and Lee, C.T. (1991). Hardnesses from electrostatic potentials. *J. Chem. Phys.* 94 (9): 6055–6056.
- 42 Chattaraj, P.K., Cedillo, A., and Parr, R.G. (1995). Variational method for determining the Fukui function and chemical hardness of an electronic system. *J. Chem. Phys.* 103 (17): 7645–7646.
- 43 Pearson, R.G. (1990). Hard and soft acids and bases—the evolution of a chemical concept. *Coord. Chem. Rev.* 100: 403–425.
- 44 Galvan, M. and Vargas, R. (1992). Spin-potential in Kohn–Sham theory. *J. Phys. Chem.* 96 (4): 1625–1630.
- 45 Chamorro, E. and Perez, P. (2005). Condensed-to-atoms electronic Fukui functions within the framework of spin-polarized density-functional theory. *J. Chem. Phys.* 123 (11): 114107.
- 46 Pinter, B., De Proft, F., Van Speybroeck, V. et al. (2007). Spin-polarized conceptual density functional theory study of the regioselectivity in ring closures of radicals. *J. Org. Chem.* 72 (2): 348–356.
- 47 Pinter, B., De Proft, F., Veszpremi, T., and Geerlings, P. (2005). Regioselectivity in the [2+2] cyclo-addition reaction of triplet carbonyl compounds to substituted alkenes (Paterno-Buchi reaction): a spin-polarized conceptual DFT approach. *J. Chem. Sci.* 117 (5): 561–571.
- 48 Franco-Perez, M., Gazquez, J.L., Ayers, P.W., and Vela, A. (2018). Thermodynamic dual descriptor. *Acta Phys. Chim. Sin.* 34 (6): 683–691.
- 49 Ceron, M.L., Echegaray, E., Gutierrez-Oliva, S. et al. (2011). The reaction electronic flux in chemical reactions. *Sci. China-Chem.* 54 (12): 1982–1988.

- 50 Matute, R.A., Perez, P., Chamorro, E. et al. (2018). Reaction electronic flux perspective on the mechanism of the zimmerman Di-pi-methane rearrangement. *J. Org. Chem.* 83 (11): 5969–5974.
- 51 Echegaray, E. and Toro-Labbe, A. (2008). Reaction electronic flux: a new concept to get insights into reaction mechanisms. Study of model symmetric nucleophilic substitutions. *J. Phys. Chem. A* 112 (46): 11801–11807.
- 52 Senet, P. (1997). Kohn–Sham orbital formulation of the chemical electronic responses, including the hardness. *J. Chem. Phys.* 107 (7): 2516–2524.
- 53 Chamorro, E., Perez, P., De Proft, F., and Geerlings, P. (2006). Philicity indices within the spin-polarized density-functional theory framework. *J. Chem. Phys.* 124 (4): 044105.
- 54 Geerlings, P., Fias, S., Boisdenghien, Z., and De Proft, F. (2014). Conceptual DFT: chemistry from the linear response function. *Chem. Soc. Rev.* 43 (14): 4989–5008.
- 55 Chamorro, E., De Proft, F., and Geerlings, P. (2005). Hardness and softness reactivity kernels within the spin-polarized density-functional theory. *J. Chem. Phys.* 123 (15): 6.
- 56 Boisdenghien, Z., Fias, S., Van Alsenoy, C. et al. (2014). Evaluating and interpreting the chemical relevance of the linear response kernel for atoms II: open shell. *Phys. Chem. Chem. Phys.* 16 (28): 14614–14624.
- 57 Fias, S., Boisdenghien, Z., De Proft, F., and Geerlings, P. (2014). The spin polarized linear response from density functional theory: theory and application to atoms. *J. Chem. Phys.* 141 (18): 12.
- 58 Miranda-Quintana, R.A. and Ayers, P.W. (2016). Systematic treatment of spin-reactivity indicators in conceptual density functional theory. *Theor. Chem. Acc.* 135 (10): 1–18.
- 59 Garza, J., Vargas, R., Cedillo, A. et al. (2006). Comparison between the frozen core and finite differences approximations for the generalized spin-dependent global and local reactivity descriptors in small molecules. *Theor. Chem. Acc.* 115 (4): 257–265.
- 60 Vargas, R., Garza, J., and Cedillo, A. (2005). Koopmans-like approximation in the Kohn–Sham method and the impact of the frozen core approximation on the computation of the reactivity parameters of the density functional theory. *J. Phys. Chem. A* 109 (39): 8880–8892.
- 61 Cardenas, C., Ayers, P.W., and Cedillo, A. (2011). Reactivity indicators for degenerate states in the density-functional theoretic chemical reactivity theory. *J. Chem. Phys.* 134 (17): 13.
- 62 Cohen, M.H. and Ganduglia-Pirovano, M.V. (1994). Electronic and nuclear chemical reactivity. *J. Chem. Phys.* 101 (10): 8988–8997.
- 63 Chamorro, E., De Proft, F., and Geerlings, P. (2005). Generalized nuclear Fukui functions in the framework of spin-polarized density-functional theory. *J. Chem. Phys.* 123 (8): 15.
- 64 Cardenas, C., Lamsabhi, A.M., and Fuentealba, P. (2006). Nuclear reactivity indices in the context of spin polarized density functional theory. *Chem. Phys.* 322 (3): 303–310.

- 65 Balawender, R., De Proft, F., and Geerlings, P. (2001). Nuclear Fukui function and Berlin's binding function: prediction of the Jahn–Teller distortion. *J. Chem. Phys.* 114 (10): 4441–4449.
- 66 Balawender, R. and Geerlings, P. (2001). Nuclear Fukui function from coupled perturbed Hartree–Fock equations. *J. Chem. Phys.* 114 (2): 682–691.
- 67 Cohen, M.H., Ganduglia-Pirovano, M.V., and Kudrnovsky, J. (1995). Reactivity kernels, the normal modes of chemical reactivity, and the hardness and softness spectra. *J. Chem. Phys.* 103 (9): 3543–3551.
- 68 Ghashghaee, M. and Ghambarian, M. (2020). Defect engineering and zinc oxide doping of black phosphorene for nitrogen dioxide capture and detection: quantum-chemical calculations. *Appl. Surf. Sci.* 523: 10.
- 69 Juarez, A.R., Villanueva, M.S., Cortes-Arriagada, D., and Anot, E.C. (2019). Fullerene-like boron nitride cages  $B_xN_y$  ( $x+y = 28$ ): stabilities and electronic properties from density functional theory computation. *J. Mol. Model.* 25 (1): 14.
- 70 Castro, M. and Anot, E.C. (2019). Growth of iron clusters on octahedral  $B_{12}N_{12}$  cage: a time-dependent-DFT analysis. *Struct. Chem.* 30 (1): 195–200.
- 71 Escobar, J.C., Villanueva, M.S., Hernandez, A.B. et al. (2019). Interactions of  $B_{12}N_{12}$  fullerenes on graphene and boron nitride nanosheets: a DFT study. *J. Mol. Graphics Modell.* 86: 27–34.
- 72 Anot, E.C., Villanueva, M.S., Hernandez, A.B. et al. (2018). Retention of carbon monoxide onto magnetic [BN fullerene:  $B_6$ ] $^-$  and [BN fullerene:  $C_6$ ] $^-$  nanocomposites. *Appl. Phys., A* 124 (9): 17.
- 73 Ortega-Moo, C., Duran, R., Herrera, B. et al. (2017). Study of antiradical mechanisms with dihydroxybenzenes using reaction force and reaction electronic flux. *Phys. Chem. Chem. Phys.* 19 (22): 14512–14519.
- 74 Lozano-Espinosa, M., Garza, J., and Galvan, M. (2017). Confinement effects on the spin potential of first row transition metal cations. *Philos. Mag.* 97 (4): 284–297.
- 75 Peng, D.G. and Yang, W.T. (2013). Fukui function and response function for nonlocal and fractional systems. *J. Chem. Phys.* 138 (18): 15.
- 76 Lamsabhi, A.M., Corral, I., Perez, P. et al. (2012). Oxygenation of the phenyl-halocarbenes. Are they spin-allowed or spin-forbidden reactions? *J. Mol. Model.* 18 (6): 2813–2821.
- 77 Du, J.G., Sun, X.Y., and Jiang, G. (2012). A theoretical study on  $Ta_n^+$  cluster cations: structural assignments, stability, and electronic properties. *J. Chem. Phys.* 136 (9): 8.
- 78 Gal, T. and Geerlings, P. (2010). Energy surface, chemical potentials, Kohn–Sham energies in spin-polarized density functional theory. *J. Chem. Phys.* 133 (14): 16.
- 79 Gal, T. and Geerlings, P. (2010). Derivative of the Lieb definition for the energy functional of density-functional theory with respect to the particle number and the spin number. *Phys. Rev. A* 81 (3): 8.
- 80 De Vleeschouwer, F., De Proft, F., and Geerlings, P. (2010). Conceptual density functional theory based intrinsic radical stabilities: application to substituted silylenes and p-benzynes. *J. Mol. Struct. THEOCHEM* 943 (1–3): 94–102.



- 81 Perez, P. and Chamorro, E. (2010). Global and local reactivity of N-heterocyclic carbenes with boron and phosphorus atoms: an analysis based on spin polarized density functional framework. *J. Mol. Struct. THEOCHEM* 943 (1–3): 110–114.
- 82 Olah, J., Veszpremi, T., De Proft, F., and Geerlings, P. (2007). Silylenes: a unified picture of their stability, acid-base and spin properties, nucleophilicity, and electrophilicity via computational and conceptual density functional theory. *J. Phys. Chem. A* 111 (42): 10815–10823.
- 83 Stuyver, T., Chen, B., Zeng, T. et al. (2019). Do diradicals behave like radicals? *Chem. Rev.* 119 (21): 11291–11351.
- 84 Stuyver, T., De Proft, F., Geerlings, P., and Shaik, S. (2020). How do local reactivity descriptors shape the potential energy surface associated with chemical reactions? The valence bond delocalization perspective. *J. Am. Chem. Soc.* 142 (22): 10102–10113.
- 85 Navarro-Santos, P., Rodriguez-Olalde, N.E., Gallo, M. et al. (2019). On the initial stages of lignin polymerization through spin-polarized density functional theory. *Chem. Phys. Lett.* 730: 289–296.
- 86 Martinez-Araya, J.I. and Glossman-Mitnik, D. (2018). Assessment of ten density functionals through the use of local hyper-softness to get insights about the catalytic activity. *J. Mol. Model.* 24 (2): 11.
- 87 Morrison, R.C. (2018). Fukui functions for the temporary anion resonance states of Be<sup>-</sup>, Mg<sup>-</sup>, and Ca. *Acta Phys. Chim. Sin.* 34 (3): 263–269.
- 88 Chamorro, E., Perez, P., Duque, M. et al. (2008). Dual descriptors within the framework of spin-polarized density functional theory. *J. Chem. Phys.* 129: 064117.
- 89 Martinez-Araya, J.I., Yepes, D., and Jaque, P. (2018). A 3D visualization of the substituent effect A brief analysis of two components of the operational formula of dual descriptor for open-shell systems. *J. Mol. Model.* 24 (1): 8.
- 90 Martinez-Araya, J.I., Grand, A., and Glossman-Mitnik, D. (2015). Towards the rationalization of catalytic activity values by means of local hyper-softness on the catalytic site: a criticism about the use of net electric charges. *Phys. Chem. Chem. Phys.* 17 (44): 29764–29775.
- 91 Araya, J.I.M. (2011). The dual descriptor: working equations applied on electronic open-shell molecular systems. *Chem. Phys. Lett.* 506 (1–3): 104–111.
- 92 Sanchez, A., Guillen-Villar, R.C., Sanchez, R. et al. (2014). Electrochemical oxidation of symmetrical amides of ferulic acid in aprotic medium. *Electrochim. Acta* 133: 546–554.
- 93 Domingo, L.R., Pérez, P., and Sáez, J.A. (2013). Understanding the local reactivity in polar organic reactions through electrophilic and nucleophilic parr functions. *RSC Adv.* 3: 1486–1494.
- 94 Gusarov, S., Dmitriev, Y.Y., Stoyanov, S.R., and Kovalenko, A. (2013). Koopmans' multiconfigurational self-consistent field (MCSCF) Fukui functions and MCSCF perturbation theory. *Can. J. Chem.* 91 (9): 886–893.

- 95 Reyes, A., Cuervo, P.A., Orozco, F. et al. (2013). Theoretical investigation of the selectivity in intramolecular cyclizations of some 2'-aminochalcones to dihydroquinolin-8-ones and indolin-3-ones. *J. Mol. Model.* 19 (9): 3611–3618.
- 96 Alcoba, D.R., Lain, L., Torre, A. et al. (2013). Fukui and dual-descriptor matrices within the framework of spin-polarized density functional theory. *Phys. Chem. Chem. Phys.* 15 (24): 9594–9604.
- 97 Zhong, A.G., Huang, L., and Jiang, H.J. (2011). Structure, spectroscopy and reactivity of H<sub>2</sub>S bonding to metal(II) porphyrins. *Acta Phys. Chim. Sin.* 27 (4): 837–845.
- 98 Gal, T., Geerlings, P., De Proft, F., and Torrent-Sucarrat, M. (2011). A new approach to local hardness. *Phys. Chem. Chem. Phys.* 13 (33): 15003–15015.
- 99 De Vleeschouwer, F., Jaque, P., Geerlings, P. et al. (2010). Regioselectivity of radical additions to substituted alkenes: insight from conceptual density functional theory. *J. Org. Chem.* 75 (15): 4964–4974.
- 100 Feng, X.T., Yu, J.G., Liu, R.Z. et al. (2010). Why iron? A spin-polarized conceptual density functional theory study on metal-binding specificity of porphyrin. *J. Phys. Chem. A* 114 (21): 6342–6349.
- 101 Bochevarov, A.D., Harder, E., Hughes, T.F. et al. (2013). Jaguar: a high-performance quantum chemistry software program with strengths in life and materials sciences. *Int. J. Quantum Chem.* 113 (18): 2110–2142.
- 102 Frisch, M.J., Trucks, G.W., Schlegel, H.B. et al. (2017). *Gaussian 16, Revision B.01*. Wallingford, CT: Gaussian, Inc.
- 103 Buchachenko, A.L. and Berdinsky, V.L. (1996). Spin catalysis of chemical reactions. *J. Phys. Chem.* 100 (47): 18292–18299.
- 104 Humphrey, W., Dalke, A., and Schulten, K. (1996). VMD - visual molecular dynamics. *J. Mol. Graphics* 14: 33–38.
- 105 Lu, T. and Chen, F.W. (2012). Multiwfn: a multifunctional wavefunction analyzer. *J. Comput. Chem.* 33 (5): 580–592.
- 106 Sureshkumar, B., Mary, Y.S., Panicker, C.Y. et al. (2020). Quinoline derivatives as possible lead compounds for anti-malarial drugs: spectroscopic, DFT and MD study. *Arabian J. Chem.* 13 (1): 632–648.
- 107 Klisuric, O.R., Armakovic, S.J., Armakovic, S. et al. (2020). Structural, biological and in-silico study of quinoline-based chalcogensemicarbazones. *J. Mol. Struct.* 1203: 12.
- 108 Sureshkumar, B., Mary, Y.S., Suma, S. et al. (2018). Spectroscopic characterization of 8-hydroxy-5-nitroquinoline and 5-chloro-8-hydroxy quinoline and investigation of its reactive properties by DFT calculations and molecular dynamics simulations. *J. Mol. Struct.* 1164: 525–538.
- 109 Bielenica, A., Beegum, S., Mary, Y.S. et al. (2020). Experimental and computational analysis of 1-(4-chloro-3-nitrophenyl)-3-(3,4-dichlorophenyl)thiourea. *J. Mol. Struct.* 1205: 10.
- 110 Menon, V.V., Mary, Y.S., Mary, Y.S. et al. (2018). Combined spectroscopic, DFT, TD-DFT and MD study of newly synthesized thiourea derivative. *J. Mol. Struct.* 1155: 184–195.

- 111** War, J.A., Jalaja, K., Mary, Y.S. et al. (2017). Spectroscopic characterization of 1-3-(1H-imidazol-1-yl)propyl-3-phenylthiourea and assessment of reactive and optoelectronic properties employing DFT calculations and molecular dynamics simulations. *J. Mol. Struct.* 1129: 72–85.
- 112** Aswathy, V.V., Mary, Y.S., Jojo, P.J. et al. (2017). Investigation of spectroscopic, reactive, transport and docking properties of 1-(3,4-dichlorophenyl)-3-(3-(trifluoromethyl)phenyl)thiourea (ANF-6): combined experimental and computational study. *J. Mol. Struct.* 1134: 668–680.
- 113** Mary, Y.S., Aswathy, V.V., Panicker, C.Y. et al. (2016). Spectroscopic, single crystal XRD structure, DFT and molecular dynamics investigation of 1-(3-chloro-4-fluorophenyl)-3-(3-(trifluoromethyl)phenyl)thiourea. *RSC Adv.* 6 (113): 111997–112015.
- 114** Mary, Y.S., Al-Shehri, M.M., Jalaja, K. et al. (2017). Synthesis, vibrational spectroscopic investigations, molecular docking, antibacterial studies and molecular dynamics study of 5-(4-nitrophenyl)acetamido-2-(4-tert-butylphenyl)benzoxazole. *J. Mol. Struct.* 1133: 557–573.
- 115** Aswathy, V.V., Alper-Hayta, S., Yalcin, G. et al. (2017). Modification of benzoxazole derivative by bromine-spectroscopic, antibacterial and reactivity study using experimental and theoretical procedures. *J. Mol. Struct.* 1141: 495–511.
- 116** Beegum, S., Mary, Y.S., Panicker, Y. et al. (2019). Spectroscopic, antimicrobial and computational study of novel benzoxazole derivative. *J. Mol. Struct.* 1176: 881–894.
- 117** Vennila, P., Govindaraju, M., Venkatesh, G. et al. (2018). A complete computational and spectroscopic study of 2-bromo-1,4-dichlorobenzene - A frequently used benzene derivative. *J. Mol. Struct.* 1151: 245–255.
- 118** Venkatesh, G., Kamal, C., Vennila, P. et al. (2018). Molecular dynamic simulations, ALIE surface, Fukui functions geometrical, molecular docking and vibrational spectra studies of tetra chloro p and m-xylene. *J. Mol. Struct.* 1171: 253–267.
- 119** Crisan, L., Borota, A., Bora, A., and Pacureanu, L. (2019). Diarylthiazole and diarylimidazole selective COX-1 inhibitor analysis through pharmacophore modeling, virtual screening, and DFT-based approaches. *Struct. Chem.* 30 (6): 2311–2326.
- 120** Thomas, R., Hossain, M., Mary, Y.S. et al. (2018). Spectroscopic analysis and molecular docking of imidazole derivatives and investigation of its reactive properties by DFT and molecular dynamics simulations. *J. Mol. Struct.* 1158: 156–175.
- 121** Hossain, M., Thomas, R., Mary, Y.S. et al. (2018). Understanding reactivity of two newly synthesized imidazole derivatives by spectroscopic characterization and computational study. *J. Mol. Struct.* 1158: 176–196.
- 122** Benzon, K.B., Sheena, M.Y., Panicker, C.Y. et al. (2017). Studies on the synthesis, spectroscopic analysis, molecular docking and DET calculations on 1-hydroxy-2-(4-hydroxyphenyl)-4,5-dimethyl-imidazol-3-oxide. *J. Mol. Struct.* 1130: 644–658.

- 123** Benzou, K.B., Mary, Y.S., Varghese, H.T. et al. (2017). Spectroscopic, DFT, molecular dynamics and molecular docking study of 1-butyl-2-(4-hydroxyphenyl)-4,5-dimethyl-imidazole 3-oxide. *J. Mol. Struct.* 1134: 330–344.
- 124** Mary, Y.S., Miniyar, P.B., Mary, Y.S. et al. (2018). Synthesis and spectroscopic study of three new oxadiazole derivatives with detailed computational evaluation of their reactivity and pharmaceutical potential. *J. Mol. Struct.* 1173: 469–480.
- 125** Al-Tamimi, A.M.S., Mary, Y.S., Miniyar, P.B. et al. (2018). Synthesis, spectroscopic analyses, chemical reactivity and molecular docking study and anti-tubercular activity of pyrazine and condensed oxadiazole derivatives. *J. Mol. Struct.* 1164: 459–469.
- 126** Mary, Y.S., Al-Omary, F.A.M., Mostafa, G.A.E. et al. (2017). Insight into the reactive properties of newly synthesized 1,2,4-triazole derivative by combined experimental (FT-IR and FR-Raman) and theoretical (DFT and MD) study. *J. Mol. Struct.* 1141: 542–550.
- 127** Devi, A.S., Aswathy, V.V., Mary, Y.S. et al. (2017). Synthesis, XRD single crystal structure analysis, vibrational spectral analysis, molecular dynamics and molecular docking studies of 2-(3-methoxy-4-hydroxyphenyl) benzothiazole. *J. Mol. Struct.* 1148: 282–292.
- 128** El-Azab, A.S., Mary, Y.S., Abdel-Aziz, A.A.M. et al. (2018). Synthesis, spectroscopic analyses (FT-IR and NMR), vibrational study, chemical reactivity and molecular docking study and anti-tubercular activity of condensed oxadiazole and pyrazine derivatives. *J. Mol. Struct.* 1156: 657–674.
- 129** Muthukkumar, M., Bhuvanewari, T., Venkatesh, G. et al. (2018). Synthesis, characterization and computational studies of semicarbazide derivative. *J. Mol. Liq.* 272: 481–495.
- 130** Murthy, P.K., Suneetha, V., Armakovic, S. et al. (2018). Synthesis, characterization and computational study of the newly synthesized sulfonamide molecule. *J. Mol. Struct.* 1153: 212–229.
- 131** Beegum, S., Mary, Y.S., Mary, Y.S. et al. (2020). Exploring the detailed spectroscopic characteristics, chemical and biological activity of two cyanopyrazine-2-carboxamide derivatives using experimental and theoretical tools. *Spectrochim. Acta, Part A* 224: 13.
- 132** Mary, S.Y., Al-Abdullah, E.S., Aljohar, H.I. et al. (2018). 4-(4-Acetylphenyl)amino -2-methylidene-4-oxobutanoic acid, a newly synthesized amide with hydrophilic and hydrophobic segments: spectroscopic characterization and investigation of its reactive properties. *J. Serb. Chem. Soc.* 83 (1): 1–18.
- 133** Ranjith, P.K., Al-Abdullah, E.S., Al-Omary, F.A.M. et al. (2017). FT-IR and FT-Raman characterization and investigation of reactive properties of N-(3-iodo-4-methylphenyl)pyrazine-2-carboxamide by molecular dynamics simulations and DFT calculations. *J. Mol. Struct.* 1136: 14–24.

- 134** Murthy, P.K., Mary, Y.S., Mary, Y.S. et al. (2017). Synthesis, crystal structure analysis, spectral investigations, DFT computations and molecular dynamics and docking study of 4-benzyl-5-oxomorpholine-3-carbamide, a potential bioactive agent. *J. Mol. Struct.* 1134: 25–39.
- 135** Bonsaii, M., Gholivand, K., Khosravi, M., and Abdi, K. (2017). Negative hyperconjugation effect on the reactivity of phosphoramidate mustard derivatives as a DNA alkylating agent: theoretical and experimental insights. *New J. Chem.* 41 (19): 11036–11052.
- 136** Beegum, S., Mary, Y.S., Varghese, H.T. et al. (2017). Vibrational spectroscopic analysis of cyanopyrazine-2-carboxamide derivatives and investigation of their reactive properties by DFT calculations and molecular dynamics simulations. *J. Mol. Struct.* 1131: 1–15.
- 137** Murthy, P.K., Krishnaswamy, G., Armakovic, S. et al. (2018). Structural and spectroscopic characterization, reactivity study and charge transfer analysis of the newly synthesized 2-(6-hydroxy-1-benzofuran-3-yl) acetic acid. *J. Mol. Struct.* 1162: 81–95.
- 138** Mary, Y.S., Mary, Y.S., Panicker, C.Y. et al. (2017). Investigation of reactive and spectroscopic properties of oxobutanoic acid derivative: combined spectroscopic, DFT, MD and docking study. *J. Mol. Struct.* 1148: 266–275.
- 139** Nayak, N., Prasad, K.S., Pillai, R.R. et al. (2018). Remarkable colorimetric sensing behavior of pyrazole-based chemosensor towards Cu(II) ion detection: synthesis, characterization and theoretical investigations. *RSC Adv.* 8 (32): 18023–18029.
- 140** Zainuri, D.A., Arshad, S., Khalib, N.C. et al. (2017). Synthesis, XRD crystal structure, spectroscopic characterization (FT-IR, H-1 and C-13 NMR), DFT studies, chemical reactivity and bond dissociation energy studies using molecular dynamics simulations and evaluation of antimicrobial and antioxidant activities of a novel chalcone derivative, (E)-1-(4-bromophenyl)-3-(4-iodophenyl)prop-2-en-1-one. *J. Mol. Struct.* 1128: 520–533.
- 141** Sureshkumar, B., Mary, Y.S., Panicker, C.Y. et al. (2017). Spectroscopic analysis of 8-hydroxyquinoline-5-sulphonic acid and investigation of its reactive properties by DFT and molecular dynamics simulations. *J. Mol. Struct.* 1150: 540–552.
- 142** Ranjith, P.K., Mary, Y.S., Panicker, C.Y. et al. (2017). New quinolone derivative: spectroscopic characterization and reactivity study by DFT and MD approaches. *J. Mol. Struct.* 1135: 1–14.
- 143** Sultan, M.A., Almansour, A.I., Pillai, R.R. et al. (2017). Synthesis, theoretical studies and molecular docking of a novel chlorinated tetracyclic: (Z/E)-3-(1,8-dichloro-9,10-dihydro-9,10-ethanoanthracen-11-yl)acrylaldehyde. *J. Mol. Struct.* 1150: 358–365.
- 144** Radanovic, M.M., Rodic, M.V., Armakovic, S. et al. (2017). Pyridoxylidene aminoguanidine and its copper(II) complexes - syntheses, structure, and DFT calculations. *J. Coord. Chem.* 70 (16): 2870–2887.

- 145** Onawole, A.T., Al-Ahmadi, A.F., Mary, Y.S. et al. (2017). Conformational, vibrational and DFT studies of a newly synthesized arylpiperazine-based drug and evaluation of its reactivity towards the human GABA receptor. *J. Mol. Struct.* 1147: 266–280.
- 146** Jalaja, K., Mary, Y.S., Panicker, C.Y. et al. (2017). Spectroscopic characterization of 4-(2-(5-Ethylpyridin-2-yl)ethoxy)benzaldehyde oxime and investigation of its reactive properties by DFT calculations and molecular dynamics simulations. *J. Mol. Struct.* 1128: 245–256.
- 147** El-Azab, A.S., Mary, Y.S., Mary, Y.S. et al. (2017). Newly synthesized dihydroquinazoline derivative from the aspect of combined spectroscopic and computational study. *J. Mol. Struct.* 1134: 814–827.
- 148** Murthy, P.K., Valverde, C., Suneetha, V. et al. (2019). An analysis of structural and spectroscopic signatures, the reactivity study of synthesized 4,6-dichloro-2-(methylsulfonyl)pyrimidine: a potential third-order nonlinear optical material. *J. Mol. Struct.* 1186: 263–275.
- 149** Al-Omary, F.A.M., Mary, Y.S., Beegum, S. et al. (2017). Molecular conformational analysis, reactivity, vibrational spectral analysis and molecular dynamics and docking studies of 6-chloro-5-isopropylpyrimidine-2,4(1H,3H)-dione, a potential precursor to bioactive agent. *J. Mol. Struct.* 1127: 427–436.
- 150** Fashe, M.M., Juvonen, R.O., Petsalo, A. et al. (2015). In silico prediction of the site of oxidation by cytochrome P450 3A4 that leads to the formation of the toxic metabolites of pyrrolizidine alkaloids. *Chem. Res. Toxicol.* 28 (4): 702–710.
- 151** El-labbad, E.M., Ismail, M.A.H., Abou El Ella, D.A. et al. (2015). Discovery of novel peptidomimetics as irreversible CHIKV Nsp2 protease inhibitors using quantum mechanical-based ligand descriptors. *Chem. Biol. Drug Des.* 86 (6): 1518–1527.
- 152** Domingo, L.R., Chamorro, E., and Perez, P. (2009). An analysis of the regioselectivity of 1,3-dipolar cycloaddition reactions of benzonitrile N-oxides based on global and local electrophilicity and nucleophilicity indices. *Eur. J. Org. Chem.* 2009 (18): 3036–3044.
- 153** Domingo, L.R., Chamorro, E., and Perez, P. (2010). Understanding the high reactivity of the azomethine ylides in [3 + 2] cycloaddition reactions. *Lett. Org. Chem.* 7 (6): 432–439.
- 154** Chamorro, E., De Proft, F., and Geerlings, P. (2005). Generalized nuclear Fukui functions in the framework of spin-polarized density-functional theory. *J. Chem. Phys.* 123 (8): 084104.
- 155** De Proft, F., Geerlings, P., and Chamorro, E. (2005). The nuclear Fukui function: generalization within spin-polarized conceptual density functional theory. *Adv. Comput. Methods Sci. Eng.* 4A–4B: 1240–1243.
- 156** Franco-Perez, M., Ayers, P.W., Gazquez, J.L., and Vela, A. (2017). Thermodynamic responses of electronic systems. *J. Chem. Phys.* 147 (9): 11.
- 157** Franco-Perez, M., Gazquez, J.L., Ayers, P.W., and Vela, A. (2017). Thermodynamic hardness and the maximum hardness principle. *J. Chem. Phys.* 147 (7): 7.

- 158** Theophilou, I., Penz, M., Ruggenthaler, M., and Rubio, A. (2020). Virial relations for electrons coupled to quantum field modes. *J. Chem. Theory Comput.* 16 (10): 6236–6243.
- 159** Flick, J., Welakuh, D.M., Ruggenthaler, M. et al. (2019). Light-matter response in nonrelativistic quantum electrodynamics. *ACS Photonics* 6 (11): 2757–2778.
- 160** Flick, J., Schafer, C., Ruggenthaler, M. et al. (2018). Ab initio optimized effective potentials for real molecules in optical cavities: photon contributions to the molecular ground state. *ACS Photonics* 5 (3): 992–1005.
- 161** Flick, J., Ruggenthaler, M., Appel, H., and Rubio, A. (2017). Atoms and molecules in cavities, from weak to strong coupling in quantum-electrodynamics (QED) chemistry. *Proc. Natl. Acad. Sci. U. S. A.* 114 (12): 3026–3034.
- 162** Flick, J., Ruggenthaler, M., Appel, H., and Rubio, A. (2015). Kohn-Sham approach to quantum electrodynamical density-functional theory: exact time-dependent effective potentials in real space. *Proc. Natl. Acad. Sci. U. S. A.* 112 (50): 15285–15290.
- 163** Ruggenthaler, M., Flick, J., Pellegrini, C. et al. (2014). Quantum-electrodynamical density-functional theory: bridging quantum optics and electronic-structure theory. *Phys. Rev. A* 90 (1): 26.

## 8

## Finite Temperature Conceptual Density Functional Theory

José L. Gázquez<sup>1</sup> and Marco Franco-Pérez<sup>2</sup>

<sup>1</sup>Universidad Autónoma Metropolitana-Iztapalapa, Departamento de Química, Av. San Rafael Atlixco 186, Ciudad de Mexico 09340, Mexico

<sup>2</sup>Universidad Nacional Autónoma de México, Cd. Universitaria, Facultad de Química, Ciudad de Mexico 04510, Mexico

### 8.1 Introduction

The framework of conceptual density functional theory (CDFT) is mainly based on the response functions that arise from changes in the electronic energy ( $E$ ) with respect to changes in the number of electrons ( $N$ ) and in the external potential  $v(\mathbf{r})$ . Through this consideration, four fundamental concepts emerge. The chemical potential [1] ( $\mu_e$ ) and the hardness [2] ( $\eta_e$ ), which are given by the first and second derivatives of the energy with respect to  $N$ , respectively, and the Fukui function [3–5] ( $f_e(\mathbf{r})$ ) and the dual descriptor [6, 7] ( $\Delta f_e(\mathbf{r})$ ) that correspond to the first and second derivatives of the electronic density,  $\rho(\mathbf{r})$ , with respect to  $N$ , respectively.

The relevance of these response functions to describe very important aspects of the global reactivity, in the case of  $\mu_e$  and  $\eta_e$ , and regioselectivity, in the case of  $f_e(\mathbf{r})$  and  $\Delta f_e(\mathbf{r})$ , comes from the fact that they provide a link with intuitive chemically meaningful concepts. The chemical potential is equal to the negative of the electronegativity [1] ( $\chi$ ) defined by Iczkowski and Margrave [8] who made a generalization of the formula proposed by Mulliken [9]. The definition given for hardness corresponds to the identification of the concept originally proposed by Pearson [10, 11]. The Fukui function was defined through the analysis of the total differential [3] of  $E$  and of  $\mu_e$  as functions of  $N$  and  $v(\mathbf{r})$ , that leads to the Maxwell relation  $(\delta\mu_e/\delta v(\mathbf{r}))_N = (\partial\rho(\mathbf{r})/\partial N)_{v(\mathbf{r})} = f_e(\mathbf{r})$ , and it reduces to the electronic density of the frontier orbitals, the highest occupied molecular orbital (HOMO) and the lowest unoccupied molecular orbital (LUMO), when the relaxation effects associated with the removal or addition of an electron from the system are neglected [3, 4].

These identifications have provided a theoretical framework to get a better understanding of commonly used principles of chemical reactivity. Thus, the electronegativity equalization principle proposed by Sanderson [12, 13] follows immediately from the relationship  $\chi = -\mu_e$ , since it indicates that it is equivalent to a chemical potential equalization in a charge-transfer process. The hard and



soft acids and bases principle [10, 11, 14, 15] and the maximum hardness principle [16, 17] proposed by Pearson can be analyzed through CDFT from several perspectives. On the other hand, from the relationship between the Fukui function and the frontier orbitals one can get important insights that provide additional support to the relevant aspects contained in the frontier orbital theory of chemical reactivity [18, 19]. In general the CDFT framework allows one to establish the conditions required for the fulfillment of these principles and its implications with respect to the interacting species [17, 20–57]. Moreover, through this approach it has been possible to introduce global, local, and non-local descriptors that have enriched the analysis of chemical reactivity in terms of a chemically meaningful language [58–80].

A very important relationship used in the analysis and understanding of the concepts and principles mentioned in the previous paragraphs is the smooth quadratic interpolation [2] between the energy of the systems with  $N_0 - 1$ ,  $N_0$ , and  $N_0 + 1$  electrons, where  $N_0$  is an integer,

$$\Delta E = \mu_e \Delta N + \frac{1}{2} \eta_e (\Delta N)^2 \quad (8.1)$$

with  $\Delta N = N - N_0$  and we have used the definitions of  $\mu_e$  and  $\eta_e$  in terms of the first and second derivatives of  $E$  with respect to  $N$  at constant  $v(\mathbf{r})$ . Since these derivatives must be evaluated at  $N_0$ , one finds that  $\mu_e = -(I + A)/2$  and  $\eta_e = I - A$ , where  $I$  and  $A$  are the vertical first ionization potential and electron affinity of the reference system, respectively. These are very important relationships because, if one makes use of the experimental values of  $I$  and  $A$ , one finds that the values obtained through them for the chemical potential (minus the Mulliken electronegativity) and the hardness follow approximately the same behavior of the qualitative scales of Pauling [81, 82] for  $\chi = -\mu_e$  and of Pearson [10, 11, 14, 15] for  $\eta_e$ . This result, derived by Parr and Pearson, strengthened the association of the first and second derivatives with  $\mu_e$  and  $\eta_e$ , and became, together with Eq. (8.1), the basis for the study of charge-transfer processes [14, 15, 49–57, 83–97] and, as mentioned, the principles associated with them.

The detailed analysis of the four concepts and the principles mentioned, together with other important indexes and complementary principles of chemical reactivity, which were derived in the framework of CDFT can be seen in several chapters of this book and in several revisions [98–108].

In this chapter we will focus on the implications associated to the fact that to evaluate the derivatives just mentioned, one needs to define the energy and the electronic density for a fractional number of electrons. In this context, the appropriate theoretical framework is given by the grand canonical ensemble and finite temperature density functional theory (DFT), [109–111] to allow the system to exchange electrons with the reservoir (bath) in which it is immersed. Through this approach the number of electrons fluctuates, so that one needs to consider the average value for the ensemble, which may be an integer or a real number. Although there have been in the past several approaches [112–121] to analyze these aspects, here we will concentrate on the development we have achieved recently [122–134].

In the process of performing this analysis, we will derive the temperature-dependent expressions of  $\mu_e$ ,  $\eta_e$ ,  $f_e(\mathbf{r})$ , and  $\Delta f_e(\mathbf{r})$ , and from them, their behavior in the limit when the temperature goes to zero and at temperatures of chemical interest

will be established. Additionally, we will discuss new concepts that arise through this approach that provide a complement to the CDFT theoretical framework, and finally, we will examine the fundamental equations for a chemical change with the temperature-dependence perspective incorporated.

## 8.2 First-Order Response Functions in the Grand Canonical Ensemble

The natural variables of the grand canonical ensemble are the chemical potential of the reservoir  $\mu_{\text{Bath}}$ , the external potential  $v(\mathbf{r})$ , and the temperature  $T$ . In this ensemble the partition function is given by

$$\Xi(\mu_{\text{Bath}}, T)[v(\mathbf{r})] = \sum_N \sum_i e^{-\beta(E_{N,i} - \mu_{\text{Bath}}N)} \quad (8.2)$$

where  $E_{N,i}$  is the energy of the  $i$ th  $N$ -electron excited state ( $i = 0$  corresponds to the ground state),  $\beta = 1/k_{\text{B}}T$ , and  $k_{\text{B}}$  is Boltzmann's constant.

By making use of the weighting factor, which is expressed in terms of the grand partition function as

$$w_{N,i} = \frac{1}{\Xi} e^{-\beta(E_{N,i} - \mu_{\text{Bath}}N)} \quad (8.3)$$

one can determine other variables in terms of their average value in the ensemble. Thus, to obtain the response functions that arise from changes in the energy and in the electronic density with respect to changes in the number of electrons and the external potential, discussed in the previous section, one must consider their average value in the ensemble, that is

$$\langle N \rangle = \sum_N \sum_i w_{N,i} N \quad (8.4)$$

$$\langle E \rangle = \sum_N \sum_i w_{N,i} E_{N,i} \quad (8.5)$$

and

$$\langle \rho(\mathbf{r}) \rangle = \sum_N \sum_i w_{N,i} \rho_{N,i}(\mathbf{r}) \quad (8.6)$$

Now, in terms of the natural variables of the grand canonical ensemble, the flux of electrons to or from the system is controlled by  $\mu_{\text{Bath}}$ . The response of the average electronic energy of the system to this change in the average number of electrons corresponds to the finite temperature definition of the chemical potential [1, 123],

$$\mu_e = \left( \frac{\partial \langle E \rangle}{\partial \langle N \rangle} \right)_{T, v(\mathbf{r})} \quad (8.7)$$

which may be expressed in terms of changes in the chemical potential of the reservoir using the chain rule, that is

$$\left( \frac{\partial \langle E \rangle}{\partial \langle N \rangle} \right)_{T, v(\mathbf{r})} = \left( \frac{\partial \langle E \rangle}{\partial \mu_{\text{Bath}}} \right)_{T, v(\mathbf{r})} \left( \frac{\partial \mu_{\text{Bath}}}{\partial \langle N \rangle} \right)_{T, v(\mathbf{r})} \quad (8.8)$$

The two derivatives in the right-hand side of this equation may be expressed in terms of the thermal fluctuations between the average energy and the average number of electrons,  $\sigma_{EN}$ , and in the average number of electrons,  $\sigma_{NN}$ ,

$$\left( \frac{\partial \langle E \rangle}{\partial \mu_{\text{Bath}}} \right)_{T, \nu(\mathbf{r})} = \beta \sigma_{EN} = \beta (\langle EN \rangle - \langle E \rangle \langle N \rangle) \quad (8.9)$$

and

$$\left( \frac{\partial \langle N \rangle}{\partial \mu_{\text{Bath}}} \right)_{T, \nu(\mathbf{r})} = \beta \sigma_{NN} = \beta (\langle N^2 \rangle - \langle N \rangle \langle N \rangle) \quad (8.10)$$

Therefore, substituting these two expressions in Eq. (8.8), and using Eq. (8.7) one obtains that

$$\mu_e = \frac{\sigma_{EN}}{\sigma_{NN}} = \frac{\langle EN \rangle - \langle E \rangle \langle N \rangle}{\langle N^2 \rangle - \langle N \rangle \langle N \rangle} \quad (8.11)$$

It is important to note that  $\mu_e$  in the grand canonical ensemble is not an independent variable, and therefore it must be determined through the thermodynamic variables  $\mu_{\text{Bath}}$  and  $T$ . In fact, one can show that the relationship between  $\mu_e$  and  $\mu_{\text{Bath}}$  is given by

$$\mu_e = \mu_{\text{Bath}} + T \left( \frac{\partial \langle S_T \rangle}{\partial \langle N \rangle} \right)_{T, \nu(\mathbf{r})} \quad (8.12)$$

where

$$\langle S_T \rangle = -k_B \sum_N \sum_i w_{N,i} \ln w_{N,i} \quad (8.13)$$

is the average electronic entropy. Thus Eq. (8.12) implies that the electronic chemical potential and the chemical potential of the bath are equal to each other only at zero temperature, because when  $T \neq 0$  there is an additional entropic contribution.

Now, to obtain a simpler expression that may be useful for studies of chemical reactivity, one can evaluate directly the derivative of the average electronic energy with respect to the average number of electrons using Eqs. (8.4) and (8.5), in combination with the three ground-states ensemble model, which is composed of the systems with  $N_0 - 1$ ,  $N_0$ , and  $N_0 + 1$  electrons in their ground state. Thus, the fractional charge, defined as the difference between the average number of electrons and  $N_0$ , evaluated for this ensemble adopts the form

$$\omega = \langle N \rangle - N_0 = \frac{\exp[\beta(A + \mu_{\text{Bath}})] - \exp[-\beta(I + \mu_{\text{Bath}})]}{1 + \exp[\beta(A + \mu_{\text{Bath}})] + \exp[-\beta(I + \mu_{\text{Bath}})]} \quad (8.14)$$

while the difference between the average energy and the ground-state energy of the reference system is given by

$$\Delta \langle E \rangle = \langle E \rangle - E_{N_0,0} = \frac{I \exp[-\beta(I + \mu_{\text{Bath}})] - A \exp[\beta(A + \mu_{\text{Bath}})]}{1 + \exp[\beta(A + \mu_{\text{Bath}})] + \exp[-\beta(I + \mu_{\text{Bath}})]} \quad (8.15)$$

From these two relationships, one can derive the expression for the energy difference in terms of the fractional charge given in Table 8.1, Eq. (T1-1), with

$$\alpha = (\omega^2 + 4(1 - \omega^2) \exp[-\beta(I - A)])^{1/2} \quad (8.16)$$

**Table 8.1** First-order response functions of the electronic energy and the electronic density evaluated with the three ground-states ensemble.<sup>a)</sup>

Electronic energy	Electronic density
<p>Temperature dependent expressions</p> $\Delta(E) = -\frac{1}{2}(I+A)\omega + \frac{1}{2}(I-A)\frac{\alpha+\omega^2}{1+\alpha} \quad (\text{T1-1})$	<p>Temperature dependent expressions</p> $\Delta(\rho(\mathbf{r})) = \frac{1}{2} [f_e^-(\mathbf{r}) + f_e^+(\mathbf{r})] \omega + \frac{1}{2} [f_e^+(\mathbf{r}) - f_e^-(\mathbf{r})] \frac{\alpha+\omega^2}{1+\alpha} \quad (\text{T1-7})$
$\mu_e = -\frac{1}{2}(I+A) + \frac{\omega}{2\alpha}(I-A) \quad (\text{T1-2})$	$f_e(\mathbf{r}) = \frac{1}{2} [f_e^-(\mathbf{r}) + f_e^+(\mathbf{r})] - \frac{1}{2} [f_e^-(\mathbf{r}) - f_e^+(\mathbf{r})] \frac{\omega}{\alpha} \quad (\text{T1-8})$
$\begin{aligned} \mu_e(\mathbf{r}) = & -\frac{1}{2} [If_e^-(\mathbf{r}) + Af_e^+(\mathbf{r})] \\ & + \frac{1}{2} [If_e^-(\mathbf{r}) - Af_e^+(\mathbf{r})] \frac{\omega}{\alpha} \quad (\text{T1-3}) \\ & - [f_e^+(\mathbf{r}) - f_e^-(\mathbf{r})] (I-A)\lambda^{-1} \end{aligned}$	$\begin{aligned} f_e(\mathbf{r}, \mathbf{r}') = & \frac{1}{2} [f_e^-(\mathbf{r})f_e^-(\mathbf{r}') + f_e^+(\mathbf{r})f_e^+(\mathbf{r}')] \\ & + \frac{1}{2} [f_e^+(\mathbf{r})f_e^+(\mathbf{r}') - f_e^-(\mathbf{r})f_e^-(\mathbf{r}')] \frac{\omega}{\alpha} \quad (\text{T1-9}) \\ & + [f_e^+(\mathbf{r}) - f_e^-(\mathbf{r}')] [f_e^-(\mathbf{r}') - f_e^+(\mathbf{r}')] \lambda^{-1} \end{aligned}$
<p>Expressions at <math>T = 0</math> and at temperatures of chemical interest</p> $\langle E \rangle = \begin{cases} (1+\omega)E_{N_0} - \omega E_{N_0-1}, & \text{for } 0 \geq \omega \geq -1 \\ (1-\omega)E_{N_0} + \omega E_{N_0+1}, & \text{for } 0 \leq \omega \leq +1 \end{cases} \quad (\text{T1-4})$	<p>Expressions at <math>T = 0</math> and at temperatures of chemical interest</p> $\langle \rho(\mathbf{r}) \rangle = \begin{cases} (1+\omega)\rho_{N_0}(\mathbf{r}) - \omega \rho_{N_0-1}(\mathbf{r}), & \text{for } 0 \geq \omega \geq -1 \\ (1-\omega)\rho_{N_0}(\mathbf{r}) + \omega \rho_{N_0+1}(\mathbf{r}), & \text{for } 0 \leq \omega \leq +1 \end{cases} \quad (\text{T1-10})$
$\mu_e = \begin{cases} -I & \omega < 0 \\ -(I+A)/2 & \omega = 0 \\ -A & \omega > 0 \end{cases} \quad (\text{T1-5})$	$f_e(\mathbf{r}) = \begin{cases} f_e^-(\mathbf{r}) & \omega < 0 \\ \frac{1}{2} [f_e^-(\mathbf{r}) + f_e^+(\mathbf{r})] & \omega = 0 \\ f_e^+(\mathbf{r}) & \omega > 0 \end{cases} \quad (\text{T1-11})$
$\mu_e(\mathbf{r}) = \begin{cases} -If_e^-(\mathbf{r}) & \omega < 0 \\ -(If_e^-(\mathbf{r}) + Af_e^+(\mathbf{r})) / 2 & \omega = 0 \\ -Af_e^+(\mathbf{r}) & \omega > 0 \end{cases} \quad (\text{T1-6})$	$f_e(\mathbf{r}, \mathbf{r}') = \begin{cases} f_e^-(\mathbf{r})f_e^-(\mathbf{r}') & \omega < 0 \\ [f_e^-(\mathbf{r})f_e^-(\mathbf{r}') + f_e^+(\mathbf{r})f_e^+(\mathbf{r}')] / 2 & \omega = 0 \\ f_e^+(\mathbf{r})f_e^+(\mathbf{r}') & \omega > 0 \end{cases} \quad (\text{T1-12})$

a) The definitions of  $\omega$  and  $\alpha$  are given in Eqs. (8.14) and (8.16).

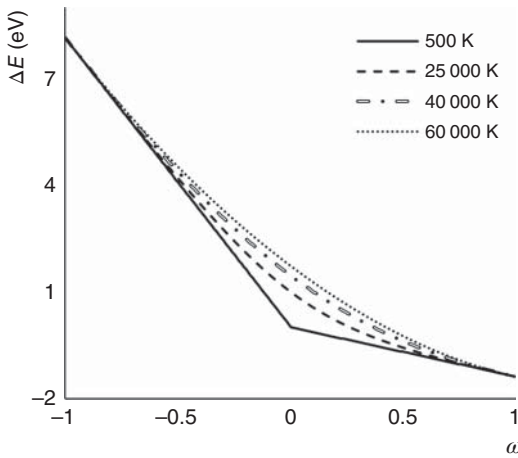


**Figure 8.1** Average energy as a function of the fractional charge at several temperatures.

One can note that Eq. (T1-1) bears some resemblance with the quadratic smooth interpolation given in Eq. (8.1). However, Eq. (T1-1) is not quadratic in  $\omega$ , because Eq. (8.16) establishes that  $\alpha$  is also a function of  $\omega$ . In fact, at zero temperature this expression reduces to the straight lines connecting the integer values of  $\langle N \rangle$  behavior established in 1982 by Perdew et al. [135–137], Eq. (T1-4).

In Figure 8.1 it may be seen that Eq. (T1-1) qualitatively resembles the piecewise continuous straight-lines shape up to rather high temperatures. Nevertheless, in general, the temperature smoothens this profile, so that the derivatives of the average energy with respect to the average number of electrons to all orders exist and can be evaluated analytically. However, it is important to note that at temperatures of chemical interest the average energy becomes practically equal to the value it has at  $T = 0$ .

In this context, the electronic chemical potential can be determined by taking the first derivative of Eq. (T1-1) with respect to the fractional charge. This procedure leads to Eq. (T1-2), that when it is evaluated at zero temperature leads to Eq. (T1-5), which, as a consequence of the piecewise straight-line shape of the energy, it shows a Heaviside step function behavior, that is qualitatively retained also up to rather high temperatures, although the effect of temperature smoothens this profile. Thus, at temperatures of chemical interest, the values for  $\mu_e$  are equal to the values at  $T = 0$ .

As in the case of the average energy, the response of the average electronic density of the system to the change in the average number of electrons corresponds to the finite temperature definition of the Fukui function [3, 122],

$$f_e(\mathbf{r}) = \left( \frac{\partial \langle \rho(\mathbf{r}) \rangle}{\partial \langle N \rangle} \right)_{T, v(\mathbf{r})} \quad (8.17)$$

which, through the chain rule, can be expressed as

$$\left( \frac{\partial \langle \rho(\mathbf{r}) \rangle}{\partial \langle N \rangle} \right)_{T, v(\mathbf{r})} = \left( \frac{\partial \langle \rho(\mathbf{r}) \rangle}{\partial \mu_{\text{Bath}}} \right)_{T, v(\mathbf{r})} \left( \frac{\partial \mu_{\text{Bath}}}{\partial \langle N \rangle} \right)_{T, v(\mathbf{r})} \quad (8.18)$$

The first derivative in the right-hand side of this equation, as in the case of the average energy, may be associated with the thermal fluctuations between the average

electron density and the average number of electrons,  $\sigma_{\rho(\mathbf{r})N}$ ,

$$\left( \frac{\partial \langle \rho(\mathbf{r}) \rangle}{\partial \mu_{\text{Bath}}} \right)_{T, v(\mathbf{r})} = \beta \sigma_{\rho(\mathbf{r})N} = \beta (\langle \rho(\mathbf{r})N \rangle - \langle \rho(\mathbf{r}) \rangle \langle N \rangle) \quad (8.19)$$

while the inverse of the second derivative in Eq. (8.18) was already identified with  $\sigma_{NN}$ , through Eq. (8.10), so that the Fukui function may be expressed as

$$f_e(\mathbf{r}) = \frac{\sigma_{\rho(\mathbf{r})N}}{\sigma_{NN}} = \frac{\langle \rho(\mathbf{r})N \rangle - \langle \rho(\mathbf{r}) \rangle \langle N \rangle}{\langle N^2 \rangle - \langle N \rangle \langle N \rangle} \quad (8.20)$$

An important consequence of the finite temperature definition of the Fukui function comes from the fact that the Maxwell relation [138]  $(\delta \mu_e / \delta v(\mathbf{r}))_N = (\partial \rho(\mathbf{r}) / \partial N)_{v(\mathbf{r})}$  is only fulfilled at  $T = 0$ , because it can be shown that, in general,

$$f_e(\mathbf{r}) = \left( \frac{\delta \mu_e}{\delta v(\mathbf{r})} \right)_{T, \langle N \rangle} - T \left[ \frac{\partial}{\partial \langle N \rangle} \left( \frac{\delta \langle S_T \rangle}{\delta v(\mathbf{r})} \right)_{T, \langle N \rangle} \right]_{T, v(\mathbf{r})} \quad (8.21)$$

Thus, one can see that there is an additional entropic contribution.

Now, to determine the temperature-dependent expression for the Fukui function, one must consider the difference between the average electronic density and the ground-state electronic density,  $\rho_{N_0,0}(\mathbf{r})$ , for the three ground-states ensemble, that is

$$\Delta \langle \rho(\mathbf{r}) \rangle = \langle \rho(\mathbf{r}) \rangle - \rho_{N_0,0}(\mathbf{r}) = \frac{f_e^+(\mathbf{r})e^{\beta(EA+\mu_{\text{Bath}})} - f_e^-(\mathbf{r})e^{-\beta(IP+\mu_{\text{Bath}})}}{1 + e^{\beta(EA+\mu_{\text{Bath}})} + e^{-\beta(IP+\mu_{\text{Bath}})}} \quad (8.22)$$

where

$$f_e^-(\mathbf{r}) = \rho_{N_0,0}(\mathbf{r}) - \rho_{N_0-1,0}(\mathbf{r}) \quad (8.23)$$

and

$$f_e^+(\mathbf{r}) = \rho_{N_0+1,0}(\mathbf{r}) - \rho_{N_0,0}(\mathbf{r}) \quad (8.24)$$

Combining the expression given in Eq. (8.22) with Eq. (8.14) one can express the electron density in terms of the fractional charge in the form given by Eq. (T1-7). As in the case of the average energy, at zero temperature this expression reduces to the straight lines connecting the integer values of  $\langle N \rangle$  behavior established also in 1982 by Perdew et al., Eq. (T1-10). Through this approach, the Fukui function can be determined by taking the first derivative of the average electronic density with respect to the fractional charge, leading to Eq. (T1-8), that at zero temperature reduces to Eq. (T1-11). This expression shows the Heaviside step function behavior, and it can be used to evaluate the Fukui function at temperatures of chemical interest.

Up to this point we have considered the first-order response functions associated with the changes in the average energy and in the average electronic density with respect to changes in the average number of electrons. In the first case one is led to a global-type indicator that characterizes the molecules as a whole, while in the second case one is led to a local type indicator that distinguishes between different sites within the molecule. However, in the first case, it is important to establish a local counterpart that describes the distribution of the global property at the local

level within the molecule, whereas in the second case one can define a non-local counterpart that distinguishes the sites or regions that make the largest contributions to the value of the property at a given point. In both cases it seems reasonable to develop these counterparts so that their integral over the whole space recovers the original global and local indicators.

To achieve this goal, one may consider first that the local counterpart of the average number of electrons is the average electronic density, since

$$\langle N \rangle = \int d\mathbf{r} \langle \rho(\mathbf{r}) \rangle \quad (8.25)$$

Then, in the case of the electronic chemical potential, one may replace the average number of electrons that appears in the numerator of Eq. (8.11) by its local counterpart, the average electronic density, to obtain that the local counterpart of  $\mu_e$ , is [127]

$$\mu_e(\mathbf{r}) = \frac{\sigma_{EN}}{\sigma_{NN}} = \frac{\langle E\rho(\mathbf{r}) \rangle - \langle E \rangle \langle \rho(\mathbf{r}) \rangle}{\langle N^2 \rangle - \langle N \rangle \langle N \rangle} \quad (8.26)$$

that clearly satisfies the condition

$$\mu_e = \int d\mathbf{r} \mu_e(\mathbf{r}) \quad (8.27)$$

and in the case of the electronic density, one can perform the same substitution in Eq. (8.20) to introduce the Fukui kernel [130], that is

$$f_e(\mathbf{r}, \mathbf{r}') = \frac{\sigma_{\rho(\mathbf{r})N}}{\sigma_{NN}} = \frac{\langle \rho(\mathbf{r})\rho(\mathbf{r}') \rangle - \langle \rho(\mathbf{r}) \rangle \langle \rho(\mathbf{r}') \rangle}{\langle N^2 \rangle - \langle N \rangle \langle N \rangle} \quad (8.28)$$

which indicates that

$$f_e(\mathbf{r}) = \int d\mathbf{r}' f_e(\mathbf{r}, \mathbf{r}') \quad (8.29)$$

Once the local chemical potential and the kernel of the Fukui function have been defined, one can proceed to establish their explicit temperature-dependent expressions, by making use of the three ground-states ensemble. This procedure leads to Eq. (T1-3) in the case of  $\mu_e(\mathbf{r})$  and to Eq. (T1-9) in the case of  $f_e(\mathbf{r}, \mathbf{r}')$ , with

$$\lambda = 4 + e^{\beta(I+\mu_{\text{Bath}})} + e^{-\beta(A+\mu_{\text{Bath}})} \quad (8.30)$$

The expressions for these two quantities, in the limit of zero temperature, and up to temperatures of chemical interest are given by Eqs. (T1-6) and (T1-12).

It is important to note that the expression for the local chemical potential at temperatures of chemical interest, Eq. (T1-6), in the case of  $\omega = 0$  leads to what could be identified as the negative of a local Mulliken electronegativity. But also, the expressions for  $\omega < 0$  and  $\omega > 0$  are very important, since they can be associated with the local ionization energy [139–144], and the local electron affinity energy [145–147], respectively. These two concepts have been used to describe the most favorable sites for electrophilic and nucleophilic attacks, and the acid–base behavior of different chemical species. On the other hand, the kernel of the Fukui function, Eq. (T1-12), is a new, important concept that allows one to study bond reactivity and stability [134].

### 8.3 Second-Order Response Functions in the Grand Canonical Ensemble

From the results established in the previous section, let us proceed to determine and analyze second-order response functions, particularly, the hardness and the dual descriptor. Thus, the finite temperature definition of the chemical hardness is expressed in terms of the second derivative of the average energy with respect to the average number of electrons, that is [123],

$$\eta_e = \left( \frac{\partial^2 \langle E \rangle}{\partial \langle N \rangle^2} \right)_{T, v(\mathbf{r})} = \left( \frac{\partial \mu_e}{\partial \langle N \rangle} \right)_{T, v(\mathbf{r})} \quad (8.31)$$

where the second equality comes from the finite temperature definition of the chemical potential given by Eq. (8.7). In a similar way, one finds the corresponding expression for the finite temperature dual descriptor, which is given by [122]

$$\Delta f_e(\mathbf{r}) = \left( \frac{\partial^2 \langle \rho(\mathbf{r}) \rangle}{\partial \langle N \rangle^2} \right)_{T, v(\mathbf{r})} = \left( \frac{\partial f_e(\mathbf{r})}{\partial \langle N \rangle} \right)_{T, v(\mathbf{r})} \quad (8.32)$$

Where we have used Eq. (8.17) to obtain the second equality.

Therefore, from the definition given by these two expressions, one can proceed to evaluate the second derivatives making use of the three ground-states ensemble, to obtain the explicit temperature-dependent equations. The results are presented in Table 8.2, Eqs. (T2-1) and (T2-9), together with their corresponding expressions for  $T = 0$ , and for temperatures of chemical interest, Eqs. (T2-5) and (T2-13). For the latter, one can note that the Heaviside step function behavior of the chemical potential and the Fukui function lead to the presence of the Dirac delta function in the hardness and in the dual descriptor, respectively [148]. As a matter of fact, although at temperatures different from zero these profiles smoothen, at temperatures of chemical interest they retain a strong Dirac delta function-like behavior. However, we had already argued that the identification of the hardness with the second derivative of the average energy with respect to the average number of electrons, and its evaluation through a smooth quadratic interpolation leads to  $\eta_e = I - A$ , which provides a satisfactory description of the intuitive concept developed by Pearson, and a similar situation applies to the dual descriptor when identified as  $\Delta f_e(\mathbf{r}) = f_e^+(\mathbf{r}) - f_e^-(\mathbf{r})$ . Therefore, one may consider alternative approaches that avoid the Dirac delta function-type behavior, to derive the second-order response functions.

In this context, one alternative consists of making use of the local chemical potential that satisfies Eq. (8.27), since one can derive this expression with respect to the average number of electrons to obtain that [127]

$$\eta_\tau = \int d\mathbf{r} \eta_\tau(\mathbf{r}) \quad (8.33)$$

where the subindex  $\tau$  is used to indicate that the origin of this hardness is based on the temperature-dependent approach through the use of Eq. (8.26). Similarly, in the case of the dual descriptor one can make use of Eq. (8.29) so that [130]

$$\Delta f_\tau(\mathbf{r}) = \int d\mathbf{r}' \Delta f_\tau(\mathbf{r}, \mathbf{r}') \quad (8.34)$$



**Table 8.2** Second-order response functions of the electronic energy and the electronic density evaluated with the three ground-states ensemble.

Electronic energy	Electronic density
Temperature dependent expressions	Temperature dependent expressions
$\eta_e = (I - A) \frac{2e^{-\beta(I-A)}}{\alpha^2}$ (T2-1)	$\Delta f_e(\mathbf{r}) = [f_e^+(\mathbf{r}) - f_e^-(\mathbf{r})] \frac{2e^{-\beta(I-A)}}{\alpha^3}$ (T2-9)
$\eta_r = \int d\mathbf{r} \eta_r(\mathbf{r}) = I - A$ (T2-2)	$\Delta f_r(\mathbf{r}) = \int d\mathbf{r}' \Delta f_r(\mathbf{r}, \mathbf{r}') = f_e^+(\mathbf{r}) - f_e^-(\mathbf{r})$ (T1-10)
$\eta_{\text{Th}} = \frac{\beta}{2} C_T (IP - EA)$ (T2-3)	$\Delta f_{\text{Th}}(\mathbf{r}) = \frac{\beta}{2} C_T [f_e^+(\mathbf{r}) - f_e^-(\mathbf{r})]$ (T2-11)
$\eta_r(\mathbf{r}) = If_e^-(\mathbf{r}) - Af_e^+(\mathbf{r})$ $+ \frac{\omega}{2} (I - A) (f_e^+(\mathbf{r}) - f_e^-(\mathbf{r}))$ (T2-4)	$\Delta f_r(\mathbf{r}, \mathbf{r}') = f_e^+(\mathbf{r})f_e^+(\mathbf{r}') - f_e^-(\mathbf{r})f_e^-(\mathbf{r}')$ $+ \frac{\omega}{2} \Delta f_e(\mathbf{r})\Delta f_e(\mathbf{r}')$ (T2-12)
Expressions at $T = 0$ and at temperatures of chemical interest	Expressions at $T = 0$ and at temperatures of chemical interest
$\eta_e = \begin{cases} 0 & \omega < 0 \\ (I - A) \delta(\omega) & \omega = 0 \\ 0 & \omega > 0 \end{cases}$ (T2-5)	$\Delta f_e(\mathbf{r}) = \begin{cases} 0 & \omega < 0 \\ [f_e^+(\mathbf{r}) - f_e^-(\mathbf{r})] \delta(\omega) & \omega = 0 \\ 0 & \omega > 0 \end{cases}$ (T2-13)
$\eta_r = \begin{cases} I - A & \omega < 0 \\ I - A & \omega = 0 \\ I - A & \omega > 0 \end{cases}$ (T2-6)	$\Delta f_r(\mathbf{r}) = \begin{cases} f_e^+(\mathbf{r}) - f_e^-(\mathbf{r}) & \omega < 0 \\ f_e^+(\mathbf{r}) - f_e^-(\mathbf{r}) & \omega = 0 \\ f_e^+(\mathbf{r}) - f_e^-(\mathbf{r}) & \omega > 0 \end{cases}$ (T2-14)
$\eta_{\text{Th}} = \begin{cases} 0 & \omega < 0 \\ \frac{\beta}{2} (I - A) & \omega = 0 \\ 0 & \omega > 0 \end{cases}$ (T2-7)	$\Delta f_{\text{Th}}(\mathbf{r}) = \begin{cases} 0 & \omega < 0 \\ \frac{\beta}{2} [f_e^+(\mathbf{r}) - f_e^-(\mathbf{r})] & \omega = 0 \\ 0 & \omega > 0 \end{cases}$ (T2-15)
$\eta_r(\mathbf{r}) \begin{cases} If_e^-(\mathbf{r}) - Af_e^+(\mathbf{r}) & \omega < 0 \\ If_e^-(\mathbf{r}) - Af_e^+(\mathbf{r}) & \omega < 0 \\ If_e^-(\mathbf{r}) - Af_e^+(\mathbf{r}) & \omega < 0 \\ -(I - A) [f_e^+(\mathbf{r}) - f_e^-(\mathbf{r})] / 2 & \omega < 0 \end{cases}$ (T2-8)	$\Delta f_r(\mathbf{r}, \mathbf{r}') \begin{cases} [f_e^+(\mathbf{r})f_e^+(\mathbf{r}') - f_e^-(\mathbf{r})f_e^-(\mathbf{r}')] & \omega < 0 \\ - [f^+(\mathbf{r}) - f^-(\mathbf{r})] [f^+(\mathbf{r}') - f^-(\mathbf{r}')] / 2 & \omega < 0 \\ f_e^+(\mathbf{r})f_e^+(\mathbf{r}') - f_e^-(\mathbf{r})f_e^-(\mathbf{r}') & \omega < 0 \\ f_e^+(\mathbf{r})f_e^+(\mathbf{r}') - f_e^-(\mathbf{r})f_e^-(\mathbf{r}') & \omega < 0 \\ - [f^+(\mathbf{r}) - f^-(\mathbf{r})] [f^+(\mathbf{r}') - f^-(\mathbf{r}')] / 2 & \omega < 0 \end{cases}$ (T1-16)

When one considers the three ground-states ensemble to obtain the explicit expressions for the quantities involved in these two relationships, one obtains Eqs. (T2-2) and (T2-4) for the hardness, and Eqs. (T2-10) and (T2-12) for the dual descriptor, while at  $T = 0$  and at temperatures of chemical interest, one finds that these expressions reduce to Eqs. (T2-6) and (T2-8) for the hardness, and Eqs. (T2-14) and (T2-16) for the dual descriptor. One can note that in the global and local counterpart of the hardness, there is no explicit dependence on the Dirac delta function, because it cancels in the derivation, so that one recovers, in the case of the global hardness, the chemically useful identification with the quantity  $(I - A)$ . The same situation occurs in the local and non-local counterpart of the dual descriptor, where one also is led to the chemically important quantity  $[f_e^+(\mathbf{r}) - f_e^-(\mathbf{r})]$ .

An additional important outcome of this procedure lies in the local hardness thus obtained, Eq. (T2-4), and particularly Eq. (T2-8), which corresponds to temperatures of chemical interest. It is well known that the original definition of local hardness based on the construction of a hierarchy of global, local, and non-local hardnesses that are inverses of the global, local, and non-local softnesses, respectively, is intrinsically ambiguous [43, 58, 61]. However, one can see that the local hardness derived from the grand canonical ensemble is well defined, it recovers the intuitive proposal of Meneses et al. [65, 67], and it provides, in general, valuable information about site selectivity. A similar result occurs with the dual descriptor kernel that contains valuable information about the balance between the electrophilic and nucleophilic characteristics of a chemical bond.

A second alternative to avoid the Dirac delta function-like behavior comes from the fact that the response of a system to changes in the chemical potential of the reservoir when the temperature and the external potential are kept constant is equivalent to the response of the system to changes in the average number of electrons, since the latter is modified through charge transfer between the system and the surroundings. Thus, to obtain the second-order responses of the energy and of the electronic density one can consider the derivatives of the chemical potential and of the Fukui function with respect to  $\mu_{\text{Bath}}$ , that is [128]

$$\eta_{\text{Th}} = \left( \frac{\partial \mu_e}{\partial \mu_{\text{Bath}}} \right)_{T, v(\mathbf{r})} \quad (8.35)$$

and [132]

$$\Delta f_{\text{Th}}(\mathbf{r}) = \left( \frac{\partial f_e(\mathbf{r})}{\partial \mu_{\text{Bath}}} \right)_{T, v(\mathbf{r})} \quad (8.36)$$

The expressions for these two derivatives associated with the three ground-states ensemble are given by Eq. (T2-3) for the thermodynamic hardness, and by Eq. (T2-11) for the thermodynamic dual descriptor, where

$$C_T = \frac{\text{sech}^2[\beta \Delta\mu] - \text{sech}[\beta \Delta\mu] e^{-\frac{\beta}{2}(I-A)}}{1 + 2 \text{sech}[\beta \Delta\mu] e^{-\frac{\beta}{2}(I-A)} \left( 1 + 4e^{-\frac{\beta}{2}(I-A)} \text{sech}[\beta \Delta\mu] \right)} \quad (8.37)$$

$\text{sech}$  is the hyperbolic secant function and  $\Delta\mu = \mu_{\text{Bath}} + (I + A)/2$ . One can also see that in the limit when  $T = 0$ , and for temperatures of chemical interest  $C_T = 1$

when  $\omega = 0$ , and  $C_T = 0$  when  $\omega < 0$  or  $\omega > 0$ , leading to the relationships expressed in Eqs. (T2-7) and (T2-15). These show that through this procedure the final expressions do not depend on the Dirac delta function and that the thermodynamic hardness and dual descriptor become proportional to  $(I - A)$  and  $[f_e^+(\mathbf{r}) - f_e^-(\mathbf{r})]$ , respectively, which are the expressions that provide good estimates of these two quantities.

## 8.4 Response Functions to Changes in the Temperature and Their Central Role in a Chemical Event

Since we are dealing with the temperature-dependent approach, it is important to consider and to analyze response functions associated with changes in the temperature – in particular the first-order responses of the average energy and the average density. The former leads to an electronic heat capacity, namely [125],

$$C_{v(\mathbf{r})} = \left( \frac{\partial \langle E \rangle}{\partial T} \right)_{\langle N \rangle, v(\mathbf{r})} \quad (8.38)$$

while the latter can be identified with a local heat capacity, that is [126],

$$C_{v(\mathbf{r})}(\mathbf{r}) = \left( \frac{\partial \langle \rho(\mathbf{r}) \rangle}{\partial T} \right)_{\langle N \rangle, v(\mathbf{r})} \quad (8.39)$$

On the other hand, in the case of second-order response functions it is important to consider the change in the electronic chemical potential with respect to the change in the temperature that leads to the following Maxwell relationship [125],

$$\left( \frac{\partial \mu_e}{\partial T} \right)_{\langle N \rangle, v(\mathbf{r})} = \left( \frac{\partial C_{v(\mathbf{r})}}{\partial \langle N \rangle} \right)_{T, v(\mathbf{r})} \quad (8.40)$$

where we have used Eqs. (8.7) and (8.38).

The explicit expressions for these three indexes associated with the three ground-states ensemble can be obtained by determining the derivative of  $\langle E \rangle$  (Eq. (T1-1)),  $\langle \rho(\mathbf{r}) \rangle$  (Eq. (T1-7)) and  $\mu_e$  (Eq. (T1-2)) with respect to  $T$ , taking into account Eq. (8.14) for  $\omega$  and Eq. (8.16) for  $\alpha$ , since these two quantities are the ones that contain the dependence on the temperature. It is found that in the low-temperature limit that includes the interval of temperatures of chemical interest, the three indexes are equal to zero for  $\omega < 0$  and  $\omega > 0$ , whereas for  $\omega = 0$  they adopt the form

$$C_{v(\mathbf{r})} = \left( \frac{\partial \langle E \rangle}{\partial T} \right)_{\langle N \rangle, v(\mathbf{r})} = \frac{e^{-\frac{\beta}{2}(I-A)}}{2k_B T^2} (I - A)^2 \quad (8.41)$$

$$C_{v(\mathbf{r})}(\mathbf{r}) = \left( \frac{\partial \langle \rho(\mathbf{r}) \rangle}{\partial T} \right)_{\langle N \rangle, v(\mathbf{r})} = \frac{e^{-\frac{\beta}{2}(I-A)}}{2k_B T^2} (I - A) [f_e^+(\mathbf{r}) - f_e^-(\mathbf{r})] \quad (8.42)$$

And

$$\left( \frac{\partial \mu_e}{\partial T} \right)_{\langle N \rangle, v(\mathbf{r})} = \left( \frac{\partial C_{v(\mathbf{r})}}{\partial \langle N \rangle} \right)_{T, v(\mathbf{r})} = -\frac{e^{-\frac{\beta}{2}(I-A)}}{4k_B T^2} (I - A)^2 \quad (8.43)$$

It is important to note that these three indexes become exactly equal to zero when  $T = 0$ , a result that is consistent with the overall discussion, since in this limit there should be no contributions from the response functions associated to changes in the temperature.

Now, let us consider the total differential for the average energy and the average electronic density. At first instance, in the grand canonical ensemble, we should consider  $\mu_{\text{Bath}}$ ,  $v(\mathbf{r})$ , and  $T$  as the independent variables that characterize the differential. However, it has been shown that one can make a transformation from this set to one in which  $\langle E \rangle$  and  $\langle \rho(\mathbf{r}) \rangle$  are treated as functions of  $\langle N \rangle$ ,  $v(\mathbf{r})$ , and  $T$ . In this framework the total differentials are expressed as

$$d\langle E \rangle = \mu_e d\langle N \rangle + \int [\langle \rho(\mathbf{r}) \rangle + T(\delta\langle S_T \rangle / \delta v(\mathbf{r}))_{T, \langle N \rangle}] \delta v(\mathbf{r}) d\mathbf{r} + (\partial\langle E \rangle / \partial T)_{\langle N \rangle, v(\mathbf{r})} dT \quad (8.44)$$

and

$$d\langle \rho(\mathbf{r}) \rangle = f_e(\mathbf{r}) d\langle N \rangle + \int (\delta\langle \rho(\mathbf{r}) \rangle / \delta v(\mathbf{r}'))_{T, \langle N \rangle} \delta v(\mathbf{r}') d\mathbf{r}' + C_{v(\mathbf{r})}(\mathbf{r}) dT \quad (8.45)$$

In the analysis of these fundamental changes, one must take into account that at the onset of a chemical interaction, the participating species have an integer average number of electrons. At this point, precisely, as we have just seen, the three indexes just described are different from zero, so that one can infer that according to Eqs. (8.41) and (8.44) there is an energy exchange associated with changes in the temperature and according to Eqs. (8.42) and (8.45) these changes also promote charge transfer, which is governed by the regioselectivity features characterized by the nucleophilic–electrophilic balance expressed in the directional Fukui functions. However, once the average number of electrons starts to adopt small fractional values, because of the charge transferred, the two response functions of Eqs. (8.41) and (8.42) become very small, so that the interaction after this point is dominated by the changes in the external potential and in the average number of electrons, rather than by changes in the temperature.

If we consider the total differential for the electronic chemical potential, then

$$d\mu_e = \eta_e d\langle N \rangle + \int [f_e(\mathbf{r}) + T(\delta^2\langle S_T \rangle / \partial\langle N \rangle \delta v(\mathbf{r}))] \delta v(\mathbf{r}) d\mathbf{r} + (\partial\mu_e / \partial T)_{\langle N \rangle, v(\mathbf{r})} dT \quad (8.46)$$

At zero temperature the entropic contribution and the last term in the right-hand side of this equation vanish, so that in this limit this differential becomes identical to the one first introduced by Parr and Yang to define the Fukui function [3]. In their work they postulated through this expression that the site preferred for a chemical interaction to occur is the one that corresponds to the largest change in the chemical potential, which implies that the sites with the largest values of the Fukui functions are the most reactive sites. Since the frontier orbitals are closely related with the Fukui function, Parr and Yang concluded that the frontier orbital theory could be seen as a consequence of the “ $|\Delta\mu|$  big is good” rule for chemical reactivity. Recently,

this last statement was proven, together with its implications in the hard and soft acids and bases principle and in the principle of maximum hardness [54, 56, 57].

Now, from the perspective of the temperature-dependent approach, at the onset of the interaction, before the charge transferred has occurred, the value of  $\langle N \rangle$  for each one of the participating species is an integer. At this point, the changes in the chemical potential arise from changes in the temperature, until charge transfer begins, when the response function given by Eq. (8.43) becomes very small, and the charge-transfer process is controlled then by the changes in the external potential and in the average number of electrons. Thus, one can see that the “ $|\Delta\mu|$  big is good” rule has two components. An initial one caused by changes in  $T$  and expressed in Eq. (8.42) combined with Eq. (8.45), and a subsequent one caused by changes in  $v(\mathbf{r})$  and  $\langle N \rangle$  and expressed in Eq. (8.21) combined with Eq. (8.46). In both cases the regioselectivity information contained in the directional Fukui functions for electrophilic and nucleophilic attacks plays an important role.

## 8.5 Concluding Remarks

Through this chapter, we have seen that the generalization of the CDFT to the grand canonical ensemble has very important consequences in the study of chemical reactivity.

In first place, we have seen that although  $\mu_{\text{Bath}}$ ,  $v(\mathbf{r})$ , and  $T$  are the natural independent variables of the grand canonical ensemble, it is more convenient to make use of the set of variables constituted by  $\langle N \rangle$ ,  $v(\mathbf{r})$ , and  $T$ , together with the average values of the energy and the electronic density in the ensemble, to determine directly the temperature-dependent derivatives associated with the definitions of the different response functions. Through this procedure, we have seen, for the particular case of the three ground-states ensemble, that when these relationships are evaluated at  $T = 0$ , they become identical to the zero-temperature expressions obtained by Perdew and collaborators in 1982. This result provides a strong support to the procedure just outlined in terms of average properties of the ensemble.

It is also important to note that quantities that are equal to each other at zero temperature, like  $\mu_e$  and  $\mu_{\text{Bath}}$ , may be, in general, different from each other at other temperatures due to the presence of additional terms that are different from zero for  $T \neq 0$ , as established in Eq. (8.12). A similar situation occurs with  $f_e(\mathbf{r})$  and  $(\delta\mu_e/\delta v(\mathbf{r}))_{T, \langle N \rangle}$ , as expressed in Eq. (8.21).

A remarkable aspect comes from the fact that dependence on the temperature smoothens the piecewise continuous straight lines behavior of the average energy and the average electron density, so that derivatives of these two quantities with respect to the average number of electrons to all orders exist and can be evaluated analytically. Although it is important to take into account that the values of the response functions at  $T = 0$  remain practically unchanged at temperatures of chemical interest, because temperatures of the order of  $10^4$  K are required to observe a significant change in their values. An important consequence of this behavior is that the three ground-states ensemble include the most relevant contributions required

to obtain a good description of the response functions, so that one really does not need to go beyond this ensemble, except for very small number of specific cases [129].

Now, the fact that the response functions retain the characteristics associated with them at  $T = 0$  up to temperatures of chemical interest implies that the chemical potential will show the Heaviside step function behavior. This aspect could be seen as a reasonable result from the chemical viewpoint, because one can expect that the response of a system to charge donation ( $\omega < 0$ ) will be different from its response to charge acceptance ( $\omega > 0$ ), and different from its response when at the end neither donates nor accepts charge ( $\omega = 0$ ).

However, the hardness will show the Dirac delta function-type behavior in the range of temperatures important for chemical reactivity, a situation which, indeed, will not lead to satisfactory description of this important index. Nevertheless we have seen that through the temperature-dependent approach we have been able to develop two alternative definitions that avoid the Dirac delta function, and, at the same time, are proportional to the quantity  $(I - A)$ , to essentially recover the main characteristics of the global hardness. Additionally, two new concepts, the local chemical potential and the local hardness, have emerged. These new concepts have been shown to be very useful to analyze regioselectivity issues in several chemical interactions.

In summary, although the contribution to the values of the response functions associated with CDFT, arising from the temperature are fundamentally negligible, with respect to the values they adopt at zero temperature, the analysis in the grand canonical ensemble is essential to get a more complete and more solid framework to study chemical reactivity through this approach.

## Acknowledgment

We thank Conacyt for grant Sinergia 1561802.

## References

- 1 Parr, R.G., Donnelly, R.A., Levy, M., and Palke, W.E. (1978). Electronegativity - density functional viewpoint. *J. Chem. Phys.* 68: 3801–3807.
- 2 Parr, R.G. and Pearson, R.G. (1983). Absolute hardness - companion parameter to absolute electronegativity. *J. Am. Chem. Soc.* 105: 7512–7516.
- 3 Parr, R.G. and Yang, W.T. (1984). Density functional approach to the frontier-electron theory of chemical reactivity. *J. Am. Chem. Soc.* 106: 4049–4050.
- 4 Yang, W.T., Parr, R.G., and Pucci, R. (1984). Electron-density, Kohn-Sham frontier orbitals, and Fukui functions. *J. Chem. Phys.* 81: 2862–2863.
- 5 Ayers, P.W. and Levy, M. (2000). Perspective on “Density functional approach to the frontier-electron theory of chemical reactivity” by Parr RG, Yang W (1984). *Theor. Chem. Accounts* 103: 353–360.

- 6 Morell, C., Grand, A., and Toro-Labbé, A. (2005). New dual descriptor for chemical reactivity. *J. Phys. Chem. A* 109: 205–212.
- 7 Morell, C., Grand, A., and Toro-Labbé, A. (2006). Theoretical support for using the delta  $f(r)$  descriptor. *Chem. Phys. Lett.* 425: 342–346.
- 8 Iczkowski, R. and Margrave, J.L. (1961). Electronegativity. *J. Am. Chem. Soc.* 83: 3547–3551.
- 9 Mulliken, R.S. (1934). A new electroaffinity scale; together with data on valence states and on valence ionization potentials and electron affinities. *J. Chem. Phys.* 2: 782–793.
- 10 Pearson, R.G. (1963). Hard and soft acids and bases. *J. Am. Chem. Soc.* 85: 3533–3539.
- 11 Pearson, R.G. (1966). Acids and bases. *Science* 151: 172–177.
- 12 Sanderson, R.T. (1951). An interpretation of bond lengths and a classification of bonds. *Science* 114: 670–672.
- 13 Sanderson, R.T. (1971). *Chemical Bonds and Bond Energy*. New York: Academic Press.
- 14 Pearson, R.G. (1988). Absolute electronegativity and hardness: application to inorganic chemistry. *Inorg. Chem.* 27: 734–740.
- 15 Pearson, R.G. (1989). Absolute electronegativity and hardness: application to organic chemistry. *J. Org. Chem.* 54: 1423–1430.
- 16 Pearson, R.G. (1987). Recent advances in the concept of hard and soft acids and bases. *J. Chem. Educ.* 64: 561–567.
- 17 Pearson, R.G. and Palke, W.E. (1992). Support for a principle of maximum hardness. *J. Phys. Chem.* 96: 3283–3285.
- 18 Fukui, K. (1982). Role of frontier orbitals in chemical-reactions. *Science* 218: 747–754.
- 19 Fukui, K., Yonezawa, T., and Shingu, H. (1952). A molecular orbital theory of reactivity in aromatic hydrocarbons. *J. Chem. Phys.* 20: 722–725.
- 20 Zhou, Z.X. and Parr, R.G. (1990). Activation hardness: new index for describing the orientation of electrophilic aromatic substitution. *J. Am. Chem. Soc.* 112: 5720–5724.
- 21 Chattaraj, P.K., Lee, H., and Parr, R.G. (1991). HSAB principle. *J. Am. Chem. Soc.* 113: 1855–1856.
- 22 Parr, R.G. and Chattaraj, P.K. (1991). Principle of maximum hardness. *J. Am. Chem. Soc.* 113: 1854–1855.
- 23 Gázquez, J.L. (1993). Hardness and softness in density functional theory. *Struct. Bond.* 80: 27–43.
- 24 Gázquez, J.L., Martínez, A., and Méndez, F. (1993). Relationship between energy and hardness differences. *J. Phys. Chem.* 97: 4059–4063.
- 25 Ghanty, T.K. and Ghosh, S.K. (1993). Correlation between hardness, polarizability, and size of atoms, molecules, and clusters. *J. Phys. Chem.* 97: 4951–4953.
- 26 Gázquez, J.L. and Méndez, F. (1994). The hard and soft acids and bases principle: an atoms in molecules viewpoint. *J. Phys. Chem.* 98: 4591–4593.

- 27 Ghanty, T.K. and Ghosh, S.K. (1994). Simple density functional approach to polarizability, hardness, and covalent radius of atomic systems. *J. Phys. Chem.* 98: 9197–9201.
- 28 Méndez, F. and Gázquez, J.L. (1994). Chemical reactivity of enolate ions: the local hard and soft acids and bases principle viewpoint. *J. Am. Chem. Soc.* 116: 9298–9301.
- 29 Chattaraj, P.K., Cedillo, A., and Parr, R.G. (1995). Variational method for determining the Fukui function and chemical hardness of an electronic system. *J. Chem. Phys.* 103: 7645–7646.
- 30 Chattaraj, P.K., Liu, G.H., and Parr, R.G. (1995). The maximum hardness principle in the Gyftopoulos-Hatsopoulos three-level model for an atomic or molecular species and its positive and negative ions. *Chem. Phys. Lett.* 237: 171–176.
- 31 Gázquez, J.L. (1997). The hard and soft acids and bases principle. *J. Phys. Chem. A* 101: 4657–4659.
- 32 Gázquez, J.L. (1997). Bond energies and hardness differences. *J. Phys. Chem. A* 101: 9464–9469.
- 33 Gázquez, J.L. (1997). Activation energies and softness additivity. *J. Phys. Chem. A* 101: 8967–8969.
- 34 Chattaraj, P.K., Fuentealba, P., Jaque, P., and Toro-Labbé, A. (1999). Validity of the minimum polarizability principle in molecular vibrations and internal rotations: an *ab initio* SCF study. *J. Phys. Chem. A* 103: 9307–9312.
- 35 Ayers, P.W. and Parr, R.G. (2000). Variational principles for describing chemical reactions: the Fukui function and chemical hardness revisited. *J. Am. Chem. Soc.* 122: 2010–2018.
- 36 Cedillo, A., Chattaraj, P.K., and Parr, R.G. (2000). Atoms-in-molecules partitioning of a molecular density. *Int. J. Quantum Chem.* 77: 403–407.
- 37 Torrent-Sucarrat, M., Luis, J.M., Durán, M., and Solá, M. (2001). On the validity of the maximum hardness and minimum polarizability principles for nontotally symmetric vibrations. *J. Am. Chem. Soc.* 123: 7951–7952.
- 38 Torrent-Sucarrat, M., Luis, J.M., Durán, M., and Solá, M. (2002). Are the maximum hardness and minimum polarizability principles always obeyed in nontotally symmetric vibrations? *J. Chem. Phys.* 117: 10561–10570.
- 39 Gómez, B., Fuentealba, P., and Contreras, R. (2003). The maximum hardness and minimum polarizability principles as the basis for the study of reaction profiles. *Theor. Chem. Accounts* 110: 421–427.
- 40 Torrent-Sucarrat, M., Luis, J.M., Durán, M., and Solá, M. (2004). The hardness profile as a tool to detect spurious stationary points in the potential energy surface. *J. Chem. Phys.* 120: 10914–10924.
- 41 Ayers, P.W. (2007). The physical basis of the hard/soft acid/base principle. *Faraday Discuss.* 135: 161–190.
- 42 Ayers, P.W. (2007). On the electronegativity nonlocality paradox. *Theor. Chem. Accounts* 118: 371–381.
- 43 Ayers, P.W. and Parr, R.G. (2008). Local hardness equalization: exploiting the ambiguity. *J. Chem. Phys.* 128: 184108.



- 44 Ayers, P.W. and Parr, R.G. (2008). Beyond electronegativity and local hardness: higher-order equalization criteria for determination of a ground-state electron density. *J. Chem. Phys.* 129: 054111.
- 45 Chattaraj, P.K., Giri, S., and Duley, S. (2010). Electrophilicity equalization principle. *J. Phys. Chem. Lett.* 1: 1064–1067.
- 46 Ayers, P.W. and Cárdenas, C. (2013). Communication: a case where the hard/soft acid/base principle holds regardless of acid/base strength. *J. Chem. Phys.* 138: 181106.
- 47 Cárdenas, C. and Ayers, P.W. (2013). How reliable is the hard-soft acid-base principle? An assessment from numerical simulations of electron transfer energies. *Phys. Chem. Chem. Phys.* 15: 13959–13968.
- 48 Gázquez, J.L., Vela, A., and Chattaraj, P.K. (2013). Local hardness equalization and the principle of maximum hardness. *J. Chem. Phys.* 138: 214103.
- 49 Ayers, P.W. (2005). An elementary derivation of the hard/soft-acid/base principle. *J. Chem. Phys.* 122: 141102.
- 50 Chattaraj, P.K. and Ayers, P.W. (2005). The maximum hardness principle implies the hard/soft acid/base rule. *J. Chem. Phys.* 123: 086101.
- 51 Ayers, P.W., Parr, R.G., and Pearson, R.G. (2006). Elucidating the hard/soft acid/base principle: a perspective based on half-reactions. *J. Chem. Phys.* 124: 194107.
- 52 Chattaraj, P.K., Ayers, P.W., and Melin, J. (2007). Further links between the maximum hardness principle and the hard/soft acid/base principle: insights from hard/soft exchange reactions. *Phys. Chem. Chem. Phys.* 9: 3853–3856.
- 53 Miranda-Quintana, R.A. (2017). Note: the minimum electrophilicity and the hard/soft acid/base principles. *J. Chem. Phys.* 146: 046101.
- 54 Miranda-Quintana, R.A. and Ayers, P.W. (2018). Dipolar cycloadditions and the "Delta mu big is good" rule: a computational study. *Theor. Chem. Accounts* 137: 177.
- 55 Miranda-Quintana, R.A. and Ayers, P.W. (2018). Note: maximum hardness and minimum electrophilicity principles. *J. Chem. Phys.* 148: 196101.
- 56 Miranda-Quintana, R.A., Heidar-Zadeh, F., and Ayers, P.W. (2018). Elementary derivation of the "delta mu big is good" rule. *J. Phys. Chem. Lett.* 9: 4344–4348.
- 57 Miranda-Quintana, R.A. and Ayers, P.W. (2019). The "delta mu big is good" rule, the maximum hardness, and minimum electrophilicity principles. *Theor. Chem. Accounts* 138: 44.
- 58 Berkowitz, M., Ghosh, S.K., and Parr, R.G. (1985). On the concept of local hardness in chemistry. *J. Am. Chem. Soc.* 107: 6811–6814.
- 59 Yang, W.T. and Parr, R.G. (1985). Hardness, softness, and the Fukui function in the electronic theory of metals and catalysis. *Proc. Natl. Acad. Sci. U. S. A.* 82: 6723–6726.
- 60 Berkowitz, M. and Parr, R.G. (1988). Molecular hardness and softness, local hardness and softness, hardness and softness kernels, and relations among these quantities. *J. Chem. Phys.* 88: 2554–2557.
- 61 Ghosh, S.K. (1990). Energy derivatives in density-functional theory. *Chem. Phys. Lett.* 172: 77–82.

- 62 Vela, A. and Gázquez, J.L. (1990). A relationship between the static dipole polarizability, the global softness and the Fukui function. *J. Am. Chem. Soc.* 112: 1490–1492.
- 63 Cohen, M.H., Ganduglia-Pirovano, M.V., and Kudrnovsky, J. (1995). Reactivity kernels, the normal modes of chemical reactivity, and the hardness and softness spectra. *J. Chem. Phys.* 103: 3543–3551.
- 64 Fuentealba, P. (1995). A local model for the hardness kernel and related reactivity parameters in density functional theory. *J. Chem. Phys.* 103: 6571–6575.
- 65 Meneses, L., Tiznado, W., Contreras, R., and Fuentealba, P. (2004). A proposal for a new local hardness as selectivity index. *Chem. Phys. Lett.* 383: 181–187.
- 66 Chattaraj, P.K., Roy, D.R., Geerlings, P., and Torrent-Sucarrat, M. (2007). Local hardness: a critical account. *Theor. Chem. Accounts* 118: 923–930.
- 67 Meneses, L., Araya, A., Pilaquinga, F. et al. (2007). Local hardness: an application to electrophilic additions. *Chem. Phys. Lett.* 446: 170–175.
- 68 Torrent-Sucarrat, M., Salvador, P., Geerlings, P., and Solá, M. (2007). On the quality of the hardness kernel and the Fukui function to evaluate the global hardness. *J. Comput. Chem.* 28: 574–583.
- 69 Torrent-Sucarrat, M., De Proft, F., Geerlings, P., and Ayers, P.W. (2008). Do the local softness and hardness indicate the softest and hardest regions of a molecule? *Chem. Eur. J.* 14: 8652–8660.
- 70 Torrent-Sucarrat, M., Salvador, P., Solá, M., and Geerlings, P. (2008). The hardness kernel as the basis for global and local reactivity indices. *J. Comput. Chem.* 29: 1064–1072.
- 71 Sablon, N., De Proft, F., and Geerlings, P. (2010). The linear response kernel: inductive and resonance effects quantified. *J. Phys. Chem. Lett.* 1: 1228–1234.
- 72 Torrent-Sucarrat, M., De Proft, F., Ayers, P.W., and Geerlings, P. (2010). On the applicability of local softness and hardness. *Phys. Chem. Chem. Phys.* 12: 1072–1080.
- 73 Gál, T. (2012). Why the traditional concept of local hardness does not work. *Theor. Chem. Accounts* 131: 1223.
- 74 Fias, S., Geerlings, P., Ayers, P., and De Proft, F. (2013). Sigma, pi aromaticity and anti-aromaticity as retrieved by the linear response kernel. *Phys. Chem. Chem. Phys.* 15: 2882–2889.
- 75 Geerlings, P., Fias, S., Boisdenghien, Z., and De Proft, F. (2014). Conceptual DFT: chemistry from the linear response function. *Chem. Soc. Rev.* 43: 4989–5008.
- 76 Zadeh, F.H., Fuentealba, P., Cardenas, C., and Ayers, P.W. (2014). An information-theoretic resolution of the ambiguity in the local hardness. *Phys. Chem. Chem. Phys.* 16: 6019–6026.
- 77 Heidar-Zadeh, F., Fias, S., Vohringer-Martinez, E. et al. (2016). The local response of global descriptors. *Theor. Chem. Accounts* 136: 19.
- 78 Polanco-Ramírez, C.A., Franco-Pérez, M., Carmona-Espíndola, J. et al. (2017). Revisiting the definition of local hardness and hardness kernel. *Phys. Chem. Chem. Phys.* 19: 12355–12364.

- 79 Franco-Pérez, M., Polanco-Ramírez, C.A., Gázquez, J.L., and Ayers, P.W. (2018). Local and nonlocal counterparts of global descriptors: the cases of chemical softness and hardness. *J. Mol. Model.* 24: 285.
- 80 Robles, A., Franco-Pérez, M., Gázquez, J.L. et al. (2018). Local electrophilicity. *J. Mol. Model.* 24: 245.
- 81 Pauling, L. (1932). The nature of the chemical bond IV the energy of single bonds and the relative electronegativity of atoms. *J. Am. Chem. Soc.* 54: 3570–3582.
- 82 Pauling, L. (1960). *The Nature of the Chemical Bond*, 3e. New York: Cornell University Press.
- 83 Parr, R.G., Von Szentpaly, L., and Liu, S.B. (1999). Electrophilicity index. *J. Am. Chem. Soc.* 121: 1922–1924.
- 84 Ayers, P.W., Anderson, J.S.M., Rodríguez, J.I., and Jawed, Z. (2005). Indices for predicting the quality of leaving groups. *Phys. Chem. Chem. Phys.* 7: 1918–1925.
- 85 Chattaraj, P.K. and Roy, D.R. (2007). Update 1 of: electrophilicity index. *Chem. Rev.* 107: PR46–PR74.
- 86 Chattaraj, P.K., Sarkar, U., and Roy, D.R. (2006). Electrophilicity index. *Chem. Rev.* 106: 2065–2091.
- 87 Gázquez, J.L., Cedillo, A., and Vela, A. (2007). Electrodonating and electroaccepting powers. *J. Phys. Chem. A* 111: 1966–1970.
- 88 Bagaria, P., Saha, S., Murru, S. et al. (2009). A comprehensive decomposition analysis of stabilization energy (CDASE) and its application in locating the rate-determining step of multi-step reactions. *Phys. Chem. Chem. Phys.* 11: 8306–8315.
- 89 Saha, S., Roy, R.K., and Pal, S. (2010). CDASE-a reliable scheme to explain the reactivity sequence between Diels-Alder pairs. *Phys. Chem. Chem. Phys.* 12: 9328–9338.
- 90 Chattaraj, P.K., Giri, S., and Duley, S. (2011). Update 2 of: electrophilicity index. *Chem. Rev.* 111: PR43–PR75.
- 91 Sarmah, A. and Roy, R.K. (2013). Understanding the interaction of nucleobases with chiral semiconducting single-walled carbon nanotubes: an alternative theoretical approach based on density functional reactivity theory. *J. Phys. Chem. C* 117: 21539–21550.
- 92 Sarmah, A. and Roy, R.K. (2015). Interaction between small gold clusters and nucleobases: a density functional reactivity theory based study. *J. Phys. Chem. C* 119: 17940–17953.
- 93 Hamid, A., Anand, A., and Roy, R.K. (2017). The charge transfer limit of a chemical adduct: the role of perturbation on external potential. *Phys. Chem. Chem. Phys.* 19: 10905–10912.
- 94 Orozco-Valencia, A.U., Gázquez, J.L., and Vela, A. (2017). Global and local partitioning of the charge transferred in the Parr-Pearson model. *J. Phys. Chem. A* 121: 4019–4029.
- 95 Orozco-Valencia, U., Gázquez, J.L., and Vela, A. (2017). Donation and back-donation analyzed through a charge transfer model based on density functional theory. *J. Mol. Model.* 23: 207.

- 96 Orozco-Valencia, U., Gázquez, J.L., and Vela, A. (2018). Role of reaction conditions in the global and local two parabolas charge transfer model. *J. Phys. Chem. A* 122: 1796–1806.
- 97 Orozco-Valencia, U., Gázquez, J.L., and Vela, A. (2018). Reactivity of indoles through the eyes of a charge-transfer partitioning analysis. *Acta Phys. - Chim. Sin.* 34: 692–698.
- 98 Parr, R.G. and Yang, W.T. (1989). *Density-Functional Theory of Atoms and Molecules*. New York: Oxford University Press.
- 99 Parr, R.G. and Yang, W.T. (1995). Density-Functional theory of the electronic-structure of molecules. *Annu. Rev. Phys. Chem.* 46: 701–728.
- 100 Chermette, H. (1999). Chemical reactivity indexes in density functional theory. *J. Comput. Chem.* 20: 129–154.
- 101 Geerlings, P., De Proft, F., and Langenaeker, W. (2003). Conceptual density functional theory. *Chem. Rev.* 103: 1793–1873.
- 102 Ayers, P.W., Anderson, J.S.M., and Bartolotti, L.J. (2005). Perturbative perspectives on the chemical reaction prediction problem. *Int. J. Quantum Chem.* 101: 520–534.
- 103 Gázquez, J.L. (2008). Perspectives on the density functional theory of chemical reactivity. *J. Mex. Chem. Soc.* 52: 3–10.
- 104 Chattaraj, P.K. (ed.) (2009). *Chemical Reactivity Theory: A Density Functional View*. Boca Raton, FL: CRC Press.
- 105 Liu, S.B. (2009). Conceptual density functional theory and some recent developments. *Acta Phys. - Chim. Sin.* 25: 590–600.
- 106 Johnson, P.A., Bartolotti, L., Ayers, P.W. et al. (2012). Charge density and chemical reactions: a unified view from conceptual DFT. In: *Modern Charge-Density Analysis* (ed. C. Gatti and P. Macchi), 715–764. Dordrecht: Springer.
- 107 Fuentealba, P. and Cardenas, C. (2015). Density functional theory of chemical reactivity. In: *Chemical Modelling: A Specialist Periodical Report*, vol. 11 (ed. J.O. Joswig and M. Springborg), 151–174. Cambridge: The Royal Society of Chemistry.
- 108 Geerlings, P., Chamorro, E., Chattaraj, P.K. et al. (2020). Conceptual density functional theory: status, prospects, issues. *Theor. Chem. Accounts* 139: 36.
- 109 Mermin, N.D. (1965). Thermal properties of inhomogeneous electron gas. *Phys. Rev.* 137: 1441–1443.
- 110 Kohn, W. and Vashishta, P. (1983). General density functional theory. In: *Theory of the Inhomogeneous Electron Gas* (ed. N.H. March), 124. New York: Plenum.
- 111 Eschrig, H. (2010).  $T > 0$  ensemble-state density functional theory via Legendre transform. *Phys. Rev. B* 82: 205120.
- 112 Gyftopoulos, E.P. and Hatsopoulos, G.N. (1968). Quantum-thermodynamic definition of electronegativity. *Proc. Natl. Acad. Sci. U. S. A.* 60: 786–793.
- 113 Sebastian, K.L. (1994). On the proof of the principle of maximum hardness. *Chem. Phys. Lett.* 231: 40–42.
- 114 Baekelandt, B.G., Cedillo, A., and Parr, R.G. (1995). Reactivity indexes and fluctuation formulas in density-functional theory - isomorphic ensembles and a new measure of local hardness. *J. Chem. Phys.* 103: 8548–8556.

- 115 Chattaraj, P.K., Cedillo, A., and Parr, R.G. (1996). Chemical softness in model electronic systems: dependence on temperature and chemical potential. *Chem. Phys.* 204: 429–437.
- 116 Malek, A. and Balawender, R. (2015). Revisiting the chemical reactivity indices as the state function derivatives. The role of classical chemical hardness. *J. Chem. Phys.* 142: 054104.
- 117 Miranda-Quintana, R.A. and Ayers, P.W. (2016). Interpolation of property-values between electron numbers is inconsistent with ensemble averaging. *J. Chem. Phys.* 144: 244112.
- 118 Miranda-Quintana, R.A. and Ayers, P.W. (2016). Fractional electron number, temperature, and perturbations in chemical reactions. *Phys. Chem. Chem. Phys.* 18: 15070–15080.
- 119 Miranda-Quintana, R.A. (2017). Thermodynamic electrophilicity. *J. Chem. Phys.* 146: 214113.
- 120 Miranda-Quintana, R.A., Chattaraj, P.K., and Ayers, P.W. (2017). Finite temperature grand canonical ensemble study of the minimum electrophilicity principle. *J. Chem. Phys.* 147: 124103.
- 121 Miranda-Quintana, R.A., Kim, T.D., Cárdenas, C., and Ayers, P.W. (2017). The HSAB principle from a finite-temperature grand-canonical perspective. *Theor. Chem. Accounts* 136: 135.
- 122 Franco-Pérez, M., Ayers, P.W., Gázquez, J.L., and Vela, A. (2015). Local and linear chemical reactivity response functions at finite temperature in density functional theory. *J. Chem. Phys.* 143: 244117.
- 123 Franco-Pérez, M., Gázquez, J.L., Ayers, P.W., and Vela, A. (2015). Revisiting the definition of the electronic chemical potential, chemical hardness, and softness at finite temperatures. *J. Chem. Phys.* 143: 154103.
- 124 Franco-Pérez, M., Gázquez, J.L., and Vela, A. (2015). Electronic chemical response indexes at finite temperature in the canonical ensemble. *J. Chem. Phys.* 143: 024112.
- 125 Franco-Pérez, M., Ayers, P.W., and Gázquez, J.L. (2016). Average electronic energy is the central quantity in conceptual chemical reactivity theory. *Theor. Chem. Accounts* 135: 199.
- 126 Franco-Pérez, M., Ayers, P.W., Gázquez, J.L., and Vela, A. (2017). Thermodynamic responses of electronic systems. *J. Chem. Phys.* 147: 094105.
- 127 Franco-Pérez, M., Ayers, P.W., Gázquez, J.L., and Vela, A. (2017). Local chemical potential, local hardness, and dual descriptors in temperature dependent chemical reactivity theory. *Phys. Chem. Chem. Phys.* 19: 13687–13695.
- 128 Franco-Pérez, M., Gázquez, J.L., Ayers, P.W., and Vela, A. (2017). Thermodynamic hardness and the maximum hardness principle. *J. Chem. Phys.* 147: 074113.
- 129 Franco-Pérez, M., Heidar-Zadeh, F., Ayers, P.W. et al. (2017). Going beyond the three-state ensemble model: the electronic chemical potential and Fukui function for the general case. *Phys. Chem. Chem. Phys.* 19: 11588–11602.

- 130** Franco-Pérez, M., Polanco-Ramirez, C.A., Ayers, P.W. et al. (2017). New Fukui, dual and hyper-dual kernels as bond reactivity descriptors. *Phys. Chem. Chem. Phys.* 19: 16095–16104.
- 131** Franco-Pérez, M., Gázquez, J.L., Ayers, P.W., and Vela, A. (2018). Thermodynamic justification for the parabolic model for reactivity indicators with respect to electron number and a rigorous definition for the electrophilicity: the essential role played by the electronic entropy. *J. Chem. Theory Comput.* 14: 597–606.
- 132** Franco-Pérez, M., Gázquez, J.L., Ayers, P.W., and Vela, A. (2018). Thermodynamic dual descriptor. *Acta Phys. - Chim. Sin.* 34: 683–691.
- 133** Gázquez, J.L., Franco-Pérez, M., Ayers, P.W., and Vela, A. (2019). Temperature-dependent approach to chemical reactivity concepts in density functional theory. *Int. J. Quantum Chem.* 119: e25797.
- 134** Franco-Pérez, M., Polanco-Ramirez, C.A., Gázquez, J.L. et al. (2020). Study of organic reactions using chemical reactivity descriptors derived through a temperature-dependent approach. *Theor. Chem. Accounts* 139: 44.
- 135** Perdew, J.P., Parr, R.G., Levy, M., and Balduz, J.L. (1982). Density-functional theory for fractional particle number - derivative discontinuities of the energy. *Phys. Rev. Lett.* 49: 1691–1694.
- 136** Yang, W.T., Zhang, Y.K., and Ayers, P.W. (2000). Degenerate ground states and a fractional number of electrons in density and reduced density matrix functional theory. *Phys. Rev. Lett.* 84: 5172–5175.
- 137** Ayers, P.W. (2008). The dependence on and continuity of the energy and other molecular properties with respect to the number of electrons. *J. Math. Chem.* 43: 285–303.
- 138** Nalewajski, R.F. and Parr, R.G. (1982). Legendre transforms and Maxwell relations in density functional theory. *J. Chem. Phys.* 77: 399–407.
- 139** Sjöberg, P., Murray, J.S., Brinck, T., and Politzer, P. (1990). Average local ionization energies on the molecular surfaces of aromatic systems as guides to chemical reactivity. *Can. J. Chem.* 68: 1440–1443.
- 140** Murray, J.S. and Politzer, P. (1998). Average local ionization energies: significance and applications. In: *Theoretical Organic Chemistry* (ed. C. Parkanyi), 189–202. Amsterdam: Elsevier.
- 141** Murray, J.S., Peralta-Inga, Z., Politzer, P. et al. (2001). Computational characterization of nucleotide bases: molecular surface electrostatic potentials and local ionization energies, and local polarization energies. *Int. J. Quantum Chem.* 83: 245–254.
- 142** Politzer, P., Murray, J.S., and Concha, M.C. (2002). The complementary roles of molecular surface electrostatic potentials and average local ionization energies with respect to electrophilic processes. *Int. J. Quantum Chem.* 88: 19–27.
- 143** Toro-Labbé, A., Jaque, P., Murray, J.S., and Politzer, P. (2005). Connection between the average local ionization energy and the Fukui function. *Chem. Phys. Lett.* 407: 143–146.

- 144** Chamorro, E. and Duque-Norena, M. (2015). Understanding the highly varying  $pK(a)$  of arylamines. A perspective from the average local ionization condensed-to-atom framework. *J. Phys. Chem. A* 119: 8156–8162.
- 145** Clark, T. (2010). The local electron affinity for non-minimal basis sets. *J. Mol. Model.* 16: 1231–1238.
- 146** Brinck, T., Carlqvist, P., and Stenlid, J.H. (2016). Local electron attachment energy and its use for predicting nucleophilic reactions and halogen bonding. *J. Phys. Chem. A* 120: 10023–10032.
- 147** Stenlid, J.H. and Brinck, T. (2017). Nucleophilic aromatic substitution reactions described by the local electron attachment energy. *J. Org. Chem.* 82: 3072–3083.
- 148** Gázquez, J.L. (2009). Chemical reactivity concepts in density functional theory. In: *Chemical Reactivity Theory: A Density Functional View* (ed. P.K. Chattaraj), 7–22. Boca Raton, FL: CRC Press.

## 9

## Chemical Reactivity in Time-Dependent Situations

Utpal Sarkar<sup>1</sup> and Pratim Kumar Chattaraj<sup>2,3</sup>

<sup>1</sup>Assam University, Department of Physics, Silchar 788011, India

<sup>2</sup>Indian Institute of Technology, Department of Chemistry, Kharagpur 721302, India

<sup>3</sup>Indian Institute of Technology, Department of Chemistry, Bombay, Powai, Mumbai 400076, India

### 9.1 Introduction

Density functional theory (DFT) [1, 2] successfully describes the electronic structure of many-electron systems and the related chemical concepts like chemical hardness [3–6], chemical potential [7], electronegativity [7], and polarizability are defined within conceptual DFT [8, 9]. The foundation of DFT has been based on the two well-known theorems given by Hohenberg and Kohn [1, 2], which mainly revolve around the density of ground state of the system. According to the theorems, all the ground-state properties of that particular system may be calculated using the density.

For an  $N$ -electronic system, associated with an external potential,  $v(\mathbf{r})$ , the Hamiltonian  $H$  may be identified by the two quantities,  $N$  and  $v(\mathbf{r})$ . In addition, as proven by Hohenberg and Kohn, the energy functional  $E[\rho]$  assumes a minimum for the true  $N$ -electron density for a given  $N$  and  $v(\mathbf{r})$ . By solving the following Euler–Lagrange equation, one can obtain the density,

$$\frac{\delta E[\rho]}{\delta \rho} = \mu \quad (9.1)$$

where  $\mu$  is the Lagrange multiplier associated with the normalization constraint. It is known as the chemical potential [10].

The energy functional  $E[\rho]$  may be given by [11],

$$E[\rho(\mathbf{r})] = F[\rho(\mathbf{r})] + \int \rho(\mathbf{r})v(\mathbf{r})d\mathbf{r} \quad (9.2)$$

where  $F[\rho(\vec{r})]$  is known as the Hohenberg–Kohn universal functional [12], given as

$$F[\rho(\vec{r})] = T[\rho(\vec{r})] + \frac{1}{2} \iint \frac{\rho(\vec{r})\rho(\vec{r}')}{|\vec{r} - \vec{r}'|} d\vec{r}d\vec{r}' + E_{\text{XC}}[\rho(\vec{r})] \quad (9.3)$$

In the above equation, the first term  $T[\rho(\vec{r})]$  corresponds to kinetic energy functional, the second term is the classical Coulomb part of the electron–electron interaction energy, and the third term  $E_{\text{XC}}[\rho(\vec{r})]$  is known as the exchange–correlation functional.



Chemical reactivity of any system can be understood by identifying  $\mu$  as the negative of electronegativity ( $\chi$ ) [5]. The stability of a molecular system may be assessed with the help of the reactivity parameters like hardness and electrophilicity [3–6, 13, 14] through the related electronic structure principles such as Pearson's hard and soft acids and bases (HSAB) principle [15–18], maximum hardness principle (MHP) [19, 20], Sanderson's electronegativity equalization principle [21, 22], minimum electrophilicity principle (MEP) [23–25], and minimum polarizability principle (MPP) [26, 27]. These principles play a major role in explaining the change in reactivity parameters, which a system undergoes during a chemical reaction [28–38].

Chemical hardness ( $\eta$ ) may be obtained by differentiating energy ( $E$ ) twice with respect to number of electrons ( $N$ ) keeping the external potential fixed as given by Parr and Pearson [5]:

$$\eta = \left( \frac{\partial^2 E}{\partial N^2} \right)_{v(\vec{r})} = \left( \frac{\partial \mu}{\partial N} \right)_{v(\vec{r})} \quad (9.4)$$

According to Koopmans' theorem [39], the energy difference (energy gap) in between the two frontier molecular orbitals, i.e. highest occupied molecular orbital (HOMO) and lowest unoccupied molecular orbital (LUMO), of any system may also be termed as chemical hardness.

Electrophilicity index, defined by Parr and coworkers, gives an indication about the stabilization energy of the corresponding system when extra amount of charge is loaded to it from the surrounding as [13, 14, 40–46],

$$\omega = \frac{\mu^2}{2\eta} \quad (9.5)$$

Inverse of global hardness is known as global softness, given by [47]:

$$S = \frac{1}{\eta} \quad (9.6)$$

Polarizability ( $\alpha$ ) of a system can be mathematically represented as the second-order variation of energy, which is defined as the linear response of the electron density when the particular system is subjected to an infinitesimally small electric field  $\mathbf{F}$  [48]:

$$\alpha_{a,b} = - \left( \frac{\partial^2 E}{\partial F_a \partial F_b} \right)_{a,b=x,y,z} \quad (9.7)$$

Again global softness is related to polarizability, i.e. with an increase in polarizability, a system becomes softer and vice versa.

Another parameter given by the name Fukui function (FF) is a local reactivity descriptor, which is used for getting knowledge on the chemical reactivity and site selectivity of any atom in a molecule [30, 49–54]:

$$f(\vec{r}) = \left[ \frac{\partial \rho(\vec{r})}{\partial N} \right]_{v(\vec{r})} = \left[ \frac{\delta \mu}{\delta v(\vec{r})} \right]_N \quad (9.8)$$

where,

$$\int f(\vec{r}) d\vec{r} = 1 \quad (9.9)$$

FFs can be of three types (nucleophilic, electrophilic, and radical) and with the help of frozen core and finite difference approximations, these may be represented as [55–57]:

For nucleophilic attack,

$$f^+(\vec{r}) = \left( \frac{\partial \rho}{\partial N} \right)_{v(\vec{r})}^+ \cong \rho_{N+1}(\vec{r}) - \rho_N(\vec{r}) \approx \rho_{\text{LUMO}}(\vec{r}) \quad (9.10)$$

For electrophilic attack,

$$f^-(\vec{r}) = \left( \frac{\partial \rho}{\partial N} \right)_{v(\vec{r})}^- \cong \rho_N(\vec{r}) - \rho_{N-1}(\vec{r}) \approx \rho_{\text{HOMO}}(\vec{r}) \quad (9.11)$$

For radical attack,

$$f^0(\vec{r}) = \left( \frac{\partial \rho}{\partial N} \right)_{v(\vec{r})}^0 \cong \frac{1}{2}(\rho_{N+1}(\vec{r}) - \rho_{N-1}(\vec{r})) \approx \frac{1}{2}(\rho_{\text{HOMO}}(\vec{r}) + \rho_{\text{LUMO}}(\vec{r})) \quad (9.12)$$

Also more the magnitude of  $f^+$ ,  $f^0$ , and  $f^-$  at any site, more will be the change in chemical potential.

One may also define a local philicity index  $\omega(\vec{r})$ , which is again divided into three different types and may be given as [44]:

$$\omega^\alpha(\vec{r}) = \omega f^\alpha(\vec{r}) \quad (9.13)$$

The superscript  $\alpha = +, -, 0$  implies electrophilic, nucleophilic, and radical attacks, respectively. Information of FF and electrophilicity is contained in this parameter. In addition, knowledge about other chemical reactivity parameters such as electronegativity, hardness, and local and global softness along with site selectivity can be realized using the local philicity index.

A time-dependent version of DFT, i.e. time-dependent density functional theory (TDDFT), gained attention of the researchers [58–61] worldwide to take care of dynamical problems. Reactivity dynamics has also been investigated using Born-Oppenheimer Molecular Dynamics (BOMD) method [62–66]. This TDDFT and quantum fluid dynamics (QFD) together resulted in a new theory, known as quantum fluid density functional theory (QFDFT), which is generally based on the solution of a generalized nonlinear Schrödinger equation (GNLSE) [67].

## 9.2 Theoretical Background

With the help of the following density functional, one may realize a time-dependent energy functional as:

$$E(t) = \frac{1}{2} \int \rho(\mathbf{r}, t) |\nabla \xi|^2 d\mathbf{r} + T[\rho] + E_{xc}[\rho] + \int v_{\text{core}}(\mathbf{r}) \rho(\mathbf{r}, t) d\mathbf{r} \\ + \frac{1}{2} \iint \frac{\rho(\mathbf{r}, t) \rho(\mathbf{r}', t)}{|\mathbf{r} - \mathbf{r}'|} d\mathbf{r} d\mathbf{r}' + \int v_{\text{ext}}(\mathbf{r}) \rho(\mathbf{r}, t) d\mathbf{r} \quad (9.14)$$

Here, for hydrogen atom,  $v_{\text{core}}(\mathbf{r}) = v1_{\text{core}}(\mathbf{r})$ , whereas, for that of helium atom,  $v_{\text{core}}(\mathbf{r}) = v2_{\text{core}}(\mathbf{r})$  for all the states.

For a dynamic system, QFDFT is used to get information about the time evolution of charge density  $\rho(\mathbf{r}, t)$  and current density  $\mathbf{j}(\mathbf{r}, t)$ . The dynamics of a helium atom in its ground state can be obtained by solving the following GNLSSE (in a.u.):

$$\left[ -\frac{1}{2}\nabla^2 + v_{\text{eff}}(\vec{r}, t) \right] \varphi(\vec{r}, t) = i\frac{\partial\varphi(\vec{r}, t)}{\partial t}, \quad i = \sqrt{-1} \quad (9.15)$$

where,

$$v_{\text{eff}} = \frac{5}{3}C_k\rho^{2/3} - \frac{4}{3}C_x\rho^{1/3} - \frac{\alpha(N)}{\mathbf{r}^2} - \frac{Q(\vec{r})}{\mathbf{r}} - \frac{1}{|\mathbf{R} - \vec{r}|} + \frac{f(\mathbf{R}, N)}{N} \quad (9.16)$$

Here,

$$\rho(\vec{r}, t) = |\varphi(\vec{r}, t)|^2 \quad (9.17)$$

$$Q(\vec{r}, t) = Z - r \int \frac{\rho(\vec{r}', t)}{|\vec{r} - \vec{r}'|} d\mathbf{r}' \quad (9.18)$$

$$\alpha(N) = \alpha_0 + \frac{\alpha_1}{N^{1/3}} + \frac{\alpha_2}{N^{2/3}} \quad \text{and} \quad f(\mathbf{R}, N) = \frac{1}{R^{12}} - \left(\frac{N}{10}\right)^{14} R^2 \exp(-0.8R) \quad (9.19)$$

Here  $v_{\text{eff}}(\vec{r}, t)$  is a pulsating dynamical external potential associated with the actual process and  $Q(\vec{r}, t)$  is screened nuclear charge.

The QFDFT approach stands on Eqs. (9.14)–(9.16). It is to be noted that for the first time, Deb and coworker have provided solution to these equations considering both time-dependent as well as time-independent cases [68].

The dynamic current density on the other hand is represented by,

$$\vec{j}(\vec{r}, t) = \varphi_{\text{re}}\nabla\varphi_{\text{im}} - \varphi_{\text{im}}\nabla\varphi_{\text{re}} \quad (9.20)$$

Herein follows some specific examples of dynamical problems analyzed through the time evolution of various reactivity descriptors using QFDFT and the dynamical variants of different associated electronic structure principles.

### 9.3 An Atom Interacting with an External Electric Field

Time-dependent reactivity parameters of helium atom when exposed to electric field strengths of  $\epsilon_0 = 10^{-6}$ , 0.01 and 100 have been studied in both ground state ( $n = 1$ ) and excited state ( $n > 1$ ) of the atom. It is observed that the hardness and electronegativity in ground state are higher than the corresponding values in excited states, which proves the validity of MHP. The system also follows maximum entropy principle with a larger value of entropy in ground state in comparison to that in the excited state. The MPP is also followed by the helium atom since it is less polarizable in ground state as compared to excited state.

Chemical potential of the system is always more in excited state over the ground state and it shows characteristic oscillations (Figure 9.1). The oscillations are found to be in sync with the applied field. One may find that for low field intensity, oscillations are out of phase with the field, but with increasing intensity, beautiful in-phase

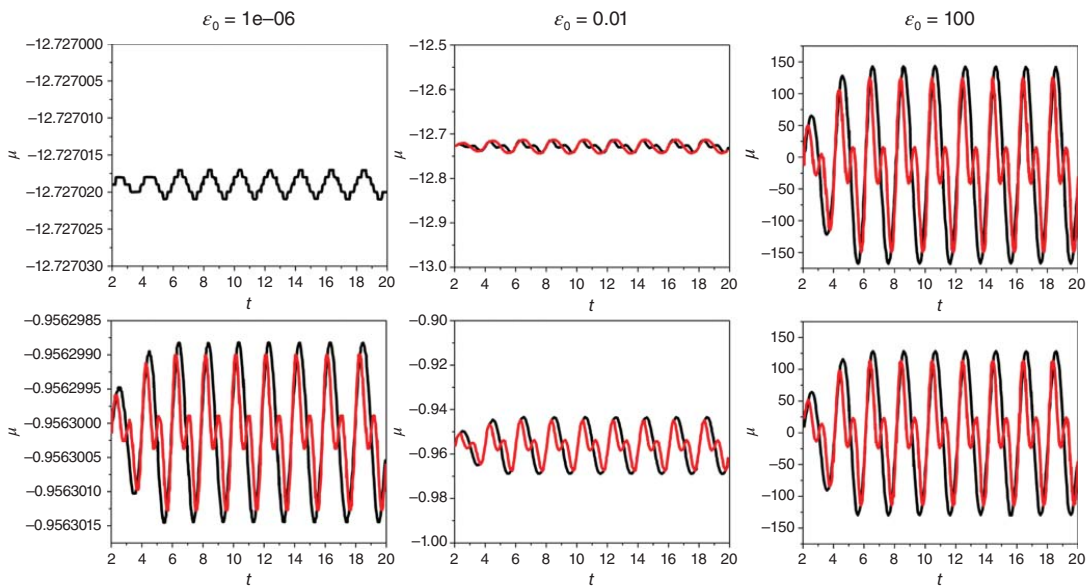


**Figure 9.1** Dynamic profile of chemical potential ( $\mu$ ) when a helium atom is subjected to external electric fields. Top row represents excited state and bottom row represents ground state. Black and red colors represent monochromatic and bichromatic pulse, respectively. Source: Chattaraj et al. [69].

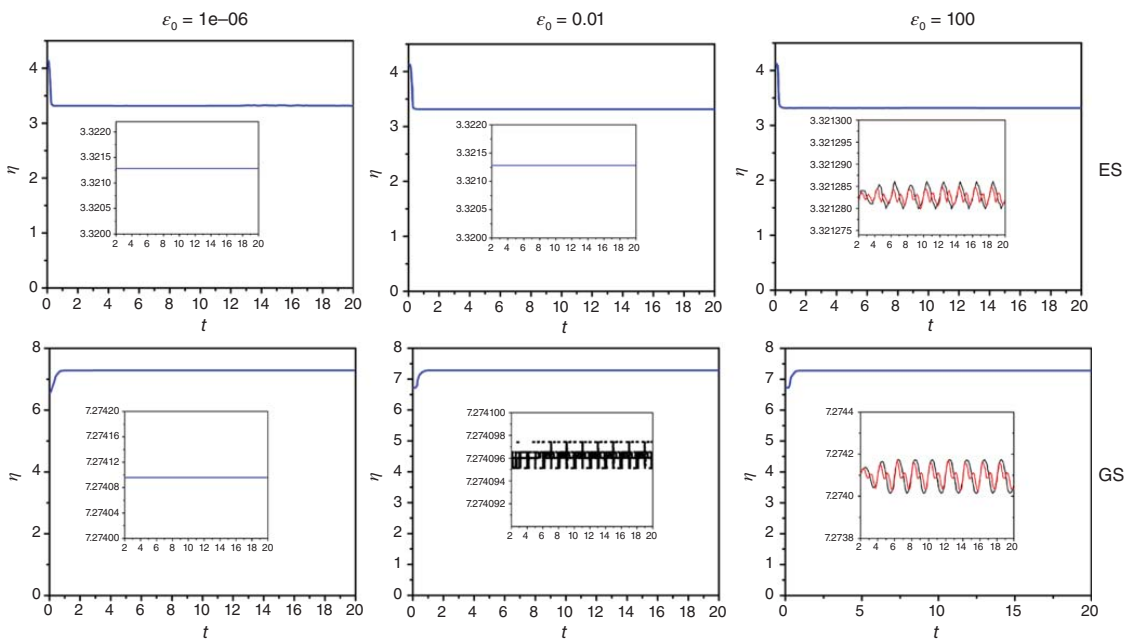


**Figure 9.2** Dynamic profile of chemical hardness ( $\eta$ ) when a helium atom is subjected to external electric fields. Black and red colors represent monochromatic and bichromatic pulse, respectively. Source: Chattaraj et al. [69].

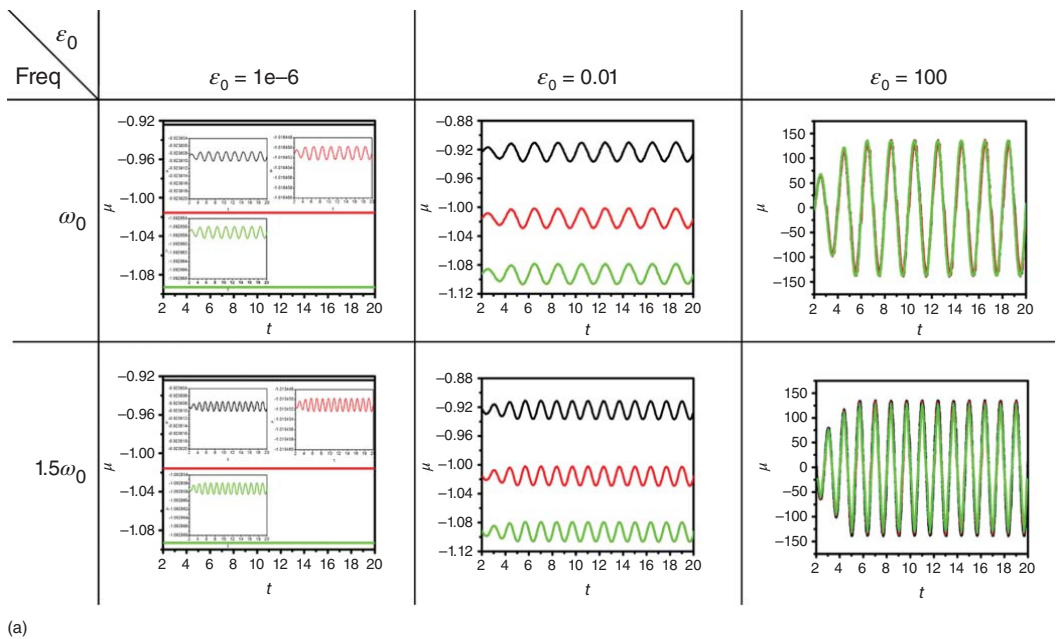
oscillations can be seen for all the studied electronic states. The chemical hardness achieves an almost consistent value just after the completion of the initial transients, but the ground-state value of hardness is larger than the excited-state value of hardness (Figure 9.2), which follows from the MHP [69].

## 9.4 An Atom Interacting with an External Electric Field in a Confined Environment

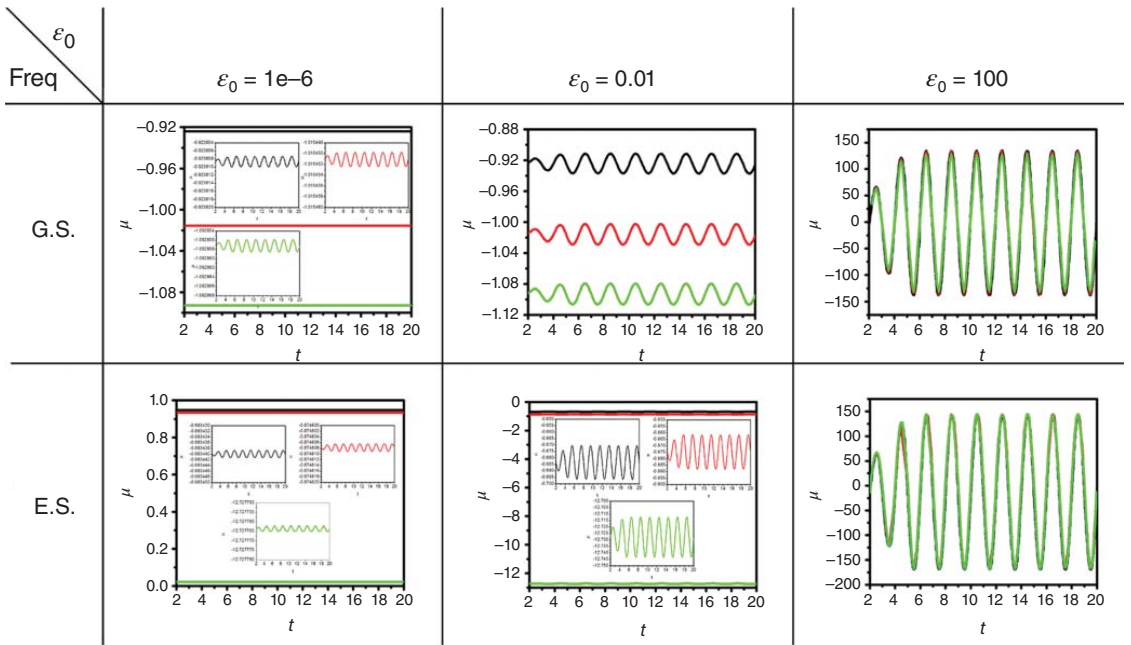
The reactivity parameters for the same system when exposed to an external electric field in the presence of confinement exhibit remarkable changes. The frequency of the applied field is taken as  $\Pi$ . The time-evolved hardness decreases as soon as the system changes from its ground state to excited state, in confined condition, which validates the MHP. On increasing the degree of compression, hardness is found to increase for all electronic states. The other reactivity descriptors like polarizability, chemical potential, electrophilicity and entropy in dynamic state are also studied by varying the laser radiation under confinement. The chemical potential of the system shows negligible change for the most intense laser field, but its magnitude lowers in ground state and rises in excited state when low and intermediate field strengths are applied (Figure 9.3). Time-dependent electrophilicity follows the chemical potential trend in low and intermediate field strengths, while it relates to that of hardness (Figure 9.4) with the higher electric field strength. Similar to ground state, dynamic polarizability follows same trend in excited state in both confined as well as unconfined situations; however, the ground-state value is lower than the excited-state one, validating the MPP. Under confinement, decrease in the ground-state value of entropy is observed (as compared to unconfined state) [70].

## 9.5 A Molecule Interacting with an External Electric Field in a Confined Environment

Changes in the time-evolved chemical reactivity parameters of hydrogen molecule subjected to an intense laser radiation in ground and excited states are analyzed. Chemical potential for the system in its ground state is lower than its corresponding excited state (Figure 9.5), in case of free state of the system. But chemical potential in the ground state decreases when the extent of confinement increases, although in the excited state it remains unchanged. Amplitude of ground-state chemical potential increases with a rise in the degree of confinement, while the excited-state value remains unchanged. According to MEP, the electrophilicity value for the free system in ground state is not as much as that of the excited state. With an increase in the extent of confinement, electrophilicity profile of the system shows a decrease in both the electronic states. The  $\eta$  value is greater in ground state than excited state (Figure 9.6) when no confinement is present for the system, validating the MHP. Confinement, however, increases the highest  $\eta$  value in both the electronic states.



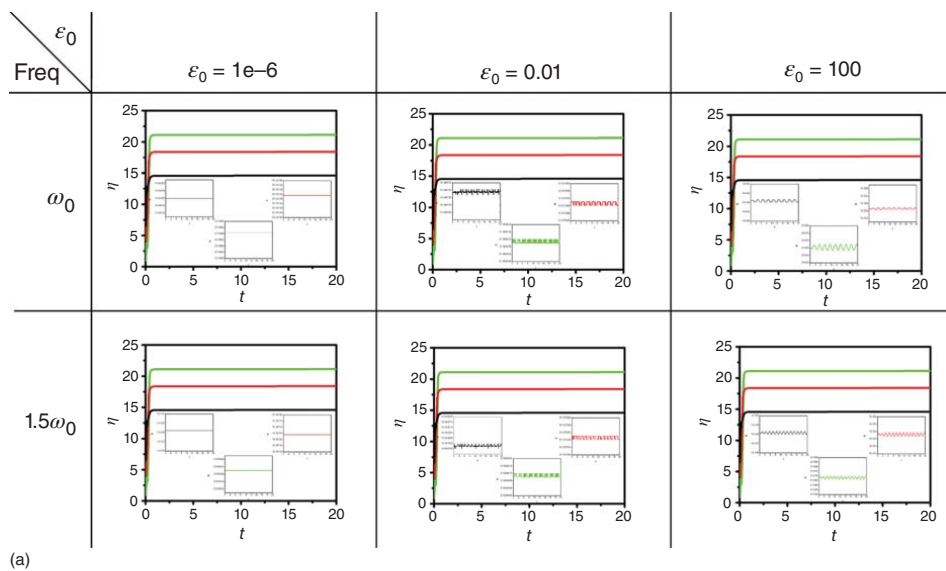
**Figure 9.3** (a) Ground-state dynamic chemical potential ( $\mu$ ) profile of helium atom under different field strength. Red and green lines represent confined system with cylinder length 4.8 and 4.2 a.u., respectively. Black line represents unconfined system with cylinder length 6 a.u., respectively. (b) Ground- and excited-state dynamic chemical potential ( $\mu$ ) profile of helium atom under different field strength. Red and green lines represent confined system with cylinder length 6.6 and 5.8 a.u., respectively. Black line represents unconfined system with cylinder length 7.2 a.u., respectively. Source: Sarkar et al. [70].



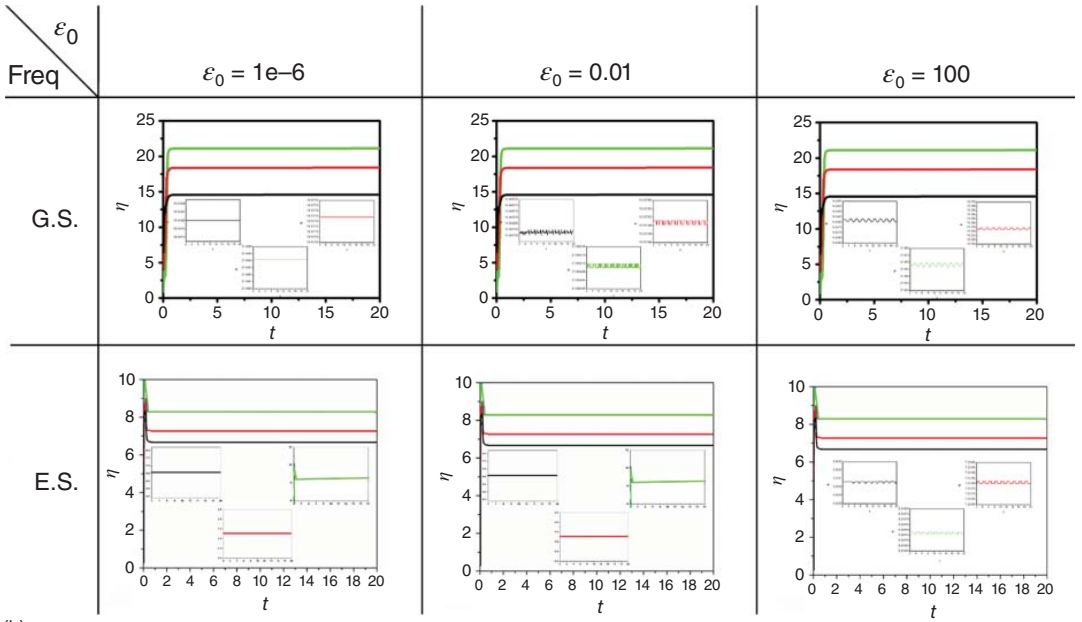
(b)

Figure 9.3 (Continued)





**Figure 9.4** (a) Ground-state dynamic chemical hardness ( $\eta$ ) profile of helium atom under different laser field, (b) Ground-state and excited-state dynamic chemical hardness ( $\eta$ ) profile of helium atom. Source: Sarkar et al. [70].



(b)

Figure 9.4 (Continued)

### Ground state

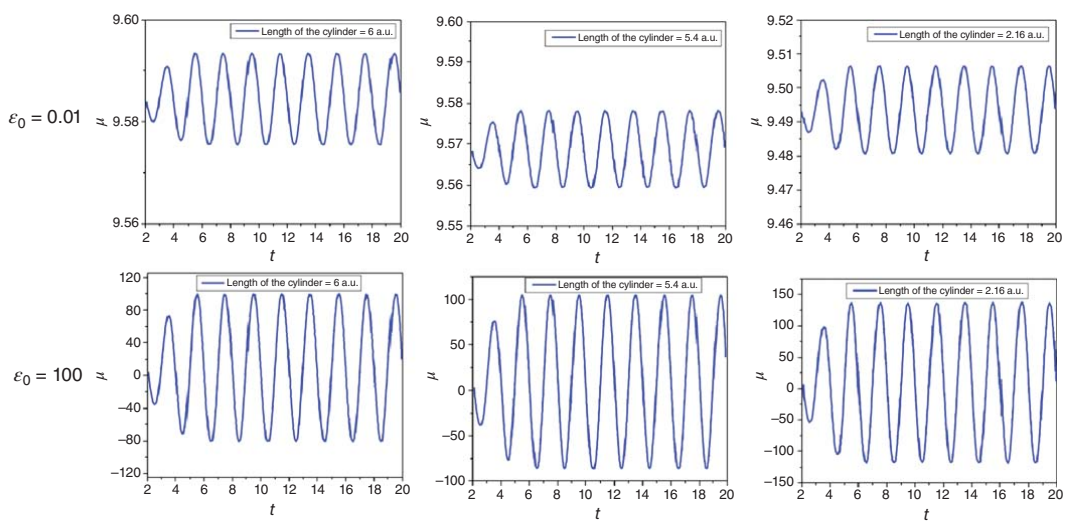


**Figure 9.5** Ground- and first excited-state dynamic chemical potential ( $\mu$ ) profile of  $H_2$  molecule under different field strength. Source: Khatua et al. [71].

Excited state

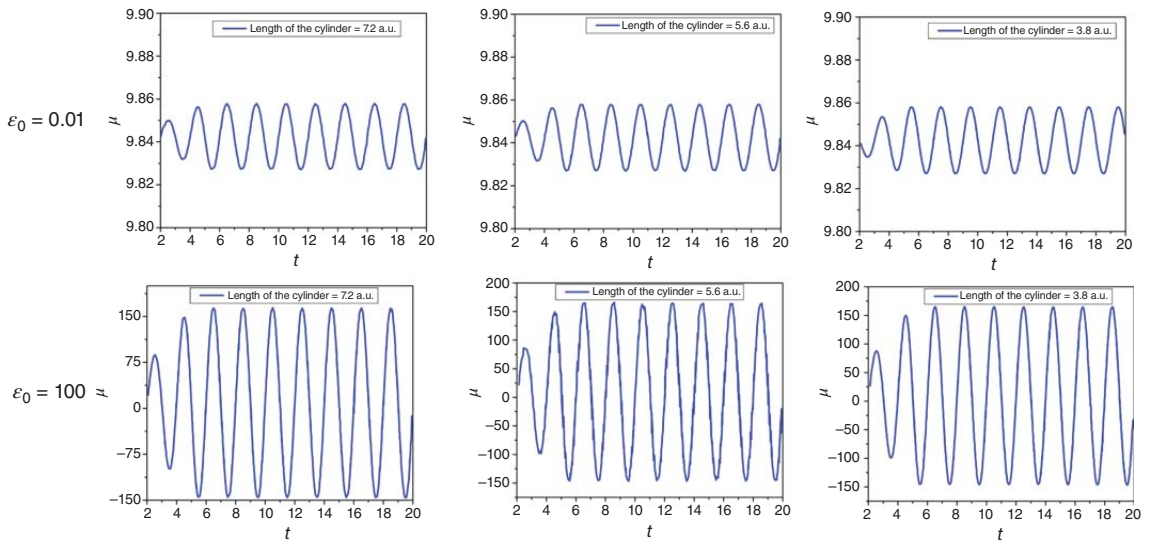
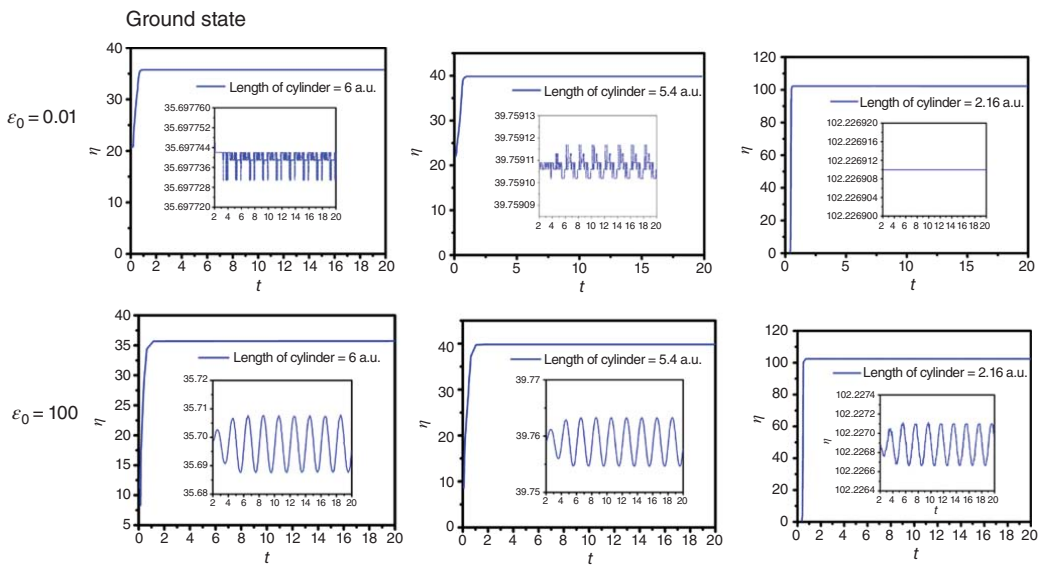


Figure 9.5 (Continued)



**Figure 9.6** Ground- and first excited-state dynamic chemical hardness ( $\eta$ ) profile of  $H_2$  molecule under different field strength. Source: Khatua et al. [71].

Excited state

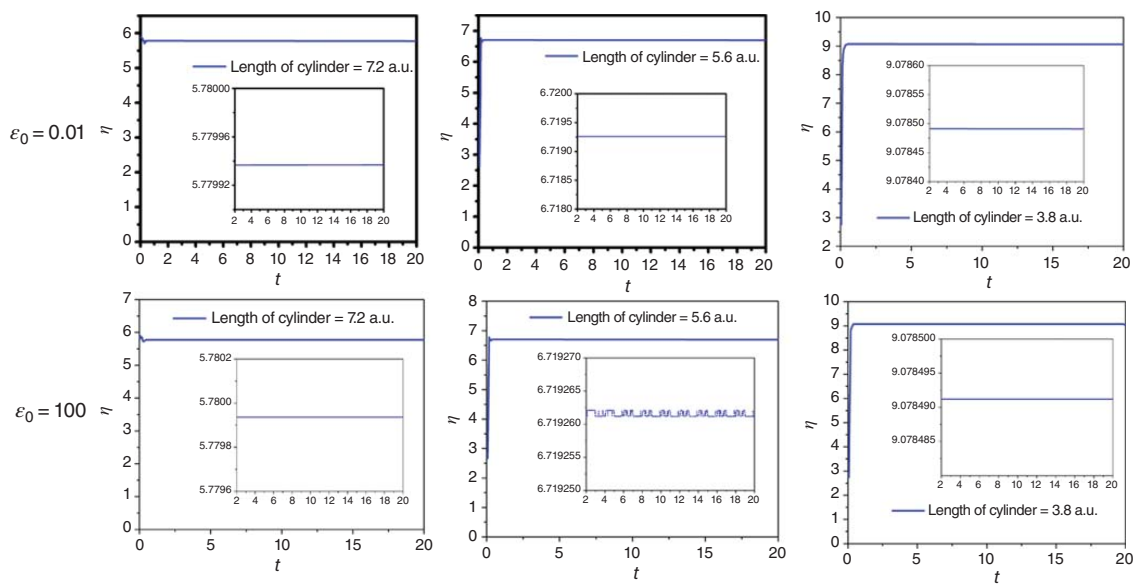


Figure 9.6 (Continued)

On the other hand, for unconfined system, the minimum value of  $\alpha$  is lower in the ground state in comparison to the excited state as expected from MPP. We may find that both in ground and excited states, the minimum polarizability value decreases, with increasing the amount of confinement [71].

## 9.6 An Atom Interacting with an External Magnetic Field in a Confined Environment

Next we present here the dynamic changes observed in chemical reactivity parameters when a hydrogen atom is placed in a magnetic field within confinement. Chemical potential profile for the system resonates with the magnetic field and when the compression on the system increases, it gets lowered for ground and excited states. The amplitude of  $\mu$  rises with the rise in the amplitude of the magnetic field. Amplitude of chemical potential increases when there is an increase in the strength of the applied field. While studying the  $\eta$  profile of the system, it is observed that its magnitude increases with the increase in the magnetic field strength, which infers that the system becomes further stabilized in stronger magnetic field. Under confinement, the  $\eta$  value in ground state is more than that in the excited state. This finding is true in case of unconfined condition as well, thus validating the MHP. Most importantly, it describes that in case of hydrogen atom there is a chance of chaotic ionization from its Rydberg state. Just like the chemical potential, electrophilicity index also oscillates in phase with the magnetic field. The excited-state electrophilicity of the system is greater than its corresponding ground-state value and with an increase in the degree of confinement, electrophilicity profile shows a decrease in its magnitude, which again implies the stability of the system by obeying the MEP [34].

## 9.7 A Molecule Interacting with an External Magnetic Field in a Confined Environment

The time-dependent chemical reactivity parameters when a hydrogen molecule subjected to magnetic field of amplitudes,  $\beta_{\max} = 0.001, 1.0, \text{ and } 50.0$  have been studied. The ground-state chemical potential of the system shows a decrease when the degree of confinement increases for lower field strength. But no such effect can be seen either for intermediate or high field since confinement does not play any significant role in these regions. The amplitude of ground-state chemical potential, however, increases with the rise in the external field strength (Figure 9.7). The excited-state chemical potential is insensitive toward confinement effect. The chemical hardness of the system does not vary with the field strength significantly in both ground and excited states. But in stronger electric field regions, change in hardness profile can be found in ground state only. One may find that the system becomes harder upon confinement, which may be based on the finding that both ground- and excited-state hardnesses increase with increasing amount of compression. Here also as expected

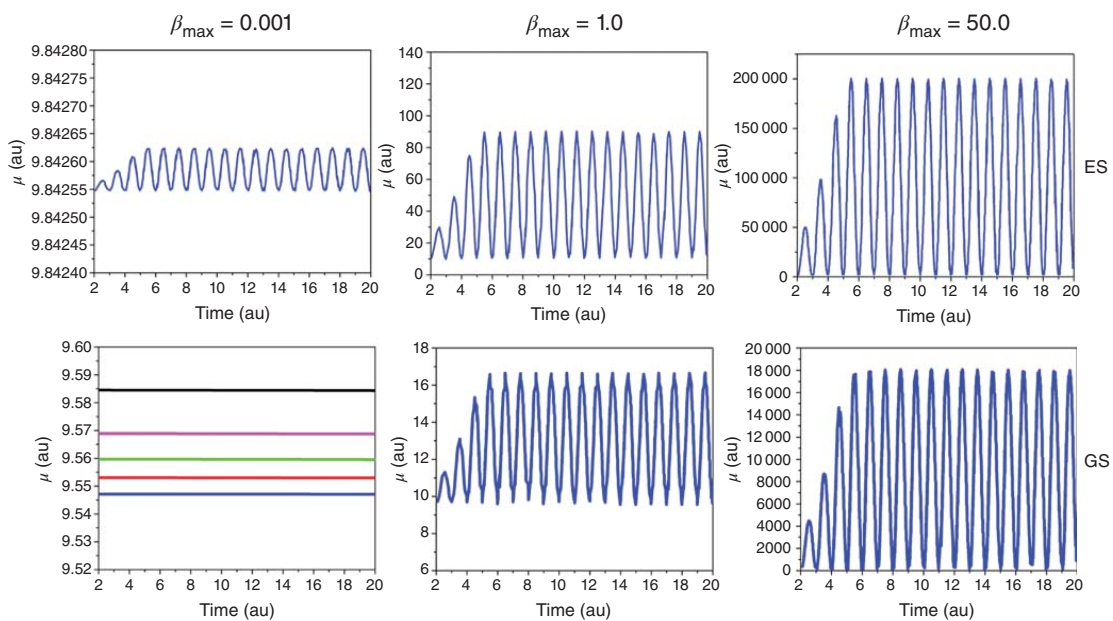


**Figure 9.7** Ground- and excited-state dynamic chemical potential ( $\mu$ ) profile of  $H_2$  molecule under different field strength. The different degrees of confinement are denoted by different colors. The unconfined system is denoted by black line and the most confined system is denoted by blue line. Source: Khatua et al. [35].



from MHP, the  $\eta$  value of excited state is less as compared to the ground-state value irrespective of confinement or in free state. When the molecule is not in confined condition, the ground-state electrophilicity is lower compared to excited-state one. However, electrophilicity profile lowers down with an increase in the confinement degree for both the electronic states, making the system attain stability upon confinement [35].

## 9.8 Ion–Atom Collision

Here we present the changes in the reactivity parameters when collision process occurs between a helium atom and an incoming proton [72]. The time evolution of the chemical potential associated with the collision process is presented in Figure 9.8. The whole collision process is described by three distinct regions namely, approach region, encounter region, and departure region. The chemical potential is not calculable in encounter zone while in the approach region, once the initial transients get over, chemical potential becomes stable. But due to rapid charge oscillations, chemical potential changes drastically, when the departure region begins and also when the approach region ends. For the ground state,  $\mu$  is negative, but for the excited state, it becomes positive as well in these time steps. In the departure zone,  $\mu$  again shows drastic change to attain a stable value, which is almost similar to that found in the approach region. The detailed insights into the collision process associated with a chemical reaction are well described by the dynamics of electronegativity. The time-dependent electronegativity profile helps us to distinguish the whole interaction into approach, encounter, and departure regimes. Time-evolved hardness profile is presented in Figure 9.9. In the approach region, hardness remains almost constant. However, it increases all of a sudden and goes through a region of maximum in the encounter region. The larger value of maximum hardness in ground state and the maximization of hardness in the encounter region clearly validate the MHP dynamically. Again in the departure zone, hardness acquires the similar constant value as found in the approach region.

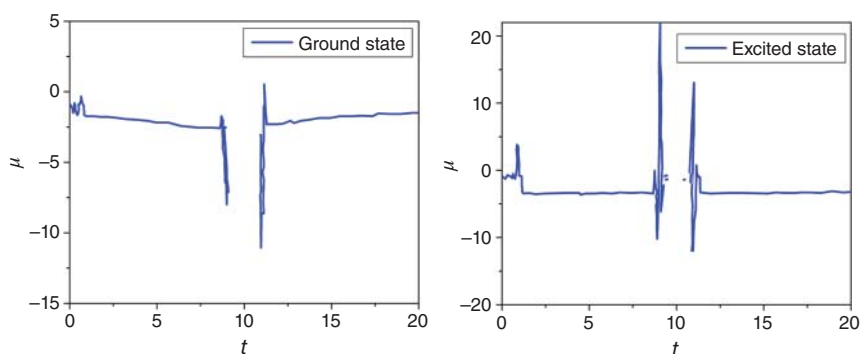


**Figure 9.8** Dynamic chemical potential ( $\mu$ ) profile during a collision process between a He atom and a proton. Source: Chattaraj et al. [72].

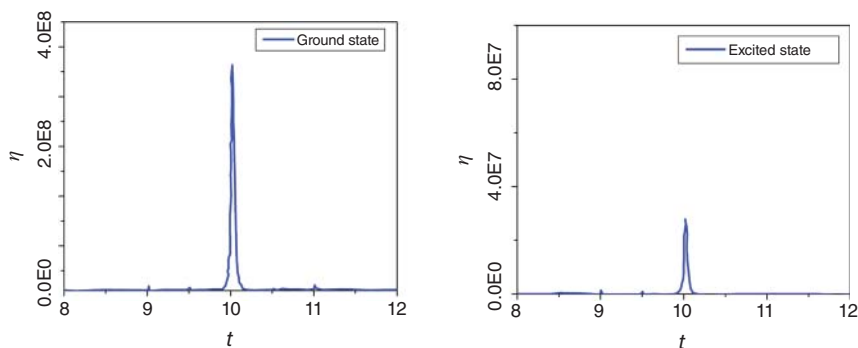


**Figure 9.9** Dynamic chemical hardness ( $\eta$ ) profile during a collision process between a He atom and a proton. Source: Chattaraj et al. [72].

The maximization of hardness and entropy and the minimization of polarizability in the encounter region for the collision process clarify that at least for a moment a  $\text{HeH}^+$  molecule is formed, which in course of time breaks into He and  $\text{H}^+$  due to the high kinetic energy of proton [72].

## 9.9 Ion-Molecule Collision

A collision process occurring between various atoms or molecules with that of an ion has been a subject of interest because of its importance in the field of nuclear physics as well as astrophysics. Dynamics of collision process starting from one-electron to many-electron systems have been investigated both theoretically and experimentally. Chemical reaction among two species may be described with the help of collision process, where the reactant species collide with one another to form the product species. To this end, ion-atom and ion-molecule reactions are studied widely by Chattaraj and group [73]. Ion-molecule reactions are important especially since they govern the chemistry of formation of molecule in dense interstellar clouds. Here we will discuss the time evolution of hardness and polarizability for collision happening between a proton and some homonuclear and heteronuclear diatomic molecules both in ground and excited states. To check the regioselectivity in a chemical reaction where multiple sites are involved, heteronuclear molecules are considered.

The densities of  $\text{N}_2$  and  $\text{F}_2$  molecules in their ground and excited electronic states are symmetric in all the electronic states. One may find that the densities at the two nuclei of the diatomic molecules are symmetric in all the electronic states. Density decreases at the nuclear sites, in the first excited state, while in the outer region it spreads out more radially for these molecules.

When these molecules are hit by a proton, hardness increases and polarizability decreases in the vicinity of the nuclei. They are found to be symmetric in ground and excited states of the studied  $\text{N}_2$  and  $\text{F}_2$  molecules. In the encounter region, due to speedy oscillations of charge (since electron density is being shared by both the nuclei),  $\eta$  becomes very large. Hardness exceptionally becomes greater when

the two nuclei come very close to each other because of the Coulomb singularity. The molecule in its first excited state is softer and consequently more polarizable, it shows lower magnitude of  $\eta_{\max}$  and higher magnitude of  $\alpha_{\min}$  on being compared to the corresponding ground-state values.

For the heteronuclear molecules, electron densities are localized in the vicinity of the nuclei of those two atoms forming the molecule (H, F atoms of HF, B, F atoms of BF, and C, O atoms of CO molecules). For the excited state, density is found to decrease at the nuclear sites, although it spreads more when one radially moves away from the nuclei. In ground as well as excited states, electron density of F nuclei in HF and BF, and O nuclei in CO are greater than H nuclei in HF, B nuclei in BF, and C nuclei in CO [70]. It has been shown that when collision process takes place under confined environment, the highest value of hardness increases and the lowest value of polarizability decreases when compared with unconfined system [70].

## 9.10 Conclusion

Time evolution of various chemical reactivity descriptors like chemical potential, chemical hardness, electrophilicity, and polarizability is tracked for the atom/molecule interaction with external electric/magnetic field and collision processes between atom/molecule and a proton in both ground and excited states. The whole study is done within the context of QFDFT. The dynamical variants of the associated electronic structure principles such as the MHP, MPP, and MEP have been found to be operative when the time evolution of different reactivity parameters involving in different processes is analyzed. In addition, confinement effects on these processes are also understood.

## Acknowledgments

Pratim Kumar Chattaraj would like to thank Professor Shubin Liu for the invitation. He also thanks DST, New Delhi, for the J. C. Bose National Fellowship and his students whose work is presented in this chapter. Utpal Sarkar would like to thank DST, New Delhi, India, for the SERB project (File No. EMR/2016/006764) for financial assistance.

## References

- 1 Hohenberg, P. and Kohn, W. (1964 November). Inhomogeneous electron gas. *Phys. Rev.* 136: B864.
- 2 Kohn, W. and Sham, L.J. (1965 Nov). Self-consistent equations including exchange and correlation effects. *Phys. Rev.* 140 (4A): A1133.
- 3 Pearson, R.G. (1963 Nov). Hard and soft acids and bases. *J. Am. Chem. Soc.* 85 (22): 3533–3539.

- 4 Pearson, R.G. (1997). *Chemical Hardness*, 198. New York: Wiley.
- 5 Parr, R.G. and Pearson, R.G. (1983 December). Absolute hardness: companion parameter to absolute electronegativity. *J. Am. Chem. Soc.* 105 (26): 7512–7516.
- 6 Miranda-Quintana, R.A., Franco-Pérez, M., Gázquez, J.L. et al. (2018 September). Chemical hardness: temperature dependent definitions and reactivity principles. *J. Chem. Phys.* 149 (12): 124110.
- 7 Parr, R.G., Donnelly, R.A., Levy, M., and Palke, W.E. (1978 August). Electronegativity: the density functional viewpoint. *J. Chem. Phys.* 68 (8): 3801–3807.
- 8 Chattaraj, P.K. and Sengupta, S. (1997 October). Dynamics of chemical reactivity indices for a many-electron system in its ground and excited states. *J. Phys. Chem. A* 101 (42): 7893–7900.
- 9 Chakraborty, D. and Chattaraj, P.K. (2021 March). Conceptual density functional theory based electronic structure principles. *Chem. Sci.* 12 (18): 6264–6279.
- 10 Sarkar, U. and Chattaraj, P.K. (2021 February). Reactivity dynamics. *J. Phys. Chem. A* 125 (10): 2051–2060.
- 11 Ghosh, S.K. and Deb, B.M. (1994). Improved local density approximation to the exchange and kinetic energy functionals for atomic systems. *J. Phys. B: At. Mol. Opt. Phys.* 27: 381–387.
- 12 Parr, R.G. and Yang, W. (1989). *Density Functional Theory of Atoms and Molecules*. Oxford, UK: Oxford University Press.
- 13 Parr, R.G., Szentpaly, L.V., and Liu, S. (1999 February). Electrophilicity index. *J. Am. Chem. Soc.* 121 (9): 1922–1924.
- 14 Chattaraj, P.K., Sarkar, U., and Roy, D.R. (2006 May). Electrophilicity index. *Chem. Rev.* 106 (6): 2065–2091.
- 15 Pearson, R.G. (1987 July). Recent advances in the concept of hard and soft acids and bases. *J. Chem. Edu.* 64 (7): 561–567.
- 16 Pearson, R.G. (1973). *Hard and Soft Acids and Bases*. Stroudsburg, PA: Dowden, Hutchinson and Ross.
- 17 Chattaraj, P.K., Lee, H., and Parr, R.G. (1991 February). HSAB principle. *J. Am. Chem. Soc.* 113 (5): 1855–1856.
- 18 Pearson, R.G. (1968 September). Hard and soft acids and bases, HSAB, part 1: fundamental principles. *J. Chem. Edu.* 45 (9): 581–587.
- 19 Parr, R.G. and Chattaraj, P.K. (1991 February). Principle of maximum hardness. *J. Am. Chem. Soc.* 113 (5): 1854–1855.
- 20 Franco-Pérez, M., Gázquez, J.L., Ayers, P.W., and Vela, A. (2017 August). Thermodynamic hardness and the maximum hardness principle. *J. Chem. Phys.* 147 (7): 074113.
- 21 Sanderson, R.T. (1951 December). An interpretation of bond lengths and a classification of bonds. *Science* 114 (2973): 670–672.
- 22 Sanderson, R.T. (1955 November). Partial charges on atoms in organic compounds. *Science* 121 (3137): 207–208.
- 23 Chamorro, E., Chattaraj, P.K., and Fuentealba, P. (2003 August). Variation of the electrophilicity index along the reaction path. *J. Phys. Chem. A* 107 (36): 7068–7072.

- 24 Chattaraj, P.K., Gutiérrez-Oliva, S., Jaque, P., and Toro-Labbé, A. (2003 November). Towards understanding the molecular internal rotations and vibrations and chemical reactions through the profiles of reactivity and selectivity indices: an ab initio SCF and DFT study. *Mol. Phys.* 101 (18): 2841–2853.
- 25 Miranda-Quintana, R.A., Chattaraj, P.K., and Ayers, P.W. (2017 September). Finite temperature grand canonical ensemble study of the minimum electrophilicity principle. *J Chem. Phys.* 147 (12): 124103.
- 26 Chattaraj, P.K. and Sengupta, S. (1996 October). Popular electronic structure principles in a dynamical context. *J. Phys. Chem.* 100 (40): 16126–16130.
- 27 Ghanty, T.K. and Ghosh, S.K. (1996 July). A density functional approach to hardness, polarizability, and valency of molecules in chemical reactions. *J. Phys. Chem.* 100 (30): 12295–12298.
- 28 Chattaraj, P.K. and Sarkar, U. (2003 December). Ground and excited states reactivity dynamics of hydrogen and helium atoms. *Int. J. Quant. Chem.* 91 (5): 633–650.
- 29 Chattaraj, P.K. and Sarkar, U. (2003 April). Chemical reactivity of spherically confined atoms. *Chem. Phys. Lett.* 372 (6): 805–809.
- 30 Chattaraj, P.K., Maiti, B., and Sarkar, U. (2003 June). Chemical reactivity of the compressed noble gas atoms and their reactivity dynamics during collision with a proton. *J. Chem. Sci.* 115: 195–218.
- 31 Elango, M., Parthasarathi, R., Subramanian, V. et al. (2005 March). Formaldehyde decomposition through profiles of global reactivity indices. *J. Mol. Struct.* 723 (1–3): 43–52.
- 32 Parthasarathi, R., Elango, M., Padmanabhan, J. et al. (2006 January). Application of quantum chemical descriptors in computational medicinal chemistry for chemoinformatics. *Ind. J. Chem. A.* 45A: 111–125.
- 33 Chattaraj, P.K., Sarkar, U., and Roy, D.R. (2007 February). Electronic structure principles and aromaticity. *J. Chem. Educ.* 84 (2): 354–357.
- 34 Khatua, M., Sarkar, U., and Chattaraj, P.K. (2014 February). Reactivity dynamics of confined atoms in the presence of an external magnetic field. *Eur. Phys. J. D* 68: 22.
- 35 Khatua, M., Sarkar, U., and Chattaraj, P.K. (2015 February). Reactivity dynamics of a confined molecule in presence of an external magnetic field. *Int. J. Quantum Chem.* 115 (3): 144–157.
- 36 Deb, J., Paul, D., Sarkar, U., and Ayers, P.W. (2018 August). Characterizing the sensitivity of bonds to the curvature of carbon nanotubes. *J. Mol. Model.* 24: 249.
- 37 Singh, N.B. and Sarkar, U. (2014 January). A density functional study of chemical, magnetic and thermodynamic properties of small palladium clusters. *Mol. Simul.* 40 (15): 1255–1264.
- 38 Singh, N.B. and Sarkar, U. (2014 December). Structure, vibrational and optical properties of platinum cluster: a density functional theory approach. *J. Mol. Model.* 20: 2537.

- 39 Koopmans, T.A. (1934 June). Über die Zuordnung von Wellenfunktionen und Eigenwerten zu den Einzelnen Elektronen Eines Atoms. *Physica* 1 (1–6): 104–113.
- 40 Maynard, A.T., Huang, M., Rice, W.G., and Covell, D.G. (1998 September). *Proc. Natl. Acad. Sci. U. S. A.* 95 (20): 11578–11583.
- 41 Roy, D.R., Parthasarathi, R., Padmanabhan, J. et al. (2006 January). Careful scrutiny of the philicity concept. *J. Phys. Chem. A* 110 (3): 1084–1093.
- 42 Chattaraj, P.K., Sarkar, U., Parthasarathi, R., and Subramanian, V. (2005 November). DFT study of some aliphatic amines using generalized philicity concept. *Int. J. Quant. Chem.* 101 (6): 690–702.
- 43 Roy, D.R., Sarkar, U., Chattaraj, P.K. et al. (2006 June). Analyzing toxicity through electrophilicity. *Mol. Divers.* 10: 119–131.
- 44 Chattaraj, P.K., Maiti, B., and Sarkar, U. (2003 May). Philicity: a unified treatment of chemical reactivity and selectivity. *J. Phys. Chem. A* 107: 4973–4975.
- 45 Chattaraj, P.K., Sarkar, U., Elango, M. et al. (2006 May). Is electrophilicity a kinetic or a thermodynamic concept? *Indian J. Chem. A* 45A: 1099–1112.
- 46 Elango, M., Parthasarathi, R., Narayanan, G.K. et al. (2005 January). The relationship between electrophilicity index, Hammett constant and nucleus independent chemical shift. *J. Chem. Sci.* 117: 61–65.
- 47 Fuentealba, P. (1995 June). A local model for the hardness kernel and related reactivity parameters in density functional theory. *J. Chem. Phys.* 103 (15): 6571.
- 48 Fuentealba, P., Simón-Manso, Y., and Chattaraj, P.K. (2000 March). Molecular electronic excitations and the minimum polarizability principle. *J. Phys. Chem. A* 104 (14): 3185–3187.
- 49 Parr, R.G. and Yang, W. (1984 July). Density functional approach to the frontier electron theory of chemical reactivity. *J. Am. Chem. Soc.* 106 (14): 4049–4050.
- 50 Fukui, K. (1987 November). Role of frontier orbitals in chemical reactions. *Science* 218 (4574): 747–754.
- 51 Ayers, P.W. and Levy, M. (2000 February). Perspective on “Density functional approach to the frontier-electron theory of chemical reactivity.”. *Theor. Chem. Acc.* 103: 353–360.
- 52 Padmanabhan, J., Parthasarathi, R., Sarkar, U. et al. (2004 November). Effect of solvation on the condensed Fukui function and the generalized philicity index. *Chem. Phys. Lett.* 383 (1–2): 122–128.
- 53 Parthasarathi, R., Padmanabhan, J., Subramanian, V. et al. (2003 December). Toxicity analysis of benzidine through chemical reactivity and selectivity profiles: a DFT approach. *Internet Electron. J. Mol. Des.* 2 (12): 798–813.
- 54 Sarkar, U., Padmanabhan, J., Parthasarathi, R. et al. (2006 January). Toxicity analysis of polychlorinated dibenzofurans through global and local electrophilicities. *J. Mol. Struct.* 758 (2–3): 119–125.
- 55 Yang, W. and Mortier, W.J. (1986 September). The use of global and local molecular parameters for the analysis of the gas-phase basicity of amines. *J. Am. Chem. Soc.* 108 (19): 5708–5711.
- 56 Lee, C., Yang, W., and Parr, R.G. (1988 January). Local softness and chemical reactivity in the molecules CO, SCN– and H<sub>2</sub>CO. *J. Mol. Struct.* 163: 305–313.

- 57 Cioslowski, J., Martinov, M., and Mixon, S.T. (1993 October). Atomic Fukui indexes from the topological theory of atoms in molecules applied to Hartree-Fock and correlated electron densities. *J. Phys. Chem.* 97 (42): 10948–10951.
- 58 Paul, D., Deb, J., and Sarkar, U. (2020 June). A detailed DFT study on electronic structures and nonlinear optical properties of doped C<sub>30</sub>. *Chem. Sel.* 5 (23): 6987–6999.
- 59 Deb, J., Paul, D., and Sarkar, U. (2020 January). Density functional theory investigation of nonlinear optical properties of T-graphene quantum dots. *J. Phys. Chem. A* 124 (7): 1312–1320.
- 60 Pegu, D., Deb, J., Paul, D., and Sarkar, U. (2018 January). Electronic, nonlinear optical and thermodynamic properties of (CdS)<sub>n</sub> clusters: a first principle study. *Comput. Condens. Matter.* 14: 40–45.
- 61 Paul, D., Dua, H., and Sarkar, U. (2020 August). Confinement effects of a noble gas dimer inside a fullerene cage: can it be used as an acceptor in a DSSC? *Front. Chem.* 8: 621.
- 62 Schlegel, H.B. (2003 June). Ab initio molecular dynamics with born-oppenheimer and extended Lagrangian methods using atom centered basis functions. *Bull. Korean Chem. Soc.* 24 (6): 837–842.
- 63 Roos, G., Loverix, S., Brosens, E. et al. (2006 May). The activation of electrophile, nucleophile and leaving group during the reaction catalysed by pI258 arsenate reductase. *ChemBioChem* 7 (6): 981–989.
- 64 Helgaker, T., Uggerud, E., and Jensen, H.J.A. (1990 October). Integration of the classical equations of motion on ab initio molecular potential energy surfaces using gradients and Hessians: application to translational energy release upon fragmentation. *Chem. Phys. Lett.* 173 (2–3): 145–150.
- 65 Liu, S. (2005 September). Dynamic behavior of chemical reactivity indices in density functional theory: a Bohn–Oppenheimer quantum molecular dynamics study. *J. Chem. Sci.* 117 (5): 477–483.
- 66 Zhong, A., Rong, C., and Liu, S. (2007 March). Structural and dynamic properties of (SiO<sub>2</sub>)<sub>6</sub> silica nanostructures: a quantum molecular dynamics study. *J. Phys. Chem. A* 111 (16): 3132–3136.
- 67 Deb, B.M. and Chattaraj, P.K. (1989 February). Density-functional and hydrodynamical approach to ion-atom collisions through a new generalized nonlinear Schrödinger equation. *Phys. Rev. A* 39 (4): 1696.
- 68 Deb, B.M. and Ghosh, S.K. (1982). Schrödinger fluid dynamics of many-electron systems in a time-dependent density-functional framework. *J. Chem. Phys.* 77 (1): 342.
- 69 Chattaraj, P.K. and Maiti, B. (2001 December). Reactivity dynamics in atom–field interactions: a quantum fluid density functional study. *J. Phys. Chem. A* 105 (1): 169–183.
- 70 Sarkar, U., Khatua, M., and Chattaraj, P.K. (2012 December). A tug-of-war between electronic excitation and confinement in a dynamical context. *Phys. Chem. Chem. Phys.* 14 (5): 1716–1727.

- 71 Khatua, M. and Chattaraj, P.K. (2013 February). Molecular reactivity dynamics in a confined environment. *Phys. Chem. Chem. Phys.* 15 (15): 5588–5614.
- 72 Chattaraj, P.K., Sengupta, S., and Poddar, A. (1998 December). Quantum fluid density functional theory of time-dependent processes. *Int. J. Quantum Chem.* 69 (3): 279–291.
- 73 Chattaraj, P.K. and Maiti, B. (2004 January). Regioselectivity in the chemical reactions between molecules and protons: a quantum fluid density functional study. *J. Phys. Chem. A* 108 (4): 658–664.



## 10

### Selectivity: An Electron Density Perspective

Mar Ríos-Gutiérrez<sup>1</sup> and Ramón Alain Miranda-Quintana<sup>2</sup>

<sup>1</sup>University of Valencia, Department of Organic Chemistry, Dr. Moliner 50, Valencia 46100, Spain

<sup>2</sup>University of Florida, Department of Chemistry and Quantum Theory Project, 165 Buckman Drive, Gainesville, FL 32611, USA

#### 10.1 Introduction

Molecular orbitals (MOs) have reigned supreme for a long time in chemistry [1, 2]. Not only our most accurate computational methods [3] (configuration interaction [4], coupled cluster [5], geminals [6], density matrix renormalization group [7], etc.) are orbital-based, chemists often “think” in terms of orbitals. Highest occupied and lowest unoccupied orbitals (HOMO and LUMO, respectively) [8–12], resonant structures [2, 13, 14], Mulliken charges [15–18], bonding and antibonding, all of these terms are deeply engraved in our chemical minds, to the point where we use them as primary descriptors of a plethora of chemical processes. All things considered, it is hard to argue against the utility of the orbital picture in modern chemistry, but as useful as they are, MOs are not directly accessible via experiments, and they cannot be univocally defined (e.g. the phase of an orbital is completely arbitrary).

The electron density is the only reality facing the MOs in many different aspects. For one, density functional theory (DFT) [19–21], while not as precise as many of the *ab initio* methods, is every bit as formally rigorous, and has the upper hand when it comes to computational efficiency and ability to treat larger systems [22]. Additionally, the electron density is directly related to seminal chemical concepts like atomic charges [23–28] and molecular electrostatic potentials [29–32], which play a large role in our understanding of molecular structures. Moreover, by the end of the 1970s, Parr et al. [33] realized that a deeper scrutiny of the foundations of DFT, combined with an incisive thermodynamic point of view, naturally led to a formalism that seamlessly accommodated much of chemical reactivity. This is what we now call density functional chemical reactivity theory, chemical reactivity from DFT, chemical DFT or, more generally, conceptual density functional theory (CDFT) [21, 34–38]. The most immediate impact of CDFT is the newfound ability to define several chemical concepts in a precise mathematical way. Moreover, CDFT also provides a framework to understand the relations between these concepts

*Conceptual Density Functional Theory: Towards a New Chemical Reactivity Theory*, First Edition.

Edited by Shubin Liu.

© 2022 WILEY-VCH GmbH. Published 2022 by WILEY-VCH GmbH.

and well-established physical principles, allowing us to provide analytical proofs for many reactivity principles [39–50].

Molecular electron density theory (MEDT) [51] is a more recent outlook on the chemical reactivity problem in which the electron density takes center stage. MEDT was proposed in 2016 by Domingo as a new reactivity theory according to which, changes in electron density, but not MO interactions as the frontier molecular orbital (FMO) proposed [52], are responsible for the chemical reactivity. Thus, the application of MEDT is intrinsically linked to the use of quantum chemical tools based only on the analysis of electron distribution functions such as the electron density or the electron localization function (ELF) [53]. For instance, besides an exhaustive exploration and characterization of reaction paths, CDFT [21, 34–38], the quantum theory of atoms in molecules (QTAIM) [54, 55], and/or bonding evolution theory (BET) [56] may be used. Thus, it is worth emphasizing that MEDT is not a mere compilation or application of already well-established quantum chemical tools, but a different rationalization of chemistry based on electron density instead on MOs. Note that MEDT can be applied even using the electron density obtained from *ab initio* methods.

In this chapter we aim to provide a pedagogical (yet, not exhaustive) discussion about how MEDT, in particular CDFT and Parr functions, can be used to study some types of selectivity, such as chemo-, regio-, and pseudocyclic selectivities. We start by presenting a brief introduction to CDFT descriptors and their relations. Given its importance, we explore the Fukui functions in particular detail (not only going over their analytical properties, but also about the ways to calculate them), and we present their several connections to FMO theory. We then discuss how the Fukui function plays a fundamental role in different matching criteria used to explain regio- and chemoselectivity patterns in the context of several reactivity principles. Finally, we discuss the close connections between the Fukui function and the dual descriptor. Then, we present a brief introduction to MEDT in which we will show the application of the empiric Parr functions [56] (presented in more detail in Chapter 24, “Polar Diels–Alder Reactions”) to predict and understand the experimental selectivities in several cycloaddition reactions.

## 10.2 Conceptual Density Functional Theory

### 10.2.1 The Fukui Function and Frontier Molecular Orbitals

The Fukui function [51, 52, 57] is defined as the response in the system’s energy with respect to changes in number of electrons and external potential:  $f(r) = \frac{\delta^2 E}{\delta v(r) N}$ . This can be re-written as the response of the chemical potential to an external perturbation:

$$f(r) = \left( \frac{\delta \mu}{\delta v(r)} \right)_N \quad (10.1)$$

However, the more popular working expressions are derived after the fact that the response of the energy to changes in the external potential is nothing more than the electron density,  $\rho(r)$ , so we can write instead:

$$f(r) = \left( \frac{\partial \rho(r)}{\partial N} \right)_{v(r)} \quad (10.2)$$

(Notice that Eqs. (10.1) and (10.2) are just Maxwell relations of each other.)

This makes it clear that the Fukui function represents a generalization of the concepts of FMOs. If we approximate the ground state of the system by a single Slater determinant formed by orbitals  $\{\phi_i\}$ , then electron density will be given by:

$$\rho(r) = \sum_i |\phi_i(r)|^2 \quad (10.3)$$

This simple picture implies that if we remove an electron (while ignoring the subsequent orbital relaxation), we must do so from the most energetic level, that is, from the highest occupied orbital, which implies that:

$$f^-(r) = |\phi_{\text{HOMO}}(r)|^2 \quad (10.4)$$

while if we add an extra electron the most stable configuration will result from doing so in the available orbital with lowest possible energy, hence:

$$f^+(r) = |\phi_{\text{LUMO}}(r)|^2 \quad (10.5)$$

(In Eqs (10.4) and (10.5) the supra-indices “-” and “+” mean removing and adding an electron, respectively, a notation that we will explore in more detail in the next section.)

In this sense, the FMOs represent a “zeroth-order” approximation to the Fukui function, but it is important to realize that the latter are a much more general concept. For one, the Fukui functions can be calculated for every electronic-structure method, independent of whether they use orbitals or not. This means that they can encapsulate electron correlation effects, which are in principle absent from the simplistic HOMO/LUMO picture.

Equations (10.4) and (10.5) are usually presented as the only link between the Fukui functions and the FMOs; however, if this was the case, it would imply that FMO theory is more fundamental than CDFT. FMO not only identifies the HOMO and LUMO as critical to explain the local reactivity of a system, but also provides a first-principles explanation for this observation based on the Klopman–Salem perturbative model [53–56, 58–62]. Thus, while we have seen that the Fukui functions can identify the regions in space associated to these orbitals, the importance of such regions is derived from FMO theory. Fortunately, Parr and Yang realized a long time ago that CDFT could also provide an explanation for this fact, based on Eq. (10.1) [63]. These authors argued that if one could show that a chemical process will tend to be favored if it entails a bigger variation in the chemical potential, this will in turn imply that regions with large values of the Fukui function will dictate the local

reactivity of a system. As they put it: “Of two different sites with generally similar dispositions for reacting with a given reagent, the reagent prefers the one which on the reagent’s approach is associated with the maximum response of the system’s chemical potential” [21]. In more succinct terms, for CDFT to provide a theoretical justification for FMO theory we need to show that: “ $|\Delta\mu|$  big is good” (DMB) [39, 64–66]. An elementary argument [64] in favor of this seminal principle can be obtained from a simple reduction of the charge transfer reaction between reagents A and B in which we only take into account the global descriptors:

$$A + B = AB \Rightarrow \Delta E_{\text{ABrxn}} = -\frac{1}{2} \frac{(\mu_B - \mu_A)^2}{(\eta_A + \eta_B)} \quad (10.6)$$

Now, noting that since the chemical potential is an intensive quantity we must calculate its variation along this reaction according to:

$$\Delta\mu_{\text{AB}} = \mu_{\text{AB}} - \frac{1}{2}(\mu_A + \mu_B) = \frac{(\mu_B - \mu_A)(\eta_A - \eta_B)}{2(\eta_A + \eta_B)} \quad (10.7)$$

We can then assume (without losing any generality) that B is the base and A is the acid, which in turn implies that: [40, 67, 68]

$$\mu_B - \mu_A > 0 \quad (10.8)$$

What is left then is noticing that:

$$\Delta E_{\text{ABrxn}} = -(\mu_B - \mu_A) \frac{\Delta\mu_{\text{AB}}}{(\eta_A - \eta_B)} \quad (10.9)$$

but since  $\frac{\Delta\mu_{\text{AB}}}{(\eta_A - \eta_B)} = \frac{(\mu_B - \mu_A)}{2(\eta_A + \eta_B)} > 0$ , we get that:

$$0 \leq \frac{\Delta\mu_{\text{AB}}^{(2)}}{\eta_A - \eta_B} = \left| \frac{\Delta\mu_{\text{AB}}^{(2)}}{\eta_A - \eta_B} \right| = \frac{|\Delta\mu_{\text{AB}}^{(2)}|}{|\eta_A - \eta_B|} \quad (10.10)$$

Eq. (10.9) then turns into:

$$\Delta E_{\text{ABrxn}}^{(2)} = -(\mu_B - \mu_A) \frac{|\Delta\mu_{\text{AB}}^{(2)}|}{|\eta_A - \eta_B|} \quad (10.11)$$

from which is clear that:

$$\frac{\partial \Delta E}{\partial |\Delta\mu|} < 0 \quad (10.12)$$

In other words, increasing  $|\Delta\mu|$  should decrease  $\Delta E$ : the DMB principle.

There are more detailed proofs of this principle, including extensions to more realistic charge transfer models than the truncated parabolic model [64], as well as studies of the validity of the principle in simple cycloaddition reactions [66], and showing its relation to other classical reactivity rules [65], but for our present purposes the most important result is that by proving the DMB principle we have established a rigorous link between CDFT and FMO theory, showing that indeed the former is a more general framework.

### 10.2.2 Calculating the Fukui Function

The simplest possible way to calculate the Fukui functions is to just use Eqs (10.4) and (10.5); however, while this is a perfectly valid approach, it is perhaps too

contrived in the sense that we will be foregoing all the power of CDFT by limiting ourselves to the standard FMO result. According to Eq. (10.2), to calculate the Fukui function we need to consider how the state of a system will change when it changes its number of particles. This is the well-known  $E$  vs.  $N$  problem. The exact  $E$  vs.  $N$  dependency for isolated systems at absolute zero is given by straight lines connecting the integer particle number states [69–73]. This means that the electron density of a system with  $N = M + \Delta N$  electrons ( $M$  being an integer, and  $0 \leq \Delta N \leq 1$ ) is:

$$\rho_{M+\Delta N}(r) = (1 - \Delta N)\rho_M(r) + \Delta N\rho_{M+1}(r) \quad (10.13)$$

While the derivative with respect to  $N$  of this expression is univocal and well defined when  $\Delta N \in (0; 1)$ , when we have an integer number of particles the pairwise-linear nature of this dependency means that we must consider directional derivatives. In other words, the derivative when the system is losing electrons:

$$f_M^-(r) = \rho_M(r) - \rho_{M-1}(r) \quad (10.14)$$

and the derivative when the system is gaining electrons:

$$f_M^+(r) = \rho_{M+1}(r) - \rho_M(r) \quad (10.15)$$

(Notice how in both cases the correct normalization is achieved.)

This simple mathematical nuance reflects the fact that a molecule will most certainly react in different ways when it encounters an electrophile or a nucleophile. It is also easy to see that these equations represent a generalization of the FMO results.

While the linear  $E$  vs.  $N$  model is perhaps the most popular at the time of calculating the Fukui function, CDFT practitioners often make use of other  $E$  vs.  $N$  dependencies that correspond to higher-order truncations of the parabolic model [74–76]. Analogous to the linear case, these models are usually interpreted as interpolations between a selected number of integer-particle states. While there are theoretical arguments against the statistical thermodynamic validity of such models [77, 78], the simplest of them (proposed by Parr and Pearson) is a mainstay in CDFT [76]. Under the assumption that the state of a system can be described as a (incoherent) superposition of three integer-particle states, we get:

$$\rho_{M+\Delta N}(r) = \left(\frac{\Delta N^2 - \Delta N}{2}\right)\rho_{M-1}(r) + (1 - \Delta N^2)\rho_M(r) + \left(\frac{\Delta N^2 + \Delta N}{2}\right)\rho_{M+1}(r) \quad (10.16)$$

One of the advantages of this approach is that now the derivative of the density with respect to the number of particles is univocally well defined in every possible state, so:

$$f_{M+\Delta N}(r) = \left(\frac{2\Delta N - 1}{2}\right)\rho_{M-1}(r) + (1 - 2\Delta N)\rho_M(r) + \left(\frac{2\Delta N + 1}{2}\right)\rho_{M+1}(r) \quad (10.17)$$

In particular, for an integer-particle state:

$$f_M(r) = \frac{\rho_{M+1}(r) - \rho_{M-1}(r)}{2} \quad (10.18)$$

This equation is often referred to (in a rather unfortunate convention) as the “radical Fukui function,” and notice that it can be rewritten as:

$$f_M(r) = \frac{f_{M+1}^+(r) + f_{M-1}^-(r)}{2} \quad (10.19)$$

so in a sense it averages the nucleophilic and electrophilic behaviors contained in Eqs (10.14) and (10.15).

In any event, the workflow to calculate the Fukui functions is pretty simple:

1. Optimize the geometry of the system with  $M$  electrons.
2. Perform single-point calculations of the systems with  $M + 1$  and  $M - 1$  electrons.

We need to keep the system’s geometry fixed in the second step because, as indicated in Eq. (10.2), the response to the change in number of electrons must be calculated at constant external potential.

Note that using this recipe we will get a 3D function, which can be very useful in identifying which regions in a molecule are more prone to a nucleophilic or electrophilic attack. However, in some cases we might want to take a closer look at which individual atoms contribute the most to the reactivity of a molecule. In this case we need the condensed (atom-resolved) form of the Fukui function [79–81]. Denoting by  $q_M^A$  the charge of atom  $A$  in a system with  $M$  electrons, the corresponding working equations can be easily obtained within the fragment of molecular response approach [80] (in the response of molecular fragment [81] approach we would have to consider the response of the atomic partition, which introduces an extra level of complexity). For the linear case:

$$\begin{aligned} f_M^-(A) &= q_{M-1}^A - q_M^A \\ f_M^+(A) &= q_M^A - q_{M+1}^A \end{aligned} \quad (10.20)$$

and for the parabolic case:

$$f_M(A) = \frac{q_{M-1}^A - q_{M+1}^A}{2} \quad (10.21)$$

Finally, it is important to remark that there are more sophisticated versions of the Fukui functions that correspond to further generalizations of the CDFT formalism. For instance, we can calculate spin-resolved Fukui functions [82–87], which play a key role in understanding the reactivity of open-shell species. On the other hand, the finite-temperature [47, 88–97] formulation of CDFT leads to very elegant expressions for the Fukui function:

$$\begin{aligned} f_{M+\Delta N}(r) &= f_M(r) - \frac{f_M^-(r) - f_M^+(r)}{2} \frac{\alpha}{\Delta N} \\ \alpha &= \sqrt{\Delta N^2 - 4(\Delta N^2 - 1) \exp[-\beta(I - A)]} \end{aligned} \quad (10.22)$$

where  $\beta = \frac{1}{kT}$ , and  $I$  and  $A$  are the ionization potential and electron affinity of the system, respectively. Note that despite the apparent complexity of this expression, the steps outlined above to calculate the zero-temperature Fukui function are still all that is necessary to calculate the finite-temperature analogue.

In 2013, Domingo proposed the Parr functions  $P(\mathbf{r})$  as an approach to the Fukui functions proposed in 1984 within CDFT. The Parr functions are given by the following equations: [56]

$$P^-(\mathbf{r}) = \rho_s^{rc}(\mathbf{r}) \quad \text{for electrophilic attacks} \quad (10.23)$$

and

$$P^+(\mathbf{r}) = \rho_s^{ra}(\mathbf{r}) \quad \text{for nucleophilic attacks} \quad (10.24)$$

where  $\rho_s^{rc}(\mathbf{r})$  is the atomic spin density (ASD) at the  $\mathbf{r}$  atom of the radical cation of a considered frozen molecule and  $\rho_s^{ra}(\mathbf{r})$  is the ASD at the  $\mathbf{r}$  atom of the radical anion. Each ASD gathered at the different atoms of the radical cation and the radical anion of a molecule provides the nucleophilic  $P_k^-$  and electrophilic  $P_k^+$  Parr functions of the neutral molecule.

### 10.2.3 Matching Criteria Based on the Fukui Function

Given the previously explored connection between FMO theory and the Fukui functions, we can arrive at the natural conclusion that the latter should play a key role in our understanding of local reactivity. We can look at this as a “matching problem,” that is, finding ways to say which atoms in a molecule A should bind to a set of atoms in a molecule B. The simplest way to this is by just looking at the Fukui functions and trying to match the regions with high values of  $f^-$  in an electron donor with the regions with large values of  $f^+$  in an electron acceptor (notice that this is just a straightforward generalization of the classical FMO rule of maximizing the overlap between the HOMO and LUMO of the reactants).

However, probably the most popular matching rule in CDFT makes use of the local hard/soft acid/base (HSAB) principle [98–105]. The global (and more fundamental) version of this principle states that “other things being equal, hard acids prefer binding to hard bases when soft acids are binding to soft bases” [68]. There are several theoretical and experimental arguments supporting the global HSAB rule, so it seems natural to extend this principle to study the reactivity of moieties inside a molecule. To fix ideas, let us focus on the case in which we have two reactants, A and B, each with two reactive centers, 1 and 2. The first step then is defining a local analogue to the (global) softness of molecule X,  $S_X = \frac{1}{\eta_X}$ , for the  $k$ th atom, which we can do with the help of the Fukui function:

$$s_{X_k} = f_{X_k} S_X \quad (10.25)$$

From the global HSAB, it makes sense now to consider a measure of how different two local softnesses are,  $d(s_{B_k}, s_{A_j})$ . For instance a  $L_1$  or  $L_2$  norm,  $|s_{B_k} - s_{A_j}|$ ,  $(s_{B_k} - s_{A_j})^2$ , respectively. Then, the matching 1-1 will be favored over the matching 2-2 if:

$$d(s_{B_1}, s_{A_1}) + d(s_{B_2}, s_{A_2}) > d(s_{B_1}, s_{A_2}) + d(s_{B_2}, s_{A_1}) \quad (10.26)$$

which means that the two molecules will react in a way that the difference between the matched local softnesses is minimal. Apparently simple at first sight, the problem

of selecting the right  $d$  is far from trivial, since seemingly equivalent difference measures can lead to selecting different reactivity patterns [106, 107]. This means that we must consider an energetic criterion to identify how to quantify the difference in hardness between the reacting sites.

This is exactly what Ponti did [108], taking into account the variation in the grand-potential,  $\Omega$ , along the reaction. Here we will illustrate his result from a simpler point of view, noting that in a general  $A + B = AB$  reaction:

$$\Delta E = \Delta E_A + \Delta E_B = \Delta \Omega_A + \Delta \Omega_B = \Delta \Omega \quad (10.27)$$

Then we just need to consider the (local) reactions:



for which:

$$\left. \begin{aligned} A_1 + B_1 \rightarrow A_1B_1, \quad \Delta E_1^1 &= -\frac{1}{2}(\mu_A - \mu_B)^2 \frac{s_{A_1}s_{B_1}}{s_{A_1} + s_{B_1}} \\ A_2 + B_2 \rightarrow A_2B_2, \quad \Delta E_2^2 &= -\frac{1}{2}(\mu_A - \mu_B)^2 \frac{s_{A_2}s_{B_2}}{s_{A_2} + s_{B_2}} \end{aligned} \right\} \rightarrow \Delta E_{12}^{12} = \Delta E_1^1 + \Delta E_2^2 \quad (10.29)$$

We can repeat this analysis and get, for the 1-2 and 2-1 interaction:

$$\left. \begin{aligned} A_1 + B_2 \rightarrow A_1B_2, \quad \Delta E_1^2 &= -\frac{1}{2}(\mu_A - \mu_B)^2 \frac{s_{A_1}s_{B_2}}{s_{A_1} + s_{B_2}} \\ A_2 + B_1 \rightarrow A_2B_1, \quad \Delta E_2^1 &= -\frac{1}{2}(\mu_A - \mu_B)^2 \frac{s_{A_2}s_{B_1}}{s_{A_2} + s_{B_1}} \end{aligned} \right\} \rightarrow \Delta E_{12}^{21} = \Delta E_1^2 + \Delta E_2^1 \quad (10.30)$$

The first matching will be the favored if:

$$\begin{aligned} \Delta E_{12}^{12} - \Delta E_{12}^{21} &< 0 \\ \frac{1}{2}(\mu_A - \mu_B)^2 &\left[ \frac{s_{A_2}s_{B_1}s_{B_2} + s_{A_1}s_{B_1}s_{B_2} + s_{A_1}s_{A_2}s_{B_2} + s_{A_1}s_{A_2}s_{B_1}}{(s_{A_1} + s_{B_1})(s_{A_2} + s_{B_2})(s_{A_1} + s_{B_2})(s_{A_2} + s_{B_1})} \right] \\ &\times (s_{A_1} - s_{A_2})(s_{B_2} - s_{B_1}) < 0 \end{aligned} \quad (10.31)$$

which (due to the energy convexity) can in turn be written as:

$$\Delta E_{12}^{12} - \Delta E_{12}^{21} < 0 \Leftrightarrow (s_{A_1} - s_{A_2})(s_{B_2} - s_{B_1}) < 0 \quad (10.32)$$

Finally, we can rewrite this as:

$$(s_{A_1} - s_{A_2})(s_{B_2} - s_{B_1}) < 0 \Leftrightarrow (s_{A_1} - s_{B_1})^2 + (s_{A_2} - s_{B_2})^2 < (s_{A_1} - s_{B_2})^2 + (s_{A_2} - s_{B_1})^2 \quad (10.33)$$

This means that, under the current assumptions, the  $L_2$  norm is the one that should give the preferred local interaction, and indeed this is the most popular formulation



of the local HSAB principle. However, this formulation has been criticized because the predictions made by it, while correct in some instances, fail catastrophically in many cases. It is thus a pressing issue to find explanations as to why the above derivation does not provide accurate results.

There are other selectivity criteria that are essentially based on “spreading out” a global descriptor into local atomic basins using the Fukui function (like matching local electrophilicities and/or nucleophilicities) [109–111], but while also popular, they lack rigorous footing.

### 10.2.4 The Dual Descriptor

The Fukui function seems like the ideal tool to describe the reactivity of a species that is either only going to gain or lose electrons. However, while these extreme cases are important and common, there are cases in which different parts of the same molecule are going to accept and/or donate electrons. A typical instance of this are cycloaddition reactions, particularly those with the presence of a well-defined dipole. This means that we need a tool to identify which predominant behavior (electrophilic or nucleophilic) will be present in different parts of a molecule. The way to do so was found by Morell coworkers [83, 112–114] and is based on the dual descriptor,  $\Delta f(r)$ :

$$\Delta f(r) = \frac{\delta^3 E}{\delta v(r) \delta N^2} = \left( \frac{\partial^2 \rho(r)}{\partial N^2} \right)_{v(r)} = \left( \frac{\partial f(r)}{\partial N} \right)_{v(r)} \quad (10.34)$$

The last expression is actually the most convenient to study the properties of this descriptor. First of all, its normalization can be easily derived:

$$\int \Delta f(r) dr = \int \left( \frac{\partial f(r)}{\partial N} \right)_{v(r)} dr = \left( \frac{\partial \int f(r) dr}{\partial N} \right)_{v(r)} = \left( \frac{\partial 1}{\partial N} \right)_{v(r)} = 0 \quad (10.35)$$

Moreover, by using a finite difference approximation to obtain a working equation for the derivative we get:

$$\Delta f(r) = f^+(r) - f^-(r) \quad (10.36)$$

It is easy to see how this satisfies the normalization condition, but more importantly, this provides a simple interpretation for the dual descriptor, since regions with positive values will indicate a larger tendency to accept electrons, while regions with negative values will be more prone to donate electrons. This provides a very convenient and unambiguous matching criterion between two reactants: just matching regions with different  $\Delta f(r)$  signs. This should provide a good estimate of how the electrons will flow during the reaction, particularly, how the new bonds will form.

Beyond this simple application, the dual descriptor has been used to highlight a deeper connection between FMO and CDFT, since it can be used to re-derive the Woodward–Hoffmann rules, without the need to consider MOs [115–120]. The other key advantage of the dual descriptor is that it can be easily generalized to include contributions from excited states [121], which can be critical to understand the reactivity patterns in complex reactions.

## 10.3 Molecular Electron Density Theory

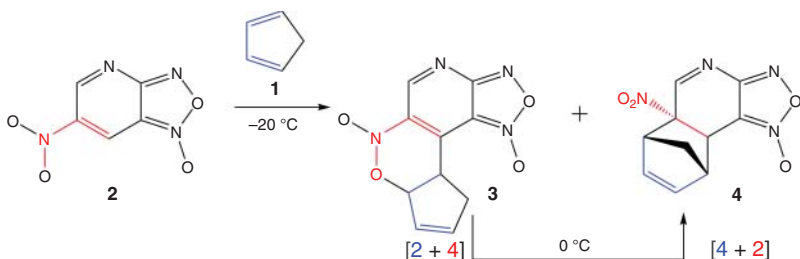
In this section, we will show how MEDT, in particular, CDFT and Parr functions, are applied to explain chemo-, regio-, and *pseudocyclic* selectivities in several types of experimental cycloaddition reactions.

### 10.3.1 Pseudocyclic Selectivity in Polar DA (P-DA) Reactions

Reactions taking place through a more or less distorted cyclic TS, in which all atoms are not necessarily bound, were recently classified as *pseudocyclic* reactions [122]. The term *pseudocyclic* selectivity refers to the selective formation of structural isomers through *pseudocyclic* reactions [123]. This type of selectivity, yielding structural isomers, can be found in highly polar DA reactions involving strong nucleophilic and electrophilic species.

#### 10.3.1.1 Competitive [2 + 4] vs. [4 + 2] Cycloadditions

The treatment of 4-aza-6-nitrobenzofuroxan (ANBF, **2**) with a large excess of cyclopentadiene (Cp) **1** overnight at room temperature led to the formation of the [4 + 2] cycloadduct **4** (see Scheme 10.1) [125]. When the reaction was initially carried out at  $-20^{\circ}\text{C}$ , the NMR spectra revealed the formation of a mixture of the [2 + 4] cycloadduct **3** and [4 + 2] cycloadduct **4**. Raising the temperature to  $0^{\circ}\text{C}$ , the complete conversion of the [2 + 4] cycloadduct **3** into the [4 + 2] cycloadduct **4** was observed [125].

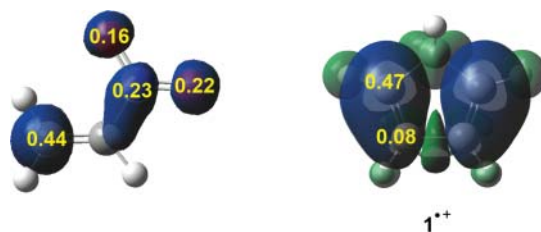


**Scheme 10.1** Competitive [2 + 4] vs. [4 + 2] cycloadditions in the P-DA reaction of Cp **1** with ANBF **2**. Source: Domingo [124]/American Chemical Society.

Only one highly asynchronous TS associated with the formation of the [2 + 4] cycloadduct **3** was found in the P-DA reaction of ANBF **2** with Cp **1**. A subsequent [3,3]-sigmatropic rearrangement on the [2 + 4] cycloadduct **3** allowed its conversion into the thermodynamically more stable formal [4 + 2] cycloadduct **4** [126].

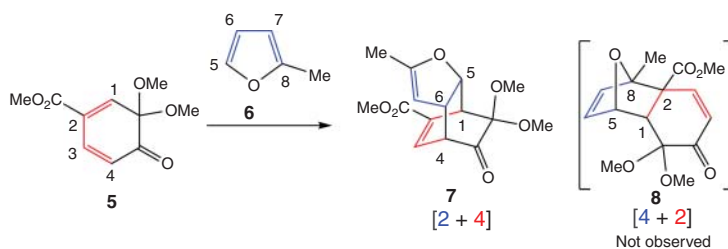
As a consequence of the high global electron density transfer (GEDT) [124] taking place at the TS of this P-DA reaction, 0.40e, which fluxes from the nucleophilic Cp **1** toward the strong electrophilic ANBF **2**, a high amount of electron density is accumulated at the nitro group of the nitroethylene framework (see the electrophilic  $P_k^+$  Parr functions of nitroethylene in Figure 10.1). Consequently, after the corresponding highly asynchronous TS, the subsequent ring closure takes place via the attack

**Figure 10.1** 3D representations of the Mulliken ASD of the radical anion of nitroethylene and the radical cation  $1^{+}$ , together with the electrophilic  $P_k^+$  and nucleophilic  $P_k^-$  Parr functions of nitroethylene and Cp **1**, respectively.



of one negatively charged oxygen of the nitro group to the positively charged allylic framework of the Cp moiety, yielding the  $[2 + 4]$  cycloadduct **3**, but the formal  $[4 + 2]$  cycloadduct **4** was found thermodynamically more stable.

A similar *pseudocyclic* selectivity was observed in the P-DA reactions of furan derivatives with masked *o*-benzoquinones [127], in which furan **6** acts as a strong nucleophilic ethylene and masked *o*-benzoquinones **5** acts as a strong electrophilic species yielding  $[2 + 4]$  cycloadducts (see Scheme 10.2). Note that the experimentalists did not expect the ethylenic behavior of furan **6** [127], a usual nucleophilic diene.



**Scheme 10.2**  $[2 + 4]$  cycloaddition in the P-DA reaction of furan derivative **6** with masked *o*-benzoquinone **5**.

Analysis of the electrophilic Parr functions at masked *o*-benzoquinone **5** shows that the C1 carbon is the most electrophilic center of this species,  $P_k^+ = 0.48$  (see Figure 10.2). After the nucleophilic attack of the non-substituted C5 position of 1-methyl-furan **6**,  $P_k^- = 0.48$ , on the C1 carbon of masked *o*-benzoquinone **5**, the subsequent ring closure takes place at the C4 position of **5**.

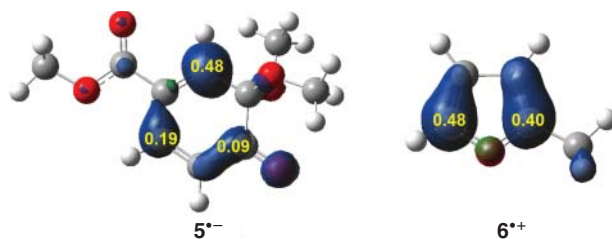
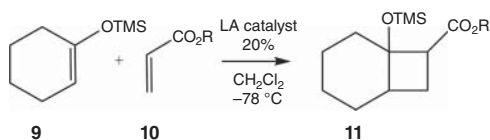


**Figure 10.2** 3D representations of the Mulliken ASD of the radical anion  $5^-$  and radical cation  $6^+$  together with the electrophilic  $P_k^+$  and nucleophilic  $P_k^-$  Parr functions of **5** and **6**, respectively.

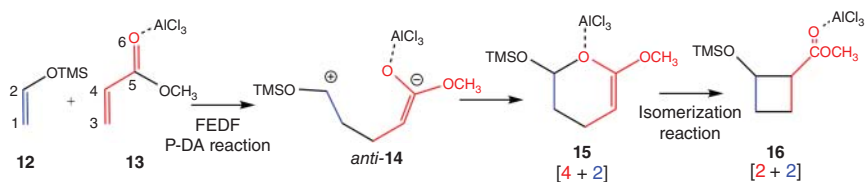
### 10.3.1.2 Competitive [4 + 2] vs. [2 + 2] Cycloadditions

In 2004, Takasu reported the catalytic [2 + 2] cycloaddition reactions of silyl enol ether **9** with the  $\alpha,\beta$ -unsaturated esters **10** leading to the formation of cyclobutane rings **11** (see Scheme 10.3) [129].



**Scheme 10.3** [2 + 2] cycloaddition reactions of silyl enol ether **9** with the  $\alpha,\beta$ -unsaturated esters **10**. Source: Domingo et al. [128]/American Chemical Society.

A study on the formation of the simpler formal [2 + 2] cycloadduct **16** [130] showed that this reaction is a domino process in which the [4 + 2] cycloadduct **15** is first kinetically formed through a stepwise P-DA reaction of forward electron density flux (FEDF) (see Scheme 10.4) [128]; however, **14** was found to be thermodynamically unstable [130]. A subsequent isomerization converts the [4 + 2] cycloadduct **14** into the thermodynamically more stable formal [2 + 2] cycloadduct **15**.



**Scheme 10.4** Domino reaction between silyl enol ether **12** and Lewis-acid complex **13** yielding cyclobutane **16**. Source: IUPAC [131]/Royal Society of Chemistry.

Similar to the reactions shown in Schemes 10.1 and 10.2, the *pseudocyclic* selectivity found in these highly polar cycloaddition reactions is controlled at the ring-closure process taking place after the highly asynchronous TSs. These P-DA reactions can take place through a *two-stage one-step* [132] or a two-step mechanism; while the reaction rate is usually determined by the nucleophilic/electrophilic interactions taking place at the beginning of the reaction, the *pseudocyclic* selectivity is played at the ring-closure step taking place at the end of the reaction.

The electrophilic and nucleophilic Parr functions at the intermediate *anti*-**14** involved in the polar cycloaddition reaction of silyl enol ether **12** with Lewis-acid complex **13** are shown in Figure 10.3. As can be seen, zwitterionic intermediate **14** has the most electrophilic  $P_k^+$  Parr function at the C2 carbon of the enol framework,  $P_k^+ = 0.84$ , and the most nucleophilic  $P_k^-$  Parr function at the C4 carbon of the  $\alpha,\beta$ -unsaturated ester moiety,  $P_k^- = 0.73$ . Consequently, from an electronic point of view, the most favorable ring closure will be that yielding cyclobutane **16**. However, some geometrical restriction associated to the formation of the cyclobutane ring might be responsible for the initial formation of the six-membered dihydropyran **15**.

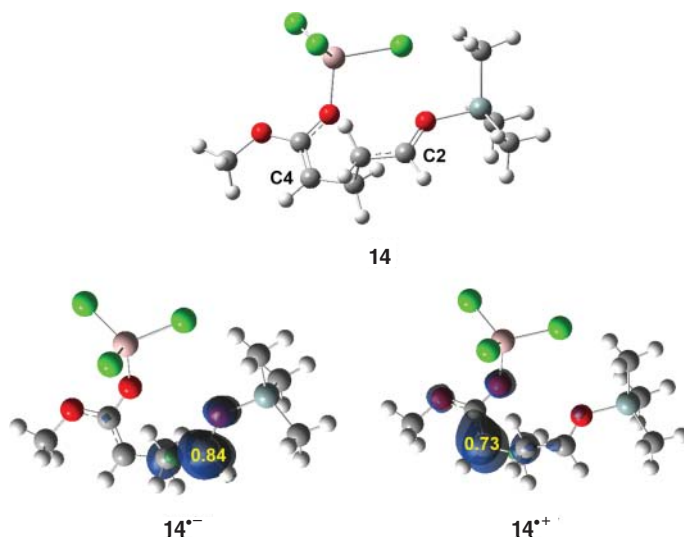
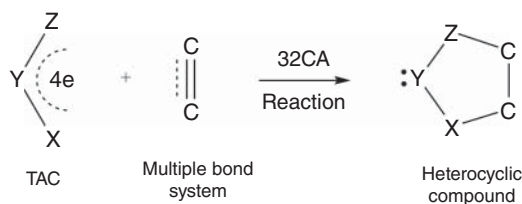


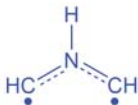
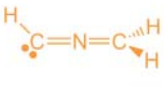
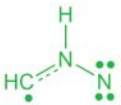
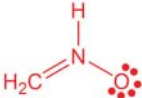
**Figure 10.3** 3D representations of the intermediate *anti*-**14** involved in the polar cycloaddition reaction of silyl enol ether **12** with Lewis-acid complex **13**, and Mulliken ASD of the radical anion and radical cation of this species together with the corresponding electrophilic  $P_k^+$  and nucleophilic  $P_k^-$  Parr functions.

### 10.3.2 Regioselectivity in [3 + 2] Cycloaddition (32CA) Reactions

A regioselective reaction is one in which one direction of bond making or breaking occurs preferentially over all other possible directions [131]. 32CA reactions consist of the addition of a multiple bond system to a three-atom component (TAC) giving rise to the formation of a five-member heterocyclic compound (see Scheme 10.5) in a more or less regioselective manner. A great number of MEDT studies of 32CA reactions have allowed finding a very good correlation between the electronic structure of TACs and their reactivity [133]. Thus, depending on the electronic structure of TACs, i.e. *pseudodiradical*, *pseudo(mono)radical*, carbenoid, and zwitterionic, 32CA reactions have been classified into the four respective types (see Chart 10.1), which present different mechanism and kinetics. For instance, while *pdr-type* 32CA reactions take place very easily even with low-polar character, *zw-type* 32CA reactions demand adequate nucleophilic/electrophilic interactions to take place.



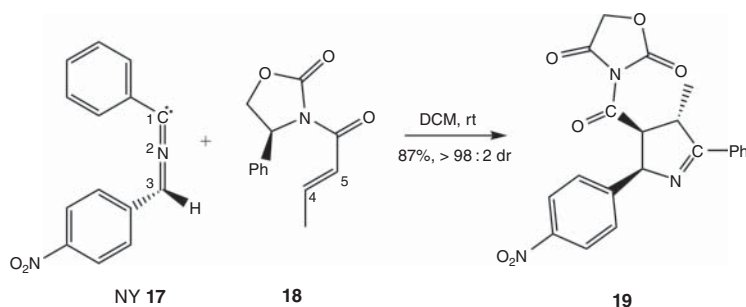
**Scheme 10.5** 32CA reaction between a TAC and a multiple bond system, yielding a five-membered heterocyclic compound.

			
Azomethine ylide	Nitrile ylide	Azomethine imine	Nitron
Structure			
<i>pseudodiradical</i>	<i>carbenoid</i>	<i>pseudoradical</i>	<i>zwitterionic</i>
Reactivity			
<i>pdr-type</i>	<i>cb-type</i>	<i>pmr-type</i>	<i>zw-type</i>

**Chart 10.1** Classification of 32CA reactions depending on the electronic structure of TACs and their reactivity.

Although 32CA reactions lack a general reactivity model like DA reactions and present lower selectivities than the latter, the local reactivity and preferred regioisomeric reaction path can be equally ascertained through the analysis of the Parr functions. In the following, we will present two representative examples.

In 2009, Sibi et al. [134] showed that the 32CA reaction of nucleophilic nitrile ylide **17** with electrophilic chiral oxazolidinone **18** takes place in high yield and high regio- and stereoselectivities (see Scheme 10.6).



**Scheme 10.6** 32CA reaction of nitrile ylide **17** with chiral oxazolidinone **18** yielding pyrrolines **19**.

Analysis of the nucleophilic  $P_k^-$  Parr functions of nitrile ylide **17** indicates that the carbenoid C1 carbon is the most nucleophilic center of this species with the maximum value of  $P_k^- = 0.59$ , while the electrophilic  $P_k^+$  Parr functions of oxazolidinone **18** indicate that the  $\beta$ -conjugated C5 carbon is the most electrophilic center,  $P_k^+ = 0.48$  (see Figure 10.4) [136]. Consequently, the most favorable interaction along this polar reaction is that between the carbenoid C1 carbon of nitrile ylide **17** and the  $\beta$ -conjugated C5 carbon, in clear agreement with the experimental outcomes.

Another example of complete regioselectivity is the 32CA reaction of nitrile oxide **20** with 2,2,4,4-tetramethyl-3-thioxocyclobutan-1-one **21** as a thioketone derivative, experimentally studied by Mlostoń et al. [137], which affords the corresponding 1-oxo-3-thio-4,5-dihydro-azole derivative **22** in good (58%) yield, quite C-S chemoselectivity, and complete regioselectivity with no formation of

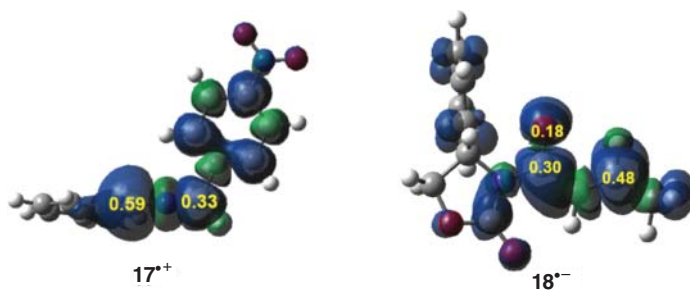
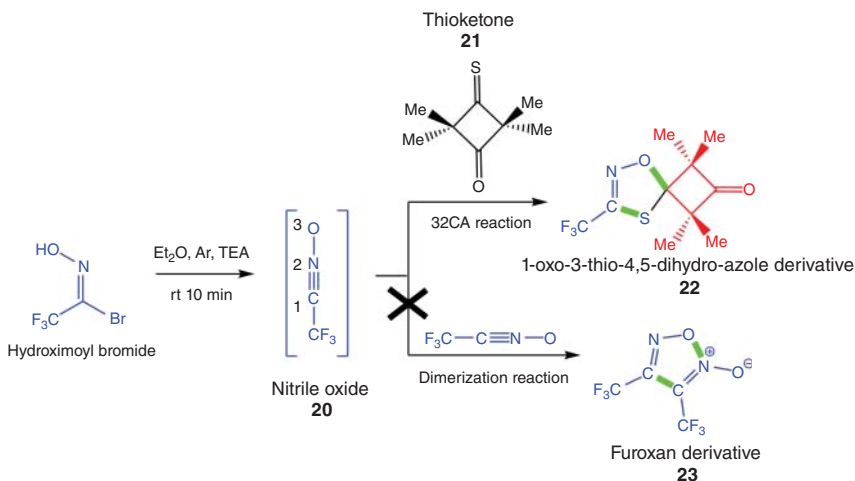


**Figure 10.4** 3D representations of the Mulliken ASD of the radical cation  $17^+$  and radical anion  $18^-$ , together with the nucleophilic  $P_k^-$  and electrophilic  $P_k^+$  Parr functions of **17** and **18**, respectively. Source: Emamian et al. [135]/Royal Society of Chemistry.

furoxan derivative **23** from the competitive dimerization process of nitrile oxide **20** (see Scheme 10.7).



**Scheme 10.7** 32CA reaction of *in situ* – generated nitrile oxide **20** with thioketone **21**, yielding cycloadduct **22** as the only product experimentally isolated.

Analysis of the calculated electrophilic  $P_k^+$  Parr functions at the reactive sites of nitrile oxide **20** indicates that the C1 carbon atom,  $P_k^+ = 0.30$ , is noticeably more electrophilic than the O3 oxygen atom,  $P_k^+ = 0.13$  [135]. Note that in this case the electrophilic  $P_k^+$  Parr functions are analyzed at the TAC framework because this reaction is classified as of reverse electron density flux (REDF) [128]. On the other hand, the nucleophilic  $P_k^-$  Parr functions in thioketone **21** indicate that while the  $P_k^-$  value at the S5 sulfur atom ( $P_k^- = 0.67$ ) is larger than that at the O7 oxygen atom ( $P_k^- = 0.21$ ) by more than three times, both C4 and C6 carbons are deactivated nucleophilic centers with negative  $P_k^-$  values. Therefore, the Parr functions predict that the most favorable path will involve the C1 carbon atom of nitrile oxide **20** and the S5 sulfur atom of thioketone **21**, in clear agreement with the chemo- and regioselectivity experimentally observed [137] (Figure 10.5).

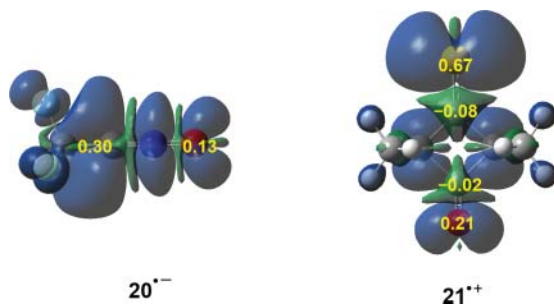
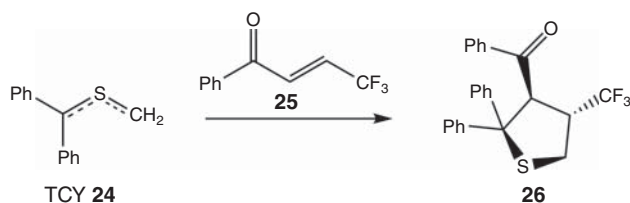


**Figure 10.5** 3D representations of the Mulliken ASD of the radical anion  $20^{\bullet-}$  and radical cation  $21^{\bullet+}$ , together with the electrophilic  $P_k^+$  and nucleophilic  $P_k^-$  Parr functions of  $20$  and  $21$ , respectively.

### 10.3.3 Chemoselectivity in 32CA Reactions

Chemoselectivity is the preferential reaction of a chemical reagent with one of two or more different functional groups [131]. In 2016, Mlostoń et al. reported the 32CA reactions of thiocarbonyl S-methanides (TCY) with fluorinated enones [138]. In the case of enones containing the  $\text{CF}_3\text{CH}=\text{CH}$  moiety, the 32CA reaction takes place chemo- and regioselectively onto the  $\text{C}=\text{C}$  double bond to give trifluoromethylated tetrahydrothiophenes (Scheme 10.8).



In these 32CA reactions, TCY **24** participates as a strong nucleophile toward the electrophilic fluorinated enone **25** [139]. Thus, the nucleophilic Parr functions were computed at TCY **24** and the electrophilic Parr functions were evaluated at enone **25**. The corresponding values are shown in Figure 10.6. Analysis of Parr functions

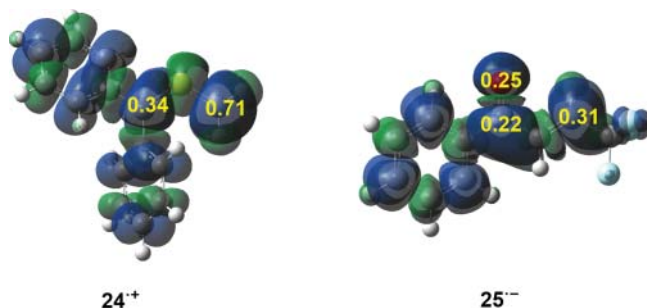
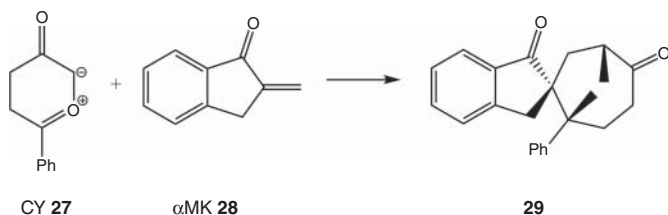


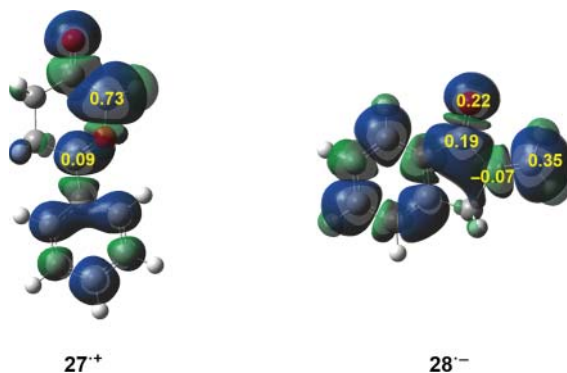
**Figure 10.6** 3D representations of the Mulliken ASD of the radical cation  $24^{\bullet+}$  and radical anion  $25^{\bullet-}$ , together with the nucleophilic  $P_k^-$  and electrophilic  $P_k^+$  Parr functions of **24** and **25**, respectively.





**Scheme 10.9** 32CA reaction of CY 27 with  $\alpha$ MK 28.

**Figure 10.7** 3D representations of the Mulliken ASD of the radical cation  $27^{+\cdot}$  and radical anion  $28^{\cdot-}$ , together with the nucleophilic  $P_k^-$  and electrophilic  $P_k^+$  Parr functions of 27 and 28, respectively.



shows that the most nucleophilic center of TCY **24** is the C2 carbon, while the most electrophilic center of enone **25** is the C3 carbon, indicating that the most favorable nucleophile–electrophile interaction is in agreement with the experimentally observed regioselectivity.

On the other hand, Muthusamy et al. [140] reported the stereo-, regio-, and chemoselective syntheses of oxa-bridged spirocycles by the 32CA reaction of the Padwa carbonyl ylide (CY) **27** with the  $\alpha$ -methylene ketone ( $\alpha$ MK) **28** (see Scheme 10.9).

As CY **27** is a strong nucleophile and  $\alpha$ MK **28** is a strong electrophile, the nucleophilic  $P_k^-$  and electrophilic  $P_k^+$  Parr functions were analyzed, respectively [141]. As can be observed in Figure 10.7, the Parr functions predict that the most favorable two-center interaction is that between the most nucleophilic C3 carbon of CY **27** and the most electrophilic C6 carbon of  $\alpha$ MK **28**, in total agreement with the regio- and the chemoselectivity experimentally observed.

## 10.4 Conclusions and Perspective

We have provided a short review of the use of the electron density as primary variable in understanding the regio-, chemo-, and pseudocyclic selectivities in cycloaddition reactions. As discussed above, while the FMO picture has certainly been of great use, the electron density gives us not only more information, but also in a more meaningful way. The very enticing prospect of relying on well-established physical

principles, and the fact that we can use a simple mathematical framework to gain further insight as to how to combine different descriptors are powerful reasons to prefer the electron density description of reactivity. This is amplified by the success of simple (and inexpensive) computational workflows, especially those used within MEDT, which provide accurate predictions over diverse families of reactions.

All of this is not to say that there are areas that deserve a closer look in the study of local reactivity. For instance, the methods described here usually perform better in polar reactions controlled by the GEDT effect, but not so much when electrostatic interactions (and/or polarization) are paramount. Other important factors, like steric effects, are also hard to incorporate into this framework. Moreover, in some cases it might be necessary to take into account the influence of the molecular surroundings on the descriptors used to understand the reactivity. These are some of the challenges facing the electron density-based description of chemical reactivity, which we anticipate will motivate further work in this field.

## References

- 1 Pauling, L. (1960). *The Nature of the Chemical Bond*, vol. 3. Ithaca: Cornell UP.
- 2 Pauling, L. (1949). A Resonating-Valence-Bond Theory of Metals and Inter-metallic Compounds. *Proceedings of the Royal Society A: Mathematical, Physical and Engineering Sciences*, vol. 196, 343.
- 3 Helgaker, T., Jørgensen, P., and Olsen, J. (2000). *Modern Electronic Structure Theory*. Chichester: Wiley.
- 4 Sharma, S., Holmes, A.A., Jeanmariet, G. et al. (2017). *J. Chem. Theory Comp.* 13: 1595.
- 5 Tribedi, S., Chakraborty, A., and Maitra, R. (2020). *J. Chem. Theory Comp.* 16: 6317.
- 6 Johnson, P.A., Limacher, P.A., Kim, T.D. et al. (2017). *Comput. Theor. Chem.* 1116: 207.
- 7 Nakatani, N. and Guo, S. (2017). *J. Chem. Phys.* 146: 094102.
- 8 Fukui, K. (1981). *Acc. Chem. Res.* 14: 363.
- 9 Fukui, K. (1975). *Theory of Orientation and Stereoselection*. Berlin: Springer-Verlag.
- 10 Fukui, K., Yonezawa, T., and Nagata, C. (1954). *Bull. Chem. Soc. Japan* 27: 423.
- 11 Fukui, K., Yonezawa, T., and Nagata, C. (1953). *J. Chem. Phys.* 21: 174.
- 12 Fukui, K., Yonezawa, T., and Shingu, H. (1952). *J. Chem. Phys.* 20: 722.
- 13 McWeeny, R. and Pickup, B.T. (1980). *Rep. Prog. Phys.* 43: 1065.
- 14 van Vleck, J.H. and Sherman, A. (1935). *Rev. Mod. Phys.* 7: 167.
- 15 Mulliken, R.S. (1955). *J. Chem. Phys.* 23: 1833.
- 16 Mulliken, R.S. (1955). *J. Chem. Phys.* 23: 1841.
- 17 Mulliken, R.S. (1955). *J. Chem. Phys.* 23: 2343.
- 18 Mulliken, R.S. (1955). *J. Chem. Phys.* 23: 2338.
- 19 Kohn, W. and Sham, L. (1965). *J. Phys. Rev.* 140: A1133.
- 20 Hohenberg, P. and Kohn, W. (1964). *Phys. Rev.* 136: B864.

- 21 Parr, R.G. and Yang, W. (1989). *Density-Functional Theory of Atoms and Molecules*. New York: Oxford UP.
- 22 Koch, W. and Holthausen, M. C. Wiley-VCH: New York, 2001; Vol. 2nd.
- 23 Heidar-Zadeh, F. and Ayers, P.W. (2015). *J. Chem. Phys.* 142: 044107.
- 24 Verstraelen, T., Ayers, P.W., Van Speybroeck, V., and Waroquier, M. (2013). *J. Chem. Theory Comp.* 9: 2221.
- 25 Bultinck, P., Ayers, P.W., Fias, S. et al. (2007). *Chem. Phys. Lett.* 444: 205.
- 26 Bultinck, P., Van Alsenoy, C., Ayers, P.W., and Carbó-Dorca, R. (2007). *J. Chem. Phys.* 126: 144111.
- 27 Ayers, P.W. (2006). *Theor. Chem. Acc.* 115: 370.
- 28 Parr, R.G., Ayers, P.W., and Nalewajski, R.F. (2005). *J. Phys. Chem. A* 109: 3957.
- 29 Bultinck, P., Cardenas, C., Fuentealba, P. et al. (2013). *J. Chem. Theory Comp.* 9: 4779.
- 30 Verstraelen, T., Sukhomlinov, S.V., Van Speybroeck, V. et al. (2012). *J. Phys. Chem. C* 116: 490.
- 31 Murray, J.S. and Politzer, P. (2011). *WIREs* 1: 153.
- 32 Van Damme, S., Bultinck, P., and Fias, S. (2009). *J. Chem. Theory Comp.* 5: 334.
- 33 Parr, R.G., Donnelly, R.A., Levy, M., and Palke, W.E. (1978). *J. Chem. Phys.* 68: 3801.
- 34 Geerlings, P., De Proft, F., and Langenaeker, W. (2003). *Chem. Rev.* 103: 1793.
- 35 Johnson, P.A., Bartolotti, L.J., Ayers, P.W. et al. (2012). *Modern Charge Density Analysis* (ed. C. Gatti and P. Macchi), 715. New York: Springer.
- 36 Miranda-Quintana, R.A. (2018). Density functional theory for chemical reactivity. In: *Conceptual Density Functional Theory and its Applications in the Chemical Domain* (ed. N. Islam and S. Kaya), 15. New Jersey: Apple Academic Press.
- 37 Ayers, P.W. and Parr, R.G. (2001). *J. Am. Chem. Soc.* 123: 2007.
- 38 Ayers, P.W. and Parr, R.G. (2000). *J. Am. Chem. Soc.* 122: 2010.
- 39 Miranda-Quintana, R.A., Heidar-Zadeh, F., and Ayers, P.W. (2018). *J. Phys. Chem. Lett.* 9: 4344.
- 40 Ayers, P.W. (2005). *J. Chem. Phys.* 122: 141102.
- 41 Miranda-Quintana, R.A. and Ayers, P.W. (2018). *J. Chem. Phys.* 148: 196101.
- 42 Chattaraj, P.K., Nath, S., and Sannigrahi, A.B. (1993). *Chem. Phys. Lett.* 212: 223.
- 43 Pearson, R.G. (1993). *Acc. Chem. Res.* 26: 250.
- 44 Pearson, R.G. and Palke, W.E. (1992). *J. Phys. Chem.* 96: 3283.
- 45 Parr, R.G. and Chattaraj, P.K. (1991). *J. Am. Chem. Soc.* 113: 1854.
- 46 Miranda-Quintana, R.A. (2017). *J. Chem. Phys.* 146: 046101.
- 47 Miranda-Quintana, R.A., Chattaraj, P.K., and Ayers, P.W. (2017). *J. Chem. Phys.* 147: 124103.
- 48 Pan, S., Sola, M., and Chattaraj, P.K. (2013). *J. Phys. Chem. A* 117: 1843.
- 49 Morell, C., Labet, V., Grand, A., and Chermette, H. (2009). *Phys. Chem. Chem. Phys.* 11: 3414.
- 50 Noorizadeh, S. (2007). *Chin. J. Chem.* 25: 1439.
- 51 Yang, W.T., Parr, R.G., and Pucci, R. (1984). *J. Chem. Phys.* 81: 2862.

- 52 Ayers, P.W. and Levy, M. (2000). *Theor. Chem. Acc.* 103: 353.
- 53 Klopman, G. and Klopman, G. (1974). *Chemical Reactivity and Reaction Paths*, 55. Wiley-Interscience: New York.
- 54 Klopman, G. (1968). *J. Am. Chem. Soc.* 90: 223.
- 55 Hudson, R.F. and Klopman, G. (1967). *Tetrahedron Lett.* 12: 1103.
- 56 Klopman, G. and Hudson, R.F. (1967). *Theor. Chim. Act.* 8: 165.
- 57 Parr, R.G. and Yang, W.T. (1984). *J. Am. Chem. Soc.* 106: 4049.
- 58 Klopman, G. (1964). *J. Am. Chem. Soc.* 86: 1463.
- 59 Salem, L. (1972). *The Molecular Orbital Theory of Conjugated Systems*. Reading, MA: W.A. Benjamin.
- 60 Salem, L. (1969). *Chem. Britain* 5: 449.
- 61 Salem, L. (1968). *J. Am. Chem. Soc.* 90: 553.
- 62 Salem, L. (1968). *J. Am. Chem. Soc.* 90: 543.
- 63 Parr, R.G. (1994). *Int. J. Quantum Chem.* 49: 739.
- 64 Miranda-Quintana, R.A., Ayers, P.W., and Heidar-Zadeh, F. (2021). *Chemistry Select* 6: 96.
- 65 Miranda-Quintana, R.A. and Ayers, P.W. (2019). *Theor. Chem. Acc.* 138: 44.
- 66 Miranda-Quintana, R.A. and Ayers, P.W. (2018). *Theor. Chem. Acc.* 137: 177.
- 67 Ayers, P.W. (2007). *Faraday Discuss.* 135: 161.
- 68 Ayers, P.W., Parr, R.G., and Pearson, R.G. (2006). *J. Chem. Phys.* 124: 194107.
- 69 Yang, W.T., Zhang, Y.K., and Ayers, P.W. (2000). *Phys. Rev. Lett.* 84: 5172.
- 70 Ayers, P.W. (2008). *J. Math. Chem.* 43: 285.
- 71 Perdew, J.P., Parr, R.G., Levy, M., and Balduz, J.L. Jr. (1982). *Phys. Rev. Lett.* 49: 1691.
- 72 Miranda-Quintana, R.A. and Bochicchio, R.C. (2014). *Chem. Phys. Lett.* 593: 35.
- 73 Bochicchio, R.C., Miranda-Quintana, R.A., and Rial, D. (2013). *J. Chem. Phys.* 139: 191101.
- 74 Parr, R.G. and Bartolotti, L.J. (1982). *J. Am. Chem. Soc.* 104: 3801.
- 75 Fuentealba, P. and Cardenas, C. (2013). *J. Mol. Model.* 19: 2849.
- 76 Parr, R.G. and Pearson, R.G. (1983). *J. Am. Chem. Soc.* 105: 7512.
- 77 Miranda-Quintana, R.A. and Ayers, P.W. (2018). Grand-canonical interpolation models. In: *Conceptual Density Functional Theory and its Applications in the Chemical Domain* (ed. N. Islam and S. Kaya), 61. New Jersey: Apple Academic Press.
- 78 Miranda-Quintana, R.A. and Ayers, P.W. (2016). *J. Chem. Phys.* 144: 244112.
- 79 Yang, W.T. and Mortier, W.J. (1986). *J. Am. Chem. Soc.* 108: 5708.
- 80 Bultinck, P., Fias, S., Alsenoy, C.V. et al. (2007). *J. Chem. Phys.* 127: 034102.
- 81 Miranda-Quintana, R.A. (2016). *Chem. Phys. Lett.* 658: 328.
- 82 Perez, P., Chamorro, E., and Ayers, P.W. (2008). *J. Chem. Phys.* 128: 204108.
- 83 Chamorro, E., Perez, P., Duque, M. et al. (2008). *J. Chem. Phys.* 129: 064117.
- 84 Chamorro, E., De Proft, F., and Geerlings, P. (2005). *J. Chem. Phys.* 123: 154104.
- 85 Chamorro, E., De Proft, F., and Geerlings, P. (2005). *J. Chem. Phys.* 123: 084104.
- 86 Chamorro, E. and Perez, P. (2005). *J. Chem. Phys.* 123: 114107.
- 87 Miranda-Quintana, R.A. and Ayers, P.W. (2016). *Theor. Chem. Acc.* 135: 239.

- 88 Miranda-Quintana, R.A., Franco-Pérez, M., Gazquez, J.L. et al. (2018). *J. Chem. Phys.* 149: 124110.
- 89 Franco-Pérez, M., Gazquez, J.L., Ayers, P.W., and Vela, A. (2018). *J. Chem. Theory Comp.* 14: 597.
- 90 Franco-Pérez, M., Heidar-Zadeh, F., Ayers, P.W. et al. (2017). *Phys. Chem. Chem. Phys.* 19: 11588.
- 91 Franco-Pérez, M., Ayers, P.W., Gazquez, J.L., and Vela, A. (2017). *Phys. Chem. Chem. Phys.* 19: 13687.
- 92 Franco-Pérez, M., Gazquez, J.L., Ayers, P.W., and Vela, A. (2017). *J. Chem. Phys.* 147: 074113.
- 93 Franco-Pérez, M., Ayers, P.W., Gazquez, J.L., and Vela, A. (2017). *J. Chem. Phys.* 147: 094105.
- 94 Franco-Pérez, M., Ayers, P., Gazquez, J.L., and Vela, A. (2015). *J. Chem. Phys.* 143: 244117.
- 95 Franco-Pérez, M., Gazquez, J.L., Ayers, P., and Vela, A. (2015). *J. Chem. Phys.* 143: 154103.
- 96 Miranda-Quintana, R.A. and Ayers, P.W. (2016). *Phys. Chem. Chem. Phys.* 18: 15070.
- 97 Miranda-Quintana, R.A. (2017). *J. Chem. Phys.* 146: 214113.
- 98 Anderson, J.S.M. and Ayers, P.W. (2014). *Comput. Theor. Chem.* 1043: 1.
- 99 Torrent-Sucarrat, M., De Proft, F., Ayers, P.W., and Geerlings, P. (2010). *Phys. Chem. Chem. Phys.* 12: 1072.
- 100 Faver, J. and Merz, K.M. (2010). *J. Chem. Theory Comp.* 6: 548.
- 101 Gayatri, G. and Sastry, G.N. (2005). *J. Chem. Sci.* 117: 573.
- 102 Pinter, B., De Proft, F., Veszpremi, T., and Geerlings, P. (2005). *J. Chem. Sci.* 117: 561.
- 103 Chandrakumar, K.R.S. and Pal, S. (2003). *J. Phys. Chem. A* 107: 5755.
- 104 Chandrakumar, K.R.S. and Pal, S. (2002). *J. Phys. Chem. A* 106: 5737.
- 105 Damoun, S., VandeWoude, G., Mendez, F., and Geerlings, P. (1997). *J. Phys. Chem. A* 101: 886.
- 106 Miranda-Quintana, R.A., Kim, T.D., Heidar-Zadeh, F., and Ayers, P.W. (2019). *J. Math. Chem.* 57: 1755.
- 107 Miranda-Quintana, R.A., Cruz-Rodes, R., Codorniu-Hernandez, E., and Batista-Leyva, A.J. (2010). *J. Math. Chem.* 47: 1344.
- 108 Ponti, A. (2000). *J. Phys. Chem. A* 104: 8843.
- 109 Chattaraj, P.K. (2007). *Indian J. Phys. Proc. Indian Assoc. Cultiv. Sci.* 81: 871.
- 110 Chattaraj, P.K., Sarkar, U., and Roy, D.R. (2006). *Chem. Rev.* 106: 2065.
- 111 Chattaraj, P.K., Maiti, B., and Sarkar, U. (2003). *J. Phys. Chem. A* 107: 4973.
- 112 Geerlings, P. and De Proft, F. (2008). *Phys. Chem. Chem. Phys.* 10: 3028.
- 113 Morell, C., Ayers, P.W., Grand, A. et al. (2008). *Phys. Chem. Chem. Phys.* 10: 7239.
- 114 Morell, C., Grand, A., and Toro-Labbé, A. (2005). *J. Phys. Chem. A* 109: 205.
- 115 Geerlings, P., Ayers, P.W., Toro-Labbe, A. et al. (2012). *Acc. Chem. Res.* 45: 683.
- 116 Jaque, P., Correa, J.V., De Proft, F. et al. (2010). *Can. J. Chem.-Revue Can. De Chim.* 88: 858.

- 117 Sablon, N., de Proft, F., and Geerlings, P. (2009). *Croat. Chem. Acta* 82: 157.
- 118 Ayers, P.W., Morell, C., De Proft, F., and Geerlings, P. (2007). *Chem., Eur. J.* 13: 8240.
- 119 De Proft, F., Ayers, P.W., Fias, S., and Geerlings, P. (2006). *J. Chem. Phys.* 125: 214101.
- 120 Chattaraj, P.K., Fuentealba, P., Gomez, B., and Contreras, R. (2000). *J. Am. Chem. Soc.* 122: 348.
- 121 Tognetti, V., Morell, C., Ayers, P.W. et al. (2013). *Phys. Chem. Chem. Phys.* 15: 14465.
- 122 Domingo, L.R., Ríos-Gutiérrez, M., Chamorro, E., and Pérez, P. (2016). *ChemistrySelect* 1: 6026–6039.
- 123 Domingo, L.R., Ríos-Gutiérrez, M., and Pérez, P. (2018). *Molecules* 23: 1913.
- 124 Domingo, L.R. (2014). *RSC Adv.* 4: 32415–32428.
- 125 Sepulcri, P., Hallé, J.C., Goumont, R. et al. (1999). *Org. Chem.* 64: 9254–9257.
- 126 Arroyo, P., Picher, M.T., Domingo, L.R., and Terrier, F. (2005). *Tetrahedron* 61: 7359–7365.
- 127 Domingo, L.R. and Aurell, M.J. (2002). *J. Org. Chem.* 67: 959–965.
- 128 Domingo, L.R., Ríos-Gutiérrez, M., and Pérez, P. (2020). *RSC Adv.* 10: 15394–15405.
- 129 Takasu, K., Ueno, M., Inanaga, K., and Ihara, M. (2004). *J. Org. Chem.* 69: 517–521.
- 130 Arnó, M., Zaragoza, R.J., and Domingo, L.R. (2005). *Eur. J. Org. Chem.* 3973–3979.
- 131 IUPAC (1997). *Compendium of Chemical Terminology, 2. (the "Gold Book")* (ed. A.D. McNaught and A. Wilkinson). Blackwell Scientific Publications, Oxford. Online version (2019-) created by S. J. Chalk. ISBN 0-9678550-9-8.
- 132 Domingo, L.R., Sáez, J.A., Zaragoza, R.J., and Arnó, M. (2008). *J. Org. Chem.* 73: 8791–8799.
- 133 Ríos-Gutiérrez, M. and Domingo, L.R. (2019). *Eur. J. Org. Chem.* 267–282.
- 134 Sibi, M.P., Soeta, T., and Jasperse, C.P. (2009). *Org. Lett.* 11: 5366.
- 135 Emamian, S., Lu, T., Domingo, L.R. et al. (2018). *Chem. Phys.* 501: 128–137.
- 136 Domingo, L.R., Ríos-Gutiérrez, M., and Pérez, P. (2016). *Org. Biomol. Chem.* 14: 10427.
- 137 Mlostoń, G., Kowalski, M.K., Objalska, E., and Heimgartner, H. (2017). *J. Fluorine Chem.* 99: 92.
- 138 Mlostoń, G., Grzelak, P., and Heimgartner, H. (2016). *J. Fluorine Chem.* 190: 56–60.
- 139 Benhamed, L., Mekelleche, S.M., Benchouk, W. et al. (2020). *ChemistrySelect* 5: 12791–12806.
- 140 Muthusamy, S., Krishnamurthi, J., and Nethaji, M. (2005). *Chem. Commun.* 3862–3864.
- 141 Benchouk, W., Mekelleche, S.M., Aurell, M.J., and Domingo, L.R. (2009). *Tetrahedron* 65: 4644–4651.

# 11

## Charge Transfer Models in Conceptual DFT

Alberto Vela<sup>1</sup>, José L. Gázquez<sup>2</sup>, and Ulises Orozco-Valencia<sup>3</sup>

<sup>1</sup>Cinvestav, Departamento de Química, Av. IPN, 07360 Alcaldía Gustavo A. Madero, CDMX, México

<sup>2</sup>Universidad Autónoma Metropolitana-Iztapalapa, Departamento de Química, Av. San Rafael Atlixco 186, 09340 Alcaldía Iztapalapa, CDMX, México

<sup>3</sup>Universidad de Sonora, Departamento de Investigación en Polímeros y Materiales, Rosales y Blvd. Luis Encinas S/N, Col. Centro, Edificio 3G, 83000 Hermosillo, México

### 11.1 Introduction

One of the aims of chemistry is to understand the outcome of putting together two or more chemicals, under some given conditions. In other words, one aspires having a predictive model for the reaction



where  $R_i$ ,  $i = 1, 2, \dots, N_R$  represents a set of  $N_R$  molecules with positions where different chemical groups are substituted,  $T$  is a fixed “target,” and within the products, there is normally one that is the desired product. As indicated in Eq. (11.1), the reactions are done under certain conditions. Determining how efficient is a reaction is evaluated by measuring thermodynamic quantities like equilibrium constants, or kinetic properties like rate constants. The scenario just described is the typical study that we call *chemical reactivity*. Therefore, after a chemical reactivity study is done, one has a table associating each of the reactant molecules  $R_i$  with either an equilibrium or a rate constant, sometimes both, or probably another property like the position of an IR or NMR signal. This information can now be used to develop a predictive model using properties of the  $R_i$  and  $T$  reactants. One of the most successful approaches in this direction is the quantitative structure–activity relation (QSAR), which is crucial in many important chemical industries like the pharmaceutical, oil, catalysis, pesticide, food, and materials [1–3]. Understanding why a reaction proceeds as it does, and with the thermodynamic and kinetic properties observed, means that one has elucidated the reaction mechanism. This reaction mechanism consists of a series of elementary steps, leading to the formation of the products. Let us assume that the energy profile of the crucial step in the mechanism has the shape depicted in Figure 11.1. This profile describes the typical behavior of the energy as a function of the reaction coordinate corresponding to an association reaction, and the

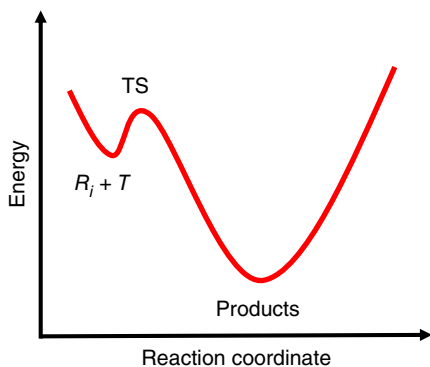


**Figure 11.1** Association reaction. Schematic representation of the energy profile of an association reaction.

point to be noted is that the difference of the values of the reaction coordinate for the reactants  $R_i + T$  and the transition state  $TS$  is small and, therefore, the geometries of the reacting species will be very similar to those of the free species. In Sections 11.3, 11.6, and 11.7, it will be shown how this association reaction is studied with the tools available in conceptual density functional theory (CDFT). It should be mentioned that within CDFT there are other approaches to describe charge transfer, like the electronegativity equalization method [4–6], which will not be discussed in this chapter. The reader is encouraged to see Chapters 2–4 for a deeper review of the fundamentals of CDFT.

## 11.2 Taylor Expansion of the Energy

From the cornerstone of density functional theory (DFT), the Hohenberg and Kohn (HK) theorems, it is concluded that the total energy  $E$  of a system with  $N$  electrons and in the presence of the external potential  $v(\mathbf{r})$  is a *function* of  $N$  and a *functional* of  $v(\mathbf{r})$ , i.e.  $E(N)[v(\mathbf{r})]$ , where the *function*-like dependence is denoted by  $(N)$  and the *functional*-like dependence by  $[v(\mathbf{r})]$ . Assuming that  $E(N)[v(\mathbf{r})]$  is differentiable with respect to both variables, one can write, up to third order, the Taylor series expansion of the energy as [7, 8]

$$\begin{aligned}
 & E(N_0 + \Delta N)[v_0(\mathbf{r}) + \Delta v(\mathbf{r})] - E(N_0)[v_0(\mathbf{r})] \\
 &= \mu \Delta N + \int d\mathbf{r} \rho(\mathbf{r}) \Delta v(\mathbf{r}) \\
 &+ \frac{1}{2} \eta (\Delta N)^2 + \int d\mathbf{r} f(\mathbf{r}) \Delta N \Delta v(\mathbf{r}) + \frac{1}{2} \iint d\mathbf{r} d\mathbf{r}' \chi(\mathbf{r}, \mathbf{r}') \Delta v(\mathbf{r}) \Delta v(\mathbf{r}') \\
 &+ \frac{1}{3!} \gamma (\Delta N)^3 + \frac{1}{2} \int d\mathbf{r} f^{(2)}(\mathbf{r}) (\Delta N)^2 \Delta v(\mathbf{r}) \\
 &+ \frac{1}{2} \iint d\mathbf{r} d\mathbf{r}' \left( \frac{\partial \chi(\mathbf{r}, \mathbf{r}')}{\partial N} \right)_{v(\mathbf{r})} \Delta N \Delta v(\mathbf{r}) \Delta v(\mathbf{r}') \\
 &+ \frac{1}{3!} \iiint d\mathbf{r} d\mathbf{r}' d\mathbf{r}'' \chi^{(2)}(\mathbf{r}, \mathbf{r}', \mathbf{r}'') \Delta v(\mathbf{r}) \Delta v(\mathbf{r}') \Delta v(\mathbf{r}'') + \dots
 \end{aligned}
 \tag{11.2}$$



In this expression, the quantities multiplying the changes in the number of electrons and/or the external potential are the reactivity coefficients, that have been studied extensively by several groups in the past three decades and that are also more deeply discussed in Chapters 2 through 4 of this book. For our purposes, one can say that these responses can be classified in **global**, **local**, and **non-local**. The global response coefficients are quantities that are associated to the chemical species as a whole, and in Eq. (11.2), we include the chemical potential,  $\mu$  [9], the chemical hardness,  $\eta$  [10, 11], and the first hyperhardness,  $\gamma$  [12]. The local response coefficients or indexes are quantities depending on one point in space and shown in the previous expansion are the electron density,  $\rho(\mathbf{r})$ , the Fukui function,  $f(\mathbf{r})$  [13, 14], and the dual descriptor,  $f^{(2)}(\mathbf{r})$  [15–17]. Finally, non-local indexes are response quantities depending on two or more points in space; so far, of the three non-local coefficients shown in Eq. (11.2), the linear response function,  $\chi(\mathbf{r}, \mathbf{r}')$  is the one that has been explored in more detail [18–20]. In Chapters 2, 3, 4, 7, 8, 14, and 15 of this book the reader can see the rich chemical information contained in these chemical response coefficients or indexes. Extracting and interpreting this information is at the heart of CDFT.

Coming back to the association reaction discussed in Section 11.1, when the values of the reaction coordinate between the reactants and the transition state are very close, then the external potential of the reactants  $v_0(\mathbf{r})$  and the external potential of the transition state  $v(\mathbf{r})$  are very similar, for every point in space, and it is reasonable assuming that for this association reaction, one can neglect the change of the external potential, i.e.  $\Delta v(\mathbf{r}) \approx 0$ . Then, the Taylor series expansion reduces to

$$\Delta E(\Delta N) = \mu \Delta N + \frac{1}{2} \eta (\Delta N)^2 + \frac{1}{3!} \gamma (\Delta N)^3 + \dots \quad (11.3)$$

meaning that in this case the change in the energy can be mainly attributed to a charge transfer process occurring between the reactants.

In Sections 11.3 and 11.6, these charge transfer processes will be explored for the case when the Taylor series expansion of the energy with respect to the number of electrons is truncated at second order, i.e.

$$\Delta E(\Delta N) = \mu \Delta N + \frac{1}{2} \eta (\Delta N)^2 \quad (11.4)$$

### 11.3 One-Parabola Model: The Venerable Parr and Pearson Model

Probably the first result that attracted the attention of the chemical community toward CDFT was the identification of the chemical potential  $\mu$  with the negative of the electronegativity. This identification was derived in a seminal paper authored by Robert G. Parr et al. [9], and it can be considered the milestone of CDFT. These authors identified the Lagrange multiplier  $\mu$ , introduced in the second HK theorem to satisfy the constraint that the electron density  $\rho(\mathbf{r})$  integrates to the correct

number of electrons  $N$ , with the chemical potential, and by the work of Iczkowski and Margrave [21], with the negative of the electronegativity,  $\chi$ , which is

$$\mu = \left( \frac{\delta E}{\delta \rho(\mathbf{r})} \right)_{v(\mathbf{r})} = \left( \frac{\partial E}{\partial N} \right)_{v(\mathbf{r})} = -\chi \quad (11.5)$$

From this identification, it is not difficult to recover, by finite differences, the definition of electronegativity provided by Robert Mulliken in 1934 [22]

$$\mu = -\chi = -\frac{I + A}{2} \quad (11.6)$$

where  $I$  is the first vertical ionization potential and  $A$  the vertical electron affinity, which are defined as

$$I = E(N - 1)[v(\mathbf{r})] - E(N)[v(\mathbf{r})] \quad (11.7)$$

and

$$A = E(N)[v(\mathbf{r})] - E(N + 1)[v(\mathbf{r})] \quad (11.8)$$

In Eqs. (11.7) and (11.8),  $E(N)[v(\mathbf{r})]$  is the ground state energy of the system with  $N$  electrons and external potential  $v(\mathbf{r})$ , using the notation introduced Section 11.2. Note that these two properties are evaluated at constant external potential, i.e. they correspond to vertical energy differences.

Few years later, in 1983, to be more specific, Parr and Pearson [10] introduced another key concept, the global hardness, defined as

$$\eta = \left( \frac{\partial^2 E}{\partial N^2} \right)_{v(\mathbf{r})} = \left( \frac{\partial \mu}{\partial N} \right)_{v(\mathbf{r})} \quad (11.9)$$

indicating that the global hardness is the concavity of the energy with respect to the number of electrons. It is also a measure of the resistance of the chemical potential to change its value when the system undergoes a change in the number of electrons. By finite differences, it can be expressed in terms of the first ionization potential and the electron affinity as

$$\eta = I - A \quad (11.10)$$

Note that the definition of the global hardness in Eq. (11.9) differs from the original by a factor of  $1/2$ . In the recent years, it has been recognized that for notational convenience, it is better dropping the  $1/2$  and, thus, defining global hardness as shown in Eq. (11.9). Together with defining hardness, Parr and Pearson, with a tremendous physical and chemical insight, made use of a continuity hypothesis for the energy and its derivatives with respect to the number of electrons, arguing that “it is convenient to consider that a smooth curve connects the various points,” where they are referring to the points of the energy corresponding to a reference number of electrons  $N_0$  and those with  $N_0 - 1$  and  $N_0 + 1$  electrons. This continuity assumption allows one writing the energy of a chemical species as a function of the number of electrons as a quadratic function (parabola) on the number of electrons shown in Eq. (11.4). This is the **one-parabola** or the **venerable Parr and Pearson (PP)** model [23]. From the discussion above, it is clear that knowing the ionization potential  $I$  and the electron affinity  $A$  suffices to obtain the chemical potential

$\mu$  and the hardness  $\eta$  that are the coefficients characterizing the parabolic PP model of Eq. (11.4).

More insight can be gained about the chemical content of this model by considering the system as an open quantum system in contact with a reservoir of electrons that fixes the chemical potential of the system and allows the exchange of electrons between the system and the bath. In this case, the grand potential  $\Omega$  determines the equilibrium and spontaneity direction of the processes. The grand potential is given by

$$\Delta\Omega(\Delta N) = \Delta E(\Delta N) - \mu_b \Delta N \quad (11.11)$$

When the chemical potential of the system,  $\mu$ , not equals that of the reservoir or bath,  $\mu_b$ , there is a spontaneous flow of electrons from the part with higher chemical potential to the part with lower chemical potential. Using Eq. (11.4), the amount of electrons involved in this process  $\Delta N$  is obtained by minimizing the change in the grand potential  $\Delta N$  and is given by

$$\Delta N = \frac{\mu_b - \mu}{\eta} \quad (11.12)$$

It is not difficult showing that the minimum energy attainable in this process corresponds to the case when the chemical potential of the bath is zero and the number of electrons exchanged in this situation is given by  $\Delta N_{\text{MAX}} = -\mu/\eta$ , which is positive. Evaluating the change in the energy for this charge transferred leads to

$$\Delta E_{\text{MIN}} = -\frac{\mu^2}{2\eta} = -\omega \quad (11.13)$$

where  $\omega$  is a new reactivity coefficient introduced by Parr et al. and is called the **electrophilicity index** [24]. This index has been widely used as it can be seen in the reviews by Chattaraj et al. [25–27].

It should be noted that the continuity of the PP model implies that the directions of charge transfer are immaterial. More precisely, with the fact that the derivative of the energy with respect to the number of electrons exists, it determines that the rate of change of the energy with respect to the number of electrons, evaluated at any integer number of electrons, is the same in any direction.

## 11.4 Derivative Discontinuities

For almost three decades, the PP model was the iconic model to study within CDFT problems where charge transfer is involved. However, it has also been severely criticized from its roots; the questionable issue is the discontinuity of the derivative of the energy with respect to the number electrons. This fundamental issue was considered from the very beginning of CDFT. In 1982, Perdew et al. [28] demonstrated that the ground state energy of a system as a function of the number of electrons, at 0 K, is composed of a series of straight lines joined at every integer number of electrons. This is the **ensemble** or **PPLB theorem**. The theorem was generalized [29, 30], and it can be stated as follows.

**Theorem 11.1** At 0 K, the dependence on the number of electrons of any size consistent property  $P$  is given by

$$P(N + \Delta N) = \begin{cases} -\Delta N P(N - 1) + (1 + \Delta N) P(N), & -1 \leq \Delta N \leq 0 \\ (1 - \Delta N) P(N) + \Delta N P(N + 1), & 0 \leq \Delta N \leq 1 \end{cases}$$

where  $N$  is any positive integer.

In this theorem, a size consistent property is defined as a property  $P$  such that if a supermolecule is composed of  $Q$  infinitely separated subsystems with wavefunctions  $\Psi_1, \Psi_2, \dots$ , and  $\Psi_Q$ , then the total value of the property in the supermolecule is the sum of the values of the properties in the subsystems, namely,

$$P_{\text{total}} = \sum_{q=1}^Q P_q \quad (11.14)$$

A very important size consistent property is the energy for which the ensemble theorem dictates that its behavior, at 0 K, as a function of the numbers of electrons is given by

$$E(N + \Delta N) = \begin{cases} E(N) + (E(N) - E(N - 1)) \Delta N, & -1 \leq \Delta N \leq 0 \\ E(N) + (E(N + 1) - E(N)) \Delta N, & 0 \leq \Delta N \leq 1 \end{cases}$$

or in terms of the ionization potential and the electron affinity,

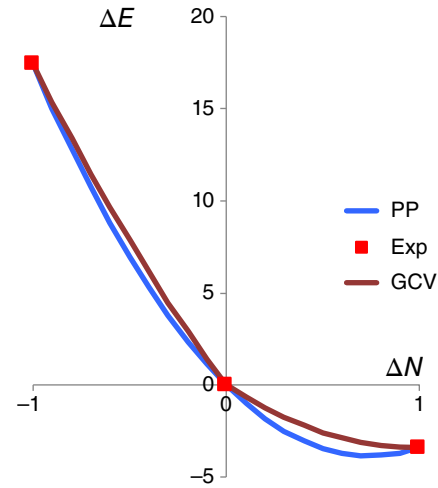
$$E(N + \Delta N) = \begin{cases} E(N) - I \Delta N, & -1 \leq \Delta N \leq 0 \\ E(N) - A \Delta N, & 0 \leq \Delta N \leq 1 \end{cases}$$

This last expression shows that indeed, at 0 K, the energy as a function of the number of electrons is a piecewise function comprised by straight lines joined at integer number of electrons. Taking  $N$  as the number of electrons of the neutral system, then the slopes of the straight lines are the negative of the ionization potential, when the number of electrons is less than  $N$ , and the negative of the electron affinity, when the number of electrons is greater than  $N$ .

## 11.5 Two-Parabola Model

A quick look of Figure 11.2 immediately tells that the PP model and the behavior predicted by the ensemble theorem are quite different. Two features are evident; first, the smooth behavior of PP going from the cation to the anion, compared with the linear behavior of the ensemble theorem, and second, the fact that at integer number of electrons, the derivatives of the energy with respect to the number of electrons coming from the left (cations) are different from those coming from the right (anions). Let us designate the derivative from the left  $\mu^-$  and that from the right  $\mu^+$ . Trying to keep the richness of the quadratic PP model but also incorporating the derivatives discontinuities was the motivation behind the two-parabola model introduced in 2007 [31]. The ansatz is very simple: it is proposed that the energy as

**Figure 11.2** Energy vs. number of electrons. The blue curve corresponds to the Parr and Pearson (PP) quadratic model, and the brown curve to the two-parabola or Gázquez, Cedillo, and Vela (GCV) model. The experimental values are for the fluorine atoms, and energies are in eV.



a function of the number of electrons is a piecewise continuous function composed of parabolas. Analytically, the function is

$$\Delta E^{+/-}(\Delta N) = \mu^{+/-} \Delta N + \frac{1}{2} \eta^{+/-} (\Delta N)^2 \quad (11.15)$$

The superindexes distinguish the cationic (−) branch from the anionic branch (+). The model has four parameters, and they are obtained imposing the following conditions: (i)  $\Delta E^{-}(-1) = I$ , (ii)  $\Delta E^{+}(1) = -A$ , (iii)  $\eta^{-} = \eta^{+} = \eta$ , and (iv)  $\eta = \mu^{+} - \mu^{-}$ . Conditions (i) and (ii) are the same used in the PP model to find the expression for  $\mu$  and  $\eta$ . Condition (iv) is supported on the fact that the derivative with respect to the number of electrons of the ensemble expression for the energy leads to a step function, and if this expression is derived again, one obtains

$$\left( \frac{\partial^2 E}{\partial N^2} \right)_{v(x)} = (\mu^{+} - \mu^{-}) \delta(\Delta N) \quad (11.16)$$

where  $\delta(x)$  is the Dirac delta function. With these conditions, one obtains the following expressions for the parameters of the model:

$$\mu^{-} = -\frac{3I + A}{4} \quad (11.17)$$

$$\mu^{+} = -\frac{I + 3A}{4} \quad (11.18)$$

and

$$\eta = \frac{I - A}{2} \quad (11.19)$$

Using Eqs. (11.15) and (11.17)–(11.19), together with the experimental values of  $I$  and  $A$  for the fluorine atom, one obtains the curves depicted in Figure 11.2. The deviations of the PP model from the ensemble theorem are noticeable, while the two-parabola model are closer to the linear behavior predicted by the ensemble theorem.

Proceeding analogously as it was done in the derivation of the electrophilicity, one can now consider an open quantum system in contact with a reservoir of electrons but with the **capability of distinguishing the direction of charge transfer**. In this case there are two grand potentials; one for the direction when the system gives away electrons, the branch labeled with the  $-$  superindex, and another corresponding to the direction when the system receives electrons, which is labeled with the  $+$  superindex. These grand potentials are

$$\Delta\Omega^{+/-}(\Delta N) = \Delta E^{+/-}(\Delta N) - \mu_b \Delta N \quad (11.20)$$

where  $\mu_b$  is the chemical potential of the reservoir. Minimizing each grand potential branch with respect to number of electrons and evaluating the corresponding energy, one obtains that

$$\Delta E^{+/-} = \frac{(\mu_b)^2 - (\mu^{+/-})^2}{2\eta} \quad (11.21)$$

Evaluating each of these energies for the case when the chemical potential of the bath is zero,  $\mu_b = 0$ , one obtains that the minimum energies for each branch are given by  $\Delta E_{MIN}^{+/-} = -\omega^{+/-}$  where  $\omega^-$  is the **electrodonating power** and  $\omega^+$  is the **electroaccepting power**, global reactivity indexes that are given by the expressions

$$\omega^{+/-} = \frac{(\mu^{+/-})^2}{2\eta} \quad (11.22)$$

that in terms of the ionization potential and electron affinity are

$$\omega^+ = \frac{1}{16} \frac{(I + 3A)^2}{(I - A)} \quad (11.23)$$

and

$$\omega^- = \frac{1}{16} \frac{(3I + A)^2}{(I - A)}$$

A deeper analysis of the charge transfer in the two-parabola model and the behavior of the electrodonating and electroaccepting powers can be found in Reference [32]. These reactivity indexes have been successfully used in classifying the observed chemical behavior of antioxidants, marine drugs, corrosion inhibitors, solar cells, and pharmaceuticals used in several neurological disorders [33–37].

As it will be discussed in Sections 11.6 and 11.7, the two-parabolas model opens the possibility of studying charge transfer reactions where the direction of electron flow can be distinguished.

## 11.6 Association Reaction

As discussed in Sections 11.1 and 11.2 of this chapter, we are interested in describing and analyzing **association reactions** of the type shown in Eq. (11.1). For notational simplicity, we will write this reactions as



where  $AB$  is the associated product. The change in the energy for this reaction is given by  $\Delta E_{AB} = E_{AB} - E_{A^0} - E_{B^0}$  where  $E_{AB}$  is the energy of the associated product and  $E_{A^0}$ ,  $E_{B^0}$  are the energies of the free reactants. Considering that the energy of the product  $AB$  as additive, i.e.  $E_{AB} \approx E_A + E_B$  where  $E_A$  and  $E_B$  are the energies of the chemical species or fragments in the molecule  $AB$ , then one can approximate the change of the energy corresponding to the association reaction by  $\Delta E_{AB} \approx \Delta E_A + \Delta E_B$ , where  $\Delta E_A = E_A - E_{A^0}$  and  $\Delta E_B = E_B - E_{B^0}$ . Recalling the consideration that the structures of  $A$  and  $B$  do not change much when they are brought from being free to be in the associated product and therefore that the changes  $\Delta v_A(\mathbf{r}) = v_A(\mathbf{r}) - v_A^0(\mathbf{r})$  and  $\Delta v_B(\mathbf{r}) = v_B(\mathbf{r}) - v_B^0(\mathbf{r})$  can be neglected, then one can write that the change of the energy of the reaction is approximately given by

$$\Delta E_{AB} \approx \Delta E_A(\Delta N_A) + \Delta E_B(\Delta N_B) \quad (11.25)$$

where it is emphasized that the only reason for the energy of the fragments to change is through changes on their corresponding number of electrons,  $N_A$  and  $N_B$ . It must be clear that provided the system is closed, the total number of electrons of the system  $N_{AB}$  is constant and equal to the sum of the number of electrons in the free fragments or species, i.e.  $N_{AB} = N_{A^0} + N_{B^0} = N_A + N_B = \text{constant}$ , implying that the changes in the number of electrons of the fragments are not independent. Rearranging the charge conservation condition, it follows that the changes in the number of electrons of the species must satisfy the *charge conservation condition*

$$\Delta N_B = -\Delta N_A \quad (11.26)$$

The amount of charge transferred in the formation of the product  $AB$  is that which minimizes the interaction energy, subject to the charge conservation constraint (Eq. (11.26)). Substituting Eq. (11.26) in Eq. (11.25) leaves only one independent variable; let us say  $\Delta N_A$ , and therefore, the amount of charge transferred is found from solving

$$\frac{\partial \Delta E_{AB}(\Delta N_A)}{\partial \Delta N_A} = \frac{\partial \Delta E_A(\Delta N_A)}{\partial \Delta N_A} + \frac{\partial \Delta E_B(-\Delta N_A)}{\partial \Delta N_A} = 0 \quad (11.27)$$

where, certainly, all the partial derivatives are taken at fixed external potential, i.e. the geometries of the species or fragments are unchanged, in compliance with our ansatz. Obtaining concrete and specific results for the amount of charge transferred in the association reaction requires establishing a model for the energy as function of the number of electrons. In Sections 11.6.1–11.6.3 and 11.7, the results provided by the PP and the two-parabola models will be discussed.

### 11.6.1 Partitioning of the Charge Transferred in the PP Model

Using the PP model for the energy (Eq. (11.4)) in the minimization condition (Eq. (11.27)) leads to solving

$$\mu_A + \eta_A \Delta N_A - \mu_B + \eta_B \Delta N_A = 0 \quad (11.28)$$

where for notational convenience we are dropping the 0 for the global reactivity indexes. Moreover, it should be clear that all these reactivity coefficients correspond

to those of the free noninteracting fragments or species. Solving this last equation for  $\Delta N_A$ , one finds that the amount of charge transferred in the association reaction is given by

$$\Delta N_A = \frac{\mu_B - \mu_A}{\eta_A + \eta_B} \quad (11.29)$$

classical and beautiful result that was derived for the first time by Sanderson [38–40] and very successfully used by Parr and Pearson in the rationalization of the hard/soft acid/base principle, the HSAB principle [41–46]. This result establishes that the gradients of the chemical potential, or electronegativity, are the driving force behind charge transfer, and it also indicates that the global hardness of the species or fragments mediates the amount of electron exchange. Another consequence is that electrons move from the fragment with higher chemical potential to that with lower. This is the spontaneous direction of electron flow.

In complete agreement with the continuity ansatz of the PP model, the total amount and direction of charge transfer is dictated by Eq. (11.29), however, it does not allow distinguishing that the processes of electron donation and electron acceptance are different, as mandated by the PPLB theorem. It has been shown [47] that one possibility to overcome this aspect of the PP model is obtained by inserting the definitions for  $\mu$  (Eq. (11.6)) and  $\eta$  (Eq. (11.10)) in Eq. (11.29), which after rearranging, it is possible to write the amount of electron transfer as the sum of two contributions:

$$\Delta N_A = - \underbrace{\frac{A_B - I_A}{2(\eta_A + \eta_B)}}_{\Delta N_A^{\text{ele}}} + \underbrace{\frac{A_A - I_B}{2(\eta_A + \eta_B)}}_{\Delta N_A^{\text{nuc}}} = -\Delta N_B \quad (11.30)$$

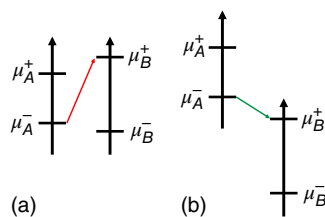
These terms can be identified as the *electrophilic (ele)* and *nucleophilic (nuc)* contributions to the total charge transferred to species *A*. The justification to call them in this way stands on the fact that considering that the global hardnesses are positive and that  $I_A > A_B \rightarrow A_B - I_A < 0$ , then  $\Delta N_A^{\text{ele}} > 0$ , species *A* is receiving electrons, and it is undergoing an electrophilic charge transfer process. A similar analysis shows that the second term indeed is negative, corresponding to a process where species *A* is donating charge, and it is undergoing a nucleophilic charge transfer process. This global partitioning of the charge transferred in the PP model was also extended to its local version. The detailed derivation of the local partitioning can be found in Reference [47]. It must be mentioned that Roy and coworkers proposed a comprehensive decomposition analysis of stabilization energy (CDASE) using an energy partitioning based on the changes of the energy of the species obtained from the PP model [48–50]

### 11.6.2 Global Charge Transfer in the Two-Parabola Model

Let us consider an association reaction  $A + B \rightarrow AB$  where *A* is donating electrons to *B* and the geometries of the fragments or species are practically unchanged when



**Figure 11.3** Alignment of chemical potentials.  
 (a) Unfavorable alignment  $\Rightarrow$  NO charge transfer.  
 (b) Favorable alignment  $\Rightarrow$  THERE IS charge transfer.



forming the association product  $AB$  from those when they are free [51, 52]. Then, since the two-parabola model distinguishes the direction of charge transfer, it is possible to write that the change in the energy to form the associated complex consists of one term related to the change in the energy of  $A$  where this species is donating electrons,  $\Delta E_A^-$ , and another related to  $B$  where this species is gaining electrons,  $\Delta E_B^+$ , that is,

$$\begin{aligned}\Delta E_{AB} &= \Delta E_A^- + \Delta E_B^+ \\ &= \mu_A^- \Delta N_A^- + \frac{1}{2} \eta_A (\Delta N_A^-)^2 + \mu_B^+ \Delta N_B^+ + \frac{1}{2} \eta_B (\Delta N_B^+)^2\end{aligned}\quad (11.31)$$

Minimizing the previous equation with respect to  $\Delta N_A^-$ , imposing charge conservation, i.e.  $\Delta N_A^- = -\Delta N_B^+$ , one obtains that the number of electrons donated from  $A$  to  $B$  is given by

$$\Delta N_A^- = \frac{\mu_B^+ - \mu_A^-}{\eta_A + \eta_B}\quad (11.32)$$

and the interaction energy is given by

$$\Delta E_{AB} = -\frac{1}{2} \frac{(\mu_B^+ - \mu_A^-)^2}{\eta_A + \eta_B}\quad (11.33)$$

It is straightforward, obtaining an expression for  $\Delta N_A^+$  considering that  $A$  is now accepting electrons from  $B$ .

Consistency in using Eq. (11.32) demands that  $\mu_A^-$  must be greater than  $\mu_B^+$ , complying that electrons flow from the species with higher chemical potential to that with smaller. However, the evaluation of the chemical potentials,  $\mu^-$  and  $\mu^+$  for the neutral and isolated species, according to Eqs. (11.17)–(11.19), will provide values aligned as shown in Figure 11.3. Figure 11.3a is the typical situation obtained for two neutral species: the chemical potentials  $\mu^-$  and  $\mu^+$  are very similar, and, as depicted, it is impossible to fulfill the condition  $\mu_A^- > \mu_B^+$ . On the contrary, Figure 11.3b clearly satisfies the condition, and, therefore, it is possible to have electron flow from  $A$  to  $B$ . To obtain this alignment, it is necessary to consider the conditions on which the reaction is taking place. Normally, one of the species in this association step has acquired charge, positive or negative, and this suffices to obtain the alignment shown. The message is that the correct application of the two-parabola model needs a clear understanding of the reaction mechanism to explain that the reacting species have their chemical potentials aligned allowing the electronic transfer among the fragments.

### 11.6.3 Local Charge Transfer in the Two-Parabola Model

The functional Taylor expansion of the energy with respect to the electron density, up to second order, is given by

$$\begin{aligned} \Delta E = & \int d\mathbf{r} \left( \frac{\delta E}{\delta \rho(\mathbf{r})} \right)_{v(\mathbf{r})} \Delta \rho(\mathbf{r}) \\ & + \frac{1}{2} \iint d\mathbf{r} d\mathbf{r}' \left( \frac{\delta^2 E}{\delta \rho(\mathbf{r}) \delta \rho(\mathbf{r}')} \right)_{v(\mathbf{r})} \Delta \rho(\mathbf{r}) \Delta \rho(\mathbf{r}') \end{aligned} \quad (11.34)$$

Substituting Eq. (11.5) for the chemical potential, identifying the second functional derivative as the hardness kernel  $\eta(\mathbf{r}, \mathbf{r}')$ , and writing the change in the electron density as  $\Delta \rho(\mathbf{r}) = f(\mathbf{r}) \Delta N$ , one has that

$$\Delta E = \int d\mathbf{r} \mu f(\mathbf{r}) \Delta N + \frac{1}{2} \iint d\mathbf{r} d\mathbf{r}' \eta(\mathbf{r}, \mathbf{r}') f(\mathbf{r}) f(\mathbf{r}') (\Delta N)^2 \quad (11.35)$$

which can be written as

$$\Delta E = \int d\mathbf{r} f(\mathbf{r}) \left[ \mu \Delta N + \frac{1}{2} \eta (\Delta N)^2 \right] = \int d\mathbf{r} \Delta \varepsilon(\mathbf{r}) \quad (11.36)$$

where we have introduced the local energy change per volume or local energy density,  $\Delta \varepsilon(\mathbf{r})$ . This equation can be written distinguishing the directions of charge transfer and using the ansatz of the two-parabola model. Then, it takes the form

$$\begin{aligned} \Delta E^{+/-} = & \int d\mathbf{r} f^{+/-}(\mathbf{r}) \left[ \mu^{+/-} \Delta N^{+/-} + \frac{1}{2} \eta (\Delta N^{+/-})^2 \right] \\ = & \int d\mathbf{r} \Delta \varepsilon^{+/-}(\mathbf{r}) \end{aligned} \quad (11.37)$$

Writing the integral over all space as a sum of integrals over the atoms comprising the molecule or fragment,

$$\begin{aligned} \Delta E^{+/-} = & \sum_k \varepsilon_k^{+/-} \\ = & \sum_k f_k^{+/-} \left[ \mu^{+/-} \Delta N^{+/-} + \frac{1}{2} \eta (\Delta N^{+/-})^2 \right] \end{aligned} \quad (11.38)$$

where the sum over  $k$  runs over the atoms in the molecule. Note that given that the term in brackets does not depend on the index  $k$ , it can be taken out of the sum, and using the fact that the integral of the Fukui function equals one, the last expression reduces correctly to the energy change in terms of the global reactivity indexes of the two-parabola model (Eq. (11.15)). Proceeding analogously as it was done in the global case, but using the local energy density  $\varepsilon$  for each of the reacting species, then, for a reaction where  $A$  gives away electrons to  $B$ , the local change in the energy density can be written as

$$\begin{aligned} \Delta \varepsilon_{ab} = & \sum_{\alpha \in A}^a \Delta \varepsilon_{\alpha}^{-} + \sum_{\beta \in B}^b \Delta \varepsilon_{\beta}^{+} \\ = & \sum_{\alpha \in A}^a f_{\alpha}^{-} \left[ \mu_{\alpha}^{-} \Delta N_{\alpha}^{-} + \frac{1}{2} \eta_{\alpha} (\Delta N_{\alpha}^{-})^2 \right] \\ & + \sum_{\beta \in B}^a f_{\beta}^{+} \left[ \mu_{\beta}^{+} \Delta N_{\beta}^{+} + \frac{1}{2} \eta_{\beta} (\Delta N_{\beta}^{+})^2 \right] \end{aligned} \quad (11.39)$$

The energy density is labeled with the indexes  $ab$  indicating that in its evaluation, one is considering  $a$  atoms from species  $A$  and  $b$  atoms from species  $B$ . The number of atoms considered must be less than the total number atoms in each fragment; otherwise, the results of the local approach will be identical to those of the local one. In the application discussed below, the determination of the number of atoms will be clarified. Minimizing Eq. (11.39) with respect to  $\Delta N_{A}^{-}$ , imposing charge conservation,  $\Delta N_{B}^{+} = -\Delta N_{A}^{-}$ , leads to the following expression for the number of electrons transferred by species  $A$  when selecting  $a$  atoms from  $A$  and  $b$  atoms from  $B$

$$\Delta N_{A,ab}^{-} = \frac{(\mu_{B}^{+} \sum_{\beta \in B}^{b} f_{\beta}^{+}) - (\mu_{A}^{-} \sum_{\alpha \in A}^{a} f_{\alpha}^{-})}{(\eta_{B} \sum_{\beta \in B}^{b} f_{\beta}^{+}) + (\eta_{A} \sum_{\alpha \in A}^{a} f_{\alpha}^{-})} \quad (11.40)$$

The successful application of the local model depends very strongly on the proper selection of the reactive atoms in species  $A$  and  $B$ , as it has been shown in the literature [53].

## 11.7 An Illustrative Application

The charge transfer models presented in Section 11.6 have been applied to the following problems: complexation reaction of nickel by alkenes (back-donation), hydration of aldehydes and ketones producing geminal diols, addition of molecular bromine to alkenes, the [4+2] Diels–Alder cycloaddition of cyclopentadiene and cyanoalkenes, back-donation of phosphines in transition metal complexes, nucleophilic reactivity of indoles, hydration of alkenes, aromatic nitration, and electron donor–acceptor complexes. These are presented and discussed in References [47, 53–57].

As an illustrative application of the formalism, the global and local two-parabola models are used to study the formation of complexes between a series of substituted nitrobenzenes and 1,3-diethylurea. These complexes are of importance in the electrochemical technique called electron transfer-controlled hydrogen bonding (ETCHB) where the strength of H-bonds is increased either by reduction of a H-acceptor or oxidation of a H-donor. The experimental binding constants ( $K_b$ ) between substituted reduced nitrobenzenes (H-acceptor) and urea derivatives (H-donor) have been recently determined [57]. The details of this problem can be found in Reference [53].

Thirteen substituted nitrobenzenes were considered. The geometries of the nitrobenzenes and 1,3-diethylurea were fully optimized, without symmetry constraints; the stationary points were characterized by a frequency analysis, showing that all the structures reported are minima on the potential energy surface. The generalized gradient approximation exchange correlation energy functional (PBE) and the split valence triple zeta with polarization basis function (TZVP) basis set were used. The condensed Fukui functions were calculated through the response-of-molecular fragment approach [58], with the scheme proposed by Yang and Mortier [59], using the Hirshfeld population analysis [60]. This problem shows very clearly the relevance of reaction conditions in the calculation of the chemical reactivity indexes necessary to evaluate the amount of charge transfer. In this case,

the electrochemical control drives the nitrobenzenes to its reduced form, i.e. they have a negative charge. Thus, the reference system nitrobenzene species is the anion, and with this reference, the chemical potentials of all nitrobenzenes are higher than the chemical potential of the diethyl urea, thus fulfilling the condition  $\mu_A^- > \mu_B^+$ . As it can be seen in Table 4 of Reference [53], the chemical potentials of the anionic nitrobenzenes are between  $-0.91$  and  $0.31$ , while the chemical potential of 1,3-diethylurea is  $-0.93$  eV. Therefore, the transfer of electrons from the nitrobenzenes to the 1,3-diethylurea is possible. The data in Table 4 of Reference [53] shows that the increase in the binding constant  $K_b$  is related with a corresponding increase in the absolute value of  $\Delta N_A^-$ . The correlation between  $K_b$  and the amount of charge transferred from the nitrobenzenes to the diethylurea is depicted in Figure 11.4. Using the values of the global reactivity indexes reported in Table 4 of Reference [53] and the condensed Fukui functions reported in this same reference, it is possible to evaluate the local charge transfer for different combinations of  $a$  atoms from the nitrobenzenes and  $b$  atoms from the 1,3-diethylurea. The protocol used in selecting the best combination or the most reactive atoms is to start with those atoms with the higher values of the condensed Fukui functions and subsequently adding atoms with lower values of the condensed Fukui functions. The pattern most frequently observed is that there are optimal combinations  $ab$  providing the best correlation coefficients. Interestingly, in several cases, the atoms associated to the best correlation do not follow the order of decreasing condensed Fukui functions. In the situation discussed here, the correlation coefficient of the linear fit is marginally better in the local model than in the global model. However, the most

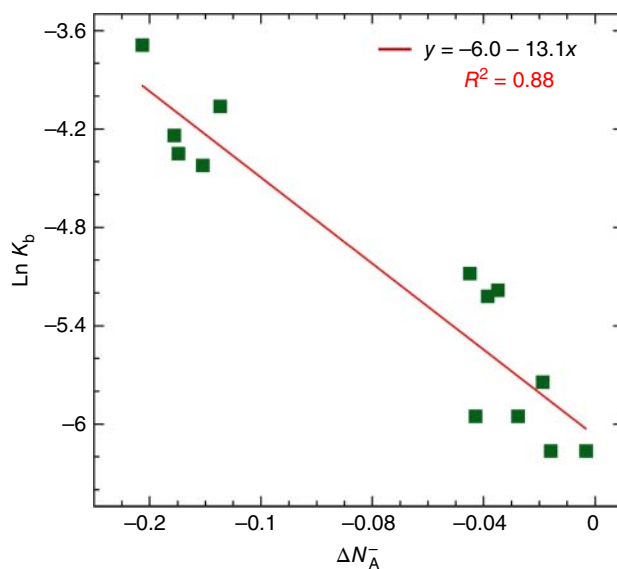


**Figure 11.4** Correlation between the binding constants  $K_b$  and the amount of GLOBAL charge transferred  $\Delta N_A^-$ . The data are from Table 4 in Reference [53]. The linear fit equation and the correlation coefficient are displayed on the top right.

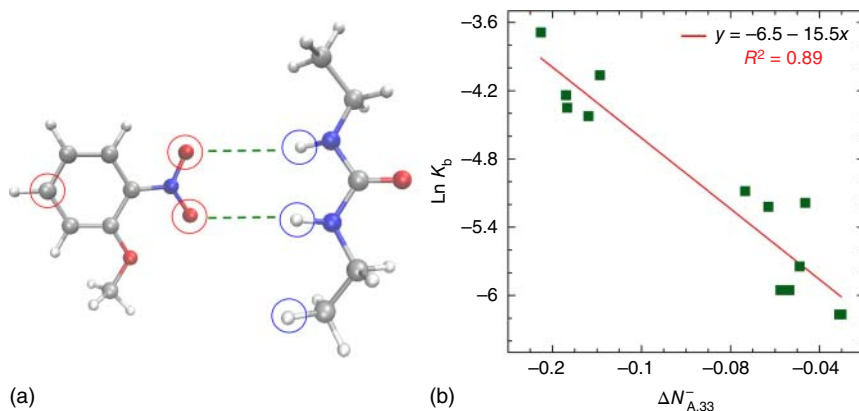


**Figure 11.5** (a) Most favourable atomic interactions predicted by the local model; (b) correlation between the binding constants  $K_b$  and the amount of LOCAL charge transferred  $\Delta N_{A,ab}^-$ . The data are from Table 4 in Reference [53]. The linear fit equation and the correlation coefficient are displayed on the top right. For this correlation, the three atoms circled in red on the nitrobenzene and the three atoms circled in blue on the 1,3-diethylurea are the ones included in the calculation of the local charge transferred. Thus, in this case,  $a = 3$  and  $b = 3$ , and consequently, the local charge transferred is denoted as  $\Delta N_{A,33}^-$ .

surprising and satisfying result is that, as it can be seen in Figure 11.5, the optimal combination of atoms in the local model, the red and blue circled atoms, is indeed those responsible for the formation of the H-bonds in the associated complex. This result shows nicely the applicability of the perturbative approach to chemical reactivity provided by CDFT.

## 11.8 Summary and Perspectives

The fundamentals of the charge transfer models developed within the context of CDFT, which are supported on the perturbative approach, were presented and used to justify that for association reactions where the geometries of the interacting species are not distorted much from their free structures, then the changes in the energy of reaction can be attributed mainly to charge transfer.

The prototypical and emblematic model proposed by Parr and Pearson, the venerable PP model, was discussed with didactic extension and intention. It was shown how from this very simple model key concepts in chemistry like electronegativity and hardness find a strong theoretical support.

The Perdew, Parr, Levy, and Balduz (PPLB), or ensemble, theorem was presented, and its consequences were briefly discussed, focusing on the behavior of the energy as a function of the number of electrons at 0 K. It was discussed that the PPLB implies that the derivatives of the energy, and any other size consistent property, with respect to the number of electrons at 0 K are discontinuous when evaluated at any positive integer number of electrons. This corollary of the ensemble theorem has important

chemical consequences, namely, the process of electron transfer is not symmetric, i.e. the processes of giving and accepting electrons at 0 K occur at different rates.

It was mentioned several times along the text that the discontinuities in the derivatives occur at 0 K. The statement was not elaborated any further to avoid opening a topic requiring more space, and it indeed is explored in detail in Chapter 8 of this book. Let us just mention that incorporating temperature in CDFT paves the way to several conflicting issues at 0 K, like the derivative discontinuities. Readers are encouraged to see Chapter 8 for more details about this issue.

Arguing that incorporating the derivatives discontinuities is very important for a better description of the charge transfer processes, the two-parabola model proposed by Gázquez, Cedillo, and Vela was presented and discussed, emphasizing that this model motivates and justifies the introduction of two new chemical reactivity indexes, the electrodonating and electroaccepting powers, having a global and local version.

For an association reaction where the external potentials of the interacting species or fragments are unchanged, the general approach to determine the amount of charge transfer is derived. This simple derivation is very well known to the expert in CDFT, but again, its presentation has mainly didactic intentions.

The amount of charge transferred was derived for the PP and the two-parabola model. For the former a very simple approach is introduced to partition the amount of charge transferred in an electrophilic and nucleophilic contribution. In the later, the direction of charge transfer is naturally and automatically incorporated by construction of the energy function. Both models have global and local versions, but for the sake of space, the local model was only explained in detail for the two-parabola case.

A representative application of the model to the description of the electrochemical formation of hydrogen bonded complexes of substituted nitrobenzenes and 1,3-diethylurea was discussed; this example shows that the CDFT charge transfer models provide excellent correlation between binding constants, reaction constants, and other properties of associated reactions where charge transfer is the most important mechanism underlying the reaction process.

Let us conclude this chapter mentioning briefly some of the avenues that, in our opinion, are opened and waiting to be explored. First and very obvious is the application of the theoretical formalism herein presented to other systems. A second direction is exploring the incorporation of terms accounting for the change in the external potentials. This will give the possibility of relaxing the assumption that the geometries of the interacting fragments or species are unchanged in the association reaction. Directly related to the previous topic, it is possible considering that this model is very well suited for a better educated approach to molecular docking and maybe force fields. Finally, the good correlations obtained can shed some light about the underlying reasons for the success of the many reactivity scales that have been empirically proposed in several branches of chemistry.

## References

- 1 Muratov, E.N., Bajorath, J., Sheridan, R.P. et al (2020). QSAR without borders. *Chem. Soc. Rev.* 49 (11): 3525–3564.
- 2 Le, T., Epa, V.A., Burden, F.R., and Winkler, D.A. (2012). Quantitative structure-property relationship modeling of diverse materials properties. *Chem. Rev.* 112 (5): 2889–2919.
- 3 Verma, R.P. and Hansch, C. (2011). Use of C-13 NMR chemical shift as QSAR/QSPR descriptor. *Chem. Rev.* 111 (4): 2865–2899.
- 4 Mortier, W.J. (1987). Electronegativity equalization and its applications. *Struct. Bond.* 66: 125–143.
- 5 Mortier, W.J., Ghosh, S.K., and Shankar, S. (1986). Electronegativity equalization method for the calculation of atomic charges in molecules. *J. Am. Chem. Soc.* 108 (15): 4315–4320.
- 6 Mortier, W.J., Van Genechten, K., and Gasteiger, J. (1985). Electronegativity equalization: application and parametrization. *J. Am. Chem. Soc.* 107 (4): 829–835.
- 7 Parr, R.G. and Yang, W. (1994). *Density-Functional Theory of Atoms and Molecules, International Series of Monographs on Chemistry*. New York, USA: Oxford University Press.
- 8 Ayers, P.W., Anderson, J.S.M., and Bartolotti, L.J. (2005). Perturbative perspectives on the chemical reaction prediction problem. *Int. J. Quantum Chem.* 101 (5, SI): 520–534.
- 9 Parr, R.G., Donnelly, R.A., Levy, M., and Palke, W.E. (1978). Electronegativity - density functional viewpoint. *J. Chem. Phys.* 68 (8): 3801–3807.
- 10 Parr, R.G. and Pearson, R.G. (1983). Absolute hardness: companion parameter to absolute electronegativity. *J. Am. Chem. Soc.* 105 (26): 7512–7516.
- 11 Pearson, R.G. (1997). *Chemical Hardness*. Wiley.
- 12 Fuentealba, P. and Parr, R.G. (1991). Higher-order derivatives in density-functional theory, especially the hardness derivative  $\Delta\eta/\Delta N$ . *J. Chem. Phys.* 94 (8): 5559–5564.
- 13 Ayers, P.W. and Levy, M. (2000). Perspective on “Density functional approach to the frontier-electron theory of chemical reactivity” - Parr, R.G., Yang, W. (1984) *J. Am. Chem. Soc.* 106: 4049–4050. *Theor. Chem. Acc.* 103 (3–4): 353–360.
- 14 Parr, R.G. and Yang, W.T. (1984). Density functional-approach to the frontier-electron theory of chemical-reactivity. *J. Am. Chem. Soc.* 106 (14): 4049–4050.
- 15 De Proft, F., Ayers, P.W., Fias, S., and Geerlings, P. (2006). Woodward–Hoffmann rules in density functional theory: initial hardness response. *J. Chem. Phys.* 125 (21). 214101–214110.
- 16 Morell, C., Grand, A., and Toro-Labbe, A. (2006). Theoretical support for using the  $\Delta f(r)$  descriptor. *Chem. Phys. Lett.* 425 (4–6): 342–346.

- 17 Morell, C., Grand, A., and Toro-Labbe, A. (2005). New dual descriptor for chemical reactivity. *J. Phys. Chem. A* 109 (1): 205–212.
- 18 Sablon, N., De Proft, F., and Geerlings, P. (2010). The linear response kernel: inductive and resonance effects quantified. *J. Phys. Chem. Lett.* 1 (8): 1228–1234.
- 19 Liu, S., Li, T., and Ayers, P.W. (2009). Potentialphilicity and potentialphobicity: reactivity indicators for external potential changes from density functional reactivity theory. *J. Chem. Phys.* 131 (11). 114106–114113
- 20 Berkowitz, M. and Parr, R.G. (1988). Molecular hardness and softness, local hardness and softness, hardness and softness kernels, and relations among these quantities. *J. Chem. Phys.* 88 (4): 2554–2557.
- 21 Iczkowski, R. and Margrave, J.L. (1961). Electronegativity. *J. Am. Chem. Soc.* 83 (17): 3547–3551.
- 22 Mulliken, R.S. (1934). A new electroaffinity scale; together with data on valence states and on valence ionization potentials and electron affinities. *J. Chem. Phys.* 2 (11): 782–793.
- 23 Miranda-Quintana, R.A., Ayers, P.W., and Heidar-Zadeh, F. (2021). Reactivity and charge transfer beyond the parabolic model: the “—Delta mu— Big is Good” principle. *ChemistrySelect* 6 (1): 96–100.
- 24 Parr, R.G., Von Szentpaly, L., and Liu, S.B. (1999). Electrophilicity index. *J. Am. Chem. Soc.* 121 (9): 1922–1924.
- 25 Chattaraj, P.K., Sarkar, U., and Roy, D.R. (2006). Electrophilicity index. *Chem. Rev.* 106 (6): 2065–2091.
- 26 Chattaraj, P.K. and Roy, D.R. (2007). Update 1 of: electrophilicity index. *Chem. Rev.* 107 (9): PR46–PR74.
- 27 Chattaraj, P.K., Giri, S., and Duley, S. (2011). Update 2 of: electrophilicity index. *Chem. Rev.* 111 (2): PR43–PR75.
- 28 Perdew, J.P., Parr, R.G., Levy, M., and Balduz, J.L. (1982). Density-functional theory for fractional particle number - derivative discontinuities of the energy. *Phys. Rev. Lett.* 49 (23): 1691–1694.
- 29 Yang, W.T., Zhang, Y.K., and Ayers, P.W. (2000). Degenerate ground states and a fractional number of electrons in density and reduced density matrix functional theory. *Phys. Rev. Lett.* 84 (22): 5172–5175.
- 30 Ayers, P.W. (2008). The dependence on and continuity of the energy and other molecular properties with respect to the number of electrons. *J. Math. Chem.* 43 (1): 285–303.
- 31 Gázquez, J.L., Cedillo, A., and Vela, A. (2007). Electrodonating and electroaccepting powers. *J. Phys. Chem. A* 111 (10): 1966–1970.
- 32 Orozco-Valencia, Á.U. and Vela, A. (2012). The electrodonating and electroaccepting powers in atoms. *J. Mex. Chem. Soc.* 56 (3): 294–301.
- 33 Yanez, O., Osorio, M.I., Areche, C. et al (2021). *Theobroma cacao* L. compounds: theoretical study and molecular modeling as inhibitors of main SARS-CoV-2 protease. *Biomed. Pharmacother.* 140. 111764–111776.
- 34 Martinez, A. (2021). Electron donor-acceptor capacity of selected pharmaceuticals against COVID-19. *Antioxidants* 10 (6). 979–990.



- 35 Goode-Romero, G., Dominguez, L., Vargas, R. et al. (2021). Analyzing the interaction energy between dopaminergic agents and DRD2: is there any difference between risperidone (antagonist), aripiprazole (partial agonist) and pramipexole (agonist)? *Comput. Theor. Chem.* 1197. 113125–113130.
- 36 Dahmani, K., Galai, M., Ouakki, M. et al. (2021). Quantum chemical and molecular dynamic simulation studies for the identification of the extracted cinnamon essential oil constituent responsible for copper corrosion inhibition in acidified 3.0 wt% NaCl medium. *Inorg. Chem. Commun.* 124. 108409–108420.
- 37 Goode-Romero, G., Winnberg, U., Dominguez, L. et al. (2020). New information of dopaminergic agents based on quantum chemistry calculations. *Sci. Rep.* 10 (1). 21581–21592.
- 38 Sanderson, R.T. (1983). Electronegativity and bond-energy. *J. Am. Chem. Soc.* 105 (8): 2259–2261.
- 39 Sanderson, R.T. (1955). Partial charges on atoms in organic compounds. *Science* 121 (3137): 207–208.
- 40 Sanderson, R.T. (1951). An interpretation of bond lengths and a classification of bonds. *Science* 114 (2973): 670–672.
- 41 Ayers, P.W. (2007). The physical basis of the hard/soft acid/base principle. *Faraday Discuss.* 135: 161–190.
- 42 Ayers, P.W., Parr, R.G., and Pearson, R.G. (2006). Elucidating the hard/soft acid/base principle: a perspective based on half-reactions. *J. Chem. Phys.* 124 (19). 194107–194114.
- 43 Chattaraj, P.K. and Ayers, P.W. (2005). The maximum hardness principle implies the hard/soft acid/base rule. *J. Chem. Phys.* 123 (8). 086101–086102.
- 44 Ayers, P.W. (2005). An elementary derivation of the hard/soft-acid/base principle. *J. Chem. Phys.* 122 (14). 141102–141104.
- 45 Chattaraj, P.K., Gomez, B., Chamorro, E. et al. (2001). Scrutiny of the HSAB principle in some representative acid-base reactions. *J. Phys. Chem. A* 105 (38): 8815–8820.
- 46 Chattaraj, P.K., Lee, H., and Parr, R.G. (1991). HSAB principle. *J. Am. Chem. Soc.* 113 (5): 1855–1856.
- 47 Orozco-Valencia, A.U., Gázquez, J.L., and Vela, A. (2017). Global and local partitioning of the charge transferred in the Parr–Pearson model. *J. Phys. Chem. A* 121 (20): 4019–4029.
- 48 Sarmah, A., Saha, S., Bagaria, P., and Roy, R.K. (2012). On the complementarity of comprehensive decomposition analysis of stabilization energy (CDASE) - scheme and supermolecular approach. *Chem. Phys.* 394 (1): 29–35.
- 49 Saha, S., Roy, R.K., and Pal, S. (2010). CDASE-A reliable scheme to explain the reactivity sequence between Diels–Alder pairs. *Phys. Chem. Chem. Phys.* 12 (32): 9328–9338.
- 50 Bagaria, P., Saha, S., Murru, S. et al. (2009). A comprehensive decomposition analysis of stabilization energy (CDASE) and its application in locating the rate-determining step of multi-step reactions. *Phys. Chem. Chem. Phys.* 11 (37): 8306–8315.

- 51 Ramirez-Ramirez, J.Z., Vargas, R., Garza, J., and Gázquez, J.L. (2010). Simple charge-transfer model for metallic complexes. *J. Phys. Chem. A* 114 (30): 7945–7951.
- 52 Vazquez-Mayagoitia, A., Garza, J., Vargas, R. et al (2010). Simple charge transfer model for one electron oxidation and reduction processes: describing reactive sites in benzocarbazolediones and gallates. *J. Mol. Struct. THEOCHEM* 943 (1–3, SI): 59–64.
- 53 Orozco-Valencia, U., Gázquez, J.L., and Vela, A. (2018). Role of reaction conditions in the global and local two parabolas charge transfer model. *J. Phys. Chem. A* 122 (6): 1796–1806.
- 54 Orozco-Valencia, U., Gázquez, J.L., and Vela A. (2018). Global and local charge transfer in electron donor-acceptor complexes. *J. Mol. Model.* 24 (9). 250–263.
- 55 Orozco-Valencia, U., Gázquez, J.L., and Vela, A. (2018). Reactivity of indoles through the eyes of a charge-transfer partitioning analysis. *Acta Phys. Chim. Sin.* 34 (6): 692–698.
- 56 Orozco-Valencia, U., Gázquez, J.L., and Vela, A. (2017). Donation and back-donation analyzed through a charge transfer model based on density functional theory. *J. Mol. Model.* 23 (7). 207–215.
- 57 Martinez-Gonzalez, E. and Frontana, C. (2014). Employment of electrodonating capacity as an index of reactive modulation by substituent effects: application for electron-transfer-controlled hydrogen bonding. *J. Org. Chem.* 79 (3): 1131–1137.
- 58 Bultinck, P., Fias, S., Van Alsenoy, C. et al. (2007). Critical thoughts on computing atom condensed Fukui functions. *J. Chem. Phys.* 127 (3). 034102–034112.
- 59 Yang, W. and Mortier, W.J. (1986). The use of global and local molecular-parameters for the analysis of the gas-phase basicity of amines. *J. Am. Chem. Soc.* 108 (19): 5708–5711.
- 60 Hirshfeld, F.L. (1977). Bonded-atom fragments for describing molecular charge-densities. *Theor. Chim. Acta* 44 (2): 129–138.

## 12

### Reaction Electronic Flux

Luis Rincon<sup>1</sup> and F. Javier Torres<sup>1,2</sup>

<sup>1</sup>Universidad San Francisco de Quito, USFQ, Instituto de Simulación Computacional, Grupo de Química Computacional y Teórica, Departamento de Ingeniería Química, Diego de Robles y Vía Interoceánica, Quito 17-1200-841, Ecuador

<sup>2</sup>Grupode Química Computacional y Teórica (QCT-UR), Facultad de Ciencias Naturales, Universidad del Rosario, Ak. 24 #63C-69, Bogotá, Colombia, 111221

#### 12.1 Introduction

The use of modern computational chemistry methodologies in the prediction of molecular properties has become increasingly popular, mainly due to significant improvements in the algorithms, the accuracy of the methods, and the advent of powerful computational resources. This is particularly true in the area of thermochemistry where researchers in industry and academia perform quantum chemistry calculations on a routinely basis. Due to the impressive success, there has been an increased interest in the application of state-of-the-art quantum chemistry methodologies in the study of physical and chemical phenomena in a wide variety of technological areas including biomedicine, chemical catalysis, environmental chemistry, combustion and alternative sources of energy, climate assessment, nanoelectronics, and the rational design of materials at the nano-scale. The field has reached such state of maturity that modern quantum chemistry methods are currently used not only for the interpretation of experimental measurements but also to guide the experimental design for measurements of novel physical and chemical properties of a wide variety of chemical system and advanced materials.

One of the areas, where major advances in quantum chemistry methodologies have made a significant impact, is the quantitative description of mechanisms, energetics, and dynamics governing chemical reactions. Today, scientists routinely employ *ab initio* quantum chemical methodologies to map potential energy surfaces (PESs) of reactive systems in the vicinity of the minimum energy path (MEP) in order to study the transformation of reactants into products. One of the most efficient ways to accomplish this entails is the use of the intrinsic reaction coordinate (IRC) concept originally developed by Fukui [1–5]. Due to the availability of analytical gradient methods [6–8], the implementation of reaction path following algorithms in the realm of *ab initio* quantum mechanical calculations has allowed

scientists to study the energetics, mechanisms, and electronic structure properties of reacting systems involving relatively large polyatomic systems [9–15].

One of the most active areas of research in density functional theory (DFT) has been the so-called “conceptual DFT” [16], which provides with a strong theoretical background, important chemical concepts, such as electronegativity, chemical hardness, and chemical softness, as well as their relations to chemical principles, such as Hard–Soft Acid–Base (HSAB), Electronegative Equalization, and Maximum Hardness. The origins of conceptual DFT can be traced back to the pivotal work of Parr who developed the theoretical formalism that establishes the direct relation between the chemical potential and the fundamental equations of DFT [17, 18]. Due to the development of computationally efficient DFT algorithms implemented in a variety of popular commercial and noncommercial quantum chemistry software packages, the literature has seen an explosion of applications employing conceptual DFT. This is particularly true in the case of chemical reactivity theory (CRT) that allows the connection between DFT concepts and the study of properties such as chemical bonding, reactivity, and dynamics. The scientific literature also abounds with applications of conceptual DFT in the study of changes of chemical reactivity indices (as well as other electronic structure properties) along reaction paths [16].

Along with a reaction path, a redistribution of the electron density among the atoms within the molecules is observed. Conceptual density functional theory is quite well suited to describe this electronic reorganization in a chemical path throughout descriptors like electronic chemical potential ( $\mu$ ) and molecular hardness ( $\eta$ ). Furthermore, the study of the profiles  $\mu$  and  $\eta$  along a reaction coordinate has been shown to be useful to rationalize different aspects of the progress of chemical reactions.

This article introduces the variation of the first derivative of the electronic energy, the reaction force (RF), and the first derivative of the chemical potential, the reaction electronic flux (REF), along the reaction coordinate. The contents of the present chapter are organized as follows: Section 12.2 introduces the RF and its interpretation. Section 12.3 introduces the REF and its decomposition. Furthermore, the application of the REF concept is briefly illustrated with the analysis of a pyrolysis reaction. Finally, Section 12.5 contains some final remarks.

## 12.2 Reaction Force

### 12.2.1 Definition

A typical potential energy profile for a reaction, denoted in the follow as  $E(\xi)$ , is depicted in Figure 12.1a for a single step reaction in which the energy of the reactant and the product is the same,  $\Delta E = 0$ . In Figure 12.1,  $\xi$  represents the IRC, or some alternative definition of the reaction coordinate. For convenience, in the rest of this manuscript,  $\xi$  is always scaled between  $\xi = \xi_R = 0$  (Reactant) and  $\xi = \xi_P = 1$  (Product). The scaled coordinate can therefore be viewed as a measure of the reaction progress going from reactants ( $\xi = 0$ ) to products ( $\xi = 1$ ), passing through a

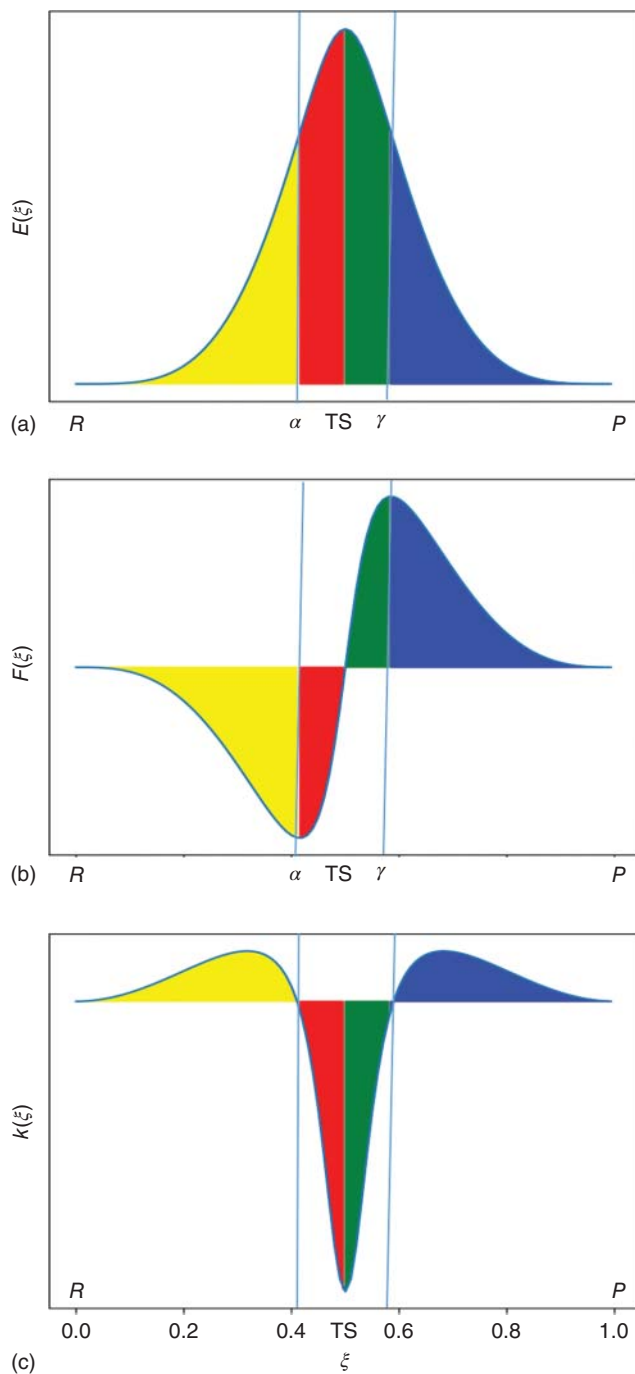


**Figure 12.1** (a) Potential energy profile,  $E(\xi)$ , for a single step reaction along the reaction coordinate,  $\xi$ . (b) Reaction force profile,  $F(\xi)$ . (c) Reaction force constant profile,  $\kappa(\xi)$ .

transition state, where  $E(\xi)$  takes its maximum at  $\xi = \xi_{\text{TS}}$ . The energy difference between the transition state maximum and the reactant minimum is the activation barrier for the forward reaction ( $\Delta E_F^\ddagger$ ). On the other hand, the difference between the transition state and the product minimum is the activation barrier for the reverse reaction ( $\Delta E_R^\ddagger$ ). Obviously, forward and reverse barriers are related through the reaction energy:  $\Delta E = \Delta E_F^\ddagger - \Delta E_R^\ddagger$ . Additional information to  $E(\xi)$  can be obtained taking their derivatives with respect  $\xi$ . In an analogy with the classical definition of mechanical force, the negative of the first-order derivative of the potential energy respect the reaction coordinate is defined as the RF [19–25]:

$$F(\xi) = -\frac{dE(\xi)}{d\xi} \quad (12.1)$$

while the second-order derivative is referred as the reaction force constant (RFC) [26–29]:

$$\kappa(\xi) = \frac{d^2E(\xi)}{d\xi^2} = -\frac{dF(\xi)}{d\xi} \quad (12.2)$$

The RF and RFC for the energy profile of Figure 12.1a is depicted in Figure 12.1b,c, respectively. A typical RF profile has a minimum value for  $\xi$  between the reactant minimum ( $\xi_R$ ) and the transition state maximum ( $\xi_{\text{TS}}$ ), this value is denoted as  $\xi_\alpha$ ; in addition, a maximum is located between the transition state maximum ( $\xi_{\text{TS}}$ ) and the product minimum ( $\xi_P$ ),  $\xi_\gamma$ . Occasionally, other extremes of the RF can be found [30]; however, for the sake of simplicity, we assume that only one minimum,  $\xi_\alpha$ , and one maximum,  $\xi_\gamma$ , are present in the RF. The extremes of the RF, along with the critical points of  $E(\xi)$ , define a partition of  $\xi$  into four regions: (i)  $\xi_R \rightarrow \xi_\alpha$ , (ii)  $\xi_\alpha \rightarrow \xi_{\text{TS}}$ , (iii)  $\xi_{\text{TS}} \rightarrow \xi_\gamma$ , and (iv)  $\xi_\gamma \rightarrow \xi_P$ . These four regions are identified by different colors in Figure 12.1: yellow, red, green, and blue, respectively. The RF in regions (i) and (ii) is negative, while in regions (iii) and (iv) is positive. By integrating the RF along the reaction coordinate, the negative of the energy between the two  $\xi$  limits can be obtained [20–25]. In this way, the activation barrier for the forward reaction can be decomposed in two contributions corresponding to regions (i) and (ii):

$$\begin{aligned} \Delta E_F^\ddagger &= E(\xi_{\text{TS}}) - E(\xi_R) \\ &= -\int_{\xi_R}^{\xi_\alpha} F(\xi)d\xi - \int_{\xi_\alpha}^{\xi_{\text{TS}}} F(\xi)d\xi \\ &= w_{(i)} + w_{(ii)} \end{aligned} \quad (12.3)$$

in an equivalent way, the activation barrier for the reverse reaction is defined in terms of the contributions of regions (iii) and (iv):

$$\begin{aligned} \Delta E_R^\ddagger &= E(\xi_{\text{TS}}) - E(\xi_P) \\ &= \int_{\xi_{\text{TS}}}^{\xi_\gamma} F(\xi)d\xi + \int_{\xi_\gamma}^{\xi_P} F(\xi)d\xi, \\ &= w_{(iii)} + w_{(iv)} \end{aligned} \quad (12.4)$$

Naturally, the reaction energy results from the contributions of the four regions:

$$\Delta E = w_{(i)} + w_{(ii)} - w_{(iii)} - w_{(iv)} \quad (12.5)$$

The RFC, Figure 12.1c, is positive in the regions (i) and (iv), while negative in the regions region of influence of the transition state, regions (ii) and (iii). The fact that the RFC is negative in the entire region between  $\xi_\alpha$  and  $\xi_\gamma$  suggests that this is in fact the transition region (associated with an imaginary frequency) [22]. The idea of employing a transition region along the reaction coordinate, and not just a single transition state point, is in full agreement with the concept of a transient state between reactant and product observed from transition state spectroscopy experiments by Polanyi and Zewail [31]. From the study of 12 double proton transfer reactions, it has been clear that the number of minima of RFC in regions (ii) and (iii) indicates the degree of synchronization of concerted reactions [27]. For most synchronous mechanisms, the profile of  $\kappa(\xi)$  has a single minimum in the transition region; in contrast, for nonsynchronous mechanisms, two minima are observed. Such assessment of the synchronicity is not easily detected by the analysis of  $E(\xi)$  or  $F(\xi)$  (Figure 12.1a,b).

### 12.2.2 Interpretation

This partition in four regions has been extensively studied for some prototypical reactions, such as  $S_N2$  mechanisms [32–34], olefin addition [35, 36], proton transfer [37–41], molecular rearrangements [42], tautomerizations [43], deamination [44], chemisorption [45], the activation of H–H and C–H bonds by frustrated Lewis pairs [46], and the C–F bond cleavage mediated by cob[I]alamin-based structures [30]. The previous list is far from exhaustive, so the reader can be referred to some reviews on this field for a more comprehensive list [25]. From the study of these reactions, some general trends have emerged [20–25]. The process observed in region (i) is typically associated with the geometric reorganization of the reactant, but a small (or negligible) bond breaking or bond formation. The regions (ii) and (iii) involve a major electronic reorganization, region (ii) represents energy uptake (negatives forces), while region (iii) represent energy release (positives forces); at the end of this region, most of the bonds are broken in the reactant and formed into the product. The region (iv) involves the geometric relaxation of the product in their path to the equilibrium structure, where the main bonding changes take place. Therefore, regions (i) and (iv) are considered the structural zones and the combination of (ii) and (iii), that include the transition state, are considered the transition region. It is important to point out that, by no means, these trends are exclusive, and small degrees of electronic reorganization are observed usually at regions (i) and (iv), conversely, region (ii) and (iii) involve small geometric changes.

## 12.3 Reaction Electronic Flux

### 12.3.1 The Chemical Potential

The electronic chemical potential ( $\mu$ ) is the central concept in understanding the changes along a reaction path [16–18]. For an  $N$ -electron system, the electronic

chemical potential is defined as the partial derivative of the energy respect to the number of electron embedded within an external nuclear potential:

$$\mu = \left( \frac{\partial E}{\partial N} \right)_v \quad (12.6)$$

This descriptor accounts for the tendency of electrons to escape from an equilibrium distribution. Moreover, the electronic chemical potential is introduced as a Lagrange multiplier in the search for an electron density that minimizes the energy for account that the density always integrate to the number of electrons. One important property of  $\mu$  is its link with the negative of the electronegativity ( $\mu = -\chi$ ) and the Sanderson's electronegativity equalization principle that state [47, 48]

When two or more atoms, initially different in electronegativity, combine chemically, their electronegativities become equalized in the molecule. The equalization of electronegativity occurs through the adjustment of the polarities of the bonds which is pictured as resulting in a partial charge on each atom. That is, electron loss causes increase, and electron gain decrease in electronegativity.

Due to the derivative discontinuity of the energy with respect to  $N$ , the usual approach is to compute the electronegativity by taking the average of the left- ( $\mu_l$ ) and right-hand-side ( $\mu_r$ ) derivatives:

$$\mu_l = E(N = N_0) - E(N = N_0 - 1) = -I \quad (12.7)$$

$$\mu_r = E(N = N_0 + 1) - E(N = N_0) = -A \quad (12.8)$$

$$\mu = \frac{1}{2}(\mu_l + \mu_r) = -\frac{1}{2}(I + A) \quad (12.9)$$

where  $I$  and  $A$  are, respectively, the ionization energy and electron affinity of the  $N_0$  electron system. It must be noted that this approach is equivalent to the use of the Mulliken definition of electronegativity. As an approximation to Eq. (12.9), and based on Koopmans' theorem, the ionization energy and electron affinity can be replaced by the highest occupied molecular orbital (HOMO) and lowest unoccupied molecular orbital (LUMO) energy ( $\epsilon_{\text{HOMO}}$  and  $\epsilon_{\text{LUMO}}$ ), respectively, yielding

$$\mu = \frac{1}{2}(\epsilon_{\text{HOMO}} + \epsilon_{\text{LUMO}}) \quad (12.10)$$

This last approximation is useful since the direct calculation of  $I$  and  $A$  is in many cases plagued on technical problems (in particular, the calculation of anionic systems). Equation (12.10) offers an useful interpretation of  $\mu$  in terms of the frozen orbitals approach. Alternatively to the finite difference approach, analytical methods have been developed to calculate energy derivatives with respect to  $N$ , leading to coupled perturbed Hartree–Fock equations. Extreme care must be exerted when comparing values obtained with different methodologies: finite difference



Koopmans-type approximation, analytical derivatives, sometimes combined with experimental data. A careful comparison of the  $\mu$  values calculated using Eqs. (12.9) and (12.10) by Komorowski and coworkers [49, 50] shows a good correlation in atomic and molecular systems.

### 12.3.2 The Reaction Electronic Flux Concept

The REF along a reaction path ( $\xi$ ) was introduced by Toro-Labbé and coworkers in the form [51–53]:

$$J_{\mu}(\xi) = Q \frac{d\mu}{d\xi} \quad (12.11)$$

What does it mean? Briefly, REF is introduced by making an analogy with the general form of the laws for macroscopic transport phenomena, for example Newton's law of viscosity, Fick's law of diffusion, or Fourier's law for heat. In one dimension, the transport law equation is  $J_X = -Q \frac{dX}{d\xi}$ , where  $J_X$  is the flux (flow rate per unit area) of property  $X$ ,  $Q$  is a transport coefficient that measures how rapidly a perturbed system returns to equilibrium, and  $\frac{dX}{d\xi}$  is the gradient force on property  $X$ . Based on this interpretation,  $J_{\mu}(\xi)$  accounts for the flow rate of the chemical potential along a reaction path. For convenience, we assume in Eq. (12.11) that  $Q = 1$ ; however, this will deserve further analysis in the next sections.

The evolution of the chemical potential along the reaction path is indicative of the electron reorganization that occurs in the system during a chemical reaction. In a further analogy with classic thermodynamics,  $J_{\mu}(\xi)$  profile can be used to describe the spontaneity of the electronic activity during the reaction. Positive values of the flux are associated with negative chemical potential, therefore account for spontaneous changes in the electronic density which are related with bond strengthening or forming processes, whereas negative values are indicative of nonspontaneous electronic reordering that can be associated with bond weakening or breaking processes.

It is expected that, along the reaction path, an electron density transfer between reactant occurs in order to stabilize the system and to equalize the chemical potential at equilibrium. This electron transfer can be scrutinized through an *ad hoc* decomposition of the REF into intra- and intermolecular electronic contributions which account for the polarization effects ( $J_p$ ) and charge transfer effects ( $J_t$ ), respectively:

$$J_{\mu}(\xi) = J_p(\xi) + J_t(\xi) \quad (12.12)$$

The intramolecular polarization can be estimated from a convenient partition of the reactants in a number of reactive chemical fragments. If this is the case, we can write  $J_p(\xi)$  as:

$$J_p(\xi) = \sum_{i=1}^n J_p^i(\xi) \quad (12.13)$$

where  $n$  is the number of reactive fragments. The  $J_p^i(\xi)$  can be obtained from a counterpoise calculation of the chemical potential of each reactive fragments along the

reaction path, and the derivation of this internal chemical potential lead to the polarization contribution to the flux in the form:

$$J_p^i(\xi) = \frac{N_i}{N} \frac{d\mu_i}{d\xi} \quad (12.14)$$

where  $N_i$  is the number of electrons of fragment  $i$  and  $N$  is the total number of electrons. The prefactor  $\frac{N_i}{N}$  ensures that each fragment contribution is proportional to their own number of electrons. The flux associated with the electronic transfer ( $J_i$ ) is taken as the difference between global  $J_\mu(\chi)$  and  $J_p(\xi)$  calculated from the isolated fragments using the counterpoise method.

It is possible to estimate the fragment contribution to  $J_\mu(\chi)$  and  $J_p(\xi)$  by appealing to the principle of equalization of the chemical potential [51–53]. According to this principle, the chemical potential of all fragments is the same, the global chemical potential ( $\mu = \mu_i$  for all  $i$ ). In this case, a convenient normalization of the contribution of each fragment to the total flux is

$$J^i(\xi) = \frac{N_i}{N} \frac{d\mu}{d\xi} \quad (12.15)$$

and the contribution of each fragment associated with electron transfer result as:

$$J_i^i(\xi) = \frac{N_i}{N} \left( \frac{d\mu}{d\xi} - \frac{d\mu_i}{d\xi} \right) \quad (12.16)$$

### 12.3.3 REF Application

The REF concept has been extensively employed in the description of the electronic activity involved in different types of chemical reactions. Some examples are the Diels–Alder reaction [54], inter- and intramolecular Proton transfer [55, 56], hydrogenation and dihydrogenation of  $\text{CO}_2$  [57, 58], decomposition, formation, and rearrangement reactions [59–61], among others. In the present section, the REF concept is illustrated by considering the theoretical description of the furfuryl acetate pyrolysis previously reported in Ref. [62]. In this study, the high-temperature decomposition of furfuryl acetate was observed to yield the uncommon methylenecyclobutenone compound and acetic acid as products, through a multistep mechanism involving two [3+3] rearrangements and a subsequent hydrogen  $\alpha$ -elimination step (Figure 12.2). It is important to point out that a detailed description of the latter reaction is not among the purposes of the present section; thus, the interested reader is referred to the main publication.

Since the  $\alpha$ -elimination was determined to be the rate-limiting step [62], the RF and REF analyses were employed to thoroughly describe this particular reaction step. Figure 12.3 depicts the results of the IRC calculation and the corresponding RF, where it is observed that, although an  $\alpha$ -elimination is customarily treated as a single concerted process, it consists of two discriminable stages in the present case. The first stage ( $\xi_R - \xi_3^{\text{SR}}$ ) is solely characterized by a gradual decrease of the O–H bond of the five-membered transition state (Figure 12.4), which goes from 2.2 to 1.8 Å. This proton transfer increases its change rate in the second stage ( $\xi_3^{\text{SR}} - \xi_1^{\text{SP}}$ ), where it reaches a final value of about  $\sim 1.0$  Å, whereas significant changes in the

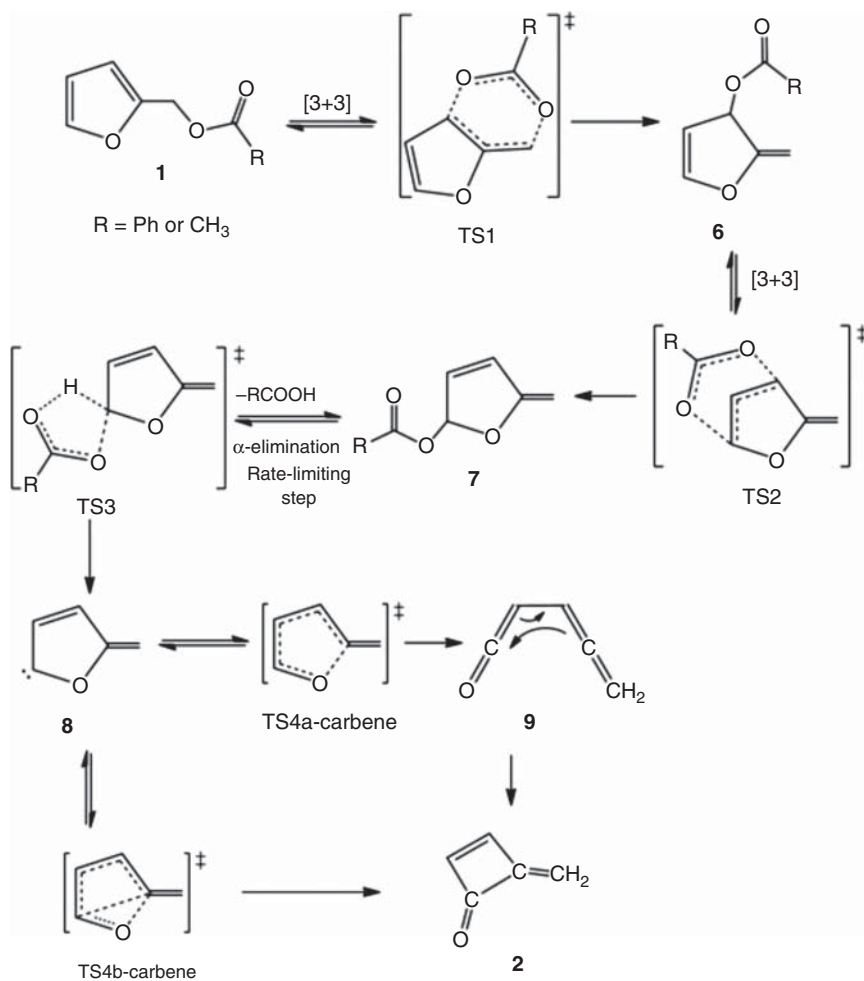


**Figure 12.2** Multistep reaction pathway of furfuryl acetate pyrolysis as reported in [62]. R represents the acetate group. Source: Mora et al. [62].

associated C–H and C–O bonds are also observed. It is important to point out that, although the RF allows the description of the  $\alpha$ -elimination in a very detailed manner, information on the electronic activity requires a further analysis by means of the REF concept.

Figure 12.5 depicts the REF profile of the  $\alpha$ -elimination process. As shown in the graphic, the first stage of the  $\alpha$ -elimination is characterized by a spontaneous electronic reorganization, which agrees with the negligible geometrical changes observed in this region of the reaction coordinate. In contrast, the second stage of the process presents a sharp nonspontaneous REF, suggesting a rapid and important electronic reorganization associated mainly with the C–O bond cleavage. The latter observation suggests that the formation of the five-membered transition state can

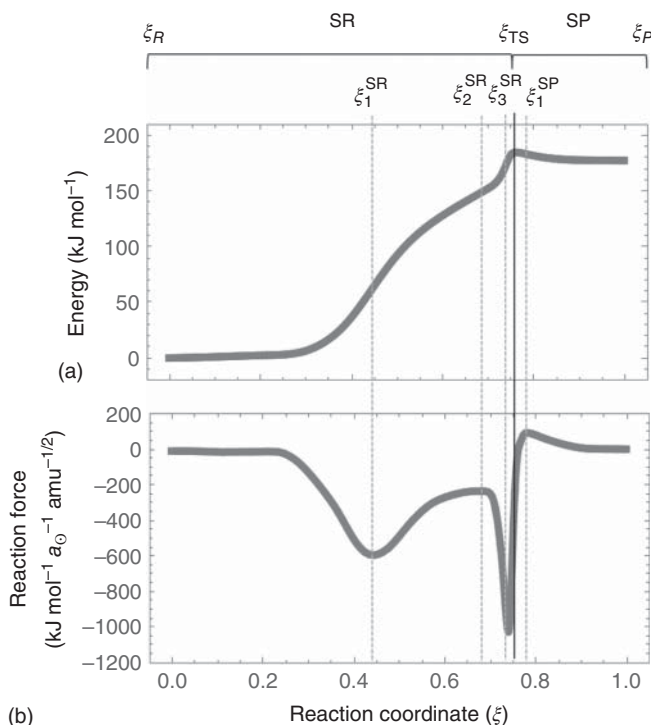


**Figure 12.3** IRC (a) and RF (b) results of the  $\alpha$ -elimination process determined as the rate-limiting step in the furfuryl acetate pyrolysis. Source: Mora et al. [62].

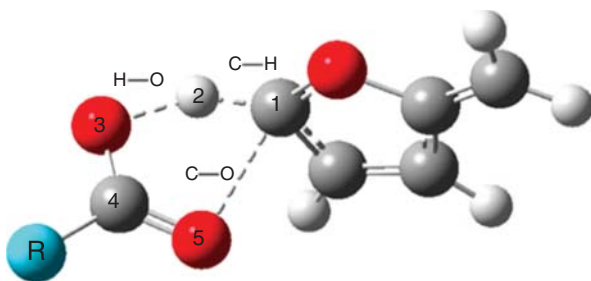


**Figure 12.4** Graphical representation of the five-membered transition state involved in the  $\alpha$ -elimination of the furfuryl acetate pyrolysis. Source: Mora et al. [62].

be significantly favored by stabilizing the partial negative charge of oxygen atom in the  $\text{C}^{\delta+} \cdots \text{O}^{\delta-}$  bond. The latter idea was confirmed in Ref. [62] by considering the  $-\text{C}_6\text{H}_5$  phenyl group as the R substituent (Figure 12.4), which was expected to actively contribute with the polarization of the C–O bond. Accordingly, the pyrolysis of the furfuryl benzoate was observed to possess a five-membered transition state that is about  $\sim 5 \text{ kJ mol}^{-1}$  more stable than its furfuryl acetate counterpart, confirming the conclusion made on the basis of the REF analysis.

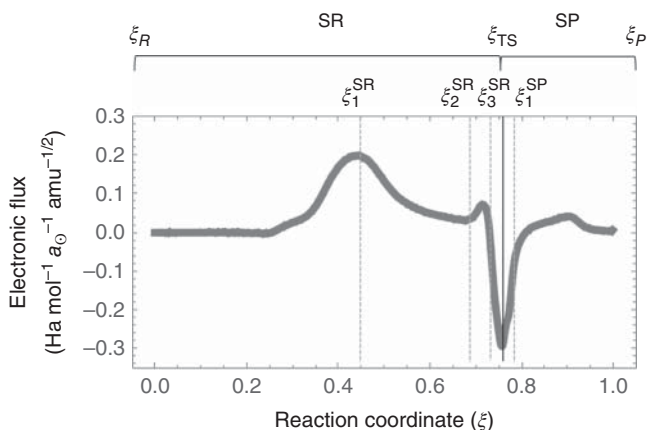


**Figure 12.5** Reaction electronic flux of the  $\alpha$ -elimination process determined as the rate-limiting step in the furfuryl acetate pyrolysis. Source: Mora et al. [62].

## 12.4 Conclusions

We have presented the RF and REF approaches as useful descriptors to characterize the electronic activity taking place during a chemical reaction, which is of great utility in conjunction with other methodologies of analysis. In this vein, it provides crucial and valuable information to characterize reaction mechanisms. The power of the REF as a descriptor to characterize the mechanism of chemical reactions has been illustrated with the analysis of a pyrolysis reaction.

The susceptibility of a molecule to various types of reactions is assessed through its response functions. Evaluating these response functions along the reaction path can provide important additional information. Specifically, studying how global and local reactivity indicators change along a reaction path can help locate transition states, reveal mechanistic insights, and connect reactivity, bonding, and kinetics. The methodologies presented in this chapter, in conjunction to others that allow the dissection of chemical reactions, have an enormous potential of future application for a number of reasons, which in our opinion are: (i) they can be envisaged as interpretative tools capable of providing a detailed picture of chemical processes, (ii) these methods do not require extreme computational costs, and (iii) their application to realistic models can be attained by considering the nowadays progress in computational architectures.

## Bibliography

- 1 Fukui, K. (1970). Formulation of the reaction coordinate. *J. Phys. Chem.* 74 (23): 4161–4163. <https://doi.org/10.1021/j100717a029>.
- 2 Ishida, K., Morokuma, K., and Komornicki, A. (1977). The intrinsic reaction coordinate. An ab initio calculation for  $hnc \rightarrow hcn$  and  $h^- + ch_4 \rightarrow ch_4 + h^-$ . *J. Chem. Phys.* 66: 2153–2156. <https://doi.org/10.1063/1.434152>.

- 3 Tachibana, A. and Fukui, K. (1978). Differential geometry of chemically reacting systems. *Theor. Chim. Acta* 49: 321–347. <https://doi.org/10.1007/BF00552483>.
- 4 Fukui, K. (1981). The path of chemical reactions—the IRC approach. *Acc. Chem. Res.* 14 (12): 363–368. <https://doi.org/10.1021/ar00072a001>.
- 5 Fukui, K. (1981). Variational principles in a chemical reaction. *Int. J. Quantum Chem.* 20: 633–642. <https://doi.org/10.1002/qua.560200866>.
- 6 Pulay, P., Fogarasi, G., Pang, F., and Boggs, J.E. (1979). Systematic ab initio gradient calculation of molecular geometries, force constants and dipole-moment derivatives. *J. Am. Chem. Soc.* 101: 2550–2560. <https://doi.org/10.1021/ja00504a009>.
- 7 El Azhary, A., Rauhut, G., Pulay, P., and Werner, H.-J. (1998). Analytical energy gradients for local second-order Möller-Plesset perturbation theory. *J. Chem. Phys.* 108: 5185–5193. <https://doi.org/10.1063/1.475955>.
- 8 Schlegel, H.B. (1982). An efficient algorithm for calculating ab initio energy gradients using s,p Cartesian Gaussians. *J. Chem. Phys.* 77: 3676–3681. <https://doi.org/10.1063/1.444270>.
- 9 Müller, K. and Brown, L.D. (1979). Location of saddle points and minimum energy paths by a constrained simplex optimization procedure. *Theor. Chim. Acta* 53: 75–93. <https://doi.org/10.1007/BF00547608>.
- 10 Cerjan, C.J. and Miller, W.H. (1981). On finding transition states. *J. Chem. Phys.* 75: 2800–2806. <https://doi.org/10.1063/1.442352>.
- 11 Bell, S. and Crighton, J.S. (1984). Locating transition states. *J. Chem. Phys.* 80: 2464–2475. <https://doi.org/10.1063/1.446996>.
- 12 Elber, R. and Karplus, M. (1987). A method for determining reaction paths in large molecules: application to myoglobin. *Chem. Phys. Lett.* 139: 375–380. [https://doi.org/10.1016/0009-2614\(87\)80576-6](https://doi.org/10.1016/0009-2614(87)80576-6).
- 13 Page, M. and McIver, J.W. (1988). On evaluating the reaction path Hamiltonian. *J. Chem. Phys.* 88: 922–935. <https://doi.org/10.1063/1.454172>.
- 14 Page, M., Doubleday, C., and McIver, J.W. (1990). Following steepest descent reaction paths. The use of higher energy derivatives with ab initio electronic structure methods. *J. Chem. Phys.* 93: 5634–5642. <https://doi.org/10.1063/1.459634>.
- 15 Hratchian, H.P. and Schlegel, H.B. (2005). Using Hessian updating to increase the efficiency of a Hessian based predictor-corrector reaction path following method. *J. Chem. Theory Comput.* 1: 61–69. <https://doi.org/10.1021/ct0499783>.
- 16 Geerlings, P., De Proft, F., and Langenaeker, W. (2003). Conceptual density functional theory. *Chem. Rev.* 103: 1793–1873. <https://doi.org/10.1021/cr990029p>.
- 17 Parr, R. and Yang, W. (1984). Density functional approach to the frontier-electron theory of chemical reactivity. *J. Am. Chem. Soc.* 106: 4049–4050. <https://doi.org/10.1021/ja00326a036>.
- 18 Parr, R. and Yang, W. (1989). *Density Functional Theory of Atoms and Molecules*. New York: Oxford University Press.
- 19 Toro-Labbé, A. (1999). Characterization of chemical reactions from the profiles of energy, chemical potential, and hardness. *J. Phys. Chem. A* 103 (22): 4398–4403. <https://doi.org/10.1021/jp984187g>.

- 20 Politzer, P., Toro-Labbé, A., Gutiérrez-Oliva, S. et al. (2005). The reaction force: three key points along the intrinsic reaction coordinate. *J. Chem. Sci.* 117 (5): 467–472. <https://doi.org/10.1007/BF02708350>.
- 21 Toro-Labbé, A., Gutiérrez-Oliva, S., Murray, J.S., and Politzer, P. (2007). A new perspective on chemical and physical processes: the reaction force. *Mol. Phys.* 105 (19–22): 2619–2625. <https://doi.org/10.1080/00268970701604663>.
- 22 Toro-Labbé, A., Gutiérrez-Oliva, S., Murray, J.S., and Politzer, P. (2009). The reaction force and the transition region of a reaction. *J. Mol. Model.* 15 (6): 707–710. <https://doi.org/10.1007/s00894-008-0431-8>.
- 23 Murray, J.S., Toro-Labbé, A., Clark, T., and Politzer, P. (2009). Analysis of diatomic bond dissociation and formation in terms of the reaction force and the position-dependent reaction force constant. *J. Mol. Model.* 15 (6): 701–706. <https://doi.org/10.1007/s00894-008-0400-2>.
- 24 Politzer, P., Reimers, J.R., Murray, J.S., and Toro-Labbé, A. (2010). Reaction force and its link to diabatic analysis: a unifying approach to analyzing chemical reactions. *J. Chem. Phys. Lett.* 1 (19): 2858–2862. <https://doi.org/10.1021/jz101135y>.
- 25 Politzer, P., Toro-Labbé, A., Gutiérrez-Oliva, S., and Murray, J.S. (2012). Perspectives on the reaction force. *Adv. Quantum Chem.* 64: 189–209. <https://doi.org/10.1016/B978-0-12-396498-4.00006-5>.
- 26 Jaque, P., Toro-Labbé, A., Politzer, P., and Geerling, P. (2008). Reaction force constant and projected force constants of vibrational modes along the path of an intermolecular proton transfer reaction. *Chem. Phys. Lett.* 456: 135–140. <https://doi.org/10.1016/cplett.2008.03.054>.
- 27 Yepez, D., Murray, J.S., Politzer, P., and Jaque, P. (2012). The reaction force constant: an indicator of the synchronicity in double proton transfer reactions. *Phys. Chem. Chem. Phys.* 14 (31): 11125–11134. <https://doi.org/10.1039/C2CP41064H>.
- 28 Politzer, P., Murray, J.S., and Jaque, P. (2013). Perspectives on the reaction force constant. *J. Mol. Model.* 19 (10): 4111–4118. <https://doi.org/10.1007/s00894-012-1713-8>.
- 29 Yepez, D., Donoso-Taуда, O., Perez, P. et al. (2013). The reaction force constant as an indicator of synchronicity/nonsynchronicity in [4 + 2] cycloaddition processes. *Phys. Chem. Chem. Phys.* 15 (19): 7311–7320. <https://doi.org/10.1039/C3CP44197K>.
- 30 Cortes-Arriaga, D., Toro-Labbé, A., Mora, J.R. et al. (2017). Theoretical analysis of C–F bond cleavage mediated by cob[I]alamin-based structures. *J. Mol. Model.* 23: 264. <https://doi.org/10.1007/s00894-017-3431-8>.
- 31 Polanyi, J.C. and Zewail, A.H. (1995). Direct observation of the transition state. *Acc. Chem. Res.* 28: 199–132. <https://doi.org/10.1021/ar00051a005>.
- 32 Politzer, P., Burda, J.V., Concha, M.C. et al. (2006). Analysis of the reaction force for a gas phase  $s_N2$  process. *J. Phys. Chem. A* 110: 756–761. <https://doi.org/10.1021/jp0582080>.
- 33 Burda, J.V., Toro-Labbé, A., Gutiérrez-Oliva, S. et al. (2007). Reaction force decomposition of activation barriers to elucidate solvent effects. *J. Phys. Chem. A* 111 (13): 2455–2457. <https://doi.org/10.1021/jp0709353>.

- 34 Giri, S., Echegaray, E., Ayers, P.W. et al. (2012). Insights into the mechanism of an  $s_N2$  reaction from the reaction force and the reaction electronic flux. *J. Phys. Chem. A* 116 (40): 10015–10026. <https://doi.org/10.1021/jp3076707>.
- 35 Burda, J.V., Morray, J.S., Toro-Labbé, A. et al. (2009). Analysis of solvent effects in the addition of HCL to propene. *J. Phys. Chem. A* 115: 6500–6505. <https://doi.org/10.1021/jp9025927>.
- 36 Jaque, P., Toro-Labbé, A., Geerling, P., and De Proft, F. (2009). Theoretical study of the regioselectivity of [2+2] photocycloaddition reaction of acrolein with olefins. *J. Phys. Chem. A* 113: 332–344. <https://doi.org/10.1021/jp807754f>.
- 37 Toro-Labbé, A., Gutiérrez-Oliva, S., Concha, M.C. et al. (2004). Analysis of two intramolecular proton transfer processes in terms of the reaction force. *J. Chem. Phys.* 121 (10): 4570–4576. <https://doi.org/10.1064/1.1777216>.
- 38 Herrera, B. and Toro-Labbé, A. (2004). The role of the reaction force to characterize local specific interactions that activate the intramolecular proton transfer in DNA bases. *J. Chem. Phys.* 121: 7096–7102. <https://doi.org/10.1064/1.1792091>.
- 39 Rincon, E., Jaque, P., and Toro-Labbé, A. (2006). A reaction force analysis of the effect of Mg(II) on the 1,3 intramolecular hydrogen transfer in thymmine. *J. Phys. Chem. A* 120: 9478–9485. <https://doi.org/10.1021/jp062870u>.
- 40 Yopez, D., Murray, J.S., Santos, J.C. et al. (2013). Fine structure in the transition region: reaction force analyses of water-assisted proton transfer. *J. Mol. Model.* 19 (7): 2689–2697. <https://doi.org/10.1007/s00894-012-1475-3>.
- 41 Inostrosa-Rivera, R., Herrera, B., and Toro-Labbé, A. (2014). Using the reaction force and the reaction electronic flux on the proton transfer of formamide derived systems. *Phys. Chem. Chem. Phys.* 16: 14489–14495. <https://doi.org/10.1039/c3cp55159h>.
- 42 Murray, J.S., Lane, P., Nieder, A. et al. (2009). Enhanced detonation sensitivities of silicon analogs of PETN: reaction force analysis and the role of  $\sigma$ -hole interactions. *Theor. Chem. Acc.* 127 (4): 345–354. <https://doi.org/10.1007/s00214-009-0723-9>.
- 43 Murray, J.S., Lane, P., Gobel, M. et al. (2009). Reaction force analysis of nitro-acid tautomerizations of trinitromethane, the elusive trinitromethanol, picric acid and 2,4-dinitro-1h-imidazole. *Theor. Chem. Acc.* 124: 355–363. <https://doi.org/10.1007/s00214-009-0630-2>.
- 44 Labet, V., Morrel, A., Grand, A., and Toro-Labbé, A. (2008). Theoretical study of cytosine deamination from the perspective of the reaction force analysis. *J. Phys. Chem. A* 112: 11487–11494. <https://doi.org/10.1021/jp8059097>.
- 45 Cortes-Arriagada, D., Gutiérrez-Oliva, S., Herrera, B. et al. (2014). The mechanism of chemisorption of hydrogen atom on graphene: insights from the reaction force and the reaction electronic flux. *J. Chem. Phys.* 141: 134701. <https://doi.org/10.1063/1.4896611>.
- 46 Villegas-Escobar, N., Toro-Labbé, A., Becera, M. et al. (2017). A DFT study of hydrogen and methane activation by  $b(c_6f_5)_3/p(t-bu)_3$  and  $al(c_6f_5)_3/p(t-bu)_3$  frustrated Lewis pairs. *J. Mol. Model.* 23: 234. <https://doi.org/10.1007/s00894-017-3404-y>.



- 47 Sanderson, R.T. (1951). An interpretation of bond lengths and a classification of bonds. *Science* 114: 670–672. <https://doi.org/10.1126/science.114.2973.670>.
- 48 Sanderson, R.T. (1955). Partial charges on atoms in organic compounds. *Science* 121: 207–208. <https://doi.org/10.1126/science.121.3137.207>.
- 49 Balawender, R., Komorowski, L., and Roszak, S. (1997). Acidic and basic molecular hardness in LCAO approximation. *Int. J. Quantum Chem.* 61 (3): 499–505.
- 50 Balawender, R. and Komorowski, L. (1998). Atomic Fukui function indices and local softness ab initio. *J. Chem. Phys.* 109: 5203. <https://doi.org/10.1063/1.477137>.
- 51 Echegaray, E. and Toro-Labbé, A. (2008). Reaction electronic flux: a new concept to get insights into reaction mechanisms. Study of model symmetric nucleophilic substitutions. *J. Phys. Chem. A* 112: 11801–11807. <https://doi.org/10.1021/jp805225e>.
- 52 Flores-Morales, P., Gutiérrez-Oliva, S., Silva, E., and Toro-Labbé, A. (2010). The reaction electronic flux: a new descriptor of the electronic activity taking place during a chemical reaction. application to the characterization of the mechanism of the Schiff's base formation in the Maillard reaction. *J. Mol. Struct. THEOCHEM* 943: 11801–11807. <https://doi.org/10.1016/j.theochem.2009.11.013>.
- 53 Ceron, M.L., Echegaray, E., Gutiérrez-Oliva, S. et al. (2011). The reaction electronic flux in chemical reactions. *Sci. China Chem.* 54: 1982–1988. <https://doi.org/10.1007/s11426-011-4447-z>.
- 54 Hernandez-Mancera, J.P., Nuñez-Zarur, F., Gutiérrez-Oliva, S. et al. (2020). Diels–Alder reaction mechanisms of substituted chiral anthracene: a theoretical study based on the reaction force and reaction electronic flux. *J. Comput. Chem.* 41: 2022–2032. <https://doi.org/10.1002/jcc.26360>.
- 55 Joseph, H.V. and Derricotte, W.D. (2020). Intramolecular proton transfer in the isomerization of hydroxyacetone: characterization based on reaction force analysis and the bond fragility spectrum. *Int. J. Quantum Chem.* 120: e26269. <https://doi.org/10.1002/qua.26269>.
- 56 Giri, S., Parida, R., Jana, M. et al. (2017). Insights into the mechanism of ground and excited state double proton transfer reaction in formic acid dimer. *J. Phys. Chem. A* 121: 9531–9543. <https://doi.org/10.1021/acs.jpca.7b09819>.
- 57 Parida, R. and Giri, S. (2019). Insights into the activation process of CO<sub>2</sub> through dihydrogenation reaction. *J. Mol. Model.* 15: 334. <https://doi.org/10.1007/s00894-019-4210-5>.
- 58 Guzman-Angel, D., Gutiérrez-Oliva, S., and Toro-Labbé, A. (2019). Hydrogenation and hydration of carbon dioxide: a detailed characterization of the reaction mechanisms based on the reaction force and reaction electronic flux analyses. *J. Mol. Model.* 25: 16. <https://doi.org/10.1007/s00894-018-3891-5>.
- 59 Azofra, L.M., Elguero, J., and Alkorta, I. (2020). A conceptual DFT study of phosphonate dimers: dianions supported by H-bonds. *J. Phys. Chem. A* 124: 2207–2214. <https://doi.org/10.1021/acs.jpca.9b10681>.
- 60 Giri, S., Inostroza-Rivera, R., and Jana, M. (2016). The Beckmann rearrangement in the framework of reaction electronic flux. *Theor. Chem. Acc.* 136: 9. <https://doi.org/10.1007/s00214-016-2025-3>.

- 61 Azofra, L.M., Alkorta, I., Elguero, J., and Toro-Labbé, A. (2012). Mechanisms of formation of hemiacetals: intrinsic reactivity analysis. *J. Phys. Chem. A* 116: 8250–8259. <https://doi.org/10.1021/jp304495f>.
- 62 Mora, J.R., Rincon, L., Torres, F.J. et al. (2019). Theoretical study of the furfuryl benzoate and furfuryl acetate pyrolysis. *J. Phys. Org. Chem.* 32: e3790. <https://doi.org/10.1002/poc.3790>.

## 13

### Mechanical Force

Tom Bettens and Frank De Proft

Research Group of General Chemistry (VUB), Vrije Universiteit Brussel (VUB), Pleinlaan 2, B-1050 Brussels, Belgium

#### 13.1 Introduction

Every process that results in the interconversion of chemical entities, i.e. chemical reactions [1], can typically be classified as either a thermochemical, electrochemical, or photochemical one. The associated subdisciplines of chemistry concern the effect of temperature, electrical current, or light on matter. In the shadow of these famed fields of study – unrightfully so – a fourth way for initiating a chemical process exists, and mankind has been aware of the unique and fascinating reaction outcomes in this field for a very long time [2]. In the fourth century before the common era, a Greek scientist by the name of Theophrastus described the formation of the liquid metal mercury by grinding cinnabar, a mineral of mercuric sulfide, in vinegar with a copper pestle and mortar [3, 4]. To date, this is the oldest preserved text on a mechanochemical reaction, i.e. a chemical process that is initiated by the direct absorption of mechanical energy by a chemical system.

Today, these primitive, manual grinding techniques have been replaced by motorized experimental equipment and mechanochemical research has been revolutionized from a slow and tedious science to an automated one with controlled procedures, the hallmark of modern mechanochemistry being ball milling [5]. Furthermore, the realization that mechanochemistry is a *dry way* of carrying out chemical reactions with unique reaction outcomes is the recurring theme that makes it a well-established research area today [6–9].

But mechanochemistry is still surrounded by a veil of mystery. The exact mechanism behind the fascinating chemical transformations achieved by mechanical activation is often poorly understood, owing largely to the bulk aspect of these *classical* techniques. A radical paradigmatic shift was initiated when atomic force microscopy (AFM) techniques were designed to study individual molecules when subjected to an external – usually pulling – force. In an AFM experiment, a scanning probe or *tip*, attached to a microcantilever, is brought in close proximity with a substrate surface. By sliding the tip over a two-dimensional *XY* area, one can measure the force on the cantilever and gain insight into the topology of the

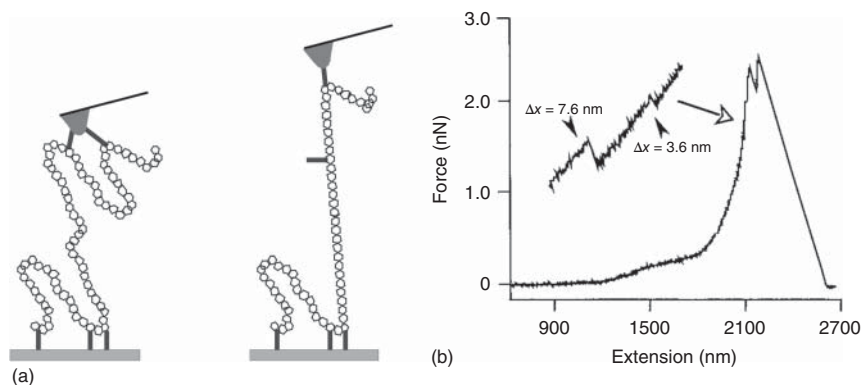


**Figure 13.1** (a) Schematic illustration of an amylose polysaccharide covalently attached to an AFM tip and substrate surface; (b) The force–extension curve shows multiple bond ruptures before the covalent link between the tip and surface is broken around 2100 nm of extension. Reproduced with permission from Ref. Grandbois et al. [11].

substrate surface with *sub*-nanometer precision [10]. Now imagine anchoring the tip to the substrate surface with a target molecule and scanning in the *Z*-direction, i.e. increasing the distance between the AFM tip and the surface. This is the exact experiment conducted by Grandbois et al. for measuring the mechanical strength of a covalent bond in an amylose backbone anchored between a silicon oxide tip and surface (Figure 13.1) [11]. In the force–extension curve, multiple irreversible bond ruptures leading to small elongations and maintaining the covalent link between tip and surface are found, before the backbone ruptures at an extension of 2100 nanometer. These single-molecule force spectroscopy (SMFS) experiments were the onset of covalent or molecular mechanochemistry and set off a train of experiments studying molecules and molecular reactions when mechanical force is applied to the molecular system [12]. In stark contrast to classical bulk mechanochemistry, properties can be investigated and chemical reactions can be initiated, in a very controlled spirit, by a pure mechanical effect on an individual molecule.

By the time of the SMFS experiment (Figure 13.1), accurate *ab initio* calculations were already a mainstream procedure in quantum and computational chemistry. Molecular mechanochemistry, therefore, witnessed a simultaneous development of experimental and theoretical techniques, which is very unique in chemistry [12–14]. Naturally, single-molecule mechanochemical reactions are usually supported by theoretical investigations. Some notable examples are the thermally forbidden ring opening of cyclobutene [15, 16], the synthesis of polyacetylene [17, 18], and the spiropyran-merocyanine isomerization [19]. These three examples demonstrate the unusual reactivity that a mechanical force can induce, the synthesis of a polymer that is enormously facilitated by single-molecule activation and a molecular force probe, i.e. a single molecule or *mechanophore* that allows for the detection and quantification of mechanical strain, respectively. The reaction mechanics of these processes are known; in no small part thanks to quantum chemical techniques.

Quantum mechanochemistry has thus played a prominent role in the evolution of molecular mechanochemistry in recent years, particularly for gaining insight into the mechanism of mechanically triggered reactions, but essential guiding principles are missing. In other words, a true understanding of how a mechanical force can influence the reactivity of a single molecule is lacking. This chapter focuses on recent efforts to understand chemical reactivity, induced by mechanical force in the context of conceptual density functional theory (DFT).

## 13.2 Quantum Mechanochemistry

Mechanical forces at the molecular level, very much like macroscopic applications, change the structure of molecules. In other words, the potential energy surface of a molecule is modified – or *tilted* – owing to the external perturbation [13, 14]. In the last two decades, which are characterized by a remarkable spike in the interest of single-molecule mechanochemistry, several theoretical approaches have been developed to simulate the structure and other properties of molecules when subjected to an external force. There are two important aspects of mechanochemical calculations. First, the force vector is applied to two atoms that define a vector  $\mathbf{R} = \mathbf{R}_j - \mathbf{R}_i$ , where  $\mathbf{R}_i$  and  $\mathbf{R}_j$  are the atomic positions of the two atoms and, second, the magnitude of the force vector is constant.

In a simulation, one either controls the bond distance  $R$  or the external force  $F_{\text{ext}}$ . The former is an indirect approach modeling the external force through the effect on the molecular structure and was the chronologically first method in quantum mechanochemistry. It is generally known by the acronym CoGEF (Constrained Geometries simulate External Force) and is still a popular method today [20]. In the CoGEF approach, a molecule is constrained by a fixed distance  $R$  and an otherwise relaxed geometry optimization is performed. When an external force with magnitude  $F_{\text{ext}}$  is applied, the molecule is elongated from its original equilibrium distance  $R_e$  by an amount  $\Delta R$  given by the condition:

$$F_{\text{ext}} = \frac{\partial V}{\partial R} \quad (13.1)$$

at the new equilibrium, meaning that the internal restoring force and the external force cancel one another. The CoGEF potential is then

$$V_{\text{CoGEF}}(\mathbf{x}, F_{\text{ext}}) = V_{\text{BO}}(\mathbf{x}) - F_{\text{ext}}(\Delta R)R \quad (13.2)$$

with  $V_{\text{BO}}$  the Born–Oppenheimer potential energy surface and  $\mathbf{x}$  the set of atomic positions. The vector character in the second term was excluded assuming the two vectors to be parallel. One can then calculate the constant force corresponding to an elongation  $\Delta R$  either numerically through Eq. (13.1) or by fitting a suitable analytic potential to the computed  $V(\Delta R)$  data points. One potential that is often used to describe bond elongations is the Morse potential (Eq. (13.3)): [21].

$$V_{\text{Morse}}(\Delta R) = D_e(1 - \exp(-\alpha\Delta R))^2 \quad (13.3)$$

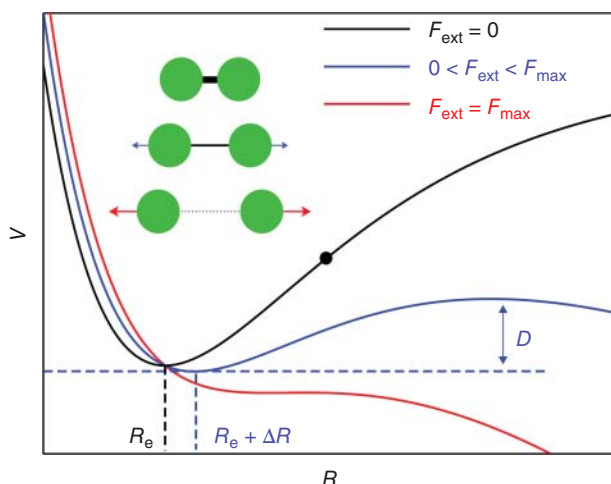


**Figure 13.2** Generic potential energy curves showing the influence of an external force in case of a diatomic molecule. Morse potential (black); a small pulling force shifts the equilibrium bond distance and lowers the bond dissociation barrier (blue); barrierless dissociation when  $F_{\text{ext}} = F_{\text{max}}$  (red). Reproduced from Ref. Bettens et al. [22] with permission from the PCCP Owner Societies.

with  $D_e$  the dissociation energy and  $\alpha$  a parameter that controls the width of the dissociation curve. Figure 13.2 shows a generic potential energy curve of a diatomic molecule that is modified or *tilted* by an external pulling force. In the absence of an external force, the bond stretching is modeled by a Morse potential. When a small external force is applied, the equilibrium distance is shifted by an amount  $\Delta R$  and, importantly, the bond dissociation energy decreases. An important consequence of applying an external force to a molecule is the susceptibility to thermal dissociation; Section 13.3.1 treats this aspect of mechanochemistry in more detail. When the external force is too large, no more equilibrium exists and the bond/molecule dissociates without energy barrier [22, 23].

An alternative approach for simulating the structure of molecules when an external force is applied is by controlling  $F_{\text{ext}}$ , in contrast to the CoGEF approach in which this parameter is obtained indirectly through a structural constraint. Ribas-Arino et al. proposed a self-consistent approach by applying the external force directly to the respective atoms: [15].

$$V_{\text{EFEI}}(\mathbf{x}, F_{\text{ext}}) = V_{\text{BO}}(\mathbf{x}) - F_{\text{ext}}R(\mathbf{x}) \quad (13.4)$$

The acronym EFEI in Eq. (13.4) means that the External Force is Explicitly Included in the electronic structure calculation. Similar isotensional approaches have been proposed simultaneously [16, 24]; however, the EFEI method is the most commonly used and has been implemented in the ORCA (version 4.0 and later) and Q-Chem (version 4.3 and later) software packages.

The isometric CoGEF and isotensional EFEI (and other) methods are very complementary and have played a prominent role into understanding the mechanical strength and mechanically induced reaction pathways during the mechanochemical

*boom* in recent years. However, one does not gain a fundamental insight into the chemical reactivity of a molecule when an external mechanical force is applied to it. Surely, force analysis tools for investigating the distribution of mechanical energy and the mechanical strength of bonds in molecules have been developed (external force does not activate one region in a molecule but the system as a whole) [25, 26]. The directional character of a force, prescribed by the pair of atoms to which it is applied, can deform – or with a chemical term *activate* – different regions in a molecule and certainly influence the molecular reactivity in different ways. But very little is known about the changes of the intrinsic reactivity of molecule when an external force is applied to it, and conceptual DFT can offer new insight into mechanochemical reactivity.

## 13.3 Mechanical Force and Conceptual DFT

### 13.3.1 Importance of a Small Force

Central in conceptual DFT is the perturbational approach to quantify changes in the energy through response functions, with particular interest for lower-order perturbations which best describe the system around its equilibrium, i.e. for small perturbations [27]. In this section, the peculiar mechanical stability of a chemical bond/system is briefly addressed, a system is as strong as its weakest bond when an external pulling force is applied. A perturbational approach thus seems naturally relevant for quantifying mechanical activation. The well-known JEDI analysis tool, for example, quantifies the strain in bonds, angles and dihedral angles based on the harmonic approximation [25].

In the CoGEF approach, a suitable analytic potential such as the Morse potential (Eq. (13.3)) can be used to simulate the elongation or compression molecule by a mechanical force. The first derivative of this potential (or the negative) is the internal restoring force the molecule experiences at a distance  $R$ :

$$\frac{\partial V_{\text{Morse}}}{\partial R} = 2D_e \alpha e^{-\alpha(R-R_e)} \left( 1 - e^{-\alpha(R-R_e)} \right) \quad (13.5)$$

According to the CoGEF formalism, the system has an equilibrium distance  $R$  when the external force is equal in magnitude to the internal restoring force but oppositely oriented. For a compressive force, meaning  $R < R_e$ , the first derivative of the Morse potential in Eq. (13.5) increases in absolute value and a larger compressive force is needed to shorten the bond length. For  $R > R_e$  on the other hand, the first derivative reaches a maximum, meaning that there exists a maximum constant pulling force  $F_{\text{max}}$  that a bond (or molecule) can sustain. The analytic expression of  $F_{\text{max}}$  can be obtained by setting the second derivative to 0 and solving this equation for  $R$ , yielding  $R_{\text{max}}$ :

$$\frac{\partial^2 V_{\text{Morse}}}{\partial R^2} = -2D_e \alpha^2 e^{-\alpha(R-R_e)} \left( 1 - 2e^{-\alpha(R-R_e)} \right) = 0 \quad (13.6)$$

$$R_{\text{max}} = R_e + \frac{1}{\alpha} \ln(2) \quad (13.7)$$

At  $R_{\max}$ , the Morse potential has an inflection point. Substituting this distance in Eq. (13.5) yields

$$F_{\max} = \frac{\alpha D_e}{2} \quad (13.8)$$

Figure 13.3a graphically illustrates Eq. (13.5) for  $H_2$  with numerical values of 1.0318, 1.404, and 0.1724 (all in a.u.) for  $\alpha$ ,  $R_e$ , and  $D_e$ , respectively. The curve reaches a maximum of 0.0889 a.u. or 7.327 nN (nano-Newton) at  $R_{\max} = 2.076$ .

While in theory any distance up to  $R_{\max}$  can be realized by applying a constant external force, the thermal stability of the chemical bond has to be considered. In

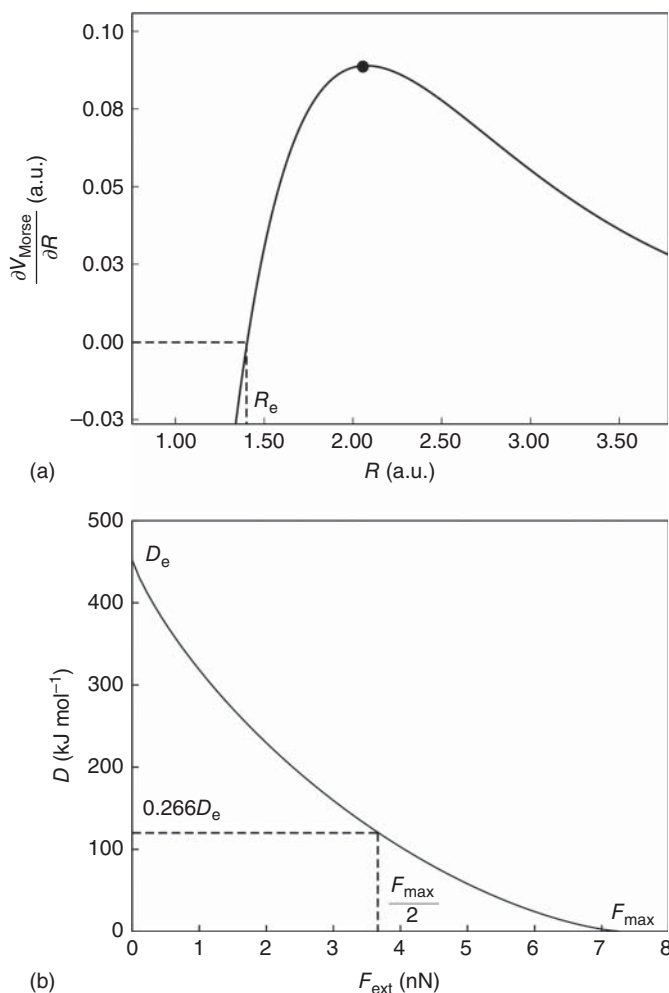


**Figure 13.3** (a) The internal restoring force of the  $H_2$  molecule. A black dot indicates the point where the internal restoring force is maximum; (b) bond dissociation barrier of  $H_2$  as a function of an external pulling force. At 50% of  $F_{\max}$ , the bond dissociation barrier decreases to  $0.266 D_e$ . Reproduced from Ref. Bettens et al. [22] with permission from the PCCP Owner Societies.



particular, pulling forces destabilize chemical bonds by lowering the dissociation energy (cf. Figure 13.2). For  $F_{\text{ext}} > 0$ , one can calculate the two stationary points of the blue curve in Figure 13.2 analytically and write the dissociation barrier  $D$  (i.e. the energy difference between the two stationary points) as a function of  $F_{\text{ext}}$ :

$$D(F_{\text{ext}}) = D_e \sqrt{1 - \frac{F_{\text{ext}}}{F_{\text{max}}}} + \frac{F_{\text{ext}}}{\alpha} \ln \left( \frac{1 - \sqrt{1 - \frac{F_{\text{ext}}}{F_{\text{max}}}}}{1 + \sqrt{1 - \frac{F_{\text{ext}}}{F_{\text{max}}}}} \right) \quad (13.9)$$

This equation is plotted for the  $\text{H}_2$  molecule in Figure 13.3b. For  $F_{\text{ext}} = 0$ , the barrier goes to  $D_e$ , corresponding to the dissociation energy in the *normal* Morse potential. For  $F_{\text{ext}} = F_{\text{max}}$ , the barrier converges to zero, which corresponds to the barrierless dissociation process in Figure 13.2. Strikingly, a rapid decrease of the dissociation energy is found, meaning that the application of an external force along a chemical bond is an effective stimulus to trigger thermal dissociation. However, when the force is applied to trigger a specific chemical reaction, (homolytic) bond dissociation owing the application of an external force is usually not desirable; instead, mechanochemical activation provokes a specific trajectory on a potential energy surface through a small perturbation of the molecular geometry. A perturbational approach for quantifying changes in the reactivity of a molecular system thus seems naturally adequate.

### 13.3.2 Mechanochemical Response Functions

Central in conceptual DFT is the energy functional  $E[N, v(\mathbf{r})]$  and the quantification of chemical reactivity through reactivity indices with a robust mathematical definition. More precisely, a perturbational approach of the molecular electronic energy,  $E$ , with respect to the number of electrons,  $N$ , and/or the external potential,  $v(\mathbf{r})$ , is used. The following question can then be asked: can this approach be extended for different external stimuli, such as an external mechanical force, and obtain response functions of the following type

$$\frac{\partial X}{\partial \mathbf{F}_{\text{ext}}} \quad (13.10)$$

where  $X$  is a reactivity index? [28] This straightforward question does not have a simple answer for a mechanochemical extension because an external force is applied to the nuclei and does not directly influence the electronic energy of a molecule.

Conceptual DFT response functions are always evaluated at a constant molecular geometry to simulate the perturbation with respect to  $N$  and/or  $v(\mathbf{r})$  at the onset of a chemical reaction. Consider, for example, the electronic potential  $\mu$  and the chemical hardness  $\eta$  being the respective first and second order derivative of the molecular energy with respect to  $N$ . The basic ingredients to calculate these response functions are the *vertical* ionization energy and *vertical* electron affinity. When calculating  $\mu$  and  $\eta$  at a constant molecular geometry, the response with respect to  $\mathbf{F}_{\text{ext}}$  will always be 0, regardless of the orientation or magnitude of the force vector: the same energy (more correct is to say *work*)  $F_{\text{ext}} R$  (cf. Eqs. (13.2) and (13.4)) will be transferred to

the  $N$ ,  $N + 1$ , and  $N - 1$  electron system. These terms will cancel each other when subtracting energies. Analogously,  $\mathbf{F}_{\text{ext}}$  does not influence the electron density  $\rho(\mathbf{r})$ , which is the basic ingredient for the evaluation of responses owing to a perturbation of  $v(\mathbf{r})$ , for a constant molecular geometry. Additionally, one is always confronted with the inevitable connection between  $v(\mathbf{r})$  and an external force: the effect of an external force, being a change in the nuclear constellation of a molecule, will always affect the potential felt by the electrons due to the nuclei.

A simple approach to circumvent the issues above is to determine force-modified geometries and evaluating the response functions at different geometries. The response of a reactivity index of the form in Eq. (13.10) can then be obtained through either a finite difference approach or by fitting a function  $X(F_{\text{ext}})$ . De Proft and coworkers adopted this method for evaluating the local effect of an external force on individual bonds (when the force is aligned with the bond axis) and bond angles (when the force is oriented perpendicular to a bond). Below, two illustrative examples are given demonstrating the changes in chemical reactivity when a mechanical force is applied to bonds (probed by the global hardness and electrophilicity) and angles (local softness) [22, 29].

### 13.3.3 Chemical Bonds Stressed by Mechanical Force

When a mechanical force is applied to two atoms in a molecule, the geometry of the entire molecule is generally affected, meaning that every chemical bond, but also angles and dihedral angles, are stressed to some degree. The effect will be largest for bonds located in the chain connecting the two pulling positions. Bettens et al. rationalized changes of the chemical hardness and the electrophilicity index, among others, for a set of 21 diatomic molecules when the bond distance is altered by an external force aligned with the bond [22]. Considering the strong decrease in the dissociation barrier with pulling forces, demonstrated in Section 13.3.1, the maximum force of the hypothetical experiments was arbitrarily set to  $0.5F_{\text{max}}$ . The authors determined the molecular geometry corresponding to 11 equidistant values of  $F_{\text{ext}}$  between  $-0.5F_{\text{max}}$  and  $0.5F_{\text{max}}$  by first fitting the Morse parameters and using the relation between  $F_{\text{ext}}$  and  $R$ , according to the CoGEF approach in Section 13.2. For each system, polynomials of second order were fit to computed  $X(F_{\text{ext}})$  values, where  $X$  represents the reactivity index, by minimizing the root-mean-square deviation (RMSD), yielding the mechanochemical response functions. The force-independent terms in these polynomials,  $X(0)$ , were calculated at  $R_e$  and were kept constant. Thus, the second-order polynomial has two parameters,  $a$  and  $b$ ,

$$X^{(2)}(F_{\text{ext}}) = aF_{\text{ext}}^2 + bF_{\text{ext}} + X(0) \quad (13.11)$$

The linear parameters in  $F_{\text{ext}}$  of the second-order polynomial are listed in Table 13.1 for the chemical hardness  $\eta$ , the global softness  $S$  (which is the inverse of  $\eta$ ) and the electrophilicity index  $\omega$ . These parameters represent the first-order change in chemical properties around the equilibrium, i.e.  $\left. \frac{\partial X^{(2)}}{\partial F_{\text{ext}}} \right|_{F_{\text{ext}}=0}$ . For clarity, the subscript  $F_{\text{ext}} = 0$  will be omitted hereafter. The discussion of mechanical response functions will primarily be based on this table, because the first-order term has

**Table 13.1** Firstorder response (in a.u.) of  $\eta$ ,  $S$  and  $\omega$  with respect to an external force oriented along the bond axis, according to a second-order polynomial fit.

	$\frac{\partial \eta^{(2)}}{\partial F_{\text{ext}}}$	$\frac{\partial S^{(2)}}{\partial F_{\text{ext}}}$	$\frac{\partial \omega^{(2)}}{\partial F_{\text{ext}}}$
H <sub>2</sub>	-0.4313	1.0196	-0.0410
HF	-0.1672	0.4436	-0.0058
HCl	-0.1222	0.5214	0.0084
HBr	-0.1312	0.6586	0.0169
F <sub>2</sub>	-0.6695	1.9945	0.3621
Cl <sub>2</sub>	-0.5374	3.4234	0.3655
Br <sub>2</sub>	-0.3992	3.3898	0.3069
FCl	-0.4124	2.0071	0.2647
FBr	-0.3597	2.1888	0.2547
ClBr	-0.4981	3.7181	0.3741
N <sub>2</sub>	-0.1457	0.3343	0.0252
P <sub>2</sub>	-0.2937	2.2166	0.0437
PN	-0.0792	0.4265	0.0373
BN	-0.1307	1.4116	-0.0030
O <sub>2</sub>	-0.0289	0.1319	0.0975
S <sub>2</sub>	-0.0459	0.5217	0.1306
SO	-0.0168	0.1346	0.0834
CO	-0.0259	0.0797	0.0196
LiF	-0.5312	3.3022	-0.0186
NaCl	-0.6475	7.0596	0.0344
MgO	-0.1902	4.3190	0.0512

Data adapted from Ref. [22].

largest contribution to the total perturbation for small forces (the importance of applying a small external force was stressed in Section 13.3.1).

The derivatives in Table 13.1 provide quantitative information on the change of a chemical property when the bond length in a diatomic molecule is altered by a small external force. In particular, the sign of these first-order response functions was rationalized in terms of the ground state geometry and electronic structure. Importantly, negative electron affinities, indicative for unstable anions, were found for H<sub>2</sub>, HF, HCl, HBr, N<sub>2</sub>, and CO; however, these were not set to 0 – as is commonly done for unstable anions [30] – because then also the derivative of the vertical electron affinity  $A$  with respect to  $F_{\text{ext}}$  would be 0 in most of these cases which nevertheless shows an intrinsically different behavior for this group of diatomics.

The response of  $\eta$  is smaller than 0 for all molecules, meaning that the chemical hardness of a diatomic molecule decreases when it is stretched by an external pulling force. Evidently, the response of  $S$  is positive for all molecules. This

observation is in agreement with the principle of maximum hardness (the two atoms arrange themselves into a configuration with maximum hardness) for pulling forces [31, 32]. However, in the case of a compressing force ( $F_{\text{ext}} < 0$ ), an increase in chemical hardness is expected by virtue of the negative response.

In order to understand the sign of this derivative, consider a frozen orbital approximation. The chemical hardness is then equal to the highest occupied molecular orbital (HOMO)–lowest unoccupied molecular orbital (LUMO) gap. For the derivative with respect to  $F_{\text{ext}}$ , one can write

$$\frac{\partial \eta}{\partial F_{\text{ext}}} \approx \frac{\partial E_{\text{LUMO}}}{\partial F_{\text{ext}}} - \frac{\partial E_{\text{HOMO}}}{\partial F_{\text{ext}}} \quad (13.12)$$

The effect of an external pulling force increases the internuclear distance of a diatomic molecule. For a diatomic system with a bonding HOMO and an antibonding LUMO, such as  $\text{H}_2$ , the decreasing orbital overlap will cause an increase in the HOMO energy and a decrease in the LUMO energy, also making the chemical bond more reactive. The approximation in Eq. (13.12) is then indeed smaller than 0. This simple proof is very straightforward and arguably trivial for a system like  $\text{H}_2$  but, nevertheless, it is important to retrieve these results. Additionally, not every chemical bond is characterized by a bonding HOMO and antibonding LUMO. Examples of such systems from Table 13.1 are the dihalogens having antibonding HOMO and LUMO as well as the ionic systems (LiF, NaCl, and MgO) with nonbonding frontier orbitals. Nevertheless, the response of  $\eta$  for these systems follows the same trend as the other chemical bonds.

Importantly, the same results were obtained for the response of  $\eta$  along vibrational modes of simple polyatomic molecules, such as  $\text{H}_2\text{O}$ ,  $\text{NH}_3$ , and  $\text{C}_2\text{H}_6$  [33]. Although a distorted geometry through molecular vibration is not identical to a force-induced equilibrium structure in a nonlinear polyatomic molecule and does not strictly fall under the proposed mechanochemical rules, modes dominated by simultaneous elongations of equivalent bonds along the normal mode of vibration can be rationalized in the same philosophy. In this work, the symmetric stretching modes in  $\text{H}_2\text{O}$ ,  $\text{NH}_3$ , and  $\text{C}_2\text{H}_6$  are dominated by simultaneous bond elongations of O–H, N–H, and C–H bonds, respectively. In the case of the ethane, all C–H bonds are significantly elongated, while there is a slight compression (five times smaller than the C–H elongation along the vibrational mode) of the C–C bond. Interestingly, all of these vibrational modes decrease the chemical hardness of the molecule, in analogy with the bond length elongations owing to an external force for diatomic molecules.

The response of the electrophilicity on the other hand is positive for all systems, except for  $\text{H}_2$ , HF, BN, and LiF which have a low negative first-order response in Table 13.1. The authors rationalized this sign by using the definition of the electrophilicity index and rewriting the derivative of  $\omega$ :

$$\omega = \frac{\mu^2}{2\eta} \quad (13.13)$$

$$\frac{\partial \omega}{\partial F_{\text{ext}}} = \frac{\partial I}{\partial F_{\text{ext}}} \left( \frac{\gamma}{2} - \frac{\gamma^2}{2} \right) + \frac{\partial A}{\partial F_{\text{ext}}} \left( \frac{\gamma}{2} + \frac{\gamma^2}{2} \right) \quad (13.14)$$

where, for  $A > 0$ ,  $\gamma$  is a positive number:

$$\gamma = \frac{\chi}{\eta} = \frac{(I + A)}{2(I - A)} \quad (13.15)$$

Because  $A$  is typically small compared to  $I$  and assuming a factor of 10 difference,  $\gamma \approx 0.6$ . The response of  $\omega$  is then more influenced by the second term (containing the derivative with respect to  $A$ ). Using again a frozen core approximation ( $A \approx E_{\text{LUMO}}$ ),  $\frac{\partial A}{\partial F_{\text{ext}}}$  is typically smaller than 0, if the LUMO is an antibonding orbital.

Similar to the chemical hardness, the electrophilicity was also found to increase upon geometric distortions along vibrational modes of  $\text{H}_2\text{O}$ ,  $\text{NH}_3$ , and  $\text{C}_2\text{H}_6$  [33]. Moreover, a positive correlation exists between the electrophilicity index and redox potentials [34, 35]. Therefore, the redox potential of molecules subjected to an external pulling force is expected to increase. Baldus and Gräter computed redox potentials of a cysteine dimer and indeed concluded that the redox potential of the dimer increases, in line with the positive response of  $\omega$  for  $\text{S}_2$  in Table 13.1 [36]. De Proft and coworkers stated that, in the case of the dicysteine system, the reduction reaction breaks the S-S bond and a pulling force increases the S-S bond distance, bringing the geometry closer to the one in the reduced form and therefore triggering the reduction. An external force should thus be oriented in a certain direction to steer a specific chemical reaction. In other words, the external force should be oriented along the reaction coordinate of the desired chemical transformation.

### 13.3.4 Bond Angles Stressed by Mechanical Force

Bond length alternations through the application of an external pulling force were shown to trigger reduction reactions, because the molecular geometry becomes distorted in the same way as a reduction process. In the same philosophy, the angular constraint on the  $\text{C}\equiv\text{C}$  bond in cyclic alkynes was translated to angular forces and the concurrent influence on its reactivity was scrutinized through conceptual DFT descriptors [29]. Alkynes can undergo 1,3-dipolar cycloaddition reactions with azides leading to the formation of 1,2,3-triazoles [37]. However, linear alkynes require a catalyst (for example Cu-based; cf. the acronym CuAAC or Copper-catalyzed Alkyne Azide Cycloaddition) or elevated reaction temperatures to trigger the cycloaddition [38, 39]. Cyclic alkynes (cyclooctynes and cycloheptynes) do not require a catalyst and can undergo strain-promoted alkyne azide cycloaddition (SPAAC) reactions under physiological reaction conditions, enabling *in vivo* biomolecule targeting and imaging [40–44].

Using the same CoGEF-based approach, Bettens et al. probed the reactivity of the  $\text{C}\equiv\text{C}$  bond through conceptual DFT indices when an alkyne is bent [29]. The authors revealed a linear relation between the force needed to bend one bond angle,  $F_{\text{ext},\perp}$ , and the angular deviation with respect to the equilibrium structure,  $\phi$ , by rewriting the force-dependent term in Eqs. (13.2) and (13.4):

$$-\int \mathbf{F}_{\text{ext}} \cdot \mathbf{R} = -\int \mathbf{F}_{\text{ext},\perp} \cdot (d\phi \times \mathbf{r}) = -\int (\mathbf{r} \times \mathbf{F}_{\text{ext},\perp}) \cdot d\phi \quad (13.16)$$

$$|\mathbf{F}_{\text{ext},\perp}| = \frac{2a\phi}{r} \quad (13.17)$$

In Eq. (13.17),  $a$  and  $r$  are the harmonic force constant of the bending and the length of the bond adjacent to the  $\text{C}\equiv\text{C}$  bond.

When both angles around the  $\text{C}\equiv\text{C}$  bond are bent away from linearity (in *syn* fashion), the molecule resembles a fragment of a cyclic alkyne, with smaller cyclic systems leading to smaller bond angles. Substituted 2-butyne fragments were used to evaluate the reactivity of cyclic alkynes. Upon bending, the  $\text{C}_{2s}$  and  $\text{C}_{2p}$  atomic orbitals start mixing with the  $\pi$  and  $\pi^*$  orbitals in the plane of the bending, while the orbitals perpendicular to the plane of bending are unaffected, lifting the degeneracy of the  $\pi$ -system [45]. As a result, the energy of the HOMO is increased, whereas the energy of the LUMO decreased. Accordingly, the global softness  $S$  of the acetylene fragment increases upon bending, i.e. perturbation to the molecular geometry away from the equilibrium, in analogy to stretching diatomic molecules (Figure 13.4).

In an alkyne-azide electrocyclization, the alkyne is typically electron-poor and interacts with the electron-rich azide [46]. Therefore, the electrophilic Fukui function, probing the difference in electron density when an electron is added to a chemical system, is more relevant than the nucleophilic analog.

$$f^+(\mathbf{r}) = \rho_{N+1}(\mathbf{r}) - \rho_N(\mathbf{r}) \quad (13.18)$$

In Eq. (13.18), one electron is added to the system. By condensing  $f^+(\mathbf{r})$  to the individual atoms by means of a population analysis, it is possible to quantify the density allocated to a specific atom when an electron is used as a model nucleophile. The Fukui function in Figure 13.5 also suggests that the reactivity of the triple bond increases upon bending. The substitution of a fluorine atom at one side of the triple

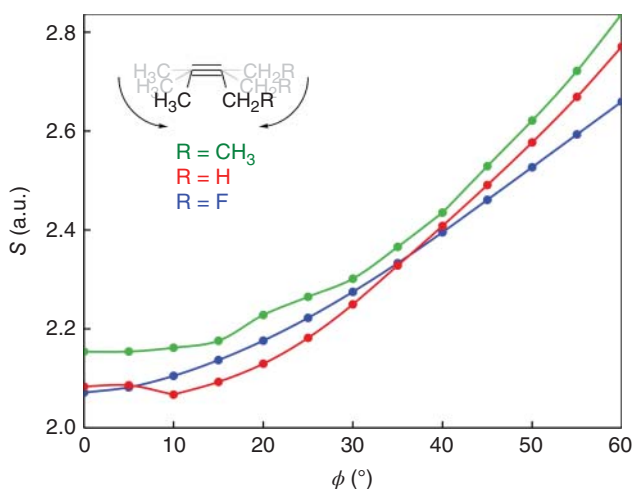


**Figure 13.4** The global softness of a 2-butyne fragment starts to increase when the triple bond is bent to an angle of  $15^\circ$  due to an increase in the in-plane  $\pi$ -HOMO energy and a decrease in the in-plane  $\pi$ -LUMO energy. Reproduced from Ref. Bettens et al. [29] with permission from the Royal Society of Chemistry.

bond also increases the Fukui function on the functional group, in accordance with the higher reaction rates of fluorinated cyclooctynes compared to the unsubstituted analog.

Interestingly, the global softness and the Fukui function do not increase rapidly for small perturbations up to  $15^\circ$ . Instead, a parabolic and sigmoid shape are retrieved, respectively. The local softness,  $s^+(\mathbf{r})$ , being the product of the softness and electrophilic Fukui function, shows the same behavior for small perturbations. Figure 13.5 conveniently illustrates the deviation from linearity around the  $\text{C}\equiv\text{C}$  bond typically found in cyclononynes, cyclooctynes, and cycloheptynes. The larger

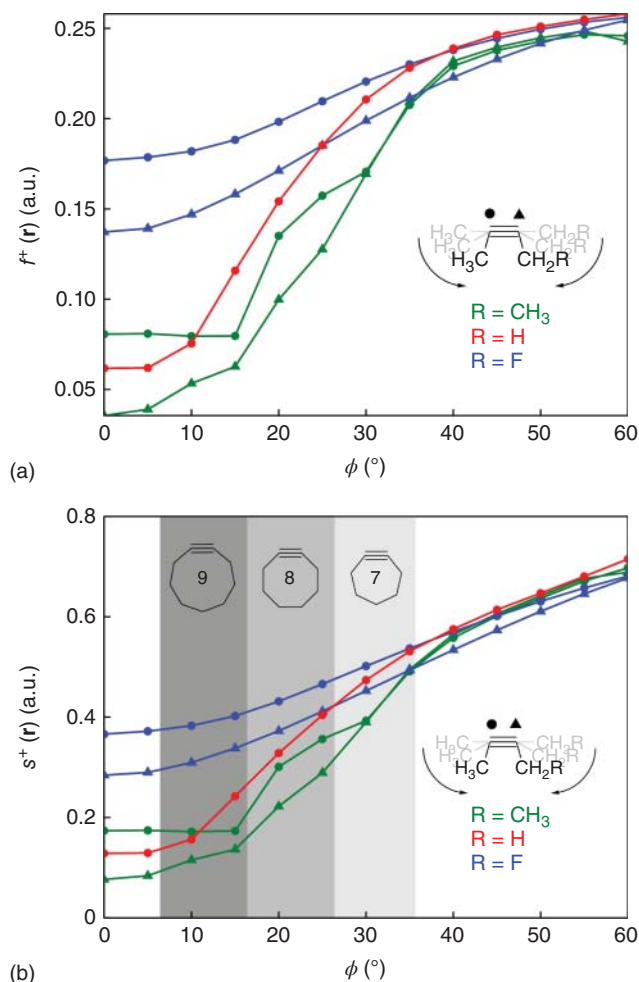


**Figure 13.5** (a) The electrophilic Fukui function of the two C-atoms in the alkyne group increases as the 2-butyne fragment is bent, indicating that smaller cyclic alkynes become more electrophilic; (b) the local softness also increases when the triple bond is bent, revealing clear trends in the reactivity of cyclic alkynes. Reproduced from Ref. Bettens et al. [29] with permission from the Royal Society of Chemistry.

cyclononynes, bearing nine atoms in the cyclic structure, are in the flat part of the curve. These larger structures do not significantly increase the reaction rate of cycloaddition reactions compared to linear alkynes, in accordance with the  $s^+(\mathbf{r})$  plot. Cyclooctynes, on the other hand, are the workhorse in SPAAC reactions and are located in the steeper part of the plot [41]. In particular, fluorinated cyclooctynes are used in SPAAC reactions for targeting biomolecules in organisms because they react faster than the parent cyclooctyne, which is also apparent from Figure 13.5. Most cycloheptynes are unstable and this family of cyclic alkynes is expected to be more reactive in cycloadditions than the cyclooctynes [47–49]. Interestingly, the difference between the curves diminishes for larger distortions because the Fukui function seems to converge at  $60^\circ$ , which corresponds to the geometry of an alkene.

Similar to the dissociation of bonds, in particular the S–S bond, in Section 13.3.3, one can interpret the increase of the Fukui function in terms of a reduction process: a disulfide can be reduced to two sulfides with two electrons and two protons; an alkyne can be reduced to an alkene with two electrons and two protons. The electrophilic Fukui function, being a measure for the electrophilic character of the alkyne, thus logically increases when the geometry of the alkyne is perturbed/bent toward the geometry of the reduced species, i.e. the alkene. The convergence of the Fukui function at  $60^\circ$  might suggest an interesting relation between mechanochemistry and redox chemistry; however, specific studies have not been conducted on this topic.

## 13.4 Conclusions and Outlook

The mechanochemistry of individual molecules which can nowadays be achieved with ingeniously setup experiments has triggered the interest in exploring the unusual reactivity of molecules induced by a slight geometric distortion owing to the application of an external mechanical force. While an array of new mechanochemical reactions with unique outcomes has been documented in recent years, demonstrating the relevance of this somewhat obscure chemical stimulus, a true understanding of the influence of mechanical activation on chemical reactivity is still lacking. The directional character of a mechanical force increases the complexity of the technique: as the system size grows, the combinations of attachment points (atoms) to which the force can be applied also increases tremendously. In view of the thermal stability of molecules subjected to an external force, the magnitude of the force vector should be small, rendering perturbational approaches appropriate for evaluating mechanochemical reactivity. Conceptual DFT, with all its successes in describing and quantifying reactivity, has been applied to some examples of unique reactions documented in literature. The evaluation of reactivity indices at distorted geometries correctly reproduce the chemical behavior to trigger specific reactions. Early work has also demonstrated the influence of a mechanical force on individual bonds and angles.

Bulk mechanochemistry, such as ball milling, has been an active field of research for many decades; however, it remains shrouded in a veil of mystery because the



size of the chemical system and the different types of interactions prevent high-level quantum chemical models. Single-molecule mechanochemistry, on the other hand, is a unique subdiscipline in chemistry as it witnessed a simultaneous development of theoretical and experimental techniques. With the emphasis on individual molecules, it is more feasible to establish a thorough theoretical framework and provide guidelines for designing new experiments.

## Bibliography

- 1 Muller, P. (1994). Glossary of terms used in physical organic chemistry (IUPAC recommendations 1994). *Pure Appl. Chem.* 66 (5): 1077–1184. <https://doi.org/doi:10.1351/pac199466051077>.
- 2 Takacs, L. (2013). The historical development of mechanochemistry. *Chem. Soc. Rev.* 42 (18): 7649–7659. ISSN 1460-4744 (Electronic) 0306-0012 (Linking). <https://doi.org/10.1039/c2cs35442j>.
- 3 Caley, E.R. and Richards, J.F.C. (1956). *Theophrastus on stones: Introduction, Greek Text, English Translation, and Commentary*. Columbus: Ohio State University.
- 4 Takacs, L. (2000). Quicksilver from cinnabar: the first documented mechanochemical reaction? *JOM* 52 (1): 12–13. <https://doi.org/10.1007/s11837-000-0106-0>.
- 5 Friscic, T., Mottillo, C., and Titi, H.M. (2020). Mechanochemistry for synthesis. *Angew. Chem. Int. Ed.* 59 (3): 1018–1029. ISSN 1521-3773 (Electronic) 1433-7851 (Linking). <https://doi.org/10.1002/anie.201906755>.
- 6 Margetić, D. and Štrukil, V. (2016). *Mechanochemical Organic Synthesis*, 55–139. Boston, MA: Elsevier. ISBN 978-0-12-802184-2. <https://doi.org/https://doi.org/10.1016/B978-0-12-802184-2.00002-9>. <https://www.sciencedirect.com/science/article/pii/B9780128021842000029>.
- 7 Howard, J.L., Cao, Q., and Browne, D.L. (2018). Mechanochemistry as an emerging tool for molecular synthesis: what can it offer? *Chem. Sci.* 9 (12): 3080–3094. ISSN 2041-6520 (Print) 2041-6520 (Linking). <https://doi.org/10.1039/c7sc05371a>.
- 8 Mateti, S., Mathesh, M., Liu, Z. et al. (2021). Mechanochemistry: a force in disguise and conditional effects towards chemical reactions. *Chem. Commun. (Camb.)* 57 (9): 1080–1092. ISSN 1364-548X (Electronic) 1359-7345 (Linking). <https://doi.org/10.1039/d0cc06581a>.
- 9 Tan, D. and Garcia, F. (2019). Main group mechanochemistry: from curiosity to established protocols. *Chem. Soc. Rev.* 48 (8): 2274–2292. ISSN 1460-4744 (Electronic) 0306-0012 (Linking). <https://doi.org/10.1039/c7cs00813a>.
- 10 Voigtländer, B. (2019). *Atomic Force Microscopy*, 1–13. Cham: Springer International Publishing. ISBN 978-3-030-13654-3. [https://doi.org/10.1007/978-3-030-13654-3\\_1](https://doi.org/10.1007/978-3-030-13654-3_1).

- 11 Grandbois, M., Beyer, M., Rief, M. et al. (1999). How strong is a covalent bond? *Science* 283 (5408): 1727–1730. ISSN 1095-9203 (Electronic) 0036-8075 (Linking). <https://doi.org/10.1126/science.283.5408.1727>.
- 12 Beyer, M.K. and Clausen-Schaumann, H. (2005). Mechanochemistry: the mechanical activation of covalent bonds. *Chem. Rev.* 105 (8): 2921–2948. ISSN 0009-2665 (Print) 0009-2665 (Linking). <https://doi.org/10.1021/cr030697h>.
- 13 Ribas-Arino, J. and Marx, D. (2012). Covalent mechanochemistry: theoretical concepts and computational tools with applications to molecular nanomechanics. *Chem. Rev.* 112 (10): 5412–5487. <https://doi.org/10.1021/cr200399q>.
- 14 Stauch, T. and Dreuw, A. (2016). Advances in quantum mechanochemistry: electronic structure methods and force analysis. *Chem. Rev.* 116 (22): 14137–14180. <https://doi.org/10.1021/acs.chemrev.6b00458>.
- 15 Ribas-Arino, J., Shiga, M., and Marx, D. (2009). Understanding covalent mechanochemistry. *Angew. Chem. Int. Ed.* 48 (23): 4190–4193. <https://doi.org/https://doi.org/10.1002/anie.200900673>.
- 16 Ong, M.T., Leiding, J., Tao, H. et al. (2009). First principles dynamics and minimum energy pathways for mechanochemical ring opening of cyclobutene. *J. Am. Chem. Soc.* 131 (18): 6377–6379. <https://doi.org/10.1021/ja8095834>.
- 17 Chen, Z., Mercer, J.A.M., Zhu, X. et al. (2017). Mechanochemical unzipping of insulating poly(ladderene) to semiconducting polyacetylene. *Science* 357 (6350): 475. <https://doi.org/10.1126/science.aan2797>.
- 18 Chen, Z., Zhu, X., Yang, J. et al. (2020). The cascade unzipping of ladderene reveals dynamic effects in mechanochemistry. *Nat. Chem.* 12 (3): 302–309. <https://doi.org/10.1038/s41557-019-0396-5>.
- 19 Davis, D.A., Hamilton, A., Yang, J. et al. (2009). Force-induced activation of covalent bonds in mechanoresponsive polymeric materials. *Nature* 459 (7243): 68–72. <https://doi.org/10.1038/nature07970>.
- 20 Beyer, M.K. (2000). The mechanical strength of a covalent bond calculated by density functional theory. *J. Chem. Phys.* 112 (17): 7307–7312. <https://doi.org/10.1063/1.481330>.
- 21 Morse, P.M. (1929). Diatomic molecules according to the wave mechanics. II. Vibrational levels. *Phys. Rev.* 34 (1): 57–64. <https://doi.org/10.1103/PhysRev.34.57>.
- 22 Bettens, T., Alonso, M., Geerlings, P., and De Proft, F. (2019). Implementing the mechanical force into the conceptual DFT framework: understanding and predicting molecular mechanochemical properties. *Phys. Chem. Chem. Phys.* 21 (14): 7378–7388. ISSN 1463-9084 (Electronic) 1463-9076 (Linking). <https://doi.org/10.1039/c8cp07349j>.
- 23 Kauzmann, W. and Eyring, H. (1940). The viscous flow of large molecules. *J. Am. Chem. Soc.* 62 (11): 3113–3125. <https://doi.org/10.1021/ja01868a059>.
- 24 Wolinski, K. and Baker, J. (2009). Theoretical predictions of enforced structural changes in molecules. *Mol. Phys.* 107 (22): 2403–2417. <https://doi.org/10.1080/00268970903321348>.
- 25 Stauch, T. and Dreuw, A. (2017). Quantum chemical strain analysis for mechanochemical processes. *Acc. Chem. Res.* 50 (4): 1041–1048. <https://doi.org/10.1021/acs.accounts.7b00038>.

- 26 Stauch, T. and Dreuw, A. (2014). A quantitative quantum-chemical analysis tool for the distribution of mechanical force in molecules. *J. Chem. Phys.* 140 (13): 134107. <https://doi.org/10.1063/1.4870334>.
- 27 Geerlings, P., De Proft, F., and Langenaeker, W. (2003). Conceptual density functional theory. *Chem. Rev.* 103 (5): 1793–1874. <https://doi.org/10.1021/cr990029p>.
- 28 Clarys, T., Stuyver, T., De Proft, F., and Geerlings, P. (2021). Extending conceptual DFT to include additional variables: oriented external electric field. *Phys. Chem. Chem. Phys.* 23 (2): 990–1005. <https://doi.org/10.1039/D0CP05277A>.
- 29 Bettens, T., Alonso, M., Geerlings, P., and De Proft, F. (2020). The hunt for reactive alkynes in bio-orthogonal click reactions: insights from mechanochemical and conceptual DFT calculations. *Chem. Sci.* 11 (5): 1431–1439. <https://doi.org/10.1039/C9SC04507D>.
- 30 Cárdenas, C., Ayers, P., De Proft, F. et al. (2011). Should negative electron affinities be used for evaluating the chemical hardness? *Phys. Chem. Chem. Phys.* 13 (6): 2285–2293. <https://doi.org/10.1039/C0CP01785J>.
- 31 Parr, R.G. and Chattaraj, P.K. (1991). Principle of maximum hardness. *J. Am. Chem. Soc.* 113 (5): 1854–1855. <https://doi.org/10.1021/ja00005a072>.
- 32 Pearson, R.G. and Palke, W.E. (1992). Support for a principle of maximum hardness. *J. Phys. Chem.* 96 (8): 3283–3285. <https://doi.org/10.1021/j100187a020>.
- 33 Parthasarathi, R., Elango, M., Subramanian, V., and Chattaraj, P.K. (2005). Variation of electrophilicity during molecular vibrations and internal rotations. *Theor. Chem. Acc.* 113 (5): 257–266. <https://doi.org/10.1007/s00214-005-0634-3>.
- 34 Moens, J., Geerlings, P., and Roos, G. (2007). A conceptual DFT approach for the evaluation and interpretation of redox potentials. *Chem. Eur. J.* 13 (29): 8174–8184. <https://doi.org/https://doi.org/10.1002/chem.200601896>.
- 35 Moens, J., Roos, G., Jaque, P. et al. (2007). Can electrophilicity act as a measure of the redox potential of first-row transition metal ions? *Chem. Eur. J.* 13 (33): 9331–9343. <https://doi.org/https://doi.org/10.1002/chem.200700547>.
- 36 Baldus, I.B. and Gräter, F. (2012). Mechanical force can fine-tune redox potentials of disulfide bonds. *Biophys. J.* 102 (3): 622–629. <https://doi.org/10.1016/j.bpj.2011.12.039>.
- 37 Huisgen, R. (1963). 1,3-dipolar cycloadditions. Past and future. *Angew. Chem. Int. Ed. Engl.* 2 (10): 565–598. <https://doi.org/https://doi.org/10.1002/anie.196305651>.
- 38 Rostovtsev, V.V., Green, L.G., Fokin, V.V., and Sharpless, K.B. (2002). A stepwise Huisgen cycloaddition process: copper(I)-catalyzed regioselective “ligation” of azides and terminal alkynes. *Angew. Chem. Int. Ed.* 41 (14): 2596–2599. [https://doi.org/https://doi.org/10.1002/1521-3773\(20020715\)41:14<2596::AID-ANIE2596>3.0.CO;2-4](https://doi.org/https://doi.org/10.1002/1521-3773(20020715)41:14<2596::AID-ANIE2596>3.0.CO;2-4).
- 39 Meldal, M. and Tornøe, C.W. (2008). Cu-catalyzed azide-alkyne cycloaddition. *Chem. Rev.* 108 (8): 2952–3015. <https://doi.org/10.1021/cr0783479>.
- 40 Sletten, E.M. and Bertozzi, C.R. (2009). Bioorthogonal chemistry: fishing for selectivity in a sea of functionality. *Angew. Chem. Int. Ed.* 48 (38): 6974–6998. <https://doi.org/https://doi.org/10.1002/anie.200900942>.

- 41 Baskin, J.M., Prescher, J.A., Laughlin, S.T. et al. (2007). Copper-free click chemistry for dynamic in vivo imaging. *Proc. Natl. Acad. Sci. U.S.A.* 104 (43): 16793. <https://doi.org/10.1073/pnas.0707090104>.
- 42 Thirumurugan, P., Matosiuk, D., and Jozwiak, K. (2013). Click chemistry for drug development and diverse chemical-biology applications. *Chem. Rev.* 113 (7): 4905–4979. <https://doi.org/10.1021/cr200409f>.
- 43 Jewett, J.C. and Bertozzi, C.R. (2010). Cu-free click cycloaddition reactions in chemical biology. *Chem. Soc. Rev.* 39 (4): 1272–1279. <https://doi.org/10.1039/B901970G>.
- 44 Li, K., Fong, D., Meichsner, E., and Adronov, A. (2021). A survey of strain-promoted azide-alkyne cycloaddition in polymer chemistry. *Chem. Eur. J.* 27 (16): 5057–5073. <https://doi.org/https://doi.org/10.1002/chem.202003386>.
- 45 Hoffman, D.M., Hoffmann, R., and Fisel, C.R. (1982). Perpendicular and parallel acetylene complexes. *J. Am. Chem. Soc.* 104 (14): 3858–3875. <https://doi.org/10.1021/ja00378a014>.
- 46 Dommerholt, J., van Rooijen, O., Borrmann, A. et al. (2014). Highly accelerated inverse electron-demand cycloaddition of electron-deficient azides with aliphatic cyclooctynes. *Nat. Commun.* 5 (1): 5378. <https://doi.org/10.1038/ncomms6378>.
- 47 Krebs, A. and Kimling, H. (1970). 3.3.6.6-tetramethyl-1-thiacycloheptin ein isolierbares siebenring-acetylen. *Tetrahedron Lett.* 11 (10): 761–764. [https://doi.org/https://doi.org/10.1016/S0040-4039\(01\)97823-2](https://doi.org/https://doi.org/10.1016/S0040-4039(01)97823-2).
- 48 Krebs, A. and Kimling, H. (1971). 3,3,7,7-tetramethylcycloheptyne, an isolable seven-membered carbocyclic alkyne. *Angew. Chem. Int. Ed. Engl.* 10 (7): 509–510. <https://doi.org/https://doi.org/10.1002/anie.197105091>.
- 49 King, M., Baati, R., and Wagner, A. (2012). New tetramethylthiepinium (TMTI) for copper-free click chemistry. *Chem. Commun.* 48 (74): 9308–9309. <https://doi.org/10.1039/C2CC35034C>.

## 14

## The Hard/Soft Acid/Base Rule: A Perspective from Conceptual Density-Functional Theory

Paul W. Ayers<sup>1</sup>, Menatalla Mohamed<sup>1</sup>, and Farnaz Heidar-Zadeh<sup>2</sup>

<sup>1</sup>McMaster University, Department of Chemistry and Chemical Biology, 25-1280 Main Street West, Hamilton, ON L8S-4M1, Canada

<sup>2</sup>Queen's University, Department of Chemistry, 90 Bader Lane, Kingston, ON K7L-3N6, Canada

### 14.1 Introduction

Nucleophilic and electrophilic substitution reactions are among the most important reactions in organic synthesis. Analogous reactions are of comparable importance in inorganic chemistry, where substitutions of Lewis acidic (electrophilic) groups and Lewis basic (nucleophilic) groups are called acid and base exchange reactions, respectively. Similar processes occur in analytical chemistry, in processes with multiple oxidizing (acidic) and reducing (basic) reagents.

The three most fundamental exchange/substitution reactions are as follows:

**Acid exchange reaction:**



**Base exchange reaction:**



**Double exchange reaction:**



Here, and in the following, the acidic and basic reagents are denoted with A and B, respectively. Determining whether the products or the reactants are favored in these equilibria is among the most fundamental questions in acid/base chemistry. While quantitative experimental and theoretical treatments of these reactions are nowadays available, it is nonetheless useful to have a unifying set of chemical concepts and associated reactivity rules for qualitatively predicting the products of these acid/base exchange reactions.

The most fundamental concept related to acid/base reactivity is the acid/base strength, and the associated reactivity rule is that strong Lewis acids and strong Lewis bases prefer to bind to each other [1]. More formally:

**Strong/weak acid/base (SWAB) Rule:** All other things being equal, a base will prefer to bind to a strong acid over a weak acid, and an acid will prefer to bind to a strong base over a weak base.



Drago and Pearson realized that acid/base strength was insufficient to fully describe acid/base reactivity preferences and that at least one additional factor was needed [2–6]. This factor was dubbed the hardness [7, 8], since it distinguishes between the reactivity preferences of smaller, highly charged, and less polarizable (i.e. hard) and larger, less charged, and more polarizable (i.e. soft) reagents [9–11]. The associated hard/soft acid/base (HSAB) reactivity rule is that hard reagents prefer each other and soft reagents prefer each other [7, 8]. More formally:

**Hard/soft acid/base (HSAB) rule:** All other things being equal, a hard acid will prefer to bind to a hard base over a soft base, and a soft acid will prefer to bind to a soft base over a hard base. Therefore:



There is a strong link to Klopman's classification of reactions as being either charge-controlled and frontier-controlled [12–15]. In particular, charge-controlled reactions tend to be electrostatically dominant and lead to bonds with significant ionic character; charge-controlled reagents tend to be surrounded by sizable electrostatic potentials, as occurs for small highly charged (i.e. hard) species. Frontier-controlled reactions tend to be driven by orbital overlap and lead to bonds with significant covalent character; frontier-controlled reagents tend to be larger, and because they have high-energy occupied orbitals and low-energy unoccupied orbitals, the reagents in frontier-controlled reactions also tend to be more polarizable (i.e. soft).

The SWAB and HSAB rules lead to additional questions:

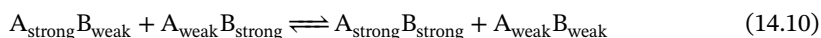
**Question:** How should the strength of an acid/base be defined?

**Question:** How should the hardness/softness of an acid/base be quantified?

**Question:** How should the “all other things being equal” assumption be interpreted?

We will return to the first two questions in Section 14.2. The third question, however, is more philosophical: in practical chemical processes, all other things are *never* equal, so forcing them to be equal restricts the scope of the SWAB and HSAB rules so severely that they become trivially true (and practically useless). To account for all the factors that are sometimes decisive in chemical reactivity – frontier orbital symmetry, low-lying nonbonding orbitals (e.g. for pi-backbonding), steric hindrance, solvation effects, geometric relaxation/rearrangement, and the like – adds so much complication and nuance that formulating simple rules-of-thumb becomes impossible. It seems appropriate to view the SWAB and HSAB rules as occupying a middle ground between meticulous analysis and vague generality: these rules are oversimplified guides-to-the-mind that neglect orbital-specific, geometry-specific, solvent-specific, relaxation/rearrangement, and other reaction-partner-specific effects [16–21]. Nonetheless, some of these effects can be treated. For example, it is commonly observed that reagents that are hard (soft) in solution are soft (hard) in the gas phase; in those cases the HSAB can not only be applied, but used to understand why the equilibrium in some reactions shifts between (polar) solvents and gas phase [9].

Much of the experimental and theoretical analysis of the SWAB and HSAB rules has featured the double-exchange reactions [9–11]:



In these double-exchange reactions, some (but not all) of the complicating reagent-specific factors (partially) cancel out, and the SWAB and HSAB rules can be studied more directly.

The purpose of this chapter is to provide a brief and personalized perspective on the HSAB rule from the viewpoint of conceptual density functional theory (DFT) [22–28]. In Section 14.2, the conceptual DFT approach to acidity/basicity and hardness/softness will be discussed. We then conclude by summarizing the current status of the HSAB rule and proposing some directions for future research.

## 14.2 Acid/Base Strength, Hardness, and Reactivity from Conceptual DFT

Acid/base reactions are defined by the approach between an electron acceptor (acid, electrophile, oxidizing agent) and an electron donor (base, nucleophile, reducing agent). If we are to assume that the “all other things being equal” caveat in the SWAB and HSAB rules indicates that reagent-specific regioselective, steric, and orbital-overlap effects are negligible, then it seems reasonable to reduce acid/base reactions to their essential electron-transfer character.

Within the framework of conceptual DFT, electron transfer to/from a reagent is modeled by expressing the reagent’s energy as a Taylor series in the number of electrons:

$$E(N_{\text{A}}^{(0)} + \Delta N_{\text{A}}) = E(N_{\text{A}}^{(0)}) + \mu_{\text{A}}^{(0)} \Delta N_{\text{A}} + \frac{1}{2} \eta_{\text{A}}^{(0)} \Delta N_{\text{A}}^2 + \dots \quad (14.12)$$

where the electronic chemical potential is defined as [22, 29–31]

$$\mu_{\text{A}}^{(0)} = \left[ \frac{\partial E(N_{\text{A}})}{\partial N_{\text{A}}} \right]_{v_{\text{A}}^{(0)}(\mathbf{r}); N_{\text{A}}=N_{\text{A}}^{(0)}} \approx -\frac{I + A}{2} \quad (14.13)$$

and the chemical hardness is defined as [32]

$$\eta_{\text{A}}^{(0)} = \left[ \frac{\partial E^2(N_{\text{A}})}{\partial N_{\text{A}}^2} \right]_{v_{\text{A}}^{(0)}(\mathbf{r}); N_{\text{A}}=N_{\text{A}}^{(0)}} \approx I - A \quad (14.14)$$

The notation indicates that the derivatives are evaluated at fixed geometry/external potential. It is not entirely unreasonable to assume that since number of terms in the Hamiltonian depends only linearly (kinetic energy and electron-nuclear attraction) and quadratically (electron-electron repulsion) on the number of electrons, cubic and higher-order terms in the Taylor series may be neglected [33–37]. This leads to the above approximations in terms of the reagent's vertical ionization potential,  $I$ , and electron affinity,  $A$  [29, 30, 38, 39]. A table of reference values of the chemical potential and hardness for atoms and atomic ions can be found in Ref. [40].

The identification of the electronic chemical potential as the quantification of (minus) the electronegativity initiated the field of conceptual DFT [29]. The idea that the second-order term might be the chemical hardness was at first speculative, but then Parr and Pearson noted that the properties of  $\eta_{\text{A}}^{(0)}$  largely mimicked the trends that had been imparted to hard (small, favoring ionic bonds, unpolarizable) and soft (large, favoring covalent bonds, polarizable) reagents [32]. That observation has been further validated both numerically and mathematically [41–65]. The identification of  $\eta_{\text{A}}^{(0)}$  as a mathematical reification of the chemical hardness was perhaps the first time conceptual DFT was used to explain a phenomenon that had been resistant to more traditional approaches, though it certainly was not the last [66–73].

If we assume that the Taylor series for the energy as a function of the number of electrons is an adequate model for electron transfer [22, 34, 74], then we can build an energy model for the fundamental acid + base reaction [32].

#### Acid + Base Reaction:



Specifically, because electrons are transferred from the base to the acid, we know that  $\mu_{\text{A}}^{(0)} < \mu_{\text{B}}^{(0)}$  and  $\Delta N := \Delta N_{\text{A}} = -\Delta N_{\text{B}} > 0$ . The energy of the simple acid + base reaction is

$$\Delta_{\text{rxn}} E = E_{\text{A}}(N_{\text{A}}^{(0)} + \Delta N) - E_{\text{A}}(N_{\text{A}}^{(0)}) + E_{\text{B}}(N_{\text{B}}^{(0)} - \Delta N) - E_{\text{B}}(N_{\text{B}}^{(0)}) \quad (14.16)$$

If we assume that the Taylor series can be truncated at second order, this becomes a quadratic expression for  $\Delta N$ , which can be minimized to determine the optimal amount of electron transfer from the base to the acid

$$\Delta N = \frac{\mu_{\text{B}}^{(0)} - \mu_{\text{A}}^{(0)}}{\eta_{\text{A}}^{(0)} + \eta_{\text{B}}^{(0)}} \quad (14.17)$$



and the associated electron-transfer energy [32]

$$\Delta_{\text{rxn}}E = -\frac{1}{2} \frac{(\mu_{\text{B}}^{(0)} - \mu_{\text{A}}^{(0)})^2}{\eta_{\text{A}}^{(0)} + \eta_{\text{B}}^{(0)}} \quad (14.18)$$

Notice that the direction of electron transfer is determined by the chemical potential and the extent of electron transfer/sharing between acid and the base is less for hard reagents (for which ionic bonds are favored) than it is for soft reagents (for which polar-covalent bonds are favored) [32]. Based on these pictures, the chemical potential can be identified as a measure of the intrinsic Lewis acidity/basicity [75]. Similarly, the chemical hardness quantifies the chemical concept of hardness [32]. The softness was subsequently defined as the reciprocal of the hardness [76]:

$$S = \frac{1}{\eta} \quad (14.19)$$

Using the reaction energy of the fundamental electron-transfer acid + base reaction, one can directly construct a model for the electron-transfer energy associated with the acid-exchange, base-exchange, and double-exchange reactions (cf. reactions 14.1–14.3) [75, 77]. Because the SWAB and HSAB rules can favor different products, they cannot always be valid. Indeed, because  $\mu$  and  $\eta$  both tend to increase when the ionization potential of a molecule increases, hard acids tend to be strong, but hard bases are often weak. (For example, the Chloride ion is rather hard, but it is also a weak base.) For example, using the definitions for the chemical potential and the hardness in Eqs. (14.13) and (14.14) and choosing to set negative electron affinities to zero [78], the Lithium cation is a stronger, harder Lewis acid than the Cesium cation, and the Iodide anion is a stronger, softer base than the Fluoride anion. Therefore the left-hand side of the following exchange reaction is favored by the SWAB, and the right-hand side is favored by the HSAB:



In this case, the HSAB rule actually overrules the SWAB rule (the reaction is exothermic by 33 kcal mol<sup>-1</sup>) [9]. This is unusual, because typically the SWAB rule is more decisive. However, the strengths of the acids and bases in this reaction are rather closely matched, while their hardnesses are quite distinct. Computational tests reveal that where the SWAB and HSAB rules are in competition with each other, the SWAB products are favored in about 75% of the cases. In cases where the SWAB-preferred and HSAB-preferred products are the same, the rules are quite reliable, but not perfectly so [79].

Alternatively, we can use a simple electrostatic model to compute the energy of the fundamental acid + base reaction [50, 75]. Typical hard acids are small and have large positive charge  $Q_{\text{A}} \gg 0$ . Similarly, typical hard bases are small and have large (in magnitude) negative charge  $Q_{\text{B}} \ll 0$ . Denoting the radius of the acid as  $r_{\text{A}}$  and the radius of the base as  $r_{\text{B}}$ , we can then write an expression for the energy of the fundamental acid + base reaction if the product is a purely ionic compound:

$$\Delta_{\text{rxn}}E = \frac{Q_{\text{A}}Q_{\text{B}}}{r_{\text{A}} + r_{\text{B}}} \quad (14.21)$$

The HSAB rule immediately follows in this purely electrostatic picture [50, 75]. We will not discuss this approach further, as it lies somewhat outside the mainstream of conceptual DFT, but it is important to note that both electrostatic/charge-driven reactions and electron-transfer/orbital-driven reactions favor the HSAB rule. With electron-transfer effects, the driving force for the HSAB product is the exceptional energetic stability of the soft acid/soft base compound. With electrostatic effects, the driving force for the HSAB product is the exceptional stability of the hard acid/hard base compound. Together, electron transfer and electrostatic interaction reinforce each other, helping the HSAB rule hold for most reactions where the “all other things being equal” caveat is not egregiously violated [50, 75].

By using either electron-transfer or electrostatic energies to estimate the energy of the double-exchange reaction, one can deduce specific and quantitative versions of the SWAB and HSAB rules.

**Quantitative Strong/Weak Acid/Base Rule:** If electron-transfer effects dominate the reaction energy of the double-exchange reaction, and the hard acid and hard base have the same hardness, and similarly the soft acid and soft base have the same hardness, then the strong acid will bond to the strong base, and the weak acid will bond to the weak base, in accord with the SWAB rule. The thermodynamic driving force for the reaction is the exceptional stability of the strong acid/strong base product [75].

**Quantitative Hard/Soft Acid/Base Rule:** If electron-transfer effects dominate the reaction energy of the double-exchange reaction, and the hard acid and soft acid have the same intrinsic strength/chemical potential, and similarly the hard base and the soft base have the same intrinsic strength/chemical potential, then the hard acid will bond to the hard base, and the soft acid will bond to the soft base, in accord with the HSAB rule. The driving force for the reaction is the exceptional stability of the soft acid/soft base product. A similar statement can be made for reactions where electrostatic effects dominate if the hard reagents are smaller and more highly charged than the soft reagents. In that case the thermodynamic driving force for the reaction is the exceptional stability of the hard acid/hard base product [75, 77, 80].

**Combined SWAB and HSAB Rules:** If electron-transfer effects dominate the reaction energy of the double-exchange reaction, the soft acid is stronger than the hard acid, and the soft base is stronger than the hard base, then the strong/soft acid prefers binding to the strong/soft base, and the weak/hard acid prefers binding to the weak/hard base, in accord with both the SWAB and HSAB rules. The thermodynamic driving force for the reaction is the exceptional stability of the strong-soft acid with the strong-soft base [81].

These and other refinements of the HSAB and SWAB provide very specific quantifications of the all-other-things-being-equal caveat. Certain non-reaction-partner-specific effects can be incorporated in this framework [49, 57, 78, 82–88]. For example, the adiabatic ionization potential and electron affinity can be used to approximately account for geometry relaxation effects, the oxidation/reduction potentials in solution can be used to approximately account for solvation effects, and

finite-temperature effects can be included. Effects that are reaction-partner specific, however, seem beyond the scope of the SWAB and HSAB rules. Nonetheless, one can incorporate some of these additional effects using more sophisticated versions of the two-reagent model.

It should be mentioned that while the SWAB rule is quite reliable for single-exchange reactions, the HSAB rule for single-exchange reactions is less robust because of the following [50, 75]:

**Case I:** For electron-transfer-driven reactions, given two reagents (either two acids or two bases) with equal strength but different hardness, the *softer* reagent tends to be more reactive.

**Case II:** For electrostatically driven reactions, given two reagents (either two acids or two bases) with equal strength but different hardness, the *harder* reagent tends to be more reactive.

Obviously, while electrostatic and electron-transfer effects reinforce each other for the double-exchange reaction, in these single-exchange reactions, that is not the case. Nonetheless, these rules are not directly in opposition to the canonical HSAB principle because reactions with soft reagents tend to be electron-transfer driven (Case I) while reactions with hard reagents tend to be electrostatically driven (Case II).

## 14.3 Summary and Future Directions

Assuming the energy of electron transfer dominates the reaction energy in acid/base reactions, and furthermore assuming that the quadratic model frequently used in conceptual DFT is valid, one identifies acid/base strength with the first derivative of the energy with respect to electron number (the electronic chemical potential) and the chemical hardness with the second derivative of the energy with respect to electron number. Within this mathematical framework, one can then deduce situations where the HSAB and SWAB rules hold. Section 14.2 summarized a few of the key results from the literature.

Nonetheless, we deliberately excluded one of the most frequently employed applications of the HSAB rule, namely, the local HSAB rule for ambident acids and bases [89–93]:



The mathematical framework for describing these reactions is much less developed, perhaps because of the difficulty of unambiguously defining a local hardness [34, 58, 94–116]. In the limit where the linker between the hard and soft reactive sites is sufficiently large, the nearsightedness principle means that these reactions

behave like the corresponding acid/base single-exchange reactions [117–120]. Developing a robust and quantitative approach to the local HSAB rule is, nonetheless, an important open problem. Experimental studies do seem to indicate that the local HSAB rule is significantly less robust than the global HSAB rule [121, 122].

At the computational level, there have been no large and no systematic tests of the global and local HSAB rules, though there are recent-developed software tools that would make such studies feasible [123, 124]. Such tests would contribute significant value, because the extent to which the all-other-things-being-equal caveat can be relaxed could be more clarified.

At the theoretical level, there are extremely suggestive links between the maximum hardness principle (MHP) [11, 125–127], the  $\mu$  big is good rule (DMB) [128, 129], and the HSAB rule. Indeed, the first mathematical treatment of the HSAB rule included the MHP perspective [80], and subsequent work on the HSAB rule has often followed, or been followed by, analogous work on MHP and DMB [128–135]. Reactions that follow the HSAB rule tend to products that are harder than the reactants (MHP), and the shift in chemical potential when forming the products seems to be larger than it was for the reactants (DMB). The concurrence of these rules is highly suggestive, but explicit mathematical links suggesting that the rules are equivalent (or clarifying when they are equivalent) are lacking.

More provocatively, we wish to suggest that alternative definitions for the intrinsic strength and hardness of acids/bases should be considered. Is it possible to find an alternative definition of intrinsic Lewis acidity/basicity so that key observations (the flow of electrons from base to acid; the SWAB rule) are more universally satisfied? Is it possible to find an alternative definition of chemical hardness so that the HSAB rule is more universally satisfied? Can one define a local hardness measure that ensures the reliability of the local HSAB rule? It seems that investigations like these would be fruitful even if they fail, because the failure of such attempts would reinforce the wise choices that Parr and his colleagues made in the formative years of conceptual DFT.

## Acknowledgments

PWA wishes to acknowledge the inspirational guidance of the late Professor Robert G. Parr, who first introduced him to the HSAB principle and consistently encouraged and guided his investigations. The authors wish to acknowledge fruitful collaborations over many years related to the HSAB rule, most notably with Carlos Cardenas, Pratim Chattaraj, Marco Franco, and Ramon Miranda-Quintana.

## References

- 1 Pauling, L. (1960). *The Nature of the Chemical Bond*. Cornell UP.
- 2 Drago, R.S. (1973). On Pearson's quantitative statement of HSAB. *Inorg. Chem.* 12 (9): 2211–2212.

- 3 Pearson, R.G. (1968). Failure of Pauling's bond energy equation. *Chem. Commun.* (2): 65–67.
- 4 Pearson, R.G. (1972). [Quantitative evaluation of the HSAB (hard-soft acid-base) concept]. Reply to the paper by Drago and Kabler. *Inorg. Chem.* 11 (12): 3146.
- 5 Drago, R.S. and Kabler, R.A. (1972). Quantitative evaluation of the HSAB [hard-soft acid-base] concept. *Inorg. Chem.* 11 (12): 3144–3145. <https://doi.org/10.1021/ic50118a064>.
- 6 Drago, R.S., Vogel, G.C., and Needham, T.E. (1971). Four-parameter equation for predicting enthalpies of adduct formation. *J. Am. Chem. Soc.* 93 (23): 6014–6026. <https://doi.org/10.1021/ja00752a010>.
- 7 Pearson, R.G. (1963). Hard and soft acids and bases. *J. Am. Chem. Soc.* 85: 3533–3539.
- 8 Pearson, R.G. (1966). Acids and bases. *Science* 151: 172–177.
- 9 Pearson, R.G. (1968). Hard and soft acids and bases (HSAB). II. Underlying theories. *J. Chem. Educ.* 45 (10): 643–648.
- 10 Pearson, R.G. (1968). Hard and soft acids and bases (HSAB). I. fundamental principles. *J. Chem. Educ.* 45 (9): 581–587.
- 11 Pearson, R.G. (1987). Recent advances in the concept of hard and soft acids and bases. *J. Chem. Educ.* 64: 561–567.
- 12 Klopman, G. (1968). Chemical reactivity and the concept of charge and frontier-controlled reactions. *J. Am. Chem. Soc.* 90: 223–234.
- 13 Fujimoto, H., Fukui, K., and Klopman, G. (1974). Intermolecular interactions and chemical reactivity. In: *Chemical Reactivity and Reaction Paths*, (ed. Gilles Klopman), 23–54. Wiley-Interscience.
- 14 Anderson, J.S.M., Melin, J., and Ayers, P.W. (2007). Conceptual density-functional theory for general chemical reactions, including those that are neither charge- nor frontier-orbital-controlled. 1. Theory and derivation of a general-purpose reactivity indicator. *J. Chem. Theory Comput.* 3 (2): 358–374. <https://doi.org/10.1021/ct600164j>.
- 15 Anderson, J.S.M., Melin, J., and Ayers, P.W. (2007). Conceptual density-functional theory for general chemical reactions, including those that are neither charge- nor frontier-orbital-controlled. 2. Application to molecules where frontier molecular orbital theory fails. *J. Chem. Theory Comput.* 3 (2): 375–389. <https://doi.org/10.1021/ct6001658>.
- 16 Pearson, R.G. (1997). *Chemical Hardness*. Wiley-VCH.
- 17 Ayers, P.W. (2000). Atoms in molecules, an axiomatic approach. I. Maximum transferability. *J. Chem. Phys.* 113 (24): 10886–10898.
- 18 Ayers, P.W., Fias, S., and Heidar-Zadeh, F. (2018). The axiomatic approach to chemical concepts. *Comput. Theor. Chem.* 1142: 83–87. <https://doi.org/10.1016/j.comptc.2018.09.006>.
- 19 Parr, R.G., Ayers, P.W., and Nalewajski, R.F. (2005). What is an atom in a molecule? *J. Phys. Chem. A* 109: 3957–3959.
- 20 Andres, J., Ayers, P.W., Boto, R.A. et al. (2019). Nine questions on energy decomposition analysis. *J. Comput. Chem.* 40 (26): 2248–2283. <https://doi.org/10.1002/jcc.26003>.

- 21 Ayers, P.W., Boyd, R.J., Bultinck, P. et al. (2015). Six questions on topology in theoretical chemistry. *Comput. Theor. Chem.* 1053: 2–16. <https://doi.org/10.1016/j.comptc.2014.09.028>.
- 22 Ayers, P.W., Anderson, J.S.M., and Bartolotti, L.J. (2005). Perturbative perspectives on the chemical reaction prediction problem. *Int. J. Quantum Chem.* 101 (5): 520–534. <https://doi.org/10.1002/qua.20307>.
- 23 Geerlings, P., De Proft, F., and Langenaeker, W. (2003). Conceptual density functional theory. *Chem. Rev.* 103: 1793–1873. <https://doi.org/10.1021/cr990029p>.
- 24 Gazquez, J.L. (2008). Perspectives on the density functional theory of chemical reactivity. *J. Mex. Chem. Soc.* 52: 3–10.
- 25 De Proft, F., Geerlings, P., and Ayers, P.W. (2014). The conceptual density functional theory perspective of bonding. In: *The Chemical Bond: Fundamental Aspects of Chemical Bonding*, vol. 1 (ed. S. Shaik and G. Frenking), 233–270. Wiley.
- 26 Johnson, P.A., Bartolotti, L.J., Ayers, P.W. et al. (2012). Charge density and chemical reactivity: a unified view from conceptual DFT. In: *Modern Charge Density Analysis* (ed. C. Gatti and P. Macchi), 715–764. Springer.
- 27 Geerlings, P., Ayers, P.W., Toro-Labbe, A. et al. (2012). The Woodward–Hoffmann rules reinterpreted by conceptual density functional theory. *Acc. Chem. Res.* 45 (5): 683–695. <https://doi.org/10.1021/ar200192t>.
- 28 Liu, S.B. (2009). Conceptual density functional theory and some recent developments. *Acta Phys. Chim. Sin.* 25: 590–600. <https://doi.org/10.3866/PKU.WHXB20090332>.
- 29 Parr, R.G., Donnelly, R.A., Levy, M., and Palke, W.E. (1978). Electronegativity: the density functional viewpoint. *J. Chem. Phys.* 68: 3801–3807.
- 30 Itzkowski, R.P. and Margrave, J.L. (1961). *J. Am. Chem. Soc.* 83: 3547.
- 31 Ayers, P.W. (2007). On the electronegativity nonlocality paradox. *Theor. Chem. Acc.* 118: 371–381.
- 32 Parr, R.G. and Pearson, R.G. (1983). Absolute hardness: companion parameter to absolute electronegativity. *J. Am. Chem. Soc.* 105: 7512–7516.
- 33 Ayers, P.W. and Parr, R.G. (2008). Beyond electronegativity and local hardness: higher-order equalization criteria for determination of a ground-state electron density. *J. Chem. Phys.* 129: 054111. <https://doi.org/10.1063/1.2957900>.
- 34 Ayers, P.W. and Parr, R.G. (2008). Local hardness equalization: exploiting the ambiguity. *J. Chem. Phys.* 128: 184108. <https://doi.org/10.1063/1.2918731>.
- 35 Parr, R.G. and Pariser, R. (2013). The parameter  $I - A$  in electronic structure theory. In: *Concepts and Methods in Modern Theoretical Chemistry: Electronic Structure and Reactivity* (ed. S.K. Ghosh and P.K. Chattaraj), 431–440. CRC Press.
- 36 Franco-Perez, M., Gazquez, J.L., Ayers, P.W., and Vela, A. (2018). Thermodynamic justification for the parabolic model for reactivity indicators with respect to electron number and a rigorous definition for the electrophilicity: the essential role played by the electronic entropy. *J. Chem. Theory Comput.* 14 (2): 597–606. <https://doi.org/10.1021/acs.jctc.7b00940>.

- 37 Ayers, P.W. (2008). The dependence on and continuity of the energy and other molecular properties with respect to the number of electrons. *J. Math. Chem.* 43 (1): 285–303. <https://doi.org/10.1007/s10910-006-9195-5>.
- 38 Parr, R.G. and Bartolotti, L.J. (1982). On the geometric mean principle for electronegativity equalization. *J. Am. Chem. Soc.* 104: 3801–3803.
- 39 Heidar-Zadeh, F., Miranda-Quintana, R.A., Verstraelen, T. et al. (2016). When is the Fukui function not normalized? The danger of inconsistent energy interpolation models in density functional theory. *J. Chem. Theory Comput.* 12 (12): 5777–5787. <https://doi.org/10.1021/acs.jctc.6b00494>.
- 40 Cardenas, C., Heidar-Zadeh, F., and Ayers, P.W. (2016). Benchmark values of chemical potential and chemical hardness for atoms and atomic ions (including unstable anions) from the energies of isoelectronic series. *Phys. Chem. Chem. Phys.* 18 (36): 25721–25734. <https://doi.org/10.1039/c6cp04533b>.
- 41 Simon-Manso, Y. and Fuentealba, P. (1998). On the density functional relationship between static dipole polarizability and global softness. *J. Phys. Chem. A* 102: 2029–2032.
- 42 Das, R., Vigneresse, J.L., and Chattaraj, P.K. (2013). Redox and Lewis acid-base activities through an electronegativity-hardness landscape diagram. *J. Mol. Model.* 19 (11): 4857–4864. <https://doi.org/10.1007/s00894-013-1986-6>.
- 43 Pearson, R.G. (2009). The hardness of closed systems. In: *Chemical Reactivity Theory: A Density Functional View* (ed. P.K. Chattaraj), 155–162. CRC Press.
- 44 Pearson, R.G. (2005). Chemical hardness and density functional theory. *J. Chem. Sci.* 117 (5): 369–377. <https://doi.org/10.1007/bf02708340>.
- 45 Patra, G.K., Hati, S., and Datta, D. (1999). Proofs for Pearson’s HSAB principle. *Indian J. Chem. Sect. A-Inorg. Bio-Inorg. Phys. Theor. Anal. Chem.* 38 (1): 1–3.
- 46 Kaya, S. and Kaya, C. (2015). A new method for calculation of molecular hardness: a theoretical study. *Comput. Theor. Chem.* 1060: 66–70. <https://doi.org/10.1016/j.comptc.2015.03.004>.
- 47 Datta, D. (1992). On Pearson HSAB principle. *Inorg. Chem.* 31 (13): 2797–2800.
- 48 Datta, D. and Singh, S.N. (1991). Pearson’s chemical hardness, heterolytic dissociation version of Pauling’s bond-energy equation and a novel approach towards understanding Pearson’s hard-soft acid-base principle. *J. Chem. Soc., Dalton Trans.* 1541–1549.
- 49 Franco-Perez, M., Gazquez, J.L., Ayers, P.W., and Vela, A. (2017). Thermodynamic hardness and the maximum hardness principle. *J. Chem. Phys.* 147 (7). <https://doi.org/10.1063/1.4998701>.
- 50 Ayers, P.W. (2007). The physical basis of the hard/soft acid/base principle. *Faraday Discuss.* 135: 161–190. <https://doi.org/10.1039/b606877d>.
- 51 Chandrakumar, K.R.S., Ghanty, T.K., and Ghosh, S.K. (2004). Relationship between ionization potential, polarizability, and softness: a case study of lithium and sodium metal clusters. *J. Phys. Chem. A* 108: 6661–6666.
- 52 Ghanty, T.K. and Ghosh, S.K. (1996). A new simple approach to the polarizability of atoms and ions using frontier orbitals from the Kohn–Sham density functional theory. *J. Mol. Struct. THEOCHEM* 366: 139–144.

- 53 Ghanty, T.K. and Ghosh, S.K. (1996). New scale of atomic orbital radii and its relationship with polarizability, electronegativity, other atomic properties, and bond energies of diatomic molecules. *J. Phys. Chem.* 100: 17429–17433.
- 54 Ghanty, T.K. and Ghosh, S.K. (1996). A density functional approach to hardness, polarizability, and valency of molecules in chemical reactions. *J. Phys. Chem.* 100: 12295–12298.
- 55 Ghanty, T.K. and Ghosh, S.K. (1994). A frontier orbital density-functional approach to polarizability, hardness, electronegativity, and covalent radius of atomic systems. *J. Am. Chem. Soc.* 116: 8801–8802.
- 56 Ghanty, T.K. and Ghosh, S.K. (1993). Correlation between hardness, polarizability, and size of atoms, molecules, and clusters. *J. Phys. Chem.* 97: 4951–4953.
- 57 Franco-Perez, M., Gazquez, J.L., Ayers, P.W., and Vela, A. (2015). Revisiting the definition of the electronic chemical potential, chemical hardness, and softness at finite temperatures. *J. Chem. Phys.* 143 (15): 154103. <https://doi.org/Artn154103> 10.1063/1.4932539.
- 58 Franco-Perez, M., Polanco-Ramirez, C.A., Gazquez, J.L., and Ayers, P.W. (2018). Reply to the “comment on “revisiting the definition of local hardness and hardness kernel”” by C. Morell, F. Guegan, W. Lamine, and H. Chermette, *Phys. Chem. Chem. Phys.*, 2018, 20, DOI: 10.1039/c7cp04100d. *Phys. Chem. Chem. Phys.* 20 (13): 9011–9014. <https://doi.org/10.1039/c7cp07974e>.
- 59 Chattaraj, P.K., Gomez, B., Chamorro, E. et al. (2001). Scrutiny of the HSAB principle in some representative acid-base reactions. *J. Phys. Chem. A* 105: 8815–8820.
- 60 Chattaraj, P.K. and Nath, S. (1994). Maximum hardness and HSAB principles: an ab initio SCF study. *Indian J. Chem., Sect. A: Inorg. Bio-Inorg. Phys. Theor. Anal. Chem.* 33A: 842–843.
- 61 Chattaraj, P.K. and Schleyer, P.R. (1994). An ab initio study resulting in a greater understanding of the HSAB principle. *J. Am. Chem. Soc.* 116: 1067–1071.
- 62 Gazquez, J.L. (1997). Bond energies and hardness differences. *J. Phys. Chem. A* 101: 9464–9469.
- 63 Gazquez, J.L. (1997). The hard and soft acids and bases principle. *J. Phys. Chem. A* 101: 4657–4659.
- 64 Roy, R., Chandra, A.K., and Pal, S. (1994). Correlation of polarizability, hardness, and electronegativity - polyatomic-molecules. *J. Phys. Chem.* 98: 10447–10450.
- 65 Shoeb, T., Gorelsky, S.I., Lever, A.B.P. et al. (2001). When does the hard and soft acid base principle apply in the gas phase? *Inorg. Chim. Acta* 315 (2): 236–239.
- 66 Melin, J., Ayers, P.W., and Ortiz, J.V. (2007). Removing electrons can increase the electron density: a computational study of negative Fukui functions. *J. Phys. Chem. A* 111: 10017–10019.
- 67 Echegaray, E., Cardenas, C., Rabi, S. et al. (2013). In pursuit of negative Fukui functions: examples where the highest occupied molecular orbital fails to dominate the chemical reactivity. *J. Mol. Model.* 19 (7): 2779–2783. <https://doi.org/10.1007/s00894-012-1637-3>.



- 68 Echegaray, E., Rabi, S., Cardenas, C. et al. (2014). In pursuit of negative Fukui functions: molecules with very small band gaps. *J. Mol. Model.* 20: 2162. <https://doi.org/10.1007/s00894-014-2162-3>.
- 69 Ayers, P.W. (2006). Can one oxidize an atom by reducing the molecule that contains it? *Phys. Chem. Chem. Phys.* 8: 3387–3390.
- 70 Bartolotti, L.J. and Ayers, P.W. (2005). An example where orbital relaxation is an important contribution to the Fukui function. *J. Phys. Chem. A* 109 (6): 1146–1151. <https://doi.org/10.1021/jp0462207>.
- 71 Flurchick, K. and Bartolotti, L. (1995). Visualizing properties of atomic and molecular-systems. *J. Mol. Graph.* 13 (1): 10–13.
- 72 Tognetti, V., Morell, C., Ayers, P.W. et al. (2013). A proposal for an extended dual descriptor: a possible solution when frontier molecular orbital theory fails. *Phys. Chem. Chem. Phys.* 15 (34): 14465–14475. <https://doi.org/10.1039/c3cp51169c>.
- 73 Cardenas, C., Rabi, N., Ayers, P.W. et al. (2009). Chemical reactivity descriptors for ambiphilic reagents: dual descriptor, local hypersoftness, and electrostatic potential. *J. Phys. Chem. A* 113: 8660–8667. <https://doi.org/10.1021/jp902792n>.
- 74 Liu, S.B. (1996). Local-density approximation, hierarchy of equations, functional expansion, and adiabatic connection in current-density- functional theory. *Phys. Rev. A* 54 (2): 1328–1336.
- 75 Ayers, P.W., Parr, R.G., and Pearson, R.G. (2006). Elucidating the hard/soft acid/base principle: a perspective based on half-reactions. *J. Chem. Phys.* 124: 194107. <https://doi.org/10.1063/1.2196882>.
- 76 Yang, W.T. and Parr, R.G. (1985). Hardness, softness, and the Fukui function in the electron theory of metals and catalysis. *Proc. Natl. Acad. Sci. U.S.A.* 82: 6723–6726.
- 77 Ayers, P.W. (2005). An elementary derivation of the hard/soft-acid/base principle. *J. Chem. Phys.* 122: 141102.
- 78 Cardenas, C., Ayers, P.W., De Proft, F. et al. (2011). Should negative electron affinities be used for evaluating the chemical hardness. *Phys. Chem. Chem. Phys.* 13: 2285–2293.
- 79 Cardenas, C. and Ayers, P.W. (2013). How reliable is the hard-soft acid-base principle? An assessment from numerical simulations of electron transfer energies. *Phys. Chem. Chem. Phys.* 15 (33): 13959–13968. <https://doi.org/10.1039/c3cp51134k>.
- 80 Chattaraj, P.K., Lee, H., and Parr, R.G. (1991). HSAB principle. *J. Am. Chem. Soc.* 113: 1855–1856.
- 81 Ayers, P.W. and Cardenas, C. (2013). Communication: A case where the hard/soft acid/base principle holds regardless of acid/base strength. *J. Chem. Phys.* 138: 181106.
- 82 Pearson, R.G. (1987). Equilibrium constants, oxidation potentials, and nucleophilicity in  $\text{SN}_2$  displacements. *J. Org. Chem.* 52: 2131–2136.
- 83 Pearson, R.G. (1995). The HSAB principle - more quantitative aspects. *Inorg. Chim. Acta* 240: 93–98.

- 84 Gázquez, J.L., Franco-Pérez, M., Ayers, P.W., and Vela, A. (2019). Temperature-dependent approach to chemical reactivity concepts in density functional theory. *Int. J. Quantum Chem.* 119 (2): e25797. <https://doi.org/10.1002/qua.25797>.
- 85 Miranda-Quintana, R.A., Martínez Gonzalez, M., and Ayers, P.W. (2016). Electronegativity and redox reactions. *Phys. Chem. Chem. Phys.* 18 (32): 22235–22243. <https://doi.org/10.1039/c6cp03213c>.
- 86 Miranda-Quintana, R.A., Kim, T.D., Cardenas, C., and Ayers, P.W. (2017). The HSAB principle from a finite-temperature grand-canonical perspective. *Theor. Chem. Acc.* 136 (12). <https://doi.org/10.1007/s00214-017-2167-y>.
- 87 Miranda-Quintana, R.A. and Ayers, P.W. (2016). Fractional electron number, temperature, and perturbations in chemical reactions. *Phys. Chem. Chem. Phys.* 18 (22): 15070–15080. <https://doi.org/10.1039/c6cp00939e>.
- 88 Ayers, P.W. (2001). Strategies for computing chemical reactivity indices. *Theor. Chem. Acc.* 106: 271–279.
- 89 Gázquez, J.L. and Mendez, F. (1994). The hard and soft acids and bases principle: an atoms in molecules viewpoint. *J. Phys. Chem.* 98: 4591–4593.
- 90 Mendez, F. and Gázquez, J.L. (1994). Chemical-reactivity of enolate ions - the local hard and soft acids and bases principle viewpoint. *J. Am. Chem. Soc.* 116: 9298–9301.
- 91 Anderson, J.S.M. and Ayers, P.W. (2007). Predicting the reactivity of ambidentate nucleophiles and electrophiles using a single, general-purpose, reactivity indicator. *Phys. Chem. Chem. Phys.* 9: 2371–2378.
- 92 Chandrakumar, K.R.S. and Pal, S. (2002). Study of local hard-soft acid-base principle to multiple-site interactions. *J. Phys. Chem. A* 106 (23): 5737–5744.
- 93 Anderson, J.S.M. and Ayers, P.W. (2014). Resolving the nature of the reactive sites of phenylsulfinate (PhSO<sub>2</sub><sup>-</sup>) with a single general-purpose reactivity indicator. *Comput. Theor. Chem.* 1043: 1–4. <https://doi.org/10.1016/j.comptc.2014.04.032>.
- 94 Berkowitz, M., Ghosh, S.K., and Parr, R.G. (1985). On the concept of local hardness in chemistry. *J. Am. Chem. Soc.* 107: 6811–6814.
- 95 Berkowitz, M. and Parr, R.G. (1988). Molecular hardness and softness, local hardness and softness, hardness and softness kernels, and relations among these quantities. *J. Chem. Phys.* 88: 2554–2557.
- 96 Harbola, M.K., Chattaraj, P.K., and Parr, R.G. (1991). Aspects of the softness and hardness concepts of density-functional theory. *Isr. J. Chem.* 31: 395–402.
- 97 Langenaeker, W., Deproft, F., and Geerlings, P. (1995). Development of local hardness related reactivity indexes - their application in a study of the SE at monosubstituted benzenes within the HSAB context. *J. Phys. Chem.* 99: 6424–6431.
- 98 Meneses, L., Tiznado, W., Contreras, R., and Fuentealba, P. (2004). A proposal for a new local hardness as selectivity index. *Chem. Phys. Lett.* 383: 181–187.
- 99 De Proft, F., Ayers, P.W., Sen, K.D., and Geerlings, P. (2004). On the importance of the “density per particle” (shape function) in the density functional theory. *J. Chem. Phys.* 120: 9969–9973.

- 100** Meneses, L., Araya, A., Pilaquinga, F. et al. (2007). Local hardness: an application to electrophilic additions. *Chem. Phys. Lett.* 446: 170–175. <https://doi.org/10.1016/j.cplett.2007.07.092>.
- 101** Chattaraj, P.K., Roy, D.R., Geerlings, P., and Torrent-Sucarrat, M. (2007). Local hardness: a critical account. *Theor. Chem. Acc.* 118: 923–930.
- 102** Torrent-Sucarrat, M., De Proft, F., Geerlings, P., and Ayers, P.W. (2008). Do the local softness and hardness indicate the softest and hardest regions of a molecule? *Chem. Eur. J.* 14: 8652–8660. <https://doi.org/10.1002/Chem.200800570>.
- 103** Torrent-Sucarrat, M., De Proft, F., Ayers, P.W., and Geerlings, P. (2010). On the applicability of local softness and hardness. *Phys. Chem. Chem. Phys.* 12: 1072–1080. <https://doi.org/10.1039/b919471a>.
- 104** Gal, T., Geerlings, P., De Proft, F., and Torrent-Sucarrat, M. (2011). A new approach to local hardness. *Phys. Chem. Chem. Phys.* 13 (33): 15003–15015. <https://doi.org/10.1039/c1cp21213c>.
- 105** Cuevas-Saavedra, R., Rabi, N., and Ayers, P.W. (2011). The unconstrained local hardness: an intriguing quantity, beset by problems. *Phys. Chem. Chem. Phys.* 13: 19594–19600. <https://doi.org/10.1039/c1cp21646e>.
- 106** Ayers, P.W., Liu, S.B., and Li, T.L. (2011). Stability conditions for density functional reactivity theory: an interpretation of the total local hardness. *Phys. Chem. Chem. Phys.* 13: 4427–4433. <https://doi.org/10.1039/c0cp01675f>.
- 107** Cardenas, C., Tiznado, W., Ayers, P.W., and Fuentealba, P. (2011). The Fukui potential and the capacity of charge and the global hardness of atoms. *J. Phys. Chem. A* 115: 2325–2331. <https://doi.org/10.1021/jp109955q>.
- 108** Gal, T. (2012). Why the traditional concept of local hardness does not work. *Theor. Chem. Acc.* 131 (7): 1223. <https://doi.org/10.1007/s00214-012-1223-x>.
- 109** Gazquez, J.L., Vela, A., and Chattaraj, P.K. (2013). Local hardness equalization and the principle of maximum hardness. *J. Chem. Phys.* 138: 214103. <https://doi.org/10.1063/1.4807887>.
- 110** Heidar-Zadeh, F., Fuentealba, P., Cardenas, C., and Ayers, P.W. (2014). An information-theoretic resolution of the ambiguity in the local hardness. *Phys. Chem. Chem. Phys.* 16 (13): 6019–6026. <https://doi.org/10.1039/c3cp52906a>.
- 111** Guégan, F., Lamine, W., Chermette, H., and Morell, C. (2018). Comment on “Revisiting the definition of local hardness and hardness kernel” by C.A. Polanco-Ramirez, M. Franco-Pérez, J. Carmona-Espindola, J.L. Gázquez, and P.W. Ayers, *Phys. Chem. Chem. Phys.* 2017, 19, 12355. *Phys. Chem. Chem. Phys.* 20 (13): 9006–9010. <https://doi.org/10.1039/C7CP04100D>.
- 112** Heidar-Zadeh, F., Fias, S., Vohringer-Martinez, E. et al. (2016). The local response of global descriptors. *Theor. Chem. Acc.* 136 (1). <https://doi.org/10.1007/s00214-016-2036-0>.
- 113** Franco-Perez, M., Ayers, P.W., Gazquez, J.L., and Vela, A. (2017). Local chemical potential, local hardness, and dual descriptors in temperature dependent chemical reactivity theory. *Phys. Chem. Chem. Phys.* 19 (21): 13687–13695. <https://doi.org/10.1039/c7cp00692f>.

- 114 Polanco-Ramirez, C.A., Franco-Perez, M., Carmona-Espindola, J. et al. (2017). Revisiting the definition of local hardness and hardness kernel. *Phys. Chem. Chem. Phys.* 19 (19): 12355–12364. <https://doi.org/10.1039/c7cp00691h>.
- 115 Ayers, P.W., Liu, S., and Li, T. (2009). Chargephilicity and chargephobicity: two new reactivity indicators for external potential changes from density functional reactivity theory. *Chem. Phys. Lett.* 480 (4): 318–321. <https://doi.org/10.1016/j.cplett.2009.08.067>.
- 116 Liu, S.B., Li, T.L., and Ayers, P.W. (2009). Potentialphilicity and potential-phobicity: reactivity indicators for external potential changes from density functional reactivity theory. *J. Chem. Phys.* 131: 114106. <https://doi.org/114106> 10.1063/1.3231687.
- 117 Kohn, W. (1996). Density functional and density matrix method scaling linearly with the number of atoms. *Phys. Rev. Lett.* 76: 3168–3171.
- 118 Prodan, E. and Kohn, W. (2005). Nearsightedness of electronic matter. *Proc. Natl. Acad. Sci. U.S.A.* 102: 11635–11638.
- 119 Bader, R.F.W. (2008). Nearsightedness of electronic matter as seen by a physicist and a chemist. *J. Phys. Chem. A* 112 (51): 13717–13728. <https://doi.org/10.1021/jp806282j>.
- 120 Fias, S., Heidar-Zadeh, F., Geerlings, P., and Ayers, P.W. (2017). Chemical transferability of functional groups follows from the nearsightedness of electronic matter. *Proc. Natl. Acad. Sci. U.S.A.* 114 (44): 11633–11638. <https://doi.org/10.1073/pnas.1615053114>.
- 121 Loos, R., Kobayashi, S., and Mayr, H. (2003). Ambident reactivity of the thiocyanate anion revisited: can the product ratio be explained by the hard soft acid base principle? *J. Am. Chem. Soc.* 125 (46): 14126–14132.
- 122 Breugst, M. and Mayr, H. (2010). Ambident reactivities of pyridone anions. *J. Am. Chem. Soc.* 132: 15380–15389. <https://doi.org/10.1021/ja106962u>.
- 123 Heidar-Zadeh, F., Richer, M., Fias, S. et al. (2016). An explicit approach to conceptual density functional theory descriptors of arbitrary order. *Chem. Phys. Lett.* 660: 307–312. <https://doi.org/10.1016/j.cplett.2016.07.039>.
- 124 Verstraelen, T., Adams, W., Pujal, L. et al. (2021). IOData: A python library for reading, writing, and converting computational chemistry file formats and generating input files. *J. Comput. Chem.* 42 (6): 458–464. <https://doi.org/10.1002/jcc.26468>.
- 125 Ayers, P.W. and Parr, R.G. (2000). Variational principles for describing chemical reactions: the Fukui function and chemical hardness revisited. *J. Am. Chem. Soc.* 122: 2010–2018.
- 126 Parr, R.G. and Chattaraj, P.K. (1991). Principle of maximum hardness. *J. Am. Chem. Soc.* 113: 1854–1855.
- 127 Pearson, R.G. and Palke, W.E. (1992). Support for a principle of maximum hardness. *J. Phys. Chem.* 96: 3283–3285.
- 128 Miranda-Quintana, R.A., Heidar-Zadeh, F., and Ayers, P.W. (2018). Elementary derivation of the “delta mu big is good” rule. *J. Phys. Chem. Lett.* 9 (15): 4344–4348. <https://doi.org/10.1021/acs.jpcclett.8b01312>.

- 129** Parr, R.G. and Yang, W. (1989). *Density-Functional Theory of Atoms and Molecules*. Oxford UP.
- 130** Miranda-Quintana, R.A. and Ayers, P.W. (2018). Dipolar cycloadditions and the “ $|\Delta\mu|$  big is good” rule: a computational study. *Theor. Chem. Acc.* 137 (12): 177. <https://doi.org/10.1007/s00214-018-2391-0>.
- 131** Miranda-Quintana, R.A. and Ayers, P.W. (2018). Note: Maximum hardness and minimum electrophilicity principles. *J. Chem. Phys.* 148 (19). <https://doi.org/10.1063/1.5033964>.
- 132** Miranda-Quintana, R.A. and Ayers, P.W. (2019). The “ $|\Delta\mu|$  big is good” rule, the maximum hardness, and minimum electrophilicity principles. *Theor. Chem. Acc.* 138 (3): 44. <https://doi.org/10.1007/s00214-019-2435-0>.
- 133** Miranda-Quintana, R.A., Ayers, P.W., and Heidar-Zadeh, F. (2021). Reactivity and charge transfer beyond the parabolic model: the “ $|\Delta\mu|$  Big is Good” principle. *ChemistrySelect* 6 (1): 96–100. <https://chemistry-europe.onlinelibrary.wiley.com/action/showCitFormats?doi=10.1002\LY1\textbackslash%2Fslct.202004055\LY1\textbackslash&mobileUi=0>.
- 134** Chattaraj, P.K., Ayers, P.W., and Melin, J. (2007). Further links between the maximum hardness principle and the hard/soft acid/base principle: insights from hard/soft exchange reactions. *Phys. Chem. Chem. Phys.* 9: 3853–3856. <https://doi.org/10.1039/b705742c>.
- 135** Chattaraj, P.K. and Ayers, P.W. (2005). The maximum hardness principle implies the hard/soft acid/base rule. *J. Chem. Phys.* 123: 086101. <https://doi.org/10.1063/1.2011395>.

## 15

### Information-Theoretic Approach

Chunying Rong<sup>1</sup>, Donghai Yu<sup>2</sup>, and Shubin Liu<sup>3</sup>

<sup>1</sup>Hunan Normal University, Key Laboratory of Chemical Biology and Traditional Chinese Medicine Research (Ministry of Education of China), 168 South Lushan Road, Changsha 410081, P.R. China

<sup>2</sup>University of Chinese Academy of Sciences, Shanghai Institute of Organic Chemistry, Key Laboratory of Organofluorine Chemistry, 345 Lingling Road, Shanghai 200032, P.R. China

<sup>3</sup>University of North Carolina, Research Computing Center, 211 Manning Drive, Chapel Hill, NC 27599-3420, USA

<sup>4</sup>Department of Chemistry, University of North Carolina, Chapel Hill, NC 27599-3290, USA

#### 15.1 Introduction

To establish a chemical reactivity theory in density functional theory (DFT) (density-based) language, aside from conceptual density functional theory (CDFT) [1, 2], which is the main theme of this book, there is a recent effort in the literature undertaking a vastly different approach [3–7]. In this case, instead of employing first- and second-order derivatives introduced in Part I, simple electron density functionals themselves are directly employed to quantify stability and reactivity properties for molecules, such as steric effect, electrophilicity, nucleophilicity, stereoselectivity, and aromaticity [6, 7]. This idea of employing density functionals to quantify molecular reactivity is indeed akin to and consistent with the original spirit of basic DFT theorems [1, 8]. This is because the electron density alone suffices in determining all properties in the ground state, so any molecular property related to stability and reactivity could similarly be expressed as a functional of the electron density, same as what noninteracting kinetic, Coulombic, and exchange-correlation energies have been done [1].

Among many different possible forms of density functionals one could think of, the simplest forms are the ones from the information theory. Originating from Claude Shannon's 1948 paper entitled "The mathematical theory of communication" [9], and still entertaining widespread applications in mathematics, statistics, computer science, physics, neurobiology, and many other disciplines, information theory studies the quantification and communication of information, which is often characterized by a probability distribution function. The electron density can be regarded as such a distribution function. Because of this reason, ever since the early days of DFT development, there have been tremendous interests in the literature to

apply information theory to DFT [10–15]. This effort is usually categorized as the information-theoretic approach (ITA) in DFT [6, 7].

There have been a few reviews [6, 7] and books [3–5] on ITA in DFT in the literature. In this chapter, we briefly overview our current understanding of the subject by highlighting three points of its theoretical framework and five topic applications. Readers with interest to know more details are referred to the recent reviews on the subject [6, 7].

## 15.2 Theoretical Framework

### 15.2.1 Three Representations

Using the electron density  $\rho(\mathbf{r})$  as the probability function in information theory, one obtains the first representation of ITA. Shannon entropy is the first such uncertainty measure widely used in the literature [9],

$$S_S = - \int \rho(\mathbf{r}) \ln \rho(\mathbf{r}) d\mathbf{r} = \int s_S(\mathbf{r}) d\mathbf{r} \quad (15.1)$$

where  $s_S(\mathbf{r})$  is the Shannon entropy density and the total electron density  $\rho(\mathbf{r})$  satisfies the following normalization condition in relation to the total number of electrons,  $N$ , of the system,

$$\int \rho(\mathbf{r}) d\mathbf{r} = N \quad (15.2)$$

Shannon entropy measures the spatial delocalization of the electronic density. The more delocalized the electron density is, the larger the measurement uncertainty and thus the Shannon entropy. It reaches the maximal value when  $\rho(\mathbf{r})$  is uniformly distributed.

The second quantity in ITA is the Fisher information [16],  $I_F$ ,

$$I_F \equiv \int i_F(\mathbf{r}) d\mathbf{r} = \int \frac{|\nabla \rho(\mathbf{r})|^2}{\rho(\mathbf{r})} d\mathbf{r} \quad (15.3)$$

where  $i_F(\mathbf{r})$  is the Fisher information density and  $\nabla \rho(\mathbf{r})$  is the density gradient. Fisher information measures the sharpness or concentration of the electron density distribution. For systems like the homogenous electron gas with  $|\nabla \rho(\mathbf{r})| = 0$ ,  $I_F$  vanishes. The larger the density heterogeneity, the larger the Fisher information. Fisher information and Shannon entropy are quantities measuring two opposite trends of a distribution function, homogeneity and heterogeneity, so, in principle, they should be independent. However, for the electron density, as will be shown below, they are intrinsically correlated [17]. This is, again, due to the basic theorems of DFT. Since the electron density contains all the information necessary to quantify any property of a molecule, its functionals become redundant and thus dependent on one another.

Also, we have earlier proved [17] that there is an equivalent expression for the Fisher information in terms of the Laplacian of the electron density  $\nabla^2 \rho$

$$I'_F \equiv \int i'_F(\mathbf{r}) d\mathbf{r} = - \int \nabla^2 \rho(\mathbf{r}) \ln \rho(\mathbf{r}) d\mathbf{r} \quad (15.4)$$

Equations (15.3) and (15.4) are equivalent in the sense that they can be derived by partial integration from one to the other, and that the two integrals have the same

value. As have been shown, however, local behaviors of the two integrands,  $i_{\text{F}}(\mathbf{r})$  and  $i'_{\text{F}}(\mathbf{r})$ , are markedly different [17].

The third quantity in ITA is the Ghosh–Berkowitz–Parr (GBP) entropy [11]

$$S_{\text{GBP}} = \int \frac{3}{2} k \rho(\mathbf{r}) \left[ c + \ln \frac{t(\mathbf{r}; \rho)}{t_{\text{TF}}(\mathbf{r}; \rho)} \right] d\mathbf{r} \quad (15.5)$$

where  $t(\mathbf{r}, \rho)$  is the kinetic energy density, satisfying

$$\int t(\mathbf{r}; \rho) d\mathbf{r} = T_{\text{S}} \quad (15.6)$$

with  $T_{\text{S}}$  as the total kinetic energy and  $t_{\text{TF}}(\mathbf{r}; \rho)$  the Thomas–Fermi kinetic energy density,  $t_{\text{TF}}(\mathbf{r}; \rho) = c_K \rho^{5/3}(\mathbf{r})$ , where  $k$  is the Boltzmann constant (set to be unity),  $c = \frac{5}{3} + \ln \frac{4\pi c_K}{3}$ , and  $c_K = \frac{3}{10} (3\pi^2)^{2/3}$ . The GBP entropy originates from the effort to transcribe the ground-state DFT into local thermodynamics through a phase-space distribution function. The specific form of the local kinetic energy  $t(\mathbf{r}; \rho)$  used is  $t(\mathbf{r}; \rho) = \sum_i \frac{1}{8} \frac{\nabla \rho_i \cdot \nabla \rho_i}{\rho_i} - \frac{1}{8} \nabla^2 \rho$ . Other quantities in ITA include the Rényi entropy [18] of order  $n$ , where  $n \geq 0$  and  $n \neq 1$ , defined as

$$R_n = \frac{1}{1-n} \ln \left[ \int \rho(\mathbf{r})^n d\mathbf{r} \right] \quad (15.7)$$

where when  $n$  approaches to 1, it is reduced to Shannon entropy and Tsallis entropy [19] of order  $n$  defined by

$$T_n = \frac{1}{n-1} \left[ 1 - \int \rho(\mathbf{r})^n d\mathbf{r} \right] \quad (15.8)$$

which is a generalization of the standard Boltzmann–Gibbs entropy. The common term in Eqs. (15.7) and (15.8) is the integral of the  $n$ -th power of the electron density, which is called the Onicescu information energy [20] of order  $n$ :

$$E_n = \frac{1}{n-1} \int \rho(\mathbf{r})^n d\mathbf{r} \quad (15.9)$$

Onicescu introduced this quantity to define a finer measure of dispersion distribution than that of Shannon entropy. These ITA quantities are all simple density functionals.

The other set of important quantities in ITA is the relative entropy or information, which is defined through a reference density. The first one is the relative Shannon entropy, also called information gain, Kullback–Leibler divergence [21], or information divergence,

$$S_{\text{r}} \equiv I_{\text{G}} \equiv \int i_{\text{G}}(\mathbf{r}) d\mathbf{r} = \int \rho(\mathbf{r}) \ln \frac{\rho(\mathbf{r})}{\rho_0(\mathbf{r})} d\mathbf{r} \quad (15.10)$$

where  $i_{\text{G}}(\mathbf{r})$  is the information gain density and  $\rho_0(\mathbf{r})$  is the reference density satisfying the same normalization condition as  $\rho(\mathbf{r})$ . This reference density can be from neutral atoms in the isolated state, from the same molecule with a different conformation, or the reactant of a chemical reaction when the transition state is investigated. Another relative entropy is the relative Rényi entropy [22] of order  $n$ ,

$$R_n^{\text{r}} = \frac{1}{n-1} \ln \left[ \int \frac{\rho^n(\mathbf{r})}{\rho_0^{n-1}(\mathbf{r})} d\mathbf{r} \right] \quad (15.11)$$



The relative Fisher information in Eq. (15.3) is [23, 24]

$${}^r_F I \equiv \int {}^r_F i(\mathbf{r}') F r d\mathbf{r} = \int \rho(\mathbf{r}) \left[ \nabla \ln \frac{\rho(\mathbf{r})}{\rho_0(\mathbf{r})} \right]^2 d\mathbf{r} \quad (15.12)$$

and the relative quantity for the alternative Fisher information in Eq. (15.4) is [25]

$${}^r_F I' \equiv \int {}^r_F i'(\mathbf{r}') d\mathbf{r} = \int \nabla^2 \rho(\mathbf{r}) \ln \frac{\rho(\mathbf{r})}{\rho_0(\mathbf{r})} d\mathbf{r} \quad (15.13)$$

with  ${}^r_F i(\mathbf{r})$  and  ${}^r_F i'(\mathbf{r})$  as the local density of the two forms of Fisher information.

Equations (15.1)–(15.13) make use of the total electron density as the local distribution function. They are all based on the first representation in ITA. There are two other representations in ITA. One is through the shape function  $\sigma(\mathbf{r})$  [26], which is related to the electron density  $\rho(\mathbf{r})$  and the total number of electrons  $N$  through the following relationship,  $\rho(\mathbf{r}) = N \sigma(\mathbf{r})$  with the normalization condition to unit  $\int \sigma(\mathbf{r}) d\mathbf{r} = 1$ . The above formulas for the two sets of ITA quantities can be rewritten accordingly in terms of the shape function. For example, for Shannon entropy and Fisher information, one has

$$S_\sigma = - \int \sigma(\mathbf{r}) \ln \sigma(\mathbf{r}) d\mathbf{r} \quad (15.14)$$

and

$$I_\sigma = \int \frac{|\nabla \sigma(\mathbf{r})|^2}{\sigma(\mathbf{r})} d\mathbf{r} \quad (15.15)$$

respectively. The third representation of ITA formulation is through the partition of atoms in molecules (AIM), where the total electron population  $N$  of the system is the summation of electron density in each atomic contribution,  $N_A$ ,

$$N = \sum_A N_A = \sum_A \int_{\Omega_A} \rho_A(\mathbf{r}) d\mathbf{r} \quad (15.16)$$

Three schemes to partition AIM are available in the literature, Becke's fuzzy atom approach [27], Bader's zero-flux AIM approach [28], and Hirshfeld's stockholder approach [29]. Within this representation, for instance, Shannon entropy and information gain can be, respectively, rewritten as

$$S_S = - \sum_A \int_{\Omega_A} \rho_A(\mathbf{r}) \ln \rho_A(\mathbf{r}) d\mathbf{r} \quad (15.17)$$

$$S_r \equiv I_G = \sum_A \int_{\Omega_A} \rho_A(\mathbf{r}) \frac{\rho_A(\mathbf{r})}{\rho_A^0(\mathbf{r})} d\mathbf{r} \quad (15.18)$$

It is important to keep in mind that (i) unlike the universal functional in DFT [1], whose exact expression is still unknown, these ITA quantities are all simple density functionals with their dependence on the electron density and its associated quantities explicitly given, and (ii) these three representations are related to each other and one can derive exact relationships among them [30]. Also, they can be separately utilized for different purposes. We will highlight some examples below.

### 15.2.2 Three Principles in ITA

The first principle in ITA, called the “*Principle of Extreme Physical Information*”, was proposed by Nagy [31]. The Euler equation of DFT for a real interacting system  $\mu = \delta E / \delta \rho$  can be recast in the model noninteracting system and becomes

$$\mu = \frac{\delta T_S}{\delta \rho(\mathbf{r})} + v_{KS}(\mathbf{r}) \quad (15.19)$$

where  $T_S$ ,  $v_{KS}$ , and  $\mu$  are the noninteracting kinetic energy, Kohn–Sham potential, and chemical potential, respectively, arising from the constraint that the total number of electrons must be fixed to  $N$ . Furthermore, the noninteracting kinetic energy can be divided into two pieces,

$$T_S = T_W + T_P \quad (15.20)$$

where  $T_W$  is the Weizsäcker kinetic energy

$$T_W = \frac{1}{8} \int \frac{|\nabla \rho(\mathbf{r})|^2}{\rho(\mathbf{r})} d\mathbf{r} \quad (15.21)$$

and  $T_P$  is the Pauli energy due to the Pauli exclusion principle. So, the Euler equation becomes

$$\mu = \frac{\delta T_W}{\delta \rho(\mathbf{r})} + v_p(\mathbf{r}) + v_{KS}(\mathbf{r}) \quad (15.22)$$

where  $v_p$  is the Pauli potential defined as the functional of derivative of  $T_P$  with respect to the electron density. With the help that

$$\frac{\delta T_W}{\delta \rho(\mathbf{r})} = \frac{1}{8} \left( \frac{\nabla \rho(\mathbf{r})}{\rho(\mathbf{r})} \right)^2 - \frac{1}{4} \frac{\nabla^2 \rho(\mathbf{r})}{\rho(\mathbf{r})} = \rho^{-1/2}(\mathbf{r}) \left( -\frac{1}{2} \nabla^2 \right) \rho^{-1/2}(\mathbf{r}) \quad (15.23)$$

Eq. (15.22) becomes

$$\left( -\frac{1}{2} \nabla^2 + v_p(\mathbf{r}) + v_{KS}(\mathbf{r}) \right) \rho^{1/2}(\mathbf{r}) = \mu \rho^{1/2}(\mathbf{r}) \quad (15.24)$$

Equation (15.24) is like the Kohn–Sham equation, but it does not require the introduction of any orbitals. It is the working formula for the orbital-free DFT (OF-DFT) approach in DFT.

As shown by Nagy [31], this OF-DFT equation can, however, be rederived from the *Principle of Extreme Physical Information*, which states that the “physical information”  $K$  of a system should be extreme:

$$K = I_F - J = \text{extreme} \quad (15.25)$$

where  $I_F$  is the Fisher information,  $J$  is the set of constraints that are to be imposed, and  $K$  is the difference between  $I_F$  and  $J$ , called the “physical information”. According to Nagy [31], these constraints are threefold. (i) The total wave function of the system is antisymmetric. As shown by Nagy [14] and Flores and Keller [32], this condition generates the Pauli potential  $v_p(\mathbf{r})$ . (ii) The total density of the noninteracting system should be the same as that of the interacting system. Same as the Kohn–Sham equation, this constraint yields the Kohn–Sham potential  $v_{KS}(\mathbf{r})$ . (iii) Lastly, the total

electron density is normalized to  $N$ , Eq. (15.2), which results in a Lagrange multiplier  $\mu$ , the chemical potential of the system. In other words, minimizing the Fisher information subject to the above three constraints should give us the same Euler equation in OF-DFT. What the *Principle of Extreme Physical Information* tells us is that one does not have to use electronic energy when deriving the Euler equation in DFT. It could be substituted by information. Information alone is adequate in determining all properties of the system. We recently demonstrated the validity of this argument within the context of so-called *Information Functional Theory* [33].

The second principle in ITA is due to Nalewajski and Parr [34], called *Minimum Information Gain Principle*. In their original work, they minimized the relative Shannon entropy in the AIM representation, Eq. (15.18), subject to the condition that atomic densities are always normalized to the total electron  $N$

$$\int \rho \, d\mathbf{r} = \sum_A \int \rho_A \, d\mathbf{r} = \sum_A \int \rho_A^0 \, d\mathbf{r} = N \quad (15.26)$$

which leads to

$$\delta \left\{ I_G - \lambda \left[ \sum_A \int \rho_A(\mathbf{r}) \, d\mathbf{r} - N \right] \right\} = 0 \quad (15.27)$$

where  $\lambda$  is the Lagrange multiplier. Functional differentiation of Eq. (15.27) with respect to all  $\rho_A$ , after some algebraic manipulations, yields that for all atoms  $A$ , we have

$$\rho_A = \frac{\rho_A^0}{\sum_A \rho_A^0} \rho \quad (15.28)$$

Equation (15.28) is the well-known “stockholder partition” of the electron density for AIM first proposed by Hirshfeld [29]. This result shows that if one employs the Hirshfeld scheme to partition atoms in a molecule, the information gain due to the formation of the molecule from the composing pieces will be minimal. In other words, AIM partitioned in this manner will preserve their identity (e.g. electrophilic and nucleophilic properties) of the reference state as much as possible. This nature of minimal information deficiency is called the *Minimum Information Gain Principle*. Since atomic charges are not associated with any physical observable, they have no unique definition. Indeed, there are many ways to quantify charge in the literature [35]. This work provides the first example to derive the definition of an atomic charge from a physiochemical principle.

The third principle in ITA is called *Information Conservation Principle* proposed by us [36]. According to the *Minimum Information Gain Principle*, atoms in molecules tend to keep their identity of their reference state as much as possible, indicating that  $\rho_A$  and  $\rho_A^0$  should be similar and the difference between the two densities could be simulated by a perturbation expansion using the Taylor series. We can define a new variable,  $x = (\rho_A - \rho_A^0)/\rho_A$  so the information gain becomes

$$I_G = \sum_A \int \rho_A \ln \frac{1}{1-x} \, d\mathbf{r} \quad (15.29)$$

Since  $x$  is expected to be small, using  $\ln \frac{1}{1-x} \approx x$  as the first-order approximation, we have

$$I_G \approx \sum_A \int (\rho_A - \rho_A^0) d\mathbf{r} = -\sum_A q_A \quad (15.30)$$

where  $q_A$  is the Hirshfeld charge on Atom (or Group) A. This result shows that under the first-order approximation, the information gain simply gives rise to the Hirshfeld charge distribution. Meanwhile, since  $\rho_A$  and  $\rho_A^0$  satisfy the same normalization condition, Eq. (15.26), the total information gain in Eq. (15.30) must vanish,

$$I_G \approx -\sum_A q_A \equiv 0 \quad (15.31)$$

suggesting that under the first-order approximation, *the information before and after a system is formed should be conserved*. We call this result the *Information Conservation Principle* [36]. This principle, which stemmed from the above first-order approximation, is a special case of the *Minimum Information Gain Principle*. The actual value of information gain in Eq. (15.30) should come from the second and other higher-order terms in the Taylor expansion in Eq. (15.44), with  $\ln \frac{1}{1-x} \approx x + \frac{x^2}{2} + \frac{x^3}{3} + \dots$

### 15.2.3 Relationships Among ITA Quantities

ITA quantities introduced above each have their own explicit formulas well-defined in terms of the electron density and its associated quantities (gradient, Laplacian, etc.). Plus, in the context of information theory, each of them has its distinct physical meaning. In this regard, it seems that they should be independent of one another. Nevertheless, due to the existence of the basic theorems in DFT and henceforth the redundancy of information included in the density functionals, they are closely related. In 2007, we proved that for the density of Shannon entropy,  $s_S(\mathbf{r})$ , and two forms of Fisher information,  $i_F(\mathbf{r})$  and  $i'_F(\mathbf{r})$ , the following identity for atoms and molecules must be valid [17],

$$s_S(\mathbf{r}) = -\rho(\mathbf{r}) + \frac{1}{4\pi} \int \frac{i_F(\mathbf{r}')}{|\mathbf{r} - \mathbf{r}'|} d\mathbf{r}' - \frac{1}{4\pi} \int \frac{i'_F(\mathbf{r}')}{|\mathbf{r} - \mathbf{r}'|} d\mathbf{r}' \quad (15.32)$$

Integrating both sides leads to

$$S_S = -N + \frac{1}{4\pi} \iint \frac{i_F(\mathbf{r}')}{|\mathbf{r} - \mathbf{r}'|} d\mathbf{r}d\mathbf{r}' - \frac{1}{4\pi} \iint \frac{i'_F(\mathbf{r}')}{|\mathbf{r} - \mathbf{r}'|} d\mathbf{r}d\mathbf{r}' \quad (15.33)$$

More recently, for the density of information gain  $i_G(\mathbf{r})$ , we proved [25] the existence of the following identity with the local density of two forms of the relative Fisher information,  ${}^r_F i(\mathbf{r})$  and  ${}^r_F i'(\mathbf{r})$ ,

$$i_G(\mathbf{r}) = -\frac{1}{4\pi} \int \frac{{}^r_F i(\mathbf{r}')}{|\mathbf{r} - \mathbf{r}'|} d\mathbf{r}' - \frac{1}{4\pi} \int \frac{{}^r_F i'(\mathbf{r}')}{|\mathbf{r} - \mathbf{r}'|} d\mathbf{r}' - \frac{1}{4\pi} \int \frac{g_2(\mathbf{r}')}{|\mathbf{r} - \mathbf{r}'|} d\mathbf{r}' \quad (15.34)$$

with

$$g_2(\mathbf{r}') = \rho(\mathbf{r}') \left[ \frac{\nabla^2 \rho(\mathbf{r}')}{\rho(\mathbf{r}')} - \frac{\nabla^2 \rho_0(\mathbf{r}')}{\rho_0(\mathbf{r}')} \right] \quad (15.35)$$

Integrating both sides of Eq. (15.34), one arrives at

$$I_G = -\frac{1}{4\pi} \iint \frac{f(\mathbf{r}')}{|\mathbf{r} - \mathbf{r}'|} d\mathbf{r}d\mathbf{r}' - \frac{1}{4\pi} \iint \frac{g_2(\mathbf{r}')}{|\mathbf{r} - \mathbf{r}'|} d\mathbf{r}d\mathbf{r}' - \frac{1}{4\pi} \iint \frac{f'(\mathbf{r}')}{|\mathbf{r} - \mathbf{r}'|} d\mathbf{r}d\mathbf{r}'. \quad (15.36)$$

These relationships show that, different from other disciplines where information theory is applied, ITA quantities in DFT are intrinsically correlated. This is due to the uniqueness of the electron density in describing molecular properties in the ground state. Numerical evidence demonstrated the validity of these identities for atoms and molecules alike [15, 25, 30].

## 15.3 Applications

In what follows, we highlight five topics where ITA quantities have been recently applied to enhance our understanding about chemical reactivity, including (i) steric effect and stereoselectivity, (ii) electrophilicity and nucleophilicity, (iii) strong covalent interactions (SCIs), (iv) cooperativity in weakly interacting systems, and (v) aromaticity and antiaromaticity.

### 15.3.1 Steric Effect and Stereoselectivity

As one of the most widely used chemical concepts, the steric effect is associated with the impact of the space-occupied atoms in molecules on chemical reactivity. Since it has no physical observable associated with it, its definition is not unique. In 2007, we proposed a quantification approach from the DFT perspective [37] using Weizsäcker kinetic energy [38],

$$T_W \equiv \frac{1}{8} \int \frac{|\nabla\rho(\mathbf{r})|^2}{\rho(\mathbf{r})} d\mathbf{r} \quad (15.37)$$

which is simply one-eighth of Fisher information [16]. Our proposal is as follows. We assume the total electronic energy  $E$  of a molecular system comes from the contribution of three independent physiochemical effects, steric  $E_S$ , electrostatic  $E_e$ , and Fermionic quantum  $E_q$

$$E \equiv E_S + E_e + E_q \quad (15.38)$$

In DFT, we have [1]

$$E = T_S + V_{ne} + J + E_{xc} + V_{nn} = T_S + E_e + E_{xc} \quad (15.39)$$

where  $T_S$ ,  $V_{ne}$ ,  $J$ ,  $V_{nn}$ , and  $E_{xc}$  are the noninteracting kinetic energy, nuclear–electron attraction, classical electron–electron Coulomb repulsion, nuclear–nuclear repulsion, and exchange–correlation energy density functionals, respectively, and  $V_{ne}$ ,  $V_{nn}$ , and  $J$  are of the electrostatic nature, so  $E_e = V_{ne} + J + V_{nn}$ . For the quantum part due to the exchange–correlation effect, we know [39, 40]

$$E_q = E_{xc} + E_{\text{Pauli}} = E_{xc} + T_S - T_W \quad (15.40)$$

where the Pauli energy is [39, 40]

$$E_{\text{Pauli}} \equiv T_{\text{S}} - T_{\text{W}} \quad (15.41)$$

which stands for the portion of the kinetic energy due to the antisymmetric requirement of the total wave function by the Pauli exclusion principle. Putting them together yields [37]

$$E_{\text{S}} = E - E_{\text{e}} - E_{\text{q}} = T_{\text{W}} = 1/8 I_{\text{F}} \quad (15.42)$$

This result suggests that (i) if the assumption in Eq. (15.38) is valid, so is the result in Eq. (15.42); (ii) the steric effect can be quantified in DFT by Weizsäcker kinetic energy,  $T_{\text{W}}$ ; and (iii) since Fisher information differs from the Weizsäcker form by only a factor of 1/8, the steric effect can be described within the ITA framework by Fisher information. To rationalize the last point, Fisher information gauges the heterogeneity of the electron density distribution, which should maximize near the nuclei. These are where most densities reside, space is occupied by AIM, and thus Fisher information can be utilized to represent the impact of the occupied space on reactivity.

One of the applications with the two schemes of total energy partition, Eqs. (15.38) and (15.39), is to provide a unified understanding about the rotation barrier height for six simple compounds, ethane  $\text{C}_2\text{H}_6$ , methylamine  $\text{CH}_3\text{NH}_2$ , methanol  $\text{CH}_3\text{OH}$ , hydrazine  $\text{N}_2\text{H}_4$ , hydroxylamine  $\text{NH}_2\text{OH}$ , and hydrogen peroxide  $\text{H}_2\text{O}_2$ , each of which has only one rotatable bond [41–43]. Figure 15.1 shows all the data points from the flexible rotation of the rotatable bond for these six molecules. The y-axis is the rotation barrier height, and the x-axis is the energy component. When

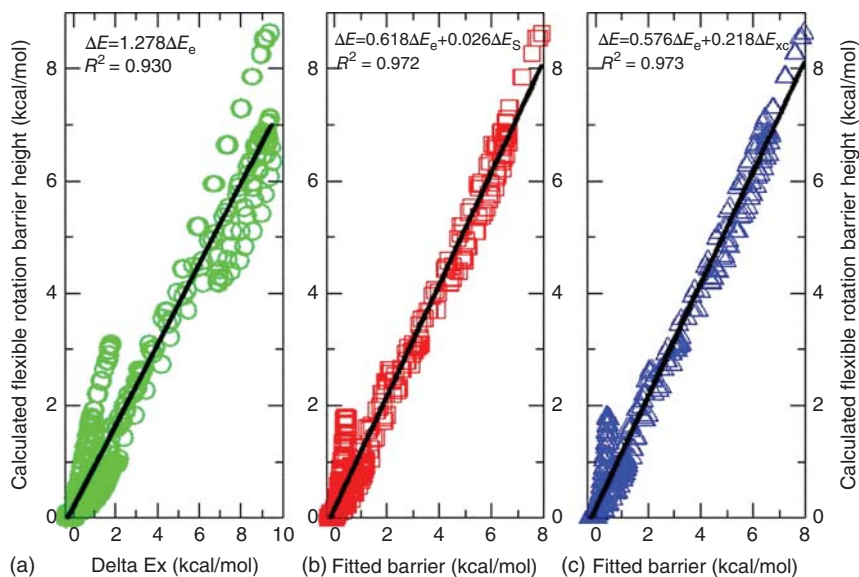


**Figure 15.1** Least-square fittings with one and two energy components for all six molecules. Source: Reprinted with permission from Liu [43], American Chemical Society.

the electrostatic component is plotted against the barrier height, as shown in Figure 15.1a, a reasonably strong linear correlation can be obtained, suggesting that the electrostatic interaction plays the dominant role. However, when it fits together with the contribution from either steric (Figure 15.1b) or exchange-correlation (Figure 15.1c) effect, much stronger correlations become possible. These results indicate that steric and quantum effects play minor but indispensable roles in determining the rotation barrier height.

Stereoselectivity is a chemical reactivity concept closely related to the steric effect. It is a tendency of a chemical reaction in which a single reactant forms an unequal mixture of stereoisomers. This selectivity difference arises from the fact that when an incoming agent attacks the reaction center, it prefers one direction over the other, due to the hindrance of the steric effect. One prominent example is the nucleophilic addition by an electrophile on the carbonyl group with different substituting groups in  $\alpha$ -carbon, where Cram's rule [44] plays important role. Using the above quantification approach of the steric effect, we can predict the stereoselectivity propensity for these reactions. This is done through the steric potential defined by the functional derivative with respect to the electron density [37, 45],

$$v_s(\mathbf{r}) = \frac{\delta E_s[\rho]}{\delta \rho(\mathbf{r})} = \frac{1}{8} \frac{|\nabla \rho(\mathbf{r})|^2}{\rho(\mathbf{r})} - \frac{1}{4} \frac{\nabla^2 \rho(\mathbf{r})}{\rho(\mathbf{r})} \quad (15.43)$$

Taking the partial derivative of Eq. (15.43) with respect to the spatial variable  $\mathbf{r}$ , we have the steric force [45]

$$\mathbf{F}_s(\mathbf{r}) = -\nabla_{\mathbf{r}} v_s(\mathbf{r}) \quad (15.44)$$

With Eq. (15.43), we can also define the steric charge  $q_s(\mathbf{r})$  using the Poisson equation [46],

$$q_s(\mathbf{r}) = -\frac{1}{4\pi} \nabla^2 v_s(\mathbf{r}) = -\frac{1}{4\pi} \nabla^2 \left( \frac{\delta E_s[\rho]}{\delta \rho(\mathbf{r})} \right) \quad (15.45)$$

It can rigorously be proven that the total steric charge of a molecular system should vanish,

$$\int q_s(\mathbf{r}) d\mathbf{r} = \sum_A \int_{\Omega_A} q_s(\mathbf{r}) d\mathbf{r} = \sum_A Q_s^A = 0 \quad (15.46)$$

where the summation is over all atoms in the molecule, the integration is over the atomic basin  $\Omega_A$ , and  $Q_s^A$  is the condensed steric charge on Atom A.

As two illustrative examples, Figure 15.2 exhibits the effectiveness of applying steric force to predict stereoselectivity. The incoming electrophile prefers the side with a smaller group in the  $\alpha$ -carbon, which is unambiguously seen by the magnitude of the steric force in Figure 15.2b. Their stereoselectivity propensity is featured by smaller steric forces on the preferred attacking side (more red area coverage and larger green arrow) of the carbonyl carbon atom. Figure 15.3 visualizes the strong linear correlation between the steric charge of the central carbon atom and the barrier height of the self-exchange  $S_N2$  reaction with the substituent groups from H to *tert*-butyl. It is well known from the experimental finding that bulky groups on the central carbon substantially increase the reaction barrier height. Our results from the steric charge clearly endorse that finding.

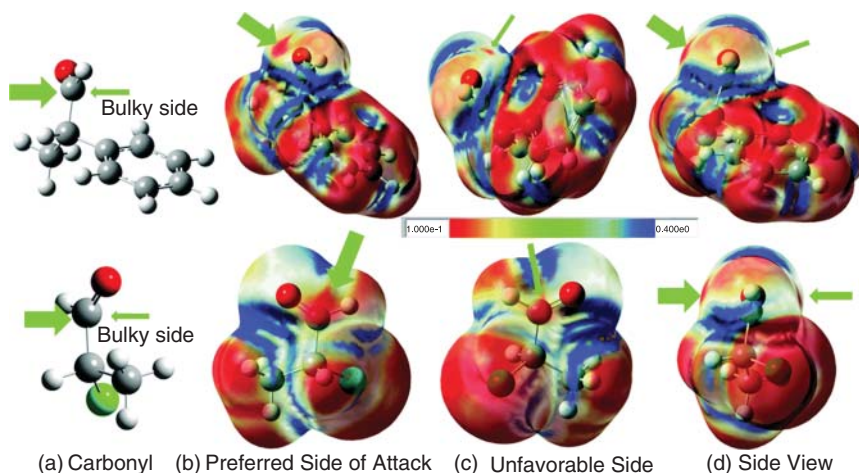


**Figure 15.2** The magnitude of the steric force mapped onto the van der Waals surface for PhMeHC-CHO and ClMeHC-CHO molecules. Source: Reprinted with permission from Liu et al. [45], Royal Society of Chemistry.

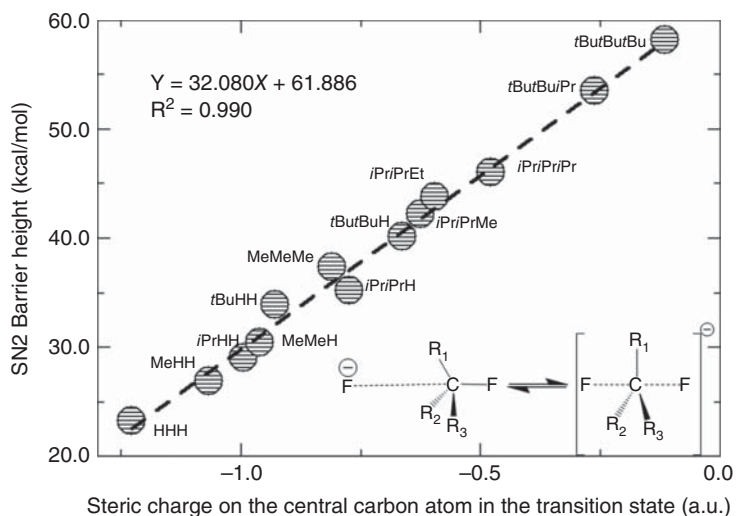


**Figure 15.3** The strong linear correlation between the steric charge of the central carbon atom and the barrier height of the self-exchange  $S_N2$  reaction. Source: Reprinted with permission from Liu et al. [46], Royal Society of Chemistry.

### 15.3.2 Electrophilicity and Nucleophilicity

Recall that there is no unique definition for the atomic charge, but the Hirshfeld charge is the first atomic charge derived from the first principles [33]. Moreover, we demonstrated that it can be employed to determine regioselectivity and simultaneously quantify electrophilicity and nucleophilicity [36]. The reason behind this is the following. According to the *Information Conservation Principle* [36], when a new



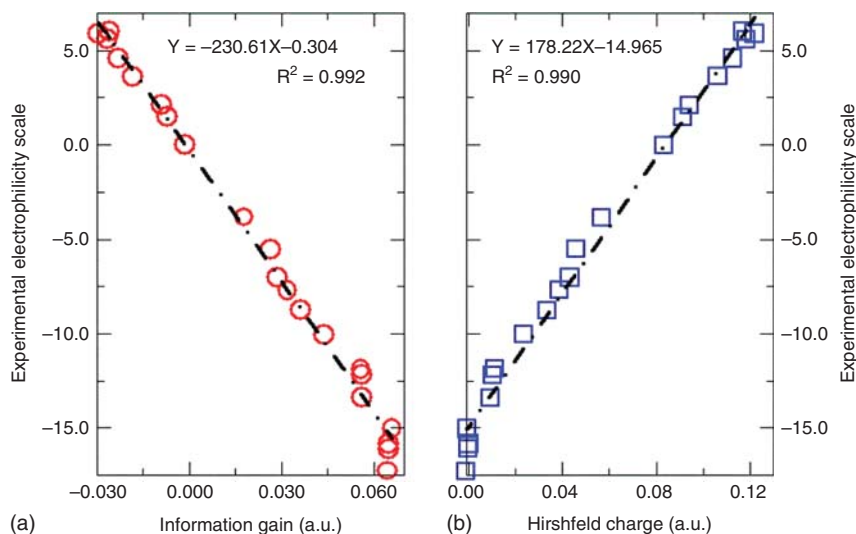


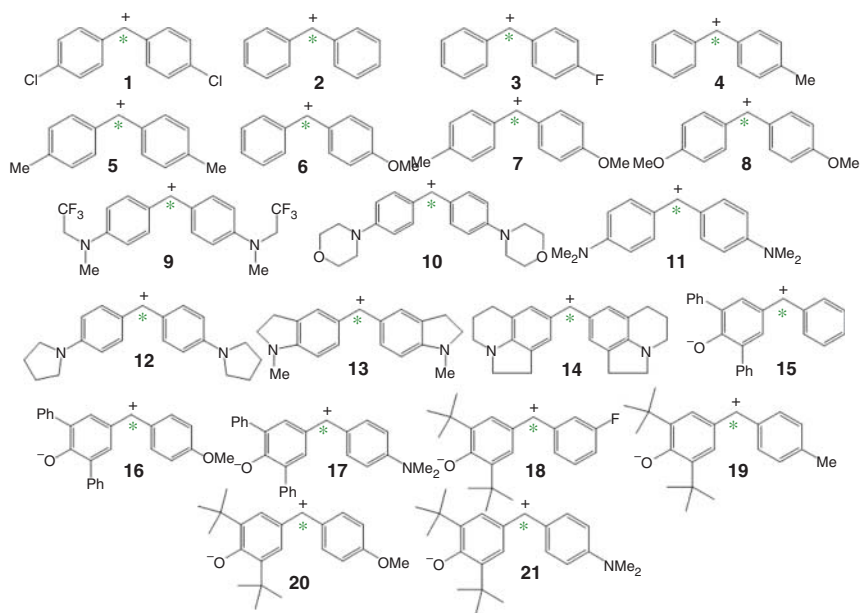
**Figure 15.4** Comparison of the experimental electrophilicity scale of Mayr et al. [47–50] with (a) information gain and (b) Hirshfeld charge for 21 systems listed in Scheme 15.1. Source: Reprinted with permission from Liu et al. [36], American Chemical Society.

system is formed, the identity of its components will be preserved. If a component is electrophilic in nature before the new system is formed, it will still be so afterward. To preserve the identity as much as possible, the newly formed system adjusts its components in such a way that each component becomes charged according to the stockholder partition scheme. Therefore, the amount of the Hirshfeld charge becomes the identity indicator of each component in the new system. To be more specific, if the Hirshfeld charge is negative, it can donate electrons, so it is nucleophilic; if the Hirshfeld charge is positive, it is able to accept electrons, so it is electrophilic. Our results are compared with experimental scales by Mayr and coworkers [47–50].

The validity and effectiveness of applying information gain and Hirshfeld charge to quantify electrophilicity and nucleophilicity have been examined [35, 36, 51–55]. Figure 15.4 shows our results compared with the experimental scale for 21 electrophilic systems in Scheme 15.1. Figure 15.5 visualizes the comparison for 22 nucleophilic molecules in Scheme 15.2. A remarkable agreement between Mayr's experimental scales and our theoretical measures has been achieved. Both information gain and the Hirshfeld charge yielded similar results. Recently, we compared our results with the Fukui function with better results from the Hirshfeld charge observed [35].

### 15.3.3 Strong Covalent Interactions

The idea of using density-based quantities to appreciate chemical bonding is not new. Electron localization function (ELF) [56] is one example and the density Laplacian is another one [28]. Recently, we unveiled that the Pauli energy, Eq. (15.41), can be applied to identify the strong covalent bonds [57–59]. This is because in regions



**Scheme 15.1** Twenty-one electrophilic molecules studied.

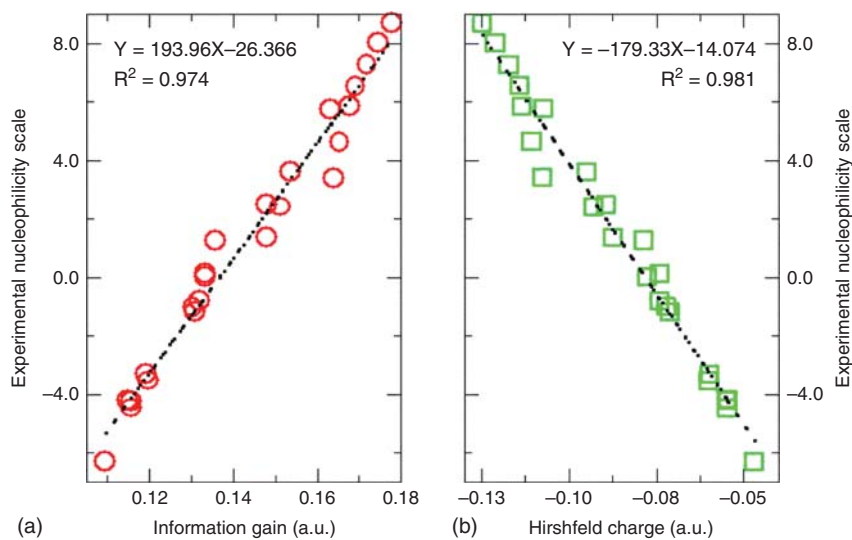
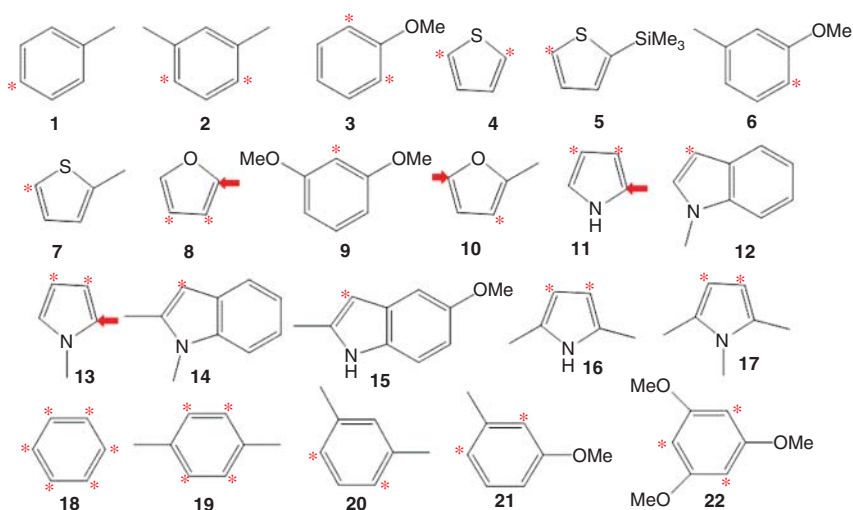


**Figure 15.5** Comparison of the experimental nucleophilicity scale by Mayr et al. [47–50] with (a) information gain and (b) Hirshfeld charge for 22 systems listed in Scheme 15.2. Source: Reprinted with permission from Liu et al. [36], American Chemical Society.



**Scheme 15.2** Twenty-two nucleophilic molecules studied.

where multiple covalent bonding occurs involving multiple pairs of electrons in limited space, strong electron repulsion originating from the Pauli repulsion principle should be present. This strong repulsion can be quantified by the Pauli energy. With the Pauli energy, we proposed a dimensional index called SCI (strong covalent interaction) index. We discovered that a signature isosurface shape of a dumbbell, donut, and four beans in the center of covalent bonding, as shown in Figure 15.6, is an indication of double, triple, and quadruple bonds, respectively. This SCI index has been applied to various organic and inorganic systems, and the above signature isosurface for systems with different covalent bond orders is always preserved, indicating the reliability and robustness of applying the Pauli energy to describe SCIs. Furthermore, with this same idea, we were able to identify quintuple and even sextet bonds. This quantity can also be applied to assess the quality of approximate kinetic energy density functionals when approximate kinetic energy functionals are employed instead of the accurate one to compute the Pauli energy [59].

### 15.3.4 Cooperativity in Noncovalent Systems

For systems with noncovalent interactions, they are often characterized by the cooperativity effect due to the competition and compromise among two or more interactions. We recently quantified the cooperativity effect using the interaction energy for systems composed of multiple copies of the same building block, and then analyzed the nature and origin of the cooperativity effect with ITA quantities [60–62]. Using simple atomic and molecular clusters as examples in Scheme 15.3, we showed that both positive and negative cooperativity is possible. Cooperativity in homogeneous molecular systems is positive, but cooperativity in charged molecular systems is negative (Figure 15.7) [62]. We unveiled that positive cooperativity is dominated

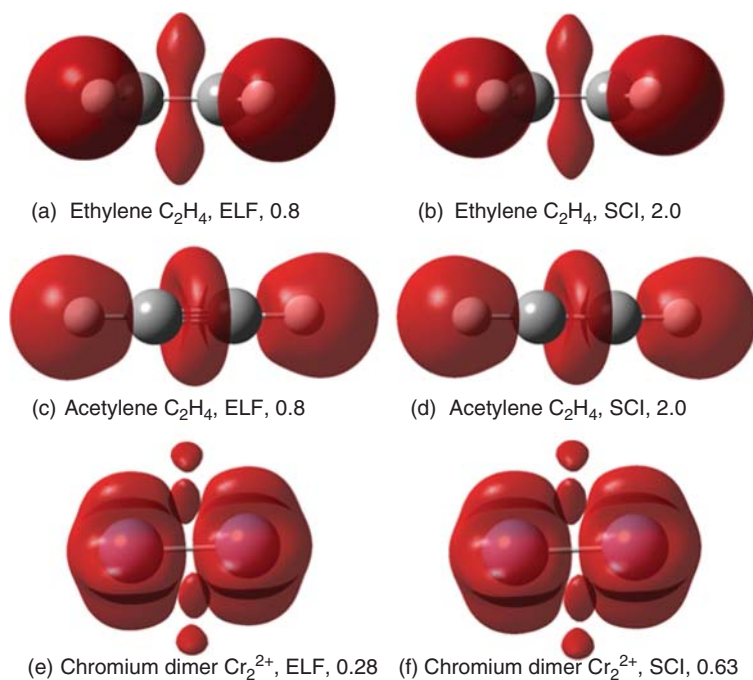
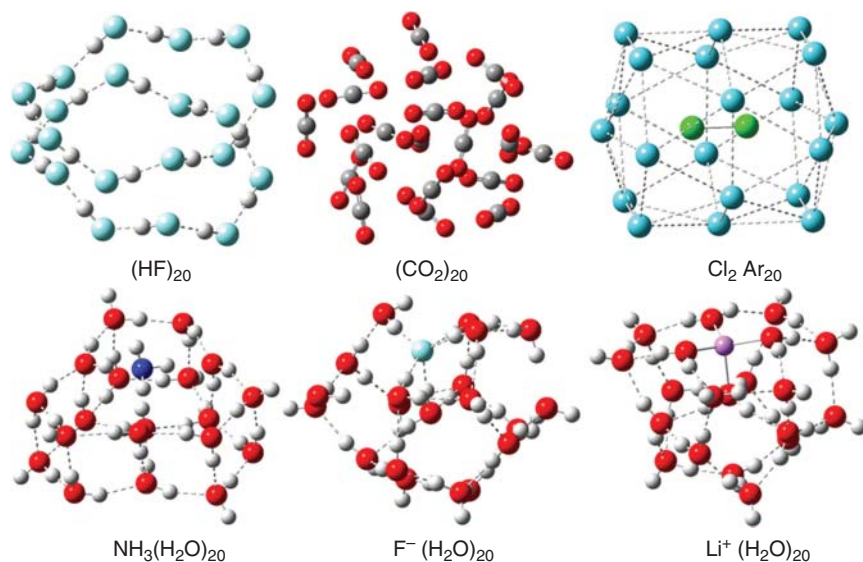


**Figure 15.6** Identification of strong covalent interactions with ELF and SCI distributions: (a, b) double, (c, d) triple, and (e, f) quadruple bonds, whose isosurface shape in the center of the strong covalent bonds is like a dumbbell, donut, and four beans, respectively. The isovalue employed to plot contour surfaces of ELF and SCI is shown for each system as well. Source: Reprinted with permission from Liu et al. [57], American Chemical Society.

by the exchange-correlation interaction and steric effect, but the negative cooperativity is dictated by the electrostatic interaction. From the ITA perspective, these two categories of systems also demonstrated vastly different yet self-consistent behaviors.

### 15.3.5 Aromaticity and Antiaromaticity

Aromaticity and antiaromaticity are another set of extremely fundamental concepts in chemistry, yet much is needed to understand their origin and nature. Many types of aromaticity have emerged, such as Hückel aromaticity, Möbius aromaticity, excited-state aromaticity, homoaromaticity, heteroaromaticity, three-dimensional aromaticity, spherical aromaticity,  $\sigma$ -aromaticity,  $\delta$ -aromaticity, and metalloaromaticity. Many kinds of aromaticity and antiaromaticity descriptors have been proposed (ASE, Harmonic Oscillator Model of Aromaticity [HOMA], para-delocalization index [PDI], FLU, NICS, and MCI) as well. However, none of them can identify all aromaticity types. Recently, we applied ITA quantities to appreciate aromaticity and antiaromaticity [63–68]. In Figure 15.8, using fulvene derivatives as illustrative examples [63], often called the chameleon of aromaticity because of their capability to switch between aromaticity and antiaromaticity by changing the substituting group, we demonstrate the usefulness of ITA quantities



**Scheme 15.3** The optimized structure for six cluster models with  $n = 20$  studied in this work. Source: Reprinted with permission from Rong et al. [62], American Chemical Society.

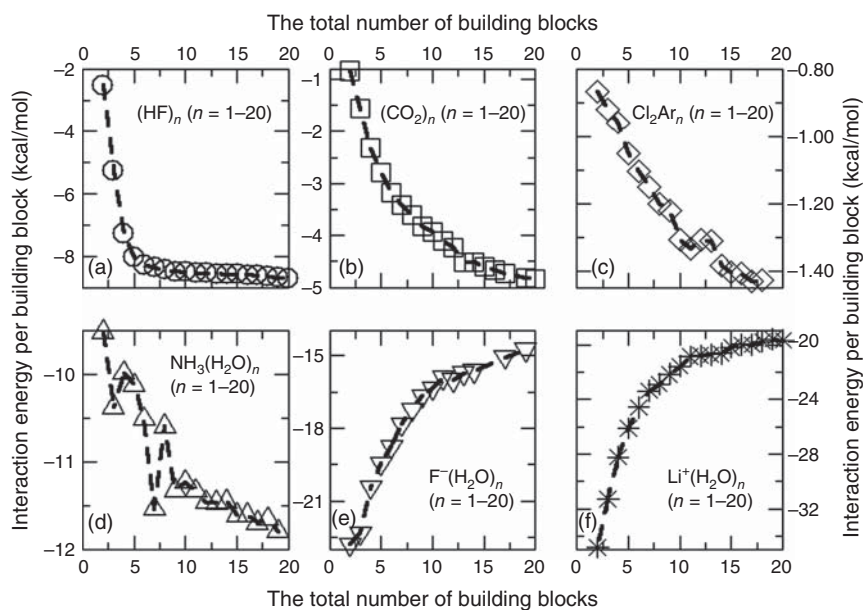


**Figure 15.7** Cooperativity profiles of the six cluster models studied in Scheme 15.3. Source: Reprinted with permission from Rong et al. [62], American Chemical Society.

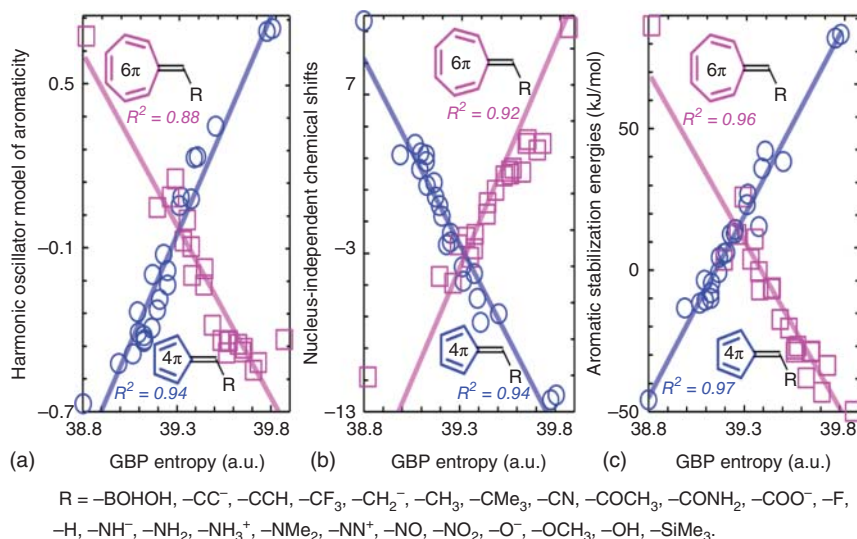


**Figure 15.8** Comparison of the GBP entropy with three aromaticity descriptors. (a) Structural index, Harmonic Oscillator Model of Aromaticity (HOMA); (b) magnetic index, nucleus-independent chemical shifts; and (c) energetic index, aromatic stabilization energies for fulvene derivatives with a total of 4 and 6  $\pi$  electrons. Source: Reprinted with permission from Ref. [63]. Copyright 2018, Royal Society of Chemistry.

in distinguishing aromaticity from antiaromaticity. We utilized the GBP entropy in this case and compared it with three aromaticity (structural, magnetic, and energetic) descriptors for two series of fulvene compounds with 4 and 6  $\pi$  electrons, respectively. As can be unambiguously seen from the figure, the ITA quantity displays opposite correlation trends for aromatic and antiaromatic systems with all three aromaticity criteria. These opposite trends of correlations can be utilized to identify aromaticity and antiaromaticity. This behavior has been observed in other systems as well [64–68].

## 15.4 Concluding Remarks

This chapter introduces the ITA and highlights a few of its recent developments as a new front of CDFT, where simple electron density functionals are directly employed to quantify chemical reactivity. Because of the space limit, we only overviewed its three theory developments and five topic applications. In retrospect, searching for accurate approximations for energetic components such as exchange and correlation energy density functionals has been the focus of DFT developments in the past few decades. Can density functionals do the same for chemical reactivity such as regioselectivity, stereoselectivity, or chemoselectivity? From what we have presented in this chapter, the answer should definitely be yes. As an extension part of this CDFT textbook, we hope that more efforts will be invested in the future along this direction toward our common goal of crafting a chemical reactivity theory in density-based language.

## References

- 1 Parr, R.G. and Yang, W. (1989). *Density Functional Theory of Atoms and Molecules*. New York: Oxford University Press.
- 2 Geerlings, P., De Proft, F., and Langenaeker, W. (2003). *Chem. Rev.* 103: 1793–1873.
- 3 Nalewajski, R.F. (2006). *Information Theory of Molecular Systems*. Amsterdam: Elsevier Science.
- 4 Nalewajski, R.F. (2010). *Information Origins of the Chemical Bond*. New York: Nova Science Publishers.
- 5 Nalewajski, R.F. (2016). *Quantum Information Theory of Molecular States*. New York: Nova Science Publishers.
- 6 Liu, S.B. (2016). *Acta Phys. -Chim. Sin.* 32: 98–118.
- 7 Rong, C.Y., Wang, B., Zhao, D.B., and Liu, S.B. (2020). *WIREs Comp. Mol. Sci.* 10: e1461.
- 8 Hohenberg, P. and Kohn, W. (1964). *Phys. Rev.* 136: B864–B871.
- 9 Shannon, C.E. (1948). *Bell Syst. Tech. J.* 27: 379–423.
- 10 Sears, S.B., Parr, R.G., and Dinur, U. (1980). *Isr. J. Chem.* 19: 165–173.
- 11 Ghosh, S.K., Berkowitz, M., and Parr, R.G. (1984). *Proc. Natl. Acad. Sci. U. S. A.* 81: 8028–8031.
- 12 Gadre, S.R. and Bendale, R.D. (1987). *Phys. Rev. A* 36: 1932.
- 13 Nalewajski, R.F. and Parr, R.G. (2001). *J. Phys. Chem. A* 105: 7391–7400.
- 14 Nagy, A. (2003). *J. Chem. Phys.* 119: 9401–9405.
- 15 Parr, R.G., Ayers, P.W., and Nalewajski, R.F. (2005). *J. Phys. Chem. A* 109: 3957–3959.
- 16 Fisher, R.A. (1925). *Proc. Camb. Philos. Soc.* 22: 700–725.
- 17 Liu, S.B. (2007). *J. Chem. Phys.* 126: 191107.
- 18 Rényi, A. (1970). *Probability Theory*. Amsterdam: North-Holland.
- 19 Tsallis, C. (1988). *J. Stat. Phys.* 52: 479–487.
- 20 Onicescu, O. (1966). *C. R. Acad. Sci. Paris A* 263: 25.
- 21 Kullback, S. and Leibler, R.A. (1951). *Ann. Math. Stat.* 22: 79–86.
- 22 Nagy, Á. and Romera, E. (2015). *Europhys. Lett.* 109: 60002.
- 23 Nagy, Á. (2020). *Int. J. Quantum Chem.* 120: e26405.
- 24 Yamano, T. (2018). *Chem. Phys. Lett.* 691: 196–198.
- 25 Liu, S.B. (2019). *J. Chem. Phys.* 151: 141103.
- 26 Baekelandt, B.G., Cedillo, A., and Parr, R.G. (1995). *J. Chem. Phys.* 103: 8548–8556.
- 27 Becke, A.D. (1988). *J. Chem. Phys.* 88: 2547–2553.
- 28 Bader, R.F.W. (1990). *Atoms in Molecules: A Quantum Theory*. Oxford, England: Oxford University Press.
- 29 Hirshfeld, F. (1977). *Theor. Chim. Acc.* 44: 129–138.
- 30 Rong, C.Y., Lu, T., Ayers, P.W. et al. (2015). *Phys. Chem. Chem. Phys.* 17: 4977–4988.
- 31 Nagy, Á. (2014). *Int. J. Quantum Chem.* 114: 114.
- 32 Flores, J.A. and Keller, J. (1992). *Phys. Rev. A* 45: 6259.

- 33 Zhou, X., Rong, C., Lu, T. et al. (2016). *J. Phys. Chem. A* 120: 3634–3642.
- 34 Nalewajski, R.F. and Parr, R.G. (2000). *Proc. Natl. Acad. Sci. U. S. A.* 97: 8879–8882.
- 35 Wang, B., Rong, C.Y., Chattaraj, P.K., and Liu, S.B. (2019). *Theor. Chem. Acc* 138: 124.
- 36 Liu, S.B., Rong, C.Y., and Lu, T. (2014). *J. Phys. Chem. A* 118: 3698–3704.
- 37 Liu, S.B. (2007). *J. Chem. Phys.* 126: 244103.
- 38 von Weizsäcker, C.F. (1935). *Z. Phys.* 96: 431–458.
- 39 March, N.H. (1986). *Phys. Lett. A* 113: 476.
- 40 Holas, A. and March, N.H. (1991). *Phys. Rev. A* 44: 5521.
- 41 Liu, S.B. and Govind, N. (2008). *J. Phys. Chem. A* 112: 6690–6699.
- 42 Liu, S.B., Govind, N., and Pedersen, L.G. (2008). *J. Chem. Phys.* 129: 094104.
- 43 Liu, S.B. (2013). *J. Phys. Chem. A* 117: 962–965.
- 44 Cram, D.J. and Elhafez, F.A.A. (1952). *J. Am. Chem. Soc.* 74: 5828–5835.
- 45 Liu, S.B., Rong, C.Y., and Lu, T. (2017). *Phys. Chem. Chem. Phys.* 19: 1496–1503.
- 46 Liu, S.B., Liu, L., Yu, D. et al. (2018). *Phys. Chem. Chem. Phys.* 20: 1408–1420.
- 47 Mayr, H. and Patz, M. (1994). *Angew. Chem. Int. Ed. Eng.* 33: 938–957.
- 48 Mayr, H., Bug, T., Gotta, M.F. et al. (2001). *J. Am. Chem. Soc.* 123: 9500–9512.
- 49 Lucius, R., Loos, R., and Mayr, H. (2002). *Angew. Chem. Int. Ed.* 41: 91–95.
- 50 Mayr, H., Kempf, B., and Ofial, A.R. (2003). *Acc. Chem. Res.* 36: 66–77.
- 51 Zhou, X.Y., Rong, C., Lu, T., and Liu, S.B. (2014). *Acta Phys. -Chim. Sin.* 30: 2055–2062.
- 52 Liu, S.B. (2014). *J. Chem. Phys.* 141: 194109.
- 53 Liu, S.B. (2015). *J. Phys. Chem. A* 119: 3107–3111.
- 54 Wu, W., Wu, Z., Rong, C. et al. (2015). *J. Phys. Chem. A* 119: 8216–8224.
- 55 Wu, Z., Rong, C., Lu, T. et al. (2015). *Phys. Chem. Chem. Phys.* 17: 27052–27061.
- 56 Becke, A.D. and Edgecombe, K.E. (1990). *J. Chem. Phys.* 92: 5397–5403.
- 57 Liu, S.B., Rong, C.Y., Lu, T., and Hao, H. (2018). *J. Phys. Chem. A* 122: 3087–3095.
- 58 Huang, Y., Liu, L., Rong, C. et al. (2018). *J. Mol. Model.* 24: 213.
- 59 Liu, S.B., Zhao, D., Rong, C. et al. (2019). *J. Chem. Phys.* 150: 204106.
- 60 Rong, C.Y., Zhao, D.B., Yu, D.H., and Liu, S.B. (2018). *Phys. Chem. Chem. Phys.* 20: 17990–17998.
- 61 Zhou, T.J., Liu, S.Y., Yu, D.H. et al. (2019). *Chem. Phys. Lett.* 716: 192–198.
- 62 Rong, C.Y., Zhao, D.B., Zhou, T.J. et al. (2019). *J. Phys. Chem. Lett.* 10: 1716–1721.
- 63 Yu, D.H., Rong, C.Y., Lu, T. et al. (2017). *Phys. Chem. Chem. Phys.* 19: 18635–18645.
- 64 Yu, D.H., Rong, C.Y., Lu, T. et al. (2018). *ACS Omega* 3: 18370–18379.
- 65 Yu, D.H., Rong, C.Y., Lu, T. et al. (2018). *Acta Phys. -Chim. Sin.* 34: 639–649.
- 66 Yu, D.H., Stuyver, T., Rong, C.Y. et al. (2019). *Phys. Chem. Chem. Phys.* 21: 18195–18210.
- 67 Yu, D.H., Rong, C.Y., Lu, T. et al. (2020). *Phys. Chem. Chem. Phys.* 22: 4715–4730.
- 68 He, X., Yu, D.H., Wu, J.Y. et al. (2020). *Chem. Phys. Lett.* 761: 138065.



## 16

# The Linear Response Function

Paul Geerlings

*Vrije Universiteit Brussel, Research Group of General Chemistry (ALGC), Faculty of Science and Bioengineering Science, Pleinlaan 2, Brussels 1050, Belgium*

## 16.1 Introduction

Response functions [1] play a fundamental role in conceptual density functional theory (CDFT) [2–9]. As outlined in the Chapter 1 and in Chapter 2, they appear in a natural way when discussing the effect of perturbations in the number of electrons  $N$  or the external potential  $v(\mathbf{r})$  on the energy  $E$  of an atom, molecule... upon a chemical reaction. A series expansion then indeed reveals the importance of partial, functional, or mixed derivatives of the type  $\partial^n E[N, v] / \partial N^m \delta v(\mathbf{r}_1) \delta v(\mathbf{r}_2) \cdots \delta v(\mathbf{r}_{m'})$  with  $(n = m + m')$  indicating the sensitivity, or response, of a system toward perturbations in  $N$  and/or  $v$ . Multiplied by the perturbation itself, they quantify the magnitude of the effect of the perturbation on the system. Hence their name: response functions. It should be stressed again (see Chapter 2) that these quantities are intrinsic properties of the system, i.e. only a function of the nature of the system, not a function of the (magnitude) of the perturbation.

In Chapter 2, the “response function tree” [3, 4, 10] was introduced, showing how, adopting the usual sequence, “pure”  $N$  derivatives are at the extreme left, “pure”  $v$  derivatives at the extreme right at a given order of perturbation  $n$ , and that when going from left to right one passes from global (i.e.  $\mathbf{r}$ -independent), to local (i.e.  $\mathbf{r}$ -dependent) to nonlocal (depending on  $\mathbf{r}, \mathbf{r}', \mathbf{r}'' \dots$ ) descriptors. In the previous chapters of the foundations part, most attention went to both  $n = 1$  derivatives (electronic chemical potential and electron density, being global and local in nature, respectively) and to two of the three  $n = 2$  derivatives (chemical hardness, electronic Fukui function, again being global and local in nature respectively). Although present in the response function tree, the utmost right  $n = 2$  derivative in Scheme 2.3 received much less attention. This second functional derivative of  $E$

with respect to the external potential at a constant number of electrons, a kernel, is commonly referred to as the linear response function (LRF) [2] for reasons that will become clear below (for reviews see Refs [11, 12]). Usually, it is written as  $\chi(\mathbf{r}, \mathbf{r}')$ . The reasons why its importance in CDFT was limited in the early years of CDFT (cf. Chapter 1) are clear: it is a complicated descriptor, the function of six variables, hard to evaluate, and after evaluation, hard to represent, let it be to give chemical significance to it. In the past 10–15 years, it, however became possible to calculate, at different levels of approximation and to represent this descriptor and show that it contains important chemical information. As an afterthought, its chemical significance is not unexpected because, in the response tree, it can be placed on equal footing as the chemical hardness, the second pure  $N$  derivative. A word of caution should be placed here. The reader may well be aware of the use of the frequency-dependent form of the LRF,  $\chi(\mathbf{r}, \mathbf{r}'; \omega)$ , which has a long-standing tradition in time-dependent DFT [13]. Thanks to pioneering work by Gross and coworkers [14, 15] and the elegant matrix formulation by Casida [16], it offers a routinely available road to compute the electronic transition energies/frequencies as its poles and on the fly its intensities and assignments; nowadays, it is implemented in many standard Quantum Chemical packages. This remarkable computational evolution, however, was not accompanied by parallel investigations on different ways of the evaluation, representation, and especially the chemical interpretation of its frequency-independent, or static congener,  $\chi(\mathbf{r}, \mathbf{r}')$ .

It should be clear that in this chapter we describe the basics of and the evolution in research and use of the time-independent LRF, which to a certain extent, has proceeded independent of its time-dependent version and, up to now, has certainly had a different finality. These things said, the chapter is structured as follows. Section 16.2 will start from the exact expression for the LRF originating from a wave functional perturbational ansatz and the different approximations in use to cope with the computational intractability of the basic expression. In Section 16.3, a selection will be made of applications varying from atoms to molecules illustrating how and which chemical information can be retrieved from the LRF, whereas its representation will also be scrutinized. In a separate subsection, we will highlight the connection between the LRF and the alchemical derivatives involving a new type of response function ( $\partial E/\partial Z_\alpha$ ), where  $Z_\alpha$  is the charge of nucleus  $\alpha$ . Introduced by von Lilienfeld, these derivatives have shown to offer promising possibilities in exploring the chemical space. In view of (i) their response function character and (ii) their direct link with the LRF theoretical and applied aspects of the alchemical derivatives are included in this chapter.

A final introductory word: although we will try to adopt as much as possible a pedagogical style in view of the aim of this book, it is absolutely impossible to give and comment on all derivations in detail. The essentials will be given, and the reader will be referred to other reviews or the original papers for further details. Note that not all basic references to CDFT are included again, as they can be found in the four chapters in Part I. On the other hand, the references to the LRF literature are comprehensive.

## 16.2 Theory and Computational Aspects

The at first awkward expression for  $\chi$

$$\chi(\mathbf{r}, \mathbf{r}') = (\delta^2 E / \delta v(\mathbf{r}) \delta v(\mathbf{r}'))_N \quad (16.1)$$

becomes more transparent when realizing that the response function tree [3, 4, 10] in Chapter 3 reveals that

$$(\delta E / \delta v(\mathbf{r}))_N = \rho(\mathbf{r}) \quad (16.2)$$

turning Eq. (16.1) into

$$\chi(\mathbf{r}, \mathbf{r}') = (\delta \rho(\mathbf{r}) / \delta v(\mathbf{r}'))_N = (\delta \rho(\mathbf{r}') / \delta v(\mathbf{r}))_N = \chi(\mathbf{r}', \mathbf{r}) \quad (16.3)$$

where the second expression results from the independence of the sequence of the two functional derivatives in Eq. (16.1). The physical interpretation of the LRF now becomes obvious: it represents the sensitivity of the density at position  $\mathbf{r}$  to a change in the external potential at position  $\mathbf{r}'$  or vice versa. The first-order change in the density  $\Delta \rho(\mathbf{r})$  upon a perturbation  $\Delta v(\mathbf{r}')$  can then be written as

$$\Delta \rho(\mathbf{r}) = \int (\delta \rho(\mathbf{r}) / \delta v(\mathbf{r}'))_N \Delta v(\mathbf{r}') d\mathbf{r}' = \int \chi(\mathbf{r}, \mathbf{r}') \Delta v(\mathbf{r}') d\mathbf{r}' \quad (16.4)$$

The terminology “linear” now becomes clear:  $\chi(\mathbf{r}, \mathbf{r}')$  is the proportionality “constant” between the change in density at position  $\mathbf{r}$  and the change (perturbation) of the potential at position  $\mathbf{r}'$ . This simple relationship between both quantities only holds when the strength of the perturbation is small, and higher-order terms can be neglected: then the response  $\delta \rho$  is linearly related to the perturbation  $\delta v$ , and one can work in the context of linear response theory with as fundamental and intrinsic property of the system  $\chi(\mathbf{r}, \mathbf{r}')$  characterizing, as stated above, the sensitivity of the density of a system at position  $\mathbf{r}$  to a change or perturbation is the external potential at position  $\mathbf{r}'$ . The reader will notice that the term “linear” is at first sight contradictory with the position of the LRF in the CDF tree introduced in Chapter 2 of the fundamentals, the reason, of course, being that this tree is based on energy derivatives and that in this context, the density itself already appears as the first derivative of the energy.

As a final remark before proceeding to the evaluation of the LRF, the reader should realize that, in analogy to macroscopic thermodynamics and using its wording, the perturbation in the external potential may bring the atomic or molecular system “out of equilibrium,” leading to the question of criteria for intrinsic equilibrium and stability of molecular systems. These criteria have been formulated by Nalewajski and Capitani and interpreted in terms of the Le Châtelier and the Le Châtelier Braun principle, further extending analogies between the Density Functional Theory and Thermodynamics [17a], put forward by Nalewajski and Parr [17b].

Passing now to the evaluation of  $\chi(\mathbf{r}, \mathbf{r}')$ , its most general expression can be obtained from standard first-order perturbation theory in a wave function theory context [2]. One starts from the density expression for a  $N$  electron system described by a (time-independent) wave function  $\psi$

$$\psi = \psi(\mathbf{x}_1, \mathbf{x}_2 \cdots \mathbf{x}_N) \quad (16.5)$$

where  $\mathbf{x}_i$  is a four-vector containing three spatial coordinates gathered in  $\mathbf{r}_i$  and a spin variable  $s_i$ . Throughout this text all wave functions will be considered as real, the extension to complex wave functions being evident. The density at position  $\mathbf{r}$ ,  $\rho(\mathbf{r})$ , is then given by

$$\rho(\mathbf{r}) = N \int \Psi(\mathbf{x}_1, \mathbf{x}_2 \cdots \mathbf{x}_N) \Psi(\mathbf{x}_1, \mathbf{x}_2 \cdots \mathbf{x}_N) ds_1 d\mathbf{x}_2 \cdots d\mathbf{x}_N \quad (16.6)$$

Consider now a one-electron perturbation in the potential

$$\Delta V = \sum_i \Delta v_i(\mathbf{r}) \quad (16.7)$$

First-order perturbation theory (not considering here the case of degeneracy) then straightforwardly yields

$$\begin{aligned} \Delta\rho(\mathbf{r}_1) &= N \int \cdots \int (\Psi - \Psi_0^{(0)} \Psi_0^{(0)}) ds_1 d\mathbf{x}_2 \cdots d\mathbf{x}_N \\ &= 2N \sum_{j>0} (E_0^{(0)} - E_j^{(0)})^{-1} \langle \Psi_j^{(0)} | \Delta V | \Psi_0^{(0)} \rangle \\ &\quad \int \cdots \int \Psi_0^{(0)} \Psi_j^{(0)} ds_1 d\mathbf{x}_2 \cdots d\mathbf{x}_N \end{aligned} \quad (16.8)$$

where the summation over  $j$  runs over all excited states  $\psi_j$ ,  $\psi_0$  denoting the ground state, with associated energy levels  $E_j$  and  $E_0$  and the superscript<sup>(0)</sup> denotes the unperturbed system. Evaluating the  $\Delta V$  matrix elements and comparing Eq. (16.8) with Eq. (16.4) then yields

$$\begin{aligned} \chi(\mathbf{r}_1, \mathbf{r}_2) &= 2N^2 \sum_{j>0} (E_0^{(0)} - E_j^{(0)})^{-1} \left( \int \Psi_j^{(0)} \Psi_0^{(0)} d\mathbf{x}_1 ds_2 d\mathbf{x}_3 \cdots d\mathbf{x}_N \right) \\ &\quad \times \left( \int \Psi_0^{(0)} \Psi_j^{(0)} ds_1 d\mathbf{x}_2 d\mathbf{x}_3 \cdots d\mathbf{x}_N \right) \end{aligned} \quad (16.9)$$

Introducing the density operator  $\rho_{\text{op}}(\mathbf{r}) = \sum_i \delta(\mathbf{r} - \mathbf{r}_i)$  allows to simplify expression (16.6) as

$$\rho(\mathbf{r}) = \int \Psi(\mathbf{x}_1, \mathbf{x}_2 \cdots \mathbf{x}_N) \rho_{\text{op}}(\mathbf{r}) \Psi(\mathbf{x}_1, \mathbf{x}_2 \cdots \mathbf{x}_N) d\mathbf{x}^N \quad (16.10)$$

Extending this density expression to “off-diagonal cases” involving two different wave functions, say,  $\psi_j^{(0)}$  and  $\psi_0^{(0)}$ , one arrives at a compact expression (changing  $\mathbf{r}_1$  and  $\mathbf{r}_2$  into  $\mathbf{r}$  and  $\mathbf{r}'$ )

$$\chi(\mathbf{r}, \mathbf{r}') = 2 \sum_{j>0} (E_0^{(0)} - E_j^{(0)})^{-1} \langle j | \rho_{\text{op}}(\mathbf{r}) | 0 \rangle \langle 0 | \rho_{\text{op}}(\mathbf{r}') | j \rangle \quad (16.11)$$

This type of expression is encountered in the context of time-dependent DFT for the frequency-dependent counterpart  $\chi(\mathbf{r}, \mathbf{r}'; \omega)$  of the LRF, usually termed the spectral density representation of the density-density response function. In the zero-frequency limit [13]. In the case of real functions, Eq. (16.11) is retrieved. The complications arising when attempting to evaluate  $\chi$  in this way are obvious, as in the infinite summation, the energies and wave functions of all excited states are needed.

Most work in this field has been done using a coupled perturbed Hartree–Fock (HF) or Kohn–Sham (KS) ansatz [11, 18], where the basic idea is that a single Slater

determinant is used for the unperturbed system involving orbitals  $\varphi_i$ , solutions of the unperturbed HF, or KS equations, whose change under perturbation is evaluated at different orders. Taking for the sake of simplicity a closed shell system and real orbitals, the density can then be written as

$$\rho^{(0)}(\mathbf{r}) = 2\sum_i \varphi_i^{(0)2}(\mathbf{r}) \quad (16.12)$$

and its first-order correction as

$$\rho^{(1)}(\mathbf{r}) = 4\sum_i \varphi_i^{(0)}(\mathbf{r})\varphi_i^{(1)}(\mathbf{r}) \quad (16.13)$$

where the first-order correction to orbital  $\varphi_i$ ,  $\varphi_i^{(1)}$ , can be expanded in terms of the zero-order functions

$$\varphi_i^{(1)}(\mathbf{r}) = \sum_a c_{ai} \varphi_a^{(0)}(\mathbf{r}) \quad (16.14)$$

Introducing this expansion into the perturbed HF or KS equations (for a complete derivation see [11, 18]), one obtains

$$\chi(\mathbf{r}, \mathbf{r}') = (\delta\rho(\mathbf{r})/\delta v(\mathbf{r}'))_N = -4 \sum_{ib} \sum_{jc} (\mathbf{M}^{-1})_{ib,jc} \varphi_i^{(0)}(\mathbf{r}) \varphi_b^{(0)}(\mathbf{r}) \varphi_j^{(0)}(\mathbf{r}') \varphi_c^{(0)}(\mathbf{r}') \quad (16.15)$$

where the  $\mathbf{M}$  matrix elements are given by

$$\text{in HF } M_{ib,jc} = (\varepsilon_c - \varepsilon_j) \delta_{ij} \delta_{bc} + 4(ib|jc) - 2(ic|jb) \quad (16.16a)$$

$$\text{in KS } M_{ib,jc} = (\varepsilon_c - \varepsilon_j) \delta_{ij} \delta_{bc} + 4(ib|jc) + 4(ib|f_{xc}(\mathbf{r}, \mathbf{r}')|jc) \quad (16.16b)$$

The  $\varepsilon_k$  stands for the orbital energies, indices  $i$  and  $j$  refer to occupied orbitals,  $b$  and  $c$  to unoccupied ones, and the integrals between curly brackets are the two-electron interaction integrals. In the KS expression, the exchange-correlation term is defined in terms of the operator  $f_{xc}(\mathbf{r}, \mathbf{r}') = \delta^2 E_{xc} / \delta\rho(\mathbf{r})\delta\rho(\mathbf{r}')$ , where  $E_{xc}$  is the exchange-correlation energy. Note the similarity of both expressions: the first, orbital energy-dependent term, is identical and is the only term in HF if the influence of the external potential perturbation on the first-order correction to the Fock operator (through the perturbed orbitals) is neglected; in KS, it is the only remaining term if the influence of the potential perturbation on the Hartree or exchange-correlation potentials is dropped. When the influence of this perturbation is maintained in the Coulomb terms, HF and KS again display the same second term, whereas when exchange (HF) or exchange-correlation effects (KS) are included, the third, now different terms in Eqs. (16.16a) and (16.16b) appear. It is easily seen that in the simplest approximation, the Independent Particle Model,  $\chi(\mathbf{r}, \mathbf{r}')$ , reduces to (dropping the superscripts to simplify the notation)

$$\chi(\mathbf{r}, \mathbf{r}') = -4 \sum_i \sum_a (\varepsilon_a - \varepsilon_i)^{-1} \varphi_i(\mathbf{r}) \varphi_a(\mathbf{r}') \varphi_i(\mathbf{r}') \quad (16.17)$$

which boils down to  $\chi_{KS}(\mathbf{r}, \mathbf{r}') (= \delta\rho(\mathbf{r})/\delta v_{KS}(\mathbf{r}'))$  the functional derivative of  $\rho$  w.r.t. the KS potential  $v_{KS}$ , as discussed by Ayers [19, 20]. Finally, note that the ‘‘Master’’ Eq. (16.11) reduces to (16.17) if one starts from a single Slater-determinant wave function and exploits (i) Slater’s rules for the 1-electron matrix elements and (ii) a Koopman’s type approach for the denominator.

The independent particle approximation is straightforward to evaluate after a standard HF or KS calculation, as present in nearly all quantum chemistry packages. The so-called random phase approximation to the LRF [18], including the Coulombic correction and the complete expressions involve the manipulation of two-electron interaction integrals, the evaluation of the exchange-correlation term in the KS approach starting from a well-chosen exchange-correlation potential, and the inversion of the  $\mathbf{M}$  matrix. In Section 16.3.3, we will have, for a particular example, a glance at the relative performance of the three levels in a KS context.

As an afterthought and preparing one of the applications in Section 16.3, the resemblance of the IPM expression (16.17) and Coulson's atom-atom polarizability  $\pi_{r,s}$  (16.18) [21] should be mentioned.  $\pi_{r,s}$  given by

$$\pi_{r,s} = (\partial q_r / \partial \alpha_s) \quad (16.18)$$

can be seen as an atom-condensed version of the LRF Eq. (16.2) with  $q_r$ , the  $\pi$  electron density on atom  $r$  in Hückel's  $\pi$  electron theory and  $\alpha_s$ , the Coulomb parameter/integral for atom  $s$  [22]. Its variation can be seen as a special, atom-condensed, case of the variation of the external potential  $\delta v(\mathbf{r})$  in Eq. (16.2). Again, using first-order perturbation theory, the resulting expression for  $\pi_{r,s}$  is given by

$$\pi_{r,s} = -4 \sum_j \sum_k (\epsilon_k - \epsilon_j)^{-1} c_{rj} c_{sj} c_{rk} c_{sk} \quad (16.19)$$

The summations over  $j$  and  $k$  run over all occupied and unoccupied orbitals, respectively, with energies  $\epsilon_j$  and  $\epsilon_k$  and the orbital coefficients  $c_{rj} \dots$  are extracting the term relevant for atom  $r$  from orbital  $j, \dots$ . The analogy with expression (16.17) is striking and will be further commented on in Section 16.3.3.

To end this section, it should be noticed that a descriptor analogous to the LRF has also been addressed in the other ensemble (cf. Chapter 2 in the Foundations), where  $v(\mathbf{r})$  is one of the two variables, namely the grand canonical ensemble  $\Omega = \Omega[\mu, v]$ . Here, the second functional derivative of  $\Omega$  with respect to  $v(\mathbf{r})$  at constant  $\mu$  emerges as an analogue of the LRF [3, 4]. One of the most interesting properties of this kernel, written as  $s(\mathbf{r}, \mathbf{r}')$  and termed the softness kernel [23, 24], is that upon integration, it yields the local softness  $s(\mathbf{r})$ , which in its turn via the expression  $s(\mathbf{r}) = S f(\mathbf{r})$  (Chapter 2), yields the global softness  $S$ . An analogous integration sequence is not recognized in the canonical ensemble for the LRF. We finally mention, without proof (see [23]), that a relationship between the two kernels has been established in the famous Berkowitz-Parr relation

$$s(\mathbf{r}, \mathbf{r}') = -\chi(\mathbf{r}, \mathbf{r}') + \eta^{-1} f(\mathbf{r}) f(\mathbf{r}') = -\chi(\mathbf{r}, \mathbf{r}') + S f(\mathbf{r}) f(\mathbf{r}') \quad (16.20)$$

where  $f(\mathbf{r})$  is the Fukui function and  $\eta$ , the hardness. Recently it was shown that, based on the convexity of  $\Omega(v)$  [24] as opposed to the concavity of  $E(v)$  [24b, 25, 26], the following inequality stands

$$s(\mathbf{r}, \mathbf{r}) \geq s(\mathbf{r})^2 / S \geq 0 \quad (16.21)$$

linking the three softness descriptors in another way and pointing out that the diagonal elements of the softness kernel should be positive or zero as opposed to those of the LRF (see Section 16.3.1).

In the context of the analogy between thermodynamics and DFT mentioned above [17], it can be shown [12, 24a], starting from the concavity property of the Gibbs Free energy  $G(T, p)$  and its analogue  $\Omega = \Omega[\mu, v]$ , that this inequality, involving the three second-order derivatives of  $\Omega$  with respect to  $\mu$  and  $v$ , bears complete analogy with the one related to the isothermal compressibility  $\kappa_T$ , the heat capacity at constant pressure  $C_p$ , and the coefficient of thermal expansion  $\alpha$ , involving the three second-order derivatives of  $G$  with respect to  $p$  and  $T$  [27].

$$\kappa_T/V \geq \alpha^2 T/C_p \quad (16.22)$$

## 16.3 Applications

### 16.3.1 Atoms: Shell Structure

The study of the non-integrated form of  $\chi(\mathbf{r}, \mathbf{r}')$  as such is, as stated above, hampered by the six-dimensional nature of this kernel but is important from a fundamental point of view before passing to atom-integrated forms (*vide infra*). Atoms are a way out to introduce some mathematical properties of the LRF and to connect these with the physical/chemical significance of this kernel. When considering a spherical potential perturbation, the 6D information of the LRF can be compacted, after integrating out any angular dependencies to a 2D contour-plot adopting a “radial distribution” representation  $r^2 \chi(r, r') r'^2$ , where  $r$  and  $r'$  denote the distance to the nucleus, situated at the origin of the points  $\mathbf{r}$  and  $\mathbf{r}'$  at which the LRF is evaluated [28].

In Figure 16.1, we show, as an example, this plot for the first three noble gases He, Ne, and Ar. In all cases (and this also turns to be the case for all atoms up to Ar as reported in Ref. [28]), negative regions are observed along the diagonal, symmetrically surrounded by positive ones, and in the case of Ne and Ar, also secondary negative regions. In the simplest case, He, only two distinct regions appear, which are multiplied when passing from one row of the periodic table to the next one, indicating already a relationship with the shell structure of atoms. To further simplify,

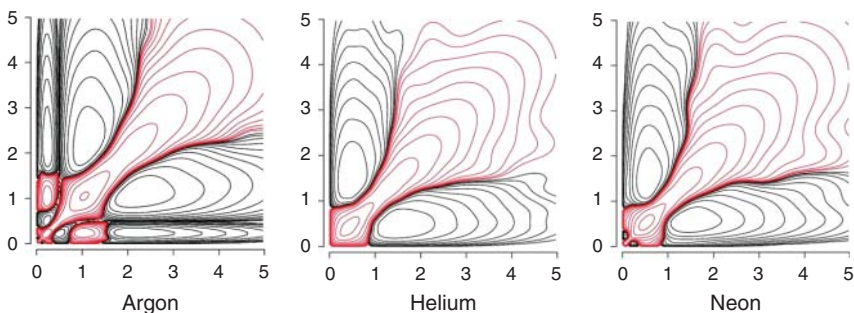


**Figure 16.1** Contour-plots of the radial distribution function  $r^2 \chi(r, r') r'^2$  for the noble gases He, Ne, Ar (PBE with aug-cc-pVTZ). Source: Reproduced from Boisdenghien et al. [28], with permission from the PCCP Owner Society.

one can turn to one-dimensional versions of these plots by keeping  $r$  or  $r'$  fixed. In Figure 16.2, we show the function  $r^2\chi(r, r')$  for  $r' = 0$ , i.e. the origin. One then generates a cross section of the full contour plot along the  $r$ -axis. There it is seen that close to  $r = 0$ ,  $r^2\chi(r, 0)$  is negative. If a positive perturbation is supposed to be active, i.e. less attractive for the electrons, as compared to  $(-Z/r)$ , essentially, the region close to the nucleus becomes less attractive, resulting in a depletion of electrons in the vicinity of the nucleus. This is an emanation of the overall negative value of the diagonal elements  $\chi(\mathbf{r}, \mathbf{r}')$  of the LRF. This behavior is intimately related to the concavity of the  $E = E[N, v]$  functional with respect to  $v$  [24–26].

$$E[N, \lambda v_1 + (1 - \lambda)v_2] \geq \lambda E[N, v_1] + (1 - \lambda) E[N, v_2] \quad \forall \lambda \in [0, 1] \quad (16.23)$$

leading to the conclusion that the LRF is negative semidefinite

$$\int \int \chi(\mathbf{r}, \mathbf{r}') \theta(\mathbf{r}) \theta(\mathbf{r}') d\mathbf{r} d\mathbf{r}' \leq 0 \quad (16.24)$$

where  $\theta(\mathbf{r})$  is any continuous function. If now the second-order variation in the energy  $\delta E^{(2)}$  upon variation of the potential  $\delta v(\mathbf{r})$  is considered, one gets

$$\delta E^{(2)} = 1/2 \int \int \chi(\mathbf{r}, \mathbf{r}') \delta v(\mathbf{r}) \delta v(\mathbf{r}') d\mathbf{r} d\mathbf{r}' \quad (16.25)$$

Adopting a delta function expression for  $\delta v(\mathbf{r}')$ ,  $V_0\delta(\mathbf{r}' - \mathbf{r}')$ , where  $V_0$  is a constant, one gets

$$\delta E^{(2)} = 1/2 V_0^2 \chi(\mathbf{r}'', \mathbf{r}'') \leq 0 \quad (16.26)$$

showing that the diagonal elements of the LRF should be negative or zero. Its physical significance is straightforward: when at a given point  $\mathbf{r}$ , the potential is increased (less negative), this unfavorable situation for the electrons will result in an electron depletion at that point with concomitant negative  $(\delta\rho(\mathbf{r})/\delta v(\mathbf{r}))_N$  value, i.e. a negative or zero diagonal  $\chi$  value  $\chi(\mathbf{r}, \mathbf{r})$ .

Returning now to the plots in Figures 16.1 and 16.2 and continuing with a point charge perturbation of the external potential located at the origin,  $\delta v(\mathbf{r}) = A\delta(\mathbf{r} - \mathbf{0})$ , where we assume  $A$  to be a positive real constant, we obtain

$$\Delta\rho(\mathbf{r}) = \int \chi(\mathbf{r}, \mathbf{r}') \delta v(\mathbf{r}') d\mathbf{r}' = A \int \chi(\mathbf{r}, \mathbf{r}') \delta(\mathbf{r}' - \mathbf{0}) d\mathbf{r}' = A\chi(\mathbf{r}, \mathbf{0}) \quad (16.27)$$

implying (cf. the Figure for  $r^2\chi(r, 0)$ ) a drop in the electron density close to the nucleus ( $r$  small) accompanied at a large distance by a positive region, as it should in view of the conservation of the number of electrons. For the LRF, this demand results in the following property

$$\int \chi(\mathbf{r}, \mathbf{r}') d\mathbf{r}' = 0 \quad (16.28)$$

indeed

$$\int \chi(\mathbf{r}, \mathbf{r}') d\mathbf{r}' = \int (\delta\rho(\mathbf{r})/\delta v(\mathbf{r}'))_N = \delta/\delta v(\mathbf{r}') \int \rho(\mathbf{r}) d\mathbf{r} = \delta N/\delta v(\mathbf{r}') = 0 \quad (16.29)$$



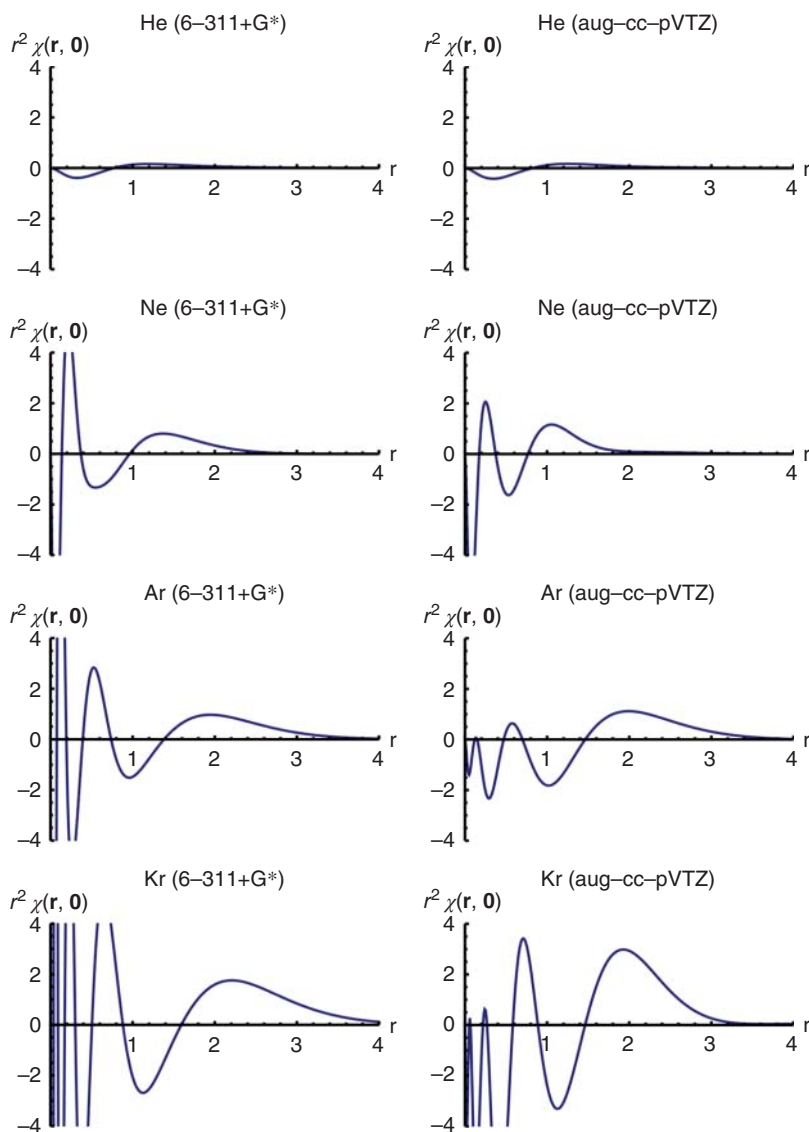


**Figure 16.2** One-dimensional plots for  $r^2 \chi(r, 0)$  for the noble gases He, Ne, Ar, Kr (PBE with aug-cc-pVTZ). Source: Reprinted with permission of Boisdenghien et al. [28], American Chemical Society.

in line with the alternating positive and negative regions for constant  $r$  or  $r'$  in Figure 16.1. In Figure 16.2, we finally compare the plots for the radial distribution functions  $r^2 \chi(r, 0)$  between the different noble gases: it is seen that upon multiplication of regions in the contour-plots of Figure 16.1 when going down in the periodic table, an increasing number of alternating positive and negative regions show up in the radial distribution function when passing from He, via Ne, and Ar to Kr.

The increasing number of nodes with a concomitant shift of the highly oscillatory regions to small  $r$  values is reminiscent of the well-known increasing number of peaks in the radial distribution function of the density offered as a visualization of the “shell structure of atoms” [29]. In other words, disentangling the complex nature of the six-dimensional LRF reveals a fundamental property of atoms: their shell structure.

### 16.3.2 Molecules: Inductive and Mesomeric Effects, Electron Delocalization, and Aromaticity

Concepts such as inductive and mesomeric effects, electron delocalization aromaticity, and anti-aromaticity are for decades at the heart of the interpretation of the structure, stability, charge distribution, and reactivity of both organic and inorganic molecules [30]. It is tempting to see if this basic chemistry, in which often the influence of a substituent on given position on another position of a chain or ring is at stake, can be retrieved from the LRF in which precisely these two ingredients, perturbation at one point and response (of the density) at another point [31], are involved. In Figure 16.3, we depict the condensed LRF for the different atoms of a few simple organic molecules: linear chains, saturated and unsaturated, with at position 1 a substituent, *in casu* an alcohol or amino group. The reader will notice that here we pass to another representation of the LRF in view of the complexity of the systems, an atom-integrated LRF, where an atom-condensed LRF matrix is introduced with elements

$$\chi_{AB} = \int_{V_A} \int_{V_B} \chi(\mathbf{r}, \mathbf{r}') d\mathbf{r} d\mathbf{r}' \quad (16.30)$$

The LRF is integrated into atomic basins in regions  $V_A$  and  $V_B$  associated to atoms A and B.

The figure shows a monotonous decrease along the saturated chain for the response of a given atom to the perturbation of the substituent at position 1, with a value vanishing after two or three bonds. This is highly reminiscent of the inductive effect, which is known to decay monotonously along a chain and dies off after two or three bonds. In the unsaturated case, different behavior is noticed with alternating maxima (at  $C_2$ ,  $C_4$ , and  $C_6$ ) and minima (at  $C_1$ ,  $C_3$ , and  $C_5$ ), corresponding to mesomeric active and passive atoms, respectively, changing their charge when one passes from one canonical form to another. The mesomeric effect (Figure 16.4) is thereby retrieved, suggesting that the LRF could be used as a measure of delocalization in, e.g. cyclic systems, and so it is natural, as a next step, to scrutinize the information content of the LRF on aromaticity [32, 33].

In Figure 16.5, we depict the LRF matrix-elements  $\chi_{C_1, C_i}$  ( $i = 2, 3, \dots, 6$ ) for cyclohexane, benzene, cyclohexanol, and phenol. Again, in the saturated systems, a monotonous decrease along the ring is observed until reaching the 4-position, typical for the inductive effect, whereas for the aromatic systems, a “zigzag” curve is obtained with maxima at the mesomerically active ortho and para positions. This result is reminiscent of the 1,4 para-delocalization index (PDI) proposed by Sola and coworkers [34], as a measure for aromaticity, suggesting that the LRF, in its

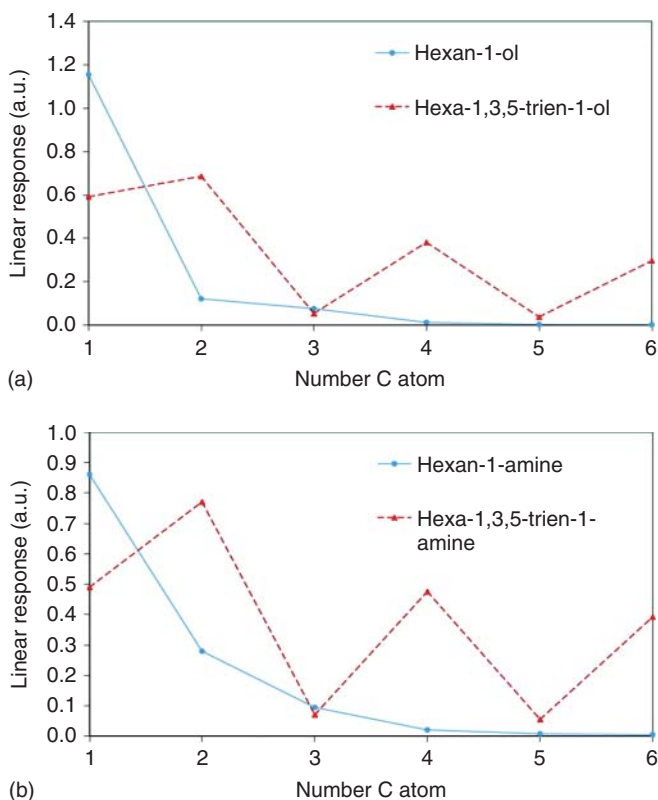


**Figure 16.3** The Linear Response matrix elements (a)  $\chi_{OX}$  and (b)  $\chi_{NX}$  with  $X = C_1, \dots, C_6$  between the oxygen (a) and nitrogen (b) atoms and the Carbon atoms of a saturated and unsaturated linear chain with OH and  $NH_2$  group at position  $C_1$ . All values are in a.u. Source: Reprinted with permission from Sablon et al. [31], American Chemical Society.

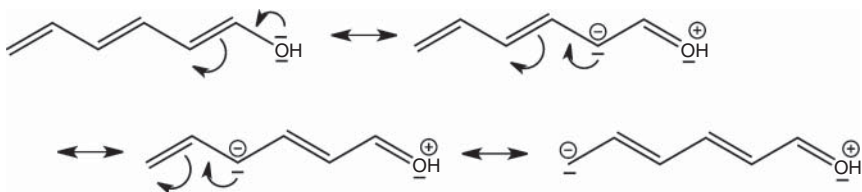


**Figure 16.4** The mesomeric effect at work in hexa-1,3,5-trien-1-ol. Source: Reprinted with permission from Sablon et al. [31], American Chemical Society.

turn, may be used as a measure of aromaticity. Figure 16.6 shows the behavior of the LRF in a number of aromatic, nonequivalent six-rings in a large series of polycyclic aromatic systems, where all rings are seen to display an outspoken zigzag pattern, the most prominent behavior being benzene itself. The LRF and PDI were shown to be linearly correlated, and within certain approximations, an analytical expression

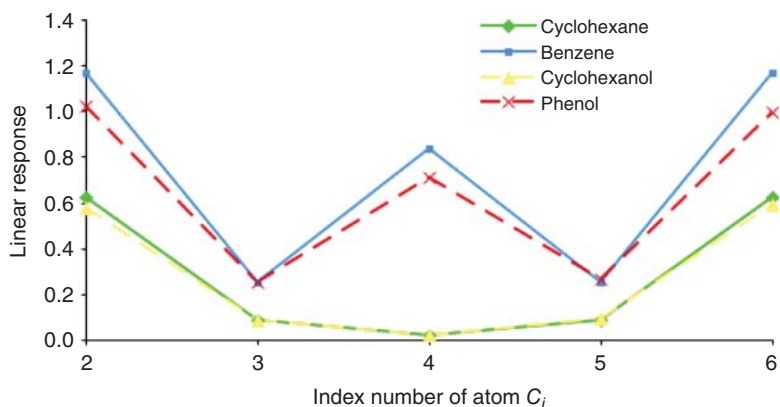


**Figure 16.5** The atom-condensed LRF matrix-elements  $\chi_{C_1, C_i}$  ( $i = 2, 3, \dots, 6$ ) for cyclohexane, benzene, cyclohexanol, and phenol (all values in a.u.). Source: Reprinted with permission from Sablon et al. [32], Elsevier.

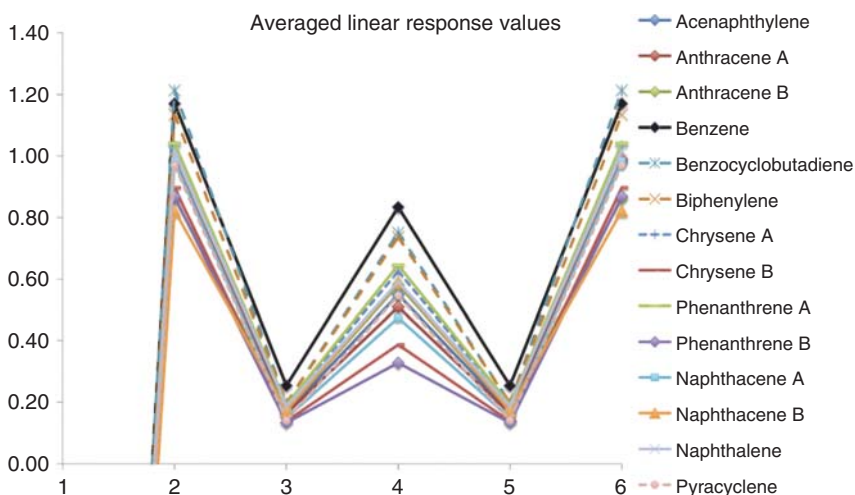


**Figure 16.6** Atom-condensed LRF matrix elements  $\chi_{C_1, C_i}$  ( $i = 2, 3, \dots, 6$ ) for non-equivalent six-membered rings in carbocyclic systems. Source: Reprinted from Geerlings et al. [11], with permission from the Royal Society of Chemistry.

justifying this behavior can be presented. Remarkably, for anti-aromatic molecules, an inverted zigzag pattern is revealed.

The results for benzene, originally obtained in the IPA version of the coupled perturbed KS ansatz, were later on compared with the two superior levels described in Section 16.2 to test the reliability of the IPA (C. Van Alsenoy et al., unpublished). In Table 16.1, the comparison is given for the matrix elements  $\chi_{C_1, C_i}$  ( $i = 2, 3, \dots, 6$ ) for benzene at the three levels.

Although the IPA values significantly differ from the two other levels, which among each other are quite close, the overall pattern at the three levels is identical;

**Table 16.1** Comparison of the condensed LRF matrix elements  $\chi_{C1,Ci}$  ( $i = 2, 3, \dots, 6$ ) for benzene obtained via coupled perturbed KS and the three levels of approximation described in Section 16.2.

Method/element	1,1	1,2	1,3	1,4	1,5	1,6
IPA	-2.663	0.535	0.281	0.503	0.281	0.535
RPA	-0.971	0.203	0.088	0.124	0.088	0.203
Full expression	-1.010	0.218	0.085	0.127	0.085	0.219

Use of the B3-LYP functional with a 6-311++G\*\* basis-set and Iterative Hirschfeld condensation; all values in a.u.) (C. Van Alsenoy et al., unpublished).

the zigzag structure prevails at all levels of theory suggesting that, despite its overestimation of the matrix-elements, the IPA may be used in a qualitative approach when looking for trends and comparisons within the same system or between systems.

As an eye-opener and in view of the success of the LRF to retrieve inductive and mesomeric effects, at the heart of the concept of transferability of functional groups, we briefly refer here to the results of a recent in-depth study on the relationship between Kohn's nearsightedness of electronic matter principle (NEM) [35, 36] and the transferability of functional groups [37] (for more details, see [38]). The former is a very deep theorem on the behavior of electronic matter under perturbation with the upshot that electronic matter is nearsighted (i.e. turns out to be under certain conditions "blind" for perturbations beyond a certain distance). The latter is a long-standing chemist's paradigm that the behavior of functional groups is transferable and, to a certain extent, independent of its environment (e.g. the chain it is attached to) and vice versa. This concept has been at the basis of an impressive systematic and structural approach to organic chemistry in the previous chemistry, as witnessed by Patai's unsurpassed book series on the "Chemistry of Functional Groups" [39]. The analytical calculations of the softness kernel  $s(\mathbf{r}, \mathbf{r}')$ , in use as Kohn's principle, is formulated at conditions of constant  $\mu$ , for a series of linear chains, confirmed its nearsightedness, providing a physical basis for the transferability concept. The physicist's NEM principle and the chemist's transferability of functional groups paradigm could thereby be reconciled.

### 16.3.3 The Link Between the Linear Response Function and Molecular Conductivity

In view of the fundamental property of the LRF of relating two positions in space, it turned out worthwhile to investigate the link between the LRF and molecular conductivity. Molecular electronics has been a vibrant area of research in recent years, and an ever-growing number of studies [40] have been devoted to the transport properties of, typically, organic molecules containing  $\pi$ -conjugated systems with the ultimate aim to incorporate them in molecular electronic devices [41]. The fundamental quantity in this type of investigations is the transmission probability at the

Fermi level  $T_{AB}(0)$  between two contacts attached to two atoms A and B. Within several approximations, e.g. only considering the  $\pi$  electron system and cutting the resonance effects between the contacts and the molecule after the molecules' first neighbor in the contact (see, e.g. [42, 43] for a detailed analysis), the following simple expression can be written down

$$T_{AB}(0) = 4 \beta^2 \Delta_{AB}^2 / \Delta^2 \quad (16.31)$$

A and B are the atoms at which the contacts are placed,  $\Delta$  is the Hückel determinant for the  $\pi$  system of the isolated molecule, and  $\Delta_{AB}$  is the determinant from which row A and column B are eliminated, and  $\beta$  is a measure of the interaction between the contact atom and its neighbor, the (first atom of) the molecule considered. The link between this expression and the LRF emerges when going back to the forerunner of the LRF, Coulson's atom-atom polarizability, mentioned in Section 16.2. Using complex analysis, circumventing, e.g. the diagonalization of the  $\Delta$  matrix to obtain the system's energy, Coulson and Longuet Higgins showed [21] that the atom-atom polarizability (cf. Eq. (16.19)) could be written as

$$\pi_{A,B} = (\partial q_A / \partial \alpha_B) = \pi^{-1} \int (\Delta_{AB}(iy) / \Delta(iy))^2 dy \quad (16.32)$$

This remarkable result shows that the integrand of  $\pi_{AB}$  is directly related to the transmission probability  $T_{AB}(0)$ : an intimate relation between numerical results for  $\pi_{AB}$  and  $T_{AB}(0)$  may therefore be foreshadowed [44]. In Figure 16.7a, we depict these two quantities for the early members of the linear acenes (benzene, naphthalene, anthracene, and tetracene), where one atom, say, A, is taken as reference atom, at which in the conductivity setup, the first contact is attached. For  $\pi_{AB}$ , the reference atom is indicated by a green circle, with a radius proportional to the self-polarizability  $\pi_{AA}$  of the atom, which (cf. the discussion of the diagonal elements of the LRF in Section 16.3.1) is always negative, as is also easily seen from Eq. (16.19) when putting there  $r = s$ . The black and red circles on the other atoms denote the atom-atom polarizability quantifying the response of the charge on a given atom B,  $q_B$ , when a perturbation in  $v$ , *in casu* the Coulomb integral  $\alpha$ , is exerted on atom A ( $\pi_{AB} > 0$  : black;  $\pi_{AB} < 0$  : red). A similar pictorial representation is followed for  $T_{AB}(0)$ , with an empty green circle at the position of the "first" contact at reference atom A and the black circle at an atom B, whose area is proportional to the magnitude of the transmission when the "second" contact is positioned at that atom (note that no negative values occur here as  $T_{AB}(0)$  lies between 0 and 1). Figure 16.7a clearly displays the analogy in the pattern between  $\pi_{AB}$  and  $T_{AB}(0)$ : a positive atom-atom polarizability between two centers turns out to be a necessary condition for non-zero transmission (a simple selection rule) with overall a larger conductivity associated with larger polarizability.

The results in the case of pentacene in Figure 16.7b strengthen this view: when varying the position of the first contact, a highly similar pattern for the response of a different atom in  $\pi_{AB}$  and the concomitant transmission probability emerges.

The final conclusion is that the "two-point" structure of the LRF (i.e. its kernel character), here used in its atom-condensed forerunner  $\pi_{AB}$ , enables a predictive

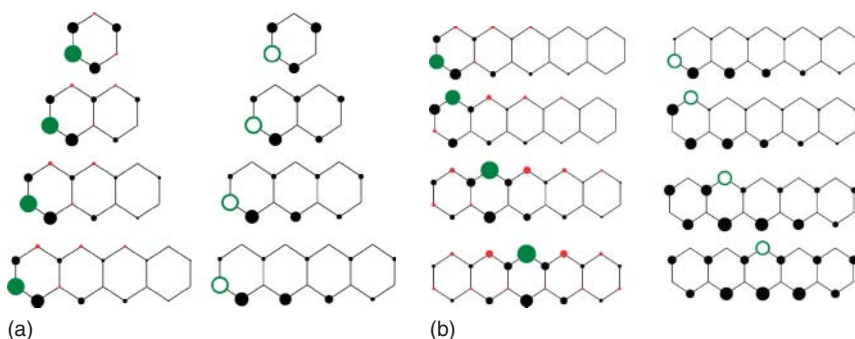


**Figure 16.7** (a) The atom–atom polarizability (left) and the transmission probability at the Fermi level (right) for a single reference atom for benzene, anthracene, and tetracene. (b) The atom–atom polarizability (left) and the transmission probability at the Fermi-level (right) for pentacene with variable reference atom. Source: Reprinted with permission of the Stuyver et al. [44], AIP Publishing.

use in discussing molecular conductivity [44, 45]. At first sight, these two quantities are somewhat distant; upon closer look, they bear important similarity when keeping in mind the analogy between the kernel structure of the LRF and the two-point connecting event in molecular conductivity.

### 16.3.4 Alchemical Derivatives and Their Relationship with the Linear Response Function

Alchemical derivatives were introduced by von Lilienfeld and coworkers [46–50] in an early attempt to efficiently explore chemical compound space [51, 52], the space populated by all imaginable chemicals with natural nuclear charges and realistic internuclear distances for which chemical interactions exist. Navigating through this space is costly, obviously for experimental chemists and theoretical chemists can and should be guiding their experimental colleagues in this endeavor by developing efficient algorithms in prospective work, e.g. by quantum-chemical calculations at a much lower cost. In this context, a very promising ansatz was launched by von Lilienfeld. In his alchemical coupling approach, two iso-electronic molecules are “coupled alchemically” through the interpolation of their external potentials [46–50]. In this approach, a key role is played by the so-called alchemical derivatives, the simplest one being  $(\partial E / \partial Z_A)_{N, Z_B \neq Z_A}$  [46, 53], i.e. the derivative of the molecular energy with respect to a nuclear charge at a constant number of electrons. These derivatives and their higher-order congeners in principle allow obtaining the energy of a “transmuted” molecule, in which a given nuclear charge has been changed, starting from the energy of the “parent” molecule through the use of a Taylor expansion [53]

$$E(Z_A', Z_B, \dots, N) = E(Z_A, Z_B, \dots, N) + (\partial E / \partial Z_A)_{N, Z_B \neq Z_A} \Delta Z_A + \frac{1}{2} (\partial^2 E / \partial Z_A^2)_{N, Z_B \neq Z_A} \Delta Z_A^2 + \dots \text{with } \Delta Z_A = Z_A' - Z_A \quad (16.33)$$

The alchemical derivatives, termed the alchemical potential  $\mu^{\text{al}}_{\text{A}} ((\partial E/\partial Z_{\text{A}})_{N, Z_{\text{B}} \neq Z_{\text{A}}})$  and alchemical hardness  $\eta^{\text{al}}_{\text{A}} ((\partial^2 E/\partial Z_{\text{A}}^2)_{N, Z_{\text{B}} \neq Z_{\text{A}}})$ , including also mixed terms (derivative with respect to  $Z_{\text{A}}$  and  $Z_{\text{B}}$ ), are a particular type of response functions, bearing an analogy the electronic  $N$  derivatives  $\mu$  and  $\eta$ . In fact, they originate from a particular choice of the derivatives with respect to the external potential  $v(\mathbf{r})$  if the change in  $v$  is concretized in a change in  $Z$  value(s). The direct link with other CDFT descriptors, such as the density and the LRF, becomes apparent starting from the explicit expression for the external potential, (cf. Chapter 2)  $(-\sum Z_{\text{A}}/|\mathbf{r} - \mathbf{R}_{\text{A}}|)$ . The first-order alchemical derivative  $(\partial E/\partial Z_{\text{A}})_{N, Z_{\text{B}} \neq Z_{\text{A}}}$  can then indeed be written as

$$(\partial E/\partial Z_{\text{A}})_{N, Z_{\text{B}} \neq Z_{\text{A}}} = \int (\delta E/\delta v(\mathbf{r})_N) (\partial v(\mathbf{r})/\partial Z_{\text{A}}) d\mathbf{r} = - \int \rho(\mathbf{r}) (|\mathbf{r} - \mathbf{R}_{\text{A}}|)^{-1} d\mathbf{r} \quad (16.34)$$

implying the electron density (in what follows, only the electronic part of the derivatives will be displayed, the nuclear part being simple derivatives of the nuclear–nuclear repulsion energy, vanishing from the third-order derivative on). For atoms, putting the nucleus at the origin, it reduces to

$$(\partial E/\partial Z)_N = - \int \rho(\mathbf{r}) r^{-1} d\mathbf{r} \quad (16.35)$$

which is the electrostatic potential at the nucleus. The second-order derivative  $(\partial^2 E/\partial Z_{\text{A}}^2)_N$  is easily seen to reduce to

$$(\partial^2 E/\partial Z_{\text{A}}^2)_N = \int \int \chi(\mathbf{r}, \mathbf{r}') (|\mathbf{r} - \mathbf{R}_{\text{A}}|)^{-1} (|\mathbf{r}' - \mathbf{R}_{\text{B}}|)^{-1} d\mathbf{r} d\mathbf{r}' \quad (16.36)$$

and in the atomic case to  $\int \int \chi(\mathbf{r}, \mathbf{r}') r^{-1} r'^{-1} d\mathbf{r} d\mathbf{r}'$  where now the LRF makes its entrance [54, 55]. It should be remarked that this expression bears strong analogy with the expression of the elements of the electric polarizability tensor  $\alpha$ , the second-order derivative of the energy with respect to the components of an external field  $\epsilon$  which can be written, say, in the case of  $\alpha_{xy}$  as

$$\alpha_{xy} = \partial^2 E/\partial \epsilon_x \partial \epsilon_y = \int \int \chi(\mathbf{r}, \mathbf{r}') x y' d\mathbf{r} d\mathbf{r}' \quad (16.37)$$

They both show a doubly integrated and distance-weighted LRF, the precise form of the weight function being dictated by the form of the perturbation in the Hamiltonian. This type of analogy shows up in a natural way when extending the number of variables in the Energy functional  $E = E[N, v]$  in CDFT to cope with the ever-increasing variability of reaction conditions [9], such as electric and magnetic fields, mechanical forces, pressure, and temperature [56] (see also Chapter 13). A perturbation in  $Z$  can in this context be considered to be completely analogous to a perturbation via  $\epsilon$ , both being special cases of changing the external potential.

Returning to the alchemical case, the alchemical hardness can be obtained by integrating the LRF weighted by functions of the  $1/r$  and  $1/r'$  type. Recently, mixed derivatives involving both  $Z$  and  $N$  were presented, leading in the simple case of an atom to expressions of the type.

$$(\partial^2 E/\partial Z \partial N) = \int f(\mathbf{r}) r^{-1} d\mathbf{r} \quad (16.38)$$



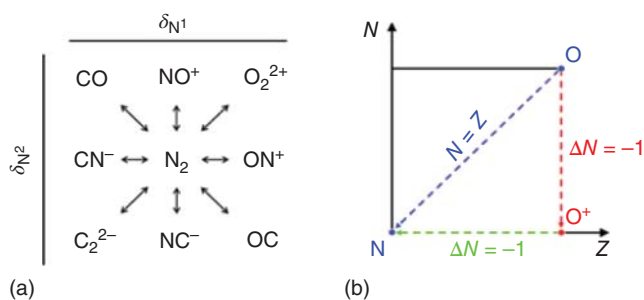


**Figure 16.8** Transmutations of (a) molecules (iso-electronic) and (b) atoms (preserving neutrality).

i.e. a  $1/r$  weighted integral of the Fukui function [57], or the Fukui potential [58, 59].

Various applications of alchemical derivatives have been presented, mainly by von Lilienfeld on the one hand and Balawender and Geerlings on the other hand, and they would need a separate chapter to be covered. The reader is referred to the original papers and reviews by these two (groups of) contributors [12, 50]. We present here, as a selection, two proof-of-concept applications by the latter group and one more direct application in the field of Catalysis by von Lilienfeld.

The two simple proof-of-concept applications are the iso-electronic transmutation of N<sub>2</sub> [54] and a recent study on the transmutation of one neutral atom in another, where the number of electrons is also changed so that neutrality is preserved [57]. In the case of the transmutation of N<sub>2</sub>, Figure 16.8a shows that changing the nuclear charge of the two N atoms by + or -1, at a constant number of electrons, generates 5 transmuted molecules (CO, NO<sup>+</sup>, CN<sup>-</sup>, O<sub>2</sub><sup>2+</sup>, C<sub>2</sub><sup>2-</sup>). At B3LYP level with a cc-pCVTZ level, the mean absolute error (MAE) between the alchemical transmutation energy (obtained with the Taylor expansion (16.33) up to second order, so including alchemical hardness) and the exact energy difference was 0.034 a.u. An exceptionally good performance for the N<sub>2</sub> to CO transmutation of 0.004 a.u., i.e. 2.5 kcal mol<sup>-1</sup>, the only neutral to neutral transformation, was noticed and ascribed to the cancellation of the odd terms in the Taylor expansion. A crucial performance issue was, not unexpected, the inclusion of tight functions, the C acronym in the basis-set for accurately representing the core region. Similar positive results when transmuted two nuclei, one upward in charge, one downward, resulting in a neutral daughter molecule, was obtained in detailed investigations on transformations of CC units to their iso-electronic BN units [54, 55], which have been shown to induce important and interesting changes in electronic, photophysical and chemical properties of the parent molecule [60]. Both planar systems, starting from benzene and leading to azaborines and 3D systems, starting from a fullerene (*in casu* C<sub>60</sub>) and leading to its BN-doped congeners, were considered. In nearly all the cases, the correct stability sequence of the isomers, its number dramatically increasing when passing from 2D to 3D and in case of multi-substitution, was successfully retrieved.

The latter finding is of practical importance in graphene chemistry, where the  $(CC)_n$  to  $(BN)_n$  substitution is a topic that received great interest in recent years [61]. At an even more fundamental level is the investigation of the transmutation of a given neutral atom into its neutral neighbor in the periodic table, where now a simultaneous increase/decrease of  $Z$  and  $N$  by  $+1$  or  $-1$  is involved. In principle, the Taylor expansion now involves also the mixed  $Z, N$  derivatives. Upon inspection, it turns out that the most successful transformation energies can be obtained by first ionizing the parent atom and then alchemically transforming it into its neutral neighbor, rather than following the “diagonal” way ( $Z = N$ ) in Figure 16.8b (blue arrow) or the route via the anion. To obtain the energy of Nitrogen starting from that of oxygen, one then first ionizes oxygen leading to  $O^+$  ( $\Delta N = -1, \Delta Z = 0$ ) (red arrow) and then alchemically transforms, at a constant number of electrons,  $O^+$  into  $N$  ( $\Delta Z = -1; \Delta N = 0$ ) (green arrow). This procedure was applied to the complete series of first- and second-row atoms ( $H \rightarrow Cl$ ) and led at a similar though higher level of theory as mentioned above (CAMB3LYP and aug-cc-pCVQZ basis-set with extension of the perturbation expansion up to third order) to a mean average deviation of  $1.6 \cdot 10^{-3}$  a.u., about  $1 \text{ kcal mol}^{-1}$ , i.e. chemical accuracy. (Ne and Na were left out of consideration due to a basis set deficiency arising when at the beginning or end of a row a sharp difference of basis-set composition arises as compared to the neighbor atom). This difference should be put in perspective with the order of magnitude of transformation energy, e.g. for N to O of 20.47 a.u. [57].

As a direct application of the alchemical approach in a broad chemical context, we take a recent study by von Lilienfeld on “Alchemical Predictions for Computational Catalysis” [62]. The case study presented there addresses the binding energy prediction of oxygen reduction reaction intermediates ( $OOH^*, O^*, OH^*$ ) on alloys of Pt, Pd, and Ni. Binding energy calculations use a fcc (111) surface model consisting of four layers, in which transmutations are considered. In one of the cases studied, the chemical nature of the surface alloy is changed by transmuted atoms of the top layer of a metal (Pt, Pd, or Ni) surface by  $\Delta Z = +/-1$ , i.e. moving to one of its neighbors, compensated by a transmutation on the bottom layer  $\Delta Z = -/+1$  to cope with the demand of a constant number of electrons. A large series of different hypothetical alloys can thereby be formed. The corresponding difference in binding energies between on the one hand those obtained alchemically starting from the reference system and the alchemical coupling with the transmuted system and on the other hand, those generated by an explicit DFT calculation, shows a MAE between 0.06 and 0.24 eV for the nine combinations arising from the three reference slabs (Pt(1,1,1), Pd(1,1,1), and Ni(1,1,1)) in combination with the three intermediates mentioned above. Note that all alchemical predictions of BEs for a given adsorbate and reference slab merely require three quantum-mechanical optimizations for the adsorbate, the substrate, and the molecular adsorbate alone and that the computational overhead for even a large number of alchemical transformations turns out, as expected, negligible (a similar situation emerges in the aforementioned BN-doped fullerene investigations).

Figure 16.9 shows the plots of the obtained differences in binding energy, alchemical vs. explicit DFT for the surface model that was discussed above (surf),

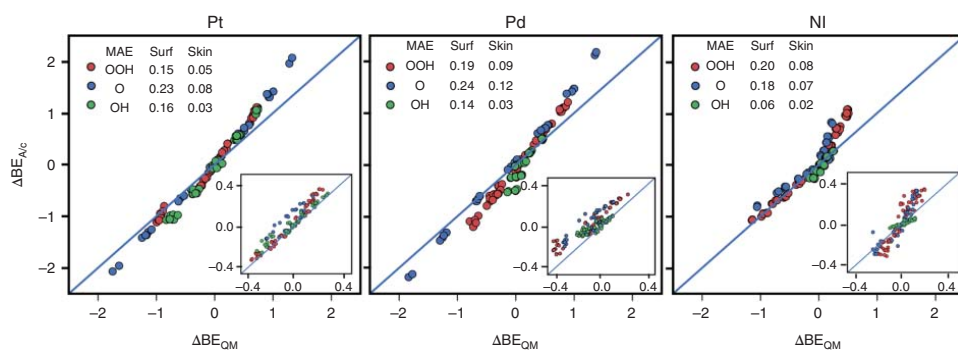


**Figure 16.9** Alchemical (Alc) vs. explicit DFT (QM) calculated differences in binding energies ( $\Delta BE$ ) between the reference and the hypothetical alloy of OOH\*, O\*, and OH\*-based on three different reference slabs (see text). The main figure depicts the data for the surface alloys discussed in the text (Surf); the insert depicts the data for the skin alloys not discussed in the text (Skin). Mean absolute errors (MAE) in eV. Source: Reprinted with permission from Saravanan et al. [62], American Chemical Society.

and (in insert) another model (skin) that was left out for the sake of brevity. The results, as can be judged from the MAE for each combination, are amazing and extremely promising for computationally screening catalysts thousands of times more efficiently than with conventional DFT methods.

## 16.4 Conclusions

Since the launching of CDFT, the LRF has received relatively little attention in its time-independent form for reasons of the complexity of its evaluation and representation and the non-evident extraction of chemical information from it. In the past ten to fifteen years, it gained increasing interest in the CDFT literature as a full-fledged second-order response function. Various approximation methods to the exact and complex expression have been proposed, offering a way to explore, at least qualitatively, at the simplest level, its physical and chemical properties. Thereby, the link between mathematical and physical properties has also been explored. The chemical content has been scrutinized for atoms and molecules, and basic concepts of the chemist's interpretational toolbox, such as inductive and mesomeric effects, electron delocalization, and aromaticity, have been retrieved. The two-point nature of the LRF kernel is at the basis of the link, established via its forerunner, Coulson's atom-atom polarizability, between the LRF and transmission probability in molecular conductivity. The linear and higher-order response functions are seen to be the key ingredients in (evaluating) second- and higher-order alchemical derivatives whose use has been intensified in recent years when looking for efficient algorithms when navigating through chemical compound space in search of molecules with optimal properties and which already yielded spectacular results, e.g. in the computational screening of catalysts.

In summary, the LRF now has the status of a full-fledged second-order derivative in the response function tree with well-established mathematical and physical properties and a clear and diverse chemical content. The awkward second-order functional derivative has gone a long way.

## Acknowledgments

The author wants to thank his colleague Shubin Liu for having invited him to contribute to this timely initiative of editing an almost comprehensive book on CDFT. He is indebted to many (co) authors of the references mentioned in the text for their enthusiastic contribution to exploring the LRF, from its basics to applications. So many thanks to (in no particular order) Frank De Proft, Nick Sablon, Stijn Fias, Zino Boisdenghien, and Thijs Stuyver from the VUB, Weitao Yang (Duke University, USA), Aron Cohen (University of Cambridge, UK), Paul Ayers and Farnaz Heider-Zadeh (Mc Master, Canada), Robert Balawender, Andrzej Holas, Meressa Welearegay, and Michael Lesiuk (Polish Academy of Sciences, Warsaw,

Poland), Christian Van Alsenoy (University of Antwerp, Belgium), Miquel Torrent and Miquel Sola (University of Girona, Spain), and Patrick Fowler (Sheffield, UK).

## References

- 1 Martin, R.M. (2004). *Electronic Structure: Basic Theory and Practical Methods*. Cambridge, New York: Cambridge University Press Appendix.
- 2 Parr, R.G. and Yang, W. (1989). *Density Functional Theory of Atoms and Molecules*. New York: Oxford University Press.
- 3 Chermette, H. (1999). *J. Comput. Chem.* 20: 129–154.
- 4 Geerlings, P., De Proft, F., and Langenaeker, W. (2003). *Chem. Rev.* 103: 1793–1873.
- 5 Ayers, P.W., Anderson, J., and Bartolotti, L.J. (2005). *Int. J. Quant. Chem.* 101: 520–524.
- 6 Geerlings, P. and De Proft, F. (2008). *PCCP* 10: 3028–3042.
- 7 Gazquez, J.L. (2008). *J. Mex. Chem. Soc.* 52: 8–10.
- 8 Liu, S.B. (2009). *Acta Phys. Chem. Sin.* 25: 590–600.
- 9 Geerlings, P., Chamorro, E., Chattaraj, P.K. et al. (2020). *Theor. Chim. Acta* 139: i36.
- 10 Senet, P. (1997). *J. Chem. Phys.* 107: 2516–2524.
- 11 Geerlings, P., Fias, S., Boisdenghien, Z., and De Proft, F. (2014). *Chem. Soc. Rev.* 43: 4989–5008.
- 12 Geerlings, P., Fias, S., Stuyver, T. et al. (2019). *Density Functional Theory* (ed. D. Glossman-Mitnik). London: IntechOpen Chapter 1.
- 13 Ullrich, C.A. (2019). *Time Dependent Density Functional Theory: Concepts and Applications*. Oxford, UK: Oxford University Press.
- 14 Runge, E. and Gross, E.K.U. (1984). *Phys. Rev. Lett.* 52: 997–1000.
- 15 Grabo, T., Pietersilka, M., and Gross, E.K.U. (2000). *J. Mol. Struct. (THEOCHEM)* 501: 353–367.
- 16 (a) Casida, M.E. (1995). *Recent Advances in Density Functional Methods*, 155–192. Singapore: World Scientific. (b) Casida, M. (2009). *J. Mol. Struct. (THEOCHEM)* 914: 3.
- 17 (a) Nalewajski, R.F. and Capitani, J.F. (1982). *J. Chem. Phys.* 77: 2514–2526. (b) Nalewajski, R.F. and Parr, R.G. (1982). *J. Chem. Phys.* 77: 399–407.
- 18 Yang, W., Cohen, A.J., De Proft, F., and Geerlings, P. (2012). *J. Chem. Phys.* 136: 144110.
- 19 Ayers, P.W. (2001). *Theor. Chem. Acc.* 106: 271–279.
- 20 Ayers, P.W. (2007). *Faraday Discuss.* 135: 161.
- 21 Coulson, C.A. and Longuet Higgins, H.C. (1947). *Proc. Roy. Soc. London Series A* 191: 39–60.
- 22 For an authoritative review see Streitwieser, E. (1961). *Molecular Orbital Theory for Organic Chemists*. New York: Wiley.
- 23 Berkowitz, M. and Parr, R.G. (1988). *J. Chem. Phys.* 88: 2554–2557.

- 24 (a) Geerlings, P., De Proft, F., and Fias, S. (2018). *Acta Phys-Chim. Sin.* 34: 699–707; (b) Geerlings, P., Boisdenghien, Z., DeProft, F., and Fias, S. (2016). *Theor. Chem. Acc.* 135: 213.
- 25 Lieb, E.H. (1983). *Int. J. Quantum Chem.* 24: 243–277.
- 26 Kvaal, S., Ekstrom, U., Teale, A.M., and Helgaker, T. (2014). *J. Chem. Phys.* 140: 18A518.
- 27 Prigogine, I. and Defay, R. (1954). *Chemical Thermodynamics*. London, UK: Longman.
- 28 (a) Boisdenghien, Z., VanAlsenoy, C., DeProft, F., and Geerlings, P. (2013). *J. Chem. Theor. Comp.* 9: 1007–1015. (b) Boisdenghien, Z., Fias, S., De Proft, F., and Geerlings, P. (2014). *Phys. Chem. Chem. Phys.* 16: 14614–14624. (c) Fias, S., Boisdenghien, Z., De Proft, F., and Geerlings, P. (2014). *J. Chem. Phys.* 141: 184107.
- 29 Pilar, F.L. (1968). *Elementary Quantum Chemistry*, 192–193. New York: Graw Hill.
- 30 (a) Smith, M.B. and March, J. (2001). *March's Advanced Organic Chemistry*, 5e. New York: Wiley-Interscience. (b) Huheey, J.E., Keiter, E.A., and Keiter, R.L. (1993). *Inorganic Chemistry*, 4e. New York: HarperCollins.
- 31 Sablon, N., De Proft, F., and Geerlings, P. (2010). *J. Phys. Chem. Lett.* 1: 1228–1234.
- 32 Sablon, N., De Proft, F., and Geerlings, P. (2010). *Chem. Phys. Lett.* 498: 192–197.
- 33 Fias, S., Geerlings, P., Ayers, P., and De Proft, F. (2013). *Phys. Chem. Chem. Phys.* 15: 2882–2889.
- 34 Poater, J., Fradera, X., Duran, M., and Sola, M. (2003). *Chem. Eur. J.* 9: 400–406.
- 35 Kohn, W. (1996). *Phys. Rev. Lett.* 76: 3168–3171.
- 36 Prodan, E. and Kohn, W. (2005). *Proc. Natl. Acad. Sci. U. S. A.* 102: 11635–11638.
- 37 Bader, R.F.W. (2008). *J. Phys. Chem. A* 112: 13717–13728.
- 38 Fias, S., Heidar-Zadeh, F., Geerlings, P., and Ayers, P.W. (2017). *Proc. Natl. Acad. Sci. U. S. A.* 114: 11633–11638.
- 39 Patai, S. *PATAI's Chemistry of Functional Groups*. Wiley <https://doi.org/10.1002/SERIES1078>.
- 40 Aviram, A. and Ratner, M.A. (1974). *Chem. Phys. Lett.* 29: 277–283.
- 41 Sun, L., Fernandez, Y.A.D., Gschneidner, T.A. et al. (2014). *Chem. Soc. Rev.* 43: 7378–7744.
- 42 Ernzerhof, M.A. (2007). *J. Chem. Phys.* 127: 204709.
- 43 Pickup, B.T. and Fowler, P.W. (2008). *Chem. Phys. Lett.* 459: 198–202.
- 44 Stuyver, T., Fias, S., De Proft, F. et al. (2015). *J. Chem. Phys.* 142: 094103.
- 45 Stuyver, T., Fias, S., De Proft, F., and Geerlings, P. (2015). *J. Phys. Chem. C* 119: 26390–26400.
- 46 von Lilienfeld, O.A., Lins, R.D., and Rothlisberger, U. (2005). *Phys. Rev. Lett.* 95: 153002.
- 47 von Lilienfeld, O.A. and Tuckerman, M.E. (2006). *J. Chem. Phys.* 125: 154104.
- 48 von Lilienfeld, O.A. and Tuckerman, M.E. (2007). *J. Chem. Theory Comp.* 3: 1083–1090.
- 49 von Lilienfeld, O.A. (2009). *J. Chem. Phys.* 131: 164102.

- 50 von Lilienfeld, O.A. (2013). *Int. J. Quant. Chem.* 113: 1676–1689.
- 51 Kirkpatrick, P. and Ellis, C. (2004). *Nature* 432: 823.
- 52 Dobson, C.M. (2004). *Nature* 432: 824–828.
- 53 Lesiuk, M., Balawender, R., and Zachara, J. (2012). *J. Chem. Phys.* 136: 034104.
- 54 Balawender, R., Welearegay, M.A., Lesiuk, M.A. et al. (2013). *J. Chem. Theory Comp.* 9: 5327–5340.
- 55 Balawender, R., Lesiuk, M., De Proft, F., and Geerlings, P. (2018). *J. Chem. Theory Comp.* 14: 1154–1168.
- 56 Clarys, T., Stuyver, T., De Proft, F., and Geerlings, P. (2021). *Phys. Chem. Chem. Phys.* 23: 990–1005.
- 57 Balawender, R., Lesiuk, M., De Proft, F. et al. (2019). *Phys. Chem. Chem. Phys.* 21: 23865–23879.
- 58 Cardenas, C., Tiznado, W., Ayers, P.W., and Fuentealba, P. (2011). *J. Phys. Chem. A* 115: 2325–2331.
- 59 Cardenas, C. (2011). *Chem. Phys. Lett.* 513: 127–129.
- 60 Campbell, P.G., Marwitz, A.J.V., and Liu, S.Y. (2012). *Angew. Chem. Intl. Ed.* 51: 6074–6092.
- 61 Kan, M., Liu, Y., and Sun, Q. (2016). *Wiley Interdiscip. Rev. Comput. Mol. Sci.* 6: 65–82.
- 62 Saravanan, K., Kitchin, J.R., von Lilienfeld, O.A., and Keith, J.A. (2017). *J. Phys. Chem. Lett.* 8: 5002–5007.

## 17

## Valence-State Concepts and Implications for CDFT

László von Szentpály<sup>1</sup> and Romola A. Bernard<sup>2</sup><sup>1</sup>Universität Stuttgart, Institut für Theoretische Chemie, Pfaffenwaldring 55, Stuttgart D-70569, Germany<sup>2</sup>University of North Georgia, Gainesville Campus, Department of Middle Grades, Secondary, and Science Education, 3820 Mundy Mill Road, Oakwood, GA 30566, USA

## 17.1 Introduction

The evolution of the active research on valence states (VS) starts well before that of conceptual DFT (CDFT). While the development of CDFT is dealt with in the chapter “Historic Overview,” we give a short introduction to two distinct VS concepts and emphasize their importance for CDFT. The picture of atoms interacting in a molecule while retaining some of their identity as atoms-in-molecules (AiMs) is a common denominator of CDFT and VS concepts. AiMs and groups-in-molecules show characteristics, which are retained in different molecular environments. Important properties of molecules are determined by valencies, hybridization, and electronegativities of their constituent AiMs. The AiM is as old as atomistic chemistry, but it is cumbersome to develop rigorous quantum chemical bases for it. Different formulations of AiMs are given by Mulliken [1, 2], Moffitt [3], Ruedenberg [4], Parr and co-workers [5, 6], and Weinhold and Landis [7], to name a few of importance for this chapter. The need to assign several valence states to atoms arose from the concept of different valencies, especially for carbon. Valency, valence states, and electronegativity are not directly measurable but are derived theoretically from the results of measurements. Interpretations are needed to characterize them and assign quantitative values to them. Following the attribution of valence states to a hybridized carbon atom by Van Vleck [8], Mulliken closely linked his absolute scale of electroaffinity, or electronegativity (EN), to promote VS energies [2]. Mulliken pointed out in his abstract of [2] that “the absolute electronegativity scale is equal to the average of ionization potential and electron affinity. These quantities must, however, in general, be calculated not an the ordinary way but for suitable ‘valence states’ of the positive and negative ion. Also, the electroaffinity of an atom has different values for different values of its valence” (p. 782). Mulliken’s valence-state ionization energy,  $I_{VS}(X) = E_{VS}(X^+) - E_{VS}(X)$ , and electron affinity,  $A_{VS}(X) = E_{VS}(X) - E_{VS}(X^-)$ , are calculated from spectroscopic data, including the directly measurable ground-state (GS) ionization energy,  $I_0(X) = E_{GS}(X^+) - E_{GS}(X)$ ,

*Conceptual Density Functional Theory: Towards a New Chemical Reactivity Theory*, First Edition.

Edited by Shubin Liu.

© 2022 WILEY-VCH GmbH. Published 2022 by WILEY-VCH GmbH.



and ground-state electron affinity,  $A_0(X) = E_{\text{GS}}(X) - E_{\text{GS}}(X^-)$ . Mulliken emphasized that “for meaningful results, valence-state quantities, first used by Van Vleck, are necessary” [1] (p. 14). Parr et al. [5] agreed that for DFT “the limitation to ground states is unfortunate, and efforts to remove this limitation should be intensified” (p. 3807). Our contributions to remove limitations of CDFT in combination of improving the VS concepts started more than 30 years ago [9, 10]. They are not limited to electronegativity, chemical potential, hardness, and electrophilicity but include the development of universal potential energy curves in connection to valence states. For the bond dissociation energy,  $D$ , we quote Mulliken: “While the empirical  $D$  is good practical measure of bond energy, in general, a theoretically more significant  $D$ , the *intrinsic*  $D$ , can be obtained, if the dissociation energy is measured from an asymptote, in which the atoms are in suitable valence states” [11] (p. 233). The concept of intrinsic  $D$  has been also very helpful in finding a universal potential energy curve for covalent and ionic bonds [9, 12]. In this chapter, however, we focus on the discussion of electronegativity because of its central role in CDFT.

## 17.2 Ground-State vs. Valence-State Energies

The differences between GS and VS energies in atoms, ions, and molecules are important in discussing bonding because the reference electron configuration of the atom-in-the-molecule is not the same as that of the free atom in its ground state. The AiMs reference energy differs from the GS energy by positive promotion energy,  $P^0 > 0$ , [2–14]. First, for hybridized AiM, a hybridization energy,  $E_{\text{hybr}} > 0$ , is present [2, 3, 8–14]. Second, the spin–orbit splitting in the free atom is largely quenched in AiMs due to the lower symmetry of the molecule [2, 3, 13]. Third, a molecule is composed of various ionic or neutral valence structures. These structures must fulfill the strict Wigner–Witmer correlation rules [15, 16], which establish symmetry constraints for atoms and molecules with respect to bond forming and breaking. Other state combinations are excluded by the symmetry constraints. The bond energy,  $D(X - Y)$ , of a singly bonded diatomic molecule is partitioned with contributions from ionic and neutral structures of weights  $c_j^2$  ( $j = 1, 2, 3$ ), as shown by (17.1), where  $\sum c_j^2 = 1$  [2].

$$D(X - Y) = c_1^2 D(X^+ : Y^-) + c_2^2 D(X^- : Y^+) + c_3^2 D(X : Y) \quad (17.1)$$

The total energy may be minimized at different levels of theory, but all bonding models and structural principles must be made consistent with the Wigner–Witmer rules. For example, the structure combining the ground-state ions,  $\text{Cl}^+$  and  $\text{F}^-$ , does not contribute to the  $\text{Cl}-\text{F}$  bond. This is because the  $\text{Cl}^+$  triplet cation,  $^3P_2$ , and the  $\text{F}^-$  singlet anion,  $^1S_0$ , do not combine to the  $\text{ClF}$  molecule in its singlet GS,  $^1\Sigma^+$ . Instead of the  $^3P_2$  state, the Wigner–Witmer rules require either the  $^1D_2$ , the  $^1S_0$ , or their averaged valence state, symbolized as,  $\text{Cl}_{\text{VS}}^+$ , to form the  $\text{Cl}^+\text{F}^-$  valence structure [2, 13–16]. The VS promotion energies,  $P^0$ ,  $P^+$ , and  $P^-$  needed to excite an atom or its positive or negative ion, respectively,

from the GS to specific VSs were originally derived from atomic spectroscopic term values according to the Slater–Condon theory of atomic structure [17]. The energy of an atom in its Van Vleck–Mulliken VS [2, 3, 8], is the averaged energy of the individual spectroscopic states belonging to a valence configuration. Mulliken’s electronegativity scale,  $\chi_{\text{VS}}$ , was *a priori* conceived to fulfill all symmetry requirements for characterizing bonds [13–16], by interplaying covalent and ionic valence-structures [1, 2, 8, 11, 13]. Extended discussions and tables of promotion energies in connection with electronegativity are given by Mulliken [2], Pritchard and Skinner [13], Hinze and Jaffé [18], and Bratsch [19]. The divalent carbon atom may serve as an example. The divalent configurational average of carbon is  $s^2p^1p^1$ , with integer occupation numbers,  $n = \{0, 1, 2\}$  in superscript. The relevant spectroscopic states are  $^3P_0$ ,  $^3P_2$ , and  $^1D_2$ . Those of the monovalent cation  $C^+$  in configuration  $s^2p^1$  are  $^2P_{1/2}$  and  $^2P_{3/2}$ . The excited  $^2D_J$  and  $^2P_J$  states contribute to the  $s^2p^2p^1$  valence configuration of the monovalent anion  $C^-$  in its VS. Thus, the valence-state electron affinity of the divalent C in  $\pi$ -bonded  $C = C$  is  $A_{\text{VS}} = 0.40$  eV [20], while the GS value of the free atom is  $A_0 = 1.263$  eV [18].

The number of half-filled orbitals of the AiM, that is, its valency with respect to covalent bonding,  $V$ , is important for Mulliken’s atomic electronegativity [2, 12–14, 18–20], and also for its generalization, the valence-pair affinity,  $\alpha_{\text{VP}}$ , [21–26], which will be discussed in Sections 17.3–17.5 below. In valence states, the valency of the ions  $X_{\text{VS}}^+$  and  $X_{\text{VS}}^-$ , is always reduced by 1, as given by (17.2).

$$V(X_{\text{VS}}^+) = V(X_{\text{VS}}^-) = V(X_{\text{VS}}) - 1 \quad (17.2)$$

This condition is independent of the different definitions of the VS energy. For the half-filled atomic orbital,  $i^1$ , of the AiM,  $X$ , the VS energies of the cation, neutral, and anion species are promoted above their GS by respective promotion energies,  $P(X^+, i^0)$ ,  $P(X, i^1)$ , and  $P(X^-, i^2)$ . Equation (17.3) defines the VS ionization energy for AiM,  $X$ , while (17.4) does the same for the VS electron affinity [2, 12–14, 18–26].

$$I_{\text{VS}}(X, i) = I_0(X) + P(X^+, i^0) - P(X, i^1) \quad (17.3)$$

$$A_{\text{VS}}(X, i) = A_0(X) + P(X, i^1) - P(X^-, i^2) \quad (17.4)$$

The VS ionization energy,  $I_{\text{VS}}(X, i)$ , is the energy needed to detach the electron from the half-filled atomic orbital,  $i$ , while the VS electron affinity,  $A_{\text{VS}}(X, i)$ , is the energy gained by attaching a second electron to the same orbital. For the AiM,  $X$ , Mulliken’s absolute orbital electronegativity, first called “electroaffinity,”  $\chi_{\text{VS}}(X, i)$ , [2, 13, 18–26] is defined by (17.5).

$$\chi_{\text{VS}}(X, i) = \frac{1}{2} [I_{\text{VS}}(X, i) + A_{\text{VS}}(X, i)] = \chi_0(X) + \frac{1}{2}P(X^+, i^0) - \frac{1}{2}P(X^-, i^2) \quad (17.5)$$

Where  $\chi_0(X) = \frac{1}{2} [I_0(X) + A_0(X)]$  is the ground-state electronegativity (GS-EN). The negative of GS-EN,  $-\chi_0(X) = \mu_0$ , is best known in CDFT as the operational chemical potential [5, 6, 27]. Equation (17.5) quantifies that the VS electronegativity

of the AiM,  $\chi_{\text{VS}}(X, i)$ , differs from the GS electronegativity of the free atom,  $\chi_0(X)$ , by the promotion energies of the cation and anion species of the AiM. It is important that  $P(X, i^1)$  does not occur in (17.5). It is canceled by averaging (17.3) and (17.4). However, Mulliken defined  $\chi_{\text{VS}}$  for atoms only. Therefore, the meaning of the  $\chi_{\text{VS}}$  in bonds needs to be specified, in due consideration of the Wigner–Witmer rules. The molecular generalization of  $\chi_{\text{VS}}$ , the valence-pair affinity,  $\alpha_{\text{VP}}$ , [21–26], will be of focus in Sections 17.3–17.5. In the finite difference approximation of CDFT [6, 27], the chemical hardness is expressed as  $\eta_0(X) = I_0(X) - A_0(X)$ , which is a global descriptor in CDFT. The VS orbital hardness,  $\eta_{\text{VS}}(X, i)$ , of the AiM is analogously defined by the difference between (17.3) and (17.4). It differs from the GS global hardness of the free atom:

$$\eta_{\text{VS}}(X, i) = I_0(X) - A_0(X) + \{P(X^+, i^0) - 2P(X, i^1) + P(X^-, i^2)\} \quad (17.6)$$

A closer examination of the neutral promotion energy,  $P(X, i^1)$ , is needed to show the differences between the Mulliken- and Ruedenberg-type VS energies. For the Mulliken VS energy, the promotion,  $P(X, i^1)$ , accounts for averaging the configuration energy, including spin–orbit splitting, plus the hybridization energy,  $E_{\text{hybr}}$ , where appropriate [1, 2, 11, 13, 14, 18–20]. Hinze and Jaffé [18] and Bratsch [19] published lists of promotion energies for Mulliken VS energies, hereafter denoted,  $P_{\text{HJB}}(X, i^1)$ . Thereby “zero-sharing penetration,” namely,  $c_1^2 = c_2^2 = 0$ , in (17.1) is assumed for homonuclear molecules,  $X_2$ . However, typical homonuclear diatomic molecules cannot be correctly described without including their ionic structures of weights,  $c_1^2 = c_2^2 > 0$ , as indicated in (17.1) [2, 4, 9, 10, 12, 21–26, 28, 29]. As highlighted by Ruedenberg [4] and modern Valence Bond (VB) theory [29], the positive Mulliken-type VS promotion energy is further increased by accounting for the ionic valence structures in AiMs. Pauling [28] and Mulliken [2] did not specify the best amount of “ionic terms,” but Ruedenberg [4] discussed the whole spectrum of contributing structures, for the case of the homonuclear diatomic molecule,  $X_2$ , up to the Molecular Orbital (MO) limit, where  $c_1^2 = c_2^2 = \frac{1}{4}$ . Ruedenberg’s [4] bond theory includes the MO and VB levels of theory as special cases and concentrates on the role of electron density,  $\rho(\mathbf{r})$ , and electron pair-density,  $\pi(\mathbf{r}_1, \mathbf{r}_2)$ . An atom is in its Ruedenberg valence state when all other atoms bonded to it are removed to infinity under the constraint that all interference-free  $\rho(\mathbf{r})$  and  $\pi(\mathbf{r}_1, \mathbf{r}_2)$  remain frozen at their molecular values [4, 9, 10, 12, 21–26]. The presence of intra-atomic electron-pair-repulsion in homonuclear bonds increases the atomic promotion energy of the Ruedenberg VS, shown in (17.7).

$$P_{\text{RVS}}(X, i^1) = P_{\text{HJB}}(X, i^1) + (\text{intra-atomic electron pair repulsion}) \quad (17.7)$$

Influenced by Ruedenberg [4], Klopman [30], and Ferreira [31], we [9, 10, 12, 21–26], model the intra-atomic pair-repulsion energy by  $c_1^2 J(X, i)$  per atom and bond, where  $J(X, i) = I_{\text{VS}}(X, i) - A_{\text{VS}}(X, i)$  is the semiempirical expression for the electron-pair repulsion energy of the doubly occupied orbital,  $i$ , of the AiM,  $X$ . Note that  $P(X^+, i^0)$  and  $P(X^-, i^2)$  contain the correct intra-atomic pair-repulsion energy, because of  $c_1^2 = 0$  and  $c_2^2 = 1$ , respectively. The neutral atom,  $X$ , in  $X_2$  is

modeled by setting  $c_1^2 = c_2^2 = \frac{1}{4}$ , as at the Restricted Hartree–Fock MO level of theory [4, 9, 12, 21–26, 30, 31]. Although the ionic structures strongly influence the charge dependence of the VS electronegativity, [10, 12, 21–26, 31] its value for the neutral AiM, (17.5), is unaffected by their admixture. However, the VS orbital hardness, (17.6), is significantly lower than the GS value. By combining (17.6) and (17.7), and modeling  $c_1^2 J(X, i) = \frac{1}{4} [I_{VS}(X, i) - A_{VS}(X, i)]$ , we obtain

$$\eta_{VS}(X, i) = I_0(X) - A_0(X) + \left\{ P(X^+, i^0) - 2P_{HJB}(X, i^1) - \frac{1}{2} [I_{VS}(X, i) - A_{VS}(X, i)] + P(X^-, i^2) \right\} \quad (17.8)$$

which simplifies to (17.9),

$$\eta_{VS}(X, i) = \frac{1}{2} [I_{VS}(X, i) - A_{VS}(X, i)] \quad (17.9)$$

Another essential difference between the GS and VS approaches to EN and hardness is the absence of hybridization in CDFT, as opposed to its pivotal role for VS energies [2, 3, 8–14]. Hybridization was introduced into theoretical chemistry in connection to the concept of localized bonds formed by electron pairs [1–3, 7, 28, 32–36]. Mulliken differentiated between isovalent hybridization, a partial hybridization without an increase of the valency, e.g. Li in LiH (see Table 17.1), and plivalent hybridization, with an increased valency, e.g. C in CH<sub>4</sub>. Discussing his electronegativity scale, Mulliken [33] pointed out that the electronegativity of an AiM should “vary greatly with the type of bonding AO it was using, and in the case of a hybrid AO, should depend strongly on the degree of hybridization” (p. 309). His conclusion was that isovalent hybridization is often very important for molecular stability, dipole moment, quadrupole moment, and intensities of molecular electronic spectra [33]. This option does not seem to fit CDFT, which almost exclusively refers to GS atoms and molecules [6, 27, 37, 38].

Table 17.1 lists GS and VS electronegativity and hardness values for first- and second-row atoms. Note that the rankings of several atomic GS values,  $\chi_0(X)$ , are at variance with chemical experience at the bench [24, 39]. For example, the  $\chi_0$  values in [37] are:  $\chi_0(N) = \chi_0(H) = 7.18$  eV. Some striking consequences of counterintuitive  $\chi_0$  rankings are discussed in [24] and shown in Section 17.3.

When more than one type of orbital is available, the bonding orbital is underlined.

### 17.3 Valence-Pair-Affinity, its Equilibration, and Partial Charges

Partitioning of the molecular charge density,  $\rho(x, y, z)$ , into atom- and/or bond-centered point charges forges a bridge to classical physico-chemical intuition. There is, however, no unique definition of atomic charge. There are several schemes designed to partition the electronic charge of a molecule among its atoms, resulting in various quantum mechanical approaches that generate different, if not contradictory charge distributions [6, 7, 10, 12, 20, 24, 32, 40–44]. The quality of an atomic

**Table 17.1** Hybridizations, electronegativity, and hardness.

Atom	Bond	p character	$\chi_{\text{VS}}/\text{eV}$	$\chi_0 = -\mu_0/\text{eV}$	$\eta_{\text{VS}}/\text{eV}$	$\eta_0/\text{eV}$
H	Single, s	0.00	7.18	7.18	6.42	12.84
Li	Single, s	0.00	3.01	3.01	2.39	4.77
	s <sup>2</sup> p [7]	0.33	2.62		2.15	
B	GS			4.29		8.02
	Single, p [19]	1.00	3.84		4.46	
C	GS			6.26		10.00
	Single, sp <sup>3</sup> [19]	0.75	8.15		5.70	
	Double, sp <sup>2</sup> , $\pi$	0.67	8.91		5.74	
	Triple, sp, $\pi$ , $\pi$	0.50	10.42		5.85	
N	GS [37]			7.18		14.71
	Single, sp <sup>3</sup> [19]	0.75	10.66		6.58	
	Triple, $\sigma$ , $\pi$ , $\pi$	1.00	7.32		6.50	
O	GS			7.54		12.16
	Double, $\sigma$ , $\pi$ [19]	1.00	9.63		7.66	
	Single, sp <sup>4</sup>	0.80	13.14		7.75	
F	GS	1.00		10.41		14.02
	Single, p [19]		12.20		8.78	
	Single, sp <sup>11</sup> [7]	0.917	14.00		8.86	

charge definition is not an inherent property but strongly depends on its use. For example, seeking the best charges to assess the charge transfer (CT) between AiMs does not necessarily lead to the best molecular electrostatic potentials [43]. We describe the charge distribution in a molecule by assigning a non-integer number of electrons,  $N$ , to atoms or groups in the molecule, and fractional occupation numbers,  $n_j$ , to atomic orbitals, AOs, or group orbitals, GOs. The problems arising from the assumption of non-integer, continuous  $N$  and  $n_j$  have been discussed from various angles, and equations have been developed for defining the energies  $E(N)$  and  $E(n_j)$  for continuous variables [3, 4, 6, 9, 10, 12, 18–26, 37, 38, 40].

The exact DFT energy,  $E_{\text{DFT}}(N)$ , consists of straight-line segments connecting the exact GS energies,  $E(N_0 - 1)$ ,  $E(N_0)$ , and  $E(N_0 + 1)$ , with slope discontinuities at integer values of  $N$  [5, 6, 45]. When applied to a single atom with  $N_0$  electrons,  $\partial E_{\text{DFT}}(N)/\partial N = -I$ , for  $N_0 - 1 < N < N_0$ , and  $-A$ , for  $N_0 < N < N_0 + 1$  [45]. However, the assumption of a differentiable function  $E(N)$  is essential for the “modern” definition of electronegativity, [6, 9–12, 14]. Nonlinear, at least quadratic  $E(N)$  and  $E(n_j)$  functions are needed in the chemical context, where the system transfers or exchanges electrons [6, 10–14, 18–27, 37, 39–41, 46]. Two basically different second-order polynomials,  $E(N)$ , have been proposed: the “ground-state-parabola” (GSP) energy,  $E_{\text{GS}}(N)$ , [6, 27, 37, 38, 40], and the valence-pair-energy,  $E_{\text{VP}}(n_j)$  of

the “valence-state-parabola” (VSP) model [9, 10, 12, 38, 40]. In CDFT, the *GSP*, is obtained by fitting a second-order polynomial,  $E_{\text{GS}}(N)$ , to the experimental GS energies of the cationic, neutral, and anionic species, at constant external potential,  $v(\mathbf{r})$  expressed by (17.10).

$$E_{\text{GS}}(N) = E_{\text{GS}}(N_0) - \frac{1}{2} [I_0 + A_0] (N - N_0) + \frac{1}{2} [I_0 - A_0] (N - N_0)^2 \quad (17.10)$$

The first and second partial derivatives of  $E_{\text{GS}}(N)$  at  $N_0$  and constant  $v(\mathbf{r})$  are operationally defined as (i) the chemical potential,

$$\mu(N_0) = \partial E_{\text{GS}}(N)/\partial N = -\chi_0(N_0) = -\frac{1}{2} [I_0 + A_0] \quad (17.11)$$

which is the negative GS-EN and (ii) the global chemical hardness [27],

$$\eta_0(N) = \partial^2 E_{\text{GS}}(N)/\partial N^2 = [I_0 - A_0] \quad (17.12)$$

As pointed out by Ferreira [31] and by Ghosh and Parr [46], the “bond-electronegativity” in the molecule is to be perceived as “pair-electronegativity” because electron pair-density,  $\pi(\mathbf{r}_1, \mathbf{r}_2)$ , is accumulated, and there is a significant probability for finding a pair of “bonding electrons” shared on an AiM. Therefore, the energy of a shared electron pair on the AiM, its “valence-pair-energy,”  $E_{\text{VP}}(X, n_i)$ , and a new scale for pair-sharing, the “valence-pair-affinity” (*VPA*), represented as  $\alpha_{\text{VP}}(X, n_i)$ , had to be introduced [21, 22, 24, 25]. We define the valence-pair-energy,  $E_{\text{VP}}(X, n_i)$ , of the *VSP* model as the differentiable function, which connects the VS energies of  $X^+$  and  $X^-$  by a second-order polynomial, such that the orbital occupancy,  $0 \leq n_i \leq 2$  is continuous [9, 10, 12, 21–26, 38, 40], as shown in (17.13).

$$E_{\text{VP}}(X, n_i) = -n_i I_{\text{VS}}(X, i) + \left(\frac{n_i}{2}\right)^2 [I_{\text{VS}}(X, i) - A_{\text{VS}}(X, i)] \quad (17.13)$$

The *VPA* of an AiM is defined quasi as a potential. It is the negative partial derivative of the  $E_{\text{VP}}(X, n_i)$  with respect to continuous atomic orbital occupation numbers,  $0 \leq n_i \leq 2$ , while the total number of electrons in the molecule is kept constant at  $N_0$ , as given in (17.14).

$$\begin{aligned} \alpha_{\text{VP}}(X, n_i) &= \left[ -\partial E_{\text{VP}}(X, n_i) / \partial n_i \right]_{N_0} \\ &= \frac{1}{2} [I_{\text{VS}}(X, i) + A_{\text{VS}}(X, i)] + \frac{1}{2} (1 - n_i) [I_{\text{VS}}(X, i) - A_{\text{VS}}(X, i)] \end{aligned} \quad (17.14)$$

The *VPA* is the measure for the potential of an atom-in-the-molecule (or functional group) to attract an *electron pair in a sharing competition* with another atom (or group) in the molecule [21, 22, 24, 25]. Note that for  $n_i = 1$  the  $\alpha_{\text{VP}}(X, n_i = 1) = \frac{1}{2} [I_{\text{VS}}(X, i) + A_{\text{VS}}(X, i)]$ , is identical to Mulliken’s EN,  $\chi_{\text{VS}}(X, i)$ , of (17.5). This identity follows from connecting the limiting values  $I_{\text{VS}}(X, i)$  and  $A_{\text{VS}}(X, i)$  by any second-order polynomial, not just by the VS parabola. However, only the  $E_{\text{VP}}(n_i)$  fulfills Janak’s theorem [45] at the boundaries  $X^+$  and  $X^-$ . To give an example comparing *GSP* and *VSP*, we consider a hydrogen atom, shown in Figure 17.1. The energy of hydrogen plotted against the number of electrons shows (i) the valence-pair-energy,  $E_{\text{VP}}(H, n_i)$ , for the *VSP* model; (ii) the  $E_{\text{GS}}(N)$  of the

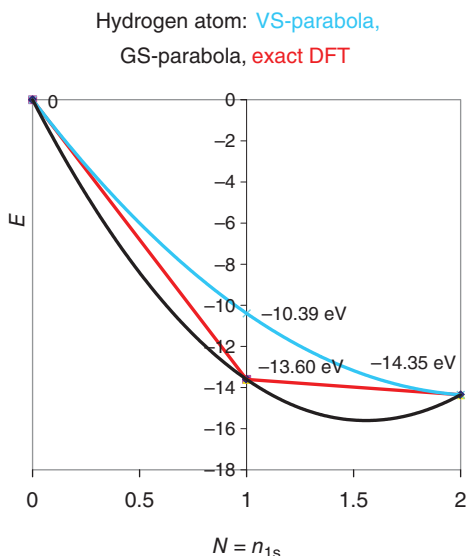


**Figure 17.1** Energy of hydrogen atom,  $E(H, N)$ , vs. electron number,  $N = n_{1s}$ . Blue represents the Valence-State-Parabola (VSP), Eq. (17.13). Red represents the exact DFT energy of the free atom [6, 45, 47]. Black represents the GSP of conceptual DFT, Eq. (17.10). Energies are in units of eV.

GSP model, which in (17.13) replaces  $\left(\frac{n_i}{2}\right)^2$  by  $\frac{1}{2}n_i(n_i - 1)$ , and (iii) the exact DFT result,  $E_{\text{DFT}}(N)$ , for a free H atom. The slope discontinuity [6, 40, 45, 47] of the exact  $E_{\text{DFT}}(N)$  at  $n_{1s} = 1$  is due to the onset of pair repulsion between the already present “spin-up electron” with  $n_{1s\uparrow} = 1$  and the gradually added “spin-down” charge,  $n_{1s\downarrow}$ , [40, 47]. In the VSP model, we have  $n_{1s\uparrow} = n_{1s\downarrow} = n_{1s}/2$ , and the spin population vanishes in the bond of the closed shell  $\text{H}_2$ ,  $\sum n_{1s\uparrow} - \sum n_{1s\downarrow} = 0$ . The intra-atomic pair-repulsion energy due to sharing-penetration is  $(n_{1s}/2)^2 [I_{\text{VS}}(H, 1s) - A_{\text{VS}}(H, 1s)]$ . The valence-pair-energy,  $E_{\text{VP}}(H, n_i)$ , starts as required by Janak’s theorem [45] at  $E_{\text{VP}}(H, n_i = 0) = 0$  with the gradient  $-\alpha_{\text{VP}}(H^+) = -I_{\text{VS}}(H) = -13.60$  eV. The anion,  $\text{H}^-$ , is reached at  $E_{\text{VP}}(H, n_i = 2) = -I(H) - A(H) = -14.35$  eV with the slope  $-\alpha_{\text{VP}}(H^-) = -A_{\text{VS}}(H) = -0.754$  eV. The valence-pair-energy parabola,  $E_{\text{VP}}(n_i)$  fulfills Janak’s theorem at both boundaries  $\text{H}^+$  and  $\text{H}^-$ . Due to the sharing penetration,  $\left(\frac{n_i}{2}\right)^2 [I_{\text{VS}}(X, i) - A_{\text{VS}}(X, i)]$ , the VS energy parabola,  $E_{\text{VP}}(H, n_i)$ , remains above the exact DFT energy. In contrast, the  $E_{\text{GS}}(N)$  of the GS-parabola is more negative than the exact  $E_{\text{DFT}}(N)$  except for integer  $N$ . In the GSP model, an electron self-interaction error is present by an unphysical electron–electron attraction, because  $\frac{1}{2}n_i(n_i - 1)$  is negative for  $n_i < 1$ , as pointed out in [9, 10, 12, 24, 31, 40]. Two maxima of this erroneous electron–electron attraction are reached at  $n_i = 0.5$  and  $1.5$ , where it amounts to  $-J(X, i)/8 = -(I(X) - A(X))/8$ , compared to the exact DFT values for free atoms. The GSP model also violates Janak’s theorem, because its initial gradient amounts to  $-\chi_0(H^+) = -\frac{3}{2}I(H) + \frac{1}{2}A(H) = -20.20$  eV, instead of  $-I(H)$  only, and its gradient at  $\text{H}^-$  is positive with  $-\chi_0(H^-) = -\frac{3}{2}A(H) + \frac{1}{2}I(H) = +5.57$  eV. The  $E_{\text{GS}}(N)$  parabola reaches its minimum already at  $N = 1.56$  electrons, accordingly the anion  $\text{H}^-$  should be unstable (Figure 17.1).

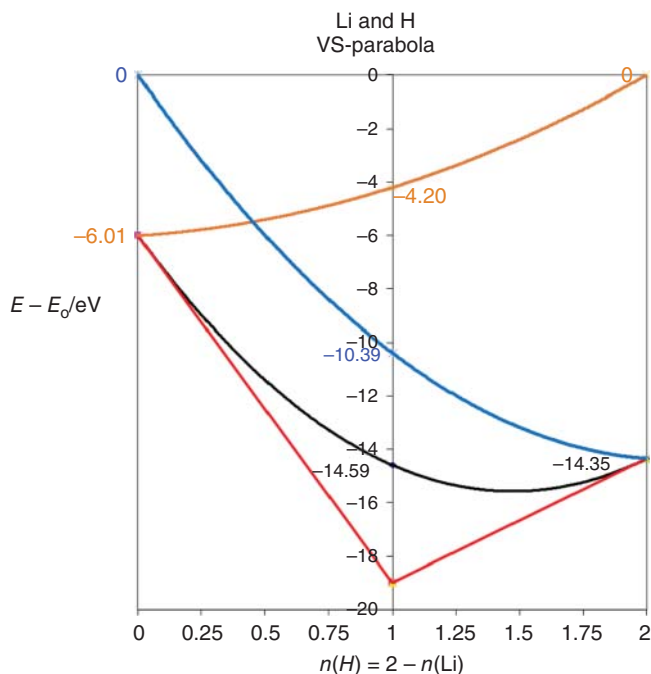


**Figure 17.2** The Valence-Pair-Energy,  $E_{VP}(S, n) - E_{VP}(S, 0)$ , for  $S = \{\text{Li, H and LiH}\}$  vs. the occupation number,  $n(\text{H})$ , according to the VSP model. Blue for H atom, orange for Li, and black for the energy sum,  $E_{VP}(\text{Li}) + E_{VP}(\text{H})$ . The sum of the exact DFT energies for the separated atoms is shown in red for comparison. Energies are in eV.

One of the aims of valence pair equilibration (VPEq) is to find charges,  $q_{VPEq}$ , consistent with those obtained by state-of-the-art population analyses [7, 30, 32, 43], and those derived from spectroscopic observations [42, 44]. An example of the distribution of an electron pair between two atoms of different electronegativity within the VSP model is shown in Figure 17.2.

For the diatomic molecule lithium hydride, LiH, Figure 17.2. provides insight into the interaction energy and charge equilibration between Li and H. For the single bond, Li - H, with partial net charges,  $1 - n(\text{Li}) = q(\text{Li}) = -q(\text{H}) = 1 - n(\text{H})$ , the sum of valence-pair-energies, given by (17.15), is minimized by charge transfer at distances beyond the onset of a covalent-type wave interference.

$$\begin{aligned}
 E_{VP}(\text{Li}, i) + E_{VP}(\text{H}, j) = & E_{VS}(\text{Li}, q = 0) + \chi_{VS}(\text{Li}, i) q(\text{Li}) + \eta_{VS}(\text{Li}, i) q(\text{Li})^2 \\
 & + E_{VS}(\text{H}, q = 0) + \chi_{VS}(\text{H}, j) q(\text{Li}) - \eta_{VS}(\text{H}, j) q(\text{Li})^2
 \end{aligned}
 \tag{17.15}$$

It is essential that the atomic valence-pair-energy parabolas,  $E_{VP}$ , and their sum remain above the energies of the neutral GS atoms. According to the Ruedenberg bond theory, the total molecular energy is further minimized by wave interference in the next bonding step [4, 22, 24, 40]. However, by charge equilibration alone, the separated atoms with fractional charges,  $q_{VPEq} \neq 0$ , are higher in energy than



the neutral atoms; thus, the variational principle is not violated. This eliminates the “dissociation catastrophe” found in CDFT and most DFT exchange-correlation approximations, [6, 48–50], for which well-separated atoms retain  $q \neq 0$  with energies below that of neutral atoms. With the notable exceptions of a fluctuating charge model by Chen and Martínez [41] and our work [21–26], the available electronegativity equalization models suffer from electron self-interaction errors and manifest delocalization errors [6, 49]. These models may result in incorrect dissociation products (“dissociation catastrophe”) [41, 48–50].

The maximum CT energy lowering,  $E_{\text{CT, VPEq}}$ , by equilibration between orbital,  $i$ , of Li and orbital,  $j$ , of H occurs at  $\partial(E_{\text{VP}}(\text{Li}) + E_{\text{VP}}(\text{H}))/\partial q(\text{Li}) = 0$ , which corresponds to the VPEq in the bond. The VPEq is equivalent to the maximization of  $E_{\text{CT, VPEq}}$  the CT contribution to the bond energy, [10, 21–26], defined by (17.16).

$$E_{\text{CT, VPEq}} = \frac{[\chi_{\text{VS}}(\text{H}, j) - \chi_{\text{VS}}(\text{Li}, i)]^2}{2 [\eta_{\text{VS}}(\text{H}, j) + \eta_{\text{VS}}(\text{Li}, i)]} \quad (17.16)$$

The equilibrated VPA value,  $\langle \alpha_{\text{VP}}(at) \rangle$ , is given by (17.17).

$$\langle \alpha_{\text{VP}}(at) \rangle = \frac{[\chi_{\text{VS}}(\text{H}, j)/\eta_{\text{VS}}(\text{H}, j) + \chi_{\text{VS}}(\text{Li}, i)/\eta_{\text{VS}}(\text{Li}, i)]}{[1/\eta_{\text{VS}}(\text{H}, j) + 1/\eta_{\text{VS}}(\text{Li}, i)]} \quad (17.17)$$

The net atomic charge,  $q$ , or the bond polarity, is the value maximizing  $E_{\text{CT, VPEq}}$ . In the case of a single bond, the charge transferred between orbital  $i$ , and orbital  $j$ , is such that  $q(\text{Li}, i) = \delta_{i,j}$  and  $q(\text{H}, j) = -\delta_{i,j}$ , where the solution of  $\delta_{i,j}$  is given by (17.18).

$$q(\text{Li})_{\text{VPEq}} = \delta_{i,j} = \frac{\chi_{\text{VS}}(\text{H}, j) - \chi_{\text{VS}}(\text{Li}, i)}{\eta_{\text{VS}}(\text{H}, j) + \eta_{\text{VS}}(\text{Li}, i)} \quad (17.18)$$

The partial charge is proportional to the electronegativity difference between the bonding orbitals and inversely proportional to the sum of their VS hardness. Equation (17.18) is equivalent to (17.19).

$$q(\text{Li})_{\text{VPEq}} = \frac{[\langle \alpha_{\text{VP}}(at) \rangle - \chi_{\text{VS}}(\text{Li}, i)]}{\eta_{\text{VS}}(\text{Li}, i)} = 0.48 \quad (17.19)$$

The partial charge,  $q(\text{Li})_{\text{VPEq}} = +0.48$ , is also seen in Figure 17.2. at the minimum of the energy sum,  $E_{\text{VP}}(\text{Li}) + E_{\text{VP}}(\text{H})$ . Partial charges of other diatomic molecules are tabulated in Table 17.2.

Equations (17.17) and (17.19) may be extended into a rough first approximation of the VPEq for polyatomic molecules by assuming an overall (“globally”) equalized VPA of the molecule. We refer to the work of Ray et al. [51], Reed [52], and Bratsch [53], who calculated the “globally” equalized electronegativity of polyatomic molecules,  $\langle \chi_0(at) \rangle$  or  $\langle \chi_{\text{VS}}(at) \rangle$ , by solving linear equations. This approach has been refined by Bergmann and Hinze [20]. The result is globally equalized  $\langle \chi_0(at) \rangle$  of the molecule, defined by (17.20), which sums over all atoms.

$$\langle \chi_0(at) \rangle = \frac{\sum \chi_0^{(X)}/\eta_0(X)}{\sum 1/\eta_0(X)} \quad (17.20)$$

**Table 17.2** Comparison of partial charges,  $q$ , on atom  $X$  (underlined) obtained by methods mentioned in the text.

$\underline{XY}$	$q_{\text{VPEq}}$ (17.23)	$q_{\text{IR}}$ [42, 44]	$q_{\text{elstat}}$ [43, 44]	$q_{\text{RHF}}$ [30]	$q_{\text{NBO}}$ [7, 32, 44]	$q_0$ (17.21)
$\underline{\text{LiH}}$	0.48 (s) <sub>Li</sub> 0.53 (s <sup>2</sup> p) <sub>Li</sub>	n. a.	n. a.	0.589		0.24
					0.529(s <sup>2</sup> p) <sub>Li</sub> [7]	
$\underline{\text{LiF}}$	0.82 (s) <sub>Li</sub> (p) <sub>F</sub> 0.96(s) <sub>Li</sub> (sp <sup>11</sup> ) <sub>F</sub>	0.84	0.84 [43]	0.882		0.39
					0.96 (sp <sup>11</sup> ) <sub>F</sub> [7]	
$\underline{\text{NaF}}$	0.84(s) <sub>Na</sub> (p) <sub>F</sub>	0.87	0.86 [43]	0.881	n. a.	0.41
$\underline{\text{NaCl}}$	0.82(s) <sub>Na</sub> (p) <sub>Cl</sub>	0.78	0.82 [43]	0.857	0.93	0.39
$\underline{\text{KCl}}$	0.91(s) <sub>K</sub> (p) <sub>Cl</sub>	0.90	n. a.	0.888	n. a.	0.45
$\underline{\text{HF}}$	0.40 (sp <sup>19</sup> ) <sub>F</sub> 0.53 (sp <sup>6</sup> ) <sub>F</sub> 0.60 (sp <sup>4</sup> ) <sub>F</sub>	0.41	0.44 [43]			0.12
				0.595	0.553(sp <sup>4</sup> ) <sub>F</sub> [7]	
$\underline{\text{ClF}}$	0.20 (p) <sub>Cl and F</sub> 0.30 (sp <sup>6</sup> ) <sub>Cl and F</sub>	n. a.	0.16	0.285	0.332 [7]	0.09
$\underline{\text{OH}}$	0.38(sp <sup>5</sup> ) <sub>O</sub> [19]	0.36	0.39 [44]	0.323	n. a.	0.02
$\underline{\text{H}_2\text{O}}$	0.29 (sp <sup>4</sup> ) <sub>O</sub>	0.33	0.37 [44] 0.28 [43]	0.318	0.458	0.01
$\underline{\text{NH}_3}$	-0.40(sp <sup>3</sup> ) <sub>N</sub>	-0.81	-0.717 [43]	n. a.	-1.05	0.00

Data from Weinhold and Landis [7]; von Szentpály [10]; Bratsch [19].

n. a. means: no data available.

The partial charge  $q_0(X)$  calculated by this ground-state electronegativity equalization (GS-ENE) method is shown in (17.21)

$$q_0(X) = \frac{[\langle \chi_0(at) \rangle - \chi_0(X)]}{\eta_0(X)} \quad (17.21)$$

Reed [52] emphasizes a decisive warning by Evans and Huheey [54] that the averaged electronegativities and partial charges are not satisfactory because electronegativity equalization fails to minimize the energy of the system. This *caveat* is supported by a large-scale assessment of GS-ENE on 210 molecules [55]. The root-mean-square deviation of the geometric mean of the atomic values,  $\langle \chi_0(at) \rangle_{\text{GM}}$ , from the molecular  $\chi_0(\text{mol}) = 1/2 [I_0(\text{mol}) + A_0(\text{mol})]$  amounts to 71% for a broad set of 210 molecules [55]. Thus, the  $\chi_0(\text{mol})$  of a large majority of investigated molecules cannot be obtained by any equalization scheme [55].

A similar set of linear equations is solved, yielding a globally equalized, thus approximate *VPA* of the molecule, defined by (17.22), such that the summation is over all the AiMs.

$$\langle \alpha_{\text{VP}}(at) \rangle \approx \frac{\sum^{XVS(X,i)} \chi_{VS(X,i)} / \eta_{VS(X,i)}}{\sum 1 / \eta_{VS(X,i)}} \quad (17.22)$$

The partial charges on the AiMs or groups-in-a molecule of polyatomic molecules are to the first approximation, given by (17.23).

$$q(X, i)_{\text{VPEq}} \approx \frac{[\langle \alpha_{\text{VP},at} \rangle - \chi_{\text{VS}}(X, i)]}{\eta_{\text{VS}}(X, i)} \quad (17.23)$$

The partial charges obtained from VPEq for diatomic molecules,  $\text{H}_2\text{O}$ , and  $\text{NH}_3$  are compared to partial charges given by population analyses and those derived from infrared (IR) spectroscopic observations in Table 17.2. Note that the charges by the natural bond orbital (NBO) population analysis [7, 32] require the total energy minimization by a sophisticated method, whereas the VPEq and the GS-ENE are based on atomic data only. Without requiring ad hoc calibrations, the VPEq bond polarities agree very well with the results of state-of-the-art population analyses and charges derived from vibrational spectra. The last column of Table 17.2 also displays the corresponding  $q_0(XY)$  results from GS-ENE. Compared to  $q_{\text{NBO}}(\text{Li}) = 0.529$  obtained as the NBO charge of the metal hydride,  $\text{LiH}$ , GS-ENE gives the very low partial charge of  $q_0(\text{Li}) = 0.24$  only. It is exactly half of the  $q_{\text{VPEq}}(\text{Li}) = 0.48$ , because the hardness in (17.21) is  $\eta_0(\text{Li}) = 2\eta_{\text{VS}}(\text{Li})$  according to (17.23). For the ionic molecule,  $\text{LiF}$ , Table 17.2 reports consistent partial charges on Li ranging from 0.82 to 0.93 for all methods except GS-ENE, which again gives a much too low value of 0.39. A similar trend is observed for other metal halides such as  $\text{NaF}$ ,  $\text{NaCl}$ , and  $\text{KCl}$ , with the metal having partial charges of 0.39 to 0.45 for values obtained from GS-ENE. The influence of hybridization on the VPEq bond polarity is notable on  $q_{\text{VPEq}}(\text{HF})$ , with the values shifted up to 50%. Here again,  $q_0(\text{HF}) = 0.12$  is far too small. To make it worse, the GS-ENE of Eq. (17.21) predicts the partial charge on the  $N$  atom in ammonia  $q_0(\text{NH}_3) = 0$ , because of  $\chi_0(N) = \chi_0(\text{H})$ , according to [37]. Similarly,  $q_0(\text{H}_2\text{O}) = 0.01$  is almost zero for  $H$  of water. The GS-ENE, according to (17.21) completely fails to assess the polarity for these hydrides. In addition, the limits of Eqs. (17.22) and (17.23) as a simplistic extension of VPEq to polyatomic molecules are documented by the too small partial charges  $q_{\text{VPEq}}$  for  $\text{H}_2\text{O}$  and  $\text{NH}_3$ . We need to improve the VPEq ansatz for polyatomic molecules.

## 17.4 Valence-Pair-Equilibration and Thermodynamic Cycles

So far, we presented support for the valence-pair-equilibration by comparing the partial charges  $q_{\text{VPEq}}$  with those given by population analyses and spectroscopic observations in Table 17.2. However, the method of choice is the direct comparison of molecular VPA values,  $\alpha_{\text{VP}}(\text{mol})$ , with equilibrated VPA values,  $\langle \alpha_{\text{VP}}(at) \rangle$ , defined either in (17.22), or by an improved model. We have to define the VPA for bonds in molecules.

We start by extending the VPA scale from AiMs to molecules,  $XY$ , with electron-pair bonds,  $b$  [21, 22, 24, 25]. The relevant states of  $XY$ ,  $XY^+$ , and  $XY^-$  are determined by the Wigner–Witmer rules in symmetry correlations to the

constituent VS atoms and their ions. Photoelectron spectra are often assigned to electron removal from a particular bond. The observed vertical ionization energy is denoted as  $I_v(XY, b)$ . The bond may be specified in complex molecules as  $\sigma$ -,  $\pi$ -,  $\delta$ -bond, according to the local symmetry behavior with respect to the particular bond. The molecular  $A_v(XY)$  values are also determined in agreement with the Wigner–Witmer constraints [21, 22, 24]. The VPA,  $\alpha_{VP}(XY, b)$ , of bond  $b$ , formed by the orbitals  $i$  of  $X$  and  $j$  of  $Y$ , is defined as

$$\alpha_{VP}(XY, b) = 1/2 [I_v(XY, b) + A_v(XY)] \quad (17.24)$$

The companion parameter of  $\alpha_{VP}(XY, b)$  is the VS hardness of the bond  $b$ ,

$$\eta_{VS}(XY, b) = 1/2 [I_v(XY, b) - A_v(XY)] \quad (17.25)$$

The factor  $1/2$  is due to the difference between the second partial derivatives of the VS and GS energy parabolas.

We specify the conditions for VPEq in association reactions,  $X + Y \rightarrow XY$ , using thermochemical cycles based on the first law of thermodynamics. Consider atoms or groups as reactants,  $R = \{X, Y\}$ , and their products,  $P = \{X_2, XY\}$ , with corresponding cations,  $P^+$ , and anions,  $P^-$ . Figure 17.3. illustrates the bond formation between  $X$  and  $Y$ , and displays the “ingredients” needed to discuss both the VPEq and GS-ENE rules. Thermochemical cycles connect the bond dissociation energies,  $D(P)$ ,  $D(P^+)$ , and  $D(P^-)$  to the ionization energies,  $I$  and electron affinities,  $A$ , of the reactants and their product [25]. We use  $I(X) \leq I(Y)$  and  $A(X) \leq A(Y)$ , thus  $\chi(Y) - \chi(X) \geq 0$  and focus on two cycles given by (17.26) and (17.27).

$$I_a(P) + D(P^+) - I(X) - D(P) = 0 \quad (17.26)$$

$$A_a(P) + D(P) - A(Y) - D(P^-) = 0 \quad (17.27)$$

The average of (17.26) and (17.27) is,

$$\alpha_{VP,a}(P) + 1/2 [D(P^+) - I(X) - A(Y) - D(P^-)] = 0 \quad (17.28)$$

The *adiabatic VPA*,  $\alpha_{VP,a}(P) = \frac{1}{2} [I_a(P) + A_a(P)]$ , is normally close to the *vertical VPA*,  $\alpha_{VP,v}(P) \approx \alpha_{VP,a}(P)$ , since  $I_a(P) \leq I_v(P)$ , but  $A_a(P) \geq A_v(P)$ . Written in terms of the bond dissociation energy, the product's *adiabatic VPA* is expressed as,

$$\alpha_{VP,a}(P) = \frac{1}{2} [D(P^-) - D(P^+) + \chi(X) + \eta(X) + \chi(Y) - \eta(Y)] \quad (17.29)$$

that simplifies to,

$$\alpha_{VP,a}(P) = \frac{1}{2} [D(P^-) - D(P^+)] + \langle \chi(R) \rangle_{AM} - \frac{1}{2} \Delta\eta(R) \quad (17.30)$$

in terms of the arithmetic mean  $\langle \chi(R) \rangle_{AM}$ , which differs from the product's *adiabatic VPA* by (17.31).

$$\langle \chi(R) \rangle_{AM} - \alpha_{VP,a}(P) = \frac{1}{2} [D(P^+) - D(P^-)] - \frac{1}{2} \Delta\eta(R) \geq \frac{1}{2} [D(P^+) - D(P^-)] \quad (17.31)$$

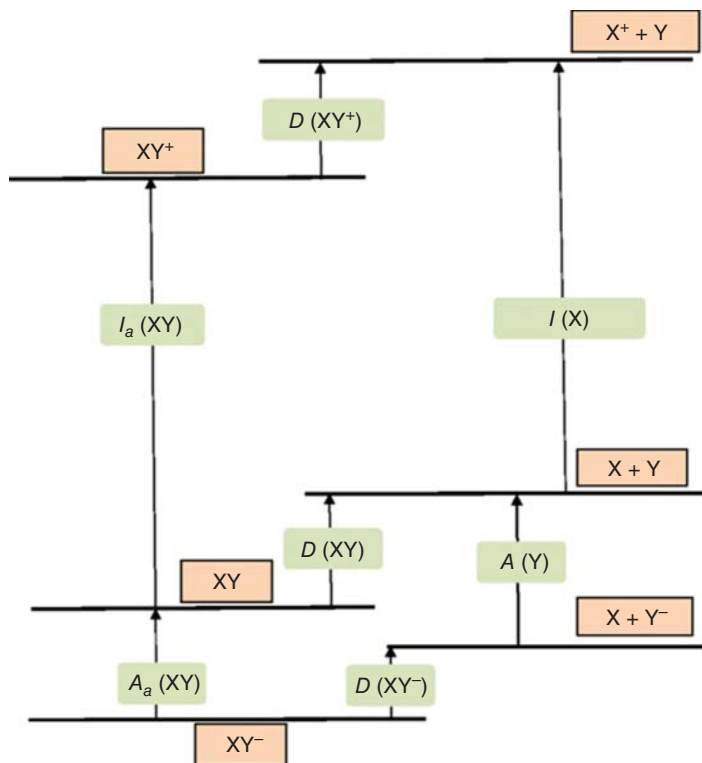


**Figure 17.3** Thermochemical cycles illustrate the bond formation between the chemical species  $X$  and  $Y$ . Adiabatic ionization energy,  $I_a(XY)$ , and electron affinity,  $A_a(XY)$ , of the product, and the  $I(X)$  and  $A(Y)$  values of reactants. Bond dissociation energies,  $D(XY)$ ,  $D(XY^+)$ , and  $D(XY^-)$ . Source: From von Szentpály [25]. Licensed under CC BY 4.0.

We have a positive  $\Delta\eta(R) = \eta(Y) - \eta(X) \geq 0$ , due to  $\Delta\chi(R) \geq 0$ , and the high-quality linear relationship between  $\chi(at)$  and  $\eta(at)$ , found by Bratsch for the main group elements [53].

$$\eta(at) = (0.60 \pm 0.11) \chi(at) \quad (17.32)$$

The thermochemical cycles provide essential support for the new *Rule: VPA* is equalized (individual deviations: <10%) by association reactions,  $X + Y \rightarrow XY$ , if the ionic dissociation energies are equal,  $D(XY^+) - D(XY^-) \approx 0$ . Changes in the external potential,  $v(\mathbf{r})$ , during the reaction are absorbed in the thermochemical cycles and do not interfere with the ENE rule. Therefore, a restriction to *vertical* ionization energies and electron affinities in the context of this rule is not mandatory. The examples in Table 17.3 evidence the main result of this chapter, that in case of  $\alpha_{VP} \neq \chi_0$ , the accuracy of *VPEq* is up to orders of magnitude better than that of *GS-ENE*. With the exception of LiH, small differences  $\frac{1}{2}[D(P^+) - D(P^-)]$  are required for the equilibration of both VS and GS electronegativities by bonding.

**Table 17.3** Bond dissociation energies,  $D(XY^+)$ ,  $D(XY^-)$ , and difference,  $\frac{1}{2}[D(XY^+) - D(XY^-)]$ . Differences  $\Delta\alpha_{\text{VP}}$  and  $\Delta\chi_0$  given as  $\Delta\chi = \langle\chi(at)\rangle_{\text{CT}} - \chi(XY)$  and  $\delta = 100 [(\Delta\chi/\chi(XY))]\%$ .

$XY$	$D(XY^+)$	$D(XY^-)$	$\frac{1}{2}[D(XY^+) - D(XY^-)]$	$\Delta\alpha_{\text{VP}}$ and $\Delta\chi_0$ [25]	$\delta(\%)$ [25]
H <sub>2</sub>	2.65	n. a.	n. a.	7.18 – 6.99 = 0.19	3
Li <sub>2</sub>	1.44	≈0.90	0.27	3.01 – 2.80 = 0.21	7
Na <sub>2</sub>	0.96	0.614	0.17	2.84 – 2.77 = 0.07	3
LiNa	0.99	≈0.69	0.15	2.92 – 2.80 = 0.12	4
LiH	0.114	2.003	–0.944	4.14 – 4.08 = 0.06	1.4
N <sub>2</sub>	VS:7.61	≈7.53	VS: ≈ 0.04	$\alpha_{\text{VP}}$ : 7.32 – 7.31 = 0.01	0.1
	GS:8.71	”	GS: ≈ 0.63	$\chi_0$ : 7.18 – 6.62 = 0.56	8.5
NO	VS:4.44	5.05	VS:–0.30	$\alpha_{\text{VP}}$ : 8.38 – 8.52 = –0.14	–1.6
	GS: 10.85	”	GS:2.90	$\chi_0$ : 7.36 – 4.50 = 2.86	64
O <sub>2</sub>	VS:4.03	4.09	VS:–0.03	$\alpha_{\text{VP}}$ :9.63 – 9.64 = –0.01	–0.1
	GS:6.66	”	GS:1.28	$\chi_0$ : 7.54 – 6.35 = 1.19	19
S <sub>2</sub>	VS:3.52	3.95	VS:–0.21	$\alpha_{\text{VP}}$ : 7.39 – 7.32 = 0.07	1
	GS:5.37	”	GS:0.71	$\chi_0$ : 6.22 – 5.43 = 0.79	15
F <sub>2</sub>	VS:1.37	1.28	VS:0.05	$\alpha_{\text{VP}}$ : 12.20 – 11.36 = 0.84	7
	GS:3.34	”	GS:1.03	$\chi_0$ : 10.41 – 8.71 = 1.70	19
Cl <sub>2</sub>	VS:1.50	1.26	VS:0.12	$\alpha_{\text{VP}}$ : 9.35 – 8.64 = 0.71	8
	GS:3.95	”	GS:1.35	$\chi_0$ : 8.29 – 6.38 = 1.91	30
IBr	VS:1.08	1.10	VS:–0.01	$\alpha_{\text{VP}}$ : 8.30 – 7.66 = 0.64	8.4
	GS:2.42	”	GS:0.65	$\chi_0$ : 7.16 – 5.74 = 1.42	25

Energies, VPAs, and electronegativities in electron Volt units (eV). The valence-state (VS,  $\Delta\alpha_{\text{VP}}$ ) and ground-state (GS,  $\Delta\chi_0$ ) data are assigned, unless they are identical.

The performances of the *VPEq* and CDFT's GS-ENE have been compared for 89 molecules with very diverse bond characters, including the “exotic” dimers Be<sub>2</sub>, Mg<sub>2</sub>, B<sub>2</sub>, C<sub>2</sub>, and Mn<sub>2</sub> [24]. The mean unsigned deviations (MUDs) are  $\text{MUD}(\alpha_{\text{VP}}) = 2.55\%$  and  $\text{MUD}(\chi_0) = 21.95\%$  for 89 molecules. The accuracy of *VPEq* is about nine times better than that of GS-ENE [24]. The conclusion is that GS-ENE between atoms gives good results, only if  $\chi_0 \approx \alpha_{\text{VP}}$ , for the atoms involved. This is the case for, e.g. H<sub>2</sub>, Li<sub>2</sub>, LiH, Cu<sub>2</sub>, and P<sub>2</sub>, but is more the exception than the rule. The large changes of the external potential,  $v(\mathbf{r})$ , during bond formation do not affect the accuracy of *VPEq*; thus, the constancy of  $v(\mathbf{r})$  is not required. If the changes of the external potential were the primary reason for the many exceptions to GS-ENE, it would be very hard to explain why *ENE* is almost perfectly realized, as long as  $\chi_0 = \alpha_{\text{VP}}$ , as, e.g. in H<sub>2</sub>, Li<sub>2</sub>, and LiH (Table 17.3).

## 17.5 Partial Charges from Valence-Pair-Equilibration in Polyatomics

In most molecules, an AiM usually forms more than one bond, and all bonds are coupled in principle. Polar bonds affect each other's polar character. A charge shift in a bond affects not only the VPA of the bond of interest but, to a lesser degree, also that of the *geminal* bonds on the same atom [24, 26, 40]. The VPA functions mutually influence each other by a kind of hardness matrix [18, 19, 24, 26, 40]. Therefore, the expression for the orbital electronegativity of the *active* orbital,  $i$ , involved in the bond under consideration must include the effects of the *geminal* orbitals,  $I$ ; that is, of the other valence orbitals not participating in the bond of interest. This coupling cannot be of long range. Otherwise, such charge equilibration models would result in the same net charges on all the AiMs of the same element, independent of the neighboring atoms, which is contrary to accepted chemical wisdom.

The *geminal* charge coefficient,  $\eta_{VS}/\kappa$ , is introduced into (17.33) to give a generalized expression for the VPA,  $\alpha_{VP,i}$ , in terms of the charge shifts within the valence orbitals,

$$\alpha_{VP,i}(\delta_i) = \chi_{VS}(X, i) + \frac{1}{\kappa} \sum_{I \neq i} \eta_{VS}(X, I) \delta_I + \eta_{VS}(X, i) \delta_i \quad (17.33)$$

The *geminal* hardness,  $\eta_{VS}(I)$ , is not expected to contribute fully to the active orbital. The inverse  $\kappa$  term,  $1/\kappa$ , is a correction factor that reduces the contributions of the VS hardness of the *geminal* orbitals to the active orbital. Therefore, for integer values,  $\kappa > 1$ , the larger the value of  $\kappa$ , the smaller the influence of the *geminal* orbitals. Here, we opt for  $\kappa = 2$ . The terms,  $\chi_{VS}(X, i)$ ,  $\eta_{VS}(X, I)$ , and  $\eta_{VS}(X, i)$  are abbreviated to simpler notations,  $\chi_{X,i}^{VS}$ ,  $\eta_{X,I}$ , and  $\eta_{X,i}$ , respectively. The VPA of the bonded orbitals equalizes to an equilibrium value by bond formation. Applying the VPEq method to each bond in the molecule results in a charge shift within each two-center two-electron bond, from which the partial charges at the atomic centers in the molecule can be determined. For instance, the charge shift,  $\delta_{i,j}$ , within the bond formed between overlapping orbitals,  $i$ , on atomic center,  $X$ , and orbital,  $j$ , on atomic center,  $Y$ , is determined by first equating the orbital electronegativity expressions, as shown in (17.34).

$$\chi_{X,i}^{VS} + \frac{1}{\kappa} \sum_{I \neq i} \eta_{X,I} \delta_{X,I} + \eta_{X,i} \delta_{X,i} = \chi_{Y,j}^{VS} + \frac{1}{\kappa} \sum_{J \neq j} \eta_{Y,J} \delta_{Y,J} + \eta_{Y,j} \delta_{Y,j} \quad (17.34)$$

The active bond between overlapping orbitals  $i$  and  $j$  is labeled,  $k$ , such that  $\delta_{X,i} = \delta_{i,j} = \delta_k$  and  $\delta_{Y,j} = -\delta_{i,j} = -\delta_k$ . Likewise, the *geminal* bonds between overlapping orbitals represented by  $I$  and  $J$  are labeled  $l$  such that  $\delta_{X,I} = \delta_{I,J} = \delta_l$  and  $\delta_{Y,J} = -\delta_{I,J} = -\delta_l$ . Omitting the labels for the atoms but including the labels for the bonds (17.34) simplifies to (17.35)

$$\left(\eta_i^k + \eta_j^k\right) \delta_k + \frac{1}{\kappa} \sum_{I \neq i} \sum_{J \neq j} \left(\eta_I^l + \eta_J^l\right) \delta_l = \left(\chi_j^{VS} - \chi_i^{VS}\right)_k, k \neq l \quad (17.35)$$

For each bond in the molecule, one such linear equation is derived. In general, if  $\delta_{i,j} = \delta_k$  denotes the charge shift between the bonded active orbitals on the respective atomic centers in the molecule, then there are  $n$  linear equations for  $n$  bonds in the molecule. A set of simultaneous linear equations is generated for the charge shifts,  $\delta_k$ , for  $k = 1, 2, 3, \dots, n$ , as the variables to be solved [56].

In matrix form, the simultaneous equations are represented by (17.36) through (17.41), such that  $k \neq l$  and  $k, l = 1, 2, 3, \dots, n$ . Matrix,  $\mathbf{A}$ , has dimensions,  $n \times n$ , and is defined by (17.36).

$$\mathbf{Ax} = \mathbf{b} \quad (17.36)$$

The diagonal elements,  $A_{kk}$ , for the active bonds are characterized by (17.37).

$$A_{kk} = \eta_i^k + \eta_j^k \quad (17.37)$$

The off-diagonal elements,  $A_{kl}$ , are given by (17.38),

$$A_{kl} = \frac{1}{\kappa} \sum_{I \neq i} \sum_{J \neq j} (\eta_I^l + \eta_J^l) \quad (17.38)$$

such that for bonds not formed by the AiM,  $A_{kl} = 0$ . Note,  $\mathbf{x}$  and  $\mathbf{b}$  are column matrices for which the elements of  $\mathbf{b}$ , shown in (17.39), are the electronegativity difference for the bonded orbitals.

$$b_k = \chi_j^{\text{VS}} - \chi_i^{\text{VS}} \quad (17.39)$$

The elements of  $\mathbf{x}$  are the charge shifts within each bond defined by (17.40).

$$x_k = \delta_k \quad (17.40)$$

The matrix  $\mathbf{A}$  is non-singular with solutions found using standard matrix inversion methods given by (17.41).

$$\mathbf{x} = \mathbf{A}^{-1}\mathbf{b} \quad (17.41)$$

Appropriate row and column operations may be performed to reduce the dimension of the problem for equivalent bonds of a given AiM [56].

In the *VPEq* method, the partial charge,  $q$ , at each atomic center in the molecule is calculated by summing all the charge shifts within the bonded orbitals of the AiM. For instance, the partial charge on atom,  $X$ , in the molecule is given by (17.42),

$$q_X = \sum_i \delta_{X,i} \quad (17.42)$$

where  $i$  represents all the bonded orbitals of atom,  $X$ . The molecule is electroneutral, since  $\sum_{k=1}^N q_k = 0$  for the  $N$  atoms in the molecule. One of the main advantages of the *VPEq* method is that the charge distributions in molecules are determined without extensive quantum mechanical calculations while retaining the intuitive idea of atomic centers within the molecule. This makes the *VPEq* method very appealing since consistent atomic charges for a wide range of molecules can be reliably determined without almost any knowledge of the molecular wave function. Table 17.4 lists the partial charges  $q_{\text{VPEq}}$  obtained from *VPEq* for polyatomic molecules, where the influences of the *geminal* bonds are included. We would like to thank Dr. Genevieve



**Table 17.4** Partial charges,  $q_{\text{VPEq}}$ , and primary electric dipole moments,  $\vec{\mu}_p$ .

Molecule	Atom	Partial charges	Calculated primary dipole moment /D	Experimental dipole moment [57] /D
Lithium fluoride	Li	0.82	6.18	6.32
LiF	F	-0.82		
Ammonia	N	-0.534	0.946	$1.471 \pm 0.01$
NH <sub>3</sub>	H	0.178		
Water	O	-0.661	1.811	$1.854 \pm 0.01$
H <sub>2</sub> O	H	0.331		
Propane	C a	-0.159	0.045	$0.084 \pm 0.001$
	C b	-0.141		
	H a	0.056		
	H b	0.062		
Propene	C a	-0.223	0.313	$0.366 \pm 0.003$
	C b	-0.213		
	C c	-0.120		
	H a	0.116		
	H b	0.120		
	H c	0.068		
Propyne	C a	-0.267	1.109	$0.784 \pm 0.008$
	C b	-0.268		
	C c	-0.023		
	H a	0.265		
	H c	0.098		
Methylamine	C	-0.078	1.277	$1.31 \pm 0.02$
	N	-0.525		
	H a	0.081		
	H b	0.181		

Henry (Susquehanna University) for her help in drawing the structures included in Table 17.4.

## 17.6 Electric Dipole Moments

In a diatomic molecule, XY, with a single bond, where Y is more electronegative than X, there is a negative partial charge,  $q_Y$ , centered at Y and an equivalent positive

partial charge,  $q_X$ , centered at  $X$ . The primary dipole moment of the  $XY$  molecule is given by (17.43),

$$\vec{\mu}_p = q_X \vec{r}_X + q_Y \vec{r}_Y \quad (17.43)$$

Where  $\vec{r}_X$  and  $\vec{r}_Y$  are position vectors of atoms  $X$  and  $Y$ , with respect to an arbitrary origin. The bond dipole moment is a consequence of the electronic charge transfer within the orbitals of the AiMs upon bond formation [56, 58, 59]. It is important to note that the primary moment represents one component of the total or resultant dipole moment of the molecule, which is the sum of the primary moment, induced moment, and the hybridization moment for molecules [56, 58–61]. However, the induced moment and the hybridization moment tend to cancel each other. We, therefore, focus on the primary dipole moment. For polyatomic molecules, the primary moment is given by (17.44),

$$\vec{\mu}_p = \sum_j q_j \vec{r}_j \quad (17.44)$$

such that  $q_j$  is the charge at the  $j$ th atomic center in the molecule and  $\vec{r}_j$  is its position vector with respect to an arbitrary assigned molecular origin.  $\vec{\mu}_p$  is independent of the position of the origin in the molecule since  $\sum_j q_j = 0$ . According to VB theory, the resultant dipole moment is a vector sum of all the bond dipole moments.

Table 17.4 lists our calculated primary dipole moments along with the experimental moments [57]. Taken from Table 17.2, the  $|q_{VPEq}(\text{LiF})| = 0.82$  produces  $|\vec{\mu}_p| = 6.18$  D just 2% off the reported experimental value. As expected, the  $O$  atom of water with a charge of  $-0.661$  is more negative than  $N$  of ammonia with a charge of  $-0.534$ . This is a direct consequence of referencing to  $\alpha_{VP}$  and  $\eta_{VS}$  for the AiM, which results in a primary dipole moment of 1.811 D in excellent agreement with the experimental value of  $1.854 \pm 0.01$  D for water. The  $VPEq$  method differentiates between the orbitals on the  $C$  atom based on its environment. The charge shifts between  $H$  and the primary vs. secondary  $C$  atoms of propane yield a primary  $H$  atom with a slightly greater charge of 0.062 compared to 0.056 for the secondary  $H$ . Conversely, the primary and secondary  $C$  atoms are different with charges of  $-0.159$  and  $-0.141$ , respectively. This is significant because the  $VPEq$  method gives a non-zero primary moment of 0.045 D for propane, which is in reasonable agreement with the experimental value of  $0.084 \pm 0.001$  D. The partial charges of the  $C$  and  $H$  atoms of the methyl group are similar for propane, propene, propyne, and methylamine with their differences rationalized by increased polarity due to multiple neighboring bonds, or the more electronegative primary amine group in the case of methylamine. This is convincing evidence that the  $\alpha_{VP}$  and  $\eta_{VS}$  of the AiM are needed, but the global  $\chi_0$  and  $\eta_0$  of CDFT are insufficient to assess dipole moments.

The errors in the primary electric dipole moment determined from the uncertainty in the partial charge and bond length are  $\pm 0.005$  D, when  $\vec{\mu}_p \leq 0.1$  D;  $\pm 0.05$  D, when  $0.1 < \vec{\mu}_p \leq 1$  D; and  $\pm 0.10$  D, when  $\vec{\mu}_p > 1$  D.

## 17.7 Summary and Conclusions

Conceptual DFT not only profoundly influences our perceptions of chemical concepts, principles, and rules but also faces challenges in its applications. We here concentrate on the implications of VS concepts on CDFT. The focus is on EN and its equalization (ENE) by bonding as a central topic of CDFT. For this purpose, Mulliken's exclusively atomic VS orbital electronegativity definition is extended to bonds in molecules. This generalized *VPA*, symbolized  $\alpha_{\text{VP}}$ , is defined as a charge-dependent pair-sharing power. It is derived in accordance with Ruedenberg's bond theory, which defines the valence-state energy by keeping the ionic valence structures of the molecule intact and frozen up to the separated atoms.

In contrast to the GS-EN,  $\chi_0$ , the  $\alpha_{\text{VP}}$  fulfils all Wigner–Witmer symmetry requirements for characterizing bonds by the interplay of covalent and ionic valence structures. Another essential difference between the GS and VS approaches to EN, especially, *VPA* is the absence of hybridization in CDFT, as opposed to its important role for VS energies. An order of magnitude improvement of the accuracy of ENE is achieved by replacing the  $\chi_0$  by the *VPA*,  $\alpha_{\text{VP}}$ , which is equilibrated in bonds (*VPEq*). Without requiring *ad hoc* calibrations, the *VPEq* bond polarities agree very well with the results of state-of-the-art population analyses, and charges derived from vibrational spectra. A conclusion is that ground-state ENE between atoms gives reasonable results, as long as  $\chi_0 \approx \alpha_{\text{VP}}$  for the atoms are involved. The large changes of the external potential,  $v(\mathbf{r})$ , during bond formation do not affect the accuracy of *VPEq*; thus, the constancy of  $v(\mathbf{r})$  is not required. The *VPEq* calculated primary dipole moments of medium-sized organic molecules reasonably reproduce the observed dipole moments. In summary, the concepts of valence states should be more emphasized in their consequences for CDFT.

## References

- 1 Mulliken, R.S. (1978). Chemical bonding. *Annu. Rev. Phys. Chem.* 29: 1–30.
- 2 Mulliken, R.S. (1934). A new electroaffinity scale; together with data on valence states and on valence ionization potentials and electron affinities. *J. Chem. Phys.* 2 (11): 782–793.
- 3 Moffitt, W. (1954). Atomic valence states and chemical binding. *Rep. Prog. Phys.* 17 (1): 173–200.
- 4 Ruedenberg, K. (1962). The physical nature of the chemical bond. *Rev. Mod. Phys.* 34 (2): 326–376.
- 5 Parr, R.G., Donnelly, R.A., Levy, M., and Palke, W.E. (1978). Electronegativity: the density functional viewpoint. *J. Chem. Phys.* 68 (8): 3801–3807.
- 6 Parr, G.R. and Yang, W. (1989). *Density-Functional Theory of Atoms and Molecules*. Oxford, UK: Oxford University Press.
- 7 Weinhold, F. and Landis, C.L. (2005). *Valency and Bonding*. Cambridge, UK: Cambridge University Press.

- 8 Van Vleck, J.H. (1934). On the theory of the structure of  $\text{CH}_4$  and related molecules: part III. *J. Chem. Phys.* 2 (1): 20–30.
- 9 von Szentpály, L. (1995). Valence states and a universal potential energy curve for covalent and ionic bonds. *Chem. Phys. Lett.* 245: 209–214.
- 10 von Szentpály, L. (1991). Studies on electronegativity equalization: Part 1. Consistent diatomic partial charges. *J. Mol. Struct. THEOCHEM* 233: 71–81.
- 11 Mulliken, R.S. (1966). The bonding characteristics of diatomic MO's. In: *Quantum Theory of Atoms, Molecules, and the Solid State* (ed. P. Löwdin), 231–241. New York, NY: Academic Press.
- 12 von Szentpály, L. and Gardner, D.O.N. (2001). Valence-state atoms in molecules. 6. Universal ionic–covalent potential energy curves. *J. Phys. Chem. A* 105 (41): 9467–9477.
- 13 Pritchard, H.O. and Skinner, H.A. (1955). The concept of electronegativity. *Chem. Rev.* 55 (4): 745–786.
- 14 Pritchard, H.O. and Sumner, F.H. (1956). The application of electronic digital computers to molecular orbital problems – II. A new approximation for hetero-atom systems. *Proceedings of the Royal Society, London*.
- 15 Wigner, E. and Witmer, E.E. (1928). Über die Struktur der zweiatomigen Molekelspektren nach der Quantenmechanik. *Z. Phys.* 51 (11–12): 859–886.
- 16 Herzberg, G. (1950). *Molecular Spectra and Molecular Structure: Vol.1. Spectra of Diatomic Molecules*, 315–322. Princeton, NJ: Van Nostrand.
- 17 Condon, E.U. and Shortley, G.H. (1953). *The Theory of Atomic Spectra*. Cambridge, UK: Cambridge University Press.
- 18 Hinze, J. and Jaffé, H.H. (1962). Orbital electronegativity of neutral atoms. *J. Am. Chem. Soc.* 84 (4): 540–546.
- 19 Bratsch, S.G. (1988). Revised Mulliken electronegativities: I. Calculation and conversion to Pauling units. *J. Chem. Educ.* 65 (1): 34–41.
- 20 Bergmann, D. and Hinze, J. (1996). Electronegativity and molecular properties. *Angew. Chem. Int. Ed.* 35 (2): 150–163.
- 21 von Szentpály, L. (2015). Symmetry laws improve electronegativity equalization by orders of magnitude and call for a paradigm shift in conceptual density functional theory. *J. Phys. Chem. A* 119 (9): 1715–1722.
- 22 von Szentpály, L. (2015). Physical basis and limitations of equalization rules and principles: valence-state electronegativity and valence-state affinity versus operational chemical potential. *Quantum Matter* 4: 47–55.
- 23 von Szentpály, L. (2017). Hardness maximization or equalization? New insights and quantitative relations between hardness increase and bond dissociation energy. *J. Mol. Model.* 23 (7): 217.
- 24 von Szentpály, L. (2018). Eliminating symmetry problems in electronegativity equalization and correcting self-interaction errors in conceptual DFT. *J. Comput. Chem.* 39 (24): 1949–1969.
- 25 von Szentpály, L. (2020). Theorems and rules connecting bond energy and bond order with electronegativity equalization and hardness maximization. *Theor. Chem. Acc.* 139 (3): 54.

- 26 von Szentpály, L., Kaya, S., and Karakuş, N. (2020). Why and when is electrophilicity minimized? New theorems and guiding rules. *J. Phys. Chem. A* 124 (51): 10897–10908.
- 27 Parr, R.G. and Pearson, R.G. (1983). Absolute hardness: companion parameter to absolute electronegativity. *J. Am. Chem. Soc.* 105 (26): 7512–7516.
- 28 Pauling, L. (1932). The nature of the chemical bond. IV. The energy of single bonds and the relative electronegativity of atoms. *J. Am. Chem. Soc.* 54 (9): 3570–3582.
- 29 Zhang, H., Danovich, D., Wu, W. et al. (2014). Charge-shift bonding emerges as a distinct electron-pair bonding family from both valence bond and molecular orbital theories. *J. Chem. Theory Comput.* 10 (6): 2410–2418.
- 30 Klopman, G. (1964). Semiempirical treatment of molecular structures. II. Molecular terms and applications to diatomic molecules. *J. Am. Chem. Soc.* 86 (21): 4550–4557.
- 31 Ferreira, R. (1968). Is one electron less than half what an electron pair is? *J. Chem. Phys.* 49 (5): 2456–2457.
- 32 Reed, A.E., Weinstock, R.B., and Weinhold, F.J. (1985). Natural population analysis. *J. Chem. Phys.* 83 (2): 735–746.
- 33 Mulliken, R.S. (1952). Magic formula, structure of bond energies and isovalent hybridization. *J. Phys. Chem.* 56 (3): 295–311.
- 34 Coulson, C. (1952). *Valence*, 2e. London, UK: Oxford University Press.
- 35 McWeeny, R. (1983). *Coulson's Valence*, 3e. Oxford, UK: Oxford University Press.
- 36 Pauling, L. (1931). The nature of the chemical bond. Application of results obtained from the quantum mechanics and from a theory of paramagnetic susceptibility to the structure of molecules. *J. Am. Chem. Soc.* 53 (4): 1367–1400.
- 37 De Proft, F., Ayers, P.W., and Geerlings, P. (2014). The conceptual density functional theory perspective of bonding. In: *The Chemical Bond. Fundamental Aspects of Chemical Bonding* (ed. G. Frenking and S. Shaik), 233–269. Weinheim: Wiley-VCH.
- 38 Parr, R.G., von Szentpály, L., and Liu, S. (1999). Electrophilicity index. *J. Am. Chem. Soc.* 121 (9): 1922–1924.
- 39 Politzer, P., Murray, J.S., and Bulat, F.A. (2010). Average local ionization energy: a review. *J. Mol. Model.* 16: 1731–1742.
- 40 von Szentpály, L. (2000). Modeling the charge dependence of total energy and its relevance to electrophilicity. *Int. J. Quantum Chem.* 76 (2): 222–234.
- 41 Chen, J. and Martínez, T.J. (2007). QTPIE: charge transfer with polarization current equalization. A fluctuation charge model with correct asymptotics. *Chem. Phys. Lett.* 438: 315–320.
- 42 Gussoni, M., Castiglioni, C., and Zerbi, G. (1984). Physical meaning of electrooptical parameters derived from infrared intensities. *J. Phys. Chem.* 88 (3): 600–604.
- 43 Orozco, M. and Luque, F.J. (1990). On the use of AM1 and MNDO wave functions to compute accurate electrostatic charges. *J. Comput. Chem.* 11 (8): 909–923.

- 44 Milani, A., Tommasini, M., and Castiglioni, C. (2012). Atomic charges from IR intensity parameters: theory, implementation and application. *Theor. Chem. Acc.* 131 (3): 1–17.
- 45 Janak, J.F. (1978). Proof that  $\partial E/\partial n_i = \epsilon$  in density-functional theory. *Phys. Rev. B* 18: 7165–7168.
- 46 Ghosh, S.K. and Parr, R.G. (1987). Toward a semiempirical density functional theory of chemical binding. *Theor. Chimica Acta* 72: 379–391.
- 47 Phillips, P. and Davidson, E.R. (1983). Chemical potential for harmonically interacting particles in a harmonic potential. *Int. J. Quantum Chem.* 23: 185–194.
- 48 Zahariev, F.E. and Wang, Y.A. (2004). Functional derivative of the universal density functional in Fock space. *Phys. Rev. A* 70: 042503.
- 49 Cohen, A.J., Mori-Sánchez, P., and Yang, W. (2012). Challenges for density functional theory. *Chem. Rev.* 112: 289–320.
- 50 Bao, J.L., Wang, Y., He, X. et al. (2017). Multiconfiguration pair-density functional theory is free from delocalization error. *J. Chem. Phys. Lett.* 8 (22): 5616–5620.
- 51 Ray, N.K., Samuels, L., and Parr, R.G. (1979). Studies of electronegativity equalization. *J. Chem. Phys.* 70: 3680–3684.
- 52 Reed, J.L. (1981). Electronegativity: an isolated atom property. *J. Phys. Chem.* 85: 148–153.
- 53 Bratsch, S.G. (1988). Revised Mulliken electronegativities: II. Applications and limitations. *J. Chem. Educ.* 65 (3): 223–227.
- 54 Evans, R.S. and Huheey, J.E. (1970). Electronegativity, acids, and bases. III. Calculation of energies associated with some hard and soft acid-base interactions. *J. Inorg. Nucl. Chem.* 32 (3): 777–793.
- 55 Datta, D., Shee, N.K., and von Szentpály, L. (2013). Chemical potential of molecules contrasted to averaged atomic electronegativities: alarming differences and their theoretical rationalization. *J. Phys. Chem. A* 117 (1): 200–206.
- 56 Bernard Rodrigues, R.A. (2000). *Effects of Electronegativity on Molecular Charge Distribution and the Enthalpy of Formation of Branched and Cyclic Alkanes [dissertation]*. Mona Campus, Kingston, JM: University of the West Indies.
- 57 Lide, D.R. (ed.) (2004). *Handbook of Chemistry and Physics*, 84e. Boca Raton, FL: CRC Press.
- 58 Ferreira, R. (1963). Principle of electronegativity equalization. Part 1.—Bond moments and force constants. *Trans. Faraday Soc.* 59: 1064–1074.
- 59 Gordy, W. and Cook, R.L. (1984). *Microwave Molecular Spectra*. New York, NY: Wiley.
- 60 Párkányi, C. and Aaron, J.J. (1998). Dipole moments of aromatic heterocycles. In: *Theoretical Organic Chemistry*, vol. 5 (ed. C. Párkányi), 233–258. Amsterdam, NL: Elsevier Science.
- 61 Housecroft, C.E. and Sharpe, A.G. (2018). *Inorganic Chemistry*, 5e. Pearson Education Limited: Harlow, UK.

## 18

## Chemical Information

Rubén Laplaza<sup>1</sup>, Julen Munárriz<sup>2</sup>, and Julia Contreras-García<sup>1</sup>

<sup>1</sup>Sorbonne Université, Laboratoire de Chimie Théorique, F. 75005 Paris, France

<sup>2</sup>Universidad de Oviedo, Departamento Química Física y Analítica, 33006 Oviedo, Spain

## 18.1 Introduction

Chemistry is the science devoted to the study of the properties, structure, and composition of substances, as well as the processes they undergo. This means that extracting chemical information from the concepts seen until now is naturally focused on the changes induced by the external potential: what happens when we change a given atom by another, or when it changes place., is all summarized in the variable  $v(\mathbf{r})$  (coordinates and nuclear charges).

This is the phenomenological approach taken for the last decades in Chemistry: the properties and reactivities of families of related compounds are predicted in terms of simple models or experimental correlations: acid and base activity and electrophilic substitutions are two textbooks examples which, from the very history of chemistry, we know to work quite well. It should be noted that this approach has recently re-seen a boost with machine learning [1, 2]. Molecular representations aimed at machine learning applications often rely in implicitly mimicking the external potential. As seen in Chemistry for decades, the external potential on its own may have a signature that is genuinely unique and can be nonlinearly mapped to the desired property (e.g. the expectation value of a given operator).

Nevertheless, this approach has limitations, which are easily seen if we go back to the energy derivatives seen in Chapter 2. We have seen that both the external potential,  $v$ , and the particle number,  $N$ , are enough to completely characterize the system, determining both the exact Hamiltonian and the exact ground state energy,  $E$ . Hence,  $dE$  can be written as:

$$dE = \left( \frac{\partial E}{\partial N} \right)_{v(\mathbf{r})} dN + \int \left( \frac{\delta E}{\delta v(\mathbf{r})} \right)_N \delta v(\mathbf{r}) d\mathbf{r} \quad (18.1)$$

The first derivative of the right-hand side is the chemical potential,  $\mu$ :

$$\mu = \left( \frac{\partial E}{\partial N} \right)_{v(\mathbf{r})} \quad (18.2)$$

which is one of the pillars of conceptual density functional theory (DFT).

*Conceptual Density Functional Theory: Towards a New Chemical Reactivity Theory*, First Edition.

Edited by Shubin Liu.

© 2022 WILEY-VCH GmbH. Published 2022 by WILEY-VCH GmbH.

Going back to our focus, *chemical information*, we now turn to the second part of Equation 18.1: the changes in the energy with respect to the external potential at constant  $N$ .

Resorting to perturbation theory, the first-order correction to the ground-state energy  $dE^{(1)}$  due to a change in the external potential.  $V = \sum_i \delta v(\mathbf{r}_i)$ , is given by:

$$dE^{(1)} = \int \phi^{(0)*} V \phi^{(0)} d\mathbf{r} = \int \rho(\mathbf{r}) \delta v(\mathbf{r}) d\mathbf{r} \quad (18.3)$$

where  $\phi^{(0)}$  is the unperturbed wavefunction. We see that the second derivative in Eq. 18.1 is thus the electron density:

$$\rho(\mathbf{r}) = \left( \frac{\partial E}{\partial v(\mathbf{r})} \right)_N \quad (18.4)$$

While the chemical potential is a scalar, in this case, we have to handle a 3D scalar field,  $\rho(\mathbf{r})$ , which is significantly more intricate. Within given families of compounds, where the 3D distributions are transferable and the particle number (charge, spin multiplicity) remains constant, the external potential might be enough to develop phenomenological models. In other cases, the analysis of the electron density is needed to interpret structure and reactivity.

In what follows, we will first review how to analyze the electron density, which provides access to thermodynamic properties by virtue of being directly connected to the energy. Then we will show how this information can be enriched by other density-derived quantities, also present in DFT. Finally, we will briefly explain how this information can be even exploited to understand errors in routine electronic structure calculations.

## 18.2 The Electron Density

### 18.2.1 General Shape

A beautiful example of the connection between the electron density and the energy can be constructed on the basis of very simple arguments. It is known that the wavefunction must have a derivative discontinuity on top of the nuclear positions  $\mathbf{R}_i$  for all nuclei  $M_i$  with nuclear charge  $Z_i$  (we refer the reader to Ref. [3] for details on the electron–electron coalescence cusp). Thus, the electron density must present this cusp as well. In this sense, Kato’s cusp condition states that when  $\mathbf{r} = \mathbf{R}_i$ :

$$\frac{d\bar{\rho}(\mathbf{r})}{d\mathbf{r}} = -2\bar{\rho}(\mathbf{r})Z_i \quad (18.5)$$

where  $\bar{\rho}$  is the electron density spherically averaged around  $\mathbf{R}_i$ . Equation (18.5) is valid for Coulomb systems assuming the Born–Oppenheimer approximation and point-like nuclei.

It is thus possible to deduce the positions of all nuclei strictly from the electron density as cusps in  $\rho(\mathbf{r})$ , the nuclear charges through derivatives as in Eq. (18.5), and the number of electrons  $N$  by integration  $N = \int \rho(\mathbf{r}) d\mathbf{r}$ . In this sense, note that the Hamiltonian of the system is completely determined just from the exact electron density  $\rho$  [4].



This is generalized to other potentials as per the Hohenberg–Kohn theorems, but the argument above, as given originally by Bright-Wilson, is a very good example on how relevant information of the system can be extracted directly from the electron density.

Beyond the maxima, the general shape of the electron density can be understood from the analysis of atomic behavior and its superposition [5]. For an atom,  $A$ , the value of the density at the nucleus can be related to its nuclear charge,  $Z_A$ , as seen before:

$$\lim_{\mathbf{r} \rightarrow \mathbf{R}_A} \left[ \frac{\delta}{\delta \mathbf{r}} + 2Z_A \right] \bar{\rho}(\mathbf{r}) = 0, \quad (18.6)$$

where  $\bar{\rho}(\mathbf{r})$  is once again the spherical average of  $\rho(\mathbf{r})$ . When going away from the nucleus of  $A$ ,  $\rho$  experiences an exponential decay that is related with the first ionization potential of the system,  $I$ :

$$\rho(\mathbf{r}) \propto e^{-2\sqrt{I}|\mathbf{r}|} \quad (18.7)$$

Further away, the electron density tends asymptotically to 0:

$$\rho(\mathbf{r} \rightarrow \infty) = 0 \quad (18.8)$$

In a molecular system, the overall shape of the electron density is dictated by the position of the nuclei (external potential), so that the final density presents cusps at all nuclear positions (related to their respective  $Z$ ). In this sense, in Figure 18.1, it can be seen how all the main features of the electron density are dictated by the position of the constituent atoms for the LiH molecule. Note the two nearly perfect exponentially decaying cusps in the inset, with the cusps located at the atomic positions.

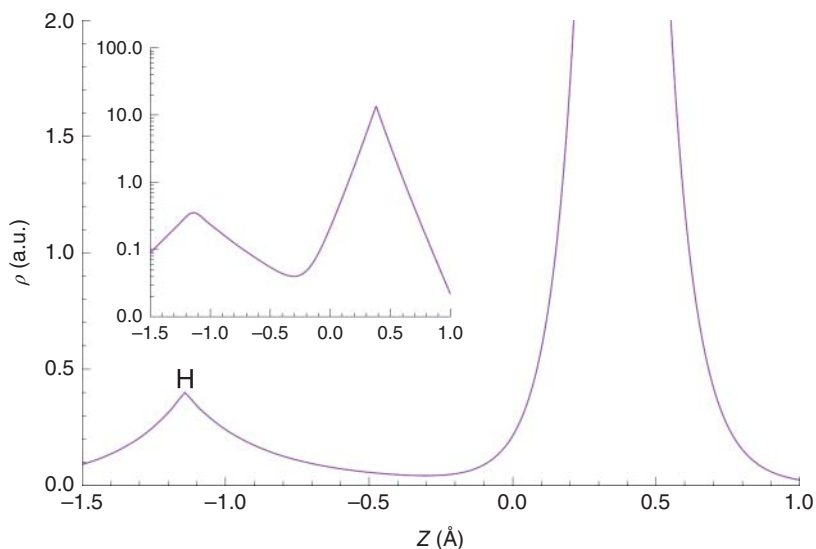


**Figure 18.1** Electron density in a.u. along the line connecting Li and H in the LiH molecule. The *inset* has a logarithmic *y*-axis to convey the exponential nature of the atomic cusps.

This illustrates what we saw above: the electron density enables identifying the position,  $\mathbf{R}_A$ , and nature of the atoms in the system,  $Z_A$ .

Notice that optimizing the wavefunction with an self consistent field (SCF) procedure leads to a relatively minor perturbation of the atomic densities. This feature is commonly used in crystallographic studies, where the initial atomic density is used as a first approximation to fit structure factors. Hence, these simple rules enable us to have a general picture of the electron density in a system. However, we need a finer analysis in order to retrieve general rules that we can relate to Chemistry. A simple framework to achieve this is proposed by the so-called quantum theory of atoms in molecules (QTAIM), as introduced by Bader and coworkers [6, 7].

### 18.2.2 Extracting Chemical Information: QTAIM

$\rho(\mathbf{r})$  is not a truly differentiable field, since there are cusps, not maxima, on top of nuclear positions. We can nevertheless build a topologically equivalent field (known as homeomorphic field) that is equal to  $\rho(\mathbf{r})$  at all points save small neighborhoods around the nuclei. In these small regions, we substitute the true non-differentiable density by an approximation showing a true local maximum. Note that this homeomorphic field is also naturally found when we introduce finite gaussian basis sets for computation (see for instance Figure 18.2).

Under these conditions, we can analyze the shape of  $\rho(\mathbf{r})$  with simple mathematical function analysis tools from the field of topology. This allows to retrieve valuable information about both atomic and bonding properties, stability, and chemical reactivity. This notion lies at the heart of the QTAIM framework that we will summarize in this section.

From Figure 18.1, we had identified the cusps which are now assumed as maxima as associated with a nuclei. For this reason, these maxima are called nuclear critical points (NCPs). If we now look closer into Figure 18.3, we can see that the density gradient is able to detect the fact that there is an interaction between atoms. Indeed, the existence of bonding interactions can also be derived directly from the electron density as well. First-order saddle points of the electron density, also known as bond

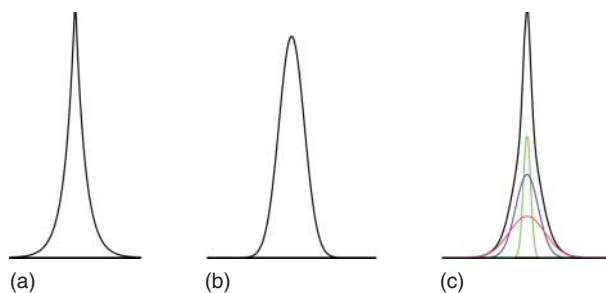


**Figure 18.2** Shape of the approximate homeomorphic  $\rho(\mathbf{r})$  cusp surrounding a nucleus, as given by a basis set composed of (a) Slater-type functions, (b) Gaussian-type functions, and (c) contracted Gaussian-type functions, where the individual Gaussian functions are shown colored.

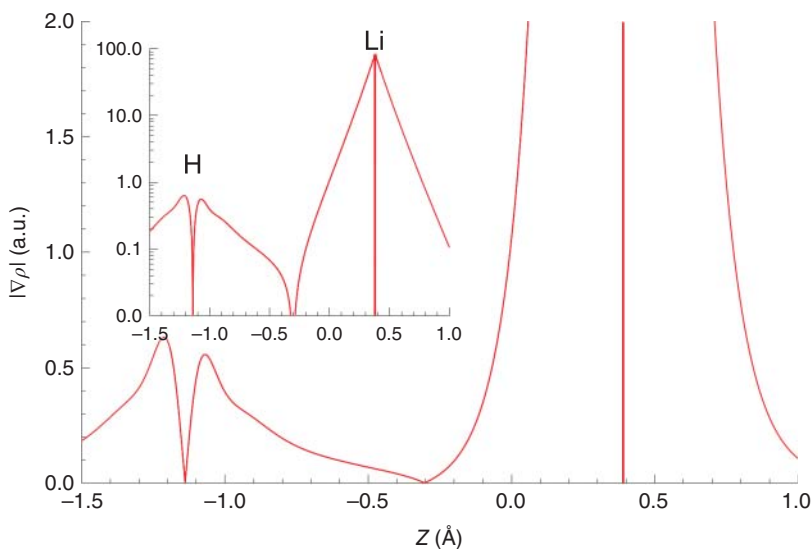


**Figure 18.3** Norm of the gradient of the electron density in a.u. along the line connecting Li and H in the LiH molecule. The *inset* has a logarithmic *y*-axis to convey the relative scale.

critical points (BCPs), appear in between bonded atoms. At the BCPs, the electron density is minimal along the bonding line and maximal across the perpendicular plane. This can be seen in Figures 18.1 and 18.4 for the simple LiH molecule, and by the existence of a point at which the gradient is 0 in Figure 18.3. In simple mathematical terms, a BCP represents the point in which the two exponentially decaying atomic densities intersect along the line that connects both nuclei.

In general, starting from the atomic densities, it is easy to showcase that the points in which the distinct atomic cusps intersect lead to saddle points of different order. The points of space in which the gradient of the density is 0, that is, the critical points (CPs) of  $\rho(\mathbf{r})$ , including NCPs and BCPs, are particularly interesting. The relationship between NCPs and the Bright-Wilson argument is evident at this point. As we will see, other CPs may require further consideration. We will analyze the different possibilities in Section 18.2.3.

### 18.2.2.1 Critical Points of the Electron Density

In order to characterize CPs of different nature (beyond NCPs and BCPs), we can analyze the components of the Hessian matrix of  $\rho(\mathbf{r})$  with respect to  $\mathbf{r} = (x, y, z)$  at the CP (Eq. (18.9)):

$$H(\rho, \mathbf{r}) = \begin{bmatrix} \partial^2 \rho / \partial x^2 & \partial^2 \rho / \partial x \partial y & \partial^2 \rho / \partial x \partial z \\ \partial^2 \rho / \partial y \partial x & \partial^2 \rho / \partial y^2 & \partial^2 \rho / \partial y \partial z \\ \partial^2 \rho / \partial z \partial x & \partial^2 \rho / \partial z \partial y & \partial^2 \rho / \partial z^2 \end{bmatrix} \quad (18.9)$$

In turn,  $H(\rho, \mathbf{r})$  can be diagonalized to produce three eigenvalues  $\lambda_1$ ,  $\lambda_2$ , and  $\lambda_3$ . The Laplacian of the electron density  $\nabla^2 \rho(\mathbf{r})$  is the sum of the diagonal elements of the Hessian. The standard notation for a CP is  $(r, g)$ , where the rank  $r$  is the number

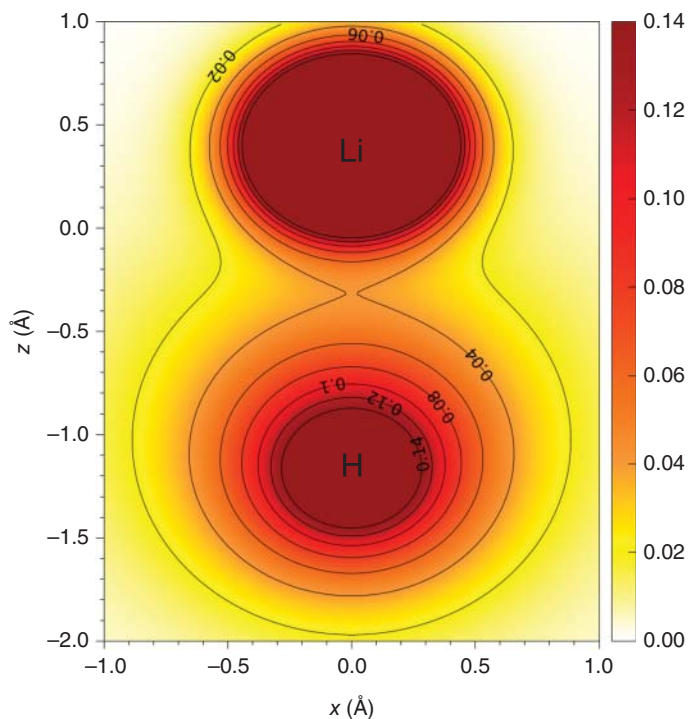


**Figure 18.4** Electron density in a.u. in the  $xz$  plane containing the LiH molecule. Note that the density is truncated to 0.14 a.u. in order to better showcase the relative magnitudes. For a complete scale, see Figure 18.1.

of nonzero eigenvalues  $\lambda_i$ , and the signature  $g$  is defined as  $\sum \lambda_i/|\lambda_i|$ . Four kinds of CPs of rank 3 (the most common ones) can be found in molecules, here listed by the aforementioned convention:

- (3,−3) points correspond to local maxima of  $\rho(\mathbf{r})$ , generally found in nuclear positions (recalling that nuclear cusps are assimilated to maxima). As previously indicated, they are often called nuclear critical points (NCPs).
- (3,−1) points correspond to a saddle point that is a maximum in two directions of space, and a minimum along the other orthogonal direction. They are associated with bonds, and hence called bond critical points (BCPs).
- (3,+1) points correspond to a saddle point that is a minimum in two directions of space, and a maximum in the other orthogonal direction. They are associated with the center of rings of covalent bonds and thus called ring critical points (RCPs).
- (3,+3) points correspond to local minima of  $\rho(\mathbf{r})$ , generally found in the center of cages of bonds. They are known as cage critical points (CCPs).

Note that representative examples of each kind of CP are provided in Figure 18.5.

Assuming that the atomic cusp of the electron density and its exponentially decaying tails are transferable, that is, an atom behaves similarly independently of the environment, the density and position of CPs uniquely determine the position

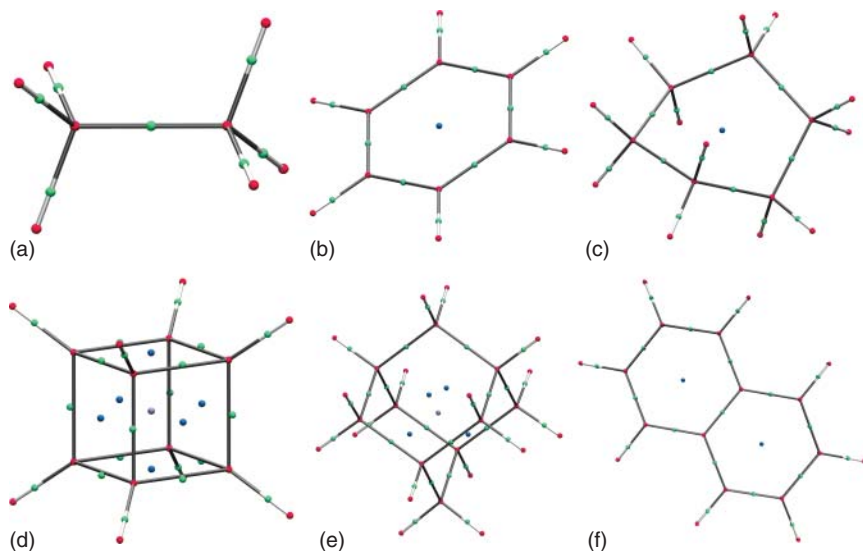


**Figure 18.5** CPs of  $\rho(\mathbf{r})$  for different molecules calculated at the HF/6-31G\* level: (a) ethane, (b) benzene, (c) cyclohexane, (d) cubane, (e) adamantane, and (f) naphthalene. CPs are shown as spheres. NCPs, BCPs, RCPs, and CCPs are colored red, green, blue, and violet respectively.

of the interacting atoms. While this is rigorously true if the density is strictly a superposition of atomic densities, the inference of molecular geometry from the CPs of the electron density is generally possible. Note that this is greatly advantageous, since this is a much reduced object than the  $\rho(\mathbf{r})$  scalar field.

The bundle of CPs of a molecular system, including the gradient paths that connect them, is often called a molecular graph. Indeed, it faithfully mimics the molecule by explicitly locating nuclei (NCPs) and interactions between them are represented by BCPs, RCPs, and CCPs. The particle number is implicitly included if the value of  $\rho(\mathbf{r})$  is given for each CP, as in a weighted graph. Molecular graphs thus allow to connect the electron density with one of the pillars of Chemistry: chemical structure.

Some molecular graphs are presented as an example in Figure 18.5. Most often, the gradient paths that connect NCPs and BCPs are almost strictly straight and match the least-distance connection between two bonded nuclei. Notable exceptions are strained bonds, in which the gradient path that connects BCPs and NCPs is slightly longer than the geometrical distance between nuclei. The difference between the two distances can be used as an indicator of strain for such contexts.

### 18.3 Electron Density-Derived Functions

The electron density has a direct connection with the energetics of the system through the Hohenberg–Kohn theorem. The Kohn–Sham (KS)-DFT formulation

sets  $F[\rho]$  as an implicit functional of the density (Eq. (18.10)):

$$F[\rho] = T_s[\rho] + E_H[\rho] + E_{xc}[\rho] \quad (18.10)$$

where  $E_H[\rho]$  is the Hartree functional and  $T_s[\rho]$  is the kinetic energy of the noninteracting KS system. This scheme simplifies the problem by setting the exchange–correlation functional  $E_{xc}[\rho]$  as the remaining piece to the exact  $F[\rho]$ . This means that the form encoded in  $E_{xc}[\rho]$  attempts to connect the density with the energy differences from the noninteracting system. This is the main goal of the vast number of approaches to new, and hopefully more accurate, density functional approximations (DFAs).

Generally speaking, DFAs are classified using Jacob’s ladder, which ranks them in terms of their degree of non-locality. The bottom three rungs are occupied by semilocal approximations of the form

$$E_{xc}[\rho] = \int \rho(\mathbf{r})\epsilon_{xc}[\rho(\mathbf{r})]d\mathbf{r}, \quad (18.11)$$

where  $\epsilon_{xc}$  is the exchange–correlation energy density per volume. According to the rung, this value is a function of the following functions [8]:

- First rung: The electron density,  $\rho$ , in the local density approximation (LDA),
- Second rung:  $\rho$  and its gradient,  $\nabla\rho$ , in the generalized gradient approximation (GGA), and
- Third rung:  $\rho$ ,  $\nabla\rho$  and the kinetic energy density and/or  $\nabla^2\rho$  in the meta-GGA approximation.

The reader will realize that the chemical information we have extracted up to now is related to the density and its gradient (first and second rungs above). Nevertheless, since the energetic description usually improves along the ladder, one could expect that the density-derived scalars used in third rung enables to extract more and richer information about the system. This is indeed the case. Many other scalar fields relevant for chemical interpretation are derived from semilocal DFAs. Among them, we can highlight the electron localization function (ELF) [9–11], the localized orbital locator (LOL) [12, 13], and the non-covalent interactions (NCI) index (i.e. the analysis of the reduced density gradient) [14] as some representative examples. We will review the chemical information of some of these functions in the coming Sections (18.3.1–18.3.3).

### 18.3.1 The Reduced Density Gradient

We have seen that the density gradient enables to extract structural information straight from the electron density (e.g. nuclear positions, chemical bonds). In DFT, the gradient is usually used in its reduced form,  $s(\mathbf{r})$ , in second rung functionals due to a second-order gradient expansion (GEA):

$$s(\mathbf{r}) = \frac{1}{C_s} \frac{|\nabla\rho(\mathbf{r})|}{\rho(\mathbf{r})^{4/3}}, \quad (18.12)$$

$$E_{xc}^{\text{GEA}} = E_x^{\text{LDA}} + \sum \int F(s)\rho^{4/3}(\mathbf{r})d\mathbf{r} \quad (18.13)$$

where  $C_s = 2(3\pi^2)^{1/3}$  and  $F(s)$  is a function of the reduced density gradient for a given spin. The  $4/3$  exponent of the density in the definition of  $s(\mathbf{r})$  ensures that it is a dimensionless quantity.

The electron density gradient is at the heart of the atoms in molecules (AIM) approach, since it becomes 0 at points where interactions are expected, such as BCPs. In fact, at any CP of  $\rho(\mathbf{r})$ , from Eq. (18.12) we see that  $s(\mathbf{r}) = 0$  by definition. Since by definition  $s \geq 0$ , CPs of  $\rho(\mathbf{r})$  are CPs of  $s(\mathbf{r})$ . However, this does not go both ways. Indeed, the reduced density gradient has a richer topology, and hence it contains more information than the gradient of the electron density.

CPs of  $s(\mathbf{r})$  that are not CPs of the electron density (i.e.  $\nabla\rho(\mathbf{r}) \neq 0$ ) occur whenever the following equality holds (Eq. (18.14)):

$$\frac{\nabla^2\rho(\mathbf{r})}{\rho(\mathbf{r})} = \frac{4}{3} \frac{(\nabla\rho(\mathbf{r}))^2}{\rho^2(\mathbf{r})}, \quad (18.14)$$

which requires a positive value for the Laplacian of  $\rho(\mathbf{r})$ . This is very convenient for DFAs in this rung, as information about the Laplacian can be derived purely from  $s(\mathbf{r})$ .

The inclusion of  $s(\mathbf{r})$  in DFAs can be interpreted chemically: it is a function that can detect interactions between atoms (i.e. deviations from exponential decay). The properties of  $s(\mathbf{r})$  have been investigated in depth in the process of developing increasingly accurate DFAs due to its deep relationship with the chemical region of the molecule (shells, bonds) [15–19].

Indeed, the reduced density gradient can be related to local density inhomogeneities:

- It takes large values in the exponentially decaying density tails far from the nuclei, where the density denominator approaches 0 more rapidly than the gradient numerator.
- Small values of  $s(\mathbf{r})$  occur throughout for the homogeneous electron gas (HEG), close to bonding regions, due to the presence of CPs, and in Lewis pairs, due to its relationship with the one-electron potential [20].

The effect of these inhomogeneities on the reduced density gradient is especially easy to visualize by plotting  $s(\mathbf{r})$  as a function of the density (Figure 18.6). Assuming a Slater-type behavior, it can be shown that graphs of  $s(\mathbf{r})$  vs.  $\rho(\mathbf{r})$  assume the form  $s(\mathbf{r}) = a\rho(\mathbf{r})^{-1/3}$ , where  $a$  is the Slater exponent. When there is overlap between atomic orbitals,  $s(\mathbf{r})$  goes to 0 and a characteristic spike appears in the  $s(\rho)$  diagram (see Figure 18.6 for an example, noticing the spike that appears for the dimer).

The reduced density gradient is related to the ratio between the Weizäcker kinetic energy density and the kinetic energy density of the HEG. As the first is the kinetic energy density of a single-orbital system and the latter is appropriate for independent particles, the ratio estimates the local relevance of electron pairing, bearing the name of  $t_{\text{bose}}$  [20], defined as:

$$t_{\text{bose}}(\mathbf{r}) = \frac{t_{\text{w}}}{t_{\text{HEG}}} = \frac{5}{6} s(\mathbf{r})^2 \quad (18.15)$$

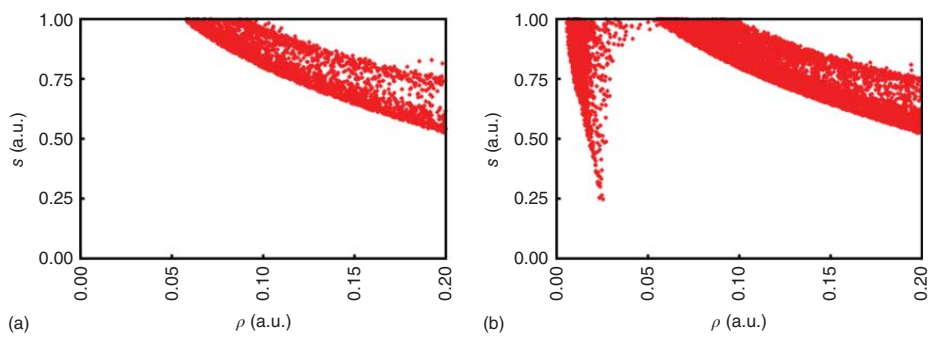


**Figure 18.6** 2D plot of  $s(r)$  against  $\rho(r)$  for (a) single water molecule and (b) water dimer.



where  $t_w$  is the von Weizsäcker kinetic energy density and  $t^{\text{HEG}}$  is the HEG value:

$$t_w = \frac{1}{8}(\nabla\rho(\mathbf{r}))^2\rho(\mathbf{r}) \quad (18.16)$$

$$t^{\text{HEG}} = \frac{3}{10}(3\pi^2)^{2/3}\rho(\mathbf{r})^{5/3} \quad (18.17)$$

Accordingly, the bosonic kinetic energy density  $t_{\text{bose}}$  reveals chemical features in situations when electrons behave like bosons: (i) paired electrons and (ii) where the density is very low. This can be visualized from the points forming  $s(\rho)$  isosurfaces with very low values of the function. Such 3D representations are able to reveal (i) Lewis features (covalent bonds, shells, and lone pairs) [21] and (ii) non-covalent bonds [14], including weak intramolecular non-covalent interactions [22]. Figure 18.7 shows the chemical features highlighted by the reduced density gradient in  $\text{N}_2$ . Core, lone pairs, and interatomic bonding regions may all be identified as minima of  $s(\mathbf{r})$ .

Nonetheless, the reduced density gradient is most commonly used to reveal non-covalent interactions, which are otherwise difficult to unravel. Consequently, the 3D analysis of  $s(\mathbf{r})$  is generally known as NCI [14]. Furthermore, these interactions are also very hard to identify from the geometry alone. Whereas covalent radii are very well defined for covalent bonds, non-covalent interactions cover a much wider range of radii and angles. In many cases, they are markedly non-pairwise, which further hampers identification (e.g.  $\pi$ -stacking interactions). The reduced density gradient is a very intuitive way to reveal them.

As an example, the reduced density gradient is able to provide intuitive insight into localized vs. delocalized interactions in a benzene crystal, as highlighted in Figure 18.8. Whereas localized CH–C interactions appear as a small atom-to-atom surfaces (C1–H3), delocalized CH– $\pi$  interactions, appearing as large flat surfaces, highlight the interaction of the hydrogen atom (H2) with the whole neighboring  $\pi$  system.

As previously discussed, DFAs in the first rung include mostly information about atoms, the second rung adds information about inhomogeneities and, to some degree, interactions between ideal atomic cusps. However, as we have also seen, by looking at the gradient we are not able to tell BCPs and RCPs from each other, for instance. That is, we are not able to characterize the CPs of  $\rho(\mathbf{r})$ . For instance, the

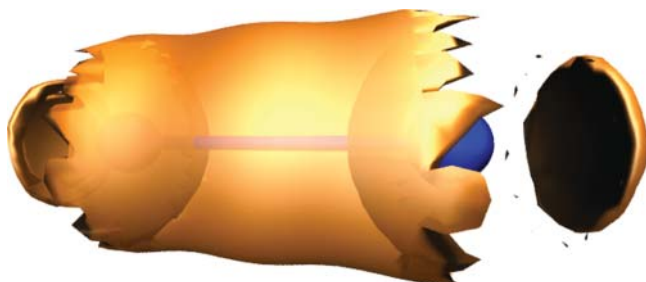


**Figure 18.7** Chemical features (bond and lone pairs) of  $\text{N}_2$  as revealed by  $s(\mathbf{r}) = 0.33$  with the isosurface colored orange. Critical points in nuclear positions are not shown.

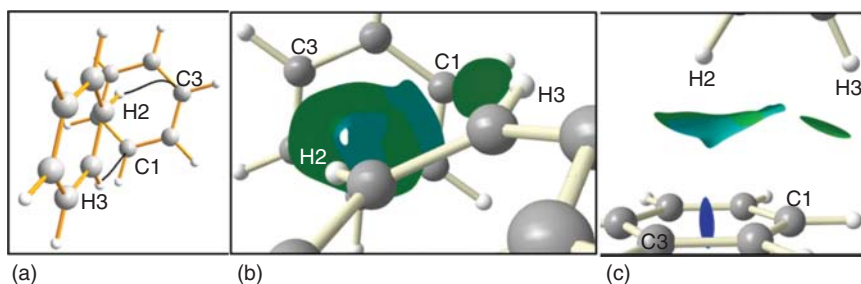


**Figure 18.8** (a) Bond paths (QTAIM); (b)  $s(\mathbf{r})$  for the intermolecular interactions in benzene crystal: localized CH–C interaction (small isosurface between C1–H3) and delocalized CH– $\pi$  interaction (bigger surface between H2 and the benzene ring of C3); and (c) lateral view of the T-shape CH– $\pi$  interaction. Reprinted with permission from Ref. [23].

local environment of a BCP between two heavy atoms and the NCP of a H atom might have the same values of density and gradient, which is a typical issue for the crystallographic determination of hydrogen atoms.

If we want to go further, we can look at higher rungs of Jacob’s ladder. DFAs in the third rung, known as meta-GGAs, include information on the Laplacian of the electron density and/or the kinetic energy density of the calculated Kohn–Sham orbitals. The first is an explicit functional of the density, while the latter is only an implicit functional of the density and requires Kohn–Sham orbitals to be computed.

### 18.3.2 The Laplacian of the Electron Density

As previously discussed, the position of nuclei and bonds are associated with CPs of the density. In a similar fashion, atomic shells, lone pairs, and other features are recovered from the Laplacian,  $\nabla^2 \rho(\mathbf{r})$ .

The main limiting behaviors for the Laplacian are the following:

- It tends to  $-\infty$  for  $\mathbf{r} \rightarrow \mathbf{R}_A$ . The behavior at the nuclei is given by:

$$\nabla^2 \rho(\mathbf{r}) = N e^{-Zr} \left( Z^2 - 2 \frac{Z}{r} \right) \quad (18.18)$$

where  $Z$  is the nuclear charge.

- Since the electron density falls exponentially to 0 at long distances, so does the Laplacian.
- In between these two asymptotes, the Laplacian in isolated atoms shows maxima and minima with spherical symmetry, which recover the number of shells. This chemical description in atomic shells is also maintained in ionic compounds.

The meaning of the Laplacian can also be understood from its relationship with the electron density gradient through the divergence theorem. According to the divergence theorem, the sign of the Laplacian of a scalar function indicates whether a net flux of the gradient of the scalar is entering (negative sign) or leaving (positive sign) an infinitesimal volume centered on a given point. Hence, the sign of the Laplacian of the density informs us on whether the electron density

is concentrating/compressing or diluting/expanding at a given point. From this, it is possible to infer a degree of charge depletion (accumulation) for a positive (negative) Laplacian [24].

Let us start from the local expression of the virial theorem,

$$\frac{1}{4}\nabla^2\rho(\mathbf{r}) = 2t(\mathbf{r}) + V(\mathbf{r}), \quad (18.19)$$

where  $t(\mathbf{r})$  is the positive definite kinetic energy density and  $V(\mathbf{r})$  is the potential energy density. Since  $t(\mathbf{r})$  is positive everywhere and  $V(\mathbf{r})$  is negative everywhere, the theorem states that the sign of  $\nabla^2\rho(\mathbf{r})$  determines which energy contribution, potential or kinetic, is in local excess relative to their average virial ratio of minus two. Thus, a negative Laplacian reveals that the potential energy is in local excess (electron sharing interactions), while a positive Laplacian denotes that the kinetic energy is locally prevailing (closed-shell interactions). Recall now that CPs of  $s(\mathbf{r})$  that are not CPs of  $\rho(\mathbf{r})$  mandate positive Laplacian values, and thus closed-shell interactions. This is in perfect agreement with the interpretation given before for non-covalent interactions, which we expect to involve little to no electron sharing.

Figure 18.9a highlights the ability of the Laplacian to reveal the shells in MgO: two for  $\text{Mg}^{2+}$  (K and L) and another two for  $\text{O}^{2-}$ . In covalent compounds, the valence becomes united (see  $\text{C}_2$  in Figure 18.9b). This different picture enables to distinguish bonding types in terms of the sign of the Laplacian [24]. It can be seen that in the first case (MgO) this leads to  $\nabla^2\rho > 0$  in the interatomic region, whereas  $\nabla^2\rho < 0$  for  $\text{C}_2$ , as expected from their respective bonding regimes.

### 18.3.3 Kinetic Energy Densities

Due to the ability of the first-order density matrix to reveal nonlocal effects, kinetic energy densities are a good option to convey extra bonding information and nonlocal information. Since the kinetic energy density is not uniquely defined, the positive definite option,  $t$ , is preferred for bonding analysis, since it is easier to interpret:

$$t(\mathbf{r}) = \frac{1}{2}(\nabla \cdot \nabla')\Gamma_1(\mathbf{r}; \mathbf{r}')|_{\mathbf{r}'=\mathbf{r}} \stackrel{\text{D}}{=} \frac{1}{2}\sum_i (\nabla\psi_i(\mathbf{r}) \cdot \nabla\psi_i^*(\mathbf{r})) \quad (18.20)$$

where  $\Gamma_1(\mathbf{r}; \mathbf{r}')$  is the first-order density matrix and “D” refers to monodeterminantal wavefunctions. As we have seen before when discussing the gradient, we can expect the kinetic energy density to be maximal near nuclei. This is quite uninteresting per se. It is often more insightful to calculate the ratio between the kinetic energy density and a reference, to see whether the electrons have more or less kinetic energy density than this reference.

#### 18.3.3.1 LOL

The LOL,  $v_{\text{LOL}}$  [12], introduced by Schmider and Becke, is defined as:

$$v_{\text{LOL}} = \frac{t^{\text{HEG}}}{t}, \quad (18.21)$$

where the HEG value is used as a reference. This eliminates the  $\rho^{5/3}$  dependence of the kinetic energy density which would otherwise hide valence characteristics due to the greater core densities [25, 26].

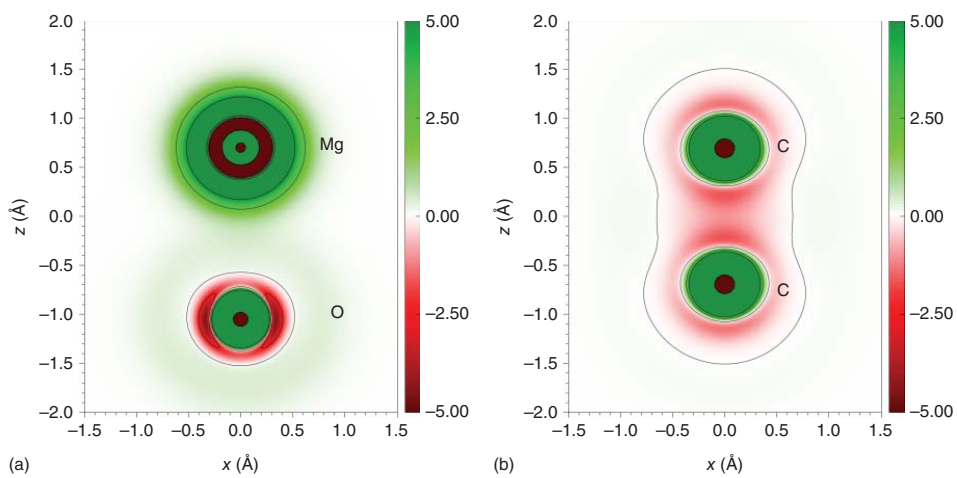


**Figure 18.9**  $\nabla^2\rho(\mathbf{r})$  in a.u. on the  $xz$  plane that contains the nuclei for (a) MgO and (b)  $C_2$ . Note that Laplacian values are truncated to  $\pm 5$  a.u. to avoid cluttering.

Since  $v_\sigma$  is bounded by 0 from below, but has no upper boundary, a Lorentzian mapping is usually used, so that the index,  $\eta_{\text{LOL}}$  runs from 0 to 1:

$$\eta_{\text{LOL}}(\mathbf{r}) = \frac{v_{\text{LOL}}}{1 + v_{\text{LOL}}} = \frac{1}{1 + v_{\text{LOL}}} \quad (18.22)$$

The name LOL owes to the ability of such a function, which identifies whether a point in space  $\mathbf{r}$  can be described by a localized orbital:

- At the positions of the stationary points of localized orbitals,  $v_{\text{LOL}}$  is driven to small values ( $\eta_{\text{LOL}} \rightarrow 0$ ).
- In regions dominated by the overlap of localized orbitals,  $v_{\text{LOL}}$  attains large values ( $\eta_{\text{LOL}} \rightarrow 1$ ).

This leads to a distribution of maxima and minima that reveals atomic shell structure and bonding patterns in 3D [12, 13]. Moreover, given its connection with localization, it is also able to reveal multicenter delocalization when averaged over atomic basins [27].

Figure 18.10 shows the evolution of  $\eta_{\text{LOL}}$  along the internuclear plane of the  $\text{CO}_2$  molecule. As it can be seen, the function identifies the position of the cores, the bond in between them and the lone pairs at each side.

### 18.3.3.2 ELF

The two previously introduced kinetic energy density measures (LOL and  $s$ ) constitute the chemical information used to construct another very well-known topological index, the ELF [9]. Its kernel,  $\chi_{\text{ELF}}$ , according to Savin's interpretation is given by [11]:

$$\chi_{\text{ELF}} = \frac{t - t_w}{t_{\text{HEG}}} = v_{\text{LOL}}^{-1} - t_{\text{bose}} \quad (18.23)$$

The numerator in Eq. (18.23) is sometimes called Pauli kinetic energy density  $t_p(\mathbf{r}) = t(\mathbf{r}) - t_w(\mathbf{r})$ . Indeed, the difference between the Kohn–Sham kinetic energy

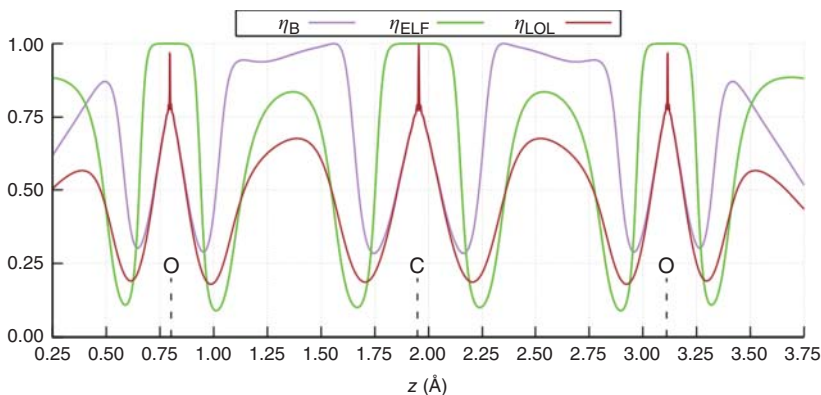


**Figure 18.10** Scaled bosonic kinetic energy density  $\eta_{\text{B}} = (1 + t_{\text{bose}})^{-1}$  (purple, Eq. (18.15)),  $\eta_{\text{ELF}}$  (green, Eq. (18.24)), and  $\eta_{\text{LOL}}$  (red, Eq. (18.22)) along the internuclear axis of the  $\text{CO}_2$  molecule.

density and the Weiszäcker one can be likened to the influence of Pauli's exclusion principle. Note here that  $t_{\text{bose}} = 5/6s^2$ . Due to the Pauli principle, electrons (fermions) are faster in average than if they were bosons. Hence,  $t_w$  is a lower limit for  $t$ , and  $t_{\text{bose}}$  is a lower limit for  $v_{\text{LOL}}^{-1}$ .

In other words, ELF is a very helpful tool to reveal Pauli behavior and its local effects on the kinetic energy. Just like in the case of LOL, the kernel of ELF is re-scaled to provide a bound function:

$$\eta_{\text{ELF}}(\mathbf{r}) = \frac{1}{1 + \chi_{\text{ELF}}(\mathbf{r})^2} \quad (18.24)$$

Since Pauli repulsion leads to electron pairing and localization, the following features can be observed in 3D representations of  $\eta_{\text{ELF}}$ :

- The upper limit,  $\eta_{\text{ELF}}(\mathbf{r}) = 1$ , corresponds to perfect localization. In general, maxima of  $\eta_{\text{ELF}}$  (although not necessarily  $\eta_{\text{ELF}}(\mathbf{r}) = 1$ ) are identified with regions of high electron localization, such as cores, lone pairs, and covalent bonds.
- The value  $\eta_{\text{ELF}}(\mathbf{r}) = 1/2$  corresponds to HEG-like behavior.
- When  $\eta_{\text{ELF}}$  tends to 0, we are in a boundary region between localization domains.  $\eta_{\text{ELF}}$  values at the saddle points have been shown [28, 29] to be related to the delocalization between fragments via the overlap of the relevant orbitals involved in the interaction.

This has been highlighted in Figure 18.10, where  $t_{\text{bose}}$  (purple line) has been plotted along with LOL (red line). In order to follow the same mapping,  $t_{\text{bose}}$  has also been scaled:  $\eta_B = 1/(1 + t_{\text{bose}})$ . Note that  $\eta_{\text{LOL}} \geq \eta_B$  at all points. In spite of some differences in the slopes, the different kinetic energy density-based functions are topologically equivalent in most cases and thus they reveal similar chemical features.

However, the pictures from Pauli's kinetic energy density are clearer. As a representative example, Figure 18.11 highlights ELF's ability to discern localization domains in  $\text{N}_2$ , simply by representing its isosurfaces (compare to Figure 18.7). Small, nearly spherical surface appear at the N cores, and larger basins bound the N–N triple bond and the lone pairs. It looks very similar to the LOL (and even to the  $s$  picture).

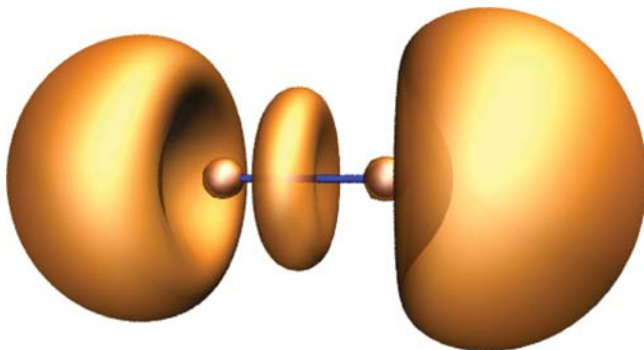


**Figure 18.11** Chemical features (cores, bond, and lone pairs) of  $\text{N}_2$  as revealed by  $\eta_{\text{ELF}}(\mathbf{r}) = 0.8$  with the isosurface colored orange.

The biggest advantage of ELF vs. other scaled kinetic energy densities is that it is soundly rooted on the Pauli principle. Hence, the topology of ELF renders a quantitative Lewis picture of chemical systems. It is also well behaved and smooth. But what is most important, it has been shown to recover the Aufbau principle for shell filling along the periodic table [30]. This is not possible with LOL nor with  $s$ .

More explicitly, we can expand the expression for  $\chi(\mathbf{r})$ , so that the  $\eta_{\text{ELF}}$  reads as:

$$\eta_{\text{ELF}}(\mathbf{r}) = \frac{1}{1 + v_{\text{LOL}}^{-2}(\mathbf{r}) + t_{\text{bose}}^2(\mathbf{r}) + 2v_{\text{LOL}}^{-1}(\mathbf{r})t_{\text{bose}}(\mathbf{r})} \quad (18.25)$$

from which we can easily see that  $\eta_{\text{ELF}}(\mathbf{r}) = 1$  only whenever  $v_{\text{LOL}}^{-1}(\mathbf{r}) = t_{\text{bose}}(\mathbf{r})$  or  $\eta_{\text{bose}}(\mathbf{r}) = \eta_{\text{LOL}}(\mathbf{r})$ . This will only happen in one-orbital regions. Localization, as given by  $v_{\text{LOL}}(\mathbf{r})$ , might be arbitrarily large or small in this sense.

However, if  $v_{\text{LOL}}(\mathbf{r})$  is very large, that is, the kinetic energy density of the system is very small compared to that of the HEG, then  $v_{\text{LOL}}^{-1}(\mathbf{r})$  will be very small. As we saw in Figure 18.10,  $t_{\text{bose}}(\mathbf{r})$  is a lower bound of the latter, and therefore  $\eta_{\text{ELF}}(\mathbf{r}) \approx 1$  forcefully. In this sense, the ELF measures localization due to fermionic character but also localization that has to do strictly with the kinetic energy density itself.

On the other hand,  $\chi(\mathbf{r})$  will be large whenever the system has a character that is significantly different from the single-orbital model in a way that is significant compared to the homogeneous kinetic energy density for that region. Then,  $\eta_{\text{ELF}}(\mathbf{r}) \rightarrow 0$ . Hence,  $\eta_{\text{ELF}}(\mathbf{r})$  is often said to be maximal (i.e. nearly 1) for spin-paired regions, minimal (nearly 0) for spin-unpaired regions, and takes the value 1/2 when the system resembles the localization of the HEG model.

This must be kept in mind. For instance, in isolated atoms, several local maxima of  $\eta_{\text{ELF}}(\mathbf{r})$  arise, describing electronic shells. For reference, the  $\eta_{\text{ELF}}(\mathbf{r})$  profiles of the C and O atoms (in two multiplicities each) are collected in Figure 18.12.

Note how the trend on the  $\eta_{\text{ELF}}(\mathbf{r})$  values of the second shell invert when passing from C to O: in the O atom it could be suggested that the higher values of  $\eta_{\text{ELF}}(\mathbf{r})$  for the second shell for the  $S = 1$  situation are due to an increased electron pairing. This

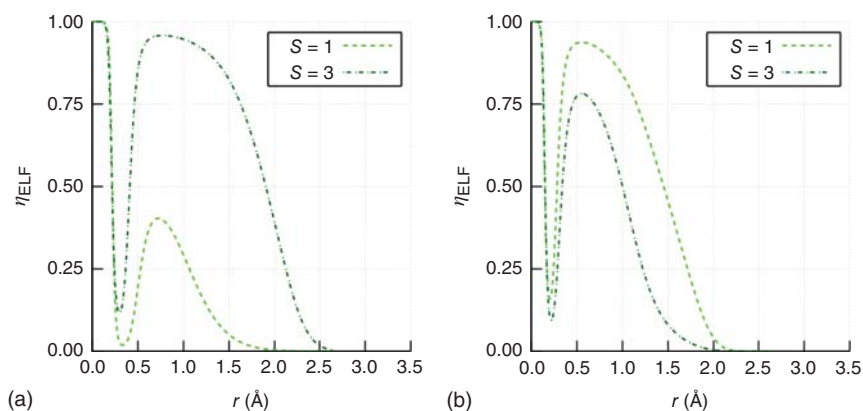


**Figure 18.12**  $\eta_{\text{ELF}}(\mathbf{r})$  a.u. along the distance  $r$  to the nuclear position of: (a) carbon atom and (b) oxygen atom. Data calculated at the CCSD/cc-PVTZ level.

is shown to be inconsistent in the case of C, and hence not true. Let this example showcase how the interpretation of the ELF solely in terms of electron pairs, if used acritically, might lead to important errors.

## 18.4 Assessing the Quality of Chemical Information

It is clear from Section 18.3 that increasing the sources of information enhances the flexibility, and thus the performance, of the various DFAs, allowing them to reproduce features that are beyond simpler approaches. However, extensive parametrization can also translate into an artificially good performance, at the expense of the underlying physical meaning of the DFA. It is worth wondering how do these parametrizations translate in the electron density and the other derived functions we have seen, and the chemical information they convey.

As previously explained, DFT typically proceeds in two steps. First, one obtains a well-behaved system wavefunction that satisfies the Kohn–Sham equations under the chosen exchange–correlation potential, and then the energy is evaluated from the electron density derived from the aforementioned wavefunction. Unfortunately, only the *exact* functional would provide the *exact* ground state energy for the *exact* ground state density  $\rho$ , and for approximate DFAs, there is not any guarantee that this process leads to a proper density or wavefunction. As a consequence, a wrong parametrization might lead to good energy results at the expense of accuracy in  $\rho(\mathbf{r})$ —and its derived scalar fields. Recall that  $\rho(\mathbf{r})$  can be expressed as the derivative of the total energy with respect to the external potential with a constant number of electrons  $N$ . This way, it is straightforward to understand that a DFA fitted to reproduce the absolute energy may be inaccurate for the derivatives of the energy, and thus provide inaccurate densities. In the coming Sections (18.4.1 and 18.4.2), we will provide some general (local and global) descriptors to understand the errors introduced by various DFAs in the chemical description of a system, so that the reader is aware of the deviations expected depending on the functional used in the calculation. We note beforehand that we will focus in covalently bound molecular systems, first and foremost, due to the impossibility of tackling the myriad of situations that might arise in computational modeling endeavors.

### 18.4.1 Electron Density Errors

In general,  $\rho(\mathbf{r})$  has been shown to be very robust with respect to the calculation level [31], as different methodologies translate into relatively small differences in the density [32]. This is in line with the fact (see above) that most properties of the electron density are determined directly from the atomic constituents.

There are many ways of identifying and quantifying the density error of a given DFA, such as the analysis of the radial distribution function of  $\rho$  [33] and the decomposition of the total error into hypothetical functional and a density contributions [34].



Another way of evaluating the quality of the density of a given molecular geometry would be the density difference function. Since the CCSD(T) methodology provides a good reference density and energy, as well as dipole moments, we may take it as the reference method, which avoids the use of the much more expensive full configuration interaction (FCI). This way, near the basis set limit, we can define  $\rho_{\text{diff}}(\mathbf{r})$  as:

$$\rho_{\text{diff}}(\mathbf{r}) = \rho_{\text{CCSD(T)}}(\mathbf{r}) - \rho(\mathbf{r}) \quad (18.26)$$

In order to avoid error compensation between positive and negative regions, the following global descriptor might be useful:

$$\Lambda_{\text{diff}} = \int |\rho_{\text{diff}}(\mathbf{r})| d\mathbf{r} \quad (18.27)$$

This scheme based on the use of  $\rho_{\text{diff}}(\mathbf{r})$  is robust from the integration point of view, and advantageous from the sampling perspective, as it captures the points in which the density error is effectively 0 without including new artificial ones.

Let us take the CO molecule calculated using HF and the PBE DFA at a fixed geometry as an example. The robustness of  $\rho(\mathbf{r})$ , in conjunction with its prevalence near nuclei, implies that distributions do not change much qualitatively. Note that  $\rho_{\text{diff}}(\mathbf{r})$  is maximal near nuclear positions, as presented in Figure 18.13, which is somehow expected, as most of the density is surrounding the nuclei.

Nonetheless, the error in relative terms is in general more important for bonding regions than for core regions, as chemical features (bonds and lone pairs) are dictated by very small density values that spread over large regions of space. This is shown in Figure 18.14 for the CO molecule. Namely, the relative error near the nuclei is less than 0.5%, while it can be more than 10% in certain chemically meaningful regions. This highlights the necessity of focusing in the valence region and the descriptors of localized electrons we have previously introduced if we want to understand (preferably in advance) the density errors we can expect from a calculation.

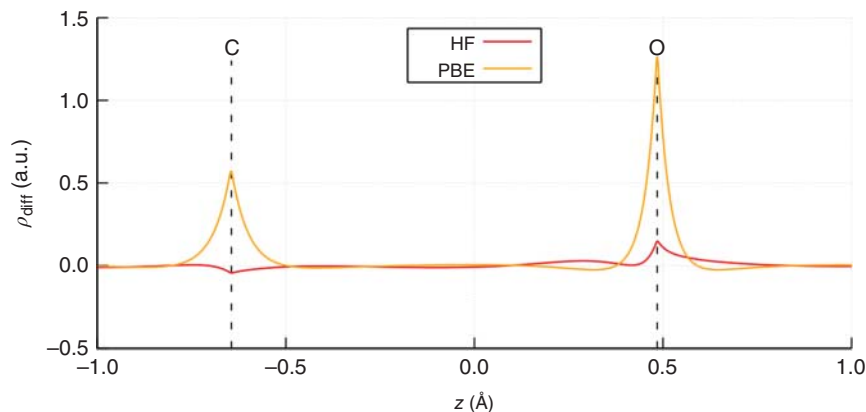


**Figure 18.13**  $\rho_{\text{CCSD(T)}}(z) - \rho(z)$  along the internuclear axis of CO. Calculated with different methods and the cc-PVDZ basis set. Dashed lines indicate the position of nuclei.

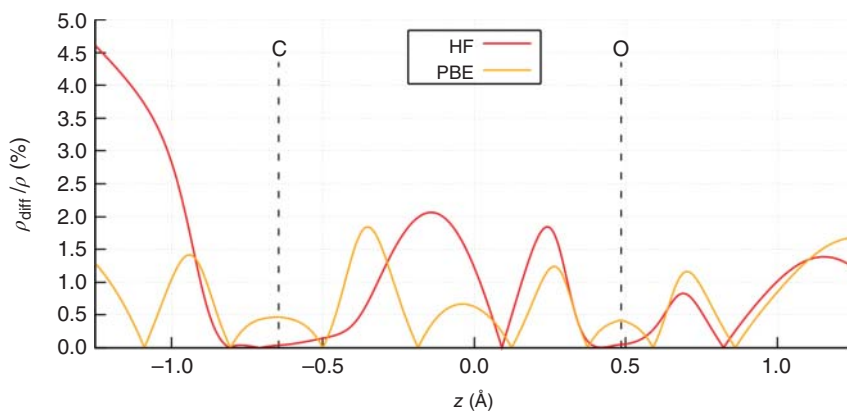


**Figure 18.14**  $\rho_{\text{diff}}$  (Eq. (18.26)) as a percentage of  $\rho_{\text{CCSD(T)}}(z)$  along the internuclear axis of CO. Calculated with different methods and the cc-PVDZ basis set. Dashed lines indicate the position of nuclei.

#### 18.4.2 Electron Localization Errors

We have seen that the density errors are larger (in relative terms) in valence regions than in core regions, and we know that valence regions are more chemically interesting. This puts forward the necessity of evaluating the quality of  $\rho(\mathbf{r})$  in localized regions of space, rather than globally. For that, we can resort to some of the previously introduced topological descriptors, given their ability to identify and characterize the various chemical regions of space. Namely, we will focus on the ELF and LOL as defined in Section 18.3.3.

As previously explained, when the kinetic energy density of the system is equivalent to that of an HEG of the same density  $\eta_{\text{LOL}}(\mathbf{r}) = 1/2$ . In this regard,  $\rho_{\text{diff}}(\mathbf{r})$  over the  $xz$  plane together with  $\eta_{\text{LOL}}(\mathbf{r}) = 1/2$  contours for the  $\text{N}_2$  molecules are provided in Figure 18.15. First of all, it should be noticed that the LOL isosurfaces reveal a distinct excess or defect of electron density depending on the method (with respect to CCSD(T), i.e. they match a  $\rho_{\text{diff}}(\mathbf{r}) = 0$  isosurface), providing very good guides on the expected errors in terms of chemical information.

The results highlight the differences observed in  $\rho_{\text{diff}}$  depending on the model Hamiltonian. HF accumulates more density than it should in the bonding region, while local bonds in local semilocal DFAs have a deficit of electron density in covalent bonds. Moreover, the LDA, GGA, and hybrid representatives (SVWN3, PBE, and TPSSh) exhibit increasing quality while following the same trend, according to which  $\rho(\mathbf{r})$  is higher than the reference one in the core region and spreads in a relatively smooth way compared to HF. Notice that hybrid DFAs are in general in between HF and local DFAs, thus providing a better density, which is expected, as HF and LDAs show clear opposite trends and represent opposite extreme Hamiltonians, so they should somehow compensate each other.

Interestingly, M06-2X shows a different error distribution over the plane, further away from just being in between HF and GGA. This result indicates that M06-2X parametrization allows for a high flexibility with respect to a simpler DFA, but it also

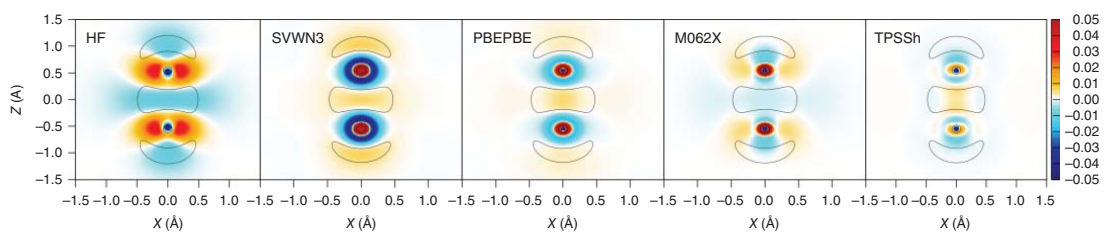


**Figure 18.15** Electron density difference ( $\rho_{diff}(\mathbf{r})$ , Eq. (18.26)) maps on the  $\sigma_v$  planes of the  $N_2$  molecule at  $R_{eq} = 1.0984 \text{ \AA}$ .  $\eta_{LOL}(\mathbf{r}) = 0.5$  isolines are shown in black. Methods are detailed in the top left corners, left to right: HF, SVWN3, PBEPBE, M06-2X, and TPSSh. Basis set is aug-cc-pCVQZ in all cases. Reproduced from Ref. [35] with permission from the PCCP Owner Societies.

**Table 18.1** Descriptors for the respective equilibrium geometries of CO.

Method	Pop. $\Omega_b$	Vol. $\Omega_b$	$R_{eq}$	$\omega_h$
PBEPBE	3.0110	59.09	1.1353	2162.47
BLYP	2.9835	54.84	1.1355	2161.34
B3LYP	3.0874	62.45	1.1237	2251.95
mPW1LYP	3.1014	63.45	1.1218	2266.82
HF	3.3040	74.56	1.1019	2426.46
SVWN3	3.0607	59.65	1.1255	2237.59
CCSD(T)	3.0741	71.51	1.1294	2168.92

Source: Population of  $\Omega_b$  in electrons, volume of  $\Omega_b$  in a.u.<sup>-3</sup>, equilibrium distances ( $R_{eq}$ ) in Å, harmonic frequencies ( $\omega_h$ ) in cm<sup>-1</sup>, and atomization energies ( $\Delta E_{atom}$ ) in kcal mol<sup>-1</sup>.

implies a less predictable behavior. Overall, and especially if one analyzes a larger dataset, we can suggest that *some* DFAs localize errors in an intuitive way, while others do not [35]. Hence, for chemical information analyses, the use of functionals with a small number of parameters, and higher upon Jacob's ladder, are expected to provide more accurate and reproducible results. In the case of non-hybrid functionals, underestimating the bonding density in covalent bonds is to be expected.

In order to quantify this effect, we can calculate the ELF population of a given covalent bond as given by integral of the electron density over the bonding basin  $\Omega_b$ . This is a powerful tool to reveal the effect of the DFA choice in chemical bonds. To better illustrate the discussion, we show the bond populations for the CO molecule calculated with HF and a set of DFAs in Table 18.1. As expected, HF provides the most populated bonds, while those derived from PBE and SVWN3 are less populated than the CCSD(T) reference, due to the delocalization error; and higher rungs DFAs yield bonding densities in between. We can expect the exact FCI result to be in between as well.

Another interesting point is that *local* errors in some regions are not directly related with the global performance of a given DFA, at least to those given by  $\Lambda_{diff}$ . In order to illustrate it, Figures 18.16 and 18.17 show analogous calculations for the CO and C<sub>2</sub>H<sub>6</sub> molecules. It can be seen at first glance that some DFAs bearing quite similar  $\Lambda_{diff}$  values have significantly different error localization patterns (e.g. BHandH and M05-2X in CO). Moreover,  $\Lambda_{diff}$  increases significantly on average when moving from CO and N<sub>2</sub> (two atoms, and thus two cusps in  $\rho$ ) to C<sub>2</sub>H<sub>6</sub> (eight cusps in  $\rho$ ), in spite of the whole set having the same number of electrons, as more cusps (on which the error is maximal) implies higher  $\Lambda_{diff}$ . This clearly showcases that global descriptors are pretty weak in terms of transferability and recalls once again the need to stay in 3D, not only for chemical interpretation, but also for predicting the errors we should expect in their calculation.

Note that there are many DFAs close to the CCSD(T) result, which thus provide very accurate results at a significantly lower cost, while some hybrids (especially

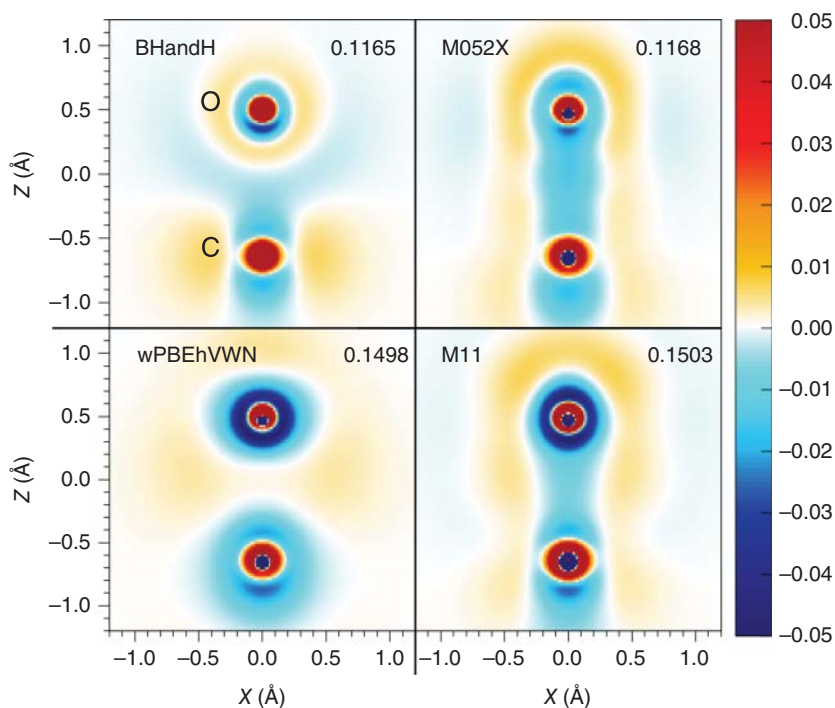


**Figure 18.16** Electron density difference ( $\rho_{\text{diff}}(\mathbf{r})$ , Eq. (18.26)) maps on the  $\sigma_v$  planes of the CO molecule at  $R_{\text{eq}}$ . Methods are detailed in the top left corners, left to right and top to bottom: BHandH, M05-2X, wPBEhVWN, and M11. Their values of  $\Lambda_{\text{diff}}$  are: 0.1165, 0.1168, 0.1498, and 0.1503 a.u. respectively. Basis set is aug-cc-pCVQZ in all cases. Reproduced from Ref. [35] with permission from the PCCP Owner Societies.

those with a high percentage of exact exchange) exhibit an expected tendency to approach the HF result.

## 18.5 Summary and Conclusions

Along this chapter, we have highlighted the need to resort to 3D scalar fields in order to gather chemical information from a system. The electron density, through its connection with the energy (both in DFAs themselves and linked to conceptual DFT) provides very valuable information to understand both structure and reactivity.

After a brief overview of its fundamentals, we have also shown the potential of other scalar functions, also present in DFT development, to reveal the Chemistry of molecular species. Functions such as the reduced density gradient, the ELF, or the LOL provide nonlocal information to various DFA formulations and can be used to gain intuitive insight about bonding and chemical structure – or vice versa. Finally, given the recent attention paid to the lackluster description of the electron density given by certain DFAs, we have put forward a detailed analysis of the errors the reader might encounter when resorting to these functions from the DFT framework.

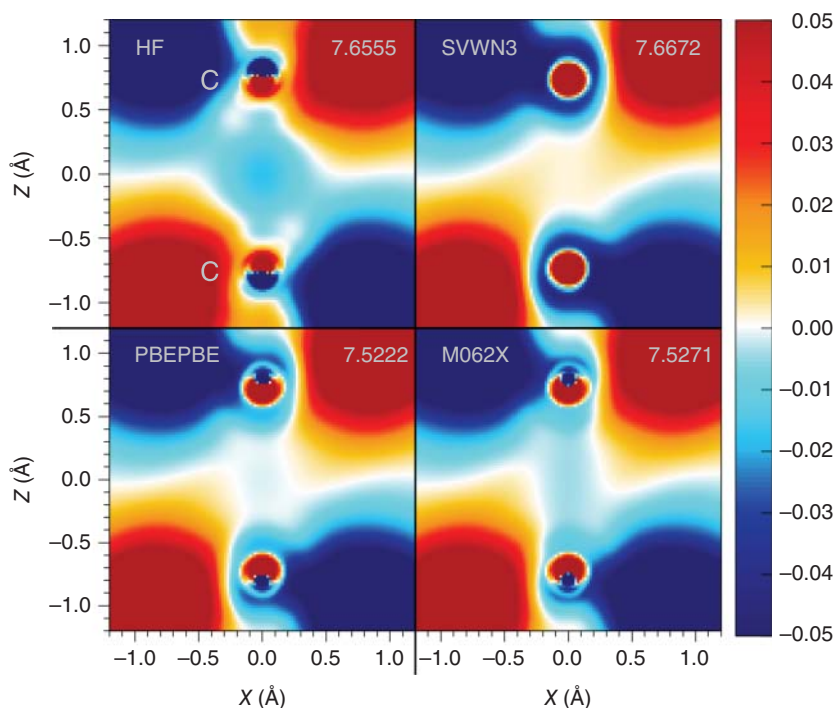


**Figure 18.17** Electron density difference ( $\rho_{\text{diff}}(\mathbf{r})$ , Eq. (18.26)) maps on the  $\sigma_v$  planes of the ethane  $\text{C}_2\text{H}_6$  molecule at  $R_{\text{eq}}$ . Methods are detailed in the top left corners, left to right and top to bottom: HF, SVWN3, PBEPBE, and M06-2X. Their values of  $\Lambda_{\text{diff}}$  are: 7.6555, 7.6672, 7.5222, and 7.5271 a.u., respectively. Basis set is aug-cc-pCVQZ in all cases. Reproduced from Ref. [35] with permission from the PCCP Owner Societies.

General guides of the expected errors and their localization have been given, albeit we duly note that different bonding regimes interact with the self-interaction error differently as well.

Overall, the information in the electron density and DFT-derived functions can provide very rich and subtle information on systems. Just now, its relevance for functional development is also seeing the light. Hopefully the knowledge accumulated on their analysis from the 3D point of view will also help to improve the DFT approaches from which they stem, thus completing a scientific feedback loop.

## Bibliography

- 1 Rupp, M., Tkatchenko, A., Müller, K.-R., and von Lilienfeld, O.A. (2012). *Phys. Rev. Lett.* 108: 058301.
- 2 Collins, C.R., Gordon, G.J., von Lilienfeld, O.A., and Yaron, D.J. (2018). *J. Chem. Phys.* 148: 241718.
- 3 Coleman, A.J. and Yakulov, V.I. (2000). *Reduced Density Matrices. Coulson's Challenge*. New York: Springer.

- 4 Parr, R.G. (1980). *Horizons of Quantum Chemistry*, 5–15. Netherlands: Springer.
- 5 Spackman, M.A. and Maslen, E.N. (1986). *J. Phys. Chem.* 90: 2020–2027.
- 6 Matta, C.F. and Boyd, R.J. (eds.) (2007). *The Quantum Theory of Atoms in Molecules*. Wiley.
- 7 Bader, R.F. (1990). *Atoms in Molecules: A Quantum Theory*. Oxford: Clarendon Press. Print. ISBN 978-0198558651.
- 8 Perdew, J.P. (2001). Jacob's ladder of density functional approximations for the exchange-correlation energy. *AIP Conference Proceedings. Density Functional Theory and Its Application to Materials*, AIP. <https://doi.org/10.1063/1.1390175>.
- 9 Becke, A.D. and Edgecombe, K.E. (1990). *J. Chem. Phys.* 92: 5397–5403.
- 10 Silvi, B. and Savin, A. (1994). *Nature* 371: 683–686.
- 11 Savin, A., Nesper, R., Wengert, S., and Fässler, T.F. (1997). *Angew. Chem. Int. Ed. Engl.* 36: 1808–1832.
- 12 Schmider, H. and Becke, A. (2000). *J. Mol. Struct. THEOCHEM* 527: 51–61.
- 13 Schmider, H.L. and Becke, A.D. (2002). *J. Chem. Phys.* 116: 3184–3193.
- 14 Johnson, E.R., Keinan, S., Mori-Sánchez, P. et al. (2010). *J. Am. Chem. Soc.* 132: 6498–6506.
- 15 Sahni, V., Gruenebaum, J., and Perdew, J.P. (1982). *Phys. Rev. B* 26: 4371–4377.
- 16 Pearson, E.W. and Gordon, R.G. (1985). *J. Chem. Phys.* 82: 881–889.
- 17 Perdew, J.P., Burke, K., and Ernzerhof, M. (1996). *Phys. Rev. Lett.* 77: 3865–3868.
- 18 Zupan, A., Burke, K., Ernzerhof, M., and Perdew, J.P. (1997). *J. Chem. Phys.* 106: 10184–10193.
- 19 Tognetti, V., Cortona, P., and Adamo, C. (2008). *Chem. Phys. Lett.* 460: 536–539.
- 20 Boto, R.A., Contreras-García, J., Tierny, J., and Piquemal, J.-P. (2015). *Mol. Phys.* 114: 1406–1414.
- 21 Boto, R.A., Piquemal, J.-P., and Contreras-García, J. (2017). *Theor. Chem. Acc.* 136. <https://doi.org/10.1007/s00214-017-2169-9>.
- 22 Lane, J.R., Contreras-García, J., Piquemal, J.-P. et al. (2013). *J. Chem. Theor. Comput.* 9: 3263–3266.
- 23 Saleh, G., Gatti, C., Lo Presti, L., and Contreras-García, J. (2012). *Chem. Eur. J.* 18: 15523–15536.
- 24 Bader, R.F.W. and Essén, H. (1984). *J. Chem. Phys.* 80: 1943–1960.
- 25 Kohout, M., Pernal, K., Wagner, F.R., and Grin, Y. (2005). *Theor. Chem. Acc.* 113: 287–293.
- 26 Silvi, B. (2003). *J. Phys. Chem. A* 107: 3081–3085.
- 27 Becke, A.D. (2000). *J. Chem. Phys.* 112: 4020–4026.
- 28 Contreras-García, J. and Recio, J.M. (2010). *Theor. Chem. Acc.* 128: 411–418.
- 29 Contreras-García, J., Pendás, A.M., Silvi, B., and Recio, J.M. (2009). *J. Phys. Chem. B* 113: 1068–1073.
- 30 Kohout, M. and Savin, A. (1996). *Int. J. Quantum Chem.* 60: 875–882.
- 31 Dobado, J.A., Martínez-García, H., Molina, J.M., and Sundberg, M.R. (1998). *J. Am. Chem. Soc.* 120: 8461–8471.
- 32 Kim, M.-C., Sim, E., and Burke, K. (2013). *Phys. Rev. Lett.* 111: 073003.
- 33 Medvedev, M.G., Bushmarinov, I.S., Sun, J. et al. (2017). *Science* 355: 49–52.

- 34 Sim, E., Song, S., and Burke, K. (2018). *J. Phys. Chem. Lett.* 9: 6385–6392. PMID: 30335392.
- 35 Laplaza, R., Polo, V., and Contreras-García, J. (2019). *Phys. Chem. Chem. Phys.* 21: 20927–20938.



## 19

### Molecular Face

*Dong-Xia Zhao, Hong Huang, and Zhong-Zhi Yang*

*Liaoning Normal University, School of Chemistry and Chemical Engineering, Department of Chemistry, Huanghe St, Shahekou District, Dalian 116029, PR China*

#### 19.1 Introduction

Shape and size are the basic concepts that govern our understanding of nature. They play a crucial role in natural phenomena. When studying a macro- or micro-object, we often consider its shape, size, and position first. Therefore, shape and size are widely studied in various fields [1].

Shape and size are the parameters that define the external form of a molecule. Additionally, these parameters are the concrete manifestation of the interaction and movement of electrons and nuclei within a molecule. The molecular shapes and the physical quantities that are derived from them are often used to determine the properties of the molecules. Further, to some extent, they may also be used to determine the interactions and reactions between molecules. The molecular shape and size are determined from the external molecular surface boundary. For studying molecular surfaces, numerous models and methods have been proposed based on both experimental facts and theoretical studies. A molecular shape is commonly idealized by a set of overlapping hard spheres with the corresponding van der Waals (vdW) radii [2]. There are mainly three kinds of surfaces based on this idea: the vdW surface (vdWS) [3–5], the solvent-accessible surface (SAS) [6], and solvent-excluded surface (SES [5]) or molecular surface (MS [7]) by rolling a probe sphere (representing the solvent, generally with a radius of 1.4 Å for water) around the vdWS of the solute. Grant and Pickup [8, 9] proposed the Gaussian shape method, in which hard vdW spheres are replaced by “soft” Gaussian spheres. Weiser et al. [10–12] presented the neighbor-list reduction optimization to accelerate the computation of hard-sphere MSs. This electron isodensity-based quantum chemical approach to decipher the molecular shape has been the subject of several studies [1, 13–22]. Bader et al. [14, 15] proposed a surface with a constant electron density (ED) (typical density values of 0.001 a.u. or 0.002 a.u.) to describe the shape and size of the diatomic molecules. Mezey et al. [1, 13, 16] established a method for the topological analysis of contour surfaces represented by electron isodensity-fused spheres.

One may wonder that what is the molecular boundary surface and how to determine it theoretically. This is a story of defining the molecular face (MF) and its applications.

In this chapter, before formulating the MF theory, we first provide a preliminary discussion on the atomic and ionic radii because atoms are the building blocks of molecules. Next to this, a description has been provided on how to define the MF, which is a molecular intrinsic characteristic contour (MICC) on that maps the ED. This MF or molecular frontier electron density (MFED) gives rise to the interaction and reactivity indicators. Additionally, some intuitive examples have been provided as well.

## 19.2 Atomic and Ionic Radii

Atomic radii, which are the fundamental parameters in chemistry and physics, have been investigated rigorously. Several atomic radii [23–36] have been defined and derived experimentally or theoretically, corresponding to different bonding conditions. Generally, three types of atomic radii exist, which have been well defined and widely used: covalent, metallic, and vdW radii. Quantum chemistry provides a powerful tool for evaluating atomic radii and exploring their types. For example, Slater [24] identified a close correlation between the atomic radii and radii corresponding to the maximum charge density in the outermost atomic shell via self-consistent field wave function calculations [37]. In discussing the chemical potential, Politzer et al. [26] found that the radial distance at which an atom's electrostatic potential equals its chemical potential is fairly close to its covalent radius. Chattaraj et al. [27] defined the atomic characteristic radius as the point where the electrostatic potential due to the Fukui function is equal to the hardness. The atomic radii values agreed excellently with experimental and covalent radii values. By expressing the atomic electronegativity as a formulation of several atomic parameters (i.e. the atomic radius, total number of valence electrons, nuclear effective charge, and orbital exponent), Putz et al. [28] derived a set of atomic radii by fixing all parameters involved in the formulation, except the atomic radius. In quantum chemistry, the main approach for defining an atomic radius is to utilize the particular contour of its total ED, which has also been widely used to describe the molecular surfaces [1, 38]. Using this method, Boyd explored the relative sizes of atoms and calculated scaled atomic radii, from hydrogen to xenon, by simulating the Pauling univalent radii of the noble gas atoms [29]. To define the radii of atoms and ions on the same basis, Deb et al. [30] adopted a universal criterion of ED, that is 0.008714 a.u., which is obtained from the ratio of Dirac's exchange constant and the Thomas–Fermi kinetic energy constant, and they found that the resulting radii correlated well with a number of atomic and ionic properties (e.g. ionization potential, electronegativity, and softness). Unfortunately, atomic radii that are obtained by this approach depend considerably upon the particular selection of the threshold value of ED. Yang et al. [31–36] proposed an approach, in which a unique radius is assigned to a certain atom, according to the classical turning point of the electronic motion. The atomic radii of the elements,

from hydrogen to xenon, are calculated via an *ab initio* method to determine the Configuration Interaction with all Single and Double substitution (SDCI) levels by using near Hartree–Fock (HF) limit basis sets.

### 19.2.1 Turning Radius of a Hydrogen Atom

One may wonder what and where is the boundary surface and how to determine it for an isolated hydrogen atom. For an isolated hydrogen atom, the ground-state electronic wave function is defined as  $\psi(\vec{r}) = 1/\sqrt{\pi}e^{-r}$ , which is the wave function for the 1s atomic orbital with the orbital energy  $-0.5$  a.u. ( $-13.6$  eV). The  $\psi^2(\vec{r})$  is equal to  $1/\pi e^{-2r}$ . This implies that the probability of finding an electron is not equal to zero, even when the electron appears very far away from the nucleus. If an electron belongs to an atom, then the atomic radius of this atom should be infinite. Oh! The electron of one hydrogen atom might fill the whole universe! However, we practically consider the hydrogen atomic radius, such as the vdW radius, to describe its spatial size. How to define an intrinsic atomic radius has been posed.

Let us consider a hydrogen atom. It contains a nucleus of positive charge 1 and one electron  $e$  of negative charge  $-1$ . Suppose the nucleus is at the origin of a spherical polar coordinate system, and the electron coordinate is  $\vec{r}$ . The electrostatic potential acting on an electron from the nucleus is stated as follows:  $V(r) = -1/r$ , which has spherical symmetry depending only on the radial distance  $r$ . The potential energy is equal to the total energy ( $=-0.5$  a.u.),  $V(r_b) = -1/r_b = -0.5$ , thus,  $R_b = 2.0$  a.u. This indicates that, at this point, the local kinetic energy of the electron is equal to zero; therefore, this point is termed as the classical turning point, which is significant for the quantum chemical analysis of the MFs. When the electron radial distance,  $r$ , is less than  $R_b = 2.0$  a.u.  $= 1.06$  Å, the corresponding region is called the classically permitted region because the electron kinetic energy remains positive. Contrarily, when the electron radial distance,  $r$ , is greater than  $R_b = 2.0$  a.u., the corresponding region is called a classically forbidden region because the electron kinetic energy becomes negative in this region. Therefore, it is proposed that the turning point  $R_b = 2.0$  a.u., called the classical turning radius, turning radius, or boundary radius represents the intrinsic radius of an isolated hydrogen atom [31, 36]. In other words, in a hydrogen atom, the classical turning surface is represented by a spherical surface of radius  $R_b = 2.0$  a.u., whose inner area is the permitted region and the outer area is the forbidden region for the motion of the electron.

In the same way, the turning radius of the H atom in an excited state with the quantum number  $n$  is defined as  $2n^2$  a.u., i.e. if  $n = 2$ , it is 8 a.u. and so on. Therefore, when the H atom is excited to an excited state, its size greatly expands. According to the same idea, for the hydrogen-like ions containing only one electron in a state denoted by  $n$ ,  $l$ , and  $m$  that are principal, angular, and magnetic quantum numbers, their turning radii are defined as  $2n^2/Z$  a.u., where  $Z$  is their corresponding nuclear charge, that is all spherical without depending on the angular and magnetic quantum number.

This idea may be extended to other atoms and molecules via required elaborate approaches.

### 19.2.2 Atomic Turning Radii for Many-Electron Atoms

In this section, we extend the idea of the hydrogen atom, discussed in the previous section, to other atoms to define their atomic turning radii. Intuitively and directly, in a many-electron atom, one electron at a local position  $\vec{r}$  interacts with the nucleus and the remaining electrons. The associated interaction potential can be expressed as follows:

$$V(\vec{r}) = -\frac{Z}{r} + \frac{1}{\rho(\vec{r})} \int \frac{\rho_2(\vec{r}, \vec{r}_2)}{|\vec{r} - \vec{r}_2|} d\vec{r}_2 \quad (19.1)$$

where  $Z$  denotes the nuclear charge,  $\vec{r}$  is the position of the considered interacting electron,  $r$  is the distance from the electron to the nucleus,  $\rho(\vec{r})$  is the total ED at position  $\vec{r}$ , and  $\rho_2(\vec{r}, \vec{r}_2)$  represents the two-ED function, which is the probability of one electron appearing at position  $\vec{r}$ , and another at position  $\vec{r}_2$ , simultaneously. This function describes the exchange interaction with the remaining electrons of the atom. Thus, the potential that acts on one electron in an atom (PAEA) consists of two parts. The first term in Eq. (19.1) is the attractive potential that acts on the considered electron due to its nucleus, and the second term is the potential created by its interaction with the remaining electrons. This second potential term includes both the Coulomb and exchange potentials.

As long as the PAEA has been calculated, the classical turning point of electronic motion  $\vec{r}$  is defined as follows [31, 33]:  $V(\vec{r}) = -I$ , where  $V(\vec{r})$  is the potential acting on one electron at  $\vec{r}$  in an atom or ion, and  $-I$  represents the negative value of the first ionization potential of the atom or ion. We use  $R_b$ , which is simply called the atomic turning radius, to denote the distance from the classical turning point to the nucleus of the atom or ion. Similar to the hydrogen atom case, this atomic turning radius is an intrinsic mark for an atom or ion.

Using the *ab initio* method, the atomic turning radii for the elements from hydrogen to xenon have been calculated [31, 36, 39]. For the atoms in the same group, the turning radii and atomic characteristic radii [31, 36, 39] show a close correlation with the commonly used atomic radii, especially the vdW atomic radii. Further, the surface derived from this turning radius is considered as the accurate classical turning point surface to resemble the results reported by Ayers [40]. These characteristic ionic radii [32, 35] also correlate well with the Pauling ionic radii [23] as well as the Shannon and Prewitt ionic radii [41].

Figure 19.1 illustrates the distinction between ionic and covalent AB-type crystals. Based on the concept of this type of atomic and ionic radii and an *ab initio* study, a criterion for defining the ionic or covalent character of AB-type crystals has been demonstrated.  $L_{\text{exp}}$  denotes the internuclear separation between positive and negative ions of the crystals measured by an X-ray diffraction experiment.  $L_{\text{br}}$  denotes the sum of the turning radii of positive and negative ions. If the  $\Delta L = L_{\text{exp}} - L_{\text{br}} > 0.0$ , the AB-type crystal is ionic, otherwise is covalent. For LiF crystal,  $L_{\text{exp}} = 2.01 \text{ \AA}$  and  $L_{\text{br}} = 1.73 \text{ \AA}$ , then  $\Delta L > 0.0$ . Distance between Li cation and F anion in LiF crystal is larger than the sum of the Li cationic turning radius and the F anionic turning radius, i.e. there is a separation region between these two spheres (two ions). Thus it is an ionic crystal [39]. The criterion states that an AB-type crystal is designated as a

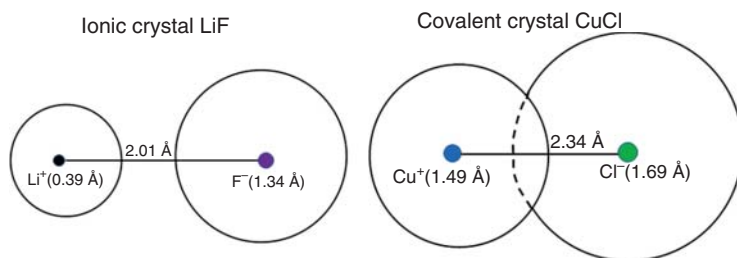


**Figure 19.1** The distinction between ionic and covalent AB-type crystals.

primarily ionic crystal if there exists a separation region, which is the classically forbidden region for the electronic motion between the pair of adjacent cation  $A^+$  and anion  $B^-$ . Further, if no such separation region exists for a pair of adjacent cation  $A^+$  and anion  $B^-$ , then the corresponding AB-type crystal is sorted as a primarily covalent one, such as CuCl crystal. This provides a platform to gain a fundamental understanding of the nature of ionic and covalent crystals. A comparison has been given between the results obtained from the application of this criterion and those obtained from the widely accepted Pauling's electronegativity criterion. This comparison demonstrates that in most cases both criteria yield the same results for the ionic or covalent characters. When there are discrepancies between the results of the two criteria, this type of criterion provides suitable estimations for the affected cases.

Soon after the above-mentioned study, Perdew and his coworkers [42] defined the sizes and shapes of atoms, molecules, and solids by using the Kohn–Sham (KS) potential, stating that their contribution is an extension of the pioneering work of Yang et al. [31, 39] They pointed out that a nonarbitrary method, along with the quantum chemical calculations, can be used to generate a pictorial representation of the MFs, which are indispensable in chemistry and condensed matter physics.

The information provided above indicates that the definition of atomic and ionic turning radii (characteristic boundary contour) is significant and widely accepted. According to DeKock et al. [43], there are five acceptable atomic radii: covalent radii, HF radii, polarizability radii, vdW radii, and turning point radii (i.e. turning radii).

### 19.3 Molecular Face Formalism

To extend the above-described model to define an MICC, i.e. the electron turning boundary surface, first, we need to study and discuss the potential acting on an electron in a molecule (PAEM). The MF is defined by mapping the ED on the MICC, showing both the molecular shape and frontier ED. For a molecule, its MF is unique, just like a person's face or fingerprint, which contains vital information that will be described.

### 19.3.1 Potential Acting on One Electron in a Molecule

As one electron of a molecule appears at a local point,  $\vec{r}$ , the potential acting on this electron is defined via the interaction energy of this local electron with respect to the remaining particles, i.e. all the nuclei and the remaining electrons [44–46]. Assuming that a molecule is in its electronic ground state, the potential acting on one electron at position  $\vec{r}$  (PAEM) can be expressed as follows:

$$V(\vec{r}) = -\sum_A \frac{Z_A}{|\vec{r} - \vec{R}_A|} + \frac{1}{\rho(\vec{r})} \int \frac{\rho_2(\vec{r}, \vec{r}_2)}{|\vec{r} - \vec{r}_2|} d\vec{r}_2 \quad (19.2)$$

where  $Z_A$  and  $\vec{R}_A$  are the nuclear charge and position of nucleus  $A$ , respectively. The electron at position  $\vec{r}$  belongs to the molecular system and has an exchange interaction, which is a quantum effect, with the remaining electrons. Therefore, the PAEM considers one internal electron, whereas the molecular electrostatic potential (MEP) considers one external test positive charge. This is the essential difference between the PAEM and MEP [46]. Notably, the PAEM potential is also different from the HF potential. For ease of explanation, the closed-shell situation is taken as an example. The canonical molecular orbital (CMO), in the HF self-consistent field molecular orbital (HFSCF-MO) theory, satisfies the HF equation; thus, the HF potential for one electron is equivalent to its interaction energy, when the said electron is located in a given CMO [47]. Although they have different forms, both PAEM and HF potentials include the quantum mechanical exchange effect.

The topological characteristics of PAEM are provided by the analysis of its associated gradient field (its minus is the FAEM) [45]. Although the topological analysis of the PAEM is very similar to that of the ED as in Bader's AIM theory, the former is distinct from the latter. Herein, a PAEM critical point (*pcp*) is a point where the gradient of the scalar field  $V(\vec{r})$  vanishes, as expressed in  $\nabla V(\vec{r})|_{\vec{r}_{pcp}} = 0$ . Thus, a *pcp* is a point where the corresponding scalar field has an extremum. To characterize the critical points of the PAEM, as usual, we assume that, for a sufficiently well-behaved scalar field, the Hessian matrix of the field, exists at a *pcp* point. Consequently, at any given *pcp* point, the Hessian matrix is able to be diagonalized and then yields three real eigenvalues,  $i$  ( $i = 1, 2, 3$ ). The corresponding eigenvectors are the principal axes. The characterization of a *pcp* depends on its rank and signature. The rank,  $R$ , of a *pcp* is the number of eigenvalues that are different from zero, and the signature,  $S$ , is the algebraic sum of the signs of the three eigenvalues:  $S = \sum_{i=1}^3 \text{sign}(\lambda_i)$ . Thus, a *pcp* is classified by the ordered pair  $(R, S)$ . A  $(3, +3)$  is a local minimum, a  $(3, +1)$ , bond critical point (*bcp*), is a minimum in two directions and a maximum in the other direction, a  $(3, -1)$ , circle critical point (*ccp*), is maximum in two directions and a minimum in the other direction.

The characteristic features of the PAEM for furan molecules are shown in Figure 19.2. A three-dimensional (3D) representation of the PAEM, reduced from a full 4D representation of the PAEM, including a 3D one-electron coordinate  $\vec{r}(x, y, z)$  and the value of  $V(\vec{r})$ , is shown in Figure 19.2a with  $z$  fixed at 0.0 a.u. As the position of one electron,  $\vec{r}$ , varies on the  $xy$  plane ( $\vec{r}(x, y, z = 0.0)$ ), the corresponding calculated values of  $V(\vec{r})$  are seen on the ordinate. In case of the PAEM of furan,

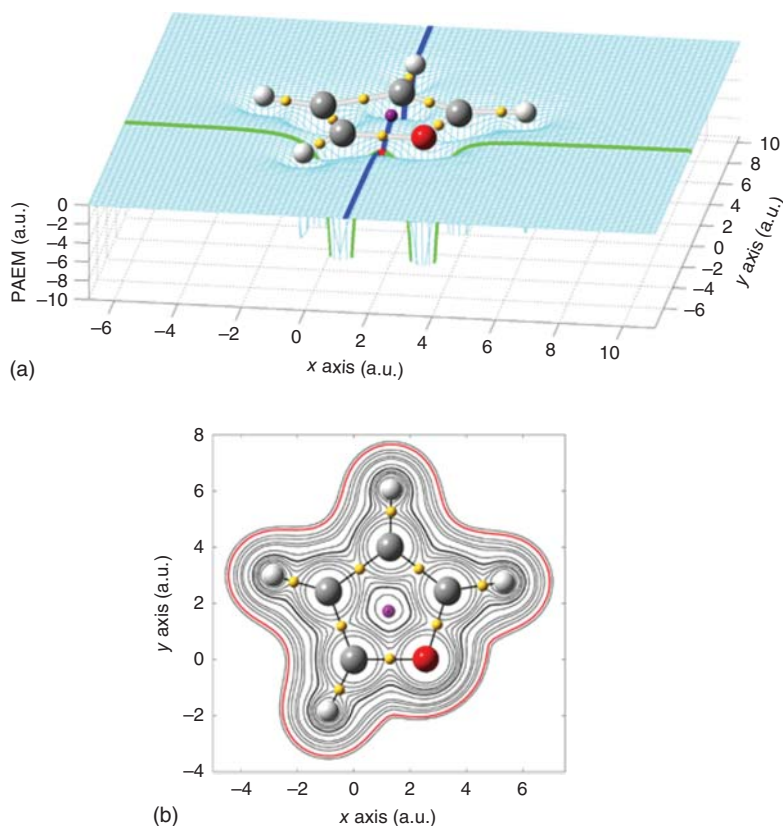


**Figure 19.2** (a) 3D graph representation of the PAEM and curves of the PAEM along (green curve) and perpendicular to (blue curve) C—O bond, electron running on the furan molecular plane. (b) Display of the iso-PAEM of the furan molecule.

nine deep potential wells originate from their corresponding nuclear positions. A significant feature of the PAEM surface is that there is a potential saddle point (*psp*) between the two bonded atoms, as shown in Figure 19.2a. Here, only one is clearly marked by a red solid star, where the PAEM value is a local maximum along the C—O chemical bond (green bold line) and a local minimum in the direction perpendicular to the C—O bond (blue bold line). The *psp* corresponds to the electronic coordinate that is marked by a yellow solid ball on the C—O bond and is called the *bcp*. As shown in Figure 19.2a,b, each bond has a *bcp*, marked by a yellow solid ball. Moreover, there is a *ccp*, which is located around the center of the furan cycle. In the remaining vast region, the potential gradually increases with increasing distance between the electron and nuclei and then approaches zero at infinity, which is the expected asymptotic behavior. As shown in Figure 19.2b, each contour represents an iso-value line of the PAEM. The potential wells around the oxygen and carbon atoms are wider than those around the hydrogen atoms.

### 19.3.2 Kohn–Sham One-Electron Potential

Following the description of PAEM, we briefly state the Kohn–Sham effective one-electron potential. The KSpot,  $v_{\text{KS}}(\vec{r})$ , is an effective electronic potential:

$$v_{\text{KS}}(\vec{r}) = -\sum_A \frac{Z_A}{|\vec{r} - \vec{R}_A|} + \int \frac{\rho(\vec{r}')}{|\vec{r} - \vec{r}'|} d\vec{r}' + v_{\text{XC}}(\vec{r}) \quad (19.3)$$

where the first term denotes the interaction from all the nuclei of a molecule, the second term denotes the interaction from the remaining electrons, and the last term  $v_{\text{XC}}(\vec{r})$  is the KS exchange-correlation potential.

Both the PAEM and Kohn–Sham effective one-electron potential (KSpot), as one-electron potential, can be used to define the MICC with similar results.

### 19.3.3 Molecular Intrinsic Characteristic Contour – A Classical Turning Surface

As a common understanding, the boundary of an object should confine the movement of all the component particles within it. Therefore, the concept of “boundary” or “surface” is classical in nature, and it is natural to define a molecular model in terms of the classical turning point of the movement of the electron within a molecule. The MICC model can be understood as follows: When an electron moves in a molecule, its kinetic energy varies with its position, relative to the other particles of the molecule. If at some point, its energy equals the PAEM (an average potential), that means, the average kinetic energy of this electron at this position is zero. Then, the position  $\vec{r}$  is called the classical turning point of movement for the considered electron. Therefore, the one-electron energy is equal to the one-electron average potential energy in this case. Moreover, if we assume that the one-electron energy at  $\vec{r}$  is equal to the negative value of the first ionization potential ( $-I$ ) of the molecule, then we can state the turning point equation for this electron as follows:

$$V(\vec{r}) = -I \quad (19.4)$$

where  $r$  is called the turning point. The set of all such points defines the classical turning surface, which can be expressed as follows:  $G(-I) = \{\vec{r} : V(\vec{r}) = -I\}$ , where  $G$  denotes the classical turning surface. The surface has a clear physical meaning as it is composed of all the classical turning points of the movement of an electron within a molecule. It is an iso-potential contour, where the potential equals the negative value of the first ionization potential (Eq. (19.4)). Thus, the inside of this contour is the classically permitted region, whereas the outside of this contour is the classically forbidden region for the electron movement.

## 19.4 Frontier Electron Density on the Molecular Face, Revealing the Reaction and Interaction Between the Molecules

The MFs not only describe the shape and size of a molecule in space, but also the MFED, which shows the physical and chemical characteristics of a molecule. Non-covalent interactions, including hydrogen, halogen, and pnictogen bonds, are widely



known because of their significant roles in both chemical reactions and biological phenomena.

### 19.4.1 Molecular Face Indicating the Hydrogen, Halogen, and Pnicogen Bonds Between the Molecules

We applied the MF theory (MFT), based on the PAEM, to the systems undergoing noncovalent interactions, such as noncovalent bond complexes [48], to visualize the reactive sites for the monomers, as shown in Figure 19.3. The MFED extremes on the MF that are considered as the local reactivity descriptors are applied to extract the regioselectivity and preferred direction for the monomers in hydrogen-, halogen-, and pnicogen-binding complexes. The corresponding results are found to be in good agreement with those of the chemical conventions and *ab initio* calculations. MFT provides a new way to demonstrate the regioselectivity and can be applied to other types of molecules in the future.

For the systems of interest, we obtained the PAEM-based ED mapping on the MF, which is equal to the negative value of the first ionization energy. Figure 19.3 displays the geometries and MFs of hydrogen (Urea–H<sub>2</sub>O), halogen (ClBr–NH<sub>3</sub>), and pnicogen (ClPH<sub>2</sub>–NH<sub>3</sub>) dimers from upper to lower. As shown in Figure 19.3a, for the urea molecule in hydrogen (Urea–H<sub>2</sub>O) dimer, the MFED shows that the dark blue region corresponds to the two lone pair (*lp*) regions of the oxygen atom and the single lone pair regions of the two nitrogen atoms (orange circle), and the four red areas correspond to the four hydrogen atoms. The urea molecule, specifically its lone pair of an oxygen atom, is an acceptor of the hydrogen bond to approach

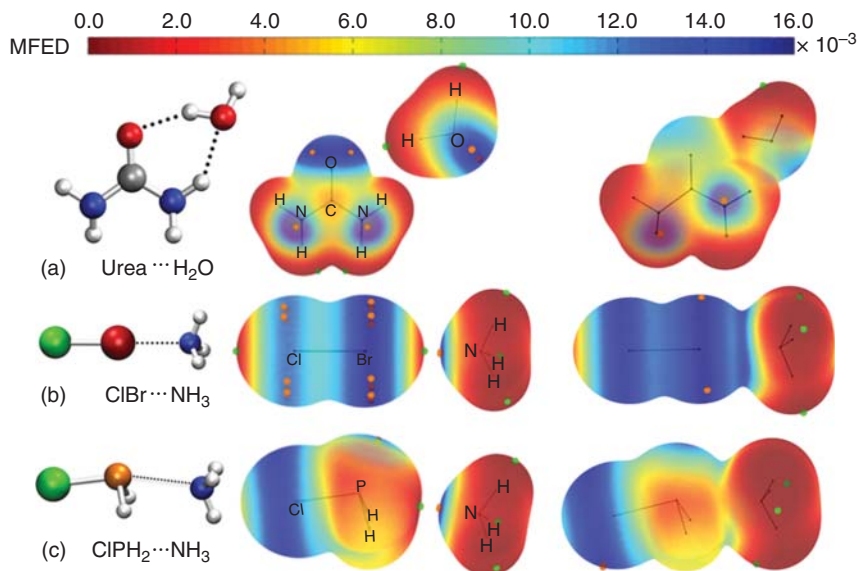


**Figure 19.3** MFs of the monomers and dimers, including the monomers in hydrogen bond (urea–H<sub>2</sub>O dimer), halogen bond (ClBr–NH<sub>3</sub>), and pnicogen bond (ClPH<sub>2</sub>–NH<sub>3</sub>). The orange spheres denote the maxima of MFED and the green ones denote the minima. All dimensions are in a.u.

a donor of H-bond. The donor interacts with the urea molecule along the direction of an oxygen atom and its lone pair. The angle of the C—O—*lp* is 120.36°, as obtained by the MFED. In the *ab initio* optimized urea–H<sub>2</sub>O dimer, the C—O…H angle, between C—O and H—O (H<sub>2</sub>O), is 109.05°. As shown in Figure 19.3b, for the ClBr monomer in the ClBr…NH<sub>3</sub> dimer, MF exhibits  $\sigma$ -holes in the Cl and Br atomic sides along the Cl—Br chemical bond axis, in which the minima of the MFED are on the right of the  $\sigma$ -hole whose definition is similar to that of the Politzer [49]. The site with the minimum MFED can easily form a halogen bond with the lone pair of the NH<sub>3</sub> molecule. We searched the sites of  $\sigma$ -holes on the various MFs in the Cl and Br atomic sides and calculate the angles of Cl—Br-extreme and found that these  $\sigma$ -holes tend to approach a donor of the halogen bond. The angle of the Cl—Br-extreme is 180.0°, as obtained by the MFED. In the *ab initio* optimized ClBr—NH<sub>3</sub> dimer, the Cl—Br…N angle is 179.8°. At this time, the halogen bond angle predicted by the MF is almost the same as that estimated by the *ab initio* calculations. In contrast to the hydrogen bond, however, similar to the halogen bond, a pnictogen bond is formed via interaction between the Lewis base nitrogen atom and the Lewis acid phosphorous atom, which shows a high degree of anisotropy, as displayed in Figure 19.3c. The lone pair on the nitrogen atom in NH<sub>3</sub> directly interacts with the site with the minimum MFED in MF around the phosphorous atomic region. The Cl—P-minimum MFED angle that is predicted from the MF is 158.90°, which is close to the Cl—P…N angle in the ClPH<sub>2</sub>—NH<sub>3</sub>. Thus, the MFED is a good local reactivity descriptor for characterizing the sites between molecular interactions and can be considered for the prediction of the regioselectivity of large molecular systems.

Further, we demonstrated the various types of MFs that originate during the formation and fracture of chemical bonds. These MFs aided us in visualizing the molecular shape change process, thereby providing new insights into the chemical change processes.

#### 19.4.2 Molecular Face Picture Indicating the Interactions and Reactions Between Atoms and Molecules

Based on the MICC model, the concept of MF is proposed as the MICC with ED mapped on it. This ED is the MFED. MF based on the PAEM has been successfully developed and applied to demonstrate the bond formation and/or breaking of H<sub>2</sub> [50], the polarization effect of hydrogen and fluorine atoms in the process of forming an HF molecule [51], the reaction mechanism of adding fluorine radical to ethylene (F + C<sub>2</sub>H<sub>4</sub>) [52], the proton transfer reaction in Be<sup>2+</sup>(H<sub>2</sub>O)*n* and the formation of hydroxide [53], and the front-side attack identity SN<sub>2</sub>(C) and SN<sub>2</sub>(Si) reactions in the gas phase [54, 55]. The PAEM-based MF model provides vivid and interesting details on the spatial changes and electron transfer mechanisms in the system.

For example, the reactivity of Markovnikov (M) addition of alkenes [56] was investigated in terms of the ED encoded on the MF. The effect of the density distribution in the initial state of the alkenes on their regioselectivity and reactivity has been discussed, as shown in Figure 19.4. We calculated and sketched the features of the MFs for the considered molecules. For HCl and CH<sub>2</sub>=CHCH<sub>3</sub>, the results are shown in

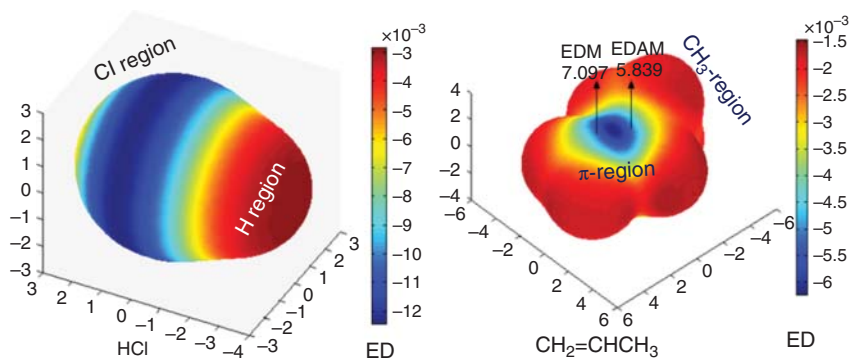


**Figure 19.4** Features of the MFs for the HCl,  $\text{CH}_2=\text{CHCH}_3$  molecules. Dark blue denotes higher densities and dark red denotes lower densities.

Figure 19.4. The magnitude of MFED is proportional to the surface using a color gradient, with dark blue areas denoting higher electron densities and dark red areas representing lower densities. When molecules approach each other, they first “see” their respective MFs, followed by subsequent recognition and interaction. The features of the MFs for HCl and  $\text{CH}_2=\text{CHCH}_3$  show that the hydrogen region of HCl is brighter than that of the other regions, indicating that the MFED of the hydrogen region of HCl is smaller than that of the other regions. However, the  $\pi$ -region for the  $\text{CH}_2=\text{CHCH}_3$  molecule is darker than those of the other regions, indicating higher MFEDs. Furthermore, when a substituent group binds to one of two carbons of the  $\text{C}=\text{C}$  double bond, the electron densities of the two carbon atom regions become nonidentical, such as for  $\text{CH}_2=\text{CHCH}_3$  in Figure 19.4; therefore, a preference for the M or anti-Markovnikov (AM) carbon atom, that is, regioselectivity, appears during the electrophilic addition reactions. Consequently, when HCl approaches an alkene, it attacks the  $\pi$ -region, especially one of the M and AM carbon atom regions with a higher MFED.

The chemistry of alkenes depends mainly on the characteristic double bond between the two carbon atoms, which can be characterized by the MFED encoded on the MF. As expected, there is a certain correlation between the regioselectivity and the MFEDs in the initial state of the alkenes. In fact, the MF is obtained by carrying out large numbers of calculations in a 3D space. However, here we have selected two characteristic points whose MFEDs are defined as follows: a straight line originating at the M (or AM) carbon atom nucleus and perpendicular to the  $\pi$ -bond plane has an intersection point with the part of the MF that faces the attacking HCl. The MFED at this point is defined as  $\text{ED}_\text{M}$  (or  $\text{ED}_\text{AM}$ ). In  $\text{CH}_2=\text{CHCH}_3$  molecule, the MFEDs of the C atoms of double bond perpendicular to the  $\pi$ -bond plane are  $7.097 \times 10^{-3}$  and  $5.839 \times 10^{-3}$ ; thus, the  $\text{ED}_\text{M}$  and  $\text{ED}_\text{AM}$  are  $7.097 \times 10^{-3}$  and  $5.839 \times 10^{-3}$ .

The dynamically changing spatial features of the MFs are described in detail for the electrophilic additions to the alkenes along the intrinsic reaction coordinate routes, as shown in Figure 19.5. We selected five states to investigate the

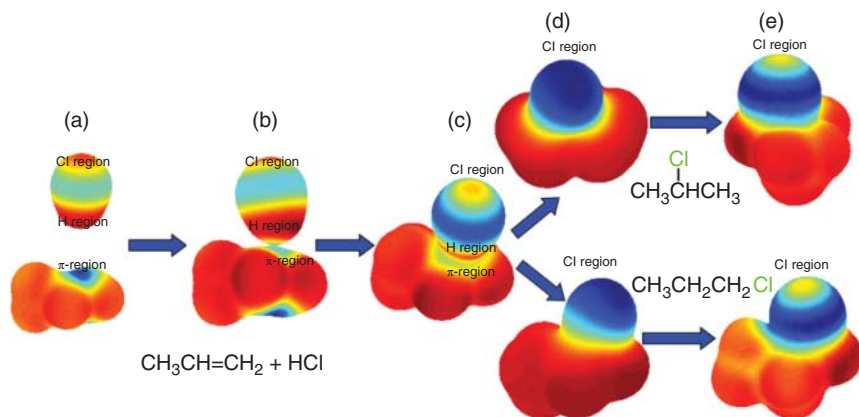


**Figure 19.5** Dynamically changing spatial features of the MFs for the electrophilic addition of HCl to  $\text{CH}_2=\text{CHCH}_3$  during the reaction.

dynamically changing spatial features of the MFs during the reaction. The  $R_a$  state represents the reactants in the initial stage. Its geometry was fully optimized with the same symmetry as that of the  $R_p\text{-C}$  state by constraining the distance between the attacking hydrogen atom and the  $\pi$ -region. The  $R_b$  state is the critical point, where the attacking hydrogen atom and  $\pi$ -region are in contact with each other. The visualized MF faces from the reactant to product states are shown in Figure 19.5 for the electrophilic addition of HCl to propene.

Considering the  $\text{CH}_2=\text{CHCH}_3+\text{HCl}$  reaction, the substituent  $\text{CH}_3$  binds to one of the carbon atoms of the  $\text{C}=\text{C}$  double bond; thus, the two carbon atoms are not identical. As the ED of the CM carbon is much larger than that of CAM, HCl attacks the M carbon (see Figure 19.5) during the reaction. Before the reactant state, the hydrogen region of HCl approaches CM, and the distance between the hydrogen atom and CM is smaller than that between hydrogen and CAM. The intermolecular polarization effect between the former pair was stronger than that between the latter pair. Consequently, the representative ED of CM decreases relative to that of the CAM. Therefore, up to the first state (reactant), the EDM of the M carbon atom is smaller than that of the EDAM. From the first to the second state, the ED of HCl gradually increases, whereas that of the  $\pi$ -region of  $\text{CH}_2=\text{CHCH}_3$  gradually decreases (Figure 19.5). This clearly indicates that electrons are transferred from  $\text{CH}_2=\text{CHCH}_3$  to HCl. In the  $R_p\text{-C}$  state, EDCl increases; however, the EDH decreases slightly, indicating that the electron is further transferred from  $\text{CH}_2=\text{CHCH}_3$  region to the Cl region via the hydrogen region. In the transition state, EDCl becomes much larger than that of the other regions of the  $[\text{CH}_2=\text{CHCH}_3\cdots\text{HCl}]^\ddagger$  system for both M (first line of Figure 19.5) and AM (second line of Figure 19.5) addition routes. This further indicates that electrons gradually transfer to HCl. In the product state, the products  $\text{CH}_3\text{CHClCH}_3$ , for the M addition route (first line of Figure 19.5) and  $\text{CH}_2\text{ClCH}_2\text{CH}_3$  for the AM addition route, are formed (second line of Figure 19.5). The electrons are completely transferred from  $\text{CH}_2=\text{CHCH}_3$  to HCl.

### 19.4.3 Showing Reactivity Ability by the Frontier Electron Density and Steric Force on the Molecular Face

In DFT [57, 58], the ED,  $\rho(r)$ , is a fundamental property of the atoms, molecules, and condensed phases of matter. The steric potential can be stated as:

$$v_s(\vec{r}) = \frac{\delta E_s[\rho]}{\delta \rho} = \frac{1}{8} \frac{|\nabla \rho(\vec{r})|^2}{\rho(\vec{r})} - \frac{1}{4} \frac{\nabla^2 \rho(\vec{r})}{\rho(\vec{r})} \quad (19.5)$$

where  $\nabla \rho(\vec{r})$  is the gradient of ED and  $\nabla^2 \rho(\vec{r})$  is the Laplace function of ED. The steric energy,  $E_s[\rho]$ , is a universal density functional, which is always a lower bound to the true kinetic energy and always nonnegative. The steric force [59, 60] is equal to the negative gradient of the steric potential and can be expressed as follows:

$$\vec{F}_s(\vec{r}) = -\nabla v_s(\vec{r}) \quad (19.6)$$

The steric force is a vector quantity. We only consider the magnitude of the steric force, i.e.  $|\vec{F}_s(\vec{r})|$ , irrespective of its direction. A higher steric force results in an equally higher spatial resistance. By defining the position resistance on the MF, the position of the molecular steric force can be extracted, which may reflect the stereoselectivity ability of the molecule.

With MFED and steric force at hand, the reactivity ability for the activity of ketones should be validated, as shown in Figure 19.6, which are classical cases to elucidate the addition activity of the carbonyl group. As can be seen from Figure 19.6a, the oxygen atom possesses a nucleophilic region, and MFED values of the oxygen atoms in acetone, cyclopentanone, and benzophenone molecules in order increase rapidly, indicating that the activity of the oxygen atom in order becomes weaker due to the increase in steric hindrance. Thus, it is intriguing that the MF is an unbiased way to exhibit steric hindrance, where these molecules have clearly demonstrated the decreasing tendency for the activity of carbonyl groups in view of the steric

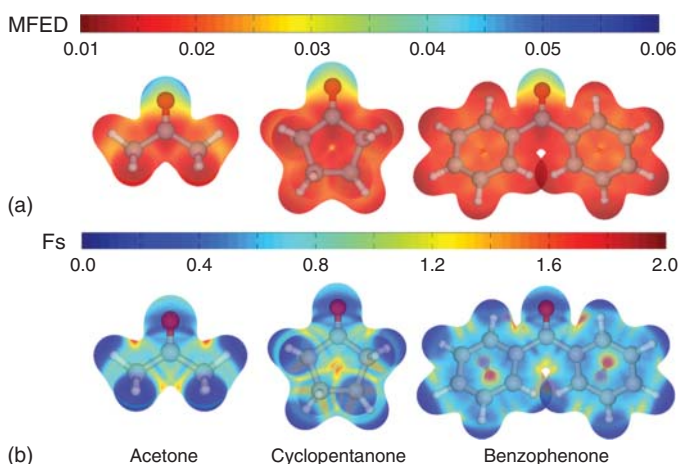


**Figure 19.6** The KSspot-based MF of acetone, cyclopentanone, and benzophenone. ED denotes electron density and  $F_s$  denotes the absolute value of the steric force.

effect. The above results are in agreement with the experimental findings, that is, decreasing the nucleophilic addition order of the carbonyl group follow the decreasing order: acetone, cyclopentanone, and benzophenone [61]. To visualize the steric hindrance and verify the conclusion drawn from the MF, we drew the steric force map. To characterize the previously studied stereoselectivity, the profiles of the steric force mapping on the defined molecular surface are plotted in Figure 19.6b. The steric effect becomes increasingly strong in order of acetone, cyclopentanone to benzophenone around the region of an oxygen atom, where we can see that the steric force increases gradually. This means that the steric hindrance becomes evident and affects the stereoselectivity when the volume of the bonded group is large. Thus, the steric hindrance can explain the order of the reactivity ability. However, instead of assigning an intuitive meaning to this term, it is more useful to visualize steric hindrance in the form of computer-generated illustrations on the MF.

This observation has been concluded from the above illustrations, KSpot-based MF-ED and MF-Fs maps. Generally, the best illustrations are based on general principles of good physical representation and graphic design; however, the link between scientific concepts and visual representation is often difficult to achieve, particularly in the educational context. We believe that the KSpot-based MF-ED and MF-Fs can construct the above-mentioned link, which bridges the connection between regioselectivity, stereoselectivity, and visualization.

## 19.5 Summary

The atomic turning radii and ionic radii are the basic parameters. It is shown that they may provide a pictorial criterion for distinguishing the ionic crystals from the covalent ones. The MF of a molecule is uniquely defined by the MICC, which maps the ED on it. The MICC is a classical turning boundary surface, whose inside area is a classically permitted region, whereas the outside area is a classically forbidden region for the electron motion. We assume a turning point on the MICC, such that the local potential acting on one electron is equal to the negative value of the first ionization potential of the molecule. The local potential can be of two types: the PAEM that is calculated by an *ab initio* method or a Kohn–Sham effective one-electron potential, which is calculated using the DFT theory. These two potentials exhibit similar behaviors and result in similar MFs and characteristics. The molecular frontier ED and the steric force on an MF are the indicators of interaction and reactivities between molecules; they even guide the reaction pathways. One could potentially add more significant quantities to the contour of an MF.

## Acknowledgment

This research was supported by the National Natural Science Foundation of China (Nos. 21473083 and 21133005).

## References

- 1 Mezey, P.G. (1993). *Shape in Chemistry: An Introduction to Molecular Shape and Topology*. New York: VCH.
- 2 Corey, R.B. and Pauling, L. (1953). *Rev. Sci. Instrum.* 24: 621.
- 3 Gibson, K.D. and Scheraga, H.A. (1987). *Mol. Phys.* 62: 1247.
- 4 Petitjean, M. (1994). *J. Comput. Chem.* 15: 507.
- 5 Greer, J. and Bush, B.L. (1978). *Proc. Natl. Acad. Sci. U. S. A.* 75: 303.
- 6 Lee, B. and Richards, F.M. (1971). *J. Mol. Biol.* 55: 379.
- 7 Richards, F.M. (1974). *J. Mol. Biol.* 82: 1.
- 8 Grant, J.A. and Pickup, B.T. (1995). *J. Phys. Chem.* 99: 3501.
- 9 Grant, J.A., Pickup, B.T., Sykes, M.J. et al. (2007). *Phys. Chem. Chem. Phys.* 9: 4913.
- 10 Weiser, J., Shenkin, P.S., and Still, W.C. (1999). *J. Comput. Chem.* 20: 688.
- 11 Weiser, J., Shenkin, P.S., and Still, W.C. (1999). *J. Comput. Chem.* 20: 217.
- 12 Weiser, J., Weiser, A.A., Shenkin, P.S., and Still, W.C. (1998). *J. Comput. Chem.* 19: 797.
- 13 Walker, P.D. and Mezey, P.G. (1994). *J. Am. Chem. Soc.* 116: 12022.
- 14 Bader, R.F.W. (1990). *Atoms in Molecules-A Quantum Theory*. New York: Oxford University Press.
- 15 Bader, R.F.W., Carroll, M.T., Cheeseman, J.R., and Chang, C. (1987). *J. Am. Chem. Soc.* 109: 7968.
- 16 Walker, P.D. and Mezey, P.G. (1993). *J. Am. Chem. Soc.* 115: 12423.
- 17 Mitchell, A.S. and Spackman, M.A. (2000). *J. Comput. Chem.* 21: 933.
- 18 Becue, A., Meurice, N., Leherte, L., and Vercauteren, D.P. (2004). *J. Comput. Chem.* 25: 1117.
- 19 Bytheway, I., Darley, M.G., and Popelier, P.L.A. (2008). *ChemMedChem* 3: 445.
- 20 Rafat, M. and Popelier, P.L.A. (2007). *J. Comput. Chem.* 28: 2602.
- 21 Smith, B.J. and Hall, N.E. (1998). *J. Comput. Chem.* 19: 1482.
- 22 Stefanovich, E.V. and Tiwong, T.N. (1995). *Chem. Phys. Lett.* 244: 65.
- 23 Pauling, L. (1960). *The Nature of the Chemical Bond*, 3e. Ithaca, NY: Cornell University Press.
- 24 Slater, J.C. (1964). *J. Chem. Phys.* 41: 3199.
- 25 Bondi, A. (1964). *J. Phys. Chem.* 68: 441.
- 26 Politzer, P., Parr, R.G., and Murphy, D.R. (1983). *J. Chem. Phys.* 79: 3859.
- 27 Chattaraj, P.K., Cedillo, A., and Parr, R.G. (1995). *J. Chem. Phys.* 103: 10621.
- 28 Putz, M.V., Russo, N., and Sicilia, E. (2003). *J. Phys. Chem. A* 107: 5461.
- 29 Boyd, R.J. (1977). *J. Phys. B: Atom. Mol. Phys.* 10: 2283.
- 30 Deb, B.M., Singh, R., and Sukumar, N. (1992). *J. Mol. Struct. THEOCHEM* 259: 121.
- 31 Yang, Z.Z. and Davidson, E.R. (1997). *Int. J. Quantum Chem.* 62: 47.
- 32 Yang, Z.Z., Li, G.H., Zhao, D.X. et al. (1998). *Chin. Sci. Bull.* 43: 1452.
- 33 Yang, Z.Z. and Niu, S.Y. (1991). *Chin. Sci. Bull.* 36: 964.
- 34 Yang, Z.Z., Niu, S.Y., Tang, S.Q., and Shen, E.Z. (1995). *Abstract PAP Am. Chem. Soc.* 210: 108.

- 35 Yang, Z.Z., Tang, S.Q., and Niu, S.Y. (1996). *Acta. Chim. Sin.* 54: 846.
- 36 Zhang, M.B., Zhao, D.X., and Yang, Z.Z. (2005). *J. Theor. Comput. Chem.* 4: 281.
- 37 Waber, J.T. and Cromer, D.T. (1965). *J. Chem. Phys.* 42: 4116.
- 38 Bader, R.F.W., Hennaker, W.H., and Cade, P.E. (1967). *J. Chem. Phys.* 44: 3341.
- 39 Zhao, D.-X., Yan, C.-Y., Zhu, Z.-W. et al. (2018). *Mol. Phys.* 116: 969.
- 40 Ayers, P.W. (2001). *Theor. Chem. Acc.* 106: 271.
- 41 Shannon, R.D. (1976). *Acta. Cryst.* A32: 751.
- 42 Ospadov, E., Tao, J., Staroverov, V.N., and Perdew, J.P. (2018). *Proc. Natl. Acad. Sci. U.S.A.* 115: E11578.
- 43 DeKock, R.L., Strikwerda, J.R., and Yu, E.X. (2012). *Chem. Phys. Lett.* 547: 120.
- 44 Wang, Z., Shaik, S., and Wang, B. (2021). *J. Am. Chem. Soc.* 143: 1005.
- 45 Zhao, D.X. and Yang, Z.Z. (2014). *J. Phys. Chem. A* 118: 9045.
- 46 Zhao, D.X., Gong, L.D., and Yang, Z.Z. (2005). *J. Phys. Chem. A* 109: 10121.
- 47 Pople, J.A. and Beberidge, D.L. (1970). *Approximate Molecular Orbital Theory*. New York: McGraw-Hill Book Company.
- 48 Zhao, D.-X., Zhao, J., Liu, X.-N. et al. (2020). *Theor. Chem. Acc.* 139: 1.
- 49 Politzer, P., Murray, J.S., and Clark, T. (2010). *Phys. Chem. Chem. Phys.* 12: 7748.
- 50 Zhao, D.X. and Yang, Z.Z. (2002). *J. Mol. Struct. (THEOCHEM)* 579: 73.
- 51 Yang, Z.Z., Zhao, D.X., and Wu, Y. (2004). *J. Chem. Phys.* 121: 3452.
- 52 Zhang, M.B. and Yang, Z.Z. (2005). *J. Phys. Chem. A* 109: 4816.
- 53 Li, X. and Yang, Z.Z. (2006). *J. Theor. Comput. Chem.* 5: 75.
- 54 Yang, Z.Z., Ding, Y.L., and Zhao, D.X. (2009). *J. Phys. Chem. A* 113: 5432.
- 55 Ding, Y.L., Gong, L.D., Zhao, D.X. et al. (2009). *J. Theor. Comput. Chem.* 8: 983.
- 56 Yang, Z.Z., Ding, Y.L., and Zhao, D.X. (2008). *Chemphyschem* 9: 2379.
- 57 Kohn, W. and Sham, L. (1965). *Phys. Rev. A* 140: 1133.
- 58 Parr, R.G. and Yang, W.T. (1989). *Density-Functional Theory of Atoms and Molecules*. New York: Oxford University Press.
- 59 Liu, S., Rong, C., and Lu, T. (2017). *Phys. Chem. Chem. Phys.* 19: 1496.
- 60 Liu, S. (2007). *J. Chem. Phys.* 126: 244103.
- 61 Smith, M.B. and March, J. (2007). *March's Advanced Organic Chemistry: Reactions, Mechanisms, and Structure*. New York: Wiley.



## 20

## Bridging Conceptual Density Functional and Valence Bond Theories

*Thijs Stuyver and Sason Shaik*

*The Hebrew University, Institute of Chemistry, Edmond J. Safra Campus at Givat Ram, Jerusalem 9190401, Israel*

### 20.1 Introduction

Kohn–Sham density functional theory (KS-DFT), as well as regular molecular orbital (MO) theory, uses delocalized electronic wave functions, i.e. each electron is considered to be “smeared out” over the system as a whole [1, 2]. In practical terms, both of these theories involve – in one way or the other – the construction of molecular/delocalized orbitals (usually by taking linear combinations of atomic orbitals), of which the shape is modulated/optimized to obtain an accurate description of the electronic structure of the chemical system under consideration.

Valence bond (VB) theory on the other hand takes an entirely different approach [3]. Here, one starts by defining localized configurations where individual atomic orbitals are populated directly by the electrons present in the chemical system. Many configurations (also called VB structures or diabatic states) can be defined in this manner, and usually these are not orthogonal, i.e. they interact significantly among themselves. By taking linear combinations and optimizing the weights of the individual configurations/structures, one ends up with the (correlated) ground- (and excited) states – also called adiabatic states – of the chemical system.

To focus our thoughts, let us consider the VB description of the wave function for the simplest possible molecule,  $H_2$ , in the case of a minimal basis set, i.e. one s-orbital on each H-moiety (Figure 20.1). For this simplistic molecule, one can distinguish a singlet-paired covalent structure  $H\bullet-\bullet H$ , also known as the Heitler–London (HL) structure, two ionic structures,  $H^+ \dots H^-$  and  $H^- \dots H^+$ , and a set of equivalent triplet structures (Figure 20.1a). Taking linear combinations of these structures, one ends up with the full, adiabatic states of  $H_2$ . As can be inferred from Figure 20.1b, the lowest state for  $H_2$ , i.e. the ground state, consists mainly of the HL structure, with a minor contribution of the ionic structures. Above the ground state, two excited singlet states can be distinguished, corresponding almost exclusively to linear combinations of the ionic structures. Finally, an additional (covalent) state can be defined, which stems exclusively from the triplet structure(s).

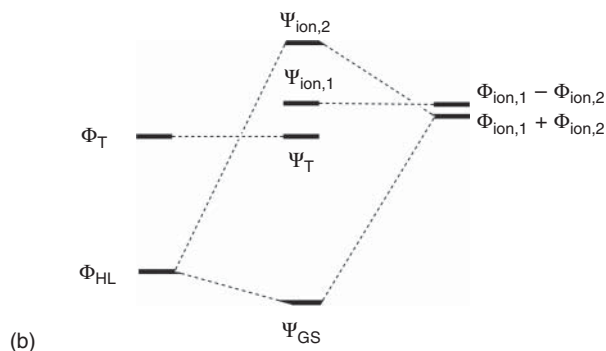
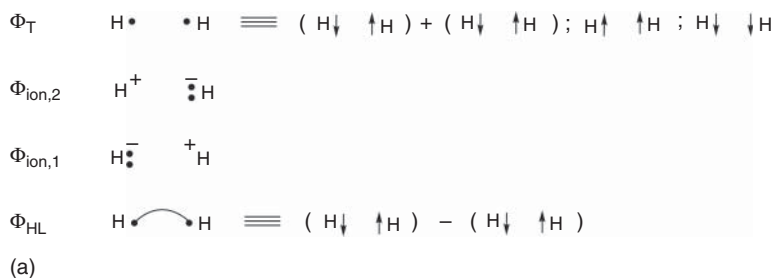


**Figure 20.1** (a) The individual VB structures which can be defined for  $\text{H}_2$ , i.e. the HL structure ( $\Phi_{\text{HL}}$ ), the ionic structures ( $\Phi_{\text{ion},1}$  and  $\Phi_{\text{ion},2}$ ), and the three equivalent triplet structures ( $\Phi_{\text{T}}$ ). Note that the arched lines in  $\Phi_{\text{HL}}$  connecting the electrons signify favorable singlet pairing. (b) The adiabatic states which can be constructed through linear combinations of these localized structures: the ground-state wave function ( $\Psi_{\text{GS}}$ ), two (mainly) ionic wave functions ( $\Psi_{\text{ion},1}$  and  $\Psi_{\text{ion},2}$ ), and the triplet wave function ( $\Psi_{\text{T}}$ ). Source: From Stuyver and Shaik [4]. American Chemical Society.

The final ground-state wave function emerging from a VB treatment is perfectly equivalent to the wave function obtained through a corresponding correlated MO treatment, cf. MO-CI (with CI corresponding to configuration interaction), and thus also agrees with the corresponding KS-DFT description – when an adequate functional is used. As such, the choice of perspective (localized vs. delocalized) is in fact the only real difference between these theories.

The fact that KS-DFT and VB descriptions are in principle equivalent, does not necessarily imply that they lead to equivalent insights as well. It has been argued and demonstrated at various instances throughout the literature that some chemical phenomena can actually be described more straightforwardly from a delocalized perspective, whereas others benefit from a localized treatment [1, 3, 5–7]. Furthermore, going back and forth between the two perspectives can in many cases be extremely productive and lead to enhanced insights in the chemical problems at hand.

In this chapter, we aim to build explicit bridges between conceptual density functional theory (CDFT) [8, 9] and qualitative VB theory, and thereby demonstrate that important synergies and new insights arise by combining both. More specifically, we will provide a concise overview of our recent work on local reactivity descriptors,



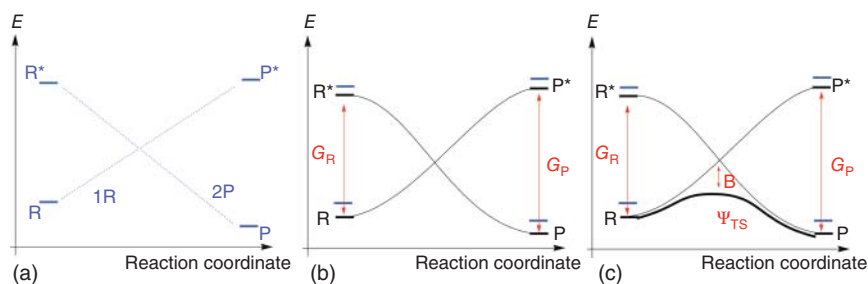


**Figure 20.3** VB reactivity diagrams, depicting the diabatic and adiabatic energy curves along the reaction coordinate connecting the reactants (R), i.e.  $\text{H}_3\text{C}\bullet$  and  $\text{H-SiH}_3$ , to the products (P), i.e.  $\text{H}_3\text{C-H}$  and  $\bullet\text{SiH}_3$ . (a) The HL structures (i.e.  $\mathbf{1}_R$  and  $\mathbf{2}_P$ ) are first-order approximations of the electronic structure of R and P, respectively. (b) The same VB diagram but now with the ionic structures mixed into the diabatic reactant and product states (resulting in a slight stabilization with respect to the curves for  $\mathbf{1}_R$  and  $\mathbf{2}_P$  in isolation).  $G_R$  and  $G_P$  denote the promotion energy gaps on the reactant- and product side, respectively. (c) The same VB diagram but now with the adiabatic curve, which arises from the mixing of the individual diabatic curves, included in bold.  $\Psi_{\text{TS}}$  corresponds to the transition state. **B** denotes the resonance interaction between the two curves in the TS geometry. Source: From Stuyver et al. [10]. American Chemical Society.

one moves away from the optimal product geometry and, at the optimal reactant geometry, this VB structure can be regarded as a first-order approximation of the promoted state of the reactant R, denoted by  $R^*$ . This way, the rudimentary shape of two crossing diabatic curves is obtained, cf. Figure 20.3a.

So far, we have focused exclusively on the main HL structures. As mentioned in the introduction, secondary structures, e.g. ionic configurations, interact with the HL ones. More specifically for our model reaction, structures **3** and **4** in Figure 20.2 can be expected to contribute to the H-SiH<sub>3</sub> Lewis bond in  $\mathbf{1}_R$ , while **5** and **6** will contribute to the full bond in  $\mathbf{2}_P$ . Often, these ionic structures are directly combined with the HL structures to form the so-called diabatic reactant and product Lewis states, offering a more accurate description of R,  $R^*$ , P, and  $P^*$  (Figure 20.3b). With the ionic structures included, it can be demonstrated that the promotion energies required to excite R to  $R^*$  and P to  $P^*$  ( $G_R$  and  $G_P$ ), can be expressed as the singlet-triplet excitation energies of the active reactant and product bonds (H-SiH<sub>3</sub>/H-CH<sub>3</sub>). These quantities correspond approximately to twice the respective bond energies [12, 14].

Next to the ionic structures, one can also distinguish charge-transfer (CT) structures, i.e. structures which involve an odd number of electrons in both the right-hand and left-hand bonds, cf. structures **7** and **8** in Figure 20.2. In the optimal reactant or product geometries, **7** and **8** generally do not interact with the main structures  $\mathbf{1}_R$  and  $\mathbf{2}_P$ . Consequently, they do not contribute to either the reactant or product diabatic states. However, their mixing does become allowed in the transition-state (TS) geometry region (cf. Figure 20.3b). As a result, the full, i.e. adiabatic, wave function, which results from the intermixing of all the diabatic states (*vide supra*), will be pushed significantly below the crossing point of the reactant and product curves. The resulting energy hill obtained (cf. Figure 20.3c) corresponds to the reaction barrier for the considered chemical reaction. The total amount of resonance stabilization of

the adiabatic state with respect to the crossing point between reactant and product state in the TS geometry is usually denoted by **B**.

Based on this rudimentary VB model of chemical reactivity, the following expression for the barrier height or activation energy associated with a generic chemical reaction can be derived [14]

$$\Delta E^\ddagger = f_0 G_0 + 0.5 \Delta E_{\text{rp}} - B \quad (20.1)$$

where  $\Delta E_{\text{rp}}$  stands for the thermodynamic driving force and  $f_0 G_0$  corresponds to a fraction ( $f_0$ ) of the average of the promotion gaps on the reactant and product side,

$$G_0 = 0.5 (G_{\text{R}} + G_{\text{P}}) \quad (20.2)$$

Let us now apply this equation to estimate quantitatively the activation energy associated with the model reaction considered, i.e. the H-abstraction from H-SiH<sub>3</sub> by H<sub>3</sub>C•. In previous studies on the properties of the diabatic curves for hydrogen abstraction reactions,  $f_0$  was determined to amount to approximately 0.348, and **B** to 50 kcal mol<sup>-1</sup>. For H-SiH<sub>3</sub>, the experimental bond dissociation enthalpy (BDE) amounts to 87 kcal mol<sup>-1</sup> and for H-CH<sub>3</sub>, this quantity amounts to 105 kcal mol<sup>-1</sup>. As such, the averaged promotion gap  $G_0$  can be crudely estimated to amount to 192 kcal mol<sup>-1</sup>. Furthermore, given that the overall effect of the hydrogen exchange reaction under consideration is the breaking of a Si-H bond and the formation of a C-H bond,  $\Delta E_{\text{rp}}$  can be approximated as the energy difference between the two corresponding BDE values, i.e.  $\Delta E_{\text{rp}} \approx -18$  kcal mol<sup>-1</sup>. Inserting all these quantities into Eq. (20.1) leads to an estimated activation energy for the reaction of approximately 7.8 kcal mol<sup>-1</sup>. These estimates agree nicely with the corresponding values calculated at UB3LYP/cc-pVTZ level-of-theory [15-17] ( $\Delta E^\ddagger = 6.9$  kcal mol<sup>-1</sup> and  $\Delta E_{\text{rp}} = -13.4$  kcal mol<sup>-1</sup>, respectively).

## 20.3 How Does Delocalization Affect the Shape of the Curves in the VB Diagram?

The model system in the previous section, H<sub>3</sub>C• + H-SiH<sub>3</sub>, involved a perfectly localized radical electron, so that both the reactant and product states could be approximated initially by a single (HL) structure. The localization of the wave function of the chemical system in such a situation is reflected among others in the spin density distribution: in the reactants, C carries a spin density of approximately unity, in the products, it is Si, which carries unity spin.

Let us now consider what happens to the shape of the potential energy surface (PES) when extensive electronic delocalization enters the picture [10]. Again, we focus on a model reaction: the hydrogen exchange between allyl• and SiH<sub>4</sub>. It should be clear that the reaction between these two reagents can result in several reaction products. For the sake of the argument that follows, let us focus specifically on the main products expected, i.e. **P1** and **P2** in Figure 20.4a. Evidently, these two products are chemically equivalent, but mathematically (when one assigns labels

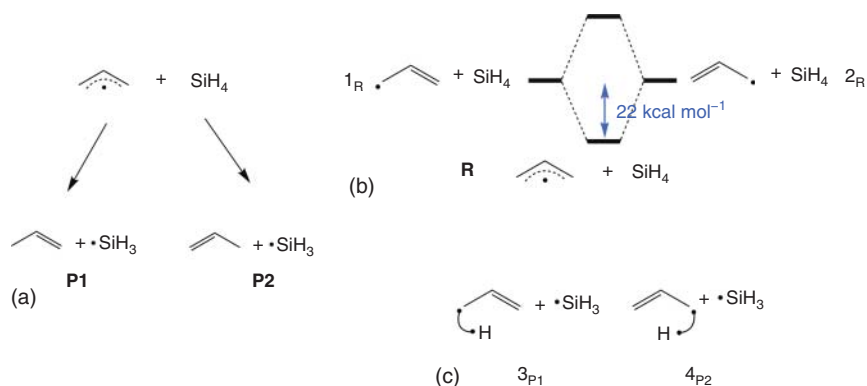


**Figure 20.4** (a) The main products formed from the reaction between allyl• and SiH<sub>4</sub>. The “+” signs denote that the species on opposing sides of this sign are perfectly separated. (b) The resonance mixing of the two localized structures and the resulting delocalized allyl•. The displayed resonance energy was calculated at VBSCF/6-311++G\*\*//UB3LYP/cc-pVTZ level-of-theory [18, 19]. (c) The major VB structures associated with the products **P1** and **P2** in panel (a), respectively. Source: From Stuyver et al. [10]. American Chemical Society.

to the individual C-atoms), or if one of the ethylenic carbons is <sup>14</sup>C, their electronic structure is described distinctively.

In contrast to the localized (radical) system discussed in the previous section, it is now impossible to define a single VB structure that adequately represents the reactant state: the wave function associated with allyl• inherently consists of a linear combination of two equivalent Lewis VB structures (Figure 20.4b). The extent of mixing of these two equivalent, localized structures taking part in the full wave function is significant; quantitative VB calculations at VBSCF/6-311++G\*\*//UB3LYP/cc-pVTZ level-of-theory [18, 19] point to an overall resonance stabilization of approximately 22 kcal mol<sup>-1</sup> for the adiabatic wave function of allyl• compared to its localized constituents. As a consequence of this delocalization, the atom-condensed spin densities on neither of the extremal carbon centers of allyl• approach unity; instead, they both amount to approximately 0.63e (the central carbon center carries a negative spin of -0.26e). The individual products on the other hand can perfectly be described by a single (Lewis) VB structure each (Figure 20.4c). As a consequence, the radical centers for these species become perfectly localized once more: the natural population analysis (NPA) spin density on the product Si approaches unity ( $\rho(\text{Si}) = 0.97e$ ).

As such, one can conclude that the resonance energy associated with the delocalization of the radical electron, which is present in the reactant, is lost once either of the possible products is reached.

Note that the impact of the loss of delocalization is reflected not only in the evolution of the spin density distribution throughout the reaction, but also in the geometry of the system. Whereas in the reactant allyl•, the two C—C bonds are equal in length due to the resonance between the two individual localized VB structures, the product

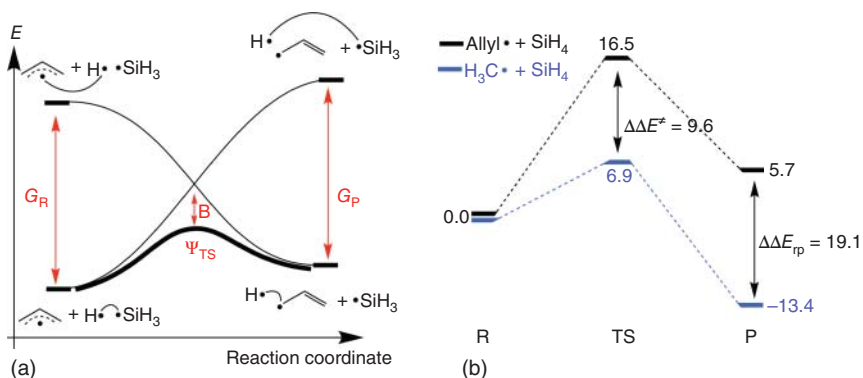


**Figure 20.5** (a) The VB reactivity diagram for the H-abstraction reaction between allyl• and H-SiH<sub>3</sub>. (b) The calculated potential energy profile for the hydrogen abstraction reaction of allyl• and H<sub>3</sub>C• with SiH<sub>4</sub>. Calculations were performed at UB3LYP/cc-pVTZ level-of-theory [15–17]. Energy values are presented in kcal mol<sup>-1</sup> (with ZPE included). Source: From Stuyver et al. [10]. American Chemical Society.

propene has two unequal C—C bonds: a short one corresponding to the double bond, and a long one corresponding to the single bond in the dominant product VB structure (cf. **3<sub>P1</sub>** in Figure 20.4c).

Let us consider now how this loss of resonance energy impacts the PES exactly by constructing the VB diagram associated with the reaction under consideration (Figure 20.5a).

In the reactant geometry, the reactant state R is resonance stabilized due to the interaction between the localized **1<sub>R</sub>** and **2<sub>R</sub>** states; *vide supra* (Figure 20.5a). The excited reactant state (R\*) can be expected to be equally delocalized in this geometry: **3<sub>P1</sub>** and **4<sub>P2</sub>** are degenerate in the reactant geometry, and hence they will each contribute to the wave function equally. On the product side, the product state P is – as discussed – localized. Since P\* corresponds to the vertical excitation of P, this state shares the same (localized) geometry of the product, and hence, it will also be mainly localized.

As such, for a delocalized species undergoing a (localization) reaction, the product states are both destabilized with respect to the reactant states in the VB diagram. The extent of destabilization is connected to the resonance energy present in the reactant state but usually does not correspond quantitatively to this quantity: geometric relaxation of the system as the reaction proceeds can be expected to increasingly accommodate – and thus stabilize – the emerging dominant product VB structure. Consequently, the resonance energy loss is partially compensated. For our model H-abstraction reaction involving the delocalized allyl•, we computationally obtain a thermodynamic driving force  $\Delta E_{rp}$  of +5.7 kcal mol<sup>-1</sup>. Since  $\Delta E_{rp}$  for the corresponding reaction involving the localized H<sub>3</sub>C• amounted to -13.4 kcal mol<sup>-1</sup> (cf. the previous section), the actual relative destabilization of the product state for this specific localized product can be estimated at 19.1 kcal mol<sup>-1</sup>. Hence, the total amount of resonance energy present in the reactant state should

be considered as an upper limit and a guide value for the actual relative product destabilization.

According to the barrier height equation introduced in the previous section (cf. Eq. (20.1)), a decrease in  $\Delta E_{\text{rp}}$  should induce an increase in the activation energy associated with the reaction. More specifically, given that  $\Delta\Delta E_{\text{rp}}$  amounted to 19.1 kcal mol<sup>-1</sup> when comparing the H-abstraction reaction involving H<sub>3</sub>C• with the one involving allyl•, one can estimate  $\Delta\Delta E^\ddagger$  to amount to approximately 9.5 kcal mol<sup>-1</sup> in our case, assuming that the other factors in the expression remain more or less constant. This is exactly what emerges from our UB3LYP/cc-pVTZ calculations:  $\Delta E^\ddagger$  amounts to 6.9 kcal mol<sup>-1</sup> for H<sub>3</sub>C•, while for allyl•,  $\Delta E^\ddagger$  is calculated to be 16.5 kcal mol<sup>-1</sup> (Figure 20.5b). Note that the same qualitative trend could also have been inferred from the Bell–Evans–Polanyi principle [20, 21].

## 20.4 The Spin Density Distribution as a Probe for the Regioselective Preference in Radical Reactions

So far, we have discussed how changes in spin delocalization affect the PES associated with a radical reaction through modification of the thermodynamic driving force. In this section, we will concisely discuss how, building on this knowledge, the spin density distribution can be cast as a natural reactivity indicator for radical molecules containing multiple reactive sites, able to infer the “most favorable” reaction pathway, i.e. the regioselectivity. Once more, we focus our attention on a simplistic model system, vinyloxy radical (H<sub>2</sub>C=CH-O•), shown in Figure 20.6a. A simple electronic structure calculation reveals that the radical electron in this compound is mainly localized on the extremal C-center: the NPA spin density on this site amounts to 0.79e, the O-moiety on the other end of the molecule carries a spin density of 0.36e.

In agreement with these calculated spin densities, we find that the localized VB structure in which the unpaired electron resides on the C-site is significantly

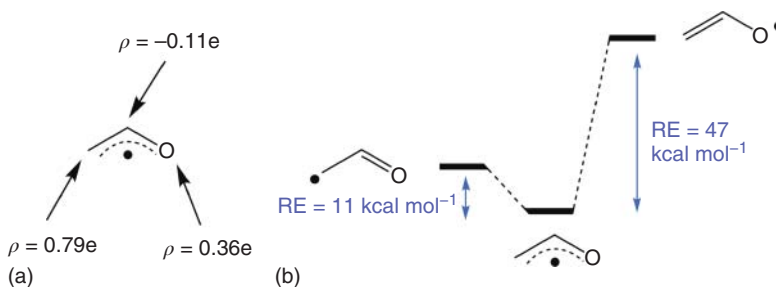


**Figure 20.6** (a) The NPA spin density distribution for vinyloxy•, calculated at UB3LYP/cc-pVTZ level of theory. (b) The interaction between the localized resonance structure giving rise to the delocalized ground state of vinyloxy•. Resonance energies were calculated at VBSCF/6-311++G\*\*/UB3LYP/cc-pVTZ level-of-theory. Source: From Stuyver et al. [10]. American Chemical Society.



**Table 20.1** Comparison of the barrier heights ( $\Delta E^\ddagger$ ), and reaction energies ( $\Delta E_{\text{rp}}$ ) of H-abstraction from  $\text{SiH}_4$  for both attack sites of vinyloxy• and their corresponding localized analogs ( $\text{H}_3\text{C}\bullet$  and  $\text{HO}\bullet$ ), calculated at UB3LYP/cc-pVTZ level-of-theory.

	H-abstraction from $\text{SiH}_4$ (C-attack)		H-abstraction from $\text{SiH}_4$ (O-attack)		
	$\Delta E^\ddagger$ (kcal mol <sup>-1</sup> )	$\Delta E_{\text{rp}}$ (kcal mol <sup>-1</sup> )	$\Delta E^\ddagger$ (kcal mol <sup>-1</sup> )	$\Delta E_{\text{rp}}$ (kcal mol <sup>-1</sup> )	
Vinyloxy•	9.8	-2.3	Vinyloxy•	18.3	9.5
$\text{H}_3\text{C}\bullet$	6.9	-13.4	$\text{HO}\bullet$	0.0	-24.9

Energy values are presented in kcal mol<sup>-1</sup> (with ZPE included). Note that the changes in  $\Delta E_{\text{rp}}$  agree qualitatively with the calculated delocalization energies (11 and 47 kcal mol<sup>-1</sup>, respectively).

more stable than the one in which the radical resides on the O-site: for the former structure, the resonance energy separating it from the delocalized resonance hybrid amounts to merely 11 kcal mol<sup>-1</sup>, whereas for the latter structure, the resonance energy amounts to almost 47 kcal mol<sup>-1</sup> (Figure 20.6b).

As such, given the analysis in the previous section, one can reasonably expect that this delocalized radical compound will preferentially engage in radical reactivity through the terminal C-center: reacting from this side of the molecule causes a much smaller loss of delocalization energy throughout the reaction. Our computations confirm this behavior: for the H-abstraction reaction from  $\text{SiH}_4$ , the decrease in thermodynamic driving forces for the two attack positions with respect to their corresponding localized analogs ( $\text{HO}\bullet$  and  $\text{H}_3\text{C}\bullet$ , respectively) is in line with the magnitude of the “delocalization penalty” associated with each site (cf. Table 20.1). Since the barrier heights increase more or less proportionally with the change in  $\Delta E_{\text{rp}}$ , reaction from the C-site is indeed unequivocally favored, both thermodynamically and kinetically.

## 20.5 Extending the VB Delocalization Perspective to Other Local Reactivity Descriptors: The Case of the Fukui Function

So far, only a single local reactivity descriptor has been considered: the spin density distribution. The goal of the present section is to demonstrate that the presented viewpoint can straightforwardly be extended to other (CDFT) reactivity descriptors as well. In particular, we will focus on the Fukui function [2, 8, 22], a local reactivity descriptor associated with nucleophilic/electrophilic reactivity. Again, let us turn to a simple model reaction: the methylation of (ambident) vinyloxy anion (cf. Figure 20.7).

Analogous to the case of vinyloxy• discussed before, vinyloxy anion can react in two different ways: either through the C-site or through the O-site. Within a conceptual DFT approach, the most nucleophilic site of this compound is traditionally inferred through consideration of the spatial distribution of the Fukui function for

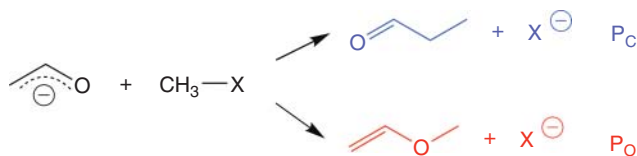


**Figure 20.7** The possible outcomes for the methylation reaction between vinyloxy anion and  $\text{CH}_3\text{X}$  ( $\text{X} = \text{F}, \text{Cl}, \text{Br}, \text{I}$ , etc.). Source: From Stuyver et al. [10]. American Chemical Society.

electrophilic attack,  $f^-(\mathbf{r})$  [8, 22, 23],

$$f^-(\mathbf{r}) = (\partial\rho(\mathbf{r})/\partial N)^- = \rho_N(\mathbf{r}) - \rho_{N-1}(\mathbf{r}) \approx \left| \Psi_{\text{HOMO}}^2 \right| \quad (20.3)$$

where  $\rho(\mathbf{r})$  corresponds to the electron density and  $N$  corresponds to the number of electrons in the compound.

Let us now explore how the Fukui function can be recovered within our qualitative VB framework by constructing the VB diagram associated with this reaction. For nucleophilic/electrophilic reactions, the product-state curve, i.e. the curve connecting the promoted reactant state ( $\text{R}^*$ ) to the product state ( $\text{P}$ ; *vide supra*), corresponds to a charge-transfer state. In the case of the reaction considered here, the relevant CT state is the one in which an electron is transferred from the vinyloxy anion to  $\text{H}_3\text{C-X}$ , as shown in Figure 20.8a. As such,  $\text{R}^*$  corresponds to mutually isolated vinyloxy $\bullet$  and radical anion  $\text{H}_3\text{C-X}^{\bullet-}$ . The vinyloxy radical species in  $\text{R}^*$  will obviously be delocalized: it is a hybrid of a localized structure in which the unpaired electron resides on the C-atom, in combination with another one in which this radical electron resides on the O-atom (*vide supra*; cf. Figure 20.6b).

As the reaction proceeds, i.e. as one advances from  $\text{R}$  to  $\text{P}$ , the resonance energy between these two localized structures in the vinyloxy $\bullet$  in the diabatic product curve will once again be lost; the methylation occurs either on the C- or O-side. As such, one can expect that the most stable product will be the one associated with the

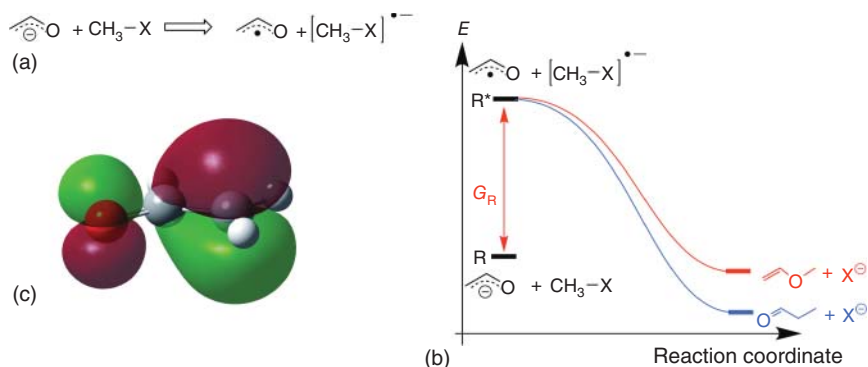


**Figure 20.8** (a) The CT state ( $\text{R}^*$  in b) in the reactant geometry corresponding to the product-state curve in the VB diagram for the methylation of vinyloxy anion. (b) The specific diabatic product curves associated with the two competing reaction pathways. (c) The HOMO-orbital of vinyloxy anion calculated at B3LYP/cc-pVTZ level-of-theory. Source: From Stuyver et al. [10]. American Chemical Society.

localized VB structure having the highest weight in the promoted product state  $R^*$ , since the corresponding mode of attack will involve the lowest “resonance penalty” to be paid. Hence, based on Figure 20.6b, one can infer that the C-attack will be the most thermodynamically favorable reaction pathway. Figure 20.8b enables one to visualize the specific product-state curves associated with the two competing reaction pathways.

Calculations performed by Mayr and coworkers confirm the analysis above: even though the computed absolute  $\Delta E_{rp}$  values in their study were observed to be highly dependent on the nature of the halogen in  $H_3C-X$ , the relative difference in thermodynamic driving force between the C- and O-attack, i.e.  $\Delta\Delta E_{rp}$ , consistently amounted to approximately  $20 \text{ kcal mol}^{-1}$  in favor of the C-attack [24].

Let us now review what we have discussed in this section so far. We have demonstrated that for nucleophilic attack involving an ambident reactant, the thermodynamic stability of the individual products is determined by the corresponding “resonance/delocalization penalty,” in a similar way as it was demonstrated to be the case for radical reactions. Contrary to our analysis in the previous sections, the resonance penalty here cannot be inferred simply from consideration of the spin density distributions. Instead, what needs to be analyzed is the delocalization of the radical electron in the ambident reactant – after one electron has been removed from this species (cf.  $R^*$  in Figure 20.8b). In practice, this delocalization can be probed by considering the distribution of the highest occupied molecular orbital (HOMO) of the nucleophile, since from an MO perspective, the radical electron resulting from the oxidation of this species will reside in this orbital. Turning back now to Eq. (20.3), one can straightforwardly see that we have effectively recovered the idea of a Fukui function as a local reactivity descriptor from a pure VB perspective! Indeed, one finds that the HOMO of vinyloxy anion is disproportionally localized on the extremal C-atom (Figure 20.8c) and accordingly, the atom-condensed Fukui function (calculated at (U)B3LYP/cc-pVTZ level-of-theory through NPA analysis in the finite difference approximation) has a significantly higher amplitude on this site as well, i.e.  $\rho(C) = 0.53e$  and  $\rho(O) = 0.34e$ .

Note that in Figure 20.8b, only the product curve is drawn. As discussed, knowledge about the evolution of this diabatic curve for different attack positions enables one to infer overall thermodynamic preferences. The kinetic preferences however cannot be inferred from information about this diabatic curve alone, since the latter preference depends on the location of the crossing point of the reactant and product states (and the amount of resonance energy  $B$ ; cf. Eq. (20.2)). Our analysis above clearly indicates that inspection of the Fukui function does not tell us anything about the evolution of the reactant curve for different attack positions, and consequently, the impact on the barrier height of an increased thermodynamic driving force may very well be canceled out by an enhanced increase of the reactant curve, resulting in a diverging thermodynamic and kinetic preference.

For the vinyloxy anion, this is exactly what one observes: even though C-attack is preferred thermodynamically (in line with the relative magnitudes of the Fukui function), the barrier for O-attack turns out to be slightly lower than for C-attack ( $\Delta E^\ddagger = 0.4 \text{ kcal mol}^{-1}$  at B3LYP/cc-pVTZ level-of-theory), i.e. the kinetic preference

is reversed and thus does not follow the trend suggested by the Fukui function [24]. As will be discussed at the end of this chapter, this “anomalous” kinetic preference can be attributed to differential electrostatic interactions in the respective TS geometries, as well as a preferential localization of the negative charge on the O-site in vinyloxy anion (i.e. the reactant curve for O-attack rises more slowly than the one for C-attack; *vide infra*).

## 20.6 Hardness and Softness from a VB Perspective

All of the local reactivity descriptors we have treated/recovered from a VB perspective up to this point (i.e. spin density and Fukui function distributions) described so-called (frontier) orbital or “soft–soft” interactions: they dealt with the pairing/re-pairing of electron pairs in the constructed VB diagram. Conceptual DFT however tells us that there is another interaction type which can drive reactivity as well: electrostatic interactions. Indeed, according to the HSAB principle [25–27], reactions ought to be dominated by either one of these two interaction types. Whichever type dominates in the reaction under consideration is then expected to determine the corresponding regioselectivity: the preferential association site for soft compounds is generally assumed to be dictated by the Fukui function distribution [22], whereas the preferential association site for hard compounds is assumed to be dictated by atom-condensed charges or molecular electrostatic potential (MEP) maps [28, 29].

Taking a delocalized perspective on electronic structure (*vide supra*), the individual magnitudes of (frontier) orbital and electrostatic interactions cannot be probed explicitly in a straightforward fashion. Consequently, there has been a heated debate and some confusion in the CDFT literature about the relative magnitude and importance of the respective electrostatic/(frontier) orbital contributions for specific reaction types [30–32]. As we will demonstrate below, VB theory enables a straightforward resolution of the respective contributions and thus enables a more profound study of the role played by the individual local descriptors in shaping the PES [11]. The key to achieve this feat is to consider ionic and HL structures separately, i.e. to refrain from mixing them together into Lewis structures as we have done in the previous sections (*vide supra*).

Let us focus here on protonation reactions (in the gas phase), since this ubiquitous reaction type in particular has been the subject of controversy in recent years.  $H^+$  is generally considered as a prototypical hard electrophile, so one could naively expect that the association of this species with a reaction partner would generally be dominated by electrostatic, i.e. hard–hard, interactions. Indeed, several researchers have reported that electrostatic descriptors, e.g. partial charges and MEP maps, are suitable guides to identify preferential/likely protonation sites in a variety of systems [33–35]. At the same time, it should be noted that the bond formed between a proton and its reaction partner is generally assumed to be covalent in nature. As such, an electron re-pairing unequivocally occurs throughout the reaction, which suggests that spin-pairing (or soft–soft) interactions most certainly are not negligible

either. Indeed, Bettens et al. recently reported that in protonation reactions of a variety of alkaline earth and transition metal complexes, e.g.  $\text{Ca}(\text{N}_2)_8$  and  $\text{Cr}(\text{N}_2)_8$ , the  $\text{H}^+$  species prefer those sites which carry the highest HOMO amplitude, i.e. they prefer to associate with the softest sites of the complex [36].

To shed some more light on this seemingly contradictory situation, let us consider a generic protonation reaction, i.e. the mutual approach of an  $\text{H}^+$  and an (organic/inorganic) molecule R, from a VB perspective [3, 11]. Just as in the case of  $\text{H}_2$  (cf. Section 20.1), three main (singlet) VB structures can be associated with the  $[\text{R}\dots\text{H}]^+$  system: a HL/covalent one ( $\text{R}^+\bullet\text{--}\bullet\text{H}$ ), as well as two ionic ones ( $\text{R}:\text{H}^+$  and  $\text{R}^{2+}:\text{H}^-$ , respectively). In the HL structure, a neutral  $\text{H}\bullet$  approaches  $\text{R}^+\bullet$  so that the only significant stabilizing interaction that can emerge stems from spin pairing. In the ionic structures, a charged species ( $\text{H}^+$  and  $:\text{H}^-$ , respectively) approaches the  $\text{R}/\text{R}^{2+}$  system, so that – depending on the polarity of the region of  $\text{R}/\text{R}^{2+}$  to which the charged species associates – either an electrostatic stabilization or destabilization will emerge. One can logically expect that the spacing at infinite separation between the HL and the ionic structures in  $[\text{R}\dots\text{H}]^+$  will determine to a significant extent the nature of the bond being formed.

The energetic separation between the main ionic structure,  $\Phi_{\text{ion},1}(\text{R}\dots\text{H}^+)$ , and the HL structure,  $\Phi_{\text{HL}}(\text{R}^+\text{--}\text{H})$ , in the dissociated geometry can be approximated as,

$$E(\Phi_{\text{ion},1}) - E(\Phi_{\text{HL}}) = A_{\text{H}^+} - I_{\text{R}} = I_{\text{H}} - I_{\text{R}} \quad (20.4)$$

with  $I_{\text{R}}$  the vertical ionization potential (IP) of R and  $A_{\text{H}^+}$  the electron affinity of the proton (which is identical to the IP of H,  $I_{\text{H}}$ ).

The spacing between the HL structure and the second ionic structure,  $\Phi_{\text{ion},2}(\text{R}^{2+}:\text{H}^-)$ , can be approximated as,

$$E(\Phi_{\text{ion},2}) - E(\Phi_{\text{HL}}) = A_{\text{H}} - I_{\text{R}^+} \quad (20.5)$$

According to Eq. (20.4),  $\Phi_{\text{ion},1}$  will be lower than  $\Phi_{\text{HL}}$  in the dissociation limit in the case that the (vertical) IP of R is larger than  $313.6 \text{ kcal mol}^{-1}$ , which is the IP of H. For most common molecules this will not be the case. To provide some perspective, the vertical IP of  $\text{H}_2\text{O}$  amounts to approximately  $295 \text{ kcal mol}^{-1}$ , for  $\text{NH}_3$ , this quantity amounts to  $251 \text{ kcal mol}^{-1}$  and for ethylene and pyridine, it amounts respectively to  $243$  and  $217 \text{ kcal mol}^{-1}$  (values calculated at B3LYP/6-31++G\*\*\*/B3LYP/def2-TZVP level-of-theory).

As such, at infinite separation, the HL structure associated with the protonated system will generally be the lowest diabatic state. However, it should be clear that the energetic spacing between this structure and  $\Phi_{\text{ion},1}$  will be on the lower side: it will range from close to a  $100 \text{ kcal mol}^{-1}$  in case of pyridine +  $\text{H}^+$  to a mere  $20 \text{ kcal mol}^{-1}$  in case of  $\text{H}_2\text{O} + \text{H}^+$ . This relatively small spacing is already an indication that the formed bond between R and  $\text{H}^+$  will most likely correspond to neither a purely covalent nor a purely ionic bond (*vide infra*).

In Figure 20.9, a concise VB analysis of the R—H bond formation process is presented for some simple single-site model systems, i.e.  $\text{H}_3\text{O}^+$ ,  $\text{NH}_4^+$ , and  $\text{H}_3\text{S}^+$  (calculations were performed at DFVB(LYP)/6-31++G\*\*\*/B3LYP/def2-TZVP

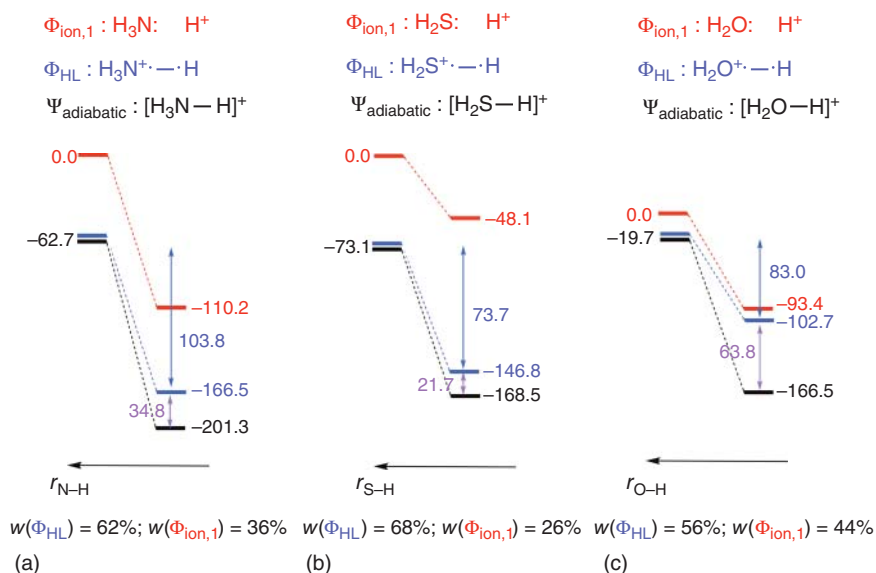


**Figure 20.9** Schematic representation of the bonding interaction and the evolution of the energy of the individual diabatic structures and the global adiabatic ground state associated with a protonation reaction for (a)  $[\text{H}_3\text{N}-\text{H}]^+$ , (b)  $[\text{H}_2\text{S}-\text{H}]^+$ , and (c)  $[\text{H}_2\text{O}-\text{H}]^+$ . Note that the curves associated with  $\Phi_{\text{ion},2}$  are not depicted in this figure due to the significant distance between this curve and the ones associated with  $\Phi_{\text{ion},1}$  and  $\Phi_{\text{HL}}$ , respectively. The spin-pairing stabilization energies associated with  $\Phi_{\text{ion},1}$  upon bond formation are depicted in blue italics; the resonance energies are denoted in magenta. At the bottom of each panel, we show the weights of the individual structures in the adiabatic wave function at the optimal bonding distance. Source: From Stuyver and Shaik [11]. American Chemical Society.

level-of-theory [37] with the XMVB code [18, 19], where R and H were selected as the local fragments from which the wave function is constructed).

A first conclusion that can be drawn from this figure is that for each of the considered bonds, the HL structure remains the main contributor to the wave function throughout the entire bond formation process (hence, there are no diabatic crossovers and protonation reactions are generally barrierless in the gas phase). Furthermore, the nature of the formed bond is indeed a reflection of the relative spacing of the VB structures at infinite separation, i.e. the relative magnitude of the IP of  $\text{NH}_3$ ,  $\text{H}_2\text{S}$ , and  $\text{H}_2\text{O}$ . It follows that the  $[\text{H}_2\text{S}-\text{H}]^+$  bond is the most covalent, followed by the  $[\text{H}_3\text{N}-\text{H}]^+$  one, and finally the  $[\text{H}_2\text{O}-\text{H}]^+$  bond (the weights of the HL structures in the wave functions exceed 68%, 61%, and 55%, respectively).

Even though our analysis indicates that the R—H bond for each of these model systems is formally covalent in nature at the optimal bonding distance, Figure 20.9 clearly demonstrates that the bulk of the protonation/bonding energy cannot be attributed exclusively to either the electrostatic or the spin-pairing interaction: the resonance contribution caused by the mixing between the individual VB structures is significant. For  $\text{H}_3\text{S}^+$ , the contribution to the full protonation energy, i.e.  $E(\Phi_{\text{ion},1}[\text{dissociated}]) - E(\Psi_{\text{adiabatic}}[\text{bonded}])$ , by the resonance energy is still

relatively limited; it is responsible for 22 kcal mol<sup>-1</sup> out of a total of 169 kcal mol<sup>-1</sup>. For NH<sub>4</sub><sup>+</sup>, the contribution by the resonance energy increases slightly to 35 kcal mol<sup>-1</sup> out of a total of 201 kcal mol<sup>-1</sup>; for H<sub>3</sub>O<sup>+</sup>, the resonance energy accounts already for close to 40% of the protonation energy: the resonance with the (electrostatics-governed) ionic structure contributes 64 out of 167 kcal mol<sup>-1</sup>.

Note that the latter resonance energy value (64 kcal mol<sup>-1</sup>) approaches 50% of the total adiabatic bonding energy (147 kcal mol<sup>-1</sup>), i.e. the energy lowering of the black curve in Figure 20.9c. As some of us have discussed before, whenever resonance becomes significant and/or starts to take over from either pure electrostatics or spin pairing as the main driver of the bonding interaction, it is arguably more appropriate to categorize the considered bond distinctively as a so-called “charge-shift” bond instead of a covalent or ionic one [38, 39].

## 20.7 Regioselectivity in Protonation Reactions: Sometimes Consideration of a Single Spin-pairing/Orbital Interaction Descriptor Is Not Enough!

From the results for the selected model systems in the previous paragraphs, one could already deduce that the R—H bond in protonated molecules can range from mainly covalent to predominantly charge shift in nature. Let us now proceed from the considered single-site model systems, toward a couple of multi-site (combined) analogs, H<sub>2</sub>NOH and H<sub>2</sub>NSH, and probe their respective regioselectivity for protonation. Experimental data indicate that proton association will preferentially occur at the N-site for both of these species [40]. Note that these model systems were also considered previously by Chattaraj and coworkers to establish the proposed hardness-dominated regioselectivity of a protonation reaction [33].

In Figure 20.10, concise VB analyses are presented for the competing protonated products for both considered species, i.e. H<sub>3</sub>N<sup>+</sup>OH vs. H<sub>2</sub>NOH<sub>2</sub><sup>+</sup> and H<sub>3</sub>N<sup>+</sup>SH vs. H<sub>2</sub>NSH<sub>2</sub><sup>+</sup>. Figure 20.11 contains an overview of some local reactivity descriptors describing hard–hard and soft–soft interactions, i.e. on one hand the electrostatic potential (ESP) partial charges together with MEP maps for the unprotonated species, and on the other hand the NPA spin densities for the (unprotonated) oxidized species (our VB-inspired analog of the Fukui function [43, 44]; *vide supra*), respectively [10].

From a first inspection of Figure 20.10, it should already be clear that the composition of the considered bonds barely differs from their corresponding single-site analogs in Figure 20.9: the weights of the individual VB structures are equivalent, and the magnitude of resonance energy between the ionic and HL structures is also not affected. Protonation energies are also barely modified; for the respective N—H bonds formed, the protonation energies have decreased by 5–10 kcal mol<sup>-1</sup>, for the corresponding O—H and S—H bonds, they have increased by a similar magnitude. These observations should not come as a big surprise: H<sub>2</sub>NOH and H<sub>2</sub>NSH are generally considered as chemically localized species, so that the individual sites can be expected to behave more or less independently.

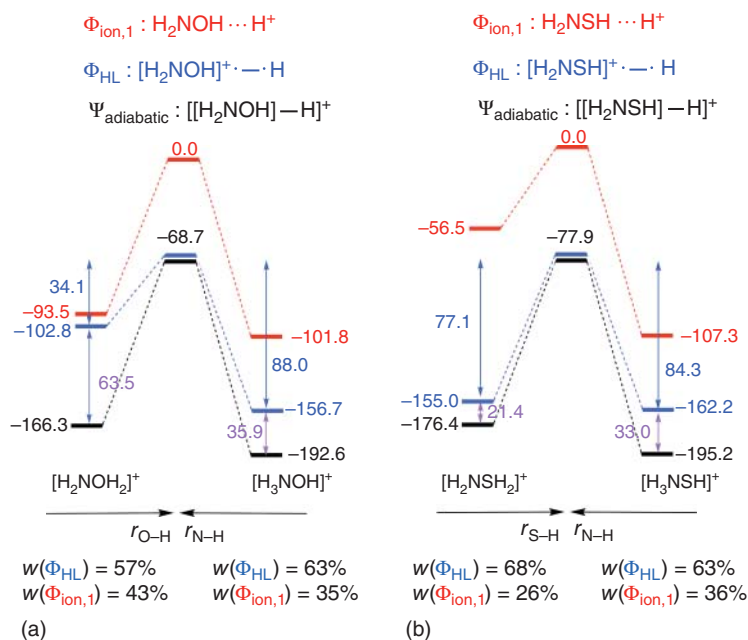


**Figure 20.10** Schematic representation of the bonding interaction and the energy evolution of the individual diabatic states and the global adiabatic state associated with the protonation of (a)  $\text{H}_2\text{NOH}$  and (b)  $\text{H}_2\text{NSH}$ . The actual protonation site is indicated by the respective products at the bottom of each energy profile. Note that the curves associated with  $\Phi_{\text{ion},2}$  are not depicted in this figure due to the significant distance between this curve and the ones associated with  $\Phi_{\text{ion},1}$  and  $\Phi_{\text{HL}}$ , respectively. The spin-pairing stabilization energies upon bond formation are depicted in blue italics; the resonance energies are denoted in magenta. The weights of the individual structures in the adiabatic wave function at the optimal bonding distance are shown at the bottom of each panel. Source: From Stuyver and Shaik [11]. American Chemical Society.

Nevertheless, one can pose the question: how do the local reactivity descriptors presented in Figure 20.11 fare in “predicting” the regioselectivity, i.e. do they enable the correct identification of the preferential protonation site in the multi-site systems?

From Figure 20.11a, one can conclude that for both of the unprotonated molecules considered, the N moiety carries the highest partial charge. This is also reflected in the MEP maps (cf. Figure 20.11b): the region of the isosurface associated with the lone pair of N colors bright red (indicating strong Coulombic attraction of a positive test-charge), the region associated with the O lone pairs has a similar – though slightly less bright – hue, but the regions corresponding to the lone pairs of sulfur clearly correspond to a much less negative electrostatic potential. Correspondingly, proton association at the N-site leads to the largest electrostatic stabilization in both systems (cf. the stabilization of the red curves in Figure 20.10).

The total protonation energy follows an identical pattern, i.e. association at the N-site is preferred for both model compounds, so that one can phenomenologically conclude that they both adhere to the hard-hard/charge-controlled paradigm,



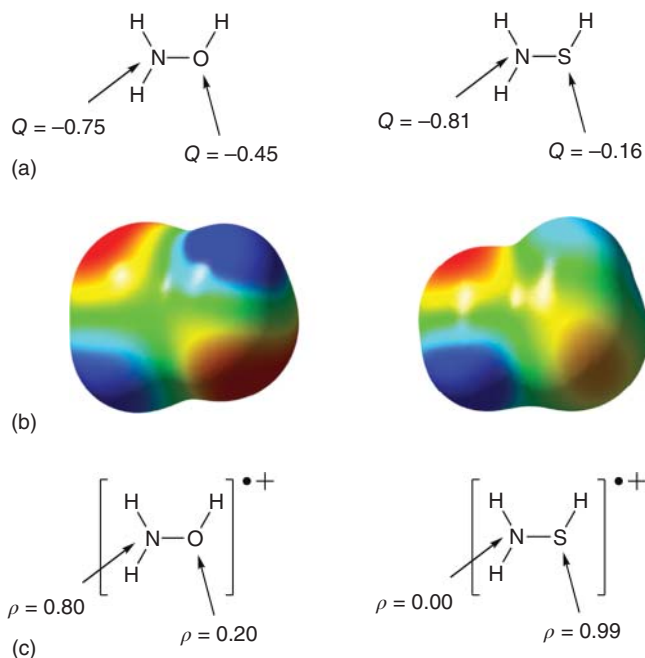


**Figure 20.11** (a) ESP charges ( $Q$ ) on the N and O/S sites of the neutral, unprotonated species; (b) corresponding MEP maps (with the scale ranges from  $-25 \text{ kcal mol}^{-1}$  (red) to  $25 \text{ kcal mol}^{-1}$  (blue)); (c) NPA spin densities ( $\rho$ ) on the N and O/S sites of the oxidized, i.e. radical cation, species. Calculations were performed at (U)B3LYP/def2-TZVP level-of-theory [15–17, 41, 42]. Source: From Stuyver and Shaik [11]. American Chemical Society.

which is in line with the previous findings by Chattaraj and coworkers [33]. What is clearly revealed by our analysis however is that this regioselective preference is not the result of the electrostatic interactions dominating in absolute terms over the spin-pairing ones: in fact, the charge interaction is not even the main driver of the bonding in either of the four regio-isomers probed!

Turning to the spin densities presented in Figure 20.11c, one can observe that for  $\text{H}_2\text{NOH}$ , this descriptor correctly probes the relative magnitudes of the spin-pairing stabilization during bond formation. The role played by the resonance penalty (*vide supra*) clearly comes to the forefront in this system. For the N-site, which carries the bulk of the spin density in  $[\text{H}_2\text{NOH}]^{+\bullet}$ , the spin-pairing/(frontier) orbital stabilization is only slightly lower than the corresponding intrinsic value, which – as mentioned before – corresponds to the spin-pairing stabilization exhibited by the localized analog, i.e.  $\text{NH}_4^+$  in Figure 20.9b ( $88.0$  vs.  $103.8 \text{ kcal mol}^{-1}$ ). For the O-site, carrying a spin density of only  $0.2e$ , the spin-pairing stabilization upon protonation is dramatically reduced compared to the corresponding value obtained from  $\text{H}_3\text{O}^+$  ( $34.1$  vs.  $83.0 \text{ kcal mol}^{-1}$ ).

In  $[\text{H}_2\text{NSH}]^{+\bullet}$ , the spin density is more or less perfectly localized on the S-site ( $\rho = 0.99e$ ). As such, one could expect that almost no resonance penalty would be associated with this moiety. Indeed, the spin-pairing stabilization for this site agrees

almost perfectly with the corresponding intrinsic value (77.1 vs. 73.7 kcal mol<sup>-1</sup>; cf. Figure 20.9b). Consequently, one could also expect at the same time a huge resonance penalty to be associated with the N-site for this compound. However, this is clearly not the case: the spin-pairing stabilization for the latter site deviates by only a moderate 20 kcal mol<sup>-1</sup> from the corresponding intrinsic value (84.3 vs. 103.8 kcal mol<sup>-1</sup>).

*Complementary reactivity modes:* Does this seemingly anomalous resonance penalty associated with the N-site constitute a failure of our reactivity descriptor? Not quite; performing a time-dependent density functional theory (TD-DFT) calculation on the oxidized radical species [H<sub>2</sub>NSH]<sup>•+</sup> straightforwardly reveals the existence of an excited radical cation state a mere 0.18 eV (~4 kcal mol<sup>-1</sup>) above the ground state. Whereas the spin density in the ground state is localized on the (lone pairs of the) S-moiety, the spin density in this – almost degenerate – excited state is primarily localized on the lone pair of the N-moiety ( $\rho_N = 0.92e$ ; cf. the spin density distributions associated to both states in Figure 20.12a).

The appearance of two close-lying states for the radical cation could in fact have been readily predicted/anticipated from a VB analysis. In the wave function of [H<sub>2</sub>NSH]<sup>•+</sup>, one can expect two main VB structures to emerge: one in which the positive charge is located on the N-moiety and another one in which the charge is located on the S-moiety. From the spacing between  $E(\Phi_{\text{ion},1})$  and  $E(\Phi_{\text{HL}})$  in

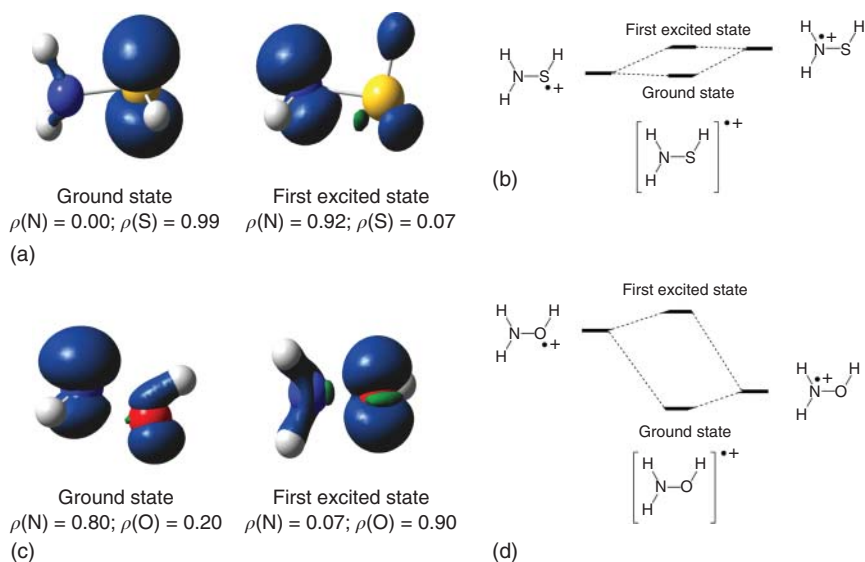


**Figure 20.12** (a) Spin density contour maps for the ground- and first excited state of [H<sub>2</sub>NSH]<sup>•+</sup>. (b) Schematic representation of the mixing between two main VB structures, giving rise to the ground- and first excited state, for [H<sub>2</sub>NSH]<sup>•+</sup>. (c) Spin density maps for the ground- and first excited state of [H<sub>2</sub>NOH]<sup>•+</sup>. (d) Schematic representation of the VB mixing for [H<sub>2</sub>NOH]<sup>•+</sup>. The contours have been drawn at 0.008 au. Condensed spin density values are presented below each respective map. Source: From Stuyver and Shaik [11]. American Chemical Society.

the dissociated geometry for  $\text{NH}_3$  and  $\text{H}_2\text{S}$  (i.e.  $A_{\text{H}^+} - I_{\text{R}}$ ; cf. Figure 20.9), one can deduce that the IP for the S-moiety is very similar to that for the N-moiety (though slightly lower; 240 vs. 251 kcal mol<sup>-1</sup>). Consequently, these two localized VB structures are expected to be almost degenerate. Whether these structures interact then depends on the overlap between the local orbitals on the individual moieties. From an inspection of the geometry of  $\text{H}_2\text{NSH}$ , one can readily deduce that the orbitals containing the lone pairs on sulfur and nitrogen lie in almost orthogonal planes (cf. Figure 20.11). Consequently, one expects very limited to no mixing between these two structures: our calculations show that  $[\text{H}_2\text{NSH}]^{+\bullet}$  indeed gives rise to two close-lying adiabatic states, one in which the spin density is localized on the S-site, and another one in which the spin density is localized on the N-site (cf. Figure 20.12c).

According to the argumentation in the previous sections, if the two localized structures lie closely, the amount of delocalization energy lost during protonation of the respective sites is more or less equal. As a consequence, the resonance penalty associated with protonation of the N-moiety is less pronounced than exclusive consideration of the spin density distribution in the adiabatic ground state of  $[\text{H}_2\text{NSH}]^{+\bullet}$  would suggest.

In the case of  $[\text{H}_2\text{NOH}]^{+\bullet}$ , the two most stable VB structures, i.e. the one in which the positive charge is located on the N-moiety and the other in which the charge is located on the O-moiety, are not close to degeneracy at all; the IP for the N-moiety is significantly lower than the IP for the O-moiety, cf. the IP for  $\text{NH}_3$  (251 kcal mol<sup>-1</sup>) vs. the IP for  $\text{H}_2\text{O}$  (293 kcal mol<sup>-1</sup>). Consequently, we do not end up with two almost degenerate states for  $[\text{H}_2\text{NOH}]^{+\bullet}$  now (cf. Figure 20.12d); for this system, there is one state that is clearly lower in energy than the other (according to our calculations, the difference amounts to 0.8 eV, i.e. 19 kcal mol<sup>-1</sup>).

In summary, the analysis above indicates that indiscriminate, exclusive consideration of the ground-state spin density distribution of the oxidized species of a molecule, corresponding to the “ground-state” (nucleophilic) Fukui function in CDFT language, is not always sufficient to infer relative protonation site propensities (or more generally speaking, electrophilic attack). The appearance of low-lying excited states for this species is generally an indication of hampered mixing between (almost) equally favorable localized states. In such a case, the spin distribution in all of the low-lying states needs to be considered; failing to do so will lead to a misinterpretation of the relative soft–soft preference toward protonation/electrophilic attack within the molecule (cf. Ref. [33]).

## 20.8 Revisiting the Reactivity of the Ambident Vinyloxy Anion

Now that we have established how hardness and softness emerge from a VB perspective, it is timely to reconsider the reactivity of the ambident vinyloxy anion, which we used as a model system to discuss Fukui functions (*vide supra*). Recall that the Fukui function correctly pointed to the thermodynamically preferred attack position

for this system, i.e. the C-moiety, but that kinetically, an opposite preference was observed, i.e. the barrier for O-attack was found to be slightly lower than for C-attack.

This observation of diverging thermodynamic and kinetic preferences is driven to a significant extent by electrostatic interactions in the TS region: the stabilizing alternation of local charges in the TS geometry for the O-attack is significantly more pronounced than for the C-attack (Figure 20.13a). This finding suggests an enhanced weight of one of the ionic states in the diabatic reactant state (Figure 20.13b), pushing the associated curve – and thus also the crossing point with the product curve – to a lower energy (Figure 20.13c). In other words, the relative stabilization of the TS for O-attack is mainly driven by enhanced hard–hard interactions. Another factor stabilizing the reactant curve can be identified as well,

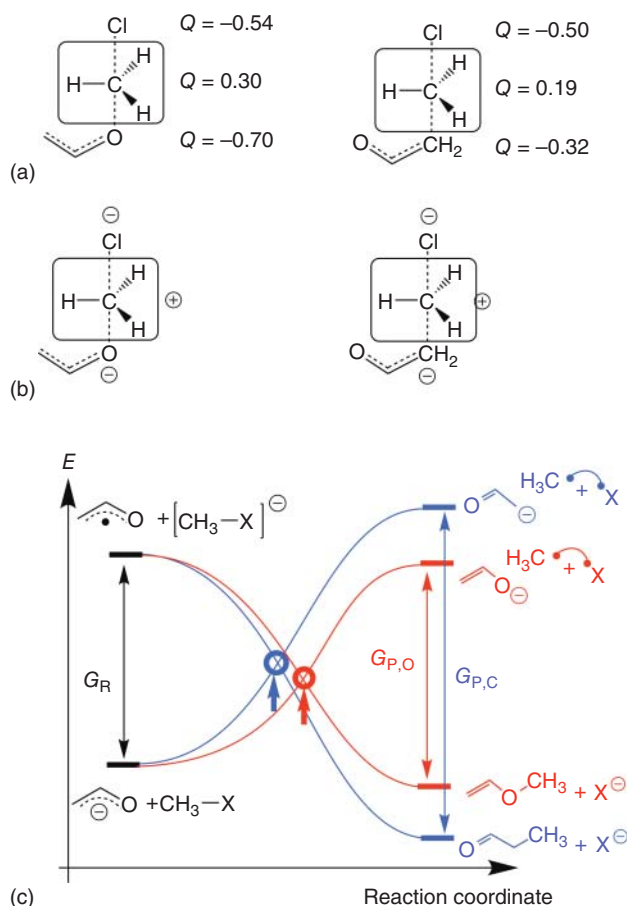


**Figure 20.13** (a) NPA charges ( $Q$ ) in the TSs for the O- and C-attack of vinyloxy anion on  $\text{CH}_3\text{Cl}$  (calculated at B3LYP/cc-pVTZ level-of-theory). (b) The respective ionic VB structures which impact the stability of the TS through electrostatic interactions. (c) Schematic VBSCD for the methylation of vinyloxy anion (cf. Figure 20.8). Note that the ionic VB structures depicted in panel (b) are implicitly incorporated into the reactant curves in the diagram.

namely that the negative charge on the vinyloxy anion will preferentially localize on the O-site (cf. Ref. [10]), but this effect can be expected to be minor in comparison to the differential electrostatic interactions.

One can expect the enhancement of ionic contributions to the wave function in the TS region (resulting – in extreme cases – in a divergent kinetic preference with respect to the trends expected from exclusive consideration of spin-pairing interactions), to be a ubiquitous phenomenon in regular electrophilic/nucleophilic reactions.

## 20.9 Conclusions

This chapter constructs bridges between two seemingly detached and irreconcilable realms within the field of theoretical chemistry: CDFT and VB theory. Focusing on various simple model systems, we have shown that a more profound understanding and enhanced insights can be achieved by combining both viewpoints.

In the first part of the chapter, we have discussed how many common (orbital-based) local reactivity descriptors, i.e. the spin density distribution for radical reactions and the Fukui function for electrophilic/nucleophilic reactions, can essentially be regarded – in one way or another – as indirect measures of delocalization, i.e. resonance stabilization, present within the reactants, from a (qualitative) VB perspective. The inherent connection between (spatial) delocalization and (energetic) resonance stabilization embedded in VB theory provides a natural and elegant framework through which the impact of these individual local reactivity descriptors on the global PES can be analyzed and understood.

In the second part of this chapter, we have expanded our analysis toward “hard–hard” reactivity descriptors as well, thus recovering the principal idea behind the HSAB principle. We demonstrated that both hard–hard and soft–soft interactions can be probed by considering appropriate local reactivity descriptors: electrostatic potential maps and/or partial charges provide information about electrostatic interactions, whereas spin density/Fukui function distributions do the same for spin-pairing interactions.

As model reactions for our analysis of the competition between spin-pairing and electrostatic interactions, we considered a set of protonation reactions, which involve  $H^+$  as a prototypical hard electrophile, in the gas phase. In contrast to previous reports, we find that most of these reactions cannot be classified as exclusively charge- (or orbital-) controlled; the two bonding contributions interact in more subtle patterns instead, only giving the impression of a clear-cut dichotomy. As such, a hybrid approach in which descriptors of both interactions types are combined is required to accurately and conclusively gauge the reactivity patterns for this reaction type [45, 46].

Finally, we also demonstrated that important complementary covalent, i.e. spin pairing, reactivity modes can remain concealed when only a single spin-pairing descriptor is considered. Including spin density distributions of low-lying excited states in the analysis alleviates this problem.

## Acknowledgments

Thijs Stuyver acknowledges the Research Foundation-Flanders (FWO) for a position as postdoctoral research fellow (1203419N). Sason Shaik acknowledges support by the Israel Science Foundation (ISF Grant 520/18).

## References

- 1 Hoffmann, R., Shaik, S., and Hiberty, P.C. (2003). A conversation on VB vs MO theory: a never-ending rivalry? *Acc. Chem. Res.* 36 (10): 750–756. <https://doi.org/10.1021/ar030162a>.
- 2 Parr, R.G. and Yang, W. (1994). *Density-Functional Theory of Atoms and Molecules, 1. International Series of Monographs on Chemistry*. New York: Oxford University Press.
- 3 Shaik, S. and Hiberty, P. (2007). *A Chemist's Guide to Valence Bond Theory*. Hoboken, NJ: Wiley.
- 4 Stuyver, T. and Shaik, S. (2021). Promotion energy analysis predicts reaction modes: nucleophilic and electrophilic aromatic substitution reactions. *J. Am. Chem. Soc.* 143 (11): 4367–4378. <https://doi.org/10.1021/jacs.1c00307>.
- 5 Hiberty, P.C. and Braïda, B. (2018). Pleading for a dual molecular-orbital/valence-bond culture. *Angew. Chem. Int. Ed.* 57 (21): 5994–6002. <https://doi.org/10.1002/anie.201710094>.
- 6 Stuyver, T., Chen, B., Zeng, T. et al. (2019). Do diradicals behave like radicals? *Chem. Rev.* 119 (21): 11291–11351. <https://doi.org/10.1021/acs.chemrev.9b00260>.
- 7 Borden, W.T., Hoffmann, R., Stuyver, T., and Chen, B. (2017). Dioxygen: what makes this triplet diradical kinetically persistent? *J. Am. Chem. Soc.* 139 (26): 9010–9018. <https://doi.org/10.1021/jacs.7b04232>.
- 8 Geerlings, P., De Proft, F., and Langenaeker, W. (2003). Conceptual density functional theory. *Chem. Rev.* 103 (5): 1793–1874. <https://doi.org/10.1021/cr990029p>.
- 9 Geerlings, P., Fias, S., Boisdenghien, Z., and De Proft, F. (2014). Conceptual DFT: chemistry from the linear response function. *Chem. Soc. Rev.* 43 (14): 4989. <https://doi.org/10.1039/c3cs60456j>.
- 10 Stuyver, T., De Proft, F., Geerlings, P., and Shaik, S. (2020). How do local reactivity descriptors shape the potential energy surface associated with chemical reactions? The valence bond delocalization perspective. *J. Am. Chem. Soc.* 142 (22): 10102–10113. <https://doi.org/10.1021/jacs.0c02390>.
- 11 Stuyver, T. and Shaik, S. (2020). Unifying conceptual density functional and valence bond theory: the hardness–softness conundrum associated with protonation reactions and uncovering complementary reactivity modes. *J. Am. Chem. Soc.* 142 (47): 20002–20013. <https://doi.org/10.1021/jacs.0c09041>.
- 12 Shaik, S. and Shurki, A. (1999). Valence bond diagrams and chemical reactivity. *Angew. Chem. Int. Ed.* 38: 586–625.

- 13 Shaik, S.S. (1981). What happens to molecules as they react? A valence bond approach to reactivity. *J. Am. Chem. Soc.* 103 (13): 3692–3701. <https://doi.org/10.1021/ja00403a014>.
- 14 Lai, W., Li, C., Chen, H., and Shaik, S. (2012). Hydrogen-abstraction reactivity patterns from A to Y: the valence bond way. *Angew. Chem. Int. Ed.* 51 (23): 5556–5578. <https://doi.org/10.1002/anie.201108398>.
- 15 Becke, A.D. (1988). Density-functional exchange-energy approximation with correct asymptotic behavior. *Phys. Rev. A* 38 (6): 3098–3100. <https://doi.org/10.1103/PhysRevA.38.3098>.
- 16 Becke, A.D. (1992). Density-functional thermochemistry. I. The effect of the exchange-only gradient correction. *J. Chem. Phys.* 96 (3): 2155–2160. <https://doi.org/10.1063/1.462066>.
- 17 Lee, C., Yang, W., and Parr, R.G. (1988). Development of the Colle-Salvetti correlation-energy formula into a functional of the electron density. *Phys. Rev. B* 37 (2): 785–789. <https://doi.org/10.1103/PhysRevB.37.785>.
- 18 Song, L., Mo, Y., Zhang, Q., and Wu, W. (2005). XMVB: a program for *ab initio* nonorthogonal valence bond computations. *J. Comput. Chem.* 26 (5): 514–521. <https://doi.org/10.1002/jcc.20187>.
- 19 Chen, Z., Ying, F., Chen, X. et al. (2015). XMVB 2.0: a new version of xiamen valence bond program. *Int. J. Quantum Chem.* 115 (11): 731–737. <https://doi.org/10.1002/qua.24855>.
- 20 Bell, R.P. (1936). The theory of reactions involving proton transfers. *Proc. R. Soc. Lond. A* 154 (882): 414–429. <https://doi.org/10.1098/rspa.1936.0060>.
- 21 Evans, M.G. and Polanyi, M. (1936). Further considerations on the thermodynamics of chemical equilibria and reaction rates. *Trans. Faraday Soc.* 32: 1333. <https://doi.org/10.1039/tf9363201333>.
- 22 Langenaeker, W., Demel, K., and Geerlings, P. (1991). Quantum-chemical study of the Fukui function as a reactivity index. *J. Mol. Struct. THEOCHEM* 234: 329–342. [https://doi.org/10.1016/0166-1280\(91\)89021-R](https://doi.org/10.1016/0166-1280(91)89021-R).
- 23 Ayers, P. and Parr, R.G. (2000). Variational principles for describing chemical reactions: the Fukui function and chemical hardness revisited. *J. Am. Chem. Soc.* 122: 2010–2018.
- 24 Breugst, M., Zipse, H., Guthrie, J.P., and Mayr, H. (2010). Marcus analysis of ambident reactivity. *Angew. Chem. Int. Ed.* 49: 5165–5169.
- 25 Pearson, R.G. (1995). The HSAB principle — more quantitative aspects. *Inorg. Chim. Acta* 240 (1–2): 93–98. [https://doi.org/10.1016/0020-1693\(95\)04648-8](https://doi.org/10.1016/0020-1693(95)04648-8).
- 26 Chattaraj, P.K., Lee, H., and Parr, R.G. (1991). HSAB principle. *J. Am. Chem. Soc.* 113 (5): 1855–1856. <https://doi.org/10.1021/ja00005a073>.
- 27 Ayers, P.W. (2007). The physical basis of the hard/soft acid/base principle. *Faraday Discuss.* 135: 161–190. <https://doi.org/10.1039/B606877D>.
- 28 Mecozzi, S., West, A.P., and Dougherty, D.A. (1996). Cation- $\pi$  interactions in aromatics of biological and medicinal interest: electrostatic potential surfaces as a useful qualitative guide. *Proc. Natl. Acad. Sci.* 93 (20): 10566–10571. <https://doi.org/10.1073/pnas.93.20.10566>.

- 29 Wheeler, S.E. and Houk, K.N. (2010). Are anion/ $\pi$  interactions actually a case of simple charge–dipole interactions? <sup>†</sup>. *J. Phys. Chem. A* 114 (33): 8658–8664. <https://doi.org/10.1021/jp1010549>.
- 30 Torrent-Sucarrat, M., De Proft, F., Geerlings, P., and Ayers, P.W. (2008). Do the local softness and hardness indicate the softest and hardest regions of a molecule? *Chem. Eur. J.* 14 (28): 8652–8660. <https://doi.org/10.1002/chem.200800570>.
- 31 Torrent-Sucarrat, M., De Proft, F., Ayers, P.W., and Geerlings, P. (2010). On the applicability of local softness and hardness. *Phys. Chem. Chem. Phys.* 12 (5): 1072–1080. <https://doi.org/10.1039/B919471A>.
- 32 Cedillo, A. (2020). The role of the density response kernel in the protonation process. *J. Phys. Chem. A* 124 (5): 858–863. <https://doi.org/10.1021/acs.jpca.9b07478>.
- 33 Melin, J., Aparicio, F., Subramanian, V. et al. (2004). Is the Fukui function a right descriptor of hard–hard interactions? *J. Phys. Chem. A* 108 (13): 2487–2491. <https://doi.org/10.1021/jp037674r>.
- 34 Zielinski, F., Tognetti, V., and Joubert, L. (2013). A theoretical study on the gas-phase protonation of pyridine and phosphinine derivatives. *J. Mol. Model.* 19 (9): 4049–4058. <https://doi.org/10.1007/s00894-013-1925-6>.
- 35 Grimmel, S.A. and Reiher, M. (2019). The electrostatic potential as a descriptor for the protonation propensity in automated exploration of reaction mechanisms. *Faraday Discuss.* 220: 443–463. <https://doi.org/10.1039/C9FD00061E>.
- 36 Bettens, T.; Pan, S.; De Proft, F.; Geerlings, P.; Frenking, G. Alkaline earth metals activate  $N_2$  and CO in cubic complexes just like transition metals do: a conceptual DFT and EDA study. *Chem. Eur. J.* 2020, 26(56):12785–12793. <https://doi.org/10.1002/chem.202001585>.
- 37 Ying, F., Su, P., Chen, Z. et al. (2012). DFVB: a density-functional-based valence bond method. *J. Chem. Theory Comput.* 8 (5): 1608–1615. <https://doi.org/10.1021/ct200803h>.
- 38 Shaik, S., Danovich, D., Wu, W., and Hiberty, P.C. (2009). Charge-shift bonding and its manifestations in chemistry. *Nat. Chem.* 1 (6): 443–449. <https://doi.org/10.1038/nchem.327>.
- 39 Shaik, S., Danovich, D., Galbraith, J.M. et al. (2020). Charge-shift bonding: a new and unique form of bonding. *Angew. Chem. Int. Ed.* 59 (3): 984–1001. <https://doi.org/10.1002/anie.201910085>.
- 40 Angelelli, F., Aschi, M., Cacace, F. et al. (1995). Gas-phase reactivity of hydroxylamine toward charged electrophiles. A mass spectrometric and computational study of the protonation and methylation of  $H_2NOH$ . *J. Phys. Chem.* 99 (17): 6551–6556. <https://doi.org/10.1021/j100017a041>.
- 41 Weigend, F. and Ahlrichs, R. (2005). Balanced basis sets of split valence, triple zeta valence and quadruple zeta valence quality for H to Rn: design and assessment of accuracy. *Phys. Chem. Chem. Phys.* 7 (18): 3297. <https://doi.org/10.1039/b508541a>.
- 42 Weigend, F. (2006). Accurate Coulomb-fitting basis sets for H to Rn. *Phys. Chem. Chem. Phys.* 8 (9): 1057. <https://doi.org/10.1039/b515623h>.



- 43** Domingo, L.R., Pérez, P., and Sáez, J.A. (2013). Understanding the local reactivity in polar organic reactions through electrophilic and nucleophilic Parr functions. *RSC Adv.* 3 (5): 1486–1494. <https://doi.org/10.1039/C2RA22886F>.
- 44** Chamorro, E., Pérez, P., and Domingo, L.R. (2013). On the nature of Parr functions to predict the most reactive sites along organic polar reactions. *Chem. Phys. Lett.* 582: 141–143. <https://doi.org/10.1016/j.cplett.2013.07.020>.
- 45** Anderson, J.S.M., Melin, J., and Ayers, P.W. (2007). Conceptual density-functional theory for general chemical reactions, including those that are neither charge- nor Frontier-orbital-controlled. 1. Theory and derivation of a general-purpose reactivity indicator. *J. Chem. Theory Comput.* 3 (2): 358–374. <https://doi.org/10.1021/ct600164j>.
- 46** Anderson, J.S.M., Melin, J., and Ayers, P.W. (2007). Conceptual density-functional theory for general chemical reactions, including those that are neither charge- nor Frontier-orbital-controlled. 2. Application to molecules where Frontier molecular orbital theory fails. *J. Chem. Theory Comput.* 3 (2): 375–389. <https://doi.org/10.1021/ct6001658>.

## **Part III**

### **Applications**

## 21

# A Conceptual Density Functional Theoretic View of Chemical Binding

Swapan K. Ghosh

*UM-DAE-Centre for Excellence in Basic Sciences, University of Mumbai, Kalina, Santacruz (East), Mumbai 400098, India*

### 21.1 Introduction

This chapter attempts to provide a physical picture of chemical binding within the theoretical framework of density functional theory (DFT) [1–3], or to be more specific, what is popularly known as conceptual density functional theory (CDFT) [4]. Molecules and materials are essentially a collection of atoms/nuclei, arranged in a particular geometrical configuration, and bonded together by the electron glue. Different systems correspond to different sets of atoms and their different spatial arrangements, and different phenomena correspond to their different types of changes from one spatial configuration to another. When two or more atoms approach each other, their electrons get partially delocalized and redistributed in space as a consequence of interatomic perturbation, thereby forming molecules, through what is known as chemical binding, an important aspect in the description of many of the systems and phenomena involved in chemical, physical, biological, and other sciences, as well.

Chemical binding is at the root of molecule (or solid) formation through electron density reorganization, manifested often through interatomic charge and spin transfer, and intra-atomic rearrangement leading to creation of atomic dipoles due to polarization from electronic responses. In this chapter, the emphasis has been on the conceptual aspects and model building through a physical picture and not so much on the accuracy of numerical prediction through a rather involved and sophisticated solution of the Schrodinger equation or its approximate variants, which are well established as computational tool.

Desire to have a deeper understanding of chemical binding leading to formation of molecules or solids is however quite old, and many attempts toward fulfilling this goal have been made in the past and the search is still on with equal vigor. This is inspired or triggered by the discovery and introduction of many new chemical concepts or providing foundation to the existing concepts. Many of these concepts have however crept in with a view to explain and rationalize experimental facts, and

are often empirical. Providing physical foundation to these chemical concepts has thus been a field of research by itself. This has been fueled, often by the availability of a new theoretical machinery within the quantum mechanical framework, since chemical binding is a quantum effect, an apt example being the availability of DFT as a theory with single-particle electron density as the basic variable. Density-based approach is most suitable for the purpose, since chemical binding is essentially an outcome of electron density reorganization, which takes place when the atoms approach each other. Although many researchers had attempted to visualize the binding process through the plots of electron density and other associated property density changes on molecule formation, a real breakthrough entered the scene when a more formal approach with sound theoretical basis was started [5] by Prof Robert G Parr in the mid-seventies, leading to the development of DFT-based approach to chemical concepts, aiming at providing a true physical picture of the chemical binding as well as chemical reactivity. The rest is history and the seed has now led to the growth of a big tree representing the field of CDFT [4], which deals with diverse conceptual aspects within the framework of DFT.

For a quantitative description of chemical binding, the energetics associated with molecule formation is to be considered and a simple model follows through consideration of the interatomic perturbation of the electron cloud, when the atoms approach closer. Since the associated energy changes are much smaller in comparison to the energies of the individual atoms, a simple perturbation-theory-based approach is quite appropriate, in view of its simplicity and general applicability. The electron density reorganization, besides intra-atomic rearrangement, might also lead to inter-atomic transfer of electrons, leading to a charge separation and hence dipole moment of the molecule. In a coarse-grained picture, the individual atoms acquire partial atomic charges and also atomic dipoles are created at each atomic site.

The direction and extent of inter-atomic charge flow have been understood by introducing the concepts of electronegativity [5] and chemical hardness [6] of the atoms, respectively. The electronegativity has been identified with the chemical potential of the electron cloud (with a negative sign). The chemical potential dictates the direction of charge flow in the same spirit as the temperature does for the direction of heat flow (from hot body to cold body), or, the electric potential determines the direction of electricity flow. Analogously, the chemical hardness parameter controls the extent of interatomic electron transfer, analogous to heat capacity determining the extent of heat flow or capacitance determining the amount of electricity flow.

There are, however, two important issues associated with the coarse-grained models that need to be addressed. Firstly, the aspects of prediction of binding energies in these models are mostly valid for the equilibrium geometry of the molecules concerned. An unphysical charge transfer will be wrongly predicted even at large interatomic separation, due to the existence of the electronegativity or chemical potential difference, the driving force for the charge transfer. The concept of a chemical contact may need to be invoked to prevent the spurious charge transfer at large separation, the objective being the prediction of the correct dissociation limit of the molecule.

The other issue stems from the fact that the electronegativity (and hardness)-based models are suitable only for ionic binding, leaving apparently the territory of covalent binding away from their invasion. An extreme case is that of the homonuclear molecules where there is no electronegativity difference, but there is chemical binding through covalent contribution. Two important aspects about covalent bond formation come to the rescue again, the first being a charge build up in the bond midpoint/region, the other being the role of unpaired electrons in the atoms for the formation of electron pair, which is synonymous with the formation of the covalent bond. While for the former, the concept of bond electronegativity and bond hardness [7–10] has been useful, for the latter, generalized concepts of up-spin and down-spin electronegativity using spin-polarized DFT [11–12] have been found to be quite successful.

This may predict an up-spin electron transfer from one atom to the other, and down-spin electron transfer in the opposite direction, leading to a net spin transfer responsible for covalent binding, although there may or may not be any resultant charge transfer. In these models, the partial atomic charges [13], or even atomic dipoles, can be useful for predicting the reactivity of reactive sites in molecules. Out of the many available reactivity indices [14], the charge-related ones are useful for the study of chemical binding [11, 15, 16]. It is worthwhile to mention some of the widely used reactivity parameters, viz. electrophilicity [17, 18], nucleophilicity, frontier orbitals [3, 19], response kernels [20, 21], and local and global hardness and softness [22–24].

The objective of this work is to present a brief overview of the developments in the field of chemical binding within the framework of CDFT. Only glimpses of the main features are discussed here, in lieu of an exhaustive account of all aspects of the whole field, which is rather vast and also fast growing. Thus, in what follows, we first introduce some of the basic chemical concepts and reactivity parameters (for spin-polarized situations), which are most widely used to provide a physical picture of chemical binding, and then demonstrate their utility and role in describing the formulation of ionic as well as covalent binding in molecular systems. A generalized picture within the basic DFT framework extended to spin and bond spaces is one of the major highlights of the presentation. The problems associated with these approaches for describing the limiting case of molecular dissociation are also briefly addressed.

## 21.2 Physical Foundation of Chemical Concepts: A View Through Conceptual DFT Window

In chemistry, many concepts have been introduced from time to time to explain, interpret, or rationalize the experimental observations, which ultimately help also in predicting novel molecules and materials with tailor-made properties. However, since many of these concepts have been born empirically, there has always been a quest to place them in a more sound theoretical footing. The CDFT, a version of DFT, has come to the rescue and extended a helping hand to deal with these interpretive

aspects. To start with, we first discuss the most basic and relevant aspects of CDFT, in the present context.

As is well known, DFT is a simpler alternative to wavefunction-based quantum mechanical framework, where the role of basic variable is played by the single-particle electron density  $\rho(r)$ , defined in terms of the many particle wavefunction  $\Psi(r_1, r_2, \dots, r_N)$  for an  $N$ -electron system, as

$$\rho(r_1) = N \iint \dots \int \Psi^*(r_1, r_2, \dots, r_N) \Psi(r_1, r_2, \dots, r_N) dr_2, \dots, dr_N \quad (21.1)$$

which can alternatively be expressed in terms of the expectation value of the density operator as

$$\rho(r) = \langle \Psi(r_1, r_2, \dots, r_N) | \sum_i \delta(r - r_i) | \Psi(r_1, r_2, \dots, r_N) \rangle \quad (21.2)$$

where the summation runs from  $i = 1$  to  $N$ . In DFT, the ground-state electronic energy of an  $N$ -particle system characterized by an external potential  $v(r)$  is expressed as a functional  $E_v[\rho]$  of the density  $\rho(r)$  given by

$$E_v[\rho] = \int v(r)\rho(r)dr + F[\rho] \quad (21.3)$$

where  $F[\rho]$  represents a universal functional of density consisting of contributions from the kinetic and electron repulsion energies. For fixed  $v(r)$ , the energy functional  $E_v[\rho]$  obeys the variational principle  $\delta[E_v[\rho] - \mu\{\int \rho(r)dr - N\}] = 0$ , corresponding to energy minimization with respect to the density variation  $\delta\rho(r)$ , subject to the normalization condition  $\int \rho(r)dr = N$ , and leads to the result

$$\mu = (\delta E_v[\rho]/\delta\rho(r)) = v(r) + (\delta F[\rho]/\delta\rho(r)) \quad (21.4)$$

Here  $\mu$ , the Lagrange multiplier corresponding to the density normalization constraint, represents the chemical potential of the electron cloud and plays a major role in the framework of CDFT. For example,  $\mu$  has been intimately linked with the concepts of electronegativity and hardness, which have been highly successful for the rationalization and prediction of many aspects of chemical binding and chemical reactivity.

The electronegativity parameter  $\chi$  is defined in terms of the first derivative of the energy  $E$  with respect to the number of electrons  $N$ , as

$$\chi = -(\partial E/\partial N)_{v(r)} \quad (21.5)$$

while the hardness parameter  $\eta$  is defined in terms of the second derivative as

$$\eta = (1/2)(\partial^2 E/\partial N^2)_{v(r)} = (1/2)(\partial\chi/\partial N)_{v(r)} \quad (21.6)$$

with the external potential  $v(r)$  kept fixed. The two derivatives can be approximated, within a finite difference approximation, in terms of the ionization potential ( $I$ ) and electron affinity ( $A$ ), as  $\chi = (I + A)/2$  and  $\eta = (I - A)/2$ . DFT permits one to express  $\chi$  as

$$\begin{aligned} \chi &= -(\partial E_v/\partial N)_{v(r)} = - \int (\delta E_v[\rho]/\delta\rho(r)) (\partial\rho(r)/\partial N) d\mathbf{r} \\ &= -\mu \int (\partial\rho(r)/\partial N) d\mathbf{r} = -\mu \end{aligned} \quad (21.7)$$

and thus identifies  $\chi$  as the negative of the chemical potential  $\mu$ . An interesting fact about the expression  $\mu = v(r) + (\delta F[\rho]/\delta\rho(r))$  is that although the right side is expressed as a sum of position-dependent terms, the left side, which represents  $\mu$ , is the same at every point. This aspect has implications toward the equalization of electronegativity of atoms during molecule formation, used widely as a principle in chemistry.

While the above definitions of the chemical potential and hardness are based on the single variable  $N$ , most of the atoms are open-shell systems, and spin-polarized DFT is the right tool for their investigation. For an  $N$ -electron system with  $N_\alpha$  and  $N_\beta$  as the numbers of spin-up and spin-down electrons, where  $N = N_\alpha + N_\beta$ , the up-spin and down-spin electronegativity and hardness parameters can be defined as a generalization, viz.

$$\chi_\alpha = -(\partial E/\partial N_\alpha)_{v(r), N_\beta}; \quad \chi_\beta = -(\partial E/\partial N_\beta)_{v(r), N_\alpha} \quad (21.8)$$

and

$$\eta_{\alpha\alpha} = (1/2)(\partial^2 E/\partial N_\alpha^2)_{v(r), N_\beta} = (1/2)(\partial\chi_\alpha/\partial N_\alpha)_{v(r), N_\beta} \quad (21.9a)$$

$$\eta_{\beta\beta} = (1/2)(\partial^2 E/\partial N_\beta^2)_{v(r), N_\alpha} = (1/2)(\partial\chi_\beta/\partial N_\beta)_{v(r), N_\alpha} \quad (21.9b)$$

$$\eta_{\alpha\beta} = \eta_{\beta\alpha} = (\partial^2 E/\partial N_\alpha \partial N_\beta)_{v(r)} = (\partial\chi_\alpha/\partial N_\beta)_{v(r)} = (\partial\chi_\beta/\partial N_\alpha)_{v(r)} \quad (21.9c)$$

where  $v(r)$  in the subscript does refer to  $\{v_\alpha(r), v_\beta(r)\}$ , if the external potential is spin-dependent.

The DFT analogue of the two electronegativities is straightforward and can be equated to the two respective chemical potentials,  $\mu_\alpha$  and  $\mu_\beta$ , viz.

$$\begin{aligned} \chi_\alpha &= -(\partial E_v/\partial N_\alpha)_{v(r), N_\beta} = -\int (\delta E_v[\rho_\alpha, \rho_\beta]/\delta\rho_\alpha(r)) (\partial\rho_\alpha(r)/\partial N_\alpha) d\mathbf{r} \\ &= -\mu_\alpha \int (\partial\rho_\alpha(r)/\partial N_\alpha) d\mathbf{r} = -\mu_\alpha \end{aligned} \quad (21.10a)$$

$$\begin{aligned} \chi_\beta &= -(\partial E_v/\partial N_\beta)_{v(r), N_\alpha} = -\int (\delta E_v[\rho_\alpha, \rho_\beta]/\delta\rho_\beta(r)) (\partial\rho_\beta(r)/\partial N_\beta) d\mathbf{r} \\ &= -\mu_\beta \int (\partial\rho_\beta(r)/\partial N_\beta) d\mathbf{r} = -\mu_\beta \end{aligned} \quad (21.10b)$$

where the up-spin and down-spin densities  $\rho_\alpha(\mathbf{r})$  and  $\rho_\beta(\mathbf{r})$  sum up to the net overall density as  $\rho(r) = \rho_\alpha(r) + \rho_\beta(r)$  and also enable one to define a spin density as  $s(r) = \rho_\alpha(r) - \rho_\beta(r)$ . Respective integrated results also follow  $\int \rho_\alpha(r) d\mathbf{r} = N_\alpha$  and  $\int \rho_\beta(r) d\mathbf{r} = N_\beta$ , clearly satisfying  $N = N_\alpha + N_\beta$ , and  $N_s = \int s(r) d\mathbf{r} = N_\alpha - N_\beta$ , with  $N_s$  denoting the number of unpaired electrons. The spin-dependent chemical potentials  $\mu_\alpha$  and  $\mu_\beta$  represent the respective functional derivatives of energy, viz.  $\mu_\alpha = (\delta E_v[\rho_\alpha, \rho_\beta]/\delta\rho_\alpha(r))$  and  $\mu_\beta = (\delta E_v[\rho_\alpha, \rho_\beta]/\delta\rho_\beta(r))$ , with respect to the density components.

Since the variables  $N$  and  $N_s$  are related to  $N_\alpha$  and  $N_\beta$  by the simple linear transformations, written in matrix form as

$$\begin{pmatrix} N \\ N_s \end{pmatrix} = \begin{pmatrix} 1 & 1 \\ 1 & -1 \end{pmatrix} \begin{pmatrix} N_\alpha \\ N_\beta \end{pmatrix}; \quad \begin{pmatrix} N_\alpha \\ N_\beta \end{pmatrix} = \frac{1}{2} \begin{pmatrix} 1 & 1 \\ 1 & -1 \end{pmatrix} \begin{pmatrix} N \\ N_s \end{pmatrix} \quad (21.11a)$$

the corresponding derivatives can also be related by a similar transformation given by

$$\begin{pmatrix} (\partial/\partial N) \\ (\partial/\partial N_s) \end{pmatrix} = \frac{1}{2} \begin{pmatrix} 1 & 1 \\ 1 & -1 \end{pmatrix} \begin{pmatrix} (\partial/\partial N_\alpha) \\ (\partial/\partial N_\beta) \end{pmatrix}; \quad \begin{pmatrix} (\partial/\partial N_\alpha) \\ (\partial/\partial N_\beta) \end{pmatrix} = \begin{pmatrix} 1 & 1 \\ 1 & -1 \end{pmatrix} \begin{pmatrix} (\partial/\partial N) \\ (\partial/\partial N_s) \end{pmatrix} \quad (21.11b)$$

Using this, the energy derivatives  $(\partial E_v/\partial N)_{v(r)}$  and  $(\partial E_v/\partial N_s)_{v(r)}$  representing the chemical potentials  $\mu_N$  and  $\mu_s$ , respectively, can easily be evaluated and found to be related to  $\mu_\alpha$  and  $\mu_\beta$  by the linear transformation

$$\begin{pmatrix} \mu_N \\ \mu_s \end{pmatrix} = \frac{1}{2} \begin{pmatrix} 1 & 1 \\ 1 & -1 \end{pmatrix} \begin{pmatrix} \mu_\alpha \\ \mu_\beta \end{pmatrix}; \quad \begin{pmatrix} \mu_\alpha \\ \mu_\beta \end{pmatrix} = \begin{pmatrix} 1 & 1 \\ 1 & -1 \end{pmatrix} \begin{pmatrix} \mu_N \\ \mu_s \end{pmatrix} \quad (21.12)$$

Analogously, the hardness parameters defined by using  $N$  and  $N_s$  variables as

$$\eta_{NN} = (1/2)(\partial^2 E/\partial N^2)_{v(r)} = (1/2)(\partial \mu_N/\partial N)_{v(r)} \quad (21.13a)$$

$$\eta_{SS} = (1/2)(\partial^2 E/\partial N_s^2)_{v(r)} = (1/2)(\partial \mu_s/\partial N_s)_{v(r)} \quad (21.13b)$$

$$\eta_{NS} = \eta_{SN} = (\partial^2 E/\partial N \partial N_s)_{v(r)} = (\partial \mu_N/\partial N_s)_{v(r)} = (\partial \mu_s/\partial N)_{v(r)} \quad (21.13c)$$

can easily be related to  $\eta_{\alpha\alpha}$ ,  $\eta_{\beta\beta}$ , and  $\eta_{\alpha\beta}$  by repeated application of the above derivative relations, through the simple linear transformation given, in matrix notation, by

$$\begin{pmatrix} \eta_{NN} \\ \eta_{SS} \\ \eta_{NS} \end{pmatrix} = \frac{1}{4} \begin{pmatrix} 1 & 1 & 2 \\ 1 & 1 & -2 \\ 1 & -1 & 0 \end{pmatrix} \begin{pmatrix} \eta_{\alpha\alpha} \\ \eta_{\beta\beta} \\ \eta_{\alpha\beta} \end{pmatrix}; \quad \begin{pmatrix} \eta_{\alpha\alpha} \\ \eta_{\beta\beta} \\ \eta_{\alpha\beta} \end{pmatrix} = \begin{pmatrix} 1 & 1 & 2 \\ 1 & 1 & -2 \\ 1 & -1 & 0 \end{pmatrix} \begin{pmatrix} \eta_{NN} \\ \eta_{SS} \\ \eta_{NS} \end{pmatrix} \quad (21.14)$$

In view of these simple interrelations [21], one can consider either of the two schemes  $(N_\alpha, N_\beta)$  or  $(N, N_s)$  and can easily switch over between the two. However, in this work we prefer to use the  $(N_\alpha, N_\beta)$  representation, for convenience and also due to the symmetry of the equations with respect to the two spins [22].

### 21.3 Energy Change of Spin-Polarized Many-Electron Systems: A Perturbation Theoretic Approach

As we know, the Hamiltonian of a many-electron system is uniquely defined by the number of electrons,  $N$ , and the external potential,  $v(r)$ , which characterizes the system. Thus, the total energy of the system becomes a function/functional of  $N$  and  $v(r)$ , i.e.  $E[N, v(r)]$ . The corresponding quantities for a spin-polarized system become  $(N_\alpha, N_\beta)$ ,  $(v_\alpha(r), v_\beta(r))$  and one has the energy functional  $E[N_\alpha, N_\beta, v_\alpha(r), v_\beta(r)]$ ,



in standard notation, assuming the external potentials to depend on the electron spin. Although one can alternatively consider  $(N, N_S)$ ,  $(v_N(r), v_S(r))$  and  $E[N, N_S, v_N(r), v_S(r)]$ , the two schemes are related, and the advantages of the former scheme have been pointed out earlier, and hence we discuss here only the former one, for convenience.

The energy change  $\Delta E$  of a system due to change in these quantities, viz.  $\delta N_\alpha$ ,  $\delta N_\beta$ ,  $\delta v_\alpha(r)$ , and  $\delta v_\beta(r)$ , can be expressed by a perturbation expansion in terms of them and one has, by retaining terms up to second order, the expression

$$\begin{aligned}
 \Delta E &= E_{v_\alpha + \delta v_\alpha, v_\beta + \delta v_\beta}[N_\alpha + \Delta N_\alpha, N_\beta + \Delta N_\beta] - E_{v_\alpha, v_\beta}[N_\alpha, N_\beta] \\
 &= \mu_\alpha \Delta N_\alpha + \mu_\beta \Delta N_\beta + (1/2)\eta_{\alpha\alpha} (\Delta N_\alpha)^2 + (1/2)\eta_{\beta\beta} (\Delta N_\beta)^2 \\
 &\quad + \eta_{\alpha\beta} (\Delta N_\alpha)(\Delta N_\beta) + \int d\mathbf{r} \delta v_\alpha(r) \rho_\alpha(r) + \int d\mathbf{r} \delta v_\beta(r) \rho_\beta(r) \\
 &\quad + (1/2) \int d\mathbf{r} \int d\mathbf{r}' \delta v_\alpha(r) \delta v_\alpha(r') \chi_{\alpha\alpha}(r, r') \\
 &\quad + (1/2) \int d\mathbf{r} \int d\mathbf{r}' \delta v_\beta(r) \delta v_\beta(r') \chi_{\beta\beta}(r, r') \\
 &\quad + \int d\mathbf{r} \int d\mathbf{r}' \delta v_\alpha(r) \delta v_\beta(r') \chi_{\alpha\beta}(r, r') \\
 &\quad + \Delta N_\alpha \int d\mathbf{r} \delta v_\alpha(r) f_{\alpha\alpha}(r) + \Delta N_\alpha \int d\mathbf{r} \delta v_\beta(r) f_{\beta\alpha}(r) \\
 &\quad + \Delta N_\beta \int d\mathbf{r} \delta v_\alpha(r) f_{\alpha\beta}(r) + \Delta N_\beta \int d\mathbf{r} \delta v_\beta(r) f_{\beta\beta}(r) \quad (21.15)
 \end{aligned}$$

where, in writing the first-order terms with respect to the variations  $\delta v_\alpha(\mathbf{r})$  and  $\delta v_\beta(\mathbf{r})$ , we have replaced the terms  $[(\delta E/\delta v_\alpha(r))_{N_\alpha, N_\beta, v_\beta}]$  and  $[(\delta E/\delta v_\beta(r))_{N_\alpha, N_\beta, v_\alpha}]$  with  $\rho_\alpha(r)$  and  $\rho_\beta(r)$  respectively, by making use of the identities

$$\rho_\alpha(r) = [(\delta E/\delta v_\alpha(r))_{N_\alpha, N_\beta, v_\beta}] \quad (21.16a)$$

and

$$\rho_\beta(r) = [(\delta E/\delta v_\beta(r))_{N_\alpha, N_\beta, v_\alpha}] \quad (21.16b)$$

Similarly in writing the second-order corrections with respect to the variations  $\delta v_\alpha(r)$  and  $\delta v_\beta(r)$ , we introduce the response kernels,  $\chi_{\alpha\alpha}(r, r')$ ,  $\chi_{\beta\beta}(r, r')$ , and  $\chi_{\alpha\beta}(r, r')$ , defined as

$$\begin{aligned}
 \chi_{\alpha\alpha}(r, r') &= [(\delta^2 E/\delta v_\alpha(r) \delta v_\alpha(r'))_{N_\alpha, N_\beta, v_\beta}] = (\delta \rho_\alpha(r')/\delta v_\alpha(r))_{N_\alpha, N_\beta, v_\beta} \\
 &= (\delta \rho_\alpha(r)/\delta v_\alpha(r'))_{N_\alpha, N_\beta, v_\beta} = \chi_{\alpha\alpha}(r', r) \quad (21.17a)
 \end{aligned}$$

$$\begin{aligned}
 \chi_{\beta\beta}(r, r') &= [(\delta^2 E/\delta v_\beta(r) \delta v_\beta(r'))_{N_\alpha, N_\beta, v_\alpha}] = (\delta \rho_\beta(r')/\delta v_\beta(r))_{N_\alpha, N_\beta, v_\alpha} \\
 &= (\delta \rho_\beta(r)/\delta v_\beta(r'))_{N_\alpha, N_\beta, v_\alpha} = \chi_{\beta\beta}(r', r) \quad (21.17b)
 \end{aligned}$$

and

$$\begin{aligned}
 \chi_{\alpha\beta}(r, r') &= [(\delta^2 E/\delta v_\alpha(r) \delta v_\beta(r'))_{N_\alpha, N_\beta}] = (\delta \rho_\beta(r')/\delta v_\alpha(r))_{N_\alpha, N_\beta} \\
 &= (\delta \rho_\alpha(r)/\delta v_\beta(r'))_{N_\alpha, N_\beta} = \chi_{\beta\alpha}(r', r) \quad (21.17c)
 \end{aligned}$$

which are known to play important role as widely useful nonlocal reactivity descriptors [23]. In the last four terms, representing the mixed second-order corrections, arising from the variations of  $\{\delta v_\alpha(r), \delta v_\beta(r)\}$  as well as  $\{\Delta N_\alpha, \Delta N_\beta\}$ , the four quantities  $f_{\alpha\alpha}(r) [=(\partial\rho_\alpha(r)/\partial N_\alpha)_{N\beta, v\beta}]$ ,  $f_{\alpha\beta}(r) [=(\partial\rho_\beta(r)/\partial N_\alpha)_{N\beta, v\alpha}]$ ,  $f_{\beta\alpha}(r) [=(\partial\rho_\alpha(r)/\partial N_\alpha)_{N\beta, v\alpha}]$ , and  $f_{\beta\beta}(r) [=(\partial\rho_\beta(r)/\partial N_\beta)_{N\alpha, v\alpha}]$ , which are known as Fukui functions, have been used to replace the four coefficients appearing in the original expansion, viz. the response functions  $[((\delta/\delta v_\alpha(r))(\partial E/\partial N_\alpha))_{N\beta, v\beta}]$ ,  $[((\delta/\delta v_\beta(r))(\partial E/\partial N_\alpha))_{N\beta, v\alpha}]$ ,  $[((\delta/\delta v_\alpha(r))(\partial E/\partial N_\beta))_{N\alpha, v\beta}]$ , and  $[((\delta/\delta v_\beta(r))(\partial E/\partial N_\beta))_{N\alpha, v\alpha}]$  in view of the identities [3, 19], as shown below, viz.

$$[((\delta/\delta v_\alpha(r))(\partial E/\partial N_\alpha))_{N\beta, v\beta}] = [(\delta\mu_\alpha/\delta v_\alpha(r))_{N\beta, v\beta}] = (\partial\rho_\alpha(r)/\partial N_\alpha)_{N\beta, v\beta} = f_{\alpha\alpha}(r) \quad (21.18a)$$

$$[((\delta/\delta v_\alpha(r))(\partial E/\partial N_\beta))_{N\alpha, v\beta}] = [(\delta\mu_\beta/\delta v_\alpha(r))_{N\alpha, v\beta}] = (\partial\rho_\alpha(r)/\partial N_\beta)_{N\alpha, v\beta} = f_{\alpha\beta}(r) \quad (21.18b)$$

$$[((\delta/\delta v_\beta(r))(\partial E/\partial N_\alpha))_{N\beta, v\alpha}] = [(\delta\mu_\alpha/\delta v_\beta(r))_{N\beta, v\alpha}] = (\partial\rho_\beta(r)/\partial N_\alpha)_{N\beta, v\alpha} = f_{\beta\alpha}(r) \quad (21.18c)$$

$$[((\delta/\delta v_\beta(r))(\partial E/\partial N_\beta))_{N\alpha, v\alpha}] = [(\delta\mu_\beta/\delta v_\beta(r))_{N\alpha, v\alpha}] = (\partial\rho_\beta(r)/\partial N_\beta)_{N\alpha, v\alpha} = f_{\beta\beta}(r) \quad (21.18d)$$

The expression for  $\Delta E$  given by Eq. (21.15) can also be written in an alternative compact form as

$$\begin{aligned} \Delta E = & \left[ \mu_\alpha + (1/2)\eta_{\alpha\alpha}(\Delta N_\alpha) + (1/2)\eta_{\alpha\beta}(\Delta N_\beta) + \int \mathbf{dr} \delta v_\alpha(r) f_{\alpha\alpha}(r) + \int \mathbf{dr} \delta v_\beta(r) f_{\beta\alpha}(r) \right] \Delta N_\alpha \\ & + \int \mathbf{dr} \delta v_\alpha(r) \left[ \rho_\alpha(r) + (1/2) \int \mathbf{dr}' \delta v_\alpha(r') \chi_{\alpha\alpha}(r, r') + (1/2) \int \mathbf{dr}' \delta v_\beta(r') \chi_{\alpha\beta}(r, r') \right] \\ & + \left[ \mu_\beta + (1/2)\eta_{\beta\beta}(\Delta N_\beta) + (1/2)\eta_{\alpha\beta}(\Delta N_\alpha) + \int \mathbf{dr} \delta v_\alpha(r) f_{\alpha\beta}(r) + \int \mathbf{dr} \delta v_\beta(r) f_{\beta\beta}(r) \right] \Delta N_\beta \\ & + \int \mathbf{dr} \delta v_\beta(r) \left[ \rho_\beta(r) + (1/2) \int \mathbf{dr}' \delta v_\beta(r') \chi_{\beta\beta}(r, r') + (1/2) \int \mathbf{dr}' \delta v_\alpha(r') \chi_{\alpha\beta}(r, r') \right] \end{aligned} \quad (21.19)$$

The energy change  $\Delta E$ , as given by the above expressions (21.15) and (21.19), corresponds to a perturbation due to the potential change  $\{\delta v_\alpha(r), \delta v_\beta(r)\}$  and also the electron number change  $\{\Delta N_\alpha, \Delta N_\beta\}$ . It will be now worthwhile to find out what will be the chemical potential in the perturbed state. This can be accomplished by taking the derivative of the energy expression with respect to the number of electrons, viz.

$$\begin{aligned} \mu_\alpha &= (\partial E_v / \partial N_\alpha)_{v\alpha(r), v\beta(r), N\beta} \\ &= \mu_\alpha^0 + \eta_{\alpha\alpha}(\Delta N_\alpha) + \eta_{\alpha\beta}(\Delta N_\beta) + \int \mathbf{dr} \delta v_\alpha(r) f_{\alpha\alpha}(r) + \int \mathbf{dr} \delta v_\beta(r) f_{\beta\alpha}(r) \end{aligned} \quad (21.20a)$$

$$\begin{aligned} \mu_\beta &= (\partial E_v / \partial N_\beta)_{v\alpha(r), v\beta(r), N\alpha} \\ &= \mu_\beta^0 + \eta_{\beta\beta}(\Delta N_\beta) + \eta_{\alpha\beta}(\Delta N_\alpha) + \int \mathbf{dr} \delta v_\alpha(r) f_{\alpha\beta}(r) + \int \mathbf{dr} \delta v_\beta(r) f_{\beta\beta}(r) \end{aligned} \quad (21.20b)$$

where  $\mu_\alpha^0$  and  $\mu_\beta^0$  refer to the unperturbed system.

The energy change  $\Delta E$  can also be estimated through a more detailed picture by considering the perturbation in terms of the electron density change  $\{\delta\rho_\alpha(r), \delta\rho_\beta(r)\}$  (which may include the electron number changes  $\{\Delta N_\alpha, \Delta N_\beta\}$  as well as the density shape changes), and of course the potential change  $\{\delta v_\alpha(r), \delta v_\beta(r)\}$ . Thus, one has, in the density and potential representation, the expression

$$\Delta E = E_{v_\alpha+\delta v_\alpha, v_\beta+\delta v_\beta}[\rho_\alpha(r) + \delta\rho_\alpha(r), \rho_\beta(r) + \delta\rho_\beta(r)] - E_{v_\alpha, v_\beta}[\rho_\alpha(r), \rho_\beta(r)] \quad (21.21)$$

which can be evaluated easily by considering the energy expression

$$E_{v_\alpha, v_\beta}[\rho_\alpha, \rho_\beta] = \int d\mathbf{r} v_\alpha(r) \rho_\alpha(r) + \int d\mathbf{r} v_\beta(r) \rho_\beta(r) + F[\rho_\alpha, \rho_\beta] \quad (21.22)$$

with  $F[\rho_\alpha, \rho_\beta]$  representing a universal functional of the spin-component densities, consisting of contributions from the kinetic energy, classical Coulomb, and exchange-correlation energy, the last two representing components of electron repulsion energy density functionals.

Thus,  $\Delta E$  can be expressed by considering the Taylor series expansion and retaining terms up to second order, viz.

$$\begin{aligned} \Delta E = & \mu_\alpha \int d\mathbf{r} \delta\rho_\alpha(r) + \mu_\beta \int d\mathbf{r} \delta\rho_\beta(r) + \int d\mathbf{r} \delta v_\alpha(r) \rho_\alpha(r) + \int d\mathbf{r} \delta v_\beta(r) \rho_\beta(r) \\ & + (1/2) \int d\mathbf{r} \int d\mathbf{r}' \eta_{\alpha\alpha}(r, r') \delta\rho_\alpha(r) \delta\rho_\alpha(r') + (1/2) \int d\mathbf{r} \\ & \times \int d\mathbf{r}' \eta_{\beta\beta}(r, r') \delta\rho_\beta(r) \delta\rho_\beta(r') \\ & + \int d\mathbf{r} \int d\mathbf{r}' \eta_{\alpha\beta}(r, r') \delta\rho_\alpha(r) \delta\rho_\beta(r') + (1/2) \int d\mathbf{r} \\ & \times \int d\mathbf{r}' \delta v_\alpha(r) \delta v_\alpha(r') \chi_{\alpha\alpha}(r, r') \\ & + (1/2) \int d\mathbf{r} \int d\mathbf{r}' \delta v_\beta(r) \delta v_\beta(r') \chi_{\beta\beta}(r, r') + \int d\mathbf{r} \\ & \times \int d\mathbf{r}' \delta v_\alpha(r) \delta v_\beta(r') \chi_{\alpha\beta}(r, r') \\ & + \int d\mathbf{r} \int d\mathbf{r}' \delta v_\alpha(r) \delta\rho_\alpha(r') \xi_{\alpha\alpha}(r, r') + \int d\mathbf{r} \int d\mathbf{r}' \delta v_\beta(r) \delta\rho_\beta(r') \xi_{\beta\beta}(r, r') \\ & + \int d\mathbf{r} \int d\mathbf{r}' \delta v_\alpha(r) \delta\rho_\beta(r') \xi_{\alpha\beta}(r, r') + \int d\mathbf{r} \int d\mathbf{r}' \delta v_\beta(r) \delta\rho_\alpha(r') \xi_{\beta\alpha}(r, r') \end{aligned} \quad (21.23)$$

In writing the first-order term, use has been made of the definitions of  $\mu_\alpha$  and  $\mu_\beta$  as  $\mu_\alpha = v_\alpha(r) + [\delta F/\delta\rho_\alpha(r)]$  and  $\mu_\beta = v_\beta(r) + [\delta F/\delta\rho_\beta(r)]$ . One can of course replace the integrals  $\int d\mathbf{r} \delta\rho_\alpha(r)$  and  $\int d\mathbf{r} \delta\rho_\beta(r)$  by  $\Delta N_\alpha$  and  $\Delta N_\beta$ , respectively, which will be done later. Similarly in writing the second-order contributions, where we have introduced the hardness kernel [24–26]

$$\eta_{\alpha\alpha}(r, r') = [(\delta^2 E/\delta\rho_\alpha(r) \delta\rho_\alpha(r'))]_{v_\alpha, v_\beta} = [(\delta^2 F/\delta\rho_\alpha(r) \delta\rho_\alpha(r'))] \quad (21.24a)$$

$$\eta_{\beta\beta}(r, r') = [(\delta^2 E/\delta\rho_\beta(r) \delta\rho_\beta(r'))]_{v_\alpha, v_\beta} = [(\delta^2 F/\delta\rho_\beta(r) \delta\rho_\beta(r'))] \quad (21.24b)$$

$$\eta_{\alpha\beta}(r, r') = [(\delta^2 E/\delta\rho_\alpha(r) \delta\rho_\beta(r'))]_{v_\alpha, v_\beta} = [(\delta^2 F/\delta\rho_\alpha(r) \delta\rho_\beta(r'))] = \eta_{\beta\alpha}(r, r') \quad (21.24c)$$

and another cross coefficient, the density–potential response function

$$\xi_{\alpha\alpha}(r, r') = [(\delta^2 E / \delta v_{\alpha}(r) \delta \rho_{\alpha}(r'))]_{v\beta, \rho\beta} \quad (21.25a)$$

$$\xi_{\beta\beta}(r, r') = [(\delta^2 E / \delta v_{\beta}(r) \delta \rho_{\beta}(r'))]_{v\alpha, \rho\alpha} \quad (21.25b)$$

$$\xi_{\alpha\beta}(r, r') = [(\delta^2 E / \delta v_{\alpha}(r) \delta \rho_{\beta}(r'))]_{v\beta, \rho\alpha} \quad (21.25c)$$

$$\xi_{\beta\alpha}(r, r') = [(\delta^2 E / \delta v_{\beta}(r) \delta \rho_{\alpha}(r'))]_{v\alpha, \rho\beta} \quad (21.25d)$$

The response functions  $\chi_{\alpha\beta}(r, r')$  are defined as follows (analogous to Eq. (21.17) but defined at constant density  $\rho$ ).

$$\chi_{\alpha\alpha}(r, r') = [(\delta^2 E / \delta v_{\alpha}(r) \delta v_{\alpha}(r'))]_{\rho\alpha, \rho\beta, v\beta} = \chi_{\alpha\alpha}(r', r) \quad (21.26a)$$

$$\chi_{\beta\beta}(r, r') = [(\delta^2 E / \delta v_{\beta}(r) \delta v_{\beta}(r'))]_{\rho\alpha, \rho\beta, v\alpha} = \chi_{\beta\beta}(r', r) \quad (21.26b)$$

$$\chi_{\alpha\beta}(r, r') = [(\delta^2 E / \delta v_{\alpha}(r) \delta v_{\beta}(r'))]_{\rho\alpha, \rho\beta} = \chi_{\beta\alpha}(r', r) \quad (21.26c)$$

On comparison of this energy expression (21.23) with that of Eqs (21.15) and (21.19), it is clear that the first-order terms are the same, while the second-order terms involving density changes and the corresponding derivatives with respect to density are different. This difference arises from the fact that in Eq. (21.15), the variable changes are  $\{\delta N_{\alpha}, \delta N_{\beta}\}$ , whereas here these variable changes are  $\{\delta \rho_{\alpha}(r), \delta \rho_{\beta}(r)\}$ . Also the response functions for the former correspond to constancy of  $N_{\alpha}$  or  $N_{\beta}$ , whereas here the variables kept constant are  $\rho_{\alpha}(r)$  or  $\rho_{\beta}(r)$ . Thus, for example, the terms with hardness parameters  $\eta_{\alpha\beta}(r, r')$ , etc. are different, and it is clear that for specific cases such as for the forms of the hardness kernel as constants, these terms in Eq. (21.23) become same as the corresponding terms in Eq. (21.15). Analogously, the terms involving the potential–density response parameters are also apparently different. However, for cases of  $\xi_{\alpha\beta}(r, r')$  being equal to the Fukui function  $f_{\alpha\beta}(r)$ , which can be rationalized by considering  $\xi_{\alpha\beta}(r, r') = [(\delta / \delta v_{\alpha}(r))(\delta E / \delta \rho_{\beta}(r'))] = [(\delta \mu_{\beta} / \delta v_{\alpha}(r))] = (\partial \rho_{\alpha}(r) / \partial N_{\beta}) = f_{\alpha\beta}(r)$ , the above-mentioned terms of Eq. (21.23) become same as the corresponding terms in Eq. (21.15). However, here we treat these response functions as parameters and can be suitably modeled.

The expressions for the chemical potentials can be obtained by taking the functional derivatives of Eq. (21.23) with respect to density, viz.

$$\begin{aligned} \mu_{\alpha} &= (\delta E / \delta \rho_{\alpha}(r))_{v\alpha(r), v\beta(r), \rho_{\beta}} \\ &= \mu_{\alpha}^0 + \int d\mathbf{r}' \eta_{\alpha\alpha}(r, r') \delta \rho_{\alpha}(r') + \int d\mathbf{r}' \eta_{\alpha\beta}(r, r') \delta \rho_{\beta}(r') \\ &\quad + \int d\mathbf{r}' \delta v_{\alpha}(r') \xi_{\alpha\alpha}(r', r) + \int d\mathbf{r}' \delta v_{\beta}(r') \xi_{\beta\alpha}(r', r) \end{aligned} \quad (21.27a)$$

$$\begin{aligned} \mu_{\beta} &= (\delta E / \delta \rho_{\beta}(r))_{v\alpha(r), v\beta(r), \rho_{\alpha}} \\ &= \mu_{\beta}^0 + \int d\mathbf{r}' \eta_{\beta\beta}(r, r') \delta \rho_{\beta}(r') + \int d\mathbf{r}' \eta_{\alpha\beta}(r, r') \delta \rho_{\alpha}(r') \\ &\quad + \int d\mathbf{r}' \delta v_{\beta}(r') \xi_{\beta\beta}(r', r) + \int d\mathbf{r}' \delta v_{\alpha}(r') \xi_{\alpha\beta}(r', r) \end{aligned} \quad (21.27b)$$

where again  $\mu_{\alpha}^0$  and  $\mu_{\beta}^0$  refer to the unperturbed system.

## 21.4 Density Functional Perturbation Approach to Energy Changes in Molecule Formation: A Coarse-Grained Procedure

We have so far considered the number of electrons or electron density along with the characterizing potentials for spin-polarized situations as the variables for a many-electron system and considered changes in them as perturbation, thus determining the changes in energy and chemical potential of the system. More specifically, we have derived the expressions for the energy change  $\Delta E$  and also the chemical potential changes  $\Delta\mu_\alpha$  and  $\Delta\mu_\beta$ , corresponding to up ( $\alpha$ )- and down ( $\beta$ )-spin electrons, by considering the perturbation in terms of the electron density change  $\{\delta\rho_\alpha(r), \delta\rho_\beta(r)\}$  (or the electron number change  $\{\Delta N_\alpha, \Delta N_\beta\}$ ) and the potential change  $\{\delta v_\alpha(r), \delta v_\beta(r)\}$ . While these expressions are of general validity and these perturbations might correspond to different physical situations, we now specialize to the case of molecule formation from the constituent atoms, where a situation of this type arises, and the participating atoms experience changes in these quantities due to mutual interatomic interaction. The unperturbed densities of the individual atoms undergo changes due to mutual interatomic interaction, with consequent changes in the potential experienced by the electrons of the individual atoms.

Thus, considering the formation of an  $N$ -electron molecular system from  $N_{\text{atom}}$  number of atoms (which are now considered as subsystems of the whole molecular system), the unperturbed system corresponds to the isolated atoms placed in a certain geometrical arrangement  $\{R_i\}$ , (for  $i = 1, \dots, N_{\text{atom}}$ , and  $R_i$  denoting the position of the  $i$ th atom), with no interatomic interaction (as happens when they are infinite distance apart), and consequently the total energy of the molecular system is just a sum of the energies of the individual atoms. This can be a suitable reference (unperturbed) state for developing the perturbation approach to molecule formation. Now if the interatomic interaction is switched on, clearly this becomes a nonequilibrium situation and the electrons will feel the effect of the new changed external potential, and the system will experience density reorganization and a new equilibrium will be established, which is a stable state of the molecule formed with new energy. The energy change associated with this process is an estimate of the binding energy of the molecule and can be evaluated by considering the expression derived earlier (Eq. (21.23)).

For simplification, we consider the total density change in the molecule as sum of the density changes at each atom, i.e.  $\delta\rho_\alpha(\mathbf{r}) = \sum_i \delta\rho_\alpha^{(i)}(r_i)$ ;  $\delta\rho_\beta(\mathbf{r}) = \sum_i \delta\rho_\beta^{(i)}(r_i)$ , and similarly the total potential change as sum over the atomic sites, i.e.  $\delta v_\alpha(\mathbf{r}) = \sum_i \delta v_\alpha^{(i)}(r_i)$ ;  $\delta v_\beta(\mathbf{r}) = \sum_i \delta v_\beta^{(i)}(r_i)$ , where  $\mathbf{r}_i = (\mathbf{r} - \mathbf{R}_i)$  denotes the  $i$ th atom centered coordinate for the electron, i.e. with the origin located at the  $i$ th atomic site and the superscript ( $i$ ) denotes that the quantity corresponds to the  $i$ th atomic region. It may be noted that the quantities  $\delta\rho_\alpha^{(i)}(r_i)$  and  $\delta\rho_\beta^{(i)}(r_i)$ , denoting the density changes over the  $i$ th atomic region, may have contributions from the shape factor ( $\sigma_\alpha^{(i)}(r)$ , for  $\rho_\alpha^{(i)}(r) = N_\alpha^{(i)}\sigma_\alpha^{(i)}(r)$  and similarly for spin  $\beta$ ) change

within the atomic region as well as the interatomic electron transfer mainly from/to the atoms bonded to the  $i$ th atom. Making these substitutions into Eq. (21.23), one can have the energy change expressed as

$$\begin{aligned}
\Delta E = & \sum_i \mu_\alpha^{(i)} \int d\mathbf{r}_i \delta \rho_\alpha^{(i)}(r_i) + \sum_i \mu_\beta^{(i)} \int d\mathbf{r}_i \delta \rho_\beta^{(i)}(r_i) \\
& + \sum_i \sum_j \int d\mathbf{r}_i \delta v_\alpha^{(j)}(r_i) \rho_\alpha^{(i)}(r_i) + \sum_i \sum_j \int d\mathbf{r}_i \delta v_\beta^{(j)}(r_i) \rho_\beta^{(i)}(r_i) \\
& + (1/2) \sum_i \sum_j \int d\mathbf{r}_i \int d\mathbf{r}_j' \eta_{\alpha\alpha}^{(ij)}(r_i, r_j') \delta \rho_\alpha^{(i)}(r_i) \delta \rho_\alpha^{(j)}(r_j') \\
& + (1/2) \sum_i \sum_j \int d\mathbf{r}_i \int d\mathbf{r}_j' \eta_{\beta\beta}^{(ij)}(r_i, r_j') \delta \rho_\beta^{(i)}(r_i) \delta \rho_\beta^{(j)}(r_j') \\
& + \sum_i \sum_j \int d\mathbf{r}_i \int d\mathbf{r}_j' \eta_{\alpha\beta}^{(ij)}(r_i, r_j') \delta \rho_\alpha^{(i)}(r_i) \delta \rho_\beta^{(j)}(r_j') \\
& + (1/2) \sum_i \sum_j \int d\mathbf{r}_i \int d\mathbf{r}_j' \delta v_\alpha^{(i)}(r_i) \delta v_\alpha^{(j)}(r_j') \chi_{\alpha\alpha}^{(ij)}(r_i, r_j') \\
& + (1/2) \sum_i \sum_j \int d\mathbf{r}_i \int d\mathbf{r}_j' \delta v_\beta^{(i)}(r_i) \delta v_\beta^{(j)}(r_j') \chi_{\beta\beta}^{(ij)}(r_i, r_j') \\
& + \sum_i \sum_j \int d\mathbf{r}_i \int d\mathbf{r}_j' \delta v_\alpha^{(i)}(r_i) \delta v_\beta^{(j)}(r_j') \chi_{\alpha\beta}^{(ij)}(r_i, r_j') \\
& + \sum_i \sum_j \int d\mathbf{r}_i \int d\mathbf{r}_j' \delta v_\alpha^{(i)}(r_i) \delta \rho_\alpha^{(j)}(r_j') \xi_{\alpha\alpha}^{(ij)}(r_i, r_j') \\
& + \sum_i \sum_j \int d\mathbf{r}_i \int d\mathbf{r}_j' \delta v_\beta^{(i)}(r_i) \delta \rho_\beta^{(j)}(r_j') \xi_{\beta\beta}^{(ij)}(r_i, r_j') \\
& + \sum_i \sum_j \int d\mathbf{r}_i \int d\mathbf{r}_j' \delta v_\alpha^{(i)}(r_i) \delta \rho_\beta^{(j)}(r_j') \xi_{\alpha\beta}^{(ij)}(r_i, r_j') \\
& + \sum_i \sum_j \int d\mathbf{r}_i \int d\mathbf{r}_j' \delta v_\beta^{(i)}(r_i) \delta \rho_\alpha^{(j)}(r_j') \xi_{\beta\alpha}^{(ij)}(r_i, r_j') \tag{21.28}
\end{aligned}$$

Within this approach, the expressions for the chemical potentials given by Eq. (21.27) simplify to

$$\begin{aligned}
\mu_\alpha^{(i)} = & \mu_\alpha^{0(i)} + \sum_j \int d\mathbf{r}_j' \eta_{\alpha\alpha}^{(ij)}(r_i, r_j') \delta \rho_\alpha^{(j)}(r_j') + \sum_j \int d\mathbf{r}_j' \eta_{\alpha\beta}^{(ij)}(r_i, r_j') \delta \rho_\beta^{(j)}(r_j') \\
& + \sum_j \int d\mathbf{r}_j' \delta v_\alpha^{(j)}(r_j') \xi_{\alpha\alpha}^{(ij)}(r_j', r_i) + \sum_j \int d\mathbf{r}_j' \delta v_\beta^{(j)}(r_j') \xi_{\beta\alpha}^{(ij)}(r_j', r_i) \tag{21.29a}
\end{aligned}$$

$$\begin{aligned}
\mu_\beta^{(i)} = & \mu_\beta^{0(i)} + \sum_j \int d\mathbf{r}_j' \eta_{\beta\beta}^{(ij)}(r_i, r_j') \delta \rho_\beta^{(j)}(r_j') + \sum_j \int d\mathbf{r}_j' \eta_{\alpha\beta}^{(ij)}(r_i, r_j') \delta \rho_\alpha^{(j)}(r_j') \\
& + \sum_j \int d\mathbf{r}_j' \delta v_\beta^{(j)}(r_j') \xi_{\beta\beta}^{(ij)}(r_j', r_i) + \sum_j \int d\mathbf{r}_j' \delta v_\alpha^{(j)}(r_j') \xi_{\alpha\beta}^{(ij)}(r_j', r_i) \tag{21.29b}
\end{aligned}$$

where again  $\mu_\alpha^{0(i)}$  and  $\mu_\beta^{0(i)}$  refer to the unperturbed  $i$ th atomic system.

## 21.5 A Coarse-Graining Procedure: Lattice Model for Molecular Systems

Equations (21.28) and (21.29) form the basis for developing a lattice model for molecules. However, the expressions for the energy and chemical potential changes,

for spin-polarized situations, as a consequence of molecule formation, depend on density and potential variables, which are functions of the coordinate  $\mathbf{r}$ , which although provide a more detailed and significant information, are more cumbersome as well. To provide simplifications, we adopt what is known as coarse-graining approach.

For this purpose, let us first consider the susceptibility or response parameters that enter the perturbation theory expressions. These quantities are: spin-dependent chemical potentials ( $\mu_\alpha^{(i)}$ ,  $\mu_\beta^{(i)}$ ), which are atomic parameters for the  $i$ th atom, and the rest are interatomic parameters, for  $i$ th and  $j$ th atoms, viz. the hardness kernels or density–density response functions ( $\eta_{\alpha\alpha}^{(ij)}(r_i, r_j')$ ,  $\eta_{\beta\beta}^{(ij)}(r_i, r_j')$ ,  $\eta_{\alpha\beta}^{(ij)}(r_i, r_j')$ ), potential–potential response functions ( $\chi_{\alpha\alpha}^{(ij)}(r_i, r_j')$ ,  $\chi_{\beta\beta}^{(ij)}(r_i, r_j')$ ,  $\chi_{\alpha\beta}^{(ij)}(r_i, r_j')$ ), density–potential response functions ( $\xi_{\alpha\alpha}^{(ij)}(r_i, r_j')$ ,  $\xi_{\beta\beta}^{(ij)}(r_i, r_j')$ ,  $\xi_{\alpha\beta}^{(ij)}(r_i, r_j')$ ,  $\xi_{\beta\alpha}^{(ij)}(r_i, r_j')$ ), and the atom–atom Fukui functions  $f_{\alpha\beta}^{(ij)}(r_i, r_j)$ . The atomic chemical potentials can easily be obtained through DFT calculation or using the expression  $(I + A)/2$ , within the finite difference approximation. Similarly the Fukui function can also be obtained through direct calculation or within finite difference approximation.

The spin-dependent response properties, viz. ( $\eta_{\gamma\delta}^{(ij)}(r_i, r_j')$ , ( $\chi_{\gamma\delta}^{(ij)}(r_i, r_j')$ , and ( $\xi_{\gamma\delta}^{(ij)}(r_i, r_j')$ , where  $\gamma$  and  $\delta$  can denote the spins  $\alpha$  or  $\beta$ , can be suitably modeled within a coarse-grained prescription so that the lattice model is recovered, which provides a rather simpler scheme to implement practical applications to large molecular systems or to generate force fields in classical molecular dynamics simulations.

For this purpose, the  $r$ -dependence (or  $(r, r')$ -dependence) of various quantities is to be modeled, for which we make use of Taylor series expansion around the atomic sites. Thus, the perturbing potentials  $\delta v_\alpha^{(i)}(r_i)$  and  $\delta v_\beta^{(i)}(r_i)$ , which are one-particle functions, can be written as

$$\begin{aligned}\delta v_\alpha^{(i)}(r_i) &= \delta v_\alpha^{(i)}(r_i = 0) + \mathbf{r}_i \cdot \nabla_i \delta v_\alpha^{(i)}(r_i) \Big|_{r_i=0} + (1/2)r_i^2 \nabla_i^2 \delta v_\alpha^{(i)}(r_i) \Big|_{r_i=0} + \dots \\ &= \delta v_\alpha^{(i)}(i) + \mathbf{r}_i \cdot \nabla_i \delta v_\alpha^{(i)}(i) + (1/2)r_i^2 \nabla_i^2 \delta v_\alpha^{(i)}(i) + \dots\end{aligned}\quad (21.30a)$$

$$\begin{aligned}\delta v_\beta^{(i)}(r_i) &= \delta v_\beta^{(i)}(r_i = 0) + \mathbf{r}_i \cdot \nabla_i \delta v_\beta^{(i)}(r_i) \Big|_{r_i=0} + (1/2)r_i^2 \nabla_i^2 \delta v_\beta^{(i)}(r_i) \Big|_{r_i=0} + \dots \\ &= \delta v_\beta^{(i)}(i) + \mathbf{r}_i \cdot \nabla_i \delta v_\beta^{(i)}(i) + (1/2)r_i^2 \nabla_i^2 \delta v_\beta^{(i)}(i) + \dots\end{aligned}\quad (21.30b)$$

by retaining terms up to second order. Similarly the two-particle response kernels  $\eta$ ,  $\chi$ , and  $\xi$ , can be written, by retaining terms up to second order, as

$$\begin{aligned}\eta_{\gamma\delta}^{(ij)}(r_i, r_j') &= \eta_{\gamma\delta}^{(ij)}(i, j) + \mathbf{r}_i \cdot \nabla_i \eta_{\gamma\delta}^{(ij)}(i, j) + \mathbf{r}_j' \cdot \nabla_j \eta_{\gamma\delta}^{(ij)}(i, j) + (1/2)r_i^2 \cdot \nabla_i^2 \eta_{\gamma\delta}^{(ij)}(i, j) \\ &\quad + (1/2)r_j'^2 \cdot \nabla_j^2 \eta_{\gamma\delta}^{(ij)}(i, j) + r_i r_j' \cdot \nabla_i \nabla_j \eta_{\gamma\delta}^{(ij)}(i, j) + \dots\end{aligned}\quad (21.31a)$$

$$\begin{aligned}\chi_{\gamma\delta}^{(ij)}(r_i, r_j') &= \chi_{\gamma\delta}^{(ij)}(i, j) + \mathbf{r}_i \cdot \nabla_i \chi_{\gamma\delta}^{(ij)}(i, j) \\ &\quad + \mathbf{r}_j' \cdot \nabla_j \chi_{\gamma\delta}^{(ij)}(i, j) + (1/2)r_i^2 \cdot \nabla_i^2 \chi_{\gamma\delta}^{(ij)}(i, j) \\ &\quad + (1/2)r_j'^2 \cdot \nabla_j^2 \chi_{\gamma\delta}^{(ij)}(i, j) + r_i r_j' \cdot \nabla_i \nabla_j \chi_{\gamma\delta}^{(ij)}(i, j) + \dots\end{aligned}\quad (21.31b)$$

$$\begin{aligned}\xi_{\gamma\delta}^{(ij)}(r_i, r_j') &= \xi_{\gamma\delta}^{(ij)}(i, j) + \mathbf{r}_i \cdot \nabla_i \xi_{\gamma\delta}^{(ij)}(i, j) + \mathbf{r}_j' \cdot \nabla_j \xi_{\gamma\delta}^{(ij)}(i, j) + (1/2)r_i^2 \cdot \nabla_i^2 \xi_{\gamma\delta}^{(ij)}(i, j) \\ &\quad + (1/2)r_j'^2 \cdot \nabla_j^2 \xi_{\gamma\delta}^{(ij)}(i, j) + r_i r_j' \cdot \nabla_i \nabla_j \xi_{\gamma\delta}^{(ij)}(i, j) + \dots\end{aligned}\quad (21.31c)$$

where the arguments ( $i$ ) and ( $i, j$ ) indicate that the relevant functions are evaluated at the atomic sites ( $r_i = 0$ ) and ( $r_i = 0, r_j' = 0$ ), i.e. ( $\mathbf{r} = \mathbf{R}_i$ ) and ( $\mathbf{r} = \mathbf{R}_i, \mathbf{r}' = \mathbf{R}_j$ ), respectively. Here, again  $\gamma$  and  $\delta$  each denote one of the two spins  $\alpha$  or  $\beta$ .

Substituting these expressions into Eqs (21.28) and (21.29), and retaining terms up to desired (first) order, the expressions for  $\Delta E$  and ( $\mu_\alpha^{(i)}, \mu_\beta^{(i)}$ ) simplify to

$$\begin{aligned}\Delta E &= \sum_i \mu_\alpha^{(i)} \int d\mathbf{r}_i \delta\rho_\alpha^{(i)}(r_i) + \sum_i \mu_\beta^{(i)} \int d\mathbf{r}_i \delta\rho_\beta^{(i)}(r_i) \\ &\quad + \sum_i \sum_j \int d\mathbf{r}_i \delta v_\alpha^{(i)}(i) \rho_\alpha^{(i)}(r_i) + \sum_i \sum_j \int d\mathbf{r}_i \delta v_\beta^{(i)}(i) \rho_\beta^{(i)}(r_i) \\ &\quad + \sum_i \sum_j \int d\mathbf{r}_i \mathbf{r}_i \cdot \nabla_i \delta v_\alpha^{(i)}(i) \rho_\alpha^{(i)}(r_i) + \sum_i \sum_j \int d\mathbf{r}_i \mathbf{r}_i \cdot \nabla_i \delta v_\beta^{(i)}(i) \rho_\beta^{(i)}(r_i) \\ &\quad + (1/2) \sum_i \sum_j \int d\mathbf{r}_i \int d\mathbf{r}_j' \eta_{\alpha\alpha}^{(ij)}(i, j) \delta\rho_\alpha^{(i)}(r_i) \delta\rho_\alpha^{(j)}(r_j') \\ &\quad + (1/2) \sum_i \sum_j \int d\mathbf{r}_i \int d\mathbf{r}_j' \mathbf{r}_i \cdot \nabla_i \eta_{\alpha\alpha}^{(ij)}(i, j) \delta\rho_\alpha^{(i)}(r_i) \delta\rho_\alpha^{(j)}(r_j') \\ &\quad + (1/2) \sum_i \sum_j \int d\mathbf{r}_i \int d\mathbf{r}_j' \mathbf{r}_j' \cdot \nabla_j \eta_{\alpha\alpha}^{(ij)}(i, j) \delta\rho_\alpha^{(i)}(r_i) \delta\rho_\alpha^{(j)}(r_j') \\ &\quad + (1/2) \sum_i \sum_j \int d\mathbf{r}_i \int d\mathbf{r}_j' \mathbf{r}_i \mathbf{r}_j' \cdot \nabla_i \nabla_j \eta_{\alpha\alpha}^{(ij)}(i, j) \delta\rho_\alpha^{(i)}(r_i) \delta\rho_\alpha^{(j)}(r_j') \\ &\quad + (1/2) \sum_i \sum_j \int d\mathbf{r}_i \int d\mathbf{r}_j' \eta_{\beta\beta}^{(ij)}(i, j) \delta\rho_\beta^{(i)}(r_i) \delta\rho_\beta^{(j)}(r_j') \\ &\quad + (1/2) \sum_i \sum_j \int d\mathbf{r}_i \int d\mathbf{r}_j' \mathbf{r}_i \cdot \nabla_i \eta_{\beta\beta}^{(ij)}(i, j) \delta\rho_\beta^{(i)}(r_i) \delta\rho_\beta^{(j)}(r_j') \\ &\quad + (1/2) \sum_i \sum_j \int d\mathbf{r}_i \int d\mathbf{r}_j' \mathbf{r}_j' \cdot \nabla_j \eta_{\beta\beta}^{(ij)}(i, j) \delta\rho_\beta^{(i)}(r_i) \delta\rho_\beta^{(j)}(r_j') \\ &\quad + (1/2) \sum_i \sum_j \int d\mathbf{r}_i \int d\mathbf{r}_j' \mathbf{r}_i \mathbf{r}_j' \cdot \nabla_i \nabla_j \eta_{\beta\beta}^{(ij)}(i, j) \delta\rho_\beta^{(i)}(r_i) \delta\rho_\beta^{(j)}(r_j') \\ &\quad + \sum_i \sum_j \int d\mathbf{r}_i \int d\mathbf{r}_j' \eta_{\alpha\beta}^{(ij)}(i, j) \delta\rho_\alpha^{(i)}(r_i) \delta\rho_\beta^{(j)}(r_j') \\ &\quad + \sum_i \sum_j \int d\mathbf{r}_i \int d\mathbf{r}_j' \mathbf{r}_i \cdot \nabla_i \eta_{\alpha\beta}^{(ij)}(i, j) \delta\rho_\alpha^{(i)}(r_i) \delta\rho_\beta^{(j)}(r_j') \\ &\quad + \sum_i \sum_j \int d\mathbf{r}_i \int d\mathbf{r}_j' \mathbf{r}_j' \cdot \nabla_j \eta_{\alpha\beta}^{(ij)}(i, j) \delta\rho_\alpha^{(i)}(r_i) \delta\rho_\beta^{(j)}(r_j') \\ &\quad + (1/2) \sum_i \sum_j \int d\mathbf{r}_i \int d\mathbf{r}_j' \mathbf{r}_i \mathbf{r}_j' \cdot \nabla_i \nabla_j \eta_{\alpha\beta}^{(ij)}(i, j) \delta\rho_\alpha^{(i)}(r_i) \delta\rho_\beta^{(j)}(r_j') \\ &\quad + (1/2) \sum_i \sum_j \int d\mathbf{r}_i \int d\mathbf{r}_j' \delta v_\alpha^{(i)}(r_i) \delta v_\alpha^{(j)}(r_j') \chi_{\alpha\alpha}^{(ij)}(i, j)\end{aligned}$$



$$\begin{aligned}
& + (1/2)\Sigma_i\Sigma_j \int d\mathbf{r}_i \int d\mathbf{r}_j' \delta v_\alpha^{(i)}(r_i)\delta v_\alpha^{(j)}(r_j')\mathbf{r}_i \cdot \nabla_i \chi_{\alpha\alpha}^{(ij)}(i,j) \\
& + (1/2)\Sigma_i\Sigma_j \int d\mathbf{r}_i \int d\mathbf{r}_j' \delta v_\alpha^{(i)}(r_i)\delta v_\alpha^{(j)}(r_j')\mathbf{r}_j \cdot \nabla_j' \chi_{\alpha\alpha}^{(ij)}(i,j) \\
& + (1/2)\Sigma_i\Sigma_j \int d\mathbf{r}_i \int d\mathbf{r}_j' \delta v_\beta^{(i)}(r_i)\delta v_\beta^{(j)}(r_j')\chi_{\beta\beta}^{(ij)}(i,j) \\
& + (1/2)\Sigma_i\Sigma_j \int d\mathbf{r}_i \int d\mathbf{r}_j' \delta v_\beta^{(i)}(r_i)\delta v_\beta^{(j)}(r_j')\mathbf{r}_i \cdot \nabla_i \chi_{\beta\beta}^{(ij)}(i,j) \\
& + (1/2)\Sigma_i\Sigma_j \int d\mathbf{r}_i \int d\mathbf{r}_j' \delta v_\beta^{(i)}(r_i)\delta v_\beta^{(j)}(r_j')\mathbf{r}_j' \cdot \nabla_j \chi_{\beta\beta}^{(ij)}(i,j) \\
& + \Sigma_i\Sigma_j \int d\mathbf{r}_i \int d\mathbf{r}_j' \delta v_\alpha^{(i)}(r_i)\delta v_\beta^{(j)}(r_j')\chi_{\alpha\beta}^{(ij)}(i,j) \\
& + \Sigma_i\Sigma_j \int d\mathbf{r}_i \int d\mathbf{r}_j' \delta v_\alpha^{(i)}(r_i)\delta v_\beta^{(j)}(r_j')\mathbf{r}_i \cdot \nabla_i \chi_{\alpha\beta}^{(ij)}(i,j) \\
& + \Sigma_i\Sigma_j \int d\mathbf{r}_i \int d\mathbf{r}_j' \delta v_\alpha^{(i)}(r_i)\delta v_\beta^{(j)}(r_j')\mathbf{r}_j' \cdot \nabla_j \chi_{\alpha\beta}^{(ij)}(i,j) \\
& + \Sigma_i\Sigma_j \int d\mathbf{r}_i \int d\mathbf{r}_j' \delta v_\alpha^{(i)}(r_i)\delta\rho_\alpha^{(j)}(r_j')\xi_{\alpha\alpha}^{(ij)}(i,j) \\
& + \Sigma_i\Sigma_j \int d\mathbf{r}_i \int d\mathbf{r}_j' \delta v_\alpha^{(i)}(r_i)\delta\rho_\alpha^{(j)}(r_j')\mathbf{r}_i \cdot \nabla_i \xi_{\alpha\alpha}^{(ij)}(i,j) \\
& + \Sigma_i\Sigma_j \int d\mathbf{r}_i \int d\mathbf{r}_j' \delta v_\alpha^{(i)}(r_i)\delta\rho_\alpha^{(j)}(r_j')\mathbf{r}_j' \cdot \nabla_j \xi_{\alpha\alpha}^{(ij)}(i,j) \\
& + \Sigma_i\Sigma_j \int d\mathbf{r}_i \int d\mathbf{r}_j' \delta v_\alpha^{(i)}(r_i)\delta\rho_\alpha^{(j)}(r_j')\mathbf{r}_i\mathbf{r}_j' \cdot \nabla_i \nabla_j \xi_{\alpha\alpha}^{(ij)}(i,j) \\
& + \Sigma_i\Sigma_j \int d\mathbf{r}_i \int d\mathbf{r}_j' \delta v_\beta^{(i)}(r_i)\delta\rho_\beta^{(j)}(r_j')\xi_{\beta\beta}^{(ij)}(i,j) \\
& + \Sigma_i\Sigma_j \int d\mathbf{r}_i \int d\mathbf{r}_j' \delta v_\beta^{(i)}(r_i)\delta\rho_\beta^{(j)}(r_j')\mathbf{r}_i \cdot \nabla_i \xi_{\beta\beta}^{(ij)}(i,j) \\
& + \Sigma_i\Sigma_j \int d\mathbf{r}_i \int d\mathbf{r}_j' \delta v_\beta^{(i)}(r_i)\delta\rho_\beta^{(j)}(r_j')\mathbf{r}_j' \cdot \nabla_j \xi_{\beta\beta}^{(ij)}(i,j) \\
& + \Sigma_i\Sigma_j \int d\mathbf{r}_i \int d\mathbf{r}_j' \delta v_\beta^{(i)}(r_i)\delta\rho_\beta^{(j)}(r_j')\mathbf{r}_i\mathbf{r}_j' \cdot \nabla_i \nabla_j \xi_{\beta\beta}^{(ij)}(i,j) \\
& + \Sigma_i\Sigma_j \int d\mathbf{r}_i \int d\mathbf{r}_j' \delta v_\alpha^{(i)}(r_i)\delta\rho_\beta^{(j)}(r_j')\xi_{\alpha\beta}^{(ij)}(i,j) \\
& + \Sigma_i\Sigma_j \int d\mathbf{r}_i \int d\mathbf{r}_j' \delta v_\alpha^{(i)}(r_i)\delta\rho_\beta^{(j)}(r_j')\mathbf{r}_i \cdot \nabla_i \xi_{\alpha\beta}^{(ij)}(i,j) \\
& + \Sigma_i\Sigma_j \int d\mathbf{r}_i \int d\mathbf{r}_j' \delta v_\alpha^{(i)}(r_i)\delta\rho_\beta^{(j)}(r_j')\mathbf{r}_j' \cdot \nabla_j \xi_{\alpha\beta}^{(ij)}(i,j) \\
& + \Sigma_i\Sigma_j \int d\mathbf{r}_i \int d\mathbf{r}_j' \delta v_\alpha^{(i)}(r_i)\delta\rho_\beta^{(j)}(r_j')\mathbf{r}_i\mathbf{r}_j' \cdot \nabla_i \nabla_j \xi_{\alpha\beta}^{(ij)}(i,j) \\
& + \Sigma_i\Sigma_j \int d\mathbf{r}_i \int d\mathbf{r}_j' \delta v_\beta^{(i)}(r_i)\delta\rho_\alpha^{(j)}(r_j')\xi_{\beta\alpha}^{(ij)}(i,j) \\
& + \Sigma_i\Sigma_j \int d\mathbf{r}_i \int d\mathbf{r}_j' \delta v_\beta^{(i)}(r_i)\delta\rho_\alpha^{(j)}(r_j')\mathbf{r}_i \cdot \nabla_i \xi_{\beta\alpha}^{(ij)}(i,j)
\end{aligned}$$

$$\begin{aligned}
& + \Sigma_j \Sigma_i \int d\mathbf{r}_i \int d\mathbf{r}_j' \delta v_\beta^{(i)}(r_i) \delta \rho_\alpha^{(j)}(r_j') \mathbf{r}_j' \cdot \nabla_j \xi_{\beta\alpha}^{(ij)}(i, j) \\
& + \Sigma_j \Sigma_i \int d\mathbf{r}_i \int d\mathbf{r}_j' \delta v_\beta^{(i)}(r_i) \delta \rho_\beta^{(j)}(r_j') \mathbf{r}_i \mathbf{r}_j' \cdot \nabla_i \nabla_j \xi_{\beta\beta}^{(ij)}(i, j)
\end{aligned} \quad (21.32)$$

Similarly, the expressions for the chemical potentials given by Eq. (21.29) simplify to

$$\begin{aligned}
\mu_\alpha^{(i)} = & \mu_\alpha^{0(i)} + \delta v_\alpha^{(i)}(i) + \mathbf{r}_i \cdot \nabla_i \delta v_\alpha^{(i)}(i) + \Sigma_j \int d\mathbf{r}_j' \eta_{\alpha\alpha}^{(ij)}(i, j) \delta \rho_\alpha(r_j') \\
& + \Sigma_j \int d\mathbf{r}_j' \eta_{\alpha\beta}^{(ij)}(i, j) \delta \rho_\beta(r_j') + \Sigma_j \int d\mathbf{r}_j' \mathbf{r}_i \cdot \nabla_i \eta_{\alpha\alpha}^{(ij)}(i, j) \delta \rho_\alpha(r_j') \\
& + \Sigma_j \int d\mathbf{r}_j' \mathbf{r}_i \cdot \nabla_i \eta_{\alpha\beta}^{(ij)}(i, j) \delta \rho_\beta(r_j') + \Sigma_j \int d\mathbf{r}_j' \mathbf{r}_j' \cdot \nabla_j \eta_{\alpha\alpha}^{(ij)}(i, j) \delta \rho_\alpha(r_j') \\
& + \Sigma_j \int d\mathbf{r}_j' \mathbf{r}_j' \cdot \nabla_j \eta_{\alpha\beta}^{(ij)}(i, j) \delta \rho_\beta(r_j') \\
& + \Sigma_j \int d\mathbf{r}_j' \mathbf{r}_i \mathbf{r}_j' \cdot \nabla_i \nabla_j \eta_{\alpha\alpha}^{(ij)}(i, j) \delta \rho_\alpha^{(i)}(r_j') \\
& + \Sigma_j \int d\mathbf{r}_j' \mathbf{r}_i \mathbf{r}_j' \cdot \nabla_i \nabla_j \eta_{\alpha\beta}^{(ij)}(i, j) \delta \rho_\beta^{(i)}(r_j') + \Sigma_j \int d\mathbf{r}_j' \delta v_\alpha(r_j') \xi_{\alpha\alpha}^{(ji)}(j, i) \\
& + \Sigma_j \int d\mathbf{r}_j' \delta v_\beta(r_j') \xi_{\beta\alpha}^{(ji)}(j, i) + \Sigma_j \int d\mathbf{r}_j' \delta v_\alpha(r_j') \mathbf{r}_i \cdot \nabla_i \xi_{\alpha\alpha}^{(ji)}(j, i) \\
& + \Sigma_j \int d\mathbf{r}_j' \delta v_\beta(r_j') \mathbf{r}_i \cdot \nabla_i \xi_{\beta\alpha}^{(ji)}(j, i) + \Sigma_j \int d\mathbf{r}_j' \delta v_\alpha(r_j') \mathbf{r}_j' \cdot \nabla_j \xi_{\alpha\alpha}^{(ji)}(j, i) \\
& + \Sigma_j \int d\mathbf{r}_j' \delta v_\beta(r_j') \mathbf{r}_j' \cdot \nabla_j \xi_{\beta\alpha}^{(ji)}(j, i)
\end{aligned} \quad (21.33a)$$

$$\begin{aligned}
\mu_\beta^{(i)} = & \mu_\beta^{0(i)} + \delta v_\beta^{(i)}(i) + \mathbf{r}_i \cdot \nabla_i \delta v_\beta^{(i)}(i) + \Sigma_j \int d\mathbf{r}_j' \eta_{\beta\beta}^{(ij)}(i, j) \delta \rho_\beta(r_j') \\
& + \Sigma_j \int d\mathbf{r}_j' \eta_{\alpha\beta}^{(ij)}(i, j) \delta \rho_\alpha(r_j') + \Sigma_j \int d\mathbf{r}_j' \mathbf{r}_i \cdot \nabla_i \eta_{\beta\beta}^{(ij)}(i, j) \delta \rho_\beta(r_j') \\
& + \Sigma_j \int d\mathbf{r}_j' \mathbf{r}_i \cdot \nabla_i \eta_{\alpha\beta}^{(ij)}(i, j) \delta \rho_\alpha(r_j') + \Sigma_j \int d\mathbf{r}_j' \mathbf{r}_j' \cdot \nabla_j \eta_{\beta\beta}^{(ij)}(i, j) \delta \rho_\beta(r_j') \\
& + \Sigma_j \int d\mathbf{r}_j' \mathbf{r}_j' \cdot \nabla_j \eta_{\alpha\beta}^{(ij)}(i, j) \delta \rho_\alpha(r_j') + \Sigma_j \int d\mathbf{r}_j' \mathbf{r}_i \mathbf{r}_j' \cdot \nabla_i \nabla_j \eta_{\beta\alpha}^{(ij)}(i, j) \delta \rho_\alpha^{(i)}(r_j') \\
& + \Sigma_j \int d\mathbf{r}_j' \mathbf{r}_i \mathbf{r}_j' \cdot \nabla_i \nabla_j \eta_{\beta\beta}^{(ij)}(i, j) \delta \rho_\beta^{(i)}(r_j') + \Sigma_j \int d\mathbf{r}_j' \delta v_\beta(r_j') \xi_{\beta\beta}^{(ji)}(j, i) \\
& + \Sigma_j \int d\mathbf{r}_j' \delta v_\alpha(r_j') \xi_{\alpha\beta}^{(ji)}(j, i) + \Sigma_j \int d\mathbf{r}_j' \delta v_\beta(r_j') \mathbf{r}_i \cdot \nabla_i \xi_{\beta\beta}^{(ji)}(j, i) \\
& + \Sigma_j \int d\mathbf{r}_j' \delta v_\alpha(r_j') \mathbf{r}_i \cdot \nabla_i \xi_{\alpha\beta}^{(ji)}(j, i) + \Sigma_j \int d\mathbf{r}_j' \delta v_\beta(r_j') \mathbf{r}_j' \cdot \nabla_j \xi_{\beta\beta}^{(ji)}(j, i) \\
& + \Sigma_j \int d\mathbf{r}_j' \delta v_\alpha(r_j') \mathbf{r}_j' \cdot \nabla_j \xi_{\alpha\beta}^{(ji)}(j, i)
\end{aligned} \quad (21.33b)$$

The higher-order terms, which will contribute to the final result, are only written here. Others are omitted for simplicity. These expressions can be further simplified in terms of coarse-grained variables. Thus the energy expression simplifies to

$$\begin{aligned}
\Delta E = & \sum_i \mu_\alpha^{(i)} \Delta N_\alpha(i) + \sum_i \mu_\beta^{(i)} \Delta N_\beta(i) \\
& + \sum_i \sum_j \delta v_\alpha^{(ij)}(i) N_\alpha^{(i)}(i) + \sum_i \sum_j \delta v_\beta^{(ij)}(i) N_\beta^{(i)}(i) \\
& + \sum_i \sum_j \mathbf{p}_\alpha^{(i)}(i) \cdot \nabla_i \delta v_\alpha^{(ij)}(i) + \sum_i \sum_j \mathbf{p}_\beta^{(i)}(i) \cdot \nabla_i \delta v_\beta^{(ij)}(i) \\
& + (1/2) \sum_i \sum_j \eta_{\alpha\alpha}^{(ij)}(i, j) \Delta N_\alpha^{(i)}(i) \Delta N_\alpha^{(j)}(j) \\
& + (1/2) \sum_i \sum_j \mathbf{p}_\alpha(i) \cdot \nabla_i \eta_{\alpha\alpha}^{(ij)}(i, j) \Delta N_\alpha^{(j)}(j) \\
& + (1/2) \sum_i \sum_j \mathbf{p}_\alpha(j) \cdot \nabla_j \eta_{\alpha\alpha}^{(ij)}(i, j) \Delta N_\alpha^{(i)}(i) \\
& + (1/2) \sum_i \sum_j \eta_{\beta\beta}^{(ij)}(i, j) \Delta N_\beta^{(i)}(i) \Delta N_\beta^{(j)}(j) \\
& + (1/2) \sum_i \sum_j \mathbf{p}_\beta(i) \cdot \nabla_i \eta_{\beta\beta}^{(ij)}(i, j) \Delta N_\beta^{(j)}(j) \\
& + (1/2) \sum_i \sum_j \mathbf{p}_\beta(j) \cdot \nabla_j \eta_{\beta\beta}^{(ij)}(i, j) \Delta N_\beta^{(i)}(i) \\
& + \sum_i \sum_j \eta_{\alpha\beta}^{(ij)}(i, j) \Delta N_\alpha^{(i)}(i) \Delta N_\beta^{(j)}(j) \\
& + (1/2) \sum_i \sum_j \mathbf{p}_\alpha(i) \cdot \nabla_i \eta_{\alpha\beta}^{(ij)}(i, j) \Delta N_\beta^{(j)}(j) \\
& + (1/2) \sum_i \sum_j \mathbf{p}_\alpha(j) \cdot \nabla_j \eta_{\alpha\beta}^{(ij)}(i, j) \Delta N_\beta^{(i)}(i) \\
& + (1/2) \sum_i \sum_j \mathbf{p}_\alpha(i) \mathbf{p}_\alpha(j) \cdot \nabla_i \nabla_j \eta_{\alpha\alpha}^{(ij)}(i, j) \\
& + (1/2) \sum_i \sum_j \mathbf{p}_\beta(i) \mathbf{p}_\beta(j) \cdot \nabla_i \nabla_j \eta_{\beta\beta}^{(ij)}(i, j) \\
& + \sum_i \sum_j \mathbf{p}_\alpha(i) \mathbf{p}_\beta(j) \cdot \nabla_i \nabla_j \eta_{\alpha\beta}^{(ij)}(i, j) \\
& + (1/2) \sum_i \sum_j \Delta v_\alpha(i) \Delta v_\alpha(j) \chi_{\alpha\alpha}^{(ij)}(i, j) \\
& + (1/2) \sum_i \sum_j \Pi_\alpha(i) \cdot \nabla_i \chi_{\alpha\alpha}^{(ij)}(i, j) \Delta v_\alpha(j) + (1/2) \sum_i \sum_j \Pi_\alpha(j) \cdot \nabla_j \chi_{\alpha\alpha}^{(ij)}(i, j) \Delta v_\alpha(i) \\
& + (1/2) \sum_i \sum_j \Delta v_\beta(i) \Delta v_\beta(j) \chi_{\beta\beta}^{(ij)}(i, j) \\
& + (1/2) \sum_i \sum_j \Pi_\beta(i) \cdot \nabla_i \chi_{\beta\beta}^{(ij)}(i, j) \Delta v_\beta(j) + (1/2) \sum_i \sum_j \Pi_\beta(j) \cdot \nabla_j \chi_{\beta\beta}^{(ij)}(i, j) \Delta v_\beta(i) \\
& + \sum_i \sum_j \Delta v_\alpha(i) \Delta v_\beta(j) \chi_{\alpha\beta}^{(ij)}(i, j) \\
& + \sum_i \sum_j \Pi_\alpha(i) \cdot \nabla_i \chi_{\alpha\beta}^{(ij)}(i, j) \Delta v_\beta(j) + \sum_i \sum_j \Pi_\beta(j) \cdot \nabla_j \chi_{\alpha\beta}^{(ij)}(i, j) \Delta v_\alpha(i) \\
& + \sum_i \sum_j \Delta v_\alpha(i) \xi_{\alpha\alpha}^{(ij)}(j, i) \Delta N_\alpha(j) + \sum_i \sum_j \Delta v_\beta(i) \xi_{\beta\beta}^{(ij)}(j, i) \Delta N_\beta(j) \\
& + \sum_i \sum_j \Delta v_\alpha(i) \xi_{\alpha\beta}^{(ij)}(j, i) \Delta N_\beta(j) + \sum_i \sum_j \Delta v_\beta(i) \xi_{\beta\alpha}^{(ij)}(j, i) \Delta N_\alpha(j) \\
& + \sum_i \sum_j \Pi_\alpha(i) \cdot \nabla_i \xi_{\alpha\alpha}^{(ij)}(i, j) \Delta N_\alpha(j) + \sum_i \sum_j \Delta v_\alpha(i) \mathbf{p}_\alpha(j) \cdot \nabla_j \xi_{\alpha\alpha}^{(ij)}(i, j) \\
& + \sum_i \sum_j \Pi_\beta(i) \cdot \nabla_i \xi_{\beta\beta}^{(ij)}(i, j) \Delta N_\beta(j) + \sum_i \sum_j \Delta v_\beta(i) \mathbf{p}_\beta(j) \cdot \nabla_j \xi_{\beta\beta}^{(ij)}(i, j) \\
& + \sum_i \sum_j \Pi_\alpha(i) \cdot \nabla_i \xi_{\alpha\beta}^{(ij)}(i, j) \Delta N_\beta(j) + \sum_i \sum_j \Delta v_\alpha(i) \mathbf{p}_\beta(j) \cdot \nabla_j \xi_{\alpha\beta}^{(ij)}(i, j) \\
& + \sum_i \sum_j \Pi_\beta(i) \cdot \nabla_i \xi_{\beta\alpha}^{(ij)}(i, j) \Delta N_\alpha(j) + \sum_i \sum_j \Delta v_\beta(i) \mathbf{p}_\alpha(j) \cdot \nabla_j \xi_{\beta\alpha}^{(ij)}(i, j) \quad (21.34)
\end{aligned}$$

where we define for  $\alpha$ -spin, the change in the number of electrons,  $\Delta N_\alpha(j) = \int d\mathbf{r}_j' \delta \rho_\alpha(r_j')$  and the atomic dipole moment  $\mathbf{p}_\alpha(j) = \int d\mathbf{r}_j' \mathbf{r}_j' \delta \rho_\alpha(r_j')$ , and the quantities  $\Delta v_\alpha^{(ij)}(j) = \int d\mathbf{r}_j' \delta v_\alpha^{(ij)}(r_j') \mathbf{r}_j'$ , all located at the  $j$ th site.

Similar expressions for  $\beta$ -spin are:  $\Delta N_\beta(j) = \int d\mathbf{r}_j' \delta \rho_\beta(r_j')$  and the atomic dipole moment  $\mathbf{p}_\beta(j) = \int d\mathbf{r}_j' \mathbf{r}_j' \delta \rho_\beta(r_j')$ , and the quantities  $\Delta v_\beta^{(ij)}(j) = \int d\mathbf{r}_j' \delta v_\beta^{(ij)}(r_j') \mathbf{r}_j'$ , again all located at the  $j$ th site.

Similarly, the chemical potential expressions become

$$\begin{aligned}
\mu_{\alpha}^{(i)} &= \mu_{\alpha}^{0(i)} + \delta v_{\alpha}^{(j)}(i) + \mathbf{r}_i \cdot \nabla_i \delta v_{\alpha}^{(j)}(i) \\
&+ \sum_j \eta_{\alpha\alpha}^{(ij)}(i, j) \Delta N_{\alpha}(j) + \sum_j \eta_{\alpha\beta}^{(ij)}(i, j) \Delta N_{\beta}(j) \\
&+ \mathbf{r}_i \cdot \sum_j \nabla_i \eta_{\alpha\alpha}^{(ij)}(i, j) \Delta N_{\alpha}(j) + \mathbf{r}_i \cdot \sum_j \nabla_i \eta_{\alpha\beta}^{(ij)}(i, j) \Delta N_{\beta}(j) \\
&+ \sum_j \mathbf{p}_{\alpha}(j) \cdot \nabla_j \eta_{\alpha\alpha}^{(ij)}(i, j) + \sum_j \mathbf{p}_{\beta}(j) \cdot \nabla_j \eta_{\alpha\beta}^{(ij)}(i, j) \\
&+ \mathbf{r}_i \cdot [\sum_j \mathbf{p}_{\alpha}(j) \cdot \nabla_i \nabla_j \eta_{\alpha\alpha}^{(ij)}(i, j) + \sum_j \mathbf{p}_{\beta}(j) \cdot \nabla_i \nabla_j \eta_{\alpha\beta}^{(ij)}(i, j)] \\
&+ \sum_j \Delta v_{\alpha}(j) \xi_{\alpha\alpha}^{(ij)}(j, i) + \sum_j \Delta v_{\beta}(j) \xi_{\beta\alpha}^{(ij)}(j, i) \\
&+ \mathbf{r}_i \cdot \sum_j \Delta v_{\alpha}(j) \nabla_i \xi_{\alpha\alpha}^{(ij)}(j, i) + \mathbf{r}_i \cdot \sum_j \Delta v_{\beta}(j) \nabla_i \xi_{\beta\alpha}^{(ij)}(j, i) \\
&+ \sum_j \Pi_{\alpha}(j) \cdot \nabla_j \xi_{\alpha\alpha}^{(ij)}(j, i) + \sum_j \Pi_{\beta}(j) \cdot \nabla_j \xi_{\beta\alpha}^{(ij)}(j, i)
\end{aligned} \tag{21.35a}$$

$$\begin{aligned}
\mu_{\beta}^{(i)} &= \mu_{\beta}^{0(i)} + \delta v_{\beta}^{(j)}(i) + \mathbf{r}_i \cdot \nabla_i \delta v_{\beta}^{(j)}(i) \\
&+ \sum_j \eta_{\beta\beta}^{(ij)}(i, j) \Delta N_{\beta}(j) + \sum_j \eta_{\alpha\beta}^{(ij)}(i, j) \Delta N_{\alpha}(j) \\
&+ \mathbf{r}_i \cdot \sum_j \nabla_i \eta_{\beta\beta}^{(ij)}(i, j) \Delta N_{\beta}(j) + \mathbf{r}_i \cdot \sum_j \nabla_i \eta_{\alpha\beta}^{(ij)}(i, j) \Delta N_{\alpha}(j) \\
&+ \sum_j \mathbf{p}_{\beta}(j) \cdot \nabla_j \eta_{\beta\beta}^{(ij)}(i, j) + \sum_j \mathbf{p}_{\alpha}(j) \cdot \nabla_j \eta_{\alpha\beta}^{(ij)}(i, j) \\
&+ \mathbf{r}_i \cdot [\sum_j \mathbf{p}_{\beta}(j) \cdot \nabla_i \nabla_j \eta_{\beta\beta}^{(ij)}(i, j) + \sum_j \mathbf{p}_{\alpha}(j) \cdot \nabla_i \nabla_j \eta_{\alpha\beta}^{(ij)}(i, j)] \\
&+ \sum_j \Delta v_{\beta}(j) \xi_{\beta\beta}^{(ij)}(j, i) + \sum_j \Delta v_{\alpha}(j) \xi_{\alpha\beta}^{(ij)}(j, i) \\
&+ \mathbf{r}_i \cdot \sum_j \Delta v_{\beta}(j) \nabla_i \xi_{\beta\beta}^{(ij)}(j, i) + \mathbf{r}_i \cdot \sum_j \Delta v_{\alpha}(j) \nabla_i \xi_{\alpha\beta}^{(ij)}(j, i) \\
&+ \sum_j \Pi_{\beta}(j) \cdot \nabla_j \xi_{\beta\beta}^{(ij)}(j, i) + \sum_j \Pi_{\alpha}(j) \cdot \nabla_j \xi_{\alpha\beta}^{(ij)}(j, i)
\end{aligned} \tag{21.35b}$$

One can also obtain the expressions for the chemical potentials by directly differentiating the energy expression of Eq. (21.34) with respect to  $\Delta N_{\alpha}(i)$  or  $\Delta N_{\beta}(i)$ , which will yield the chemical potential of  $i$ th atom.

From the expressions of the chemical potentials as given by Eq. (21.35), it is clear that since left side is position-independent, right side can be evaluated at any value of the position and evaluate the left side, which is the chemical potential. Thus, by evaluating at  $r_i = 0$ , one has the result

$$\begin{aligned}
\mu_{\alpha}^{(i)} &= \mu_{\alpha}^{0(i)} + \delta v_{\alpha}^{(j)}(i) + \sum_j \eta_{\alpha\alpha}^{(ij)}(i, j) \Delta N_{\alpha}(j) + \sum_j \eta_{\alpha\beta}^{(ij)}(i, j) \Delta N_{\beta}(j) \\
&+ \sum_j \mathbf{p}_{\alpha}(j) \cdot \nabla_j \eta_{\alpha\alpha}^{(ij)}(i, j) + \sum_j \mathbf{p}_{\beta}(j) \cdot \nabla_j \eta_{\alpha\beta}^{(ij)}(i, j) \\
&+ \sum_j \Delta v_{\alpha}(j) \xi_{\alpha\alpha}^{(ij)}(j, i) + \sum_j \Delta v_{\beta}(j) \xi_{\beta\alpha}^{(ij)}(j, i) \\
&+ \sum_j \Pi_{\alpha}(j) \cdot \nabla_j \xi_{\alpha\alpha}^{(ij)}(j, i) + \sum_j \Pi_{\beta}(j) \cdot \nabla_j \xi_{\beta\alpha}^{(ij)}(j, i)
\end{aligned} \tag{21.36a}$$

$$\begin{aligned}
\mu_{\beta}^{(i)} &= \mu_{\beta}^{0(i)} + \delta v_{\beta}^{(j)}(i) + \sum_j \eta_{\beta\beta}^{(ij)}(i, j) \Delta N_{\beta}(j) + \sum_j \eta_{\alpha\beta}^{(ij)}(i, j) \Delta N_{\alpha}(j) \\
&+ \sum_j \mathbf{p}_{\beta}(j) \cdot \nabla_j \eta_{\beta\beta}^{(ij)}(i, j) + \sum_j \mathbf{p}_{\alpha}(j) \cdot \nabla_j \eta_{\alpha\beta}^{(ij)}(i, j) \\
&+ \sum_j \Delta v_{\beta}(j) \xi_{\beta\beta}^{(ij)}(j, i) + \sum_j \Delta v_{\alpha}(j) \xi_{\alpha\beta}^{(ij)}(j, i) \\
&+ \sum_j \Pi_{\beta}(j) \cdot \nabla_j \xi_{\beta\beta}^{(ij)}(j, i) + \sum_j \Pi_{\alpha}(j) \cdot \nabla_j \xi_{\alpha\beta}^{(ij)}(j, i)
\end{aligned} \tag{21.36b}$$

By comparing Eqs (21.35) and (21.36), one also obtains the relations

$$\begin{aligned} \nabla_i \delta v_\alpha^{(j)}(i) + (\sum_j \nabla_i \eta_{\alpha\alpha}^{(ij)}(i, j) \Delta N_\alpha(j) + \sum_j \nabla_i \eta_{\alpha\beta}^{(ij)}(i, j) \Delta N_\beta(j) + \sum_j \Delta v_\alpha(j) \nabla_i \xi_{\alpha\alpha}^{(ji)}(j, i) \\ + \sum_j \Delta v_\beta(j) \nabla_i \xi_{\beta\alpha}^{(ji)}(j, i) + [\sum_j \mathbf{p}_\alpha(j) \cdot \nabla_i \nabla_j \eta_{\alpha\alpha}^{(ij)}(i, j) + \sum_j \mathbf{p}_\beta(j) \cdot \nabla_i \nabla_j \eta_{\alpha\beta}^{(ij)}(i, j)]) = 0 \end{aligned} \quad (21.37a)$$

and

$$\begin{aligned} \nabla_i \delta v_\beta^{(j)}(i) + (\sum_j \nabla_i \eta_{\beta\beta}^{(ij)}(i, j) \Delta N_\beta(j) + \sum_j \nabla_i \eta_{\alpha\beta}^{(ij)}(i, j) \Delta N_\alpha(j) + \sum_j \Delta v_\beta(j) \nabla_i \xi_{\beta\beta}^{(ji)}(j, i) \\ + \sum_j \Delta v_\alpha(j) \nabla_i \xi_{\alpha\beta}^{(ji)}(j, i) + [\sum_j \mathbf{p}_\alpha(j) \cdot \nabla_i \nabla_j \eta_{\alpha\alpha}^{(ij)}(i, j) + \sum_j \mathbf{p}_\beta(j) \cdot \nabla_i \nabla_j \eta_{\alpha\beta}^{(ij)}(i, j)]) = 0 \end{aligned} \quad (21.37b)$$

Here, the quantities  $\nabla_i \delta v_\alpha^{(j)}(i)$  and  $\nabla_i \delta v_\beta^{(j)}(i)$  represent the electric field arising from the change in external potential. It may include any external applied electric field.

Now, separating out the self terms and cross terms from the summations in Eq. (21.36), one can write

$$\begin{aligned} \mu_\alpha^{(i)} = \mu_\alpha^{0(i)} + \delta v_\alpha^{(j)}(i) + \eta_{\alpha\alpha}^{(ii)}(i, i) \Delta N_\alpha(i) + \eta_{\alpha\beta}^{(ii)}(i, i) \Delta N_\beta(i) \\ + \sum_{j \neq i} \eta_{\alpha\alpha}^{(ij)}(i, j) \Delta N_\alpha(j) + \sum_{j \neq i} \eta_{\alpha\beta}^{(ij)}(i, j) \Delta N_\beta(j) \\ + \mathbf{p}_\alpha(i) \cdot \nabla_j \eta_{\alpha\alpha}^{(ij)}(i, j) \Big|_{j=i} + \mathbf{p}_\beta(i) \cdot \nabla_j \eta_{\alpha\beta}^{(ij)}(i, j) \Big|_{j=i} \\ + \sum_{j \neq i} \mathbf{p}_\alpha(j) \cdot \nabla_j \eta_{\alpha\alpha}^{(ij)}(i, j) + \sum_{j \neq i} \mathbf{p}_\beta(j) \cdot \nabla_j \eta_{\alpha\beta}^{(ij)}(i, j) \\ + \sum_j \Delta v_\alpha(j) \xi_{\alpha\alpha}^{(ji)}(j, i) + \sum_j \Delta v_\beta(j) \xi_{\beta\alpha}^{(ji)}(j, i) \\ + \sum_j \Pi_\alpha(j) \cdot \nabla_j \xi_{\alpha\alpha}^{(ji)}(j, i) + \sum_j \Pi_\beta(j) \cdot \nabla_j \xi_{\beta\alpha}^{(ji)}(j, i) \end{aligned} \quad (21.38a)$$

$$\begin{aligned} \mu_\beta^{(i)} = \mu_\beta^{0(i)} + \delta v_\beta^{(j)}(i) + \eta_{\beta\beta}^{(ii)}(i, i) \Delta N_\beta(i) + \eta_{\alpha\beta}^{(ii)}(i, i) \Delta N_\alpha(i) \\ + \sum_{j \neq i} \eta_{\beta\beta}^{(ij)}(i, j) \Delta N_\beta(j) + \sum_{j \neq i} \eta_{\alpha\beta}^{(ij)}(i, j) \Delta N_\alpha(j) \\ + \mathbf{p}_\beta(i) \cdot \nabla_j \eta_{\beta\beta}^{(ij)}(i, j) \Big|_{j=i} + \mathbf{p}_\alpha(i) \cdot \nabla_j \eta_{\alpha\beta}^{(ij)}(i, j) \Big|_{j=i} \\ + \sum_{j \neq i} \mathbf{p}_\beta(j) \cdot \nabla_j \eta_{\beta\beta}^{(ij)}(i, j) + \sum_{j \neq i} \mathbf{p}_\alpha(j) \cdot \nabla_j \eta_{\alpha\beta}^{(ij)}(i, j) \\ + \sum_j \Delta v_\beta(j) \xi_{\beta\beta}^{(ji)}(j, i) + \sum_j \Delta v_\alpha(j) \xi_{\alpha\beta}^{(ji)}(j, i) \\ + \sum_j \Pi_\beta(j) \cdot \nabla_j \xi_{\beta\beta}^{(ji)}(j, i) + \sum_j \Pi_\alpha(j) \cdot \nabla_j \xi_{\alpha\beta}^{(ji)}(j, i) \end{aligned} \quad (21.38b)$$

Let us now interpret the various response parameters. The quantities  $\eta_{\alpha\alpha}^{(ii)}(i, i)$  and  $\eta_{\beta\beta}^{(ii)}(i, i)$  are the diagonal elements with respect to atom indices as well as spin indices, and are analogous to the conventional hardness parameter, while the parameter  $\eta_{\alpha\beta}^{(ii)}(i, i)$  is diagonal in atom index but off-diagonal in spin index, which is again similar but refers to one derivative with up-spin and the other with down-spin electron. These three parameters can be evaluated, within a finite difference approximation, using the ionization potential and electron affinity parameters  $I_\alpha$ ,  $A_\alpha$ ,  $I_\beta$ , and  $A_\beta$  for both the spins. Thus, one can have  $\eta_{\alpha\alpha}^{(ii)}(i, i) = (I_\alpha - A_\alpha)/2$ ,  $\eta_{\beta\beta}^{(ii)}(i, i) = (I_\beta - A_\beta)/2$ , and  $\eta_{\alpha\beta}^{(ii)}(i, i) = [(I_\alpha - A_\beta) + (I_\beta - A_\alpha)]/4$ .

The atom-atom cross parameters  $\eta_{\alpha\alpha}^{(ij)}(i, j)$ ,  $\eta_{\beta\beta}^{(ij)}(i, j)$ , and  $\eta_{\alpha\beta}^{(ij)}(i, j)$  can either be evaluated by using the simple model of averaging the atomic softnesses (inverse

of hardness) of the  $i$ th and  $j$ th atoms, thus writing as  $1/\eta_{\gamma\delta}^{(ij)}(i, j) = (1/2)[1/\eta_{\gamma\gamma}^{(ii)}(i, i) + 1/\eta_{\delta\delta}^{(jj)}(j, j)]$ , for  $\gamma, \delta = \alpha$  or  $\beta$ . These quantities however denote essentially the multiplicative factor for the charge on the  $j$ th atom, for generating the potential at the  $i$ th atom. Thus, in one level of approximation, it can be just a Coulombic term,  $1/R_{ij}$ , which is true only for point charges. However, better approximations can be made by taking clue from semiempirical quantum chemistry, e.g. by using Mataga–Nishimoto-type empirical formula [11] given by  $\eta_{\gamma\delta}^{(ij)}(i, j) = (a_{ij}^{\gamma\delta} + R_{ij})^{-1}$ , where  $a_{ij}^{\gamma\delta}$  is a constant and can be related to the hardness parameters of the  $i$ th and  $j$ th atoms. The coefficients of the atomic dipole moments are related to the atomic polarizabilities and dipolar (or charge-dipole) hardnesses for the self terms and some kind of Coulomb-like terms for the cross coefficients.

Equation (21.38) represents essentially the spin-dependent chemical potentials of an atom (say,  $i$ th atom) in the molecular species of interest, within the approximations of superposed atomic site densities and consideration of only the first two moments (zeroth and first), viz. the up- and down-spin atomic charges  $q_{\alpha}(i) (= -\Delta N_{\alpha}(i))$ ,  $q_{\beta}(i) (= -\Delta N_{\beta}(i))$  and the atomic dipole moments  $\mathbf{p}_{\alpha}(i)$ ,  $\mathbf{p}_{\beta}(i)$ , respectively. Thus, in this lattice model, a molecule represents a collection of atom centers with point charges and dipoles, determined through the chemical potential equalization, by equating each of the two spin chemical potentials  $\mu_{\alpha}^{(i)}$  and  $\mu_{\beta}^{(i)}$  (as expressed by Eq. (21.38)) for all the atom centers. For each spin, two sets of equation pairs will result, one by equating on both sides the constant terms and the other from terms linear in  $\mathbf{p}_{\alpha}(i)$  or  $\mathbf{p}_{\beta}(i)$ , respectively. For a molecule with  $N_{\text{atom}}$  number of atoms, one obtains a set of  $N_{\text{atom}} - 1$  equations from equating the scalar chemical potentials for up-spin for all the atoms and another set of  $N_{\text{atom}} - 1$  equations for down-spin. The additional two equations are given by the charge conservation for each spin (neutrality for a neutral molecule)  $\sum_i \Delta N_{\alpha}(i) = 0$ ,  $\sum_i \Delta N_{\beta}(i) = 0$ . Besides this set of  $2N_{\text{atom}}$  scalar equations, one has  $2N_{\text{atom}}$  vector equations, corresponding to atomic dipole moment vectors for the two spins (see Eq. (21.37)). These equations, which are essentially  $8N_{\text{atom}}$  number of scalar equations, being linear in nature, can easily be solved by matrix methods to obtain the atomic charges (scalars), and the atomic dipoles (vectors) corresponding to both the spins at each of the atomic sites.

## 21.6 Miscellaneous Aspects: Inclusion of Bond Space, Covalent Binding, and Correct Asymptotics

It may be noted that the charge transfer due to chemical potential difference between atoms leads to binding, which is essentially ionic binding. For describing the covalent binding within an electronegativity or chemical potential–based picture, several other considerations are in fact needed. The first one is inspired by the presence of unpaired electrons, which can be quantified by assuming spin-dependent chemical potential for each atom, within the spin-polarized DFT, which has already been discussed in the earlier section. Another approach makes use of the fact that there is

charge accumulation at the bond region in covalent binding, which can be investigated by considering the bond sites as additional sites in the lattice model, in addition to the atomic sites. These additional bond sites can be located in between (say middle of the bond) the two atoms in each bonded atom pair. This is the so-called introduction or inclusion of the bond space, in which chemical potential and hardness parameters ( $\mu^{\text{bond}}$  and  $\eta^{\text{bond}}$ ) are assigned for the bond region. This is quite appropriate in view of the fact that in DFT the chemical potential is defined at all points in space. Spin-polarized DFT can be used for this purpose as well. The formalism is analogous to that discussed in the previous section. But a direct coarse-grained picture in terms of the atomic and bond charges can be a simple one.

As far as the parametrizations of the different quantities are concerned, the bond chemical potential can be thought of as approximately the electrostatic potential at the atomic radius sites and hence a simple prescription can be in terms of the sum of the two associated atoms, viz.  $\mu_{ij}^{\text{bond}} = K(\mu_i^0 + \mu_j^0)$ , with  $K$  as an empirical constant. There will be several types of bond hardness parameters, associated with different bonds, in the same spirit as that of the different mutual hardness parameters, defined for the atom–atom cases. Thus, one can define the mutual atom–bond hardness  $\eta_{i,kl}^{\text{atom/bond}}$  corresponding to  $i$ th atom and bond between the  $k$ -th and  $l$ -th atoms. Similarly for the mutual bond–bond hardness  $\eta_{ij,kl}^{\text{bond/bond}}$  two bonds are involved, one between the  $i$ th atom and  $j$ th atom while the other is between the  $k$ -th atom and  $l$ -th atom. The diagonal element of the quantity  $\eta_{ij,kl}^{\text{bond/bond}}$  is essentially the self bond hardness and can be denoted as  $\eta_{ij,ij}^{\text{bond}}$ . The resulting charges on the atoms and the bond regions are independent quantities and can easily be calculated using the formalism similar to the case of atomic sites alone. For diatomic molecules, there are less number of parameters, the equations as well as the calculation are simple [7–10, 27]. A combined approach with spin-dependent chemical potential and hardness parameters along with the inclusion of the bond space can be more successful to predict the binding energy.

Another limitation of these types of approaches is the lack of models with correct dissociation limits. To prevent the spurious charge transfer at large separation, the concept of a chemical contact for the charge transfer to take place may need to be introduced. There have been many attempts to address this important issue. For example, the atom–atom mutual hardness parameter can be assumed [28] to be dependent on the distance, with strong inverse dependence, with the implication that charge transfer will not take place when the distance is large. The works of Mathieu [29] and Valone and Atlas [30] in this direction have led to interesting conclusions in this context. But much more studies are needed to arrive at a better model with proper dissociation behavior. This will also help in application to the generation of “on the fly” atomic charges and dipoles leading to a better force field in molecular dynamics simulation [31]. Many other conceptual aspects, such as near sightedness [32], linear response functions [33], and mutual polarizabilities [34], might also throw light into these descriptions. Time-dependent extensions of DFT [35] and its conceptual counterpart [36] also have much in store for future directions.

## 21.7 Concluding Remarks

This work has presented some of the aspects of description of chemical binding through CDFT-based view of how coarse-grained atom (or bond)-centered variables can lead to estimation of charge transfer, spin transfer, atomic dipole moment, and binding energy of simple molecular systems. It is gratifying to note that the seed planted through the introduction of the concept of chemical potential of the electron cloud in DFT, and its identification with the electronegativity parameter in chemistry 45 years ago in the laboratory of Professor Robert Parr, has now grown into a big tree. A whole new field of research, the so-called CDFT has in fact been born. The present discussion has, however, been limited to a small subset of this vast area, enriched by so many novel ideas, even within the domain of chemical binding. Much broader aspects lie outside what has been covered.

## Acknowledgments

The work and views reported here have been possible due to enlightening discussions I had with many teachers, collaborators, and friends. In particular, I express my gratefulness to Prof B M Deb and Prof Robert G Parr, from whom I have learnt a lot over the years. I also thank my colleagues Dr Alok Samanta, Dr Tapan Ghanty, Dr KRS Chandrakumar, Dr Amita Wadehra, and many others for helpful discussions and collaborations. Finally I am thankful to Prof Shubin Liu for inviting me to contribute this chapter and for showing enormous patience and encouragement during the course of its completion.

## References

- 1 Hohenberg, P. and Kohn, W. (1964). Inhomogeneous electron gas. *Phys. Rev.* 136: B864.
- 2 Kohn, W. and Sham, L.J. (1965). Self-consistent equations including exchange and correlation effects. *Phys. Rev.* 140: A1133.
- 3 Parr, R.G. and Yang, W. (1989). *Density-Functional Theory of Atoms and Molecules*. New York: Oxford University Press, and Clarendon Press, Oxford.
- 4 Geerlings, P., Chamorro, E., Chattaraj, P.K. et al. (2020). Conceptual density functional theory: status, prospects, issues. *Theor. Chem. Acc.* 139: 36. <https://doi.org/10.1007/s00214-020-2546-7>.
- 5 Parr, R.G., Donnelly, R.A., Levy, M., and Palke, W.E. (1978). Electronegativity: the density functional viewpoint. *J. Chem. Phys.* 68 (8): 3801–3807.
- 6 Parr, R.G. and Pearson, R.G. (1983). Absolute hardness: companion parameter to absolute electronegativity. *J. Am. Chem. Soc.* 105 (26): 7512–7516.
- 7 Ghosh, S.K. and Parr, R.G. (1987). Toward a semiempirical density functional theory of chemical binding. *Theor. Chim. Acta* 72: 379–391.



- 8 Ghanty, T.K. and Ghosh, S.K. (1991). Electronegativity and covalent binding in homonuclear diatomic molecules. *J. Phys. Chem.* 95 (17): 6512–6514.
- 9 Ghanty, T.K. and Ghosh, S.K. (1992). Electronegativity, hardness, and chemical binding in simple molecular systems. *Inorg. Chem.* 31 (10): 1951–1955.
- 10 Ghanty, T.K. and Ghosh, S.K. (1994). A new simple density functional approach to chemical binding. *J. Phys. Chem.* 98 (7): 1840–1843.
- 11 Ghosh, S.K. (1994). Electronegativity, hardness, and a semiempirical density functional theory of chemical binding. *Int. J. Quantum Chem.* 49: 239–251.
- 12 Ghanty, T.K. and Ghosh, S.K. (1994). Spin-polarized generalization of the concepts of electronegativity and hardness and the description of chemical binding. *J. Am. Chem. Soc.* 116 (9): 3943–3948.
- 13 Mortier, W.J., Ghosh, S.K., and Shankar, S. (1986). Electronegativity-equalization method for the calculation of atomic charges in molecules. *J. Am. Chem. Soc.* 108 (15): 4315–4320.
- 14 Chattaraj, P.K. (ed.) (2009). *Chemical Reactivity Theory: A Density Functional View*. Boca Raton: CRC Press.
- 15 Wadehra, A. and Ghosh, S.K. (2005). A density functional theory-based chemical potential equalisation approach to molecular polarizability. *J. Chem. Sci.* 117: 401–409.
- 16 Ghosh, S.K. (2010). A coarse grained density functional theory, chemical potential equalization and electric response in molecular systems. *J. Mol. Struct. THEOCHEM* 943: 178–182.
- 17 Parr, R.G., Szentpály, L., and Liu, S. (1999). Electrophilicity index. *J. Am. Chem. Soc.* 121 (9): 1922–1924.
- 18 Chattaraj, P.K., Sarkar, U., and Roy, D.R. (2006). Electrophilicity index. *Chem. Rev.* 106: 2065–2091.
- 19 Parr, R.G. and Yang, W. (1984). Density functional approach to the frontier-electron theory of chemical reactivity. *J. Am. Chem. Soc.* 106: 4049–4050.
- 20 Ghosh, S.K. (1990). Energy derivatives in density-functional theory. *Chem. Phys. Lett.* 172: 77–82.
- 21 Garza, J., Vargas, R., Cedillo, A. et al. (2006). Comparison between the frozen core and finite differences approximations for the generalized spin-dependent global and local reactivity descriptors in small molecules. *Theor. Chem. Acc.* 115: 257–265.
- 22 Perez, P., Chamorro, E., and Aiyers, P.W. (2008). Unusual mathematical identities in DFT: results from three different spin-resolved representations. *J. Chem. Phys.* 128: 204108.
- 23 Davari, N., Haghani, S., Astrand, P.-O., and Schatz, G.C. (2015). Local electric field factors by a combined charge transfer and point-dipole interaction model. *RSC Adv.* 5: 31594–31605.
- 24 Berkowitz, M., Ghosh, S.K., and Parr, R.G. (1986). On the concept of local hardness in chemistry. *J. Am. Chem. Soc.* 107 (24): 6811–6814.
- 25 Ghosh, S.K. and Berkowitz, M. (1985). A classical fluid-like approach to the density-functional formalism of many-electron systems. *J. Chem. Phys.* 83 (6): 2976–2983.

- 26 Berkowitz, M. and Parr, R.G. (1988). Molecular hardness and softness, local hardness and softness, hardness and softness kernels, and relations among these quantities. *J. Chem. Phys.* 88: 2554–2557.
- 27 Chen, J., Hundertmark, D., and Martínez, T.J. (2008). A unified theoretical framework for fluctuating-charge models in atom-space and in bond-space. *J. Chem. Phys.* 129: 214113.
- 28 Chen, J. and Martinez, T.J. (2007). QTPIE: charge transfer with polarization current equalization: a fluctuating charge model with correct asymptotics. *Chem. Phys. Lett.* 438: 313–320.
- 29 Mathieu, D. (2007). Split charge equilibration method with correct dissociation limits. *J. Chem. Phys.* 127: 224103.
- 30 Valone, S.M. and Atlas, S.R. (2004). An empirical charge transfer potential with correct dissociation limits. *J. Chem. Phys.* 120: 7262–7273.
- 31 York, D.M. and Yang, W. (1996). A chemical potential equalization method for molecular simulations. *J. Chem. Phys.* 104 (1): 159–172.
- 32 Fias, S., Helder-Zadeh, F., Geerlings, P., and Ayers, P.W. (2017). Chemical transferability of functional groups follows from the nearsightedness of electronic matter. *Proc. Nat. Acad. Sci. USA* 114: 11633–11638.
- 33 Geerlings, P., Fias, S., Boisdenghien, Z., and De Proft, F. (2014). Conceptual DFT: chemistry from the linear response function. *Chem. Soc. Rev.* 43: 4989–5008.
- 34 Chakkamalayath, J., Chandrakumar, K.R.S., and Ghosh, S.K. (2020). Reactivity parameters and substitution effect in organic acids. *J. Phys. Chem. A* 124: 3770–3777.
- 35 Ghosh, S.K. and Dhara, A.K. (1988). Density-functional theory of many-electron systems subjected to time-dependent electric and magnetic fields. *Phys. Rev. A* 38: 1149–1158.
- 36 Chattaraj, P.K. and Maiti, B. (2001). Reactivity dynamics in atom–field interactions: a quantum fluid density functional study. *J. Phys. Chem. A* 105 (1): 169–183.

## 22

### Molecular Acidity, PCET, and Metal Specificity

Dongbo Zhao<sup>1</sup> and Shubin Liu<sup>2</sup>

<sup>1</sup>Yunnan University, Institute of Biomedical Research, Wujiajiing Street, Kunming 650504, P.R. China

<sup>2</sup>University of North Carolina, Research Computing Center and Department of Chemistry, Chapel Hill, NC 27599-3420, USA

#### 22.1 Introduction

Conceptual density functional theory (CDFT) [1, 2], sometimes also called density functional reactivity theory or chemical density functional theory (DFT), employs concepts and formalisms from DFT to obtain both qualitative and quantitative insights into chemical reactivity. It started in the 1980s with the renaissance of the chemical potential function, equivalent to electronegativity, and has since developed into a suite of useful reactivity indexes such as hardness, softness, Fukui function, electrophilicity, and many others. Recent developments also include the dual descriptor [3–8], quantification of steric effect [9], etc. In this chapter, we mainly stay focused on three applications of CDFT, molecular acidity for organic and inorganic compounds [7, 8], proton-coupled electron transfer (PCET) reactions for biologically relevant complexes [10, 11], and metal specificity for porphyrin systems [12, 13] to elucidate the usefulness and robustness of CDFT in real-world applications.

#### 22.2 Molecular Acidity

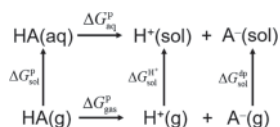
The acid–base dissociation constant, represented by the  $pK_a$  value, is the measure of the strength of an acid or a base and plays the key role in understanding and quantifying the acid–base processes in solution, closely related to chemical synthesis, pharmacokinetics, drug design and metabolism, toxicology, and environmental protection. In the literature, lots of efforts have been devoted to developing accurate and efficient computational protocols to predict or estimate the  $pK_a$  value.

In quantum chemistry, however, to accurately compute  $pK_a$  values for large systems such as proteins using standard *ab initio* and DFT methods is a formidable challenge. Since the experimental  $pK_a$  values are obtained in solution, in practice

*Conceptual Density Functional Theory: Towards a New Chemical Reactivity Theory*, First Edition.

Edited by Shubin Liu.

© 2022 WILEY-VCH GmbH. Published 2022 by WILEY-VCH GmbH.



**Scheme 22.1** The thermodynamic cycle.

one has to resort to the thermodynamic cycle (Scheme 22.1) where a series of free energy changes must be simulated [14, 15]:

$$2.303 RT \cdot \text{p}K_{\text{a}} = \Delta G_{\text{aq}}^{\text{p}} = \Delta G_{\text{sol}}^{\text{dp}} + \Delta G_{\text{sol}}^{\text{H}^+} - \Delta G_{\text{sol}}^{\text{p}} + \Delta G_{\text{gas}}^{\text{p}} \quad (22.1)$$

where  $R$  is the Rydberg gas constant and  $T$  is the absolute temperature.  $\Delta G_{\text{aq}}^{\text{p}}$  is the sum of the free energy of deprotonation of the gas-phase species  $\Delta G_{\text{gas}}^{\text{p}}$ , the free energies of desolvation of the protonated form  $-\Delta G_{\text{sol}}^{\text{p}}$ , and solvation of the deprotonated form  $\Delta G_{\text{sol}}^{\text{dp}}$ , and the free energy of solvation for the proton  $\Delta G_{\text{sol}}^{\text{H}^+}$ . Suffice to note that for large systems, *ab initio* simulations are extremely difficult or frequently intractable, even equipped with the most advanced software and hardware.

An alternative to avoid computation of free energies is to seek linear correlations of  $\text{p}K_{\text{a}}$  values and quantum descriptors, among which are highest occupied molecular orbital (HOMO) energies [16], localized reactive orbital, frontier effective-for-reaction molecular orbitals (FERMO) [17], electrophilicity or group-philicity [18, 19], just to name a few. The core idea behind these relationships is that proton or electron donor-acceptor reactions are driven by frontier molecular orbitals. Yet, the relations were often only observed for compounds like phenols in the same family.

Recently, we have proposed to employ two interdependent quantum descriptors to accurately and efficiently estimate molecular  $\text{p}K_{\text{a}}$  values. The two quantum descriptors are molecular electrostatic potential (MEP) on an acidic atom (such as N, O, or S nucleus) and the sum of the valence natural atomic orbital energies, NAO, of the same acidic atom. The philosophy behind is that molecular acidity is a local property at a particular acidic atom and that the impact of the environment is reflected through the changes to that atom.

To numerically verify the rationale, we selected a series of molecular systems (228 in total), including 154 primary, secondary, and tertiary amines and anilines, 59 carboxylic acids and alcohols, and 15 sulfonic acids and thiols. Calculations were carried out at the DFT B3LYP/6-311+G(2d,2p) level for both structure optimization and harmonic vibrational analysis. Molecular properties, such as MEP values on each nucleus and NAO energies resulted from a full NBO (natural bond orbital) [20] analysis, were obtained on top of a fully optimized structure.

Shown in Figure 22.1 are strong correlations between experimental  $\text{p}K_{\text{a}}$  values and each of these two quantities for each of the three categories. Moreover, if the MEP is subtracted by the isolated atomic MEP for each category of compounds, in Figure 22.2, we observe a single unique linear relationship between the resultant MEP difference and experimental  $\text{p}K_{\text{a}}$  data. These results can generally be utilized to simultaneously estimate  $\text{p}K_{\text{a}}$  values at multiple sites with a single calculation for either relatively small molecules in drug design or amino acids in proteins and

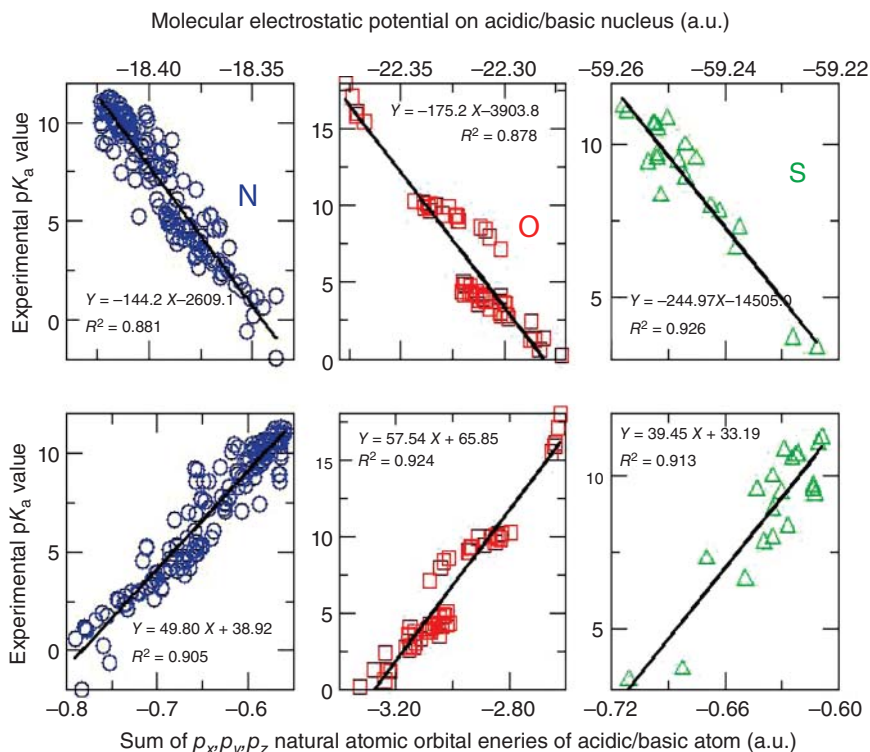


**Figure 22.1** Linear relationships between molecular electrostatic potential on acidic nucleus and experimental  $pK_a$  values for amines (N), carboxylic acids and alcohols (O), and sulfonic acids and thiols (S) (a); and linear relationships between the sum of three valence NAO 2p/3p orbitals and  $pK_a$  values (b). Source: Reprinted with permission from Liu and Pedersen [7], American Chemical Society.

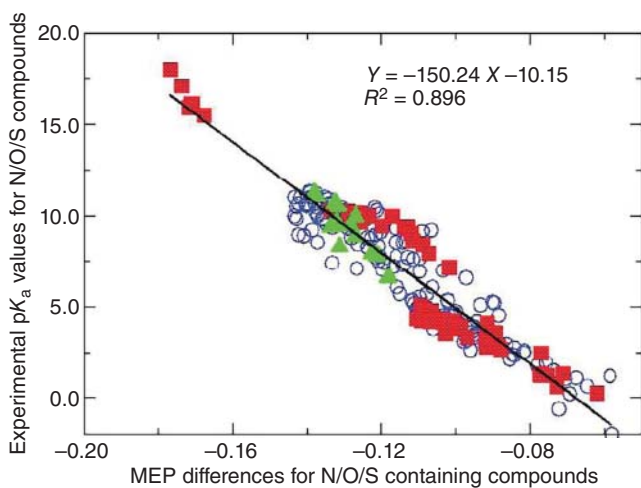


**Figure 22.2** Linear relationship between the MEP difference and experimental  $pK_a$  values for all 228 data points. The MEP reference values for N, O, and S compounds are  $-18.28$ ,  $-22.20$ , and  $-59.12$  au, respectively. Symbols: N, blue  $\circ$ ; O, red  $\blacksquare$ ; S, green  $\blacktriangle$ . Source: Reprinted with permission from Ref. Liu and Pedersen [7], American Chemical Society.

macromolecules. Additionally, similar results have been observed by Cao et al. [21] for singly and doubly substituted benzoic acids, singly substituted benzenesulfonic acids, benzeneseleninic acids, phenols, and alkylcarboxylic acids, and by Zhao et al. [22] for 20 natural  $\alpha$ -amino acids and 5 DNA/RNA bases, together with a few other biologically relevant species. These results collectively show the great potential of MEP and NAO in appreciating molecular acidity/basicity.

$$V_{R_A} = \sum_{i \neq A} \frac{Z_i}{|\mathbf{R}_i - \mathbf{R}_A|} - \int \frac{\rho(\mathbf{r})}{|\mathbf{r} - \mathbf{R}_A|} d\tau \quad (22.2)$$

In CDFT, the total energy change  $\Delta E$  is related to changes in the number of electrons  $\Delta N$  and the external potential  $\Delta v(\mathbf{r})$ , which reads:

$$\begin{aligned} \Delta E &= E[v(\mathbf{r}) + \Delta v(\mathbf{r}); N + \Delta N] - E[v(\mathbf{r}); N] \\ &= \left\{ \left( \frac{\partial E}{\partial N} \right)_{v(\mathbf{r})} \Delta N + \int \left( \frac{\delta E}{\delta v(\mathbf{r})} \right)_N \Delta v(\mathbf{r}) d\mathbf{r} \right\} \\ &\quad + \frac{1}{2} \left[ \left( \frac{\partial^2 E}{\partial N^2} \right) (\Delta N)^2 + 2\Delta N \int \frac{\delta \Delta E}{\delta v(\mathbf{r}) \partial N} \Delta v(\mathbf{r}) d\mathbf{r} \right. \\ &\quad \left. + \iint \left( \frac{\delta^2 E}{\delta v(\mathbf{r}') \delta v(\mathbf{r})} \right)_N \Delta v(\mathbf{r}) \Delta v(\mathbf{r}') d\mathbf{r} d\mathbf{r}' \right] \\ &\quad + (\text{third and higher order terms}) \end{aligned} \quad (22.3)$$

The terms in braces  $\{\}$  and brackets  $[\ ]$  are the first- and second-order terms, respectively.

The process of proton dissociation from an acid can be approximated by the above expansion. It involves one proton dissociation; thus, the total number of electrons in the acid system remains a constant and only the external potential  $\Delta v(\mathbf{r})$  varies. With  $\Delta N = 0$ , in the simplest case when only the first-order term is considered, Eq. (22.3) becomes

$$\Delta E[\Delta v(\mathbf{r})] = \int \rho(\mathbf{r}) \Delta v(\mathbf{r}) d\mathbf{r} \quad (22.4)$$

Now, for the special case of Eq. (22.2), the change in the external potential,  $\Delta v(\mathbf{r}, \mathbf{R}_H)$ , resulted from the dissociation of a proton, can explicitly be obtained, giving

$$\Delta v(\mathbf{r}, \mathbf{R}_H) = \sum_{i \neq H} \frac{Z_i}{|\mathbf{R}_i - \mathbf{R}_H|} - \frac{1}{|\mathbf{r} - \mathbf{R}_H|} \quad (22.5)$$

The first term in Eq. (22.5) signifies the repulsive potential between the leaving proton  $\mathbf{R}_H$  and the other nuclei  $\mathbf{R}_i$ , and the second term means the attractive interaction between an electron at position  $\mathbf{r}$  and the leaving proton at  $\mathbf{R}_H$ .

With Eqs. (22.5) and (22.4), one can have

$$\Delta E[\Delta v(\mathbf{r}, \mathbf{R}_H)] = \sum_{i \neq H} \frac{Z_i Z_H}{|\mathbf{R}_i - \mathbf{R}_H|} - \int \frac{\rho(\mathbf{r})}{|\mathbf{r} - \mathbf{R}_H|} d\tau \quad (22.6)$$

where  $Z_H = 1$ . The meaning of Eq. (22.6) is that the total electronic energy change resulted from dissociation of a proton in an acid is nothing but the electrostatic potential on the same proton. Implication of Eq. (22.6) is straightforward that the MEP of the leaving proton can serve as a linear predictor of the  $pK_a$  of the acid.

$$pK_a \propto \sum_{i \neq H} \frac{Z_i}{|\mathbf{R}_i - \mathbf{R}_H|} - \int \frac{\rho(\mathbf{r})}{|\mathbf{r} - \mathbf{R}_H|} d\tau \quad (22.7)$$

It is worthwhile to mention that to obtain Eq. (22.7), we have assumed that (i) thermodynamic contributions from solvent and temperature effects are negligible and the entropic effect is trivial; thus, we employed the total electronic energy difference in Eq. (22.6) to approximate the Gibbs free energy change in Eq. (22.1). (ii) The first order of the Taylor expansion in Eq. (22.3) suffices. (iii) Before and after a proton dissociation, the structural relaxation in the conjugate base  $A^-$  has little effect on the external potential, so that the external potential change is only related to the removal of a proton from the acid. Notice that Eqs. (22.5) and (22.6) have the same format, but Eq. (22.5) describes a potential variation and is used for the acidic atom in an acid such as O in carboxyl acid and alcohols, N in amines and anilines, and S in sulfonic acids and thiols, whereas Eq. (22.6) represents an energy variation and is used for the nuclear MEP of the leaving proton. Our studies show that MEP of acidic atoms and the leaving proton are strongly correlated. This is the reason why they can both be employed to predict  $pK_a$  values. Also, these MEP values are majorly resulted from the electron density in the valence orbitals. That is the reason why NAO could be equivalently applied for the same purpose.

In another application [8], we employed a total of 27 metal–water complexes,  $M(H_2O)_n^{m+}$  ( $M = Al, Ba, Be, Ca, Co, Cr, Fe, Ga, Hf, In, K, Li, Mg, Mn, Na, Ni, Sc, Sr, Ti, Tl, Zn,$  and  $Zr; m = 1, 2, 3, 4; n = 4, 6$ ), whose charge on the metal cation ranges from +1 (Li, K, Na, and Tl) to +4 (Hf, Sn, Ti, and Zr). Each metal cation is coordinated by six water molecules with two exceptions  $Be(H_2O)_4^{2+}$  and  $Tl(H_2O)_4^{3+}$ . Experimental  $pK_a$  values of these species span  $\sim 19$  orders of magnitude, ranging from  $-4.0$  in  $Ti(H_2O)_6^{4+}$  to  $+14.7$  in  $Na(H_2O)_6^+$ . Plotted in Figure 22.3a are strong linear relationships between MEP at the oxygen nucleus, the sum of valence NAO energies of oxygen, experimental  $pK_a$  values, and chemical potential (arithmetic mean value of HOMO and lowest unoccupied molecular orbital [LUMO] energies) for the 27  $M(H_2O)_n^{m+}$  complexes. Furthermore, we have revealed similar results for the leaving protons in Figure 22.3b. With these linear correlations, we can readily reproduce the experimental  $pK_a$  results. These computational results corroborate that the accuracy of our approach is statistically similar to that of the conventional method through the thermodynamic cycle, while maintaining great advantage of simplicity and efficiency.

Taken together, we have unraveled that molecular acidity can be well appreciated and quantified in CDFT only by employing two equivalent quantum descriptors MEP and NAO at the acidic atom or leaving proton, which can have wide potential applications in biological systems.

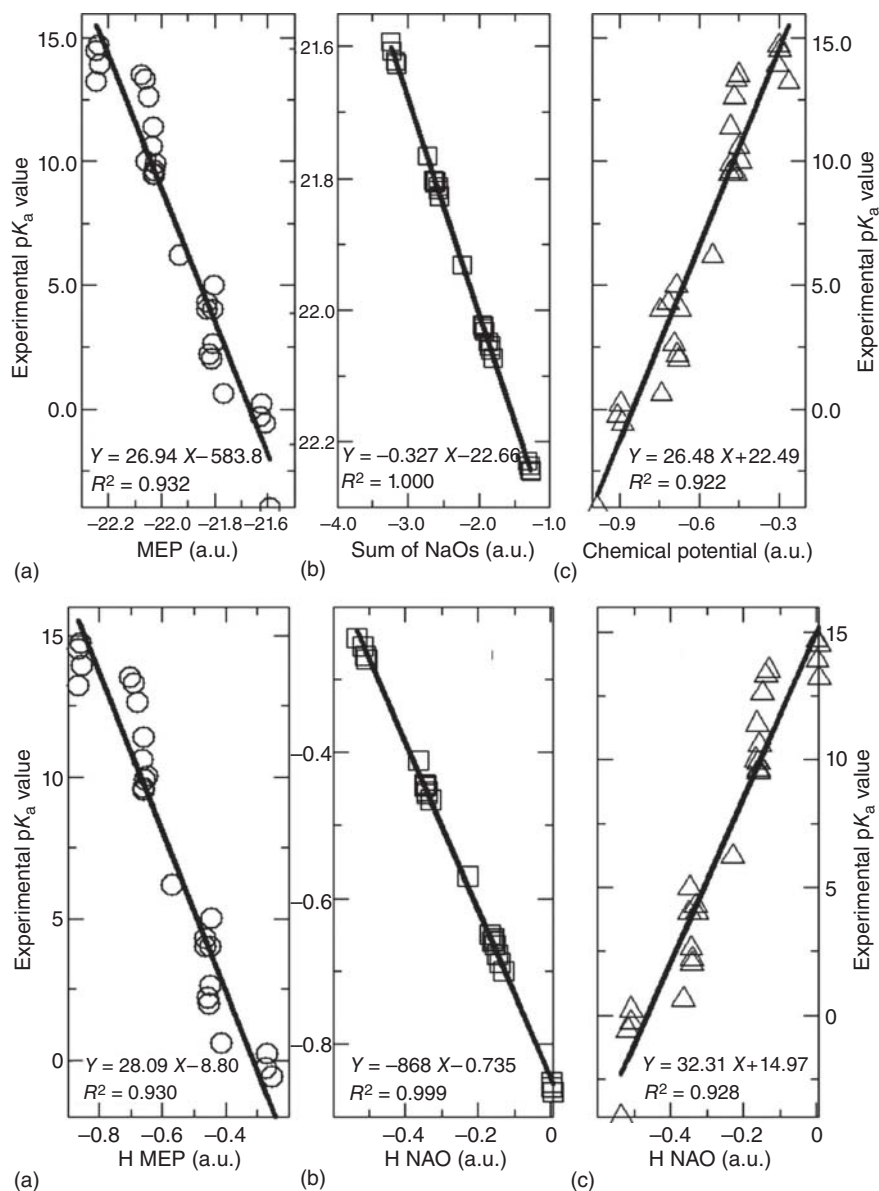
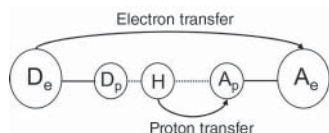


**Figure 22.3** Linear relationships between MEP at oxygen/hydrogen nucleus, the sum of valence NAO energies of oxygen/hydrogen, experimental  $pK_a$  values, and chemical potential derived from HOMO and LUMO energies for the 27  $M(H_2O)_n^{m+}$  complexes. Source: Reprinted with permission from Liu et al. [8], American Institute of Physics.



## 22.3 Proton-coupled Electron Transfer

Electron transfer accompanied by a proton transfer is a ubiquitous phenomenon for reactants with dissociable protons. Two possible mechanisms have been proposed in the literature. One is the so-called PCET mechanism [23–26], where the proton and the electron can be transferred to different orbitals or sites of a molecular system and these transfers are simultaneous (Scheme 22.2). The other is the hydrogen atom transfer (HAT) mechanism [27, 28] where the proton and the electron are transferred to the same location in a radical pathway. PCET is implicated in many biological and solar energy conversion processes, among which are photosynthesis in the oxygen-evolving complex of photosystem II and cytochrome P450, etc. PCET has attracted great interest in the literature since its role in the redox chemistry of ruthenium bipyridine complexes was first unveiled. These biological and organometallic PCET mechanisms share a common feature that an electron is often transferred to a site often far away from the proton acceptor site.



**Scheme 22.2** Proton-coupled electron transfer (PCET).

We employed density-based reactivity descriptors, such as dual descriptor in CDFT, to characterize changes in the electron density. Dual descriptor is defined as [3–6]

$$f^{(2)}(\mathbf{r}) = \left( \frac{\partial f(\mathbf{r})}{\partial N} \right)_{v(\mathbf{r})} \quad (22.8)$$

where  $N$  is the total number of electrons in the system,  $v(\mathbf{r})$  is the external potential from the atomic nuclei, and  $f(\mathbf{r})$  is the Fukui function, which relates the change in electron density,  $\rho(\mathbf{r})$ , with change in electron number,  $N$ ,  $f(\mathbf{r}) = (\delta\rho(\mathbf{r})/\delta N)_{v(\mathbf{r})}$ . To feature the electrophilic capability of a system, one uses

$$f^+(\mathbf{r}) = \rho_{N+1}(\mathbf{r}) - \rho_N(\mathbf{r}) \approx \rho_{\text{LUMO}}(\mathbf{r}) \quad (22.9)$$

and to measure its nucleophilic power, one employs

$$f^-(\mathbf{r}) = \rho_N(\mathbf{r}) - \rho_{N-1}(\mathbf{r}) \approx \rho_{\text{HOMO}}(\mathbf{r}) \quad (22.10)$$

where  $\rho_{N+1}(\mathbf{r})$ ,  $\rho_N(\mathbf{r})$ , and  $\rho_{N-1}(\mathbf{r})$  denote the electron density for the  $N + 1$ ,  $N$ , and  $N - 1$  systems, respectively, with the molecular structure held fixed and  $\rho_{\text{LUMO}}(\mathbf{r})$  and  $\rho_{\text{HOMO}}(\mathbf{r})$  are the LUMO and HOMO densities, respectively. The first equality in Eqs. (22.9) and (22.10) is resulted from the finite difference approximation, and the second approximate equality uses the frozen orbital approximation. The  $f^+(\mathbf{r})/f^-(\mathbf{r})$  function measures the response of the electron density change following an addition/removal of an electron, and thus it is a reactivity descriptor

to quantify electrophilicity/nucleophilicity. Under the above two approximations, dual descriptor becomes

$$f^{(2)}(\mathbf{r}) = f^+(\mathbf{r}) - f^-(\mathbf{r}) \approx \rho_{\text{LUMO}}(\mathbf{r}) - \rho_{\text{HOMO}}(\mathbf{r}) \quad (22.11)$$

In addition, the condensed-to-atoms version of the Fukui functions and dual descriptor is also available [29] where the electron densities in Eqs. (22.9)–(22.11) are replaced by atomic charges resulted from population analysis.

The dual descriptor  $f^{(2)}(\mathbf{r})$  can be used to identify electrophilic and nucleophilic domains in a donor–acceptor complex. If these electrophilic and nucleophilic regions are sufficiently separated in space, there will be a propensity for charge separation. When  $f^{(2)}(\mathbf{r})$  is plotted over a supramolecular complex consisting of the reactants, an electrophilic region is indicated by a positive  $f^{(2)}(\mathbf{r})$  function value (red region) and a nucleophilic region is indicated by a negative  $f^{(2)}(\mathbf{r})$  function value (green region). The complex is aligned with an assumption of the direction of proton transfer. The location of the electron transfer might be determined by the electrophilic region from the dual descriptor or electrophilic Fukui function quantities. If the electrophilic region does not include the proton acceptor site, then spatial separation between the proton and electron transfer may occur in a PCET mechanism. Notice that the current approach is thermodynamic in nature, so it is not kinetic. It cannot predict whether concerted or stepwise electron–proton transfer will occur.

Experimental evidence suggests that the electron and proton transfer between phenol and  $\text{ArO}^\bullet$  radical proceeds through a PCET mechanism [30]. Figure 22.4a shows the dual descriptor plot for the reactant complex of phenol with  $\text{ArO}^\bullet$  radical. The electron-donating region (green) is located on the phenol  $\pi$ -system and the electron-accepting region (red) is on the  $\pi$ -system of the  $\text{ArO}^\bullet$  radical. The key point from this analysis is that no red surface is situated at the oxygen atom of  $\text{ArO}^\bullet$ , showing that this site is not the electrophilic site of the complex. This suggests that an electron may be transferred to the aryl  $\pi$ -system rather than the oxygen atom, leading to charge separation in a PCET mechanism. The electron and proton transfer between phenol and the  $\text{CH}_3\text{OO}^\bullet$  radical occurs via a HAT mechanism. Figure 22.4b

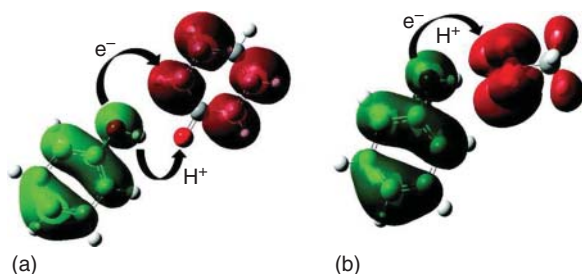


**Figure 22.4** Plot of dual descriptor contour surfaces (value of 0.0004 au) for reactant complexes of (a)  $\text{ArOH} + \text{ArO}^\bullet$ ; and (b)  $\text{ArOH} + \text{CH}_3\text{OO}^\bullet$  reactions. Surfaces in red are the electrophilic regions and those in green are nucleophilic regions. A proton/charge transfer separation is seen in (a) but not in (b). Source: Reprinted with permission from Liu et al. [10], American Chemical Society.

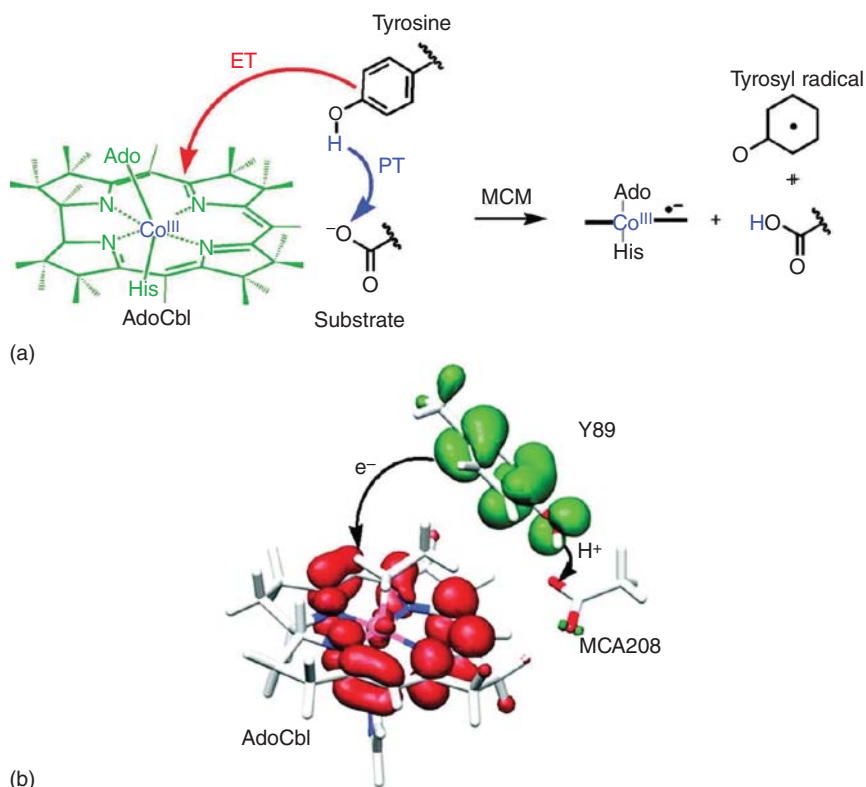


**Figure 22.5** (a) Proposed PCET mechanistic route for MCM enzyme. (b) Dual descriptor contour surface of the minimal structural model of MCM enzyme. Source: Reprinted with permission from Kumar et al. [11], American Chemical Society.

shows the dual descriptor plot for the reactant complex of phenol with the  $\text{CH}_3\text{OO}^\cdot$  radical. In contrast to the phenol case, the proton is transferred to an oxygen atom that has significant electrophilic character, suggesting that charge separation is less likely for the latter reaction.

Shown in Figure 22.5 is a minimal structural model to mimic of the MCM (methylmalonyl-CoA mutase) enzyme in which all the side chains of the cofactor were replaced by hydrogen atoms and axial ligands were simplified. Based on the model, we aim to employ the dual descriptor in CDFT to characterize the charge separation propensity of AdoCbl–Tyr–Sub complex. The dual descriptor plot of the reactant complex reveals that the electron-donating region (green surface) is located on the Y89 residue, while the electron-accepting region (red surface) is on the  $\pi$ -system of the corrin ring of the AdoCbl cofactor. Because the two regions are separated, it indicates that there would exist a propensity of charge separation if one assumes that the system is aligned in the direction of a proton transfer. This strongly supports that the substrate is not implicated in charge separation; rather, it is exclusively susceptible for the proton shift. Importantly, a minimal structural model suggests that an electron can be transferred from aryl system of

tyrosine to coenzyme B12, that is, leading to charge separation through the PCET mechanism. Moreover, we computed the condensed-to-atoms dual descriptor values of the nucleophilic and electrophilic sites. The total value of the Y89 residue is  $-0.508$ , which shows that this site is the most nucleophilic, whereas the total value of AdoCbl is  $+0.735$ , indicating that AdoCbl is the most electrophilic site in the model system.

In a nutshell, we have shown that PCET can be well appreciated in terms of the dual descriptor. It is anticipated that more complex phenomena such as double PCET should witness some success in the future.

## 22.4 Metal Specificity

As the core cofactor of hemoproteins, heme is a metal-binding porphyrin consisting of a heterocyclic organic ring made from four pyrrole subunits linked via methine bridges. Hemoglobin is most commonly found in its oxygen-binding state where the bonded metal cation is a divalent iron. Other porphyrin-binding divalent metal ions have also been found such as Mn, Mg, Zn, Cr, Cu, etc. When in its resting or functional state, up to two axial ligands are required to bond with the metal cation to carry out the catalytic process. Here, we will try to figure out the metal specificity of Fe metal-porphyrin complex using CDFT and its spin-polarized variant, SP-CDFT.

In CDFT, several global and local reactivity descriptors have been introduced and applied to lots of problems. These reactivity indices include chemical potential  $\mu$ , electronegativity  $\chi$ , hardness  $\eta$ , softness  $S$ , Fukui function  $f(\mathbf{r})$ , and electrophilicity  $\omega$ . For a closed-shell system with  $N$ -electrons and external potential  $v$  and total energy  $E$ , these indices can be defined as follows:

$$\mu = \left( \frac{\partial E}{\partial N} \right)_v = -\chi \approx \frac{I + A}{2} \quad (22.12)$$

$$\eta = \left( \frac{\partial^2 E}{\partial N^2} \right)_v = \left( \frac{\partial \mu}{\partial N} \right)_v = I - A = \frac{1}{S} \quad (22.13)$$

$$\omega = \frac{\mu^2}{2\eta} \quad (22.14)$$

with  $I$  and  $A$  as the vertical ionization potential and electron affinity, respectively, which can be obtained via  $I \approx -\varepsilon_{\text{HOMO}}$  and  $A \approx -\varepsilon_{\text{LUMO}}$ .

The SP-CDFT approach, which provides a general treatment for processes involving both electron transfer and spin polarization, has both the charge density,  $\rho_N = \rho_\alpha + \rho_\beta$ , and spin density,  $\rho_S = \rho_\alpha - \rho_\beta$ , as the basic variables. The changes in the total energy can be proceeded in the standard Euler equation manner, giving two Lagrange multipliers,  $\mu_N$  and  $\mu_S$ ,

$$\mu_N = \left( \frac{\partial E}{\partial N} \right)_{N_S, v(\mathbf{r}), B(\mathbf{r})} \quad (22.15)$$

and

$$\mu_S = \left( \frac{\partial E}{\partial N_S} \right)_{N, v(\mathbf{r}), B(\mathbf{r})} \quad (22.16)$$

where  $v(\mathbf{r})$  is the external potential and  $B(\mathbf{r})$  is the external magnetic field.  $\mu_N$  is equivalent to the chemical potential  $\mu$  in the spin-restricted case, and  $\mu_S$  measures the tendency to undergo spin transfer, at constant  $N$ , which can further be obtained by

$$\mu_N^+ \approx \frac{\epsilon_{\text{LUMO}}^\alpha - \epsilon_{\text{HOMO}}^\beta}{2} \quad (22.17)$$

and

$$\mu_S^+ \approx \frac{\epsilon_{\text{HOMO}}^\alpha - \epsilon_{\text{LUMO}}^\beta}{2} \quad (22.18)$$

Equations (22.17) and (22.18) correspond to the two possible ways of spin transfer, one from  $\beta$  spin to  $\alpha$  spin and the other from  $\alpha$  spin to  $\beta$  spin. A larger value of  $\mu_S^+$  means that the system is less likely to increase the spin number because of the bigger HOMO/LUMO gap. Similarly, we can define the spin-hardness, viewed as the response of the spin potential relative to changes in the spin number,

$$\eta_{\text{SS}}^+ = \left( \frac{\partial^2 E}{\partial N_S^2} \right)_{N, v(\mathbf{r}), B(\mathbf{r})} = \left( \frac{\partial \mu_S}{\partial N_S} \right)_{N, v(\mathbf{r}), B(\mathbf{r})} \approx \frac{\mu_S^{*-} - \mu_S^+}{2} \quad (22.19)$$

where  $\mu_S^+$  is the spin potential of the ground state and  $\mu_S^{*-}$  stands for the spin potential for the  $N_S + 2$  state. For example, if the ground state  $N_S$  is singlet,  $N_S + 2$  will be triplet. Note that unlike the spin-restricted counterpart, where  $\eta$  is always positive, this is no longer the case for  $\eta_{\text{SS}}^+$ ; indeed, it is always negative because the spin potential of the  $N_S + 2$  state is smaller than that of the ground state.

Under the condition of a fixed external potential and total number of electrons, we can investigate the total energy change as a function of the spin number change through the following Taylor series:

$$\Delta E_{N, v(\mathbf{r})} = \mu_S \Delta N_S + \frac{1}{2} \eta_{\text{SS}} \Delta N_S^2 \quad (22.20)$$

With the maximum increase or decrease in spin multiplicity,  $\Delta N_S^\pm = -\mu_S^\pm / \eta_{\text{SS}}$ , the maximum energy change,  $\Delta E_{\text{max}}^\pm$ , is given by

$$\Delta E_{\text{max}}^\pm = -\frac{(\mu_S^\pm)^2}{2\eta_{\text{SS}}} = \omega_S^\pm > 0 \quad (22.21)$$

where  $\omega_S^+$  and  $\omega_S^-$  denote the spin-philicity and spin-donicity, respectively, serving as the estimation of system's capability to change its spin multiplicity. Since values of  $\Delta E$  are always positive, the  $\omega_S^\pm$  descriptor will always be positive. Therefore, the lower the  $\omega_S^\pm$  value, the easier the system changes spin multiplicity. Notice that these descriptors do not involve electron transfer because the total number of electrons is held fixed in Eq. (22.20).

In SP-CDFT, two kinds of spin Fukui functions can also be introduced and they are defined as

$$f_{\text{NS}}(\mathbf{r}) = \left( \frac{\partial \rho(\mathbf{r})}{\partial N_S} \right)_{N, v(\mathbf{r}), B(\mathbf{r})} = \left( \frac{\delta \mu_S}{\delta v(\mathbf{r})} \right)_{N, N_S, B(\mathbf{r})} \quad (22.22)$$

and

$$f_{SS}(\mathbf{r}) = \left( \frac{\partial \rho_S(\mathbf{r})}{\partial N_S} \right)_{N,u(\mathbf{r}),B(\mathbf{r})} = -\frac{1}{\mu_B} \left( \frac{\delta \mu_S}{\delta B(\mathbf{r})} \right)_{N,N_S,u(\mathbf{r})} \quad (22.23)$$

respectively. These local functions are discontinuous with respect to  $N_S$  and can also be condensed to an atom  $k$ . Using the frozen core approximation,  $f_{SS,k}^+(\mathbf{r})$  and  $f_{SS,k}^-(\mathbf{r})$  can be obtained as follows [31, 32]:

$$f_{SS,k}^+(\mathbf{r}) \approx \frac{1}{2} [|\Phi_{\text{LUMO},\alpha,k}(\mathbf{r})|^2 + |\Phi_{\text{HOMO},\beta,k}(\mathbf{r})|^2] \quad (22.24)$$

$$f_{SS,k}^-(\mathbf{r}) \approx \frac{1}{2} [|\Phi_{\text{HOMO},\alpha,k}(\mathbf{r})|^2 + |\Phi_{\text{LUMO},\beta,k}(\mathbf{r})|^2] \quad (22.25)$$

whereas  $f_{NS,k}^+$  and  $f_{NS,k}^-$  can be approximated by

$$f_{NS,k}^+(\mathbf{r}) \approx \frac{1}{2} [|\Phi_{\text{LUMO},\alpha,k}(\mathbf{r})|^2 - |\Phi_{\text{HOMO},\beta,k}(\mathbf{r})|^2] \quad (22.26)$$

$$f_{NS,k}^-(\mathbf{r}) \approx \frac{1}{2} [|\Phi_{\text{HOMO},\alpha,k}(\mathbf{r})|^2 - |\Phi_{\text{LUMO},\beta,k}(\mathbf{r})|^2] \quad (22.27)$$

where  $\Phi_{\text{HOMO},\alpha,k}(\mathbf{r})$ ,  $\Phi_{\text{HOMO},\beta,k}(\mathbf{r})$ ,  $\Phi_{\text{LUMO},\alpha,k}(\mathbf{r})$ , and  $\Phi_{\text{LUMO},\beta,k}(\mathbf{r})$  are HOMO and LUMO orbitals for  $\alpha$  and  $\beta$  electrons, respectively. A larger value  $f_{SS,k}^\pm$  for a region  $k$  implies that the region is more likely to change its spin density. If  $f_{NS,k}^\pm > 0$ , the region  $k$  gains electrons as the total spin number changes, and if  $f_{NS,k}^\pm < 0$ , the region is more likely to lose electrons. These local descriptors can be termed as “spin reactivity indices” describing the tendency of molecular areas to gain or lose electrons or spin electrons when the total spin number of the system is changed.

Charge distributions from the natural population analyses (NPA) and the donor–acceptor back-bonding interactions, etc. are collected in Table 22.1 for a selected list of atoms. One can see that Fe, Co, Ni, and Ru ions, especially Ru, and their corresponding N(Ppy) atoms have relatively smaller NPA charges, meaning that these M–N(Pph) bonds are more characteristic of covalent bonds. We observed that for most of the complexes the charges on the metal ion changed little from p1 to p2, with all  $< 0.1$ . Yet, for Fe and Ru, the charge decreased by about 0.4 and 0.2, respectively, from p1 to p2. Since p2 is the functional state for porphyrin complexes in proteins, this large reduction of charge may well be a prerequisite of the catalyst, thus providing clues to why the Fe ion is favored over others for porphyrin metalation in hemoproteins.

Also shown in Table 22.1 are the donor–acceptor back-bonding interactions between porphyrin (donor) and the metal ion (Pph  $\rightarrow$  M and M  $\rightarrow$  Pph) and between pyridine and the metal ion (Py  $\rightarrow$  M and M  $\rightarrow$  Py). Overall, these interaction energies are large. Large back-bonding energies from the Ru complex account for the fact that it has a smaller charge distribution and larger covalent contributions. Looking at the M  $\rightarrow$  Py and Py  $\rightarrow$  M energies of the first-row transition metal ions for p2, we find that Fe has the largest sum of these back-bonding interactions. This strong interaction between the Fe ion and axial ligands elucidates why there is a substantial decrease of the NPA charge on Fe from p1 to p2. This substantial enhancement of interactions in p2 may also be an indication of the uniqueness of this metal ion in forming complexes with porphyrin. However, the CDFT indices

**Table 22.1** NPA charge distribution and second-order perturbation theory analyses of the three systems in Scheme 22.3.

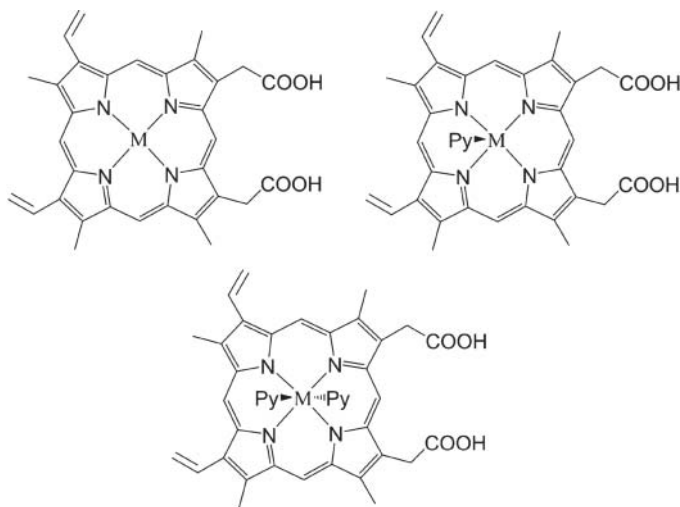
py No.	Type	Cr	Mn	Fe	Co	Ni	Cu	Ru
0	M	1.268	1.518	1.075	1.079	1.018	1.304	0.898
	N (Pph)	-0.626	-0.680	-0.588	-0.588	-0.558	-0.626	-0.539
	Pph → M	517.0	320.8	434.7	404.5	392.2	289.8	709.2
	M → Pph	147.7	153.4	268.6	131.3	229.4	71.4	2056.7
1	M	1.245	1.463	1.126	1.082	1.439	1.333	0.713
	N (Py)	-0.490	-0.537	-0.488	-0.478	-0.501	-0.486	-0.323
	N (Pph)	-0.612	-0.655	-0.571	-0.557	-0.623	-0.618	-0.490
	Pph → M	596.8	384.2	533.7	214.8	359.3	293.2	956.6
	M → Pph	401.2	475.0	456.4	260.0	339.3	224.4	5284.9
	Py → M	7.2	57.0	12.1	14.6	18.4	17.9	15.5
	M → Py	42.9	91.7	30.1	25.3	25.2	18.0	609.2
2	M	1.273	1.391	<b>0.747</b>	1.043	1.320	1.352	<b>0.549</b>
	N (Py)	-0.456	-0.488	-0.400	-0.459	-0.475	-0.462	-0.374
	N (Pph)	-0.600	-0.643	-0.506	-0.544	-0.610	-0.616	-0.467
	Pph → M	1035.2	480.9	901.8	538.6	389.1	274.3	1467.7
	M → Pph	1369.8	505.0	1340.0	600.4	554.5	317.1	7251.2
	Py → M	156.8	18.6	265.2	27.6	81.2	13.9	379.4
	M → Py	301.5	90.7	<b>502.3</b>	88.7	162.1	35.5	<b>811.7</b>

Units are in kcal mol<sup>-1</sup>. Charges listed are those on the metal ion, M, and nitrogen atoms of porphyrin, N(Pph), and pyridine, N(Py). L → M stands for the donor-acceptor interaction between L (porphyrin and pyridine) and M (metal).

Source: Reprinted with permission from Feng et al. [12], American Chemical Society.

are similar (results not shown) for all the species considered indicating that spin polarization should come into play.

The spin potential  $\mu_S^+$  of the ground state, the spin potential  $\mu_S^{*-}$  of the  $N_S + 2$  excited state, the spin hardness  $\eta_{SS}^+$ , and the spin-philicity  $\omega_S^+$  for the (pyridine) $_n$ -metal-porphyrin complexes (Scheme 22.3) are collected in Table 22.2. It is clear that the values of spin potentials  $\mu_S^+$  and  $\mu_S^{*-}$ , spin hardnesses  $\eta_{SS}^+$ , and spin-philicities  $\omega_S^+$  decrease as the number of axial pyridine groups increases from 0 to 2. This indicates that after the coordination of the metal-porphyrin complex with pyridine, its capability of increasing its spin multiplicity in general also increases, a distinct feature commonly seen in hemoproteins when undergoing redox reactions in the active site. In comparison with other metal complexes with the same number of pyridine groups, the Fe-porphyrin complex stands up and often possesses the smallest value for each of the SP-CDFT quantities in most cases, indicating that the Fe system is most likely to increase the total spin number. For example, in the p0 case,  $\omega_S^+$  of the Fe-porphyrin complex is 0.81 eV, the smallest among the eleven complexes;  $\eta_{SS}^+$  is  $-1.34$  eV, also the smallest among the series. For p1 and p2 series, the small values of  $\mu_S^+$  and  $\eta_{SS}^+$  of the Fe-porphyrin complex also result in small values for the spin-philicity. Also in these cases, it is consistently the smallest except for two cases, the p1-Co-porphyrin and the p2-Cr-porphyrin, suggesting that these species can take up spin more easily than others within the series. When looking at  $\mu_S^+$  for  $n = 0$ , we observe that the Ru-porphyrin complex possesses the highest tendency to raise  $N_S$  (smallest  $\mu_S^+$  value). This is not necessarily in contradiction with its spin-philicity, because the spin potential probes the maximum tendency of energy change with respect to the optimal spin number change. The latter descriptor also includes the contribution from the spin hardness,  $\eta_{SS}^+$ , which can be seen as the response of the spin potential to the change in the spin number  $N_S$ . These results



**Scheme 22.3** (Pyridine) $_n$ -metal(M)-porphyrin systems with divalent metal ions  $M = \text{Mg, Ca, Cr, Mn, Co, Ni, Cu, Zn, Ru, and Cd}$  and  $n = 0, 1, \text{ and } 2$ .



**Table 22.2** Global reactivity descriptors from spin-polarized conceptual DFT, including spin potentials of ground state and  $N_S + 2$  state ( $\mu_S^+$  and  $\mu_S^{*-}$ ), spin hardness ( $\eta_{SS}^+$ ), and spin-philicity ( $\omega_S^+$ ) for pyridine–metal(II)–porphyrin complexes.

py No.	Metal ion	$2S + 1$	$\mu_S^+$	$\mu_S^{*-}$	$\eta_{SS}^+$	$\omega_S^+$
0	Mg	1	1.45	0.74	−0.53	2.01
	Ca	1	1.43	0.68	−0.54	1.90
	Cr	5	1.50	0.53	−0.48	2.32
	Mn	6	1.47	0.75	−0.53	2.03
	Fe	3	1.47	<b>−0.27</b>	<b>−1.34</b>	<b>0.81</b>
	Co	2	1.48	0.87	−0.49	2.23
	Ni	1	1.49	0.87	−0.50	2.24
	Cu	2	1.47	0.80	−0.51	2.12
	Zn	1	1.47	0.84	−0.49	2.18
	Ru	3	1.30	0.34	−0.46	1.83
	Cd	1	1.46	0.73	−0.54	2.00
	Average			1.45	0.66	−0.58
1	Mg	1	1.43	0.68	−0.54	1.90
	Ca	1	1.42	0.84	−0.47	2.15
	Cr	5	1.49	0.81	−0.52	2.14
	Mn	6	1.46	0.72	−0.54	1.97
	Fe	3	<b>1.24</b>	<b>0.35</b>	<b>−0.59</b>	<b>1.29</b>
	Co	2	1.49	−0.27	−1.36	0.82
	Ni	3	1.47	0.76	−0.53	2.04
	Cu	2	1.46	0.73	−0.53	2.00
	Zn	1	1.44	0.85	−0.48	2.18
	Ru	1	1.42	0.72	−0.51	1.96
	Cd	1	1.41	0.85	−0.46	2.16
	Average			1.43	0.64	−0.59
2	Mg	1	1.38	0.61	−0.54	1.77
	Cr	3	0.63	−0.11	−0.57	0.35
	Mn	6	1.43	0.65	−0.55	1.85
	Fe	1	1.45	<b>−0.13</b>	<b>−1.17</b>	<b>0.90</b>
	Co	2	1.48	0.78	−0.53	2.08
	Ni	3	1.40	0.63	−0.54	1.80
	Cu	2	1.45	0.71	−0.54	1.95
	Zn	1	1.42	0.86	−0.46	2.17
	Ru	1	1.38	0.63	−0.53	1.80
	Average			1.34	0.51	−0.60

Units in eV.

Source: Reprinted with permission from Feng et al. [13], American Chemical Society.

from SP-CDFT differ much from those obtained from the spin-restricted CDFT results, where we found that global CDFT indices behaved similarly for both Fe- and Ru-porphyrin complexes. Put together, these results show that to answer the question of why Nature selects Fe over Ru, besides their abundance difference: in metalation with porphyrin in hemoproteins one has to resort to the SP-CDFT, since spin states play an important in catalytic reactions of the enzymes.

The peculiarity of the Fe-porphyrin system is further verified in other properties. For example, the spin potential  $\mu_S^{*-}$  of the p0-Fe system, that is,  $\mu_S^-$  of its  $N_S + 2$  state (i.e. quintet), is  $-0.27$  eV, the only case of a negative value for the p0 series (Table 22.2), indicating that the  $N_S + 2$  state of the p0-Fe system is more stable than other metal species of the same nature. Its counterpart for the multiplicity increasing process,  $\mu_S^{*+}$  of the p0-Fe system, that is,  $\mu_S^+$  of its  $N_S + 2$  state is found to be  $+1.45$  eV (not shown). Combining its negative  $\mu_S^-$  and positive  $\mu_S^+$  for the  $N_S + 2$  state, we find that the p0-Fe system is unique in relative stability, compared to other systems in p0 series, which have both positive  $\mu_S^-$  and  $\mu_S^+$  values. This large difference between the two states indicates that the higher spin state of the p0-Fe system could be a stable or intermediate state, accessible during the catalytic reactions in physiological conditions. To confirm this, we also computed the dual descriptor of p0-Fe\* and found that it is considerably larger than that of the triplet ground state, with  $f_M^{*(2)} = 0.693$  and  $f_M^{(2)} = 0.052$ , meaning that the higher spin state of p0-Fe is much more electrophilic than the ground state. Note that  $\mu_S^{*-}$  of p1-Co, p2-Cr, and p2-Fe are also negative, and that their  $\mu_S^{*+}$  (not shown in Table 22.2) are positive. Their dual descriptor values, however, behave differently, with  $f_{p1-Co}^{*(2)} = 0.457$ ,  $f_{p2-Cr}^{*(2)} = 0.153$ ,  $f_{p2-Fe}^{*(2)} = 0.236$  (all positive) for the  $N_S + 2$  state and  $f_{p1-Co}^{(2)} = -0.146$ ,  $f_{p2-Cr}^{(2)} = -0.022$ ,  $f_{p2-Fe}^{(2)} = -0.289$  (all negative), for the  $N_S$  ground state, respectively. Compared to p0-Fe, these three systems exhibit a tendency to be electrophilic in the excited state with the  $N_S + 2$  multiplicity, but the former shows unique reactivity: both  $N_S$  and  $N_S + 2$  states are electrophilic.

We further investigate the behavior of local descriptors from SP-CDFT, given in Table 22.3, where the condensed spin polarized Fukui functions,  $f_{SS}^+$  and  $f_{NS}^+$  are given for three atoms, the metal cation M in the porphyrin inner cavity, the nitrogen atom, N-Pph, bonded with the metal ion, and the carbon atom, C-Pph, at the *meso* position of the porphyrin ring. The spin uptake process mainly takes place at the site having the largest value of  $f_{SS}^+$ . We find that in the p0 cases, both the Fe and Ru systems have the markedly larger values for this quantity than both the other metal ions as well as the N and C atoms, suggesting that the metal cation of these two complexes is the center of electron oxidation and the most involved in the spin uptake, in agreement with the experiment. For the p1 and p2 systems, however, the  $f_{SS}^+$  value of Fe and Ru is very different, showing that Fe is much more preferred than other metal ions as the metal oxidation site among the series. This uniqueness of regioselectivity in metal oxidation distinguishes the Fe complex from others in this study, exhibiting the preferred metal-binding specificity of porphyrin with the Fe cation. Also shown in Table 22.3 are the results for the other condensed spin-polarized Fukui function  $f_{NS}^+$  for the same atoms of the three systems. This quantity provides the information for the response of the total electron density condensed on atom  $k$  with respect to

**Table 22.3** Selected local descriptors from SP-CDFT such as spin-polarized Fukui function  $f_{SS,k}^+$  and  $f_{NS,k}^+$  for p0-, p1-, and p2-Metal(l)-Porphyrin complexes, where  $k$  is M (metal cation), N-Pph (nitrogen atom on the porphyrin ring), and C-Pph (bridging/meso carbon atoms on the porphyrin ring).

py No.	Metal ion	$f_{SS,k}^+$			$f_{NS,k}^+$		
		M	N-Pph	C-Pph	M	N-Pph	C-Pph
0	Mg	0.001	0.042	0.063	0.000	0.029	0.006
	Ca	0.021	0.088	0.057	-0.006	-0.023	0.011
	Cr	0.048	0.043	0.063	0.048	0.041	0.003
	Mn	0.013	0.044	0.063	0.012	0.033	0.005
	Fe	<b>0.224</b>	0.042	0.057	<b>-0.185</b>	0.039	0.011
	Co	0.019	0.040	0.062	0.017	0.039	0.002
	Ni	0.021	0.041	0.064	0.020	0.039	0.004
	Cu	0.007	0.040	0.064	0.006	0.036	0.005
	Zn	0.004	0.039	0.064	0.002	0.036	0.005
	Ru	0.264	0.082	0.046	-0.057	0.028	0.015
	Cd	0.010	0.059	0.060	-0.004	0.007	0.009
	Average	0.057	0.051	0.060	-0.013	0.028	0.007
1	Mg	0.361	0.142	0.056	-0.329	-0.066	0.013
	Ca	0.051	0.104	0.050	-0.046	-0.047	0.006
	Cr	0.081	0.046	0.062	0.064	0.041	0.003
	Mn	0.202	0.095	0.060	-0.089	0.002	0.009
	Fe	<b>0.765</b>	0.052	0.040	<b>-0.690</b>	0.035	0.024
	Co	0.089	0.047	0.064	-0.003	0.035	0.004
	Ni	0.264	0.071	0.062	-0.150	0.020	0.006
	Cu	0.226	0.108	0.058	-0.184	-0.027	0.011
	Zn	0.397	0.143	0.054	-0.275	-0.037	0.011
	Ru	0.263	0.060	0.038	-0.214	0.029	0.020
	Cd	0.055	0.116	0.056	0.029	-0.025	0.013
	Average	0.250	0.089	0.054	-0.171	-0.004	0.011
2	Mg	0.180	0.158	0.054	-0.162	-0.089	0.014
	Cr	0.180	0.053	0.057	-0.112	0.029	0.007
	Mn	0.308	0.165	0.054	-0.252	-0.084	0.013
	Fe	<b>0.764</b>	0.052	0.039	<b>-0.620</b>	0.027	0.027
	Co	0.585	0.175	0.055	-0.489	-0.092	0.013
	Ni	0.594	0.181	0.054	-0.503	-0.103	0.014
	Cu	0.251	0.141	0.055	-0.189	-0.056	0.013
	Zn	0.358	0.154	0.054	-0.275	-0.060	0.014
	Ru	0.425	0.071	0.040	-0.119	0.041	0.022
	Average	0.405	0.128	0.051	-0.302	-0.043	0.015

Source: Reprinted with permission from Feng et al. [13], American Chemical Society.

the increase of the total spin number. A negative  $f_{\text{NS},k}^+$  indicates that the atom is more likely to be oxidized once excited as a better electron donor has a larger HOMO spin density and thus a more negative  $f_{\text{NS},k}^+$ . From Table 22.3, we found out on average that the  $f_{\text{NS},k}^+$  value of metal cations is  $-0.013$  for p0,  $-0.171$  for p1, and  $-0.302$  for p2. This finding verifies that as more pyridine groups are coordinated to the metal ion in the complex, the metal ion itself becomes a better electron donor, in line with other results from the CDFT. Another prominent feature of the  $f_{\text{NS},k}^+$  results in Table 22.3 is that in all three cases the Fe cation has the smallest  $f_{\text{NS},k}^+$  value, indicating that the Fe center possesses the largest electron donation capability. Recall that in our earlier work Ru and Fe were found to have similar reactivities in CDFT. From both  $f_{\text{SS},k}^+$  and  $f_{\text{NS},k}^+$  results in Table 22.3, in addition to the global indices in Table 22.2, we can see that in the spin polarization these two metal complexes differ much in reactivity properties.

## 22.5 Concluding Remarks

We have applied CDFT and its spin-polarized variant, SP-CDFT, to understand molecular acidity, PCET, and metal specificity for a number of systems. We have unraveled that for acidic atoms, electrostatic molecular potential and the sum of natural valence orbital energies are two reliable descriptors to predict experimental  $\text{p}K_{\text{a}}$  values. They are originated from the first-order approximation in CDFT. Using the dual descriptor in CDFT, PCET reaction mechanism can be qualitatively appreciated and predicted through direct visual inspections. We also made use of a series of reactivity indices both in CDFT and SP-CDFT to dissect the origin and nature of metal specificity for metal-porphyrin complexes. In a nutshell, as illustrated by three examples in this chapter, CDFT can be a robust and effective tool with predictive power in explaining complex physicochemical phenomena.

## References

- 1 Parr, R.G. and Yang, W. (1989). *Density Functional Theory of Atoms and Molecules*. New York: Oxford University Press.
- 2 Geerlings, P., De Proft, F., and Langenaeker, W. (2003). *Chem. Rev.* 103 (5): 1793–1873.
- 3 Morell, C., Grand, A., and Toro-Labbé, A. (2005). *J. Phys. Chem. A* 109 (1): 205–212.
- 4 Morell, C., Grand, A., and Toro-Labbé, A. (2006). *Chem. Phys. Lett.* 425 (4–6): 342–346.
- 5 Geerlings, P. and De Proft, F. (2008). *Phys. Chem. Chem. Phys.* 10 (21): 3028–3042.
- 6 Martínez, J., Cruz, V., Ramos, J. et al. (2008). *J. Phys. Chem. C* 112 (13): 5023–5028.
- 7 Liu, S. and Pedersen, L.G. (2009). *J. Phys. Chem. A* 113 (15): 3648–3655.

- 8 Liu, S., Schauer, C., and Pedersen, L.G. (2009). *J. Chem. Phys.* 131 (16): 164107.
- 9 Liu, S. (2007). *J. Chem. Phys.* 126 (24): 244103.
- 10 Liu, S., Ess, D.H., and Schauer, C.K. (2011). *J. Phys. Chem. A* 115 (18): 4738–4742.
- 11 Kumar, N., Liu, S., and Kozlowski, P.M. (2012). *J. Phys. Chem. Lett.* 3 (8): 1035–1038.
- 12 Feng, X., Yu, J., Lei, M. et al. (2009). *J. Phys. Chem. B* 113 (40): 13381–13389.
- 13 Feng, X., Yu, J., Liu, R. et al. (2010). *J. Phys. Chem. A* 114 (21): 6342–6349.
- 14 Jorgensen, W.L., Briggs, J.M., and Gao, J. (1987). *J. Am. Chem. Soc.* 109 (22): 6857–6858.
- 15 Pliego, J.R. Jr., (2003). *Chem. Phys. Lett.* 367 (1–2): 145–149.
- 16 De Proft, F., Amira, S., Choho, K., and Geerlings, P. (1994). *J. Phys. Chem.* 98 (20): 5227–5233.
- 17 Da Silva, G., Kennedy, E.M., and Dlugogorski, B.Z. (2006). *J. Phys. Chem. A* 110 (39): 11371–11376.
- 18 Deka, R.C., Roy, R.K., and Hirao, K. (2004). *Chem. Phys. Lett.* 389 (1–3): 186–190.
- 19 Gupta, K., Roy, D.R., Subramanian, V., and Chattaraj, P.K. (2007). *J. Mol. Struct. (THEOCHEM)* 812 (1–3): 13–24.
- 20 Glendening, E.D., Badenhop, J.K., Reed, A.E. et al. (2001). NBO 5.0. Theoretical Chemistry Institute, University of Wisconsin, Madison.
- 21 Cao, X., Rong, C., Zhong, A. et al. (2018). *J. Comput. Chem.* 39: 117–129.
- 22 Zhao, D., Rong, C., Yin, D., and Liu, S. (2013). *J. Theor. Comput. Chem.* 12 (05): 1350034.
- 23 Hammes-Schiffer, S. (2009). *Acc. Chem. Res.* 42 (12): 1881–1889.
- 24 Huynh, M.H.V. and Meyer, T.J. (2007). *Chem. Rev.* 107 (11): 5004–5064.
- 25 Mayer, J.M. (2004). *Annu. Rev. Phys. Chem.* 55: 363–390.
- 26 Hammes-Schiffer, S. (2001). *Acc. Chem. Res.* 34 (4): 273–281.
- 27 Warren, J.J. and Mayer, J.M. (2010). *Proc. Natl. Acad. Sci. U. S. A.* 107 (12): 5282–5287.
- 28 Tishchenko, O., Truhlar, D.G., Ceulemans, A., and Nguyen, M.T. (2008). *J. Am. Chem. Soc.* 130 (22): 7000–7010.
- 29 Yang, W. and Mortier, W.J. (1986). *J. Am. Chem. Soc.* 108 (19): 5708–5711.
- 30 O'Malley, P.J. (2002). *Chem. Phys. Lett.* 364 (3–4): 318–322.
- 31 Galvan, M., Vela, A., and Gazquez, J.L. (1988). *J. Phys. Chem.* 92 (22): 6470–6474.
- 32 Galvan, M. and Vargas, R. (1992). *J. Phys. Chem.* 96 (4): 1625–1630.

## 23

### On the Mechanisms of Chemical Reactions

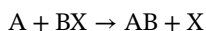
Soledad Gutiérrez-Oliva<sup>1</sup>, Angie Carolay Forero-Girón<sup>1</sup>, Nery Villegas-Escobar<sup>2</sup>, and Alejandro Toro-Labbé<sup>1</sup>

<sup>1</sup>Universidad Católica de Chile, Facultad de Química y de Farmacia, Laboratorio de Química Teórica Computacional (QTC), Santiago, Chile

<sup>2</sup>Universidad Bernardo O'Higgins, Centro Integrativo de Biología y Química Aplicada (CIBQA), Santiago, Chile

#### 23.1 Introduction

One can picture a chemical reaction as a sequence of chemical events that are structural and electronic changes taking place along a reaction coordinate to produce a chemical transformation. These chemical events are basically bond-forming and bond-breaking processes that are main actions, although not the only ones, necessary to produce the structural and electronic changes that achieve a chemical reaction. For example, a simple substitution reaction as



involves a weak initial attractive interaction that allows the approach of the reactants A and BX to initiate the reaction. This is followed by the breaking of the B–X bond and the formation of the A–B bond; depending on the reaction, these two events may, or may not, take place simultaneously. The reaction is achieved when the products AB and X are formed and interacting through non-covalent interactions. It is possible to define a hierarchy of chemical events that can be distinguished empirically, but also in terms of the amount of energy they involve and, in most cases, for the position along the reaction coordinate in which they take place. Bond-breaking and bond-forming processes are primary events, bond weakening and strengthening are secondary events, and non-covalent interactions can be considered as tertiary events. These chemical events shows up at different degrees of progress of the reaction, as shown in Figure 23.1. Discovering how and where, along the reaction coordinate, chemical events shows up unveils the very whole reaction mechanism, the processes by which chemical substances are transformed into other substances are then at hand.

The first key quantity involved in a chemical process is the reaction energy ( $\Delta E^\circ$ ), which is the net energy change between reactants and products; it defines the chemical equilibrium and characterizes the thermodynamics of the reaction.

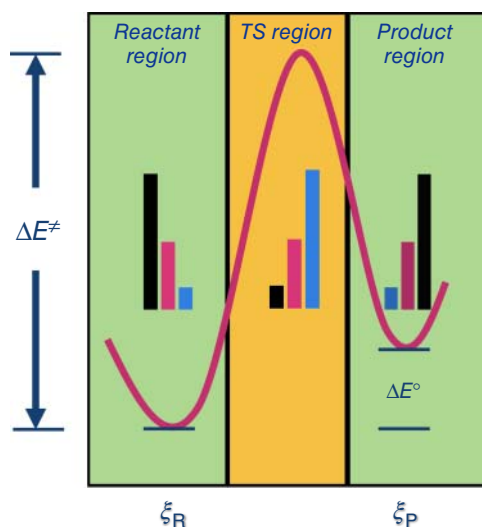


**Figure 23.1** The partition of the reaction coordinate provided by the reaction force analysis and projected on a schematic energy profile of an elementary step along the reaction coordinate  $\xi$ . The pair  $\{\Delta E^\circ, \Delta E^\ddagger\}$  are the reaction and activation energies. The bars on each reaction region indicate qualitatively the expected intensity of primary (blue), secondary (pink), and tertiary (black) chemical events along the reaction coordinate.

Frequently, there are many ways a chemical reaction may take place. Among all possible mechanisms, the most probable is the one that follows the minimum energy path (MEP) connecting the reactants with the products and passing by a transition state [1–3]. The MEP corresponds to the path with the lower activation energy, which is the energy necessary to reach the transition state, and to do so, chemical events have to be put at play. An energy profile represented in Figure 23.1 has three key points, two minima at the reactants ( $\xi_R$ ) and products ( $\xi_P$ ) and one maximum at the transition state. The activation energy ( $\Delta E^\ddagger$ ) reveals, through the transition state theory (TST) [4–6], the kinetic aspects of an elementary step or how much time it takes for the whole process. Reaction thermodynamics, kinetics, and mechanism are the three most relevant dimensions of a chemical reaction, and they are intimately related. Therefore, a complete characterization of a chemical reaction necessarily requires the knowledge of these three aspects.

Reaction rate and the activation energy are connected through the Arrhenius equation

$$k = Ae^{-\Delta E^\ddagger/RT} \quad (23.1)$$

where  $k$  is the rate constant,  $A$  is the pre-exponential coefficient often referred to as the frequency factor,  $R$  is the universal gas constant, and  $T$  is the temperature. More sophisticated theories have been developed later being the most important one the Eyring, Polanyi, and Evans TST [4, 5] based on the assumption that activated complexes are in quasi-equilibrium with the reactants. This leads to the Eyring equation [6, 7]

$$k = \left( \frac{k_B T}{h\nu} \right) e^{-\Delta G^\ddagger/RT} \quad (23.2)$$

where  $k_B$  is the Boltzmann constant,  $h$  is the Planck constant,  $\nu$  is the frequency of an specific vibrational mode (chemical event) responsible for converting the

activated complex to the product, and  $\Delta G^\ddagger$  is the activation Gibbs free energy. Therefore, the knowledge of the activation energy of a chemical reaction produces fundamental kinetic information such as the time needed to produce the chemical transformation.

In the past, due to the impossibility to get reliable estimation of activation energies, empirical relationships between kinetic and thermodynamic data have been suggested. A linear relationship between the activation energy and the reaction energy of an elementary reaction is known as Brönsted–Evans–Polanyi (BEP) principle [8, 9]:

$$\Delta E^\ddagger = E_0 + \beta \Delta E^\circ \quad (23.3)$$

where  $E_0$  is a reference energy and  $\beta$  is the Brönsted coefficient that measures the resemblance between the transition state and the product. Following the Leffler postulate [10],  $\beta$  is formally defined as

$$\beta = \left( \frac{d\Delta E^\ddagger}{d\Delta E^\circ} \right) \quad (23.4)$$

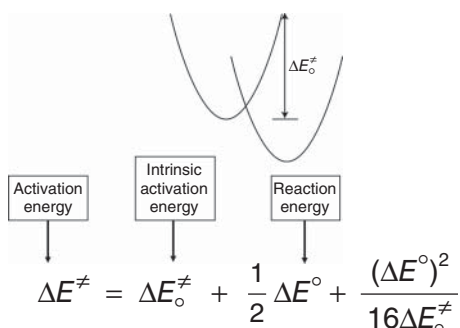
This simple equation may provide interesting insights on kinetic and thermodynamic patterns of similar reactions. The Marcus equation (ME) for predicting activation energies results from the interpolation of two local potentials,  $E_R(\xi)$  and  $E_P(\xi)$ , describing the reactants and the products. These potentials are linked through a reaction coordinate  $\xi$  and intersect in the transition state. Marcus equation is conceived at the intersection of the two wells, which correspond to the actual transition state (TS) of the reaction; see Figure 23.2 [11, 12]:

$$\Delta E^\ddagger = \Delta E^\ddagger_\circ + \frac{1}{2} \Delta E^\circ + \frac{(\Delta E^\circ)^2}{16\Delta E^\ddagger_\circ} \quad (23.5)$$

It is interesting to note that in the ME, the linear relationship between activation and reaction energies already found in the BEP model is recovered, although the constant slope of  $\beta = 0.5$  is slightly different from the  $\beta$  coefficient obtained in the BEP model, in the Marcus equation, a corrected Brönsted coefficient emerges:

$$\beta = \left( \frac{d\Delta E^\ddagger}{d\Delta E^\circ} \right) = \frac{1}{2} + \frac{\Delta E^\circ}{8\Delta E^\ddagger_\circ} \quad (23.6)$$

**Figure 23.2** The Marcus equation is obtained from interpolation of two potentials localized at the reactants and products. The intersecting point defines the location of the transition state with the associated activation energy  $\Delta E^\ddagger$ . The intrinsic activation energy is the energy involved in distorting the reactants to reach the position of the products.





As observed, the correction to the one half factor of Eq. (23.6) is due to a balance between reaction and intrinsic activation energies, and it is normally small since in most cases  $\Delta E_0^\ddagger \gg \Delta E^\circ$ . The Brönsted coefficient, as defined in Eq. (23.6), measures the compliance of the Hammond postulate [13] stating that for exergonic reactions ( $\Delta E^\circ < 0$ ) the transition state is located closer to the reactants ( $\beta < 0.5$ ), whereas for endergonic reactions ( $\Delta E^\circ > 0$ ) the TS is located closer to the products ( $\beta > 0.5$ ). This is the basis of the Marcus theory of electron transfer reactions that was originally formulated to link the rate of the reactions with the thermodynamics of the process [7, 11, 12]. As indicated in Figure 23.2, a key quantity in the Marcus theory is the reorganization energy or Marcus' intrinsic activation energy,  $\Delta E_0^\ddagger$ , which corresponds to the energy associated to the reorganization of the reactant at the equilibrium configuration of the product.

Although not intended to describe chemical reactions, the Marcus equation became a keystone in the characterization of the kinetics and thermodynamics of any kind chemical process [14, 15]. The three stationary points on the energy profile along a reaction coordinate were enough to get this information, and the profiles of energy became crucial to get kinetic and thermodynamic data of a chemical process although it never gave a clue on the reaction mechanisms. An important leap further on the direction of elucidating reaction mechanisms was the introduction of the reaction force since it provided a rational partition of the reaction coordinate into the so-called reaction regions in which specific mechanisms might be operating [16–22].

In this chapter, we are going to review all three aspects of a chemical reaction on the basis of the Marcus' equation that relates activation and reaction energies. Reaction mechanisms will be rationalized within the frame of the reaction force analysis (RFA) that allows a partition of the reaction coordinate in *reaction regions* in which different mechanisms might be operating. On the other hand, chemical events explaining the reaction mechanism will be characterized through the reaction electronic flux (REF) that is a density functional theory (DFT)-based descriptor of the electronic activity taking place during a chemical reaction.

## 23.2 Theory of the Mechanism of Chemical Reactions

### 23.2.1 The Reaction Force Analysis

As already mentioned, a major leap on the characterization of reaction mechanism was the introduction of the reaction force, defined as [16]

$$F(\xi) = - \left( \frac{dE(\xi)}{d\xi} \right) \quad (23.7)$$

So, to any energy profile it corresponds a reaction force profile that is obtained through numerical or analytic differentiation of  $E(\xi)$ , as illustrated in Figure 23.3. The five key points on the reaction force profile are the same as for the energy profile, reactant, transition state, and product to which the reaction force minimum

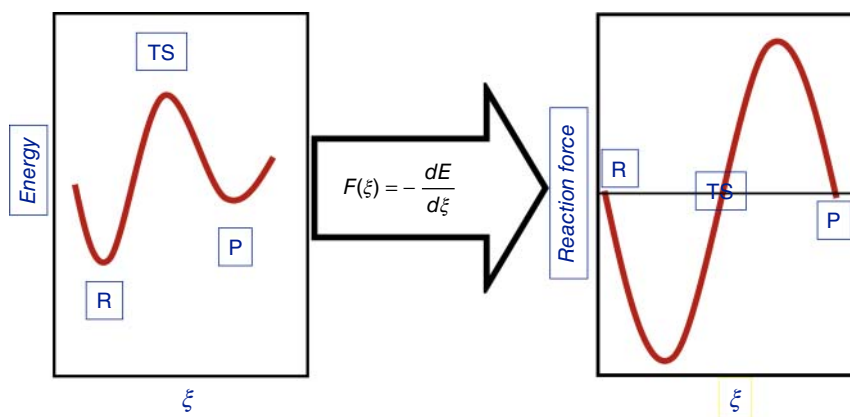
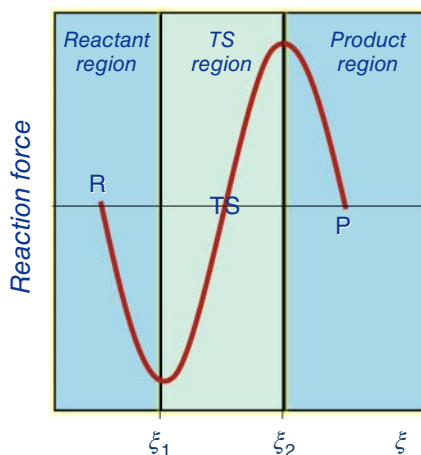


**Figure 23.3** Correspondence between energy and reaction force profiles. The energy profile has three key points, whereas the reaction force profile exhibits five points of interest.

**Figure 23.4** Reaction regions defined for an elementary step. The force minimum and the force maximum define the borders for the regions.



and maximum have to be added. These five points are used to define reaction regions along  $\xi$  as indicated in Figure 23.4, in which different mechanisms might be operating, as indicated in Figure 23.4.

The reactant and product regions are structurally intensive. In the reactant region, structural rearrangements prepare the reaction, whereas in the product region the structural relaxation leads to the products [23–27]. These two regions are characterized mainly by secondary and tertiary chemical events. In contrast to this, the transition state region is mostly electronically intensive. Here, most electronic activity takes place through primary chemical events; see Figure 23.1 [20, 28]. In fact the transition state region hosts activated reactants and products, which are unstable species that appear and disappear, promoting the reaction in one sense or the other. Significantly, the numerical value of the definite integral of reaction force

(RF) in given intervals along  $\xi$  gathers information about the energy associated with specific chemical events that might be driving the reaction within those intervals, defining reaction works as [17]

$$W_i = - \int_{\xi_i}^{\xi_i + \delta\xi} F(\xi) d\xi \quad (23.8)$$

In this way, it is possible to quantify the energetic expenditure of specific chemical events taking place anywhere along the reaction coordinate. In particular, and with the aim of providing a natural partition of activation and reaction energies, reaction works  $W_1$ ,  $W_2$ ,  $W_3$ , and  $W_4$ , consistent with the already defined reaction region, are given by

$$W_1 = - \int_{\xi_R}^{\xi_1} F(\xi) d\xi > 0; \quad W_2 = - \int_{\xi_1}^{\xi_0} F(\xi) d\xi > 0 \quad (23.9)$$

$$W_3 = - \int_{\xi_0}^{\xi_2} F(\xi) d\xi < 0; \quad W_4 = - \int_{\xi_2}^{\xi_P} F(\xi) d\xi < 0 \quad (23.10)$$

where  $\xi_0$  is the position of the transition state. The above-defined reaction works introduce a new perspective into activation and reaction energies, which can be expressed as

$$\Delta E^\circ = (W_1 + W_2 + W_3 + W_4) \quad (23.11)$$

and

$$\Delta E^\ddagger = (W_1 + W_2) \quad (23.12)$$

Note that since the reaction works are defined within regions in which structural or electronic effects prevails over the other, the physical nature of these key energies is then revealed in terms of the relative weight of structural and electronic effects. In this context a new perspective on activation processes is obtained, illustrated in Figure 23.5.

In summary, the RFA provides a reliable framework to analyze the different reaction mechanisms that might be operating within the different reaction regions. It

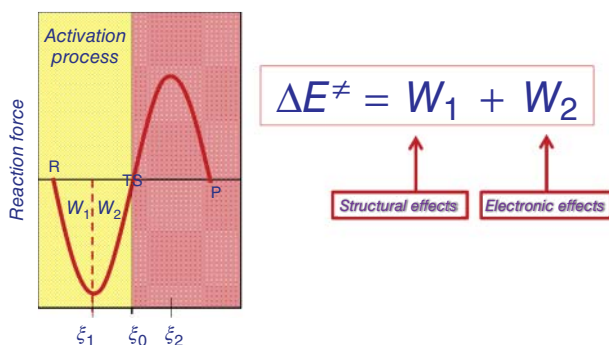


**Figure 23.5** The activation process from the perspective of the reaction force.

is important to note that for multistep reactions, more reaction regions have to be defined and a  $n$ -step reaction will have  $(2n + 1)$  reaction regions with  $n$  transition state and  $(n - 1)$  intermediate regions, besides the reactant and product regions [19, 23, 29–33]. The energy involved in activation and relaxation can be easily quantified through the reaction works evaluated within the different regions, thus allowing to identify their physical nature.

### 23.2.2 The Marcus Potential Function

Recently a potential function consistent with the Marcus equation has been proposed [34], which is given by

$$E^{(m)}(\xi) = -\frac{1}{4}\Delta E_o^\ddagger \xi^4 + \Delta E_o^\ddagger \xi^2 + \frac{1}{4}\Delta E^\circ \xi^2 \quad (23.13)$$

As it can be seen, the Marcus potential ( $E^{(m)}(\xi)$ ) is a two-parameter polynomial function. Both parameters have known physical meaning, the intrinsic activation energy  $\Delta E_o^\ddagger$  accounting for structural distortion and the reaction energy ( $\Delta E^\circ$ ) accounting for the thermodynamic driving force of the chemical process. Therefore, the Marcus potential can be defined by having the energy of the reactants, products, and the TS. This potential naturally spans in an interval  $\{0,2\}$  yielding an energy profile over  $\xi$  that recovers the activation energy and the reaction energy. The position of the transition state for  $E^{(m)}(\xi)$  is given by

$$\left( \frac{dE^{(m)}(\xi)}{d\xi} \right)_{\xi_0} = 0 \rightarrow \xi_0 = \left[ 2 + \frac{1}{2} \left( \frac{\Delta E^\circ}{\Delta E_o^\ddagger} \right) \right] \quad (23.14)$$

When Eq. (23.13) is evaluated at  $\xi_0$ , the Marcus equation is recovered. Therefore, the classical ME is a particular case of the Marcus potential.

### 23.2.3 The Reaction Force Analysis of $E^{(m)}(\xi)$

It is possible to perform the RFA using the analytic Marcus' potential function given in Eq. (23.11). The reaction force in the context of the Marcus potential is given by [34]

$$F^{(m)}(\xi) = - \left( \frac{dE^{(m)}}{d\xi} \right) = \Delta E_o^\ddagger \xi^3 - 2\Delta E_o^\ddagger \xi - \frac{1}{2}\Delta E^\circ \xi \quad (23.15)$$

The reaction force  $F^{(m)}(\xi)$  vanished at the reactant and transition state. After the TS, it continues to increase so that it can only be used for activation processes although relaxation can be treated as a reverse activation. Another important result is that the minimum of the Marcus' reaction force ( $\xi_1$ ) can be derived analytically:

$$\xi_1^2 = \frac{1}{3}\xi_0^2 = \frac{1}{3} \left[ 2 + \frac{1}{2} \left( \frac{\Delta E^\circ}{\Delta E_o^\ddagger} \right) \right] \quad (23.16)$$

and therefore, integrating  $F^{(m)}(\xi)$  within the right intervals will lead to analytic forms for reaction works  $W_1^{(m)}$  and  $W_2^{(m)}$ :

$$\begin{aligned} W_1^{(m)} &= \int_{\xi_R}^{\xi_1} F^{(m)}(\xi) d\xi \\ &= -\frac{1}{4} \Delta E_o^\ddagger \left( \frac{1}{9} \xi_0^4 \right) + \Delta E_o^\ddagger \left( \frac{1}{3} \xi_0^2 \right) + \frac{1}{4} \Delta E^\circ \left( \frac{1}{3} \xi_0^2 \right) \\ &= \frac{5}{9} \Delta E_o^\ddagger + \frac{5}{18} \Delta E^\circ + \frac{5}{144} \left[ \frac{(\Delta E^\circ)^2}{\Delta E_o^\ddagger} \right] \end{aligned} \quad (23.17)$$

and

$$\begin{aligned} W_2^{(m)} &= \int_{\xi_1}^{\xi_0} F^{(m)}(\xi) d\xi \\ &= -\frac{1}{4} \Delta E_o^\ddagger \left( \frac{8}{9} \xi_0^4 \right) + \Delta E_o^\ddagger \left( \frac{2}{3} \xi_0^2 \right) + \frac{1}{4} \Delta E^\circ \left( \frac{2}{3} \xi_0^2 \right) \\ &= \frac{4}{9} \Delta E_o^\ddagger + \frac{4}{18} \Delta E^\circ + \frac{4}{144} \left[ \frac{(\Delta E^\circ)^2}{\Delta E_o^\ddagger} \right] \end{aligned} \quad (23.18)$$

with

$$W_1^{(m)} + W_2^{(m)} = \Delta E_m^\ddagger \quad (23.19)$$

where  $\Delta E_m^\ddagger$  is the same expression for the activation energy given in Eq. (23.4), and a subindex (m) has been added to  $\Delta E^\ddagger$  to stress its analytic origin. A relevant result is that within the framework of the Marcus' potential function, the reaction work  $W_1^{(m)}$  represents 56% of the activation energy, confirming the preponderance of structural reorganizations over electronic reordering, a fact that has been empirically observed in many reactions.

### 23.3 The Reaction Electronic Flux

The REF measures the electronic activity taking place along the reaction coordinate, which is defined as [35–37]

$$J(\xi) = -\frac{d\mu}{d\xi} \quad (23.20)$$

where  $\mu$  is the electronic chemical potential accounting for the escaping tendency of electrons from equilibrium [38–40], defined as

$$\mu = \left( \frac{dE}{dN} \right)_{v(\vec{r})} \approx -\frac{1}{2}(\text{IP} + \text{EA}) \approx \frac{1}{2}(\epsilon_H + \epsilon_L) \quad (23.21)$$

where  $N$  is the total number of electron of the system,  $v(\vec{r})$  is the external potential, and the pairs {IP, EA} and  $\{\epsilon_H, \epsilon_L\}$  are the ionization potential and electron affinity; and the frontier molecular orbital energies, highest occupied molecular orbital (HOMO) and lowest unoccupied molecular orbital (LUMO), respectively. To obtain the working formulae given in the above equation from the differential

definition of  $\mu$ , it is necessary to invoke the finite difference approximation [41] and the Koopmans theorem [42]. In this context, the simple knowledge of frontier molecular orbital energies along  $\xi$  is enough to get a profile for the chemical potential,  $\mu(\xi)$ , which produces crucial information about the electronic activity that drives a chemical reaction [25, 29, 43]. It has been established that positive values of  $J(\xi)$  are associated with spontaneous electronic activity driven by bond strengthening/forming processes, whereas negative values are associated with non-spontaneous electronic activity that is conducted by bond weakening/cleavage processes [28, 43].

### 23.3.1 Physical Partition of the REF

To better rationalize results from REF, a physical partition of  $J(\xi)$  was proposed [30, 37, 44] in terms of electronic polarization and transfer effects (Figure 23.6):

$$J(\xi) = (J_p(\xi) + J_t(\xi)) \quad (23.22)$$

where  $J_p(\xi)$  and  $J_t(\xi)$  are polarization and transfer fluxes, respectively. In this way, it is possible to characterize the nature of the electronic activity that drives the reaction along  $\xi$ .

### 23.3.2 Chemical Partition of the REF

A chemical partition of the REF is also available [45], which is derived from the electrophilicity index  $\omega$ :

$$\omega = \frac{\mu^2}{2\eta} \quad (23.23)$$

where  $\eta$  is the hardness expressed in the frame of conceptual DFT as the derivative of  $\mu$  with respect to the total number of electrons. Therefore,

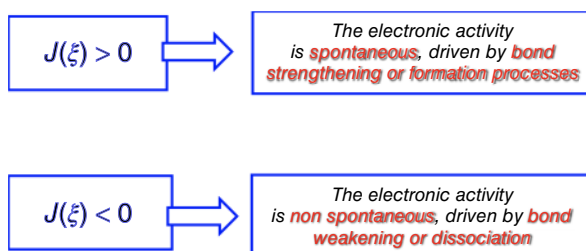
$$J(\xi) = \frac{1}{2} \Delta N_{\max}(\xi) \left( \frac{d\eta}{d\xi} \right) + \frac{1}{\Delta N_{\max}(\xi)} \left( \frac{d\omega}{d\xi} \right) \quad (23.24)$$

$$= (J_\eta(\xi) + J_\omega(\xi)) \quad (23.25)$$

with  $\Delta N_{\max} = -\mu/\eta$  being the maximum number of electrons the system can accept. Therefore, the following component of the reaction flux emerges

$$J_\eta(\xi) = \frac{1}{2} \Delta N_{\max}(\xi) \left( \frac{d\eta}{d\xi} \right) \quad (23.26)$$

**Figure 23.6** Conceptual interpretation of the reaction electronic flux.



and

$$J_{\omega}(\xi) = \frac{1}{\Delta N_{\max}(\xi)} \left( \frac{d\omega}{d\xi} \right) \quad (23.27)$$

The pair  $\{J_{\eta}, J_{\omega}\}$  can be used to rationalize results of REF in terms of well-known reactivity descriptors such as hardness and electrophilicity index.

### 23.3.3 REF, Electronic Populations, and Bond Orders

To complement the REF results, it is possible to link the REF with local electronic properties such as bond orders, atomic charges, and electronic populations. The link comes from the very definition of the chemical potential in DFT [38, 39]:

$$\mu = \int f(\vec{r}) \delta v(\vec{r}) d\vec{r} \rightarrow \mu \approx \sum_k v_k f_k \quad (23.28)$$

and therefore, the REF can be written in terms of condensed to atoms quantities:

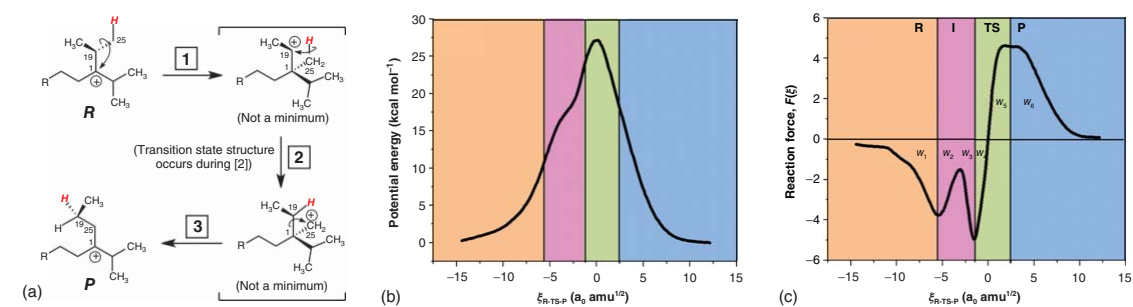
$$J(\xi) \approx -\frac{1}{N} \sum_k \left( \frac{dv_k}{d\xi} \right) \cdot \rho_k - \frac{1}{N} \sum_k \left( \frac{d\rho_k}{d\xi} \right) \cdot v_k \quad (23.29)$$

where, since the condensed external potential  $v_k$  remains constant all along the reaction coordinate, the first term of the right-hand side can be overlooked. In this context the REF becomes proportional to the derivative of electronic population on atom  $k$  weighted by the constant external potential. Following the above equation, it is possible to use bond orders to identify specific bond processes (forming/cleavage) that might be prime responsible for the electronic activity evidenced by the REF.

## 23.4 Selected Applications

### 23.4.1 Reaction Force Analysis and REF

Carbocation rearrangements are involved in many enzyme-catalyzed biochemical reactions; in particular, the carbocation triple shift (CCTS) reaction is one of the most unusual types of rearrangements discovered. The CCTS consists in concerted processes that are characterized by three main events, which are [1] 1,2-methyl shift, [2] 1,3-hydride shift, and [3] 1,2-alkyl shift [46]. In this study, the reactant, product, and transition state geometries were optimized at the B3LYP/6-31+G(d,p) level using the Gaussian 09 package, which has proven to be a good methodology for the description of this mechanism. Results are summarized in Figure 23.7. It can be observed that the reaction force profile suggests the existence of intermediates, thus leading to four reaction regions, as indicated by the different colors on the figures. The table indicate that all chemical events that drive a portion of the progress of the reaction have associated a value of energy adsorbed or released indicating that the RFA provides a very detailed scrutiny of the energy involved in the chemical transformation. On the other hand, it can be observed on the right-bottom panel that the REF is basically constructed from the contributions, at different stages of



Reaction	Chemical shift	Region	Primary (p)/secondary(s) chemical events	$W_i$ (kcal mol <sup>-1</sup> )
CCTS	1,2-methyl shift	R	C1-C25 bond forming (p) C19-C25 bond weakening (s)	11.81
		I	C1-C25 bond forming (p) C19-C25 bond weakening (s) H-C19 bond forming (p)	10.53
	1,3-hydride shift	TS	H-C19 bond forming (p) H-C25 bond breaking (p)	4.58
	1,2-alkyl shift		C1-C19 bond breaking (p) C1-C25 bond forming (p) C19-C25 bond strengthening (s)	-5.47
			C1-C19 bond breaking (p) C19-C25 bond strengthening (s)	-21.74
		P	H-C25 bond breaking (p)	

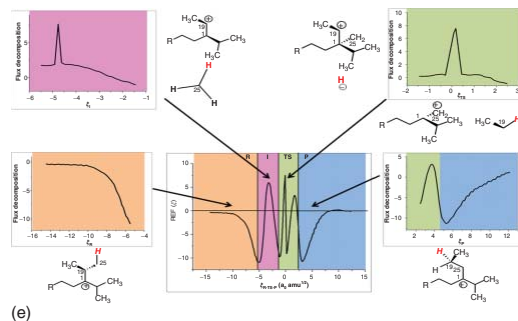


**Figure 23.7** Composition of results concerning the triple shift rearrangement. (a) The scheme of the triple shift rearrangement, the (b) energy and (c) reaction force profiles, (d) the energy associated to each chemical event that drives a portion of the progress of the reaction along  $\xi$ , and (e) REF that is clearly built up from local fragments REFs. Source: Ortega et al. [46].



the reaction, of the specific chemical event, the REFs to which are determined by fragmentation of the supermolecule into relevant topologic fragment containing the chemical event under study.

### 23.4.2 Physical and Chemical Partition of REF

To illustrate the chemical and physical partition of the REF, we will analyze the two-step mechanism of the formation of aminoacetonitrile ( $\text{NH}_2\text{CH}_2\text{CN}$ ) from methanimine ( $\text{NHCH}_2$ ) and hydrogen isocyanide ( $\text{CNH}$ ). The interest of this reaction comes from the fact that aminoacetonitrile is a direct precursor of glycine and the reaction may take place in the interstellar medium, where both reactants have been observed [45]. The reaction takes place following two steps as indicated in Figure 23.8. It can be observed in the Figure 23.8 that in step 1 physical and chemical components of the partition match each other very closely and in step 2 the situation consistency is more qualitative.

The physical and chemical representations of the REF for R1 and R2 are given in left and right bottom panels, where each one includes four plots. (a) Red and blue curves correspond to  $J_p(\xi)$  and  $J_t(\xi)$ , respectively; black curve is the total REF:  $J(\xi) = J_p(\xi) + J_t(\xi)$ . (b) Red and blue curves correspond to  $J_\eta(\xi)$  and  $J_\omega(\xi)$ , respectively; black curve is the total REF:  $J(\xi) = J_\eta(\xi) + J_\omega(\xi)$ . The inset on the Figure 23.8 shows the variation of  $\Delta N_{\text{max}}(\xi)$ . (c) Comparison between  $J_t(\xi)$  and  $J_\eta(\xi)$ . (d) Comparison between  $J_p(\xi)$  and  $J_\omega(\xi)$ . Consistency between the two approaches was reached for the case of the formation reaction of aminoacetonitrile. A very good correspondence between the pairs  $\{J_p, J_\omega\}$  and  $\{J_t, J_\eta\}$  was obtained, thus giving new conceptual insights on the physical interpretation of the REF and its components.

## 23.5 Conclusions

In this chapter, we have given an overview of a protocol based on the RFA to characterize the most frequently elusive mechanism of chemical reactions. The bunch of tools we reviewed starts with the characterization of transition states and the activation energy. This can be achieved using simple empirical models such as the BEP or the Marcus' equation. The usefulness of energy profiles to track specific events that drive the reaction has been put in value; numerical and analytic profiles can be used to rationalize them. In this context, an analytic potential was formulated to extend the validity of the ME and to characterize energies associated to specific stages as the reaction progress, energies that are crucial in the unfolding of the mechanism. It has been proven that the RFA is a very powerful tool to define a framework based on the reaction coordinate to zoom-in into the specific effects that drive a chemical reaction.

REF emerged as a very useful tool to characterize the electronic activity that takes place at every step of the reaction; the coupling between conceptual DFT and the classical physical chemistry of reactions is then achieved. Physical and chemical partitions of the REF provide different ways to rationalize the electronic

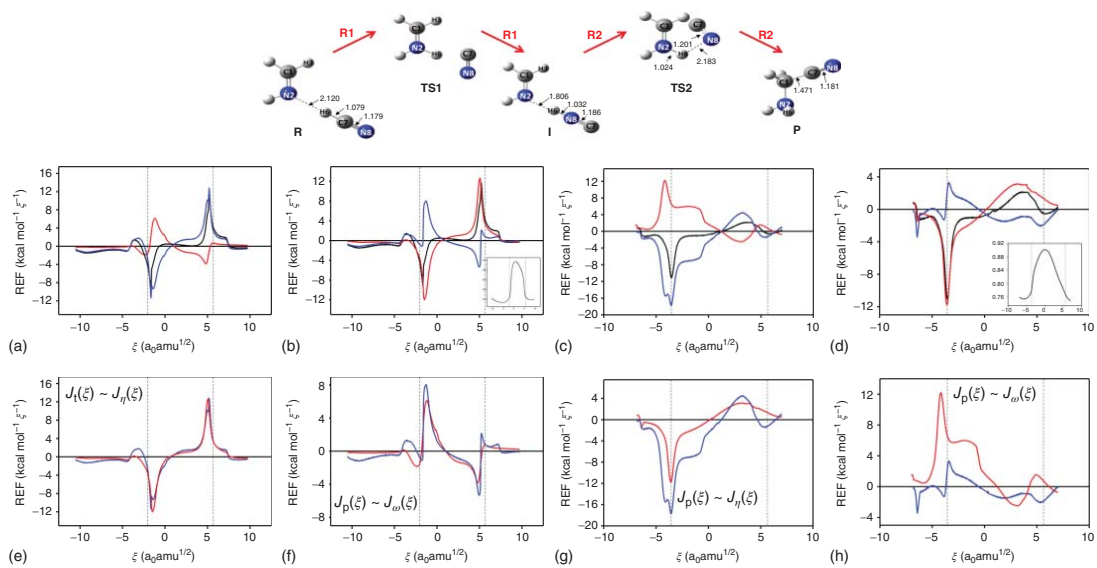


**Figure 23.8** Composition of results concerning the comparison of physical and chemical partitioning of REF. Source: Gutiérrez-Oliva et al. [45].

activity: the first one uses polarization and transfer effects, and the second one involves well-known DFT descriptors of chemical reactivity. In this context, the link between both approaches provides new interpretative resources to analyze any chemical process.

Integration of different tools, global and local properties of a chemical reaction, produces a very powerful protocol to analyze chemical events and to assign them the relevance they have in a given step of the reaction. Like a musical piece made of musical notes that are going on and off along the whole artwork, a chemical reaction is made of chemical events that show up and disappear sequentially or synchronously as part of a vast ensemble of events that remain active until completion of the desired chemical change, where equilibrium is reached.

## Acknowledgments

The authors are indebted to Professor Shubin Liu for his kind invitation to participate in this book. Financial support from FONDECYT (ANID-Chile) through Projects Nos. 1181072 and 1201617 are gratefully acknowledged.

## References

- 1 Fukui, K. (1981). The path of chemical reactions. The IRC approach. *Acc. Chem. Res.* 14 (12): 363–368.
- 2 Hratchian, H.P. and Schlegel, H.B. (2004). Accurate reaction paths using a Hessian based predictor-corrector integrator. *J. Chem. Phys.* 120: 9918–9924.
- 3 Hratchian, H.P. and Schlegel, H.B. (2005). Using Hessian updating to increase the efficiency of a Hessian based predictor-corrector reaction path following method. *J. Chem. Theory Comput.* 1: 61–69.
- 4 Eyring, H. (1935). The activated complex in chemical reactions. *J. Chem. Phys.* 3: 107–115.
- 5 Evans, M.G. and Polanyi, M. (1935). Some applications of the transition state method to the calculation of reaction velocities, especially in solution. *Trans. Faraday Soc.* 31: 875–894.
- 6 Laidler, K.J. and King, M.C. (1983). The development of transition-state theory. *J. Phys. Chem.* 87: 2657–2664.
- 7 Pross, A. (1945). *Theoretical and Physical Principles of Organic Reactivity*. Wiley.
- 8 Brønsted, J.N. (1928). Acid and basic catalysis. *Chem. Rev.* 5 (3): 231–338.
- 9 Evans, M.G. and Polanyi, M. (1938). Inertia and driving force of chemical reactions. *Trans. Faraday Soc.* 34: 11–24.
- 10 Leffler, J.E. (1953). Parameters for the description of transition states. *Science* 117: 340–341.
- 11 Marcus, R.A. (1964). Chemical and electrochemical electron-transfer theory. *Annu. Rev. Phys. Chem.* 15 (1): 155–196.

- 12 Marcus, R.A. (1993). Electron transfer reactions in chemistry. Theory and experiment. *Rev. Mod. Phys.* 65: 599–610.
- 13 Hammond, G.S. (1955). A correlation of reaction rates. *J. Am. Chem. Soc.* 77 (2): 334–338.
- 14 Cárdenas-Jirón, G.I., Toro-Labbé, A., Bock, C.W., and Maruani, J. (1995). *Characterization of Rotational Isomerization Processes in Monorotor Molecules*, 97–120. Dordrecht: Springer Netherlands.
- 15 Martínez, J. and Toro-Labbé, A. (2004). Energy and chemical force profiles from the Marcus equation. *Chem. Phys. Lett.* 392 (1–3): 132–139.
- 16 Toro-Labbé, A. (1999). Characterization of chemical reactions from the profiles of energy, chemical potential, and hardness. *J. Phys. Chem. A* 103 (22): 4398–4403.
- 17 Herrera, B. and Toro-Labbé, A. (2004). The role of the reaction force to characterize local specific interactions that activate the intramolecular proton transfers in DNA basis. *J. Chem. Phys.* 121 (15): 7096–7102.
- 18 Gutiérrez-Oliva, S., Herrera, B., Toro-Labbé, A., and Chermette, H. (2005). On the mechanism of hydrogen transfer in the  $\text{HSCH(O)} \rightleftharpoons \text{(S)CHOH}$  and  $\text{HSNO} \rightleftharpoons \text{SNOH}$  reactions. *J. Phys. Chem. A* 109 (8): 1748–1751.
- 19 Politzer, P., Toro-Labbé, A., Gutiérrez-Oliva, S. et al. (2005). The reaction force: three key points along an intrinsic reaction coordinate. *J. Chem. Sci.* 117 (5): 467–472.
- 20 Rincón, E., Jaque, P., and Toro-Labbé, A. (2006). Reaction force analysis of the effect of  $\text{Mg(II)}$  on the 1,3 intramolecular hydrogen transfer in thymine. *J. Phys. Chem. A* 110 (30): 9478–9485.
- 21 Toro-Labbé, A., Gutiérrez-Oliva, S., Murray, J.S., and Politzer, P. (2009). The reaction force and the transition region of a reaction. *J. Mol. Model.* 15: 707–710.
- 22 Politzer, P., Murray, J.S., Yepes, D., and Jaque, P. (2014). Driving and retarding forces in a chemical reaction. *J. Mol. Model.* 20 (8): 2351.
- 23 Durán, R. and Herrera, B. (2020). Theoretical study of the mechanism of catalytic enantioselective N-H and O-H insertion reactions. *J. Phys. Chem. A* 124 (1): 2–11.
- 24 Villegas-Escobar, N., Gutiérrez-Oliva, S., and Toro-Labbé, A. (2015). Catalytic mechanism of  $\text{H}_2$  activation by a carbenoid aluminum complex. *J. Phys. Chem. C* 119 (47): 26598–26604.
- 25 Villegas-Escobar, N., Larsen (Née Vilhelmsen), M.H., Gutiérrez-Oliva, S. et al. (2017). Double gold activation of 1-ethynyl-2-(phenylethynyl)benzene toward 5-exo-dig and 6-endo-dig cyclization reactions. *Chem. Eur. J.* 23 (54): 13360–13368.
- 26 Villegas-Escobar, N., Schaefer, H.F., and Toro-Labbé, A. (2020). Formation of formic acid derivatives through activation and hydroboration of  $\text{CO}_2$  by low-valent group 14 (Si, Ge, Sn, Pb) catalysts. *J. Phys. Chem. A* 124 (6): 1121–1133.
- 27 Hernández Mancera, J.P., Núñez-Zarur, F., Gutiérrez-Oliva, S. et al. (2020). Diels–Alder reaction mechanisms of substituted chiral anthracene: a theoretical study based on the reaction force and reaction electronic flux. *J. Comput. Chem.* 41 (23): 2022–2032.

- 28 Guzmán-Angel, D., Gutiérrez-Oliva, S., and Toro-Labbé, A. (2019). Hydrogenation and hydration of carbon dioxide: a detailed characterization of the reaction mechanisms based on the reaction force and reaction electronic flux analyses. *J. Mol. Model.* 25 (1): 16.
- 29 Herrera, B. and Toro-Labbé, A. (2007). The role of reaction force and chemical potential in characterizing the mechanism of double proton transfer in the adenine-uracil complex. *J. Phys. Chem. A* 111 (26): 5921–5926.
- 30 Duarte, F. and Toro-Labbé, A. (2011). The mechanism of H<sub>2</sub> activation by (amino)carbenes. *J. Phys. Chem. A* 115 (14): 3050–3059.
- 31 Martínez-Araya, J.I., Quijada, R., and Toro-Labbé, A. (2012). The mechanism of ethylene polymerization reaction catalyzed by group IVB metallocenes. A rational analysis through the use of reaction force. *J. Phys. Chem. C* 116 (40): 21318–21325.
- 32 Martínez, J. and Toro-Labbé, A. (2009). The reaction force. A scalar property to characterize reaction mechanisms. *J. Math. Chem.* 45 (4): 911–927.
- 33 Politzer, P., Toro-Labbé, A., Gutiérrez-Oliva, S., and Murray, J.S. (2012). Perspectives on the reaction force. In: *Advances in Quantum Chemistry*, (ed. E.J. Brändas) vol. 64, 189–209. Academic Press.
- 34 Gutiérrez-Oliva, S., Herrera, B., and Toro-Labbé, A. (2018). An extension of the Marcus equation: the Marcus potential energy function. *J. Mol. Model.* 24: 104.
- 35 Cerón, M.L., Echegaray, E., Gutiérrez-Oliva, S. et al. (2011). The reaction electronic flux in chemical reactions. *Sci. China Chem.* 54 (12): 1982–1988.
- 36 Vogt-Geisse, S. and Toro-Labbé, A. (2016). Chemical potential and reaction electronic flux in symmetry controlled reactions. *J. Comput. Chem.* 37 (19): 1794–1800.
- 37 Echegaray, E. and Toro-Labbé, A. (2008). Reaction electronic flux: a new concept to get insights into reaction mechanisms. Study of model symmetric nucleophilic substitutions. *J. Phys. Chem. A* 112 (46): 11801–11807.
- 38 Parr, R.G. and Yang, W. (1989). *Density-Functional Theory of Atoms and Molecules*. New York: Oxford University Press.
- 39 Geerlings, P., De Proft, F., and Langenaeker, W. (2003). Conceptual density functional theory. *Chem. Rev.* 103 (5): 1793–1874.
- 40 Parr, R.G., Donnelly, R.A., Levy, M., and Palke, W.E. (2003). Electronegativity: the density functional viewpoint. *J. Chem. Phys.* 68 (8): 3801–3807.
- 41 Janak, J.F. (1978). Proof that  $\frac{\partial e}{\partial n_i} = \epsilon$  in density-functional theory. *Phys. Rev. B* 18: 7165–7168.
- 42 Koopmans, T. (1934). Über die Zuordnung von Wellenfunktionen und Eigenwerten zu den Einzelnen Elektronen Eines Atoms. *Physica* 1 (1–6): 104–113.
- 43 Matute, R.A., Pérez, P., Chamorro, E. et al. (2018). Reaction electronic flux perspective on the mechanism of the Zimmerman Di- $\pi$ -methane rearrangement. *J. Org. Chem.* 83 (11): 5969–5974.
- 44 Vogt-Geisse, S. and Toro-Labbé, A. (2009). The mechanism of the interstellar isomerization reaction  $\text{HOC}^+ \rightarrow \text{HCO}^+$  catalyzed by H<sub>2</sub>: new insights from the reaction electronic flux. *J. Chem. Phys.* 130 (24): 244308. Gutiérrez-Oliva, Díaz and Toro-Labbé in., (Editors)

- 45 Gutiérrez-Oliva, S., Díaz, S., and Toro-Labbé, A. (2021). Chemical reactivity in confined systems: theory, modelling and applications. In: *Unveiling the Mysterious Mechanisms of Chemical Reactions*, Chapter 5 (ed. P.K. Chattaraj and D. Chakraborty). Wiley. 81–98.
- 46 Ortega, D.E., Gutiérrez-Oliva, S., Tantillo, D.J., and Toro-Labbé, A. (2015). A detailed analysis of the mechanism of a carbocationic triple shift rearrangement. *Phys. Chem. Chem. Phys.* 17: 9771–9779.

## 24

# Application of Reactivity Indices in the Study of Polar Diels–Alder Reactions

Luis R. Domingo and Mar Ríos-Gutiérrez

University of Valencia, Department of Organic Chemistry, Dr. Moliner 50, Burjassot, Valencia E-46100, Spain

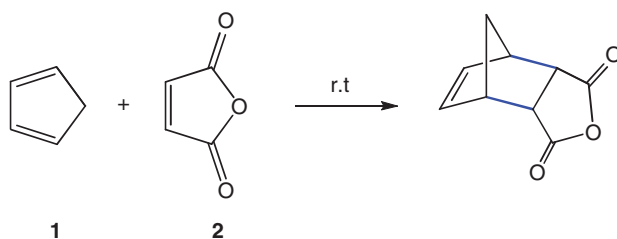
### 24.1 Introduction

After the establishment of the mechanism of polar Diels–Alder (P-DA) reactions in 2009, the use of conceptual density functional theory (CDFT)-based electrophilicity  $\omega$  index and Domingo's empirical nucleophilicity  $N$  index has become a powerful tool in organic chemistry for the study of polar organic reactions. On the other hand, the proposal of the Parr functions in 2013 as an estimation of the Fukui functions in CDFT permitted the study of the regio- and chemoselectivity in polar reactions. Despite the nucleophilicity  $N$  index is not a CDFT index per se, the analysis of these CDFT-based reactivity indices, easily accessible for experimentalists, are today a valuable tool in organic chemistry to study the reactivity. In this chapter, the application of these reactivity indices in the study of experimental P-DA reactions is presented.

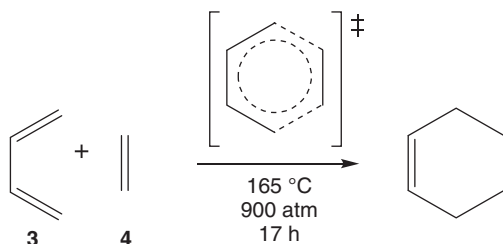
### 24.2 The Diels–Alder Reaction. The Polar Mechanism

The Diels–Alder (DA) reaction between a conjugated diene and an ethylene derivative to yield a cyclohexene, reported for the first time by Diels and Alder in 1928 [1], is one of the most studied organic reactions from a synthetic as well as a theoretical viewpoint (see Scheme 24.1) [2, 3].

The DA reaction between butadiene **3** and ethylene **4**, inadequately classified by Woodward and Hoffmann as a “pericyclic” reaction in 1969 [4], was chosen as the paradigm of DA reactions (see Scheme 24.2) [5]. However, while the experimental DA reaction between cyclopentadiene (Cp, **1**) and maleic anhydride **2** takes place easily at room temperature (see Scheme 24.1) [1], the DA reaction between butadiene **3** and ethylene **4** does not take place easily in the laboratory (see Scheme 24.2); it must be forced to take place: after 17 hours at 165 °C and 900 atmospheres, it gives a 78% yield [6].



**Scheme 24.1** DA reaction between cyclopentadiene (Cp) **1** and maleic anhydride **2** reported in 1928 by O. Diels and K. Alder.



**Scheme 24.2** Proposed pericyclic mechanism for the DA reaction between butadiene **3** and ethylene **4**.

Recently, a molecular electron density theory (MEDT) [7] study of the five reactions classified by Woodward and Hoffmann as “pericyclic” in 1969 proved that the bonding changes along these hydrocarbon reactions are non-concerted [8].

After studying numerous experimental DA reactions during 1995–2009, the very good correlation found between the activation energy and the global electron density transfer (GEDT) [9] for a series of DA reactions between Cp **1** and 12 ethylenes of increased electrophilicity,  $R^2 = 0.89$ , made it possible to establish the P-DA mechanism, followed by most experimental reactions [10, 11]. That study allowed establishing a very good correlation between the increase of the electrophilicity  $\omega$  index [12] of the ethylenes and the reduction of the activation barrier associated with these DA reactions ( $R^2 = 0.92$ ) (see Figure 24.1) [10]. Thus, while non-polar Diels–Alder (N-DA) reactions do not take place easily in the laboratory, the feasibility of P-DA reactions increases with the nucleophilic character of the diene and the electrophilic character of the ethylene, or vice versa [10]. Afterward, the analysis of the electrophilicity [12]  $\omega$  and nucleophilicity [13]  $N$  indices became an effective tool for the study of reactivity in cycloaddition reactions [14–16].

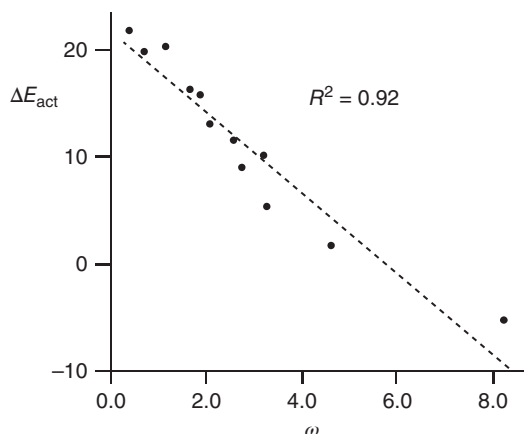
### 24.3 The Electrophilicity $\omega$ and Nucleophilicity $N$ Indices in the Study of P-DA Reactions

The electrophilicity  $\omega$  index [12], proposed in 1999 by Parr, gives a measure of the energy stabilization of a molecule when it acquires an additional amount of electron density from the environment. It is given by the simple expression:

$$\omega = \frac{\mu^2}{2\eta} \quad (24.1)$$



**Figure 24.1** Plot of the activation barriers ( $\Delta E_{\text{act}}$  in kcal mol<sup>-1</sup>) vs. the electrophilicity  $\omega$  index of the ethylenes, in eV,  $R^2 = 0.92$ , for the DA reactions between Cp **1** and the substituted ethylene series of increased electrophilic character.



where  $\mu$  is the electronic chemical potential [17] and  $\eta$  is the chemical hardness [18]. Thus, a good electrophile is a species characterized by a high  $|\mu|$  value and a low  $\eta$  value. The electronic chemical potential  $\mu$  and the chemical hardness  $\eta$  are expressed as  $\mu = (E_{\text{HOMO}} + E_{\text{LUMO}})/2$  and as  $\eta = (E_{\text{LUMO}} - E_{\text{HOMO}})$ . Note that these energies are considered only as an approach to the molecular ionization potential and electron affinity.

A comprehensive study carried out in 2002 on the electrophilicity  $\omega$  of a series of reagents participating in DA reactions allowed establishing a single electrophilicity  $\omega$  scale, which allowed the classification of organic molecules as strong electrophiles with  $\omega \geq 1.5$  eV, moderate electrophiles with  $0.8 \leq \omega < 1.5$  eV and marginal electrophiles with  $\omega < 0.8$  eV (see Table 24.1) [19]. Note that only strong electrophiles work experimentally.

For the short series of marginal electrophiles **4**, **14–16** given in Table 24.1, a good correlation between the inverse of the electrophilicity  $\omega$  index and the expected nucleophilicity was found; i.e. for these marginal electrophilic species, the less electrophilic they are, the more nucleophilic. Thus, for the series of simple molecules given in Table 24.1, a good correlation between the difference of electrophilicity  $\Delta\omega$  between the reagents and the feasibility of the DA reaction was established; i.e. the higher the  $\Delta\omega$ , the faster the DA reaction [19]. Hence, the high  $\Delta\omega$  value found for the reaction between Cp **1** and maleic anhydride **2**, experimentally reported by Diels and Alder in 1928 (see Scheme 24.1) [1],  $\Delta\omega = 2.51$  eV, accounts for the feasibility of this DA reaction, which contrasts with the DA reaction between butadiene **3** and ethylene **4**,  $\Delta\omega = 0.32$  eV, chosen by Woodward and Hoffmann as the reaction model of DA reactions (see Scheme 24.2) [4].

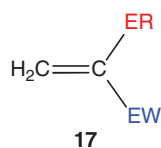
While  $\Delta\omega$  allowed explaining the reactivity in DA reactions involving simple molecules, it fails in the study of DA reactions involving complex molecules having several functional groups of different electronic nature. This is the case of the captodative ethylenes **17** given in Scheme 24.3, amphiphilic species concurrently displaying both electrophilic and nucleophilic behaviors [13].

In 2008, Domingo proposed an empirical (relative) nucleophilicity  $N$  index for closed-shell organic molecules based on the HOMO energies,  $E_{\text{HOMO}}$ , obtained within the Kohn–Sham scheme [20], defined as [13]:

$$N = E_{\text{HOMO}}(\text{Nu}) - E_{\text{HOMO}}(\text{TCE}) \quad (24.2)$$

**Table 24.1** B3LYP/6-31G(d) electrophilicity  $\omega$  index, in eV, of some common reagents involved in DA reactions.

Molecules	$\omega$
<i>Strong electrophiles</i>	
(CN) <sub>2</sub> C=C(CN) <sub>2</sub> <b>5</b>	5.96
Maleic anhydride <b>2</b>	3.24
CH <sub>2</sub> =CHCHO—BH <sub>3</sub> <b>6</b>	3.20
CH <sub>2</sub> =C(CN) <sub>2</sub> <b>7</b>	2.82
CH <sub>3</sub> O <sub>2</sub> C≡CCO <sub>2</sub> CH <sub>3</sub> <b>8</b>	2.27
CH <sub>2</sub> =CHNO <sub>2</sub> <b>9</b>	2.61
CH <sub>2</sub> =CHCHO <b>10</b>	1.84
CH <sub>2</sub> =CHCN <b>11</b>	1.74
CH <sub>2</sub> =CHCO <sub>2</sub> CH <sub>3</sub> <b>12</b>	1.51
<i>Moderate electrophiles</i>	
CH <sub>2</sub> =CH—CH=CH <sub>2</sub> <b>3</b>	1.05
CH <sub>2</sub> =CH—C(OSi(CH <sub>3</sub> ) <sub>3</sub> )=CH <sub>2</sub> <b>13</b>	0.88
Cyclopentadiene <b>1</b>	0.83
<i>Marginal electrophiles (nucleophiles)</i>	
CH <sub>2</sub> =CH <sub>2</sub> <b>4</b>	0.73
CH≡CH <b>14</b>	0.54
CH <sub>2</sub> =CHOCH <sub>3</sub> <b>15</b>	0.42
CH <sub>2</sub> =CHN(CH <sub>3</sub> ) <sub>2</sub> <b>16</b>	0.27



Captodative ethylenes

ER groups =  $-\text{N}(\text{CH}_3)_2$ ,  $-\text{OCOPh}$ ,  $-\text{OCOCH}_3$   
 EW groups =  $-\text{NO}$ ,  $-\text{COCH}_3$ ,  $-\text{COOCH}_3$ ,  $\text{CN}$

**Scheme 24.3** Captodative ethylenes **17** having both electrophilic and nucleophilic behaviors.

The nucleophilicity  $N$  index was referred to tetracyanoethylene (TCE) **5**, which is the most electrophilic neutral species in Table 24.1.

Analysis of a series of common nucleophilic species participating in polar organic reactions allowed a further classification of organic molecules as strong nucleophiles,  $N \geq 3.0$  eV, moderate nucleophiles,  $2.0 \leq N < 3.0$  eV, and marginal nucleophiles,  $N < 2.0$  eV (see Table 24.2) [21]. As can be seen, butadiene **3**, with an

**Table 24.2** B3LYP/6-31G(d) nucleophilicity  $N$  index, in eV, of some common nucleophilic reagents involved in DA reactions.

Molecule	$N$
<i>Strong nucleophiles</i>	
$\text{CH}_2=\text{CHN}(\text{CH}_3)_2$ <b>16</b>	4.28
$\text{CH}_2=\text{C}(\text{OCH}_3)_2$ <b>18</b>	3.51
Cyclopentadiene <b>1</b>	3.37
$\text{CH}_2=\text{CHOCH}_3$ <b>15</b>	3.18
$(\text{CH}_3)_2\text{C}=\text{C}(\text{CH}_3)_2$ <b>19</b>	3.35
<i>Moderate nucleophiles</i>	
$\text{CH}_2=\text{CH}-\text{CH}=\text{CH}_2$ <b>3</b>	2.93
$\text{CH}_2=\text{C}(\text{CH}_3)_2$ <b>20</b>	2.60
$\text{CH}_3\text{C}\equiv\text{CCH}_3$ <b>21</b>	2.57
$\text{CH}_2=\text{CHCH}_3$ <b>22</b>	2.32
<i>Marginal nucleophiles</i>	
$\text{CH}_2=\text{CH}_2$ <b>4</b>	1.86
$\text{CH}\equiv\text{CH}$ <b>14</b>	1.45

$N = 2.93$  eV, is found on the borderline of moderate nucleophiles, while Cp **1**, with an  $N = 3.37$  eV, is classified as a strong nucleophile participating in P-DA reactions toward strong electrophilic ethylenes. On the other hand, ethylene **4**,  $\omega = 0.73$  eV, and acetylene **14**,  $\omega = 0.54$  eV, are classified both as marginal electrophiles (see Table 24.1) and as marginal nucleophiles,  $N = 1.86$  and 1.45 eV, respectively (see Table 24.2). Consequently, neither ethylene **4** nor acetylene **14** can participate in P-DA reactions.

Captodative ethylene **17**, having one of the most electron-withdrawing (EW) groups, i.e. the nitroso NO, and one of the most electron-releasing (ER) groups, the amino  $-\text{N}(\text{CH}_3)_2$  (see Scheme 24.3), presents a high electrophilicity  $\omega$  index, 2.52 eV, being classified as a strong electrophile, and a high nucleophilicity  $N$  index, 3.29 eV, being also classified as a strong nucleophile, in clear agreement with its expected amphiphilic reactivity [13].

## 24.4 P-DA Reactions of Forward (FEDF) and Reverse (REDF) Electron Density Flux

Based on the frontier molecular orbital (FMO) theory [22], in 1972, Sustmann and coworker classified cycloaddition reactions into three types [23]: (i) in *type-I* (generally referred to as “*normal electron demand [NED]*”), the dominant FMO interaction is that between  $\text{HOMO}_{\text{TAC}}$  and  $\text{LUMO}_{\text{ethylene}}$ ; (ii) in *type-II*, FMO

energies of the TAC and the ethylene derivative are similar, so that both have to be considered; and finally, (iii) *type-III* cycloadditions (generally referred to as “*inverse electron demand [IED]*”) are dominated by interactions between  $\text{LUMO}_{\text{TAC}}$  and  $\text{HOMO}_{\text{ethylene}}$ . Although this classification was widely accepted [24], many authors have emphasized that it is sometimes confusing, leading to interpretations contrary to the experimental observations [25–28].

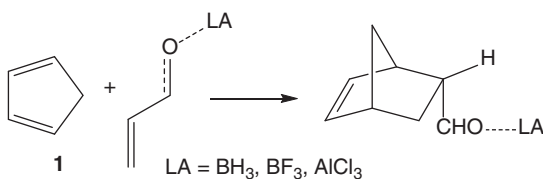
At the zwitterionic transition state structures (TSS) of P-DA reactions, the electron density always fluxes from the nucleophilic species to the electrophilic one. Analysis of the GEDT [9] at the TSS unambiguously determines the direction of the electron density flux in a P-DA reaction. On the other hand, CDFT reactivity indices such as the electronic chemical potential  $\mu$ , [17] the electrophilicity  $\omega$ , [12] and the nucleophilicity  $N$  [13] indices also permit to predict the direction of the electron density flux in polar reactions.

Due to the significance of the characterization of the direction of the electron density flux in P-DA reactions, they were recently classified as reactions of *forward electron density flux* (FEDF), when the electron density fluxes from a nucleophilic diene toward an electrophilic ethylene, and reactions of *reverse electron density flux* (REDF), when the electron density fluxes from a nucleophilic ethylene toward an electrophilic diene [29, 30]. In  $[m + n]$  cycloadditions, FEDF reactions are those in which the more unsaturated molecule is the nucleophile; i.e. the diene in P-DA reactions, a  $[4 + 2]$  cycloaddition reaction. As many  $[3 + 2]$  cycloaddition (32CA) reactions have a low polar character, cycloaddition reactions having GEDT values lower than 0.05 e have been classified as *null electron density flux* (NEDF) reactions [30].

Thus, the N-DA reaction between butadiene **3** and ethylene **4**, which had been classified as a NED DA reaction, should be classified as an NEDF DA reaction as it presents a  $\text{GEDT} = 0.0 \text{ e}$  [9].

## 24.5 Lewis Acid–Catalyzed P-DA Reactions of FEDF

Lewis acid (LA) catalysts play an important role in cycloaddition reactions since, in addition to the expected acceleration of the reactions, they notably increase selectivities, yielding in most cases only one cycloadduct. Analysis of the electrophilicity  $\omega$  index at the corresponding LA complexes allows explaining the role of the LA catalyst in P-DA reactions [10, 31, 32]. The LA-catalyzed P-DA reaction between Cp **1** and acrolein **10** is shown in Scheme 24.4, while the electrophilicity  $\omega$  and nucleophilicity  $N$  indices of the reagents are given in Table 24.3.



**Scheme 24.4** LA-catalyzed P-DA reactions between Cp **1** and acrolein **10**.

**Table 24.3** B3LYP/6-31G(d) electrophilicity  $\omega$  and nucleophilicity  $N$  indices, in eV, for the reagents involved in the LA-catalyzed P-DA reactions between Cp **1** and acrolein **10** given in Scheme 24.4.

Molecule	$\omega$	$N$
Acrolein–AlCl <sub>3</sub> <b>23</b>	4.61	1.24
Acrolein–BF <sub>3</sub> <b>24</b>	3.29	0.00
Acrolein–BH <sub>3</sub> <b>25</b>	3.20	1.92
Acrolein <b>10</b>	1.84	2.13
Cyclopentadiene <b>1</b>	0.83	3.37

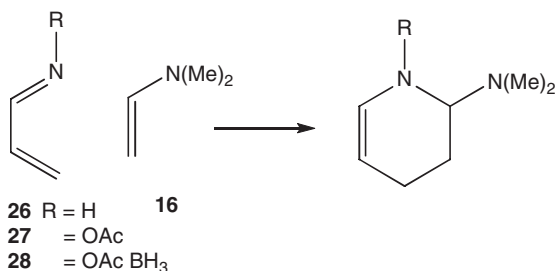
As commented on earlier, P-DA reactions require the participation of strong electrophiles and strong nucleophiles. The strong nucleophilic character of Cp **1**,  $N = 3.37$  eV, allows its participation in many P-DA reactions toward strong electrophiles without any electronic activation [10]. The electrophilicity  $\omega$  index of acrolein **10**, 1.84 eV, allows its classification as a strong electrophile, favoring the corresponding P-DA reaction of FEDF. Coordination of BH<sub>3</sub> LA to the carbonyl oxygen atom of acrolein **10** notably increases the electrophilicity  $\omega$  index of the corresponding acrolein–BH<sub>3</sub> complex **25**, 3.20 eV [10, 31]. As the acidic character of the LA increases, the electrophilicity  $\omega$  index of the corresponding complex increases, accelerating the P-DA reaction (see Table 24.3). Thus, while the DA reaction between Cp **1** and acrolein **10** must be heated, the LA-catalyzed P-DA reactions take place at room temperature, even at  $-78^\circ\text{C}$ .

A recent MEDT study on LA-catalyzed DA reactions has emphasized that while the coordination of the LA to the electrophilic ethylene does not substantially modify the electronic structure of the corresponding complex, its electrophilicity  $\omega$  index accounts for its reactivity in polar reactions [31].

## 24.6 P-DA Reactions of REDF. The H-DA Reactions

The synthetic usefulness of DA reactions, besides the substitution in both the diene and the ethylene, also arises from the exchange of one or more carbon atoms of the unsaturated compounds by a heteroatom such as O, N, S, and P, thus enabling the synthesis of heterocyclic compounds through the well-known hetero Diels–Alder (H-DA) reactions.

Thus, for instance, the aza Diels–Alder (A-DA) reactions of 1-aza-1,3-butadienes (1ABD) are a valuable methodology for the synthesis of six-membered nitrogen heterocycles (see Scheme 24.5). Unfortunately, A-DA reactions of the simplest 1ABD **26** are rarely observed due to its moderate nucleophilic and electrophilic character,  $N = 2.17$  eV and  $\omega = 1.47$  eV (see Table 24.4). However, this problem can be avoided by introducing either EW or ER groups into the nitrogen atom [33].



**Scheme 24.5** A-DA reactions of 1ABDs **26–28** with dimethylvinylamine **16**.

**Table 24.4** B3LYP/6-31G(d) electronic chemical potential  $\mu$ , chemical hardness  $\eta$ , global electrophilicity  $\omega$  and global nucleophilicity  $N$  indices, in eV, for the reagents involved in the A-DA of 1ABD derivatives.

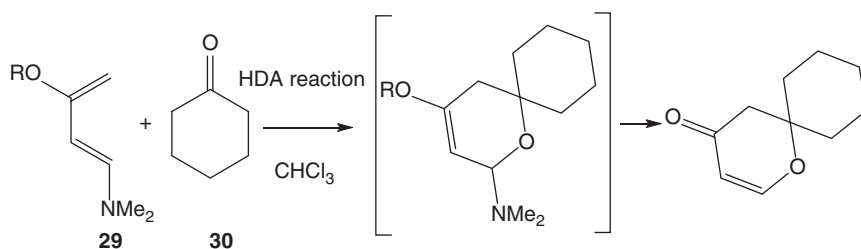
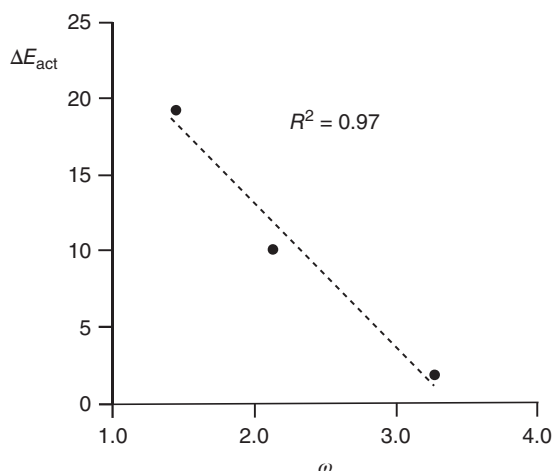
Molecule	$\mu$	$\eta$	$\omega$	$N$
CH <sub>2</sub> =CH—CH=NOAc BH <sub>3</sub> <b>28</b>	−5.05	3.93	3.24	2.11
CH <sub>2</sub> =CH—CH=NOAc <b>27</b>	−4.42	4.57	2.14	2.42
CH <sub>2</sub> =CH—CH=NH <b>26</b>	−4.09	5.72	1.47	2.17
CH <sub>2</sub> =CH—CH=CH <sub>2</sub> <b>4</b>	−3.42	5.62	1.05	2.89
CH <sub>2</sub> =CHN(CH <sub>3</sub> ) <sub>2</sub> <b>16</b>	−1.87	6.50	0.27	4.00

Thus, while the A-DA reaction of the simplest 1ABD **26** with *N,N*-dimethylvinylamine **16**, one of the most nucleophilic ethylenes,  $N = 4.00$  eV, (see Table 24.2), presents a high activation energy, 19.5 kcal mol<sup>−1</sup>, that of acetyl derivative **27** presents an activation energy of 10.2 kcal mol<sup>−1</sup>. As expected, when acetyl derivative **27** was coordinated to the BH<sub>3</sub> LA, the activation energy associated to the corresponding LA-catalyzed A-DA reaction involving complex **28** was found to be only 2.1 kcal mol<sup>−1</sup> [34]. Note that these A-DA reactions are classified as REDF reactions in which the diene acts as the electrophilic species.

A good correlation between the electrophilicity  $\omega$  index of these 1ABD derivatives and the activation energies of the corresponding A-DA reactions can be established (see Figure 24.2). An appealing conclusion can be drawn from this short series of A-DA reactions: despite the supernucleophilic character [35] of dimethylvinylamine **16**,  $N \geq 4.0$  eV, the H-DA reaction with the moderate electrophile 1ABD **26**,  $\omega = 1.47$  eV, presents a high activation energy, 19.5 kcal mol<sup>−1</sup>. This behavior supports the aforementioned proposal that at least one of the two reagents participating in a polar reaction should be a strong electrophile.

In 2002, Huang and Rawal reported the oxa Diels–Alder (O-DA) reactions of carbonyl compounds promoted by formation of hydrogen bonds (HBs) (see Scheme 24.6) [36]. These authors found that these O-DA reactions in chloroform, HCCl<sub>3</sub>, were 10 times faster than those in the more polar solvent acetonitrile, CH<sub>3</sub>CN.

**Figure 24.2** Plot of the activation energies,  $\Delta E_{\text{act}}$  in kcal mol<sup>-1</sup>, of the A-DA reactions between 1ABD derivatives **26–28** and dimethylvinilamine **16**, vs. the electrophilicity  $\omega$  index, in eV, of 1ABDs.



**Scheme 24.6** O-DA reactions of cyclohexanone **30** promoted by formation of hydrogen bonds.

A further theoretical study of the O-DA reaction between diene **29** (R=Me), a strong nucleophile, and acetone emphasized that the formation of one or two non-classical HBs between the hydrogen of chloroform and the carbonyl oxygen of acetone reduced the activation energy by 5.1 (one HB) and 9.0 (two HBs) kcal mol<sup>-1</sup>, in complete agreement with the experimental outcomes [37].

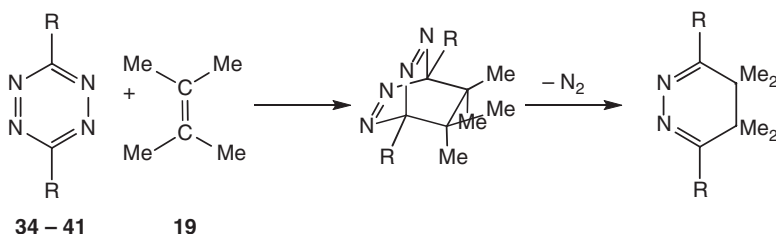
Analysis of the nucleophilicity  $N$  and electrophilicity  $\omega$  indices of the reagents allows explaining the experimental enhanced reactivity of cyclohexanone **30** by HB formation. While diene **29** is a strong nucleophile,  $N = 4.35$  eV, cyclohexanone **30** is classified as a moderate electrophile,  $\omega = 0.95$  eV. Despite the supernucleophilic character of diene **29**, cyclohexanone **30** is not electrophilic enough to favor this O-DA reaction. However, when one or two molecules of chloroform are bound by HBs to the carbonyl oxygen of cyclohexanone **30**, a noticeable increase of the electrophilicity of the corresponding hetero ethylenes is observed,  $\omega = 1.27$  eV (one HB) and 1.53 eV (two HBs) (see Table 24.5), respectively. This behavior accounts for the enhanced reactivity experimentally found by Huang and Rawal [36].

Unlike butadiene **3**, benzene **33** is a poor diene participating in DA reactions due to its inherent aromatic character [38, 39]. However, substitution of carbon atoms on benzene by nitrogen ones favors the corresponding A-DA reaction, in such a manner that tetrazine **34** easily participates in P-DA reactions of REDF [39].

**Table 24.5** B3LYP/6-31G(d) electronic chemical potential  $\mu$ , chemical hardness  $\eta$ , global electrophilicity  $\omega$  and global nucleophilicity  $N$  indices, in eV, for cyclohexanone **30** and cyclohexanone bound to one and two discrete molecules of chloroform by HBs.

Molecule	$\mu$	$\eta$	$\omega$	$N$
Cyclohexanone-2 HCCl <sub>3</sub> <b>32</b>	-4.34	6.14	1.53	1.71
Cyclohexanone-1 HCCl <sub>3</sub> <b>31</b>	-3.93	6.07	1.27	2.16
Cyclohexanone <b>30</b>	-3.35	6.05	0.93	2.74
TBSO <b>29</b>	-2.28	5.00	0.52	4.35

The reactions of seven disubstituted tetrazines **35–41** of increased electrophilic character with nucleophilic tetramethyl ethylene **19** was recently studied within the MEDT [39]. These reactions are domino processes comprising an A-DA reaction followed by an extrusion of molecular nitrogen, yielding a dihydropyridazine. Analysis of the CDFT indices showed the increase of the electrophilicity  $\omega$  and the decrease of the nucleophilicity  $N$  of tetrazines with the increase of the EW character of the substituent  $R$  (see Table 24.7). A very good correlation between the GEDT at the TSs and the activation enthalpies for these A-DA reactions of REDF was found [39] (Scheme 24.7; Table 24.6).

**Scheme 24.7** Domino reactions of disubstituted tetrazines **34–41** with tetramethyl ethylene **19**.

A good correlation between the electrophilicity  $\omega$  indices of tetrazines **34–41** and the activation energies could also be established,  $R = 0.91$  (see Figure 24.3), in such a manner that the increase of the electrophilicity  $\omega$  index of tetrazines **34–41** is accompanied by a decrease of the activation energy. Thus, while the reactions of tetrazines **40** ( $R = \text{OMe}$ ) and **41** ( $R = \text{Me}$ ), substituted by two ER groups, present high activation energies, ca.  $20 \text{ kcal mol}^{-1}$ , that involving tetrazine **35**, containing two strong EW  $\text{NO}_2$  groups, presents an unappreciable barrier of  $1.1 \text{ kcal mol}^{-1}$ .

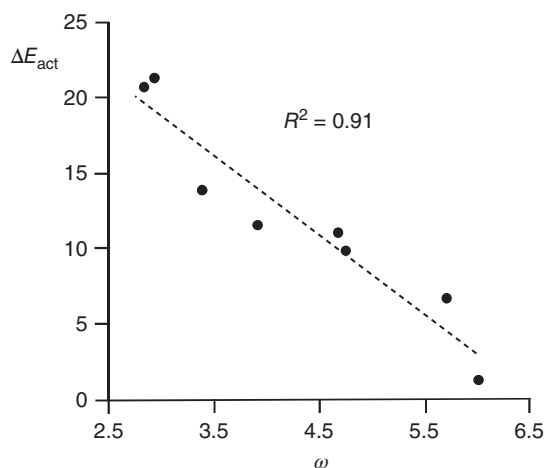
## 24.7 P-DA Reactions Between Electrophilic Species. A Challenge for the FMO Theory

In 2004, Spino et al. reported an experimental study of the DA reactions of electrophilic diene **42** with a wide variety of nucleophilic ethylenes, such as **43**, as well



**Table 24.6** B3LYP/6-31G(d) electronic chemical potential  $\mu$ , chemical hardness  $\eta$ , global electrophilicity  $\omega$  and global nucleophilicity  $N$  indices, in eV, for disubstituted tetrazines **34–41** and tetramethyl ethylene **19**.

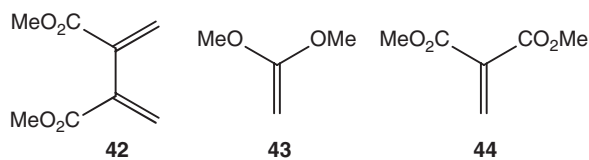
Molecule	R	$\mu$	$\eta$	$\omega$	N
<b>35</b>	NO <sub>2</sub>	-6.59	3.63	5.99	0.72
<b>36</b>	COCF <sub>3</sub>	-6.09	3.26	5.69	1.40
<b>37</b>	CF <sub>3</sub>	-5.85	3.66	4.68	1.44
<b>38</b>	CHO	-5.71	3.44	4.74	1.70
<b>39</b>	COMe	-5.26	3.53	3.91	2.10
<b>34</b>	H	-4.98	3.67	3.38	2.30
<b>40</b>	OMe	-4.63	3.65	2.93	2.67
<b>41</b>	Me	-4.50	3.58	2.83	2.83
(CH <sub>3</sub> ) <sub>2</sub> C=C(CH <sub>3</sub> ) <sub>2</sub> <b>19</b>		-2.46	6.94	0.43	3.20

**Figure 24.3** Plot of the activation enthalpies,  $\Delta H_{\text{act}}$  in kcal mol<sup>-1</sup>, of the A-DA reactions between disubstituted tetrazines **34–41** and tetramethyl ethylene **19** vs. the electrophilicity  $\omega$  index, in eV, of tetrazines.

as electrophilic ethylenes, such as **44**, finding that the reactivity of electrophilic ethylene **44** with electrophilic diene **42** was similar to that of nucleophilic ethylene **43** (see Scheme 24.8) [27].

FMO theory [22] was used to predict the reactivity of these reagents in a DA reaction. Spino et al. concluded that, *in the NED DA reaction, FMO theory could predict the relative reactivity, while in the case of the IED one, it could not* [27].

A theoretical study of the experimental Spino's P-DA reactions showed that the activation energy associated with the DA reaction of diene **42** with nucleophilic ethylene **43**, 15.3 kcal mol<sup>-1</sup>, was found only 1.0 kcal mol<sup>-1</sup> below that involving electrophilic ethylene **44**, 16.3 kcal mol<sup>-1</sup> [28]. Analysis of the electrophilicity  $\omega$  and nucleophilicity  $N$  indices allowed explaining the behaviors of these P-DA reactions. The reactivity indices of **42**, **43**, and **44** are given in Table 24.7.



**Scheme 24.8** P-DA reactions of electrophilic diene **42** with nucleophilic **43** and electrophilic **44** ethylenes.

**Table 24.7** B3LYP/6-31G(d) electronic chemical potential  $\mu$ , chemical hardness  $\eta$ , global electrophilicity  $\omega$  and global nucleophilicity  $N$  indices, in eV, of diene **42** and ethylenes **43** and **44**.

Molecule	$\mu$	$\eta$	$\omega$	$N$
<b>44</b>	-4.58	5.81	1.81	1.64
<b>42</b>	-4.27	5.68	1.60	2.01
<b>42'</b>	-3.92	5.52	1.39	2.45
Butadiene <b>3</b>	-3.42	5.62	1.04	2.89
Ethylene <b>4</b>	-3.37	7.77	0.73	1.87
<b>43</b>	-1.97	7.28	0.27	3.52

Analysis of the reactivity indices of diene **42** indicates that it is a strong electrophile,  $\omega = 1.60$  eV, and, as expected, a moderate nucleophile,  $N = 2.01$  eV. As can be seen, disubstituted ethylene **44** is the most electrophilic species in Table 24.7,  $\omega = 1.81$  eV, being classified as a strong electrophile. On the other hand, disubstituted ethylene **43** is the most nucleophilic species of this series,  $N = 3.52$  eV, being classified as a strong nucleophile.

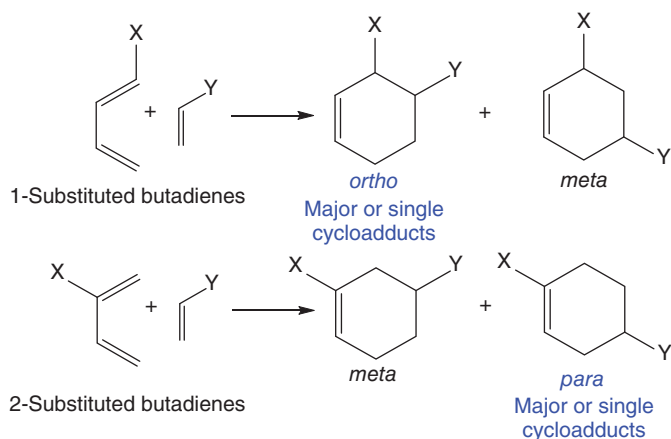
The DA reaction between electrophilic diene **42** and nucleophilic ethylene **43** has polar character, presenting an activation energy of ca. 9 kcal mol<sup>-1</sup> less than that associated to the N-DA of butadiene **3** with ethylene **4**, 24.8 kcal mol<sup>-1</sup> [9]. Analysis of the corresponding electronic chemical potentials  $\mu$  clearly indicates that the electron density will flux from nucleophilic ethylene **43** toward electrophilic diene **42**; the P-DA reaction being classified as an REDF reaction.

*What happens in the DA reaction between the two electrophilic species?* The 1,1-disubstituted ethylene **44**,  $\omega = 1.81$  eV, is more electrophilic than diene **42**,  $\omega = 1.60$  eV. On the other hand, diene **42**,  $N = 2.10$  eV, is less nucleophilic than butadiene **4**,  $N = 2.89$  eV, a nucleophilic species participating in P-DA reactions. The electrophilic behavior of diene **42** is a consequence of the presence of the two EW CO<sub>2</sub>Me groups in the diene system, which efficiently delocalizes the electron density transferred in polar processes of REDF. To realize this phenomenon efficiently, the CO<sub>2</sub>Me groups should be coplanar to the unsaturated molecules. Thus, when the two EW CO<sub>2</sub>Me groups are in a perpendicular conformation, the electrophilicity  $\omega$  index of diene **42'** decreases to 1.39 eV, and the nucleophilicity  $N$  index increases to 2.45 eV (see **42'** in Table 24.7). Consequently, the DA reaction

between diene **42'** and ethylene **44** will have polar character, in which ethylene **44** acts as a strong electrophile and diene **42'** acts as a moderate nucleophile. Thus, while the P-DA reaction of diene **42** with nucleophilic ethylene **43** is classified as an REDF reaction, that with strong electrophilic ethylene **44** is classified as FEDF.

## 24.8 Regioselectivity and Chemoselectivity in P-DA Reactions. The Parr Functions

The participation of non-symmetric reagents in P-DA reactions allows the formation of two regioisomeric cycloadducts (see Scheme 24.9). Generally, P-DA reactions of 1- or 2-substituted 1,3-butadienes are highly regioselective, yielding the formation of only of *ortho* or *meta* regioisomeric cycloadduct, respectively (see Scheme 24.9) [40].



**Scheme 24.9** Regioisomeric cycloadducts formed in P-DA reactions.

In addition, the presence of several unsaturated centers in an organic molecule makes the formation of structural isomeric cycloadducts possible. Frequently, P-DA reactions are also highly chemoselective, yielding the formation of only one structural isomeric cycloadduct.

### 24.8.1 The Parr Functions

A great number of bonding evolution theory (BET) [41] studies of cycloaddition reactions allowed Domingo to propose, in 2014, that along both non-polar and polar cycloaddition reactions the formation of new C—C single bonds takes place within the short range of 2.0–1.9 Å by the C-to-C coupling of two *pseudoradical* centers [42, 43] generated along the reaction path (see Figure 24.4) [9]. In polar reactions, the formation of these *pseudoradical* centers, which come from the depopulation of the C—C double bonds, is favored by the GEDT taking place from the nucleophilic

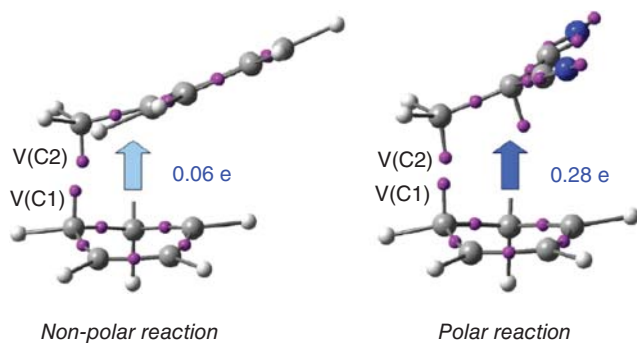


**Figure 24.4** Pseudoradical species involved in the C–C bond formation in N-DA and P-DA reactions. The blue arrows indicate the direction of the GEDT.

to the electrophilic species. In non-symmetric molecules, a non-symmetric distribution of the transferred electron density takes place at the two interacting frameworks. Thus, while at the nucleophile some atoms lose less electron density, in the electrophile some of them gather more electron density. These atoms correspond to the most nucleophilic and most electrophilic centers of the reactant molecules [9].

In case that an amount of electron density equivalent to one electron is transferred, the nucleophile becomes a radical cation, while the electrophile becomes a radical anion. Interestingly, analysis of the atomic spin density (ASD) distribution at the radical cation of the nucleophile and the radical anion of the electrophile provides a picture of the electron density distribution in both reagents when they approach each other along the reaction progress.

Based on these findings, in 2013, Domingo proposed the Parr functions  $P(\mathbf{r})$ , which are given by the following equations [44]:

$$P^-(\mathbf{r}) = \rho_s^{\text{rc}}(\mathbf{r}) \quad \text{for electrophilic attacks} \quad (24.3)$$

and

$$P^+(\mathbf{r}) = \rho_s^{\text{ra}}(\mathbf{r}) \quad \text{for nucleophilic attacks} \quad (24.4)$$

where,  $\rho_s^{\text{rc}}(\mathbf{r})$  is the ASD at the  $\mathbf{r}$  atom of the radical cation of a considered frozen molecule and  $\rho_s^{\text{ra}}(\mathbf{r})$  is the ASD at the  $\mathbf{r}$  atom of the radical anion. Each ASD gathered at the different atoms of the radical cation and the radical anion of a molecule provides the nucleophilic  $P_k^-$  and electrophilic  $P_k^+$  Parr functions of the neutral molecule.

The Parr functions can be understood as an estimation to the Fukui functions proposed in 1984 within CDFT [45]. The Fukui function  $f(\mathbf{r})$  represents the changes in electron density at a point  $\mathbf{r}$  with respect to the variation of the number of electrons  $N$  at a fixed external potential  $v(\mathbf{r})$ :

$$f(\mathbf{r}) = \left( \frac{\partial \rho(\mathbf{r})}{\partial N} \right)_{v(\mathbf{r})} \quad (24.5)$$

Although, in principle, the electron density of a neutral or  $N_{0 \pm 1 \text{electron}}$  molecule contains all information needed for the evaluation of the Fukui function, many

studies have been carried out by using the so-called finite difference method, proposed in 1986 by Yang and Mortier (YM) [46], in which the Fukui functions are approximated as:

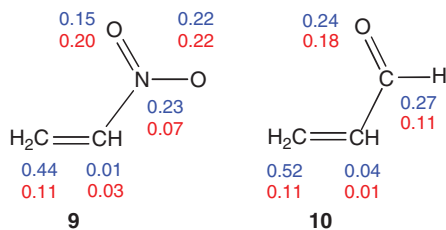
$$f^+(\mathbf{r}) \approx \rho_{N_{O+1}}(\mathbf{r}) - \rho_{N_O}(\mathbf{r}) \quad \text{for nucleophilic attacks} \quad (24.6)$$

and

$$f^+(\mathbf{r}) \approx \rho_{N_0}(\mathbf{r}) - \rho_{N_{0-1}}(\mathbf{r}) \quad \text{for electrophilic attacks} \quad (24.7)$$

where  $\rho_{N_0}$ ,  $\rho_{N_{0+1}}$ , and  $\rho_{N_{0-1}}$  are the atomic charges in the neutral, anionic, and cationic species.

A comparative analysis of the electrophilic  $P_k^+$  Parr functions and the YM electrophilic  $f_k^+$  Fukui functions of common reagents participating in P-DA reactions, such as nitroethylene **9** and acrolein **10** (see Scheme 24.10), have shown that YM Fukui functions do not account for the local reactivity of these species in P-DA reactions [14, 44]. Note that the conjugated ethylenic position is the most electrophilic center of these species, the corresponding P-DA reactions being completely chemo- and regioselective.



**Scheme 24.10** Electrophilic  $P_k^+$  Parr functions, in blue, and YM electrophilic  $f_k^+$  Fukui functions, in red, of nitroethylene **9** and acrolein **10**.

With the electrophilic  $P_k^+$  and nucleophilic  $P_k^-$  Parr functions at hand, the local electrophilicity [40]  $\omega_k$  and the local nucleophilicity [47]  $N_k$  indices can be expressed as follows [14]:

$$\omega_k = \omega P_k^+ \quad (24.8)$$

and

$$N_k = N P_k^- \quad (24.9)$$

Therefore, analysis of the Parr functions permits to characterize the most electrophilic and the most nucleophilic centers in a molecule. These centers are those with the highest electron density developed during the GEDT involved in polar processes.

### 24.8.2 Regioselectivity in P-DA Reactions

In polar reactions, the more favorable regioisomeric reaction path is that involving the two-center interaction between the most nucleophilic and electrophilic centers of the two interacting molecules [48]. Analysis of the Parr functions at the reagents allows characterizing these relevant centers. The electrophilic  $P_k^+$  and nucleophilic  $P_k^-$  Parr functions of four ethylene derivatives participating in polar cycloaddition reactions are shown in Figure 24.5. As can be seen, both the electrophilic, **10**, **9**, and **6**, and the nucleophilic, **15**, ethylenes have the most electrophilic and nucleophilic centers at the non-substituted carbon atoms.

In Figure 24.6, the nucleophilic  $P_k^-$  Parr functions of 1-methoxy-butadiene **45** and 2-methoxy-butadiene **46** are shown. As can be seen, 1-methoxy-butadiene **45** presents the most nucleophilic activation at the diene C4 carbon, while at 2-methoxy-butadiene **46** the most nucleophilic activation is at the diene C1 carbon. Consequently, the most favorable two-center nucleophilic/electrophilic interaction along a P-DA reaction involving 1-methoxy-butadiene **45** will take place between the C4 carbon of this diene and the non-substituted carbon of the electrophilic ethylene (see Figures 24.5 and 24.6), yielding the *ortho* cycloadduct, while in a P-DA reaction involving 2-methoxy-butadiene **46**, this two-center interaction will take place with the C1 carbon of this diene, yielding the *para* cycloadduct (see Scheme 24.9).

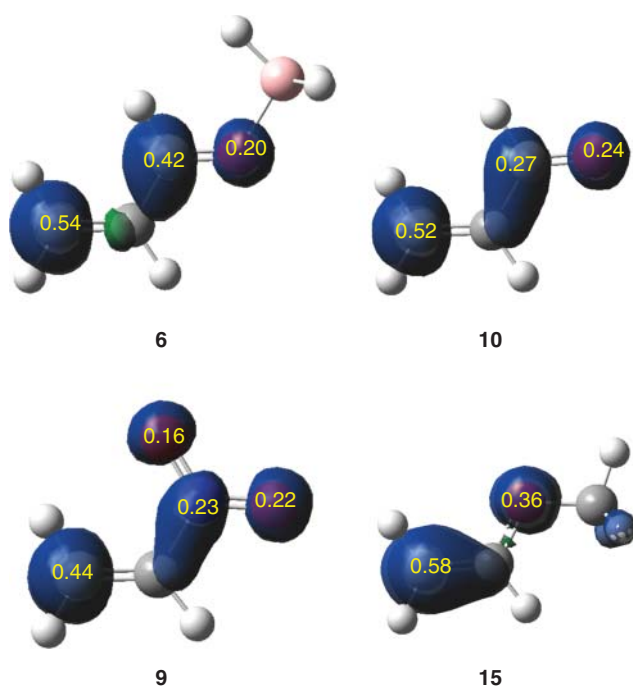
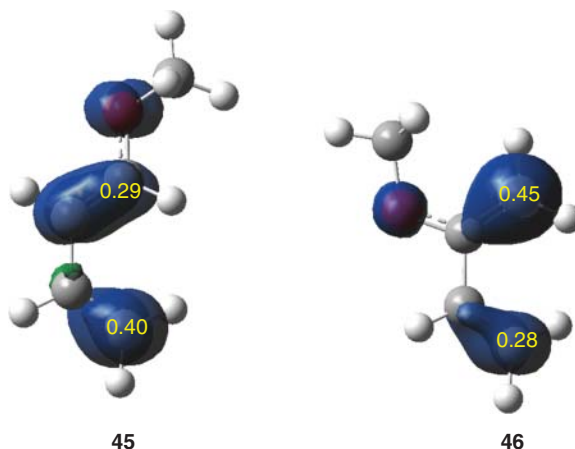


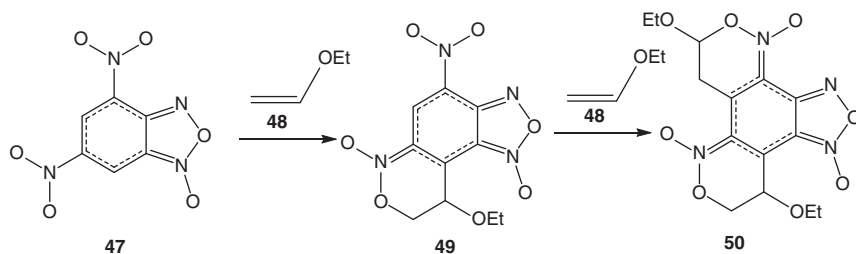
**Figure 24.5** 3D representations of the Mulliken ASD of the radical anions **6**<sup>•-</sup>, **9**<sup>•-</sup>, and **10**<sup>•-</sup>, and the radical cation **15**<sup>•+</sup>, together with the electrophilic  $P_k^+$  Parr functions of **6**, **9**, and **10**, and the nucleophilic  $P_k^-$  Parr functions of **15**.

**Figure 24.6** 3D representations of the Mulliken ASD of the radical cations **45**<sup>•+</sup> and **46**<sup>•+</sup>, together with the nucleophilic  $P_k^-$  Parr functions of 1-methoxy-butadiene **45** and a 2-methoxy-butadiene **46**.



### 24.8.3 Chemoselectivity in P-DA Reactions

In 1997, Terrier reported the P-DA reaction of 4,6-dinitrobenzofuroxan (DNBF, **47**) with ethyl vinyl ether **48**. The reaction of DNBF **47** with ethyl vinyl ether **48** (2 equiv) produced **49** exclusively (see Scheme 24.11) [49]. Using a large excess of the vinyl ether **48** afforded the adduct **50**.



**Scheme 24.11** Chemoselective P-DA reactions of DNBF **47** with vinyl ether **48**.

Analysis of the CDFT indices allows explaining the experimental outcomes. DNBF **47**,  $\omega = 5.46$  eV [50], is classified as a superelectrophile [51, 52], while vinyl ether **48**,  $N = 3.23$  eV, is a strong nucleophile. Consequently, the corresponding DA reaction will have a high polar character. Analysis of the electrophilic  $P_k^+$  Parr functions at DNBF **47** indicates that the C7 carbon, 0.40, is four times as electrophilically activated as the C5 one, 0.01, indicating that the most favorable two-center interaction will take place between the most nucleophilic center of vinyl ether **48**, the non-substituted carbon of the ethylene (see the nucleophilic  $P_k^-$  Parr functions of vinyl ether **15** in Figure 24.5) and the most electrophilic center of DNBF **47**, the C7 carbon, in complete agreement with the total regio- and chemoselectivity experimentally observed. Note that the most electrophilic center of DNBF **47** determines both the regio- and the chemoselectivity of this P-DA reaction (Figure 24.7; Table 24.8).

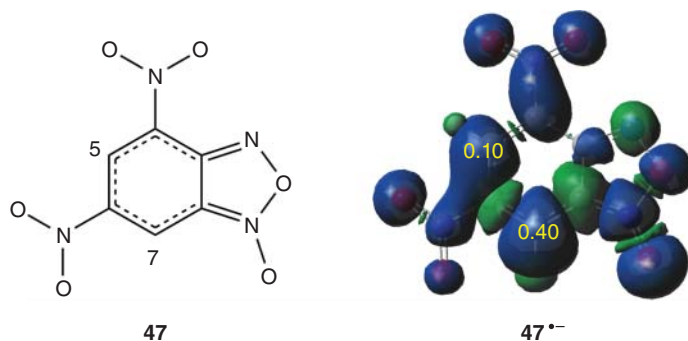


**Figure 24.7** 3D representations of the Mulliken ASD of the radical anion  $47^{\bullet-}$ , together with the electrophilic  $P_k^+$  Parr functions of DNBF **47**.

**Table 24.8** B3LYP/6-31G(d) electronic chemical potential  $\mu$ , chemical hardness  $\eta$ , global electrophilicity  $\omega$  and global nucleophilicity  $N$  indices, in eV, of the reagents involved in the P-DA reactions between DNBF **47** and ANBF **54**.

Molecule	$\mu$	$\eta$	$\omega$	$N$
DNBF <b>47</b>	-5.93	3.21	5.46	1.59
ANBF <b>54</b>	-5.67	3.34	4.81	1.78
Vinyl methyl ether <b>15</b>	-2.45	6.99	0.43	3.18
Vinyl ethyl ether <b>48</b>	-2.40	6.99	0.41	3.23

## 24.9 Conclusions

After the proposal of the P-DA mechanism in 2009 [10], which is followed by most of the experimental DA reactions, with the use CDFT-based reactivity indices, the feasibility of a DA reaction can be easily established analyzing the electrophilic and nucleophilic behaviors of the reagents participating in the reaction; i.e. the more electrophilic one of the reagents and more the nucleophilic other one, the more polar and faster the DA reaction. Many P-DA reactions involve non-symmetric electrophilic ethylenes; these reactions, which take place through highly asynchronous TSs associated to a two-center interaction between the most electrophilic center of the electrophile and the most nucleophilic center of the nucleophile, are completely regioselective, being successfully characterized by the analysis of the Parr functions.

In this context, CDFT-based reactivity indices, such as electrophilicity [12]  $\omega$  and nucleophilicity [13]  $N$  indices, as well as Parr functions [44], have become powerful tools for experimentalists to understand, even predict, DA reactions [14]. Thus, while analysis of the electrophilicity  $\omega$  and the nucleophilicity  $N$  indices allows predicting the feasibility of a DA reaction, analysis of the Parr functions accounts for the regio- and chemoselectivity in P-DA reactions.



## Acknowledgments

This work has been supported by the Ministerio de Ciencias, Innovación y Universidades of the Spanish Government, project PID2019-110776GB-I00 (AEI/FEDER, UE). This work has also received funding from the European Union's Horizon 2020 research and innovation programme under the Marie Skłodowska-Curie Grant Agreement No. 846181 (MRG).

## References

- 1 Diels, O. and Alder, K. (1928). Synthesen in der hydroaromatischen Reihe. *Justus Liebigs Ann. Chem.* 460: 98–122.
- 2 Carruthers, W. (1978). *Some Modern Methods of Organic Synthesis*, 2e. Cambridge: Cambridge University Press.
- 3 Carruthers, W. (1990). *Cycloaddition Reactions in Organic Synthesis*. Oxford: Pergamon.
- 4 Woodward, R.B. and Hoffmann, R. (1969). The conservation of the orbital symmetry. *Angew. Chem. Int. Ed. Engl.* 8: 781–853.
- 5 Houk, K.N., González, J., and Li, Y. (1995). Pericyclic reaction transition states: passions and punctilios, 1935–1995. *Acc. Chem. Res.* 28: 81–90.
- 6 Rowley, D. and Steiner, H. (1951). Kinetics of diene reactions at high temperatures. *Discuss Faraday Soc.* 10: 198–213.
- 7 Domingo, L.R. (2016). Molecular electron density theory: a modern view of reactivity in organic chemistry. *Molecules* 21: 1319.
- 8 Domingo, L.R., Mar Ríos-Gutiérrez, M., Silvi, B., and Pérez, P. (2018). The mysticism of pericyclic reactions: a contemporary rationalisation of organic reactivity based on electron density analysis. *Eur. J. Org. Chem.* 2018: 1107–1120.
- 9 Domingo, L.R. (2014). A new C–C bond formation model based on the quantum chemical topology of electron density. *RSC Adv.* 4: 32415–32428.
- 10 Domingo, L.R. and Sáez, J.A. (2009). Understanding the mechanism of polar Diels–Alder reactions. *Org. Biomol. Chem.* 7: 3576–3583.
- 11 Domingo, L.R., Arnó, M., Contreras, R., and Pérez, P. (2002). Density functional theory study for the cycloaddition of 1,3-butadienes with dimethyl acetylenedicarboxylate. Polar stepwise vs concerted mechanisms. *J. Phys. Chem. A* 106: 952–961.
- 12 Parr, R.G., Szentpaly, L.V., and Liu, S. (1999). Electrophilicity index. *J. Am. Chem. Soc.* 121: 1922–1924.
- 13 Domingo, L.R., Chamorro, E., and Pérez, P. (2008). Understanding the reactivity of captodative ethylenes in polar cycloaddition reactions. A theoretical study. *J. Org. Chem.* 73: 4615–4624.
- 14 Domingo, L.R., Ríos-Gutiérrez, M., and Pérez, P. (2016). Applications of the conceptual density functional theory indices to organic chemistry reactivity. *Molecules* 21: 748.

- 15 Pérez, P., Domingo, L.R., Aizman, A., and Contreras, R. (2007). The electrophilicity index in organic chemistry. In: *Theoretical Aspects of Chemical Reactivity*, vol. 9 (ed. A. Toro-Labbe), 139–201. Amsterdam: Elsevier.
- 16 Domingo, L.R. and Pérez, P. (2011). The nucleophilicity N index in organic chemistry. *Org. Biomol. Chem.* 9: 7168–7175.
- 17 Parr, R.G. and Yang, W. (1989). *Density Functional Theory of Atoms and Molecules*. New York: Oxford University Press.
- 18 Parr, R.G. and Pearson, R.G. (1983). Absolute hardness: companion parameter to absolute electronegativity. *J. Am. Chem. Soc.* 105: 7512–7516.
- 19 Domingo, L.R., Aurell, M.J., Pérez, P., and Contreras, R. (2002). Quantitative characterization of the global electrophilicity power of common diene/dienophile pairs in Diels–Alder reactions. *Tetrahedron* 58: 4417–4423.
- 20 Kohn, W. and Sham, L.J. (1965). Self-consistent equations including exchange and correlation effects. *Phys. Rev.* 140: 1133–1138.
- 21 Jaramillo, P., Domingo, L.R., Chamorro, E., and Pérez, P. (2008). A further exploration of a nucleophilicity index based on the gas-phase ionization potentials. *THEOCHEM J. Mol. Struct.* 865: 68–72.
- 22 Fukui, K. (1964). *Molecular Orbitals in Chemistry, Physics, and Biology*, 525. New York: Academic Press.
- 23 Sustmann, R. and Trill, H. (1972). Substituent effects in 1,3-dipolar cycloadditions of phenyl azide. *Angew. Chem. Int. Ed. Engl.* 11: 838–840.
- 24 Houk, K.N., Sims, J., Watts, C.R., and Luskus, L.J. (1973). Origin of reactivity, regioselectivity, and periselectivity in 1,3-dipolar cycloadditions. *J. Am. Chem. Soc.* 95: 7301–7315.
- 25 Kiselev, V.D. and Konovalov, A.I. (1989). Factors that determine the reactivity of reactants in normal and catalyzed Diels–Alder reactions. *Russ. Chem. Rev.* 58: 230–249.
- 26 Anh, N.T. and Maurel, F. (1997). Use and misuse of frontier orbital theory. *New J. Chem.* 21: 861–871.
- 27 Spino, C., Rezaei, H., and Dory, Y.L. (2004). Characteristics of the two frontier orbital interactions in the Diels–Alder cycloaddition. *J. Org. Chem.* 69: 757–764.
- 28 Domingo, L.R. (2004). Why do electron-deficient dienes react rapidly in Diels–Alder reactions with electron-deficient ethylenes? A density functional theory analysis. *Eur. J. Org. Chem.* 2004: 4788–4793.
- 29 Domingo, L.R., Ríos-Gutiérrez, M., and Pérez, P.A. (2020). Molecular electron density theory study of the reactivity of tetrazines in Aza-Diels–Alder reactions. *RSC Adv.* 10: 15394–15405.
- 30 Domingo, L.R., Kula, K., and Ríos-Gutiérrez, M. (2020). Unveiling the reactivity of cyclic azomethine ylides in [3+2] cycloaddition reactions within the molecular electron density theory. *Eur. J. Org. Chem.* 2020: 5938–5948.
- 31 Domingo, L.R., Ríos-Gutiérrez, M., and Pérez, P. (2020). Unveiling the Lewis acid catalysed Diels–Alder reactions through the molecular electron density theory. *Molecules* 25: 2535.

- 32 Emamian, S., Domingo, L.R., Hosseini, S.J., and Ali-Asgari, S. (2020). A molecular electron density theory study on an oxa-Diels–Alder reaction: exploration of different impacts of  $\text{AlCl}_3$  as a Lewis acid catalyst. *ChemistrySelect* 5: 5341–5348.
- 33 Boruah, R.C., Ahmed, S., Sharma, U., and Sandhu, J.S. (2000). A convenient preparation of *N*-acyl-1-aza-1,3-diene from  $\beta$ -formylenamide and its utility in inverse electron demand Diels–Alder reactions. *J. Org. Chem.* 65: 922–925.
- 34 Domingo, L.R. (2002). A density functional theory study for the Diels–Alder reaction between *N*-acyl-1-aza-1,3-butadienes and vinylamines. Lewis acid catalyst and solvent effects. *Tetrahedron* 58: 3765–3774.
- 35 Chamorro, E., Duque-Noreña, M., Gutiérrez-Sánchez, N. et al. (2020). A close look to the oxaphosphetane formation along the Wittig reaction: a [2+2] cycloaddition? *J. Org. Chem.* 85: 6675–6686.
- 36 Huang, Y. and Rawal, V.H. (2002). Hydrogen-bond-promoted hetero-Diels–Alder reactions of unactivated ketones. *J. Am. Chem. Soc.* 124: 9662–9663.
- 37 Domingo, L.R. and Andrés, J. (2003). Enhancing reactivity of carbonyl compounds via hydrogen-bond formation. A DFT study of the hetero-Diels–Alder reaction between butadiene derivative and acetone in chloroform. *J. Org. Chem.* 68: 8662–8866.
- 38 Manoharan, M., De Proft, F., and Geerlings, P. (2000). A computational study of aromaticity-controlled Diels–Alder reactions. *J. Chem. Soc. Perkin Trans. 2*: 1767–1773.
- 39 Domingo, L.R., Ríos-Gutiérrez, M., and Pérez, P. (2020). A molecular electron density theory study of the enhanced reactivity of aza aromatic compounds participating in Diels–Alder reactions. *Org. Biomol. Chem.* 18: 292–304.
- 40 Domingo, L.R., Aurell, M.J., Pérez, P., and Contreras, R. (2002). Quantitative characterization of the local electrophilicity of organic molecules. Understanding the regioselectivity on Diels–Alder reactions. *J. Phys. Chem. A* 106: 6871–6875.
- 41 Krokidis, X., Noury, S., and Silvi, B. (1997). Characterization of elementary chemical processes by catastrophe theory. *J. Phys. Chem. A* 101: 7277–7282.
- 42 Domingo, L.R., Chamorro, E., and Pérez, P. (2010). Understanding the high reactivity of the azomethine ylides in [3 + 2] cycloaddition reactions. *Lett. Org. Chem.* 7: 432–439.
- 43 Domingo, L.R. and Sáez, J.A. (2011). Understanding the electronic reorganization along the nonpolar [3 + 2] cycloaddition reactions of carbonyl ylides. *J. Org. Chem.* 76: 373–379.
- 44 Domingo, L.R., Pérez, P., and Sáez, J.A. (2013). Understanding the local reactivity in polar organic reactions through electrophilic and nucleophilic Parr functions. *RSC Adv.* 3: 1486–1494.
- 45 Parr, R.G. and Yang, W. (1984). Density functional approach to the frontier-electron theory of chemical reactivity. *J. Am. Chem. Soc.* 106: 4049–4050.
- 46 Yang, W. and Mortier, W.J. (1986). The use of global and local molecular parameters for the analysis of the gas-phase basicity of amines. *J. Am. Chem. Soc.* 108: 5708–5711.

- 47 Pérez, P., Domingo, L.R., Duque-Noreña, M., and Chamorro, E. (2009). A condensed-to-atom nucleophilicity index. An application to the director effects on the electrophilic aromatic substitutions. *J. Mol. Struct. THEOCHEM* 895: 86–91.
- 48 Aurell, M.J., Domingo, L.R., Pérez, P., and Contreras, R. (2004). A theoretical study on the regioselectivity of 1,3-dipolar cycloadditions using DFT-based reactivity indexes. *Tetrahedron* 60: 11503–11509.
- 49 Hallé, J.C., Vichard, D., Pouet, M.-J., and Terrier, F. (1997). A new cycloaddition process involving nitro group participation in polynitroaromatic chemistry. *J. Org. Chem.* 62: 7178–7182.
- 50 Arroyo, P., Picher, M.T., and Domingo, L.R. (2004). The domino reaction between 4,6-dinitrobenzofuroxan and cyclopentadiene. Insights on the nature of the molecular mechanism. *J. Mol. Struct. (THEOCHEM)* 709: 45–52.
- 51 Terrier, F., Sebban, M., Goumont, R. et al. (2000). Dual behavior of 4-aza-6-nitrobenzofuroxan. A powerful electrophile in hydration and  $\sigma$ -complex formation and a potential dienophile or heterodiene in Diels–Alder type reactions. *J. Org. Chem.* 65: 7391–7398.
- 52 Domingo, L.R. and Pérez, P. (2020). The lithium cation catalysed benzene Diels–Alder reaction. Insights on the molecular mechanism within the molecular electron density theory. *J. Org. Chem.* 85: 13121–13132.

## 25

### Interaction Locality in Molecular Crystals

Kanupriya Verma and Tonglei Li

Purdue University, Department of Industrial and Physical Pharmacy, Robert E. Heine Pharmacy Building, 575 Stadium Mall Drive, West Lafayette, IN 47907, USA

#### 25.1 Introduction

Viewing a three-dimensional crystal structure on the computer, we often become mesmerized by the symmetric tessellation of molecules. The strength and directionality of intermolecular interactions, governed by structural diversity and conformational flexibility of the molecule, dictate its crystal formation. Subtle variation in molecular interactions often results in the polymorphism of crystal packing, largely realized by changes in crystallization conditions. Understanding the supramolecular chemistry of crystallization not only satisfies our curiosity but also enables us to create new structures and materials of novel properties.

For any given organic molecule, we will always get the same crystal structures faithfully back, over and over again through crystallization. Occasionally, a few more distinct crystals may be identified under different experimental conditions. A molecule clearly “knows” which parts of its structure will interact with a counterpart, resulting in unique intermolecular interacting patterns or synthons [1], such as hydrogen bonding and  $\pi$ - $\pi$  stacking. There have been some efforts reported in the literature to characterize the locality of intermolecular interaction. Quantum theory of atoms in molecules (QTAIM) [2] analyzes the gradient field of the electron density (ED), knowing that electrons are the “glue” that sticks atoms and then molecules together. Interatomic surface (IAS) shared by two bonded atoms characterizes the physical nature of the atomic bonding by analyzing electron density at the bond critical point (BCP) [3] – a point on IAS where the gradient of ED is zero. In a study to differentiate hydrogen bonds from van der Waals interactions, Koch and Popelier identified a correlation between the energy of hydrogen bond and potential energy and interpreted it as the energetic response of the hydrogen bond to the force exerted on the electrons around BCPs [4]. For strong intermolecular hydrogen bonds, such correlation resembles that of an intramolecular bond. The importance of intermolecular interactions can also be evaluated through the analysis of atomic polarizabilities, in particular, their deformation concerning noninteracting

molecules. One approach is the electron localization function (ELF), which enables visualization of covalent bonds, electron lone pairs, and atomic shell structures by partitioning the ED and evaluating distributed atomic polarizabilities [5]. Bui et al. attempted to rationalize halogen bonding based on deformation density and visualization of  $\sigma$ -hole (which was first anticipated by Politzer [6, 7]) and examined major contributions to the electrostatic interaction [8]. Stone demonstrated that some stereochemical features of the halogen-bonded packing originate from the necessity to minimize the inter-atomic repulsion, rather than forming a stabilizing, though weak, electrostatic interaction [9]. A noteworthy study of charge density analysis is to utilize a reduced electron density gradient (RDG), which is conceived by Yang and coworkers [10–12]. RDG is calculated from the ED and its first derivative; plotting RDG vs. ED is utilized to explore the regions with reduced gradients. The concept is indicative of noncovalent interactions (NCIs).

While these studies explore molecular interactions through analyzing local electron densities, most of them rely on examining molecular pairs that are already packed or interacted. Such a posteriori practice cannot satisfy the need to seek the governing properties of a molecule that determine its locality of interaction preference or strength. Because a molecule always forms the same packing motif – or a few when the polymorphism arises – in the crystalline state, we posit that the chemical information determining the interaction locality is embedded in the molecule and can be directly obtained from the molecule. There is no need to subject it to explicit interactions with another molecule. For this purpose, we have resorted to conceptual density functional theory (CDFT) to unveil the root cause of intermolecular interactions.

Over the last several decades, DFT has evolved into two branches, one for energy calculations [13–15], and the other, generally referred to as CDFT, for theoretically exploring the fundamental linkage between electron density and molecular properties [16–19]. Among various concepts derived by CDFT, the Fukui function is particularly appealing [20–28]. It is a local, spatial function; it exhibits the intrinsic characteristics of local polarizability and electronic softness, thus utilized to characterize intermolecular interactions [29–34]. Other efforts also explore local hardness for characterizing molecular interactions, including  $\pi$ – $\pi$  stacking in biomolecules [35–37]. Nonetheless, the application of CDFT to study intermolecular interactions in organic crystals is not extensively investigated by others. Since the early 2000s, our group has explored this aspect of CDFT, especially the concept of the Fukui function for characterizing the locality of intermolecular interactions [23, 38, 39]. We explored CDFT quantities to examine several properties of organic crystals, including surface energy [23], reactivity [40–42], crystal packing [43, 44], thermal liberation [45, 46], hydrogen bonding [47], electron and charge philicity [48–50], intermolecular interaction [38, 51], nucleation mechanism [52, 53], and crystal engineering [54, 55]. We developed several CDFT concepts as well, including face-integrated Fukui function [23], crystallization force [38], and natural orbital Fukui function [56], to facilitate our understanding of molecular interactions. All these efforts demonstrate great potentials for using CDFT in analyzing electronic structures of organic molecules and gaining fundamental insights into crystal packing.

In essence, our efforts of analyzing intermolecular interactions in organic crystals stem from Pearson's HSAB (hard and soft acids and bases) principle, which states that hard acids prefer hard bases and soft acids prefer soft bases, both thermodynamically and kinetically [57–61]. The principle may be extended to characterizing the locality/regioselectivity of intermolecular interactions [62–64]. Intuitively, a soft region or functional group of a molecule prefers interacting with a soft region of another molecule; vice versa for the matching of local hardness. This remains as our foundation and motivation for studying molecular interactions. We have attempted to seek local electronic properties to characterize local softness and hardness. In light of HSAB, proper matching between local softness or hardness governs the locality of intermolecular interactions that a molecule can form. In this chapter, we illustrate some of our studies of using CDFT quantities to uncover the locality of interactions in crystal and its manifestation in solid-state reactivity, surface energy, and thermal stability.

## 25.2 Characterizing Solid-state Reaction of Organic Crystals

The crystalline state constitutes the most significant and the most widely employed form of solid active pharmaceutical ingredients (APIs) [65]. Solid-state reactions are frequently observed in organic crystalline materials, which play a crucial role in handling and processing pharmaceutical materials and ensuring product quality. The long-range order of crystals introduces a different type of complexity when compared with liquid-phase reactions, making crystals highly anisotropic and heterogeneous as reaction originates on the surface. The kinetics of these reactions is greatly influenced by polymorphism and growth morphology [66–68].

DFT-based concepts, including nuclear Fukui functions, have been employed to identify the impact of crystal packing on solid-state reactions of organic crystals at the electronic level. This section explores several systems, ranging from the polymorphs of flufenamic acid and indomethacin to the energetic materials such as RDX (1,3,5-trinitro-1,3,5-triazine), triacetone triperoxide (TATP), and diacetone diperoxide (DADP), showcasing our efforts of using nuclear Fukui functions in probing the influence by crystal packing on the reactivity of organic crystals.

The nuclear Fukui function essentially depicts the energetic response of an atom (in a molecule) to electronic perturbation. The quantity is thus intuitive to characterize the solid-state reactivity of organic crystals in light of the anisotropy in crystal packing at the electronic level [16, 18, 40, 41, 69]. The concept of nuclear Fukui function stems from the Hellmann–Feynman force, which is defined as the force upon nucleus  $\alpha$  within a molecular system, given as [70, 71]:

$$\mathbf{F}_\alpha = Z_\alpha \left[ \int \rho(\mathbf{r}) \frac{\mathbf{r}_\alpha}{r_\alpha^3} d\mathbf{r} - \sum_{\beta \neq \alpha} Z_\beta \frac{\mathbf{R}_{\alpha\beta}}{R_{\alpha\beta}^3} \right] \quad (25.1)$$

where the electron density at point  $\mathbf{r}$  is denoted by  $\rho(\mathbf{r})$ ;  $\mathbf{r}_\alpha$  is defined as the displacement vector between the position of nucleus  $\alpha$  and point  $\mathbf{r}$ ; the displacement vector

between the nucleus  $\alpha$  with charge  $Z_\alpha$  and nucleus  $\beta$  with charge  $Z_\beta$  is given by  $\mathbf{R}_{\alpha\beta}$ . The nuclear Fukui function ( $\Phi_\alpha$ ) is thus derived by the following equation, which describes the response of the force ( $\mathbf{F}_\alpha$ ) to electronic perturbation [72]:

$$\Phi_\alpha = \left( \frac{\partial \mathbf{F}_\alpha}{\partial N} \right)_v \quad (25.2)$$

where,  $N$  refers to the number of electrons in the system and  $v$  is the external potential.

Because of the discontinuity in  $N$ , nuclear Fukui function can be further defined for describing a nucleophilic or electrophilic attack, given by the following equations [72]:

$$\Phi_\alpha^+ = \mathbf{F}_\alpha^+ - \mathbf{F}_\alpha^0 \quad (25.3)$$

$$\Phi_\alpha^- = \mathbf{F}_\alpha^0 - \mathbf{F}_\alpha^- \quad (25.4)$$

where,  $\Phi_\alpha^+$  and  $\Phi_\alpha^-$  correspond to the nucleophilic and electrophilic nuclear Fukui function, respectively;  $\mathbf{F}_\alpha^+$ ,  $\mathbf{F}_\alpha^-$ , and  $\mathbf{F}_\alpha^0$  refer to the forces acting on the same nucleus  $\alpha$  of anionic, cationic, and neutral systems, respectively.

Additionally, the chemical reactivity of a given system has been described as nuclear stiffness, shown below [73, 74]:

$$\mathbf{G}_i = \left( \frac{\partial \eta}{\partial \mathbf{Q}_i} \right)_N \quad (25.5)$$

where  $\eta$  is the hardness and  $\mathbf{Q}_i$  is the displacement vector of atom  $i$  from its equilibrium position  $\mathbf{R}_{i,0}$  ( $\mathbf{R}_i - \mathbf{R}_{i,0}$ ). As nuclear reactivity index can also be expressed as a derivative of electronic chemical potential,  $\mu$ , with respect to atomic displacement [72]:

$$\Phi_i = - \left( \frac{\partial \mu}{\partial \mathbf{Q}_i} \right)_N \quad (25.6)$$

Thus,  $\mathbf{G}_i$  and  $\Phi_i$  describe a chemical reaction by characterizing individual atoms in terms of bond shortening or stretching and electron-accepting/donating ability of a molecule [74]. And because they are local quantities, reactivity variations due to crystal packing may be better revealed.

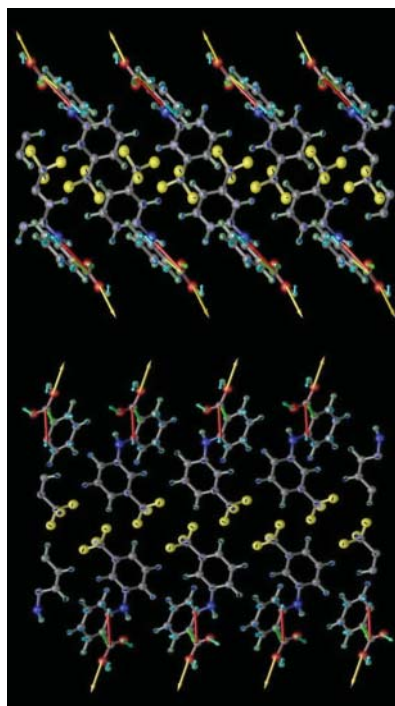
### 25.2.1 Reactivity of Pharmaceutical Crystals

We have studied the chemical reactivities of two polymorphs of flufenamic acid (2-[[3-(trifluoromethyl)phenyl]amino]benzoic acid) [40] and indomethacin (1-(4-chlorobenzoyl)-5-methoxy-2-methyl-1*H*-indole-3-acetic acid) [41]. The influence of crystal packing was elucidated through the use of electron-density-based concepts, including nuclear Fukui functions.

Out of the six possible polymorphs of flufenamic acid, two polymorphs (forms I and III), are routinely crystallized and hence studied. Experimental studies on the chemical reactivity of these polymorphs with ammonia gas indicated their reaction rates to be quite different [75]. The electronic structures, nuclear Fukui functions along with the surface energies of the two polymorphs were computed by



**Figure 25.1** Respective (100A) crystallographic faces of flufenamic acid of forms I (top) and III (bottom). Nuclear Fukui functions are shown as color-coded arrows whose lengths are commensurate with their magnitudes. Source: Adapted from Feng and Li [40], with permission granted.



CRYSTAL03, a periodic Gaussian wave-based *ab initio* program [76]. Flufenamic acid undergoes deprotonation on its reaction with ammonia and thus, the nucleophilic nuclear Fukui function ( $\Phi_{\alpha}^{+}$ , Equation (25.3)) was calculated for the analysis. The nuclear Fukui functions for the (100A) face of the two polymorphs (Figure 25.1) revealed that the carboxylic group exposed on (100A) in both forms show the highest value as compared with all other atoms and is; therefore, the most affected moiety during the nucleophilic attack by ammonia. The position of the carboxylic group affects the values of the nuclear Fukui function. In the (100A) slab, where the group is exposed, the value is significantly higher than that in (100B), where it is embedded in the middle. Between the two forms, nuclear Fukui functions of form I's carboxylic group are higher than those in form III, indicating that form I is more reactive than form III (Figure 25.2). Possible effects of mechanical strength on the chemical reactivity were also described by the surface energy of (100A) being greater than (100B), attributed to the hydrogen bonding between COOH groups in (100A). The (100B) exposure of each form is expected to be dominant for the (100) face, owing to smaller surface energies, while the more reactive (100A) is likely to be exposed as defects and initiators of the chemical reaction.

Similar to flufenamic acid, nucleophilic nuclear Fukui functions were computed for analyzing the reactivity difference between two polymorphs of indomethacin ( $\alpha$  and  $\gamma$ ) to account for the deprotonation on its reaction with ammonia. These polymorphs are known to exhibit different reactive kinetics with ammonia gas [68]. The  $\alpha$ -form consists of three symmetrically different conformers (labeled as #1, #2,

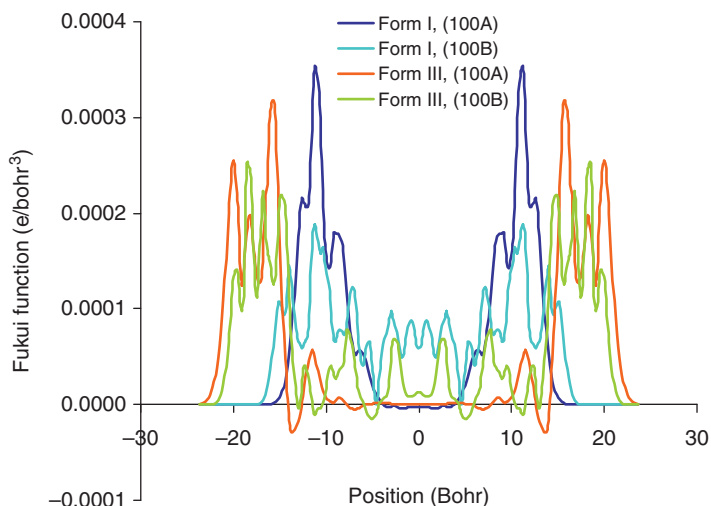


**Figure 25.2** Fukui functions integrated over various sections of (100A) and (100B) slabs of forms I and III as a function of their positions. The height of the form I slab is of one unit cell, whereas that of form III slab is of half unit cell. Source: Adapted from Feng and Li [40], with permission granted.

and #3). As shown in Figure 25.3, the carboxylic moiety of molecule #3 was found to exhibit greater values of nuclear Fukui functions in comparison to the respective atoms in #1 and #2, as well as to those in the  $\gamma$ -form. This difference in the values of nuclear Fukui functions was interpreted to be the primary reason behind the reactivity difference between the two polymorphs. A large nuclear Fukui function implies large physical stress on an atom due to perturbation in electron density. Deprotonation of the carboxylic group in #3 of the  $\alpha$ -form is the most active under a nucleophilic attack. Moreover, the carbonyl group between the indole and phenyl rings and the neighboring atoms displays higher values of nuclear Fukui functions, attributed to the steric tension between the two aromatic rings. The two aromatic rings incline to realign themselves and maximize the overlapping of their p orbitals. Molecular orbitals of a single indomethacin molecule corroborate this argument, wherein, the highest occupied molecular orbital (HOMO) is primarily delocalized on the indole ring without extending to phenyl, and lowest unoccupied molecular orbital (LUMO), on the other hand, spreads over to chlorobenzoyl of the molecule.

### 25.2.2 Reactivity of Energetic Materials

Electronic calculations and nuclear Fukui functions were employed to study the initiation mechanism of decomposition of energetic materials, including RDX, TATP, and DADP [42, 77]. RDX is regularly studied as a model system of explosive materials [73]. Various reaction pathways have been proposed for its decomposition mechanisms, but few succeeded in providing tangible answers [78–80]. Our electronic studies were hoped to provide an insight into the initial mechanism of decomposition in both the vapor and crystal phases. The reactivity of the peroxide-based explosives,

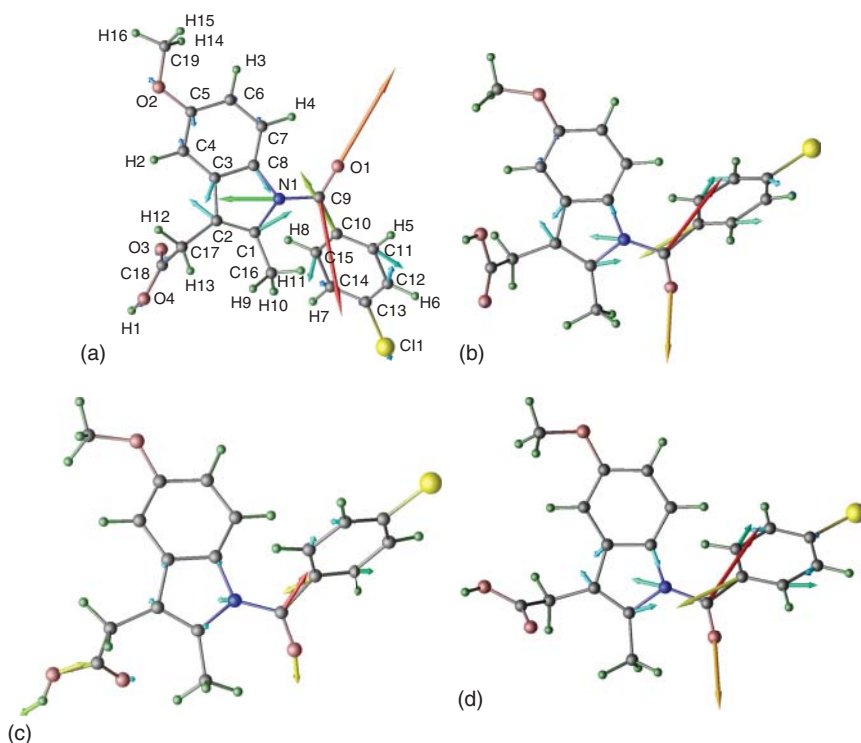


**Figure 25.3** Nuclear Fukui functions of three asymmetric molecules in the  $\alpha$ -form (a–c) and (d) the molecule in the  $\gamma$ -form of indomethacin represented as arrows. The color-coding of the arrows represents values from red (largest) to green and to blue (smallest). Source: Reproduced from Li and Feng [41], with permission granted.

TATP and DADP, was also investigated by computing nuclear Fukui functions [77]. Despite close structural similarities between TATP and DADP, these reactivity differences of the solid-state warrant a detailed study of their decomposition mechanism. There are reports accounting for isolated molecules without considering the molecular environment in crystal lattice [81–83]. In our studies, DFT-based concepts were calculated from respective crystal structures and examined.

The vapor-phase studies on RDX revealed the possibility of interconversion between the AAA, AAE, and AEE conformers, while EEE, being the least stable conformer, is the least probable [78, 84–86]. Contrary to previous experimental studies, which suggest the concerted fission mechanism as the initial decomposition step in RDX vapor, our studies indicate that breaking of the N–N bond initiates the decomposition of the more stable AAA and AAE conformers [42]. This is supported by higher nucleophilic responses of the nitro group nuclei and strong electrophilic responses of the bonded N atoms. This fact was strengthened by the magnitudes and directions of their respective nuclear Fukui functions (Figure 25.4a–h).

Calculations of RDX crystal unveiled higher magnitudes of nucleophilic nuclear Fukui function of the atoms in axial N–NO<sub>2</sub> groups. Along with strong electrophilic

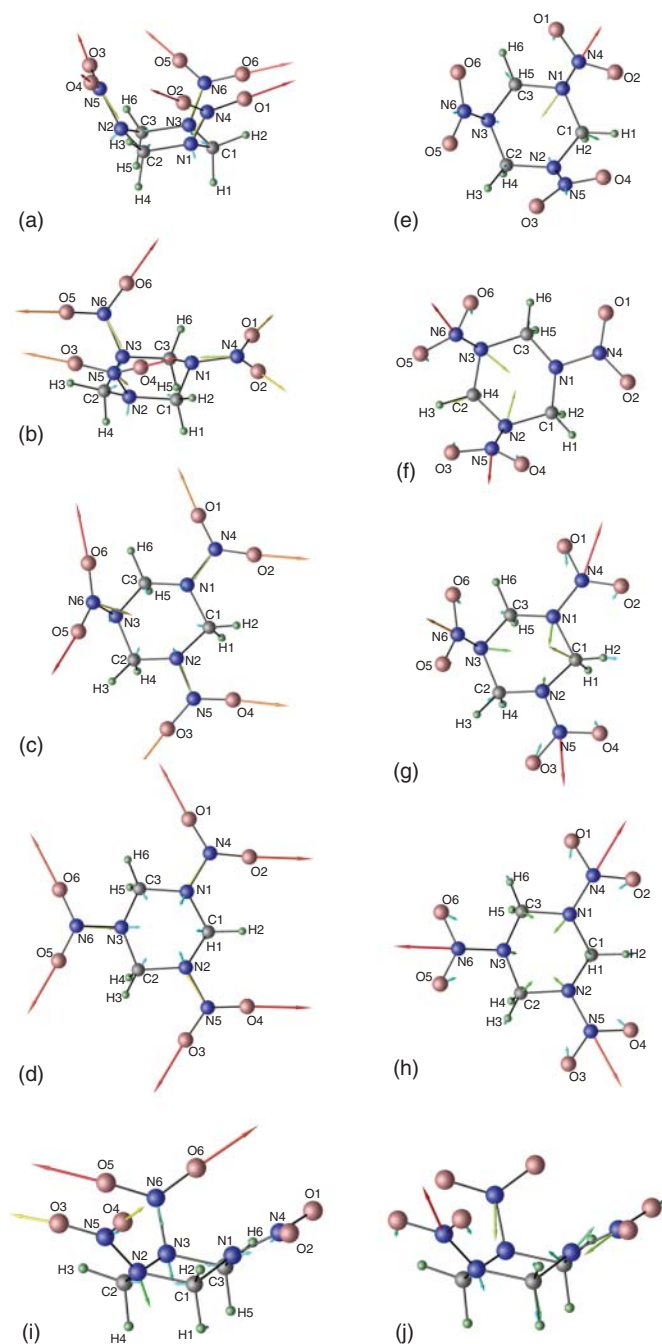


**Figure 25.4** Nucleophilic (a–d) and electrophilic (e–h) nuclear Fukui functions of AAA (a, e), AAE (b, f), AEE (c, g), and EEE (d, h) conformers of single RDX molecule, and the molecule in the crystal (i, j). Values of the nuclear Fukui functions are indicated by the length and color-coding of the arrows. Source: Adapted from Swadley and Li [42], with permission granted.

N–N responses, the N–N homolysis mechanism is plausible in the crystal. Moreover, the large electrophilic responses on the C1 and H2 nuclei coupled with the proximity of H2 to O4 of a reactive axial nitro group also hints at the possibility of HONO elimination. Nuclear Fukui functions of crystal RDX (Figure 25.4i, j) further indicated that symmetrically similar atoms bear rather different values (magnitudes and directions), which are contrary to the vapor phase. The response to electronic perturbation is conformation-dependent in the crystal.

TATP and DADP exhibit highly distinct chemical reactivities, rooted in the electronic properties of their crystal structures [77]. The decomposition sensitivity of crystalline TATP is higher than that of crystalline DADP [82]. From both gas phase and crystal structure studies, the homolytic breaking of the peroxide bond is known to be the initiating and the rate-determining step [81–83]. The nuclear Fukui functions of TATP's peroxide bonds in the crystal phase are greater; and therefore, more stressed in comparison with DADP (Figure 25.5), indicating that the former is more prone to bond breakage. While the DADP crystal seems to retain the same electronic symmetry as displayed by a single molecule in the gas phase, the TATP crystal, according to its nuclear Fukui function values, shows no symmetry of the molecular skeleton (Figure 25.5). Frontier orbitals of the single TATP and DADP molecules retain their geometric symmetry upon electronic perturbation, evidenced by the shapes of HOMO and LUMO. HOMO spreads out uniformly across symmetrically similar regions in both TATP and DADP. Similarly, LUMO, upon the addition of an electron, becomes symmetrically extended.

To summarize, these studies demonstrated the feasibility of using nuclear Fukui functions in exploring the solid-state reactivity of organic crystal systems. The role of symmetry in the crystal was illustrated by both the magnitudes and directions of the nuclear Fukui functions. Electronic calculation and DFT-based concepts enabled the probing of mechanistic details of the unimolecular decomposition of RDX and the peroxide-based explosives such as TATP and DADP.

### 25.3 Crystal–Solvent Interaction and Wettability Anisotropy

Our computational studies of the wettability of organic crystals centered around exploring electronic Fukui functions. The wettability of a crystal is anisotropic; the individual faces of a crystal differ in their respective wettability or surface energy values, also implying that a crystal may have a very different overall wettability if its growth morphology and/or structure changes. Understanding and controlling this property is particularly crucial in drug development [87]. Contact angle measurement of a solid surface enables a good estimate of the surface's wettability. A stronger solid–liquid interaction typically leads to a smaller contact angle. As the Fukui function is regarded as a descriptor of the local softness of a molecular system [88], we attempted to use face-integrated Fukui functions to characterize the relative

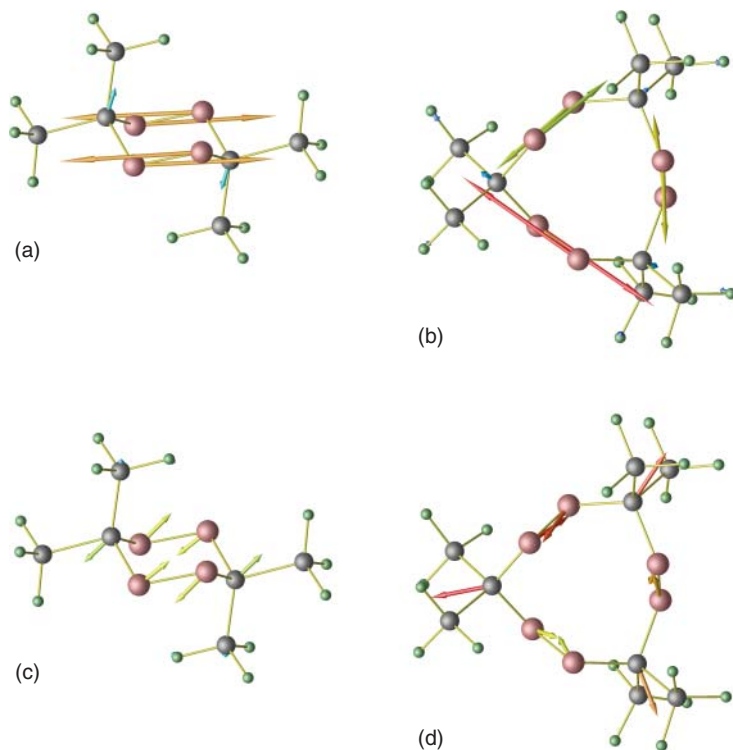


**Figure 25.5** Nucleophilic nuclear Fukui function (a, b) and electrophilic Fukui function (c, d) of DADP (a, c) and TATP (b, d) crystals, respectively. Values of the nuclear Fukui functions are indicated by the length and color-coding of the arrows. Source: Reproduced from Swadley et al. [77], with permission granted.

softness of various faces of a crystal [23]. This concept is illustrated by the following equation:

$$F(\mathbf{p}) = \int_{\mathbf{p}} f(\mathbf{r}) d\mathbf{r} / A(\mathbf{p}) \quad (25.7)$$

where,  $f(\mathbf{r})$  is Fukui function at position  $\mathbf{r}$ ; a specific crystallographic face with its relative position in the unit cell is denoted by  $\mathbf{p}$ ; the surface area of the integrated face is  $A(\mathbf{p})$ , to normalize to the integrated quantity allowing the comparison among individual crystallographic faces.

Face-integrated Fukui functions were computed to characterize the wettability of major faces of two crystal systems, aspirin, and *n,n*-octyl-*D*-gluconamide (OGA) [23]. The Fukui functions were evaluated from the electron density differences between the neutral and the anionic forms of the crystals. It was found that in aspirin, the Fukui functions were greater in the hydrogen-bonding regions. The (100) face of aspirin has two distinct ways of surface exposure. One possibility goes through the hydrogen bonds between carboxylic groups, denoted as (100b), and the other is between methyl groups without exposing any hydrogen-bonded dimers, (100a). On the other hand, the (001) face has only one way of exposure.

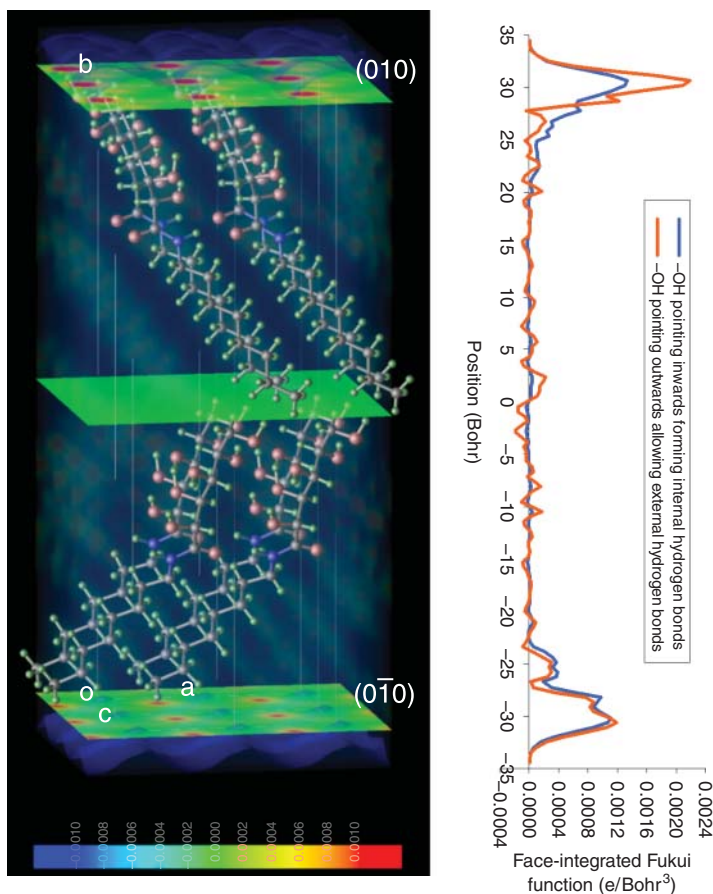


**Figure 25.6** (010) slab of OGA crystal with three highlighted slices that are mapped with Fukui functions (left panel) and corresponding face-integrated values along various positions of the slab (right panel). The orientation of the terminal  $\text{-OH}$  group influences the Fukui function values, illustrated by two curves (red and blue). Source: Adapted from Li et al. [23], with permission granted.

The face-integrated Fukui functions were found to be higher on the (100b) slab of the crystal, due to the exposed carboxylic groups, indicating that this surface is softer than the other two. Overall, this face results in stronger solid–liquid interactions, and subsequently, a smaller contact angle, as corroborated by experiments.

Due to the non-centrosymmetric structure of OGA crystal, the octyl group points toward the (0 $\bar{1}0$ ) side and the gluconamide points toward the (010) (Figure 25.6). In addition, OGA, being a polar crystal, forms stronger hydrogen-bonding interactions with water on (0 $\bar{1}0$ ), indicated by the contact angle of  $76^\circ$ , while the angle is  $43^\circ$  on (010) [89, 90]. The calculated face-integrated Fukui functions support the contact angle data and show the polar side of the crystal being softer (Figure 25.6). Hence, the face-integrated Fukui function is a useful tool to elucidate the relative softness of individual faces of a crystal, especially the interaction anisotropy of the surface.

## 25.4 Atomic Libration in Organic Crystals

CDFT concepts were explored in our studies to understand the large librational motion experienced by the terminal methyl group in aspirin and acetaminophen crystals [45, 46]. The mechanistic correlation was identified between the thermal motion of the methyl groups mainly by nuclear Fukui functions. Further quantitative correlations were derived between force constants of the nuclear thermal librations in crystals and respective nuclear Fukui functions.

Neutron diffraction studies of aspirin and acetaminophen crystals discovered large librational motions by the terminal methyl groups, compared with the other atoms in the crystals (Figure 25.7) [91, 92]. Anisotropic displacement parameters (ADP) [93], along with anisotropic and equivalent isotropic temperature factors, were found to be significantly higher for the hydrogen atoms of the terminal methyl than other atoms.

The librational motion of an atom may be characterized by a harmonic oscillator model using the so-called mean square displacement amplitude (MSDA), which is related with the force constant or energy barrier,  $k$ , of the oscillator [94, 95]:

$$\langle \chi^2 \rangle = \frac{RT}{k} \quad (25.8)$$

where  $\chi^2$  is the MSDA in a 1-D harmonic potential, the universal gas constant is denoted by  $R$ , and the absolute temperature by  $T$ . As such, from the reported neutron diffraction studies,  $k$  could be obtained for each atom in the crystals and further compared with nuclear Fukui functions calculated for these systems.

CDFT calculations revealed that nuclear Fukui functions of the C atom of the methyl group in either aspirin or acetaminophen are considerably smaller than those of other non-hydrogen atoms [45]. To account for the divergence, molecular orbitals of aspirin and acetaminophen were calculated. It is interesting to note that the methyl group is excluded from both HOMO and LUMO, leading to the smallest response of nuclear force on C9 to electronic perturbation. A similar trend was observed in the case of acetaminophen crystal wherein the methyl group is again isolated from any of the frontier orbitals, leaving C8 unaffected by electronic perturbation and hence accounting for its lowest value of nuclear Fukui function in comparison to other non-hydrogen atoms. The smaller values of nuclear Fukui functions on the methyl groups indicate lesser physical stress on these atoms, compared with other atoms. It is thus likely that these nuclei bear larger degrees of freedom in motion without causing significant variations in the overall electronic structure.

The relationship could be further illustrated by quantitatively correlating the energy barrier of libration,  $k$  (Equation (25.8)), and the nuclear Fukui function. By plotting the equivalent isotropic displacement parameter,  $U_{eq}$ , against the absolute temperatures, force constants of all atoms in aspirin and acetaminophen crystals could be derived from the slopes of linearly fitted lines. A linear correlation was then identified between the derived  $k$  and calculated  $\Phi_{\alpha}^{+}$  or  $\Phi_{\alpha}^{-}$  for all the atoms in aspirin and acetaminophen single crystals (Figure 25.8). It is known that the force constant is directly related to the energy barrier that defines the thermal motion



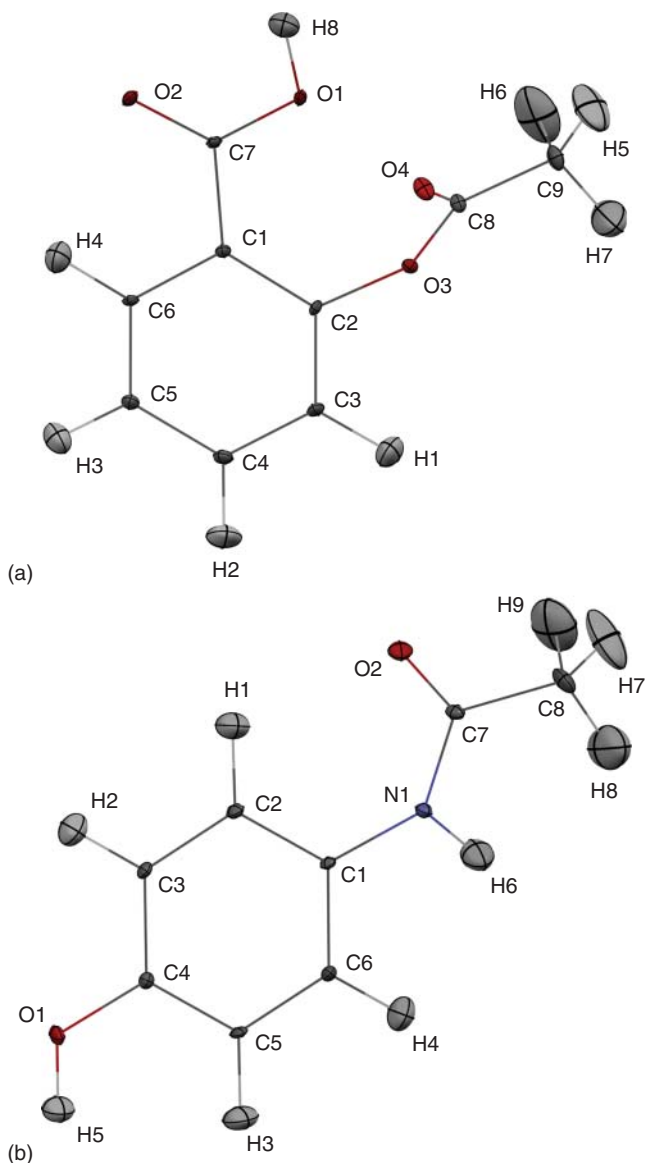


**Figure 25.7** Aspirin (a) and acetaminophen (b) molecule in their respective crystal structures. Atoms are numbered and displayed with thermal ellipsoids determined by neutron diffraction at 20 K. Source: Adapted from Li [45], with permission granted.

of an atom [94]. Thus, the relationship demonstrates that nuclear Fukui functions are also capable of unveiling local interatomic interactions, which are manifested by thermal motions of atoms in a crystal. Given that a nuclear Fukui function may be regarded as a condensed index of electronic Fukui function around a nucleus, the connection identified between thermal motions and nuclear Fukui functions

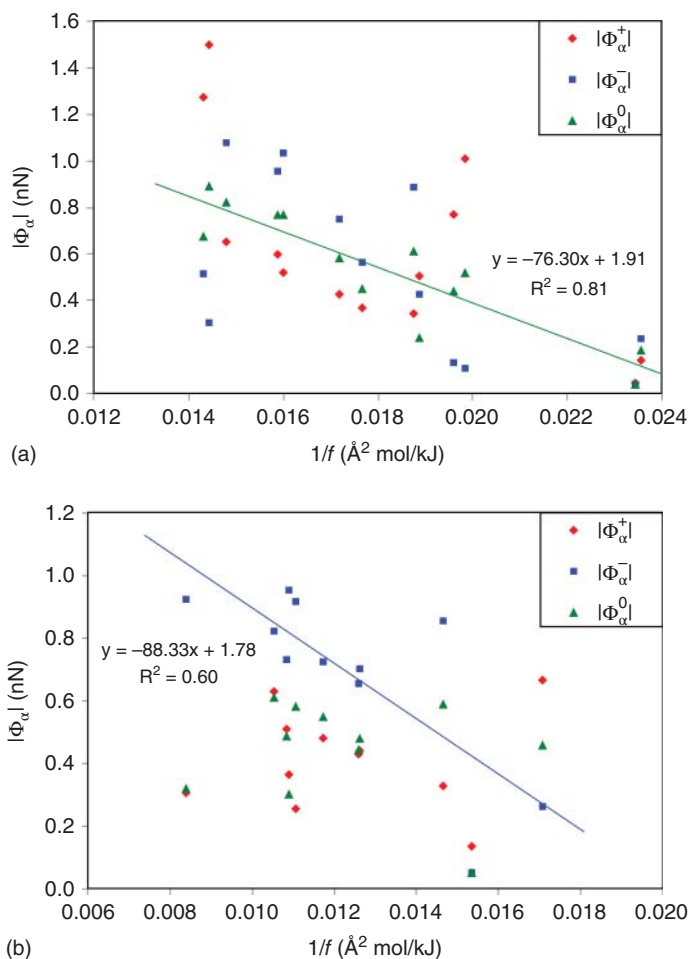


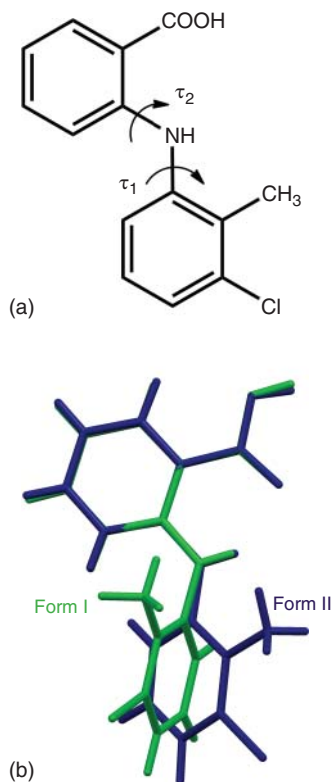
**Figure 25.8** Nuclear Fukui functions of aspirin (a) and acetaminophen (b) vs. corresponding inverse of force constants. The lines are respective linear fittings of  $|\Phi_{\alpha}^0|$  (for aspirin) and  $|\Phi_{\alpha}^{-}|$  (for acetaminophen). Source: Adapted from Li [46], with permission granted.

points to the importance of local softness defining intermolecular interactions in an organic crystal.

## 25.5 Hydrogen-bonding Strength

Hydrogen bonding plays a critical role in the formation and packing of organic crystals [96, 97]. Various synthons or hydrogen-bonding motifs have been studied in crystals and are widely utilized in crystal engineering [98, 99]. In our studies of using CDFT concepts in understanding crystal packing, we particularly focused on the role of hydrogen bonding in the interplay between intramolecular interactions, manifested by conformational flexibility of the molecule, and intermolecular interactions.

**Figure 25.9** Tolfenamic acid with major torsion angles marked,  $\tau_1$  and  $\tau_2$  (a) and overlay of TFA molecules in forms I and II (b).



Such interplay exists ubiquitously in organic crystals, leading to the conformational polymorphism of the same molecule [100, 101]. We have examined the role of hydrogen bonding on the polymorphic formation of tolfenamic acid (TFA) [44, 102] and 2-(phenylamino)nicotinic acid (2-PNA) [47].

TFA displays conformational polymorphism wherein the molecules in its two commonly occurring crystal structures form similar hydrogen-bonded dimers but bear distinct conformations (Figure 25.9). The conformation in the two forms differs primarily in the torsional angle  $\tau_1$  linking the amino and chlorinated phenyl ring. The bonding–antibonding interaction between the lone pair of the amino and carboxylated aromatic ring is much higher than that between the lone pair and the chlorinated aromatic ring, indicating a higher tendency of the nitrogen atom to share electrons with the carboxylated aromatic ring. In addition to the  $\pi$ -conjugation, there is also steric repulsion occurring when the two rings rotate against each other, collectively resulting in the distribution of  $\tau_1$ . Condensed Fukui functions were evaluated, both in the gas phase and in implicit solvent models (ethanol and tetrachloromethane), to study how conformation affects hydrogen-bonding strength. The dual descriptor values of the carbonyl oxygen indicate that the hydrogen-bonding acceptor can form stronger hydrogen bonding at an unfavorable conformation (Figure 25.10). This is significant as the CDFT concept can truly quantify the physical nature of hydrogen bonding – while it

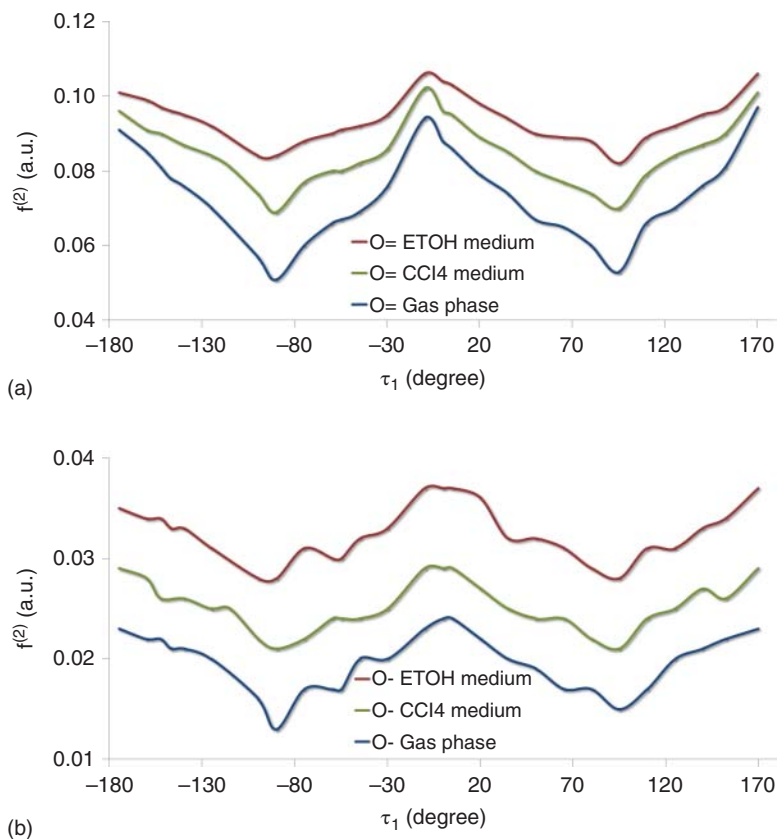
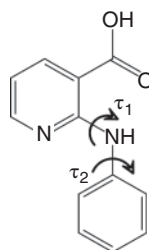


**Figure 25.10** Condensed dual descriptors of carbonyl oxygen (a) and hydroxyl oxygen (b) of TFA single-molecule calculated as a function of  $\tau_1$  in gas phase, tetrachloromethane, and ethanol implicit solvent media. Source: Reproduced from Mattei and Li [44], with permission granted.

behaves as a hydrogen-bonding acceptor, the carbonyl oxygen is an unwilling one and still electrophilic. It can form stronger hydrogen bonding only when its electrophilicity decreases, as indicated by the dual descriptor. The analysis also suggests that, without explicitly invoking molecular pairs, the intermolecular hydrogen-bonding strength as a relation of conformation can be estimated, at least relatively, by examining the single molecule.

The interplay between molecular conformation and intermolecular interaction is also revealed by the study of crystal forms of 2-PNA, which consists of both carboxyl and pyridinyl moieties (Figure 25.11). Four polymorphs of 2-PNA have been identified with two packed by acid–acid hydrogen-bonded dimers and the other two by acid–pyridine hydrogen-bonded chains [103]. Molecules in the dimer form bear planar conformations, whereas molecules in the chain adopt twisted or warped conformations, indicated by the torsional angles,  $\tau_1$  and  $\tau_2$  (Figure 25.11). The primary questions addressed in our study are (i) the effect of the difference in strength between the homo- and hetero-synthons on the molecular conformation

Figure 25.11 2-PNA.



and crystal packing and (ii) the reason behind pyridine N acting as a better hydrogen bond acceptor. Toward this direction, the crystal structures were studied with CRYSTAL06 [104] and electronic structures of single molecules were evaluated with GAUSSIAN09 [105] at the B3LYP/6-21G(d,p) and MP2/6-31G+(d,p) levels. These calculations showed that acid–pyridine hydrogen bonding is stronger than that of acid–acid homosynthon. Furthermore, Fukui functions and dual descriptors were calculated for the pyridine N, amino N, and carbonyl O in 2-PNA single-molecule (Figure 25.12) [47]. Carbonyl O is electrophilic with the highest positive value of dual descriptor and amino N is nucleophilic with the lowest negative value. The pyridine N lies in the middle (with a value of  $-0.001 e$ ), indicating it to be nucleophilic and a better hydrogen-bonding acceptor than carbonyl O. From electronic calculations, it was further revealed that pyridinyl N is sterically blocked for hydrogen-bonding access at a planar conformation. Calculation results of the twisted conformers in the  $\delta$  form showed that the pyridine N becomes more nucleophilic by an order of magnitude and thus a better hydrogen-bonding acceptor.

Through the studies of TFA and 2-PNA, the interplay between molecular conformation and intermolecular interaction is elucidated. Aided by CDFT concepts including Fukui functions, the hydrogen-bonding strength and overall intermolecular interactions in the polymorphic systems reflect the compromise between conformational stability and lattice energy. The plot of dual descriptor as a function of conformation (e.g. against a major torsion angle) is particularly powerful in unveiling the interplay in light of conformational polymorphism.

## 25.6 Locality of Intermolecular Interactions in Organic Crystals

Intermolecular interactions, including hydrogen bonding and van der Waals forces, dominate in organic crystals, determining crystallization outcome and kinetics [38, 106]. The locality of intermolecular interactions underlines the essence of crystal formation and has been explored in our studies with CDFT concepts [38, 39, 51, 107].

Intending to study intermolecular interactions in organic crystals, we developed a concept called crystallization force [38]. This CDFT concept elucidates the local variation in the electronic structure of a molecular system through the self-assembly process of crystallization. The concept is a normalized nuclear Fukui function, where

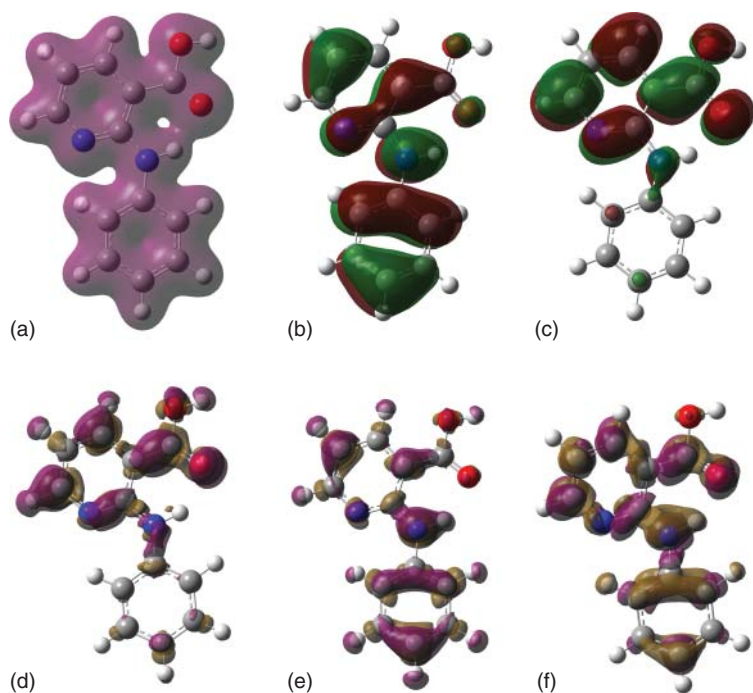


**Figure 25.12** Electronic isosurfaces of the most stable conformation of 2-PNA: electron density (a), HOMO (b), LUMO (c), nucleophilic Fukui function (d), electrophilic Fukui function (e), and dual descriptor (f). The iso-values are 0.02 (a–c) and 0.002 a.u. (d–f), respectively. Positive or negative dual descriptors are shown in pink or brown. Source: Reproduced from Li et al. [47], with permission granted.

the normalization reflects the electronic perturbation connected with crystallization. The total crystallization force of a crystal can be written as the sum of the magnitudes of the individual crystallization forces and characterizes the binding strength to form a crystal [38]:

$$G = \sum_{\substack{\alpha \\ dq_{\alpha} > 0 \\ f_{\alpha}^{+} > 0}} | \Phi_{\alpha}^{+} | \frac{dq_{\alpha}}{f_{\alpha}^{+}} - \sum_{\substack{\alpha \\ dq_{\alpha} < 0 \\ f_{\alpha}^{-} > 0}} | \Phi_{\alpha}^{-} | \frac{dq_{\alpha}}{f_{\alpha}^{-}} \quad (25.9)$$

where,  $G$  is the total crystallization force of the crystal;  $\Phi_{\alpha}^{+}$  and  $\Phi_{\alpha}^{-}$  are the nucleophilic and electrophilic nuclear Fukui functions, respectively;  $dq_{\alpha} = q_{\alpha}(\text{gas}) - q_{\alpha}(\text{crystal})$ .

An interesting example to illustrate the concept of crystallization force is a system commonly referred to as ROY (5-methyl-2-[(2-nitrophenyl)amino]-3-thiophenecarbonitrile), which has the highest number of solved polymorphs reported to date [108–111]. Its rich polymorphism was found to be a collective result of the various functional groups (nitro, nitrile, amino, and aromatic rings) contributing to a wide range of intermolecular interactions. The molecular structure of ROY along with the computed crystallization forces for its seven polymorphs is shown

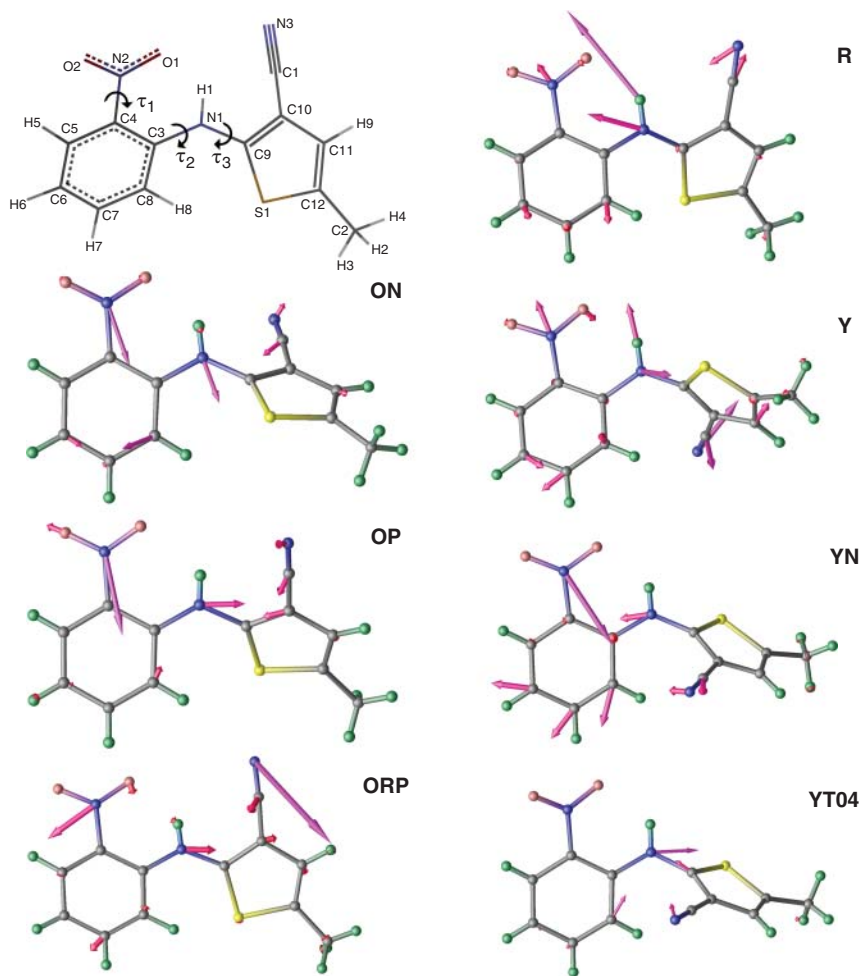


**Figure 25.13** Molecular structure of ROY and molecules in respective polymorphs with crystallization forces represented by magnitude-scaled arrows. Source: Adapted from Li et al. [38], with permission granted.

in Figure 25.13. The nitro group exhibits a larger crystallization force, involving 10 out of the 20 close contacts identified in the polymorphs. The nitrile group is involved in five close contacts; stacking of phenyl and thiophene rings accounts for the rest of the five contacts. The correlation demonstrates using crystallization force in describing the locality of intermolecular interactions in crystals. This was further corroborated by computing the lattice energy of the polymorphs with an empirically augmented DFT method [112] and plotting against the total crystallization forces [38]. It was found that linear correlations exist between the total crystallization force and lattice energy, further suggesting the underlying connection between crystallization force and intermolecular interaction (Figure 25.14).

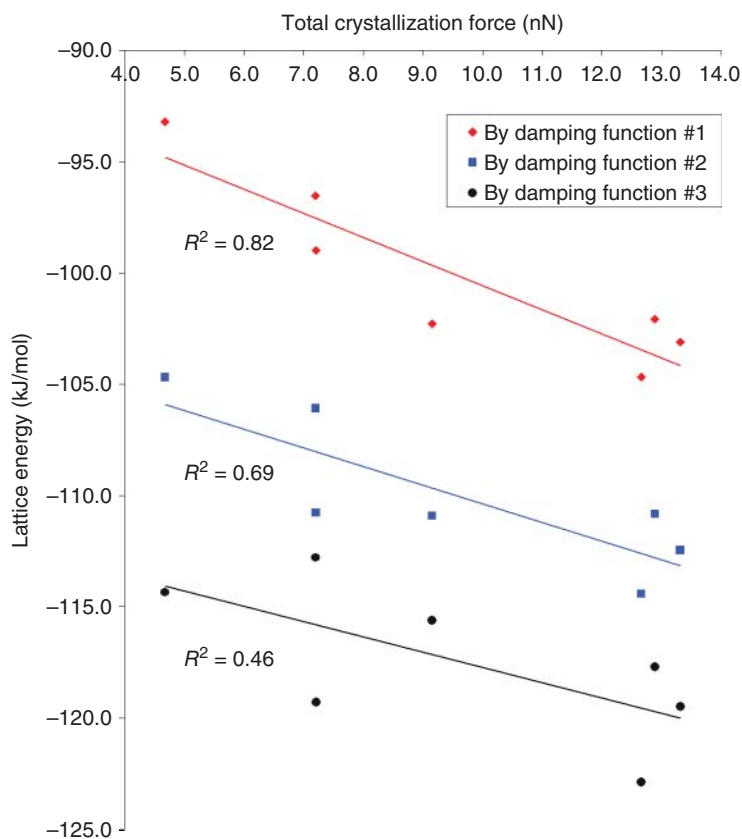


**Figure 25.14** Lattice energy versus total crystallization force of respective ROY polymorphs. Three different damping functions were used to calculate van der Waals energies for augmenting the lattice energy calculations by DFT. Source: Modified from Figure 6 in Li et al. [38], with permission granted.

To further explore the locality with CDFT concepts, Hirshfeld surface was employed in our studies to sample and visualize electronic properties, such as the Fukui function, in a crystal structure [39, 107]. A Hirshfeld surface is defined by partitioning the electron density around a molecule according to whether the contribution comes from the enclosed molecule or its neighboring molecules [113–115].

$$w_A(\mathbf{r}) = \rho_{\text{pro-molecule}}(\mathbf{r}) / \rho_{\text{pro-crystal}}(\mathbf{r}) \quad (25.10)$$

where  $\rho_{\text{pro-molecule}}(\mathbf{r})$  refers to the electron density contributed by the molecule under consideration ( $A$ ) and  $\rho_{\text{pro-crystal}}(\mathbf{r})$  is the electron density contributed by neighboring molecules in the crystal. The surface when  $w_A = 0.5$  is typically used. By mapping the Hirshfeld surface in a crystal with local electronic properties such as Fukui functions and ESP, it is possible to assess the locality of intermolecular interactions. It is also possible to integrate these electronic properties over the contact area on the Hirshfeld surface between two neighboring molecules to quantify the strength of



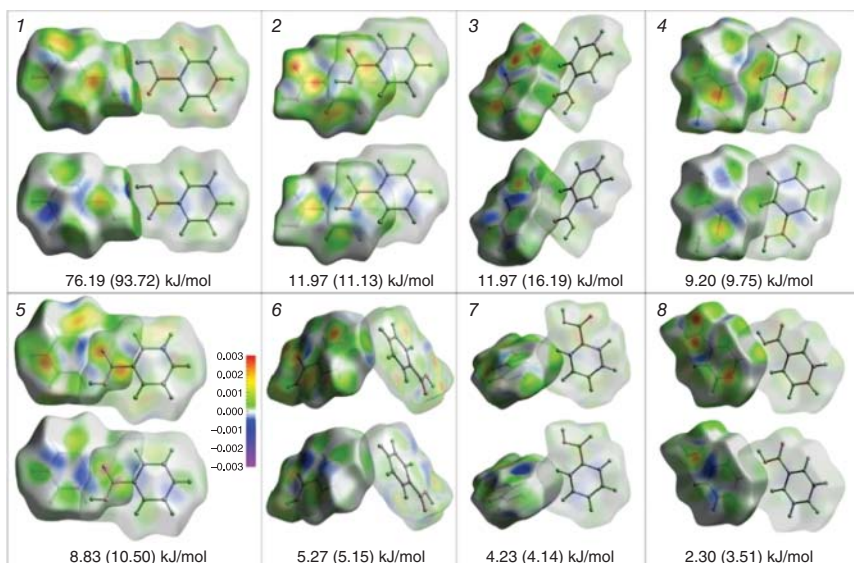


**Figure 25.15** Hirshfeld surfaces mapped with dual descriptors calculated based on the crystal (top) or single-molecule (bottom) of eight interacting pairs of benzoic acid. Intermolecular interaction energies are shown under each pair, computed at the MP2 and DFT-D (in parentheses) levels of theory. Source: Reproduced from Zhang and Li [39], with permission granted.

the interaction. This was done in our studies of intermolecular interactions in two diverse systems, viz. benzoic acid [39] and ROY [107].

In the study of benzoic acid, eight unique pairs of intermolecular contacts were identified in the crystal, and Fukui functions and ESP calculated from a single molecule or the crystal were mapped on the Hirshfeld surface. Figure 25.15 shows the Hirshfeld surface of the eight packing motifs of benzoic acid mapped with the crystal and molecule-based dual descriptor ( $f^2$ ). It is clear that the intermolecular packing motifs couple with hot spots containing larger Fukui functions. The hydrogen bonding between COOH groups is the dominant interaction and involves larger electrophilic Fukui functions ( $f^-$ ) on =O against larger nucleophilic Fukui functions ( $f^+$ ) on -OH. Moreover, the  $\pi$ - $\pi$  stacking between neighboring carboxyl groups matches against regions of larger nucleophilic Fukui functions. The weakest interactions associate with smaller, albeit noticeable  $f^+$  and  $f^-$  spots. The matching of the electronic properties defines the strength of the intermolecular interactions, thus displaying the importance of Fukui functions in quantifying the intermolecular interactions directly from analyzing the electronic properties of the single-molecule. Quantitative relationships were explored by integrating the local electronic properties over the contacting area of Hirshfeld surfaces and plotting against values of the intermolecular interactions (Figure 25.16). It is clear that even without including the hydrogen bonding in the plots, other weaker interactions still demonstrate convincing connections with the Fukui functions. It is important to note that the molecule-based electronic properties show much better correlations

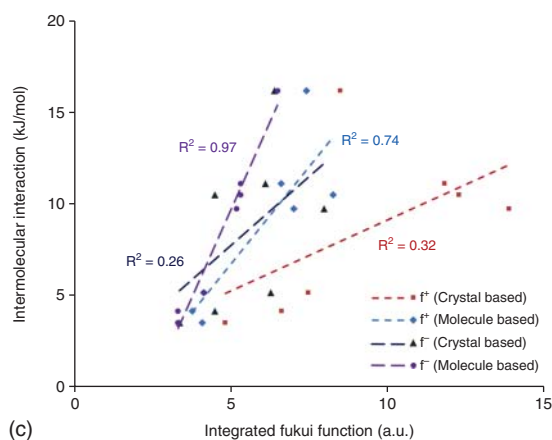
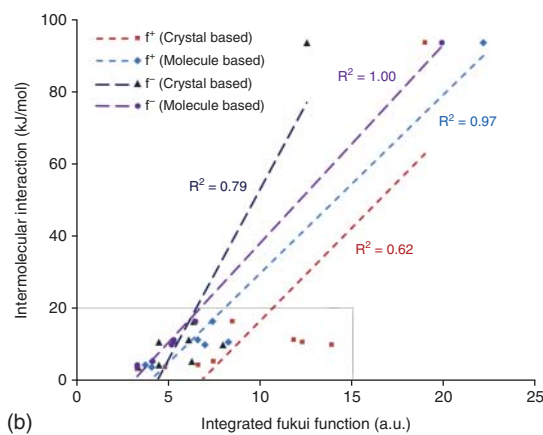
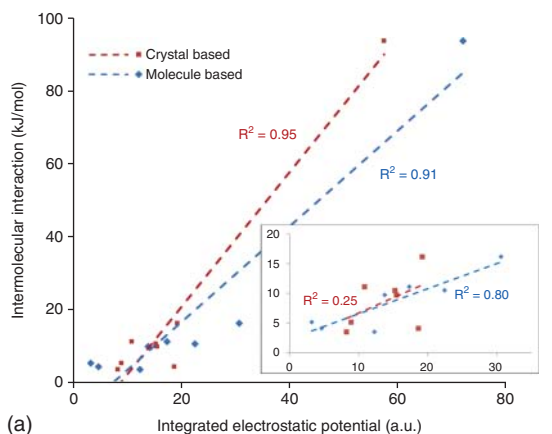


**Figure 25.16** Intermolecular interaction energy vs. integrated electronic properties over the contacting area on Hirshfeld surfaces of each interacting pair of benzoic acid: electrostatic potential (a), Fukui functions (b), and Fukui functions excluding the hydrogen-bonded pair (c). Dashed lines are respective linear regressions of corresponding data values. Source: Reproduced from Zhang and Li [39], with permission granted.

with the strengths of intermolecular interactions than the properties evaluated directly from the crystal. This suggests that the information of intermolecular interaction is already embedded in the molecule itself, regarding both the strength and locality. Similar observations were obtained by studying ROY [107].

## 25.7 Conclusion

We have studied intermolecular interactions of organic crystals based on the inherent electronic properties of a molecule within the framework of CDFT. We have utilized Fukui function, electrostatic potential, and other local electronic concepts to exploit Pearson's HSAB principle (i.e. hard acids prefer hard bases and soft acids prefer soft bases) for understanding the locality or regioselectivity and strength of intermolecular interactions with respect to crystal packing. Our findings unveiled quantitative relationships between the local electronic properties and molecular interaction energies in a crystal, shedding light on the thermodynamics and kinetics of crystallization.

## References

- 1 Desiraju, G.R. (1995). Supramolecular synthons in crystal engineering – a new organic synthesis. *Angew. Chem.* 34 (21): 2311–2327.
- 2 Bader, R.F.W. (1985). Atoms in molecules. *Acc. Chem. Res.* 18 (1): 9–15.
- 3 Bader, R.F.W. (1998). A bond path: a universal indicator of bonded interactions. *J. Phys. Chem. A* 102 (37): 7314–7323.
- 4 Koch, U. and Popelier, P.L.A. (1995). Characterization of c–h–o hydrogen-bonds on the basis of the charge-density. *J. Phys. Chem.* 99 (24): 9747–9754.
- 5 Becke, A.D. and Edgecombe, K.E. (1990). A simple measure of electron localization in atomic and molecular-systems. *J. Chem. Phys.* 92 (9): 5397–5403.
- 6 Brinck, T., Murray, J.S., and Politzer, P. (1993). Molecular-surface electrostatic potentials and local ionization energies of group-v-vii hydrides and their anions-relationships for aqueous and gas-phase acidities. *Int. J. Quantum Chem.* 48 (2): 73–88.
- 7 Brinck, T., Murray, J.S., and Politzer, P. (1992). Surface electrostatic potentials of halogenated methanes as indicators of directional intermolecular interactions. *Int. J. Quantum Chem.* 44 (19): 57–64.
- 8 Bui, T.T.T., Dahaoui, S., Lecomte, C. et al. (2009). The nature of halogen-halogen interactions: a model derived from experimental charge-density analysis. *Angew. Chem. Int. Ed.* 48 (21): 3838–3841.
- 9 Stone, A.J. (2013). Are halogen bonded structures electrostatically driven? *J. Am. Chem. Soc.* 135 (18): 7005–7009.
- 10 Contreras-Garcia, J., Johnson, E.R., Keinan, S. et al. (2011). Nciplot: a program for plotting noncovalent interaction regions. *J. Chem. Theory Comput.* 7 (3): 625–632.

- 11 Contreras-Garcia, J., Yang, W., and Johnson, E.R. (2011). Analysis of hydrogen-bond interaction potentials from the electron density: integration of noncovalent interaction regions. *J. Phys. Chem. A* 115 (45): 12983–12990.
- 12 Johnson, E.R., Keinan, S., Mori-Sanchez, P. et al. (2010). Revealing noncovalent interactions. *J. Am. Chem. Soc.* 132 (18): 6498–6506.
- 13 Andzelm, J. and Wimmer, E. (1992). Density functional gaussian-type-orbital approach to molecular geometries, vibrations, and reaction energies. *J. Chem. Phys.* 96 (2): 1280–1303.
- 14 Becke, A.D. (1993). Density-functional thermochemistry. III. The role of exact exchange. *J. Chem. Phys.* 98 (7): 5648–5652.
- 15 Politzer, P. and Seminario, J.M. (1995). *Modern Density Functional Theory: A Tool for Chemistry, Theoretical and Computational Chemistry*. Amsterdam: Elsevier.
- 16 Hohenberg, P. and Kohn, W. (1964). Inhomogeneous electron gas. *Phys. Rev. B* 136 (3B): B864–B871.
- 17 Parr, R.G. and Yang, W. (1989). *Density-Functional Theory of Atoms and Molecules*. New York, NY: Oxford University Press.
- 18 Kohn, W., Becke, A.D., and Parr, R.G. (1996). Density functional theory of electronic structure. *J. Phys. Chem.* 100 (31): 12974–12980.
- 19 Geerlings, P., De Proft, F., and Langenaeker, W. (2003). Conceptual density functional theory. *Chem. Rev.* 103 (5): 1793–1873.
- 20 Yang, W., Parr, R.G., and Pucci, R. (1984). Electron-density, kohn-sham frontier orbitals, and fukui functions. *J. Chem. Phys.* 81 (6): 2862–2863.
- 21 Gazquez, J.L., Vela, A., and Galvan, M. (1987). Fukui function, electronegativity and hardness in the kohn-sham theory. *Struct. Bond.* 66: 79–97.
- 22 Mendez, F. and Gazquez, J.L. (1994). The fukui function of an atom in a molecule – a criterion to characterize the reactive sites of chemical-species. *Proc. Indian Acad. Sci.* 106 (2): 183–193.
- 23 Li, T.L., Liu, S.B., Feng, S.X., and Aubrey, C.E. (2005). Face-integrated fukui function: understanding wettability anisotropy of molecular crystals from density functional theory. *J. Am. Chem. Soc.* 127 (5): 1364–1365.
- 24 Ayers, P.W. and Melin, J. (2007). Computing the fukui function from ab initio quantum chemistry: approaches based on the extended koopmans’ theorem. *Theor. Chem. Accounts* 117 (3): 371–381.
- 25 Li, Y. and Evans, J.N.S. (1995). The fukui function – a key concept linking frontier molecular-orbital theory and the hard-soft-acid-base principle. *J. Am. Chem. Soc.* 117 (29): 7756–7759.
- 26 Ayers, P.W. (2007). The physical basis of the hard/soft acid/base principle. *Faraday Discuss.* 135: 161–190.
- 27 Berkowitz, M. and Parr, R.G. (1988). Molecular hardness and softness, local hardness and softness, hardness and softness kernels, and relations among these quantities. *J. Chem. Phys.* 88 (4): 2554–2557.
- 28 Simon-Manso, Y. and Fuentealba, P. (1998). On the density functional relationship between static dipole polarizability and global softness. *J. Phys. Chem. A* 102 (11): 2029–2032.

- 29 Chermette, H. (1999). Chemical reactivity indexes in density functional theory. *J. Comput. Chem.* 20 (1): 129–154.
- 30 Ayers, P.W. and Parr, R.G. (2000). Variational principles for describing chemical reactions: the fukui function and chemical hardness revisited. *J. Am. Chem. Soc.* 122 (9): 2010–2018.
- 31 Thanikaivelan, P., Padmanabhan, J., Subramanian, V., and Ramasami, T. (2002). Chemical reactivity and selectivity using fukui functions: basis set and population scheme dependence in the framework of b3lyp theory. *Theor. Chem. Accounts* 107 (6): 326–335.
- 32 Balawender, R. and Geerlings, P. (2005). DFT-based chemical reactivity indices in the Hartree-Fock method. II. Fukui function, chemical potential, and hardness. *J. Chem. Phys.* 123 (12): 124102.
- 33 Borgoo, A., Tozer, D.J., Geerlings, P., and De Proft, F. (2009). Confinement effects on excitation energies and regioselectivity as probed by the Fukui function and the molecular electrostatic potential. *Phys. Chem. Chem. Phys.* 11 (16): 2862–2868.
- 34 Fuentealba, P., Florez, E., and Tiznado, W. (2010). Topological analysis of the fukui function. *J. Chem. Theory Comput.* 6 (5): 1470–1478.
- 35 Mignon, P., Loverix, S., De Proft, F., and Geerlings, P. (2004). Influence of stacking on hydrogen bonding: quantum chemical study on pyridine-benzene model complexes. *J. Phys. Chem. A* 108 (28): 6038–6044.
- 36 Mignon, P., Loverix, S., and Geerlings, P. (2005). Interplay between  $\pi$ - $\pi$  interactions and the H-bonding ability of aromatic nitrogen bases. *Chem. Phys. Lett.* 401 (1–3): 40–46.
- 37 Mignon, P., Loverix, S., Steyaert, J., and Geerlings, P. (2005). Influence of the  $\pi$ - $\pi$  interaction on the hydrogen bonding capacity of stacked DNA/RNA bases. *Nucleic Acids Res.* 33 (6): 1779–1789.
- 38 Li, T.L., Ayers, P.W., Liu, S.B. et al. (2009). Crystallization force—a density functional theory concept for revealing intermolecular interactions and molecular packing in organic crystals. *Chem. Eur. J.* 15 (2): 361–371.
- 39 Zhang, M. and Li, T. (2014). Intermolecular interactions in organic crystals: gaining insight from electronic structure analysis by density functional theory. *CrystEngComm* 16 (31): 7162–7171.
- 40 Feng, S.X. and Li, T.L. (2005). Understanding solid-state reactions of organic crystals with density functional theory-based concepts. *J. Phys. Chem. A* 109 (32): 7258–7263.
- 41 Li, T.L. and Feng, S.X. (2005). Study of crystal packing on the solid-state reactivity of indomethacin with density functional theory. *Pharm. Res.* 22 (11): 1964–1969.
- 42 Swadley, M.J. and Li, T.L. (2007). Reaction mechanism of 1,3,5-trinitro-s-triazine (RDX) deciphered by density functional theory. *J. Chem. Theory Comput.* 3 (2): 505–513.
- 43 Li, T.L. (2007). Understanding the polymorphism of aspirin with electronic calculations. *J. Pharm. Sci.* 96 (4): 755–760.

- 44 Mattei, A. and Li, T.L. (2011). Interplay between molecular conformation and intermolecular interactions in conformational polymorphism: a molecular perspective from electronic calculations of tolfenamic acid. *Int. J. Pharm.* 418 (2): 179–186.
- 45 Li, T.L. (2006). Understanding the large librational motion of the methyl group in aspirin and acetaminophen crystals: insights from density functional theory. *Cryst. Growth Des.* 6 (9): 2000–2003.
- 46 Li, T.L. (2008). Further understanding of the thermal motions of atoms in aspirin and acetaminophen crystals with conceptual density functional theory. *Cryst. Growth Des.* 8 (4): 1110–1112.
- 47 Li, T.L., Zhou, P.P., and Mattei, A. (2011). Electronic origin of pyridinyl N as a better hydrogen-bonding acceptor than carbonyl O. *CrystEngComm* 13 (21): 6356–6360.
- 48 Ayers, P.W., Liu, S.B., and Li, T.L. (2009). Chargephilicity and chargephobicity: two new reactivity indicators for external potential changes from density functional reactivity theory. *Chem. Phys. Lett.* 480 (4–6): 318–321.
- 49 Liu, S.B., Li, T.L., and Ayers, P.W. (2009). Potentialphilicity and potentialphobicity: reactivity indicators for external potential changes from density functional reactivity theory. *J. Chem. Phys.* 131 (11): 114106.
- 50 Ayers, P.W., Liu, S.B., and Li, T.L. (2011). Stability conditions for density functional reactivity theory: an interpretation of the total local hardness. *Phys. Chem. Chem. Phys.* 13 (10): 4427–4433.
- 51 Li, T.L. (2008). Visualizing the locality of intermolecular interactions in organic crystals. *J. Mol. Graph. Model.* 26 (6): 962–965.
- 52 Mattei, A. and Li, T.L. (2012). Polymorph formation and nucleation mechanism of tolfenamic acid in solution: an investigation of pre-nucleation solute association. *Pharm. Res.* 29 (2): 460–470.
- 53 Mattei, A., Mei, X.N., Miller, A.F., and Li, T.L. (2013). Two major pre-nucleation species that are conformationally distinct and in equilibrium of self-association. *Cryst. Growth Des.* 13 (8): 3303–3307.
- 54 Long, S.H. and Li, T.L. (2009). Controlled formation of the acid-pyridine heterosynthon over the acid-acid homosynthon in 2-anilinonicotinic acids. *Cryst. Growth Des.* 9 (12): 4993–4997.
- 55 Long, S.H. and Li, T.L. (2010). Enforcing molecule's  $\pi$ -conjugation and consequent formation of the acid-acid homosynthon over the acid-pyridine heterosynthon in 2-anilinonicotinic acids. *Cryst. Growth Des.* 10 (6): 2465–2469.
- 56 Zhou, P.P., Ayers, P.W., Liu, S.B., and Li, T.L. (2012). Natural orbital Fukui function and application in understanding cycloaddition reaction mechanisms. *Phys. Chem. Chem. Phys.* 14 (28): 9890–9896.
- 57 Pearson, R.G. (1963). Hard and soft acids and bases. *J. Am. Chem. Soc.* 85 (22): 3533–3539.
- 58 Pearson, R.G. (1966). Acids and bases. *Science* 151 (3707): 172–177.
- 59 Parr, R.G. and Pearson, R.G. (1983). Absolute hardness- companion parameter to absolute electronegativity. *J. Am. Chem. Soc.* 105 (26): 7512–7516.

- 60 Chattaraj, P.K., Lee, H., and Parr, R.G. (1991). HSAB principle. *J. Am. Chem. Soc.* 113 (5): 1855–1856.
- 61 Ayers, P.W., Parr, R.G., and Pearson, R.G. (2006). Elucidating the hard/soft acid/base principle: a perspective based on half-reactions. *J. Chem. Phys.* 124 (19): 194107.
- 62 Torrent-Sucarrat, M., De Proft, F., Geerlings, P., and Ayers, P.W. (2008). Do the local softness and hardness indicate the softest and hardest regions of a molecule? *Chem. Eur. J.* 14 (28): 8652–8660.
- 63 Torrent-Sucarrat, M., De Proft, F., Ayers, P.W., and Geerlings, P. (2010). On the applicability of local softness and hardness. *Phys. Chem. Chem. Phys.* 12 (5): 1072–1080.
- 64 Cardenas, C. and Ayers, P.W. (2013). How reliable is the hard-soft acid-base principle? An assessment from numerical simulations of electron transfer energies. *Phys. Chem. Chem. Phys.* 15 (33): 13959–13968.
- 65 Hadjittofis, E., Isbell, M.A., Karde, V. et al. (2018). Influences of crystal anisotropy in pharmaceutical process development. *Pharm. Res.* 35 (100): 2374–2379.
- 66 Byrn, S.R., Sutton, P.A., Tobias, B. et al. (1988). The crystal structure, solid-state NMR spectra, and oxygen reactivity of five crystal forms of prednisolone tert-butylacetate. *J. Am. Chem. Soc.* 110 (5): 1609–1614.
- 67 Kishi, Y. and Matsuoka, M. (2010). Phenomena and kinetics of solid-state polymorphic transition of Caffeine. *Cryst. Growth Des.* 10 (7): 2916–2920.
- 68 Chen, X.M., Morris, K.R., Griesser, U.J. et al. (2002). Reactivity differences of indomethacin solid forms with ammonia gas. *J. Am. Chem. Soc.* 124 (50): 15012–15019.
- 69 Parr, R.G. and Yang, W.T. (1995). Density-functional theory of the electronic structure of molecules. *Annu. Rev. Phys. Chem.* 46 (1): 701–728.
- 70 Feynman, R.P. (1939). Forces in molecules. *Phys. Rev.* 56 (4): 340–343.
- 71 Hellmann, H. (1937). *Einführung in Die Quantenchemie*. Leipzig: F Deuticke.
- 72 Cohen, M.H., Gandugliapirovano, M.V., and Kudrnovsky, J. (1994). Electronic and nuclear chemical reactivity. *J. Chem. Phys.* 101 (10): 8988–8997.
- 73 Luty, T., Ordon, P., and Eckhardt, C.J. (2002). A model for mechanochemical transformations: applications to molecular hardness, instabilities and shock initiation of reaction. *J. Chem. Phys.* 117 (4): 1775–1785.
- 74 Ordon, P. and Komorowski, L. (1998). Nuclear reactivity and nuclear stiffness in density functional theory. *Chem. Phys. Lett.* 292 (1–2): 22–27.
- 75 Chen, X.M., Li, T.L., Morris, K.R., and Byrn, S.R. (2002). Crystal packing and chemical reactivity of two polymorphs of flufenamic acid with ammonia. *Mol. Cryst. Liq. Cryst.* 381 (1): 121–131.
- 76 Doll, K., Saunders, V.R., and Harrison, N.M. (2001). Analytical hartree-fock gradients for periodic systems. *Int. J. Quantum Chem.* 82 (1): 1–13.
- 77 Swadley, M.J., Zhou, P., and Li, T. (2015). Reactivity of triacetone triperoxide and diacetone diperoxide: Insights from nuclear Fukui function. *Front. Chem. Sci. Eng.* 9 (1): 114–123.

- 78 Chakraborty, D., Muller, R.P., Dasgupta, S., and Goddard, W.A. (2000). The mechanism for unimolecular decomposition of RDX (1,3,5-Trinitro-1,3,5-triazine), an ab initio study. *J. Phys. Chem. A* 104 (11): 2261–2272.
- 79 Behrens, R. and Bulusu, S. (1992). Thermal decomposition of energetic materials. 3. Temporal behaviors of the rates of formation of the gaseous pyrolysis products from condensed-phase decomposition of 1,3,5-Trinitrohexahydro-s-triazine. *J. Phys. Chem.* 96 (22): 8877–8891.
- 80 Behrens, R. and Bulusu, S. (1992). Thermal decomposition of energetic materials. 4. Deuterium isotopic effects and isotopic scrambling in condensed phase decomposition of 1,3,5-Trinitrohexahydro-s-triazine. *J. Phys. Chem.* 96 (22): 8891–8897.
- 81 Dubnikova, F., Kosloff, R., Almog, J. et al. (2005). Decomposition of triacetone triperoxide is an entropic explosion. *J. Am. Chem. Soc.* 127 (4): 1146–1159.
- 82 Oxley, J.C., Smith, J.L., and Chen, H. (2002). Decomposition of a multi-peroxidic compound: triacetone triperoxide (TATP). *Propellants Explos. Pyrotech.* 27 (4): 209–216.
- 83 Pacheco-Londono, L.C., Primera-Pedrozo, O.M., and Hernandez-Rivera, S.P. (2004). Experimental and theoretical model of reactivity and vibrational detection modes of triacetone triperoxide (TATP) and homologues. *Proc. SPIE* 5617: 190–201.
- 84 Boyd, S., Gravelle, M., and Politzer, P. (2006). Nonreactive molecular dynamics force field for crystalline hexahydro-1,3,5-trinitro-1,3,5-triazine. *J. Chem. Phys.* 124 (10): 104508–104510.
- 85 Harris, N.J. and Lammertsma, K. (1997). Ab initio density functional computations of conformations and bond dissociation energies for hexahydro-1,3,5-trinitro-1,3,5-triazine. *J. Am. Chem. Soc.* 119 (28): 6583–6589.
- 86 Rice, B.M. and Chabalowski, C.F. (1997). Ab initio and nonlocal density functional study of 1,3,5-trinitro-s-triazine (RDX) conformers. *J. Phys. Chem. A* 101 (46): 8720–8726.
- 87 Verma, S. and Varma, R. (2015). Wetting kinetics: an alternative approach towards understanding the enhanced dissolution rate for amorphous solid dispersion of a poorly soluble drug. *AAPS PharmSciTech* 16 (5): 1079–1090.
- 88 Yang, W. and Parr, R.G. (1985). Hardness, softness, and the Fukui function in the electronic theory of metals and catalysis. *Proc. Natl Acad. Sci. USA* 82 (20): 6723–6726.
- 89 Wang, J.-L., Lahav, M., and Leiserowitz, L. (1991). Direct chiral assessment of absolute configuration of chiral alkyl gluconamides by wettability. *Angew. Chem. Int. Ed. Eng.* 30 (6): 696–698.
- 90 Muster, T.H. and Prestidge, C.A. (2002). Face specific surface properties of pharmaceutical crystals. *J. Pharm. Sci.* 91 (6): 1432–1444.
- 91 Wilson, C.C. (2000). Variable temperature study of the crystal structure of paracetamol (p-hydroxyacetanilide) by single crystal neutron diffraction. *Z. Kristallogr. Krist.* 215 (11): 693.



- 92 Wilson, C.C. (2002). Interesting proton behavior in molecular structures. Variable temperature neutron diffraction and ab initio study of acetylsalicylic acid: characterizing librational motions and comparing protons in different hydrogen bonding potentials. *New J. Chem.* 26 (12): 1733–1739.
- 93 Trueblood, K.N., Burgi, H.-B., Burzlaff, H. et al. (1996). Atomic displacement parameter nomenclature. Report of a subcommittee on atomic displacement parameter nomenclature. *Acta Cryst A*52: 770–781.
- 94 Trueblood, K.N. and Dunitz, J.D. (1983). Internal molecular motions in crystals. the estimation of force constants, frequencies and barriers from diffraction data. A feasibility study. *Acta Cryst B*39: 120–133.
- 95 Dunitz, J.D., Schomaker, V., and Trueblood, K.N. (1988). Interpretation of atomic displacement parameters from diffraction studies of crystals. *J. Phys. Chem.* 92 (4): 856–857.
- 96 Aakeroy, C.B. and Seddon, K.R. (1993). The hydrogen bond and crystal engineering. *Chem. Soc. Rev.* 22 (6): 397–407.
- 97 Subramanian, S. and Zaworotko, M.J. (1994). Exploitation of the hydrogen bond: recent developments in the context of crystal engineering. *Coord. Chem. Rev.* 137: 357–401.
- 98 Etter, M.C. (1991). Hydrogen bonds as design elements in organic chemistry. *J. Phys. Chem.* 95 (12): 4601–4610.
- 99 Bernstein, J., Davis, R.E., Shimoni, L., and Chang, N.-L. (1995). Patterns in hydrogen bonding: functionality and graph set analysis in crystals. *Angew. Chem. Int. Ed. Eng.* 34 (15): 1555–1573.
- 100 Bernstein, J. and Hagler, A.T. (1978). Conformational polymorphism. The influence of crystal structure on molecular conformation. *J. Am. Chem. Soc.* 100 (3): 673–681.
- 101 Vippagunta, S.R., Brittain, H.G., and Grant, D.J.W. (2001). Crystalline solids. *Adv. Drug Deliv. Rev.* 48 (1): 3–26.
- 102 Mattei, A. and Li, T. (2014). Nucleation of conformational polymorphs: a computational study of Tolfenamic acid by explicit solvation. *Cryst. Growth Des.* 14 (6): 2709–2713.
- 103 Long, S., Parkin, S., Siegler, M.A. et al. (2008). Polymorphism and phase behaviors of 2-(Phenylamino)nicotinic acid. *Cryst. Growth Des.* 8 (11): 4006–4013.
- 104 Dovesi, R., Saunders, V.R., Roetti, R. et al. *Crystal06 User's Manual*. Torino: University of Torino.
- 105 Frisch, M.J., Trucks, G.W., Schlegel, H.B. et al. (2009). *Gaussian 09*. Wallingford, CT, USA: Gaussian Inc.
- 106 Stein, M. and Heimsaat, M. (2019). Intermolecular interactions in molecular organic crystals upon relaxation of lattice parameters. *Crystals* 9 (12): 665.
- 107 Bhattacharjee, R., Verma, K., Zhang, M., and Li, T. (2019). Locality and strength of intermolecular interactions in organic crystals: using conceptual density functional theory (CDFT) to characterize a highly polymorphic system. *Theor. Chem. Accounts* 138: 121.

- 108 Yu, L., Stephenson, G.A., Mitchell, C.A. et al. (2000). Thermochemistry and conformational polymorphism of a hexamorphic crystal system. *J. Am. Chem. Soc.* 122 (4): 585–591.
- 109 Chen, S., Guzei, I.A., and Yu, L. (2005). New polymorphs of ROY and a new record for coexisting polymorphs of solved structures. *J. Am. Chem. Soc.* 127 (27): 9881–9885.
- 110 Yu, L. (2010). Polymorphism in molecular solids: an extraordinary system of red, orange, and yellow crystals. *Acc. Chem. Res.* 43 (9): 1257–1266.
- 111 Li, X., Ou, X., Rong, H. et al. (2020). The twelfth solved structure of ROY: single crystals of Y04 grown from melt microdroplets. *Cryst. Growth Des.* 20 (11): 7093–7097.
- 112 Feng, S. and Li, T. (2006). Predicting lattice energy of organic crystals by density functional theory with empirically corrected dispersion energy. *J. Chem. Theory Comput.* 2 (1): 149–156.
- 113 McKinnon, J.J., Mitchell, A.S., and Spackman, M.A. (1998). Hirshfeld surfaces: a new tool for visualising and exploring molecular crystals. *Chem. Eur. J.* 4 (11): 2136–2141.
- 114 Spackman, M.A. and Jayatilaka, D. (2009). Hirshfeld surface analysis. *CrystEngComm* 11 (1): 19–32.
- 115 Spackman, M.A. (2013). Molecules in crystals. *Phys. Scr.* 87 (4): 048103.

## 26

## A Conceptual DFT Approach Toward Analyzing Hydrogen Storage Potential

Arindam Chakraborty<sup>1</sup>, Sukanta Mondal<sup>2</sup>, Rakesh Parida<sup>3</sup>, Santanab Giri<sup>3</sup>, and Pratim K. Chattaraj<sup>4,5</sup>

<sup>1</sup>Jatragachi Pranabananda High School, Faculty of Science, New Town, Kolkata 700161, India

<sup>2</sup>Assam University, Department of Education, A. M. School of Educational Sciences, Silchar 788011, India

<sup>3</sup>Haldia Institute of Technology, School of Applied Science and Humanities, Haldia 721657, India

<sup>4</sup>Indian Institute of Technology Kharagpur, Department of Chemistry, Kharagpur 721302, India

<sup>5</sup>Indian Institute of Technology Bombay, Department of Chemistry, Powai 400076, India

### 26.1 Introduction

Energy is the primal requirement of the entire living race on earth. Living organisms, including the human race, require energy for their existence, growth, and progress. And in this process, the human race has thrived on the usage of energy in the conventional form, which was easily available as buried fossil fuels. An uncontrolled usage of the fossil fuels in our daily lives, especially in the industrial sectors and automobiles, has created panic regarding its availability in future. Dearth of fossil fuel reserves is alarming, as these underground resources are the prime stored energy reserves of this planet. According to the Intergovernmental Panel on Climate Change (IPCC), it is almost certain that an awfully fast growth in global warming is a direct result of such human activities [1]. The resulting climate change owing to the emission of greenhouse gases is linked to significant environmental impacts that are connected to the disappearance of animal species [2, 3], decreased agricultural yield [4–6], increasingly frequent extreme weather events [7, 8], human migration [9–11], and conflicts [12–14]. With an aim to arrest such a negative impact on the global climate, there is an increasing momentum to reduce the global emissions of greenhouse gases. For example, France approved the law no. 2015-992, which requires a 40% reduction of greenhouse gases by 2030 compared to 1990 [15]. Usage of fossil fuels undoubtedly accounts for the major source of greenhouse gases and, in this regard, reports from the United States Environmental Protection Agency show that fossil fuels account for 76% of all US emissions due to human activities [16]. In 2017, more than 85% of the energy produced globally came from fossil fuels [17]. Thus, it has become quite clear that a significant reduction of greenhouse gas emissions implies the reduction in the usage of fossil fuels. But an immediate abolition of the usage of fossil fuels would result in an

*Conceptual Density Functional Theory: Towards a New Chemical Reactivity Theory*, First Edition.

Edited by Shubin Liu.

© 2022 WILEY-VCH GmbH. Published 2022 by WILEY-VCH GmbH.

acute energy crisis [18–20]. This aspect represents a significant problem to find suitable energy sources. And, in this regard, the usage and utilities of alternative non-conventional and renewable energy resources creep in. Such resources should function as energy reservoirs and energy carriers as well. Hydrogen, due to its abundance [21] and diverse production sources, is becoming a viable, clean, and green option for energy transportation and storage. Hydrogen demonstrates itself as one of the simplest chemical systems and upon combustion produces water as a harmless by-product.  $\text{NO}_x$ ,  $\text{SO}_x$ ,  $\text{CO}_2$ , and other harmful particulates have no truly positive impact on decarbonization. Hydrogen has thus been conceived as a clean fuel source unlike the oil and natural gas resources and therefore seldom pollutes the environment. Moreover, hydrogen has the highest energy density per kilogram as compared to other combustible fuels, particularly natural gas. However, the use of hydrogen as a fuel source depends on its effective and safe means of storage. Hydrogen is extremely reactive in nature and therefore is not easy to control. It readily participates in combustion process and is also highly flammable, which may be a concern for its steady usage in passenger vehicles plying on ordinary terrain roads. The hydrogen tank, unlike the common fuel tanks, requires to be mounted beneath the vehicle in a more protected manner to avoid any friction/collision with road debris. Again, hydrogen in its gaseous state and at normal atmospheric pressure occupies a large volume. It requires very high pressure and cryogenic conditions to be liquefied and stored in manageable quantities. Maintenance of such extreme temperature and pressure conditions seems practically quite improbable for daily purposes. The main hurdle behind the use of hydrogen as an effective fuel appears to be the lack of proper storage materials that can be produced at large scale, easily handled under normal conditions, and which can also efficiently bind and store hydrogen in manageable gravimetric and volumetric amounts in a reversible fashion. The storage solution requires some breakthroughs in producing materials having better performance abilities thereby meeting the standard criteria set up by the US Department of Energy (DOE). In this regard, during the last two decades, scientists have been quite successful in the modeling and development of novel molecular networks that can efficiently bind and store hydrogen under ambient conditions. Numerous reviews on hydrogen storage have been published [22–27]. A few recent articles portraying the plausible usages of several materials as trapping agents [28–31] and renewable energy storage media [32–36] for hydrogen are worth mentioning. Moradi and Groth [37], in their recent article, have made a detailed review of the state-of-the-art techniques in hydrogen storage and delivery and the associated risk and reliability issues.

Several attempts have been made to find suitable molecular materials and frameworks that can serve as potential templates for hydrogen storage. The high reactivity of hydrogen has motivated the scientists to design several kinds of molecular templates containing both metal and non-metal as their active sites. There are so many active sites for hydrogen storage as sheet like graphene, nanomaterials containing the tubular nanostructures/nanoribbons, [38–45] fullerene-type cages and clathrate compounds, [46–66] metal hydrides and metal cluster assemblies, [67–77] or the

metal organic frameworks (MOFs)/covalent organic framework [78–98]. In this chapter, we have made an attempt to briefly describe the major forms of molecular materials and frameworks that can serve as potential templates for hydrogen storage by using a conceptual density functional theory (CDFT) based approach.

## 26.2 Conceptual DFT Approach for Hydrogen Storage Materials

CDFT, over the last few decades, has established itself as a powerful mathematical algorithm toward elucidating the ground-state properties of molecules [99–103]. The given theory is the brainchild of Chattaraj [104], who is credited as the founder of a vast DFT community that has eventually introduced some important mathematical response functions better known as the conceptual DFT-based reactivity descriptors. The variations of these molecular descriptors correspond very well with the changes in the structure, bonding, and reactivity of chemical systems. The important reactivity descriptors include the parameters like electronegativity ( $\chi$ ) [105, 106], hardness ( $\eta$ ) [107, 108], and electrophilicity ( $\omega$ ) [109–112], which have already been established quantitatively to understand molecular reactivity. An in-depth analysis of the reactivity of a specific atomic site in a molecule can be rationalized by a scrutiny of the various local reactivity descriptors like atomic charges ( $Q_k$ ) [113] and Fukui functions ( $f_k$ ) [114], which indeed play a key role toward determining the site selectivity of a chemical species. For an  $N$ -electron system, the electronegativity ( $\chi$ ) [105] and hardness ( $\eta$ ) [107] can be defined as follows:

$$\chi = -\left(\frac{\partial E}{\partial N}\right)_{v(r)} = -\mu \quad (26.1)$$

$$\eta = \left(\frac{\partial^2 E}{\partial N^2}\right)_{v(r)} \quad (26.2)$$

and

$$\omega = \left(\frac{\chi^2}{2\eta}\right) = \left(\frac{\mu^2}{2\eta}\right) \quad (26.3)$$

with  $v(r)$  and  $\mu$  as the external and chemical potentials, respectively.

Using finite difference method, electronegativity and hardness can be expressed as follows:

$$\chi = \frac{(I + A)}{2} \text{ and } \eta = (I - A) \quad (26.4)$$

where  $I$  and  $A$  represent the ionization potential and electron affinity of the system, respectively, and are computed in terms of the energies of  $N$  and  $N \pm 1$  electron systems. For an  $N$ -electron system with energy  $E(N)$ , these may be expressed as follows:

$$I \approx E(N + 1) - E(N) \quad (26.5)$$

$$A \approx E(N) - E(N - 1) \quad (26.6)$$

If  $E_{\text{HOMO}}$  and  $E_{\text{LUMO}}$  are the energies of the highest occupied and lowest unoccupied molecular orbitals, then Eq. (26.4) can be written using Koopmans' theorem as:

$$\chi = -\frac{(E_{\text{HOMO}} + E_{\text{LUMO}})}{2}$$

and  $\eta = (E_{\text{LUMO}} - E_{\text{HOMO}})$  (26.7)

The local reactivity descriptor, Fukui function (FF) [114], measures the change in electron density at a given point when an electron is added to or removed from a system at constant  $v(\mathbf{r})$ . It may be written as Eq. (26.8):

$$f(r) = \left( \frac{\partial \rho(r)}{\partial N} \right)_{v(r)} = \left( \frac{\delta \mu}{\delta v(r)} \right)_N$$
 (26.8)

Condensation of this Fukui function  $f(r)$  [115] to an individual atomic site  $k$  in a molecule gives rise to the following expressions in terms of electron population  $P_k$

$$f_k^+ = P_k(N + 1) - P_k(N)$$

For nucleophilic attack (26.9a)

$$f_k^- = P_k(N) - P_k(N - 1)$$

For electrophilic attack (26.9b)

$$f_k^0 = [P_k(N + 1) - P_k(N - 1)]/2$$

For radial attack (26.9c)

The site selectivity for a particular atomic site in a molecule can be obtained from their local philicity ( $\omega_k^\alpha$ ) also. The condensed-to-atom local philicity ( $\omega_k^\alpha$ ;  $\alpha = +, -, 0$  representing nucleophilic, electrophilic, and radical attacks, respectively) variants for the  $k$ th atomic site in a molecule is expressed as:

$$\omega_k^\alpha = \omega \cdot f_k^\alpha$$
 (26.10)

A variation of the above reactivity parameters along the reaction path of a favorable chemical process also obeys some allied molecular electronic structure principles, viz. the maximum hardness principle (MHP) [116, 117], minimum polarizability principle (MPP) [118, 119], and minimum electrophilicity principle (MEP) [120, 121]. These molecular electronic structure principles in conjunction with the thermodynamic parameters like interaction energy ( $IE$ ), gain in energy ( $GE$ ), reaction enthalpy ( $\Delta H$ ), and dissociative chemisorption energy ( $\Delta E_{\text{CE}}$ ) help determine the mode of hydrogen binding on to the various molecular clusters that have been modeled theoretically. The  $IE$ ,  $GE$ , and  $\Delta E_{\text{CE}}$  are expressed as:

$$IE = E_{n\text{H}_2\text{X}} - [E_X + nE_{\text{H}_2}]; \quad n = \text{no. of molecular H}_2$$
 (26.11)

$$GE = E_{(n-1)\text{H}_2\text{X}} + E_{\text{H}_2} - E_{n\text{H}_2\text{X}}$$
 (26.12)

$$\Delta E_{\text{CE}} = \frac{2}{n} \left[ E_X + \frac{n}{2} E_{\text{H}_2} - E_{\text{XH}_2} \right]; \quad n = \text{no. of H atoms}$$
 (26.13)

where  $E_X$  denotes the energy of the parent moiety.

Additional insights into the stability of these structural motifs can be gained by the criterion of “all-metal aromaticity” [122–124], which can be mathematically assessed from an evaluation of various aromaticity indices like nuclear-independent chemical shift [125] (NICS). NICS(0) for a planar ring molecule signifies the amount of absolute magnetic shielding computed at ring center. Subsequently NICS(1) defines the same computed at a distance of 1 Å perpendicular to the ring plane. The NICS rate at a given distance ( $r$ ) from the ring center is calculated with the following mathematical formula given as [126–129] Eq. (26.14):

$$\text{NICS}_{\text{rate}}(r) = \frac{d\text{NICS}}{dr} = \text{Lim}_{\Delta r \rightarrow 0} \frac{\text{NICS}(r + \Delta r) - \text{NICS}(r)}{\Delta r} \quad (26.14)$$

### 26.3 Computational Details

All the geometries presented here have been optimized at several levels of theory (B3LYP, MP2, MPW1K, MO52X) using various basis sets (cc-pvdz, 6-31G, 6-31+G(d), 6-311+G(d), 6-311+G(d,p)). All the computations have been performed using GAUSSIAN 03 [130] program package. The choice of the level of theory and basis set varies with the systems under study. All the structures reported were fully optimized without any symmetry constraint. Zero numbers of imaginary frequencies (NIMAG) for all optimized molecular structures confirm that they correspond to minima (global or local) on their respective potential energy surfaces (PESs). The ionization potential ( $I$ ) and electron affinity ( $A$ ) values were either calculated with the aid of Koopmans’ theorem [131] or by using a  $\Delta$ SCF technique. The atomic charges ( $Q_k$ ) and Fukui functions ( $f(\mathbf{r})$ ) were computed using the Mulliken population analysis (MPA) or the natural population analysis (NPA) scheme.

### 26.4 Designing of Hydrogen-Binding Building Blocks

It has been observed [132] that the trigonal aromatic all-metal  $\text{Li}_3$  as well as non-metallic  $\text{H}_3^+$  species can bind a number of noble gases (He–Kr). Extending this idea, Giri et al. [133] have investigated the possibility of trapping hydrogen molecules by all-metal aromatic clusters  $\text{Li}_3^+$  and  $\text{Na}_3^+$ . The use of  $\text{Mg}_n$  and  $\text{Ca}_n$  ( $n = 8$ –10) cages as a trap for hydrogen is also studied. The endohedrally trapped single  $\text{H}_2$  molecule retains its molecular form inside the cages except for the  $\text{Ca}_{10}\text{H}_2$  complex. Here it is stabilized in its atomic form. For the aromatic  $\text{Li}_3^+$  and  $\text{Na}_3^+$  systems, hydrogen remains in molecular form upon binding with Li/Na atoms. After binding with  $\text{H}_2$ , the  $\text{Li}_3^+$  and  $\text{Na}_3^+$  retain their planarity. Figure 26.1 presents the optimized molecular geometries of the  $\text{H}_2$ -trapped  $\text{Mg}_n$  and  $\text{Ca}_n$  ( $n = 8$ –10) cages along with hydrogen-loaded  $\text{Li}_3^+$  and  $\text{Na}_3^+$ .

A detailed study of various  $\text{H}_2$ -bound  $\text{Li}_3^+$  and  $\text{Na}_3^+$  systems shows that the total energy ( $E$ ) of the system gradually decreases upon increasing the number of hydrogens. Further understanding from the changes in hardness ( $\eta$ ) and

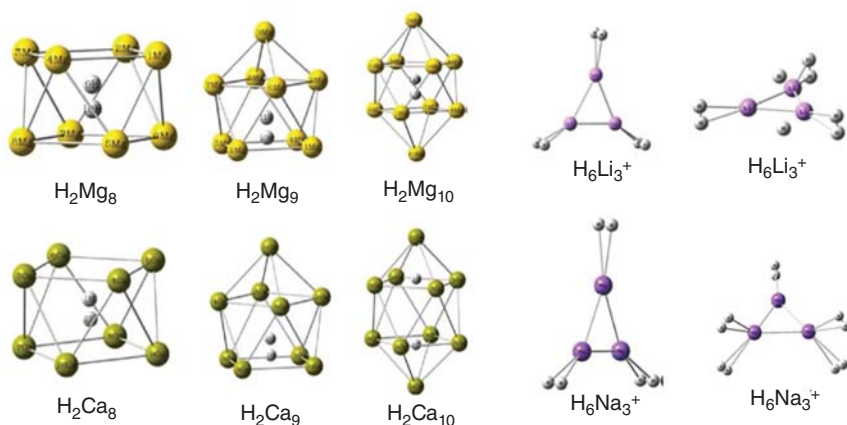


**Figure 26.1** Optimized geometries of hydrogen-absorbed Mg/Ca and Li<sub>3</sub><sup>+</sup>/Na<sub>3</sub><sup>+</sup> clusters. Source: Reproduced from Ref. [133] with permission from Springer-Verlag, Berlin, Germany.

electrophilicity ( $\omega$ ) shows that with increasing cluster size the  $\omega$  values exhibit a uniform decline indicating molecular reactivity. To see the aromatic nature of these systems, NICS (0,1) values for the upper and lower rings of the H<sub>2</sub>-trapped Mg<sub>*n*</sub> and Ca<sub>*n*</sub> (*n* = 8–10) cages were calculated. The negative NICS value reveals that the metallic cage clusters possess aromatic stability. Analogous NICS<sub>zz</sub> trends for the Li<sub>3</sub><sup>+</sup> and Na<sub>3</sub><sup>+</sup> clusters and their various H<sub>2</sub>-loaded complexes establish the existence of a favorable aromaticity criterion for gradual hydrogen adsorption. The negative reaction energy ( $\Delta E$ ) values for gradual H<sub>2</sub> adsorption on the Li<sub>3</sub><sup>+</sup> and Na<sub>3</sub><sup>+</sup> molecules lend thermodynamic support behind the spontaneity of the given reactions and the usage of the all-metal trigonal motifs as plausible hydrogen storage materials. Not only these alkali systems, but also the efficiency of the transition metal–ethylene complexes as an effective media for hydrogen binding has been further studied [134] from a conceptual DFT viewpoint. Transition metals like Sc, Ti, Fe, and Ni coupled with the C<sub>2</sub>H<sub>4</sub> molecule comprise the base moiety, M<sub>*n*</sub> – (C<sub>2</sub>H<sub>4</sub>) (M = Sc, Ti, Fe, Ni; *n* = 1, 2), where the metal atom acts as the hydrogen-binding site via Kubas interaction. Figure 26.2 illustrates some representative hydrogen-bonded molecular structures.

The total energy (*E*) of the H<sub>2</sub>-trapped complexes decreases as usual upon gradual loading. However, the trends in the associated  $\eta$  and  $\omega$  values do not follow any particular pattern for the Sc- and Ti-bound ethylene complexes. However, the  $\eta$  and  $\omega$  values of the associated H<sub>2</sub>-bound complexes corroborate with each other for the Fe- and Ni-bound ethylene molecules at the B3LYP level.

Here, the  $\eta$  values uniformly increase with increasing number of H<sub>2</sub>. The associated  $\omega$  values follow exactly opposite trend. The principles of maximum hardness and minimum electrophilicity are obeyed well in these cases. Important parameters like the *IE*, reaction electrophilicity ( $\Delta\omega$ ), and the associated reaction enthalpy ( $\Delta H$ ) are negative in most of the cases, which justify the spontaneity of the H<sub>2</sub> adsorption on metal–ethylene complexes. The dissociative chemisorption energy ( $\Delta E_{\text{CE}}$ ) values for the given reactions are all positive, which gradually decrease with increasing



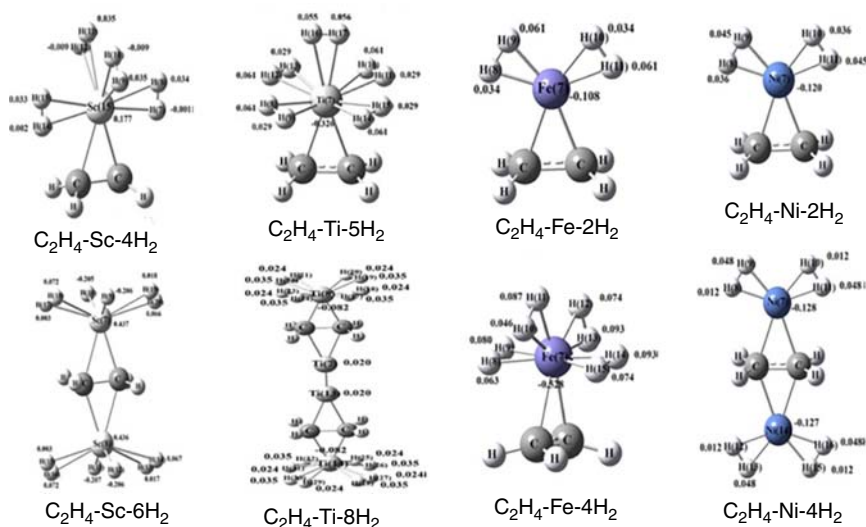


**Figure 26.2** M-ethylene (M=Sc, Ti, Fe, Ni) complex and its corresponding H<sub>2</sub>-trapped analogues. Source: Reproduced from Ref. [134] with permission from Springer-Verlag, Berlin, Germany.

hydrogen coverage. A positive  $\Delta E_{CE}$  value triggers favorable hydrogen binding with the metal center, while a decline in the same reveals that upon gradual hydrogen loading the driving force for hydrogen dissociation decreases further [135]. Thus the potency of metal-ethylene complexes for the H<sub>2</sub> trapping can be analyzed by using conceptual DFT descriptors.

Apart from that, Chattaraj and coworkers [136, 137] have investigated the use of cage-like clathrate hydrate molecules as well as the (BN)<sub>12</sub> clusters as possible hydrogen storage materials. The number of H<sub>2</sub> molecules encapsulated within the clathrate hydrate clusters depends on the cage size. It is observed that for the 5<sup>12</sup> and 5<sup>12</sup>6<sup>2</sup> cages, encapsulation of two H<sub>2</sub> molecules is energetically favorable, while the 5<sup>12</sup>6<sup>8</sup> moiety allows up to six H<sub>2</sub> molecules to bind endohedrally. Some model conformations involving the encapsulation of as many as five H<sub>2</sub> molecules in the 5<sup>12</sup> and 5<sup>12</sup>6<sup>2</sup> cages and six hydrogens in the 5<sup>12</sup>6<sup>8</sup> system are illustrated in Figure 26.3.

A variation in the conceptual DFT-based reactivity descriptors in conjunction with the favorable *IE* values builds a strong rationale toward justifying the stability of the H<sub>2</sub>-encapsulated clathrate complexes. An increase in the hardness values is well complemented by a decrease in the allied electrophilicities. The stability of the H<sub>2</sub>-trapped clathrate complexes increases with an increase in the number of H<sub>2</sub> molecules bound in an endohedral fashion. However, in spite of some dependence on the level of computations invoked, the clathrate molecules are found to be quite useful for the purpose of hydrogen storage. Srivastava et al. in a recent communication have further analyzed the efficacy of the 5<sup>12</sup>6<sup>8</sup>-clathrate cage toward incorporating more hydrogens. This study reports that the encapsulation of up to eight H<sub>2</sub> molecules in the 5<sup>12</sup>6<sup>8</sup> cage is favorable with gradually decreasing

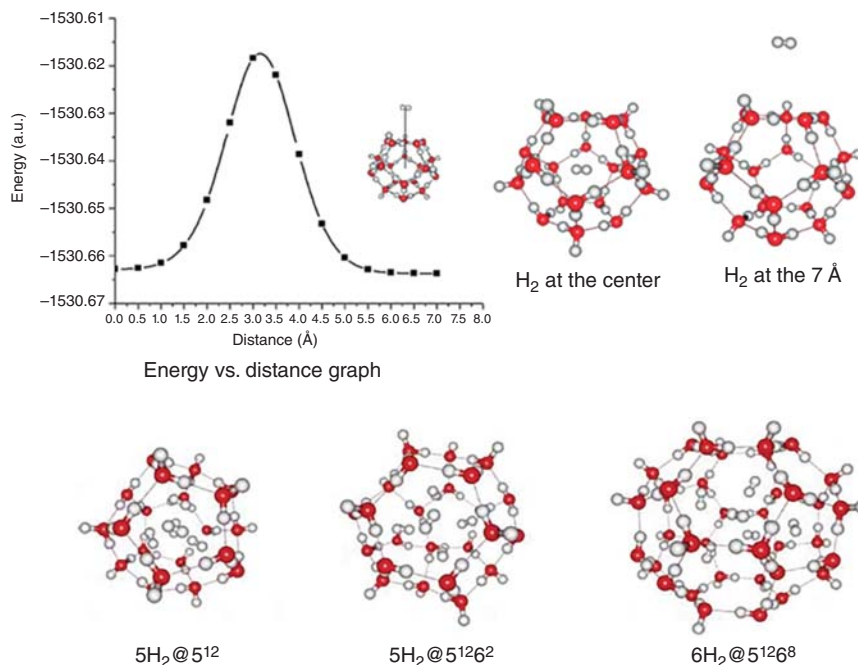


**Figure 26.3** Schematic representation for encapsulation of hydrogen trapping within different clathrate cages at B3LYP/6-31G(d) level of theory. Source: Reproduced from Ref. [136] with permission from American Chemical Society, Washington DC, USA.

*IE* values. However, for further  $\text{H}_2$  incorporation, the *IE* values increase but still remain negative up to 15  $\text{H}_2$  molecules. An attempt to bind another molecule remains unsuccessful at the given level of theory [B3LYP/6-31G(d)]. In further efforts, Chattaraj and coworkers [138] reported doped hydrate cages via the replacement of one water molecule in the clathrate assembly by one HF molecule. Moreover, they mentioned that by means of HF doping stability of water cages increases substantially without any significant change in the skeleton and shape. Thermochemical data and conceptual DFT results reveal that HF doping in  $5^{12}$ ,  $5^{12}6^2$ ,  $5^{12}6^8$ ,  $5^{12}6^4$ , and  $4^35^66^3$ , as well as in  $\text{CH}_4@5^{12}$ ,  $\text{CH}_4@5^{12}6^8$ ,  $\text{CH}_4@5^{12}6^4$ , and  $\text{CH}_4@4^35^66^3$  systems is feasible. Maximum six numbers of  $\text{H}_2$  molecules can be encapsulated by the  $5^{12}6^8$  clathrate, whereas  $\text{HF}5^{12}$ ,  $\text{HF}5^{12}6^2$  can encapsulate up to two hydrogen molecules (see Figure 26.4). Inference conceived by the thermochemical data and CDFT results is further supported by the *ab initio* molecular dynamics (AIMD) simulations on the doped systems up to 500 fs at different temperatures. It was noted that HF-doped  $5^{12}$  and  $5^{12}6^8$  systems remain stable up to 500 fs at 200 K. On the other hand, development of water trimer and tetramer was noted from 125 fs in the HF-doped  $5^{12}6^2$ . Excluding the case of  $5^{12}6^2$ , AIMD studies help in inferring the fact that HF doping facilitates the  $\text{H}_2$  uptake by clathrate hydrates. In addition to this, AIMD results reveal the more kinetic stability of the studied HF-doped hydrates in comparison to their undoped analogues.

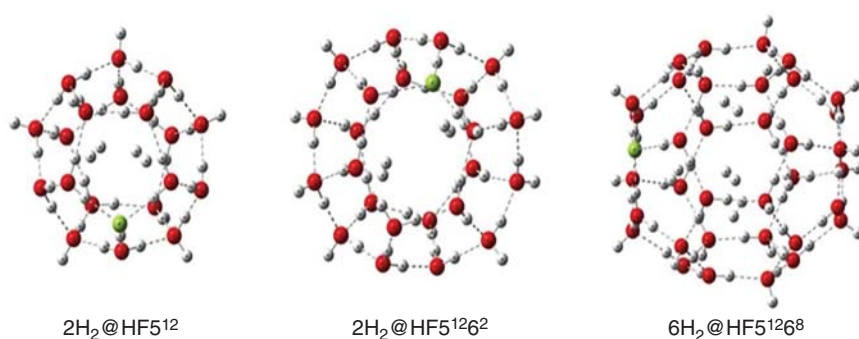


**Figure 26.4** Hydrogen-encapsulated forms of  $\text{HF}_5^{12}$ ,  $\text{HF}_5^{12}6^2$ , and  $\text{HF}_5^{12}6^8$  at DFT-D-B3LYP/6-311+G(d,p) level of theory. Source: This figure is reproduced from the work of Chattaraj et al. [136] with permission from American Chemical Society.

The research group of Chattaraj et al. further studied the noble gas hydrates and their HF-doped analogues in view of He, Ne, and Ar as the guest entities. In accordance with the cavity size of the gas hydrates and size of the considered noble gas atoms, it was found and reported that the dodecahedron hydrate cavity and the HF-doped counterpart can engage up to five He atoms, three Ne atoms, and two Ar atoms. But, according to the thermodynamical data, encapsulation of only one noble gas (He, Ne, and Ar) atom is feasible. The bigger hosts,  $5^{12}6^8$  and its HF-doped analogue, can encapsulate up to 9 He/6 Ne/6 Ar atoms and 10 He/6 Ne/6 Ar atoms, respectively. In a nutshell, HF doping improves the noble gas encapsulation capacity. Moreover, it is disclosed that bigger size of the Ng atom as well as smaller cavity size of the host water cage favors the encapsulation most significantly. On the other hand, it is understood that HF doping makes the encapsulation of one Ng atom thermodynamically most favorable. Interaction between the noble gas atoms and the host water cage, particularly, Ng–O, Ng–F, and Ng–Ng contacts, is found to be noncovalent in nature. AIMD study disclosed the fact that at 298 K the dodecahedron hydrate cage and the HF-doped analogue can keep one He/Ne/Ar guest up to 500 fs. Contrastingly, the icosahedron hydrate and the HF-doped analogue can keep up to 8 and 10 He atoms at 225 and 298 K, respectively, up to 500 fs [109]. It is important to mention here that the HF-doped moiety developed minor distortion in the cage wall. In the same time scale at 225 and 150 K temperatures, the  $5^{12}6^8$  and  $\text{HF}_5^{12}6^8$  hydrates, respectively, can engage up to 6 Ne atoms. In case of Ar gas encapsulation, it was noted that the icosahedron and HF-doped analogue hosts can retain maximum six atoms up to 500 fs, but at 298 K temperature the hydrate skeleton collapses in to the formation of water trimer and tetramer rings within the host wall.

The  $\text{B}_{12}\text{N}_{12}$  cage templates as opposed to the clathrate hydrates, however, prefer not to encapsulate the hydrogen molecules inside the cage framework. It prefers to form stable  $\text{H}_2$ -bound complexes through an exohedral arrangement of the incoming  $\text{H}_2$  molecules around the  $\text{B}_{12}\text{N}_{12}$  core as envisaged in Figure 26.5.

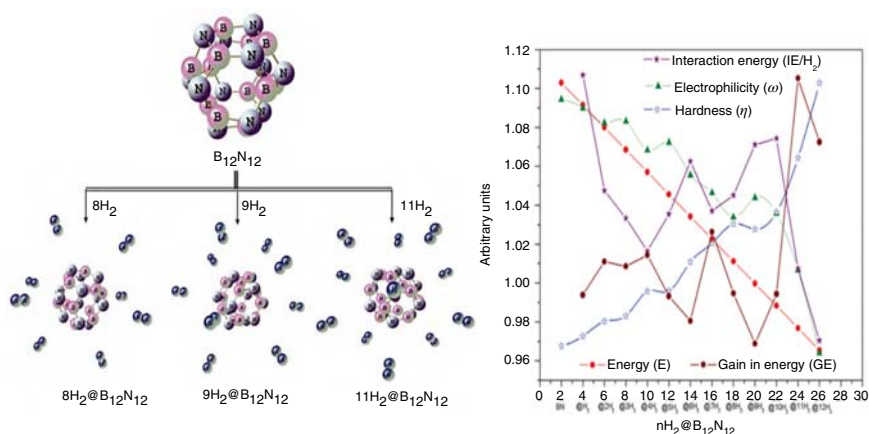


**Figure 26.5** Optimized geometries (B3LYP/6-311+G(d)) of  $B_{12}N_{12}$  and some representative  $nH_2@B_{12}N_{12}$  structures and their corresponding interaction energy with hydrogen atoms along with electrophilicity and hardness indexes. Source: Reproduced from Ref. [137] with permission from Co-action Publishing, Sweden.

An in-depth analysis of the  $nH_2@B_{12}N_{12}$  ( $n = 1-12$ ) clusters under the paradigm of conceptual DFT approach displays some unique trends in terms of their stability and reactivity patterns. The electronegativity ( $\chi$ ) values of the  $nH_2@B_{12}N_{12}$  ( $n = 1-12$ ) clusters decline upon increasing hydrogen coverage, a trend that clearly depicts the unwillingness of the cluster complexes toward attracting electrons upon cluster growth. The larger  $nH_2@B_{12}N_{12}$  ( $n = 1-12$ ) complexes thus tend to evade interactions. The variation of the chemical hardness ( $\eta$ ) and electrophilicity ( $\omega$ ) values of the hydrogen-bound  $nH_2@B_{12}N_{12}$  ( $n = 1-12$ ) complexes show a reverse trend upon gradual hydrogen loading, where the  $\eta$  values rise and  $\omega$  values fall upon increasing complexation. This trend does signify the veracity of the molecular electronic structure principles like maximum hardness principle (MHP) and MEP toward justifying molecular stability. For a set of some plausible  $H_2$ -binding reactions with the  $B_{12}N_{12}$  cage, the associated parameters depict favorable and spontaneous processes. The GE values in spite of showing some unusual patterns however increase with gradual hydrogen loading. This eventually establishes the stability of the  $nH_2$ -trapped ( $n = 1-12$ )  $B_{12}N_{12}$  clusters as compared to the bare  $B_{12}N_{12}$  cage system. The cage aromaticity of the bare as well as  $nH_2$ -trapped ( $n = 1-12$ )  $B_{12}N_{12}$  complexes computed in terms of the NICS(0) values specifies that the cage moiety is aromatic and hence stable. Yet, the aromaticity criterion may not always be considered as the sole determinant toward determining molecular stability. For the  $nH_2@B_{12}N_{12}$  ( $n = 1-12$ ) complexes, the conceptual DFT-based reactivity descriptors ( $\Delta\omega$ , governing reaction spontaneity) along with the vital energy parameters like  $IE$  per  $H_2$  molecule,  $GE$ , reaction enthalpy ( $\Delta H$ ) play a pivotal role toward determining the stability of the  $H_2$ -loaded clusters. A favorable aromaticity criterion in terms of a negative NICS value for the  $B_{12}N_{12}$  cage thus justifies the usage of the given cage cluster as an effective hydrogen storage material.

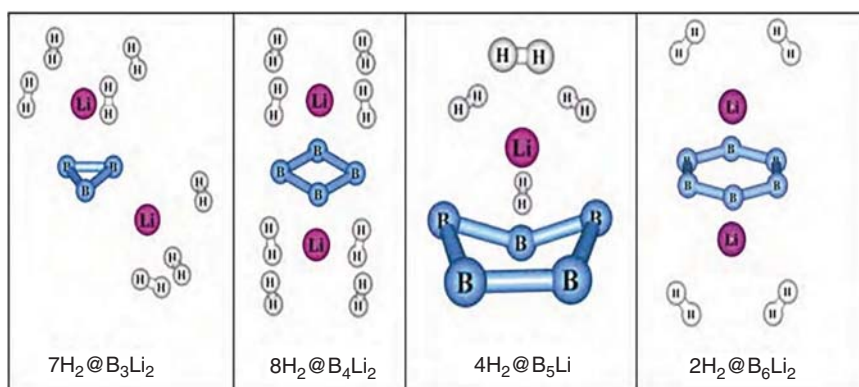


**Figure 26.6**  $B_xLi_y$  ( $x = 3-6$ ;  $y = 1, 2$ ) and its hydrogen-trapped analogues at MP2/6-311\_G(d) level of theory. Source: Reproduced from Ref. [139] with permission from John Wiley & Sons, Inc., New York.

Now, considering the ability of metal atoms/ions as good hydrogen-trapping sites, metal-doped non-metallic clusters can be designed as suitable hydrogen-binding templates. A glimpse of this idea is the simple metal–ethylene complexes where a metal atom upon binding with the ethylene moiety acts as an active site for trapping  $H_2$  molecules. Studies by Bandaru et al. [139] on some uniquely designed small-to-medium Li-doped boron–lithium ( $B_xLi_y$ ,  $x = 2-6$ ;  $y = 1, 2$ ) neutral and charged cluster molecules (Figure 26.6) reflect the potential of such metal-doped non-metallic clusters as hydrogen storage materials. Further studies under the paradigm of CDFT-based descriptor approach reveal that the clusters carrying a formal charge are more keen toward trapping hydrogen, which is evident from the higher  $\omega$  values of the  $H_2$ -loaded charged complexes as compared to the corresponding neutral templates. A clear distinction in the orientation of the B and Li atoms of the parent  $B_xLi_y$  moiety ( $x = 2-6$ ;  $y = 1, 2$ ) is observed among some of the associated neutral and charged analogues. Moreover, the molecular geometry of the parent  $B_xLi_y$  cluster undergoes a noticeable change upon gradual hydrogen loading.

The atomic charges ( $q_M$ ) on the Li-sites fall with gradual hydrogen loading. This is a sure indication of a metal–ligand interaction between the central metal core and the approaching dihydrogen ligands thus imitating the Kubas model of hydrogen binding. The  $IE$ , reaction enthalpy ( $\Delta H$ ), and reaction electrophilicity ( $\Delta\omega$ ) of all the stepwise hydrogen-binding reactions are negative, which warrants a steady hydrogen upload on the given neutral and cationic boron–lithium  $B_xLi_y$  ( $x = 2-6$ ;  $y = 1, 2$ ) cluster motifs. The reaction electrophilicity values of all the probable trapping reactions of the neutral and charged systems are negative, which is at par with the MEP, an essential criterion toward explaining molecular stability. A steady decline in the chemisorption energy ( $\Delta E_{CE}$ ) values of the stepwise hydrogen-binding reactions with the neutral and charged B–Li clusters lends additional support for a spontaneous  $H_2$  coverage and establishes the plausible usage of the above metal-doped non-metallic clusters as effective templates for

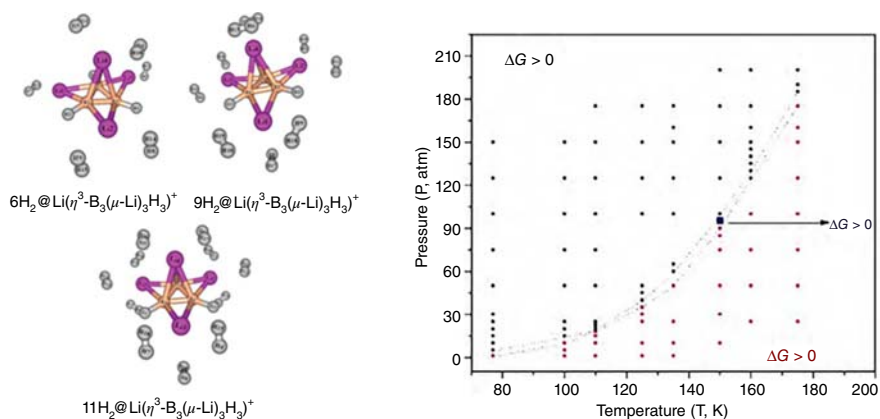


**Figure 26.7** Temperature–pressure phase diagram showing the variation of  $\Delta G$  for the 6H<sub>2</sub> adsorption process on B<sub>3</sub>(μ-Li)<sub>3</sub>H<sub>3</sub><sup>+</sup> cluster. Source: Reproduced from Ref. [140] with permission from John Wiley & Sons, New York.

hydrogen binding. Further studies [140] show that under suitable gravimetric conditions, the aromatic B<sub>3</sub>H<sub>3</sub><sup>2-</sup> unit along with its various Li/Li<sup>+</sup>-doped variants are capable of trapping hydrogen molecules. The computed energy parameters and NICS values favor a spontaneous hydrogen binding. A graphical investigation of the variation of the Gibbs' free energy ( $\Delta G$ ) of the reaction process with its temperature ( $T$ ) and pressure ( $P$ ) ( $T$ – $P$  phase diagram) clearly indicates the  $T$ – $P$  zone where the  $\Delta G$  values are negative (Figure 26.7). Thus, in these regions the hydrogen adsorption process at the given temperatures and pressures turns out to be a thermodynamically favorable one. The  $T$ – $P$  regions having positive  $\Delta G$  values, unlike the preceding process, favor a dissociative reaction mechanism that involves desorption of hydrogen from the B-Li-loaded clusters. The region depicting a  $\Delta G = 0$  value corresponds to an equilibrium state. Such  $T$ – $P$  phase diagrams, therefore, become an extremely helpful probe for the experimentalists regarding their choice of an optimal temperature–pressure condition to be exercised for a favorable reversible hydrogen storage process.

Aromatic/antiaromatic annular ring systems upon complexation with suitable counterions can be utilized as plausible hydrogen-trapping templates. A study by Duley et al. [141] elaborated the ability of planar N<sub>4</sub><sup>2-</sup> and N<sub>6</sub><sup>4-</sup> rings to adsorb hydrogen molecules upon binding with suitable counterions. A marked increase in the aromaticity of the planar N<sub>6</sub><sup>4-</sup> ring is observed upon binding with the two Ca<sup>2+</sup> counter cations (through cation– $\pi$  interactions), which is evident from the highly negative NICS(0) values. Further negative values of the allied NICS(0.5) and NICS(1) for the N<sub>6</sub><sup>4-</sup> ring do manifest the existence of a favorable  $\pi$ -ring current above and below the hexagonal plane. The N<sub>4</sub><sup>2-</sup> ring is antiaromatic with a positive NICS(0) value and continues to remain the same upon binding with two Li<sup>+</sup> counterions. However, the NICS(0.5) and NICS(1) values of the N<sub>4</sub>Li<sub>2</sub> system become increasingly more negative, which favors the existence of a  $\pi$ -aromaticity above and below the ring plane. It may be mentioned that the N<sub>4</sub><sup>2-</sup> ring in analogy

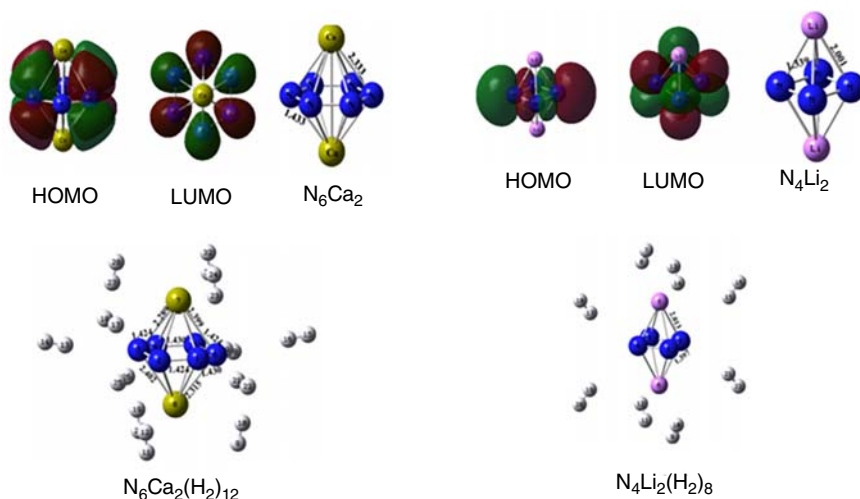


**Figure 26.8** Optimized geometry, HOMO, LUMO of  $N_6Ca_2$  and  $N_4Li_2$  and their hydrogen-trapped complexes. Source: Reproduced from Ref. [141] with permission from Elsevier, Amsterdam, The Netherlands.

with the  $Al_4^{4-}$  system exhibits a conflicting aromaticity in the sense that both  $\sigma$ -antiaromaticity and  $\pi$ -aromaticity are equally discernible [142]. The optimized structures of  $N_6Ca_2$  and  $N_4Li_2$  and the corresponding hydrogen-trapped complexes are depicted in Figure 26.8.

The adsorption energies ( $\Delta E_{\text{ads}}$ ) of the  $N_6Ca_2$  and  $N_4Li_2$  molecules show a favorable trend upon gradual hydrogen loading. So, the counterion-bound aromatic  $N_6Ca_2$  and  $N_4Li_2$  molecules become suitable stuffs for an effective hydrogen storage. The efficacy of this strategy to dope counter-ions in an all-metal aromatic framework and its further usage as hydrogen storage templates are well illustrated by Srinivasu et al. [143]. In their study, planar all-metal aromatic anionic systems like  $Be_3^{2-}$ ,  $Mg_3^{2-}$ , and  $Al_4^{2-}$  are bonded with alkali metal counter-cations to produce  $Be_3M_2$ ,  $Mg_3M_2$ , and  $Al_4M_2$  ( $M = Li, Na, \text{ and } K$ ) clusters. Among the two different metal sites in each of these clusters, the alkali metal sites owing to their higher charge/radius ratio seem to be more prone toward capturing hydrogen molecules. Thus, the alkali metal atom becomes the active binding site in these clusters. The overall efficiency of hydrogen adsorption in these all-metal clusters can also be figured out from the favorable  $\Delta H$  and  $\Delta\omega$  values of the associated hydrogen-binding reactions.

In another study by Giri et al. [144], the H atoms of some well-known planar aromatic/antiaromatic hydrocarbon systems like  $C_4H_4$ ,  $C_5H_5^-$ , and  $C_6H_6$  are substituted by the alkali metal Li to design some novel star-shaped molecular moieties formulated as  $C_4Li_4$ ,  $C_5Li_5^-$ , and  $C_6Li_6$ . These unique star-like clusters are then further investigated to see their potential as hydrogen-binding templates where the Li center owing to its higher charge density is supposed to serve as the active binding site as portrayed in Figure 26.9. In addition to that, mononuclear aromatic/antiaromatic systems starting from the smallest  $C_3$ -ring to

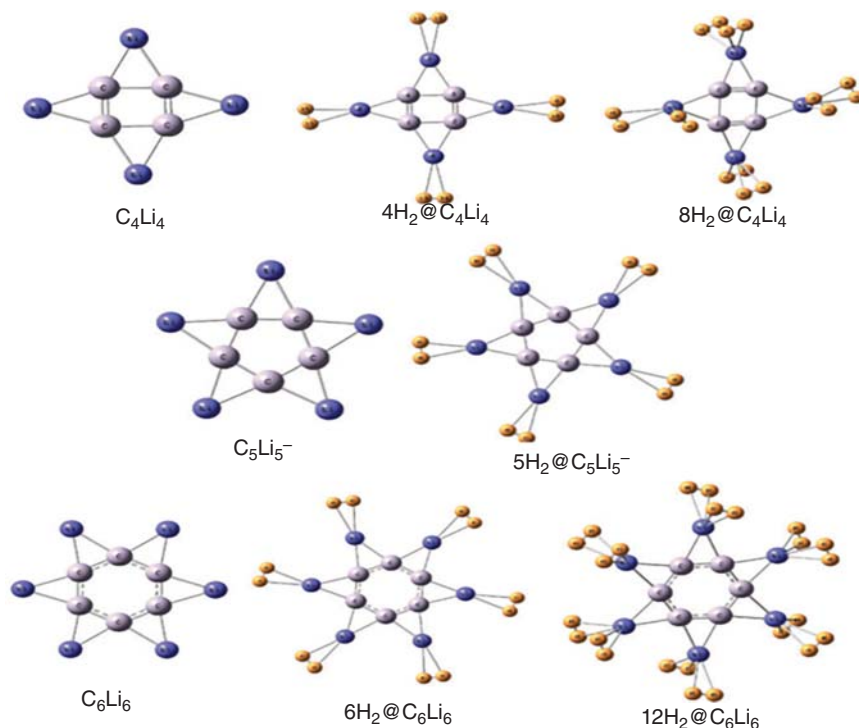


**Figure 26.9** Optimized molecular geometries of the Li-decorated “star-like” molecules and their associated hydrogen-bound complexes. Source: Reproduced from Ref. [144] with permission from Royal Society of Chemistry, London, UK.

the  $C_7$ -analogue (tropylium cation) as well as some polyaromatic hydrocarbons (PAHs) like naphthalene, anthracene, and phenanthrene are also doped with suitable  $Li^+/F^-$  counterions. A conceptual DFT approach is adopted to investigate the capability of these counterion-bound annular complexes toward effective hydrogen adsorption. Figure 26.10 represents some model conformations of the hydrogen-loaded mononuclear and polynuclear ring systems. An in-depth study of the effect of the aromaticity/antiaromaticity criterion of the central ring on the hydrogen-loading potential of these complexes, accompanied by some drastic changes if any (conversion from aromatic to antiaromatic or vice versa), is also carefully done. The results show that the aromaticity/antiaromaticity phenomenon of these planar rings, assessed in terms of the NICS criterion, hardly shows any radical change upon gradual hydrogen loading. The formal charge developed on the active binding site (the counterion) of the complexes therefore has a direct bearing on the potential of hydrogen uptake on these clusters. Additional insights into the efficacy of hydrogen loading in these complexes can be understood from a scrutiny of the associated energy parameters. The designing of these molecular clusters as potential hydrogen-binding templates therefore rests upon the conjoint effects of the changes in atomic charges on the counterion upon gradual increasing coverage followed by a favorable energy criterion. The sustenance of an aromaticity/



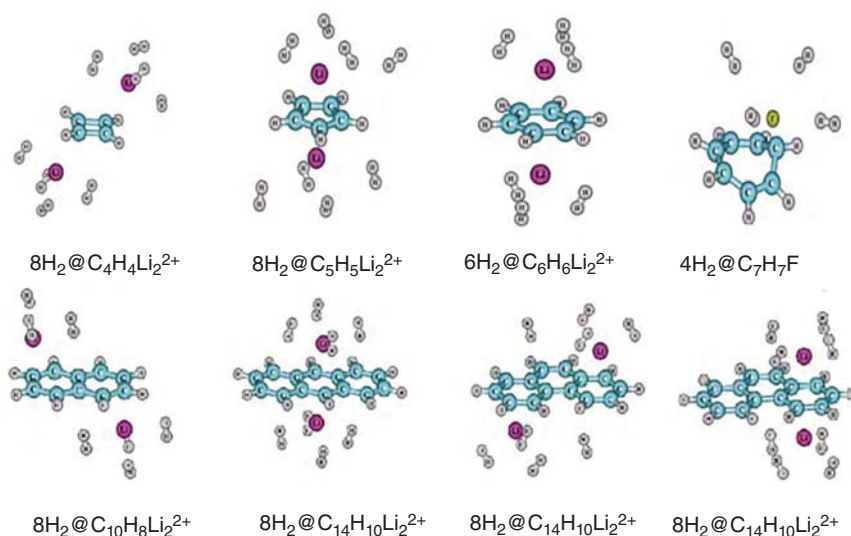


**Figure 26.10** Optimized geometries of the  $\text{Li}^+/\text{F}^-$  - doped aromatic/antiaromatic hydrocarbons and polyaromatic hydrocarbons (PAHs) and their associated hydrogen-bound complexes. Source: Reproduced from Ref. [144] with permission from Royal Society of Chemistry, London, UK.

antiaromaticity criterion in the resulting complexes adds a further dimension toward establishing their stability. The “star-like” complexes are quite unique and upon binding with suitable “linkers” can be envisaged as the building blocks for designing larger macromolecular cluster motifs suitable for storing hydrogen in bulk gravimetric amounts under ambient temperature and pressure conditions (Figure 26.10).

## 26.5 Concluding Remarks

An array of various benchmark experimental techniques along with some sophisticated theoretical algorithms have been implemented to design some novel molecular assemblies that can be used as potential templates for hydrogen storage. The powerful theoretical techniques of conceptual DFT in association with the various global and local reactivity descriptors are adopted as a yardstick to rationalize the stability of these molecular clusters and their efficacy toward hydrogen binding. The stability and reactivity of these molecular assemblies toward an efficient hydrogen binding have been explained from the dual perspectives of the important molecular electronic structure principles on one hand and a favorable energy criterion governing the reaction spontaneity on the other. The existence of an aromaticity/antiaromaticity criterion in some of the molecular clusters does add further insights into justifying the stability of the given complexes upon increasing the hydrogen coverage. The atomic charges on the respective local hydrogen-binding

sites of the clusters have a direct bearing on their gross hydrogen-loading aptitude. In summary, this chapter has made an attempt to employ modern methodologies within a conceptual DFT framework, in designing novel molecular assemblies that can serve as a potential and profitable media for the storage of hydrogen, an alternative future fuel for automobile and industrial applications.

## Acknowledgments

PKC would like to thank Professor Shubin Liu for the invitation. He also thanks DST, New Delhi, for the J. C. Bose National Fellowship and his students whose work is presented in this chapter.

## References

- 1 Stocker, T.F., Qin, D., Plattner, G.K. et al. (ed.) (2013). *IPCC, Climate Change 2013: The Physical Science Basis, contribution of Working Group I to the Fifth Assessment Report of the Intergovernmental Panel on Climate Change*, 1535. Cambridge, UK and New York, NY, USA: Cambridge University Press.
- 2 Walsh, B.S., Parratt, S.R., Hoffmann, A.A. et al. (2019). *Trends Ecol. Evol.* 34: 249.
- 3 CaraDonna, P.J., Cunningham, J.L., and Iler, A.M. (2018). *Funct. Ecol.* 32: 2345.
- 4 Hernandez-Ochoa, I.M., Asseng, S., Kassie, B.T. et al. (2018). *Agric. For. Meteorol.* 263: 373.
- 5 Kontgis, C., Schneider, A., Ozdogan, M. et al. (2019). *Appl. Geogr.* 102: 71.
- 6 Raymundo, R., Asseng, S., Robertson, R. et al. (2018). *Eur. J. Agron.* 100: 87.
- 7 Mazdiyasi, O. and AghaKouchak, A. (2015). *Proc. Natl. Acad. Sci. U. S. A.* 112: 11484.
- 8 Ogburn, S.P. (2014). *Indian monsoons are becoming more extreme*. Scientific American. <https://www.scientificamerican.com/article/indian-monsoons-are-becoming-more-extreme/>.
- 9 Warner, K., Ehrhart, C., de Sherbinin, A. et al. (2009). *Climate Change*. London, UK: CARE International.
- 10 Black, R., Bennett, S.R., Thomas, S.M., and Beddington, J.R. (2011). *Nature* 478: 447.
- 11 McLeman, R. and Smit, B. (2006). *Clim. Chang.* 76: 31.
- 12 Reuveny, R. (2007). *Polit. Geogr.* 26: 656.
- 13 Nordås, R. and Gleditsch, N.P. (2007). *Polit. Geogr.* 26: 627.
- 14 Barnett, J. (2003). *Glob. Environ. Chang.* 13: 7.
- 15 AFHYPAC and FNCCR (2018). Déployer les stations hydrogène dans votre territoire. <http://www.afhypac.org/documents/divers/GUIDE-STATION-HYDROGENE-WEB.pdf> (accessed 13 February 2019).
- 16 United States Environmental Protection Agency (2017). Inventory of U.S. greenhouse gas emissions and sinks:1990–2015. <https://www.epa.gov/sites/>

- production/files/201702/documents/2017\_complete\_report.pdf (accessed 13 February 2019).
- 17 (2018). B P statistical review of world energy. 67<sup>th</sup> ed. <https://www.bp.com/content/dam/bp/en/corporate/pdf/energy-economics/statistical-review/bp-stats-review-2018-full-report.pdf> (accessed 12 October 2018).
  - 18 Saito, S. (2010). *J. Nucl. Mater.* 398: 1.
  - 19 Salameh, M.G. (2003). *Appl. Energy* 75: 33.
  - 20 Friedrichs, J. (2010). *Energy Policy* 38: 4562.
  - 21 Mildred, D., Crabtree, G., and Buchanan, M. (2003). Basic research needs for the hydrogen economy, (Argonne National Laboratory, US Department of Energy, Office of Science Laboratory) 15 May 2003, <http://www.sc.doe.gov/bes/hydrogen.pdf>.
  - 22 Züttel, A. (2003). *Mater. Today* 6: 24.
  - 23 Abdalla, A.M., Hossain, S., Nisfindy, O.B. et al. (2018). *Energy Convers. Manag.* 165: 602.
  - 24 Durbin, D. and Malardier-Jugroot, C. (2013). *Int. J. Hydrogen Energy* 38: 14595.
  - 25 Wang, L. and Yang, R.T. (2008). *Energy Environ. Sci.* 1: 268.
  - 26 Jain, I., Jain, P., and Jain, A. (2010). *J. Alloy Compd.* 503: 303.
  - 27 Fakioglu, E., Yürüm, Y., and Nejat Veziroglu, T. (2004). *Int. J. Hydrogen Energy* 29: 1371.
  - 28 Jena, P. (2011). *J. Phys. Chem. Lett.* 2: 206.
  - 29 Zhou, L. (2005). *Renew. Sustain. Energy Rev.* 9: 395.
  - 30 Züttel, A. (2004). *Naturwissenschaften* 91: 157.
  - 31 Steriotis, T.A., Charalambopoulou, G.C., and Stubos, A.K. (2017). Advanced materials for hydrogen storage. In: *Nanoporous Materials* (ed. N. Kanellopoulos), 513. Greece: CRC Press.
  - 32 Züttel, A., Borgschulte, A., and Schlapbach, L. (2011). *Hydrogen as a Future Energy Carrier*, 441. Hoboken, NJ: Wiley.
  - 33 Winter, C.-J. and Nitsch, J. (1988). *Hydrogen as an Energy Carrier*, 380. Berlin/Heidelberg, Germany: Springer.
  - 34 Mazloomi, K. and Gomes, C. (2012). *Energy Rev.* 16: 3024.
  - 35 Cipriani, G., Di Dio, V., Genduso, F. et al. (2014). *Int. J. Hydrog. Energy* 39: 8482–8494.
  - 36 Züttel, A., Remhof, A., Borgschulte, A., and Friedrichs, O. (2010). *Philos. Trans. R. Soc. A Math. Phys. Eng. Sci.* 368: 3329–3342.
  - 37 Moradi, R. and Groth, K.M. (2019). *Int. J. Hydrog. Energy* 44: 12254.
  - 38 Srinivasu, K., Chandrakumar, K.R.S., and Ghosh, S.K. (2008). *Phys. Chem. Chem. Phys.* 10: 5832.
  - 39 Ataca, C., Aktürk, E., Ciraci, S., and Ustunel, H. (2008). *Appl. Phys. Lett.* 93: 043123.
  - 40 Kim, G., Jhi, S.-H., Lim, S., and Park, N. (2009). *Phys. Rev. B* 79: 155437.
  - 41 Liu, C.-S. and Zeng, Z. (2010). *Appl. Phys. Lett.* 96: 123101.
  - 42 Subrahmanyam, K.S., Kumar, P., Maitra, U. et al. (2011). *Proc. Natl. Acad. Sci. U. S. A.* 108: 2674.
  - 43 Okamoto, Y. and Miyamoto, Y. (2001). *J. Phys. Chem. B* 105: 3470.

- 44 Patchkovskii, S., Tse, J., Yurchenko, S. et al. (2005). *Proc. Natl. Acad. Sci. U. S. A.* 102: 10439.
- 45 Lin, Y., Ding, F., and Yakobson, B.I. (2008). *Phys. Rev. B* 78: 041402(R).
- 46 Kroto, H.W., Heath, J.R., O'Brien, S.C. et al. (1985). *Nature* 318: 162.
- 47 Iijima, S. (1991). *Nature* 354: 56.
- 48 Iijima, S. and Ichihashi, T. (1993). *Nature* 363: 603.
- 49 Bethune, D.S., Kiang, C.H., de Vries, M.S. et al. (1993). *Nature* 363: 605.
- 50 Sloan, E.D. (1998). *Clathrate Hydrates of Natural Gas*, 2e. New York: Marcel Dekker.
- 51 Dillon, A.C., Jones, K.M., Bekkedahl, T.A. et al. (1997). *Nature (London)* 386: 377.
- 52 Ding, R.G., Lu, G.Q., Yan, Z.F., and Wilson, M.A. (2001). *J. Nanosci. Nanotechnol.* 1: 7.
- 53 Hirscher, M. and Becher, M. (2003). *J. Nanosci. Nanotechnol.* 3: 3.
- 54 Jiménez, V., Sánchez, P., Díaz, J.A. et al. (2010). *Chem. Phys. Lett.* 485: 152.
- 55 Ferre-Vilaplana, A. (2005). *J. Chem. Phys.* 122: 214724.
- 56 Mpourmpakis, G., Tylianakis, E., and Froudakis, G. (2006). *J. Nanosci. Nanotechnol.* 6: 87.
- 57 Kowalczyk, P., Holyst, R., Terrones, M., and Terrones, H. (2007). *Phys. Chem. Chem. Phys.* 9: 1786.
- 58 Firlej, L., Roszak, S., Kuchta, B. et al. (2009). *J. Chem. Phys.* 131: 164702.
- 59 Wu, X., Gao, Y., and Zeng, X.C. (2008). *J. Phys. Chem. C* 112: 8458.
- 60 Meng, S., Kaxiras, E., and Zhang, Z. (2007). *Nano Lett.* 7: 663.
- 61 Mpourmpakis, G., Froudakis, G.E., Lithoxoos, G.P., and Samios, J. (2006). *Nano Lett.* 6: 1581.
- 62 Yildirim, T. and Ciraci, S. (2005). *Phys. Rev. Lett.* 94: 175501.
- 63 Tarakeshwar, P., Dhilip Kumar, T.J., and Balakrishnan, N. (2009). *J. Chem. Phys.* 130: 114301.
- 64 Han, S.S., Kang, J.K., Lee, H.M. et al. (2005). *J. Chem. Phys.* 123: 114704.
- 65 Li, Y., Zhou, Z., Shen, P. et al. (2009). *Nanotechnology* 20: 215701.
- 66 Wang, Q., Sun, Q., Jena, P., and Kawazoe, Y. (2009). *ACS Nano* 3: 621.
- 67 Weast, R.C., Astle, M.J., and Beyer, W.H. (1983). *CRC Handbook of Chemistry and Physics*, 64e. Boca Raton, FL: CRC Press.
- 68 Schüth, F., Bogdanović, B., and Felderhoff, M. (2004). *Chem. Commun.* 20: 2249.
- 69 Sakintuna, B., L-Darkrimb, F., and Hirscher, M. (2007). *Int. J. Hydrog. Energy* 32: 1121.
- 70 Hagström, M.T., Lund, P.D., and Vanhanen, J.P. (1995). *Int. J. Hydrog. Energy* 20: 897.
- 71 Bogdanović, B. and Schwickardi, M. (1997). *J. Alloys Compd.* 253: 1.
- 72 McClaine, A. W., Breault, R. W., Larsen, C. et al. (2000). Hydrogen Transmission/Storage with a Metal Hydride-Organic Slurry and Advanced Chemical Hydride/Hydrogen for PEMFC Vehicles. *Proceedings of the US DOE Hydrogen Program Review*.

- 73 Schmidt, W. R. (2001). Hydrogen Storage in Polymer-Dispersed Metal Hydrides (PDMH). *Proceedings of the US DOE Hydrogen Program Preview*.
- 74 Zaluska, A., Zaluski, L., and Ström-Olsen, J.O. (2001). *Appl. Phys. A* 72: 157.
- 75 Alapati, S.V., Johnson, J.K., and Sholl, D.S. (2006). *J. Phys. Chem. B* 110: 8769.
- 76 Wang, J., Ebner, A.D., and Ritter, J.A. (2007). *J. Phys. Chem. C* 111: 14917.
- 77 Bogdanović, B., Felderhoff, M., and Streukens, G. (2009). *J. Serb., Chem. Soc.* 74: 183.
- 78 James, S.L. (2003). *Chem. Soc. Rev.* 32: 276.
- 79 Eddaoudi, M., Moler, D.B., Li, H. et al. (2001). *Acc. Chem. Res.* 34: 319.
- 80 Britt, D., Tranchemontagne, D., and Yaghi, O.M. (2008). *Proc. Natl. Acad. Sci. U. S. A.* 105: 11623.
- 81 Rosi, N.L., Eckert, J., Eddaoudi, M. et al. (2003). *Science* 300: 1127.
- 82 Zhao, X., Xiao, B., Fletcher, A.J. et al. (2004). *Science* 306: 1012.
- 83 Murray, L.J., Dincă, M., and Long, J.R. (2009). *Chem. Soc. Rev.* 38: 1294.
- 84 Rowsell, J.L.C. and Yaghi, O.M. (2005). *Angew. Chem. Int. Ed.* 44: 4670.
- 85 Rowsell, J.L., Millward, A.R., Park, K.S., and Yaghi, O.M. (2004). *J. Am. Chem. Soc.* 126: 5666.
- 86 Collins, D.J. and Zhou, H.C. (2007). *J. Mater. Chem.* 17: 3154.
- 87 Hu, Y.H. and Zhang, L. (2010). *Adv. Mater.* 22: 117.
- 88 Meek, S.T., Greathouse, J.A., and Allendorf, M.D. (2011). *Adv. Mater.* 23: 249.
- 89 Han, S.S., Deng, W.-Q., and Goddard, W.A. III, (2007). *Angew. Chem. Int. Ed.* 46: 6289.
- 90 Dincă, M. and Long, J.R. (2008). *Angew. Chem. Int. Ed.* 47: 6766.
- 91 Dincă, M., Dailly, A., Liu, Y. et al. (2006). *J. Am. Chem. Soc.* 128: 16876.
- 92 Peterson, V.K., Liu, Y., Brown, C.M., and Kepert, C.J. (2006). *J. Am. Chem. Soc.* 128: 15578.
- 93 Kesanli, B., Cui, Y., Smith, M.R. et al. (2005). *Angew. Chem. Int. Ed.* 44: 72.
- 94 Kaye, S.S., Dailly, A., Yaghi, O.M., and Long, J.R. (2007). *J. Am. Chem. Soc.* 129: 14176.
- 95 Zhao, D., Yuan, D., and Zhou, H.-C. (2008). *Energy Environ. Sci.* 1: 222.
- 96 Ma, S. and Zhou, H.-C. (2010). *Chem. Commun.* 46: 44.
- 97 Kuc, A., Heine, T., Seifert, G., and Duarte, H.A. (2008). *Chem. Eur. J.* 14: 6597.
- 98 Klontzas, E., Tylianakis, E., and Froudakis, G.E. (2010). *Nano Lett.* 10: 452.
- 99 Parr, R.G. and Yang, W. (1989). *Density Functional Theory of Atoms and Molecules*. New York: Oxford University Press.
- 100 Giri, S., Roy, D.R., and Chattaraj, P.K. (2009). Variation of local reactivity during molecular vibrations. In: *Internal Rotations, and Chemical Reactions* (ed. P.K. Chattaraj), 323. Florida: Taylor & Francis/CRC Press.
- 101 Geerlings, P., De Proft, F., and Langenaeker, W. (2003). *Chem. Rev.* 103: 1793.
- 102 Chattaraj, P.K. and Giri, S. (2009). *Ann. Rep. Prog. Chem. Sect. C Phys. Chem.* 105: 13.
- 103 Chakraborty, A., Duley, S., Giri, S., and Chattaraj, P.K. (2011). *An Understanding of the Origin of Chemical Reactivity from a Conceptual DFT Approach* (ed. N. Sukumar), 157. New York: John Wiley and Sons.

- 104 Chattaraj, P.K. (1992). *J. Indian Chem. Soc.* 69: 173.
- 105 Parr, R.G., Donnelly, R.A., Levy, M., and Palke, W.E. (1978). *J. Chem. Phys.* 68: 3801.
- 106 Parr, R.G. and Pearson, R.G. (1983). *J. Am. Chem. Soc.* 105: 7512.
- 107 Pearson, R.G. (1997). *Chemical Hardness: Applications from Molecules to Solids*. Weinheim: Wiley-VCH.
- 108 Parr, R.G., von Szentpaly, L., and Liu, S. (1999). *J. Am. Chem. Soc.* 121: 1922.
- 109 Chattaraj, P.K., Sarkar, U., and Roy, D.R. (2006). *Chem. Rev.* 106: 2065.
- 110 Chattaraj, P.K. and Roy, D.R. (2007). *Chem. Rev.* 107: PR46.
- 111 Chattaraj, P.K., Giri, S., and Duley, S. (2011). *Chem. Rev.* 111: PR43.
- 112 Mulliken, R.S. (1955). *J. Chem. Phys.* 23: 1833.
- 113 Parr, R.G. and Yang, W. (1984). *J. Am. Chem. Soc.* 106: 4049.
- 114 Yang, W. and Mortier, W.J. (1986). *J. Am. Chem. Soc.* 108: 5708.
- 115 Pearson, R.G. (1987). *J. Chem. Edu.* 64: 561.
- 116 Parr, R.G. and Chattaraj, P.K. (1991). *J. Am. Chem. Soc.* 113: 1854.
- 117 Ayers, P.W. and Parr, R.G. (2000). *J. Am. Chem. Soc.* 122: 2010.
- 118 Chattaraj, P.K. and Sengupta, S. (1996). *J. Phys. Chem.* 100: 16126.
- 119 Fuentealba, P., Simon-Manso, Y., and Chattaraj, P.K. (2000). *J. Phys. Chem. A* 104: 3185.
- 120 Chamorro, E., Chattaraj, P.K., and Fuentealba, P. (2003). *J. Phys. Chem. A* 107: 7068.
- 121 Parthasarathi, R., Elango, M., Subramanian, V., and Chattaraj, P.K. (2005). *Theor. Chem. Acc.* 113: 257.
- 122 Li, X., Kuznetsov, A.E., Zhang, H.-F. et al. (2001). *Science* 291: 859.
- 123 Watson, M.D., Fechtenkötter, A., and Müllen, K. (2001). *Chem. Rev.*, (Special Issue on Aromaticity) 101: 1267.
- 124 Boldyrev, A.I. and Wang, L.S. (2005). *Chem. Rev.* 105: 3716.
- 125 Schleyer, P.v.R., Maerker, C., Dransfeld, A. et al. (1996). *J. Am. Chem. Soc.* 118: 6317.
- 126 Stanger, A. (2006). *J. Org. Chem.* 71: 883.
- 127 Jimenez-Halla, J.C., Matito, E., Blancafort, L. et al. (2009). *J. Comp. Chem.* 30: 2764.
- 128 Li, Z., Zhao, C., and Chen, L. (2008). *J. Mol. Struct. (Theochem)* 854: 46.
- 129 Noorzadeh, S. and Dardaba, M. (2010). *Chem. Phys. Lett.* 493: 376.
- 130 Gaussian, Inc. (2003). *GAUSSIAN 03, rev B.03*. Pittsburgh, PA: Gaussian, Inc.
- 131 Koopmans, T.A. (1933). *Physica* 1: 104.
- 132 Chakraborty, A., Giri, S., and Chattaraj, P.K. (2010). *N. J. Chem.* 34: 1936.
- 133 Giri, S., Chakraborty, A., and Chattaraj, P.K. (2011). *J. Mol. Model.* 17: 777.
- 134 Chakraborty, A., Giri, S., and Chattaraj, P.K. (2011). *Struct. Chem.* 22: 823.
- 135 Chen, L., Cooper, A.C., Pez, G.P., and Cheng, H. (2007). *J. Phys. Chem. C* 111: 5514.
- 136 Chattaraj, P.K., Bandaru, S., and Mondal, S. (2011). *J. Phys. Chem. A* 115: 187.
- 137 Giri, S., Chakraborty, A., and Chattaraj, P.K. (2011). *Nano Rev.* 2: 5767.

- 138** Mondal, S., Giri, S., and Chattaraj, P.K. (2013). *J. Phys. Chem. C* 117 (22): 11625.
- 139** Bandaru, S., Chakraborty, A., Giri, S., and Chattaraj, P.K. (2012). *Int. J. Quant. Chem.* 112: 695.
- 140** Pan, S.G. and Chattaraj, P.K. (2012). *J Comp Chem* 33: 425.
- 141** Duley, S., Giri, S., Sathymurthy, N. et al. (2011). *Chem. Phys. Lett.* 506: 315.
- 142** Kuznetsov, A., Birch, K., Boldyrev, A.I. et al. (2003). *Science* 300: 622.
- 143** Srinivasu, K., Ghosh, S.K., Das, R. et al. (2012). *RSC Adv.* 2: 2914.
- 144** Giri, S., Bandaru, S., Chakraborty, A., and Chattaraj, P.K. (2011). *Phys. Chem. Chem. Phys.* 13: 20602.

## 27

## The Fukui Function in Extended Systems: Theory and Applications

Carlos Cárdenas<sup>1</sup>, Andrea Echeverry<sup>1,2</sup>, Trinidad Novoa<sup>1,2</sup>,  
Andrés Robles-Navarro<sup>1,2</sup>, T. Gomez<sup>3</sup>, and Patricio Fuentealba<sup>1,2</sup>

<sup>1</sup>Centro para el Desarrollo de la Nanociencia y la Nanotecnología (CEDENNA), Avda. Ecuador 3493, Santiago 9170124, Chile

<sup>2</sup>Universidad de Chile, Facultad de Ciencias, Departamento de Física, Casilla 635, Santiago, Chile

<sup>3</sup>Universidad Autónoma de Chile, Theoretical and Computational Chemistry Center, Institute of Applied Chemical Sciences, Faculty of Engineering, El Llano Subercaceaux 2801, Santiago 8930843, Chile

### 27.1 Introduction

Chemical reactivity can be thought of, in an abstract way, as the response of a molecular system to disturbances induced by attacking agents. Since the electronic Hamiltonian explicitly depends on the number of electrons,  $N$ , and the external potential due to the electrostatic attraction of the nuclei,  $v(r)$ , one can measure, in principle, the chemical response (reactivity) as variations of the energy with respect to the number of electrons,  $\Delta N$ , and the external potential,  $\delta v(r)$ . Note that this is consistent with the common classification of chemical reactions as controlled by electron transfer or by electrostatic effects. This classification corresponds to limit cases in which the reactions are governed only by one of the two effects. In actual reactions, both effects are always present. Klopman and Salem were the first to point this out from a formal point of view [1, 2]. Despite this, reactions mostly controlled by electron transfer are of outermost importance to chemistry because this corresponds to the case of most reactions in which covalent bonds are broken and created. It was Fukui who first realized that the reactivity of a molecule participating in an electron transfer reaction is dictated by the density of the frontier molecular orbitals (FMOs) [3]. That is, the density of the highest occupied molecular orbital (HOMO) dictates the reactivity of molecules prone to donate electrons (here electrophiles), while the density of the lowest unoccupied molecular orbital (LUMO) does it for molecules prone to accept electrons (here nucleophiles). That simple idea is the basis of the FMO theory. Salem and Klopman provided theoretical basis for the FMO theory by using molecular orbital perturbation theory with wavefunctions corresponding to single determinant, such as in the Hartree–Fock method. That is, FMO theory was linked to an approximation and not to the exact wavefunction. In this regard, Mulliken’s words are already famous: “[...]the more accurate the calculations

*Conceptual Density Functional Theory: Towards a New Chemical Reactivity Theory*, First Edition.

Edited by Shubin Liu.

© 2022 WILEY-VCH GmbH. Published 2022 by WILEY-VCH GmbH.



became the more the concepts tended to vanish into thin air". However, a strict generalization of Fukui's ideas is possible within the mathematical framework of the density functional theory (DFT). In 1978, Robert Parr et al. [4] realized that the Lagrange multiplier of the Euler–Lagrange equations of the DFT is the electronic chemical potential,  $\mu$ , of the molecule and that its negative provides a non-empirical scale of electronegativity. This pioneering work was the first step to construct a unified corpus of chemical reactivity using DFT, or what is known today as chemical DFT or conceptual DFT [5–10]. The chemical potential of a molecule is a constant, being the same for all parts of the molecule. Hence, the chemical potential has to change in the course of a chemical reaction due to either a flow of electrons or a change in the external potential. If a molecule is perturbed in its number of electrons and its external potential, the change to the first order of the chemical potential is

$$d\mu = \left( \frac{\partial \mu}{\partial N} \right)_{v(\mathbf{r})} dN + \int \left( \frac{\delta \mu}{\delta v(\mathbf{r})} \right)_N \delta v(\mathbf{r}) d\mathbf{r} \quad (27.1)$$

Consequently, the most reactive a molecule is the easier it is to change its chemical potential. Parr called this the “ $d\mu$  big is good” rule, for which a recent proof is available [11–13]. Therefore, for a nondegenerate ground state [14–17], a disturbance will be more effective in changing the chemical potential if such disturbance (a reactant) occurs in places where  $\left( \frac{\delta \mu}{\delta v(\mathbf{r})} \right)_N$  is large. It is straightforward to show, using a Maxwell's relationship, that this functional derivative is also equal to the response of the electron density to changes in the number of electrons,

$$f(\mathbf{r}) \equiv \left( \frac{\delta \mu^\pm}{\delta v(\mathbf{r})} \right)_N = \left( \frac{\partial \rho(\mathbf{r})}{\partial N^\pm} \right)_{v(\mathbf{r})} \quad (27.2)$$

$f(\mathbf{r})$  is called the Fukui function because it generalizes the FMO theory. That is better seen when the Fukui functions are written in terms of the Kohn–Sham (KS) orbitals:

$$f^\pm(\mathbf{r}) \equiv \left| \phi_{\text{HOMO/LUMO}}(\mathbf{r}) \right|^2 + \sum_{i=1}^N \left( \frac{\partial |\phi_i(\mathbf{r})|}{\partial N} \right) \quad (27.3)$$

The Fukui function comprises two terms, the density of the HOMO (or LUMO) and a relaxation term. Note that there are two Fukui functions, one for donation of electrons (–, oxidation) and one for accepting electrons (+, reduction). That is so because of the discontinuity of the density as a function of the number of electrons [18]. In molecules, the relaxation term is usually small because of the discrete nature of the spectra of the KS orbitals [19]. This, however, is not the case in an extended system, such as a nanostructure, surface, or solid. Let us look at the difference between a solid and a molecule. As a bound quantum system – one in which the energy spectrum is discrete – increases in size, the energy eigenvalues become closer to each other. In the case of the solid, each eigenvalue of energy,  $\epsilon$ , associated with the atoms that make it up unfolds into a continuous band of energy. In the case of medium molecules, the HOMO and the internal HOMO- $n$  orbitals are clearly separated in energy. The further apart they are, the smaller the participation of the internal orbitals. For example, the orbital perturbation theory interaction

energy of the occupied orbitals of a nucleophile A with the LUMO of an electrophile B is approximately given by:

$$\sum_{i \text{ occupied} \in A} \frac{|\langle \phi_i^A | \hat{h}_{AB} | \phi_{\text{LUMO}}^B \rangle|^2}{\epsilon_i^A - \epsilon_{\text{LUMO}}^B} \quad (27.4)$$

where  $\hat{h}_{AB}$  is the total mono-electronic Hamiltonian of the system. Note that the absolute value of the denominator is largest for the term of the sum associated with the inner orbitals of the nucleophile. In a medium molecule, the term associated with HOMO is the one that contributes the most to the sum. In the case of a solid, there will be a band with infinite states associated with HOMO; therefore, the states close to it will contribute significantly to the sum. In summary, in extended systems, the relaxation contribution of the orbitals around the Fermi level (frontier states) is important and it must be taken into account.

Imagine a solid that is metallic. The distinction between the occupied and unoccupied frontier states is impossible since the system lacks a fundamental energy gap. In such a case, it seems difficult to define the Fukui function from Eq. (27.3). However, it is still possible to define the Fukui function from its analogous function for open systems, the local softness,  $s(\mathbf{r})$ :

$$s(\mathbf{r}) = \left( \frac{\partial \rho(\mathbf{r})}{\partial \mu} \right)_{v(\mathbf{r})} = \left( \frac{\partial \rho(\mathbf{r})}{\partial N} \right)_{v(\mathbf{r})} \left( \frac{\partial N}{\partial \mu} \right)_{v(\mathbf{r})} = f(\mathbf{r}) S \quad (27.5)$$

where  $S$  is the global softness ( $S = \int s(\mathbf{r}) d\mathbf{r}$ ). For any system, finite or not, the density can be written in terms of the local density of states  $g(\mathbf{r}; E)$  (LDOS):

$$g(\mathbf{r}; E) = \frac{1}{\pi} \text{Im} G(\mathbf{r}\mathbf{s}, \mathbf{r}\mathbf{s}; E^-) \quad (27.6)$$

and the electron density is

$$\rho(\mathbf{r}) = \int^{\mu} \frac{1}{\pi} \text{Im} G(\mathbf{r}, \mathbf{r}; E^-) dE = \int^{\mu} g(\mathbf{r}; E) dE \quad (27.7)$$

where  $G(\mathbf{r}\mathbf{s}, \mathbf{r}\mathbf{s}; E^-)$  is the retarded Green's function and  $\mu$  is the chemical potential which at 0 K equals the Fermi level.  $E^- = \lim_{\delta \rightarrow 0^+} E - i\delta$  avoids divergence at the poles of  $G$ .

The local softness is obtained directly from deriving Eq. (27.7) with respect to  $\mu$ :

$$s(\mathbf{r}) = \left( \frac{\partial \rho(\mathbf{r})}{\partial \mu} \right)_{v(\mathbf{r})} = g(\mathbf{r}; \mu) + \int^{\mu} \left( \frac{\partial g(\mathbf{r}; E)}{\partial \mu} \right) dE \quad (27.8)$$

and the Fukui function is recovered after normalization of  $s(\mathbf{r})$  with the global softness. Note that this expression, originally deduced by Cohen et al. [20], for the local softness has the same structure as the Fukui function of the Eq. (27.3). That is, it is composed of the density of states at the Fermi level (boundary states) and an integral that takes into account the contribution of the states around the Fermi level (relaxation term). The latter accounts for the change of  $g(\mathbf{r}, E)$  due to the fact that changing the Fermi level will change the density of occupied states. In a infinite (solid) or semi-infinite (surface) system, the continuous nature of the KS states implies that the contribution to the chemical response of states below and above the Fermi level

cannot be neglected. This is easily seen from Eq. (27.3) by changing the sum by an integral: the contribution to it of states infinitesimally close to the Fermi level decays with the difference of energy of these states and the Fermi level but it remains finite.

Cohen et al. showed that both the Fukui function (for a system with a gap) and the local softness can be expressed as the density of the frontier state modulated by a nonlocal potential [20]:

$$f^\pm(\mathbf{r}) = \int |\phi_{\text{LUMO/HOMO}}(\mathbf{r}_2)|^2 K^{-1}(\mathbf{r}, \mathbf{r}_2) d\mathbf{r}_2 \quad (27.9)$$

and

$$s(\mathbf{r}) = \int g(\mathbf{r}_2; \mu) K^{-1}(\mathbf{r}, \mathbf{r}_2) d\mathbf{r}_2 \quad (27.10)$$

where  $K(\mathbf{r}, \mathbf{r}_2)$ ,

$$K(\mathbf{r}, \mathbf{r}_2) = \delta(\mathbf{r}, \mathbf{r}_2) - \int^\mu \frac{1}{\pi} \text{Im} \left( \int G(\mathbf{r}, \mathbf{r}_3; E^-) \left( \frac{\delta v_{\text{KS}}(\mathbf{r}_3)}{\delta \rho(\mathbf{r}_2)} \right) G(\mathbf{r}_3, \mathbf{r}; E^-) \right) d\mathbf{r}_3 \quad (27.11)$$

is a kernel related to the dielectric function of electrons.

Although from a quantum mechanical calculation one could construct Green's functions and with them construct  $K$ , this strategy leads to a more complex problem than the computation of the system itself. Therefore, it escapes the very spirit of the construction of reactivity indices, which includes providing simple elements for the interpretation of the chemical response. This explains the need to build simple models of reactivity in extended systems that allow the calculation of the chemical response to be as routine as it is in the case of molecules [21].

## 27.2 Models of Local Softness: The Case of Metallic Carbon Nanotubes

As far as we know, there are only a handful of models that try to approximate the relaxation contribution to the local softness of extended systems. Santos et al. [22, 23] proposed to weight the local density of states with the product of the global softness and number of electrons ( $\int_{\mu-\Delta}^\mu g(E)dE$ ) within an arbitrary energy window,  $\Delta$ , around the Fermi level. For simplicity, we will focus on the response to oxidation of the systems, that is, the regions prone to donate electrons:

$$s^S(\mathbf{r}) = \left( \frac{\int_{\mu-\Delta}^\mu g(\mathbf{r}, E)dE}{\int_{\mu-\Delta}^\mu g(E)dE} \right) S \quad (27.12)$$

This expression is not exactly the local softness but its chemical interpretation is similar, as they demonstrated in applications to zeolites [22, 23]. Brommer et al. [24], Geerlings and coworkers [25], and Cardenas et al. [26] proposed a similar integration around the Fermi level to calculate the local softness:

$$s^I(\mathbf{r}) = \lim_{\delta\mu \rightarrow 0} \frac{1}{\delta\mu} \int_{\mu-\delta\mu}^\mu g(\mathbf{r}, E)dE \quad (27.13)$$

This equation is inspired in the fact that the derivative in Eq. (27.5) can be written as a limit:

$$\left(\frac{\partial \rho(\mathbf{r})}{\partial \mu}\right)_{\nu(\mathbf{r})} = \lim_{\delta\mu \rightarrow 0} \frac{\rho(\mathbf{r}; \mu + \delta\mu) - \rho(\mathbf{r}; \mu)}{\delta\mu} \quad (27.14)$$

Despite Eqs. (27.12) and (27.13) look similar, their implementations are different because in the  $s^I(\mathbf{r})$  model the value of  $\delta\mu$  is taken as the smallest possible for which the local softness converges rather than an arbitrary large window of energy below the Fermi level. The KS states within a band are either degenerate or pseudodegenerate, which implies that  $\delta\mu$  should be of the order of the coupling between the external perturbation and the system (typically a fraction of an eV). Nevertheless, both models use the same strategy to include contributions from states below the Fermi level and, depending on the way the local density of states is computed, they correspond to a population analysis in a portion of the valence band. Both models weight all the states in the considered energy range equally. But, from perturbation theory, one can conclude that the contribution of inner states decreases with the energetic distance to the Fermi level: the deeper the state, the smaller its contribution (see Eq. (27.4)).  $s^I(\mathbf{r})$  has been applied to describe the reactivity of Si(111)-(7 × 7) reconstructed surface, single-wall carbon nanotubes, and alkaline earth oxides' surfaces [26].

Recently, we proposed a new method which uses the exact long-range behavior of the local softness to weight the contribution of states around the Fermi level [27]:

$$s^{II}(\mathbf{r}) = \frac{1}{\delta\mu} \int_{\mu-\delta\mu}^{\mu+\delta\mu} \frac{g(\mathbf{r}, E)}{\sqrt{|E - \mu|}} dE \quad (27.15)$$

### 27.2.1 Carbon Nanotube

C(5,5) single-walled-capped carbon nanotubes (SWCCNTs) obey a series with chemical formula  $C_{10n+60}$  with alternating symmetry between  $D_{5h}$  ( $n$  odd) and  $D_{5d}$  ( $n$  even) [28]. The length at which a C( $N,N$ ) SWCCNT can be considered metallic depends on the method of calculation. Geerlings and coworkers [25] showed that a tight binding model (Hückel) captures well enough the electronic structure needed to describe the chemical reactivity of these nanotubes. In tight binding, the molecular orbital energies are just  $\epsilon = \alpha + \lambda_i \beta$ , where  $\lambda_i$  are the eigenvalues of the adjacency matrix of the structure [29]. Instead of using specific values of site energies ( $\alpha$ ) and hopping strength ( $\beta$ ) for carbon, we simplified equations by working in units of  $\beta$ . For evaluating the LDOS and density of states (DOS), each molecular orbital energy has been broadened as a Gaussian function with standard deviation of 0.076 (0.15 eV for carbon) and the smallest  $\delta\mu$  used is equal to 0.3  $\beta$ . Also, to avoid the use of a atomic orbital basis set, we found more illustrative to use condensed-to-atoms values of the local softness,  $s_k$  [30]. More details on the methodology and implementation of models of local softness are available elsewhere [27].

In Figure 27.1, the condensed local softness of the  $C_{360}(5,5)$  SWCCNT is plotted as a function of the belt number to which the C atom belongs. Due to the  $D_{5d}$  symmetry, all atoms in a belt are equivalent. Two models of softness are shown,  $s^I$  and  $s^{II}$ . We focus first in the sidewall of the nanotube (belts 5–35). Both models

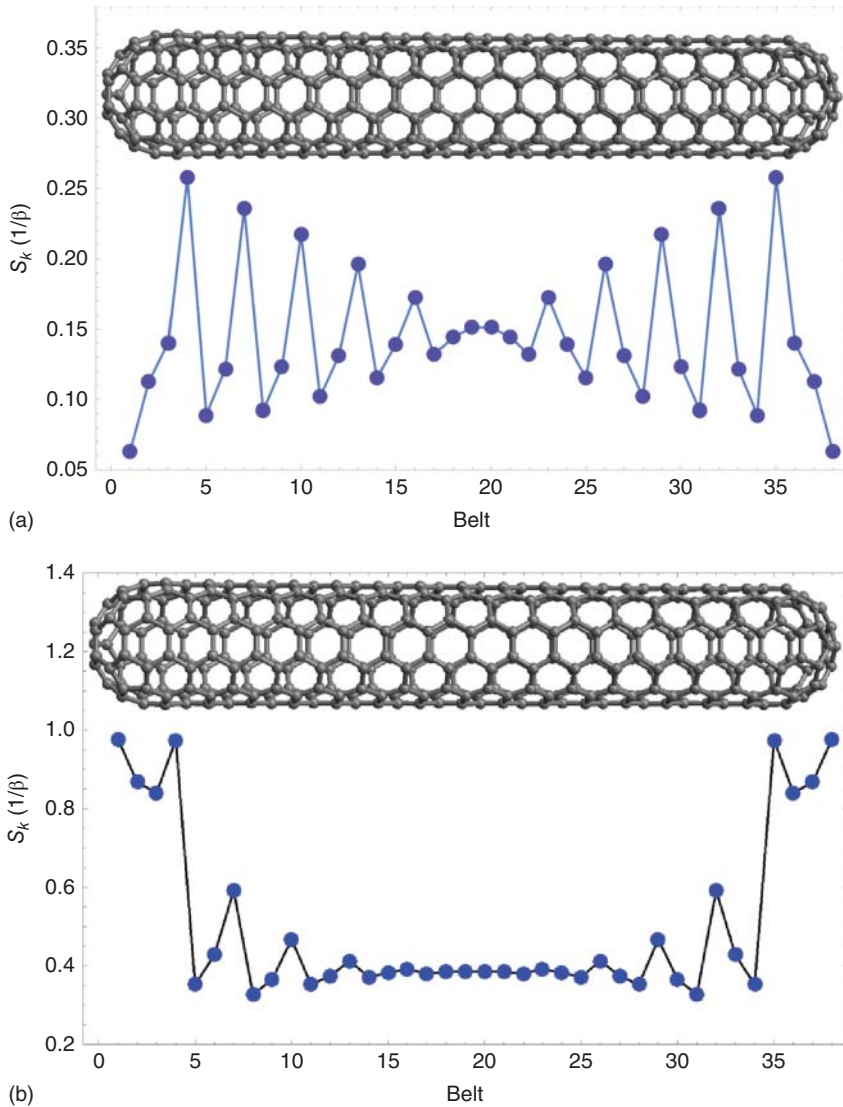


**Figure 27.1** Condensed-to-atoms local softness of capped single-wall carbon nanotube  $C_{360}(5,5)$  evaluated with a model,  $s^I(\mathbf{r})$ , that equally weights the contribution of all states (a) and, a model,  $s^{II}(\mathbf{r})$ , that weights the contribution of inner states according to how deep below the Fermi they lay (b).

predict an oscillatory character with a period of three belts, with the average softness decreasing toward the center of the nanotube. However, for model  $s^I$  this decrease is quite slow, while in model  $s^{II}$  the softness is almost constant after 10 belts measured from the cap.

As the softness kernel is nearsighted [31], the local softness in the center of a metallic capped nanotube should be smaller and almost independent of the

position. Hence, the quality of the model for the local softness can be assessed through its inherent nearsightedness. In that sense, model  $s^{\text{II}}$  performs much better than model  $s^{\text{I}}$ . That is, weighting correctly the contribution to the local softness of the occupied states below the Fermi level is essential for describing the right trend of reactivity far from the ends of the nanotube. Note that the slow decaying oscillations in model  $s^{\text{I}}$  could be, however, caused by the finite size of the  $C_{360}(5,5)$  nanotube.

Let us now see how both models describe the reactivity at the ends of the nanotube. Model  $s^{\text{I}}$  predicts that the most reactive sites of the nanotube are those corresponding to the union of the caps to the cylinder shell. This is an expected behavior because those atoms have a large deviation of the ideal  $sp^2$  hybridization of the graphene sheet. However, notice that this model totally fails in predicting that the other atoms in the caps also have enhanced reactivity. In indeed,  $s^{\text{I}}$  wrongly predicts that the outermost pentagonal belt of the nanotube is the least reactive. On the contrary, model  $s^{\text{II}}$  correctly predicts that atoms in the caps are the most reactive and that the outermost pentagonal belt along with the belt where the sidewall and the cap merge are the most reactive sites. These results suggest that, in metallic systems, models of softness should be such that the contribution of inner states to the chemical response depends explicitly on how deep below the Fermi level these state lay (Figure 27.1b). More ways to weight the contribution of inner states have been discussed elsewhere [27, 32, 33].

### 27.3 Models of Fukui Function: The Case of Alkaline Metal Oxides Bulks and (100) Surfaces

It is clear from Eq. (27.5) that given an approximation for the local softness, a corresponding approximation for the Fukui function is given by normalizing the local softness by its integral over the whole space. This is true for a system which has a gap between the valence band and the conduction band. As it was already mentioned, in a gapless system, the global softness defined as the inverse of the gap diverges and the Fukui function is ill defined by Eq. (27.5). Fortunately, this is not the case of systems with a gap, such as insulators and semiconductors at low temperature. In such a case, the Fukui function can be evaluated from models that use the density of states or from the actual variation of the density due to changes in the number of electrons. In the first case, the Fukui function corresponding to the model  $s^{\text{I}}(\mathbf{r})$  will be given by:

$$f^{-\text{I}}(\mathbf{r}) = \lim_{\delta\mu \rightarrow 0} \frac{\int_{\mu-\delta\mu}^{\mu} g(\mathbf{r}, E) dE}{\int_{\mu-\delta\mu}^{\mu} g(\mathbf{r}, E) d\mathbf{r} dE} \quad (27.16)$$

Before discussing how the Fukui function of an extended system could be computed from Eq. (27.2), let us see how this performed for a finite system, e.g. a molecule. Perdew et al. [18] proved that density of an open system with  $N_0 \pm \Delta N$  electrons, with  $N_0$  an integer, is a linear combination of the densities of the systems

with the closest integer number of electrons. Therefore, the derivatives of the density with respect to the number of electrons takes the form of a “finite difference” [34, 35]:

$$f^{-,FD}(\mathbf{r}) = \rho^N(\mathbf{r}) - \rho^{N-1}(\mathbf{r}) \quad (27.17)$$

where  $N$  stands for the system of interest and  $N - 1$  for its vertical cation. A similar expression exists for  $f^+$ . It is important to highlight that Eq. (27.17) is not an approximation to the derivative of Eq. (27.2), but it is, in principle, exact. Any departure from exactness from Eq. (27.17) comes from the approximations used to compute the density. In the special case of DFT, approximations to the exchange–correlation functional are designed to give good densities for integer number of electrons, but not for non-integer numbers [36].

A natural extension of Eq. (27.17) to extended systems suggests to compute the Fukui function by removing/adding electrons from/to the neutral system. However, this procedure entails a technical problem in solids and surfaces when they are modeled using periodic boundary conditions (PBCs), which is that it leaves a charged cell or supercell, the images of which will interact electrostatically. Consequently, adding or removing a whole electron could add a non-negligible nonphysical external potential to the unit cell.

Because the Coulomb interaction is long-ranged, it does not matter how large the unit cell is, it never converges to 0. Therefore, one cannot take for granted that increasing the size of the unitary cell will fix this problem. The magnitude of the effect of this electrostatic disturbance is not easy to determine *a priori*, but it is expected to be more significant in soft systems where the polarizability is large. Although approximations for canceling the electrostatic fields of charged images on the total energy are available, these methods are usually limited to cubic unit cells. Despite this, Eq. (27.17) has been satisfactorily used to identify the regions that maximize the Fukui function in  $V_2O_5$  systems, allowing a qualitative visual inspection of the different oxygen surface sites [37], as well as a comparison of different vanadium-based systems.

An advantage of computing the Fukui function from calculations with different number of electrons is that it easily allows to incorporate relaxation effects, but it has the trouble of creating a fictitious electric field when PBCs are used. The approach based on the LDOS (Eq. (27.16)) fixes that problem, but relaxation effects are not strictly incorporated. An alternative is using finite differences with fractional number of electrons. Importantly, reducing the step in the number of electrons in Eq. (27.17) does not fix the problem of the electric field of charged images unless  $\Delta N$  is taken at the zero limit. A computational way to take that limit is to compute the density of the neutral system,  $\rho(\mathbf{r}, N_0)$ , and several slightly charged systems,  $\rho(\mathbf{r}, N_0 + \delta)$ ,  $\rho(\mathbf{r}, N_0 + 2\delta)$  . . . . Then, for every point in the space, a linear interpolation of the density as a function of the number of electrons can be made. The slope of such interpolation is the Fukui function because

$$\rho(\mathbf{r}, N) = \rho(\mathbf{r}, N_0) + \frac{\partial \rho(\mathbf{r}, N)}{\partial N} (N - N_0) + \dots \quad (27.18)$$

Of course, this approximation will be valid only if the charge of the charged systems is small enough to fall within the linear regime of  $\rho$  vs.  $N$ .

This interpolation approach fixes the charged images problem and takes into account the relaxation of inner states. However, it introduces a new difficulty, which is the lack of accuracy of approximate functionals to describe the electron density of systems with fractional number of electrons. It is well known that LDA, all GGAs and most hybrids and long-range corrected functionals fail to predict the piecewise structure of  $E$  vs.  $N$  [36]. All those functionals follow the same trend, which is a convex underestimation of  $E$  vs.  $N$ . This underestimation results in a delocalization error in the density. That is, the density of systems with fractional number of electrons computed with approximated functionals is less compact than the exact one.

In what follows we will use Eqs. (27.16)–(27.18) to compute the Fukui function in the bulk and most stable surface ((100)) of the family of alkaline earth metal oxides rocksalt MgO, CaO, SrO, and BaO solids. Full details of the calculations can be found elsewhere [38]. Briefly, all DFT calculations with PBCs were done with the Vienna ab initio package (VASP) [39–41] using the GGA PBE exchange and correlation functional proposed by Perdew et al. [42]. Bulk was computed using a conventional unit cell with four formula units. Surfaces were cut from the optimized bulk structure, 6 oxide layers thick, and each supercell contain 12 formula units. Before comparison was done, we condensed  $f^-$  to atoms using the partition of the space induced by Voronoi polyhedral. To do this, we used the “Bader” program of Henkelman’s group [43]. Because  $f^-$  is mostly localized in the oxygen atoms, only those values are reported. As the Fukui function integrates to 1 independently of the size of the system, we decided to report the Fukui function times the number of formula units. This is especially important if one is to compare values of  $f$  for systems where the cell/supercell has different number of formula units.

Each of the models for the Fukui function depends on different parameters.  $f^l(\mathbf{r})$  depends on what value of  $\delta\mu$  is considered small enough to be representative of the  $\delta\mu \rightarrow 0$  limit. As it can be seen in Table 27.1, for  $|\delta\mu| \leq 0.15$  eV the values

**Table 27.1**  $f^{-,l}$  obtained with the DOS for the four bulk systems of the alkaline earth metal oxide series.

$\delta\mu$	MgO	CaO	SrO	BaO
−0.05	0.947	0.964	0.956	0.876
−0.10	0.947	0.960	0.956	0.876
−0.15	0.947	0.956	0.944	0.880
−0.20	0.947	0.952	0.936	0.884
−0.25	0.936	0.944	0.928	0.888
−0.30	0.936	0.944	0.928	0.888
−1.00	0.912	0.900	0.896	0.888
$\Delta N$	MgO	CaO	SrO	BaO
−1.00	0.672	0.676	0.684	0.640

The last row corresponds to  $f^{-,FD}$  obtained with finite differences (Eq. (27.17)).



of the Fukui function are almost constant within each series: MgO (0.947), CaO (0.956–0.964), SrO (0.944–0.956), and BaO (0.880–0.876).

Despite values of the Fukui function from the model  $f^{-,FD}$  follow the same trend as those computed from the density of states,  $f^{-,FD}$  values are always smaller than those from  $f^{-,I}(\mathbf{r})$  (see last row in Table 27.1). We attribute part of this to fact that  $f^{-,I}(\mathbf{r})$  misses a part of the relaxation term of the exact expression of the softness (Eq. (27.13)). For both models, the oxygen in BaO has the smallest  $f^{-}$ . For instance,  $f^{-,FD}$  in BaO is 0.64, compared with MgO, CaO, and SrO that oscillate around 0.676. The slightly lower value of  $f^{-}$  in BaO can be understood as a consequence of its larger softness and the condensation scheme. As Ba is the softest metal in the series, the frontier density is expected to be less localized around the oxygen atom. Hence, the Voronoi polyhedrons may not be an accurate representation of the space belonging to atoms. Summarizing, the method based on the density of states overestimates the Fukui function when compared to the finite difference approach. Nevertheless, we cannot say what method does better because  $f^{-,FD}$  suffers from the fictitious electric field induced by charged cells.

The most robust method to compute the Fukui function is the interpolation method,  $f^{-,int}$ , introduced in Eq. (27.18). This method includes relaxation because it comes from self-consistent calculations with different number of electrons. It also reduces the nonphysical electric field of charged cells because it takes the limit when  $\Delta N = 0$ . So, the error in  $f^{-,int}$  comes from the delocalization error in the exchange–correlation functional. Computed  $f^{-,int}$  of the bulk is shown in Table 27.2. Different interpolation schemes were used by choosing different charged states ( $\Delta N$ ) from which the interpolation of  $\partial\rho/\partial N$  is constructed ( $\Delta N$  ranging between  $-0.30$  and  $0.0e$ ). These values of  $\Delta N$  are small enough to fall within the linear response of the electron density. To be sure of this, we check that the correlation coefficient of the linear regression is at least  $R^2 = 0.99$  for every point of the grid used to compute  $f^{-,int}$ . We used the same grid used by VASP to integrate the density in real space. Condensation scheme is the same that the one used for the previous models. The results show that the values of condensed  $f^{-,int}$  on the oxygen sites are robust and do not exhibit significant deviations for a given composition:  $f^{-,int}$  is always 0.672 for MgO, and it oscillates between 0.680 and 0.692 for CaO and SrO, and between 0.628 and 0.632 for BaO. No significant change is observed by including the neutral density in the interpolation. Note that the values of  $f^{-,int}$

**Table 27.2**  $f^{-}$  condensed to O atoms obtained with the interpolation method for the four bulk systems of the alkaline earth metal oxide series.

Interpolation scheme	MgO	CaO	SrO	BaO
$\Delta N = -0.15/-0.10/-0.05/0.00$	0.672	0.680	0.688	0.628
$\Delta N = -0.30/-0.20/-0.10/0.00$	0.672	0.688	0.684	0.628
$\Delta N = -0.15/-0.10/-0.05$	0.672	0.688	0.688	0.628
$\Delta N = -0.30/-0.20/-0.10$	0.672	0.692	0.684	0.632

are closer to those obtained with finite differences than with the density of states (Table 27.1). If we take  $f^{-,\text{int}}$  as the reference values, all indicates that using the local density of states tends to overestimate the Fukui function. This is consistent with the observation that the model for  $f^{-,l}$  weights equally the contribution of the Fermi level and the states below it. That is, Eq. (27.16) overestimates the relaxation term.

### 27.3.1 Application to Surfaces

Now, we move to the description of reactivity of the most stable surfaces of same oxide for which the bulk was analyzed. That surface corresponds to the (100). For this, we have used slab models to represent the surfaces and a portion of the bulk. We discuss two models of slabs commonly used in the literature (see Figure 27.2) [26, 44, 45]. One of them allows relaxation of atoms in both layers of the slab (symmetric slab), which avoids the emergence of a finite dipole in the supercell. In the other one, (asymmetric slab) only atoms on one side of the slab are relaxed. As we will see, the local reactivity is affected by the selection of the model.

It is expected that surface sites are more reactive than bulk sites due to the low coordination of the former that raises electronic levels. We analyze if such behavior is captured by the Fukui function  $f^-$  of oxygen atoms located at the surface and in bulk positions. We have chosen to compare the interpolation method (Eq. (27.18)) with DOS one (Eq. (27.16)).

The  $f^-$  of the oxygen atoms on the surface of the asymmetric slab is always larger than of the atoms inner layers 2–4 independently of the method and the interpolation scheme used (see Tables 27.3 and 27.4). Adding or not the neutral system ( $\Delta N = 0$ ) in the interpolation has a marginal effect on  $f^{-,\text{int}}$ . The Fukui function

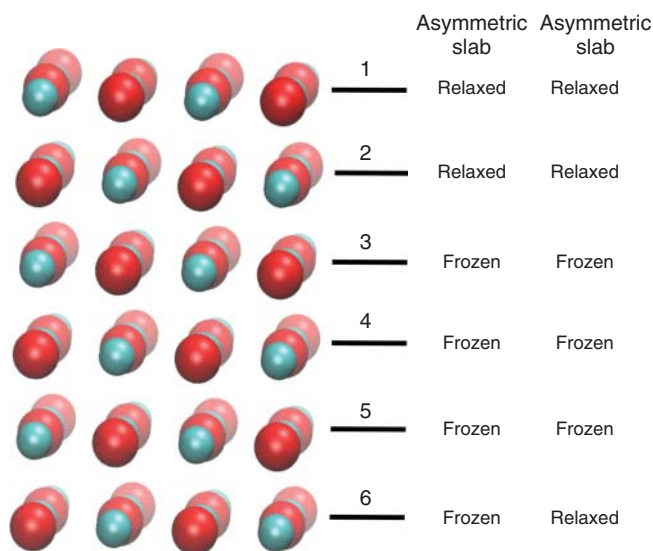


**Figure 27.2** Slab models of the alkaline earth oxides (100) surfaces. Layers are labeled with numbers 1–6.

**Table 27.3**  $f^-$  condensed to O atoms obtained with the interpolation method for the asymmetric slabs.

Layer	MgO	CaO	SrO	BaO
$\Delta N = -0.3/-0.2/-0.1/0.0$				
1	0.792	0.928	1.024	0.896
2	0.304	0.216	0.184	0.200
3	0.28	0.288	0.368	0.184
4	0.288	0.176	0.136	0.128
5	0.368	0.200	0.096	0.064
6	0.672	0.920	1.120	1.032
$\Delta N = -0.3/-0.2/-0.1$				
1	0.808	0.896	0.976	0.864
2	0.304	0.216	0.224	0.240
3	0.272	0.184	0.192	0.216
4	0.288	0.176	0.160	0.144
5	0.368	0.200	0.104	0.064
6	0.680	0.880	1.072	0.976

**Table 27.4** Comparison of  $f^-$  obtained by integration of the DOS ( $\delta\mu = -0.20$  eV) and the interpolation of  $\delta N = 0.30/ - 0.20/ - 0.10/0.0$  for asymmetric and symmetric slabs of MgO and BaO.

Layer	Asymmetric		Symmetric	
	DOS	Interpolation	DOS	Interpolation
MgO				
1	0.808	0.808	0.904	0.824
2	0.552	0.304	0.520	0.288
3	0.568	0.272	0.448	0.248
4	0.632	0.288	0.448	0.256
5	0.672	0.368	0.52	0.360
6	0.536	0.680	0.928	0.720
BaO				
1	1.288	0.896	1.464	0.904
2	0.096	0.2	0.208	0.184
3	0.064	0.184	0.136	0.16
4	0.024	0.128	0.136	0.16
5	0.016	0.064	0.2	0.176
6	2.136	1.032	1.456	0.904

of the surface oxygen sites ranges from 0.672–0.792 for MgO to 1.12–1.024 for SrO in the first interpolation scheme (considering the neutral system in the interpolation leads to similar results). Meanwhile, the Fukui of the oxygen atoms in the inner layers takes values from 0.064 for BaO to 0.368 for MgO and SrO. This is a clear indication of exaltation of the reactivity of surface sites compared to inner positions. Note that the condensed  $f^-$  values are extensive in a calculations with PBCs, i.e.  $f^-$  always integrates to 1 independently of the number of atoms. This can be fixed by multiplying every value of  $f^-$  by the volume of the supercell. This, however, introduces the difficulty that the volume of the supercell containing the slab will depend on the vacuum left between images of the slab. For this reason, we multiply the originally normalized  $f^-$  with the number of formula units in the supercell. Therefore, condensed values of  $f^-$  larger than 1 are possible.

It is interesting to note that structural relaxation of the surfaces leads to a variation in the value of  $f^-$  for all the oxides but for CaO, oxygen in layer 1 and in layer 6 seem to react in a different manner to the removal of electrons, which is reasonable considering that the electronic states around the Fermi level are localized mostly on the surfaces. There is not a clear trend within in the oxides, since in MgO the O on relaxed surface layer 1 is grater than those in the unrelaxed layer 6 (0.792 relaxed vs. 0.672 unrelaxed, respectively). Those values are similar in CaO (0.928 vs. 0.920), larger for the unrelaxed O in SrO (1.024 relaxed vs. 1.120 unrelaxed) and BaO (0.896 relaxed vs. 1.032 unrelaxed). What is clear from these data is that in assessing the reactivity of surfaces, an accurate relaxation of them is of uttermost importance. Small changes in geometry may not change the energy significantly, but they change the position (relative to the Fermi Level) of surface states.

We also used the method based on the DOS to compute  $f^{-I}$ . Table 27.4 shows the data obtained for MgO and BaO with asymmetric and symmetric slabs, with selected values for  $\delta\mu$  and a given interpolation scheme. It can be observed that the two approaches account for the increase in reactivity of the surface sites compared to inner positions. Also, the symmetric slabs reflect the same value for layers 1 and 6 as expected from the relaxation, whereas the unrelaxed sites of layer 6 show lower values than layer 1 in MgO and higher in BaO, following the trend discussed above. However, the calculation of  $f^{-I}$  is found to be very sensitive to the value of  $\delta\mu$  used for the integration in Eq. (27.16). From extensive data not shown here, we can conclude that in the case of the  $f^{-I}$  the values are less dependent on  $\delta\mu$  for symmetric slabs than for the asymmetric. It seems that small integration ranges lead to large variations in condensed values that maybe due to numerical instabilities of the integration. Values of  $\delta\mu$  of  $-0.20$  and  $-0.30$  lead to results close to those of the interpolation approach with  $\Delta N = -0.30/ -0.20/ -0.10/0.0$ .

The Fukui function  $f^-$  condensed to oxygen atoms appears to be a good descriptor for the surface reactivity within a given material. The different approaches tested give the same qualitative results: the surface O atoms are more reactive (the  $f^-$  is larger) than the inner layers atoms. The interpolation of Eq. (27.18) is a robust way to obtain  $f^-$  in non-charged systems and is found to be sensitive enough to capture effects of relaxation of the surface. Attention must be paid to the parameters used to obtain  $f^-$ , i.e. the partial charges,  $\Delta N$ , in the charged systems and the  $\delta\mu$  range

to integrate the DOS, which should not be too small. Comparison between surfaces and bulk, or between MgO–CaO–SrO–BaO is not straightforward, because the computed  $f^-$  always normalizes to one independently of the nature of the system and the number of atoms in the simulation cell. Comparison of reactivity between systems of the same size could be achieved by using the local softness instead of the Fukui function. As for the matter of extensivity of the condensed Fukui function, we propose to standardize its values multiplying by the number of unit formulas in the cell.

## 27.4 Conclusions

In this chapter, we have reviewed different methods to calculate the Fukui function of extended systems with and without a fundamental gap. The case of metallic carbon nanotubes serve to illustrate the importance of correctly weighing the contributions of internal states. In these gapped systems, using density-of-state-based softness models seems to be the best alternative. In the case of systems with a gap and with PBCs, we have shown that a strategy similar to that used in molecules is possible. This consists of calculating slightly charged systems and interpolating the density in function of the number of electrons for each point in space. A program written in Python is available upon request.

## Acknowledgments

This work was financed by: (i) FONDECYT through project No. 1181121, (ii) CONICYT, REDES 190102, and (iii) Center for the Development of Nanoscience and Nanotechnology CEDENNA AFB180001. Powered@NLHPC: This research was partially supported by the supercomputing infrastructure of the NLHPC (ECM-02).

## References

- 1 Klopman, G. (1968). Chemical reactivity and the concept of charge and frontier-controlled reactions. *J. Am. Chem. Soc.* 90: 223–234.
- 2 Salem, L. (1968). Intermolecular orbital theory of the interaction between conjugated systems. I. General theory. *J. Am. Chem. Soc.* 90: 543–552.
- 3 Fukui, K. (1982). Role of frontier orbitals in chemical reactions. *Science* 218: 747–754.
- 4 Parr, R.G., Donnelly, R.A., Levy, M., and Palke, W.E. (1978). Electronegativity: the density functional viewpoint. *J. Chem. Phys.* 68: 3801–3807.
- 5 Chermette, H. (1999). Chemical reactivity indexes in density functional theory. *J. Comput. Chem.* 20: 129–154.
- 6 Geerlings, P., De Proft, F., and Langenaeker, W. (2003). Conceptual density functional theory. *Chem. Rev.* 103: 1793–1873.

- 7 Liu, S.B. (2009). Conceptual density functional theory and some recent developments. *Acta Phys. Chim. Sin.* 25: 590–600.
- 8 Gazquez, J. (2008). Perspectives on density functional theory of chemical reactivity. *J. Mexican Chem. Soc.* 52: 3–10.
- 9 Fuentealba, P. and Cardenas, C. (2015). Density functional theory of chemical reactivity. In: *Chemical Modelling*, vol. 11 (ed. J.-O. J. Michael Springborg), 151–174. The Royal Society of Chemistry.
- 10 Geerlings, P. and De Proft, F. (2008). Conceptual DFT: the chemical relevance of higher response functions. *Phys. Chem. Chem. Phys.* 10: 3028–3042.
- 11 Miranda-Quintana, R.A., Heidar-Zadeh, F., and Ayers, P.W. (2018). Elementary derivation of the “ $\Delta\mu$  big is good” rule. *J. Phys. Chem. Lett.* 9: 4344–4348.
- 12 Miranda-Quintana, R.A. and Ayers, P.W. (2019). The “ $|\Delta\mu|$  big is good” rule, the maximum hardness, and minimum electrophilicity principles. *Theor. Chem. Acc.* 138: 44.
- 13 Parr, R.G. (1994). Companions in the search. *Int. J. Quantum Chem.* 49: 739–770. ProCite field [12]: In File NOT IN FILE IJQC.
- 14 Cardenas, C., Ayers, P.W., and Cedillo, A. (2011). Reactivity indicators for degenerate states in the density-functional theoretic chemical reactivity theory. *J. Chem. Phys.* 134: 174103–174113.
- 15 Bultinck, P., Cardenas, C., Fuentealba, P. et al. (2013). Atomic charges and the electrostatic potential are ill-defined in degenerate ground states. *J. Chem. Theory Comput.* 9: 4779–4788.
- 16 Bultinck, P., Cardenas, C., Fuentealba, P. et al. (2013). How to compute the Fukui matrix and function for systems with (quasi-)degenerate states. *J. Chem. Theory Comput.* 10: 202–210.
- 17 Bultinck, P., Jayatilaka, D., and Cardenas, C. (2015). A problematic issue for atoms in molecules: impact of (quasi-)degenerate states on Quantum Theory Atoms in Molecules and Hirshfeld-I properties. *Comput. Theor. Chem.* 1053: 106–111.
- 18 Perdew, J.P., Parr, R.G., Levy, M. et al. (1982). Density-functional theory for fractional particle number: derivative discontinuities of the energy. *Phys. Rev. Lett.* 49: 1691–1694.
- 19 EcheGARAY, E., Rabi, S., Cardenas, C. et al. (2014). In pursuit of negative Fukui functions: molecules with very small band gaps. *J. Mol. Model.* 20: 1–7.
- 20 Cohen, M.H., Ganduglia-Pirovano, M.V., and Kudrnovsky, J. (1994). Electronic and nuclear chemical reactivity. *J. Chem. Phys.* 101: 8988.
- 21 Fuentealba, P., Cardenas, C., Pino-Rios, R., and Tiznado, W. (2016). *Applications of Topological Methods in Molecular Chemistry*, 227–241. Springer International Publishing.
- 22 Santos, J.C., Contreras, R., Chamorro, E., and Fuentealba, P. (2002). Local reactivity index defined through the density of states describes the basicity of alkaline-exchanged zeolites. *J. Chem. Phys.* 116: 4311.
- 23 Santos, J.C., Contreras, R., Chamorro, E., and Fuentealba, P. (2004). Local reactivity index as descriptor of benzene adsorption in cluster models of exchanged zeolite-Y. *Chem. Phys. Lett.* 383: 612.

- 24 Brommer, K., Galván, M., Dal Pino, A., and Joannopoulos, J. (1994). Theory of adsorption of atoms and molecules on Si(111)-(7×7). *Surf. Sci.* 314: 57.
- 25 Nguyen, L., De Proft, F., Amat, M. et al. (2003). Local softness versus local density of states as reactivity index. *J. Phys. Chem. A* 107: 6837.
- 26 Cardenas, C., De Proft, F., Chamorro, E. et al. (2008). Theoretical study of the surface reactivity of alkaline earth oxides: local density of states evaluation of the local softness. *J. Chem. Phys.* 128: 034708.
- 27 Cárdenas, C., Mu noz, M., Contreras, J. et al. (2018). Understanding chemical reactivity in extended systems: exploring models of chemical softness in carbon nanotubes. *Acta Phys. Chim. Sin.* 34: 631–638.
- 28 Fowler, P. and Manopoulos, D. (1995). *An Atlas of Fullerene*. Oxford: Oxford University Press.
- 29 Fowler, P. (1996). Fullerene stability and structure. *Contemp. Phys.* 37: 235.
- 30 Yang, W. and Mortier, W. (1986). The use of global and local molecular parameters for the analysis of the gas-phase basicity of amines. *J. Am. Chem. Soc.* 108: 5708.
- 31 Cárdenas, C., Rabi, N., Ayers, P.W. et al. (2009). Chemical reactivity descriptors for ambiphilic reagents: dual descriptor, local hypersoftness, and electrostatic potential. *J. Phys. Chem. A* 113: 8660–8667.
- 32 Pino-Rios, R., Yañez, O., Inostroza, D. et al. (2017). Proposal of a simple and effective local reactivity descriptor through a topological analysis of an orbital-weighted Fukui function. *J. Comput. Chem.* 38: 481–488.
- 33 Cedillo, A. and Cárdenas, C. (2019). Reactivity of carbon molecular clusters from a Hückel-type model. *J. Phys. Chem. A* 123: 8696–8701.
- 34 Sablon, N., Proft, F.D., and Geerlings, P. (2009). Molecular orbital-averaged Fukui function for the reactivity description of alkaline earth metal oxide clusters. *J. Chem. Theory Comput.* 5: 1245–1253.
- 35 Cerón, M.L. and Calatayud, M. (2017). Application of dual descriptor to understand the activity of Cu/ZrO<sub>2</sub> catalysts in the water gas shift reaction. *J. Mol. Model.* 23: 34.
- 36 Cohen, A.J., Mori-Sanchez, P., and Yang, W.T. (2008). Insights into current limitations of density functional theory. *Science* 321: 792–794.
- 37 Calatayud, M., Tielens, F., and De Proft, F. (2008). Reactivity of gas-phase, crystal and supported V<sub>2</sub>O<sub>5</sub> systems studied using density functional theory based reactivity indices. *Chem. Phys. Lett.* 456: 59–63.
- 38 Cerón, M.L., Gomez, T., Calatayud, M., and Cárdenas, C. (2020). Computing the Fukui function in solid-state chemistry: application to alkaline earth oxides bulk and surfaces. *J. Phys. Chem. A* 124: 2826–2833.
- 39 Kresse, G. and Hafner, J. (1993). Abinitio molecular-dynamics for liquid-metals. *Phys. Rev. B* 47: 558–561.
- 40 Kresse, G. and Furthmuller, J. (1996). Efficiency of ab-initio total energy calculations for metals and semiconductors using a plane-wave basis set. *Comput. Mater. Sci.* 6: 15–50.
- 41 Kresse, G. and Furthmüller, J. (1996). Efficient iterative schemes for ab initio total-energy calculations using a plane-wave basis set. *Phys. Rev. B* 54: 11169.

- 42 Perdew, J.P., Burke, K., and Ernzerhof, M. (1996). Generalized gradient approximation made simple. *Phys. Rev. Lett.* 77: 3865–3868.
- 43 Tang, W., Sanville, E., and Henkelman, G. (2009). A grid-based Bader analysis algorithm without lattice bias. *J. Phys. Condens. Matter* 21: 084204.
- 44 Logsdail, A.J., Mora-Fonz, D., Scanlon, D.O. et al. (2015). Structural, energetic and electronic properties of (100) surfaces for alkaline earth metal oxides as calculated with hybrid density functional theory. *Surf. Sci.* 642: 58–65.
- 45 Calatayud, M., Ruppert, A., and Weckhuysen, B.M. (2009). Theoretical study on the role of surface basicity and Lewis acidity on the etherification of glycerol over alkaline earth metal oxides. *Chem. Eur. J.* 15: 10864–10870.



## 28

**Fermi Softness: A Local Perspective on Surface Activity***Bing Huang<sup>1</sup> and Lin Zhuang<sup>2,3</sup>*<sup>1</sup>University of Vienna, Faculty of Physics, Kolingasse 14, 1090 Vienna, Austria<sup>2</sup>Wuhan University, College of Chemistry and Molecular Sciences, Luojiaoshan 16, 430072 Wuhan, China<sup>3</sup>Wuhan University, Institute for Advanced Studies, Luojiaoshan 16, 430072 Wuhan, China**28.1 Introduction**

Since the very early days of theoretical chemical research, people have been enthusiastic in understanding how structure, be it geometrical or electronic, translates into the behavior of a chemical species, being either inherent property of the species per se or its interaction strength with the other incoming species. Of particular interest is the latter problem concerning the interaction between two reactive species, which also constitutes part of the grand challenge in modern pursuit of conceptual understanding of the mysterious nature of chemical bonds [1–9].

Admittedly, it would be very complicated (and likely demanding) problem to accurately examine the interaction process in detail, which typically relies on expensive quantum chemical calculations (or machine learning techniques [10]), or through sophisticated experimental setups. A vast swathe of studies have been conducted in this direction, and a lot of insights have been obtained thereafter.

Yet, a different approach is to distill the most vital information from a single (or very few) static calculation(s) of the stand-alone species involved in interaction, or some simple experimental quantities (e.g. ionization potential). In the second approach, we are most interested about the general trend of interaction strengths and some derived simple physical quantity across different systems (even better if the established reactivity model offers quantitatively correct predictions), with only one constitute varying (e.g. A interacts with a series of B's, where B's are not very different but share some common feature in geometrical/electronic structure).

As can be seen, the second approach emphasizes the conceptual aspect of chemical interaction and offers insight into chemistry in spite of the fact that its application is limited (cf. the first *ab initio* approach) and may only make qualitatively correct predictions.

Early such practices comprise almost exclusively simple linear (or low-dimensional) correlations, with the underlying physics largely unknown, and one of the most notable of which being the so-called free energy relationships,

e.g. Bell–Evans–Polanyi (BEP) principle [11, 13]. With the advent of quantum theory, in particular density functional theory, relevant stories have been completely rewritten: most of the previous empirically proposed chemical concepts such as electronegativity [14], hardness/softness [15–17], etc., could be rationalized. This specific subject, dubbed “conceptual density functional theory” (CDFT for short), pioneered by Parr and Yang [18], has been extensively developed ever since and championed by many, including Geerlings et al. [19–21].

Within the first-principle view, the distillation can be viewed as an irreversible process of abstracting essential information from the system wavefunction  $\Psi$  (obtained through solving Schrodinger equation of stand-alone entities before interaction). The distilled quantity is often termed “descriptor” and in principle to obtain which it should not be too involved. Note that how the distillation is carried out depends on the nature of the problem at hand, and hardly there exists a universal descriptor that controls every behavior of a system interacting with the other.

For molecules, profuse knowledge has been accumulated through decades of theoretical research. For a comprehensive review, the reader is referred to Greeing’s several review papers [20, 21]. When it comes to solid and solid surface, however, well-established reactivity descriptors for molecule cease to work within their native form. And often, extension of the same quantity to solid/surface is highly non-trivial or not feasible at all primarily due to the significant difference between the electronic structure of molecule and solid/surface. More specifically, solid/surface possess much more complicated electronic structure compared to that of molecule, i.e. continuous band structure for the former vs. discrete energy levels for the latter. Another unfavorable consequence is the new emerging interaction patterns between empty states of adsorbate and that of surface, further plagues the problem. For a comprehensive review on these conceptual understanding, the reader is referred to the pioneering work done by Hoffman [22, 23]. Therefore, discovery of new working descriptors for surface is usually not a smooth process, and it is not trivial to derive such descriptor purely from fundamental theories. Nevertheless, a multitude of descriptors regarding solid surface have been proposed, including early experimental discovery of the correlation between the catalytic reaction rate and the work function for some solid surface by Vayenas et al. [24], and the more concerned theoretical works, among which, notable ones consist of Yang and Parr’s work of extending the concept of softness/hardness from molecule to metallic surface [16], Wilke et al.’s local isoelectronic reactivity of solid surfaces [25], and recently Calle-Vallejo et al.’s generalized coordination number [26–28], Ma and Xin’s orbital-wise coordination number for predicting adsorption properties of metal nanocatalysts [29], etc.

Generally speaking, reactivity theory mainly deals with early stages of chemical reaction. This is especially true for interactions involving two (or more) molecules, as atoms would rearrange themselves to an extent, such that information about the reactant would be lost at the final stage of reaction. Put it another way, reactivity theory is likely to fail for such “complicated” interactions. In contrast, solid surfaces or nanoparticles (NPs) are relatively open, and its interaction with simple

molecular species (e.g. a free O atom or a small radical OH) would barely cause any significant rearrangement of the constituting atoms. Therefore, the knowledge obtained (through quantum chemical calculation or experiment) for reactants, e.g. relative magnitude of some reactivity index, may be preserved for products and may translate well into the trend of interaction strength among different systems. This openness may be responsible for the success of a wide range of surface reactivity indices, and we will come back to this point later.

Hereafter, unless otherwise stated, the systems we deal with throughout this text are all metallic (i.e. no gap in band structure), as this type of system is most studied and represents the most common catalyst in practice.

### 28.1.1 Fermi Softness

#### 28.1.1.1 Basic Idea

As has already been widely acknowledged [23, 30], both occupied and unoccupied states of solid surface are active when interacting with the adsorbate, though each state (be it occupied or not) may interact differently with the highest occupied molecular orbital (HOMO) and lowest unoccupied molecular orbital (LUMO) of the adsorbate, and accordingly, each results in different contribution to the surface bonding.

Here, we analyze in detail the energetic consequences for overall 15 types of orbital interactions, being combinations of 3 different types of adsorbate electronic states (half-occupied HOMO, fully occupied HOMO and empty LUMO) with five representative electronic states of surface band with varied position relative to Fermi level, as depicted in Figure 28.1.

Let the active state of the adsorbate be half-occupied HOMO. Consider its interaction with the half-filled Fermi level of the surface, there will be energy gain upon bonding for both of the two involved electrons, as they both descend into a lower-energy bonding state. By shifting the surface electronic state to a state slightly below Fermi level, which is now doubly occupied, the outcome would be slightly different due to the occurrence of a net “transfer” of one surface electron from below Fermi level to Fermi level, causing a small magnitude of energy penalty (i.e. raising of orbital energy of single-electron state). As the energy penalty is small, the total single-electron energy (that is, the sum of red bars minus the sum of green bars (if any) in Figure 28.1) decreases, i.e. the whole system is stabilized. As the surface electronic state moves further away from Fermi level, its interaction with the HOMO of the adsorbate becomes weaker, resulting from the larger magnitude of energy penalty, as indicated by the longer green bar in the third column of Figure 28.1a. Similar weakening happens when we shift the surface electronic state upward from Fermi level (which is now empty), as illustrated in the fourth column of Figure 28.1a. The major differences (cf. column 2 and 3 in Figure 28.1a) are twofold: (i) no energy penalty happens and (ii) the internal transfer of electrons of surface persists, but with reversed direction, i.e. there is a net transfer of electron from higher energy levels to lower ones within the surface band, further stabilizing the system.

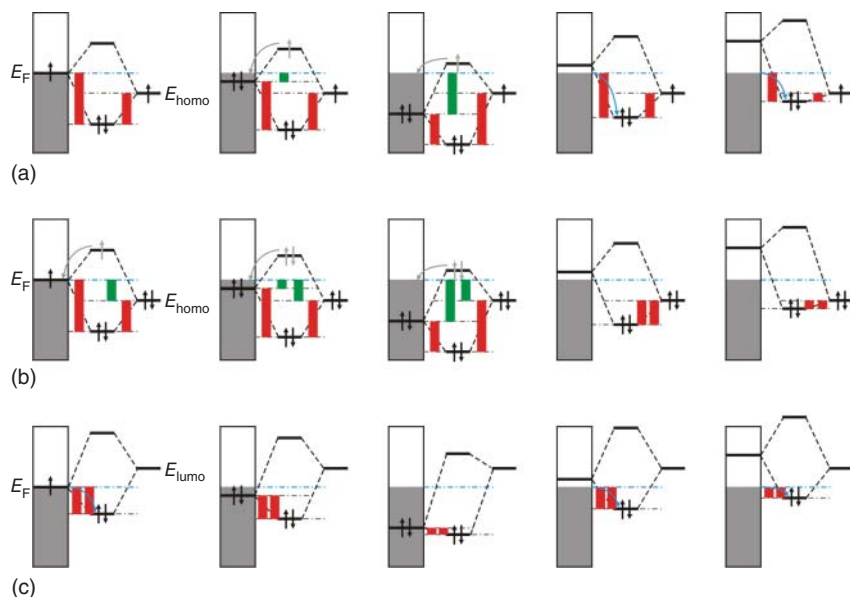


**Figure 28.1** Orbital interactions of surface band and three types of adsorbate orbital: half-occupied HOMO (a), doubly occupied HOMO (b), and empty LUMO (c). The five columns, respectively, correspond to five different states of surface band, being at Fermi level, slightly below  $\epsilon_F$ , well below  $\epsilon_F$ , slightly above  $\epsilon_F$ , and well above  $\epsilon_F$ . Red bar: magnitude of energy gain after orbital interaction; green bar: magnitude of energy penalty upon orbital interaction; solid upward (downward) pointing arrow: electron with spin up (down) occupying some electronic state; gray arrow: electron occupying some “intermediate” electronic state that is about to fill the unoccupied state at the Fermi level of surface band. Reprinted from ref. Huang et al. [31] with permission from Wiley.

When the HOMO of the adsorbate is fully occupied, similar statements could be made as in the case of singly occupied HOMO. While notable differences would be expected when the active orbital of the adsorbate is the empty LUMO. As displayed in Figure 28.1c, all five types of interaction tend to stabilize the system, free of energy penalty, differing primarily in the magnitude of energy gain. Of particular interest are the last two types of interaction in Figure 28.1c, where the interaction is between non-occupied state, yet there is still energy gain. This is unique to surface interaction, as was proposed decades ago by Hoffman [22].

Based on the analysis above, we could draw one revealing conclusion: the closer the state is to the Fermi level, the greater its contribution to bonding. Hence, to qualitatively correct describe the reactivity of a surface, one may propose a quantity as a function of the density of states ( $g(\epsilon)$ ) and some weight function ( $w(\epsilon)$ ) peaking at the Fermi level. The sum of the weighted contribution ( $\int g(\epsilon)w(\epsilon)d\epsilon$ ) is conceived to act as a reactivity descriptor of a surface.

Now the problem boils down to what form of weight function  $w(\epsilon)$  should one choose. Among the many options, herein, we assign  $w(\epsilon)$  to the derivative of the Fermi–Dirac distribution (dFDD for short, see Figure 28.2 for graphical illustration)

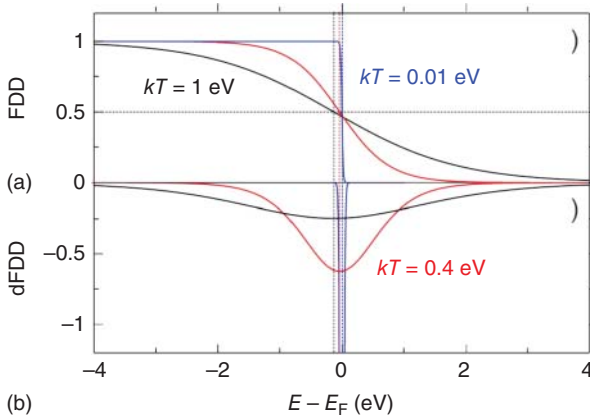


**Figure 28.2** Plot of (a) Fermi-Dirac distribution (FDD for short) function and (b) its derivative (dFDD for short) at three representative electronic temperatures: 0.01, 0.4, and 1 eV. The dashed vertical lines indicate the Fermi level at different  $kT_{\text{el}}$  values, to maintain constant electron number.

function at a nonzero electronic temperature  $\sigma = kT_{\text{el}}$ , i.e.

$$w(\varepsilon) = -f'(\varepsilon) = -\frac{df(\varepsilon)}{d\varepsilon} = \frac{\exp\left(\frac{\varepsilon-\mu}{\sigma}\right)}{\left[\exp\left(\frac{\varepsilon-\mu}{\sigma}\right) + 1\right]^2} \quad (28.1)$$

where the Fermi-Dirac distribution (FDD) is written as  $f(\varepsilon) = f(\varepsilon - \mu) = 1/(1 + e^{(\varepsilon-\mu)/\sigma})$  and the negative sign before  $f'(\varepsilon)$  ensures that the weight function is positive everywhere. As displayed in Figure 28.2, dFDD peaks at  $E_F$  as required and diminishes to zero as the eigenvalue of single electron state moves away from the Fermi level. The resulting weighted sum of the reactivity contribution is dubbed Fermi softness (labeled as  $S_F$ ) and expressed as:

$$S_F = \int_{-\infty}^{\infty} w(\varepsilon)g(\varepsilon)d\varepsilon = - \int_{-\infty}^{\infty} f'(\varepsilon)g(\varepsilon)d\varepsilon \quad (28.2)$$

where the spreading of  $f'(\varepsilon)$  can be changed by adjusting the parameter electronic temperature  $\sigma = kT_{\text{el}}$ .

Much the same as there exists a spatially resolved version of the density of state (being a function of both energy and space), i.e. the local density of state  $g(\varepsilon, r)$ , there is also a local version of  $S_F$ , the local Fermi softness  $s_F(r)$ , i.e.

$$s_F(r) = \int_{-\infty}^{\infty} w(\varepsilon)g(\varepsilon, r)d\varepsilon = - \int_{-\infty}^{\infty} f'(\varepsilon)g(\varepsilon, r)d\varepsilon \quad (28.3)$$

And similar to how we obtain the electron number  $N$  through integrating  $\rho(r)$  within the whole space, the global softness  $S_F$  and its local version  $s_F(r)$  have the following relationship:

$$S_F = \int_{-\infty}^{\infty} s_F(r)dr \quad (28.4)$$

It turns out that  $S_F$  and  $s_F(r)$  are not just some random quantities that happen to serve well as reactivity indices (as will be shown shortly), rather, they naturally arise from CDFT. It can be easily shown that at finite electronic temperature, the global softness of the system  $S_\sigma$  under fixed external potential ( $v_{\text{ext}}$ ) has the following form:

$$S_\sigma = \left( \frac{\partial N}{\partial \mu} \right)_{v_{\text{ext}}} \approx \int_{-\infty}^{\infty} g(\epsilon) \frac{\partial f(\epsilon)}{\partial \mu} d\epsilon = - \int_{-\infty}^{\infty} f'(\epsilon) g(\epsilon) d\epsilon \quad (28.5)$$

where we have used the expression for total electron number ( $N$ ) at finite  $kT_{\text{el}}$ , i.e.  $N = \int_{-\infty}^{\infty} f(\epsilon) g(\epsilon) d\epsilon$ . The local version of Fermi softness could be derived in a similar fashion.

We note by passing that dFDD is normalized, regardless of the value  $kT$  takes, i.e.

$$- \int_{-\infty}^{\infty} f'(\epsilon) d\epsilon = 1 \quad (28.6)$$

This feature is coveted as it is the density of states that enters as the sole factor determining the reactivity of a surface.

Due to the existence of locality of electronic systems aforementioned, we have to extract the contribution to  $S_F$  from some surface atom (say atom with index  $I$ ) only. There exists several approaches to do this. One straightforward way is to partition the space into atomic contributions (e.g. Bader scheme, Voronoi scheme, or simply Wigner–Seitz scheme, etc.) and then integrate  $s_F(r)$  within the subspace associated with atom  $I$ , i.e.

$$S_F^{(I)} = \int_{\Omega_I} s_F(r) dr \quad (28.7)$$

where  $\Omega_I$  is the space partitioned to atom  $I$ . Due to the fact that space partitioning could be time-consuming (especially true for Bader scheme for large systems), an alternative  $s_F(\epsilon)$ -based approach may be adopted, in which we have to obtain the density of states projected to surface atom  $I$  first and then employ the following equation to calculate  $S_F^{(I)}$  (see Figure 28.3 for graphical illustration):

$$S_F^{(I)} = \int_{-\infty}^{\infty} g^{(I)}(\epsilon) f'(\epsilon) d\epsilon \quad (28.8)$$

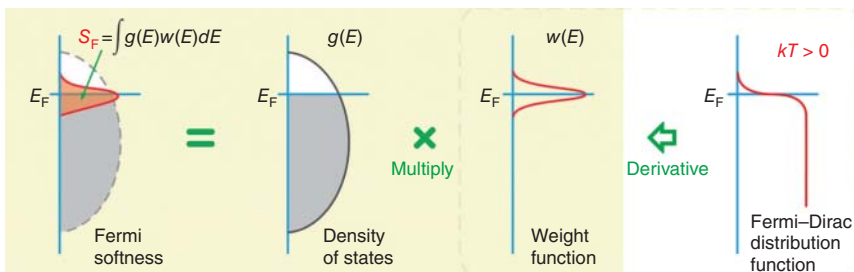


**Figure 28.3** Graphical illustration of  $S_F$ , defined as a weighted sum of the density of states  $\int g(\epsilon)w(\epsilon)d\epsilon$ , where the weight function  $w(\epsilon)$  is chosen as the derivative of the Fermi–Dirac distribution function at nonzero electronic temperature. Reprinted from ref. Huang et al. [31] with permission from Wiley.

where  $s_F^{(I)}(\epsilon)$  is the projected energy-resolved Fermi softness of surface atom  $I$ , and  $g^{(I)}(\epsilon)$  is the total density of states projected to  $I$ , including all possible angular components of atom  $I$ .

Before leaving this section, it is necessary to clarify the exact meaning of being global or local. Here, global refers to a single scalar quantity, for instance, electron number, or the global Fermi softness ( $S_F$ ). Note that  $S_F$  may also refer to a specific surface atom, i.e.  $S_F^{(I)}$ , and it is the default meaning of  $S_F$  whenever we mention  $S_F$  hereafter, unless otherwise stated. When speaking of a local picture, we mean there is a scalar value associated with every point in the three dimensional space, for instance, charge density and the local Fermi softness  $s_F(r)$ .

### 28.1.1.2 Fermi Softness vs. d-Band Center

Perhaps one of the most successful descriptors to date for transition metal surface is the so-called d-band center model developed by Hammer and Nørskov [30, 32], which states that the reactivity of a transition metal surface could be approximately characterized by the first moment ( $\epsilon_d$ ) of the projected density of states to the localized d-orbitals of surface atom ( $I$ ), i.e.  $\int_{-\infty}^{\infty} (\epsilon - \epsilon_F) g_d^I(\epsilon) d\epsilon$ .

There are three major differences between d-band model and Fermi softness: (i) Fermi softness offers both global and spatial picture of surface reactivity, while d-band model offers only the global picture. (ii) Fermi softness describes the response of the whole electron density with respect to change in chemical potential, i.e. it includes the contribution from both s-, p-, and d-orbitals, while d-band model, as its name implies, considers only projection to d-orbitals (the projection amplitude does depend on projection amplitude to the other angular channels though). Note that this does not suggest better performance of Fermi softness model (cf. d-band model), as the contribution to interaction from sp-band is similar across different transition metal surfaces. By subtracting this part of contribution, the relative magnitude of Fermi softness across transition metal surfaces would not change. That is, at least for transition metal surface, sp-band has minor effect on the relative magnitude of Fermi softness. However, for other gapless systems, such as sp-block metal surface or nonmetal surfaces, Fermi softness may stand out as a more competitive descriptor due to its response nature. (iii) d-band model is theoretically more rigorous than Fermi softness, as the former offers a direct link between chemisorption strength and d-band center (though it is much approximated) based on simplified quantum model. Fermi softness, like most CDFT-based descriptor, is lack of such direct relationship and often assumed to describe only the early stages of interaction.

In principle, both d-band model and Fermi softness are applicable to systems sharing some similarity only, but for somewhat different reasons. More specifically, for Fermi softness, the interaction types/trends in early stages are similar, so are the interaction types/trends in late stages (which determine the final interaction strength), and therefore the relative interaction strengths persist throughout. For d-band model, similar coupling matrix element between adsorbate state and surface d band would be desired [33].

## 28.2 Applications

In this section, we demonstrate the usefulness of Fermi softness, including both its global and local picture through a few representative applications. For more use cases, the reader is referred to the original publication [31].

### 28.2.1 Correlation with Adsorption Energy

In Figure 28.4, we have already demonstrated that the global Fermi softness as a reactivity index exhibits a nice correlation with oxygen adsorption energy for Pt-derived metal surfaces. Here, we offer two more examples.

The first one is for Pd(111) and supported Pd monolayer on various transition metal surfaces. The property investigated is still oxygen adsorption energy. Again, an approximate monotonic trend is observed: as the global Fermi softness of surface Pd atom increases, the surface reactivity is enhanced, resulting in stronger chemical bond. As a comparison, correlation of oxygen adsorption energy and d-band center for the same set of systems, is also plotted, as displayed in Figure 28.5b. The latter correlation to  $\epsilon_d$  is more scattered and notably worse than the former correlation with  $S_F$ . The same statement could be made for Pt and other transition metal-derived systems. This seems to suggest that the global Fermi softness is a very robust surface reactivity descriptor.

To further support our finding, more numerical results are necessary. As such, we consider further the adsorption of a saturated molecule carbon monoxide (CO) on a series of Pd, Pt, and Au NPs, with results for Pt NPs shown in Figure 28.6. The overall correlation of  $\Delta E_{\text{ads}}^{\text{CO}}$  with  $S_F$  is very good and resembles much the correlation with d-band center. Similar correlations could be found for other NPs (not shown here).

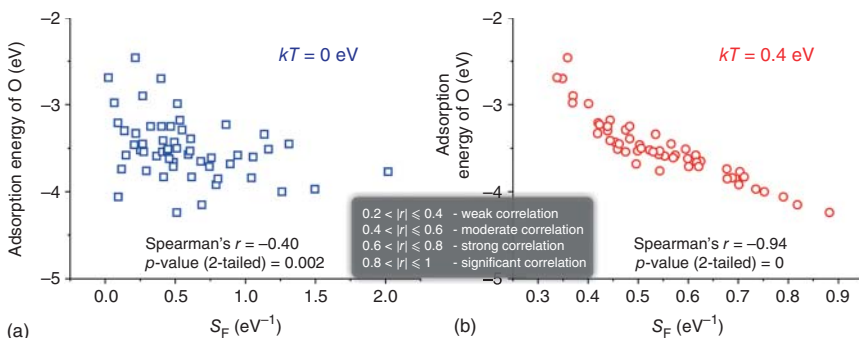


**Figure 28.4** Comparison of correlations between oxygen adsorption energy ( $\Delta E_{\text{O}}$ ) on Pt-related surfaces and  $S_F$  of surface Pt atom at two electronic temperatures: 0 eV ((a), no spreading in dFDD) and 0.4 eV (b). How well  $\Delta E_{\text{O}}$  is correlated with  $S_F$  is measured by the Spearman's  $r$  and larger absolute value indicates better correlation. Reprinted from ref. Huang et al. [31] with permission from Wiley.



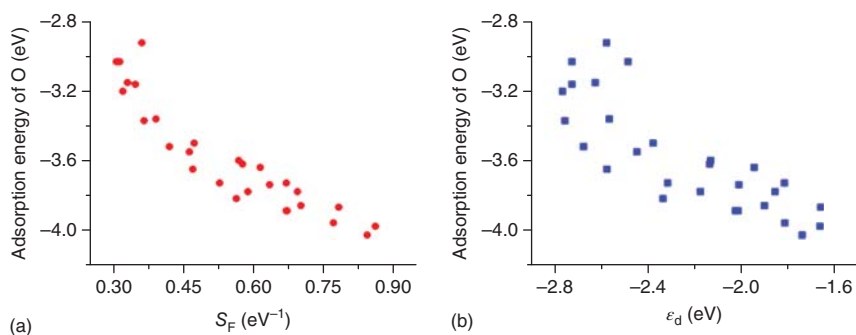


**Figure 28.5** (a) Correlation between the global Fermi softness ( $S_F$ ) and the surface reactivity as indicated by the oxygen adsorption strength on Pd-derived surfaces (see the supplementary material of Ref. [31] for details). (b) Correlation between the d-band center and the surface reactivity for the same systems as in (a). Reprinted from ref. Huang et al. [31] with permission from Wiley.

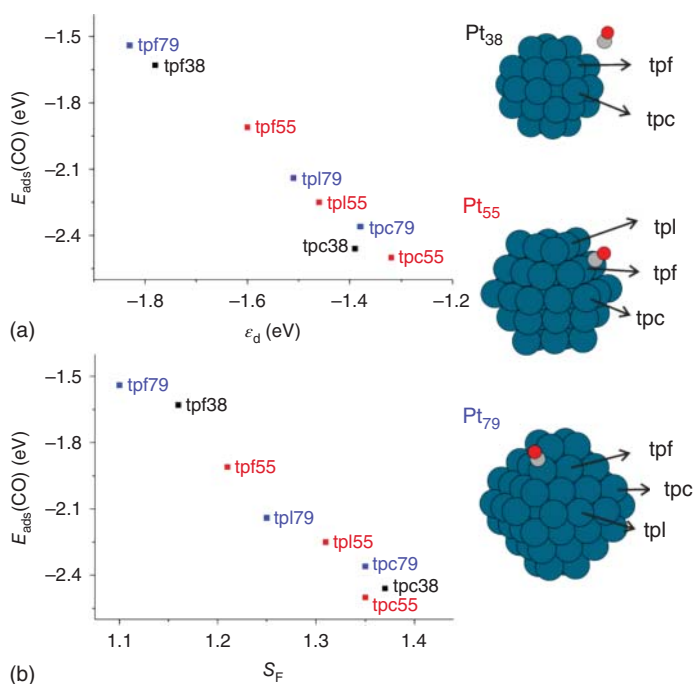


**Figure 28.6** Demonstration of the correlation between the Fermi softness ( $S_F$ ) and the reactivity of various top sites (tpf, tpc, and tpl, as shown in the inset) on Pt nanoparticles as represented by the CO adsorption strength (b). For comparison, correlation with the  $d$ -band center is also presented (a). tpl79: top site on Pt atom in Pt nanoparticle made up of 79 Pt atoms.

### 28.2.2 Active Sites of MoS<sub>2</sub>

The local picture of Fermi softness is particularly valuable when dealing with heterogeneous surface structure, which represents a wider range of catalysts in real-world applications. Here, we demonstrate its power through only one example: a one-dimensional (1D) MoS<sub>2</sub> edge, which is responsible for the high catalytic activity toward hydrogen evolution reaction [34–36].

The structure of 1D MoS<sub>2</sub> is displayed in Figure 28.7a and exhibits much richer local atomic environments than previously studied transition metal-derived surfaces. More specifically, it covers three types of sulfur atoms, including S#1, S#2, and S#3, as well as two types of Mo atoms, i.e. Mo#1 and Mo#2. Among all the S sites, the dimer consisting of two S#1 atoms (along *y* direction, see Figure 28.7a) stands out as the most prominent local environments, i.e. around which the reactivity distribution of  $s_F(r)$  exhibits a magnitude significantly larger than that of any of the rest S environments, which is totally consistent with the experimental finding [35, 36]. The sharp peak around Fermi level in the projected density of states (DOS) plot in Figure 28.7b also support the observation. More intriguing is the tilted p-orbital-like distribution of  $s_F(r)$  around S#1, which reveals the subtle information that the reactivity of the S#1 dimer edge is spatially anisotropic: the reactivity field over the aforementioned S dimer is stronger than between the two S#1 atoms lying along *x* direction. In particular, the distance between the two centers of the crown of  $s_F(r)$  of two S#1 atoms in the S dimer matches the interatomic distance of two H atoms in H<sub>2</sub> and is therefore ideal for catalyzing the formation reaction of H<sub>2</sub> from two adsorbed H atoms. To verify such a hypothesis, we have calculated the reaction profile of H–H bond formation reaction  $2H_{ad} \rightarrow H_2$  at two kinds of bridge sites: br-*x* (intra-dimer site) or br-*y* (inter-dimer site, see the inset of Figure 28.7e) on the S#1 dimer edge. The computational results clearly show that the barrier at the br-*x* site is significantly lower compared to that at the br-*y* site, regardless of the direction of the reaction. This is in full agreement with the anisotropic nature suggested by  $s_F(r)$ , an insight previously unknown and could not be unraveled by any other reactivity descriptors, to the best of our knowledge.

## 28.3 Conclusion and Outlook

To recap, we have reviewed the detailed theory of Fermi softness, and some representative applications. Numerical evidences suggest that Fermi softness could serve as a very useful reactivity descriptor for solid surface due to its robustness as well as low computational cost. While the d-band model is limited to transition metal surfaces and NPs, the potential applicability of Fermi softness is largely unlimited, thanks to its response nature, as well as its deep connection to the CDFFT. Currently, only a small amount of applications have been reported, and its power to tackle more complicated systems and ultimately help with catalysts design still awaits to be fully unleashed in the future.

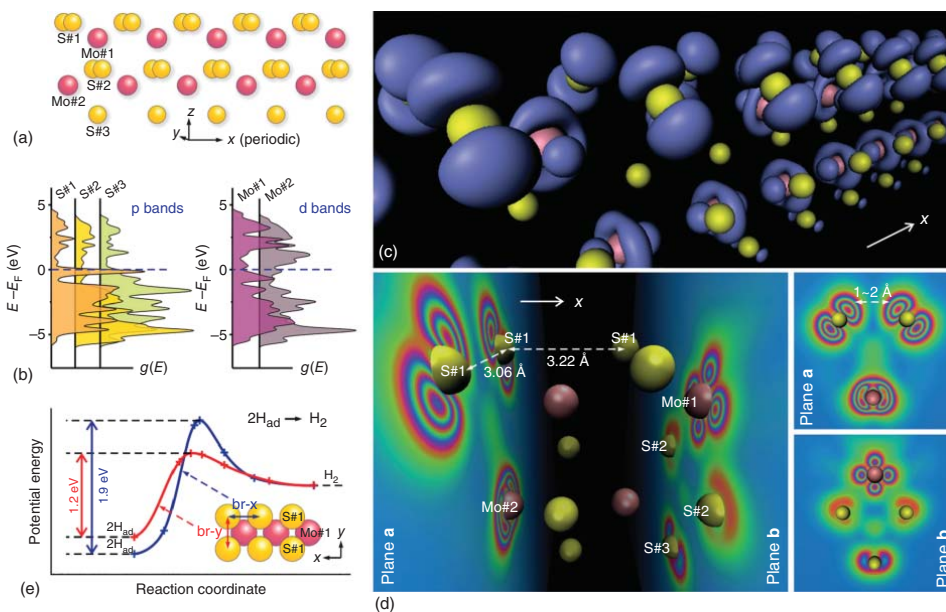


**Figure 28.7** Spatially resolved chemical reactivity of a 1D MoS<sub>2</sub> edge. (a) The geometrical structure of MoS<sub>2</sub>, with three typical local sulfur environments (S#1, S#2, and S#3) and two typical molybdenum atom environments (Mo#1 and Mo#2). (b) The projected density of states ( $g(\epsilon)$ ) of specific sulfur and molybdenum atoms. (c) A 3D perspective of the local Fermi softness  $s_F(r)$ , as represented by some isosurface (blue). (d) The  $s_F(r)$  is plotted as projection onto two planes normal to the  $x$  direction: plane **a** intersects two S#1 and one Mo#2 atoms, and plane **b** contains one Mo#1, two S#2, and one S#3 atoms. (e) Reaction energy profiles for the reaction  $2\text{H}_{\text{ad}} \rightarrow \text{H}_2$  at two kinds of bridge sites (br-x or br-y, see the inset) on the S#1 dimer edge, obtained from nudged elastic band calculations. Reprinted from ref. Huang et al. [31] with permission from Wiley.

## Acknowledgments

B.H. acknowledges funding from the Swiss National Science Foundation (No. PP00P2\_138932 and 407540\_167186 NFP 75 Big Data). This research was partly supported by NCCR MARVEL, funded by the Swiss National Science Foundation.

## Bibliography

- 1 Pauling, L. (1960). *The Nature of the Chemical Bond and the Structure of Molecules and Crystals: An Introduction to Modern Structural Chemistry*. Cornell University Press.
- 2 Ruedenberg, K. (1962). The physical nature of the chemical bond. *Rev. Mod. Phys.* 34 (2): 326–376.
- 3 de Sousa, D.W.O. and Nascimento, M.A.C. (2017). Are one-electron bonds any different from standard two-electron covalent bonds? *Acc. Chem. Res.* 50 (9): 2264–2272.
- 4 Huang, B., Zhuang, L., Xiao, L., and Lu, J. (2013). Bond-energy decoupling: principle and application to heterogeneous catalysis. *Chem. Sci.* 4 (2): 606–611.
- 5 Shaik, S., Danovich, D., Wu, W., and Hiberty, P.C. (2009). Charge-shift bonding and its manifestations in chemistry. *Nat. Chem.* 1 (6): 443–449.
- 6 Shaik, S., Danovich, D., Galbraith, J.M. et al. (2020). Charge-shift bonding: a new and unique form of bonding. *Angew. Chem. Int. Ed.* 59 (3): 984–1001.
- 7 Levine, D.S. and Head-Gordon, M. (2017). Energy decomposition analysis of single bonds within Kohn–Sham density functional theory. *Proc. Natl. Acad. Sci. U.S.A.* 114 (48): 12649–12656.
- 8 Levine, D.S. and Head-Gordon, M. (2017). Quantifying the role of orbital contraction in chemical bonding. *J. Phys. Chem. Lett.* 8 (9): 1967–1972.
- 9 Levine, D.S. and Head-Gordon, M. (2020). Clarifying the quantum mechanical origin of the covalent chemical bond. *Nat. Commun.* 11 (1): 4893.
- 10 Huang, B. and von Lilienfeld, O.A. (2021). Ab initio machine learning in chemical compound space. *Chem. Rev.* 121 (16): 10001–100360.
- 11 Bell, R.P. and Hinshelwood, C.N. (1936). The theory of reactions involving proton transfers. *Proc. R. Soc. London, Ser. A - Math. Phys. Sci.* 154 (882): 414–429.
- 12 Evans, M.G. and Polanyi, M. (1936). Further considerations on the thermodynamics of chemical equilibria and reaction rates. *Trans. Faraday Soc.* 32 (0): 1333–1360.
- 13 van Santen, R.A., Neurock, M., and Shetty, S.G. (2010). Reactivity theory of transition metal surfaces: a Bronsted–Evans–Polanyi linear activation energy free energy analysis. *Chem. Rev.* 110 (4): 2005–2048.
- 14 Mulliken, R.S. (1934). A new electroaffinity scale; together with data on valence states and on valence ionization potentials and electron affinities. *J. Chem. Phys.* 2 (11): 782–793.

- 15 Parr, R.G. and Pearson, R.G. (1983). Absolute hardness: companion parameter to absolute electronegativity. *J. Am. Chem. Soc.* 105 (26): 7512–7516.
- 16 Yang, W. and Parr, R.G. (1985). Hardness, softness, and the Fukui function in the electronic theory of metals and catalysis. *Proc. Natl. Acad. Sci. U.S.A.* 82 (20): 6723–6726.
- 17 Nguyen, L.T., De Proft, F., Amat, M.C. et al. (2003). Local softness versus local density of states as reactivity index. *J. Phys. Chem. A* 107 (35): 6837–6842.
- 18 Parr, R.G. and Yang, W. (1994). *Density-Functional Theory of Atoms and Molecules*. Springer.
- 19 Ayers, P.W. and Parr, R.G. (2000). Variational principles for describing chemical reactions: the Fukui function and chemical hardness revisited. *J. Am. Chem. Soc.* 122 (9): 2010–2018.
- 20 Geerlings, P., De Proft, F., and Langenaeker, W. (2003). Conceptual density functional theory. *Chem. Rev.* 103 (5): 1793–1874.
- 21 Geerlings, P., Fias, S., Boisdenghien, Z., and Proft, F.D. (2014). Conceptual DFT: chemistry from the linear response function. *Chem. Soc. Rev.* 43 (14): 4989–5008.
- 22 Hoffmann, R. (1987). How chemistry and physics meet in the solid state. *Angew. Chem. Int. Ed. Engl.* 26 (9): 846–878.
- 23 Hoffmann, R. (1988). A chemical and theoretical way to look at bonding on surfaces. *Rev. Mod. Phys.* 60 (3): 601–628.
- 24 Vayenas, C.G., Bebelis, S., and Ladas, S. (1990). Dependence of catalytic rates on catalyst work function. *Nature* 343 (6259): 625–627.
- 25 Wilke, S., Cohen, M.H., and Scheffler, M. (1996). Local isoelectronic reactivity of solid surfaces. *Phys. Rev. Lett.* 77 (8): 1560–1563.
- 26 Calle-Vallejo, F., Martínez, J.I., García-Lastra, J.M. et al. (2014). Fast prediction of adsorption properties for platinum nanocatalysts with generalized coordination numbers. *Angew. Chem. Int. Ed.* 53 (32): 8316–8319.
- 27 Calle-Vallejo, F., Tymoczko, J., Colic, V. et al. (2015). Finding optimal surface sites on heterogeneous catalysts by counting nearest neighbors. *Science* 350 (6257): 185–189.
- 28 Calle-Vallejo, F., Loffreda, D., Koper, M.T.M., and Sautet, P. (2015). Introducing structural sensitivity into adsorption energy scaling relations by means of coordination numbers. *Nat. Chem.* 7 (5): 403–410.
- 29 Ma, X. and Xin, H. (2017). Orbitalwise coordination number for predicting adsorption properties of metal nanocatalysts. *Phys. Rev. Lett.* 118 (3): 036101.
- 30 Hammer, B. and Nørskov, J.K. (1995). Why gold is the noblest of all the metals. *Nature* 376 (6537): 238–240.
- 31 Huang, B., Xiao, L., Lu, J., and Zhuang, L. (2016). Spatially resolved quantification of the surface reactivity of solid catalysts. *Angew. Chem.* 128 (21): 6347–6351.
- 32 Hammer, B. and Nørskov, J.K. (1995). Electronic factors determining the reactivity of metal surfaces. *Surf. Sci.* 343 (3): 211–220.
- 33 Nilsson, A., Pettersson, L., and Nørskov, J.K. (2008). *Chemical Bonding at Surfaces and Interfaces*. Elsevier.

- 34 Tsai, C., Abild-Pedersen, F., and Nørskov, J.K. (2014). Tuning the MoS<sub>2</sub> edge-site activity for hydrogen evolution via support interactions. *Nano Lett.* 14 (3): 1381–1387.
- 35 Bollinger, M.V., Lauritsen, J.V., Jacobsen, K.W. et al. (2001). One-dimensional metallic edge states in MoS<sub>2</sub>. *Phys. Rev. Lett.* 87 (19): 196803.
- 36 Jaramillo, T.F., Jørgensen, K.P., Bonde, J. et al. (2007). Identification of active edge sites for electrochemical H<sub>2</sub> evolution from MoS<sub>2</sub> nanocatalysts. *Science* 317 (5834): 100–102.

## 29

### ABEEM Polarizable Force Field

*Dong-Xia Zhao and Zhong-Zhi Yang*

*School of Chemistry and Chemical Engineering, Liaoning Normal University, Shahekou district, Dalian, 116029, P. R. China*

#### 29.1 Introduction

Potential energy surface (PES) is the potential energy of a molecular system by using atomic or nuclear coordinates as variables [1]. It is a necessary and basic quantity for the study of both molecular static properties and dynamic behaviors. In the framework of Born–Oppenheimer approximation; however, accurate calculation and construction of a PES through solving the Schrödinger equation of the electronic motion by a suitable quantum chemical method for a large molecule is not accessible. Therefore, theoretical chemists intelligently construct an empirical form of PES for a large molecular system, the molecular potential energy function called the force field that is based on plenty of both experimental data and theoretical results. This kind of attempt has begun since the 1930s [2]. Here, we will not trace the history of the development of the force field in detail, and only want to focus on the content related to the title.

With the fast pace of development of computer techniques, molecular modeling and simulations on the computer have become more and more powerful and popular tools for scientists. In this respect, for treating large complex molecular systems, a force field or molecular mechanics (MM) plays a fundamental role, even as it is combined with quantum mechanics (QM). The core of a force field is the potential energy function of molecular systems at the atomistic level. In fact, it is an effective expression of the PES for large molecular systems in molecular modeling or molecular dynamics (MDs) simulations.

#### 29.2 Classical Force Fields with the Fixed Atomic Partial Charges

The classical force fields were proposed and used as early as 1930s [2], and the general force fields, such as MMx ( $x = 2-4$ ) [3–5], CHARMM [6], OPLS [7–10], AMBER [11, 12], etc. arose during 1970s. The details of describing various force fields can be

found in many literatures and excellent textbooks. The main difference between the old and new generation of force fields is that the latter treat the polarization effect explicitly and/or make the partial atomic charges fluctuating in the geometry optimization and dynamic simulation rather than using the fixed atomic charges. There has been a steady interest since the 1970s in the development and use of polarizable force fields (PFFs) with early work focusing on liquid water and ions in water. Nevertheless, it is generally accepted, the development of a new generation of the molecular force field is a fundamental, challenging, and difficult work [13].

### 29.2.1 The Potential Energy Function in a Force Field

The general form of the potential energy function in a force field for both old and new generations is usually written as a sum of empirical terms, each describing the energy required for distorting a molecule in a specific fashion:

$$E_T = E_b + E_\theta + E_\phi + E_{\text{imptors}} + E_{\text{vdw}} + E_{\text{elec}} \quad (29.1)$$

Here,  $E_b$  is the energy function for stretching a bond between two atoms,  $E_\theta$  represents the energy required for bending an angle,  $E_\phi$  is the torsional energy for rotation around a bond,  $E_{\text{imptors}}$  is the improper dihedral angle term,  $E_{\text{vdw}}$  describes the van der Waals (vdW) or nonbonded atom–atom interaction, and  $E_{\text{elec}}$  is the electrostatic interaction energy. Usually, the first two terms are simply expressed in accordance with harmonic (or Morse) function forms as Eqs. (29.2) and (29.3):

$$E_b(r) = \sum_{\text{bonds}} k_r (r - r_{\text{eq}})^2 \quad (29.2)$$

$$E_\theta(\theta) = \sum_{\text{angles}} k_\theta (\theta - \theta_{\text{eq}})^2 \quad (29.3)$$

where  $k_r$  and  $k_\theta$  represent the force constants of the stretching and bending;  $r$  and  $\theta$  are the actual values of bond length and bond angle. The subscripts of  $r_{\text{eq}}$  and  $\theta_{\text{eq}}$  are used to denote the equilibrium values of the bond length and bond angle.

The torsional term takes the form as Eq. (29.4) and the improper dihedral angle term is written as Eq. (29.5):

$$E_\phi(\phi) = \sum_{\text{torsions}} \left\{ \frac{v_1}{2} [1 + \cos(\phi)] + \frac{v_2}{2} [1 - \cos(2\phi)] + \frac{v_3}{2} [1 + \cos(3\phi)] \right\} \quad (29.4)$$

$$E_{\text{imptors}} = \sum_{\text{imptors}} v [1 - \cos(2\phi)] \quad (29.5)$$

where  $\phi$  is the dihedral angle, and  $v_1$ ,  $v_2$ ,  $v_3$ , and  $v$  are the dihedral angle and improper dihedral angle force constants, respectively.

The vdW atom–atom interaction term,  $E_{\text{vdw}}$ , usually takes the Lennard–Jones 12-6 form (in some force fields it may take other sophisticated forms):

$$E_{\text{vdw}} = \sum_{i < j} 4f_{ij} \epsilon_{ij} \left( \sigma_{ij}^{12} / r_{ij}^{12} - \sigma_{ij}^6 / r_{ij}^6 \right) \quad (29.6)$$

Usually, the geometric combining rules for the Lennard–Jones coefficients are employed:  $\sigma_{ij} = (\sigma_{ii} \sigma_{jj})^{1/2}$  and  $\epsilon_{ij} = (\epsilon_{ii} \epsilon_{jj})^{1/2}$ . The summation runs over all of the pairs



of atoms  $i < j$  on molecules A and B for intermolecular interactions or A and A for the intramolecular interactions. Moreover, in the latter case, the coefficient  $f_{ij} = 0.0$  for any  $i$ - $j$  pair connected by a valence bond (1-2 pairs) or a valence bond angle (1-3 pairs),  $f_{ij} = 0.5$  for 1-4 interactions (atoms separated by exactly three bonds) and  $f_{ij} = 1.0$  for all of the other cases.

The term electrostatic interaction energy  $E_{\text{elec}}$  is usually expressed as following effective Coulombic form:

$$E_{\text{elec}} = \sum_{i < j} q_i q_j / r_{ij} \quad (29.7)$$

where  $i$  and  $j$  stand for the partial charge sites;  $q_i$  and  $q_j$  are the partial charges of sites  $i$  and  $j$ ;  $r_{ij}$  is the separation of sites  $i$  and  $j$ .

Each term in the energy function (29.1) may take a different form from the one given in Eqs. (29.2)–(29.7) and may also add the crossing terms, depending on the designer's consideration.

The classical force fields keep all the partial charges fixed during the process of molecular modeling or dynamic simulations.

However, as well known, for more accurate description, there are polarization effects between atoms and molecules that should not be neglected.

### 29.2.2 Charge Distribution and Polarization

From a more microscopic view, a molecule consists of nuclei and electrons. An arrangement of the nuclei or atoms in a molecule leads to electron density (or intuitively, electron cloud) re-distribution around the nuclear framework and vice versa. However, the electron density is still very difficult to be intuitively represented and particularly to be visualized except very simple cases, as well as to be applied to large molecular systems for calculating the electrostatic energy of both intramolecular and intermolecular interactions. Instead, very simply, chemists like to partition a molecule into individual atomic regions, each containing a nucleus and related electron cloud around it, and hence say atomic partial charges (condensed atomic charges, including both a nuclear charge and electron cloud charge around). This is not only an intuitive picture but also a meaningful model for discussing many molecular properties. Most importantly, this model simplifies the treating and greatly decreases the calculations involved in MD simulations for large molecular systems.

Theoretically, atomic charges of a molecule can be calculated by various approaches, such as quantum chemical methods through a number of the electron population analyses, such as famous Mulliken's [14], Lowdin's [15], NBO's (natural bond orbital) [16], and Hirshfeld's [17]. Experimentally, although electron density may, in principle, be determined by X-ray diffraction for a crystal, its practical application is very limited. But some experimental data, such as dipole moments of various molecules, may provide valuable information about partial atomic charges for small molecules.

Certainly, a proper and consistent assignment or calculation of the partial atomic charges is essential for the development of a force field, particularly a PFF. However, just as Cramer pointed out [18]: “There is no universally agreed upon ‘best’ procedure for obtaining partial atomic charge. This failure to agree is, in some sense, inevitable, because partial atomic charges are used in different ways within the context of different quantitative and qualitative models in chemistry. Therefore, there is no reason to expect a single procedure for determining such charge to be optimal for all purposes.”

Now we talk about polarization a little bit. In chemistry, polarization usually describes both spatial distortion and electron density change of the electron cloud due to intramolecular or intermolecular interaction or an external electric field. The intramolecular polarization implies the distortion of the electron cloud of a fragment or an atom relative to that of an isolated one or a reference one. In fact, the electron cloud or electron distribution around an atom or nucleus in a molecule, particularly in the bonding region, is always different from the electron cloud of an isolated one. The polarization process can be intuitively represented by the change of the molecular face (MF, Chapter 19), the frontier electron density on the molecular intrinsic characteristic counter.

Mainly, in the PFFs, there are two sorts of models to represent the polarization effect. In the first model, the polarization is described by assumed induced dipole moment (multipole) or Drude model located on each atomic site or a partial electron being connected to each atomic site while all atomic charges being fixed during geometry change or simulation process. In contrast, in the second model, the partial charge of every site changes or fluctuates during the simulation process whence the polarization effect is naturally included during the simulation process. In the following sections, we will give brief descriptions of the two models, respectively.

### 29.3 Polarizable Force Fields

MDs simulations have become a very active research field due to interpretive and predictive significance on structures and properties of various systems [19–22]. For increasing the accuracy and reliability of MD simulations, a lot of efforts have been made to develop the new generation of force fields, the PFFs that can treat polarization effect explicitly in a real environment that varies during the simulation process. In this respect, OPLS [7–10], CHARMM [22–26], NEMO [27–29], QMPFF [30–32], AMBER [33–38], AMOEBA [39–42], etc. force fields have made a lot of progresses. In many PFFs, such as in the AMOEBA force field [42], the potential energy function is expressed by containing some orders of induced multipoles, such as dipole moments, quadrupole moments, and even higher order of multipoles at atomic sites besides the partial atomic charges. In the new era, it is noticed that Xie and Gao have designed and developed a new generation force field, called the X-POL potential, which is based on a quantum mechanical model to avoid deficiencies in the usual force fields [43]. Mackerell and his coworkers have developed CHARMM Drude PFF [44–49], applied to nucleic acid bases and accurate calculation of the hydration free

energies [45, 49], and also to peptides and proteins, ethers, sulfur-containing compounds, and alkanes [44, 46–48]. This model has been used by the Robinson group to investigate cholesterol and sphingomyelin [50], and by the Best group for multi-scale simulations of the condensed phase [51]. van Gunsteren group is developing PFFs by using Drude-type approaches for MDs simulation of liquid hydrocarbons [52]. There are also inducible point dipole models, such as in the AMBER FF02 PFF. Duan et al. have developed it for simulations of proteins and peptides [36]; Mancera group presented it for calculations of the free energy of interaction of the c-Fos–c-Jun coiled-coil [53]; Sagui et al. presented it for MDs simulations of DNA [54].

At the same period of time, a few fluctuating charge models for PFFs have also been proposed and applied by some groups, such as Rick et al. [55–57], Patel and Brooks [58, 59], van der Graaf and coworkers [60, 61], Rappé and Goddard [62, 63], Chelli and Procacci [64, 65], Stern and Berne [66, 67], Oberhofer and coworkers [68], and Yang and his coworkers [69–90]. The fluctuating charge model for calculating the charge distribution is based on the electronegativity equalization method (EEM) [91, 92], the charge equilibration (QEq) [93], chemical potential equalization principle (CPE) [94, 95], atom-condensed Kohn–Sham density functional theory (DFT) approximated to second-order (ACKS2) [96] or the atom–bond electronegativity equalization method (ABEEM) [97–100]. The advantage of this method is its clear significance of the partial region charges and fast computation by solving a set of linear equations without any iteration procedures.

Evaluation of electrostatic interaction in a force field is an important and challenging task. A proper and consistent assignment or calculation of the charge distribution and polarization effect is an essential step in the representation of a force field.

### 29.3.1 Induced Dipole Moment (Multipole) Model and Drude Model

In the induced dipole (multipoles) model used in the PFFs, taking an *N*-methylacetamide (NMA) molecule as an example as shown in Figure 29.1, it is assumed that there exists a permanent partial atomic charge for an atom and then an induced atomic dipole (and multipoles) at each atomic region is produced due to the electric field given by the other permanent atomic charges. These sets of the induced atomic dipoles can be evaluated by the atomic polarizabilities. In the induced dipole PFF; therefore, the potential energy function is augmented by an inductive term from the induced dipoles. The contribution of the electrostatic interaction comes from both permanent charges and induced dipole moments, obtained from the atomic polarizabilities through an iterative procedure [101]. Karlström and coworkers [29] have demonstrated the importance of the quadrupole moment. Higher-order multipoles were included in AMOEBA PFF [102].

In the Drude model, to describe the polarization of a molecule, it is proposed that every atom other than hydrogen is attached a negative charge  $q_{\text{att}}$  at some position bound to the nucleus by a harmonic force constant where the involved parameters are determined by an iterative optimization.

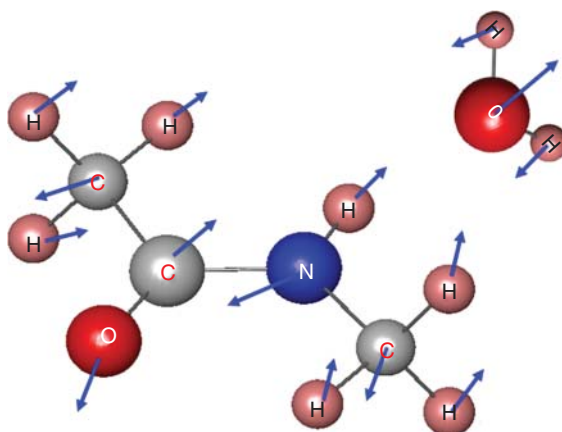


**Figure 29.1** The atomic regions and the induced atomic dipoles of *N*-methylacetamide (NMA) molecule and water molecule.

### 29.3.2 Electronegativity Equalization Method for Calculating the Charge Distribution

In a PFF, the main characteristic is the expression of its electrostatic interaction. Here, we describe the methods that give rise to calculate the partial site charges in terms of the EEM.

#### 29.3.2.1 EEM Method

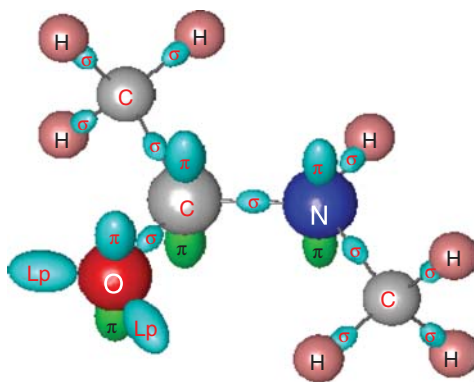
Conventional EEM methods partition a molecular system into individual atomic regions, each having one partial atomic charge. The atomic charges are calculated by the EEM whose basis is conceptual DFT [103, 104]. In the usual EEM scheme, by using the atomic partial charges and three characteristic parameters per atom, the molecular energy is represented as:

$$E = \sum_a (E_a^* + \chi_a^* q_a + \eta_a^* q_a^2) + \sum_{a<b} k_{ab} \frac{q_a q_b}{R_{ab}} \quad (29.8)$$

where  $E_a^*$  is the energy of atom  $a$  at its neutral valence state,  $q_a$  is the atomic partial charge at a region (atom and/or specified one),  $\chi_a^*$  and  $\eta_a^*$  are the valence-state electronegativity and valence-state hardness of region  $a$ ,  $R_{ab}$  is the separation between regions  $a$  and  $b$ , and the summation for both  $a$  and  $b$  is overall sites. In DFT, the effective electronegativity  $\chi_a$  of a site  $a$  is equal to the partial derivative of the electrostatic energy with respect to the partial charge  $q_a$  of site  $a$ .  $k_{ab}$  is a correction factor of the Coulombic interaction energy between the partial charges  $q_a$  and  $q_b$ , which stems from the reality that  $q_a$  and  $q_b$  involve the electron clouds rather than the ideal point charges.

Based on DFT, the effective electronegativity  $\chi_a$  of every site  $a$  is expressed as the partial derivative of the electrostatic energy with respect to the partial charge  $q_a$  of site  $a$ . According to the EEM, at the equilibrium state, the effective electronegativities of all sites are equal to the global molecular electronegativity  $\chi_{\text{mol}}$  for every molecule, which constitutes the electronegativity equalization equation, i.e.  $\chi_a = \chi_b = \dots = \chi_{\text{mol}}$ . It can be shown that the number of the equations of EEM is equal to the number of the sites of molecules. These equations, together with

**Figure 29.2** The sketch of all regions in *N*-methylacetamide (NMA) molecule defined in ABEEM method, which contains the regions or sites of the atoms, bonds, and lone pairs.



the charge constraint and given parameters (valence-state electronegativity  $\chi_a^*$  and valence-state hardness  $\eta_a^*$  of region a), can be explicitly and quickly solved to give the global molecular electronegativity  $\chi_{\text{mol}}$  and the partial charge  $q_a$  on each site a.

There are several fine implementations of EEM to allow rapid calculations of the partial charge distribution in molecules [91–95]. Particularly, the ACKS2 method [96] has given a systematic derivation and extension of the EEM of Mortier et al. [91, 92], demonstrating the limitation of the EEM and related methods in terms of the atom-condensed Kohn-Sham DFT ACKS2.

### 29.3.2.2 Atom–Bond Electronegativity Equalization Method (ABEEM)

In Figure 29.2, as an example, we draw the charts of all regions in NMA molecule in the ABEEM method. In addition to atomic sites, some new virtual sites including lone pair, and  $\sigma$  and  $\pi$  bond sites are placed according to the physical meaning. The C atom of carbonyl connects two single bonds and one double bond. The geometry around this C atom is trigonally planar. The geometry around the O atom is also trigonally planar too because the O atom of carbonyl connects one double bond and two lone pairs. The oxygen atom involves six partial charges, namely, one centered on the oxygen nucleus, one  $\sigma$  region, two  $\pi$  separate upper and lower regions, and two lone pairs.  $\sigma$  bond partial charge shared by oxygen and carbon atoms is on the bond at the point that partitions the bond length according to the ratio of covalent radii between O and C atoms; the  $\pi$  bond partial charges are placed above and below the O atom at the covalent radius (0.74 Å) of O atom perpendicular to the plane formed by the  $\sigma$  bonds and may have different values depending on the environment; the two lone pair partial charges are placed in the covalent radius of the oxygen atom (0.74 Å). A pair of electrons of the N atom can be used to make a delocalized  $\pi$  bond with carbonyl. There are also similar  $\pi$  bond partial charges for the nitrogen atom and carbon atom of carbonyl in NMA. So the nitrogen atom involves six partial charges, including one atom, three  $\sigma$ , and two  $\pi$  regions. As a whole, besides 12 atomic sites, an NMA molecule has additional 19 sites: 11  $\sigma$  bond sites, 6  $\pi$  bond sites, and 2 lone pair sites. Therefore, partial charges of these sites may fairly reflect the charge distribution, including anisotropic polarization around an atom.

The potential energy function of ABEEM PFF takes the same form as usual force fields as expressed by Eq. (29.1), but the electrostatic interaction energy term  $E_{\text{elec}}$  is

particularly expressed as:

$$E_{\text{elec}} = \sum_{i<j} k_{ij} q_i q_j / r_{ij} \quad (29.9)$$

In Eq. (29.9),  $i$  and  $j$  stand for the sites,  $q_i$  and  $q_j$  are the partial charges of sites  $i$  and  $j$  (including lone pair,  $\sigma$  and  $\pi$  bond sites),  $r_{ij}$  is the separation of sites  $i$  and  $j$ ;  $k_{ij} = 0$ , when the shortest linking path relationship between sites  $i$  and  $j$  is smaller than 1,6;  $k_{ij} = k_{\text{H-bond}}$ , when  $i$  and  $j$  are in the hydrogen bond interaction regions (HBIR);  $k_{ij} = 0.57$  for all the other cases as used [75, 76, 79, 84, 86]. The partial charges  $q_i$  and  $q_j$  are calculated in terms of the ABEEM method. The parameter  $k_{ij}$  may overcome the limitation of EEM to some extent, and here simply taking as a constant of 0.57.

The fine ABEEM [97–100] total energy of a system can be expressed as:

$$E[q] = E^* + \sum_i [\chi_i^* q_i + \eta_i^* q_i^2] + k \sum_{i<j} \frac{q_i q_j}{R_{ij}} \quad (29.10)$$

In a fluctuating charge PFF, the valence state electronegativity and hardness are important parameters, which are the first and second order expansion coefficients of the potential energy function with respect to the partial charges of the regions. According to conceptual DFT theory, the valence-state electronegativities  $\chi_i^*$  and valence-state hardnesses  $\eta_i^*$  for region  $i$  in a molecule are defined by the first partial derivative of the  $E[q]$  with respect to the partial charge  $q_i$  of region  $i$ :  $\chi_i^* = \left( \frac{\partial E}{\partial q_i} \right)_{q_j, R_{ij}}$ ,  $2\eta_i^* = \left( \frac{\partial^2 E}{\partial q_i^2} \right)_{q_j, R_{ij}}$ , where  $E$  is the molecular potential energy function as expressed by Eq. (29.10),  $q_i$  and  $q_j$  are the partial charges of regions  $i$  and  $j$ , and  $R_{ij}$  is the distance between regions  $i$  and  $j$ . Working out the partial derivatives, we obtain the following expression of the effective electronegativity  $\chi_i$  of a region  $i$ :

$$\chi_i = \chi_i^* + 2\eta_i^* q_i + k \sum_{j(\neq i)} \frac{q_j}{R_{ij}} \quad (29.11)$$

According to the electronegativity equalization principle, all the effective electronegativity  $\chi_i$  are equal to a global molecular electronegativity  $\chi_{\text{mol}}$ :

$$\chi_1 = \chi_2 = \dots = \chi_M = \chi_{\text{mol}} \quad (29.12)$$

Equations (29.12) and (29.13) represent linear associated equations with respect to the partial charges  $q_i$  as variables. In addition, there is a constraint of the total charge which means that the system may have an apparent charge  $q_{\text{mol}}$ :

$$\sum_i q_i = q_{\text{mol}} \quad (29.13)$$

By solving these linear associated equations, the partial charges  $q_i$  of all the regions can be obtained as long as the valence state electronegativity  $\chi_i^*$ , valence state hardness  $\eta_i^*$ , and parameter  $k$  are known. Different molecules may accordingly take different concrete forms.

It is noted that these equations are geometry-dependent. When the geometry or conformation of the system considered has a change, the region partial charges or

charge distributions have changes correspondingly. In this way, the ABEEM fluctuating charge method is adopted to be a PFF. Particularly, its multi-partial charge regions around an atom can well reflect the polarization effect and charge transfer as the geometry and/or the environment vary.

### 29.3.3 Calibration of the Parameters

Calibration of parameters for any force field is a highly cumbersome task with a huge amount of tests, calculations, and analyses. This is a systematic and long-term work; even the framework of a force field has been established.

It is well known that parameters for the hard degrees of freedom (bond stretching and angle bending) can be transferred from one FF to another with little modification. For example, for some bonds and angles in the amide system, the same force constants, equilibrium bond lengths, and bond angles are used in both OPLS-AA [7] and AMBER [11] FFs. Therefore, we refer and take the parameters of bond stretching and angle bending for protein from OPLS-AA FF and for DNA from AMBER FF with minor modification. The torsional terms are often regarded as “soft” degrees of freedom, in which most of the variations in structure and relative energy are due to the complex interplay between the torsional and nonbonded contributions. In ABEEM PFF, the torsional and improper torsional parameters of OPLS-AA or AMBER are taken as a reference, refitting them through the least square optimization procedure to make the conformation energies and the key dihedral angles RMSD of the model molecules be in good agreement with those calculated by high-level *ab initio* method. In addition, the Lennard–Jones parameters are determined by fitting *ab initio* conformational energies, dimer binding energies, dipole moments, and so on, using regression and least-squares method.

For the parameter calibration of ABEEM fluctuating charge force field for usual chemical (mainly organic) and biological molecules, we have chosen more than 3000 model molecules that involve a large number of organic and biological species. A great amount of effort has been devoted to optimize the ABEEM parameters to make them consistent, transferable, and applicable to reproduce and/or predict structural, energetic, and dynamic properties of various species with proper accuracy.

## 29.4 Molecular Dynamic Simulations

### 29.4.1 Water Clusters and Water Solution

As shown in Figure 29.3, the ABEEM model, i.e. ABEEM-7P or TIP7P model for a water molecule, in addition to three usual atomic sites, four new virtual sites are placed, including two lone pairs and two OH  $\sigma$  bond sites. This model means that a water molecule contains seven electron cloud regions in three atoms, two  $\sigma$  bonds whose angle is  $104.5^\circ$ , and two lone pairs whose angle is  $109.47^\circ$ . As seen, there are four electron pairs around the oxygen atom, which are spread to point roughly toward the vertexes of a tetrahedron. Every atomic charge is placed in the position

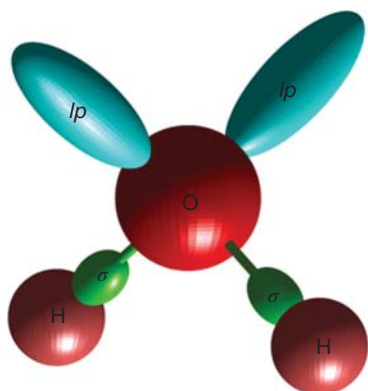


**Figure 29.3** A sketch map of the ABEEM-7P water molecule sites, including one oxygen atomic region, two hydrogen atomic regions, two O–H  $\sigma$  bond regions, and two lone pair regions.

of the corresponding atom. The  $\sigma$  bond charge is assumed to locate on the point that partitions the bond length according to the ratio of covalent atomic radii of two bonded atoms, and the lone pair sites are placed on the points, which are 0.74 Å far from the oxygen nucleus with an intervening angle of 109.47° between two lone pairs on the oxygen atom in the ABEEM model.

In the practical treatment of our ABEEM-7P model, it is a nonrigid body and fluctuating charge model, which is a transferable, intermolecular, seven-point approach (ABEEM-7P), in which the bond and angle are allowed to vibrate and the partial charges on charged sites are treated to respond to changes in their environments. The partial charges of regions are obtained by using the ABEEM. The bond stretching is represented by the Morse function. When extending the ABEEM method to a system containing many molecules, such as a water system, special attention must be given to the description of the intermolecular PES. In the water system, many of the special properties are due to the ability of water molecules to form hydrogen bonds with other water molecules; thus, a correct description of the hydrogen bond is essential. Yang et al. [70] have introduced a “HBIR,” in which the interaction between the lone-pair electron of the O atom of one water molecule and the H atom of the other is dependent on their distance until the hydrogen bond is formed, and they have used a new fitted function that is introduced to better account for hydrogen bonding between water molecules.

Small water clusters  $(\text{H}_2\text{O})_n$  ( $n = 1-6$ ) are chosen for the first application of ABEEM-7P model [70]. The ABEEM-7P model is an improved alternative one that differs from the previous TIP4P-FQ, POL5, and other models for the water system in two aspects. The Morse potential function is selected for bond stretching in the ABEEM-7P model because it can characterize a wide range of behavior from the equilibrium geometry to dissociation, and for vdW interaction the ABEEM-7P model takes oxygen–oxygen, hydrogen–hydrogen, oxygen–hydrogen interaction into account to calculate the 12-6 Lennard-Jones interaction energy.

Furthermore, the ABEEM-7P model has been used to study larger water clusters  $(\text{H}_2\text{O})_n$  ( $n = 7-34$ ) and water liquid [105], the obtained geometries, combination energies, and successive combination energies, and dipole moments are in fair



agreement with the results from experimental measurements or high-level ab initio calculations (such as MP2 method), which demonstrates that ABEEM-7P model works much better than those with fixed charge models [106–111], such as TIP3P, SPC, TIP4P, and TIP5P.

This ABEEM-7P model is also employed to study ion–water, water–amide acids, water–peptides, water–proteins, and water–bases systems.

### 29.4.2 Chemical and Biological Systems as Well as in Their Aqueous Solution

Many chemical and biological molecular systems, including in aqueous solution, have been investigated in terms of the ABEEM PFF. The water model is the ABEEM-7P flexible water model as given above.

The interaction between various molecules, water and biological molecules, such as peptides and proteins, bases and DNA, ion and biomolecules, has been described by means of the ABEEM model. The ABEEM potential functions for these systems have been constructed, sometimes combined with QM, and MDs simulations have been performed.

Just to give one example, the structures of a protein, Crambin, from the protein data bank were used as the initial geometries of MD simulations. The MD simulations were performed using the modified TINKER program in the NVT ensemble with Berendsen thermostats, the velocity Verlet integrator, and the time step of 1 fs. The systems were initially heated over 5 ps to 285 K. The cutoff radius for nonbonding interactions was 10.0 Å with the minimum image convention if the periodic boundary condition was used. For all simulations, 0.5 ns of MD run for equilibration was performed, followed by 9.5 ns of simulations for the calculation of various properties. We recomputed the partial charges of all sites using the ABEEM method in every 0.1 ps. The obtained structure of Crambin is quite close to that in the crystal.

The exhaustive conformations of Ala, Gly, and Val dipeptides and tripeptides have been investigated at B3LYP/6-311++G(d,p) theory of level at the gaseous phase. Total 17 stable structures of these dipeptides and 83 stable structures of tripeptides are obtained by optimizing at the same level. Force fields containing OPLS/AA, AMBER99sb, CHARMM27, AMOEBA, and ABEEM are employed in reproducing all minima. By scanning  $\varphi$  and  $\psi$ , which are dihedral angles at the backbone of amino acids, the PESs are investigated by both the B3LYP/6-311++G(d,p) and ABEEM. ABEEM method locates all minima with the least mean absolute deviation values. The distributions of energy regions by ABEEM agree well with that from B3LYP/6-311++G(d,p). ABEEM depicts two energy barrier regions at  $\varphi = 0^\circ$  and  $150^\circ$  throughout  $\psi$  ( $-180^\circ \sim 180^\circ$ ). Because of the feature, which is that the charge in each region fluctuates simultaneously with the changing geometry and surroundings, ABEEM describes the charge distributions as credible and reasonable and further obtains reliable region distributions. MDs simulations for four dipeptides in explicit water are performed to examine the conformational properties in aqueous with the same parameters. The preference of ABEEM in locating minima of short

peptides consists of the *ab initio* method. The energy barrier benefits the simulation of amino acid conformations and the location of stable structures.

Hydrogen-bonding and stacking interactions play a unique role in the structure and replication of DNA. When adenine in DNA is oxidized, it increases the number of hydrogen bond donor and acceptor sites and may lead to various mutations. 8-oxo-A is the most common oxidative product of adenine. Taking high-level *ab initio* calculations as benchmarks, we developed the ABEEM PFF and investigated the charges, structures, energies, and mutations of base pairs containing canonical bases and 8-oxo-A [86]. During this process, we do a great deal of *ab initio*, ABEEM, and other force field calculations for investigation, testing, and calibration. Comparing the results of *ab initio* with those of ABEEM, the linear correlation coefficients of the charges, dipole moments, and interaction energies are 0.99, 0.96, and 0.96, respectively; and the ABEEM force field provides reliable information on hydrogen bonding, stacking interactions, and mutation processes. In the DNA double helix, the mutations of AT → GC, AT → TA, or AT → CG would happen. Meanwhile, the active centers of nucleophilic or electrophilic reaction transfer during AT → GC, AT → TA, and AT → CG mutations. The results also indicate that the performance of the ABEEM PFF is generally better than that of the common force fields, and its accuracy can compare with that of the MP2 method.

We have performed many studies on the chemical and biological systems and achieved fruitful results, demonstrating ABEEM PFF is also a promising one.

## Acknowledgment

This research was supported by the National Natural Science Foundation of China (Nos. 21473083 and 21133005).

## References

- 1 Leach, A.R. (2001). *Molecular Modeling-Principles and Applications*, 2nde. Essex, England: Pearson Education Limited.
- 2 Andrews, D.H. (1930). *Phys. Rev.* 36: 544.
- 3 Burkert, U. and Allinger, N.L. (1982). *Molecular Mechanics*. Washington DC: American Chemistry Society.
- 4 Allinger, N.L., Yuh, Y.H., and Lii, J.H. (1989). *J. Am. Chem. Soc.* 111: 8551.
- 5 Nevins, N. and Allinger, N.L. (1996). *J. Comput. Chem.* 17: 730.
- 6 Kurplus, M. and McCammon, J.A. (1983). *Annu. Rev. Biochem.* 52: 263.
- 7 Jorgensen, W.L., Maxwell, D.S., and Tirado-Rives, J. (1996). *J. Am. Chem. Soc.* 118: 11225.
- 8 Jorgensen, W.L. and Tirado-Rives, J. (1988). *J. Am. Chem. Soc.* 110: 1657.
- 9 Jorgensen, W.L., Jensen, K.P., and Alexandrova, A.N. (2007). *J. Chem. Theory Comput.* 3: 1987.

- 10 Kaminski, G.A., Friesner, R.A., Tirado-Rives, J., and Jorgensen, W.L. (2001). *J. Phys. Chem. B* 105: 6474.
- 11 Cornell, W.D., Cieplak, P., Bayly, C.I. et al. (1995). *J. Am. Chem. Soc.* 117: 5179.
- 12 Małolepsza, E., Strodel, B., Khalili, M. et al. (2010). *J. Comput. Chem.* 31: 1402.
- 13 Warshel, A., Kato, M., and Pisliakov, A.V. (2007). *J. Chem. Theory Comput.* 3: 2034.
- 14 Mulliken, R.S. (1955). *J. Chem. Phys.* 23: 1841.
- 15 Löwdin, P.O. (1955). *Phys. Rev.* 97: 1474.
- 16 Reed, A.E., Weinstock, R.B., and Weinhold, F. (1985). *J. Chem. Phys.* 83: 735.
- 17 Hirshfeld, F.L. (1977). *Theor. Chim. Acta* 44: 129.
- 18 Cramer, C.J. (2004). *Essentials of Computational Chemistry*. England: Wiley.
- 19 Banci, L. (2003). *Curr. Opin. Chem. Biol.* 7: 143.
- 20 Hu, L.H. and Ryde, U. (2011). *J. Chem. Theory Comput.* 7: 2452.
- 21 Neves, R.P.P., Sousa, S.F., Fernandes, P.A., and Ramos, M.J. (2013). *J. Chem. Theory Comput.* 9: 2718.
- 22 MacKerell, A.D., Bashford, D., Bellott, R. et al. (1998). *J. Phys. Chem. B* 102: 3586.
- 23 Zhu, X., Lopes, P.E.M., and MacKerell, A.D. Jr., (2012). *WIREs Comput. Mol. Sci.* 2: 167.
- 24 Denning, E.J., Priyakumar, U.D., Nilsson, L., and MacKerell, A.D. Jr., (2011). *J. Comput. Chem.* 32: 1929.
- 25 Hart, K., Foloppe, N., Baker, C.M. et al. (2012). *J. Chem. Theory Comput.* 8: 348.
- 26 Best, R.B., Zhu, X., Shim, J. et al. (2012). *J. Chem. Theory Comput.* 8: 3257.
- 27 Engkvist, O., Åstrand, P.-O., and Karlström, G. (2000). *Chem. Rev.* 100: 4087.
- 28 Holt, A. and Karlström, G. (2008). *J. Comput. Chem.* 29: 1084.
- 29 Holt, A., Bostrom, J., Karlström, G., and Lindh, R. (2010). *J. Comput. Chem.* 31: 1583.
- 30 Khoruzhii, O., Donchev, A.G., Galkin, N. et al. (2008). *PNAS* 105: 10378.
- 31 Donchev, A.G., Galkin, N.G., Illarionov, A.A. et al. (2006). *Proc. Natl. Acad. Sci. U. S. A.* 103: 8613.
- 32 Donchev, A.G., Ozhin, V.D., Subbotin, M.V. et al. (2005). *PNAS* 102: 7829.
- 33 Wang, J., Cieplak, P., and Kollman, P.A. (2000). *J. Comput. Chem.* 21: 1049.
- 34 Wang, J., Cieplak, P., Li, J. et al. (2012). *J. Phys. Chem. B* 116: 7088.
- 35 Case, D.A., Cheatham, T.E., Darden, T. et al. (2005). *J. Comput. Chem.* 26: 1668.
- 36 Wang, Z.X., Zhang, W., Wu, C. et al. (2006). *J. Comput. Chem.* 27: 781.
- 37 Gaillard, T. and Case, D.A. (2011). *J. Chem. Theory Comput.* 7: 3181.
- 38 Zgarbová, M., Otyepka, M., Šponer, J.i. et al. (2011). *J. Chem. Theory Comput.* 7: 2886.
- 39 Grossfield, A., Ren, P., and Ponder, J.W. (2003). *J. Am. Chem. Soc.* 125: 15671.
- 40 Ponder, J.W., Wu, C., Ren, P. et al. (2010). *J. Phys. Chem. B* 114: 2549.
- 41 Ren, P. and Ponder, J.W. (2002). *J. Comput. Chem.* 23: 1497.
- 42 Ren, P., Wu, C., and Ponder, J.W. (2011). *J. Chem. Theory Comput.* 7: 3143.
- 43 Xie, W. and Gao, J. (2007). *J. Chem. Theory Comput.* 3: 1890.
- 44 Lopes, P.E.M., Huang, J., Shim, J. et al. (2013). *J. Chem. Theory Comput.* 9: 5430.

- 45 Baker, C.M., Anisimov, V.M., and MacKerell, A.D.J. (2011). *J. Phys. Chem. B* 115: 580.
- 46 Zhu, X. and Mackerell, A.D.J. (2010). *J. Comput. Chem.* 31: 2330.
- 47 Baker, C.M. and MacKerell, A.D. (2010). *J. Mol. Model.* 16: 567.
- 48 Vorobyov, I.V., Anisimov, V.M., and MacKerell, A.D. (2005). *J. Phys. Chem. B* 109: 18988.
- 49 Baker, C.M., Lopes, P.E.M., Zhu, X. et al. (2010). *J. Chem. Theory Comput.* 6: 1181.
- 50 Robinson, D. (2013). *J. Chem. Theory Comput.* 9: 2498.
- 51 Baker, C.M. and Best, R.B. (2013). *J. Chem. Theory Comput.* 9: 2826.
- 52 Szklarczyk, O.M., Bachmann, S.J., and van Gunsteren, W.F. (2014). *J. Comput. Chem.* 35: 789.
- 53 Zuo, Z.L., Gandhi, N.S., and Mancera, R.L. (2010). *J. Chem. Inf. Model.* 50: 2201.
- 54 Babin, V., Baucom, J., Darden, T.A., and Sagui, C. (2006). *J. Phys. Chem. B* 110: 11571.
- 55 Rick, S.W. (2001). *J. Chem. Phys.* 114: 2276.
- 56 Rick, S.W. and Berne, B.J. (1996). *J. Am. Chem. Soc.* 118: 672.
- 57 Rick, S.W., Stuart, S.J., and Berne, B.J. (1994). *J. Chem. Phys.* 101: 6141.
- 58 Patel, S. and Brooks, C.L. III, (2004). *J. Comput. Chem.* 25: 1.
- 59 Patel, S. and Brooks, C.L. III, (2006). *Mol. Simul.* 32: 231.
- 60 Smirnovt, K.S. and van de Graaf, B. (1996). *J. Chem. Soc. Faraday Trans.* 92: 2469.
- 61 van Duin, A.C.T., Baas, J.M.A., and van de Graaf, B. (1996). *J. Chem. Soc. Faraday Trans.* 92: 353.
- 62 Rappé, A.K., Casewit, C.J., Colwell, K.S. et al. (1992). *J. Am. Chem. Soc.* 114: 10024.
- 63 Casewit, C.J., Colwell, K.S., and Rappé, A.K. (1992). *J. Am. Chem. Soc.* 114: 10046.
- 64 Chelli, R. and Procaccia, P. (2002). *J. Chem. Phys.* 117: 9175.
- 65 Chelli, R., Procacci, P., Righini, R., and Califano, S. (1999). *J. Chem. Phys.* 111: 8569.
- 66 Stern, H.A., Kaminski, G.A., Banks, J.L. et al. (1999). *J. Phys. Chem. B* 103: 4730.
- 67 Stern, H.A., Rittner, F., Berne, B.J., and Friesner, R.A. (2001). *J. Chem. Phys.* 115: 2237.
- 68 Gütlein, P., Blumberger, J., and Oberhofer, H. (2020). *J. Chem. Theory Comput.* 16: 5723–5735.
- 69 Wu, Y. and Yang, Z.Z. (2004). *J. Phys. Chem.* 108: 7563.
- 70 Yang, Z.Z., Wu, Y., and Zhao, D.X. (2004). *J. Chem. Phys.* 120: 2541.
- 71 Li, X. and Yang, Z.Z. (2005). *J. Phys. Chem. A* 109: 4102.
- 72 Yang, Z.Z. and Li, X. (2005). *J. Phys. Chem. A* 109: 3517.
- 73 Yang, Z.Z. and Li, X. (2005). *J. Chem. Phys.* 123: 094507.
- 74 Zhang, Q. and Yang, Z.Z. (2005). *Chem. Phys. Lett.* 403: 242.
- 75 Yang, Z.Z. and Qian, P. (2006). *J. Chem. Phys.* 125: 064311.

- 76 Yang, Z.Z. and Zhang, Q. (2006). *J. Comput. Chem.* 27: 1.
- 77 Wang, F.F., Zhao, D.X., and Yang, Z.Z. (2009). *Chem. Phys.* 360: 141.
- 78 Yu, L. and Yang, Z.Z. (2010). *J. Chem. Phys.* 132: 174109.
- 79 Zhao, D.X., Liu, C., Wang, F.F. et al. (2010). *J. Chem. Theory Comput.* 6: 795.
- 80 Chen, S.L., Zhao, D.X., and Yang, Z.Z. (2011). *J. Comput. Chem.* 32: 338.
- 81 Yu, C.Y. and Yang, Z.Z. (2011). *J. Phys. Chem. A* 115: 2615.
- 82 Zhao, D.X., Yu, L., Gong, L.D. et al. (2011). *J. Chem. Phys.* 134: 194115.
- 83 Liu, C., Zhao, D.-X., and Yang, Z.-Z. (2012). *J. Comput. Chem.* 33: 379.
- 84 Yang, Z.Z., Wang, J.J., and Zhao, D.X. (2014). *J. Comput. Chem.* 35: 1690.
- 85 Xu, S., Zhao, D.X., Gong, L.D. et al. (2015). *Chem. Phys. Lett.* 618: 147.
- 86 Liu, C., Li, Y., Han, B.Y. et al. (2017). *J. Chem. Theory Comput.* 13: 2098.
- 87 Li, H., Wang, D., Zhao, X. et al. (2019). *J. Comput. Chem.* 40: 1141.
- 88 Liu, C., Zhao, J., Yang, Z.Z., and Zhao, D.X. (2020). *J. Chem. Theory Comput.* 16: 7618.
- 89 Lu, L.N., Liu, C., and Yang, Z.Z. (2020). *J. Phys. Chem. A* 124: 8614.
- 90 Shi, H., Gong, L.D., Liu, C. et al. (2020). *J. Phys. Chem. A* 124: 5963.
- 91 Mortier, W.J., Ghosh, S.K., and Shankar, S. (1986). *J. Am. Chem. Soc.* 108: 4315.
- 92 Mortier, W.J., Van Genechten, K., and Gasteiger, J. (1985). *J. Am. Chem. Soc.* 107: 829.
- 93 Rappé, A.K. and Goddard, W.A. III, (1991). *J. Phys. Chem.* 95: 3358.
- 94 York, D.M. (1995). *Int. J. Quantum Chem.* 29: 385.
- 95 York, D.M. and Yang, W. (1996). *J. Chem. Phys.* 104: 159.
- 96 Verstraelen, T., Ayers, P.W., Van Speybroeck, V., and Waroquier, M. (2013). *J. Chem. Phys.* 138.
- 97 Yang, Z.Z. and Wang, C.S. (1997). *J. Phys. Chem. A* 101: 6315.
- 98 Wang, C.S. and Yang, Z.Z. (1999). *J. Chem. Phys.* 110: 6189.
- 99 Cong, Y. and Yang, Z.Z. (2000). *Chem. Phys. Lett.* 316: 324.
- 100 Yang, Z.Z. and Cui, B.Q. (2007). *J. Chem. Theory Comput.* 3: 1561.
- 101 Rasmussen, T.S., Ren, P., Ponder, J.W., and Jensen, F. (2007). *Int. J. Quantum Chem.* 107: 1390.
- 102 Kaminsky, J. and Jensen, F. (2007). *J. Chem. Theory Comput.* 3: 1774.
- 103 Parr, R.G. and Yang, W.T. (1989). *Density-Functional Theory of Atoms and Molecules*. New York: Oxford University Press.
- 104 Gerrlings, P., De Profit, F., and Langenaeker, W. (2003). *Chem. Rev.* 103: 1793.
- 105 Qian, P., Lu, L.N., Song, W., and Yang, Z.Z. (2009). *Theor. Chem. Accounts* 123: 487.
- 106 Jorgensen, W.L. (1981). *J. Am. Chem. Soc.* 103: 335.
- 107 Dang, L.X. and Pettitt, B.M. (1987). *J. Phys. Chem.* 91: 3349.
- 108 Mahoney, M.W. and Jorgensen, W.L. (2000). *J. Chem. Phys.* 112: 8910.
- 109 Jorgensen, W.L., Chandrasekhar, J., Madura, J.D. et al. (1983). *J. Chem. Phys.* 79: 926.
- 110 Mahoney, M.W. and Jorgensen, W.L. (2000). *J. Chem. Phys.* 114: 363.
- 111 Glättli, A., Daura, X., and van Gunsteren, W.F. (2002). *J. Chem. Phys.* 116: 9811.

## 30

## Charge Transfer and Polarization in Force Fields: An *Ab Initio* Approach Based on the (Atom-Condensed) Kohn–Sham Equations, Approximated by Second-Order Perturbation Theory About the Reference Atoms (ACKS2)

Paul W. Ayers

McMaster University, Department of Chemistry and Chemical Biology, 25-1280 Main Street West, Hamilton, ON L8S-4M1, Canada

### 30.1 Introduction

Traditional fixed-charge molecular mechanics force fields play a key role in computational chemistry because they are the most computationally affordable model with atomistic resolution [1–4]. When atomistic coarse-graining fails, the straightforward approach is to revert to solving the electronic Schrödinger equation. However, in doing so, the dimensionality of the problem increases by an order of magnitude or more, and more expensive quantum-mechanical equations must be solved. This motivates the construction of models that are intermediate between fixed-charge classical molecular mechanics force fields and *ab initio* molecular dynamics. In that liminal space reside polarizable force fields [5–10] and (generalized) electronegativity equalization methods (EEMs) [11–22]. EEMs relax the requirement of fixed charges, allowing for charge transfer within, and between, molecules in response to their environment while nonetheless retaining an essentially classical description of the system. They are arguably the most straightforward, and rigorous, approach to coarse-graining the electronic Schrödinger equation to provide a classical potential energy surface for the atomic nuclei.

Density functional theory (DFT) plays a key role in the development of EEM [23–29]. The key quantities in EEM are atoms' charges (and possibly multipoles) that are determined by the balance between their electronic population and their nuclear charge. Atomic electronic population is defined by their (atomic) electron densities. Therefore, insofar as atomic charges/multipoles are coarse-grained models for molecular electronic densities, EEM energy models are course-grained DFT. Traditionally, such models were conceived using orbital-free DFT, but such models had inherent shortcomings related to the absence of a derivative discontinuity [30–34]. This motivated the development of a Kohn–Sham-based EEM, the atom-condensed Kohn–Sham (ACKS) model, where it is, for practical reasons, typically truncated at second order (ACKS2). The motivation for, and formulation of, the ACKS2 model is the topic of this chapter [15, 19, 35–38].

In Section 30.2, we motivate the use of EEM methods in general and ACKS2 in particular, followed by the pedagogical presentation of the ACKS2 framework. We conclude by listing some challenging systems that ACKS2, and other emerging force field methods, should be tested against.

## 30.2 Motivation: Where Do Current Approaches Fail

Before delving into the formulation of EEM in general, and ACKS2 in particular, it seems appropriate to mention the inherent difficulties faced by atomistic force fields in general [4, 35, 39] and traditional EEM in particular [35]. Of these difficulties, only the last (degenerate electronic ground states) is inherently beyond the scope of the ACKS approach.

### 30.2.1 Challenge: Molecular Polarizability and Hyperpolarizability

A traditional fixed-charge force field can model the vibrational contribution to the polarizability but cannot capture the electronic component of polarizability. To mimic the true (vibrational + electronic) polarizability with a fixed-charge force field, the values of the atomic charges and various electrostatic screening parameters must be adjusted to have “effective values,” but these adjustments are not very reliable, since the precise balance between electronic and vibrational polarization is highly system specific. Some atomic charges are typically amplified to mimic induction effects. For example, one might increase atomic charges on an electronegativity atom and a hydrogen atom to mimic the inductive polarization of a hydrogen bond, but these increased atomic charges will lead to unrealistic interactions when the associated moiety is not participating in a hydrogen bond.

The simplest strategy to treat polarization is to allow atomic dipoles (or even multipoles) to be induced on the atoms. This captures a component of the electronic polarization. However, if one partitions the electron density of a molecule in an external electric field, typically about half the polarization is associated with charge transfer between atoms. This is most notable in chemical bonds, where electrons tend to flow in opposition to the electric field, so that the atom with higher field (lower potential) tends to decrease in charge. To mimic this effect, classical fixed-charge polarizable force fields tend to have exaggerated atomic dipole polarizabilities, which compromise their ability to treat other types of interactions [10, 40, 41]. Attempting to model the polarizability tensor in molecules with highly directional polarization is especially challenging; treating long-range charge separation in chain-like molecules or metal clusters is inherently beyond the scope of local polarization models.

Traditional EEM models allow charge transfer between atoms but, as we shall discuss later, they typically exaggerate the polarizability [42]. Emerging machine-learned (ML) force fields have great potential, as they can (implicitly or explicitly) learn atomic charges. However, the models the author is aware of presume a level of locality that is inappropriate for externally imposed fields or for cases where the electric field on an atom is induced by charged atoms that are very

far away. It is also expected at ML-based force fields will, for larger molecules, suffer from some of the same overpolarization effects as traditional EEM models, as their (often implicit) underlying models for atomic energies/charges are smooth.

Modelling hyperpolarizabilities is even more difficult. In fact, accurately computing the hyperpolarizability is challenging even for many *ab initio* methods, because hyperpolarizability is exquisitely sensitive to the quality of the electron correlation model [43–46]. Likewise, phenomena that are superficially measurements of atoms' structure and motion but are sensitive to vibronic coupling (e.g. various types of Raman spectroscopy) are, and likely to remain, extremely challenging for all atomistic force field models [47].

### 30.2.2 Challenge: Charge and Spin States

Traditional molecular mechanics force fields determine the force on the atomic nuclei based only on the nuclear positions and therefore have no knowledge of molecular charge and spin states. Molecules must be parameterized separately for each charge/spin state of interest. This is not particularly problematic except for molecular processes (charge transfer, spin transfer) and reactions where electron transfer or spin-crossover occurs. As long as one presumes that the reaction occurs on the ground-state potential energy surface, reactive force fields, whether based on electronegativity equalization or models or machine learning, can (implicitly) address these changes. In practice, however, it is challenging to accurately model spin crossover from a singlet to a triplet carbene, or from a high-spin to a low-spin transition metal complex, with standard (single-reference) quantum chemistry methods, and it is expected that this will also be very challenging for atomistic force fields. It is even harder to describe systems where changes in charge/spin state are associated with wholesale rearrangements in molecular electronic structure [48–54].

### 30.2.3 Challenge: Molecular Dissociation and Long-Range Electron Transfer

Traditional classical force fields do not describe bond fracture and formation at all, but reactive force fields (and even some correlated electronic structure theory approaches [55–58]) also struggle because, in the absence of symmetry, isolated molecular fragments always have integer charge and spin. As a pernicious example, a force field must dissociate KCl into neutral atoms, but  $\text{NK}_4\text{Cl}$  to ions [59]. This is extremely challenging. Traditional EEM tends to dissociate molecules into fractionally charged species [15, 35, 37, 38, 60–65] because they do not address the inherent nonlocality of the electronic chemical potential [66]. Machine-learned (ML) force fields are typically incapable of including the effects of extremely distant reagents and thus cannot distinguish between two Cl centers, one of which is far away from K and the other of which is far away from  $\text{NK}_4$  [67–69]. The ACKS approach is capable of addressing this issue because it explicitly accounts for both the nonlocality of the electronic chemical potential (like all EEM) and the derivative



discontinuity (like Kohn–Sham DFT). Nonetheless, as currently formulated, ACKS2 only supports changes up to  $\pm 1$  electron.

### 30.2.4 Challenge: (Near) Degeneracy

In atomistic force fields, atoms' charges and multipoles are used to mimic the molecular electrostatic potential. However, the electron density, and consequently the electrostatic potential, is not uniquely defined for a degenerate ground state [70–72]. The response of the system to an external field is therefore nondifferentiable. A particular pernicious, yet important, example is nitric oxide, NO, where any fixed-charge force field will give errors of more than  $10 \text{ kJ mol}^{-1}$  for the differential interaction energy for positive and negatively charged ions [71]. For molecules with nearly degenerate ground states, the problem is mitigated in amplitude but not effect: very different parameterizations for the charges/multipoles and polarization parameters are needed, depending on the nature of the intermolecular interaction that is being considered [73]. As a practical example, consider the way a 1,3-dipolar compound can shift between zwitterionic and diradicaloid electronic structures depending on its molecular environment [74–77].

Fixed-charge and polarizable force fields are intrinsically incapable of describing such phenomena, as are straightforward EEM models. One can choose the parameters in a force field to provide a reliable lower bound on the interaction energy, but this bound is usually very loose [70]. ML models seem more promising here, but because the atomic properties change discontinuously with respect to the atomic environment, traditional ML force fields are unlikely to work well here also [68]. In addition, acquiring adequate training data is difficult since systems with (near) degeneracy are inherently multireference, and the reliability of standard protocols for constructing *ab initio* training data is doubtful. While ACKS2 is an inherently perturbative approach and is therefore incapable of describing (nearly) degenerate electronic ground states, the ACKS framework is exact in principle and could possibly be used to develop a practical approach for molecules with degenerate electronic states.

## 30.3 The Atom-Condensed Kohn–Sham Framework

### 30.3.1 Explicit Demonstration That Atomistic Force Fields Can Be Derived from DFT

In traditional DFT, the electron density is determined by the variational principle [78, 79]

$$\rho(\mathbf{r}) = \arg \min_{\substack{\rho(\mathbf{r}) \geq 0 \\ \int \rho(\mathbf{r}) d\mathbf{r} = N}} E_v[\rho] + V_{\text{nn}}[v] \quad (30.1)$$

where  $V_{\text{nn}}[v]$  denotes the self-repulsion of the external potential (normally just the nuclear–nuclear repulsion energy) [80],

$$V_{\text{nn}}[v] = \frac{1}{32\pi^2} \iint_{\mathbf{r} \neq \mathbf{r}'} \frac{\nabla_{\mathbf{r}}^2 v(\mathbf{r}) \nabla_{\mathbf{r}'}^2 v(\mathbf{r}')}{|\mathbf{r} - \mathbf{r}'|} d\mathbf{r} d\mathbf{r}' \quad (30.2)$$

and  $E_v[\rho]$  is the density functional for the electronic energy, which can be decomposed as [81]

$$E_v[\rho] = T_s[\rho] + E_{xc}[\rho] + J[\rho] + V_{ne}[\rho, v] \quad (30.3)$$

The expressions for the classical Coulomb repulsion between the density and the interaction of the electrons with the external potential (normally just the electron-nuclear attraction energy) are

$$J[\rho] = \iint \frac{\rho(\mathbf{r})\rho(\mathbf{r}')}{|\mathbf{r} - \mathbf{r}'|} d\mathbf{r}d\mathbf{r}' \quad (30.4)$$

and

$$V_{ne}[\rho, v] = \int \rho(\mathbf{r})v(\mathbf{r})d\mathbf{r} \quad (30.5)$$

respectively. Note that  $V_{nn}$ ,  $J$ , and  $V_{ne}$  are all electrostatic in nature. These terms, then, are especially amenable to an atomistic force field treatment, as they can be approximated by the interaction energy between the atomic charges/multipoles:

$$\begin{aligned} U_q &= J[\rho] + V_{ne}[\rho] + V_{nn}[v] \\ &\approx \sum_{A=1}^{N_{\text{atoms}}} \sum_{1 \leq B < A}^{N_{\text{atoms}}} \frac{q_A q_B}{|\mathbf{R}_A - \mathbf{R}_B|} + \frac{(q_A \mathbf{d}_B - q_B \mathbf{d}_A) \cdot (\mathbf{R}_A - \mathbf{R}_B)}{|\mathbf{R}_A - \mathbf{R}_B|^3} + \dots \end{aligned} \quad (30.6)$$

The Kohn–Sham kinetic energy,  $T_s$ , and the exchange–correlation energy,  $E_{xc}$ , do not have simple equations in terms of atomic charges and multipoles. However, their expressions can be formulated using constrained DFT [82–84]. Specifically, the Hohenberg–Kohn functional

$$F[\rho] = T_s[\rho] + E_{xc}[\rho] + J[\rho] \quad (30.7)$$

can be defined through the Levy constrained search [85, 86]

$$F[\rho] = \min_{\Psi \rightarrow \rho} \langle \Psi | \hat{T} + \hat{V}_{ee} | \Psi \rangle \quad (30.8)$$

Relaxing the constraint where the density is specified, and forcing only the atomic charges/multipoles to be specified, gives the Hohenberg–Kohn *function* of the atomic charges/multipoles:

$$F\left(\left\{m_A^{\ell,m}\right\}\right) = \min_{\Psi \rightarrow \left\{m_A^{\ell,m}\right\}} \langle \Psi | \hat{T} + \hat{V}_{ee} | \Psi \rangle \quad (30.9)$$

This, or an equivalent formulation in terms of the Legendre transform [35, 87–89], establishes that it is theoretically possible to define an atom-condensed force field, even for a near-degenerate or excited state [90–95], directly from quantum mechanics [96, 97]. To actually construct such a force field, however, we need to explicitly specify what we mean by an atom in a molecule (AIM) and how this changes during chemical processes [98–106].

### 30.3.2 Atoms in a Molecule (AIM)

The electron density of molecules and materials can be *condensed* into atomic contributions by choosing a set of atomic weights,  $\{w_A(\mathbf{r})\}$ . These weights must be nonnegative, and every point in space should be fully assigned to one (or more) atoms. The atomic weights are therefore a partition of unity [98, 99, 102]:

$$0 \leq w_A(\mathbf{r}) \quad (30.10)$$

$$1 = \sum_{A=1}^{N_{\text{atoms}}} w_A(\mathbf{r}) \quad (30.11)$$

The atomic electron densities are then defined as

$$\rho_A(\mathbf{r}) = w_A(\mathbf{r})\rho_{\text{total}}(\mathbf{r}) \quad (30.12)$$

For simplicity, the notation and nomenclature in this paper assumes that the coarse graining is performed at the atomic level. However, larger moieties (e.g. functional groups) can be treated without significant changes to the subsequent analysis. The atomic charge density is then

$$q_A(\mathbf{r}) = Z_A\delta(\mathbf{r} - \mathbf{R}_A) - \rho_A(\mathbf{r}) \quad (30.13)$$

and the atomic charges, dipoles, and higher-order multipoles can be computed directly therefrom. For example, the Cartesian multipoles are determined by integration:

$$m_A^{k_x, k_y, k_z} = \int (x - X_A)^{k_x} (y - Y_A)^{k_y} (z - Z_A)^{k_z} \rho_A(\mathbf{r}) d\mathbf{r} \quad (30.14)$$

The ACKS2 method is agnostic about the choice of partitioning. However, some partitioning methods perform much better than others. For example, it is desirable if the atomic densities are compact (with little long-range structure), nearly spherical (so that the multipole expansion of the charge density converges quickly), and insensitive to molecular conformation [102, 106, 107]. It is often convenient if the atomic weights do not change when the atomic charges/multipoles change [26, 108–110]. This suggests the use of a Hirshfeld partitioning [110–112]:

$$w_A(\mathbf{r}) = \frac{\rho_A^{(0)}(\mathbf{r})}{\sum_{B=1}^{N_{\text{atoms}}} \rho_B^{(0)}(\mathbf{r})} \quad (30.15)$$

where  $\rho_A^{(0)}(\mathbf{r})$  is the density of a reference pro-atom, which need not be neutral [113].

### 30.3.3 Energy Difference from Changes in Molecular Density

To model the potential energy surface with DFT, one needs to understand how a system's energy changes when its electron density changes. The electrostatic energy (Eq. (30.6)) is already easily expressed in terms of the nuclear positions and electron density, so the challenge is to expression how the kinetic exchange–correlation energy

$$E_{\text{txc}}[\rho] = T_s[\rho] + E_{\text{xc}}[\rho] \quad (30.16)$$

changes with respect to electron-density changes. Such changes can be modeled with the functional Taylor series [114, 115]

$$\begin{aligned} E_{\text{txc}} \left[ \rho_{\text{total}}^{(0)} + \Delta \rho_{\text{total}} \right] - E_{\text{txc}} \left[ \rho_{\text{total}}^{(0)} \right] \\ = \int \left[ \frac{\delta E_{\text{txc}}}{\delta \rho(\mathbf{r})} \right]_{\rho_{\text{total}}^{(0)}} \Delta \rho_{\text{total}}(\mathbf{r}) d\mathbf{r} \\ + \frac{1}{2} \iint \left[ \frac{\delta^2 E_{\text{txc}}}{\delta \rho(\mathbf{r}) \delta \rho(\mathbf{r}')} \right]_{\rho_{\text{total}}^{(0)}} \Delta \rho_{\text{total}}(\mathbf{r}) \Delta \rho_{\text{total}}(\mathbf{r}') d\mathbf{r} d\mathbf{r}' + \dots \quad (30.17) \end{aligned}$$

We have assumed the functional derivatives exist: that is not true in general, but it is true if  $E_{\text{txc}}$  is modeled using traditional orbital-free density functional approximations [87, 88, 116, 117].

### 30.3.4 The Electronegativity Equalization Method (EEM): Energy Difference from Changes in Atomic Densities

To decompose Eq. (30.17) as atomic contributions, we introduce a basis set for the density changes. Since we would like to have atomic contributions, and since we would like to be able to easily compose atomic contributions into multipoles, we choose a basis that is a product of atom-centered radial functions and spherical harmonic functions:

$$\sigma_A^{n,\ell,m}(\mathbf{r}) = \zeta_A^n(|\mathbf{r} - \mathbf{R}_A|) \times |\mathbf{r} - \mathbf{R}_A|^\ell Y_\ell^m(\theta, \phi) \quad (30.18)$$

While any (complete) basis can work [96, 118], one can argue that the most intuitive choice is to choose the spherically averaged atomic Fukui function, dual descriptor, and hyperdual descriptors for the radial functions [119–132]:

$$\zeta_A^n(r) = \left\langle f_A^{(n)}(\mathbf{r}) \right\rangle_{\text{spherical average}} \quad (30.19)$$

These descriptors describe how the atomic density changes when electrons are added/removed therefrom.

The change in molecular density can then be decomposed into atomic contributions:

$$\Delta \rho_{\text{total}}(\mathbf{r}) = \sum_{A=1}^{N_{\text{atoms}}} \sum_{n=1}^{n_{\text{max}}} \sum_{\ell=0}^{\ell_{\text{max}}} \sum_{m=-\ell}^{m=\ell} c_A^{n,\ell,m} \sigma_A^{n,\ell,m}(\mathbf{r}) \quad (30.20)$$

The change in energy can then be written as a Taylor series in the coefficients  $\{c_A^{n,\ell,m}\}$ , i.e. Eq. (30.17) can be rewritten as

$$\begin{aligned} \Delta E_{\text{txc}} \left( \{c_A^{n,\ell,m}\} \right) = \sum_{A,n,\ell,m} \left[ \frac{\partial E_{\text{txc}}}{\partial c_A^{n,\ell,m}} \right]_{c_A^{n,\ell,m}=0} c_A^{n,\ell,m} \\ + \frac{1}{2} \sum_{A,n,\ell,m} \sum_{A',n',\ell',m'} \left[ \frac{\partial^2 E_{\text{txc}}}{\partial c_A^{n,\ell,m} \partial c_{A'}^{n',\ell',m'}} \right]_{c_A^{n,\ell,m}=0} c_A^{n,\ell,m} c_{A'}^{n',\ell',m'} + \dots \quad (30.21) \end{aligned}$$

In the context of conceptual DFT [108, 115, 133–137], the coefficients in Eq. (30.21) are referred to as (atom-condensed) chemical potentials [138]

$$\mu_A^{n,\ell,m} = \left[ \frac{\partial E_{\text{txc}}}{\partial c_A^{n,\ell,m}} \right]_{c_A^{n,\ell,m}=0} \quad (30.22)$$

and the (atom-condensed) hardness kernel (or matrix) [139]

$$\eta_{A,A'}^{n,\ell,m;n',\ell',m'} = \left[ \frac{\partial^2 E_{\text{txc}}}{\partial c_A^{n,\ell,m} \partial c_{A'}^{n',\ell',m'}} \right]_{c_A^{n,\ell,m}=c_{A'}^{n',\ell',m'}=0} \quad (30.23)$$

The EEM results when the sum of the electrostatic (cf. Eq. (30.6)) and kinetic exchange–correlation (cf. Eq. (30.21)) energies is minimized with respect to the unknown atomic density change coefficients,  $\{c_A^{n,\ell,m}\}$ , subject to the constraint that the total number of electrons is preserved. If, for concreteness, we assume that a radial basis of (hyper)Fukui functions is used, then because the Fukui function is normalized to one, and the (hyper)dual descriptors are normalized to zero, the normalization constraint is that [129, 130, 140]

$$0 = \sum_{A=1}^{N_{\text{atoms}}} \sum_{n=1}^{n_{\text{max}}} c_A^{n,0,0} \quad (30.24)$$

The EEM method then amounts to the minimization

$$\Delta E_{\text{EEM}} = \min_{\left\{ c_A^{n,\ell,m} \mid 0 = \sum_{A,n} c_A^{n,0,0} \right\}} \Delta E_{\text{txc}} \left( \left\{ c_A^{n,\ell,m} \right\} \right) + U_q \left( \left\{ c_A^{n,\ell,m} \right\} \right) \quad (30.25)$$

The electrostatic energy expression is a quadratic functional of the density; if the Taylor series for  $\Delta E_{\text{txc}}$  is also truncated at second order, then the unknown atomic density change expansion coefficients,  $\{c_A^{n,\ell,m}\}$ , can be determined by a system of linear equations.

### 30.3.5 *Ab Initio* Parameterization of EEM

To parameterize EEM directly from *ab initio* data, one needs to construct an electrostatic model, and one needs to determine the derivatives in Eq. (30.21) from a density functional approximation. The electrostatic model is often approximated in terms of atomic charges and multipoles, which is quite easy if the basis in Eq. (30.18) is used. However, charge penetration effects can be modeled by explicitly evaluating the interatomic Coulomb attractions and repulsions:

$$V_A^{n,\ell,m} = \int \sigma_A^{n,\ell,m}(\mathbf{r}) v(\mathbf{r}) d\mathbf{r} \quad (30.26)$$

$$J_{A,A'}^{n,\ell,m;n',\ell',m'} = \iint \frac{\sigma_A^{n,\ell,m}(\mathbf{r}) \sigma_{A'}^{n',\ell',m'}(\mathbf{r}')}{|\mathbf{r} - \mathbf{r}'|} d\mathbf{r} d\mathbf{r}' \quad (30.27)$$

where, for economy of notation, the reference atomic density is assigned as the zeroth-order radial basis function

$$\sigma_A^{0,0,0}(\mathbf{r}) = \rho_A^{(0)}(\mathbf{r}) \quad (30.28)$$

The method for expanding functional derivatives in a basis is quite standard and can be easily adapted to the unknown partial derivatives in Eq. (30.21). Specifically, the atom-condensed chemical potentials,  $\mu_A^{n,\ell,m}$ , can be parameterized using the chain rule for functional derivatives:

$$\begin{aligned} \mu_A^{n,\ell,m} &= \left[ \frac{\partial E_{\text{txc}}}{\partial c_A^{n,\ell,m}} \right]_{c_A^{n,\ell,m}=0} = \int \left[ \frac{\delta E_{\text{txc}}}{\delta \rho(\mathbf{r})} \right]_{\rho_{\text{total}}^{(0)}} \left[ \frac{\partial \rho(\mathbf{r})}{\partial c_A^{n,\ell,m}} \right]_{c_A^{n,\ell,m}=0} d\mathbf{r} \\ &= \int \left[ \frac{\delta E_{\text{txc}}}{\delta \rho(\mathbf{r})} \right]_{\rho_{\text{total}}^{(0)}} \sigma_A^{n,\ell,m}(\mathbf{r}) d\mathbf{r} \end{aligned} \quad (30.29)$$

The strategy for parameterizing the atom-condensed hardness kernel is similar: one uses the chain rule to derive the equation

$$\eta_{A,A'}^{n,\ell,m,n',\ell',m'} = \iint \left[ \frac{\delta^2 E_{\text{txc}}}{\delta \rho(\mathbf{r}) \delta \rho(\mathbf{r}')} \right]_{\rho_{\text{total}}^{(0)}} \sigma_A^{n,\ell,m}(\mathbf{r}) \sigma_{A'}^{n',\ell',m'}(\mathbf{r}') d\mathbf{r} d\mathbf{r}' \quad (30.30)$$

Note that the same expressions for  $\mu_A^{n,\ell,m}$  and  $\eta_{A,A'}^{n,\ell,m,n',\ell',m'}$  are obtained by direct substitution of Eq. (30.18) into Eq. (30.21).

### 30.3.6 Kohn–Sham DFT: Fixing the Failures of Orbital-Free DFT and Traditional EEM

It is clear from Section 30.3.5 that EEM is merely a (re)parameterization of orbital-free DFT, and, as such, it is subject to the same caveats [141–144]. For example, traditional orbital-free density functional approximations suffer from extremely large delocalization errors because they do not have any derivative discontinuity. However, without a derivative discontinuity, it is always favorable to donate electrons from the fragment with higher chemical potential to the fragment with lower chemical potential, no matter how far the fragments are apart [66].

In Kohn–Sham DFT, the derivative discontinuity in the energy is regained by explicitly using a wavefunction — namely, the wavefunction of the Kohn–Sham reference system of noninteracting electrons — in the functional [145, 146]. In most (but not all) cases, Kohn–Sham DFT gives appropriate dissociation products [58]. The remaining failures of Kohn–Sham DFT, which mostly result from the tendency of electrons to delocalize to minimize the unphysical self-interaction error, are acceptable, at least insofar as an atomistic force field that could retain the accuracy of an underlying local and semilocal (gradient-corrected) exchange–correlation density functional would be acceptable.

### 30.3.7 Atom-Condensed Kohn–Sham DFT (ACKS-DFT)

In an atomistic force field, there is no concept of orbital, so direct construction of the Kohn–Sham energy expression is infeasible. Thus, instead of the atom-condensed constrained-search functional

$$T_s \left( \left\{ c_A^{n,\ell,m} \right\} \right) = \min_{\Psi \rightarrow \left\{ c_A^{n,\ell,m} \right\}} \langle \Psi | \hat{T} | \Psi \rangle \quad (30.31)$$

we use the Legendre transform technique [87]. The Legendre transform expression for the Kohn–Sham density functional is

$$T_s[\rho] = \sup_w E_s[w; N] - \int \rho(\mathbf{r})w(\mathbf{r})d\mathbf{r} \quad (30.32)$$

where  $E_s[w; N]$  is the energy of a system of  $N$  noninteracting fermions bound by the effective potential  $w(\mathbf{r})$ .

Inspired by the strategy for deriving an atom-condensed version of orbital-free DFT, we obtain an atom-condensed version of  $T_s[\rho]$  by using a Taylor series approximation to  $E_s[w; N]$ :

$$\begin{aligned} E_s[w; N] &= E_s[w^{(0)}; N] + \int \left[ \frac{\delta E_s}{\delta w(\mathbf{r})} \right]_{w^{(0)}(\mathbf{r}), N} \Delta w_s(\mathbf{r})d\mathbf{r} \\ &+ \frac{1}{2} \iint \left[ \frac{\delta^2 E_s}{\delta w(\mathbf{r})\delta w(\mathbf{r}')} \right]_{w^{(0)}(\mathbf{r}), N} \Delta w_s(\mathbf{r})\Delta w_s(\mathbf{r}')d\mathbf{r}d\mathbf{r}' \end{aligned} \quad (30.33)$$

Let us assume that we know the exact Kohn–Sham effective potential,  $w^{(0)}(\mathbf{r})$ , for a reference molecular density,  $\rho_{\text{total}}^{(0)}(\mathbf{r})$ . For this reference system, we have

$$T_s[\rho_{\text{total}}^{(0)}] = E_s[w^{(0)}; N] - \int \rho_{\text{total}}^{(0)}(\mathbf{r})w^{(0)}(\mathbf{r})d\mathbf{r} \quad (30.34)$$

The key functional derivatives are [147–151]

$$\left[ \frac{\delta E_s}{\delta w(\mathbf{r})} \right]_{w^{(0)}(\mathbf{r}), N} = \rho_{\text{total}}^{(0)}(\mathbf{r}) \quad (30.35)$$

and

$$\left[ \frac{\delta^2 E_s}{\delta w(\mathbf{r})\delta w(\mathbf{r}')} \right]_{w^{(0)}(\mathbf{r}), N} = \chi_s^{(0)}(\mathbf{r}, \mathbf{r}') \quad (30.36)$$

$\chi_s^{(0)}(\mathbf{r}, \mathbf{r}')$  is the Kohn–Sham linear response function, which is a standard quantity available in time-dependent DFT and conceptual DFT software [130, 152]. The Taylor series expansion, truncated at second order, is

$$\begin{aligned} T_s[\rho_{\text{total}}^{(0)} + \Delta\rho_{\text{total}}] - T_s[\rho_{\text{total}}^{(0)}] &= \sup_{\Delta w} \left[ \frac{1}{2} \iint \chi_s^{(0)}(\mathbf{r}, \mathbf{r}')\Delta w(\mathbf{r})\Delta w(\mathbf{r}')d\mathbf{r}d\mathbf{r}' \right. \\ &\quad \left. - \int \Delta\rho_{\text{total}}(\mathbf{r})(w^{(0)}(\mathbf{r}) + \Delta w(\mathbf{r}))d\mathbf{r} \right] \end{aligned} \quad (30.37)$$

To use this expression, we need to decompose both the density and the potential as a sum of atomic contributions. We (re)introduce the basis set for the density

$$\rho_{\text{total}}(\mathbf{r}) = \rho_{\text{total}}^{(0)}(\mathbf{r}) + \sum_{A=1}^{N_{\text{atoms}}} \sum_{n=1}^{n_{\text{max}}} \sum_{\ell=0}^{\ell_{\text{max}}} \sum_{m=-\ell}^{m=\ell} c_A^{n,\ell,m} \sigma_A^{n,\ell,m}(\mathbf{r}) \quad (30.38)$$

and define a basis set for the potential

$$w(\mathbf{r}) = w^{(0)}(\mathbf{r}) + \sum_{A=1}^{N_{\text{atoms}}} \sum_{n=1}^{n_{\text{max}}} \sum_{\ell=0}^{\ell_{\text{max}}} \sum_{m=-\ell}^{m=\ell} w_A^{n,\ell,m} v_A^{n,\ell,m}(\mathbf{r}) \quad (30.39)$$

Constructing a good basis set for a potential can be rather tricky; one strategy is to choose the potential basis functions,  $\{v_A^{n,\ell,m}(\mathbf{r})\}$ , to be identical to the density

basis functions. A somewhat more rigorous approach is to define the potential basis functions as dual to the density basis functions. For example, if a Coulomb kernel were used, then [153–158]

$$v_A^{n,\ell,m}(\mathbf{r}) = \int \frac{\sigma_A^{n,\ell,m}(\mathbf{r}')}{|\mathbf{r} - \mathbf{r}'|} d\mathbf{r}' \quad (30.40)$$

Note that the number of density and potential basis functions need not be identical, though it is traditional to keep the sets balanced.

The change in kinetic energy is then

$$\begin{aligned} \Delta T_s \left[ \left\{ c_A^{n,\ell,m} \right\} \right] &= \sum_{A,n,\ell,m} \mu_{s:A}^{n,\ell,m} c_A^{n,\ell,m} + \max_{\left\{ w_A^{n,\ell,m} \right\}_{A,A',n,n',\ell,\ell',m,m'}} \sum \\ &\times \left( \frac{1}{2} w_A^{n,\ell,m} w_{A'}^{n',\ell',m'} \chi_{s:A,A'}^{n,n',\ell,\ell',m,m'} - c_A^{n,\ell,m} w_{A'}^{n',\ell',m'} S_{A,A'}^{n,n',\ell,\ell',m,m'} \right) \end{aligned} \quad (30.41)$$

where the supremum has been replaced by a maximum and the following terms have been defined:

$$\mu_{s:A}^{n,\ell,m} = - \int \sigma_A^{n,\ell,m}(\mathbf{r}) w^{(0)}(\mathbf{r}) d\mathbf{r} \quad (30.42)$$

$$\chi_{s:A,A'}^{n,n',\ell,\ell',m,m'} = \iint v_A^{n,\ell,m}(\mathbf{r}) \chi_s^{(0)}(\mathbf{r}, \mathbf{r}') v_{A'}^{n',\ell',m'}(\mathbf{r}') d\mathbf{r} d\mathbf{r}'$$

$$S_{A,A'}^{n,n',\ell,\ell',m,m'} = \int \sigma_A^{n,\ell,m}(\mathbf{r}) v_{A'}^{n',\ell',m'}(\mathbf{r}) d\mathbf{r} \quad (30.43)$$

The final expression for the EEM is obtained by substituting Eq. (30.41) into Eq. (30.25), obtaining a quadratic objective function to optimize and, therefore, a linear system of equations to solve. These final equations will be summarized in Section 30.4.

## 30.4 Recapitulation

The atom-condensed Kohn–Sham (second-order) (ACKS2) strategy for discretizing the Kohn–Sham equations relies on only three approximations:

- *An approximate exchange–correlation functional without a derivative discontinuity is used.* This means that the ACKS model will fail where semilocal density functional approximations fail. To remedy this assumption, one would need to either:
  - Develop a practical Legendre transform strategy for generalized Kohn–Sham methods. Then, one could use any modern density functional approximation, including hybrid functionals, range-separated hybrid functionals, double-hybrid functionals, and various random phase approximation approaches to parameterize the model.
  - Use the Legendre transform for the Hohenberg–Kohn functional. The resulting method would appear similar to this one, but one would need to evaluate interacting linear response functional.



- An limited basis of atom-centered density/potential functions is used. In practice, this assumption can be relaxed by increasing the basis. However, as the basis increases, the cost of the method increases, and the transferability of the parameters decreases.
- The Taylor series expansions of the exchange–correlation energy functional and the Kohn–Sham noninteracting energy functional are truncated at second order. This assumption is helpful because it leads to a linear system of equations to solve for the unknown parameters. However, the resulting equations need not always have a solution. Computing the higher-order Kohn–Sham responses is expensive, so the cost of parameterization also increases. The other case where the Taylor series approximation fails is when the Kohn–Sham system has a (nearly) degenerate ground state. The mathematical treatment necessary to resolve such cases is known [70], but the Taylor series coefficients would then depend on the perturbation, which is an unpleasant (and computationally demanding) complication.

After these three assumptions are made, one needs to evaluate the following quantities:

$$N_k = \int \sigma_k(\mathbf{r}) d\mathbf{r} \quad (30.44)$$

$$V_k = \int \sigma_k(\mathbf{r}) v(\mathbf{r}) d\mathbf{r} \quad (30.45)$$

$$J_{kl} = \iint \frac{\sigma_k(\mathbf{r}) \sigma_l(\mathbf{r}')}{|\mathbf{r} - \mathbf{r}'|} d\mathbf{r} d\mathbf{r}' \quad (30.46)$$

$$\mu_k = \int \sigma_k(\mathbf{r}) \left( v_{\text{xc}}^{(0)}(\mathbf{r}) - w^{(0)}(\mathbf{r}) \right) d\mathbf{r} \quad (30.47)$$

$$\chi_{s;kl} = \iint v_k(\mathbf{r}) \chi_s^{(0)}(\mathbf{r}, \mathbf{r}') v_l(\mathbf{r}') d\mathbf{r} d\mathbf{r}' \quad (30.48)$$

$$E_{\text{xc};kl} = \iint \sigma_k(\mathbf{r}) f_{\text{xc}}^{(0)}(\mathbf{r}, \mathbf{r}') \sigma_l(\mathbf{r}') d\mathbf{r} d\mathbf{r}' \quad (30.49)$$

$$S_{kl} = \int \sigma_k(\mathbf{r}) v_l(\mathbf{r}) d\mathbf{r} \quad (30.50)$$

where  $\sigma_k(\mathbf{r})$  and  $v_l(\mathbf{r})$  denote the (atomic) density and potential basis sets, respectively. (Specific useful choices for these basis sets are recommended in Eqs. (30.18) and (30.40).)  $v(\mathbf{r})$  denotes the external potential, which specifies the molecular geometry. The reference system about which the Taylor series is expanded has electron density  $\rho_{\text{total}}^{(0)}(\mathbf{r})$ , exchange–correlation potential  $v_{\text{xc}}^{(0)}(\mathbf{r})$ , exchange–correlation kernel  $f_{\text{xc}}^{(0)}(\mathbf{r}, \mathbf{r}')$ , Kohn–Sham potential  $w^{(0)}(\mathbf{r})$ , and noninteracting (Kohn–Sham) linear response  $\chi_s^{(0)}(\mathbf{r}, \mathbf{r}')$ . Note that  $J + V + V_{\text{nn}}$  is just the classical electrostatic energy associated with the external potential  $v(\mathbf{r})$  and the electron density

$$\rho_{\text{total}}(\mathbf{r}) = \rho_{\text{total}}^{(0)}(\mathbf{r}) + \sum_k c_k \sigma_k(\mathbf{r}) \quad (30.51)$$

This leads to an energy functional that must be minimized with respect to the coefficients of the atomic density basis set and maximized with respect to the coefficients

of the atomic potential basis set [35, 96]:

$$\Delta E_{\text{EEM}} = \min_{\left\{c_k \mid 0 = \sum_k c_k N_k\right\}} \max_{\{w_k\}} \Delta E_{\text{xc}}(\{c_k\}) + U_q(\{c_k\}) + \Delta T_s(\{c_k\}, \{w_k\}) \quad (30.52)$$

Depending on the potential basis set, it may also be necessary to constrain the  $\{w_k\}$ , so shifts of the potential by a constant (i.e. arbitrary changes in the zero of energy) are not allowed; this is not necessary, however, if all the potential basis functions decay to zero asymptotically. The objective function can be re-expressed using the precomputed integrals defined above:

$$\begin{aligned} \Delta E_{\text{xc}}(\{c_k\}) + U_q(\{c_k\}) + \Delta T_s(\{c_k\}, \{w_k\}) \\ = V_{\text{nn}}[v] + \sum_k c_k (\mu_k + V_k) + \frac{1}{2} \sum_{k,l} c_k c_l (J_{kl} + E_{\text{xc};kl}) \\ - \sum_{k,l} c_k w_l S_{kl} + \frac{1}{2} \sum_{k,l} w_k w_l \chi_{s;kl} \end{aligned} \quad (30.53)$$

where  $V_{\text{nn}}[v]$  denotes the nuclear–nuclear repulsion energy contribution to the electrostatic energy  $U_q$ . There would always a unique energy if the exact exchange–correlation were used (because the exact density functional is nonconcave, while the exact potential functional is nonconvex) [87, 159, 160]. However, while the (approximate) Kohn–Sham response is still concave, the approximate density functional may not be convex. A unique solution, which equals the variational solution when the density functional is convex, can be found by solving the linear system of equations:

$$\begin{aligned} \mu_k + V_k &= -\sum_l J_{kl} c_l - \sum_n S_{kn} w_n + \mu_{\text{mol}} \\ 0 &= \sum_l S_{lm} c_l - \sum_n \chi_{s;mn} w_n \\ 0 &= \sum_l N_l c_l \end{aligned} \quad (30.54)$$

where  $k$  and  $l$  are the density basis functions,  $m$  and  $n$  are the potential basis functions, and  $\mu_{\text{mol}}$  is the electronic chemical potential of the molecule, which appears as the Lagrange multiplier for the normalization constraint on the total density.

## 30.5 Challenges

### 30.5.1 Parameterization of the ACKS2 Model

The ACKS approach and its quadratic approximation (ACKS2) can resolve many of the difficulties that thwarted previous electronegativity equalization approaches and provide a strong basis for further work [35]. Arguably the greatest strength of the ACKS2 model is that it can be directly parameterized from *ab initio* calculations [96]. This, however, is also its greatest weakness. The traditional charge/multipole

and bond terms in ACKS2 are readily transferable and do not change much between conformers, or even when sufficiently large fragments/monomers combine to form large structures. The ACKS polarizability is not so transferable: it is conformationally dependent. In addition, the atom-condensed polarizability is inherently a two-site nonlocal quantity. As yet, there is no robust method to construct the atom-condensed polarizability of a macromolecule from its fragments, though methods based on (approximate) decomposition of the linear response kernel are promising [161, 162].

### 30.5.2 Tests for Atomistic Force-Field Models

While the shortcomings of the ACKS2 model, and atomistic force-field approaches in general, can always be resolved by resorting to accurate molecular quantum mechanics methods, coarse-grained atom-condensed quantum mechanics is many times more computationally efficient and allows much longer length scales to be probed and much larger molecules to be simulated. With this in mind, a few salient difficulties and associated computational tests are listed here.

Whether one uses traditional explicitly parameterized molecular mechanics force fields or the emerging machine-learned models, modeling chemical reactions is still extremely difficult. Even if reasonable models for bond dissociation energies were accessible, models for molecular dissociation products are extremely challenging. Two generic tests that should be employed are as follows:

- Diatomic molecules always dissociate into neutral atoms. In most cases, this means the potential energy curve's asymptotic decay is  $\approx -R^{-6}$ , though this is different when both atoms have permanent quadrupole moments (i.e. total angular momentum  $L = 1$ ). For example, the asymptotic decay of the fluorine dimer is  $\approx -R^{-5}$  [163].
- Molecules always dissociate into fragments with integer charge, and the choice of charge depends relative ionization potentials and electron affinities of the fragments. Therefore, KCl dissociates into neutral atoms (and the potential energy curve's asymptotic decay is  $\approx -R^{-6}$ ), but  $\text{NK}_4\text{Cl}$  dissociates into ions, and the potential energy curve's asymptotic decay is  $\sim -R^{-1}$  [59].

ACKS2 was created to solve the molecular dissociation problem and can describe both neutral-fragment and ionic-fragment dissociation. Unfortunately, because the Taylor series expansion of the Kohn–Sham energy functional converges only up to  $\pm 1$  electron, one can only consider ionic fragments that differ by  $\pm 1$  from the reference state that was used in the parameterization [115, 145].

Faced with these difficulties, one might reasonably decide to focus on nonreactive force fields, in which the identity and connectivity of atoms are unchanged. However, due to the (near) degeneracy, the electrostatic potential of a molecule can change dramatically depending on its environment. Some tests (with increasing levels of difficulty) are as follows:

- Nitric oxide (NO). The ground state has an exact spatial degeneracy [71].
- 1,3-Butadiene radical cation. The ground state is degenerate for the symmetric structure and nearly degenerate otherwise [71].

- Molecules where zwitterionic and diradical structures are nearly degenerate. (These molecules are also very challenging for machine-learned atomic charges, because small changes in molecular environment/composition can lead to vast changes in molecular dipole moment.) A few special cases include the following:
  - A small set of tetramethylenes and trimethylenes near the zwitterionic/diradical threshold was compiled by Jug and Kölle. One very special case is 1-methoxy-4,4-dicyanotetramethylene, whose dipole moment changes from 2.7 Debye (diradical) in the gas phase to 24.8 Debye (zwitterion) in water [164].
  - Organic ring compounds, especially carbazole-based diradicals, also show strong competition between diradical and zwitterionic states [165, 166].
  - Other fused-ring heteroaromatic compounds show similar effects [167]. For example, tetraphenylhexaazaanthracene is primarily zwitterionic, tetraphenylhexaazapentacene has predominately singlet diradical character, and tetraphenylhexaazaoctacene has a triplet diradical ground state [168].

In general, ACKS2 will struggle to describe near degeneracy because the Taylor series expansion of the ACKS kinetic energy is unreliable in such cases.

At this stage, one might reasonably decide to dramatically lower one's expectations of a force-field method and focus on molecules with relatively rigid electronic structure. (Exactly how to quantify this is an open question, but closed-shell molecules with single Lewis structures are usually safe. Some simple aromatic systems could also be treated.) The next main difficulty is the description of molecular response to external fields. Such effects are important also for describing how molecules' charges adapt in the presence of solvent, especially if the solvent has high ionic strength. Describing the (hyper)polarizability of molecules is therefore critical. A couple simple, but challenging, cases include the following [169, 170]:

- **Polyynes:** Polyynes have high (hyper)polarizability. Describing the linear growth of polarizability with chain length is a challenge for traditional EEM methods and even some *ab initio* electronic structure theory approaches [44].
- **Cumulenes:** Cumulenes are superficially similar to polyynes, but electrons are less delocalized. In addition, odd and even cumulenes behave in qualitatively different ways. Describing the difference in (hyper)polarizability of odd/even cumulenes and polyynes is likely to be quite challenging, even though both families of molecules possess only a single dominant resonant structure.

In general, ACKS2 is able to describe molecular polarization as well as the underlying Kohn–Sham method used in the parameterization. (This indicates that a range-separated Kohn–Sham DFT method is to be preferred in the parameterization phase [171].) However, because the Taylor expansion of the ACKS energy function is truncated at second order, molecular hyperpolarizabilities are expected to be far too small.

In summary, the ACKS approach overcomes many of the difficulties of traditional fixed-charge and polarizable force fields and also some of the problems that are likely to plague machine-learned force-field models. However, ACKS2 should not be used to describe molecular hyperpolarizabilities or molecules with nearly

degenerate ground states. Such molecules and molecular properties, however, are already difficult to describe by single-reference quantum chemistry methods (like Kohn–Sham DFT), so these limitations are not unexpected, nor should they be considered unduly discouraging.

## Acknowledgments

I wish to thank Toon Verstraelen, the co-creator of ACKS2, for his longstanding collaborative friendship and the insights it has led to. In addition, I wish to thank Farnaz Heidar-Zadeh for the penetrating comments/discussions about the strengths/weaknesses of machine-learned atomistic force fields. Financial support and computational resources from NSERC and Compute Canada are gratefully acknowledged.

## References

- 1 Frenkel, D. and Smit, B. (1996). *Understanding Molecular Simulation: From Algorithms to Applications*. Academic Press.
- 2 Schlick, T. (2002). *Molecular Modeling and Simulation: An Interdisciplinary Guide*. Springer.
- 3 Wales, D.J. (2003). *Energy Landscapes, Cambridge Molecular Science*. Cambridge University Press. ISBN 0-521-81415-4.
- 4 Berendsen, H.J.C. (2007). *Simulating the Physical World: Hierarchical Modeling from Quantum Mechanics to Fluid Dynamics*. Cambridge University Press. ISBN 9780521835275. <https://doi.org/10.1017/CBO9780511815348>. <https://www.cambridge.org/core/books/simulating-the-physical-world/DEF7E50D46450E57053A5B1236E7A4EC>.
- 5 Li, H., Chowdhary, J., Huang, L. et al. (2017). Drude polarizable force field for molecular dynamics simulations of saturated and unsaturated zwitterionic lipids. *J. Chem. Theory Comput.* 13 (9): 4535–4552. <https://doi.org/10.1021/acs.jctc.7b00262>.
- 6 Piquemal, J.-P. and Cisneros, G.A. (2016). Status of the Gaussian electrostatic model, a density-based polarizable force field, pp. 269–299. <https://doi.org/10.1201/b21343-11>.
- 7 Warshel, A., Kato, M., and Pisliakov, A.V. (2007). Polarizable force fields: history, test cases, and prospects. *J. Chem. Theory Comput.* 3 (6): 2034–2045. <https://doi.org/10.1021/ct700127w>.
- 8 Lamoureux, G. and Roux, B. (2003). Modeling induced polarization with classical Drude oscillators: theory and molecular dynamics simulation algorithm. *J. Chem. Phys.* 119 (6): 3025–3039. <https://doi.org/10.1063/1.1589749>.
- 9 Baker, C.M. (2015). Polarizable force fields for molecular dynamics simulations of biomolecules. *WIREs Comput. Mol. Sci.* 5 (2): 241–254. <https://doi.org/10.1002/wcms.1215>.

- 10 Jing, Z., Liu, C., Cheng, S.Y. et al. (2019). Polarizable force fields for biomolecular simulations: recent advances and applications. *Annu. Rev. Biophys.* 48 (1): 371–394. <https://doi.org/10.1146/annurev-biophys-070317-033349>.
- 11 Islam, Md.M., Kolesov, G., Verstraelen, T. et al. (2016). eReaxFF: a pseudo-classical treatment of explicit electrons within reactive force field simulations. *J. Chem. Theory Comput.* 12 (WOS:000381320200006): 3463–3472. <https://doi.org/10.1021/acs.jctc.6b00432>.
- 12 Senftle, T.P., Hong, S., Islam, Md.M. et al. (2016). The ReaxFF reactive force-field: development, applications and future directions. *NPJ Comput. Mater.* 2 (WOS:000426821500004). <https://doi.org/10.1038/npjcompumats.2015.11>.
- 13 Leven, I. and Head-Gordon, T. (2019). C-GeM: Coarse-grained electron model for predicting the electrostatic potential in molecules. *J. Phys. Chem. Lett.* 10 (WOS:000495805100055): 6820–6826. <https://doi.org/10.1021/acs.jpcllett.9b02771>.
- 14 Guan, X., Leven, I., Heidar-Zadeh, F., and Head-Gordon, T. (2021). Protein C-GeM: a coarse-grained electron model for fast and accurate protein electrostatics prediction. *J. Chem. Inf. Model.* 61 (9): 4357–4369. <https://doi.org/10.1021/acs.jcim.1c00388>.
- 15 Valone, S.M. and Atlas, S.R. (2004). An empirical charge transfer potential with correct dissociation limits. *J. Chem. Phys.* 120 (16): 7262–7273.
- 16 Chelli, R., Procacci, P., Righini, R., and Califano, S. (1999). Electrical response in chemical potential equalization schemes. *J. Chem. Phys.* 111 (18): 8569–8575. <https://doi.org/10.1063/1.480198>.
- 17 Rappe, A.K. and Goddard, W.A. (1991). Charge equilibration for molecular-dynamics simulations. *J. Phys. Chem.* 95 (8): 3358–3363.
- 18 Nistor, R.A. and Muser, M.H. (2009). Dielectric properties of solids in the regular and split-charge equilibration formalisms. *Phys. Rev. B* 79: 104303. <https://doi.org/10.1103/PhysRevB.79.104303>.
- 19 Nistor, R.A., Polihronov, J.G., Muser, M.H., and Mosey, N.J. (2006). A generalization of the charge equilibration method for nonmetallic materials. *J. Chem. Phys.* 125: 094108. <https://doi.org/10.1063/1.2346671>.
- 20 Rick, S.W., Stuart, S.J., and Berne, B.J. (1994). Dynamical fluctuating charge force fields: application to liquid water. *J. Chem. Phys.* 101 (7): 6141–6156. <https://doi.org/10.1063/1.468398>.
- 21 Zhong, Y. and Patel, S. (2010). Nonadditive empirical force fields for short-chain linear alcohols: methanol to butanol. Hydration free energetics and Kirkwood–Buff analysis using charge equilibration models. *J. Phys. Chem. B* 114 (34): 11076–11092. <https://doi.org/10.1021/jp101597r>.
- 22 York, D.M. and Yang, W.T. (1996). A chemical potential equalization method for molecular simulations. *J. Chem. Phys.* 104: 159–172.
- 23 Mortier, W.J., Vangenechten, K., and Gasteiger, J. (1985). Electronegativity equalization: application and parameterization. *J. Am. Chem. Soc.* 107: 829–835.
- 24 Mortier, W.J., Ghosh, S.K., and Shankar, S. (1986). Electronegativity equalization method for the calculation of atomic charges in molecules. *J. Am. Chem. Soc.* 108: 4315–4320.

- 25 Mortier, W.J. (1987). Electronegativity equalization and its applications. *Struct. Bond.* 66: 125–143.
- 26 Yang, W.T. and Mortier, W.J. (1986). The use of global and local molecular parameters for the analysis of the gas-phase basicity of amines. *J. Am. Chem. Soc.* 108: 5708–5711.
- 27 Itskowitz, P. and Berkowitz, M.L. (1997). Chemical potential equalization principle: direct approach from density functional theory. *J. Phys. Chem. A* 101: 5687–5691.
- 28 Itskowitz, P. and Berkowitz, M.L. (1998). Molecular polarizability and atomic properties: density functional approach. *J. Chem. Phys.* 109: 10142–10147.
- 29 Itskowitz, P. and Berkowitz, M.L. (1998). Molecular and atomic dipole moments in heteronuclear and homonuclear diatomics. Density functional approach. *J. Phys. Chem. A* 102: 4808–4812.
- 30 Perdew, J.P., Parr, R.G., Levy, M., and Balduz, J.L. (1982). Density-functional theory for fractional particle number: derivative discontinuities of the energy. *Phys. Rev. Lett.* 49: 1691–1694. <https://doi.org/10.1103/PhysRevLett.49.1691>.
- 31 Yang, W.T., Zhang, Y.K., and Ayers, P.W. (2000). Degenerate ground states and fractional number of electrons in density and reduced density matrix functional theory. *Phys. Rev. Lett.* 84: 5172–5175. <https://doi.org/10.1103/PhysRevLett.84.5172>.
- 32 Ayers, P.W. (2008). The dependence on and continuity of the energy and other molecular properties with respect to the number of electrons. *J. Math. Chem.* 43 (1): 285–303. <https://doi.org/10.1007/s10910-006-9195-5>.
- 33 Yang, X.D., Patel, A.H.G., Miranda-Quintana, R.A. et al. (2016). Communication: two types of flat-planes conditions in density functional theory. *J. Chem. Phys.* 145 (3): 4. <https://doi.org/10.1063/1.4958636>.
- 34 Cohen, A.J., Mori-Sanchez, P., and Yang, W.T. (2008). Insights into current limitations of density functional theory. *Science* 321: 792–794. <https://doi.org/10.1126/science.1158722>.
- 35 Verstraelen, T., Ayers, P.W., Van Speybroeck, V., and Waroquier, M. (2013). ACKS2: Atom-condensed Kohn–Sham DFT approximated to second order. *J. Chem. Phys.* 138 (7). <https://doi.org/10.1063/1.4791569>.
- 36 Verstraelen, T., Bultinck, P., Van Speybroeck, V. et al. (2011). The significance of parameters in charge equilibration models. *J. Chem. Theory Comput.* 7: 1750–1764. <https://doi.org/10.1021/ct200006e>.
- 37 Cioslowski, J. and Stefanov, B.B. (1993). Electron flow and electronegativity equalization in the process of bond formation. *J. Chem. Phys.* 99: 5151–5162.
- 38 Chen, J. and Martinez, T.J. (2009). Charge conservation in electronegativity equalization and its implications for the electrostatic properties of fluctuating-charge models. *J. Chem. Phys.* 131 (4): 044114. <https://doi.org/10.1063/1.3183167>.
- 39 Ayers, P.W. (2005). Some problems related to electronegativity equalization. In: *Advances in Computational Methods in Sciences and Engineering 2005, Lecture Series on Computer and Computational Sciences*, vol. 4A-4B (ed. T. Simos

- and G. Maroulis), Boca Raton: CRC Press. 1175–1177. ISBN 1573-419690-6764-443-9.
- 40 Lemkul, J.A., Huang, J., Roux, B., and MacKerell, A.D. Jr. (2016). An empirical polarizable force field based on the classical Drude oscillator model: development history and recent applications. *Chem. Rev.* 116 (9, SI): 4983–5013. <https://doi.org/10.1021/acs.chemrev.5b00505>.
- 41 Cisneros, G.A., Karttunen, M., Ren, P., and Sagui, C. (2014). Classical electrostatics for biomolecular simulations. *Chem. Rev.* 114 (1): 779–814. <https://doi.org/10.1021/cr300461d>.
- 42 Verstraelen, T., Van Speybroeck, V., and Waroquier, M. (2009). The electronegativity equalization method and the split charge equilibration applied to organic systems: parametrization, validation, and comparison. *J. Chem. Phys.* 131: 044127. <https://doi.org/10.1063/1.3187034>.
- 43 Helgaker, T., Coriani, S., Jorgensen, P. et al. (2012). Recent advances in wave function-based methods of molecular-property calculations. *Chem. Rev.* 112 (1): 543–631. <https://doi.org/10.1021/cr2002239>.
- 44 Wouters, S., Limacher, P.A., Van Neck, D., and Ayers, P.W. (2012). Longitudinal static optical properties of hydrogen chains: finite field extrapolations of matrix product state calculations. *J. Chem. Phys.* 136: 134110. and <https://doi.org/10.1063/1.3700087>.
- 45 Mohammed, A.A.K., Limacher, P.A., and Champagne, B. (2013). Finding optimal finite field strengths allowing for a maximum of precision in the calculation of polarizabilities and hyperpolarizabilities. *J. Comput. Chem.* 34 (17): 1497–1507. <https://doi.org/10.1002/jcc.23285>.
- 46 Patel, A.H.G., Mohammed, A.A.K., Limacher, P.A., and Ayers, P.W. (2017). Finite field method for nonlinear optical property prediction using rational function approximants. *J. Phys. Chem. A* 121 (28): 5313–5323. <https://doi.org/10.1021/acs.jpca.7b04049>.
- 47 Verstraelen, T. and Bultinck, P. (2015). Can the electronegativity equalization method predict spectroscopic properties? *Spectrochim. Acta, Part A* 136: 76–80. <https://doi.org/10.1016/j.saa.2013.10.124>. Special Issue on Spectroscopy.
- 48 Ayers, P.W. (2006). Can one oxidize an atom by reducing the molecule that contains it? *Phys. Chem. Chem. Phys.* 8: 3387–3390.
- 49 Min, K.S., DiPasquale, A.G., Rheingold, A.L. et al. (2009). Observation of redox-induced electron transfer and spin crossover for dinuclear cobalt and iron complexes with the 2,5-di-tert-butyl-3,6-dihydroxy-1,4-benzoquinonate bridging ligand. *J. Am. Chem. Soc.* 131: 6229–6236. <https://doi.org/10.1021/ja900909u>.
- 50 Echegaray, E., Toro-Labbe, A., Dikmenli, K. et al. (2017). Negative condensed-to-atom Fukui functions: a signature of oxidation-induced reduction of functional groups. In: *Correlations in Condensed Matter under Extreme Conditions: A tribute to Renato Pucci on the Occasion of his 70th Birthday* (ed. A. La Magna and G.G.N. Angilello), 269–278. Springer International Publishing. ISBN 978-3-319-53664-4.



- 51 Echegaray, E., Cardenas, C., Rabi, S. et al. (2013). In pursuit of negative Fukui functions: examples where the highest occupied molecular orbital fails to dominate the chemical reactivity. *J. Mol. Model.* 19 (7): 2779–2783. <https://doi.org/10.1007/s00894-012-1637-3>.
- 52 Echegaray, E., Rabi, S., Cardenas, C. et al. (2014). In pursuit of negative Fukui functions: molecules with very small band gaps. *J. Mol. Model.* 20: 2162. <https://doi.org/10.1007/s00894-014-2162-3>.
- 53 Bartolotti, L.J. and Ayers, P.W. (2005). An example where orbital relaxation is an important contribution to the fukui function. *J. Phys. Chem. A* 109 (6): 1146–1151. <https://doi.org/10.1021/jp0462207>.
- 54 Kaim, W. (2012). The shrinking world of innocent ligands: conventional and non-conventional redox-active ligands. *Eur. J. Inorg. Chem.* (3): 343–348. <https://doi.org/10.1002/ejic.201101359>.
- 55 Van Aggelen, H., Bultinck, P., Verstichel, B. et al. (2009). Incorrect diatomic dissociation in variational reduced density matrix theory arises from the flawed description of fractionally charged atoms. *Phys. Chem. Chem. Phys.* 11: 5558–5560. <https://doi.org/10.1039/b907624g>.
- 56 Verstichel, B., van Aggelen, H., Van Neck, D. et al. (2010). Subsystem constraints in variational second order density matrix optimization: curing the dissociative behavior. *J. Chem. Phys.* 132: 114113. <https://doi.org/10.1063/1.3354911>.
- 57 van Aggelen, H., Verstichel, B., Bultinck, P. et al. (2011). Variational second order density matrix study of F-3(-): importance of subspace constraints for size-consistency. *Journal of Chemical Physics* 134: 054115. <https://doi.org/10.1063/1.3532409>.
- 58 Ruzsinszky, A., Perdew, J.P., Csonka, G.I. et al. (2006). Spurious fractional charge on dissociated atoms: pervasive and resilient self-interaction error of common density functionals. *J. Chem. Phys.* 125: 194112. <https://doi.org/10.1063/1.2387954>.
- 59 Zhang, Z. and Chen, H. (2019). Superalkali  $NM_4$  ( $M=Li, Na, K$ ): stabilities and electronic structures. *Phys. Lett. A* 383 (33): 125952. <https://doi.org/10.1016/j.physleta.2019.125952>.
- 60 Valone, S.M. and Atlas, S.R. (2006). Electron correlation, reference states and empirical potentials. *Philos. Mag.* 86 (17): 2683–2711.
- 61 Valone, S.M., Li, J.B., and Jindal, S. (2008). Quantum-based models of charge-dependent potential energy surfaces: three-state models. *Int. J. Quantum Chem.* 108: 1452–1464. <https://doi.org/10.1002/qua.21659>.
- 62 Valone, S.M. (2011). A concept of fragment hardness, independent of net charge, from a wave-function perspective. *J. Phys. Chem. Lett.* 2: 2618–2622. <https://doi.org/10.1021/jz200968a>.
- 63 Valone, S.M. (2011). Quantum mechanical origins of the Iczkowski–Margrave model of chemical potential. *J. Chem. Theory Comput.* 7: 2253–2261. <https://doi.org/10.1021/ct200283y>.
- 64 Li, H., Xu, B., Jin, H. et al. (2021). Two improved electronegativity equalization methods for charge distribution in large scale non-uniform

- system. *Comput. Math. Appl.* 81 (WOS:000600778500036): 693–701. <https://doi.org/10.1016/j.camwa.2019.12.017>.
- 65 Leven, I., Hao, H., Tan, S. et al. (2021). Recent advances for improving the accuracy, transferability, and efficiency of reactive force fields. ISSN 1549-9626.
- 66 Ayers, P.W. (2007). On the electronegativity nonlocality paradox. *Theor. Chem. Acc.* 118: 371–381. ISSN 1432-881X.
- 67 Noé, F., Tkatchenko, A., Müller, K.-R., and Clementi, C. (2020). Machine learning for molecular simulation. *Annu. Rev. Phys. Chem.* 71 (1): 361–390. <https://doi.org/10.1146/annurev-physchem-042018-052331>.
- 68 Dral, P.O. (2020). Quantum chemistry in the age of machine learning. *J. Phys. Chem. Lett.* 11 (6): 2336–2347. <https://doi.org/10.1021/acs.jpcclett.9b03664>.
- 69 Haghghatdari, M., Li, J., Heidar-Zadeh, F. et al. (2020). Learning to make chemical predictions: the interplay of feature representation, data, and machine learning methods. *Chem* 6 (7): 1527–1542. <https://doi.org/https://doi.org/10.1016/j.chempr.2020.05.014>.
- 70 Cardenas, C., Ayers, P.W., and Cedillo, A. (2011). Reactivity indicators for degenerate states in the density-functional theoretic chemical reactivity theory. *J. Chem. Phys.* 134: 174103. <https://doi.org/174103> 10.1063/1.3585610.
- 71 Bultinck, P., Cardenas, C., Fuentealba, P. et al. (2013). Atomic charges and the electrostatic potential are ill-defined in degenerate ground states. *J. Chem. Theory Comput.* 9 (11): 4779–4788. <https://doi.org/10.1021/ct4005454>.
- 72 Ayers, P.W., Liu, S.B., and Li, T.L. (2011). Stability conditions for density functional reactivity theory: an interpretation of the total local hardness. *Phys. Chem. Chem. Phys.* 13: 4427–4433. <https://doi.org/10.1039/c0cp01675f>.
- 73 Cardenas, C., Munoz, M., Contreras, J. et al. (2018). Understanding chemical reactivity in extended systems: exploring models of chemical softness in carbon nanotubes. *Acta Phys. Chim. Sin.* 34 (6): 631–638. <https://doi.org/10.3866/pku.whxb201710201>.
- 74 Verstraelen, T., Pauwels, E., De Proft, F. et al. (2012). Assessment of atomic charge models for gas-phase computations on polypeptides. *J. Chem. Theory Comput.* 8 (2): 661–676. <https://doi.org/10.1021/ct200512e>.
- 75 Miranda-Quintana, R.A. and Ayers, P.W. (2016). Charge transfer and chemical potential in 1,3-dipolar cycloadditions. *Theor. Chem. Acc.* 135 (7). <https://doi.org/10.1007/s00214-016-1924-7>.
- 76 Miranda-Quintana, R.A., Gonzalez, M.M., Hernandez-Castillo, D. et al. (2017). Conceptual DFT analysis of the regioselectivity of 1,3-dipolar cycloadditions: nitrones as a case of study. *J. Mol. Model.* 23 (8). <https://doi.org/10.1007/s00894-017-3382-0>.
- 77 Miranda-Quintana, R.A. and Ayers, P.W. (2018). Dipolar cycloadditions and the “ $|\Delta\mu|$  big is good” rule: a computational study. *Theor. Chem. Acc.* 137 (12): 177. <https://doi.org/10.1007/s00214-018-2391-0>.
- 78 Hohenberg, P. and Kohn, W. (1964). Inhomogeneous electron gas. *Phys. Rev.* 136: B864–B871. <https://doi.org/10.1103/PhysRev.136.B864>.

- 79 Ayers, P.W. and Yang, W. (2003). Density functional theory. In: *Computational Medicinal Chemistry for Drug Discovery* (ed. P. Bultinck, H. de Winter, W. Langenaeker, and J.P. Tollenaere), 571–616. Dekker.
- 80 Ayers, P.W. and Parr, R.G. (2001). Variational principles for describing chemical reactions. Reactivity indices based on the external potential. *J. Am. Chem. Soc.* 123: 2007–2017.
- 81 Kohn, W. and Sham, L.J. (1965). Self-consistent equations including exchange and correlation effects. *Phys. Rev.* 140: A1133–A1138.
- 82 Dederichs, P.H., Blügel, S., Zeller, R., and Akai, H. (1984). Ground states of constrained systems: application to cerium impurities. *Phys. Rev. Lett.* 53 (26): 2512–2515. <https://doi.org/10.1103/PhysRevLett.53.2512>.
- 83 Wu, Q. and Van Voorhis, T. (2005). Direct optimization method to study constrained systems within density-functional theory. *Phys. Rev. A* 72: 024502.
- 84 Wu, Q., Ayers, P.W., and Zhang, Y.K. (2009). Density-based energy decomposition analysis for intermolecular interactions with variationally determined intermediate state energies. *J. Chem. Phys.* 131: 164112. <https://doi.org/10.1063/1.3253797>.
- 85 Levy, M. (1979). Universal variational functionals of electron-densities, 1st-order density-matrices, and natural spin-orbitals and solution of the V-representability problem. *Proc. Natl. Acad. Sci. U.S.A.* 76: 6062–6065. <https://doi.org/10.1073/pnas.76.12.6062>.
- 86 Ayers, P.W. and Levy, M. (2018). Levy constrained search in Fock space: an alternative approach to noninteger electron number. *Acta Phys. Chim. Sin.* 34 (6): 625–630. <https://doi.org/10.3866/pku.whxb201711071>.
- 87 Lieb, E.H. (1983). Density functionals for Coulomb systems. *Int. J. Quantum Chem.* 24: 243–277.
- 88 Ayers, P.W. (2006). Axiomatic formulations of the Hohenberg–Kohn functional. *Phys. Rev. A* 73 (1). <https://doi.org/10.1103/PhysRevA.73.012513>.
- 89 Ayers, P.W. and Fuentealba, P. (2009). Density-functional theory with additional basic variables: extended legendre transform. *Phys. Rev. A* 80: 032510. <https://doi.org/10.1103/PhysRevA.80.032510>.
- 90 Gorling, A. (1996). Density-functional theory for excited states. *Phys. Rev. A* 54: 3912–3915. <https://doi.org/10.1103/PhysRevA.54.3912>.
- 91 Ayers, P.W. and Levy, M. (2009). Time-independent (static) density-functional theories for pure excited states: extensions and unification. *Phys. Rev. A* 80: 012508. <https://doi.org/10.1103/PhysRevA.80.012508>.
- 92 Nagy, A., Levy, M., and Ayers, P.W. (2009). Time-independent theory for a single excited state. In: *Chemical Reactivity Theory: A Density Functional View* (ed. P.K. Chattaraj), p. 121. Taylor and Francis.
- 93 Ayers, P.W., Nagy, A., and Levy, M. (2012). Time-independent density-functional theory for excited states of Coulomb systems. *Phys. Rev. A* 85: 042518. <https://doi.org/10.1103/PhysRevA.85.042518>.
- 94 Ayers, P.W., Levy, M., and Nagy, A. (2015). Communication: Kohn–Sham theory for excited states of Coulomb systems. *J. Chem. Phys.* 143 (19): 4. <https://doi.org/10.1063/1.4934963>.

- 95 Ayers, P.W., Levy, M., and Nagy, Á. (2018). Time-independent density functional theory for degenerate excited states of Coulomb systems. *Theor. Chem. Acc.* 137 (11): 152. <https://doi.org/10.1007/s00214-018-2352-7>.
- 96 Verstraelen, T., Vandenbrande, S., and Ayers, P.W. (2014). Direct computation of parameters for accurate polarizable force fields. *J. Chem. Phys.* 141 (19). <https://doi.org/10.1063/1.4901513>.
- 97 Vandenbrande, S., Waroquier, M., Van Speybroeck, V., and Verstraelen, T. (2017). The monomer electron density force field (MEDFF): a physically inspired model for noncovalent interactions. *J. Chem. Theory Comput.* 13 (1): 161–179. <https://doi.org/10.1021/acs.jctc.6b00969>.
- 98 Bader, R.F.W. (1991). A quantum-theory of molecular structure and its applications. *Chem. Rev.* 91: 893–928.
- 99 Ayers, P.W. (2000). Atoms in molecules, an axiomatic approach. I. Maximum transferability. *J. Chem. Phys.* 113 (24): 10886–10898.
- 100 Ayers, P.W., Fias, S., and Heidar-Zadeh, F. (2018). The axiomatic approach to chemical concepts. *Comput. Theor. Chem.* 1142: 83–87. <https://doi.org/10.1016/j.comptc.2018.09.006>.
- 101 Ayers, P.W., Boyd, R.J., Bultinck, P. et al. (2015). Six questions on topology in theoretical chemistry. *Comput. Theor. Chem.* 1053: 2–16. <https://doi.org/10.1016/j.comptc.2014.09.028>.
- 102 Heidar-Zadeh, F., Ayers, P.W., Verstraelen, T. et al. (2018). Information-theoretic approaches to atoms-in-molecules: Hirshfeld family of partitioning schemes. *J. Phys. Chem. A* 122 (17): 4219–4245. <https://doi.org/10.1021/acs.jpca.7b08966>.
- 103 Parr, R.G., Ayers, P.W., and Nalewajski, R.F. (2005). What is an atom in a molecule? *J. Phys. Chem. A* 109: 3957–3959.
- 104 Ayers, P.W. (2006). Information theory, the shape function, and the Hirshfeld atom. *Theor. Chem. Acc.* 115: 370–378.
- 105 Heidar-Zadeh, F. and Ayers, P.W. (2015). How pervasive is the Hirshfeld partitioning? *J. Chem. Phys.* 142 (4): 044107. <https://doi.org/10.1063/1.4905123>.
- 106 Verstraelen, T., Vandenbrande, S., Heidar-Zadeh, F. et al. (2016). Minimal basis iterative stockholder: atoms in molecules for force-field development. *J. Chem. Theory Comput.* 12 (8): 3894–3912. <https://doi.org/10.1021/acs.jctc.6b00456>.
- 107 Fias, S., Heidar-Zadeh, F., Geerlings, P., and Ayers, P.W. (2017). Chemical transferability of functional groups follows from the nearsightedness of electronic matter. *Proc. Natl. Acad. Sci. U.S.A.* 114 (44): 11633–11638. <https://doi.org/10.1073/pnas.1615053114>.
- 108 Ayers, P.W., Morrison, R.C., and Roy, R.K. (2002). Variational principles for describing chemical reactions: condensed reactivity indices. *J. Chem. Phys.* 116: 8731–8744.
- 109 Saha, S., Roy, R.K., and Ayers, P.W. (2009). Are the Hirshfeld and Mulliken population analysis schemes consistent with chemical intuition? *Int. J. Quantum Chem.* 109 (9): 1790–1806. <https://doi.org/10.1002/qua.21901>.
- 110 Bultinck, P., Fias, S., Van Alsenoy, C. et al. (2007). Critical thoughts on computing atom condensed Fukui functions. *J. Chem. Phys.* 127 (3): 11. <https://doi.org/10.1063/1.2749518>.

- 111 Hirshfeld, F.L. (1977). Bonded-atom fragments for describing molecular charge densities. *Theor. Chim. Acta* 44: 129–138.
- 112 Nalewajski, R.F. and Parr, R.G. (2000). Information theory, atoms in molecules, and molecular similarity. *Proc. Natl. Acad. Sci. U.S.A.* 97: 8879–8882.
- 113 Bultinck, P., Van Alsenoy, C., Ayers, P.W., and Carbó-Dorca, R. (2007). Critical analysis and extension of the Hirshfeld atoms in molecules. *J. Chem. Phys.* 126: 144111. <https://doi.org/10.1063/1.2714111>.
- 114 Wang, Y.A., Liu, S.B., and Parr, R.G. (1997). Laurent series expansions in density functional theory. *Chem. Phys. Lett.* 267 (1): 14–22.
- 115 Ayers, P.W., Anderson, J.S.M., and Bartolotti, L.J. (2005). Perturbative perspectives on the chemical reaction prediction problem. *Int. J. Quantum Chem.* 101 (5): 520–534. <https://doi.org/10.1002/qua.20307>.
- 116 Englisch, H. and Englisch, R. (1984). Exact density functionals for ground-state energies. 1. General results. *Phys. Status Solidi B* 123: 711–721.
- 117 Englisch, H. and Englisch, R. (1984). Exact density functionals for ground-state energies. 2. Details and remarks. *Phys. Status Solidi B* 124: 373–379.
- 118 Guetlein, P., Lang, L., Reuter, K. et al. (2019). Toward first-principles-level polarization energies in force fields: a Gaussian basis for the atom-condensed Kohn–Sham method. *J. Chem. Theory Comput.* 15 (WOS:000480826800021): 4516–4525. <https://doi.org/10.1021/acs.jctc.9b00415>.
- 119 Ayers, P.W. and Levy, M. (2000). Perspective on “density functional approach to the frontier-electron theory of chemical reactivity” - Parr, R.G. and Yang, W. (1984). *J. Am. Chem. Soc.* 106: 4049–4050. *Theor. Chem. Acc.* 103 (3): 353–360. <https://doi.org/10.1007/s002149900093>.
- 120 Parr, R.G. and Yang, W.T. (1984). Density functional approach to the frontier-electron theory of chemical reactivity. *J. Am. Chem. Soc.* 106: 4049–4050.
- 121 Yang, W.T., Parr, R.G., and Pucci, R. (1984). Electron density, Kohn–Sham Frontier orbitals, and Fukui functions. *J. Chem. Phys.* 81: 2862–2863.
- 122 Ayers, P.W., Yang, W.T., and Bartolotti, L.J. (2009). Fukui function. In: *Chemical Reactivity Theory: A Density Functional View* (ed. P.K. Chattaraj), 255–267. CRC Press.
- 123 Morell, C., Grand, A., and Toro-Labbé, A. (2005). New dual descriptor for chemical reactivity. *J. Phys. Chem. A* 109: 205–212.
- 124 Morell, C., Grand, A., and Toro-Labbé, A. (2006). Theoretical support for using the  $\chi(r)$  descriptor. *Chem. Phys. Lett.* 425: 342–346.
- 125 De Proft, F., Ayers, P.W., Fias, S., and Geerlings, P. (2006). Woodward–Hoffmann rules in conceptual density functional theory: initial hardness response and transition state hardness. *J. Chem. Phys.* 125: 214101.
- 126 Ayers, P.W., Morell, C., De Proft, F., and Geerlings, P. (2007). Understanding the Woodward–Hoffmann rules by using changes in electron density. *Chem. Eur. J.* 13 (29): 8240–8247. <https://doi.org/10.1002/chem.200700365>.
- 127 Geerlings, P., Ayers, P.W., Toro-Labbe, A. et al. (2012). The Woodward–Hoffmann rules reinterpreted by conceptual density functional theory. *Acc. Chem. Res.* 45 (5): 683–695. <https://doi.org/10.1021/ar200192t>.

- 128 Cardenas, C., Rabi, N., Ayers, P.W. et al. (2009). Chemical reactivity descriptors for ambiphilic reagents: dual descriptor, local hypersoftness, and electrostatic potential. *J. Phys. Chem. A* 113: 8660–8667. <https://doi.org/10.1021/jp902792n>.
- 129 Ayers, P.W. and Parr, R.G. (2008). Beyond electronegativity and local hardness: higher-order equalization criteria for determination of a ground-state electron density. *J. Chem. Phys.* 129: 054111. <https://doi.org/054111.10.1063/1.2957900>.
- 130 Heidar-Zadeh, F., Richer, M., Fias, S. et al. (2016). An explicit approach to conceptual density functional theory descriptors of arbitrary order. *Chem. Phys. Lett.* 660: 307–312. <https://doi.org/10.1016/j.cplett.2016.07.039>.
- 131 Cardenas, C., Echegaray, E., Chakraborty, D. et al. (2009). Relationships between third-order reactivity indicators in chemical density-functional theory. *J. Chem. Phys.* 130: 244105.
- 132 Geerlings, P. and De Proft, F. (2008). Conceptual DFT: the chemical relevance of higher response functions. *Phys. Chem. Chem. Phys.* 10: 3028–3042. <https://doi.org/10.1039/b717671f>.
- 133 Geerlings, P., De Proft, F., and Langenaeker, W. (2003). Conceptual density functional theory. *Chem. Rev.* 103: 1793–1873. <https://doi.org/10.1021/cr990029p>.
- 134 Gazquez, J.L. (2008). Perspectives on the density functional theory of chemical reactivity. *J. Mex. Chem. Soc.* 52: 3–10.
- 135 De Proft, F., Geerlings, P., and Ayers, P.W. (2014). The conceptual density functional theory perspective of bonding. In: *The Chemical Bond: Fundamental Aspects of Chemical Bonding*, vol. 1 (ed. S. Shaik and G. Frenking), 233–270. Wiley.
- 136 Johnson, P.A., Bartolotti, L.J., Ayers, P.W. et al. (2012). Charge density and chemical reactivity: a unified view from conceptual DFT. In: *Modern Charge Density Analysis* (ed. C. Gatti and P. Macchi), 715–764. Springer.
- 137 Liu, S.B. (2009). Conceptual density functional theory and some recent developments. *Acta Phys. Chim. Sin.* 25: 590–600. [https://doi.org/10.3866/ PKU.WHXB20090332](https://doi.org/10.3866/PKU.WHXB20090332).
- 138 Parr, R.G., Donnelly, R.A., Levy, M., and Palke, W.E. (1978). Electronegativity: the density functional view point. *J. Chem. Phys.* 68: 3801–3807.
- 139 Berkowitz, M. and Parr, R.G. (1988). Molecular hardness and softness, local hardness and softness, hardness and softness kernels, and relations among these quantities. *J. Chem. Phys.* 88: 2554–2557.
- 140 Heidar-Zadeh, F., Miranda-Quintana, R.A., Verstraelen, T. et al. (2016). When is the Fukui function not normalized? The danger of inconsistent energy interpolation models in density functional theory. *J. Chem. Theory Comput.* 12 (12): 5777–5787. <https://doi.org/10.1021/acs.jctc.6b00494>.
- 141 Haunschild, R., Henderson, T.M., Jimenez-Hoyos, C.A., and Scuseria, G.E. (2010). Many-electron self-interaction and spin polarization errors in local hybrid density functionals. *J. Chem. Phys.* 133: 134116. <https://doi.org/134116.10.1063/1.3478534>.
- 142 Mori-Sanchez, P., Cohen, A.J., and Yang, W.T. (2008). Localization and delocalization errors in density functional theory and implications for band-gap prediction. *Phys. Rev. Lett.* 100: 146401.

- 143 Mori-Sanchez, P., Cohen, A.J., and Yang, W.T. (2009). Discontinuous nature of the exchange-correlation functional in strongly correlated systems. *Phys. Rev. Lett.* 102: 066403. <https://doi.org/066403> 10.1103/PhysRevLett.102.066403.
- 144 Cuevas-Saavedra, R., Chakraborty, D., Rabi, S. et al. (2012). Symmetric non local weighted density approximations from the exchange-correlation hole of the uniform electron gas. *J. Chem. Theory Comput.* 8 (11): 4081–4093. <https://doi.org/10.1021/ct300325t>.
- 145 Percus, J.K. (1999). Further comment on eigenvalue spectrum of the independent-fermion kinetic-energy kernel. *Phys. Rev. A* 60 (3): 2601–2602.
- 146 Liu, S.B. and Ayers, P.W. (2004). Functional derivative of noninteracting kinetic energy density functional. *Phys. Rev. A* 70: 022501.
- 147 Ayers, P.W. (2001). Strategies for computing chemical reactivity indices. *Theor. Chem. Acc.* 106: 271–279.
- 148 Senet, P. (1997). Kohn–Sham orbital formulation of the chemical electronic responses, including the hardness. *J. Chem. Phys.* 107: 2516–2524.
- 149 Sablon, N., De Proft, F., Ayers, P.W., and Geerlings, P. (2010). Computing second-order functional derivatives with respect to the external potential. *J. Chem. Theory Comput.* 6 (12): 3671–3680. <https://doi.org/10.1021/ct1004577>.
- 150 Ayers, P.W., De Proft, F., Borgoo, A., and Geerlings, P. (2007). Computing Fukui functions without differentiating with respect to electron number. I. Fundamentals. *J. Chem. Phys.* 126: 224107. <https://doi.org/224107> Artn 224107.
- 151 Liu, S.B., Li, T.L., and Ayers, P.W. (2009). Potentialphilicity and potential-phobicity: reactivity indicators for external potential changes from density functional reactivity theory. *J. Chem. Phys.* 131: 114106. <https://doi.org/114106> 10.1063/1.3231687.
- 152 Geerlings, P., Fias, S., Boisdenghien, Z., and De Proft, F. (2014). Conceptual DFT: chemistry from the linear response function. *Chem. Soc. Rev.* 43 (14): 4989–5008. <https://doi.org/10.1039/c3cs60456j>.
- 153 Mintmire, J.W. and Dunlap, B.I. (1982). Fitting the coulomb potential variationally in linear-combination-of-atomic-orbitals density-functional calculations. *Phys. Rev. A* 25 (1): 88–95.
- 154 Dunlap, B.I., Rosch, N., and Trickey, S.B. (2010). Variational fitting methods for electronic structure calculations. *Mol. Phys.* 108: 3167–3180. <https://doi.org/10.1080/00268976.2010.518982>.
- 155 Dunlap, B.I. (1983). Fitting the Coulomb potential variationally in X-alpha molecular calculations. *J. Chem. Phys.* 78 (6): 3140–3142.
- 156 Wu, Q., Ayers, P.W., and Yang, W. (2003). Density-functional theory calculations with correct long-range potentials. *J. Chem. Phys.* 119 (6): 2978–2990. <https://doi.org/10.1063/1.1590631>.
- 157 Wu, Q. and Yang, W.T. (2003). A direct optimization method for calculating density functionals and exchange-correlation potentials from electron densities. *J. Chem. Phys.* 118 (6): 2498–2509.
- 158 Cuevas-Saavedra, R., Rabi, N., and Ayers, P.W. (2011). The unconstrained local hardness: an intriguing quantity, beset by problems. *Phys. Chem. Chem. Phys.* 13: 19594–19600. <https://doi.org/10.1039/c1cp21646e>.

- 159** Ayers, P.W. and Yang, W.T. (2006). Legendre-transform functionals for spin-density-functional theory. *J. Chem. Phys.* 124: 224108.
- 160** Ayers, P.W., Golden, S., and Levy, M. (2006). Generalizations of the Hohenberg–Kohn theorem: I. Legendre transform constructions of variational principles for density matrices and electron distribution functions. *J. Chem. Phys.* 124: 054101.
- 161** Gütlein, P., Blumberger, J., and Oberhofer, H. (2020). An iterative fragment scheme for the ACKS2 electronic polarization model: application to molecular dimers and chains. *J. Chem. Theory Comput.* 16 (9): 5723–5735. <https://doi.org/10.1021/acs.jctc.0c00151>.
- 162** Neugebauer, J. (2007). Couplings between electronic transitions in a subsystem formulation of time-dependent density functional theory. *J. Chem. Phys.* 126 (13). <https://doi.org/10.1063/1.2713754>.
- 163** Bytautas, L., Matsunaga, N., Nagata, T. et al. (2007). Accurate ab initio potential energy curve of F<sub>2</sub>. II. Core-valence correlations, relativistic contributions, and long-range interactions. *J. Chem. Phys.* 127 (20): 204301. <https://doi.org/10.1063/1.2801989>.
- 164** Jug, K. and Kölle, C. (1998). Solvation effects on diradicals and zwitterions: tetramethylenes and trimethylenes. *J. Phys. Chem. B* 102: 6605–6611. <https://doi.org/10.1021/jp981822+>.
- 165** Xue, G., Hu, X., Chen, H. et al. (2020). Understanding the nature of quinoidal and zwitterionic states in carbazole-based diradicals. *Chem. Commun.* 56 (38): 5143–5146. <https://doi.org/10.1039/D0CC01948H>.
- 166** Mohamed, R.K., Peterson, P.W., and Alabugin, I.V. (2013). Concerted reactions that produce diradicals and zwitterions: electronic, steric, conformational, and kinetic control of cycloaromatization processes. *Chem. Rev.* 113 (9): 7089–7129. <https://doi.org/10.1021/cr4000682>.
- 167** Wannere, C.S., Schleyer, P.R., and Schaefer, H.F. (2016). The design of “neutral” carbanions with intramolecular charge compensation. *J. Org. Chem.* 81 (5): 1885–1898. <https://doi.org/10.1021/acs.joc.5b02695>.
- 168** Khurana, R., Bajaj, A., and Ali, Md.E. (2021). Tuning the Magnetic Properties of Diamagnetic Di-Blatter’s Zwitterion to Antiferro- and Ferromagnetic Diradical. <https://doi.org/10.26434/chemrxiv.14420255.v1>. <https://chemrxiv.org/engage/chemrxiv/article-details/60c7578e337d6c0a29e29049>.
- 169** Bryce, M.R. (2021). A review of functional linear carbon chains (oligoynes, polyynes, cumulenes) and their applications as molecular wires in molecular electronics and optoelectronics. *J. Mater. Chem. C* 9 (33): 10524–10546. <https://doi.org/10.1039/D1TC01406D>.
- 170** Yu, X., Li, X., Lin, H. et al. (2020). Bond-scission-induced structural transformation from cumulene to diyne moiety and formation of semiconducting organometallic polyynes. *J. Am. Chem. Soc.* 142 (18): 8085–8089. <https://doi.org/10.1021/jacs.0c01925>.
- 171** Limacher, P.A., Mikkelsen, K.V., and Luthi, H.P. (2009). On the accurate calculation of polarizabilities and second hyperpolarizabilities of polyacetylene oligomer chains using the CAM-B3LYP density functional. *J. Chem. Phys.* 130 (19): 194114. <https://doi.org/10.1063/1.3139023>.



## **Part IV**

### **Implementations**

## 31

# Realization of Conceptual Density Functional Theory and Information-Theoretic Approach in Multiwfn Program

Tian Lu and Qinxue Chen

Beijing Kein Research Center for Natural Sciences, 11-1-301, Nanli 4th Yard, Sanjianfang, Beijing 100024, P. R. China

### 31.1 Introduction

Multiwfn is a highly integrated analysis code for processing electronic wave function produced by quantum chemistry programs. It has been contiguously developed by one of us since 2009. At present, this code has been cited more than 6000 times by users in more than 70 countries. The latest version of Multiwfn provides rich functions in studying the quantities defined under the framework of conceptual density functional theory (CDFT) and the information-theoretic approach (ITA). In this chapter, we will present an overview of relevant functions.

This chapter is organized as follows: In Section 31.2, we first introduce some relevant knowledge that is closely related to Multiwfn and practical calculations. In Section 31.3, we describe, in turn, the various kinds of CDFT analyses that Multiwfn can realize. The capacity of evaluation of ITA quantities in Multiwfn will be mentioned in Section 31.4. Finally, in Section 31.5, we make concluding remarks.

### 31.2 Some Relevant Knowledge

#### 31.2.1 Basic Features of Multiwfn

Multiwfn is an open-source program and has a very wide range of functions, which can be used in studying various problems such as chemical bonds, charge distribution, aromaticity, weak interaction, electronic excitation, reaction site prediction, molecular property prediction, and so on. For a complete list of supported functions, see the main page of the Multiwfn website (<http://sobereva.com/multiwfn>). From the website, the source code, executable files, and manual of Multiwfn can be freely downloaded. The compiled code can be run on all popular platforms, including Windows, Linux, and Mac OS. Multiwfn was developed by Fortran 95; all the time-consuming codes have been substantially parallelized by OpenMP technique.

Multiwfn is designed as an interactive program. Generally, users can easily complete various analyses simply by following the prompts on the screen. Most parts of Multiwfn are text-based, but when the calculation results are needed to be visualized, a graphical user interface will be available upon request by users. This hybrid interface design not only makes wave function analysis very convenient but also enables Multiwfn to be run using a command line and thus be embedded into shell scripts for batch analysis of a large number of systems.

Most analyses supported by Multiwfn are based on the electronic wave function, which needs to be generated by quantum chemistry programs. Multiwfn supports various common file formats for wave function exchange, including wfn, wfx, fch/fchk, and molden. Multiwfn also defines a private format “mwfn,” which is stricter and contains more comprehensive information than other formats. Ref. [1] contains a full introduction to these file formats. Nearly all mainstream quantum chemistry programs can export at least one kind of wave function file supported by Multiwfn.

### 31.2.2 Evaluation of Electron Density

Almost all quantities defined under the framework of CDFT and ITA are directly dependent on electron density and/or its derivatives. Electron density is calculated via the following expression.

$$\rho(\mathbf{r}) = \sum_i \eta_i |\varphi_i(\mathbf{r})|^2 \quad (31.1)$$

where the index  $i$  loops over all orbitals,  $\eta$  stands for orbital occupation number,  $\mathbf{r}$  is coordinate vector, and  $\varphi$  corresponds to orbital wave function, which is represented as a linear combination of basis functions,  $\chi$ , or linear combination of primitive Gaussian-type functions,  $\phi$

$$\varphi_i(\mathbf{r}) = \sum_{\mu} C_{\mu,i} \chi_{\mu}(\mathbf{r}) \quad (31.2)$$

$$\varphi_i(\mathbf{r}) = \sum_l \tilde{C}_{l,i} \phi_l(\mathbf{r}) \quad (31.3)$$

The linear transformation between the  $\phi$  and  $\chi$ , and thus between the  $\tilde{\mathbf{C}}$  and  $\mathbf{C}$ , is defined by contraction coefficients of the basis set employed in the calculation. The definition of  $\phi$  or  $\chi$ , as well as that of coefficient matrix  $\tilde{\mathbf{C}}$  or  $\mathbf{C}$ , can be loaded by Multiwfn from the inputted wave function file.

Multiwfn is able to perform CDFT and ITA analyses for any common type of wave function. Hartree–Fock (HF) and Kohn–Sham density functional theory (KS–DFT) wave functions can be analyzed if the wave function file records their molecular orbitals (MOs). The analyses are also applicable to multiconfiguration wave functions such as those produced by post-HF, complete active space self-consistent field (CASSCF), and multi-reference methods; the requirement is that the wave function file contains their natural orbitals. Analyzing excited state wave functions is also possible in Multiwfn as long as the excited state wave function can be passed to Multiwfn in terms of natural orbitals. Many quantum chemistry codes

such as Gaussian are able to generate natural orbitals of excited states calculated at the popular time-dependent density functional theory (TDDFT), state-average CASSCF, and EOM-CCSD levels and export them as wave function files.

### 31.2.3 Atomic Space Partition and Integration

Atomic CDFT and ITA quantities, such as condensed Fukui function and atomic Shannon entropy, directly depend on how to partition the whole molecular space into atomic spaces. A very common type of partition is real space partition, and the subspace belonging to an atom is represented by an atomic weighting function. Next, all atomic weighting functions supported by Multiwfn will be briefly outlined.

The very popular Hirshfeld weighting function is defined as follows.

$$w_A^{\text{Hirsh}}(\mathbf{r}) = \frac{\rho_A^0(\mathbf{r})}{\rho^{\text{pro}}(\mathbf{r})} \quad (31.4)$$

where  $\rho_A^0$  is spherically averaged electron density of atom A at its isolated state, and the  $\rho^{\text{pro}}$  is known as promolecular density, which is expressed as

$$\rho^{\text{pro}}(\mathbf{r}) = \sum_A \rho_A^0(\mathbf{r}) \quad (31.5)$$

In Multiwfn, there are two choices of the  $\rho^0$  utilized in the practical calculation: (i) The ones evaluated based on the atomic wfn files generated by invoking Gaussian program via Multiwfn (ii) Directly using the built-in  $\rho^0$  library, see Appendix 3 of Multiwfn manual for detail.

The Hirshfeld-I is a variant of Hirshfeld partition [2]; it iteratively updates atomic weighting functions until convergence to improve the representation of atomic spaces. Hirshfeld-I calculation requires radial electron density of all elements in the present system at various oxidation states, which can be automatically generated by Multiwfn via invoking Gaussian. Users can also choose to directly use the high-quality atomic radial density library that comes with the Multiwfn package, which covers almost all elements at all oxidation states possibly involved in the Hirshfeld-I calculation.

Another supported partition method is Becke's method, which originally comes from the integration algorithm proposed in Ref. [3]. Becke's partition does not depend on atomic densities in isolated states but relies on element radii. With proper choice of element radii, Becke's partition could be chemically meaningful. Details of the implementation of Becke's partition in Multiwfn can be found in the supplemental material of Ref. [4].

All aforementioned definitions of atomic weighting functions are collectively known as a fuzzy partition; the weighting function goes from 1 to 0 smoothly as the coordinate moves from the present atom to adjacent atoms. For integrating real space functions in an atomic space defined in this way, the algorithm based on atomic-center grids is employed in Multiwfn. Specifically, the second Gauss-Chebyshev quadrature and Lebedev quadrature are employed for radial and angular parts, respectively. The integration accuracy and computational cost are

simultaneously determined by the number of radial and angular integration points, which can be controlled by users.

Multiwfn also supports many other kinds of partitions, such as Mulliken [5], Voronoi [6], SCPA [7], and so on. Among these, the well-known atoms in molecules (AIM) partition [8, 9] is worth noting here, and it can be employed in the evaluation of some atomic CDFT and ITA quantities in Multiwfn [10]. AIM is a discrete partition of molecular space, namely the boundary between two adjacent atoms is clear rather than fuzzy. The interatomic boundary is defined as the zero-flux surface of the gradient of electron density. In Multiwfn, the near-grid method [11] is employed by default for the construction of AIM atomic spaces, each of which is represented by a batch of uniformly distributed grids. Then, the integration of the real space function is realized by a special algorithm proposed by us, namely the regions close to nuclei are integrated by atomic-center grids, while the other regions are integrated based on uniform grids, and the two parts are finally combined together by a switching function. Our experiences show that this integration method is not only efficient but also robust.

### 31.3 Conceptual Density Functional Theory Analysis in Multiwfn

Many different kinds of CDFT analyses can be realized in Multiwfn; they will be mentioned in turn in the next sections.

#### 31.3.1 Automatic Calculation of Common CDFT Quantities

To make the CDFT study as convenient as possible, we have developed a module in Multiwfn that can calculate all real space functions and quantities involved in common CDFT analyses at one time; all data are printed in a compact and readable format. This module also enables quantum chemistry beginners to readily and correctly apply CDFT analysis in their practical research. In addition, if combining this module with shell scripts, CDFT-based descriptors can be easily gathered for a huge number of chemical systems, which may then be used in, e.g. building quantitative structure–property relationship (QSPR) and training machine learning models.

In this module, all quantities listed below can be automatically calculated by simply providing wave function files of  $N$ ,  $N-1$ , and  $N+1$  electron states, where  $N$  is the number of electrons of the original state of the present system. It does not matter even if the users have little knowledge about quantum chemistry calculation, because the corresponding input files of Gaussian or ORCA program can be directly prepared by this module, one just needs to provide a file containing reasonable geometry corresponding to  $N$  electron state in a popular format such as pdb, xyz, and mol2.

- Global indices for the whole system
  - Vertical ionization potential (VIP):  $E(N-1) - E(N)$ , where  $E$  denotes electronic energy, similarly hereinafter
  - Vertical electron affinity (VEA):  $E(N) - E(N+1)$

- Mulliken electronegativity ( $\chi$ ):  $(VIP + VEA)/2$
- Chemical potential ( $\mu$ ):  $-\chi$
- Hardness ( $\eta$ ):  $VIP - VEA$
- Softness ( $S$ ):  $1/\eta$
- Parr's electrophilicity index ( $\omega$ ):  $\mu^2/(2\eta)$
- Nucleophilicity index ( $N_{Nu}$ ): [12]  $E_{HOMO}(Nu) - E_{HOMO}(TCE)$ , where Nu (nucleophile) corresponds to the present system, TCE denotes tetracyanoethylene
- Real space functions
  - Fukui function in different forms:  $f^+(\mathbf{r}), f^-(\mathbf{r}), f^0(\mathbf{r})$
  - Dual descriptor:  $\Delta f(\mathbf{r})$
  - Local softness in different forms:  $s^+(\mathbf{r}) = Sf^+(\mathbf{r}), s^-(\mathbf{r}) = Sf^-(\mathbf{r}), s^0(\mathbf{r}) = Sf^0(\mathbf{r})$
  - Local electrophilicity index:  $\omega^{loc}(\mathbf{r}) = \omega f^+(\mathbf{r})$
  - Local nucleophilicity index:  $N_{Nu}^{loc}(\mathbf{r}) = N_{Nu} f^-(\mathbf{r})$
- Atomic indices. Hirshfeld partition is employed for this purpose
  - Hirshfeld atomic charges of  $N, N - 1$  and  $N + 1$  states
  - Condensed Fukui function ( $f_A$ ) and condensed dual descriptor ( $\Delta f_A$ )
  - Condensed local softness in different forms:  $s_A^+ = Sf_A^+, s_A^- = Sf_A^-, s_A^0 = Sf_A^0$
  - Relative electrophilicity index:  $s_A^+/s_A^-$
  - Relative nucleophilicity index:  $s_A^-/s_A^+$
  - Condensed local electrophilicity index:  $\omega^A = \omega f_A^+$
  - Condensed local nucleophilicity index:  $N_{Nu}^A = N_{Nu} f_A^-$

In addition, Multiwfn can also calculate an alternative form of electrophilicity index,  $\omega_{cubic}$  [13]

$$\omega_{cubic} = \omega \left( 1 + \frac{\mu}{3\eta^2} \gamma \right) \quad (31.6)$$

This definition considered higher-order term than Parr's electrophilicity index and is thus physically more rigorous.

A detailed example of using this module to calculate the aforementioned CDFT quantities and visualize the real space functions can be found in Section 4.22.1 of Multiwfn manual. As an illustration, Figure 31.1 shows the three kinds of Fukui functions and dual descriptor of phenol directly plotted by Multiwfn. The corresponding grid data can also be exported to cube file so that they can be further utilized in other codes or rendered in third-part visualization software such as VMD [14].

### 31.3.2 Orbital-Weighted Fukui Function and dual Descriptor

The Fukui function ( $f$ ) and dual descriptor ( $\Delta f$ ) in the conventional form usually do not work reasonably when frontier MOs are degenerate or quasi-degenerate. In addition, when the system shows point group symmetry, such as  $C_{60}$  fullerene and cyclo[18]carbon, the distributions of  $f$  and  $\Delta f$  are usually inconsistent with molecular symmetry, giving rise to an apparently misleading picture.

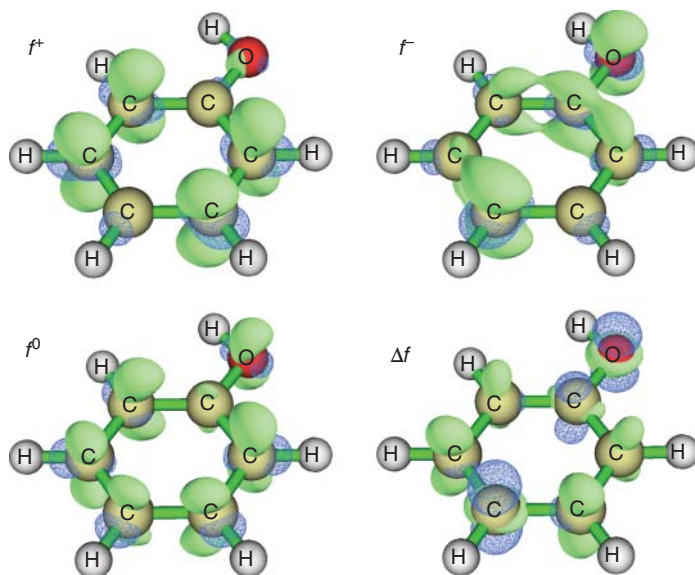


**Figure 31.1** Isosurface map of Fukui functions and dual descriptor of phenol plotted by Multiwfn. Isovalue is chosen to be 0.007 a.u. Solid and mesh surfaces correspond to positive and negative parts, respectively.

To address these problems, orbital-weighted Fukui function ( $f_w$ ) [15] and orbital-weighted dual descriptor ( $\Delta f_w$ ) [16] were proposed; they have been supported in the same module of Multiwfn as described in the last section. Three forms of  $f_w$  as well as  $\Delta f_w$  are defined as follows

$$\begin{aligned}
 f_w^+(\mathbf{r}) &= \sum_{i=\text{LUMO}}^{\infty} w_i |\varphi_i(\mathbf{r})|^2 & w_i &= \frac{\exp\left[-\left(\frac{\mu-\varepsilon_i}{\Delta}\right)^2\right]}{\sum_{i=\text{LUMO}}^{\infty} \exp\left[-\left(\frac{\mu-\varepsilon_i}{\Delta}\right)^2\right]} \\
 f_w^-(\mathbf{r}) &= \sum_i^{\text{HOMO}} w_i |\varphi_i(\mathbf{r})|^2 & w_i &= \frac{\exp\left[-\left(\frac{\mu-\varepsilon_i}{\Delta}\right)^2\right]}{\sum_i^{\text{HOMO}} \exp\left[-\left(\frac{\mu-\varepsilon_i}{\Delta}\right)^2\right]} \\
 f_w^0(\mathbf{r}) &= [f_w^+(\mathbf{r}) + f_w^-(\mathbf{r})] / 2 \\
 \Delta f_w(\mathbf{r}) &= f_w^+(\mathbf{r}) - f_w^-(\mathbf{r})
 \end{aligned} \tag{31.7}$$

where  $\varepsilon_i$  is the energy of orbital  $i$ . The chemical potential  $\mu$  is approximately calculated as  $(E_{\text{HOMO}} + E_{\text{LUMO}})/2$  in this context. The  $\Delta$  is an adjustable parameter; its most suitable value is the one able to make these functions have ideal predictability of local reactivity. According to our experiences, the  $\Delta$  between 0.05 and 0.10 Hartree works reasonably for most cases. Compared to the frozen orbital approximation form of  $f^-$ , namely  $f_{\text{F}}^- = |\varphi_{\text{HOMO}}|^2$ , the obvious advantage of  $f_w^-$  is that it takes all occupied MOs

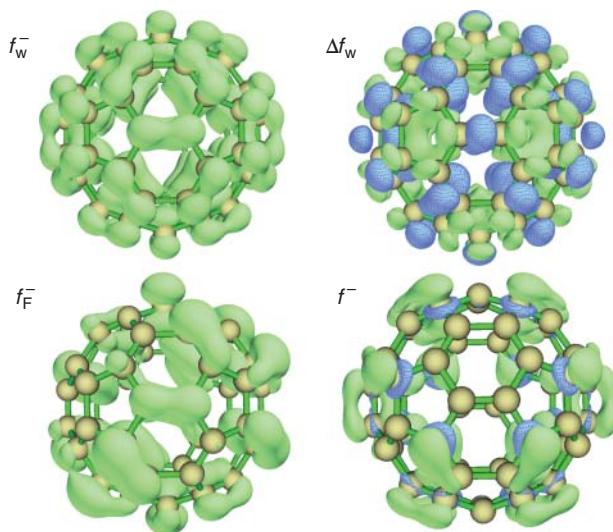


**Figure 31.2** Isosurface maps of different forms of Fukui function and dual descriptor of  $C_{60}$  plotted by Multiwfn. Isovalue is set to 0.0005 a.u. for  $f_w^-$  and  $f_F^-$ , 0.0002 a.u. for  $\Delta f_w$ , and 0.001 a.u. for  $f^-$ . Solid and solid + mesh surfaces represent positive and negative parts, respectively.

into account with different weights,  $w$ . According to Eq. (31.7), the closer orbital energy to the HOMO energy, the greater the weight of the orbital in  $f_w^-$ .

Multiwfn can also print condensed  $f_w$  and  $\Delta f_w$ , which are simply evaluated by integrating  $f_w$  and  $\Delta f_w$  in each atomic space under Hirshfeld partition.

Section 4.22.2 of Multiwfn manual presents some analysis examples, from which the readers will fully recognize the unique value of  $f_w$  and  $\Delta f_w$ . Only a representative example,  $C_{60}$  fullerene, is given here. Figure 31.2 shows various forms of Fukui function,  $f^-$  (calculated as  $\rho_N - \rho_{N-1}$ ),  $f_w^-$ ,  $f_F^-$  as well as  $\Delta f_w$ . It can be clearly seen that distributions of  $f_w^-$  and  $\Delta f_w$  are fully in line with molecular symmetry, both of them correctly indicate that all C—C bonds shared by two adjacent six-membered rings are the preferential sites for electrophilic reaction. In contrast,  $f_F^-$  and  $f^-$  are only distributed over some of the bonds and thus failed to exhibit the realistic regioselectivity.

### 31.3.3 Evaluation of Contribution of Orbitals to Fukui Function

Multiwfn has a function to evaluate the contribution of each of selected orbitals to a given density difference,  $\Delta\rho$  so that one can understand which orbitals are the main contributors of change in electron density distribution. In this module, it is assumed that  $\Delta\rho$  can be approximately represented as a linear combination of the probability density of a set of orbitals, that is

$$\Delta\rho(\mathbf{r}) \approx \Delta\rho'(\mathbf{r}) = \sum_i p_i |\varphi_i(\mathbf{r})|^2 \quad (31.8)$$



The optimal coefficients  $\{p\}$ , namely contributions of considered orbitals, can be derived via least-squares fitting to  $\Delta\rho$ , see Section 3.200.13 of Multiwfn manual for implementation details.

Expanding Fukui function as a linear combination of natural bond orbitals (NBOs) is particularly useful, and this idea has been visited in Ref. [17]. NBO is a kind of highly localized orbital, and the Lewis-type of NBO usually has a clear chemical meaning [18]. By approximately projecting Fukui function to various Lewis NBOs with imposing the constraint  $\sum_i p_i = 1$  due to the normalization condition of Fukui function via the aforementioned way, the nature of Fukui function can be explained according to the NBOs having the largest contributions. As an example, we characterize  $f^-$  of furan based on Lewis NBOs. One should first use Multiwfn to generate grid data of  $f^-$  and export it as a cube file, then use NBO program to yield NBO plot files. After that, Multiwfn will be able to calculate the fitted Fukui function  $f_{\text{fit}}^-$ , which corresponds to  $\Delta\rho'$  in Eq. (31.8), and contributions of Lewis NBO orbitals. The result is shown in Figure 31.3. It can be seen that the fitting quality is generally satisfactory, since  $f_{\text{fit}}^-$  qualitatively reproduces the major character of  $f^-$ . It is found that the  $f_{\text{fit}}^-$  is almost solely contributed by the two NBOs shown at the bottom of Figure 31.3, each one has contribution of about 50%. Since they, respectively correspond to the  $\pi$  orbital of the two C—C bonds on both sides of the furan, the  $f^-$  essentially reflects that the  $\pi$  electrons on the two C—C bonds are easiest to participate in electrophilic reactions. This example demonstrates that it is not only possible to quantify atomic contributions to Fukui function in Multiwfn but also feasible to study bond contributions with the help of NBO orbitals. Detailed steps and more

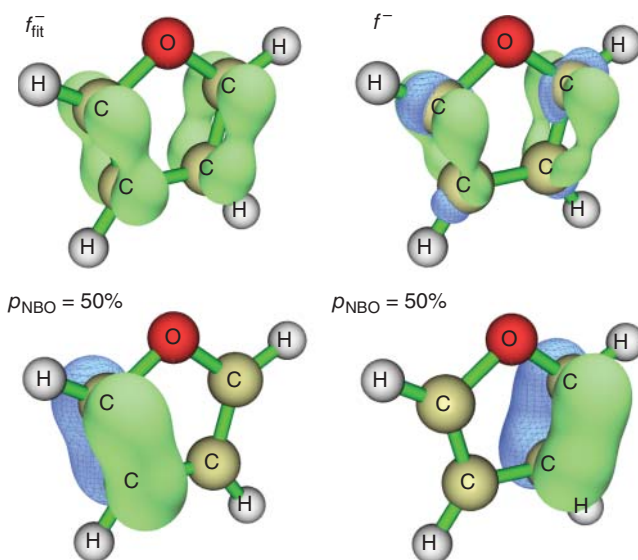


**Figure 31.3** Isosurface map of  $f^-$  and  $f_{\text{fit}}^-$  of furan with isovalue of 0.01 a.u. plotted by Multiwfn. The two NBOs having largest contribution are also shown with isovalue of 0.1 a. u. Solid and solid + mesh surfaces correspond to positive and negative parts, respectively.

examples of performing this kind of analysis can be found in Section 4.200.13 of Multiwfn manual.

### 31.3.4 Other CDFT Analyses

Due to the comprehensive functions, flexible design, and high integration, Multiwfn can also realize many other CDFT-related analyses by combinedly using multiple functions. For example, Multiwfn has a quantitative molecular surface analysis module [19], which is able to locate extrema for arbitrary mapped real space functions on isosurface of any supported real space function. In addition, various statistical data of mapped real space function over the whole surface or over the local surfaces corresponding to user-defined fragments can be derived. Therefore, one can use this module to quantitatively study the distribution of  $f$ ,  $\Delta f$ ,  $f_w$ ,  $\Delta f_w$ , etc. on the molecular surface defined by the specific isosurface of  $\rho$ . The result of this kind of analysis for a typical molecule benzaldehyde is shown in Figure 31.4, the isosurface of  $\rho = 0.01$  a.u. is taken as the molecular surface. The occurrence of surface minima of  $\Delta f_w$  above the two carbons at *meta*-sites indicates that the *meta*-carbons are most likely to undergo electrophilic attack because the  $\Delta f_w$  values at these positions are more negative than the surroundings. The  $\Delta f_w$  averaged over local molecular surfaces corresponding to different carbon atoms further consolidates this conclusion. This theoretical prediction is fully in line with experimental observation, namely aldehyde group is a *meta*-positioning group. Realization of this analysis can be learned from examples in Section 4.12 of Multiwfn manual.

It is worth noting that Multiwfn has powerful plotting functions, which can draw any aforementioned function as a curve map, various types of plane maps,

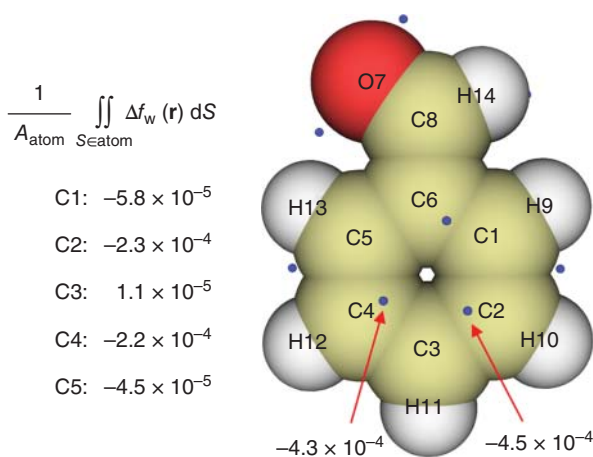


**Figure 31.4** Quantitative molecular surface analysis of  $\Delta f_w$  for benzaldehyde.  $\Delta$  parameter of 0.1 a.u. is employed. Molecular surface is defined as  $\rho = 0.01$  a.u. isosurface. Surface minima of  $\Delta f_w$  are shown as small spheres and their  $\Delta f_w$  values are labeled. Average  $\Delta f_w$  over local surface corresponding to each carbon atom that may participate in electrophilic substitution reaction is given at left side along with calculation formula, in which the  $A_{\text{atom}}$  denotes surface area occupied by the corresponding atom.

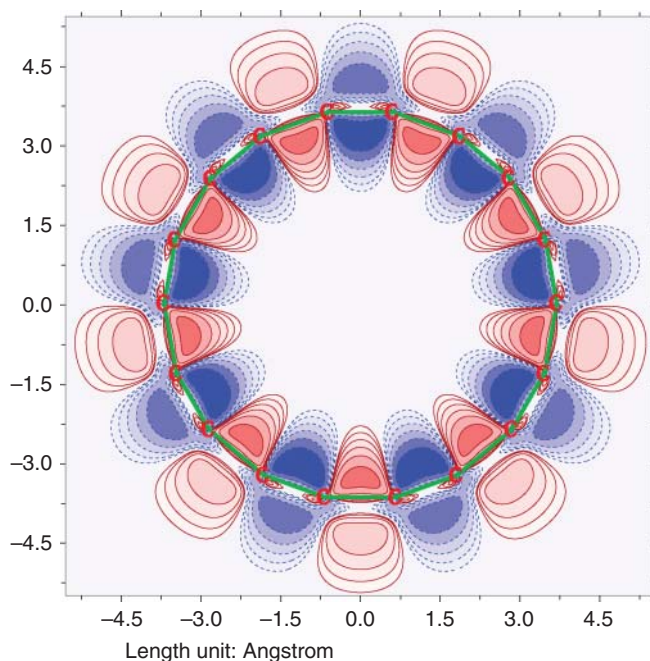


**Figure 31.5** Color-filled contour line map of  $\Delta f_w$  of cyclo [18] carbon on its molecular plane.  $\Delta$  parameter of 0.1 was employed. Positive and negative parts are represented by solid and dashed lines, respectively.

and isosurface maps. As an example, the color-filled contour line map of  $\Delta f_w$  for cyclo[18]carbon directly plotted by Multiwfn is given as Figure 31.5. This molecule consists of 18 carbon atoms and has two kinds of C—C bonds occurring alternately [20–22]. According to the sign of  $\Delta f_w$  around different bonds shown in Figure 31.5, it can be clearly recognized that the shorter and longer C—C bonds tend to participate in electrophilic and nucleophilic reactions, respectively.

## 31.4 Information-Theoretic Approach Analysis in Multiwfn

In this section, we will list all quantities defined under the ITA framework [23] that can be calculated by Multiwfn. The numerical integration algorithm employed for them has been mentioned in Section 31.2.3. Detailed calculation examples can be found in Ref. [24].

### 31.4.1 Shannon Entropy

Shannon entropy density is defined as

$$s_S(\mathbf{r}) = -\rho(\mathbf{r}) \ln \rho(\mathbf{r}) \quad (31.9)$$

In Multiwfn, this function can be integrated over the whole space to derive Shannon entropy for the whole system. Multiwfn is also able to integrate it within atomic spaces to obtain the Shannon entropy of various atoms. This can be realized by fuzzy analysis module based on Hirshfeld, Hirshfeld-I or Becke partition, or by basin analysis module using AIM partition.

It is noteworthy that the basin analysis module in Multiwfn is quite universal; it can partition the entire space into subspaces (basins) using zero-flux conditions based on any real space function. For example, zero-flux surfaces of electron localization function (ELF), localized orbital locator (LOL) [25, 26], valence electron density [27], electrostatic potential [28, 29], and even electron density difference may be used for this purpose. Basins generated in different ways may have different chemical significances; for example, it was shown that some basins of valence electron density correspond to the atomic valence regions involved in forming covalent bonds [27]. Obviously, integrating Shannon entropy density in properly selected basins could bring valuable information in understanding electronic structure.

### 31.4.2 Fisher Information and Ghosh–Berkowitz–Parr Entropy

In Multiwfn, the following functions can be integrated over the whole space or within any kind of local space, like the case of Shannon entropy density.

Fisher information density:

$$i_{\text{F}}(\mathbf{r}) = |\nabla\rho(\mathbf{r})|^2/\rho(\mathbf{r}) \quad (31.10)$$

Second Fisher information density:

$$i'_{\text{F}}(\mathbf{r}) = -\nabla^2\rho(\mathbf{r}) \ln \rho(\mathbf{r}) \quad (31.11)$$

Ghosh–Berkowitz–Parr (GBP) entropy density:

$$s(\mathbf{r}) = (3/2)\rho(\mathbf{r})\{\lambda + \ln[t(\mathbf{r})/t_{\text{TF}}(\mathbf{r})]\} \quad (31.12)$$

where  $t(\mathbf{r})$  is Lagrangian kinetic energy density and  $t_{\text{TF}}(\mathbf{r})$  is Thomas–Fermi kinetic energy density.

Note that since  $i'_{\text{F}}$  varies sharply in some regions, to achieve a relatively high integration accuracy, a very large number of radial and angular integration points should be employed, such as 400 and 2702, respectively. In the practical calculation of ITA quantities, we encourage users to perform a convergence test for the integration grid to ensure that the quality of the employed integration grid is high enough for the present case.

### 31.4.3 Relative Shannon Entropy and Relative Fisher Entropy

Relative Shannon entropy and relative Fisher entropy of an atom are also known as information gain; they characterize the variation of atomic entropy in a molecular environment with respect to an isolated state. These two quantities are defined as follows

$$\Delta S_{\text{S}}^{\text{A}} = \int \rho_{\text{A}}(\mathbf{r}) \ln \frac{\rho_{\text{A}}(\mathbf{r})}{\rho_{\text{A}}^0(\mathbf{r})} d\mathbf{r} \quad (31.13)$$

$$\Delta I_F^A = \int \rho_A(\mathbf{r}) \left| \frac{\nabla \rho_A(\mathbf{r})}{\rho_A(\mathbf{r})} - \frac{\nabla \rho_A^0(\mathbf{r})}{\rho_A^0(\mathbf{r})} \right|^2 d\mathbf{r} \quad (31.14)$$

where  $\rho_A = w_A^{\text{Hirsh}} \rho$  is atomic electron density based on Hirshfeld partition,  $\nabla \rho_A$  is simply evaluated as  $w_A^{\text{Hirsh}} \nabla \rho$ .

Relative Shannon and Fisher entropies under AIM partition are also supported by Multiwfn and are evaluated in the following forms

$$\Delta S_S^A = \int_{\Omega_A} \rho(\mathbf{r}) \ln \frac{\rho(\mathbf{r})}{\rho_A^0(\mathbf{r})} d\mathbf{r} \quad (31.15)$$

$$\Delta I_F^A = \int_{\Omega_A} \rho(\mathbf{r}) \left| \frac{\nabla \rho(\mathbf{r})}{\rho(\mathbf{r})} - \frac{\nabla \rho_A^0(\mathbf{r})}{\rho_A^0(\mathbf{r})} \right|^2 d\mathbf{r} \quad (31.16)$$

where the  $\Omega_A$  indicates that the integration is constrained in the basin of atom A.

#### 31.4.4 Rényi Entropy

Rényi entropy of two forms can be calculated in Multiwfn for the whole system

$$\text{Quadratic form : } -\log \int [\rho(\mathbf{r})]^2 d\mathbf{r}$$

$$\text{Cubic form : } -(1/2) \log \int [\rho(\mathbf{r})]^3 d\mathbf{r}$$

At the same time,  $\int w_A^{\text{Hirsh}} [\rho(\mathbf{r})]^2 d\mathbf{r}$  and  $\int w_A^{\text{Hirsh}} [\rho(\mathbf{r})]^3 d\mathbf{r}$  for each atom are also printed to help users understand the role played by various atoms.

Two forms of molecular relative Rényi entropy can also be calculated based on Hirshfeld partition:

$$\text{Quadratic form : } -\log \sum_A \int [\rho_A(\mathbf{r})]^2 / \rho_A^0(\mathbf{r}) d\mathbf{r}$$

$$\text{Cubic form : } -\log \sum_A \int [\rho_A(\mathbf{r})]^3 / [\rho_A^0(\mathbf{r})]^2(\mathbf{r}) d\mathbf{r}$$

#### 31.4.5 Other Quantities Theoretically Related to ITA

It was shown that the arithmetic mean of some information-theoretic quantities of the atoms constituting a conjugated ring has a good linear relationship with many widely accepted aromaticity indices [27]. In the fuzzy analysis module of Multiwfn, there is a function dedicated to performing this kind of calculation, see Section 3.18.11 of Multiwfn manual for a detailed explanation.

The strong covalent interaction (SCI) defined based on Pauli kinetic energy density was shown to be very useful for identifying very strong covalent bonds [30, 31]. SCI can be visually or quantitatively studied in many different ways in Multiwfn.

The energy decomposition analysis proposed by Shubin Liu divides the total molecular energy as the sum of steric energy ( $E_{\text{steric}}$ ), energy of classical electrostatic interaction, and energy due to quantum effect [23]. Multiwfn is able to calculate

$E_{\text{steric}}$  and automatically derive other terms by loading proper information in Gaussian output file, making this analysis convenient to realize. A detailed example is given in Section 4.21.2 of Multiwfn manual.

Four real space functions related to steric effect, including steric energy density, steric potential, steric charge, and magnitude of steric force, are available in Multiwfn as different user-defined functions. They can be integrated over the whole space or within atomic spaces defined by any supported partition method. They can also be easily plotted as various types of maps to visually study distribution characters.

### 31.5 Concluding Remarks

The purpose of our relentless development of the Multiwfn program is to provide the most powerful, most efficient, and most straightforward-to-use analysis program so that various valuable analysis methods based on wave function or its derivatives available in the literature can be conveniently utilized by computational chemists and create value in practical applications. Due to the importance of CDFT and ITA in analyzing molecular chemical reactions and chemical properties, Multiwfn provides many related analysis functions, which have been overviewed in this chapter. Due to the limitation of the length of the article, usage details and complete examples cannot be given. We strongly recommend readers to refer to corresponding parts of the very detailed and easy-to-understand program manual. Readers will find that Multiwfn makes CDFT analysis unprecedentedly convenient and flexible.

CDFT and ITA are still in rapid development. In the future, new analysis methods, real space functions, and quantitative indices will surely emerge, and those with high value will be added to the future version of Multiwfn.

At present, Multiwfn mainly analyzes isolated systems such as molecules and clusters. In the future, we will consider making an investigation of periodic systems fully supported in Multiwfn, and at that time, some CDFT and ITA analyses may also be applicable to solid materials, liquids, and other condensed phase systems, thereby providing chemically significant information for a broader system.

## References

- 1 Lu, T. and Chen, Q. (2020). mwfn: a strict, concise and extensible format for electronic wavefunction storage and exchange. *ChemRxiv* <https://doi.org/10.26434/chemrxiv.11872524>.
- 2 Bultinck, P., Van Alsenoy, C., Ayers, P.W., and Carbo-Dorca, R. (2007). Critical analysis and extension of the Hirshfeld atoms in molecules. *J. Chem. Phys.* 126: 144111–144119.
- 3 Becke, A.D. (1988). A multicenter numerical integration scheme for polyatomic molecules. *J. Chem. Phys.* 88: 2547–2553. <https://doi.org/10.1063/1.454033>.
- 4 Lu, T. and Chen, F. (2013). Bond order analysis based on the laplacian of electron density in fuzzy overlap space. *J. Phys. Chem. A* 117: 3100–3108. <https://doi.org/10.1021/jp4010345>.

- 5 Mulliken, R.S. (1955). Electronic population analysis on LCAO-MO molecular wave functions. II. Overlap populations, bond orders, and covalent bond energies. *J. Chem. Phys.* 23: 1841–1846.
- 6 Bickelhaupt, F.M., van Eikema Hommes, N.J.R., Fonseca Guerra, C., and Baerends, E.J. (1996). The carbon-lithium electron pair bond in (CH<sub>3</sub>Li)<sub>n</sub> (n = 1, 2, 4). *Organometallics* 15: 2923–2931. <https://doi.org/10.1021/om950966x>.
- 7 Ros, P. and Schuit, G.C.A. (1966). Molecular orbital calculations on copper chloride complexes. *Theor. Chem. Accounts* 4: 1–12.
- 8 Bader, F.W. (1994). *Atoms in Molecules: A Quantum Theory*. Oxford University Press: New York.
- 9 Matta, C.F. and Boyd, R.J. (2007). *The Quantum Theory of Atoms in Molecules – From Solid State to DNA and Drug Design*. Weinheim: WILEY-VCH Verlag GmbH & Co. KGaA.
- 10 Rong, C., Lu, T., and Liu, S. (2014). Dissecting molecular descriptors into atomic contributions in density functional reactivity theory. *J. Chem. Phys.* 140: 024109. <https://doi.org/10.1063/1.4860969>.
- 11 Tang, W., Sanville, E., and Henkelman, G. (2009). A grid-based Bader analysis algorithm without lattice bias. *J. Phys. Condens. Matter* 21: 084204. <https://doi.org/10.1088/0953-8984/21/8/084204>.
- 12 Domingo, L.R., Chamorro, E., and Pérez, P. (2008). Understanding the reactivity of captodative ethylenes in polar cycloaddition reactions. A theoretical study. *J. Org. Chem.* 73: 4615–4624. <https://doi.org/10.1021/jo800572a>.
- 13 Hoffmann, G., Tognetti, V., and Joubert, L. (2020). Electrophilicity indices and halogen bonds: some new alternatives to the molecular electrostatic potential. *J. Phys. Chem. A* 124: 2090–2101. <https://doi.org/10.1021/acs.jpca.9b10233>.
- 14 Humphrey, W., Dalke, A., and Schulten, K. (1996). VMD: visual molecular dynamics. *J. Mol. Graph.* 14: 33–38. [https://doi.org/10.1016/0263-7855\(96\)00018-5](https://doi.org/10.1016/0263-7855(96)00018-5).
- 15 Pino-Rios, R., Yañez, O., Inostroza, D. et al. (2017). Proposal of a simple and effective local reactivity descriptor through a topological analysis of an orbital-weighted fukui function. *J. Comput. Chem.* 38: 481–488. <https://doi.org/10.1002/jcc.24699>.
- 16 Pino-Rios, R., Inostroza, D., Cárdenas-Jirón, G., and Tiznado, W. (2019). Orbital-weighted dual descriptor for the study of local reactivity of systems with (Quasi-) degenerate states. *J. Phys. Chem. A* 123: 10556–10562. <https://doi.org/10.1021/acs.jpca.9b07516>.
- 17 Sánchez-Márquez, J., Zorrilla, D., García, V., and Fernández, M. (2017). Introducing a new bond reactivity index: Philicities for natural bond orbitals. *J. Mol. Model.* 24: 25. <https://doi.org/10.1007/s00894-017-3553-z>.
- 18 Weinhold, F. (1998). Natural bond orbital methods. In: *Encyclopedia of Computational Chemistry*, vol. 2 (ed. P.v.R. Schleyer), 1792–1811. West Sussex: Wiley.
- 19 Lu, T. and Chen, F. (2012). Quantitative analysis of molecular surface based on improved Marching Tetrahedra algorithm. *J. Mol. Graph. Model.* 38: 314–323. <https://doi.org/10.1016/j.jmglm.2012.07.004>.

- 20 Liu, Z., Lu, T., and Chen, Q. (2020). An sp-hybridized all-carboatomic ring, cyclo[18]carbon: electronic structure, electronic spectrum, and optical nonlinearity. *Carbon* 165: 461–467. <https://doi.org/10.1016/j.carbon.2020.05.023>.
- 21 Liu, Z., Lu, T., and Chen, Q. (2020). An sp-hybridized all-carboatomic ring, cyclo[18]carbon: bonding character, electron delocalization, and aromaticity. *Carbon* 165: 468–475. <https://doi.org/10.1016/j.carbon.2020.04.099>.
- 22 Liu, Z., Lu, T., and Chen, Q. (2021). Intermolecular interaction characteristics of the all-carboatomic ring, cyclo[18]carbon: focusing on molecular adsorption and stacking. *Carbon* 171: 514–523. <https://doi.org/10.1016/j.carbon.2020.09.048>.
- 23 Rong, C., Wang, B., Zhao, D., and Liu, S. (2020). Information-theoretic approach in density functional theory and its recent applications to chemical problems. *WIREs Comput. Mol. Sci.* 10: e1461. <https://doi.org/10.1002/wcms.1461>.
- 24 Lu T. (2020). Calculating information-theoretic quantities and some relevant quantities by Multiwfn. <http://sobereva.com/multiwfn> (accessed 30 December 2020).
- 25 Schmider, H.L. and Becke, A.D. (2000). Chemical content of the kinetic energy density. *J. Mol. Struct. (THEOCHEM)* 527: 51–61. [https://doi.org/10.1016/s0166-1280\(00\)00477-2](https://doi.org/10.1016/s0166-1280(00)00477-2).
- 26 Lu, T. and Chen, Q. (2020). A simple method of identifying  $\pi$  orbitals for non-planar systems and a protocol of studying  $\pi$  electronic structure. *Theor. Chem. Accounts* 139: 25. <https://doi.org/10.1007/s00214-019-2541-z>.
- 27 Yu, D., Rong, C., Lu, T. et al. (2018). Baird's rule in substituted fulvene derivatives: an information-theoretic study on triplet-state aromaticity and antiaromaticity. *ACS Omega* 3: 18370–18379. <https://doi.org/10.1021/acsomega.8b02881>.
- 28 Lu, T. and Chen, Q. (2020). van der Waals potential: an important complement to molecular electrostatic potential in studying intermolecular interactions. *ChemRxiv* <https://doi.org/10.26434/chemrxiv.12148572>.
- 29 Murray, J.S. and Politzer, P. (2011). The electrostatic potential: an overview. *WIREs: Comp. Mol. Sci.* 1: 153–163. <https://doi.org/10.1002/wcms.19>.
- 30 Liu, S., Rong, C., Lu, T., and Hu, H. (2018). Identifying strong covalent interactions with Pauli energy. *J. Phys. Chem. A* 122: 3087–3095. <https://doi.org/10.1021/acs.jpca.8b00521>.
- 31 Huang, Y., Liu, L., Rong, C. et al. (2018). SCI: a robust and reliable density-based descriptor to determine multiple covalent bond orders. *J. Mol. Model.* 24: 213. <https://doi.org/10.1007/s00894-018-3721-9>.



## 32

# ChemTools: Gain Chemical Insight from Quantum Chemistry Calculations

Leila Pujal\*, Alireza Tehrani\*, and Farnaz Heidar-Zadeh

Queen's University, Department of Chemistry, 90 Bader Lane, Kingston, ON K7L-3N6, Canada

## 32.1 Introduction

When a computational chemist runs a quantum mechanics (QM) calculation, the immediate output is the approximate energy and wavefunction of the chemical system under study. Most often, at the end of these calculations, some key chemical data (e.g. atomic populations) are provided. These data help scientists make sense of the gigabytes of raw wavefunction data, but most QM software only includes a few of the simplest interpretative tools, typically tools from the 1930s and 1940s (Mulliken populations, Boys–Wannier orbitals, etc.). For this reason, researchers have developed stand-alone postprocessing packages that incorporate more recent interpretive tools.

These postprocessing packages are often developed based on the scientific goals of a specific research group(s); as a result, the codes may have limited functionality and a small development team. Being limited in scope, the code structure can make it difficult to implement new features and to extend the package's utility. In addition, being an in-house code, most existing codes do not follow the latest quality assurance (QA) protocols and software development practices. Thus, the package is likely to have a monolithic source code with sparse documentation, few tests, and a rigid application programming interface (API). Thus, we believe that it is crucial to have an established and thoroughly tested framework for easy and rapid development and distribution of conceptual tools.

These motivated us to develop ChemTools, a free and open-source Python library, to provide a platform for collaborative research in conceptual quantum chemistry and promote precepts of sustainable software development. Our goal is to make it easy for theorists to test their ideas and help experimental and computational chemists use advanced interpretive tools. ChemTools strives to provide unbiased support for all mathematically rigorous postprocessing tools, not just the conceptual tools that we actively develop ourselves. Further, it strives to establish an open and collaborate environment by inviting researchers to contribute to its growth and

\*These authors contributed equally to this work.

*Conceptual Density Functional Theory: Towards a New Chemical Reactivity Theory*, First Edition.

Edited by Shubin Liu.

© 2022 WILEY-VCH GmbH. Published 2022 by WILEY-VCH GmbH.

extend its scope. This provides researchers the opportunity to be listed as a contributor and makes their research accessible and reproducible to others.

This chapter will start with characterizing ChemTools in Section 32.2. This is followed by listing its features in Section 32.3, outlining various computations that a user can (currently and in the near future) perform with ChemTools, and discussing our software design principles in Section 32.4. Our future prospects are summarized in Section 32.5 to portray potential pathways for our users and contributors.

## 32.2 Getting Started with ChemTools

Upon installation, ChemTools can be used as either a Python library or a set of command-line scripts. We have developed ChemTools using widely established and vastly used Python libraries for scientific computing and visualization, like NumPy, SciPy, SymPy, and Matplotlib. As a result, even a beginner (Python) programmer can easily and quickly get started with using ChemTools as a Python library. This is greatly facilitated by the existing example gallery described in Section 32.2.2. For less programming proficient users, we have developed a set of command-line scripts, which expose a great portion, but not all, of ChemTools functionality. These scripts have an elaborate help command to assist the user in providing correct input arguments and customize their functionality through various flags.

ChemTools has an intuitive API, with extensive documentation, to help users incorporate it for studying their chemical systems of interest. In addition, ChemTools includes sensible default parameters but allows one to customize calculations and combine tools in innovative ways.

### 32.2.1 Input and Output

As an input, ChemTools uses output file(s) from a broad range of quantum chemistry software packages. Currently, the supported file formats include Gaussian formatted checkpoint files (\*.fchk), wavefunction files (\*.wfn), extended wavefunction files (\*.wfx), Molden files (\*.molden), Molekel files (\*.mkl), Mol2 files (\*.mol2), basic XYZ Cartesian coordinate files (\*.xyz), extended XYZ files containing additional atomic properties (\*.extxyz), and cube files (\*.cube). The wavefunction information, which is available in most of these formatted files, is then analyzed by ChemTools and translated into chemical language. In addition, ChemTools can use scalar properties evaluated on a grid (as stored in a cube file) and compute pro-molecular electron density for certain type of analysis.

As an output, ChemTools produces numerical values (e.g. global descriptors like the electronegativity, gradient of electron density), tabular data (e.g. the electrophilicity of different atoms in a molecule), and a broad variety of graphical tools (both raw data like cube files and scripts for external interactive visualization software) that reveal molecular electronic structure and chemical reactivity. Section 32.3 provides an extensive list of analysis that can be performed with ChemTools,

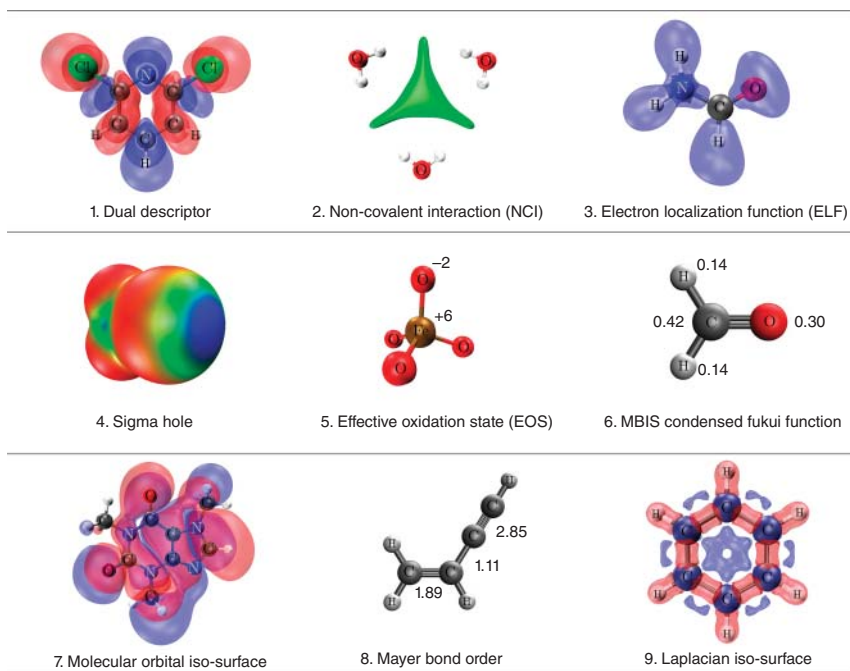


**Figure 32.1** Examples of chemical descriptors computed by ChemTools including 1. dual descriptor of dichloropyridine (iso-surface = 0.0005 a.u.), 2. non-covalent interaction (NCI) of  $[\text{H}_2\text{O}]_3$ , 3. electron localization function (ELF) of formamide (iso-surface = 0.09 a.u.), 4. electron density isosurface colored with electrostatic potential values showing the sigma hole of  $\text{F}_3\text{CBr}$  (iso-surface = 0.001 a.u., min = 0.003, max = 0.03), 5. effective oxidation state (EOS) of  $[\text{FeO}_4]^{2-}$ , 6. condensed Fukui function with minimal basis iterative stockholder (MBIS) charges of  $\text{CH}_2\text{O}$ , 7. highest occupied molecular orbital (HOMO) iso-surface of caffeine molecule (iso-surface = 0.0045 a.u.), 8. Mayer bond order of vinylacetylene, and 9. Laplacian iso-surface of Benzene (isosurface = 0.185 a.u.).

and Figure 32.1 exemplifies some of those chemical descriptors. Currently, we delegate visualization to free, third-party packages like Visual Molecular Dynamics (VMD) [1], USCF ChimeraX [2], Matplotlib, and RDKit packages and generate required cube files and scripts to facilitate visualization.

### 32.2.2 Example Gallery

From early on, we included an example gallery on the ChemTools website to facilitate user training. We use Sphinx-Gallery (a Sphinx extension that builds an HTML gallery of examples from a set of Python scripts) to showcase ChemTools functionality and flexibility. With one click, users can download the example files as a Python script or Jupyter notebook and easily modify them to new chemical systems. These examples show how ChemTools can be used as a Python library, allow users to quickly generate quality results, and give the developers an opportunity to identify “pain points” when writing ChemTools examples.

In addition, we encourage and invite researchers who use ChemTools in their research to contribute their scripts and notebooks to ChemTools example gallery, so that their published results can be easily reproduced and utilized by others.

## 32.3 ChemTools Features

The main six modules of ChemTools, sketched in Figure 32.2, are briefly discussed here to showcase numerous conceptual tools that it can compute. This also demonstrates the flexible framework of ChemTools for implementation and extension of a wide range of conceptual chemistry tools. For each module, the existing features are listed alongside their envisioned future extensions. While individual modules are designed to be used independently, it is often useful and interesting to combine tools from different modules. For example, to compute the electrophilicity of a given atom in a molecule, one needs to first compute the local electrophilicity (using conceptual density functional theory [DFT] module discussed in Section 32.3.1) and then determine how much of this local quantity is associated with a given atom (using atoms-in-molecules [AIM] partitioning module discussed in Section 32.3.2). Hence, ChemTools framework allows the user to combine various approaches for computing local electrophilicity with various approaches for partitioning it into atomic contributions.

We strive to ensure that the source code and website of ChemTools are both comprehensively documented, including tests, scripts, and examples. As that documentation is maintained with the software, providing code snippets and examples here seems unwise as they will eventually be outdated. For the most updated documentation and examples on how to use ChemTools, please refer to its website.

### 32.3.1 Conceptual Density Functional Theory

This module aims at understanding chemical reactivity and predicting the outcome of chemical reactions, by computing the changes in the energy with respect to the number of electrons and external potential. In other words, it computes the global, local, mixed, and condensed reactivity indicators from frontier molecular orbital (MO) theory or finite-difference approaches using linear [3, 4], quadratic [5, 6], exponential [7], and other user-defined energy models [8]. Currently, it allows one to compute the popular reactivity indicators [9] like chemical potential [5], chemical hardness [6], electrophilicity [10], and Fukui function [11, 12] and generate scripts and required cube files to visualize the local reactivity descriptors (e.g. plotting property isosurfaces and/or coloring it with another property) and condensed reactivity descriptors (e.g. drawing a chemical structure and labeling each atom with the corresponding reactivity descriptor value). It is being extended to compute spin-resolved and non-local reactivity descriptors, aromaticity indices, ring currents, alchemical derivatives (using response theory or finite difference), and reaction force analysis.

### 32.3.2 Atoms-in-Molecules Partitioning Schemes

This module aims at decomposing molecules into atomic subsystems by dividing the molecular electron density between constituent atoms. Currently, it includes the Hirshfeld [13], iterative Hirshfeld (HI) [14], iterative stockholder analysis (ISA) [15], minimal basis iterative stockholder (MBIS) [16], and Becke [17] partitioning schemes. This is being extended to include additive variational Hirshfeld (AVH) [18, 19] and quantum theory of atoms-in-molecules (QTAIM) [20], alongside adding the periodic boundary conditions to extend these methods to solid state.

### 32.3.3 Chemical Topological Analysis

This module aims at identifying and characterizing critical points (i.e. points with zero gradient) and topological basins of any scalar field. Currently, it includes critical point finder for any scalar property using its analytical first and second derivatives. However, it is being extended to compute and visualize topological basins, identify inter-atomic surfaces, quantify components of interaction energy between atomic basins, and calculate the (de)localization index.

### 32.3.4 Density Functional Theory Tools

This module aims at analyzing electronic structure by identifying where electrons are concentrated and depleted, within molecules. Currently, it includes computing various kinetic energy densities like Thomas Fermi, von Weizsacker, Lagrangian, and gradient expansion kinetic energy densities, non-covalent interactions (NCI) [21], electron localization function (ELF) [22, 23], and localized orbital locator (LOL) [24]. It is being extended to compute information-theoretic descriptors like the Shannon/Fisher and steric entropies [25], density overlap regions indicator (DORI) [26], and interconversion of density-like and potential-like reactivity descriptors.

### 32.3.5 Conceptual Density Matrix Functional Theory

This module aims at computing reactivity indicators based on density matrices. Currently, it computes the Fukui matrix [27], dual-descriptor matrix [28], and higher-order terms. It is being extended to compute the atomic overlap matrix, electron oxidation state (EOS) [29], localized orbital bonding analysis (LOBA) [30], probability distribution function analysis, and identifying/visualizing electron pairs.

### 32.3.6 Molecular Orbital Theory

This module aims at describing the electronic structure of molecules by analyzing MO. Currently, it computes the local ionization potential, temperature dependent density, temperature dependent local density of states, electrostatic potential, and population analysis methods like Mulliken and Löwdin [31, 32]. It is being

extended to generate MO diagrams and compute the orbital localization methods like Boys–Wannier [33] and Pipek–Mezey [34], intrinsic atomic orbitals (IAO) [35], quasi-atomic minimal basis orbital (QUAMBO) [36], bond orders and multicenter indices like shared-electron delocalization index (SEDI) [37], Cioslowski and Mayer covalent bond order [38, 39], domain-averaged Femi hole (DAFH) [40, 41],  $\sigma$ -hole,  $\pi$ -hole, orbital decomposition, and entanglement analysis.

## 32.4 ChemTools Design Principles

As software becomes ubiquitous in scientific research, the need for robust, reliable, and sustainable software becomes more acute. Modern software engineering practices for sustainable software development are attuned to these needs [42, 43], but not always aligned with the needs of scientific researchers. When scientists create software, they rarely anticipate possible use cases for different scientific disciplines. Similarly, software engineers often lack the domain knowledge to effectively anticipate the most common use cases [44].

Researchers usually develop software motivated by their own individual scientific goals, and these goals constantly shift as scientific results (re)direct the project. This favors an incremental development pattern, which makes it difficult to write a complete specification document for a software package ahead of time, which in turn makes it difficult to apply modern software engineering practices [44, 45]. On the other hand, reproducibility, readability, verifiability, and collaboration are highly valued by both software engineers and scientific researchers. This section declares the guiding principles that ChemTools uses to balance its dual goals of advancing scientific research while adhering to best practices from modern software engineering.

### 32.4.1 Open-Source Software

The open science movement encourages researchers to make their data and code publicly available to facilitate accessibility and collaboration in science [46]. Similarly, open-source software allows an individual to contribute to the development of the software and openly share any problems with the community. There are many examples of successful open, online, and community-based collaborations like Wikipedia, Linux, NumPy, and SciPy. This is unfortunately rare in research, because scientists are recognized based on publications, citations, patents, grants, etc. [47] that incentivizes maintaining control over ones scientific output and discourages efforts to advance the whole community [48].

To encourage contribution and collaboration, ChemTools contributors are all listed on GitHub that gives a transparent view of their implementation. In addition, ChemTools supports citation of key publications for each conceptual quantum chemistry tool implemented or each notebook that reproduces published results. As a result, researchers are recognized when they utilize ChemTools to distribute their scientific findings and make them accessible to a broader audience. On the other hand, users can publicly post any problems they encounter when installing or

using ChemTools through GitHub's issue tracking system that opens another level of transparency and community engagement.

### 32.4.2 Modularity

Modularity, a fundamental concept in software engineering, separates a software into its components, called modules, where each component satisfies one task and is independent of other components. This greatly reduces the complexity of software down to its individual modules, thus allowing easier maintenance of large code bases, easier testing of smaller modules, and ease of extensions. Further, modularity allows the components to become highly specialized to the expertise of the contributor while minimizing their interaction with other specialized components.

ChemTools modular structure is sketched in Figure 32.2. At the core, there are six independent modules with non-overlapping functionality. As described in Section 32.3, these six modules include conceptual density functional theory (DFT), atoms-in-molecules (AIM) partitionings, chemical topology, DFT descriptors, conceptual density matrix functional theory (DMFT), and molecular orbital theory. Each of these six modules contain key computations to support different types of conceptual quantum chemistry tools and can be modified independently. However, there are fundamental computations (e.g. file parsing, numerical integration and differentiation, evaluating integrals and functions using Gaussian basis sets) that are used by almost every module of ChemTools. To ensure that modules remain insensitive to the nature of these computational utilities, these computations are performed through Wrappers and Toolbox modules. This makes ChemTools easily maintainable since if the API of one of these external packages changes, the effects of this change are localized only to the Wrappers module.

Currently, we only have wrappers for pure Python libraries including IOData [49] (for handling input/output of chemical file formats), GBasis (for Gaussian basis functions evaluations and integrals), and Grid (for numerical molecular integration grids), which are parts of the HORTON3 (helpful open-source research tools for N-fermion systems) software package. However, to improve ChemTools performance, we are extending the Wrappers module to support PySCF [50] and Psi4 [51], which have similar functionality and utility but, as a C++/Fortran code with a veneer of Python, are often faster. The Wrappers functionality and the six core modules are connected through Toolbox module that allows combining utilities from different modules.

### 32.4.3 Robustness and Quality Assurance

Version control allows programmers to keep track of code changes, make changes without affecting the main source code, and revert unwanted changes. In addition, it facilitates collaboration and brings transparency to contributions made [43]. Alongside version control, continuous integration frameworks are used to make software development robust. This means that any change to the code triggers a series of

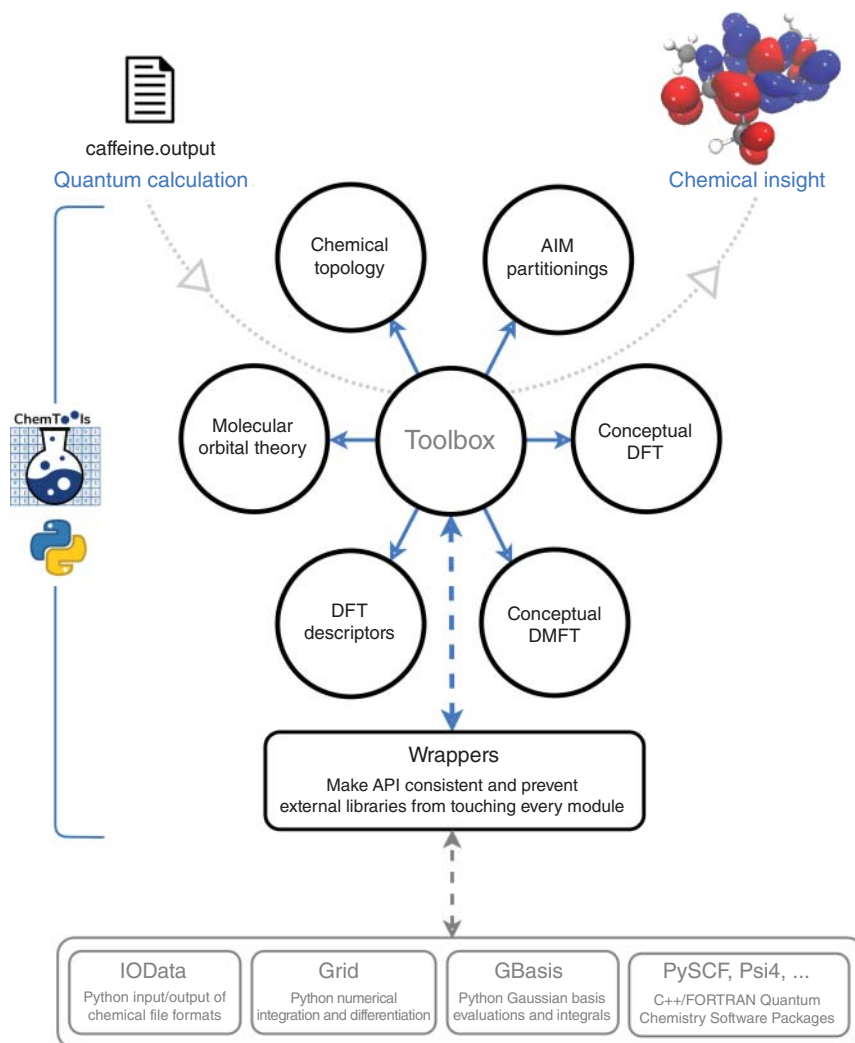


**Figure 32.2** Schematic representation of ChemTools architecture including its modules and dependencies.

automatic tests to make sure it satisfies the software's quality standard by being tested, readable, and well-documented and following its coding style. These checks can be either run manually by the contributor, or it is ran automatically whenever the code is added to the main source code.

ChemTools uses Git for version control and uses various software testing resources as part of its continuous integration and delivery framework that is also crucial for scaling quality assurance (QA) process as more features are added. Because manual testing is time-consuming, error-prone, and limited in scope, we have developed automated scripts to quickly and repeatedly run tests upon making changes to the code or making a release. To deliver a bug-free and high-quality code, as part of



ChemTools continuous integration workflow, we incorporate automatic measures for the following:

- **Testing code correctness** to ensure that code changes are working as expected without degrading functionality. This includes (i) unit tests for independent testing of individual functions and classes at a low level, (ii) integration tests to verify that different modules work well together and test new features plus existing functionality at a higher-level, and (iii) end-to-end tests to replicate a user behavior by frequently running examples and tutorials as part of ChemTools automatic test suite.
- **Testing code quality** to ensure that code changes are not degrading code quality and ChemTools coding standards. This includes (i) linters (like `pycodestyle`, `pyflakes`, and `pylint`) to check that the code adheres to coding standards (PEP8) and is well-documented (PEP257), (ii) `black` formatter to automatically and consistently improve code's readability, and (iii) code coverage to ensure that every line of code is tested.
- **Testing code built** to check that the code properly installs and tests run successfully for different operating systems and versions of Python.

#### 32.4.4 Ease of Extension and Contribution

Being modular and well-documented, it is very easy to add a new feature to ChemTools. In addition, the source code is hosted on GitHub where contributors can easily share and discuss their code and obtain the latest version of the development branch. We welcome new contributions and, to facilitate that, have included an elaborate and inclusive “Contributing Guidelines” on the ChemTools website. By contributing to ChemTools, one can join the open-source community and publicly distribute their research methods and findings, so that others can reproduce and utilize them.

## 32.5 Future Prospects

ChemTools is under active development to better cater to its audience. Currently, we are focusing on (i) extending our support for other domain-specific quantum chemistry packages like `PySCF` [50] and `Psi4` [51], (ii) improving ChemTools visualization capabilities by extending our support for other third-party visualization packages like `PyMol` or `UCSF ChimeraX`, (iii) extending existing modules to include more descriptors as described in Section 32.3, (iv) improving ChemTools computation speed, (v) improving ChemTools API to be more intuitive, and (vi) expanding the notebooks and scripts in Examples Gallery and increase reproducibility of scientific results. Even though using ChemTools command-line scripts is very straightforward and requires no knowledge of Python, we are taking advantage of various libraries to transform the command-line functionality into a user-friendly graphical user interface (GUI). We provide these alternatives to facilitate user training and on-boarding.

## Acknowledgments

We wish to acknowledge various contributions and refinements to the ChemTools library from Stijn Fias, Xiaotian Derrick Yang, Taewon David Kim, Michael Richer, Esteban Vöhringer-Martinez, Toon Verstraelen, Paul W. Ayers, and the QC-Devs development team. A.T. acknowledges support from School of Graduate Studies (SGS) doctoral scholarship at Queen's University. F.H.-Z. acknowledges Natural Sciences and Engineering Research Council (NSERC) of Canada, Queen's University Research Initiation Grant, and Compute Canada for financial and computational support.

## References

- 1 Humphrey, W., Dalke, A., and Schulten, K. (1996). VMD: visual molecular dynamics. *J. Mol. Graphics* 14 (1): 33–38.
- 2 Goddard, T.D., Huang, C.C., Meng, E.C. et al. (2018). UCSF ChimeraX: Meeting modern challenges in visualization and analysis. *Protein Sci.* 27 (1): 14–25. <https://doi.org/10.1002/pro.3235>.
- 3 Perdew, J.P., Parr, R.G., Levy, M., and Balduz, J.L. (1982). Density-functional theory for fractional particle number: derivative discontinuities of the energy. *Phys. Rev. Lett.* 49 (23): 1691–1694. <https://doi.org/10.1103/PhysRevLett.49.1691>.
- 4 Ayers, P.W. (2008). The dependence on and continuity of the energy and other molecular properties with respect to the number of electrons. *J. Math. Chem.* 43 (1): 285–303. <https://doi.org/10.1007/s10910-006-9195-5>.
- 5 Parr, R.G., Donnelly, R.A., Levy, M., and Palke, W.E. (1978). Electronegativity: the density functional viewpoint. *J. Chem. Phys.* 68 (8): 3801–3807. <https://doi.org/10.1063/1.436185>.
- 6 Parr, R.G. and Pearson, R.G. (1983). Absolute hardness: companion parameter to absolute electronegativity. *J. Am. Chem. Soc.* 105 (26): 7512–7516. <https://doi.org/10.1021/ja00364a005>.
- 7 Parr, R.G. and Bartolotti, L.J. (1982). On the geometric mean principle for electronegativity equalization. *J. Am. Chem. Soc.* 104 (14): 3801–3803. <https://doi.org/10.1021/ja00378a004>.
- 8 Heidar-zadeh, F., Miranda-quintana, A., Verstraelen, T. et al. (2016). When is the Fukui function not normalized? The danger of inconsistent energy interpolation models in density functional theory. *J. Chem. Theory Comput.* 12 (12): 5777–5787. <https://pubs.acs.org/doi/10.1021/acs.jctc.6b00494>.
- 9 Heidar-Zadeh, F., Richer, M., Fias, S. et al. (2016). An explicit approach to conceptual density functional theory descriptors of arbitrary order. *Chem. Phys. Lett.* 660: 307–312. <https://doi.org/10.1016/j.cplett.2016.07.039>.
- 10 Parr, R.G., Szentpály, L.V., and Liu, S. (1999). Electrophilicity index. *J. Am. Chem. Soc.* 121 (9): 1922–1924. <https://doi.org/10.1021/ja983494x>.
- 11 Fukui, K. (1982). Role of frontier orbitals in chemical reactions. *Science* 218 (4574): 747–754. <https://doi.org/10.1126/science.218.4574.747>.

- 12 Parr, R.G. and Yang, W. (1984). Density functional approach to the frontier-electron theory of chemical reactivity. *J. Am. Chem. Soc.* 106 (14): 4049–4050. <https://doi.org/10.1021/ja00326a036>.
- 13 Hirshfeld, F.L. (1977). Bonded-atom fragments for describing molecular charge densities. *Theor. Chim. Acta* 44 (2): 129–138. <https://doi.org/10.1007/BF00549096>.
- 14 Bultinck, P., Van Alsenoy, C., Ayers, P.W., and Carbó-Dorca, R. (2007). Critical analysis and extension of the Hirshfeld atoms in molecules. *J. Chem. Phys.* 126 (14). <https://doi.org/10.1063/1.2715563>.
- 15 Lillestolen, T.C. and Wheatley, R.J. (2008). Redefining the atom: atomic charge densities produced by an iterative stockholder approach. *Chem. Commun.* 7345 (45): 5909–5911. <https://doi.org/10.1039/b812691g>.
- 16 Verstraelen, T., Vandenbrande, S., Heidar-Zadeh, F. et al. (2016). Minimal basis iterative stockholder: atoms in molecules for force-field development. *J. Chem. Theory Comput.* 12 (8): 3894–3912. <https://doi.org/10.1021/acs.jctc.6b00456>.
- 17 Becke, A.D. (1988). A multicenter numerical integration scheme for polyatomic molecules. *J. Chem. Phys.* 88 (4): 2547–2553. <https://doi.org/10.1063/1.454033>.
- 18 Heidar-Zadeh, F. and Ayers, P.W. (2015). How pervasive is the Hirshfeld partitioning? *J. Chem. Phys.* 142 (4). <https://doi.org/10.1063/1.4905123>.
- 19 Heidar-Zadeh, F., Ayers, P.W., Verstraelen, T. et al. (2018). Information-theoretic approaches to atoms-in-molecules: Hirshfeld family of partitioning schemes. *J. Phys. Chem. A* 122 (17): 4219–4245. <https://doi.org/10.1021/acs.jpca.7b08966>.
- 20 Bader, R.F.W. (1990). *Atoms in Molecules: A Quantum Theory*. Oxford: Oxford University Press.
- 21 Johnson, E.R., Keinan, S., Mori-Sánchez, P. et al. (2010). Revealing noncovalent interactions. *J. Am. Chem. Soc.* 132 (18): 6498–6506. <https://doi.org/10.1021/ja100936w>.
- 22 Becke, A.D. and Edgecombe, K.E. (1990). A simple measure of electron localization in atomic and molecular systems. *J. Chem. Phys.* 92 (9): 5397–5403. <https://doi.org/10.1063/1.458517>.
- 23 Silvi, B. and Savin, A. (1994). Classification of chemical bonds based on topological. *Nature* 371 (64991): 683–686. <http://www.lct.jussieu.fr/pagesperso/savin/papers/nature/SilSav-94.pdf>.
- 24 Schmider, H.L. and Becke, A.D. (2000). Chemical content of the kinetic energy density. *J. Mol. Struct. THEOCHEM* 527 (1–3): 51–61. [https://doi.org/10.1016/S0166-1280\(00\)00477-2](https://doi.org/10.1016/S0166-1280(00)00477-2).
- 25 Rong, C., Wang, B., Zhao, D., and Liu, S. (2020). Information-theoretic approach in density functional theory and its recent applications to chemical problems. *Wiley Interdiscip. Rev. Comput. Mol. Sci.* 10 (4): 1–22. <https://doi.org/10.1002/wcms.1461>.
- 26 De Silva, P. and Corminboeuf, C. (2014). Simultaneous visualization of covalent and noncovalent interactions using regions of density overlap. *J. Chem. Theory Comput.* 10 (9): 3745–3756. <https://doi.org/10.1021/ct500490b>.
- 27 Bultinck, P., Clarisse, D., Ayers, P.W., and Carbo-Dorca, R. (2011). The Fukui matrix: a simple approach to the analysis of the Fukui function

- and its positive character. *Phys. Chem. Chem. Phys.* 13 (13): 6110–6115. <https://doi.org/10.1039/c0cp02268c>.
- 28 Alcoba, D.R., Tiznado, W., Oña, O.B. et al. (2012). Fukui and dual-descriptor matrices in the basis-set representation: a spin-free approach. *Chem. Phys. Lett.* 533: 114–117. <https://doi.org/10.1016/j.cplett.2012.03.009>.
- 29 Ramos-Cordoba, E., Postils, V., and Salvador, P. (2015). Oxidation states from wave function analysis. *J. Chem. Theory Comput.* 11 (4): 1501–1508. <https://doi.org/10.1021/ct501088v>.
- 30 Thom, A.J.W., Sundstrom, E.J., and Head-Gordon, M. (2009). LOBA: A localized orbital bonding analysis to calculate oxidation states, with application to a model water oxidation catalyst. *Phys. Chem. Chem. Phys.* 11 (47): 11297–11304. <https://doi.org/10.1039/b915364k>.
- 31 Mulliken, R.S. (1955). Electronic population analysis on LCAO-MO molecular wave functions. IV. Bonding and antibonding in LCAO and valence-bond theories. *J. Chem. Phys.* 23 (12): 2343–2346. <https://doi.org/10.1063/1.1741877>.
- 32 Löwdin, P.O. (1950). On the non-orthogonality problem connected with the use of atomic wave functions in the theory of molecules and crystals. *J. Chem. Phys.* 18 (3): 365–375. <https://doi.org/10.1063/1.1747632>.
- 33 Foster, J.M. and Boys, S.F. (1960). Canonical configurational interaction procedure. *Rev. Mod. Phys.* 32: 300–302. <https://doi.org/10.1103/RevModPhys.32.300>.
- 34 Pipek, J. and Mezey, P.G. (1989). A fast intrinsic localization procedure applicable for ab initio and semiempirical linear combination of atomic orbital wave functions. *J. Chem. Phys.* 90 (9): 4916–4926. <https://doi.org/10.1063/1.456588>.
- 35 Knizia, G. (2013). Intrinsic atomic orbitals: an unbiased bridge between quantum theory and chemical concepts. *J. Chem. Theory Comput.* 9 (11): 4834–4843.
- 36 Lu, W.C., Wang, C.Z., Schmidt, M.W. et al. (2004). Molecule intrinsic minimal basis sets. I. Exact resolution of ab initio optimized molecular orbitals in terms of deformed atomic minimal-basis orbitals. *J. Chem. Phys.* 120 (6): 2629–2637. <https://doi.org/10.1063/1.1638731>.
- 37 Ponec, R. and Cooper, D.L. (2007). Anatomy of bond formation. Bond length dependence of the extent of electron sharing in chemical bonds from the analysis of domain-averaged Fermi holes. *Faraday Discuss* 135: 31–42. <https://pubs.rsc.org/en/content/articlelanding/2007/fd/b605313k>
- 38 Cioslowski, J. and Mixon, S.T. (1991). Covalent bond orders in the topological theory of atoms in molecules. *J. Am. Chem. Soc.* 113 (11): 4142–4145. <https://doi.org/10.1021/ja00011a014>.
- 39 Mayer, I. (1983). Charge, bond order and valence in the AB initio SCF theory. *Chem. Phys. Lett.* 97 (3): 270–274. [https://doi.org/10.1016/0009-2614\(83\)80005-0](https://doi.org/10.1016/0009-2614(83)80005-0).
- 40 Ponec, R. (1997). Electron pairing and chemical bonds. Chemical structure, valences and structural similarities from the analysis of the Fermi holes. *J. Math. Chem.* 21 (3): 323–333.
- 41 Ponec, R. (1998). Electron pairing and chemical bonds. Molecular structure from the analysis of pair densities and related quantities. *J. Math. Chem.* 23 (1–2): 85–103.

- 42 Baxter, S.M., Day, S.W., Fetrow, J.S., and Reisinger, S.J. (2006). Scientific software development is not an oxymoron. *PLoS Comput. Biol.* 2 (9): e87. <https://doi.org/10.1371/journal.pcbi.0020087>.
- 43 Wilson, G., Aruliah, D.A., Brown, C.T. et al. (2014). Best practices for scientific computing. *PLoS Biol.* 12 (1): e1001745. <https://doi.org/10.1371/journal.pbio.1001745>.
- 44 Segal, J. (2009). Some challenges facing software engineers developing software for scientists. *2009 ICSE Workshop on Software Engineering for Computational Science and Engineering*, pp. 9–14. <https://doi.org/10.1109/SECSE.2009.5069156>.
- 45 Hannay, J.E., MacLeod, C., Singer, J. et al. (2009). How do scientists develop and use scientific software? *2009 ICSE Workshop on Software Engineering for Computational Science and Engineering*, pp. 1–8. IEEE. <https://doi.org/10.1109/SECSE.2009.5069155>.
- 46 Nielsen, M. (2011). *Reinventing Discovery: The New Era of Networked Science*. Princeton University Press.
- 47 Howison, J. and Herbsleb, J.D. (2013). Incentives and integration in scientific software production. *Proceedings of the 2013 Conference on Computer Supported Cooperative Work*, pp. 459–470. <https://doi.org/10.1145/2441776.2441828>.
- 48 Turk, M.J. (2013). Scaling a code in the human dimension. *XSEDE'13: Proceedings of the Conference on Extreme Science and Engineering Discovery Environment: Gateway to Discovery*, number 69, pp. 1–7. <https://doi.org/10.1145/2484762.2484782>.
- 49 Verstraelen, T., Adams, W., Pujal, L. et al. (2020). IOData: A python library for reading, writing, and converting computational chemistry file formats and generating input files. *J. Comput. Chem.* 458–464. <https://doi.org/10.1002/jcc.26468>.
- 50 Sun, Q., Zhang, X., Banerjee, S. et al. (2020). Recent developments in the PySCF program package. *J. Chem. Phys.* 153 (2): 024109.
- 51 Smith, D.G.A., Burns, L.A., Simmonett, A.C. et al. (2020). Psi4 1.4: Open-source software for high-throughput quantum chemistry. *J. Chem. Phys.* 152 (18): 184108.

## Index

### **a**

- ABEEM. *see* atom-bond electronegativity equalization method (ABEEM)
- ABEEM-7P model 597
- ab initio* calculations 246
- ab initio* methods 187
- ab initio* molecular dynamics (AIMD) simulations 540
- ab initio* quantum mechanical 229
- ab initio* simulations 444
- acid and base exchange reactions 263
- acid/base reaction 265–268
- acid exchange reaction 263
- ACKS2. *see* atom-condensed Kohn-Sham (second order) (ACKS2)
- active pharmaceutical ingredients (APIs) 505
- Additive Variational Hirshfeld (AVH) 653
- adiabatic states 391
- adsorption energies ( $\Delta E_{\text{ads}}$ ) 545
- alchemical derivatives 315
- alkyne-azide electrocyclization 256
- all-metal aromaticity 537
- $\alpha$ -methylene ketone ( $\alpha$ MK) 203
- amylose polysaccharide 246
- anisotropic displacement parameters (ADP) 514
- antiaromaticity 295
- anti-aromaticity 310
- anti-bonding LUMO 254
- antibonding orbital 87
- application programming interface (API) 649
- aromatic/antiaromatic annular ring systems 544
- aromaticity 281, 295–297
- Arrhenius equation 464
- association reaction 216–217
- atom-bond electronegativity equalization method (ABEEM) 587
- charge distribution and polarization 589–590
- classical force fields 587–588
- molecular dynamic simulations
- chemical and biological molecular systems 597–598
- water clusters and water solution 595–597
- polarizable force fields 590–591
- calibration of parameters 595
- Drude model 591–592
- electronegativity equalization method 592–595
- induced dipole moment (multipole) model 591–592
- potential energy function 588–589
- atom-condensed Kohn-Sham (second order) (ACKS2) 603–604, 608, 613, 615–616
- atom-condensed Kohn-Sham density functional theory (ACKS-DFT) 611, 613

- atom-condensed Kohn-Sham (ACKS) model 603, 615
- atomic charge 103–104, 330
- atomic force microscopy (AFM) 245
- atomic libration, in organic crystals 514–516
- atomic radii 376
- atom in a molecule (AIM) 607
- atomistic force field 606, 616, 618
- atoms in molecule (AIM) 325, 608
- atoms-in-molecules partitioning schemes 653
- aza Diels-Alder (A-DA) reactions 487
  
- b**
- “Bader” program 563
- Bader’s atoms in molecules (AIM) approach 25
- Bader scheme 578
- base exchange reaction 263
- Becke’s method 635
- Bell-Evans-Polanyi (BEP) principle 574
- Berkowitz-Parr relation 33
- $B_{12}N_{12}$  cage templates 541–542
- Boltzmann constant 18, 68, 139, 464
- Boltzmann-Gibbs entropy 283
- bond critical points (BCPs) 353–354, 503
- bond dissociation energy 248
- Bonding Evolution Theory (BET) 188, 493
- Born-Oppenheimer approximation 96, 118
- Born Oppenheimer Molecular Dynamics (BOMD) method 163
- Bright-Wilson argument 353
- Brønsted coefficient 466
- Brønsted-Evans-Polanyi (BEP) 465, 474
- Bürgi-Dunitz angle of attack 87
  
- c**
- cage critical points (CCPs) 354
- canonical ensemble 49–50
- canonical molecular orbital (CMO) 380
- carbonyl ylide (CY) 203
- chaotic ionization 66
- charge and spin states 605
- charge density rearrangement 122
- Chattaraj’s philicity index 32
- chemical binding
  - bond space 438–439
  - coarse grained procedure 429–430
  - correct asymptotics 438
  - covalent binding 438
  - definition 419
  - electronegativity 420–421
  - energy change of spin-polarised many-electron systems 424–428
  - lattice model for molecular systems 430–438
  - molecules formation 419
  - physical foundation 421–424
  - quantitative description of 420
  - quantum effect 420
- chemical density functional theory 7, 443
- chemical hardness ( $\eta$ ) 162
- chemical information 350
  - extracting 352–355
  - quality of 366
- chemical potential 161
  - locality 79–81
- chemical principles 116
- chemical reactivity 36–38, 229, 556
  - atom interacting with an external electric field 164–167, 167
  - atom interacting with an external magnetic field 176
  - electronic spectra and 81
  - ion-atom collision 178–179
  - ion-molecule collision 179–180
  - molecule interacting with an external electric field in confined environment 167–176
  - molecule interacting with an external magnetic field in a confined environment 176–178
  - theoretical background 163
- chemical reactivity theory (CRT) 230, 281

- chemical topological analysis 653  
 the Chemist's DFT 7  
 ChemTools 650  
   design principles 654–657  
   example 651–652  
   features 652–654  
   input and output 650–651  
   modularity 655  
   robustness and quality assurance  
     655–657  
 classical Coulomb self repulsion 19  
 classical force fields 587  
 coarse grained models 420  
 CoGEF (Constrained Geometries simulate  
   External Force) 247  
 CoGEF approach 249  
 combined SWAB and HSAB rules 268  
 complementary reactivity modes 408  
 comprehensive decomposition analysis of  
   stabilization energy (CDASE)  
     218  
 conceptual density functional theory  
   (CDFT) 7, 47, 62, 78, 93–94, 103,  
     111, 188, 210, 443, 504, 514, 519,  
     574, 652  
   automatic calculation 636  
   bond angles stressed 255–258  
   chemical binding 419  
   chemical bonds stressed 252–255  
   ensembles 49  
   evaluation of contribution 639  
   hydrogen storage 535  
   mechanical force 249–251, 504  
   mechanochemical response functions  
     251–252  
   orbital-weighted Fukui function and  
     dual descriptor 637  
 conceptual density matrix functional  
   theory 653  
 condensed local softness 559  
 condensed-to-atom variant 64  
 constrained DFT 607  
 Coulomb interaction 562  
 crystal-solvent interaction 511  
 [3+2] cycloaddition (32CA) reactions  
     199–202  
 cyclopentadiene (Cp) 196
- d**
- d-band center 579  
 degenerate states 94, 97, 104  
 del dot del 18  
 delocalization error 21  
 (de)localization index 653  
 density based models 3  
 density-based reactivity descriptors 449  
 density functional approximations (DFAs)  
     356  
 density functional reactivity theory 443  
 density functional theory (DFT) 3, 17,  
     61, 161, 419, 603  
   applications 12  
   atomic and molecular descriptors  
     8–10  
   concept 5  
   electronic chemical potential  
     identification 5–6  
   history 4–5  
   principles 10–12  
   response function tree 9  
   tools 653  
 density-potential response function 428  
 DFT descriptors 476  
 diacetone diperoxide (DADP) 505, 508,  
     509, 511  
 diatomic molecule 248  
 didactic approach 100  
 Diels-Alder (DA) reaction  
   electrophilic species 490–493  
   forward electron density flux 485–486  
   H-DA reactions 487–490  
   Lewis acid catalysts 486–487  
   Parr functions 493–498  
   polar mechanism 481  
 Dirac delta function 95, 215  
 disarmingly simple 3  
 dissociation energy 248  
 distillation 574



- domain-averaged Femi hole (DAFH)
  - 654
- double-exchange reactions 263, 265
- Drude model 591
- dual descriptor (DD) 26–31, 57, 64, 79,
  - 137, 637
  - FMO approximation 83
  - kernel 147
- dynamic current density 164
- dynamic polarizability 167
- dynamics of electronegativity 178
- e**
- electroaccepting powers 216
- electroaffinity 327
- electrodonating power 216
- electrofugality indices 26
- electron delocalization aromaticity 310
- electron density (ED) 62, 63, 100, 101,
  - 282, 503
  - critical points of 353–355
  - errors 366, 368
  - functions 355–356
  - general shape 350–352
  - kinetic 361–366
  - Laplacian of 360–361
  - reduced density gradient 356–360
- electron density gradient (RDG) 504
- electron density reorganization 420
- electronegative equalization 230
- electronegativity 21, 22, 65, 329, 420, 574
- electronegativity equalization methods
  - (EEM) 234, 591, 592, 603, 610
  - ab initio* parameterization 610–611
  - energy difference in atomic densities 609–610
  - failures of orbital-free DFT and traditional 611
- electronegativity equalization principle
  - (EEP) 10, 65, 137
- electronegativity parameter 422
- electron-electron repulsion 17, 266
- electronic chemical potential 20, 22, 62,
  - 470
- electronic energy 112, 137
- electronic entropy 68, 140
- electronic heat capacity 148
- electronic Schrödinger equation 603
- electronic structure principles
  - electronegativity based principle 65–66
  - electronic entropy based principle 68
  - electrophilicity based principles 67–68
  - hardness based principles 66–67
- electron localization errors 368
- electron localization function (ELF) 64,
  - 363, 366, 504, 653
- electron-nuclear attraction energy 607
- electron polarization rationalized
  - 85–89
- electron spin-density functions 114
- electron transfer controlled hydrogen
  - bonding (ETCHB) 221
- electron-transfer energy 268
- electron-transfer reaction 555
- Electrophilic Aromatic Substitution (EAS)
  - 84
- electrophilic Fukui function 78, 257
- electrophilicity 24, 281, 291, 482
- electrophilicity based principles 67
- electrophilicity index 65, 162, 176, 213
- electrostatic effects 555
- electrostatic energies 268
- electrostatic energy expression 610
- electrostatic interaction energy 589
- electrostatic potential 95, 101–103
- energetic materials reactivity 508
- energy density
  - Pauli kinetic 363
  - Weizäcker kinetic 357
- ethylene 79
- Euler equation 18
- Euler-Lagrange equation 62, 161, 556
- E* vs. *N* model 191
- exchange-correlation
  - energy 19, 607
  - function 562
  - potential 19

excitation energy 81  
 excited states, electron polarization  
     rationalized with 85, 88  
 Eyring equation 464

**f**

face-integrated Fukui functions  
     512  
 Fe-porphyrin complex 456  
 Fe-porphyrin system 458  
 Fermi-Dirac distribution (FDD) 577  
 Fermi level 557  
 Fermi softness  
     active sites of MoS<sub>2</sub> 582  
     basic data 575–579  
     correlation with adsorption energy  
       580–581  
     d-band center 579  
     heuristics 575  
 finite temperature conceptual density  
     functional theory  
     first order response functions, in grand  
       canonical ensemble 139–144  
     response functions 148–150  
     second order response functions, in  
       grand canonical ensemble  
       145–148  
 first order response functions, in grand  
     canonical ensemble 139–144  
 Fisher information 68, 282, 284, 643  
 fixed-charge force fields 606  
 flufenamic acid 506  
 force field 587  
 forward electron density flux 485  
 fractional charge 140  
 Fragment of the Molecular Response  
     (FMR) approach 29  
 frontier molecular orbital theory (FMOT)  
     27, 28, 38, 78, 79, 83, 84, 188, 485,  
     555  
 Fukui function (FF) 26, 31, 63, 95, 101,  
     104, 105, 120, 137, 162, 188, 221,  
     504, 511, 637  
     alkaline metal oxides bulks and (100)  
     surfaces 561–565

    application 565–567  
     calculation 190  
     carbon nanotube 559–560  
     criteria 193  
     definition 556  
     dual descriptor 195  
     frontier molecular orbitals 188–190  
     metallic carbon nanotubes 558  
 functional expansion approach 58  
 furfuryl acetate pyrolysis 237, 238  
 fuzzy partition 635

**g**

Gaussian shape method 375  
 generalized gradient approximation  
     (GGA) 4, 356  
 generalized nonlinear Schrödinger  
     equation (GNLSE) 163  
 geometric relaxation 80, 233  
 Ghosh/Berkowitz definition 34  
 Ghosh-Berkowitz-Parr (GBP) entropy  
     283, 643  
 Gibb's free energy 47, 465  
 global and local reactivity descriptors  
     63  
 global electron density transfer (GEDT)  
     196, 482  
 global softness 162  
 grand canonical ensemble 50, 52  
     first order response functions 139  
     second order response functions  
     145  
 grand isomorphic ensemble 50  
 grand potential functionals 62  
 grant isomorphic ensemble 54  
 Green's functions 558  
 ground-state electronegativity (GS-EN)  
     331  
 ground state electronegativity  
     equalization (GS-ENE) 339  
 ground state electronic density 143  
 ground-state-parabola (GSP) 330  
 ground state theory 89  
 ground state (GS), vs. valence state  
     energies 326

**h**

hard and soft acids and bases (HSAB) 23, 505

hardness 66, 329

hardness equalization principle 66

hardness kernels 33, 35

hard-soft acid-base (HSAB) 65, 230, 264

Hartree-Fock equations 234

Heaviside step function behavior 151

Hellmann-Feynman formula 49, 118, 505

Helmholtz free energy 47, 62

hemoglobin 452

hemoproteins 452

heteronuclear molecules 180

highest occupied molecular orbital (HOMO) 162, 444, 555

Hirshfeld-I 635

Hirshfeld population analysis 63

Hirshfeld surface 522, 523

Hirshfeld weighting function 635

Hohenberg and Kohn theorem 62

Hohenberg-Kohn energy 19

Hohenberg-Kohn function 4, 17, 33, 50, 62, 77, 79, 80, 93, 351, 355, 607

homogeneous electron gas (HEG) 357

HOMO-LUMO gap 23, 254

hot excited state 80

hybridization 329

hydrogen atom transfer (HAT) mechanism 449

hydrogen-bonding strength 516

hydrogen storage

- CDFT 535–537
- computations 537
- hydrogen binding building blocks 537–547
- mathematical algorithm 535

hyperbolic secant function 147

hyperpolarizability 604–605

**i**

imaginary frequency 233

information conservation principle 286

Information Functional Theory 286

information gain 283

information-theoretic approach (ITA) 642

applications 288

- aromaticity and antiaromaticity 295–297
- electrophilicity and nucleophilicity 291–292
- noncovalent systems 294–295
- steric effect and stereoselectivity 288–291
- strong covalent interactions 292–294

Fisher information 282

GBP entropy 283

principle 285

quantities 283, 287

Rényi entropy 283

inter-atomic charge flow 420

inter-atomic surface (IAS) 503

Intergovernmental Panel on Climate Change (IPCC) 533

intermolecular interactions 519

internal rotations 66

intrinsic reaction coordinate (IRC) 229, 238

inverse electron demand (IED) 486

ion-atom collision 178

ion-molecule collision 179

isomorphic ensemble 53

Iterative Stockholder Analysis (ISA) 653

**j**

JEDI analysis tool 249

**k**

kinetic energy density 18, 68, 361, 366

kinetic-exchange-correlation 610

Klopman-Salem equation 38

Klopman's classification 264

Kohnendash Sham one-electron potential 382

Kohn-Sham-based EEM 603

Kohn-Sham DFT (KS-DFT) 391, 611

Kohn-Sham equation 19, 285

- Kohn-Sham frontier molecular orbitals 27
- Kohn-Sham HOMO orbital energy 25
- Kohn-Sham kinetic energy 607
- Kohn-Sham (KS) orbitals 28, 556
- Kohn-Sham potential 19
- Kohn-Sham theory 104
- Kohn-Sham total energy 19
- Koopmans' theorem 24, 63, 162, 234, 536
- Koopmans-type approximation 235
- Kubas model of hydrogen binding 543
- Kullback-Leibler information 68
- L**
- Lagrange multiplier 18, 62, 161, 234
- Legendre-transform 48
- Lewis acid (LA) catalysts 486
- linear response function (LRF) 33, 35, 302
- applications
- alchemical derivatives 315–320
- electron delocalization, aromaticity 310–313
- inductive and mesomeric effects 310
- molecular conductivity 313–315
- theory and computational aspects 303–307
- local Berlin function 119
- Local Density Approximation (LDA) 4
- local hardness 31, 33, 55
- local heat capacity 148
- localized orbital locator (LOL) 361, 363, 653
- local philicity index 163
- local softness 31, 33
- long-range electron transfer 605, 606
- lowest unoccupied molecular orbital (LUMO) 29, 162, 555
- m**
- Marcus equation (ME) 465, 466, 474
- marcus potential function 469
- The mathematical theory, of
- communication 281
- matrix diagonalization 28
- maximum hardness principle (MHP) 11, 66, 81, 162, 230, 536
- Maxwell's relationship 51, 137, 556
- Maynard-Parr description 67
- mean-square displacement amplitude (MSDA) 514
- mean unsigned deviations (MUD) 339
- mechanical force 249, 251
- bond angles stressed by 255–258
- chemical bonds stressed by 252–255
- mechanochemical response functions 251
- mesomeric effects 310
- meta-GGA approximation 356
- metallic carbon nanotubes 573
- metal nanocatalysts 574
- metal-water complexes 447
- methylmalonyl-CoA mutase (MCM) enzyme 451
- Minimal Basis Iterative Stockholder (MBIS) 653
- minimum electrophilicity principle (MEP) 67, 162, 167, 536
- minimum energy path (MEP) 229, 464
- Minimum Information Gain Principle 286
- minimum magnetizability principle (MMP) 67
- minimum polarizability principle (MPP) 12, 67, 162, 164, 536
- modularity 655
- molecular acidity
- acid-base dissociation constant 443
- metal-water complexes 447
- molecular electrostatic potential 445
- proton dissociation 446
- quantum chemistry 443
- quantum descriptors 444
- total energy change 446
- molecular density, energy difference in 608, 609
- molecular dissociation 605, 606

- molecular dynamics (MD) simulations
    - 590
    - chemical and biological molecular systems 597–598
    - water clusters and water solution 595–597
  - molecular electron density theory (MEDT) 188, 482
    - in polar DA (P-DA) reactions
      - chemoselectivity in 32CA reactions 202
      - competitive [2+4] *versus* [4+2] cycloadditions 196–197
      - competitive [4+2] *versus* [2+2] cycloadditions 198
      - in [3+2] cycloaddition (32CA) reactions 199–202
  - molecular electrostatic potential (MEP) 64, 86, 444
  - molecular face (MF) 376
    - atomic and ionic radii 376
    - electron atoms 378–379
    - hydrogen atom 377
  - formalism 379
    - Kohn-Sham one-electron potential 382
    - molecular intrinsic characteristic contour 382
    - potential acting 380–382
  - frontier electron density 382
  - hydrogen, halogen, and pnictogen bonds 383–384
    - picture indicating 384–386
    - reactivity ability 387
  - molecular frontier electron density (MFED) 384
  - molecular graph 355
  - molecular intrinsic characteristic contour (MICC) 382
  - molecular mechanics (MM) 587
  - molecular mechanochemistry 246
  - molecular orbital (MO) 187, 391, 653, 654
  - molecular polarizability 604, 605
  - molecular vibrations 66
  - Morse potential 247, 249
  - Mulliken electronegativity 144
  - Mulliken population(s) 29
  - Mulliken population analysis (MPA) 63, 103, 537
  - Mulliken's electronegativity 6, 327
  - multiphilic descriptor 32, 64
  - Multiwfn 633
    - atomic space partition and integration 635–636
    - basic features 633–634
    - conceptual density functional theory analysis 636
    - automatic calculation 636–637
    - comprehensive functions 641–642
    - evaluation of contribution 639–641
    - orbital-weighted Fukui function and dual descriptor 637–639
    - electron density evaluation 634–635
    - information-theoretic approach analysis 642–645
- n**
- natural extensions 9
  - natural orbitals for chemical valence (NOCV) 28, 84
  - natural population analysis (NPA) 454, 537
  - natural valence orbital energies 460
  - 3*N*-dimensional wave function 61
  - N*-electronic system 161
  - N*-electron molecular system 429
  - Net Reactivity Index (NRI) 25
  - n,n*-octyl-D-gluconamide (OGA) 512
  - non-covalent interactions (NCI) 294, 504, 653
  - non-degenerate state 94, 97
  - noninteracting kinetic energy 285
  - non-vanishing current density 64
  - normal electron demand (NED) 485
  - normalisation constant 86
  - nuclear critical points (NCP) 352, 354
  - nuclear Fukui function 505, 506
  - nuclear independent chemical shift (NICS) 537

- nuclear reactivity descriptors 118  
 nuclear reactivity index 31  
 nucleofugality indices 26  
 nucleophilicity 281, 291, 482  
 null electron density flux (NEDF) 486
- O**
- one-parabola model 211, 213  
 Onicescu information energy 68, 283  
 open-source software 654, 656  
 optimum spin-densities 114  
 orbital-free DFT 603  
 orbital-perturbation-theory interaction 556  
 orbital relaxation 27  
 orbital-wise coordination number 574  
 organic crystals  
   atomic libration 514–516  
   intermolecular interactions locality 519–525  
   solid-state reaction 505–511  
 organic solid-state reaction  
   energetic materials 508–511  
   pharmaceutical crystals 506–508  
 Oriented External Electric Fields (OEEF) 9
- P**
- pair-electronegativity 331  
 Parr functions 193, 493, 495  
 particular density functional theory 574  
 Paterno-Buchi reactions 80  
 Pauli Exclusion Principle 285  
 Pauli kinetic energy density 363  
 Pearson's hard and soft acids and bases (HSAB) 162  
 Pearson's notation 82  
 periodic boundary conditions (PBC) 562  
 perturbation theory 106, 559  
 pharmaceutical crystals reactivity 506  
 2-(phenylamino)nicotinic acid (2-PNA) 517, 518  
 photochemical cycloadditions 81  
 photochemical reactivity 78  
 photoexcitation 77  
 physical information 285  
 $\pi$ - $\pi$  stacking 503  
 planar aromatic/antiaromatic hydrocarbon systems 545  
 Planck constant 464  
 polar Diels-Alder (P-DA) reaction 481  
   chemoselectivity 497–498  
   electrophilicity 482–485  
   electrophilic species 490–493  
   H-DA reactions 487–490  
   Lewis acid catalysts 486–487  
   nucleophilicity 482–485  
   Parr functions 493–495  
   regioselectivity 496–497  
   reverse electron density flux 485–486  
 polarisation energy 87  
 polarizability 162  
 polarizable force fields 590, 606  
 polyacetylene 246  
 polymorphism of crystal 503  
 potential energy surface (PES) 229, 537, 587  
 PPLB theorem 218  
 PP model 217, 218  
 Principle of Extreme Physical Information 286  
 Principle of Maximum Hardness 82  
 promolecular density 635  
 protonation energy 406  
 proton-coupled electron transfer (PCET) 449  
 pseudodegenerate 559  
 pseudodiradical 199  
 pseudo(mono)radical 199  
 pyrolysis reaction 230
- Q**
- quadratic model 26  
 quantitative hard/soft acid/base rule 268  
 quantitative strong/weak acid/base rule 268  
 Quantitative Structure-Activity Relation (QSAR) 209  
 quantum chemical community 4  
 quantum effect 420

- quantum fluid density functional theory (QFDFT) 163
  - quantum fluid dynamics (QFD) 163
  - quantum mechanics (QM) 587, 649
  - quantum mechanochemistry 247–249
  - quantum potential 64
  - quantum theory of atoms in molecules (QTAIM) 352, 355, 503, 653
  - quasi-atomic minimal basis-orbital (QUAMBO) 654
  - quasi-degenerate states 106
- r**
- Raman scattering intensity 31
  - Rayleigh-Schrödinger perturbation theory 22, 82
  - reactant minimum 232
  - reaction electronic flux (REF) 230, 470–471
    - application 236–239, 472, 474
    - chemical partition of 471–472, 474
    - chemical potential 233–235
    - concept 235–236
    - electronic populations and bond orders 472
    - physical partition of 471, 474
    - and reaction force analysis 472, 473
  - reaction energy 267
  - reaction force (RF) 230
    - definition 230, 232–233
    - interpretation 233
  - reaction force analysis (RFA) 466–470
    - and REF 472–473
  - reaction regions 466
  - reaction thermodynamics 464
  - reactivity descriptors 472
  - real space function 636
  - recapitulation 613, 615
  - regioselectivity 405
  - relative Fisher entropy 643
  - relative Shannon entropy 643
  - relaxation effects 562
  - Rényi entropy 68, 283, 644
  - response function tree 38, 301
  - response of molecular fragment (RMF) approach 29
  - reverse electron density flux (REDF) 485, 486
  - Ring Critical Points (RCPs) 354
- S**
- Sanderson's electronegativity equalization principle 162
  - Savin's interpretation 363
  - Schrödinger equation 18, 61, 419
  - second and higher order global derivatives 23–26
  - second-order gradient expansion (GEA) 356
  - second order response functions in the grand canonical ensemble 145
  - second-order taylor expansions 55
  - Shannon entropy 68, 282
    - density 642
  - shared-electron delocalization index (SEDI) 654
  - simply Wigner-Seitz scheme 578
  - singled-walled-capped carbon nanotubes (SWCCNTs) 559
  - single-molecule force spectroscopy (SMFS) 246
  - single-particle density 61
  - Slater determinant 18
  - smooth quadratic interpolation 138
  - softness kernel 33, 35, 560
  - solid-state reactions 505
  - spin density 407
  - spin density functional theory, non-relativistic 112
  - Spin-dependent Chemical potentials 431
  - spin electronegativity 423
  - spin Fukui functions 453
  - spin multiplicity 456
  - spin-orbitals 18
  - spin-polarised many-electron systems 424
  - spin-polarized conceptual DFT framework (SP-CDFT) 453

- spin-polarized density functional theory (SP-DFT) 63, 439
- applications 119–121
  - electronic descriptors 114–116
    - finite-difference approximations 117–118
    - global and local 116–117
    - non-local 117
  - Fukui descriptors 121–123
  - nuclei-related descriptors 118–119
- spin polarized version, of reactivity descriptors 63
- spin reactivity indices 454
- spiropyran-merocyanine isomerization 246
- “star-like” complexes 547
- state-specific dual descriptor (SSDD) 80, 83
- stereoselectivity 281, 290
- steric effect 281
- stockholder partition 286
- strain-promoted alkyne azide cycloaddition (SPAAC) 255
- strong covalent interaction (SCI) 292, 644
- strong/weak acid/base (SWAB) Rule 264
- t**
- Taylor expansion of energy 210, 211
- Taylor series 82
  - coefficients 104
- 2,2,4,4-tetramethyl-3-thioxocyclobutan-1-one 200
- thermodynamic driving force 469
- thermodynamic dual descriptor 147
- thiocarbonyl S-methanides (TCY) 202
- Thomas-Fermi-Dirac ansatz (TFD) 34
- three-atom-component (TAC) 199
- time-dependent chemical reactivity parameters 176
- time-dependent density functional theory (TDDFT) 33, 77, 163
- time-dependent electronegativity profile 178
- time-dependent electrophilicity 167
- time-dependent extensions 439
- time-dependent reactivity parameters 164
- time dependent situations 66
- time evolved hardness profile 178
- time-independent (and time-dependent) Schrodinger equation 61
- tolfenamic acid (TFA) 517
- total local hardness 34
- transition state theory (TST) 464
- triacetone triperoxide (TATP) 505, 511
- 1,3,5-trinitro-s-triazine (RDX) 508, 509
- 1,3,5-trinitro-1,3,5-triazine 505
- triple zeta with polarization basis function (TZVP) 221
- Tsallis entropy 283
- turning point 382
- two-parabolas model 216
  - global charge transfer in 218–219
  - local charge transfer in 220–221
- v**
- valence bond (VB) theory 391
  - ambident vinyloxy anion 409–411
  - delocalization 395–398
  - hardness and softness 402–405
  - local reactivity 399
  - qualitative reactivity 393–395
  - regioselectivity 405
  - spin density distribution 398–399
- valence-pair-affinity (VPA) 331
- valence-pair-energy 331
- valence-pair-equilibration (VPEq) 336–339
  - in polyatomics 340–342
- valence-state-parabola (VSP) 331
- valence states (VS) 325
  - electric dipole moments 342
  - ground state vs. 326–329
  - ionization energy 327
  - thermodynamic cycles 336
  - valence-pair-affinity 329–336
  - valence-pair-equilibration 336–339
    - in polyatomics 340–342
- van der Waals forces 519



venerable Parr and Pearson (PP) model  
212  
vertical ionization energy 251  
vinyloxy anion 401  
Voronoi polyhedral 563  
Voronoi scheme 578

**W**

water clusters 595  
wave function 17, 61  
wavefunction quantum chemistry 17  
Weizäcker kinetic energy density 357  
wettability anisotropy 511  
Wheland intermediate 35  
whole collision process 178

Wigner-Witmer correlation 326  
Woodward-Hoffmann rules 66  
Woodward-Hoffmann rules 78–79,  
195

**X**

X-POL potential 590

**Z**

zero number of imaginary frequencies  
(NIMAG) 537  
zero sharing penetration 328  
zero-temperature Fukui function 192  
zeroth-order approximation 189  
zeroth-order radial basis function 610